Deep Space Network

DSN Telecommunications Link Design Handbook

http://deepspace.jpl.nasa.gov/dsndocs/810-005/

TMOD No. **810-005, Rev. E**
Issue Date: November 30, 2000
JPL D-19379, Rev.E

Jet Propulsion Laboratory
California Institute of Technology

DSN Telecommunications Link Design Handbook

810-005
Rev. E

Deep Space Network

DSN Telecommunications Link Design Handbook

Prepared by:

Signature Provided 01/11/2024
Christine Chang Date

Approved by:

Signature Provided 01/11/2024
Timothy Pham Date
DSN Communication System Chief Engineer

Released by:

Signature Provided 01/11/2024
DSN Document Release Date

DSN No. **810-005**
Issue Date: January 11, 2024
JPL D-19379

Jet Propulsion Laboratory
California Institute of Technology

Users must ensure that they are using the current version in DSN Telecommunications Link Design Handbook website: https://deepspace.jpl.nasa.gov/dsndocs/810-005

This page intentionally left blank

Document Change Log

Rev.	Issue Date	Modules Affected	Change Summary
Initial	3/1/70	All	New document.
A	10/1/70	All	Complete revision.
B	4/15/72	All	Complete revision.
C	—	All	Complete revision.
D	2/15/75	All	New modular format first appeared.
E	1/15/2001	All	Title changed from DSN Flight Project Interface Design Handbook; all modules renumbered and revised or reformatted. Volume 2 deleted as proposed capabilities are now Ied within the modules of this revision. Modules not related to telecommunications link design have been deleted from this document and will be incorporated in a new document, 810-007, DSMS Mission Interface Design Handbook.
Change 1	2/10/2003	105, 202, 205	Added monthly weather statistics for all frequency bands to module 105, Added discussion of one-way Doppler error and X-Up/Sdown Solar Phase Scintillation errors to module 202. Provided characteristics of new DSMS command equipment in module 205.
Change 2	6/13/2003	207, 301	Added concatenated codes, QPSK/OQPSK, and improved turbo code information to module 207, Identified 11-m subnet as non-operational, expressed geodetic coordinates in WGS84 ellipsoid and added DSS 55 to module 301.
Change 3	8/18/2003	101, 305, 901	Documents new feedcone at DSS 63, L-band at all 70-m stations, and S-band low noise cone at DSS 43. Provided information on test support. Added information and corrected Glossary.
Change 4	2/10/2004	104, 301	Provided latest capability and performance information for all BWG stations. Corrected locations of DSS-26, 54, and 55. Provides final receive and transmit masks for DSS-55.
Change 5	3/31/2004	101A, 208, 214, 304	Corrects Figures 1 and 5 in module 101, Rev. A. Corrects Figures 3 and 17 in module 208. Adds module 214, Pseudo-noise and Regenreative Ranging, and module 304, Frequency and Timing.
Change 6	7/15/2004	210	Provides capabilities of Delta Differential One-way Ranging in the DSN.

Document Change Log (Continued)

Rev.	Issue Date	Modules Affected	Change Summary
Change 7	10/7/2004	206, 302, 901A	Adds overview of telemetry and antenna positioning capability. Revises Glossary to accommodate new and revised modules.
Change 8	5/9/05	212	Provides capabilities of telemetry equipment installed in the DSN 26-m subnet stations.
Change 9	8/10/05	104, 106	Provides revised X-band and new Ka-band capability for DSS-34. Adds module 106, Solar Corona and Solar Wind Effects.
Change 10	10/21/05	106, 301B, 901B	Corrects errors in module 106, provides revised location, coverage and horizon mask for recently relocated DSS-65, and updates Glossary.
Change 11	2/20/06	203	Incorporate changes resulting from improve-ments in sequential ranging implementation.
Change 12	5/26/06	105B, 107. 305A	Provides new weather models and methods of calculating system temperature, Adds a radio source catalog. Updates capabilities of test facilities.
Change 13	8/25/06	101B, 211	Revises 70-m module to be consistent with module 105B and to delete DSS-43 S-band Ultracone. Adds description of wideband VLBI capabilities.
Change 14	4/2/07	103A, 203A	Revises 34-m HEF module to be consistent with module 105B and to Ie DSS-45 & DSS-65 S-band uplink capability. Restores information on recommended range of *Pr*/*N*0 to module 203.
Change 15	9/15/08	103A, 104B, 201, 206A, 301C	Revises 34-m HEF module to provide measured S-band uplink performance. Modifies 34-m BWG module to document current status of K and Ka-band implementation, Modifies frequency assignments module to Ie 26-GHz band. Modifies Coverage and Telemetry General Information modules to document effects of decommissioned antennas and 26GHz.
Change 16	9/18/08	104C, 208	Adds antenna performance at 26 GHz. Revises coding module and deletes obsolete code types.
Change 16.5	5/18/2009	104D, 208A	Revises antenna performance at 26 GHz for DSS 24,-34, and 54. Adds Low Density Parity-Check (LDPC) codes as a proposed capability.
Change 17	8/1/2009	105C	Updates weather models for the 26-GHz support capability. Removes references to all 26-m stations.

Document Change Log (Continued)

Rev.	Issue Date	Modules Affected	Change Summary
Change 18	9/15/2009	101C, 102, 104E, 105D, 204, 212, 213	Updates the 400-kW S-band uplink capability and its supported frequency range. Revises DSS-54 and DSS-55 G and T information. Removes the document modules and all references to the decommissioned 26-m stations.
Change 19	10/31/2009	203C, 206B, 305B, 901D	Revises these document modules to reflect organizational changes and to eliminate references to the 26-m subnet stations.
Change 20	12/15/2009	201B, 205B, 301E, 302A	Revises these document modules to reflect organizational changes and to eliminate references to the 26-m subnet stations.
Change 21	4/1/2010	Introductory Materials, 001A	Revises introductory materials (Cover & Title pages, Change Log, Foreword, Table of Contents) and Module 001A with up-to-date information and to reflect organizational changes.
Change 22	6/1/2010	Introductory Materials, 104F, 205C, 209A, 301F, 302B	Revises these document modules to reflect organizational changes.
Change 23	9/30/2010	Introductory Materials, 106B, 202B, 304A	Revises these document modules to reflect organizational changes.
Change 24	4/29/2011	Introductory Materials, 101D, 107A, 211A, 901E	Revises introductory materials and Module 101D, 107A, 211A with up-to-date information.
Change 25	3/22/2012	Introductory Materials, 301G, 901F	Revises introductory materials and Module 301G with updated information. Revises the abbreviation list on Module 901F.
Change 26	10/17/2012	Introductory Materials, 301H	Revises introductory materials and Module 301H with updated information for DSS-54 and DSS-55.
Change 27	03/12/2013	Introductory Materials, 104G, 208B	Revises introductory materials. Revises 104G and 208B with up-to-date information.
Change 28	04/08/2013	Introductory Materials, 107B	Revises introductory materials. Revises 107B with up-to-date information.
Change 29	09/18/2013	Introductory Materials, 101E	Revises introductory materials. Revises 101E with up-to-date information.
Change 30	06/12/2014	Introductory	Revises introductory materials. Revises 301I with up-to-date information.

		Materials, 301I	
Change 31	08/01/2014	Introductory Materials, 103C	Revises introductory materials. Revises 103C with up-to-date information.
Change 32	09/10/2014	Introductory Materials, 301J	Revises introductory materials. Revises 301J with up-to-date information.
Change 33	12/15/2014	Introductory Materials, 107C, 201C, 205D, 304B	Revises introductory materials. Revises 107C, 201C, 205D, 304B with up-to-date information.
Change 34	02/09/2015	Introductory Materials, 209B, 210A, 211B, 302C	Revises introductory materials. Revises 209B, 210A, 211B, and 302C with up-to-date information.
Change 35	04/01/2015	Introductory Materials, 104H	Revises introductory materials. Revises 104H with up-to-date information.
Change 36	08/05/2015	Introductory Materials, 101F	Revises introductory materials. Revises 101F with up-to-date information.
Change 37	10/22/2015	Introductory Materials, 105E, 107D	Revises introductory materials. Revises 105E and 107D with up-to-date information.
Change 38	10/28/2015	Introductory Materials, 214A	Revises introductory materials. Revises 214A with up-to-date information.
Change 39	09/13/2016	Introductory Materials, 301K	Revises introductory materials. Revises 301K with up-to-date information.
Change 40	11/17/2016	Introductory Materials, 205E, 209C	Revises introductory materials. Revises 205E and 209C with up-to-date information.
Change 41	02/10/2017	Introductory Materials, 104I, 210B, 211C, 302D, 901G	Revises introductory materials. Revises 104I, 210B, 211C, 302D, and 901G with up-to-date information.
Change 42	05/03/2017	Introductory Materials, 206C	Revises introductory materials. Revises 206C with up-to-date information.
Change 43	0/12/2018	Introductory Materials, 104J	Revises introductory materials. Revises 104J with up-to-date information.
Change 44	07/03/2018	Introductory Materials,	Revises introductory materials. Revises 211D with up-to-date information. Revises 301L with up-to-date information.

		211D, 301L	
Change 45	01/22/2019	Introductory Materials, 202C	Revises introductory materials. Revises 202C with up-to-date information.
Change 46	02/14/2019	Introductory Materials, 209D	Revises introductory materials. Revises 209D with up-to-date information.
Change 47	06/06/2019	Introductory Materials, 210C	Revises introductory materials. Revises 210C with up-to-date information.
Change 48	07/17/2019	Introductory Materials, 104K, 203D, 214B	Revises introductory materials. Revises 104K, 203D, 214B with up-to-date information.
Change 49	09/04/2019	Introductory Materials, 101G	Revises introductory materials. Revises 101G with up-to-date information.
Change 50	10/16/2019	Introductory Materials, 104L	Revises introductory materials. Revises 104L with up-to-date information.
Change 51	12/23/2019	Introductory Materials, 211E	Revises introductory materials. Revises 211E with up-to-date information.
Change 52	09/04/2020	Introductory Materials, 201D, 301M	Revises introductory materials. Revises 201D and 301M with up-to-date information.
Change 53	11/12/2020	Introductory Materials, 108	Revises introductory materials. Initial version for 108
Change 54	02/05/2021	Introductory Materials, 201E, 209E, 210D, 304C, 901H	Revises introductory materials. Revises 201E, 209E, 210D, 304C, and 901H with up-to-date information.
Change 55	04/02/2021	Introductory Materials, 104M, 107E, 205F	Revises introductory materials. Revises 104M, 107E, and 205F with up-to-date information.
Change 56	06/07/2021	Introductory Materials, 104N	Revises introductory materials. Revises 104N with up-to-date information.
Change 57	09/01/2021	Introductory Materials, 202D, 206D	Revises introductory materials. Revises 202D and 206D with up-to-date information.
Change 58	04/15/2022	Introductory Materials, 301N	Revises introductory materials. Revises 301N with up-to-date information.
Change 59	05/04/2022	Introductory Materials, 201F	Revises introductory materials. Revises 201F with up-to-date information.

Change 60	06/07/2022	Introductory Materials, 211F	Revises introductory materials. Revises 211F with up-to-date information.
Change 61	07/19/2022	Introductory Materials, 202E	Revises introductory materials. Revises 202E with up-to-date information.
Change 62	08/09/2022	Introductory Materials, 104O	Revises introductory materials. Revises 104O with up-to-date information.
Change 63	03/23/2023	Introductory Materials, 205G	Revises introductory materials. Revises 205G with up-to-date information.
Change 64	08/03/2023	Introductory Materials, 103D, 214C	Revises introductory materials. Revises 103D and 214C with up-to-date information.
Change 65	10/10/2023	Introductory Materials, 206E	Revises introductory materials. Revises 206E with up-to-date information.
Chang 66	01/11/2024	Introductory Materials, 209F, 210E, 211G	Revises introductory materials. Revises 209F, 201E, and 211G with up-to-date information.

Foreword

This modular handbook has been approved by the Deep Space Network (DSN) Project Office and is provided as a source of technical information for all flight projects using the DSN. It provides information useful to flight projects contemplating the design of hardware and software, with reasonable assurance that the resulting project telecommunications interfaces will be compatible with the established or planned DSN configurations.

The handbook is primarily concerned with performance parameters of equipment that supports the forward and return telecommunications link interfaces between spacecraft and the DSN. The handbook consists of modules that present technical information applicable to the current DSN configuration and preliminary information applicable to future DSN configurations. The modules will be revised to reflect new capabilities when these new capabilities have been planned and budgeted for by the DSN Project Office.

For matters of interpretation or questions concerning this handbook, contact the Deep Space Network Project Office, Organization 920, Jet Propulsion Laboratory, California Institute of Technology, 4800 Oak Grove Drive, Pasadena, California, 91109.

Table of Contents

Designator	Release	Modular Document Title
210, Rev. E	January 11, 2024	Delta Differential One-way Ranging
211, Rev. G	January 11, 2024	Wideband Very Long Baseline Interferometry
212	September 15, 2009	26-m Subnet Telemetry (Decommissioned)
213	September 15, 2009	26-m Subnet Command (Decommissioned)
214, Rev. C	August 03, 2023	Pseudonoise and Regenerative Ranging
Ground Station Properties		
301, Rev. N	April 15, 2022	Coverage and Geometry
302, Rev. D	February 10, 2017	Antenna Positioning
303	January 15, 2001	Media Calibration
304, Rev. C	February 05, 2021	Frequency and Timing
305, Rev. B	October 31, 2009	Test Support
Supplementary Information		
901, Rev. H	February 05, 2021	Handbook Glossary

Deep Space Network (DSN)
Telecommunications Link Design Handbook

001, Rev. B
Handbook Introduction

April 29, 2011

Prepared by:

[Signature on file at DSN Library]
Christine Chang Date
Editor

Approved by:

[Signature on file at DSN Library]
Timothy Pham Date
DSN Communication System Chief Engineer

Released by:

[Signature on file at DSN Library]
DSN Document Release Date

Change Log

Rev	Issue Date	Affected Paragraphs	Change Summary
Initial	11/30/2000	All	All
A	4/1/2010	All	Updates names, titles, and website references due to organizational changes.
B	4/29/2011	All	Update names, titles due to organizational changes.

Contents

1 Introduction

1.1 Purpose

This modular handbook has been approved by the Deep Space Network (DSN) Project Office and is published as a source of interface design data for all flight projects using the DSN. It provides information useful to flight projects contemplating the design of hardware and software, with reasonable assurance that the resulting project telecommunications interfaces will be compatible with the established or planned DSN configurations.

1.2 Scope

The handbook consists of modules that present technical information applicable to the current DSN configuration and preliminary information applicable to future DSN configurations. These modules will be revised to reflect new capabilities and distributed to all users as these capabilities are in the plan and budgeted for by DSN Project Office.

This handbook is primarily concerned with performance parameters of equipment that supports the forward and return telecommunications link interfaces between spacecraft and the DSN.

1.3. Distribution

This handbook is published as an electronic document. The latest copy of the entire document series may be downloaded from this publicly accessible website:

http://deepspace.jpl.nasa.gov/dsndocs/810-005/

Notification of revisions will be distributed by electronic mail only. Requests for e-mail address changes should be submitted to the Editor of this document.

2 General Information

2.1 Constraints

The disclosure of a capability by this handbook does not assure that it can be made available to all potential DSN users. Specific support commitments must be negotiated between individual flight projects and the DSN/Mission Services Planning & Management Office <http://deepspace.jpl.nasa.gov/advmiss/>. Furthermore, this handbook does not relieve projects of the responsibility for obtaining frequency spectrum support for their equipment designs. Contact the DSN/Mission Services Planning & Management Office for assistance in obtaining spectrum support from the JPL Frequency Manager.

In seeking viable solutions to telecommunications or data processing problems, flight projects are not necessarily constrained by the effective design parameters contained in this handbook. However, flight project requirements that could require DSN interface design beyond what is specified by this handbook are subject to negotiation with the DSN/Mission Services Planning & Management Office.

The term *user* appears throughout this handbook whenever a mode of operation or parameter must be selected by a flight project. It must be understood that it is only in rare cases that these decisions can be made in real time. All DSN activities are planned well in advance and conducted by highly skilled personnel trained in handling contingencies. Changes to planned operations must be made in accordance with DSN procedures that are beyond the scope of this document.

2.2 Types of Data

It is the intent of this handbook to provide data verified by measurement and, therefore, representing actual performance. Unless clearly marked to the contrary, data in this handbook should be assumed to comply with this intent.

Sometimes it is necessary to include DSN design performance data that have not been verified by measurement. These data will be clearly identified in the associated text or by appropriate marking.

As hardware and software are tested and evaluated under operational conditions throughout the DSN, performance parameters will be upgraded to represent actual performance and published in the next revision of the appropriate module.

2.3 Proposed Capabilities

Whenever sufficient information is known about a capability being implemented in the DSN and having adequate maturity to be considered for spacecraft mission and equipment design, this information will be included in the appropriate modules under the heading of *Proposed Capabilities*. Telecommunications engineers are advised that anything discussed under this heading cannot be committed to except by negotiation with the DSN/Mission Services Planning & Management Office.

2.4 Document Layout

The modules in this revision of 810-005 have been divided into major sections that can be identified by their module numbers and the color of the index/tab at the on-line document website.

This module is part of an introductory section that may be expanded in the future to include tutorial or summary information. Modules in this section have yellow tabs and numbers starting with 0.

The next section, Space Link Interfaces, contains modules that provide information to those concerned with antenna selection and propagation effects. Modules in this section have blue tabs and numbers starting with 1.

The third section, Station Data Processing, contains modules that provide capabilities and performance of equipment installed in the Signal Processing Center (SPC) portion of each DSN location. This information will be of interest both to telecommunications engineers and spacecraft mission designers. Modules in this section have green tabs and numbers starting with 2.

The fourth section in this revision, Ground Station Properties, contains modules that provide information about the underlying technologies relating to many of the Space Link Interfaces and Station Data Processing modules. These modules have been grouped to consolidate this information in one place. Modules in this section have brown tabs and numbers starting with 3.

2.5 Module Revision and Control

The modules contained in this handbook are approved for publication under the authority of the cover page signatories. Revisions are indicated by a revision letter following the module designator.

A summary of the changes and additions can be accessed on the home page of the document website, provided in Section 1.3 and as listed on the cover and title page of this document. Currency of modules in printed copies can be verified against the information in the Table of Contents supplied with each revision or by comparison with the version downloaded from the website.

Persons requesting additions of modules to the handbook should direct their request to the DSN Project Office. Persons requesting changes, corrections, or additions to existing modules should direct their comments to either of the cover page signatories or to the Editor of this document. All modules are subject to the review and approval process of DSN

Standard Practice in: DSN Documentation Structure, Standards, and Definitions, DSN Document 810-001.

2.6 Abbreviations

Abbreviations are normally defined after their first textual usage and are compiled in module 901, Handbook Glossary. It should be recognized, however, that certain common abbreviations or acronyms used in this handbook might not defined. External users may refer to any of several compilations of electronic terms for omitted definitions. Users with access to the JPL Intranet can find additional abbreviations at the DSN Acronym Reference Tool website: http://dsnprocess.jpl.nasa.gov/dart/

2.7 Applicable Documents

The latest issues of the following documents are referenced by modules in this handbook or are the source of requirements for this handbook or the capabilities described herein.

2.7.1 DSN External Documents

The following documents either are public documents or may be made available to organizations or individuals under contract to, or having received a request for a proposal from, NASA or one of its Centers.

1. The Interplanetary Network Progress Report, On-line document: http://eis.jpl.nasa.gov/tmo/index.cfm
2. DSN External Interface Specifications, DSN Document 820-013
3. Deep Space Network Services Catalog, DSN Document 820-100

2.7.2 DSN Internal Documents

The following DSN internal documents are referenced by, or provide requirements for, this handbook and may be found at the Product Data Management System web site: https://pdms.jpl.nasa.gov/CMTOOLS/

1. DSN Standard Practice, DSN Documentation Structure, Standards, and Definitions, DSN Document 810-001
2. DSN Subsystem Requirements; DSN Document Series 834

Deep Space Network

101
70-m Subnet
Telecommunications Interfaces

Document Owner:

Signature provided	07/23/2019
Stephen D. Slobin Antenna System Engineer	Date

Approved by:

Signature provided	07/19/2019
Timothy Pham Communications Systems Chief Engineer	Date

Prepared by:

Signature provided	07/23/2019
Stephen D. Slobin Antenna System Engineer	Date

Released by:

Signature provided	07/23/2019
Christine Chang DSN Document Release Authority	Date

DSN No. **810-005, 101, Rev. G**
Issue Date: September 04, 2019
JPL D-19379; CL#19-5458

Jet Propulsion Laboratory
California Institute of Technology

Users must ensure that they are using the current version in DSN Telecommunications Link Design Handbook website:
https://deepspace.jpl.nasa.gov/dsndocs/810-005/

Review Acknowledgment

By signing below, the signatories acknowledge that they have reviewed this document and provided comments, if any, to the signatories on the Cover Page.

Signature provided	07/23/2019
Jeff Berner DSN Project Chief Engineer	Date

Signature provided	07/23/2019
John Cucchissi Antenna System Engineer	Date

Signature provided	07/22/2019
Timothy Cornish Uplink System Engineer	Date

Document Change Log

Rev	Issue Date	Prepared By	Paragraphs Affected	Change Summary
Initial	1/15/2001	Stephen Slobin Robert Sniffin	All	
A	07/30/2003	Stephen Slobin Robert Sniffin	All	Revised gain and noise temperature reference point to feedhorn aperture. Documented installation of new feedcone at DSS 63. Provided diagrams of L-band microwave equipment and Low-noise S-band cone at DSS 43.
Chg 1	3/31/2004	Stephen Slobin Robert Sniffin	Figures 1, 5	Corrected S-band amplifier types in Figure 1. Replaced Figure 5 with correct graphic
B	8/25/2006	Stephen Slobin Robert Sniffin	All	Documents removal of DSS-43 Ultracone. Revised T_{AMW} formulation for noise temperature to be consistent with Rev. B of module 105.
C	9/15/2009	Stephen Slobin Robert Sniffin	Pages 1, 6, Table 1, Figure 1.	Replaced DSMS with DSN. Correctly stated that 400-kW S-band uplink is available at DSS-43 only. Included frequency range for support for this capability. DSS-14 S-band radar transmitter removed.
D	4/21/2011	Stephen Slobin Christine Chang	Tables 2, 4, 5, 6, A-3. Figures 1, 8, 9, 10.	S-band LNA-1 maser at DSS-14 replaced with a HEMT, giving 1.8 K higher noise temperature. LNA numbering updated.
E	9/18/2013	Stephen Slobin Christine Chang	Tables 2, 4, 7, 8, A-3 Section 2, Table 1 Figures 9, 10 Tables 4, A-2	S-band LNA-1 maser at DSS-43 replaced with a HEMT, giving 1.8 K higher noise temperature. DSS-63 S-band transmit frequency restriction. Transmit elevation angle restrictions for all antennas. DSS-43 400 kW transmit power restriction. New temperature profiles for DSS-43. Minor numerical changes.

F	08/05/2015	Stephen Slobin Christine Chang	Tables 2, 4-10 Table 4 Figure 1 Figures 4-6 Figures 8-10 Figures 11-13 Table A-2 Table A-3	New DSS-63 S-band LNA-1 HEMT T_{AMW} values. Recalculated DSS-14 and DSS-43 S-band T_{AMW} and T_{op} with LNA-1 HEMT. New S-band T_{AMW} and T_{op} values. New X-band T_{sky} and T_{op} values. Relabeled S-band LNA-1 HEMT. Redrawn for new X-band A_{zen} values. Redrawn for new S-band T_{AMW} values. Redrawn for new X-band T_{sky} values. New X-band A_{zen} values. New S-band LNA-1 T_1 values.
G	09/04/2019	Stephen Slobin Christine Chang	Section 2 Section 4 Table 1 Table 2 Figure 1	2090-2110 MHz uplink no longer supported on 70-m antennas. DSS-43 400 kW S-band transmitter limited to 100 kW and 17.4 degree elevation restriction. Proposed Capabilities added. Changed S-band 400 kW transmitter power and EIRP to 100 kW limit. 2090-2110 MHz uplink no longer supported on 70-m antennas. Corrected 2270-2300 MHz to 2200-2300 MHz (one place). Changed to indicate 100 kW limit for DSS-43 400 kW transmitter.

Contents

Paragraph **Page**

Illustrations

Figure **Page**

Tables

Table **Page**

1 Introduction

1.1 Purpose

This module provides the performance parameters for the Deep Space Network (DSN) 70-meter antennas that are necessary to perform the nominal design of a telecommunications link. It also summarizes the capabilities of these antennas for mission planning purposes and for comparison with other ground station antennas.

1.2 Scope

References here (e.g., “Module 105”) are to the DSN Telecommunications Link Design Handbook, DSN Document Number 810-005. The scope of this module is limited to providing those parameters that characterize the RF performance of the 70-meter antennas. These are discussed in Module 105, Atmospheric and Environmental Effects. The parameters do not include effects of weather, such as reduction of system gain and increase in system noise temperature that are common to all antenna types. This module also does not discuss mechanical restrictions on antenna performance that are covered in Module 302, Antenna Positioning, or the effects of terrain masking that are covered in Module 301, Coverage and Geometry.

2 General Information

The DSN 70-m Antenna Subnet contains three 70-meter diameter antennas. Deep Space Station (DSS) 14 is located at Goldstone, California, DSS-43 is near Canberra, Australia, and DSS-63 is near Madrid, Spain. The precise station locations are given in Module 301, Coverage and Geometry. All antennas support L-, S-, and X-band reception, and S-band and X-band transmission.

Figure 1 is a block diagram of the S-band and X-band microwave and transmitter equipment at DSS-14, DSS-43, and DSS-63 that is common to all three stations. Additionally a 400 kW S-band transmitter is shown for DSS-43, but its use is limited to 100 kW. A block diagram of the L-band equipment at the three stations is shown in Figure 2.

For S-band, the stations utilize the S-band Polarization Diversity (SPD) feedcone that contains the feed, the primary low-noise amplifier (LNA) and its support equipment, the diplexer, and the required switches and other waveguide. The backup LNA and the S-band transmitters are located in an area beneath the feedcones referred to as the Module III area. The S-band feed employs an orthomode junction that permits simultaneous right hand circular polarization (RCP) and left hand circular polarization (LCP) to be used. The polarizer may be switched so that either polarization may be directed to the non-diplexed path with the opposite polarization appearing on the diplexed path. The lower-noise non-diplexed path (orthomode upper arm) is used for listen-only reception, or if the spacecraft transmits and receives on opposite polarizations. If the spacecraft receives and transmits simultaneously with the same polarization, the diplexed path must be used for reception and the system operating noise temperature is higher.

A 20-kW S-band transmitter is provided for normal spacecraft communication at all three sites. The uplink frequency band 2090-2110 MHz is no longer supported on 70-meter

antennas. An additional 400-kW S-band transmitter is available at DSS-43 (Canberra), but its power output is limited to 100 kW. In no case can the 400-kW transmitter be used below 17.4 degrees elevation, no matter what the power is. At DSS-63 (Madrid) S-band uplink in the deep space frequency band (2110-2120 MHz) is not available due to conflict with IMT-2000 users, per agreement between NASA and Secretaria de Estado de Telecomunicaciones par la Sociedad de la Informacion (SETSI), January, 2001. Deep-space S-band is also not available at the Madrid DSS-54 BWG antenna or the DSS-65 HEF antenna. Transmission below 10 degrees elevation by any antenna at any frequency is not allowed. Additional horizon mask transmission limitations can be seen in the figures in Module 301, Coverage and Geometry.

All three 70-meter antennas employ the X-band Transmit-Receive feedcone (the XTR cone). The XTR cone employs a unique feed design that includes a diplexing junction to inject the transmitted signal directly into the feed. This eliminates the need for a waveguide diplexer and a common path for the received and transmitted signals. As a result, much of the received path can be cryogenically cooled with a significant reduction in system operating noise temperature. The S/X dichroic plate can also be retracted when S-band is not required, for a further improvement in X-band performance – lower noise temperature and higher gain. When the S/X dichroic is retracted, both the X-band transmit and receive beams are moved to the left (looking outward from the antenna, minus cross-elevation direction, smaller azimuth) about 8.5 mdeg relative to the X-band beam in the S/X configuration. This beam movement is corrected for by existing pointing models, however the appropriate model must be chosen by an operator prior to observing a spacecraft. The XTR feed includes a fixed circular polarizer and an orthomode junction to enable both circular polarizations to be received simultaneously. Each polarization is routed to one of two identical high-electron-mobility transistor (HEMT) low-noise amplifiers located within the cryogenic package. A separate, switchable polarizer is provided for the X-band transmitter so that the transmitted signal can be of either polarization

The 70-m antennas are equipped with an L-band feed (Figure 2) mounted on the outside of the XTR cone. The feed normally receives LCP, but could be disassembled and reconfigured to receive RCP. The low noise amplifiers, an L-band to S-band upconverter for the received signal, and an S-band to L-band downconverter for test signals are located in the Module III area. The output of the L-band to S-band upconverter is substituted for one of the two S-band receive channels. However, the need to position the antenna subreflector to illuminate the L-band feed prevents the other frequencies from being simultaneously available.

The L-, S- and X-band feeds are provided with phase calibration couplers and comb generators so the stations can be used for very-long baseline interferometry reception in addition to spacecraft tracking.

The Goldstone site also has an X-band radar transmitter (Goldstone Solar System Radar, GSSR) in a third cone that operates near the normal receive frequency band. In this third cone is also a Ku-band (22 GHz) receive feed for radio astronomy investigations. The third feedcone position at DSS 43 is now occupied with host-country equipment for non-DSN use. At DSS-63, a third feedcone has been installed that contains a Ku-band radio astronomy feed.

3 Telecommunications Parameters

The significant parameters of the 70-meter antennas that influence telecommunications link design are listed in Tables 1 and 2. Variations in these parameters that

are inherent in the design of the antennas are discussed below. Other factors that degrade link performance are discussed in Modules 105 (Atmospheric and Environmental Effects) and 106 (Solar Corona and Wind Effects).

3.1 Antenna Gain

The antenna gains in Tables 1 and 2 do not include the effect of atmospheric attenuation and should be regarded as vacuum gain referenced to the feedhorn aperture.

3.1.1 Frequency Effects

Antenna gains are specified at the indicated frequency (f_0). For operation at higher frequencies in the same band, the gain (dBi) must be increased by 20 log (f/f_0). For operation at lower frequencies in the same band, the gain must be reduced by 20 log (f/f_0).

3.1.2 Elevation Angle Effects

Structural deformation causes a reduction in gain when the antenna operates at an elevation angle other than the angle where the reflector panels were aligned. The net gain of the antenna is also reduced by atmospheric attenuation that is a function of elevation angle and weather condition. These effects are illustrated in Figures 3 through 6 which show the estimated gain versus elevation angle for the hypothetical vacuum condition (structural deformation only) and with 0%, 50%, and 90% weather conditions, designated as CD (cumulative distribution) = 0.00, 0.50, and 0.90. A CD of 0.00 (0%) means the minimum weather effect (exceeded 100% of the time). A CD of 0.90 (90%) means that effect which is exceeded only 10% of the time. Qualitatively, a CD of 0.00 corresponds to the driest, lowest-loss condition of the atmosphere; a CD of 0.50 corresponds to humid or very light clouds; and 0.90 corresponds to very cloudy, but with no rain. A CD of 0.25 corresponds to average clear weather. Comprehensive S-band and X-band weather effects models (for weather conditions up to 99% cumulative distribution) are provided in Module 105 for detailed design control table use.

Figure 3 depicts the S-band (2295 MHz) net gains for all stations as a function of elevation angle and weather condition, including the vacuum condition. Net gain means vacuum-condition gain as reduced by atmosphere attenuation. The L-band gain curve shapes should be considered identical to the S-band curve shapes, except that they are reduced in value by the differences shown in Table 2 and Appendix Table A-1. Figures 4, 5, and 6 present the X-band (8420 MHz) net gains of the DSS-14, DSS-43, and DSS-63 antennas as a function of elevation angle and weather condition, including the vacuum condition, using the XTR feedcone with the S/X dichroic plate retracted (the X-only configuration). The equations and parameters of these curves are given in Appendix A. The models use a flat-Earth, horizontally stratified atmosphere approximation.

It should be noted in Appendix Table A-1, that the gain parameters do not vary for different S-band configurations (e.g., LNA-1 non-diplexed vs. LNA-1 diplexed), as they do in Table A-3 for the noise temperature parameters. This is due to the fact that the gain is referenced to the feedhorn aperture, and configurations “downstream” (e.g., orthomode and diplexer paths) do not affect the value of gain at the aperture. The observed differences in antenna G/T are attributed to different values of noise temperature when G and T are referred to the feedhorn aperture. When G and T are referenced to the LNA input, both the G and T

parameters vary with antenna configuration. For X-band, which is always in a fixed diplexed configuration, the S/X dichroic position in front of the feedhorn affects both the gain and noise temperature parameters at the feedhorn aperture.

Under normal operation of the antenna, the subreflector is moved in the axial (Z-direction, in-out) and lateral (Y-direction, up-down) directions several centimeters to compensate for main reflector and quadripod gravitational distortion and to maintain antenna gain at an optimum level. As the antenna moves from 6 degrees to 90 degrees in elevation, the total subreflector axial movement, relative to the quadripod, is 3.744 cm. The subreflector movement alone contributes a phase change of –666 degrees at X-band. (The sign convention is that a longer path length results in a smaller value of phase). Quadripod distortion contributes +195 degrees, and main reflector distortion contributes –172 degrees. The net effect of these three motions is a phase change of –643 degrees at X-band.

Fixing the subreflector movement at a Y/Z value appropriate for a particular elevation angle, as is done in certain very-long baseline interferometry (VLBI) and spacecraft experiments, greatly reduces the net phase change over the range of elevation angles needed to track a radio source or spacecraft. In the 6–90 degree elevation example above, the net total phase change is reduced to +23 degrees. The downside of fixing the subreflector motion is that the antenna gain will be reduced many tenths of a dB, up to 1 dB, for deviations in elevation angle of 10–20 degrees from the nominal elevation angle. These effects should be thoroughly investigated if there is any question of having adequate margin to complete the telecommunications link. Further discussion can be found in S. D. Slobin and D. A. Bathker, “DSN 70-Meter Antenna X-Band Gain, Phase, and Pointing Performance, With Particular Application for Voyager 2 Neptune Encounter,” *TDA Progress Report 42-95*, pp. 237-245, July-September 1988.

3.1.3 Wind Loading

The gain reductions at S- and X-band due to wind loading are listed in Table 3. The tabular data are for structural deformation of the main reflector only and assume that the antenna is maintained on-point by conical scan (CONSCAN, discussed in Module 302) or an equivalent process. In addition to structural deformation, wind introduces a blind-pointing error that is related to the antenna elevation angle, the angle between the antenna and the wind, and the wind speed. Cumulative probability distributions of wind velocity at Goldstone are given in Module 105.

3.2 System Operating Noise Temperature

The system operating noise temperature (T_{op}) varies as a function of elevation angle due to changes in the path length through the atmosphere and ground noise received by the sidelobe pattern of the antenna. Figures 7 through 13 show the combined effects of these factors at L-, S-, and X-bands in a hypothetical vacuum (no atmosphere) and no cosmic noise condition for selected antenna configurations, and with the three weather conditions, including cosmic noise, as described above. The equations and parameters for these curves are provided in Appendix A of this module. The models use a flat-Earth, horizontally stratified atmosphere approximation.

The system operating noise temperature, T_{op}, consists of two parts, an *antenna-microwave component*, T_{AMW}, for the contribution of the antenna and microwave hardware only, and a *sky component*, T_{sky}, that consists of the atmosphere noise plus the cosmic microwave background noise, attenuated by the atmosphere loss. T_{AMW} is shown in Figures 7, 8, 11, 12, and 13 as "ANT-UWV". The system operating noise temperature is given by

$$T_{op}(\theta) = T_{AMW} + T_{sky} = \left[T_1 + T_2 e^{-a\theta}\right] + \left[T_{atm}(\theta) + T'_{CMB}(\theta)\right]$$

where

$T_{sky} = T_{atm}(\theta) + T'_{CMB}(\theta)$

T_1, T_2, and a are coefficients and exponent given in Appendix A, Table A-3

T_{atm} is the atmosphere contribution term, calculated from Module 105

T'_{CMB} is the attenuated cosmic contribution, calculated from Module 105

More details of this calculation are given in Appendix A of this module.

Figure 7 shows the L-band (1668 MHz) system noise temperature as a function of elevation angle, for all antennas, referenced to the feedhorn aperture. Figure 8 shows the S-band (2295 MHz) system noise temperature curves for DSS 14, LNA-1, non-diplexed, referenced to the feedhorn aperture. S-band curves for other antennas and configurations can be calculated by using the parameters given in Appendix A. Figures 9 and 10 show S-band system noise temperatures at 6 degrees elevation for all antennas at the eastern and western horizons. These data were measured specifically for rise and set azimuth ranges appropriate for the Galileo spacecraft during the time period 1995 through 1998, but are usable with any spacecraft operating at S-band. All S-band noise temperatures presented here are for an antenna configuration where both LNAs are HEMTs. The X-band (8420 MHz) system noise temperatures referenced to the feedhorn aperture for the three antennas are shown in Figures 11 through 13. Each figure shows the noise temperature with the antenna in the lowest noise, X-only configuration, with the S/X dichroic reflector retracted. The higher S/X configuration noise temperatures can be calculated using the parameters given in Appendix A.

The T_{AMW} noise temperature values in Table 2 are stated with reference to the feedhorn aperture and arise from antenna and microwave hardware contribution only. No atmosphere or cosmic background contribution is included. Table 4 presents values (for all antenna frequencies and configurations, at zenith, with average-clear CD = 0.25 weather) of T_{AMW}, T_{sky}, and T_{op}. The values of T_{sky} in Table 4 are calculated by methods presented in Module 105, using year-average attenuation values in Tables 10–15 of that module

Tables 5 through 10 give S-band system noise temperatures to be expected during average clear weather conditions at elevation angles near the horizon, corresponding to rise and set azimuths of spacecraft with declinations of approximately –15° to –25°. These data were gathered specifically to support the Galileo Mission during the 1995 through 1998 period.

Tables 5 and 6 are for rise and set azimuths at DSS-14 (Goldstone) using the S-band SPD cone (the standard S-band receiving system with a HEMT LNA). Tables 7 and 8 are for rise and set azimuths at DSS-43 (Canberra) using the SPD cone with a HEMT LNA, and Tables 9 and 10 give rise and set noise temperatures for DSS-63 (Madrid) using the SPD cone

with a HEMT LNA. S-band noise temperatures above the maximum angles given in the tables can be calculated using the parameters given in Appendix A.

3.3 Pointing

Figure 15 shows the effects of pointing error on effective transmit and receive gain of the antenna (pointing loss) for the S-band transmit and the L- and S-band receive frequencies. The effects of pointing error at the X-band transmit and receive frequencies are shown in Figure 16. These curves are Gaussian approximations based on theoretical antenna beamwidths. Data have been normalized to eliminate elevation and wind-loading effects. The equation used to generate the curves is provided in Appendix A.

The Gaussian approximation underestimates the exact gain drop off by about 0.3 dB at the –5 dB pointing-loss position, and about 0.5 dB at the –6 dB position. Beyond this, the Gaussian approximation will greatly underestimate the pointing loss, as the actual pattern has a null at a position off boresight approximately equal to the full half-power beamwidth. If this is a concern, the exact antenna beam shape should be obtained and pointing loss estimates from that should be made.

4 Proposed Capabilities

All 70-meter antennas will receive significant upgrades to their S-band and X-band transmitting systems over the next several years. The S-band 20 kW and the DSS-43 400 kW transmitters will be replaced by 100 kW transmitters. The X-band 20 kW transmitters will be replaced by 80 kW transmitters. The X-band uplink frequency band will be widened to 7145-7235 MHz, up from the present 7145-7190 MHz. The X-band feeds will be modified to allow high-power transmission.

Following an approximately 10-month downtime, the following return-to-service dates for the 70-meter antennas are expected to be:

DSS-43, December 2020

DSS-63, December 2022

DSS-14, December 2024

Table 1. S- and X-Band Transmit Characteristics

Parameter	Value	Remarks
ANTENNA		
Gain		At elevation angle of peak gain, referenced to feedhorn aperture for matched polarization; no atmosphere included
S-band (2115 MHz)	62.95 ± 0.2 dBi	All stations, S/X dichroic extended
X-band (7145 MHz)	73.23 ± 0.2 dBi	All stations, S/X dichroic retracted
X-band (7145 MHz)	72.92 ± 0.2 dBi	All stations, S/X dichroic extended
Transmitter Waveguide Loss		
S-band		
	0.2 ± 0.02 dB	400-kW transmitter output to feedhorn aperture (DSS-43 only)
	0.3 ± 0.02 dB	20-kW transmitter output to feedhorn aperture (All stations)
X-band	0.45 ± 0.02 dB	20-kW transmitter output to feedhorn aperture (All stations)
Half-Power Beamwidth		Angular width (2-sided) between half-power points at specified frequency
S-band	0.128 ± 0.013 deg	
X-band	0.038 ± 0.004 deg	Note: When operating in the X-only configuration (S/X dichroic retracted), the transmit beam is moved approximately 8.5 mdeg to the left (XEL direction, looking outward from the antenna) relative to the beam in S/X configuration. Existing pointing models correct for this.
Polarization	RCP or LCP	One polarization at a time, remotely selected
Ellipticity, RCP or LCP		Ellipticity is defined as the ratio of peak-to-trough received voltages with a rotating, linearly polarized source and a circularly (elliptically) polarized receiving antenna. Ellipticity (dB) = 20 log (V_2/V_1).
S-band	2.2 dB (max)	All stations
X-band	≤1.0 dB	All stations

Table 1. S- and X-Band Transmit Characteristics (Continued)

Parameter	Value	Remarks
ANTENNA (Continued)		
Pointing Loss		
Angular	See Module 302	Also, see Figures 14 and 15.
CONSCAN		
S-band		
	0.1 dB	Recommended value
	0.03 dB	At S-band, using X-band CONSCAN reference set for 0.1 dB loss
X-band		
	0.1 dB	Recommended value
EXCITER AND TRANSMITTER		
RF Power Output		Nominal output power, referenced to transmitter port; settability is limited to 0.25 dB by measurement equipment precision
S-band		Can be used only above 10-deg elevation (above 17.4-deg for the 400-kW transmitter).
20-kW Power Amplifier	73.0, +0.0, –1.0 dBm 70.0, +0.0, –1.0 dBm	2110 to 2118 MHz 2118 to 2120 MHz 2110 to 2120 MHz not available at DSS-63 due to NASA/SETSI agreement.
400-kW Power Amplifier – Limited to 100 kW.	80.0, +0.0, –1.0 dBm	2110 to 2118 MHz Only available at DSS-43. Cannot be used above 100 kW. No operation below 17.4 degrees elevation is allowed, no matter what the power is.
X-band		Can be used only above 10-deg elevation.
20-kW Power Amplifier	73.0, +0.0, –1.0 dBm	
Both S-band and X-band transmitters employ variable-beam klystron power amplifiers. The output from this kind of amplifier varies across the bandwidth and may be as much as 1 dB below the nominal rating, as indicated by the tolerance. Performance will also vary from tube to tube. Normal procedure is to run the tubes saturated, but unsaturated operation is also possible. The point at which saturation is achieved depends on drive power and beam voltage. The 20-kW tubes are normally saturated for power levels greater than 60 dBm (1 kW) and the 400-kW tubes are saturated above 83 dBm (200 kW), however the 400 kW transmitter at DSS-43 is not used above 100 kW. Minimum power out of the 20-kW tubes is about 53 dBm (200 W) and about 73 dBm (20 kW) for the 400-kW tubes. Efficiency of the tubes drops off rapidly below nominal rated output.		

Table 1. S- and X-Band Transmit Characteristics (Continued)

Parameter	Value	Remarks
EXCITER AND TRANSMITTER (Continued)		
EIRP		At elevation angle of peak gain, referenced to feedhorn aperture
S-band	135.6, +0.0, –1.0 dBm 132.6, +0.0, –1.0 dBm	20-kW transmitter, S/X dichroic extended 2110 to 2118 MHz 2118 to 2120 MHz 2110 to 2120 MHz not available at DSS-63 due to NASA/SETSI agreement.
	142.7, +0.0, –1.0 dBm	DSS-43 400-kW transmitter at 100 kW, S/X dichroic extended, 2110 to 2118 MHz.
X-band	145.8, +0.0, –1.0 dBm	20-kW transmitter, S/X dichroic retracted
	145.5, +0.0, –1.0 dBm	20-kW transmitter, S/X dichroic extended
Frequency Range Covered		
S-band		
1-dB Bandwidth	2110 to 2118 MHz	Power decreases above 2118 MHz
Coherent with Deep Space S-band D/L Allocation	2110.2 to 2117.7 MHz	240/221 turnaround ratio
Coherent with Deep Space X-band D/L Allocation	2110.2 to 2119.8 MHz	880/221 turnaround ratio
X-band		
1-dB Bandwidth	7145 to 7190 MHz	
Coherent with Deep Space S-band D/L Allocation	7147.3 to 7177.3 MHz	240/749 turnaround ratio
Coherent with Deep Space X-band D/L Allocation	7149.6 to 7188.9 MHz	880/749 turnaround ratio
Tunability		At S-band or X-band transmitter output frequency
Phase Continuous Tuning Range	2.0 MHz	About any frequency within covered frequency ranges
Maximum Tuning Rate	± 12.1 kHz/s	

Table 1. S- and X-Band Transmit Characteristics (Continued)

Parameter	Value	Remarks
EXCITER AND TRANSMITTER (Continued)		
Frequency Error	0.012 Hz	Average over 100 ms with respect to frequency specified by predicts
Ramp Rate Error	0.001 Hz/s	Average over 4.5 s with respect to rate calculated from frequency predicts
S-Band Stability		At transmitter output frequency
Output Power Stability		12-h period
Saturated Drive	± 0.25 dB	20-kW transmitter
Saturated Drive	± 0.5 dB	400-kW transmitter, with 100-kW limit
Unsaturated Drive	± 1.0 dB	20-kW and 400-kW transmitters
Frequency ($\Delta f/f$), 1000-s Averaging	5×10^{-15}	Allan deviation
Phase Stability		In 1-Hz bandwidth
1–10 Hz Offset	–60 dBc	Below carrier
10 Hz–1 kHz Offset	–70 dBc	Below carrier
Group Delay Stability	≤3.3 ns	Ranging modulation signal path over 12-h period (see Module 203)
Spurious Output		
2nd Harmonic	–85 dBc	Below carrier
3rd Harmonic	–85 dBc	Below carrier
4th Harmonic	–140 dBm	20-kW transmitter
4th Harmonic	TBD	400-kW transmitter – limited to 100 kW.
X-Band Stability		At transmitter output frequency
Output Power Stability		12-h period
Saturated Drive	± 0.25 dB	
Unsaturated Drive	± 1.0 dB	
Frequency ($\Delta f/f$), 1000-s Averaging	2.3×10^{-15}	Allan deviation

Table 1. S- and X-Band Transmit Characteristics (Continued)

Parameter	Value	Remarks
EXCITER AND TRANSMITTER (Continued)		
X-Band Stability (Continued)		At transmitter output frequency
Phase Stability		In 1-Hz bandwidth
1–10 Hz Offset	–50 dBc	Below carrier
10 Hz–1 kHz Offset	–60 dBc	Below carrier
Group Delay Stability	≤1.0 ns	Ranging modulation signal path over 12 h period (see Module 203)
Spurious Output		
2nd Harmonic	–75 dBc	Below carrier
3rd, 4th & 5th Harmonics	–60 dBc	Below carrier

Table 2. L-, S-, and X-Band Receive Characteristics

Parameter	Value	Remarks
ANTENNA		
Gain		At elevation angle of peak gain for matched polarization, no atmosphere included. Favorable (+) and adverse (–) tolerances have a triangular PDF. See Figures 3–6 for elevation dependency.
L-Band (1668 MHz)	61.04 ± 0.3 dBi	Referenced to feedhorn aperture
S-Band (2295 MHz), All Stations	63.59 ± 0.1 dBi	Referenced to feedhorn aperture. S/X dichroic extended.
X-Band (8420 MHz), X-only Configuration		Referenced to feedhorn aperture. S/X dichroic retracted.
DSS-14	74.55 ± 0.1 dBi	
DSS-43	74.63 ± 0.1 dBi	
DSS-63	74.66 ± 0.1 dBi	
X-Band (8420 MHz), S/X Configuration		Referenced to feedhorn aperture. S/X dichroic extended.
DSS-14	74.35 ± 0.1 dBi	
DSS-43	74.36 ± 0.1 dBi	
DSS-63	74.19 ± 0.1 dBi	
Half-Power Beamwidth		Angular width (2-sided) between half-power points at specified frequency
L-Band (1668 MHz)	0.162 ± 0.016 deg	
S-Band (2295 MHz)	0.118 ± 0.012 deg	
X-Band (8420 MHz)	0.032 ± 0.003 deg	Note: When operating in the X-only configuration (S/X dichroic retracted) the receive beam is moved approximately 8.5 mdeg to the left (XEL direction, looking outward from the antenna) relative to the beam in S/X configuration. Existing pointing models correct for this.

Table 2. L-, S-, and X-Band Receive Characteristics (Continued)

Parameter	Value	Remarks
ANTENNA (Continued)		
Polarization		
L-Band, All Stations	LCP	RCP available by changing mechanical configuration of feed
S-Band, All Stations	RCP and LCP	Both polarizations are available simultaneously. Choice of diplexed or non-diplexed path is remotely selectable.
X-Band, All Stations	RCP and LCP	Both polarizations are available simultaneously.
Ellipticity		See definition in Table 1.
L-Band	2.0 dB (max)	
S-Band	0.6 dB (max)	
X-Band	0.8 dB (max)	
Pointing Loss		
Angular	See Module 302	Also, see Figures 14 and 15.
CONSCAN		
S-Band	0.03 dB, 3 sigma	At S-band using X-band CONSCAN reference set for 0.1 dB loss at X-band
	0.1 dB, 3 sigma	Recommended value when using S-band CONSCAN reference
X-Band	0.1 dB, 3 sigma	Recommended value when using X-band CONSCAN reference
LOW NOISE AMPLIFIERS AND RECEIVERS		Two tracking receivers are normally provided, which may be operated as one S- and one X-band receiver. RCP and LCP are simultaneously available at S- and X-bands so one receiver can be used on each polarization. When tracking at L-band, S- and X-band are not available. Additional receivers per polarization can be scheduled subject to availability.

Table 2. L-, S-, and X-Band Receive Characteristics (Continued)

Parameter	Value	Remarks
LOW NOISE AMPLIFIERS AND RECEIVERS (Continued)		
Frequency Ranges Covered		1 dB bandwidth
L-Band	1628 to 1708 MHz	
S-Band	2200 to 2300 MHz	
X-Band	8200 to 8600 MHz	deep space downlink telemetry allocation is 8400 to 8450 MHz
Recommended Maximum Signal Power	–80.0 dBm	At LNA input terminal
Antenna-Microwave Noise Temperature (T_{AMW})		Near zenith, no atmosphere (vacuum) or cosmic noise included. See Table 4 for 25% CD average clear sky noise contribution. Favorable (–) and adverse (+) tolerances have triangular PDF.
L-Band, all stations (1628–1708 MHz) LNA-1 or -2, HEMT	26.68 ± 2 K	With respect to feedhorn aperture. See Figure 7 for elevation dependency.
S-Band (2200–2300 MHz)		With respect to feedhorn aperture. See Figure 8 for DSS-14 elevation dependency.
DSS-14, LNA-1, HEMT, non-diplexed	12.22 ± 1 K	
DSS-14, LNA-1, HEMT, diplexed	15.86 ± 1 K	
DSS-14, LNA-2, HEMT, non-diplexed	18.80 ± 1 K	
DSS-14, LNA-2, HEMT, diplexed	23.74 ± 1 K	
DSS-43, LNA-1, HEMT, non-diplexed	13.57 ± 1 K	
DSS-43, LNA-1, HEMT, diplexed	17.67 ± 1 K	

Table 2. L-, S-, and X-Band Receive Characteristics (Continued)

Parameter	Value	Remarks
LOW NOISE AMPLIFIERS AND RECEIVERS (Continued)		
Antenna-Microwave Noise Temperature (T_{AMW})		
S-Band (2200–2300 MHz), (Continued)		
DSS-43, LNA-2, HEMT, non-diplexed	19.59 ± 1 K	
DSS-43, LNA-2, HEMT, diplexed	24.72 ± 1 K	
DSS-63, LNA-1, HEMT, non-diplexed	15.30 ± 1 K	
DSS-63, LNA-1, HEMT, diplexed	19.00 ± 1 K	
DSS-63, LNA-2, HEMT, non-diplexed	21.24 ± 1 K	
DSS-63, LNA-2, HEMT, diplexed	26.85 ± 1 K	
X-Band (8400–8500 MHz), X-Only Configuration		Referenced to feedhorn aperture. No atmosphere (vacuum) or cosmic noise included. S/X dichroic plate retracted. See Figures 11–13 for elevation dependency.
DSS-14, LNA-1/-2, HEMT	11.65 ± 1 K	
DSS-43, LNA-1/-2, HEMT	12.10 ± 1 K	
DSS-63, LNA-1/-2, HEMT	11.46 ± 1 K	
X-Band (8400–8500 MHz) S/X Configuration		Referenced to feedhorn aperture. No atmosphere (vacuum) or cosmic noise included. S/X dichroic plate extended.
DSS-14, LNA-1/-2, HEMT	12.59 ± 1 K	
DSS-43, LNA-1/-2, HEMT	13.32 ± 1 K	
DSS-63, LNA-1/-2, HEMT	12.64 ± 1 K	
Carrier Tracking Loop Noise B/W	0.25 – 200 Hz	Effective one-sided, noise-equivalent carrier loop bandwidth (B_L). See Module 202.

Table 3. Gain Reduction Due to Wind Loading, 70-m Antenna

Wind Speed		Gain Reduction (dB)*	
km/h	**mph**	**S-Band**	**X-Band**
32	20	Negligible	0.1
48	30	Negligible	0.3
72	45	0.15	1.5

* Assumes antenna is maintained on-point using CONSCAN or an equivalent. L-band gain reduction is negligible for wind speeds up to 72 km/h (45 mph). Worst case with antenna in most adverse orientation for wind.

Table 4. T_{AMW}, T_{sky}, and T_{op} for CD=25% Average Clear Weather at Zenith, Referenced to Feedhorn Aperture

Configuration and Stations	Noise Temperatures, K		
	T_{AMW}	T_{sky}	T_{op}
L-band, all stations, LNA-1 or -2, HEMT, LCP, non-diplexed	26.68	4.78	31.46
S-band, DSS 14, SPD cone, LNA-1, HEMT, non-diplexed	12.22	4.68	16.90
S-band, DSS 14, SPD cone, LNA-1, HEMT, diplexed	15.86	4.68	20.54
S-band, DSS 14, Mod III, LNA-2, HEMT, non-diplexed	18.80	4.68	23.48
S-band, DSS 14, Mod III, LNA-2, HEMT, diplexed	23.74	4.68	28.42
S-band, DSS 43, SPD cone, LNA-1, HEMT, non-diplexed	13.57	4.86	18.43
S-band, DSS 43, SPD cone, LNA-1, HEMT, diplexed	17.67	4.86	22.53
S-band, DSS 43, Mod III, LNA-2, HEMT, non-diplexed	19.59	4.86	24.45
S-band, DSS 43, Mod III, LNA-2, HEMT, diplexed	24.72	4.86	29.58
S-band, DSS 63, SPD cone, LNA-1, HEMT, non-diplexed	15.30	4.80	20.10
S-band, DSS 63, SPD cone, LNA-1, HEMT, diplexed	19.00	4.80	23.80
S-band, DSS 63, Mod III, LNA-2, HEMT, non-diplexed	21.24	4.80	26.04
S-band, DSS 63, Mod III, LNA-2, HEMT, diplexed	26.85	4.80	31.65

Table 4. T_{AMW}, T_{sky}, and T_{op} for CD=25% Average Clear Weather at Zenith, Referenced to Feedhorn Aperture (Continued)

Configuration and Stations	Noise Temperatures, K		
	T_{AMW}	T_{sky}	T_{op}
X-band, DSS 14, XTR cone, LNA-1, HEMT, RCP, X-only mode	11.65	5.04	16.69
X-band, DSS 14, XTR cone, LNA-2, HEMT, LCP, X-only mode	11.65	5.04	16.69
X-band, DSS 14, XTR cone, LNA-1, HEMT, RCP, S/X mode	12.59	5.04	17.63
X-band, DSS 14, XTR cone, LNA-2, HEMT, LCP, S/X mode	12.59	5.04	17.63
X-band, DSS 43, XTR cone, LNA-1, HEMT, RCP, X-only mode	12.10	5.39	17.49
X-band, DSS 43, XTR cone, LNA-2, HEMT, LCP, X-only mode	12.10	5.39	17.49
X-band, DSS 43, XTR cone, LNA-1, HEMT, RCP, S/X mode	13.32	5.39	18.71
X-band, DSS 43, XTR cone, LNA-2, HEMT, LCP, S/X mode	13.32	5.39	18.71
X-band, DSS 63, XTR cone, LNA-1, HEMT, RCP, X-only mode	11.46	5.27	16.73
X-band, DSS 63, XTR cone, LNA-2, HEMT, LCP, X-only mode	11.46	5.27	16.73
X-band, DSS 63, XTR cone, LNA-1, HEMT, RCP, S/X mode	12.64	5.27	17.91
X-band, DSS 63, XTR cone, LNA-2, HEMT, LCP, S/X mode	12.64	5.27	17.91

NOTE: T_{sky} calculated from attenuation values in Module 105, Tables 10-15.

Table 5. DSS 14 Eastern Horizon S-Band T_{op} (K) with SPD Cone

ELEV, deg	AZIMUTH, deg																				
	110	111	112	113	114	115	116	117	118	119	120	121	122	123	124	125	126	127	128	129	130
20.0	22.8	22.9	22.8	22.8	22.8	22.9	22.8	22.8	22.8	22.9	22.9	23.0	22.9	22.9	22.9	22.9	22.9	22.9	22.9	22.9	22.9
19.0	23.3	23.3	23.3	23.3	23.3	23.3	23.4	23.5	23.5	23.5	23.4	23.4	23.5	23.5	23.5	23.6	23.6	23.5	23.4	23.4	23.4
18.0	23.9	23.8	23.8	23.8	23.8	23.7	23.7	23.8	23.8	23.8	23.9	23.8	23.8	23.8	23.9	23.9	23.8	23.8	23.8	23.7	23.8
17.0	24.1	24.0	24.0	24.0	23.9	24.0	24.0	24.1	24.0	24.0	24.0	24.0	24.0	24.0	24.0	24.0	24.1	24.0	24.0	24.1	24.1
16.0	24.5	24.5	24.5	24.4	24.5	24.4	24.4	24.4	24.5	24.5	24.4	24.5	24.5	24.5	24.4	24.5	24.5	24.5	24.5	24.7	24.8
15.0	25.0	25.0	25.0	25.0	25.0	25.0	25.1	25.1	25.0	25.1	25.2	25.3	25.3	25.3	25.3	25.3	25.4	25.4	25.4	25.4	25.5
14.0	25.5	25.5	25.5	25.6	25.6	25.6	25.7	25.7	25.7	25.8	25.9	25.9	25.8	25.8	25.8	25.8	25.9	26.1	26.1	26.0	26.0
13.0	26.4	26.3	26.3	26.4	26.4	26.3	26.3	26.4	26.4	26.4	26.4	26.5	26.5	26.5	26.6	26.6	26.5	26.6	26.6	26.7	26.7
12.0	27.0	27.0	27.0	27.0	27.0	27.0	27.1	27.1	27.1	27.2	27.2	27.1	27.2	27.2	27.1	27.1	27.2	27.2	27.2	27.3	27.3
11.0	27.8	27.9	27.9	27.9	27.8	27.9	27.9	27.9	27.9	27.9	28.0	28.0	28.0	28.0	28.0	28.0	28.1	28.1	28.1	28.2	28.3
10.0	28.9	29.0	29.0	28.9	29.0	28.9	29.0	29.0	28.9	29.0	29.0	29.1	29.1	29.1	29.2	29.1	29.1	29.2	29.2	29.3	29.2
9.5	29.2	29.3	29.3	29.4	29.3	29.4	29.4	29.4	29.4	29.4	29.4	29.5	29.6	29.4	29.5	29.5	29.6	29.7	29.8	29.7	29.8
9.0	29.7	29.6	30.0	30.0	29.6	29.6	29.6	29.6	29.6	29.7	29.7	29.8	29.8	29.8	29.8	29.9	29.9	30.3	30.3	30.0	30.0
8.5	31.0	31.0	30.9	30.9	31.0	30.9	30.8	30.8	30.9	30.9	30.9	30.9	31.0	31.1	31.3	31.3	31.2	31.1	31.2	31.3	31.3
8.0	31.4	31.4	31.5	31.5	31.7	31.7	31.6	31.5	31.6	31.6	31.6	31.8	31.8	31.7	31.7	31.7	31.7	31.8	31.8	31.9	31.9
7.5	32.2	32.1	32.1	32.2	32.2	32.2	32.3	32.2	32.2	32.3	32.2	32.3	32.6	32.4	32.4	32.5	32.5	32.5	32.6	32.6	32.7
7.0	32.9	33.0	33.0	33.0	33.0	33.2	33.2	33.0	33.1	33.1	33.1	33.1	33.1	33.2	33.2	33.2	33.3	33.3	33.3	33.4	33.5
6.5	33.9	34.0	34.3	34.1	34.1	34.4	34.2	34.2	34.2	34.3	34.3	34.4	34.3	34.3	34.3	34.4	34.5	34.4	34.5	34.6	34.6
6.0	34.1	34.6	34.8	34.8	34.8	34.8	34.9	35.0	35.0	35.0	35.1	35.1	35.1	35.1	35.1	35.2	35.3	35.4	35.4	35.4	35.6

	AZIMUTH, deg																				
	130	131	132	133	134	135	136	137	138	139	140	141	142	143	144	145	146	147	148	149	150
20.0	22.9	22.9	22.9	22.9	22.9	23.0	23.0	23.5	23.4	22.9	23.0	23.0	23.0	23.0	22.9	22.9	23.0	23.0	23.0	23.0	23.0
19.0	23.4	23.4	23.4	23.4	23.4	23.4	23.3	23.5	23.9	23.6	23.4	23.6	23.8	23.4	23.4	23.9	23.7	23.4	23.4	23.4	23.4
18.0	23.8	23.8	23.7	23.7	23.7	23.8	23.8	23.7	23.8	23.9	23.9	23.9	24.3	24.4	23.9	24.0	24.6	24.3	23.9	24.1	24.6
17.0	24.1	24.2	24.3	24.4	24.3	24.3	24.3	24.2	24.3	24.3	24.4	24.4	24.4	24.4	24.3	24.3	24.3	24.4	24.3	24.4	24.5
16.0	24.8	24.6	24.6	24.7	24.7	24.7	24.8	24.8	24.9	24.9	24.9	25.0	25.1	25.0	24.9	25.1	25.1	24.9	24.9	25.0	25.0
15.0	25.5	25.4	25.4	25.5	25.4	25.4	25.4	25.5	25.5	25.5	25.6	25.6	25.6	25.6	25.6	25.5	25.5	25.6	25.6	25.5	25.5
14.0	26.0	26.0	26.0	26.0	26.3	26.7	26.4	26.3	26.3	26.3	26.3	26.2	26.2	26.3	26.3	26.3	26.3	26.5	26.8	26.4	26.4
13.0	26.7	26.7	26.8	26.8	26.9	27.0	26.8	26.6	26.8	26.9	27.0	27.0	27.1	27.1	27.1	27.1	27.1	27.3	27.3	27.3	27.3
12.0	27.3	27.3	27.3	27.4	27.4	27.4	27.4	27.4	27.5	27.5	27.5	27.6	27.6	27.7	27.7	27.7	27.7	27.8	27.8	27.8	27.9
11.0	28.3	28.3	28.3	28.7	29.3	28.6	28.6	29.1	28.6	28.4	28.4	28.5	28.4	28.5	28.5	28.5	28.5	28.6	28.7	28.7	28.7
10.0	29.2	29.3	29.3	29.5	29.5	29.4	29.5	29.5	29.5	29.6	29.6	29.7	29.6	29.6	29.5	29.7	29.7	29.7	29.7	29.8	29.9
9.5	29.8	29.8	29.9	29.9	30.0	29.9	29.9	29.9	29.9	30.0	30.0	30.1	30.1	30.1	30.2	30.2	30.2	30.3	30.2	30.2	30.2
9.0	30.0	30.1	30.1	30.2	30.2	30.2	30.3	30.3	30.4	30.4	30.3	30.4	30.5	30.6	30.5	30.6	30.6	30.7	30.7	30.7	30.7
8.5	31.3	31.4	31.5	31.4	31.5	31.7	31.7	31.7	31.8	31.4	31.7	31.9	31.6	31.6	31.8	31.8	31.7	31.7	31.8	31.8	31.8
8.0	31.9	31.9	32.0	32.0	32.1	32.3	32.2	32.1	32.2	32.3	32.2	32.3	32.2	32.1	32.3	32.4	32.4	32.4	32.4	32.5	32.6
7.5	32.7	32.7	32.7	32.9	33.0	33.0	33.0	33.0	33.1	33.2	33.3	33.2	33.2	33.2	33.3	33.3	33.3	33.3	33.4	33.5	33.6
7.0	33.5	33.6	33.7	33.6	33.8	33.9	33.9	34.0	33.9	33.8	33.9	34.0	34.0	34.0	34.0	34.0	34.1	34.2	34.3	34.6	34.7
6.5	34.6	34.7	34.7	34.8	34.9	35.0	35.0	35.0	35.0	35.1	35.4	35.3	35.2	35.2	35.2	35.3	35.4	35.5	35.7	35.9	36.0
6.0	35.6	35.6	35.6	35.8	35.8	35.8	35.9	35.9	35.9	36.1	36.1	36.2	36.2	36.3	36.4	36.4	36.5	36.6	36.8	37.0	37.2

Table 6. DSS 14 Western Horizon S-Band T_{op} (K) with SPD Cone

ELEV, deg	AZIMUTH, deg																				
	210	211	212	213	214	215	216	217	218	219	220	221	222	223	224	225	226	227	228	229	230
9.0	31.5	31.8	32.8	33.8	33.3	32.4	31.8	31.4	31.1	31.1	31.0	30.9	30.8	30.8	30.6	30.8	30.8	30.9	30.8	30.8	30.8
8.5	32.8	33.1	34.1	34.1	33.0	32.4	32.1	31.8	31.7	31.5	31.5	31.5	31.4	31.4	31.3	31.3	31.3	31.3	31.3	31.3	31.3
8.0	29.0	33.3	33.7	34.9	35.6	34.2	33.1	32.9	32.8	32.5	32.4	32.3	32.3	32.6	32.2	32.1	32.2	32.5	32.3	32.2	32.3
7.5	36.5	36.7	36.7	36.7	36.3	35.1	34.1	33.8	33.5	33.2	33.1	33.0	33.0	33.0	33.0	33.0	32.9	32.8	32.7	32.8	32.9
7.0	36.1	36.1	36.1	36.0	36.0	36.0	35.6	34.8	34.3	34.0	33.9	33.5	33.7	33.7	33.7	33.6	33.6	33.6	33.5	33.5	33.6
6.5	36.2	36.1	36.0	36.1	36.0	35.6	35.2	34.8	34.7	34.8	34.6	34.6	34.6	34.6	34.8	34.6	34.6	34.5	34.5	34.5	34.5
6.0	36.4	35.9	36.5	36.6	36.6	36.5	36.2	35.8	35.6	35.5	35.5	35.5	35.5	35.5	35.4	35.4	35.4	35.3	35.4	35.3	35.4
	AZIMUTH, deg																				
	230	231	232	233	234	235	236	237	238	239	240	241	242	243	244	245	246	247	248	249	250
9.0	30.8	30.7	30.7	30.7	30.9	30.9	30.7	30.9	31.2	30.7	30.6	30.6	30.6	30.5	30.6	30.6	30.5	30.5	30.6	30.7	30.8
8.5	31.3	31.2	31.2	31.2	31.3	31.5	31.3	31.3	31.2	31.1	31.2	31.2	31.2	31.2	31.2	31.2	31.2	31.3	31.3	31.3	31.3
8.0	32.3	32.1	32.0	32.0	31.9	32.0	32.0	31.7	31.8	31.9	32.0	32.0	32.0	31.9	31.9	31.9	31.8	31.9	32.0	32.0	32.1
7.5	32.9	32.8	32.8	32.8	32.7	32.7	32.7	32.8	32.8	32.7	32.4	32.7	32.9	32.8	32.8	32.9	32.7	32.7	32.7	32.5	32.3
7.0	33.6	33.6	33.5	33.5	33.6	33.6	33.5	33.5	33.5	33.5	33.5	33.5	33.4	33.4	33.4	33.2	33.4	33.5	33.5	33.4	33.5
6.5	34.5	34.4	34.4	34.4	34.4	34.4	34.4	34.4	34.4	34.4	34.4	34.3	34.3	34.4	34.4	34.3	34.3	34.3	34.4	34.3	34.3
6.0	35.4	35.5	35.4	35.5	35.7	35.7	35.6	35.6	35.7	35.6	35.6	35.6	35.6	35.5	35.5	35.5	35.5	35.5	35.6	35.6	35.6

Table 7. DSS 43 Eastern Horizon S-Band T_{op} (K) with SPD Cone

ELEV, deg	AZIMUTH, deg																				
	90	91	92	93	94	95	96	97	98	99	100	101	102	103	104	105	106	107	108	109	110
20.0	25.6	25.3	24.8	25.5	25.0	25.3	25.6	25.4	25.0	25.3	25.4	25.1	24.8	25.5	25.2	25.3	24.9	25.6	24.9	24.7	25.3
19.0	26.0	26.1	25.9	25.8	26.1	26.7	26.2	26.0	25.9	25.9	25.5	25.3	25.8	26.0	25.4	26.0	25.6	25.6	25.5	25.7	25.4
18.0	26.9	26.6	26.8	26.2	26.3	26.5	26.7	26.8	26.7	26.5	26.8	26.2	26.8	26.7	26.5	26.4	26.2	26.1	26.6	26.2	26.0
17.0	27.7	27.8	27.0	27.2	27.5	27.0	27.8	27.4	27.8	27.7	27.3	27.5	27.4	27.0	27.0	27.5	27.5	26.9	26.8	26.9	27.3
16.0	28.1	28.1	27.7	28.3	27.9	28.1	28.0	28.2	28.0	27.7	28.2	27.9	28.2	27.9	28.0	28.1	28.1	27.8	27.8	27.3	27.6
15.0	29.4	29.3	28.6	29.0	28.8	28.9	28.6	29.3	28.7	29.3	28.9	28.8	29.0	28.9	28.2	28.7	28.9	28.9	28.6	28.4	28.4
14.0	29.9	30.2	29.8	30.1	30.1	29.6	29.9	29.7	29.7	29.8	29.8	30.1	29.9	29.9	29.4	29.5	29.6	29.7	29.0	29.4	29.0
13.0	30.9	30.3	30.6	30.9	30.4	31.2	30.7	30.3	30.6	30.9	30.3	30.5	30.5	30.7	30.4	30.4	30.3	30.4	30.6	30.1	30.2
12.0	31.7	31.9	31.8	32.3	31.8	32.1	32.0	32.0	31.8	32.2	31.7	31.9	31.6	31.6	31.5	31.6	31.7	31.5	31.0	31.4	31.2
11.0	33.1	33.5	33.0	32.6	32.7	33.3	32.9	33.5	34.1	33.4	33.7	34.1	33.5	33.4	33.6	32.6	32.6	32.7	32.6	32.5	32.4
10.0	40.2	39.4	37.2	36.3	36.0	36.0	36.7	39.9	46.5	58.0	64.9	65.7	62.7	55.2	43.7	37.3	35.3	34.4	34.6	33.9	33.8
9.5	57.1	56.7	53.5	48.3	45.1	45.8	51.6	60.5	74.1	88.8	101	105	101	89.0	73.9	59.9	46.9	38.3	36.5	35.6	34.3
9.0	83.6	82.7	78.2	73.2	71.6	76.3	87.1	103	121	138	148	149	140	123	103	84.5	67.0	52.4	45.2	40.7	37.9
8.5	118	119	118	114	111	111	119	132	150	168	184	194	191	180	162	141	118	97.5	81.7	71.0	61.2
8.0	158	157	155	152	153	158	168	184	202	218	229	230	222	208	189	167	148	131	116	103	88.8
7.5	197	198	198	195	192	194	202	214	229	241	247	247	245	243	234	218	202	185	172	160	141
7.0	226	227	227	225	223	227	234	243	247	249	249	248	247	247	245	239	229	219	210	197	178
6.5	242	243	244	244	243	243	246	247	250	251	251	250	249	248	248	249	248	245	243	237	227
6.0	246	247	246	246	247	247	248	249	250	250	250	250	249	248	249	249	249	248	248	246	240
	AZIMUTH, deg																				
	110	111	112	113	114	115	116	117	118	119	120	121	122	123	124	125	126	127	128	129	130
20.0	25.3	24.9	24.9	24.3	24.7	24.0	24.5	24.3	24.7	24.2	24.6	24.2	24.0	24.1	24.1	24.6	24.5	24.5	23.8	24.1	24.3
19.0	25.4	25.3	25.5	25.5	25.6	24.9	25.4	25.0	25.1	25.3	25.0	24.4	24.9	24.5	25.2	24.6	24.7	24.5	24.6	24.8	24.4
18.0	26.0	26.4	26.1	26.3	25.8	26.1	25.6	25.4	25.8	25.4	25.5	25.5	25.4	25.5	25.5	25.3	25.1	25.5	25.1	25.3	25.5
17.0	27.3	26.7	26.9	26.5	26.9	26.2	27.1	26.2	26.2	26.2	26.4	26.4	26.1	26.1	26.2	26.1	26.0	25.9	26.1	25.6	25.3
16.0	27.6	27.4	27.9	27.5	27.4	27.5	27.3	26.7	27.0	27.4	26.9	26.4	27.0	26.4	26.8	26.4	26.5	26.7	26.3	26.6	27.5
15.0	28.4	28.2	28.2	28.1	28.1	28.1	27.9	28.1	27.9	27.6	27.9	27.9	27.5	27.5	27.9	27.5	27.5	27.2	27.4	27.3	26.9
14.0	29.0	29.0	29.0	29.3	29.0	29.0	28.8	28.8	28.9	28.7	28.7	28.2	28.5	28.3	28.4	28.3	28.5	28.3	27.7	27.9	27.7
13.0	30.2	30.6	29.8	29.9	29.9	29.8	29.7	29.5	29.6	29.6	29.6	30.3	29.3	29.1	29.8	29.0	28.9	28.8	29.2	29.4	28.7
12.0	31.2	30.9	30.4	30.9	30.9	30.8	30.7	30.5	30.8	30.0	30.4	29.9	30.3	30.6	30.4	30.4	30.1	30.2	30.1	29.9	29.9
11.0	32.4	32.4	32.1	32.1	31.9	31.5	31.7	31.8	31.9	31.2	31.6	31.5	31.2	31.9	31.5	31.8	31.2	31.4	30.9	31.4	31.7
10.0	33.8	33.9	33.7	32.9	33.1	33.0	32.8	33.4	32.7	32.7	32.6	32.9	32.8	33.0	32.9	33.9	34.6	33.9	33.0	32.8	32.8
9.5	34.3	35.1	35.0	33.7	34.4	33.8	33.6	33.6	33.3	33.2	33.6	33.0	33.3	33.8	33.2	33.5	33.1	33.5	33.4	33.1	33.1
9.0	37.9	36.3	35.4	35.4	35.2	34.8	34.8	34.5	34.6	34.5	34.3	33.8	34.1	34.1	34.0	34.1	33.8	34.1	34.1	34.1	33.3
8.5	61.2	48.2	40.2	36.6	36.3	35.6	35.4	35.7	35.8	35.3	35.1	35.1	35.0	35.3	35.2	35.0	35.5	35.1	35.5	35.0	34.8
8.0	88.8	70.2	52.9	42.7	38.2	37.1	36.4	36.1	36.6	36.3	36.1	35.9	36.1	36.2	36.2	36.0	37.0	36.6	37.0	36.2	36.5
7.5	141	120	95.6	74.6	57.4	44.6	39.7	38.0	37.7	38.1	38.0	37.4	37.9	38.1	38.1	38.0	38.0	37.9	38.4	38.0	38.1
7.0	178	154	129	103	80.7	59.3	43.7	40.6	39.8	40.4	40.1	39.9	40.7	40.4	40.5	40.9	40.6	40.0	40.4	40.2	39.3
6.5	227	207	185	160	133	106	78.6	55.0	44.8	42.8	43.5	44.0	44.2	46.2	47.8	49.1	48.0	45.1	43.8	42.6	43.3
6.0	240	226	206	182	155	123	92.3	67.7	53.5	49.3	49.4	52.9	59.1	66.8	71.2	70.0	63.3	55.2	49.6	46.6	46.0

Table 8. DSS 43 Western Horizon S-Band T_{op} (K) with SPD Cone

ELEV, deg	AZIMUTH, deg																				
	230	231	232	233	234	235	236	237	238	239	240	241	242	243	244	245	246	247	248	249	250
20.0	24.0	23.9	24.0	24.1	23.9	24.2	24.0	24.1	24.3	24.1	24.1	24.1	24.0	24.2	24.3	24.0	24.2	24.2	24.1	24.2	24.1
19.0	24.6	24.6	24.8	24.7	24.8	24.8	24.7	24.8	24.7	24.9	24.9	24.8	24.9	25.1	24.9	24.8	24.7	24.8	24.9	24.9	24.8
18.0	25.3	25.2	25.3	25.3	25.4	25.6	25.4	25.3	25.5	25.6	25.6	25.5	25.5	25.6	25.4	25.5	25.5	25.4	25.5	25.5	25.3
17.0	26.0	25.9	26.1	26.0	26.0	26.0	26.0	26.2	26.1	26.0	26.2	26.1	26.2	26.0	26.1	26.0	26.0	26.1	25.9	26.1	26.1
16.0	26.6	26.7	26.6	26.8	27.0	26.8	26.8	26.9	26.9	26.8	26.9	26.9	26.8	26.7	26.8	26.8	27.0	26.7	26.8	26.7	26.9
15.0	27.5	27.5	27.6	27.5	27.6	27.6	27.6	27.6	27.7	27.7	27.6	27.7	27.7	27.7	27.6	27.6	27.6	27.5	27.7	27.8	27.5
14.0	28.5	28.3	28.2	28.2	28.2	28.3	28.5	28.4	28.5	28.4	28.5	28.5	28.6	28.5	28.5	28.5	28.5	28.4	28.4	28.3	28.3
13.0	29.1	29.1	29.3	29.2	29.2	29.2	29.2	29.3	29.2	29.3	29.3	29.4	29.4	29.2	29.4	29.3	29.3	29.3	29.4	29.3	29.1
12.0	30.1	30.0	30.0	30.1	30.1	30.2	30.3	30.2	30.3	30.2	30.5	30.3	30.4	30.5	30.4	30.5	30.4	30.3	30.3	30.3	30.3
11.0	31.5	31.6	31.7	31.8	31.7	31.8	31.9	32.0	31.9	32.0	31.8	31.9	32.0	32.0	32.1	32.1	32.0	31.9	31.9	31.8	31.6
10.0	32.5	32.6	33.2	34.0	34.0	34.0	35.4	38.0	38.6	38.0	36.3	36.1	38.7	37.8	36.4	39.4	39.3	35.6	34.0	33.7	33.7
9.5	34.3	34.6	34.6	36.9	39.4	39.2	39.6	41.9	45.2	45.9	46.2	43.6	43.4	45.1	44.5	44.0	45.9	44.4	40.8	38.0	37.0
9.0	40.6	41.0	43.0	46.0	47.8	50.3	51.1	54.6	55.1	56.9	57.9	56.6	55.1	55.7	56.8	56.1	54.4	51.6	49.2	45.2	46.3
8.5	47.0	49.4	53.1	56.1	57.1	61.6	65.3	67.9	68.6	68.5	73.3	72.7	71.0	69.4	72.3	71.8	68.6	65.0	64.2	62.1	57.7
8.0	61.2	66.3	71.0	69.8	75.8	81.2	84.3	84.8	84.9	90.5	91.6	90.1	87.4	89.8	90.7	86.7	81.4	80.0	80.3	75.0	70.7
7.5	75.2	76.6	84.7	88.3	87.1	95.4	101	104	103	105	111	113	110	108	111	111	103	98.6	99.2	98.7	92.1
7.0	93.3	99.3	108	105	110	119	125	123	125	128	135	132	130	131	134	127	119	120	120	117	110
6.5	113	118	127	127	128	137	145	144	145	148	152	156	152	151	154	153	145	140	142	140	134
6.0	136	143	150	148	151	161	166	166	168	171	177	175	173	175	176	173	166	162	163	159	152

	AZIMUTH, deg																				
	250	251	252	253	254	255	256	257	258	259	260	261	262	263	264	265	266	267	268	269	270
20.0	24.1	24.2	23.9	24.2	23.9	24.0	24.0	24.1	24.0	24.0	24.0	24.0	24.0	24.0	23.9	24.1	24.1	24.0	23.9	24.0	24.2
19.0	24.8	24.8	24.8	24.7	24.7	24.8	24.6	24.7	24.6	24.6	24.6	24.7	24.7	24.6	24.6	24.5	24.5	24.5	24.5	24.4	24.6
18.0	25.3	25.5	25.4	25.4	25.5	25.4	25.4	25.3	25.2	25.2	25.2	25.2	25.2	25.2	25.1	25.2	25.1	25.2	25.1	25.1	25.2
17.0	26.1	25.9	25.7	26.1	26.0	25.9	25.8	25.8	25.7	25.8	25.9	25.8	25.8	25.8	25.5	25.6	25.7	25.8	25.6	25.6	25.6
16.0	26.9	26.9	26.8	26.8	26.6	26.7	26.7	26.7	26.6	26.6	26.6	26.5	26.6	26.5	26.5	26.4	26.5	26.4	26.3	26.4	26.0
15.0	27.5	27.4	27.6	27.6	27.5	27.5	27.5	27.4	27.4	27.5	27.5	27.5	27.5	27.4	27.2	27.3	27.3	27.1	27.1	27.2	27.0
14.0	28.3	28.4	28.5	28.2	28.4	28.3	28.3	28.3	28.3	28.4	28.1	28.3	28.3	28.3	28.1	28.0	28.1	28.0	28.1	28.0	28.1
13.0	29.1	29.3	29.2	29.2	29.2	29.2	29.2	29.2	29.2	29.1	29.2	29.2	29.2	29.1	29.0	29.0	28.9	28.9	29.1	28.8	29.1
12.0	30.3	30.4	30.3	30.4	30.2	30.2	30.3	30.2	30.2	30.1	30.1	30.2	30.1	30.2	30.1	30.0	30.0	29.9	30.0	29.9	29.6
11.0	31.6	31.7	31.7	31.5	31.5	31.4	31.4	31.4	31.2	31.3	31.3	31.0	31.2	31.1	31.1	31.0	31.1	31.0	30.9	30.9	30.9
10.0	33.7	34.1	34.0	33.1	33.3	33.1	32.7	32.5	32.5	32.4	32.3	32.4	32.3	32.3	32.2	32.2	32.4	32.2	32.1	32.0	31.9
9.5	37.0	38.7	39.8	37.2	35.9	36.8	35.2	33.8	33.3	33.3	33.2	33.0	33.0	33.1	32.9	32.8	32.9	32.8	32.8	32.7	32.4
9.0	46.3	47.6	45.0	42.4	42.2	39.9	36.7	34.9	34.4	34.1	34.0	33.9	33.9	33.7	33.6	33.5	33.7	33.6	33.5	33.5	33.6
8.5	57.7	57.1	55.4	55.0	52.9	47.5	42.9	41.9	37.9	35.8	35.0	34.9	34.7	34.6	34.4	34.4	34.4	34.4	34.3	34.3	34.1
8.0	70.7	69.5	70.6	67.7	62.5	55.1	54.1	50.5	43.8	38.5	36.3	35.8	35.7	35.4	35.7	35.3	35.4	35.2	35.4	35.2	35.1
7.5	92.1	87.7	86.8	87.0	82.6	74.6	69.7	66.5	58.4	49.9	42.7	38.7	37.2	37.0	36.8	36.7	36.8	36.6	36.8	36.4	36.6
7.0	110	105	105	104	97.9	89.5	86.2	78.3	67.7	58.6	50.4	43.5	40.5	39.1	38.2	37.9	37.9	37.8	37.7	37.8	37.8
6.5	134	126	125	126	122	112	108	100	87.6	77.7	68.3	59.0	51.4	47.4	42.5	40.5	39.9	39.5	39.4	39.4	39.4
6.0	152	147	147	148	139	132	127	116	103	92.6	83.0	72.4	63.6	58.8	51.7	45.6	43.8	44.1	43.5	42.3	42.0

Table 9. DSS 63 Eastern Horizon S-Band T_{op} (K) with SPD Cone

ELEV, deg	AZIMUTH, deg																				
	110	111	112	113	114	115	116	117	118	119	120	121	122	123	124	125	126	127	128	129	130
40.0	23.0	23.2	23.1	23.0	23.1	22.9	22.7	22.7	22.7	22.7	22.7	22.9	22.9	23.0	22.8	22.7	22.8	22.8	22.8	22.8	22.8
35.0	23.3	23.3	23.4	23.3	23.3	23.3	23.2	23.2	23.2	23.2	23.1	23.1	23.1	23.1	23.1	23.0	23.1	23.1	23.1	23.1	23.2
30.0	23.5	23.6	23.7	23.6	23.6	23.6	23.5	23.7	23.6	23.6	23.6	23.7	23.6	23.6	23.8	23.7	23.7	23.7	23.9	23.8	23.7
25.0	24.6	24.5	24.7	24.7	24.7	24.7	24.7	24.6	24.6	24.6	24.5	24.5	24.6	24.5	24.4	24.3	24.4	24.4	24.4	24.4	24.5
20.0	26.1	26.1	26.2	26.3	26.2	26.3	26.3	26.4	26.3	26.2	26.0	26.0	26.0	26.1	26.3	26.4	26.4	26.3	26.1	26.1	26.2
19.0	26.4	26.4	26.5	26.5	26.5	26.5	26.5	26.5	26.5	26.6	26.7	26.7	26.9	26.6	26.7	26.5	26.5	26.4	26.3	26.5	26.5
18.0	27.4	27.5	27.5	27.8	27.9	27.6	27.7	27.6	27.5	27.6	27.4	27.6	27.5	27.6	27.6	27.5	27.4	27.5	27.3	27.3	27.2
17.0	27.4	27.4	27.4	27.6	27.4	27.3	27.5	27.5	27.4	27.6	27.6	27.5	27.7	27.6	27.5	27.6	27.7	27.5	27.4	27.6	27.6
16.0	28.5	28.7	28.8	28.7	28.4	28.6	28.6	28.5	28.3	28.2	28.3	28.1	28.1	28.3	28.2	28.1	28.2	28.1	28.0	28.0	28.2
15.0	29.0	29.0	29.0	29.0	29.1	29.0	29.0	28.9	29.0	28.8	29.1	29.0	29.1	29.2	29.3	29.3	29.3	29.3	29.3	29.4	29.3
14.0	29.6	29.5	29.7	29.7	29.7	29.7	29.9	29.9	29.8	29.9	29.9	29.9	29.9	29.9	29.8	29.8	29.9	29.8	29.9	29.9	29.9
13.0	30.8	30.8	30.8	30.8	30.8	30.9	30.8	30.9	30.9	31.0	30.9	30.8	30.9	31.0	30.9	30.9	30.6	30.6	30.7	30.8	30.8
12.0	32.0	32.1	32.2	32.0	31.9	32.0	31.9	32.0	31.9	31.7	31.9	31.7	31.7	31.8	31.8	31.8	31.9	32.0	32.1	32.1	32.0
11.0	32.7	32.8	32.7	32.7	32.5	32.5	32.6	32.6	32.5	32.6	32.7	32.6	32.5	32.6	32.3	32.6	32.7	32.8	32.6	32.6	32.3
10.0	34.8	34.7	34.5	34.6	34.4	34.5	34.3	34.4	34.2	34.0	33.9	33.9	33.8	33.7	33.6	33.6	33.8	33.7	33.8	33.9	33.8
9.5	34.9	34.9	34.9	34.8	34.8	34.6	34.8	34.6	34.7	34.7	34.4	34.3	34.1	34.1	34.0	34.0	34.2	34.1	34.0	34.1	34.1
9.0	34.9	34.9	35.2	34.7	34.7	34.9	34.8	34.9	35.0	34.8	34.6	34.6	34.4	34.4	34.4	34.4	34.5	34.4	34.6	34.7	34.7
8.5	35.7	35.9	35.7	35.5	35.4	35.3	35.4	35.5	35.7	35.7	35.9	35.8	35.7	35.7	35.7	35.7	35.8	35.6	35.6	35.6	35.8
8.0	36.8	37.1	37.2	37.0	37.2	37.0	37.2	36.9	37.2	37.0	36.9	36.9	37.1	37.1	37.2	37.1	37.1	37.0	37.0	36.9	36.8
7.5	37.8	38.0	38.0	37.8	37.8	37.9	38.1	38.1	38.2	38.1	38.0	37.9	38.0	38.2	38.1	38.1	38.0	38.0	38.0	38.0	37.9
7.0	39.2	39.2	39.1	38.9	39.0	39.0	39.1	39.0	39.2	39.2	39.2	39.3	39.2	39.4	39.3	38.9	39.2	39.2	39.1	39.3	39.4
6.5	40.4	40.9	40.6	40.8	40.5	40.6	40.6	40.4	40.5	40.5	40.5	40.5	40.4	40.3	40.7	40.4	40.2	40.3	40.2	40.4	40.4
6.0	42.1	42.2	42.2	42.1	42.2	42.1	42.1	41.9	41.8	41.8	41.9	42.0	41.8	41.8	41.9	41.8	41.7	41.6	41.8	41.6	41.7

	AZIMUTH, deg																				
	130	131	132	133	134	135	136	137	138	139	140	141	142	143	144	145	146	147	148	149	150
40.0	22.8	22.9	22.9	22.9	22.9	22.9	22.9	23.0	23.0	23.0	22.7	22.6	22.7	22.7	22.8	22.8	23.0	23.1	23.1	22.9	22.9
35.0	23.2	23.1	23.1	23.3	23.3	23.3	23.5	23.5	23.5	23.4	23.3	23.2	23.1	23.0	23.1	23.1	23.2	23.3	23.3	23.4	23.4
30.0	23.7	23.8	23.7	23.9	23.7	23.8	23.9	23.9	23.8	23.9	23.7	23.7	23.6	23.8	23.7	23.6	23.8	23.7	23.8	23.8	23.7
25.0	24.5	24.5	24.6	24.6	24.7	24.7	24.8	24.7	24.6	24.6	24.6	24.5	24.5	24.5	24.5	24.5	24.3	24.4	24.7	24.7	24.6
20.0	26.2	26.2	26.3	26.2	26.3	26.4	26.4	26.4	26.5	26.2	26.3	26.4	26.3	26.3	26.2	26.2	26.3	26.5	26.4	26.3	26.3
19.0	26.5	26.6	26.6	26.6	26.5	26.6	26.9	26.7	26.8	26.7	26.6	26.6	26.6	26.7	26.7	26.9	26.9	26.8	26.9	26.8	26.7
18.0	27.2	27.2	27.3	27.0	27.3	27.3	27.2	27.3	27.4	27.4	27.4	27.4	27.4	27.2	27.2	27.1	27.0	27.2	27.3	27.3	27.2
17.0	27.6	27.5	27.5	27.4	27.5	27.5	27.5	27.4	27.5	27.5	27.7	27.8	28.0	28.1	28.1	28.1	28.1	28.0	28.0	28.1	28.1
16.0	28.2	28.1	28.1	27.9	27.8	27.9	28.0	28.3	28.2	28.3	28.4	28.4	28.3	28.3	28.4	28.6	28.4	28.5	28.7	28.9	28.7
15.0	29.3	29.2	29.1	29.3	29.4	29.3	29.2	29.2	29.2	29.1	28.9	28.8	28.7	29.0	29.2	29.0	29.1	29.0	28.9	28.9	28.9
14.0	29.9	29.9	30.0	30.1	29.9	29.8	30.0	29.9	29.8	29.9	29.9	30.0	30.0	30.0	30.2	30.1	30.1	30.2	29.9	29.9	29.8
13.0	30.8	30.7	30.7	30.9	31.0	30.9	30.8	31.0	30.9	30.9	30.9	31.0	30.8	30.7	30.7	30.7	30.8	31.0	30.9	30.9	30.9
12.0	32.0	31.9	32.0	32.1	31.8	32.0	31.8	32.0	31.7	31.8	31.6	31.6	31.5	31.7	31.5	31.7	31.4	31.5	31.4	31.6	31.8
11.0	32.3	32.6	32.7	32.5	32.4	32.5	32.7	32.8	33.2	33.3	33.2	33.3	33.4	33.5	33.5	33.4	33.4	33.3	33.5	33.4	33.3
10.0	33.8	33.9	33.7	33.8	33.9	33.8	33.9	34.0	33.9	33.9	33.8	33.7	33.8	33.8	33.7	33.7	33.7	33.8	33.9	33.9	34.0
9.5	34.1	33.9	34.1	34.1	33.8	34.1	34.0	33.8	34.1	34.1	33.8	33.7	34.0	33.8	33.8	34.0	33.9	34.0	34.0	33.9	34.0
9.0	34.7	34.8	34.9	34.9	35.2	35.0	35.0	35.2	35.2	35.2	35.0	35.0	35.2	35.2	35.1	35.0	35.1	35.0	34.7	34.9	34.7
8.5	35.8	35.7	35.5	35.6	35.5	35.3	35.2	35.0	34.9	34.8	35.1	35.1	35.2	35.1	34.9	34.8	34.8	34.9	35.0	35.1	35.3
8.0	36.8	36.5	36.3	36.5	36.4	36.5	36.4	36.3	36.2	36.1	36.1	36.6	36.2	36.1	35.9	36.4	36.4	36.0	36.1	35.9	35.7
7.5	37.9	38.0	37.9	37.7	37.7	37.6	37.5	37.1	37.4	37.2	37.4	37.3	37.4	37.5	37.4	37.4	37.3	37.2	37.3	37.3	37.3
7.0	39.4	39.2	39.3	39.2	39.1	38.9	38.9	38.7	38.7	38.7	38.5	38.4	38.4	38.4	38.8	38.4	38.4	38.2	38.2	37.9	37.9
6.5	40.4	40.4	40.3	40.3	40.4	40.2	40.3	40.2	40.3	40.1	40.0	40.1	40.0	40.2	40.2	40.0	40.0	39.9	39.8	39.8	39.8
6.0	41.7	41.6	41.7	41.7	41.7	41.4	41.4	41.3	41.4	41.3	41.5	41.4	41.2	41.3	41.3	41.1	41.3	40.8	40.8	40.7	40.7

Table 10. DSS 63 Western Horizon S-Band T_{op} (K) with SPD Cone

ELEV, deg	AZIMUTH, deg																				
	210	211	212	213	214	215	216	217	218	219	220	221	222	223	224	225	226	227	228	229	230
40.0	30.8	25.0	24.2	24.3	24.0	24.2	24.8	25.1	26.2	31.2	26.9	24.8	24.2	24.1	23.7	23.7	23.8	23.8	23.9	23.8	23.7
35.0	24.1	24.1	24.5	24.4	24.6	24.8	25.0	25.3	26.6	30.4	26.2	25.2	24.9	24.7	24.5	24.4	24.3	24.3	24.2	24.3	24.3
30.0	25.0	25.2	25.3	25.5	25.6	26.4	28.8	27.5	26.5	26.1	25.6	25.4	25.4	25.3	25.2	25.1	25.1	25.1	25.0	25.0	24.8
25.0	25.8	25.9	25.8	26.1	26.3	27.6	31.2	29.0	27.2	26.7	26.4	26.1	25.9	26.0	25.8	25.7	25.7	25.7	25.7	25.7	25.5
20.0	27.5	28.0	28.3	28.6	30.1	31.0	29.2	28.4	28.1	27.7	27.6	27.3	27.4	27.3	27.2	27.0	27.0	27.0	27.2	27.3	27.1
19.0	28.1	28.2	28.4	28.9	30.3	32.0	30.1	29.2	28.6	28.2	27.9	27.8	28.0	27.6	27.8	27.6	27.6	27.5	27.5	27.6	27.5
18.0	28.9	29.6	32.8	35.1	30.7	29.9	29.1	28.8	28.4	28.3	28.2	28.2	28.1	28.2	28.0	28.0	28.0	28.0	28.0	28.0	28.1
17.0	29.4	29.6	31.9	31.9	31.4	30.3	29.5	29.3	29.1	28.8	28.8	28.7	28.6	28.6	28.6	28.6	28.6	28.6	28.5	28.6	28.5
16.0	30.4	31.8	32.6	31.2	30.3	30.0	29.5	29.3	29.2	29.2	29.1	29.4	29.4	29.4	29.2	29.3	29.2	29.2	29.3	29.3	29.1
15.0	31.7	32.4	34.4	32.2	31.9	31.0	30.3	30.1	30.2	30.0	29.9	30.2	29.9	29.9	29.9	30.6	32.2	30.1	29.7	29.8	29.6
14.0	34.1	39.9	33.3	31.5	31.2	30.9	30.9	30.6	30.8	30.6	30.7	30.7	30.6	30.7	30.8	30.6	30.6	30.6	30.7	30.6	30.7
13.0	39.6	46.7	34.9	32.7	32.1	32.0	31.6	31.4	31.6	31.4	31.4	31.5	31.3	31.4	31.5	31.6	31.5	31.4	31.5	31.4	31.4
12.0	35.3	34.2	33.2	32.8	32.5	32.5	32.3	32.1	32.3	32.1	32.1	32.1	32.1	32.1	32.1	32.2	32.3	32.4	32.3	32.4	32.4
11.0	35.9	35.4	34.4	33.8	33.5	33.3	33.0	33.0	33.2	33.1	33.1	33.2	33.1	33.1	33.1	33.0	33.0	33.3	33.2	33.2	33.2
10.0	34.4	34.5	34.4	34.2	34.1	34.0	33.9	34.0	33.9	34.0	34.1	34.0	33.9	34.3	34.1	34.1	34.0	34.1	34.1	34.3	34.3
9.5	35.2	35.0	34.8	34.9	34.7	34.7	34.7	34.7	34.8	34.7	34.9	34.9	34.6	34.6	35.2	34.9	34.7	34.9	35.0	34.8	34.8
9.0	35.5	35.5	35.4	35.3	35.5	35.2	35.4	35.3	35.4	35.3	35.7	35.4	35.3	35.3	35.5	35.4	35.5	35.3	35.7	35.4	35.6
88.5	36.1	36.1	36.0	36.2	36.3	36.1	36.0	36.1	36.0	36.0	35.9	35.9	35.8	35.8	35.9	35.9	35.8	36.0	35.9	35.9	35.9
8.0	36.9	36.7	36.5	36.9	36.7	36.7	36.8	36.5	37.0	36.8	36.9	36.8	37.0	36.9	36.6	36.8	37.0	37.0	37.0	37.1	37.1
7.5	37.7	37.8	37.5	38.1	37.6	37.6	37.9	37.6	37.5	38.0	37.8	37.9	37.8	37.7	38.0	38.1	37.8	37.9	37.8	37.8	38.1
7.0	38.5	39.1	38.4	38.9	38.9	38.7	38.6	38.6	38.9	38.9	39.2	38.9	38.9	39.1	39.3	39.4	39.2	39.3	39.3	39.1	39.1
6.5	39.0	38.8	39.3	39.4	39.3	39.4	39.0	39.1	39.0	39.4	39.1	39.5	39.4	39.3	39.6	39.8	39.8	39.9	39.8	39.8	40.0
6.0	40.0	39.9	40.3	40.8	40.1	40.5	40.4	40.4	40.7	41.2	41.3	40.9	41.4	41.5	41.5	41.6	41.7	41.5	41.8	41.9	41.7

	AZIMUTH, deg																				
	230	231	232	233	234	235	236	237	238	239	240	241	242	243	244	245	246	247	248	249	250
40.0	23.7	23.6	23.5	23.5	23.5	23.4	23.4	23.4	23.5	23.4	23.4	23.5	23.5	23.5	23.5	23.5	23.5	23.5	23.5	23.5	23.6
35.0	24.3	24.1	24.2	24.0	23.9	24.1	24.0	23.9	24.1	24.0	23.8	23.8	24.0	24.0	23.8	23.7	23.8	23.9	24.0	23.8	23.8
30.0	24.8	24.9	24.8	24.8	24.9	24.8	24.8	24.7	24.7	24.6	24.7	24.6	24.5	24.6	24.6	24.7	24.7	24.6	24.8	24.8	24.8
25.0	25.5	25.5	25.8	25.7	25.4	25.5	25.5	25.5	25.5	25.5	25.6	25.6	25.6	25.6	25.7	25.7	25.7	25.7	25.7	25.7	25.6
20.0	27.1	27.2	27.3	27.1	27.2	27.2	27.1	27.5	27.3	27.3	27.2	27.1	27.1	27.1	27.2	27.2	27.2	27.2	27.2	27.3	27.4
19.0	27.5	27.6	27.6	27.6	27.6	27.6	27.6	27.6	27.6	27.8	27.7	27.8	27.8	27.7	27.7	27.7	27.7	27.7	27.8	27.8	27.8
18.0	28.1	28.1	28.1	28.1	28.2	28.2	28.3	28.3	28.3	28.4	28.4	28.5	28.4	28.3	28.3	28.3	28.3	28.3	28.4	28.4	28.4
17.0	28.5	28.5	28.7	28.7	28.7	28.7	28.7	28.7	28.9	28.9	28.9	28.9	28.8	28.8	28.8	28.8	28.8	28.8	28.8	28.9	28.9
16.0	29.1	29.2	29.3	29.3	29.3	29.4	29.4	29.4	29.4	29.5	29.3	29.3	29.2	29.2	29.3	29.4	29.5	29.4	29.5	29.5	29.5
15.0	29.6	29.8	29.8	29.8	29.7	29.9	29.8	29.9	29.9	29.9	30.2	30.0	30.1	30.1	30.1	30.2	30.2	30.2	30.1	30.3	30.2
14.0	30.7	30.6	30.7	30.7	30.8	30.8	30.8	30.9	30.8	30.9	31.0	30.9	30.9	30.9	31.0	31.0	31.0	31.1	31.2	31.1	31.2
13.0	31.4	31.5	31.4	31.4	31.4	31.5	31.5	31.5	31.5	31.6	31.6	31.6	31.7	31.7	31.7	31.7	31.7	31.7	31.8	31.8	31.9
12.0	32.4	32.2	32.3	32.3	32.4	32.4	32.4	32.4	32.5	32.6	32.5	32.5	32.5	32.5	32.6	32.6	32.6	32.7	32.7	32.8	32.8
11.0	33.2	33.2	33.1	33.1	33.2	33.1	33.2	33.4	33.3	33.3	33.5	33.4	33.4	33.4	33.4	33.5	33.5	33.5	33.5	33.6	33.6
10.0	34.3	34.1	34.1	34.1	34.2	34.2	34.2	34.3	34.4	34.5	34.4	34.4	34.5	34.5	34.6	34.6	34.6	34.6	34.7	34.7	34.7
9.5	34.8	35.0	34.9	34.9	34.9	34.9	34.8	35.1	35.0	35.0	35.2	35.1	35.2	35.2	35.2	35.3	35.4	35.3	35.2	35.3	35.3
9.0	35.6	35.4	35.6	35.5	35.7	35.6	35.6	35.7	35.7	35.9	35.8	35.9	36.0	35.9	36.0	36.0	36.0	36.0	36.0	36.1	36.2
8.5	35.9	35.9	36.1	36.1	36.0	36.1	36.2	36.3	36.2	36.4	36.4	36.6	36.4	36.5	36.7	36.6	36.8	36.8	36.9	36.9	37.0
8.0	37.1	37.0	37.1	37.0	36.9	37.1	37.3	37.3	37.4	37.5	37.4	37.5	37.5	37.6	37.5	37.6	37.7	37.8	37.9	37.9	38.1
7.5	38.1	37.9	37.7	37.9	38.0	38.1	38.2	38.2	38.4	38.5	38.6	38.5	38.7	38.9	38.8	39.3	39.1	39.2	39.1	39.2	39.3
7.0	39.1	39.2	39.1	39.1	39.1	39.3	39.1	39.2	39.3	39.5	39.7	40.0	40.0	40.1	40.2	40.4	40.7	40.9	41.1	41.0	41.1
6.5	40.0	40.0	40.0	40.3	40.6	40.5	40.6	40.4	39.9	40.3	40.4	40.8	41.1	41.4	41.8	42.5	43.6	46.9	50.5	49.1	43.8
6.0	41.7	41.8	41.7	41.6	41.9	41.9	41.8	42.1	42.1	42.5	43.0	43.8	46.2	52.1	54.0	62.0	94.2	117	127	122	110

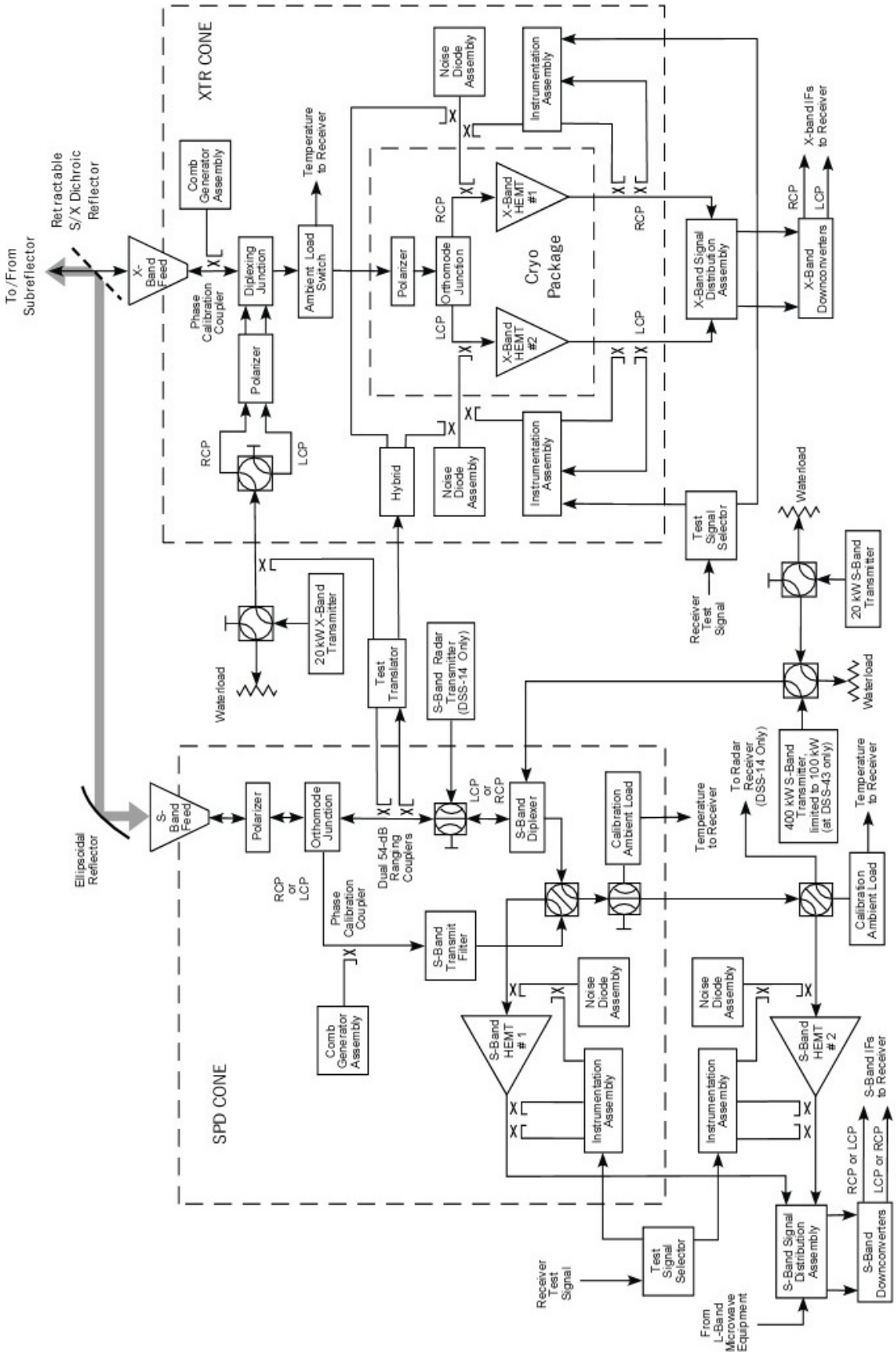

Figure 1. Functional Block Diagram of S-Band and X-Band Microwave and Transmitter Equipment

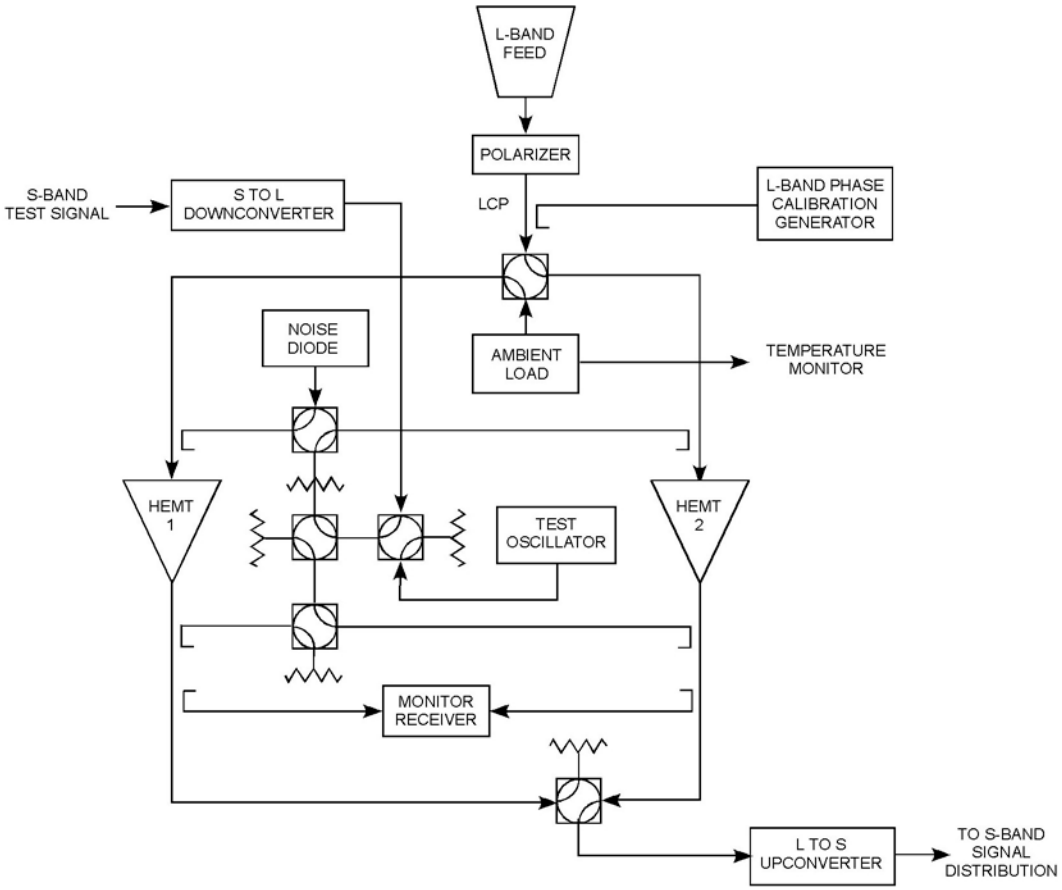

Figure 2. Functional Block Diagram of L-Band Microwave Equipment

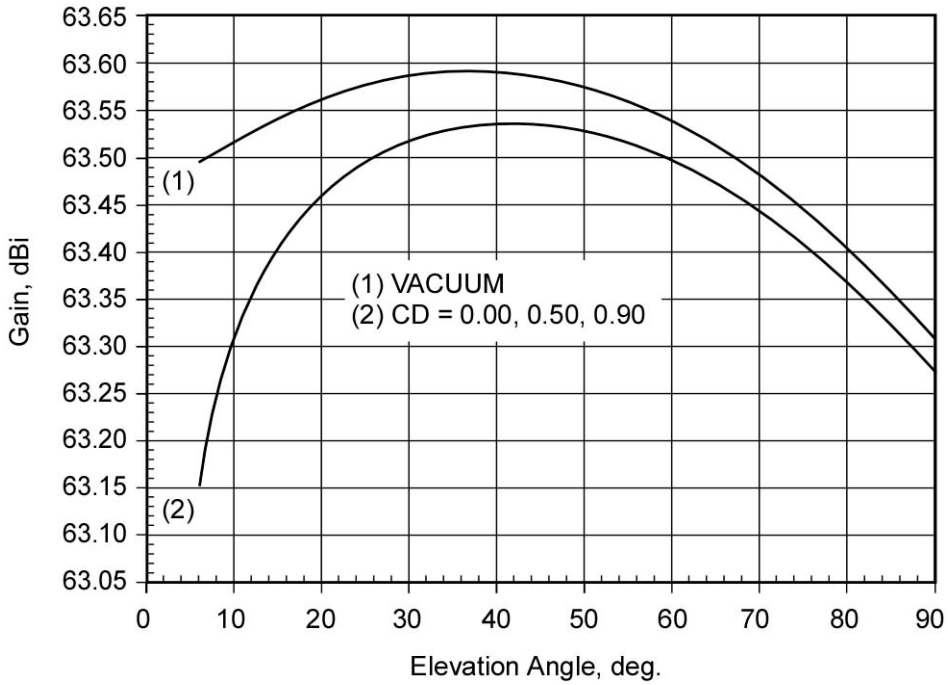

Figure 3. S-Band Receive Gain, All Stations, at Feedhorn Aperture

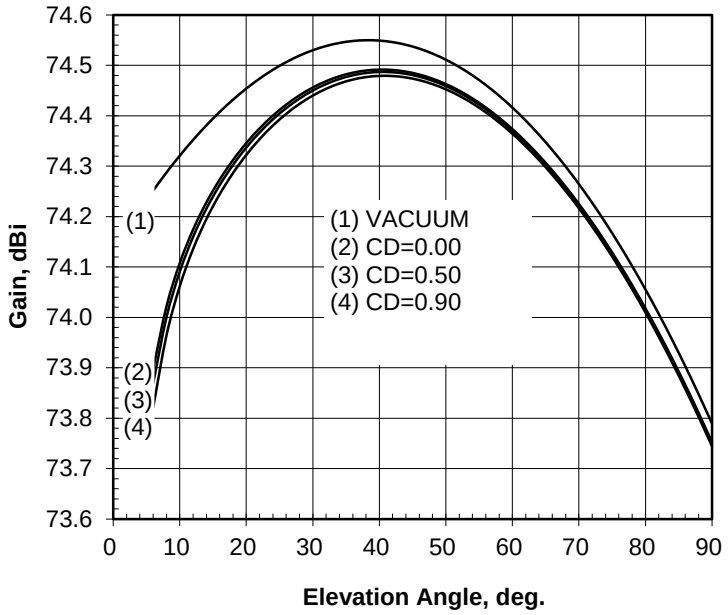

Figure 4. X-Band Receive Gain, DSS 14 Antenna, X-Only Configuration (S/X Dichroic Retracted), at Feedhorn Aperture

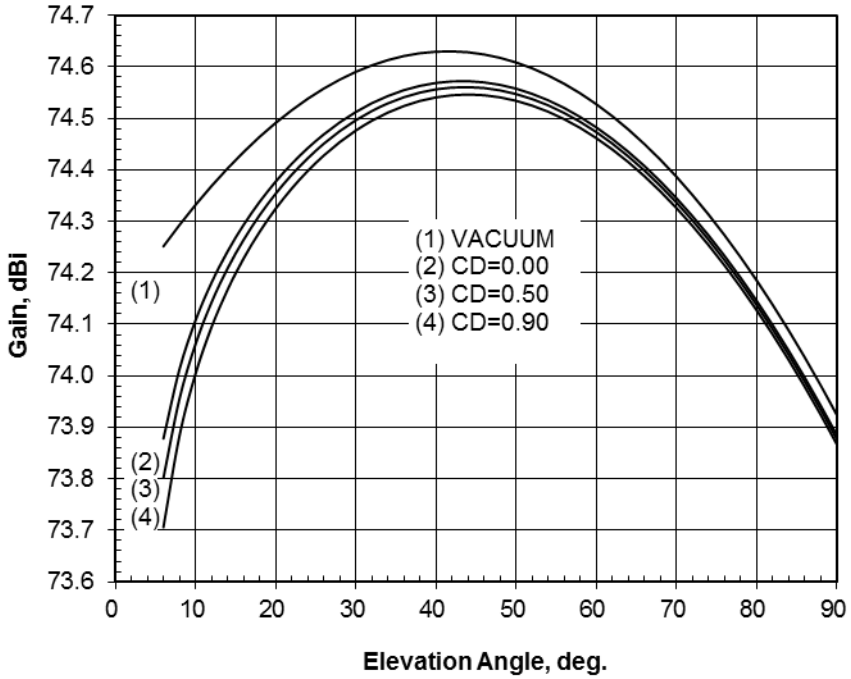

Figure 5. X-Band Receive Gain, DSS 43 Antenna, X-Only Configuration (S/X Dichroic Retracted), at Feedhorn Aperture

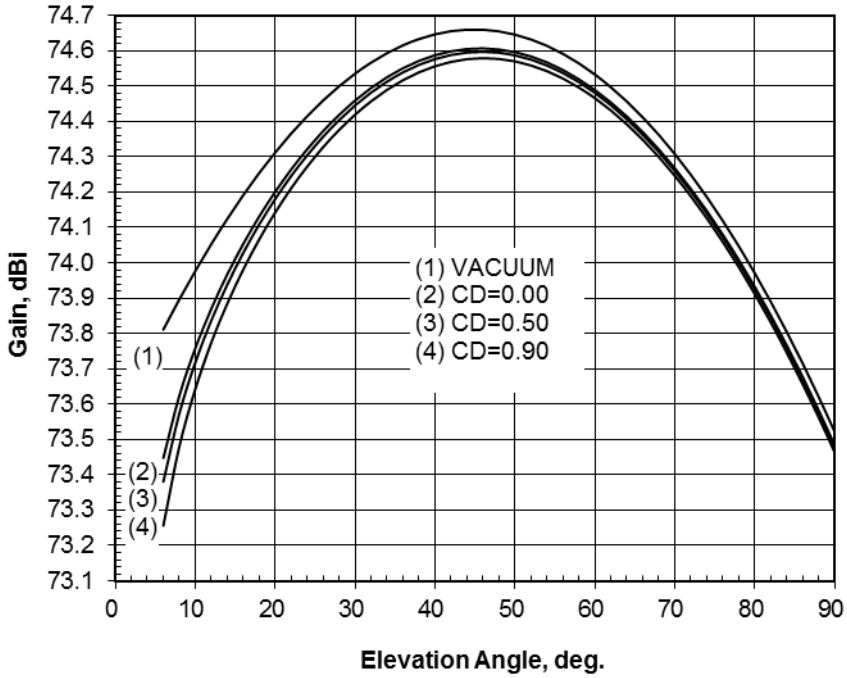

Figure 6. X-Band Receive Gain, DSS 63 Antenna, X-Only Configuration (S/X Dichroic Retracted), at Feedhorn Aperture

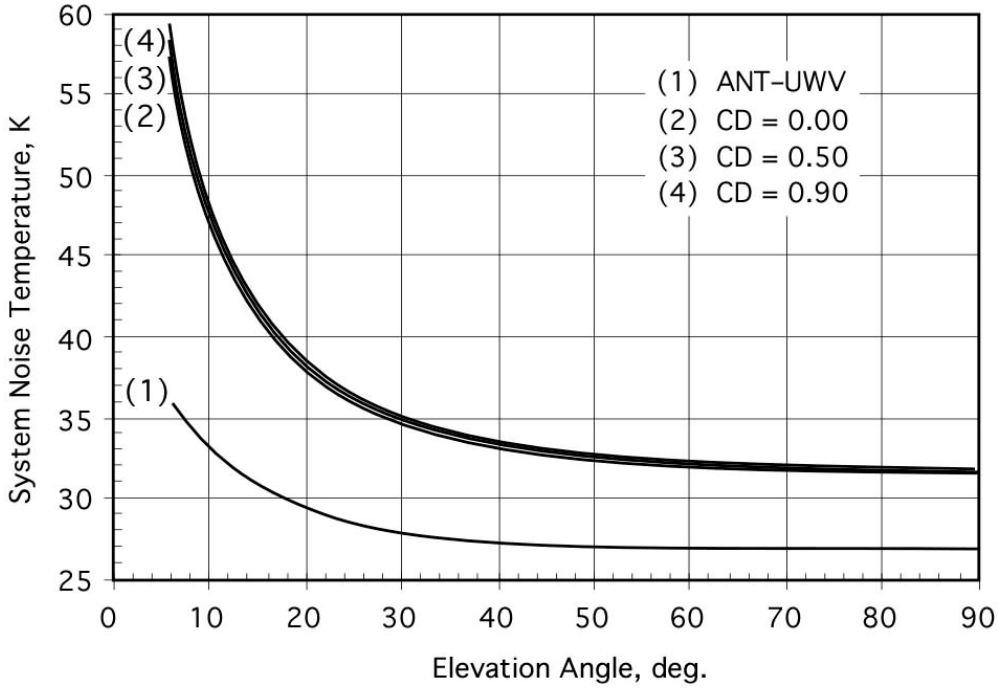

Figure 7. L-Band System Noise Temperature, All Stations, at Feedhorn Aperture

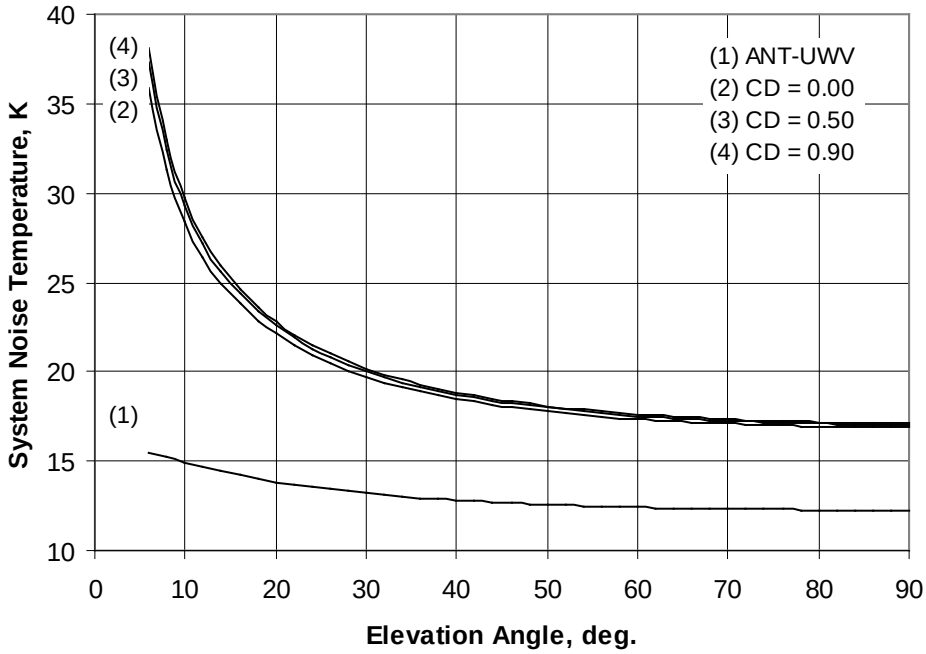

Figure 8. S-Band System Noise Temperature, DSS 14 Antenna, LNA-1, Non-Diplexed, at Feedhorn Aperture

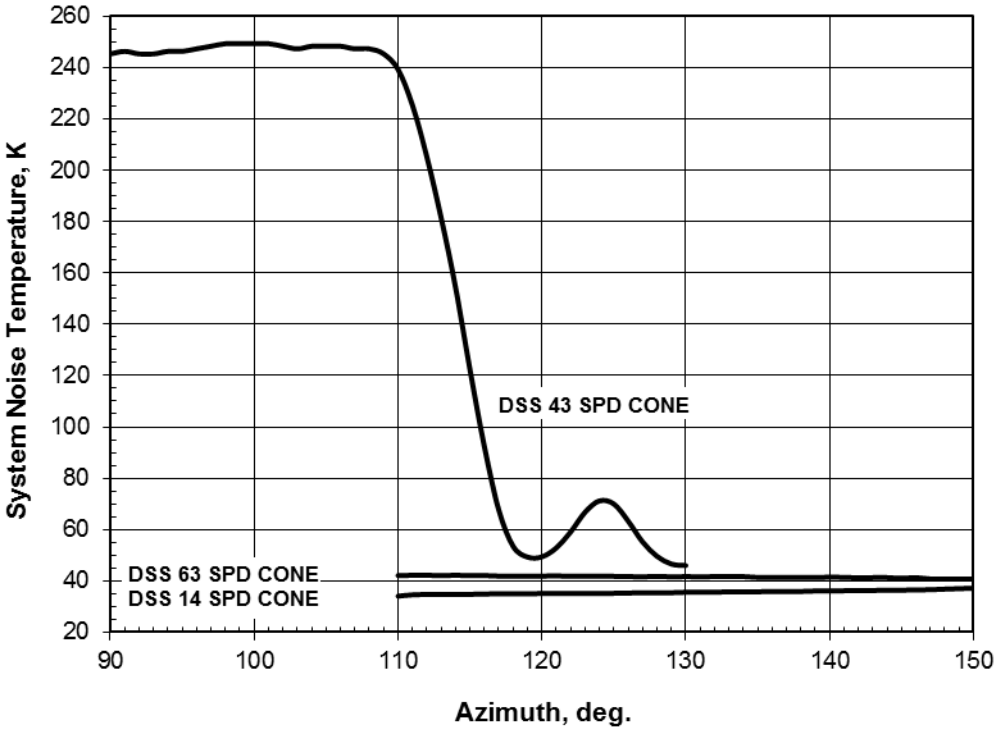

Figure 9. Eastern Horizon S-Band System Noise Temperature at 6° Elevation Angle

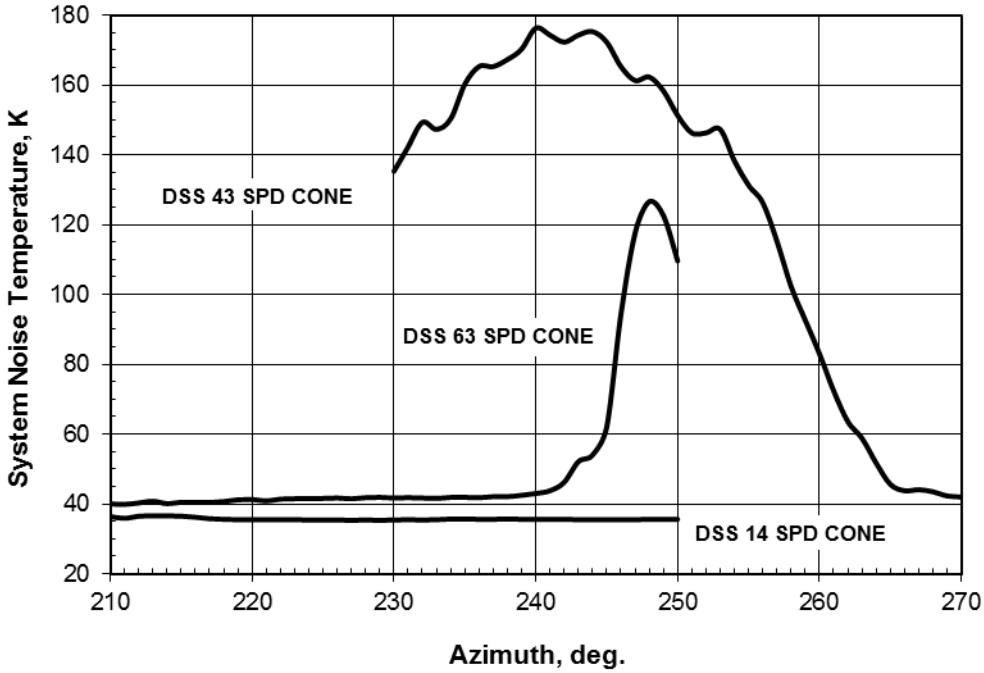

Figure 10. Western Horizon S-Band System Noise Temperature at 6° Elevation Angle

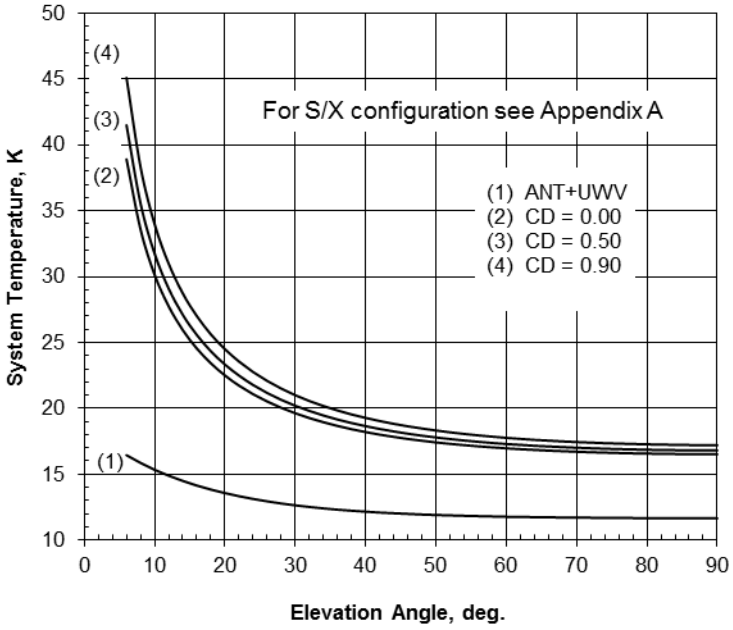

Figure 11. X-Band System Noise Temperature, DSS 14 Antenna, LNA-1 or LNA-2, X-Only Configuration (S/X Dichroic Retracted)

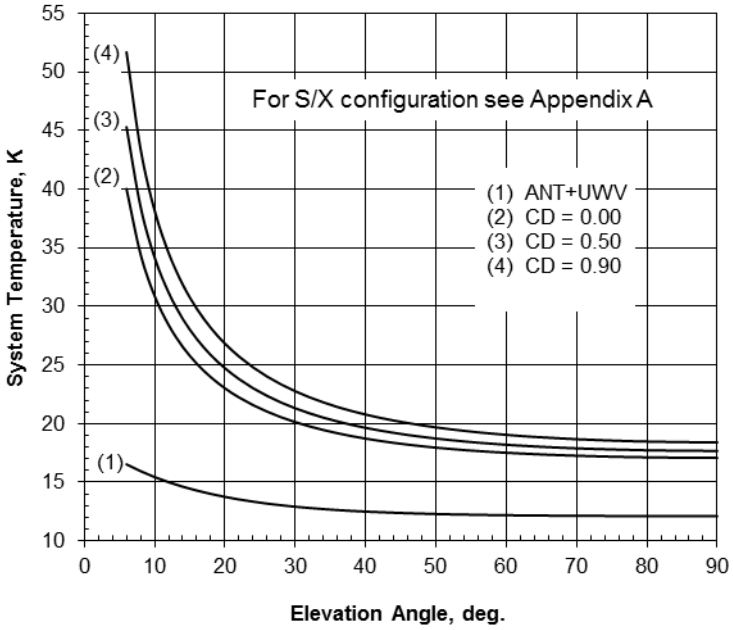

Figure 12. X-Band System Noise Temperature, DSS 43 Antenna, LNA-1 or LNA-2, X-Only Configuration (S/X Dichroic Retracted)

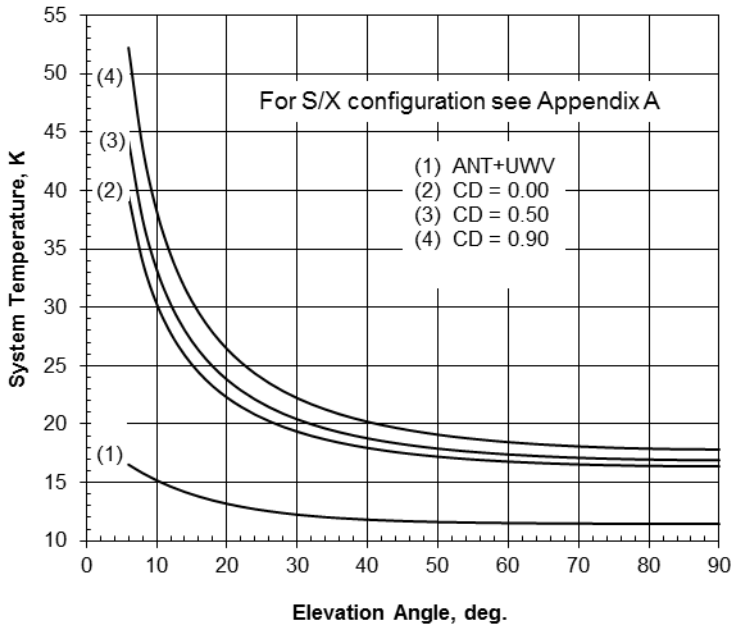

Figure 13. X-Band System Noise Temperature, DSS 63 Antenna, LNA-1 or LNA-2, X-Only Configuration (S/X Dichroic Retracted)

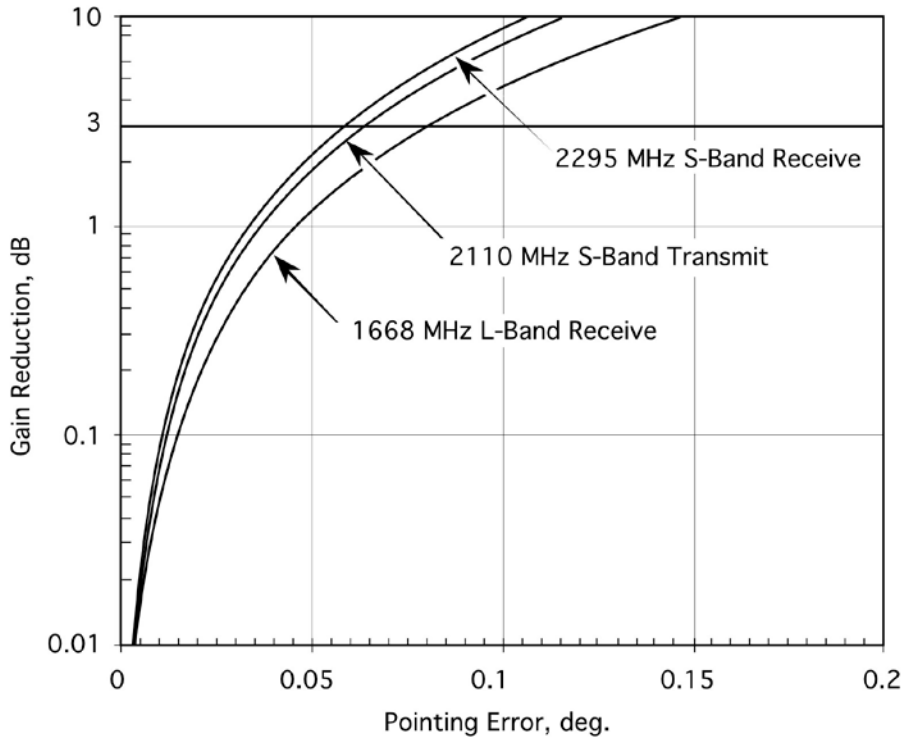

Figure 14. L-Band and S-Band Pointing Loss Versus Pointing Error

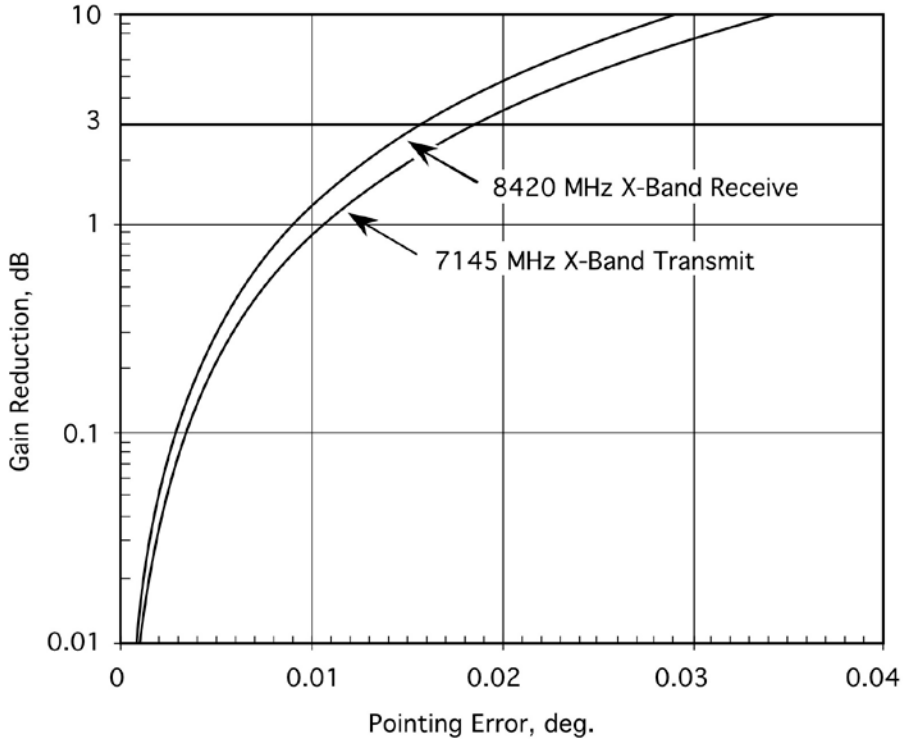

Figure 15. X-Band Pointing Loss Versus Pointing Error

Appendix A
Equations for Modeling

A.1 Equations for Gain Versus Elevation Angle

The following equation can be used to generate L-band receive, and S- and X-band transmit and receive gain versus elevation curves for DSS 14, DSS 43, and DSS 63. The gains are referenced to feedhorn aperture so different configurations (e.g., LNA-1 non-diplexed and LNA-2 diplexed) will have the same gain values. Examples of these curves are shown in Figures 3 through 6, for S- and X-bands. See paragraph 2.1.1.1 for frequency effect modeling and Module 105 for atmospheric attenuation at weather conditions corresponding to cumulative distributions from 0% to 99%. The year-average atmosphere attenuations for CD = 0.00, 0.50, and 0.90 are also given in Table A-2.

$$G(\theta) = G_0 - G_1(\theta - \gamma)^2 - \frac{A_{ZEN}}{\sin\theta}, \text{ dBi} \tag{A1}$$

where

θ	=	antenna elevation angle (deg.) $6 \le \theta \le 90$
G_0, G_1, γ	=	parameters from Table A-1
A_{ZEN}	=	zenith atmospheric attenuation from Table A-2 or from Tables 10 through 15 in Module 105, dB.

A.2 Equations for System Noise Temperature Versus Elevation Angle

The following equations can be used to generate L-, S-, and X-band receive system noise temperature versus elevation curves for DSS 14, DSS 43, and DSS-63. Examples of these curves are shown in Figures 7, 8, and 11 through 13. See Module 105 for atmospheric attenuation at weather conditions corresponding to cumulative distributions from 0% to 99%. Atmosphere attenuations for CD = 0.00, 0.50, and 0.90 are also given in Table A-2.

System operating noise temperature:

$$T_{op}(\theta) = T_{AMW} + T_{sky} = \left[T_1 + T_2 e^{-a\theta}\right] + \left[T_{atm}(\theta) + T'_{CMB}(\theta)\right] \tag{A2}$$

Sky noise contribution:

$$T_{sky} = T_{atm}(\theta) + T'_{CMB}(\theta) \tag{A3}$$

Atmospheric attenuation:

$$A(\theta) = \frac{A_{zen}}{\sin(\theta)}, \text{ dB} \tag{A4}$$

Atmospheric loss factor:

$$L(\theta) = 10^{\frac{A(\theta)}{10}}, \text{ dimensionless, } >1.0 \tag{A5}$$

Atmosphere mean effective radiating temperature:

$$T_M = 255 + 25 \times CD, \text{ K} \tag{A6}$$

Atmospheric noise contribution:

$$T_{atm}(\theta) = T_M\,[1\text{-}1/L(\theta)], \text{ K} \tag{A7}$$

Effective cosmic background noise:

$$T'_{CMB}(\theta) = \frac{T_{CMB}}{L(\theta)}, \text{ K} \tag{A8}$$

where

θ	=	antenna elevation angle (deg.), $6 \le \theta \le 90$
T_1, T_2, a	=	antenna-microwave noise temperature parameters from Table A-3
A_{ZEN}	=	zenith atmospheric attenuation, dB, from Table A-2 or from Tables 10 through 15 (L-, S-, X-bands) in Module 105 as a function of frequency, station, and cumulative distribution (CD)
CD	=	cumulative distribution, $0 \le CD \le 0.99$, used to select A_{ZEN} from Table A-2 or from Tables 10 through 15 in Module 105
T_{CMB}	=	2.725 K, cosmic microwave background noise temperature

A.3 Equation for Gain Reduction Versus Pointing Error

The following equation can be used to generate gain-reduction versus pointing error curves, examples of which are depicted in Figures 14 and 15.

$$\Delta G(\theta) = 10 \log \left(e^{\frac{2.773\theta^2}{HPBW^2}} \right), \text{ dBi} \tag{A9}$$

where

θ = pointing error (deg.)

$HPBW$ = half-power beamwidth in degrees (from Tables 1 or 2).

Table A-1. Vacuum Component of Gain Parameters, Referenced to Feedhorn Aperture

Configuration and Stations	Parameters†			
	G_0 (Transmit)	G_0 (Receive)	G_1	γ
L-Band, All Stations	—	61.04	0.000084	45
S-Band, All Stations	62.95	63.59	0.0001	37
X-Band, X-only Configuration				
DSS 14	73.17	74.55	0.000285	38.35
DSS 43	73.25	74.63	0.000300	41.53
DSS 63	73.28	74.66	0.000560	44.93
X-Band, S/X Configuration				
DSS 14	72.97	74.35	0.000365	44.19
DSS 43	72.98	74.36	0.000300	41.53
DSS 63	72.81	74.19	0.000550	45.57

NOTE:
† G_0 values are nominal at the frequency specified in Table 1 or Table 2. Other parameters apply to all frequencies within the same band.

Table A-2. Zenith Year-Average Atmosphere Attenuation Above Vacuum (A_{ZEN})

Weather Condition†	A_{ZEN}, dB*				
	L-Band	S-Band	X-Band		
	All Stations	All Stations	DSS 14	DSS 43	DSS 63
Vacuum	0.000	0.000	0.000	0.000	0.000
CD = 0.00	0.035	0.035	0.037	0.039	0.038
CD = 0.50	0.035	0.035	0.040	0.047	0.045
CD = 0.90	0.036	0.036	0.045	0.057	0.058

NOTES:
* From Tables 10 through 15 in Module 105, L- and S-band values are averages for all stations.
† CD = cumulative distribution.

Table A-3. Antenna-Microwave Noise Temperature Parameters, Referenced to Feedhorn Aperture

Configuration and Stations	Parameters		
	T_1	T_2	a
L-band, all stations, LNA-1 or -2, HEMT, LCP, non-diplexed	26.67	15.66	0.09
S-band, DSS 14, SPD cone, LNA-1, HEMT, non-diplexed	12.17	4.49	0.05
S-band, DSS 14, SPD cone, LNA-1, HEMT, diplexed	15.81	4.55	0.05
S-band, DSS 14, Mod III, LNA-2, HEMT, non-diplexed	18.74	4.61	0.05
S-band, DSS 14, Mod III, LNA-2, HEMT, diplexed	23.69	4.67	0.05
S-band, DSS 43, SPD cone, LNA-1, HEMT, non-diplexed	13.57	21.95	0.14
S-band, DSS 43, SPD cone, LNA-1, HEMT, diplexed	17.67	22.26	0.14
S-band, DSS 43, Mod III, LNA-2, HEMT, non-diplexed	19.59	22.51	0.14
S-band, DSS 43, Mod III, LNA-2, HEMT, diplexed	24.72	22.83	0.14
S-band, DSS 63, SPD cone, LNA-1, HEMT, non-diplexed	15.27	4.70	0.057
S-band, DSS 63, SPD cone, LNA-1, HEMT, diplexed	18.98	4.76	0.057
S-band, DSS 63, Mod III, LNA-2, HEMT, non-diplexed	21.20	4.82	0.057
S-band, DSS 63, Mod III, LNA-2, HEMT, diplexed	26.82	4.88	0.057
X-band, DSS 14, LNA-1, HEMT, RCP, X-only configuration	11.63	7.11	0.065
X-band, DSS 14, LNA-2, HEMT, LCP, X-only configuration	11.63	7.11	0.065
X-band, DSS 14, LNA-1, HEMT, RCP, S/X configuration	12.57	7.11	0.065
X-band, DSS 14, LNA-2, HEMT, LCP, S/X configuration	12.57	7.11	0.065
X-band, DSS 43, LNA-1, HEMT, RCP, X-only configuration	12.09	6.76	0.070
X-band, DSS 43, LNA-2, HEMT, LCP, X-only configuration	12.09	6.76	0.070
X-band, DSS 43, LNA-1, HEMT, RCP, S/X configuration	13.32	10.49	0.100
X-band, DSS 43, LNA-2, HEMT, LCP, S/X configuration	13.32	10.49	0.100
X-band, DSS 63, LNA-1, HEMT, RCP, X-only configuration	11.45	8.07	0.077
X-band, DSS 63, LNA-2, HEMT, LCP, X-only configuration	11.45	8.07	0.077
X-band, DSS 63, LNA-1, HEMT, RCP, S/X configuration	12.62	4.84	0.060
X-band, DSS 63, LNA-2, HEMT, LCP, S/X configuration	12.62	4.84	0.060

Deep Space Network

103
34-m HEF Subnet Telecommunications Interface

Document Owner:		Approved by:	
Signature provided	06/27/2023	Signature provided	06/08/2023
Stephen D. Slobin Antenna System Engineer	Date	Timothy Pham Communications Systems Chief Engineer	Date

Prepared by:		Released by:	
Signature provided	06/27/2023	Signature provided	08/03/2023
Stephen D. Slobin Antenna System Engineer	Date	Christine Chang DSN Document Release Authority	Date

DSN No. **810-005, 103, Rev. D**
Issue Date: August 03, 2023
JPL D-19379; CL#23-3962

Jet Propulsion Laboratory
California Institute of Technology

Users must ensure that they are using the current version in DSN Telecommunications Link Design Handbook website:
https://deepspace.jpl.nasa.gov/dsndocs/810-005/

Review Acknowledgment

By signing below, the signatories acknowledge that they have reviewed this document and provided comments, if any, to the signatories on the Cover Page.

Signature provided	06/26/2023	Signature not provided	
Jeff Berner DSN Project Chief Engineer	Date	John Cucchissi Antenna System Engineer	Date

Document Change Log

Rev	Issue Date	Prepared By	Affected Sections or pages	Change Summary
Initial	11/30/2000	Stephen Slobin Robert Sniffin	All	New Module
A	04/02/2007	Stephen Slobin Robert Sniffin	ALL	Documents installation of a 200 W S-band uplink at DSS-45 and DSS-65. Revised *TAMW* formulation for noise temperature to be consistent with Rev. B of module 105.
B	09/19/2008	Stephen Slobin Robert Sniffin	2. Table 1 & 2	Provides measured performance of S-band uplink at DSS 45 and DSS 65 and editorial changes.
C	08/01/2014	Stephen Slobin	Table 1 Table 3 Table 4 Table 5 Table A-3 Figure 1a Figure 1b Figure 7	Updated to include DSS-15 S-band transmitter. New DSS-15 Tamw for X-band dual-HEMT feed. New DSS-15/45/65 Tamw for low-gain mode. New wind-effect gain model. New Tamw and Top for DSS-15/45/65 X-band. New T1, T2, a for DSS-15/45/65 X-band. New for DSS-15. Re-numbered to include DSS-45/65 only. New noise temperatures for DSS-15 X-band.
D	08/03/2023	Stephen Slobin Christine Chang	Sections 1 and 2 Tables 1, 2, 3, 5 A-1, A-3 Old Figures 3, 4 7, 8 New Figures 3-7	DSS-15 and DSS-45 decommissioned. Parameters shown only for DSS-65. Gain and noise temperature for DSS-15 and DSS-45 shown as N/A. Removed Renumbered

Contents

Paragraph **Page**

Illustrations

Figure **Page**

Tables

Table **Page**

1 Introduction

1.1 Purpose

This module provides the performance parameters for the Deep Space Network (DSN) High-efficiency (HEF) 34-meter antennas that are necessary to perform the nominal design of a telecommunications link. It also summarizes the capabilities of these antennas for mission planning purposes and for comparison with other ground station antennas. As of the issue date of this module, only DSS-65 (Madrid) is operational. DSS-15 (Goldstone) and DSS-45 (Canberra) have been decommissioned, but the antennas still exist at their original locations. Some information about the decommissioned antennas has been retained in this module, for historical/archive purposes. As such, in the Tables where different Values are shown for the different antennas, the values for DSS-15 and DSS-45 are given as "N/A", but the Parameter and Remarks columns have been retained.

In the future, when/if DSS-15 and DSS-45 are reactivated, their configurations are very likely to be slightly different than shown in the block diagrams (Figures 1a and 1b). It is likely that all HEF antennas will end up having two X-band HEMTs, one for RCP and one for LCP, as shown in the block diagram for DSS-15.

1.2 Scope

The scope of this module is limited to providing those parameters that characterize the RF performance of the 34-meter HEF antennas. The parameters do not include effects of weather, such as reduction of system gain and increase in system noise temperature that are common to all antenna types. These are discussed in module 105, Atmospheric and Environmental Effects. This module also does not discuss mechanical restrictions on antenna performance that are covered in module 302, Antenna Positioning, or the effects of terrain masking that are covered in Module 301, Coverage and Geometry.

2 General Information

The DSN 34-m Antenna HEF Subnet contains three 34-meter diameter high-efficiency antennas. Only DSS-65 (Madrid) is still operational. Information about the equipment and configurations of the decommissioned antennas is retained in this section for historical purposes. These antennas employ an elevation over azimuth (AZ-EL) axis configuration, a single dual-frequency feedhorn, and a dual-shaped reflector design. Although this subnet is referred to as the High-Efficiency Subnet, the efficiency of the antennas is approximately the same as all other DSN antennas. The subnet was constructed when a subnet of lower-efficiency antennas (34m HA-DEC and 26m X-Y) was in existence, and the name has been retained. One antenna (DSS-15) is located at Goldstone, California; one (DSS-45) near Canberra, Australia; and one (DSS-65) near Madrid, Spain. The precise station locations are shown in Module 301, Coverage and Geometry.

Block diagrams of the 34-meter HEF microwave and transmitter equipment are shown in Figures 1a (DSS-15) and 1b (DSS-45 and DSS-65). Most of the microwave and transmitter equipment has been removed from DSS-15 and DSS-45. DSS-15 contained dual X-band HEMTs (one for RCP and one for LCP), while DSS-45 contained the older X-band maser and X-band HEMT configuration, with RCP and LCP, non-diplexed and diplexed, available for each low-noise amplifier (LNA). DSS-65 presently has a configuration identical to what existed at DSS-45. Additionally, DSS-65 offers a low-gain mode (−20 dB) for use at high received signal power levels for spacecraft near the Earth. DSS-65 has an orthomode junction for X-band that permits simultaneous RCP and LCP operation, although one polarization is in the non-diplexed mode and the other is in the higher-noise diplexed mode. DSS-15 was considered to be always-diplexed at X-band because it had a diplexing junction, and no lower-noise configuration was available. For X-band listen-only operation at DSS-65, or when transmitting and receiving on opposite polarizations, the low-noise path (orthomode upper arm) is used for reception. If the spacecraft receives and transmits simultaneously with the same polarization, the diplexed path must be used and the noise temperature will be higher. A waveguide labyrinth is used to couple S-band signals into and out of the feed. This would provide simultaneous RCP and LCP reception, although the presence of only one S-band low noise amplifier and receiver channel limits the use to selectable RCP or LCP. At DSS-65, the S-band polarization selection switch is used to implement a diplexed signal path in addition to the (non-simultaneous) non-diplexed, low-noise signal path. Either polarization can be low-noise or diplexed.

A 20 kW X-band transmitter is available at DSS-65. There is also a 250 W S-band transmitter intended for near-earth spacecraft support as an alternative to the beam waveguide (BWG) antennas DSS-24, -26, -34, -36, -54, and -56 described in module 104. The 250 W S-band transmitters at DSS-15 and DSS-45 have been removed and installed in the -6 BWG antennas, although they are still shown in the block diagrams for those antennas (Figures 1a and 1b). In addition to spacecraft tracking, the DSN 34-m antenna subnet is also used for very-long baseline interferometry and radio-source catalog maintenance.

2.1 Telecommunications Parameters

The significant parameters of the DSS-65 34-meter HEF antenna that influence telecommunications link design are listed in Tables 1, 2, and 3. Variations in these parameters that are inherent in the design of the antennas are discussed below. Other factors that degrade link performance are discussed in modules 105 (Atmospheric and Environmental Effects) and 106 (Solar Corona and Wind Effects). Values for DSS-15 and DSS-45 are shown as N/A, to indicate that those antennas have been decommissioned.

2.1.1 Antenna Gain Variation

The antenna gains in Tables 1, 2, and 3 do not include the effect of atmospheric attenuation and should be regarded as vacuum gain at the specified reference point.

2.1.1.1 Frequency Effects

Antenna gains are specified at the indicated frequency (f_0). For operation at higher frequencies in the same band, the gain (dBi) must be increased by 20 log (f/f_0). For operation at lower frequencies in the same band, the gain must be reduced by 20 log (f/f_0).

2.1.1.2 Elevation Angle Effects

Structural deformation causes a reduction in gain whenever the antenna is operated at an elevation angle other than the angle where the reflector panels were aligned. The effective gain of the antenna is also reduced by atmospheric attenuation, which is a function of elevation. Figures 2 and 3 show the estimated DSS-65 gain versus elevation angle for the hypothetical vacuum condition (structural deformation only) and with 0%, 50%, and 90% weather conditions, designated as CD (cumulative distribution) = 0.00, 0.50, and 0.90. A CD of 0.00 (0%) means the minimum weather effect (exceeded 100% of the time). A CD of 0.90 (90%) means that effect which is exceeded only 10% of the time. Qualitatively, a CD of 0.00 corresponds to the driest condition of the atmosphere; a CD of 0.50 corresponds to humid or very light clouds; and 0.90 corresponds to very cloudy, but with no rain. A CD of 0.25 corresponds to average clear weather and often is used when comparing gains of different antennas. Comprehensive S-band and X-band weather effects models (for weather conditions up to 99% cumulative distribution) are provided in module 105 for detailed design control table use. Equations and parameters for the curves in Figures 2 through 5 are provided in Appendix A.

Figure 2 depicts the S-band (2295 MHz) net gain for DSS-65 as a function of elevation angle and weather condition, including the vacuum condition. Net gain means vacuum-condition gain as reduced by atmosphere attenuation. Figure 3 presents the X-band (8420 MHz) net gain for DSS-65. All gains are referred to the feedhorn aperture, and the equations and parameters of these curves are given in Appendix A. The models use a flat-Earth, horizontally stratified atmosphere approximation.

It should be noted in Appendix A, Table A-1, that the gain parameters do not vary for different configurations (e.g., LNA-1 non-diplexed vs. LNA-1 diplexed), as they do in Table A-3 for the noise temperature parameters. This is due to the fact that the gain is referenced to the feedhorn aperture, and configurations "downstream" (e.g., orthomode and diplexer paths) do not affect the value of gain at the aperture. When G and T are referenced to the LNA input, both the G and T parameters vary with antenna configuration. When referenced to the feedhorn aperture, only T varies with configuration. The observed differences in antenna G/T are attributed only to different values of noise temperature, because G and T are both referenced to the feedhorn aperture.

2.1.1.3 Wind Loading

The gain reduction at X-band due to wind loading is listed in Table 4. The tabular data are for structural deformation only and presume that the antenna is maintained on-point by conical scan (CONSCAN, discussed in module 302) or an equivalent process. In addition to structural deformation, wind introduces a pointing error that is related to the antenna elevation angle, the angle between the antenna and the wind, and the wind speed. The effects of pointing

error are discussed below. Cumulative probability distributions of wind velocity at Goldstone are given in module 105.

2.1.2 System Noise Temperature Variation

The operating system temperature (T_{op}) varies as a function of elevation angle due to changes in the path length through the atmosphere and ground noise received by the sidelobe pattern of the antenna. Figures 4 and 5 show the combined effects of these factors at S- and X-bands for DSS-65 in a hypothetical vacuum (no atmosphere) and no cosmic noise condition (T_{sky} = 0, see Appendix A.2), for non-diplexed antenna configurations, and with the three weather conditions described above. The equations and parameters for these curves are provided in Appendix A of this module. The models use a flat-Earth, horizontally stratified atmosphere approximation.

The system operating noise temperature, T_{op}, consists of two parts, an *antenna-microwave component*, T_{AMW}, for the contribution of the antenna and microwave hardware only, and a *sky component*, T_{sky}, that consists of the atmosphere noise plus the cosmic microwave background noise attenuated by the atmosphere loss. T_{AMW} is shown in Figures 4 and 5 as "ANT-UWV". The system operating noise temperature is given by

$$T_{op}(\theta) = T_{AMW} + T_{sky} = \left[T_1 + T_2 e^{-a\theta}\right] + \left[T_{atm}(\theta) + T'_{CMB}(\theta)\right]$$

where

$T_{sky} = T_{atm}(\theta) + T'_{CMB}(\theta)$

T_1, T_2 and a are coefficients and exponent given in Appendix A, Table A-3

T_{atm} is the atmosphere contribution term, calculated from Module 105

T'_{CMB} is the attenuated cosmic contribution, calculated from Module 105

More details of this calculation are given in Appendix A of this module.

Figure 4 shows the S-band (2295 MHz) system noise temperature curves for DSS-65, LNA-1 (HEMT), non-diplexed, referenced to the feedhorn aperture. The DSS-65 X-band (8420 MHz) system temperature referenced to the feedhorn aperture is shown in Figure 5, for LNA-1, RCP HEMT, non-diplexed. The diplexed configuration higher noise temperatures can be calculated using the parameters given in Appendix A.

The T_{AMW} noise temperature values in Table 3 are stated with reference to the feedhorn aperture and arise from antenna and microwave hardware contribution only. No atmosphere or cosmic background contribution is included. Table 5 presents values for DSS-65 in all configurations at zenith, with average-clear CD = 0.25 weather. The values of T_{AMW}, T_{sky}, and T_{op} in Table 5 are calculated by methods presented in Module 105 using year-average attenuation values in Tables 10–15 of that module.

When two low-noise amplifiers (LNAs) are available for use, as at X-band, the amplifier in the lowest noise configuration is designated as LNA-1. Under some conditions, LNA-2 may be used, and the higher noise temperature values apply.

2.1.3 Pointing Accuracy

Figures 6 and 7 show the effects of pointing error on effective transmit and receive gain of the antenna. These curves are Gaussian beam-shape approximations based on measured and predicted antenna beamwidths. Data have been normalized to eliminate elevation and wind-loading effects. The equations used to derive the curves are provided in Appendix A.

Table 1. S-Band Transmit Characteristics, DSS-65

Parameter	Value	Remarks
ANTENNA		
Gain at 2070 MHz (near-earth)	55.40 ±0.2 dBi	At elevation angle of peak gain, referenced to feedhorn aperture for matched polarization; no atmosphere included
Transmitter Waveguide Loss	0.6 ±0.1 dB	250 W transmitter output terminal (waterload switch) to feedhorn aperture
Half-Power Beamwidth	0.258 ±0.004 deg	Angular width (2-sided) between half-power points at specified frequency
Polarization	RCP or LCP	Remotely selected.
Ellipticity	1.0 dB (max)	Peak-to-peak axial ratio defined as the ratio of peak-to-trough received voltages with a rotating linearly polarized source and the feed configured as a circularly (elliptically) polarized receiving antenna
Pointing Loss		
Angular	See module 302	See also Figure 6
CONSCAN	0.03 dB	At S-band, using X-band CONSCAN reference set for 0.1 dB loss
	0.1 dB	At S-band, using S-band CONSCAN reference set for 0.1 dB loss
EXCITER AND TRANSMITTER		
RF Power Output	47.0–54.0, ±0.25 dBm	Referenced to 250-W transmitter output terminal (waterload switch). Settability is limited to 0.25 dB by measurement equipment precision
Power output varies across the bandwidth and may be as much as 0.5 dB below the set value if the frequency is adjusted to a value other than where the power was set. In general, amplitude drift and variation with frequency will be less at higher output power, but specified performance is guaranteed over the operating range of 50 to 250 Watts.		
EIRP (maximum)	108.8, ±0.35 dBm	

Table 1. S-Band Transmit Characteristics, DSS-65 (Continued)

Parameter	Value	Remarks
EXCITER AND TRANSMITTER (Continued)		
Frequency Range Covered	2025 to 2110 MHz	Near-earth
Instantaneous 1-dB Bandwidth	>85 MHz	
Coherent with Earth Orbiter S-Band D/L Allocation	2028.8–2108.7 MHz	240/221 turnaround ratio
Tunability		At transmitter output frequency
Phase Continuous Tuning Range	2.0 MHz	
Maximum Tuning Rate	±12.1 kHz/s	
Frequency Error	0.012 Hz	Average over 100 ms with respect to frequency specified by predicts
Ramp Rate Error	0.001 Hz/s	Average over 4.5 s with respect to rate calculated from frequency predicts
Stability		At transmitter output frequency
Output Power Stability	–0.5, +1.0 dB	From initial calibration value over an 8-h period at a fixed frequency
Group Delay Stability	≤3.0 ns, RMS	Ranging modulation signal path over an 8-h period (see module 203)
Frequency Stability		Allan deviation
1 s	9.0×10^{-13}	
10 s	9.0×10^{-14}	
1000–3600 s	3.0×10^{-15}	
Spurious Output		Below carrier
1–10 Hz	–60 dB	
10 Hz–1.5 MHz	–70 dB	
1.5 MHz–8 MHz	–80 dB	
2nd Harmonic	–80 dB	
3rd, 4th & 5th Harmonics	–90 dB	

Table 2. X-Band Transmit Characteristics, DSS-65

Parameter	Value	Remarks
ANTENNA		
Gain at 7145 MHz (deep-space)	67.05 ±0.2 dBi	At elevation angle of peak gain, referenced to feedhorn aperture for matched polarization; no atmosphere included
Transmitter Waveguide Loss	0.25 ±0.05 dB	20-kW transmitter output terminal (waterload switch) to feedhorn aperture
Half-Power Beamwidth	0.0777 ±0.004 deg	Angular width (2-sided) between half-power points at specified frequency
Polarization	RCP or LCP	One polarization at a time, remotely selected
Ellipticity	1.0 dB (max)	Peak-to-peak axial ratio defined as the ratio of peak-to-trough received voltages with a rotating linearly polarized source and the feed configured as a circularly (elliptically) polarized receiving antenna
Pointing Loss		
Angular	See module 302	See also Figure 7
CONSCAN	0.1 dB	X-band CONSCAN reference set for 0.1 dB loss
EXCITER AND TRANSMITTER		
RF Power Output	73.0, +0.0, –1.0 dBm	Referenced to 20-kW transmitter output terminal (waterload switch). Settability is limited to 0.25 dB by measurement equipment precision
Power output varies across the bandwidth and may be as much as 1 dB below nominal rating. Performance will also vary from tube to tube. Normal procedure is to run the tubes saturated, but unsaturated operation is also possible. The point at which saturation is achieved depends on drive power and beam voltage. The 20-kW tubes are normally saturated for power levels greater than 63 dBm (2 kW). Minimum power out of the 20-kW tubes is about 53 dBm (200 W). Efficiency of the tubes drops off rapidly below nominal rated output.		
EIRP	139.8, +0.2, –1.0 dBm	

Table 2. X-Band Transmit Characteristics, DSS-65 (Continued)

Parameter	Value	Remarks
EXCITER AND TRANSMITTER (Continued)		
Frequency Range Covered	7145 to 7190 MHz	Deep-space
Instantaneous 1-dB Bandwidth (MHz)	45 MHz	
Coherent with Deep Space S-Band D/L Allocation	7151.9–7177.3 MHz	240/749 turnaround ratio
Coherent with Deep Space S-Band D/L Allocation	7151.9–7188.9 MHz	880/749 turnaround ratio
Tunability		At transmitter output frequency
Phase Continuous Tuning Range	2.0 MHz	
Maximum Tuning Rate	±12.1 kHz/s	
Frequency Error	0.012 Hz	Average over 100 ms with respect to frequency specified by predicts
Ramp Rate Error	0.001 Hz/s	Average over 4.5 s with respect to rate calculated from frequency predicts
Output Power Stability		From initial calibration value over an 8-h period at a fixed frequency
Saturated Drive	± 0.3 dB, peak	
Unsaturated Drive	± 0.5 dB, peak	
Output Power Variation		Across any 2 MHz segment
Saturated Drive	≤ 0.3 dB, p-p	
Unsaturated Drive	≤ 0.5 dB, p-p	
Group Delay Stability	≤ 1.5 ns, RMS	Ranging modulation signal path over 8 h period (see module 203)
Frequency Stability		Allan deviation
1 s	1.0×10^{-12}	
10 s	1.0×10^{-13}	
1000–3600 s	3.0×10^{-13}	

Table 2. X-Band Transmit Characteristics, DSS-65 (Continued)

Parameter	Value	Remarks
Spurious Output		Below carrier
1–10 Hz	–50 dB	
10 Hz–1.5 MHz	–60 dB	
1.5 MHz–8 MHz	–45 dB	
2nd Harmonic	–75 dB	
3rd, 4th & 5th Harmonics	–60 dB	

Table 3. S- and X-Band Receive Characteristics, DSS-65

Parameter	Value	Remarks
ANTENNA		
Gain (deep-space)		At elevation angle of peak gain for matched polarization, no atmosphere included. Favorable (+) and adverse (–) tolerances have a triangular PDF. See Figures 2 and 3 for elevation dependency.
S-Band (2295 MHz)	56.07 ±0.25 dBi	Referenced to feedhorn aperture
X-Band (8420 MHz)	68.41 ±0.2 dBi	Referenced to feedhorn aperture
Half-Power Beamwidth (deg.)		Angular width (2-sided) between half-power points at specified frequency
S-Band	0.242 ±0.020 deg	
X-Band	0.0660 ±0.004 deg	
Polarization		Remotely selected
S-Band	RCP or LCP	
X-Band	RCP or LCP	Same or opposite from transmit polarization
Ellipticity (dB)	0.7 dB	Peak-to-peak voltage axial ratio, RCP and LCP. See definition in Table 1.
S-Band	≤1.0 dB	
X-Band	≤0.8 dB	

Table 3. S- and X-Band Receive Characteristics, DSS-65 (Continued)

Parameter	Value	Remarks
ANTENNA (Continued)		
Pointing Loss		
Angular	See module 302	See also Figures 6 and 7
CONSCAN		
S-Band	0.03 dB, 3-sigma	Loss at S-band when using X-band CONSCAN reference set for 0.1 dB loss at X-band
	0.1 dB, 3-sigma	Recommended value when using S-band CONSCAN reference
X-Band	0.1 dB, 3-sigma	Recommended value when using X-band CONSCAN reference
RECEIVER		
Frequency Ranges Covered (MHz))		
S-Band	2200–2300 MHz	Deep-space
X-Band		Deep-space
Telemetry	8400–8500 MHz	
VLBI	8200–8600 MHz	Wide-band HEMT LNA
Recommended Maximum Signal Power	-90.0 dBm -70.0 dBm	At LNA input terminal (high-gain mode) AT LNA input terminal (low-gain mode)
Antenna-Microwave Noise Temperature (T_{AMW})		Near zenith, no atmosphere (vacuum) or cosmic noise included. See Table 5 for 25% CD average clear sky noise contribution. Favorable (–) and adverse (+) tolerances have triangular PDF. See Figures 4 and 5 for elevation dependency.
S-Band (2200–2300 MHz)		With respect to feedhorn aperture
DSS-65	34.00 ±2 K	LNA-1, HEMT, non-diplexed path
DSS-65	41.76 ±2 K	LNA-1, HEMT, diplexed path

Table 3. S- and X-Band Receive Characteristics, DSS-65 (Continued)

Parameter	Value	Remarks
RECEIVER (continued)		
X-Band Dual-HEMT LNAs		With respect to feedhorn aperture
High-Gain Mode		normal configuration
DSS-15, LNA-1, HEMT, RCP	N/A	diplexed, 8200-8600 MHz
DSS-15, LNA-2, HEMT, LCP	N/A	diplexed, 8200-8600 MHz
DSS-15, LNA-1, HEMT, RCP	N/A	diplexed, w/ radar filter, 8200-8500 MHz
DSS-15, LNA-2, HEMT, LCP	N/A	diplexed, w/ radar filter, 8200-8500 MHz
Low-Gain Mode		high spacecraft received power
DSS-15, LNA-1, HEMT, RCP	N/A	diplexed, 8200-8600 MHz
DSS-15, LNA-2, HEMT, LCP	N/A	diplexed, 8200-8600 MHz
DSS-15, LNA-1, HEMT, RCP	N/A	diplexed, w/ radar filter, 8200-8500 MHz
DSS-15, LNA-2, HEMT, LCP	N/A	diplexed, w/ radar filter, 8200-8500 MHz
X-Band Maser/HEMT LNAs, High-Gain Mode, RCP/LCP		
DSS-45	N/A	LNA-1, maser, non-diplexed path, 8400-8500 MHz
DSS-65	15.43 ±2 K	
DSS-45	N/A	LNA-1, maser, diplexed path, 8400-8500 MHz
DSS-65	24.83 ±2 K	
DSS-45	N/A	LNA-2, HEMT, non-diplexed path, 8200-8600 MHz (wide-band)
DSS-65	32.16 ±2 K	
DSS-45	N/A	LNA-2, HEMT, diplexed path, 8400-8500 MHz (narrowed due to diplexer)
DSS-65	41.56 ±2 K	

Table 3. S- and X-Band Receive Characteristics, DSS-65 (Continued)

Parameter	Value	Remarks
X-Band Maser/HEMT LNAs, Low-Gain Mode, RCP/LCP		
DSS-45	N/A	LNA-1, maser, non-diplexed path, 8400-8500 MHz
DSS-65	20.52 ±2 K	
DSS-45	N/A	LNA-1, maser, diplexed path, 8400-8500 MHz
DSS-65	29.92 ±2 K	
DSS-45	N/A	LNA-2, HEMT, non-diplexed path, 8200-8600 MHz (wide-band)
DSS-65	43.16 ±2 K	
DSS-45	N/A	LNA-2, HEMT, diplexed path, 8400-8500 MHz (narrowed due to diplexer)
DSS-65	52.56 ±2 K	
Carrier Tracking Loop Noise B/W	0.25 – 200 Hz	Effective one-sided, noise-equivalent carrier loop bandwidth (B_L)

Table 4. Gain Reduction Due to Wind Loading, 34-m HEF Antennas

Wind Speed		X-Band Gain Reduction (dB)*
(km/hr)	(mph)	
10	6	0.0
30	19	0.01
50	31	0.06
70	43	0.21

* Assumes antenna is maintained on-point using CONSCAN or equivalent closed-loop pointing technique.
S-band gain reduction is less than 0.02 dB for wind speeds up to 70 km/hr.
Worst case, with most adverse wind orientation.

Table 5. T_{AMW}, T_{sky}, and T_{op} for CD=25% Average Clear Weather at Zenith, Referenced to Feedhorn Aperture

Configuration and Stations	Noise Temperatures, K		
	T_{AMW}	T_{sky}	T_{op}
S-band DSS-65:			
S-band, DSS-65, LNA-1, HEMT, non-diplexed	34.00	4.80	38.80
S-band, DSS-65, LNA-1, HEMT, diplexed	41.76	4.80	46.56
DSS-15 X-band High-Gain Mode (normal configuration):			
X-band, DSS-15, LNA-1, HEMT, RCP, diplexed	N/A	5.04	N/A
X-band, DSS-15, LNA-2, HEMT, LCP, diplexed	N/A	5.04	N/A
X-band, DSS-15, LNA-1, HEMT, RCP, diplexed, w/ narrow-band radar filter	N/A	5.04	N/A
X-band, DSS-15, LNA-2, HEMT, LCP, diplexed, w/ narrow-band radar filter	N/A	5.04	N/A
DSS-15 X-band Low-Gain Mode (high s/c received power):			
X-band, DSS-15, LNA-1, HEMT, RCP, diplexed	N/A	5.04	N/A
X-band, DSS-15, LNA-2, HEMT, LCP, diplexed	N/A	5.04	N/A
X-band, DSS-15, LNA-1, HEMT, RCP, diplexed, w/ narrow-band radar filter	N/A	5.04	N/A
X-band, DSS-15, LNA-2, HEMT, LCP, diplexed, w/ narrow-band radar filter	N/A	5.04	N/A
DSS-45 Maser/HEMT High-Gain Mode, RCP/LCP:			
X-band, DSS-45, LNA-1, maser, non-diplexed	N/A	5.39	N/A
X-band, DSS-45, LNA-1, maser, diplexed	N/A	5.39	N/A
X-band, DSS-45, LNA-2, HEMT, non-diplexed	N/A	5.39	N/A
X-band, DSS-45, LNA-2, HEMT, diplexed	N/A	5.39	N/A
DSS-45 Maser/HEMT Low-Gain Mode, RCP/LCP:			
X-band, DSS-45, LNA-1, maser, non-diplexed	N/A	5.39	N/A
X-band, DSS-45, LNA-1, maser, diplexed	N/A	5.39	N/A
X-band, DSS-45, LNA-2, HEMT, non-diplexed	N/A	5.39	N/A
X-band, DSS-45, LNA-2, HEMT, diplexed	N/A	5.39	N/A

Table 5. T_{AMW}, T_{sky}, and T_{op} for CD=25% Average Clear Weather at Zenith, Referenced to Feedhorn Aperture (Continued)

Configuration and Stations	Noise Temperatures, K		
	T_{AMW}	T_{sky}	T_{op}
DSS-65 Maser/HEMT High-Gain Mode RCP/LCP:			
X-band, DSS-65, LNA-1, maser, non-diplexed	15.43	5.27	20.70
X-band, DSS-65, LNA-1, maser, diplexed	24.83	5.27	29.10
X-band, DSS-65, LNA-2, HEMT, non-diplexed	32.16	5.27	37.43
X-band, DSS-65, LNA-2, HEMT, diplexed	41.56	5.27	46.83
DSS-65 Maser/HEMT Low-Gain Mode, RCP/LCP:			
X-band, DSS-65, LNA-1, maser, non-diplexed	20.52	5.27	25.79
X-band, DSS-65, LNA-1, maser, diplexed	29.92	5.27	35.19
X-band, DSS-65, LNA-2, HEMT, non-diplexed	43.16	5.27	48.43
X-band, DSS-65, LNA-2, HEMT, diplexed	52.56	5.27	57.83

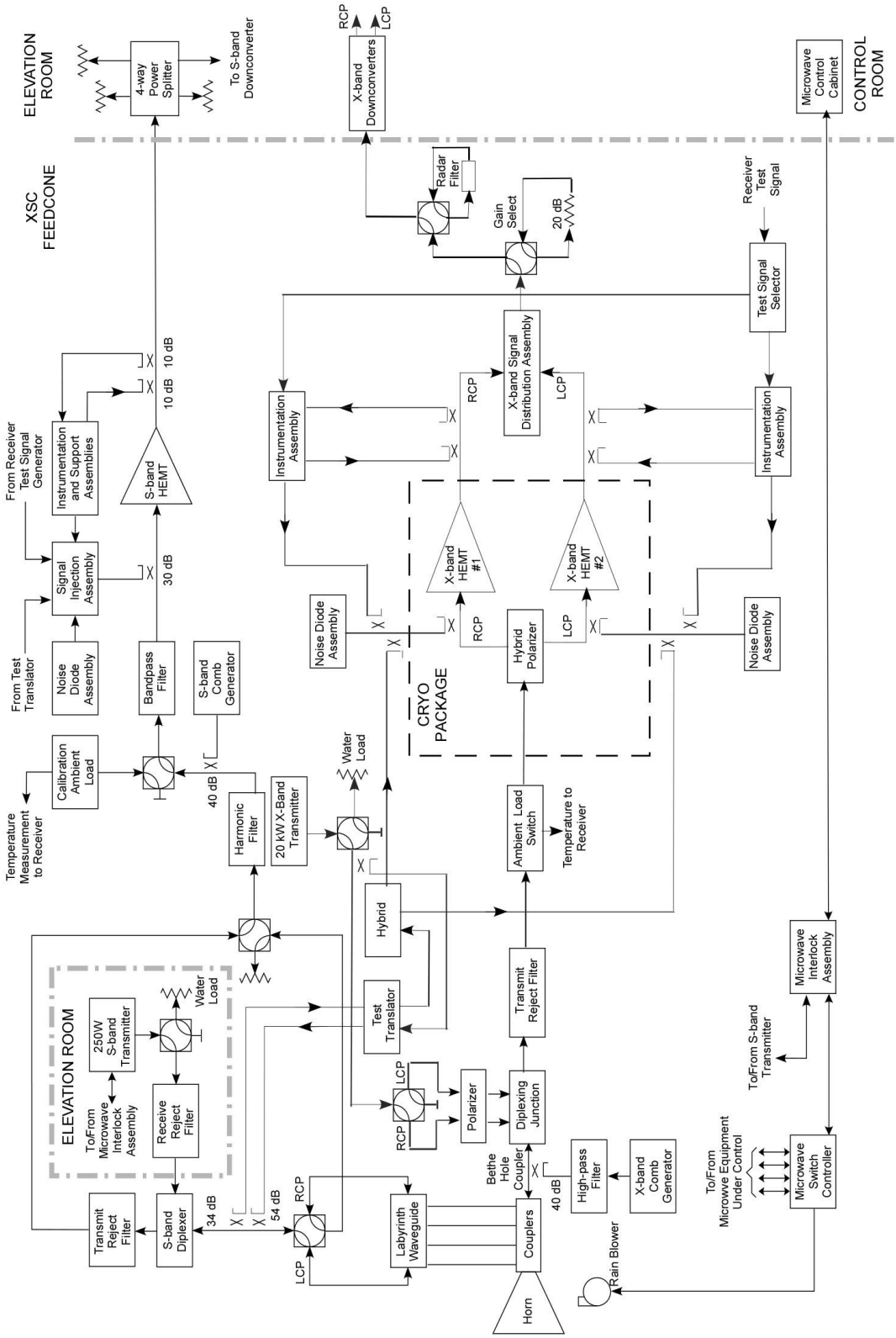

Figure 1a. Functional Block Diagram of the DSS-15 HEF Antenna (Decommissioned)

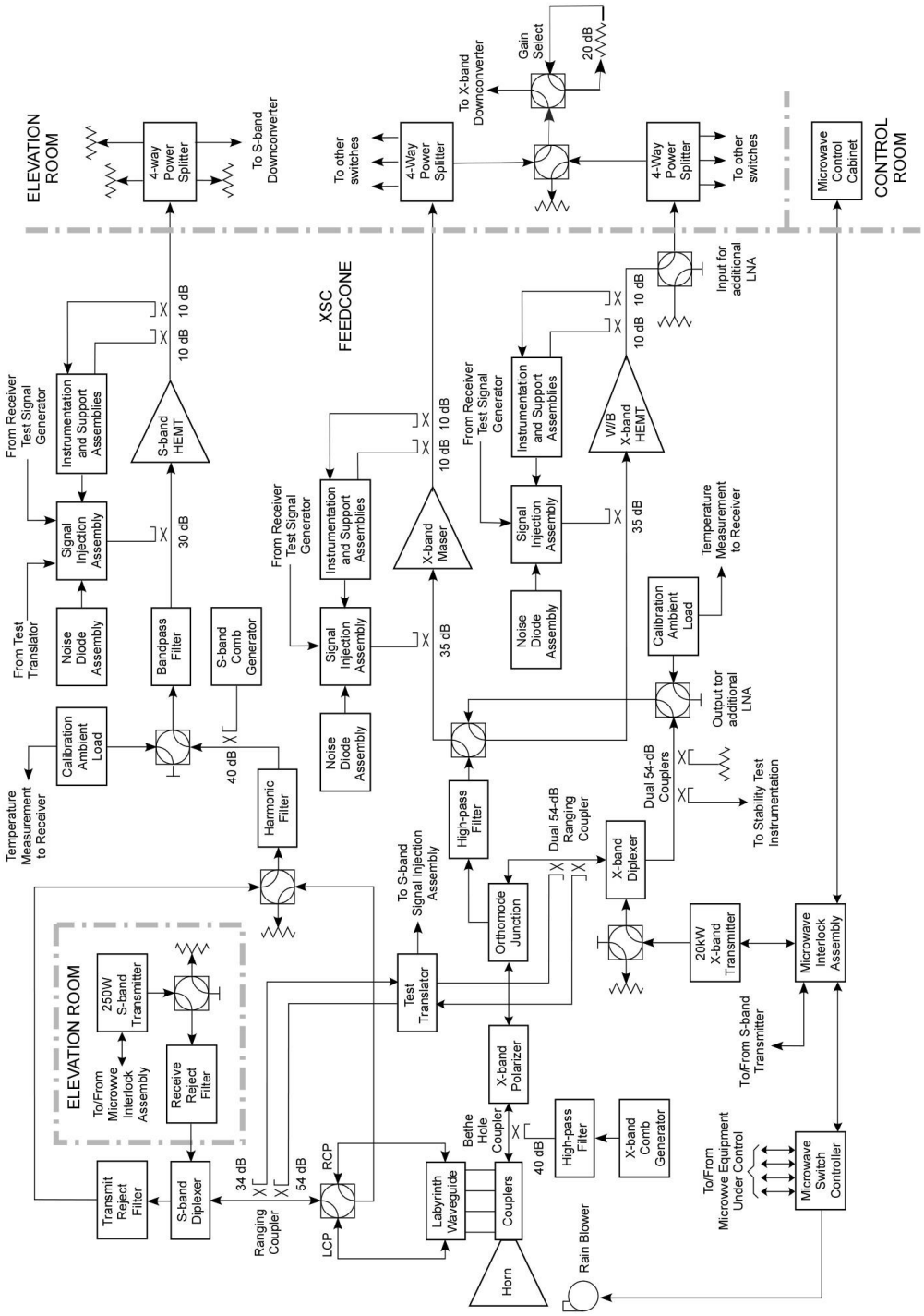

Figure 1b. Functional Block Diagram of the DSS-45 (Decommissioned) and DSS-65 HEF Antennas

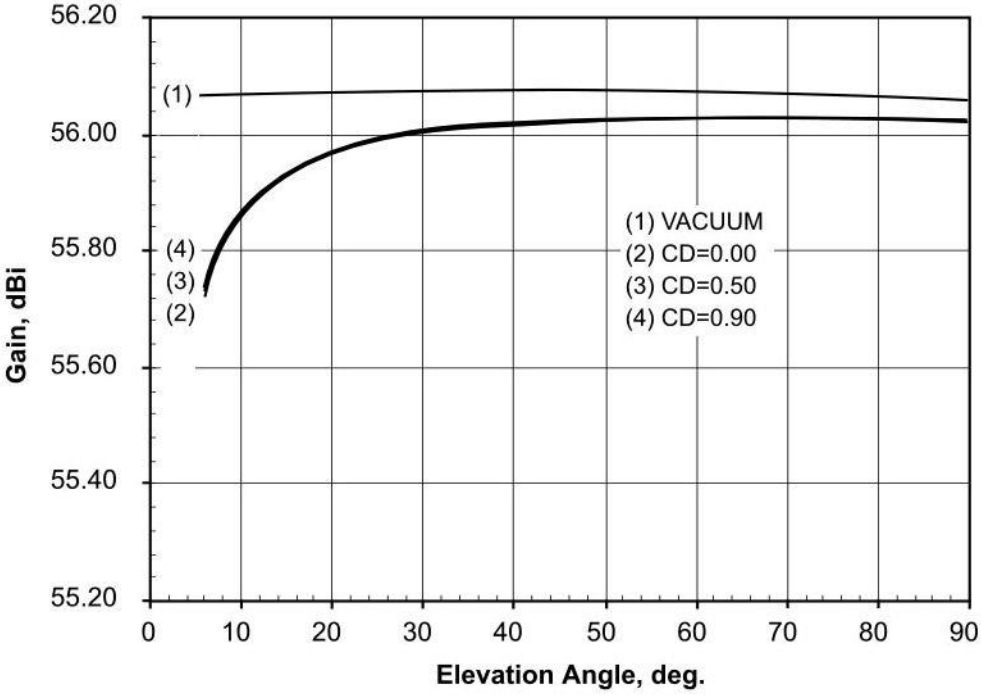

Figure 2. S-Band Receive Gain, DSS-65 Antenna, at Feedhorn Aperture

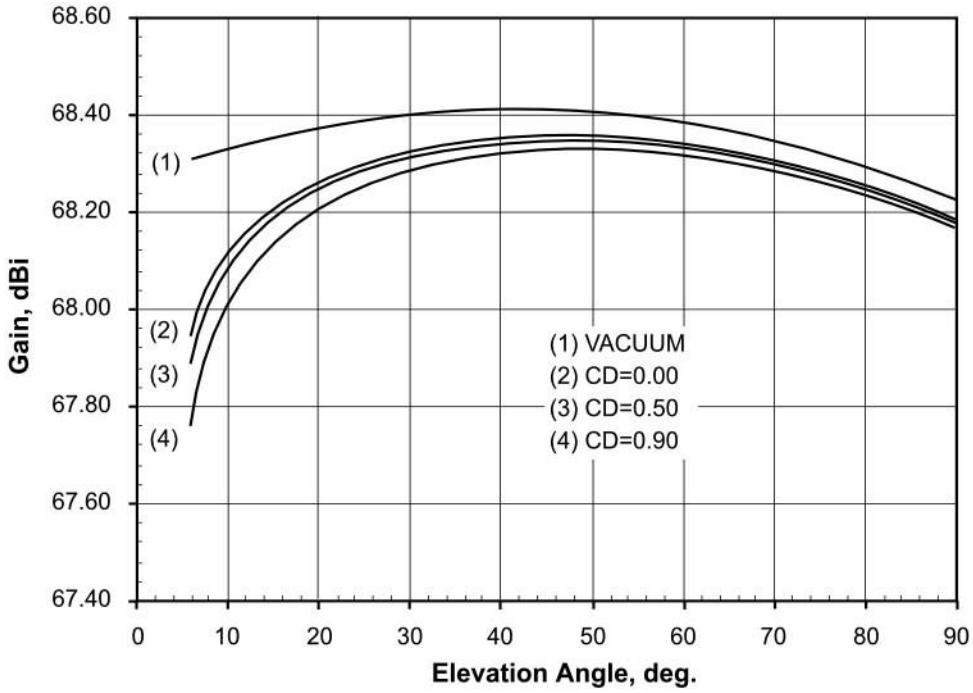

Figure 3. X-Band Receive Gain, DSS-65 Antenna, at Feedhorn Aperture

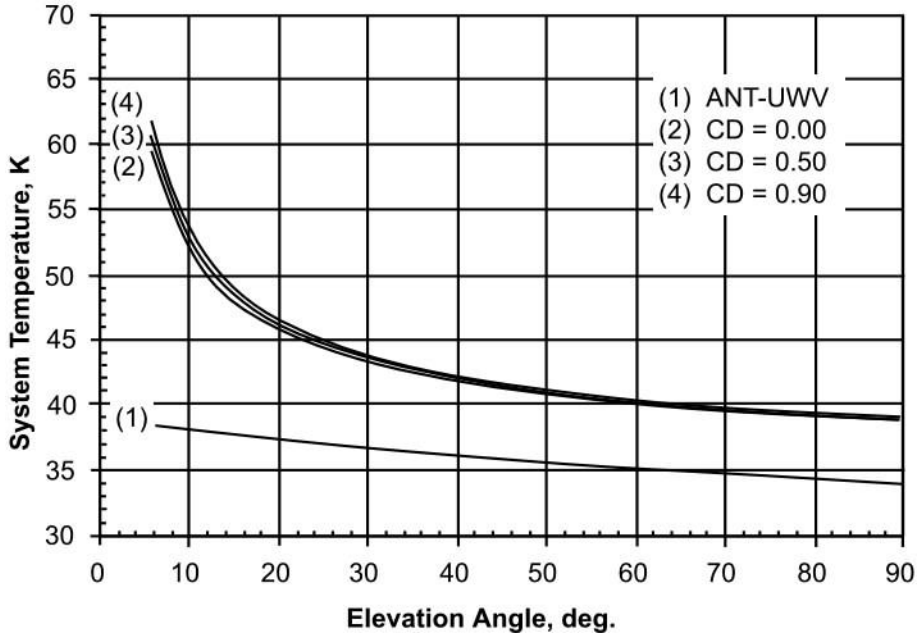

Figure 4. S-band System Noise Temperature, DSS-65, LNA-1, Non-Diplexed, at Feedhorn Aperture

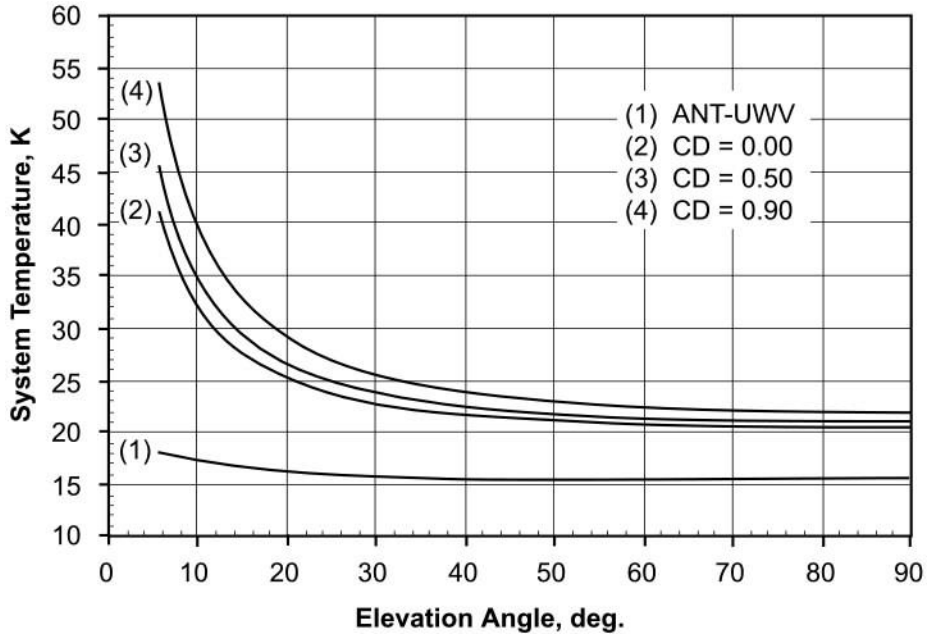

Figure 5. X-Band System Noise Temperature, DSS-65, LNA-1, Non-Diplexed, at Feedhorn Aperture

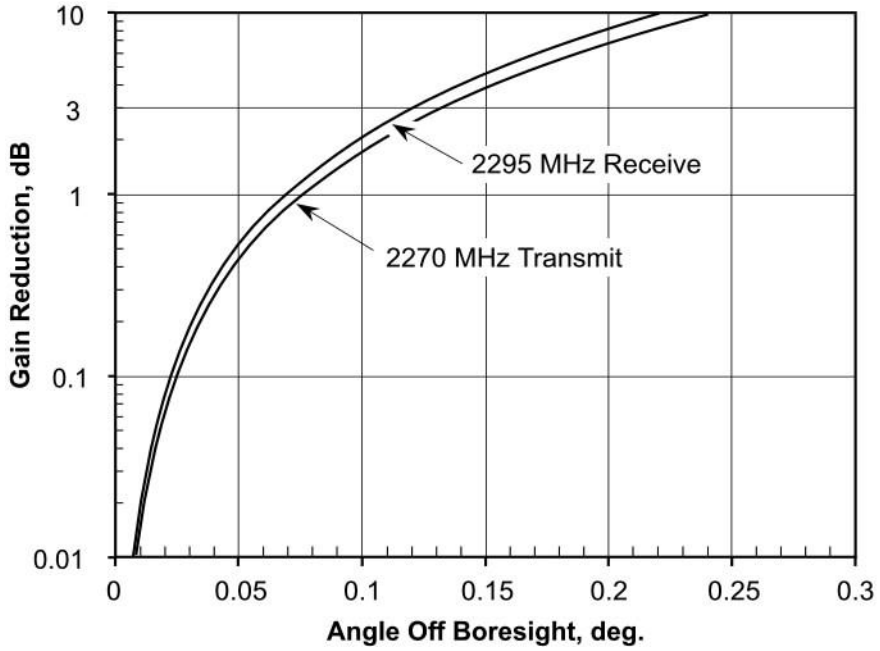

Figure 6. S-Band Gain Reduction Versus Angle Off Boresight

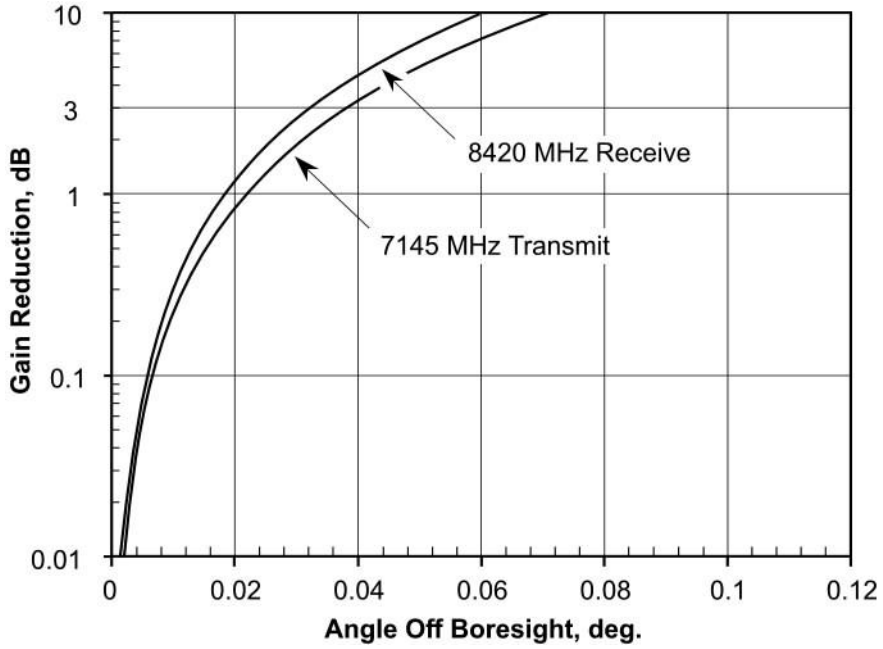

Figure 7. X-Band Gain Reduction Versus Angle Off Boresight

Appendix A
Equations for Modeling

A.1 Equations for Gain Versus Elevation Angle

The following equation can be used to generate S- and X-band transmit and receive gain versus elevation curves for DSS-65. The gains are referenced to the feedhorn aperture, so different configurations (e.g., LNA-1 non-diplexed and LNA-2 diplexed) will have the same gain values. Examples of these curves are shown in Figures 2 and 3 for S- and X-bands. See paragraph 2.1.1.1 for frequency effect modeling and Module 105 for atmospheric attenuation at weather conditions corresponding to cumulative distributions from 0% to 99%. The year-average atmosphere attenuations for CD = 0.00, 0.50, and 0.90 are also given in Table A-2.

$$G(\theta) = G_0 - G_1(\theta - \gamma)^2 - \frac{A_{ZEN}}{\sin\theta}, \text{ dBi} \qquad \text{(A1)}$$

where

θ	=	antenna elevation angle (deg.) $6 \le \theta \le 90$
G_0, G_1, γ	=	parameters from Table A-1
A_{ZEN}	=	zenith atmospheric attenuation from Table A-2 or from Tables 10 through 15 in Module 105, dB.

A.2 Equations for System Noise Temperature Versus Elevation Angle

The following equations can be used to generate S- and X-band receive system noise temperature versus elevation curves for DSS-65. Examples of these curves are shown in Figures 4 and 5. See Module 105 for atmospheric attenuation at weather conditions corresponding to cumulative distributions from 0% to 99%. Atmosphere attenuations for CD = 0.00, 0.50, and 0.90 are also given in Table A-2.

System operating noise temperature:

$$T_{op}(\theta) = T_{AMW} + T_{sky} = \left[T_1 + T_2 e^{-a\theta}\right] + \left[T_{atm}(\theta) + T'_{CMB}(\theta)\right] \qquad \text{(A2)}$$

Sky noise contribution:

$$T_{sky} = T_{atm}(\theta) + T'_{CMB}(\theta) \qquad \text{(A3)}$$

Atmospheric attenuation:

$$A(\theta) = \frac{A_{zen}}{\sin(\theta)}, \text{ dB} \qquad \text{(A4)}$$

Atmospheric loss factor:

$$L(\theta) = 10^{\frac{A(\theta)}{10}}, \text{ dimensionless, } >1.0 \qquad \text{(A5)}$$

Atmospheric physical temperature:

$$T_p = 255 + 25 \times CD, \text{ K} \qquad \text{(A6)}$$

Atmospheric noise contribution:

$$T_{atm}(\theta) = T_p\left[1 - \frac{1}{L(\theta)}\right], \text{ K} \qquad \text{(A7)}$$

Effective cosmic background noise:

$$T'_{CMB}(\theta) = \frac{T_{CMB}}{L(\theta)}, \text{ K} \qquad \text{(A8)}$$

where

θ	=	antenna elevation angle (deg.), $6 \le \theta \le 90$
T_1, T_2, a	=	antenna-microwave noise temperature parameters from Table A-3
A_{ZEN}	=	zenith atmospheric attenuation, dB, from Table A-2 or from Tables 10 through 15 (S-, X-bands) in Module 105 as a function of frequency, station, and cumulative distribution (CD)
CD	=	cumulative distribution, $0 \le CD \le 0.99$, used to select A_{ZEN} from Table A-2 or from Tables 10 through 15 in Module 105
T_{CMB}	=	2.725 K, cosmic microwave background noise temperature

A.3 Equation for Gain Reduction Versus Pointing Error

The following equation can be used to generate gain-reduction versus pointing error curves examples of which are depicted in Figures 6 and 7.

$$\Delta G(\theta) = 10\log\left(e^{\frac{2.773\theta^2}{HPBW^2}}\right) \quad , \quad \text{dB} \tag{3}$$

where

θ = pointing error (deg.)

$HPBW$ = half-power beamwidth in degrees (from Tables 1, 2, or 3)

Table A-1. Vacuum Component of Gain Parameters

Configuration and Stations	Parameters†			
	G_0* (Transmit)	G_0* (Receive)	G_1	γ
S-band, DSS-65 (Figure 2)	55.40	56.07	0.000006	42.0
X-band, DSS-65 (Figure 3)	67.05	68.41	0.00008	42.0

NOTES:

† G_0 values are nominal at the frequency specified in Tables 1, 2, and 3. Other parameters apply to all frequencies within the same band.

* Favorable tolerance = +0.5 dB, adverse tolerance = –0.5 dB, with a triangular PDF.

Table A-2. S- and X-Band Year-Average Zenith Atmosphere Attenuation Above Vacuum (A_{ZEN})

Weather Condition †	A_{ZEN}, dB*					
	S-band			X-band		
	DSS-15 Goldstone	DSS-45 Canberra	DSS-65 Madrid	DSS-15 Goldstone	DSS-45 Canberra	DSS-65 Madrid
Vacuum	0.000	0.000	0.000	0.000	0.000	0.000
CD = 0.00	0.033	0.036	0.035	0.037	0.039	0.038
CD = 0.50	0.034	0.036	0.035	0.041	0.047	0.044
CD = 0.90	0.034	0.037	0.036	0.045	0.058	0.057

NOTES:

* From Tables 10 through 15 in module 105

† CD = cumulative distribution.

Table A-3. Antenna-Microwave Noise Temperature Parameters, Referenced to Feedhorn Aperture

Configuration and Stations	Parameters		
	T_1*	T_2	a
S-band, DSS-65:			
S-band, DSS-65, LNA-1, HEMT, non-diplexed	31.80	7.10	0.013
S-band, DSS-65, LNA-1, HEMT, diplexed	39.40	7.60	0.013
DSS-15, X-band, High-Gain Mode (normal configuration):			
X-band, DSS-15, LNA-1, HEMT, RCP, diplexed	N/A	N/A	N/A
X-band, DSS-15, LNA-2, HEMT, LCP, diplexed	N/A	N/A	N/A
X-band, DSS-15, LNA-1, HEMT, RCP, diplexed, w/ narrow-band radar filter	N/A	N/A	N/A
X-band, DSS-15, LNA-2, HEMT, LCP, diplexed, w/ narrow-band radar filter	N/A	N/A	N/A
DSS-15, X-band, Low-Gain Mode (high s/c received power):			
X-band, DSS-15, LNA-1, HEMT, RCP, diplexed	N/A	N/A	N/A
X-band, DSS-15, LNA-2, HEMT, LCP, diplexed	N/A	N/A	N/A
X-band, DSS-15, LNA-1, HEMT, RCP, diplexed, w/ narrow-band radar filter	N/A	N/A	N/A
X-band, DSS-15, LNA-2, HEMT, LCP, diplexed, w/ narrow-band radar filter	N/A	N/A	N/A
DSS-45, Maser/HEMT, High-Gain Mode, RCP/LCP:			
X-band, DSS-45, LNA-1, maser, non-diplexed	N/A	N/A	N/A
X-band, DSS-45, LNA-1, maser, diplexed	N/A	N/A	N/A
X-band, DSS-45, LNA-2, HEMT, non-diplexed	N/A	N/A	N/A
X-band, DSS-45, LNA-2, HEMT, diplexed	N/A	N/A	N/A
DSS-45, Maser/HEMT, Low-Gain Mode, RCP/LCP:			
X-band, DSS-45, LNA-1, maser, non-diplexed	N/A	N/A	N/A
X-band, DSS-45, LNA-1, maser, diplexed	N/A	N/A	N/A
X-band, DSS-45, LNA-2, HEMT, non-diplexed	N/A	N/A	N/A
X-band, DSS-45, LNA-2, HEMT, diplexed	N/A	N/A	N/A

Table A-3. Antenna-Microwave Noise Temperature Parameters, Referenced to Feedhorn Aperture (Continued)

Configuration and Stations	Parameters		
	T_1*	T_2	a
DSS-65, Maser/HEMT, High-Gain Mode, RCP/LCP:			
X-band, DSS-65, LNA-1, maser, non-diplexed	15.43	5.00	0.10
X-band, DSS-65, LNA-1, maser, diplexed	24.83	6.10	0.10
X-band, DSS-65, LNA-2, HEMT, non-diplexed	32.16	5.50	0.10
X-band, DSS-65, LNA-2, HEMT, diplexed	41.56	6.60	0.10
DSS-65, Maser/HEMT, Low-Gain Mode, RCP/LCP:			
X-band, DSS-65, LNA-1, maser, non-diplexed	20.52	5.00	0.10
X-band, DSS-65, LNA-1, maser, diplexed	29.92	6.10	0.10
X-band, DSS-65, LNA-2, HEMT, non-diplexed	43.16	5.50	0.10
X-band, DSS-65, LNA-2, HEMT, diplexed	52.56	6.60	0.10

NOTES:

* Favorable tolerance = –2 K, adverse tolerance = +2 K, with a triangular PDF.

Deep Space Network

104
34-m BWG Stations Telecommunications Interfaces

Document Owner:		Approved by:	
Signature provided	07/27/2022	Signature provided	07/27/2022
Stephen D. Slobin Antenna System Engineer	Date	Timothy T. Pham Communications Systems Chief Engineer	Date

Prepared by:		Released by:	
Signature provided	07/27/2022	Signature provided	08/09/2022
Stephen D. Slobin Antenna System Engineer	Date	Christine Chang DSN Document Release Authority	Date

DSN No. **810-005, 104, Rev. O**
Issue Date: August 09, 2022
JPL D-19379; CL#22-4056

Jet Propulsion Laboratory
California Institute of Technology

Users must ensure that they are using the current version in DSN Telecommunications Link Design Handbook website:
https://deepspace.jpl.nasa.gov/dsndocs/810-005/

Review Acknowledgment

By signing below, the signatories acknowledge that they have reviewed this document and provided comments, if any, to the signatories on the Cover Page.

Signature Provided	07/27/2022	Signature Provided	07/27/2022
Jeff Berner DSN Project Chief Engineer	Date	John Cucchissi Antenna System Engineer	Date
Signature not provided		Signature not provided	
Michael Settember Uplink System Engineer	Date	David Rochblatt Antenna System Engineer	Date
Signature Provided	07/27/2022		
Harvey Soldan System Engineering Group Supervisor	Date		

Document Change Log

Rev	Issue Date	Prepared By	Affected Paragraphs	Change Summary
Initial	11/30/2000	S. Slobin R. Sniffin	All	All
A	2/5/2004	S. Slobin R. Sniffin	All	Added performance information for Ka-band capability at DSS-26 and for new station, DSS-55. Incorporated latest measurements for other stations. Incorporated text improvements.
B	8/1/2005	S. Slobin R. Sniffin	Tables 4, 5, A-1, A-2, A-3, Figures 4, 9, 14, 20, and 25.	Revised performance information for DSS-34 to reflect addition of Ka-band and X-band improvements. Required splitting of Table 4 into Tables 4 and 5, renumbering subsequent tables, revision of Figures 9 and 20, and addition of Figures 4, 14, and 25.
C	9/19/2008	S. Slobin R. Sniffin	Sections 2.1.3, 3.0; All Tables; Figures 1, 3, 4, 6 - 27	Documents installation of an X-band acquisition capability at DSS-24, -34, and -54. Revised T_{AMW} formulation for noise temperature to be consistent with Rev. B of module 105. Added proposed 26 GHz capability at DSS-24, -34, and -54.
D	5/15/2009	S. Slobin R. Sniffin	Tables 6, 11 Figures 13-15, 27-29, 36 Table A-3	Add K-band gain and noise temperature performance for DSS-24, -34, and -54.
E	9/15/2009	S. Slobin	Table A-4	Updated Ka-band G and T parameters for DSS-54 and DSS-55. HEMT numbering has also been corrected in that Table.
F	6/1/2010	S. Slobin	Table 6 Table 11 Figures 27, 28, 29 Table A-3	New K-band receive Tamw values New K-band receive Tamw and Top values New figures for K-band New K-band Tamw parameters Eliminated the Rev. E designation for the document series

Rev	Issue Date	Prepared By	Affected Paragraphs	Change Summary
G	03/05/2013	S. Slobin	Table 10 Section 2.1.1.3 Table A-5 Figures 16-19 and 30-33;	Revised references to wind effects. Section 2.1.1.3 re-written to address gain and pointing effects due to wind. Values in Table A-5 changed slightly. Figures 16-19 and 30-33 changed slightly. Minor cosmetic changes throughout.
H	04/01/2015	Stephen Slobin Christine Chang	Rev.G Tables 3,9 Figures 5,7,21 Section 2 & Table 1 Table 1 Tables 1,4 Table 3 Tables 6 & 7 Table 7 Table 8 Table 9 Figure 2 Figure 3 Figures 9, 18, 24, 33 Tables A-2 & A-4 Table A-3 Sections 2, 3 Tables 1, 3	Deleted. DSS-27 HSB antenna decommissioned. Added DSS-35 capabilities. Clarified no simultaneous X-band RCP and LCP for DSS-34 and -54. Clarified simultaneous Ka-band RCP and LCP operation. Corrected S-band uplink power. Updated Ka-band uplink power. Added DSS-35 transmit values. Clarified location of X-band acquisition antennas. Added note about low-gain mode noise temperature increase at X- and Ka-bands. Added DSS-35 receive values. Corrected Ka-band polarizations. Revised X-band HEMT bandwidths. Updated wind effect gain reduction. Added DSS-35 Tamw and Top values. Removed note on transmit table. Added DSS-35 to caption. Added DSS-35 X- and Ka-band gain and noise temperatures. Added DSS-35 gain and noise temperature parameters. Added notes about low-gain mode noise temperature increase at X- and Ka-bands. Added note about low-gain mode noise temperature increase at K-band. Added details of 80 kW X-band transmitter at DSS-26.

Rev	Issue Date	Prepared By	Affected Paragraphs	Change Summary
I	02/10/2017	Stephen Slobin Christine Chang	Sections 2, 3 Table 1 Tables 1, 2, 3, 5, 7, 9 Figure 3 Figure 5 Figure 6 Figures 7, 24 Figures 12, 22 Figures 29, 39 Figures 1-44 Tables A-1, A-2, A-4 Table A-1	Implementation dates for future antennas DSS-33, -53, -56, and 80 kW X-band transmitter additions at future antennas DSS-33, -53. DSS-36 added. DSS-55 removed, new high-power X-band feed shown. New for DSS-36. New for DSS-55. Re-drawn for DSS-34, replacing DSS-24. New for DSS-36 X- and Ka-band gain. New for DSS-36 X- and Ka-band noise temperatures. Renumbered to accommodate four new DSS-36 figures and two additional block diagrams. DSS-36 added. S-band G_0 uplink gains for DSS-24, -34, -54 re-calculated.
J	01/12/2018	Stephen Slobin Christine Chang	Tables 1, 2, A-1 Table 2 Table 3 Table 4 Table 5 All tables, including Appendix Tables A1, A2, A4 Figure 2 Figures 3, 4, 5, 6 Figure 4	DSS-36 S-band uplink clarified – near-earth only. S-band gains and EIRP re-calculated. X-band gains and EIRP re-calculated. Ka-band gains and EIRP re-calculated. New tolerances for K-band Tamw in S/K-mode. Uplink and downlink bands center frequencies stated accurately. Uplink and downlink gain adjustments noted for near-earth bands. Ka-band hyperboloid redrawn. Ka-band downconverter outputs clarified. X-band downconverter outputs clarified.

Rev	Issue Date	Prepared By	Affected Paragraphs	Change Summary
K	07/17/2019	Stephen Slobin Christine Chang	Section 3 Table 1 Tables 2, 5, 9 Tables 4, 7, 9 Figures 1-12 Appendix A-1 Appendix A-2 Appendix A-4 Figures 14, 31 Figures 24, 41	Updated operational dates New DSS-26 added for S-band New DSS-25 G, T Re-drawn and re-numbered DSS-26 added for S-band New DSS-25 X-band G, T New DSS-25 Ka-band G, T New DSS-25 X-band G, T New DSS-25 Ka-band G, T
L	10/16/2019	Stephen Slobin Christine Chang	Section 2 Table 1 Table 2	Changed to indicate DSS-54 not usable in S-band G, T deep-space band (2110-2120 MHz)
M	02/15/2021	Stephen Slobin Christine Chang	Section 3 Table 1 Tables 1, 3 Tables 2, 3, 5, 7, 9, A-1, A-2, A-3, A-4 All tables and appendices Table 9 Table A-5 Figures 1, 5, 9, 12 Figures 4, 8	Added new implementations and revised dates Corrected DSS-24 X-band polarization Removed 5.7 kW X-band transmit limit for near-earth Added performance values for DSS-56 Placeholders added for future antennas and implementations Updated Tsky values to agree with module 105, Rev. E Latest module 105 (Rev. E) atmosphere attenuation values added Block diagrams added for future DSS-23, -33, -53, and new -56 K-band equipment added
N	06/07/2021	Stephen Slobin Christine Chang	Table A-2	Removed redundant rows from Table A-2 Added the G0 Transmit values for DSS-56

Rev	Issue Date	Prepared By	Affected Paragraphs	Change Summary
O	08/09/2022	Stephen Slobin Christine Chang	Section 3	Updated
			Table 2	New, for M6 and M7 reflectors
			Table 5	New, for K-band transmit
			Tables 6-11	Re-numbered from previous revision
			Table 11	Updated for DSS-53 (X&Ka-bands) and DSS-26 (K-band)
			Table A-2	Added DSS-53 X-band G, T
			Table A-3	Added DSS-26 K-band G, T
				Added NOTES regarding K-band uplink
			Table A-4	Added DSS-53 Ka-band G, T
			Figures 2, 4, 6, 8, 10, 12	K-band uplink equipment added

Table of Contents

List of Tables

List of Figures

Section 1
Introduction

1.1 Purpose

This module provides the performance parameters for the Deep Space Network (DSN) 34m Beam Waveguide (BWG) antennas that are necessary to perform the nominal design of a telecommunications link. It also summarizes the capabilities of these antennas for mission planning purposes and for comparison with other ground station antennas.

Because of the large number of BWG antennas, the four frequency bands, and the large number of operating modes and configurations, the reader will find it helpful to refer to Tables A-1 through A-4, in addition to Table 1, to keep the capabilities and differences among the antennas clear. Reference to the antenna block diagrams (Figures 1 through 12) will clearly show the microwave equipment configurations

1.2 Scope

The scope of this module is limited to providing those parameters that characterize the RF performance of the 34-meter BWG antennas, including the effects of weather for a limited number of weather conditions. A more complete discussion of weather effects is given in module 105, Atmospheric and Environmental Effects. This module does not discuss mechanical restrictions on antenna performance covered in module 302, Antenna Positioning.

Section 2
General Information

The 34-meter diameter BWG (beam waveguide) antennas are the latest generation of antennas built for use in the DSN. These antennas differ from more conventional antennas (for example, the 34-meter HEF antennas, described in module 103) in the fact that a series of mirrors, approximately 2.4 meters in diameter, direct microwave energy from the region above the main reflector to a location in a pedestal room at the base of the antenna. The pedestal room is located below the azimuth track of the antenna and is below ground level.

In this configuration, several "positions" of microwave equipment contained in the pedestal room can be accessed by rotation of an ellipsoidal mirror located in the center of the pedestal room floor beneath the azimuth axis of the antenna. This enables great versatility of design and allows tracking with equipment at one position while equipment installation or maintenance is carried out at the other positions. Since cryogenic low-noise amplifiers (LNAs) do not tip as they do when located above the elevation axis, certain state-of-the-art low noise amplifier and feed designs can be implemented.

The capabilities of each antenna differ depending on the microwave transmitting and receiving equipment installed. A summary of these capabilities is provided in Table 1. Functional block diagrams for each antenna are provided in Figures 1 through 12. K-band equipment is shown in the block diagrams, even though this equipment is not presently installed at some antennas. See the implementation dates in Section 3 and Tables 1 and 2. Future Ka-uplink equipment will be added to the block diagrams for DSS-35 (Figure 7) and DSS-55 (Figure 11) at a future date. Block diagrams for future antennas DSS-23 and DSS-33 are also shown. In general, each antenna has at least one LNA for each supported frequency band. However, stations that can support simultaneous right circular polarization (RCP) and left circular polarization (LCP) in the same band have an LNA for each. In addition, the stations that support Ka-band contain an additional LNA to enable monopulse tracking when using RCP polarization. Each antenna also has at least one transmitter. S-band uplink can be used in conjunction K-band uplink, and X-band uplink can be used in conjunction with K-band uplink, when the appropriate K-band equipment is installed at the -4 and -6 antennas in the future.

There are six stations, DSS-24, -26, -34, -36, -54, and -56 that are capable of receiving selectable (one polarization at a time) RCP or LCP at S-band. DSS-24, -34, and -54 are also capable of simultaneously (with S-band) or independently receiving selectable (one polarization at a time) RCP or LCP at X-band due to the fact that there is only a single LNA at DSS-24, and a single X-band downconverter at DSS-34, and -54. The remaining BWG stations, DSS-25, -26, -35, -36, -55, and -56 can receive both X-band polarizations simultaneously. K-band (26 GHz) receive capability with selectable (one polarization at a time) RCP or LCP presently exists at DSS-24, -26, -34, -54. and -56. Ka-band capability, including monopulse-assisted tracking of RCP signals, exists at DSS-25, -26, -34, -35, -36, -53, -54, -55, and -56. These stations can also receive Ka-band RCP and LCP simultaneously for radio science investigations, without monopulse-assisted tracking. Future antennas DSS-23 and DSS-33 are not discussed here at this time. Their proposed capabilities are shown in Table 1.

The K-band 26 GHz receive capability can be used independently, or in combination with the station's S-band capability (with an M6A S/K dichroic) or X-band capability (with an M7A X/K

dichroic), to provide a high data rate capability for spacecraft operating at near-Earth distances (less than 2×10^6 km). The implementation dates for the X/K dichroics are coincident with the K-band uplink dates given in Section 3 and Tables 1 and 2. A low-gain mode is included to accommodate high signal levels that are expected during the early post-launch phase of 26 GHz missions. Prior to receiving the M7A X/K dichroic, those antennas with X-band or Ka-band capabilities will be unable to receive X-band or Ka-band because the retractable mirror over the X-band or X/Ka-band feeds must be retracted for K-band reception. S-band performance in the S/X and S/K modes is identical. The S-band transmitters at DSS-26, -36, and -56 are 250 W, and due to the low power are usable only for near-earth applications. The S-band transmitters at DSS-24, -34, -54 are 20 kW, however DSS-54 is not available for use in the deep space frequency band (2110-2120 MHz) due to conflict with IMT-2000 users, per agreement between NASA and Secretaria de Estado de Telecomunicaciones y para la Sociedad de la Informacion (SETSI), January, 2001. These S-band transmitters, and the X-band transmitter at DSS-24, are coupled into the microwave path using a frequency-selective diplexer. Because the diplexer increases the operating system noise temperature, a non-diplexed path for receive-only operation is provided at all of these antennas. The X-band diplexing function at DSS-25, -26, -34, -35, -36, -53, -54, -55, and -56 is accomplished using the frequency-selective characteristics of the feed in conjunction with an external polarizing network. This technique does not affect the operating system temperature, so these antennas are considered to be always-diplexed and no lower-noise non-diplexed configuration is available. All BWG antennas have a 20 kW X-band transmitter; and additionally, DSS-26 has an 80 kW X-band transmitter.

When an S-band uplink is required, the received S-band polarization must be the same as is being transmitted. X-band uplinks can be of either polarization, independent of the polarization of any signals being received. X-band uplinks are not available in conjunction with S-band downlinks due to bandwidth restrictions of the S/X dichroic plate. This dichroic plate must be retracted for X-band uplink operation, and simultaneous S-band downlink is no longer available; thus the X-band uplink gain for the S/X mode is shown as “N/A” in Table A-2.

An S/X or S/K dichroic must be extended for operation at S-band (uplink and/or downlink). DSS-24, -26, -34, -36, -54, and -56 have a retractable S/X dichroic plate to enable operation in an S/X downlink mode, or X-only if the dichroic plate is retracted. Additionally, DSS-24, -26, -34, -54, and -56 also have a retractable S/K (S/26 GHz) dichroic plate for operation in an S/K mode, or K-only if both dichroic plates are retracted. DSS-26 has a second-generation S/K dichroic [M6A(2)]) which allows simultaneous S-up/down and K-up/down operation,

The S-band transmitters at DSS-24, -34, and -54, when operated near their maximum power rating, produce sufficient 13th harmonic power to adversely affect telemetry reception in the 26 GHz band. Mission designers selecting an uplink frequency between 2025 and 2076.9 MHz and requiring a radiated power in excess of 5.0 kW should select a downlink frequency such that the 13th harmonic of the uplink frequency does not fall within the bandwidth required for their telemetry.

When simultaneous X-band uplink and downlink of the same polarization are required at the only station with a waveguide diplexer (DSS-24), reception must be through the diplexer, and the noise will be increased over that of the non-diplexed path. DSS-25, -26, -34, -35, -36, -54, -55, and -56 have two X-band LNAs, one for each polarization. As these stations do not have waveguide diplexers, the system noise temperature in each polarization is approximately the

same. Although there are two X-band LNAs at DSS-34 and DSS-54, there is only a single-channel X-band downconverter, thus simultaneous RCP and LCP reception is not possible.

Additionally, all BWG antennas offer a low-gain mode (−20 dB) for use at high received signal power levels for spacecraft near the Earth. The X- and Ka-band low-gain equipment is not shown in the antenna block diagrams in this module (only K-band is, for DSS-24, -34, and -54). Reference to the HEF antenna block diagrams of 810-005 module 103 will show the X-band low-gain equipment for those antennas.

2.1 Telecommunications Parameters

The significant parameters of the 34-meter BWG antennas that influence the design of the telecommunications link are listed in Tables 3-9, and 11. Variations of these parameters that are inherent in the design of the antennas are discussed below. Other factors that degrade link performance are discussed in modules 105 (Atmospheric and Environmental Effects) and 106 (Solar Corona and Solar Wind Effects).

The values in Tables 3-9 do not include the effects of the atmosphere. Table 11 gives system noise temperature, T_{op}, including 25% CD (cumulative distribution) average-clear weather. The attenuation and noise-temperature effects of weather for three specific weather conditions are included in the figures at the end of the module so that they may be used for a quick estimate of telecommunications link performance for those specific conditions, without reference to module 105. For detailed design control table use, the more comprehensive and detailed S-, X-, K-, and Ka-band weather effects models (for weather conditions up to 99% cumulative distribution) in module 105 should be used.

2.1.1 Antenna Gain Variation

Because the gain is referenced to the feedhorn aperture, such items as diplexers and waveguide runs to alternate LNAs that are “downstream” (below the feedhorn aperture, toward the LNA), do not affect the gain at the reference plane. Dichroic plates that are “upstream” of the feedhorn aperture cause a reduction in gain.

2.1.1.1 Frequency Effects

Antenna gains are specified at the indicated frequency (f_0). The gain varies as frequency-squared. For operation at higher or lower frequencies in the same band, the gain (dBi) must be increased or reduced, respectively, by 20 log (f/f_0).

2.1.1.2 Elevation Angle Effects

Structural deformation causes a reduction in gain when the antenna is operated at an elevation angle other than where the reflector panels were aligned, at approximately 45 degrees. The effective gain of the antenna is also reduced by atmospheric attenuation, which is a function of elevation. Figures 13 through 29 show representative curves of gain versus elevation angle for selected stations and configurations. These figures typically show the highest gain configuration for each stated antenna and frequency band (e.g, X-band for DSS-34 in the X/Ka-mode with the S/X dichroic retracted, rather than in the S/X-mode with the S/X dichroic extended). The gain curves show the hypothetical vacuum (no atmosphere) condition, and the gain with 0%, 50%,

and 90% weather conditions, designated as CD (cumulative distribution) = 0.00, 0.50, and 0.90. 0% means minimum weather effect (exceeded 100% of the time); 90% means that effect which is exceeded only 10% of the time. Qualitatively, 0% corresponds to the driest, lowest-loss condition of the atmosphere; 25% corresponds to average clear; 50% corresponds to humid or very light clouds; and 90% corresponds to very cloudy, but with no rain. Appendix A provides the complete set of parameters from which these curves were created. The atmospheric parameters used to generate these curves are from module 105, Rev. D, as shown in Table A-5. These parameters, in combination with the weather effects parameters from module 105, can be used to calculate the gain versus elevation angle curves for any antenna, in any configuration, for weather conditions up to 99% CD.

2.1.1.3 Wind Effects

A study of tracking data from the Kepler spacecraft at Ka-band during windy conditions shows minimal effects on gain degradation (due to structural deformation of the antenna) and pointing loss (due to gusty winds of varying direction). A realistic upper limit of these effects at Ka-band can be considered to be 0.8 dB for wind speeds up to 50 km/hr. The effects at S-, X-, and K-bands, all lower frequencies, are expected to be even less than at Ka-band. Cumulative probability distributions of wind velocity at Goldstone are given in module 105. At Goldstone, the windiest of the DSN antenna locations, 50 km/hr wind is exceeded about 2% of the year and 5% of the worst month (April). An estimate of these effects at S-, X-, K-, and Ka-bands at wind speeds of 10, 30, and 50 km/hr is shown in Table 10.

2.1.2 System Noise Temperature Variation

The operating system temperature (T_{op}) varies as a function of elevation angle due to changes in the path length through the atmosphere and ground noise received by the sidelobe pattern of the antenna. Figures 30 through 46 show the combined effects of these factors for the same set of stations and configurations selected above. These figures typically show the lowest noise configuration for each stated antenna and frequency band (e.g., X-band for DSS-34 in the X/Ka-mode with the S/X dichroic retracted, rather than in the S/X-mode the S/X dichroic extended). The figures show the antenna and microwave contribution alone, and also the system operating noise temperature (T_{op}) with 0%, 50%, and 90% weather conditions. The equations and parameters for these curves are provided in Appendix A.2 and can be used, in combination with the weather effects parameters from module 105, to calculate the system temperature versus elevation curve for any antenna, in any configuration, for weather conditions up to 99% CD. The values of zenith atmospheric attenuation (A_{zen}) used in generating these figures are given in Table A-5, using module 105, Rev. D values.

The system operating noise temperature, T_{op}, consists of two parts, an *antenna-microwave component*, T_{AMW}, for the contribution of the antenna and microwave hardware only, and a *sky component*, T_{sky}, that consists of the atmosphere noise, plus the cosmic microwave background (CMB) noise attenuated by the atmosphere loss. T_{AMW} is shown in Figures 30 through 46 as "ANT-UWV". The system operating noise temperature is given by

$$T_{op}(\theta) = T_{AMW} + T_{sky} = \left[T_1 + T_2 e^{-a\theta}\right] + \left[T_{atm}(\theta) + T'_{CMB}(\theta)\right]$$

where

T_1, T_2 and a are coefficients and exponent given in Appendix A, Table A-1 through Table A-4

T_{atm} is the atmosphere contribution term, calculated from Module 105

T'_{CMB} is the attenuated cosmic contribution, calculated from Module 105

More details of this calculation are given in Appendix A of this module.

The T_{AMW} noise temperature values in Tables 7-9 are stated with reference to the feedhorn aperture and arise from antenna and microwave hardware contribution only. No atmosphere or cosmic background contribution is included. Table 11 presents values of T_{AMW}, T_{sky}, and T_{op} for all antenna frequencies and configurations at zenith, with average-clear CD = 0.25 weather. The values of T_{sky} in Table 11 are calculated by methods presented in Module 105, using year-average attenuation values of that module. The values of A_{zen} used in calculating T_{sky} for average clear weather are given in Table A-5 (Module 105, Rev. E).

System noise temperature increases in the low-gain mode can be approximated for telecom modeling purposes as +20 K at X-band, +180 K at K-band, and +70 K at Ka-band.

2.1.3 Antenna Pointing

2.1.3.1 Pointing Accuracy

The pointing accuracy of an antenna, often referred to as its *blind-pointing* performance, is the difference between the calculated (or commanded) beam direction and the actual beam direction. The error is typically random (after the systematic contributions have been removed by a "blind pointing model") and can be divided into two major categories. The first of these includes the computational errors and uncertainties associated with the radio sources used to calibrate the antenna, and the location of the spacecraft provided by its navigation team. The second has many components associated with converting a calculated beam direction to the physical positioning of a large mechanical structure. Included are such things as atmospheric wind and refraction effects, servo and encoder errors, thermally and gravitationally induced structural deformation, azimuth track leveling (for an azimuth-elevation antenna), and both seismic and diurnal ground tilt.

Blind pointing is modeled by assuming equal pointing performance in the elevation (EL) and cross-elevation (XEL) directions. That is, the random pointing errors in each direction have uncorrelated Gaussian distributions with the same standard deviation. This results in a Rayleigh distribution for pointing error where the mean radial error is 1.2533 times the standard deviation of the EL and XEL components. For a Rayleigh distribution, the probability that the pointing error will be less than or equal to the mean radial error is 54.4%. Conversely, the probability that the mean radial error will be exceeded is 45.6%.

810-005 module 302 (Antenna Positioning) presents blind pointing performance (mean radial error) for the DSN antennas.

2.1.3.2 Pointing Loss

Figures 47 through 49 show the effects of pointing error on effective transmit and receive gain of the antenna. These curves are Gaussian approximations based on measured and predicted antenna beamwidths. The equations used to derive the curves are provided in Appendix A.3.

2.1.3.3 CONSCAN-aided Pointing

CONSCAN (conical scan) pointing is accomplished during tracking by moving the antenna beam in a circular motion around the predicted position of a spacecraft, with a radius such that the pointing loss is typically a constant 0.1 dB, as given in Tables 3-9. When the predicted spacecraft position deviates from the actual spacecraft position (for example, due to errors in the blind-pointing model), a "sinusoidal" error signal is generated, and a small correction to antenna pointing is applied so as to maintain the constant 0.1 dB pointing loss. A further description of CONSCAN pointing is given in 810-005 module 302.

2.1.3.4 Monopulse-aided Pointing

Ka-band monopulse-aided pointing uses a monopulse tracking coupler within the cryogenic feed package to establish a feed pattern with a theoretical null on-axis. The magnitude of the pointing error is proportional to the magnitude of the signal received by this pattern and the azimuthal error is proportional to the phase difference between the sum and difference outputs of the coupler. Thus, by measuring the complex ratio of the sum and difference signals, pointing corrections can be generated to instruct the antenna servo system to drive the pointing error to zero. The system achieves its specified performance when the ratio of the signal in the sum channel (that is, the signal from which tracking and telemetry information will be derived) to the noise level in the difference channel is greater than 26 dB-Hz.

2.1.3.5 Ka-Band Aberration Correction

The extremely narrow beamwidth at Ka band requires that a Ka-band uplink signal be aimed at where the spacecraft will be when the signal arrives, while simultaneously receiving a signal that left the spacecraft one one-way light-time previously. This is accomplished by mounting the Ka-band transmit feed at DSS-25 on a movable X-Y platform that can displace the transmitted beam as much as 30 millidegrees from the received beam.

DSS-25 is the only antenna with a Ka-band transmit capability. In the future, DSS-35 and DSS-55 will also receive a Ka-band uplink. The fact that the transmit feed is displaced from its optimum focus causes the gain reduction depicted in Figure 50. The equation used to generate this curve is provided in Appendix A.4.

2.1.3.6 X-Band Acquisition

A 1.2-m X-band acquisition antenna and receiver has been installed at the quadripod apex (above the subreflector) of the DSS-24, DSS-34, and DSS-54 antennas. The acquisition receiver employs the monopulse technique to develop pointing commands for the antenna during the launch phase when launch time and trajectory uncertainties make predict-driven pointing impractical. During acquisition, the acquisition system is responsible for antenna pointing, however uplink and downlink services are provided by the main antenna beam. The

characteristics of the acquisition antennas are given in Table 7 (for DSS-24) and in Table 8 (for DSS-34 and DSS-54).

Section 3
Proposed Capabilities

The DSN is in the process of increasing the number of 34m BWG antennas. Future BWG antennas will be:

DSS-56 (Madrid), 12/2020, (S-up/down, X-up/down, K-down, Ka-down) (completed)

DSS-53 (Madrid), 12/2021, (X-up/down, Ka-down) (completed)

DSS-23 (Goldstone), 12/2025, (X-up/down, Ka-down)

DSS-33 (Canberra), 9/2028, (X-up/down, Ka-down)

K-band (26 GHz) downlink will be installed in the following antennas:

DSS-26 (Goldstone), 2/2022 (completed)

DSS-36 (Canberra), 12/2022

250 W K-band uplink will be installed in the following antennas:

DSS-26 (Goldstone), 2/2022 (completed)

DSS-36 (Canberra), 12/2022

DSS-24 (Goldstone), 10/2023

DSS-56 (Madrid), 4/2024

DSS-34 (Canberra), 7/2025

DSS-54 (Madrid), 9/2026

800 W Ka-band uplink will be installed in the following antennas:

DSS-35 (Canberra), 9/2026

DSS-55 (Madrid), 6/2027

DSS-25 (Goldstone), 6/2028

DSS-36 and DSS-56 will receive 80 kW X-band uplink at some time in the future, but the dates have not been presently established.

Table 1. Summary of Available Configurations for Each Antenna

ANTENNA		S-UP	S-DOWN	X-UP	X-DOWN	Ka-UP	Ka-DOWN	K-UP/DOWN	OTHER
DEEP SPACE	nominal freq	2115 MHz	2295 MHz	7167.5 MHz	8425 MHz	34450 MHz	32050 MHz	-----	
	band	2110-2120	2290-2300	7145-7190	8400-8450	34.2-34.7 GHz	31.8-32.3 GHz	-----	
NEAR EARTH	nominal freq	2067.5 MHz	2245 MHz	7212.5 MHz	8475 MHz	-----	-----	26250 MHz	
	band	2025-2110 MHz	2200-2290 MHz	7190-7235 MHz	8450-8500 MHz	-----	-----	25.5-27.0 GHz uplink 22.55-23.15 GHz	
ANTENNA		S-UP	S-DOWN	X-UP	X-DOWN	Ka-UP	Ka-DOWN	K-UP/DOWN	OTHER
DSS-23 Goldstone 12/2025	Figure 1	-----	-----	20 kW (DS+NE) (17.4 kW) high power feed	RCP and LCP	-----	RCP and LCP or RCP monopulse	-----	
DSS-24 Goldstone	Figure 2	20 kW DS+NE (17.4 kW)	RCP or LCP	20 kW (DS+NE) (18.2 kW)	RCP or LCP	-----	-----	RCP or LCP 250 W uplink 10/2023	X-band Acq Aid

Table 1. Summary of Available Configurations for Each Antenna (Continued)

ANTENNA		S-UP	S-DOWN	X-UP	X-DOWN	Ka-UP	Ka-DOWN	K-UP/DOWN	OTHER
DSS-25 Goldstone	Figure 3	-----	-----	20 kW (DS+NE) (17.4 kW)	RCP and LCP	300 W (DS) (283 W) LCP only 800 W (DS) (6/2028)	RCP and LCP or RCP monopulse	-----	
DSS-26 Goldstone	Figure 4	250 W NE (200 W)	RCP or LCP	20 kW (DS+NE) (17.4 kW) 80 kW (DS+NE) (67.6 kW) high power feed	RCP and LCP	-----	RCP and LCP or RCP monopulse	RCP or LCP 250 W uplink	
DSS-33 Canberra 9/2028	Figure 5	-----	-----	20 kW (DS+NE) (17.4 kW) high power feed	RCP and LCP	-----	RCP and LCP or RCP monopulse	-----	

Table 1. Summary of Available Configurations for Each Antenna (Continued)

ANTENNA		S-UP	S-DOWN	X-UP	X-DOWN	Ka-UP	Ka-DOWN	K-UP/DOWN	OTHER
DSS-34 Canberra	Figure 6	20 kW DS+NE (17.4 kW)	RCP or LCP	20 kW (DS+NE) (17.4 kW)	RCP or LCP	-----	RCP and LCP or RCP monopulse	RCP or LCP 250 W uplink 7/2025	X-band Acq Aid
DSS-35 Canberra	Figure 7	-----	-----	20 kW (DS+NE) (17.4 kW) high power feed	RCP and LCP	800 W (DS) (9/2026)	RCP and LCP or RCP monopulse	-----	
DSS-36 Canberra	Figure 8	250 W NE (200 W)	RCP or LCP	20 kW (DS+NE) (17.4 kW) high power feed 80 kW (future)	RCP and LCP	-----	RCP and LCP or RCP monopulse	RCP or LCP 12/2022 250 W uplink 12/2022	
DSS-53 Madrid	Figure 9	-----	-----	20 kW (DS+NE) (17.4 kW) high power feed	RCP and LCP	-----	RCP and LCP or RCP monopulse	-----	

Table 1. Summary of Available Configurations for Each Antnna (Continued)

ANTENNA		S-UP	S-DOWN	X-UP	X-DOWN	Ka-UP	Ka-DOWN	K-UP/DOWN	OTHER
DSS-54 Madrid	Figure 10	20 kW NE only (17.4 kW)	RCP or LCP	20 kW (DS+NE) (17.4 kW)	RCP or LCP	-----	RCP and LCP or RCP monopulse	RCP or LCP 250 W uplink 9/2026	X-band Acq Aid
DSS-55 Madrid	Figure 11	-----	-----	20 kW (DS+NE) (17.4 kW)	RCP and LCP	800 W (DS) (6/2027)	RCP and LCP or RCP monopulse	-----	
DSS-56 Madrid	Figure 12	250 W NE (200 W)	RCP or LCP	20 kW (DS+NE) (17.4 kW) high power feed 80 kW (future)	RCP and LCP	-----	RCP and LCP or RCP monopulse	RCP or LCP 250 W uplink 4/2024	

NOTES:
1. DS = deep-space. NE = near-earth.
2. (200 W), (17.4 kW) is power at feedhorn aperture, after transmitter waveguide loss
3. X-band uplink is not available when S-band downlink is required (S/X dichroic in place)
4. Simultaneous X-band RCP and LCP not available at DSS-34 and DSS-54 due to having only a single-channel X-band downconverter, thus RCP "or" LCP.
5. DSS-26, -36, -56 n/a for S-band deep-space uplink due to low transmit power (250 W). DSS-54 n/a for S-band deep-space uplink due to frequency restriction.
6. Simultaneous Ka-band RCP and LCP prevents use of RCP monopulse.
7. Simultaneous K-band RCP and LCP not available due to having only a single K-band downconverter, thus RCP "or" LCP.
8. ORANGE highlight = future antennas. GREEN highlight = low-power S-band transmitters. YELLOW highlight = future Ka-band 800 W transmitters.

Table 2. M6 and M7 Reflector Locations and Implementation Dates

ANTENNA	M6 REFLECTORS			M7 REFLECTORS		
	M6-dichroic S/X SSX	M6A(1)-dichroic S/K SSK	M6A(2)-dichroic S/K SSKK	M7-mirror X/Ka XXKa	M7-dichroic X/Ka XXKaKa	M7A-dichroic X/K XXKK
	S-down S-up X-down	S-down S-up K-down	S-down S-up K-down K-up	X-down X-up Ka-down	X-down X-up Ka-down Ka-up	X-down X-up K-down K-up
DSS-23				12/2025		
DSS-24	X	X -->>	10/2023	X		10/2023
DSS-25					X--(6/2028)	
DSS-26	X		X	X		X
DSS-33				9/2028		
DSS-34	X	X -->>	7/2025	X		7/2025
DSS-35				X	9/2026	
DSS-36	X		12/2022	X		12/2022
DSS-53				X		
DSS-54	X	X -->>	9/2026	X		9/2026
DSS-55				X	6/2027	
DSS-56	X	X -->>	4/2024	X		4/2024

NOTES:

1. Mirror/dichroic descriptions current as of date of Module 104.
2. "X" indicates existing mirror/dichroic.

3. "X-->>" indicates that existing M6A(1) dichroic will be replaced by new M6A(2) dichroic on date to the right.
4. Dates for DSS-23 and DSS-33 are new-antenna operational dates with M7-mirror.
5. Dates for M6A(2) and M7A are when antenna will receive dichroics and 250 W K-band uplink.
6. Dates for M7-dichroic are when antenna will receive 800 W Ka-band uplink (DSS-25,35,55) and new M7 dichroic (DSS-35,55).

Table 3. S-Band Transmit Characteristics, DSS-24, -26, -34, -36, -54, and -56

Parameter	Value	Remarks
ANTENNA		
Gain at 2067.5 MHz (center of near-earth band, 2025-2110 MHz)	55.9 +0.2/–0.3 dBi (DSS-24, -26, -34 ,-36, -54, -56)	At peak of gain versus elevation curve, referenced to feedhorn aperture for matched polarization; no atmosphere included; triangular probability density function (PDF) tolerance.
Gain at 2115 MHz (center of deep-space band, 2110-2120 MHz)	56.2 +0.2/–0.3 dBi (DSS-24, -34 only) (DSS-26, -36, -54, -56 n/a for deep space)	At peak of gain versus elevation curve, referenced to feedhorn aperture for matched polarization; no atmosphere included; triangular probability density function (PDF) tolerance
Transmitter Waveguide Loss	0.6 ±0.1 dB 1.0 ±0.1 dB	20-kW transmitter output terminal (waterload switch) to feedhorn aperture (DSS-24,-34,-54) DSS-26,-36,-56, 250-W transmitter
Half-Power Beamwidth	0.263 ±0.020 deg	Angular width (2-sided) between half-power points at specified frequency
Polarization	RCP or LCP	One polarization at a time, remotely selected. Polarization must be the same as received polarization.
Ellipticity	1.0 dB (max)	Peak-to-peak axial ratio defined as the ratio of peak-to-trough received voltages with a rotating linearly polarized source and the feed configured as a circularly (elliptically) polarized receiving antenna.
Pointing Loss		
Angular	See module 302	See also Figure 47.
CONSCAN	0.01 dB	S-band loss using X-band CONSCAN
	0.1 dB	S-band loss using S-band CONSCAN

Table 3. S-Band Transmit Characteristics, DSS-24, -26, -34, -36, -54, and -56 (Continued)

Parameter	Value	Remarks
EXCITER AND TRANSMITTER		
Frequency Range Covered	2025–2120 MHz	Power amplifier is step-tunable over the specified range in six 20-MHz segments, with 5-MHz overlap between segments. Tuning between segments can be accomplished in 30 seconds.
Instantaneous 1-dB bandwidth	20 MHz	
Coherent with near-earth S-band D/L allocation	2028.8–2108.7 MHz	240/221 turnaround ratio
Coherent with deep space S-band D/L channels	2110.2–2117.7 MHz	240/221 turnaround ratio
Coherent with deep space X-band D/L channels	2110.2–2119.8 MHz	880/221 turnaround ratio
RF Power Output		Referenced to transmitter output terminal (waterload switch). Setability is limited to 0.25 dB by measurement equipment precision.
2025–2110 MHz (near-earth band) 2110-2120 MHz (deep-space band)	53.0–73.0 +0.0/-1.0 dBm 54.0 +0.0/-1.0 dBm	DSS-24,-34 (200 W – 20 kW, near-earth and deep-space bands) DSS-54 (200 W − 20 kW, near-earth band only) DSS-26,-36,-56 (250 W, near-earth band only)
Power output varies across the bandwidth and may be as much as 1 dB below nominal rating. Performance will also vary from tube to tube. Normal procedure is to run the tubes saturated, but unsaturated operation is also possible. The point at which saturation is achieved depends on drive power and beam voltage. The 20-kW tubes are normally saturated for power levels greater than 60 dBm (1 kW). Minimum power out of the 20-kW tubes is about 53 dBm (200 W). Efficiency of the tubes drops off rapidly below nominal rated output.		
EIRP (maximum, near-earth band)	128.3 +0.2/–1.0 dBm (DSS-24, -34, -54) 108.9 +0.2/−1.0 dBm (DSS-26, -36, -56)	At gain set elevation angle, referenced to feedhorn aperture
EIRP (maximum, deep-space band)	128.6 +0.2/-1.0 dBm (DSS-24, -34 only)	At gain set elevation angle, referenced to feedhorn aperture. DSS-26, -36, -54, -56 n/a for deep-space.

Table 3. S-Band Transmit Characteristics, DSS-24, -26, -34, -36, -54, and -56 (Continued)

Parameter	Value	Remarks
Tunability		At transmitter output frequency
Phase Continuous Tuning Range	2.0 MHz	
Maximum Tuning Rate	±12.1 kHz/s	
Frequency Error	0.012 Hz	Average over 100 ms with respect to frequency specified by predicts
Ramp Rate Error	0.001 Hz/s	Average over 4.5 s with respect to rate calculated from frequency predicts
Stability		At transmitter output frequency
Output Power Stability		From initial calibration value over 8 hours at a fixed frequency
Saturated Drive	±0.3 dB peak	
Unsaturated Drive	±0.5 dB peak	
Output Power Variation		Across any 600 kHz segment
Saturated Drive	≤0.3 dB p-p	
Unsaturated Drive	≤0.5 dB p-p	
Group Delay Stability	≤ 3.5 ns rms	Ranging modulation signal path (see module 203) over 8 h period
Spurious Output	1–10 Hz -50 dB 10 Hz–1.5 MHz -60 dB 1.5 MHz–8 MHz -45 dB	Below carrier
2nd Harmonic	-85 dB	
3rd Harmonic	–85 dB	
4th Harmonic	–140 dB	At input to X-band horn, with transmitter set for 20-kW output
13th Harmonic		The 13th harmonic of the transmitter lies within the 25.5 – 27.0 GHz allocation for transmitter frequencies from 2025 to 2076.9 MHz and is presently unfiltered – of concern for 20 kW only

Table 4. X Band Transmit Characteristics, DSS-23, -24, -25, -26, -33, -34, -35, -36, -53, -54, -55, and -56

Parameter	Value	Remarks
ANTENNA		
Gain at 7167.5 MHz (center of 7145-7190 MHz deep-space band) Gain at 7212.5 MHz (center of 7190-7235 MHz near-earth band)	66.98 +0.2/–0.3 dBi 67.03 +0.2/-0.3 dBi	At peak of gain versus elevation angle curve, referenced to feedhorn aperture for matched polarization; no atmosphere included; triangular PDF tolerance.
Transmitter Waveguide Loss		20 kW or 80 kW transmitter output terminal (waterload switch) to feedhorn aperture
DSS-24	0.4 ±0.1 dB	20 kW transmitter
DSS-23, -25, -26, -33, -34, -35, -36, -53, -54, -55, -56	0.6 ±0.1 dB 0.7 ±0.1 dB	20 kW transmitter 80 kW transmitter (DSS-26)
Half-Power Beamwidth	0.077 ±0.004 deg	Angular width (2-sided) between half-power points at specified frequency
Polarization	RCP or LCP	One polarization at a time, remotely selected, independent of received polarization.
Ellipticity	1.0 dB (max)	Peak-to-peak axial ratio. See Table 3 for definition.
Pointing Loss		
Angular	See module 302	See also Figure 48.
CONSCAN	0.1 dB	X-band loss with X-band CONSCAN reference set for 0.1 dB loss
EXCITER AND TRANSMITTER		
Frequency range covered	7145–7235 MHz	S-band downlink is not available with X-band uplink because S/X Dichroic Plate will not pass X-band uplink frequencies.
Coherent with deep space X-band D/L channels	7149.6–7188.9 MHz	880/749 turnaround ratio
Coherent with deep space Ka-band D/L allocation	7149.6–7234.6 MHz	3344/749 turnaround ratio. Note: X-band uplink frequencies greater than 7190 MHz are outside deep space X-band uplink allocation.

Table 4. X-Band Transmit Characteristics, DSS-23, -24, -25, -26, -33, -34, -35, -36, -53, -54, -55, and -56 (Continued)

Parameter	Value	Remarks
RF Power Output		Referenced to 20/80-kW transmitter output terminal (waterload switch). Setability is limited to 0.25 dB by measurement equipment precision.
7145.0–7190.0 MHz	53.0–73.0 ±0.5 dBm	Deep-space uplink allocation, 20 kW xmtr.
7145.0–7190.0 MHz	53.0–79.0 ±0.5 dBm	Deep-space uplink allocation, 80 kW xmtr. (DSS-26 only).
7190.0–7235.0 MHz	53.0–73.0 ±0.5 dBm	Near-earth uplink allocation, 20 kW transmitter.
7190.0–7235.0 MHz	53.0–79.0 ±0.5 dBm	Near-earth uplink allocation, 80 kW transmitter (DSS-26 only).
Power output varies across the bandwidth and may be as much as 1 dB below nominal rating. Performance will also vary from tube to tube. Normal procedure is to run the tubes saturated, but unsaturated operation is also possible. The point at which saturation is achieved depends on drive power and beam voltage. Minimum power out of the 20-kW and 80-kW tubes is about 53 dBm (200 W). Efficiency of the tubes drops off rapidly below nominal rated output.		
EIRP (maximum)		At gain set elevation angle, referenced to feedhorn aperture
DSS-24		
7145.0–7190.0 MHz	139.6 ±0.7 dBm	Deep-space allocation, 20 kW transmitter.
7190.0–7235.0 MHz	139.7 ±0.7 dBm	Near-earth allocation, 20 kW transmitter.
DSS-23, -25, -26, -33, -34, -35, -36, -53, -54, -55, -56		
7145.0–7190.0 MHz	139.4 ±0.7 dBm	Deep-space allocation, 20 kW transmitter.
7145.0–7190.0 MHz	145.2 ±0.7 dBm	Deep-space allocation, 80 kW transmitter (DSS-26 only).
7190.0–7235.0 MHz	139.5 ±0.7 dBm	Near-earth allocation, 20 kW transmitter.
7190.0–7235.0 MHz	145.3 ±0.7 dBm	Near-earth allocation, 80 kW transmitter (DSS-26 only).

Table 4. X-Band Transmit Characteristics, DSS-23, -24, -25, -26, -33, -34, -35, -36, -53, -54, -55, and -56 (Continued)

Parameter	Value	Remarks
Tunability		At transmitter output frequency
Phase Continuous Tuning Range	2.0 MHz	
Maximum Tuning Rate	±12.1 kHz/s	
Frequency Error	0.012 Hz	Average over 100 ms with respect to frequency specified by predicts
Ramp Rate Error	0.001 Hz/s	Average over 4.5 s with respect to rate calculated from frequency predicts
Stability		At transmitter output frequency
Output Power Stability		From initial calibration value over 8 hours at a fixed frequency
Saturated Drive	±0.3 dB peak	
Unsaturated Drive	±0.5 dB peak	
Output Power Variation		Across any 2 MHz segment
Saturated Drive	≤0.3 dB p-p	
Unsaturated Drive	≤0.5 dB p-p	
Group Delay Stability	≤ 1.5 ns rms	Ranging modulation signal path over 8 h period (see module 203)
Spurious Output		Below carrier
1–10 Hz	–50 dB	
10 Hz–1.5 MHz	–60 dB	
1.5 MHz–8 MHz	–45 dB	
2nd Harmonic	–75 dB	
3rd, 4th & 5th Harmonics	–60 dB	

Table 5. K-band Transmit Characteristics, DSS-24, -26, -34, -36, -54, and -56

Parameter	Value	Remarks
ANTENNA		
Gain at 22850 MHz (center of 22550-23150 MHz near-earth band)	76.1 +0.2/-0.3 dB	At peak of gain versus elevation angle curve, referenced to feedhorn aperture for matched polarization; no atmosphere included; triangular PDF tolerance.
Transmitter Waveguide Loss	2.4 ±0.1 dB	250W power amplifier output terminal (before filters) to feedhorn aperture
Half-Power Beam width	0.024 ±0.002 deg	Angular width (2-sided) between half-power points at specified frequency
Polarization	RCP or LCP	One polarization at a time, remotely selected, independent of received polarization.
Ellipticity	1.0 dB (max)	Peak-to-peak axial ratio. See Table 3 for definition.
Pointing Loss		
Angular	See module 302	See also Figure 48.
CONSCAN	0.1 dB	K-band loss with K-band CONSCAN reference set for 0.1 dB loss
EXCITER AND TRANSMITTER		
Frequency range covered	22550 - 23150 MHz	Near-earth allocation, 250W transmitter. See implementation dates in Section 3.
	22565.6 - 23150 MHz 22550 - 23150 MHz 22550 - 23078.5 MHZ	2720/2407 turnaround ratio 2760/2407 turnaround ratio 2816/2407 turnaround ratio
RF Power Output	40.0 – 54.0 ±0.5 dBm (10W – 250W)	Referenced to 250W transmitter power amplifier output terminal (before filters and air load switch). Setability is limited to 0.25 dB by measurement equipment precision.
EIRP (maximum)	127.7 ±0.7 dBm	At gain set elevation angle, referenced to feedhorn aperture

Table 5. K-Band Transmit Characteristics, DSS-24, -26, -34, -36, -54 and -56 (Continued)

Parameter	Value	Remarks
Tunability		At transmitter output frequency
Phase Continuous Tuning Range	4.0 MHz	
Maximum Tuning Rate	±60.5 kHz/s	
Frequency Error	0.012 Hz	Average over 100 ms with respect to frequency specified by predicts
Ramp Rate Error	0.001 Hz/s	Average over 4.5 s with respect to rate calculated from frequency predicts
Stability		At transmitter output frequency
Output Power Stability	±0.5 dB peak	From initial calibration value over 8 hours at a fixed frequency
Output Power Variation	≤0.5 dB p-p	Across any 10 MHz segment
Group Delay Stability	≤1.0 ns rms	Ranging modulation signal path over 8 h period (see module 203)
Spurious Output		Below carrier
1–10 Hz	–50 dBc	
10 Hz–100 MHz	–50 dBc	
2nd Harmonic	–29 dBc	
3rd, 4th, 5th Harmonics	–54 dBc	

Table 6. Ka-Band Transmit Characteristics, DSS-25

Parameter	Value	Remarks
ANTENNA		
Gain at 34450 MHz		At peak of gain versus elevation angle curve, referenced to feedhorn aperture for matched polarization; no atmosphere included; triangular PDF tolerance.
X/Ka-mode	79.03 +0.2/–0.3 dBi	
Transmitter Waveguide Loss	0.25 ±0.1 dB	300 W transmitter output terminal (waterload switch) to feedhorn aperture
Half-Power Beamwidth	0.016 ±0.001 deg	Angular width (2-sided) between half-power points at specified frequency
Polarization	LCP	RCP is available by changing mechanical configuration of feed
Ellipticity	1.0 dB (max)	Peak-to-peak axial ratio. See Table 3. for definition.
Pointing Loss	0.12 dB	Monopulse aided tracking with minimum required signal level
Angular	See module 302	See also Figure 49 and Figure 50.

Table 6. Ka-Band Transmit Characteristics, DSS-25 (Continued)

Parameter	Value	Remarks
EXCITER AND TRANSMITTER		
Frequency range covered		
Exciter	34200-34700 MHz	
Transmitter	34315-34415 MHz	
Coherent with deep space Ka-band D/L channels	34317.8-34406.3 MHz	3360/3599 turnaround ratio
Coherent with deep space X-band D/L channels	34354.3-34409.8 MHz	880/3599 turnaround ratio
RF Power Output	47.0–54.8 ±0.5 dBm 59.0 dBm	Referenced to 300 W transmitter output terminal (transmitter RF drawer rear panel flange). Settability is limited to 0.25 dB by measurement equipment precision. 800 W transmitter (DSS-25 in 6/2028, DSS-35 in 9/2026, DSS-55 in 6/2027)
Minimum power output is about 47 dBm (50 W) and may operate unsaturated.		
EIRP (maximum)	133.6 +0.6/-0.5 dBm	At gain set elevation angle, referenced to feedhorn aperture. 300 W transmitter.
Output Power Variation	$\leq \pm$1.0 dB	Across frequency band over 8 hours
Spurious Output		Below carrier
1–10 Hz	–50 dB	
10 Hz–1.5 MHz	–60 dB	

Table 7. S- and K-Band Receive Characteristics, DSS-24, -26, -34, -36, -54, and -56

Parameter	Value	Remarks
ANTENNA		
Gain		At peak of gain versus elevation angle curve, referenced to feedhorn aperture (feed and feedline losses are accounted for in system temperature), for matched polarization; no atmosphere included; triangular PDF tolerance. See Figure 13 and Figures 21 – 23 for representative gain versus elevation curves.
S-band (2295 MHz)	56.74 +0.1/–0.2 dBi	
K-band (26250 MHz)	77.2 +0.0/–0.2 dBi	See implementation dates in Section 3.
Half-Power Beamwidth		Angular width (2-sided) between half-power points at specified frequency
S-band	0.242 ±0.020 deg	
K-band	0.021 ±0.002 deg	
Polarization	RCP or LCP	Remotely selected. S-band must be same as transmit polarization
Ellipticity	≤1.0 dB	Peak-to-peak voltage axial ratio, RCP and LCP. See definition in Table 3.
Pointing Loss		
Angular	See module 302	See also Figure 47 and Figure 49.
CONSCAN	0.1 dB	Recommended value for S-, X, or K-band tracking
S-BAND RECEIVER		
Frequency Range Covered	2200–2300 MHz	
Recommended Maximum Signal Power	-85.0 dBm	At HEMT input terminal
Antenna-Microwave Noise Temperature (T_{AMW})		Near zenith, no atmosphere or cosmic noise included. See also Table 11. Favorable (–) and adverse (+) tolerances have triangular PDF.
Non-Diplexed Path		Referenced to feedhorn aperture. LNA = HEMT-1
DSS-24	26.10 –1.0/+2.0 K	
DSS-26	17.60 –1.0/+2.0 K	
DSS-34	24.88 –1.0/+/2.0 K	
DSS-36	21.57 –1.0/+2.0 K	
DSS-54	25.73 –1.0/+2.0 K	

Table 7. S- and K-Band Receive Characteristics, DSS-24, -26, -34, -36, -54, and -56 (Continued)

Parameter	Value	Remarks
S-BAND RECEIVER (Continued)		
DSS-56	20.63 –1.0/+2.0 K	
Diplexed Path	Add 8.00 K to above	DSS-24, -26, -34, -36, -54, -56
K-BAND RECEIVER		
Frequency Range Covered	25500–27000 MHz	
Recommended Maximum Signal Power		At HEMT input terminal
Normal Mode	–85.0 dBm	
Low-gain Mode	–65.0 dBm	For high received power levels
Antenna-Microwave Noise Temperature (T_{AMW})		RCP/LCP average at 26000 MHz. Referenced to feedhorn aperture. See also Table 11.
DSS-24 K-only mode	20.7 –1.0/+3.0 K	
DSS-24 S/K-mode	26.5 –1.0/+3.0 K	
DSS-26 K-only mode	31.3 –1.0/+3.0 K	
DSS-26 S/K mode	39.9 –1.0/+3.0 K	
DSS-34 K-only mode	25.6 –1.0/+3.0 K	.
DSS-34 S/K-mode	31.4 –1.0/+3.0 K	
DSS-36 K-only mode	Not presently available	Available in 12/2022
DSS-36 S/K mode	Not presently available	Available in 12/2022
DSS-54 K-only mode	28.8 –1.0/+3.0 K	
DSS-54 S/K-mode	34.6 –1.0/+3.0 K	
DSS-56 K-only mode	33.8 –1.0/+3.0 K	
DSS-56 S/K-mode	39.6 –1.0/+3.0 K	
Low-Gain Mode		Required for signal levels in excess of –85.0 dBm
K-only (All Stations)	156 –11.0/+33.0 K	
S/K-only (All Stations)	185 –11.0/+33.0 K	
Tunability	1 Hz resolution	
Carrier Tracking Loop Noise B/W	0.1% of symbol rate	Effective one-sided, noise-equivalent carrier loop bandwidth (B_L)
Symbol Loop Acquisition B/W	0.3% of symbol rate	

Table 8. X-Band Receive Characteristics, DSS-24

Parameter	Value	Remarks
MAIN ANTENNA		
Gain (8425 MHz)		At peak of gain versus elevation angle curve, referenced to feedhorn aperture (feed and feedline losses are accounted for in system temperature), for matched polarization; no atmosphere included; triangular PDF tolerance.
X-only Mode	68.24 +0.1/–0.2 dBi	S/X and S/K dichroic plates retracted.
S/X Mode	68.19 +0.1/–0.2 dBi	S/X dichroic plate extended.
Half-Power Beamwidth	0.066 ±0.004 deg	Angular width (2-sided) between half-power points at specified frequency
Polarization	RCP or LCP	Remotely Selected. Same as or opposite from transmit polarization
Ellipticity	≤0.7 dB	Peak-to-peak voltage axial ratio, RCP and LCP. See definition in Table 3..
Pointing Loss		
Angular	See module 302	See also Figure 48.
CONSCAN	0.1 dB	Recommended value when using X-band CONSCAN reference
RECEIVER		
Frequency Range Covered	8400–8500 MHz	
Recommended Maximum Signal Power	-90.0 dBm	At maser input terminal
Antenna-Microwave Noise Temperature (T_{AMW})	Low-gain mode add +20 K to values below	Near zenith, no atmosphere or cosmic noise included. See also Table 11. Favorable (–) and adverse (+) tolerances have triangular PDF.
Non-Diplexed Path (8400–8500 MHz) LNA = MASER-1	21.28 –1.0/+2.0 K	X-band-only operation (S/X-band dichroic plate retracted). Referenced to feedhorn aperture.
Diplexed Path (8400–8500 MHz) LNA = MASER-1	30.39 –1.0/+2.0 K	X-band-only operation (S/X-band dichroic plate retracted). Referenced to feedhorn aperture.
Non-Diplexed Path (8400–8500 MHz) LNA = MASER-1	22.72 –1.0/+2.0 K	S/X-band operation (S/X-band dichroic plate extended). Referenced to feedhorn aperture.
Diplexed Path (8400–8500 MHz) LNA = MASER-1	31.89 –1.0/+2.0 K	S/X-band operation (S/X-band dichroic plate extended). Referenced to feedhorn aperture.
Tunability	Continuous	
Carrier Tracking Loop Noise B/W (Hz)	0.25 – 200	Effective one-sided, noise-equivalent carrier loop bandwidth (B_L)

Table 8. X-Band Receive Characteristics, DSS-24 (Continued)

Parameter	Value	Remarks
ACQUISITION ANTENNA AND RECEIVER – DSS-24		
Gain (8425 MHz)	38.0 ±0.5 dB	Referenced to acquisition downconverter input terminals (includes feedline losses)
Half-Power Beamwidth	2.1 deg	Angular width (2-sided) between half-power points at specified frequency
Polarization	RCP	LCP is available by manual selection at feed
Frequency Range Covered	8400–8500 MHz	
System Temperature	280 ±30K.	Near Zenith
Tracking Bandwidths		Two-sided bandwidths
Residual Carrier	4 kHz	
Frequency Acquisition	±150 kHz	
Doppler Tracking	±400 kHz	
Suppressed Carrier	280 kHz	Open-loop operation
Tunability	1 kHz resolution	
Signal Acquisition Range		
Residual Carrier	–90 to –135 dBm	
Suppressed Carrier	–90 to –119 dBm.	

Table 9. X- and Ka-Band Receive Characteristics, DSS-23, -25, -26, -33, -34, -35, -36, -53, -54, -55, and -56

Parameter	Value	Remarks
MAIN ANTENNA		
Gain		At peak of gain versus elevation angle curve, referenced to feedhorn aperture (feed and feedline losses are accounted for in system temperature), for matched polarization; no atmosphere included; triangular PDF tolerance. See Figures 14 – 20 and Figures 24 – 29 for representative gain versus elevation curves.
X-band (8425 MHz)	68.27 +0.1/–0.2 dBi	DSS-26, -34, -36, -54, -56, S/X-band operation (S/X dichroic plate extended). DSS-23, -25, -33, -35, -53, -55 do not have S-band capability.
X-band (8425 MHz)	68.32 +0.1/–0.2 dBi	DSS-23, -25, -26, -33, -34, -35, -36, -53, -54, -55, -56, X/Ka-band operation
Ka-band (32050 MHz)	79.0 +0.3/–0.3 dBi	DSS-23, -25, -26, -33, -34, -35, -36, -53, -54, -55, -56, X/Ka-band operation
Half-Power Beamwidth		Angular width (2-sided) between half-power points at specified frequency
X-band	0.066 ±0.004 deg	
Ka-band	0.017 ±0.002 deg	
Polarization		
X-band DSS-23, -25, -26, -33, -35, -36, -53, -55, -56	RCP and LCP	Simultaneously
X-band DSS-24, -34, -54	RCP or LCP	Remotely selected. Independent of transmit polarization. Only one X-band downconverter at DSS-34/-54, thus “or”.
Ka-band DSS-23, -25, -26, -33, -34, -35, -36, -53, -54, -55, & -56	RCP and LCP	Monopulse is available only at RCP.
Ellipticity		Peak-to-peak voltage axial ratio. See definition in Table 3.
X-band	≤0.7 dB	RCP and LCP
Ka-band	≤1.0 dB	RCP and LCP
Pointing Loss		
Angular	See module 302	See also Figures 48 and 49.
CONSCAN		
X-band	0.1 dB	Recommended value when using X-band CONSCAN

Table 9. X- and Ka-Band Receive Characteristics, DSS-23, -25, -26, -33, -34, -35, -36, -53, -54, -55, and -56 (Continued)

Parameter	Value	Remarks
Ka-band	0.1 dB	Recommended value when using Ka-band CONSCAN if monopulse not available or for dual-polarization Ka-band reception.
Monopulse		
X-band	0.007 dB	Using Ka-band monopulse reference
Ka-band	0.11 dB	Sum channel signal to error channel noise ratio ≥ 26 dB-Hz
RECEIVER		
Frequency Ranges		
X-band	8200-8600 MHz	General frequency range. Specific antenna bandwidth restrictions listed below.
Ka-band	31800–32300 MHz	Tracking receiver covers bandwidth with 5 overlapping bands of 160 MHz
Recommended Maximum Signal Power	-85.0 dBm -65.0 dBm	At HEMT input terminal (DSS-23, -25, -26, -33, -34, -35, -36, -53, -54, -55, -56) At HEMT input terminal (DSS-23, -25, -26, -33, -34, -35, -36, -53, -54, -55, -56) for high received power level in low-gain mode.
Antenna-Microwave Noise Temperature (T_{AMW})	Low-gain mode add +20 K for X-band, +70 K for Ka-band, to values below	Near zenith, no atmosphere or cosmic noise included. See also Table 11. Favorable (–) and adverse (+) tolerances have triangular PDF.
X-band (8200–8600 MHz)		DSS-23,-25,-26,-33,-34,-35,-36,-53,-54,-55,-56 with always-diplexed dual-HEMT X/X/Ka feed. With or without transmitter operating. Referenced to feedhorn aperture.
DSS-23 (RCP)	TBD	X/Ka-mode, LNA = HEMT-1
DSS-23 (RCP)	TBD	X/Ka-mode, LNA = HEMT 2
DSS-25 (RCP)	16.2 –1.0/+2.0 K	X/Ka-mode, LNA = HEMT-1
DSS-25 (LCP)	16.0 –1.0/+2.0 K	X/Ka-mode, LNA = HEMT-2
DSS-26 (RCP)	16.29 –1.0/+2.0 K	X/Ka-mode, LNA = HEMT-1
DSS-26 (LCP)	15.43 –1.0/+2.0 K	X/Ka-mode, LNA = HEMT-2
DSS-26 (RCP)	18.01 –1.0/+2.0 K	S/X-mode, LNA = HEMT-1
DSS-26 (LCP)	17.15 –1.0/+2.0 K	S/X-mode, LNA = HEMT-2
DSS-33 (RCP)	TBD	X/Ka-mode, LNA = HEMT-1
DSS-33 (LCP)	TBD	X/Ka-mode, LNA = HEMT-2
DSS-34 (RCP)	16.28 –1.0,+2.0 K	X/Ka-mode, LNA = HEMT-1

Table 9. X- and Ka-Band Receive Characteristics, DSS-23, -25, -26, -33, -34, -35, -36, -53, -54, -55, and -56 (Continued)

Parameter	Value	Remarks
DSS-34 (LCP)	16.71 –1.0/+2.0 K	X/Ka-mode, LNA = HEMT-2
DSS-34 (RCP)	17.99 –1.0/+2.0 K	S/X-mode, LNA = HEMT-1
DSS-34 (LCP)	18.43 –1.0/+2.0 K	S/X-mode, LNA = HEMT-2
DSS-35 (RCP)	14.7 –1.0/+2.0 K	X/Ka-mode, LNA = HEMT-1
DSS-35 (LCP)	15.0 –1.0/+2.0 K	X/Ka-mode, LNA = HEMT-2
DSS-36 (RCP)	12.59 –1.0/+2.0 K	X/Ka-mode, LNA = HEMT-1
DSS-36 (LCP)	13.95 –1.0/+2.0 K	X/Ka-mode, LNA = HEMT-2
DSS-36 (RCP)	14.31 –1.0/+2.0 K	S/X-mode, LNA = HEMT-1
DSS-36 (LCP)	15.67 –1.0/+2.0 K	S/X-mode, LNA = HEMT-2
DSS-53 (RCP)	13.1 –1.0/+2.0 K	X/Ka-mode, LNA = HEMT-1
DSS-53 (LCP)	13.2 –1.0/+2.0 K	X/Ka-mode, LNA = HEMT-2
DSS-54 (RCP)	18.31 –1.0/+2.0 K	X/Ka-mode, LNA = HEMT-1
DSS-54 (LCP)	18.31 –1.0/+2.0 K	X/Ka-mode, LNA = HEMT-2
DSS-54 (RCP)	20.03 –1.0/+2.0 K	S/X-mode, LNA = HEMT-1
DSS-54 (LCP)	20.03 –1.0/+2.0 K	S/X-mode, LNA = HEMT-2
DSS-55 (RCP)	17.42 –1.0/+2.0 K	X/Ka-mode, LNA = HEMT-1
DSS-55 (LCP)	17.82 –1.0/+2.0 K	X/Ka-mode, LNA = HEMT-2
DSS-56 (RCP)	14.47 –1.0/+2.0 K	X/Ka-mode, LNA = HEMT-1
DSS-56 (LCP)	13.96 –1.0/+2.0 K	X/Ka-mode, LNA = HEMT-2
DSS-56 (RCP)	16.19 –1.0/+2.0 K	S/X-mode, LNA = HEMT-1
DSS-56 (LCP)	15.68 –1.0/+2.0 K	S/X-mode, LNA = HEMT-2
Ka-band (31800–32300 MHz)		X/Ka-band operation referenced to feedhorn aperture,
DSS-23 (RCP)	TBD	LNA = HEMT-1
DSS-23 (RCP Error)	TBD	LNA = HEMT-2
DSS-23 (LCP)	TBD	LNA = HEMT-3
DSS-25 (RCP)	24.2 –1.0/+2.0 K	LNA = HEMT-1
DSS-25 (RCP Error)	25.7 –1.0/+2.0 K	LNA = HEMT-2
DSS-25 (LCP)	23.0 –1.0/+2.0 K	LNA = HEMT-3
DSS-26 (RCP)	19.36 –1.0/+2.0 K	LNA = HEMT-1
DSS-26 (RCP Error)	24.55 –1.0/+2.0 K	LNA = HEMT-2
DSS-26 (LCP)	20.77 –1.0/+2.0 K	LNA = HEMT-3
DSS-33 (RCP)	TBD	LNA = HEMT-1
DSS-33 (RCP Error)	TBD	LNA = HEMT-2
DSS-33 (LCP)	TBD	LNA = HEMT-3
DSS-34 (RCP)	19.38 –1.0/+2.0 K	LNA = HEMT-1

Table 9. X- and Ka-Band Receive Characteristics, DSS-23, -25, -26, -33, -34, -35, -36, -53, -54, -55, and -56 (Continued)

Parameter	Value	Remarks
DSS-34 (RCP Error)	23.25 –1.0/+2.0 K	LNA = HEMT-2
DSS-34 (LCP)	19.61 –1.0/+2.0 K	LNA = HEMT-3
DSS-35 (RCP)	17.3 –1.0/+2.0 K	LNA = HEMT-1
DSS-35 (RCP Error)	TBD	LNA = HEMT-2
DSS-35 (LCP)	17.2 –1.0/+2.0 K	LNA = HEMT-3
DSS-36 (RCP)	12.54 –1.0/+2.0 K	LNA = HEMT-1
DSS-36 (RCP Error)	TBD	LNA = HEMT-2
DSS-36 (LCP)	12.18 –1.0/+2.0 K	LNA = HEMT-3
DSS-53 (RCP)	13.0 –1.0/+2.0 K	LNA = HEMT-1
DSS-53 (RCP Error)	18.0 –1.0/+2.0 K	LNA = HEMT-2
DSS-53 (LCP)	13.4 –1.0/+2.0 K	LNA = HEMT-3
DSS-54 (RCP)	21.80 –1.0/+2.0 K	LNA = HEMT-1
DSS-54 (RCP Error)	25.00 –1.0/+2.0 K	LNA = HEMT-2
DSS-54 (LCP)	21.80 –1.0/+2.0 K	LNA = HEMT-3
DSS-55 (RCP)	20.80 –1.0/+2.0 K	LNA = HEMT-1
DSS-55 (RCP Error)	21.98 –1.0/+2.0 K	LNA = HEMT-2
DSS-55 (LCP)	19.83 –1.0/+2.0 K	LNA = HEMT-3
DSS-56 (RCP)	16.5 –1.0/+2.0 K	LNA = HEMT-1
DSS-56 (RCP Error)	TBD	LNA = HEMT-2
DSS-56 (LCP	17.0 –1.0/+2.0 K	LNA = HEMT-3
Carrier Tracking Loop Noise B/W	0.25 – 200 Hz	Effective one-sided, noise-equivalent carrier loop bandwidth (B_L). See module 202

Table 9. X- and Ka-Band Receive Characteristics, DSS-23, -25, -26, -33, -34, -35, -36, -53, -54, -55, and -56 (Continued)

Parameter	Value	Remarks
ACQUISITION ANTENNA AND RECEIVER – DSS-34 AND DSS-54		
Gain (8425 MHz)	38.0 ±0.5 dB	Referenced to acquisition downconverter input terminals (includes feedline losses)
Half-Power Beamwidth	2.1 deg	Angular width (2-sided) between half-power points at specified frequency
Polarization	RCP	LCP is available by manual selection at feed
Frequency Range Covered	8400–8500 MHz	
System Temperature	280 ±30K.	Near Zenith
Tracking Bandwidths		Two-sided bandwidths
Residual Carrier	4 kHz	
Frequency Acquisition	±150 kHz	
Doppler Tracking	±400 kHz	
Suppressed Carrier	280 kHz	Open-loop operation
Tunability	1 kHz resolution	
Signal Acquisition Range		
Residual Carrier	–90 to –135 dBm	
Suppressed Carrier	–90 to –119 dBm.	

Table 10. Gain Reduction Due to Wind Effects on Structural Deformation and Pointing Error

Wind Speed		Gain Reduction (dB)*			
(km/hr)	(mph)	S-Band	X-Band	K-Band	Ka-Band
10	6	negligible	negligible	0.02	0.03
30	18	negligible	0.02	0.19	0.29
50	30	negligible	0.06	0.53	0.80

* Maximum total combined effects of structural deformation and pointing error at various wind speeds.

Table 11. T_{AMW}, T_{sky}, and T_{op} for CD=25% Average Clear Weather at Zenith, Referenced to Feedhorn Aperture

Frequency, Station, and Configuration	Noise Temperatures, K		
	T_{AMW}	T_{sky}	T_{op}
S-band, DSS-24, S/X or S/K, HEMT-1, RCP or LCP, non-diplexed	26.10	4.68	30.78
S-band, DSS-24, S/X or S/K, HEMT-1, RCP or LCP, diplexed	33.47	4.68	38.15
S-band, DSS-26, S/X or S/K, HEMT-1, RCP or LCP, non-diplexed	17.6	4.68	22.3
S-band, DSS-26, S/X or S/K, HEMT-1, RCP or LCP, diplexed	23.4	4.68	28.1
S-band, DSS-34, S/X or S/K, HEMT-1, RCP or LCP, non-diplexed	24.88	4.86	29.74
S-band, DSS-34, S/X or S/K, HEMT-1, RCP or LCP, diplexed	34.46	4.86	39.32
S-band, DSS-36, S/X or S/K, HEMT-1, RCP or LCP, non-diplexed	21.57	4.86	26.43
S-band, DSS-36, S/X or S/K, HEMT-1, RCP or LCP, diplexed	30.43	4.86	35.29
S-band, DSS-54, S/X or S/K, HEMT-1, RCP or LCP, non-diplexed	25.73	4.80	30.53
S-band, DSS-54, S/X or S/K, HEMT-1, RCP or LCP, diplexed	35.35	4.80	40.15
S-band, DSS-56, S/X or S/K, HEMT-1, RCP or LCP, non-diplexed	20.63	4.80	25.43
S-band, DSS-56, S/X or S/K, HEMT-1, RCP or LCP, diplexed	27.33	4.80	32.13
X-band, DSS-23, X/Ka, HEMT-1, RCP, diplexed	TBD	5.04	TBD
X-band, DSS-23, X/Ka, HEMT-2, LCP, diplexed	TBD	5.04	TBD
X-band, DSS-24, X-only, MASER-1, RCP or LCP, non-diplexed	21.28	5.04	26.32
X-band, DSS-24, X-only, MASER-1, RCP or LCP, diplexed	30.39	5.04	35.43
X-band, DSS-24, S/X, MASER-1, RCP or LCP, non-diplexed	22.72	5.04	27.76
X-band, DSS-24, S/X, MASER-1, RCP or LCP, diplexed	31.89	5.04	36.93
X-band, DSS-25, X/Ka, HEMT-1, RCP, diplexed	16.2	5.04	21.2
X-band, DSS-25, X/Ka, HEMT-2, LCP, diplexed	16.0	5.04	21.0
X-band, DSS-26, X/Ka, HEMT-1, RCP, diplexed	16.29	5.04	21.33
X-band, DSS-26, X/Ka, HEMT-2, LCP, diplexed	15.43	5.04	20.47
X-band, DSS-26, S/X, HEMT-1, RCP, diplexed	18.01	5.04	23.05
X-band, DSS-26, S/X, HEMT-2, LCP, diplexed	17.15	5.04	22.19
X-band, DSS-33, X/Ka, HEMT-1, RCP, diplexed	TBD	5.39	TBD
X-band, DSS-33, X/Ka, HEMT-2, LCP, diplexed	TBD	5.39	TBD
X-band, DSS-34, X/Ka, HEMT-1, RCP, diplexed	16.28	5.39	21.67
X-band, DSS-34, X/Ka, HEMT-2, LCP, diplexed	16.71	5.39	22.10
X-band, DSS-34, S/X, HEMT-1, RCP, diplexed	17.99	5.39	23.38
X-band, DSS-34, S/X, HEMT-2, LCP, diplexed	18.43	5.39	23.82
X-band, DSS-35, X/Ka, HEMT-1, RCP, diplexed	14.7	5.39	20.09
X-band, DSS-35, X/Ka, HEMT-2, LCP, diplexed	15.0	5.39	20.45
X-band, DSS-36, X/Ka, HEMT-1, RCP, diplexed	12.59	5.39	17.98
X-band, DSS-36, X/Ka, HEMT-2, LCP, diplexed	13.95	5.39	19.34
X-band, DSS-36, S/X, HEMT-1, RCP, diplexed	14.31	5.39	19.70
X-band, DSS-36, S/X, HEMT-2, LCP, diplexed	15.67	5.39	21.06

Table 11. T_{AMW}, T_{sky}, and T_{op} for CD=25% Average Clear Weather at Zenith, Referenced to Feedhorn Aperture (Continued)

Frequency, Station, and Configuration	Noise Temperatures, K		
	T_{AMW}	T_{sky}	T_{op}
X-band, DSS-53, X/Ka, HEMT-1, RCP, diplexed	13.1	5.27	18.37
X-band, DSS-53, X/Ka, HEMT-2, LCP, diplexed	13.2	5.27	18.47
X-band, DSS-54, X/Ka, HEMT-1, RCP, diplexed	18.31	5.27	23.58
X-band, DSS-54, X/Ka, HEMT-2, LCP, diplexed	18.31	5.27	23.58
X-band, DSS-54, S/X, HEMT-1, RCP, diplexed	20.03	5.27	25.30
X-band, DSS-54, S/X, HEMT-2, LCP, diplexed	20.03	5.27	25.30
X-band, DSS-55, X/Ka, HEMT-1, RCP, diplexed	17.42	5.27	22.69
X-band, DSS-55, X/Ka, HEMT-2, LCP, diplexed	17.82	5.27	23.09
X-band, DSS-54, X/Ka, HEMT-1, RCP, diplexed	14.47	5.27	19.74
X-band, DSS-54, X/Ka, HEMT-2, LCP, diplexed	13.96	5.27	19.23
X-band, DSS-54, S/X, HEMT-1, RCP, diplexed	16.19	5.27	21.46
X-band, DSS-54, S/X, HEMT-2, LCP, diplexed	15.68	5.27	20.95
K-band, DSS-24, K-only, HEMT-1, RCP, non-diplexed, 25.5 GHz	19.8	10.3	30.1
K-band, DSS-24, K-only, HEMT-2, LCP, non-diplexed, 25.5 GHz	27.3	10.3	37.6
K-band, DSS-24, S/K, HEMT-1, RCP, non-diplexed, 25.5 GHz	30.4	10.3	40.7
K-band, DSS-24, S/K, HEMT-2, LCP, non-diplexed, 25.5 GHz	37.9	10.3	48.2
K-band, DSS-24, K-only, HEMT-1, RCP, non-diplexed, 26.0 GHz	17.7	10.1	27.8
K-band, DSS-24, K-only, HEMT-2, LCP, non-diplexed, 26.0 GHz	23.7	10.1	33.8
K-band, DSS-24, S/K, HEMT-1, RCP, non-diplexed, 26.0 GHz	23.6	10.1	33.7
K-band, DSS-24, S/K, HEMT-2, LCP, non-diplexed, 26.0 GHz	29.6	10.1	39.7
K-band, DSS-24, K-only, HEMT-1, RCP, non-diplexed, 27.0 GHz	21.0	10.1	31.1
K-band, DSS-24, K-only, HEMT-2, LCP, non-diplexed, 27.0 GHz	25.6	10.1	35.7
K-band, DSS-24, S/K, HEMT-1, RCP, non-diplexed, 27.0 GHz	30.6	10.1	40.7
K-band, DSS-24, S/K, HEMT-2, LCP, non-diplexed, 27.0 GHz	35.2	10.1	45.3
K-band, DSS-26, K-only, HEMT-1, RCP, diplexed, 26.0 GHz	31.8	10.1	41.9
K-band, DSS-26, K-only, HEMT-2, LCP, diplexed, 26.0 GHz	30.8	10.1	40.9
K-band, DSS-26, S/K, HEMT-1, RCP, diplexed, 26.0 GHz	40.4	10.1	50.5
K-band, DSS-26, S/K, HEMT-2, LCP, diplexed, 26.0 GHz	39.4	10.1	49.5
K-band, DSS-34, K-only, HEMT-1, RCP, non-diplexed, 25.5 GHz	25.1	13.3	38.4
K-band, DSS-34, K-only, HEMT-2, LCP, non-diplexed, 25.5 GHz	26.5	13.3	39.8
K-band, DSS-34, S/K, HEMT-1, RCP, non-diplexed, 25.5 GHz	35.7	13.3	49.0
K-band, DSS-34, S/K, HEMT-2, LCP, non-diplexed, 25.5 GHz	37.1	13.3	50.4
K-band, DSS-34, K-only, HEMT-1, RCP, non-diplexed, 26.0 GHz	25.5	13.0	38.5
K-band, DSS-34, K-only, HEMT-2, LCP, non-diplexed, 26.0 GHz	25.6	13.0	38.6
K-band, DSS-34, S/K, HEMT-1, RCP, non-diplexed, 26.0 GHz	31.4	13.0	44.4

Table 11. T_{AMW}, T_{sky}, and T_{op} for CD=25% Average Clear Weather at Zenith, Referenced to Feedhorn Aperture (Continued)

Frequency, Station, and Configuration	Noise Temperatures, K		
	T_{AMW}	T_{sky}	T_{op}
K-band, DSS-34, S/K, HEMT-2, LCP, non-diplexed, 26.0 GHz	31.5	13.0	44.5
K-band, DSS-34, K-only, HEMT-1, RCP, non-diplexed, 27.0 GHz	23.9	12.8	36.7
K-band, DSS-34, K-only, HEMT-2, LCP, non-diplexed, 27.0 GHz	24.7	12.8	37.5
K-band, DSS-34, S/K, HEMT-1, RCP, non-diplexed, 27.0 GHz	33.5	12.8	46.3
K-band, DSS-34, S/K, HEMT-2, LCP, non-diplexed, 27.0 GHz	34.3	12.8	47.1
K-band, DSS-36, K-only, HEMT-1, RCP, non-diplexed, 26.0 GHz	TBD	13.0	TBD
K-band, DSS-36, K-only, HEMT-2, LCP, non-diplexed, 26.0 GHz	TBD	13.0	TBD
K-band, DSS-36, S/K, HEMT-1, RCP, non-diplexed, 26.0 GHz	TBD	13.0	TBD
K-band, DSS-36, S/K, HEMT-2, LCP, non-diplexed, 26.0 GHz	TBD	13.0	TBD
K-band, DSS-54, K-only, HEMT-1, RCP, non-diplexed, 25.5 GHz	28.4	11.9	40.3
K-band, DSS-54, K-only, HEMT-2, LCP, non-diplexed, 25.5 GHz	30.9	11.9	42.8
K-band, DSS-54, S/K, HEMT-1, RCP, non-diplexed, 25.5 GHz	39.0	11.9	50.9
K-band, DSS-54, S/K, HEMT-2, LCP, non-diplexed, 25.5 GHz	41.5	11.9	53.4
K-band, DSS-54, K-only, HEMT-1, RCP, non-diplexed, 26.0 GHz	28.3	11.7	40.0
K-band, DSS-54, K-only, HEMT-2, LCP, non-diplexed, 26.0 GHz	29.2	11.7	40.9
K-band, DSS-54, S/K, HEMT-1, RCP, non-diplexed, 26.0 GHz	34.2	11.7	45.9
K-band, DSS-54, S/K, HEMT-2, LCP, non-diplexed, 26.0 GHz	35.1	11.7	46.8
K-band, DSS-54, K-only, HEMT-1, RCP, non-diplexed, 27.0 GHz	26.9	11.6	38.5
K-band, DSS-54, K-only, HEMT-2, LCP, non-diplexed, 27.0 GHz	26.8	11.6	38.4
K-band, DSS-54, S/K, HEMT-1, RCP, non-diplexed, 27.0 GHz	36.5	11.6	48.1
K-band, DSS-54, S/K, HEMT-2, LCP, non-diplexed, 27.0 GHz	36.4	11.6	48.0
K-band, DSS-56, K-only, HEMT-1, RCP, non-diplexed, 26.15 GHz	33.8	11.7	45.5
K-band, DSS-56, K-only, HEMT-2, LCP, non-diplexed, 26.15 GHz	33.8	11.7	45.5
K-band, DSS-56, S/K, HEMT-1, RCP, non-diplexed, 26.15 GHz	39.8	11.7	51.5
K-band, DSS-56, S/K, HEMT-2, LCP, non-diplexed, 26.15 GHz	39.8	11.7	51.5
Ka-band, DSS-23, X/Ka, HEMT-1, RCP, non-diplexed	TBD	11.50	TBD
Ka-band, DSS-23, X/Ka, HEMT-2, RCP-error, non-diplexed	TBD	11.50	TBD
Ka-band, DSS-23, X/Ka, HEMT-3, LCP, non-diplexed	TBD	11.50	TBD
Ka-band, DSS-25, X/Ka, HEMT-1, RCP, diplexed	24.2	11.50	35.70
Ka-band, DSS-25, X/Ka, HEMT-2, RCP-error, diplexed	25.7	11.50	37.20
Ka-band, DSS-25, X/Ka, HEMT-3, LCP, diplexed	23.0	11.50	34.50
Ka-band, DSS-26, X/Ka, HEMT-1, RCP, non-diplexed	19.36	11.50	30.86
Ka-band, DSS-26, X/Ka, HEMT-2, RCP-error, non-diplexed	24.55	11.50	36.05
Ka-band, DSS-26, X/Ka, HEMT-3, LCP, non-diplexed	20.77	11.50	32.27
Ka-band, DSS-33, X/Ka, HEMT-1, RCP, non-diplexed	TBD	14.81	TBD

Table 11. T_{AMW}, T_{sky}, and T_{op} for CD=25% Average Clear Weather at Zenith, Referenced to Feedhorn Aperture (Continued)

Frequency, Station, and Configuration	Noise Temperatures, K		
	T_{AMW}	T_{sky}	T_{op}
Ka-band, DSS-33, X/Ka, HEMT-2, RCP-error, non-diplexed	TBD	14.81	TBD
Ka-band, DSS-33, X/Ka, HEMT-3, LCP, non-diplexed	TBD	14.81	TBD
Ka-band, DSS-34, X/Ka, HEMT-1, RCP, non-diplexed	19.38	14.81	34.19
Ka-band, DSS-34, X/Ka, HEMT-2, RCP-error, non-diplexed	23.25	14.81	38.06
Ka-band, DSS-34, X/Ka, HEMT-3, LCP, non-diplexed	19.61	14.81	34.42
Ka-band, DSS-35, X/Ka, HEMT-1, RCP, diplexed (9/2026)	17.3	14.81	32.11
Ka-band, DSS-35, X/Ka, HEMT-2, RCP-error, diplexed (9/2026)	TBD	14.81	TBD
Ka-band, DSS-35, X/Ka, HEMT-3, LCP, diplexed (9/2026)	17.2	14.81	32.01
Ka-band, DSS-36, X/Ka, HEMT-1, RCP, non-diplexed	12.54	14.81	27.35
Ka-band, DSS-36, X/Ka, HEMT-2, RCP-error, non-diplexed	TBD	14.81	TBD
Ka-band, DSS-36, X/Ka, HEMT-3, LCP, non-diplexed	12.18	14.81	26.99
Ka-band, DSS-53, X/Ka, HEMT-1, RCP, non-diplexed	13.0	13.91	26.91
Ka-band, DSS-53, X/Ka, HEMT-2, RCP-error, non-diplexed	TBD	13.91	TBD
Ka-band, DSS-53, X/Ka, HEMT-3, LCP, non-diplexed	13.4	13.91	27.31
Ka-band, DSS-54, X/Ka, HEMT-1, RCP, non-diplexed	21.80	13.91	35.71
Ka-band, DSS-54, X/Ka, HEMT-2, RCP-error, non-diplexed	25.00	13.91	38.91
Ka-band, DSS-54, X/Ka, HEMT-3, LCP, non-diplexed	21.80	13.91	35.71
Ka-band, DSS-55, X/Ka, HEMT-1, RCP, diplexed (6/2027)	20.80	13.91	34.71
Ka-band, DSS-55, X/Ka, HEMT-2, RCP-error, diplexed (6/2027)	21.98	13.91	35.89
Ka-band, DSS-55, X/Ka, HEMT-3, LCP, diplexed (6/2027)	19.83	13.91	33.74
Ka-band, DSS-56, X/Ka, HEMT-1, RCP, non-diplexed	16.5	13.91	30.41
Ka-band, DSS-56, X/Ka, HEMT-2, RCP-error, non-diplexed	TBD	13.91	TBD
Ka-band, DSS-56, X/Ka, HEMT-3, LCP, non-diplexed	17.0	13.91	30.91

NOTE: For low-gain mode add +20 K (X-band), +180 K (K-band), +70 K (Ka-band)

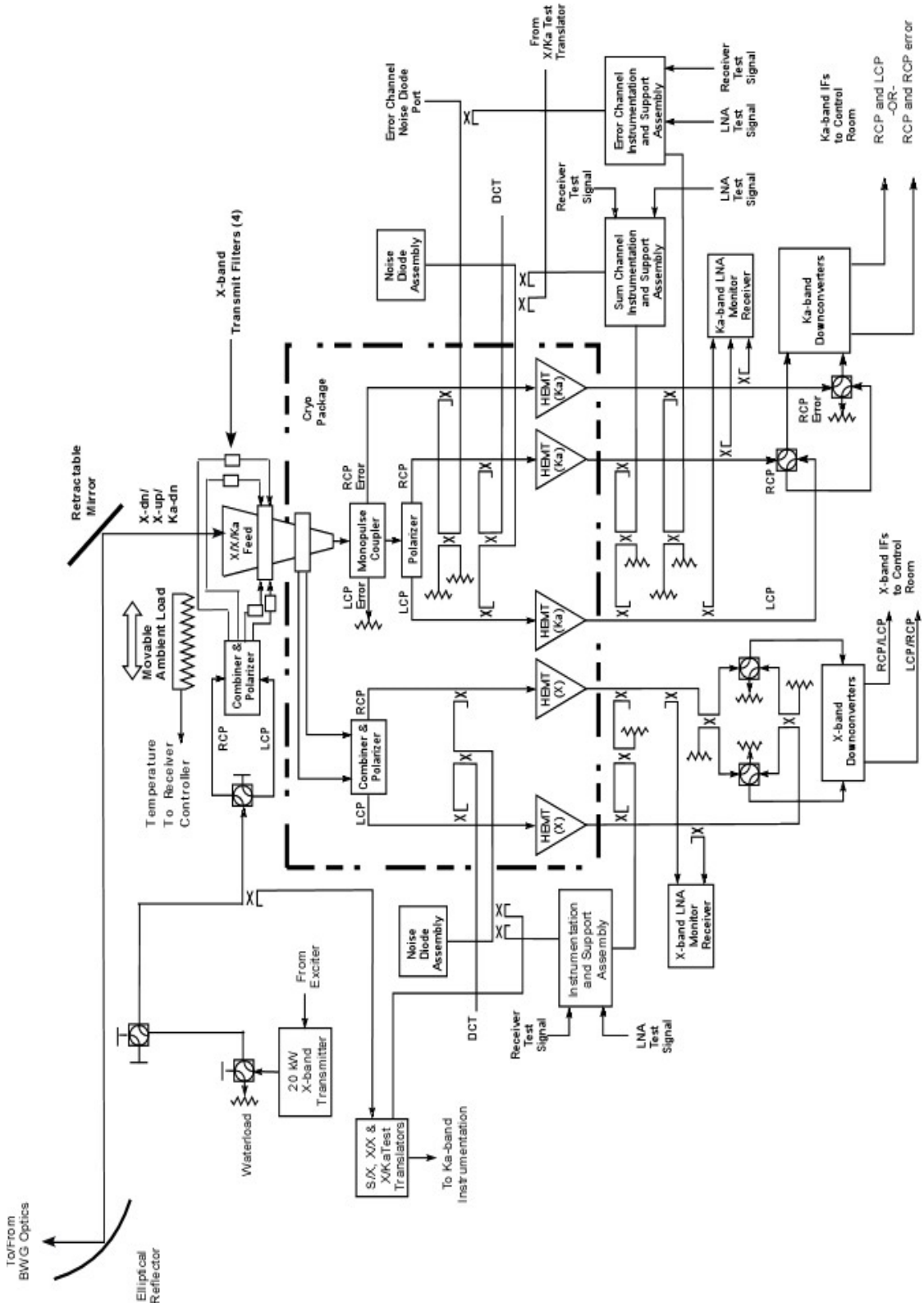

Figure 1. Functional Block Diagram of the DSS-23 Antenna.

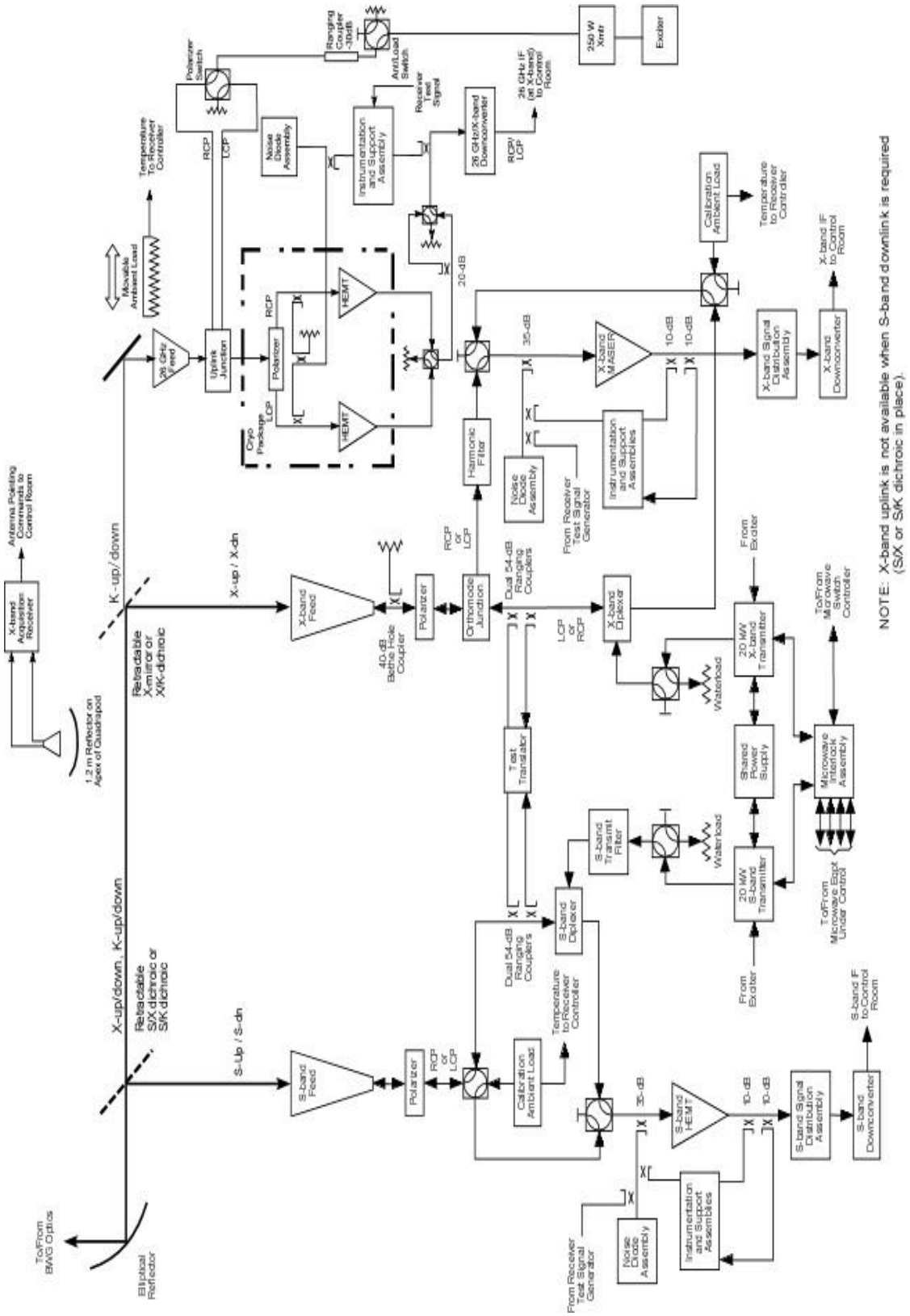

Figure 2. Functional Block Diagram of the DSS-24 Antenna.

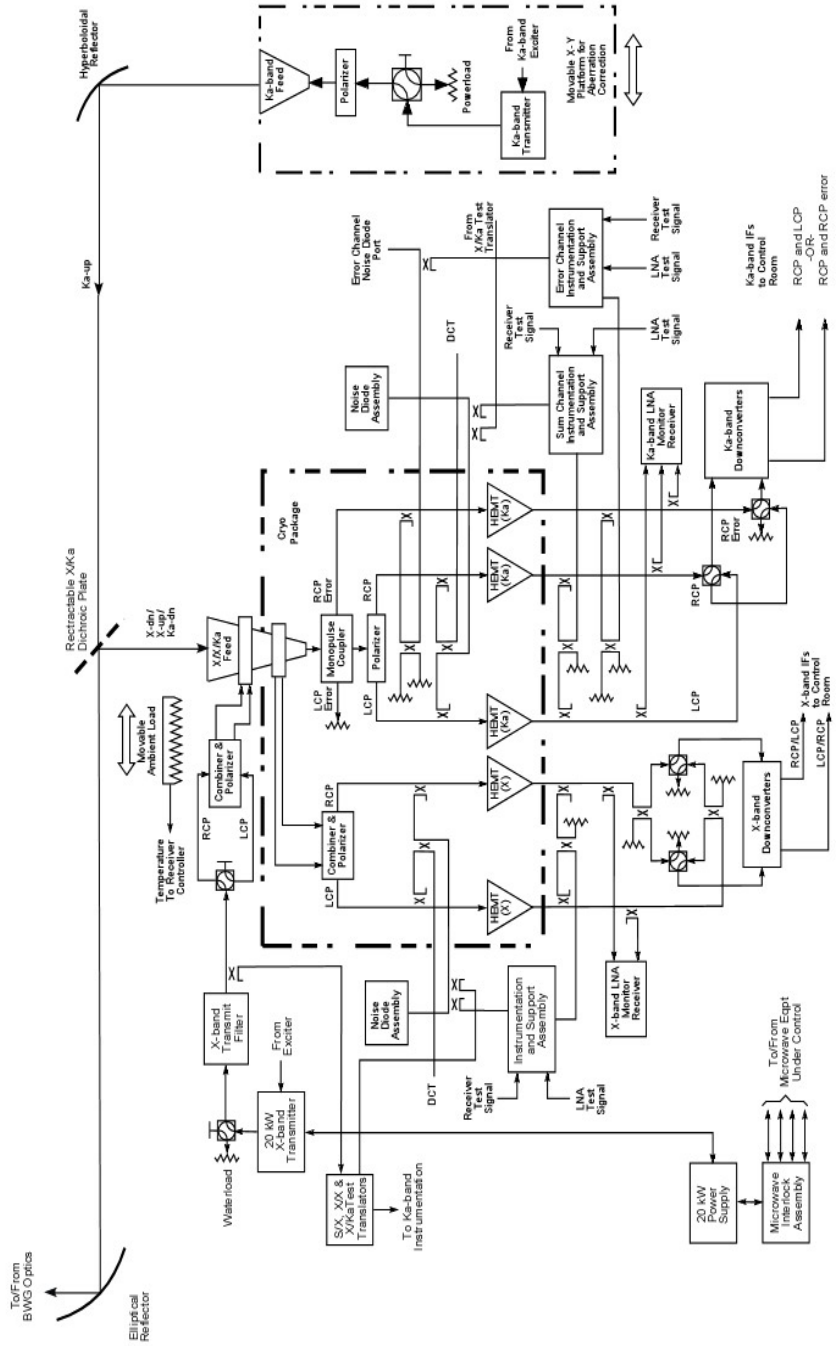

Figure 3. Functional Block Diagram of the DSS-25 Antenna.

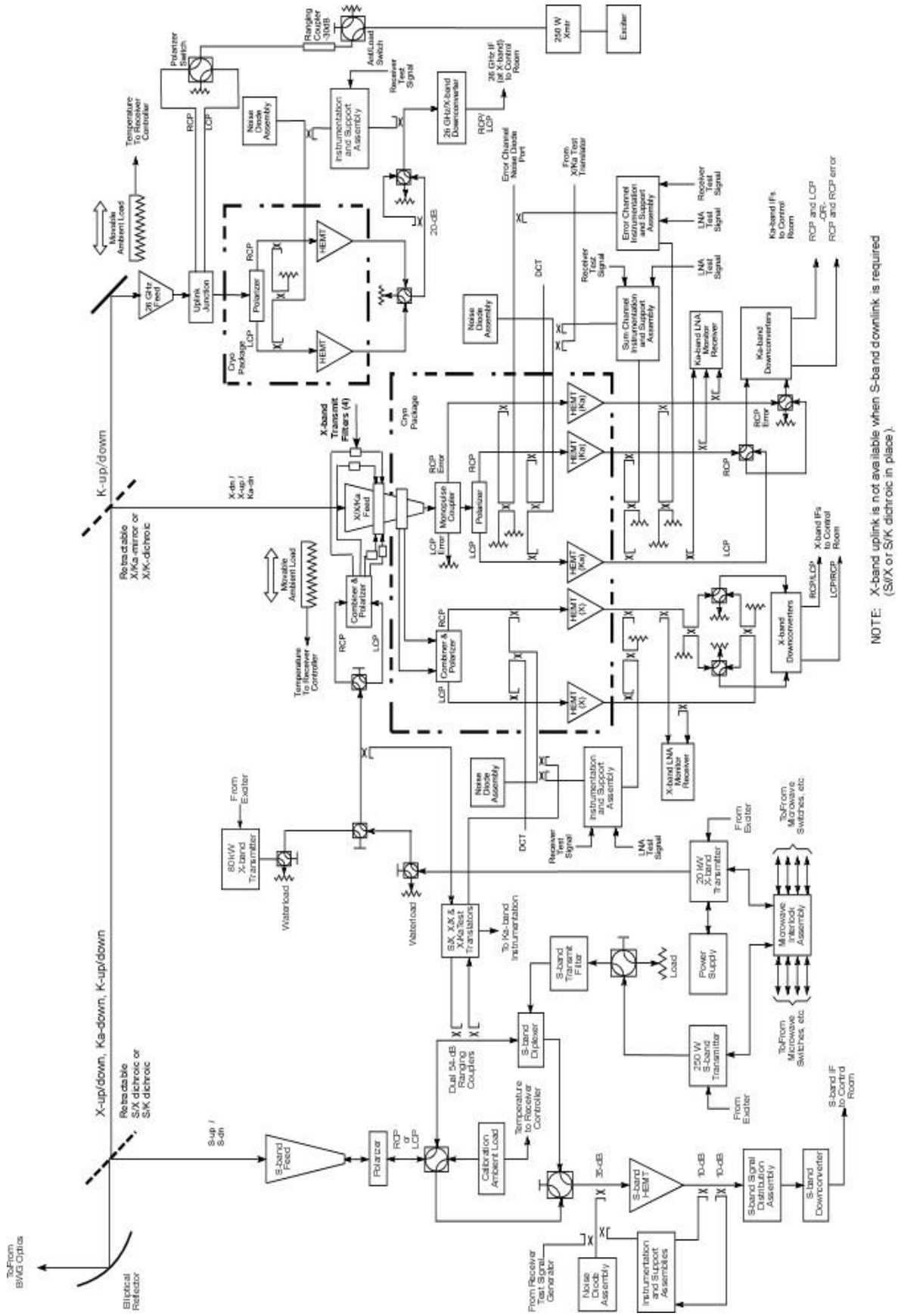

NOTE: X-band uplink is not available when S-band downlink is required (S/X or S/K dichroic in place).

Figure 4. Functional Block Diagram of the DSS-26 Antenna.

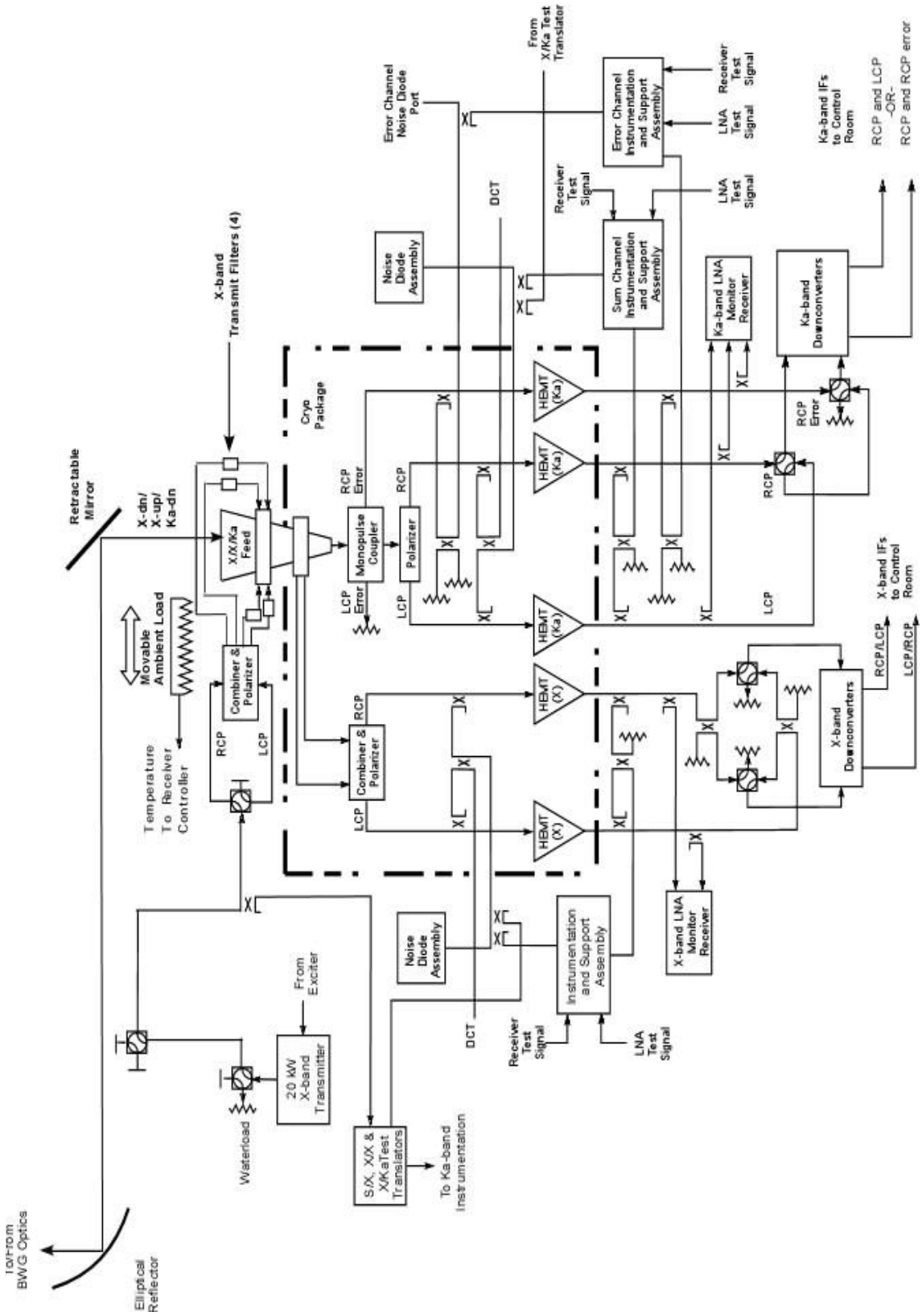

Figure 5. Functional Block Diagram of the DSS-33 Antenna.

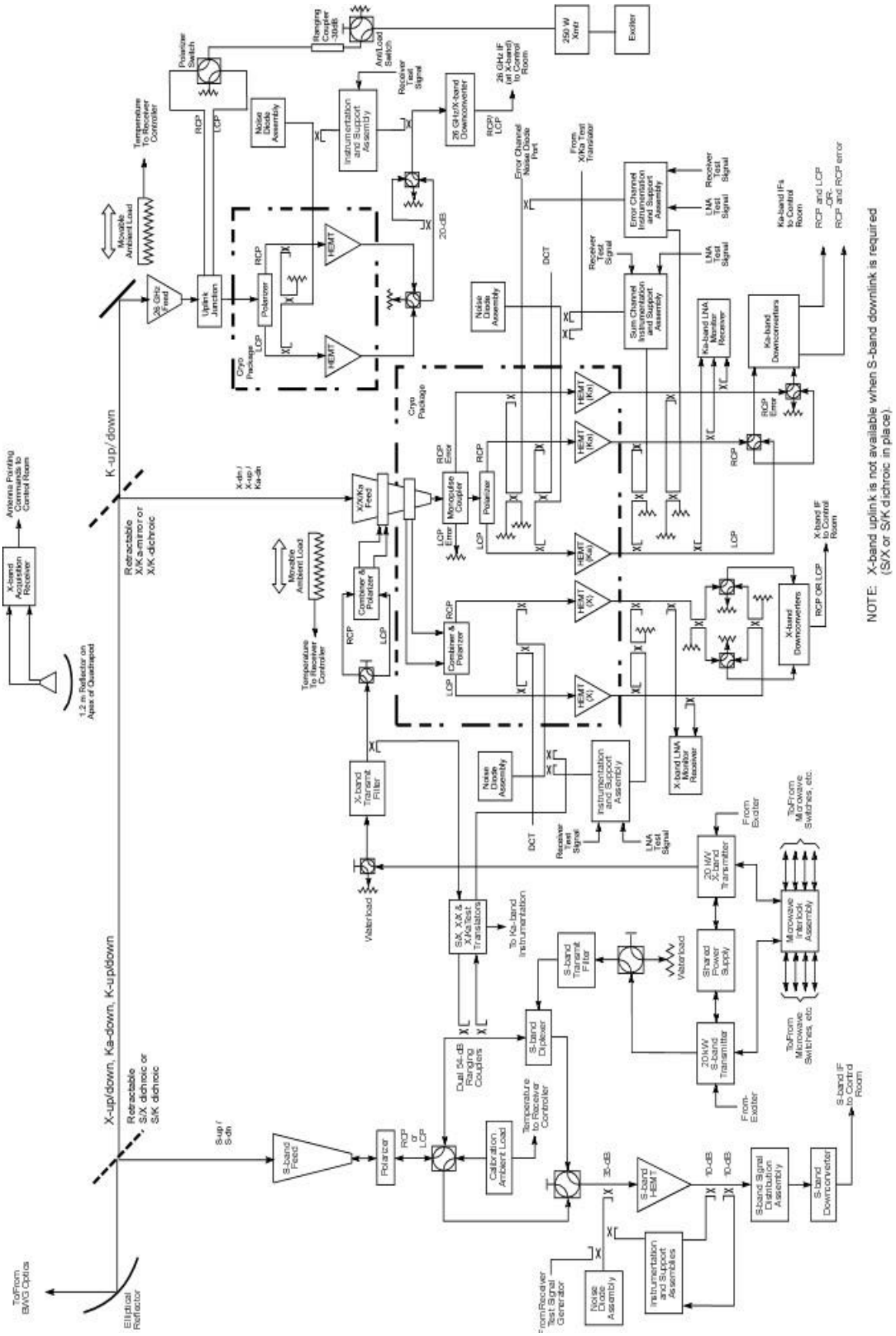

NOTE: X-band uplink is not available when S-band downlink is required (S/X or S/K dichroic in place).

Figure 6. Functional Block Diagram of the DSS-34 Antenna.

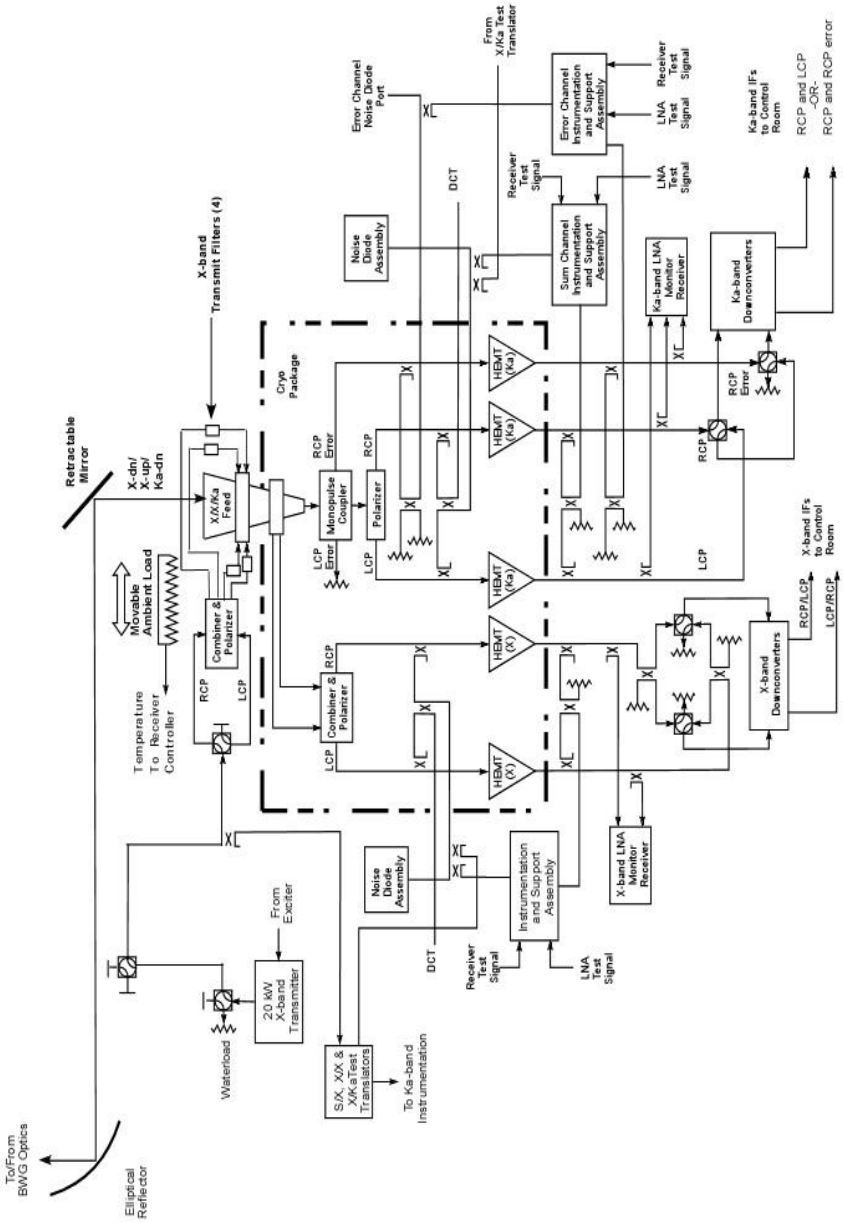

Figure 7. Functional Block Diagram of the DSS-35 Antenna.

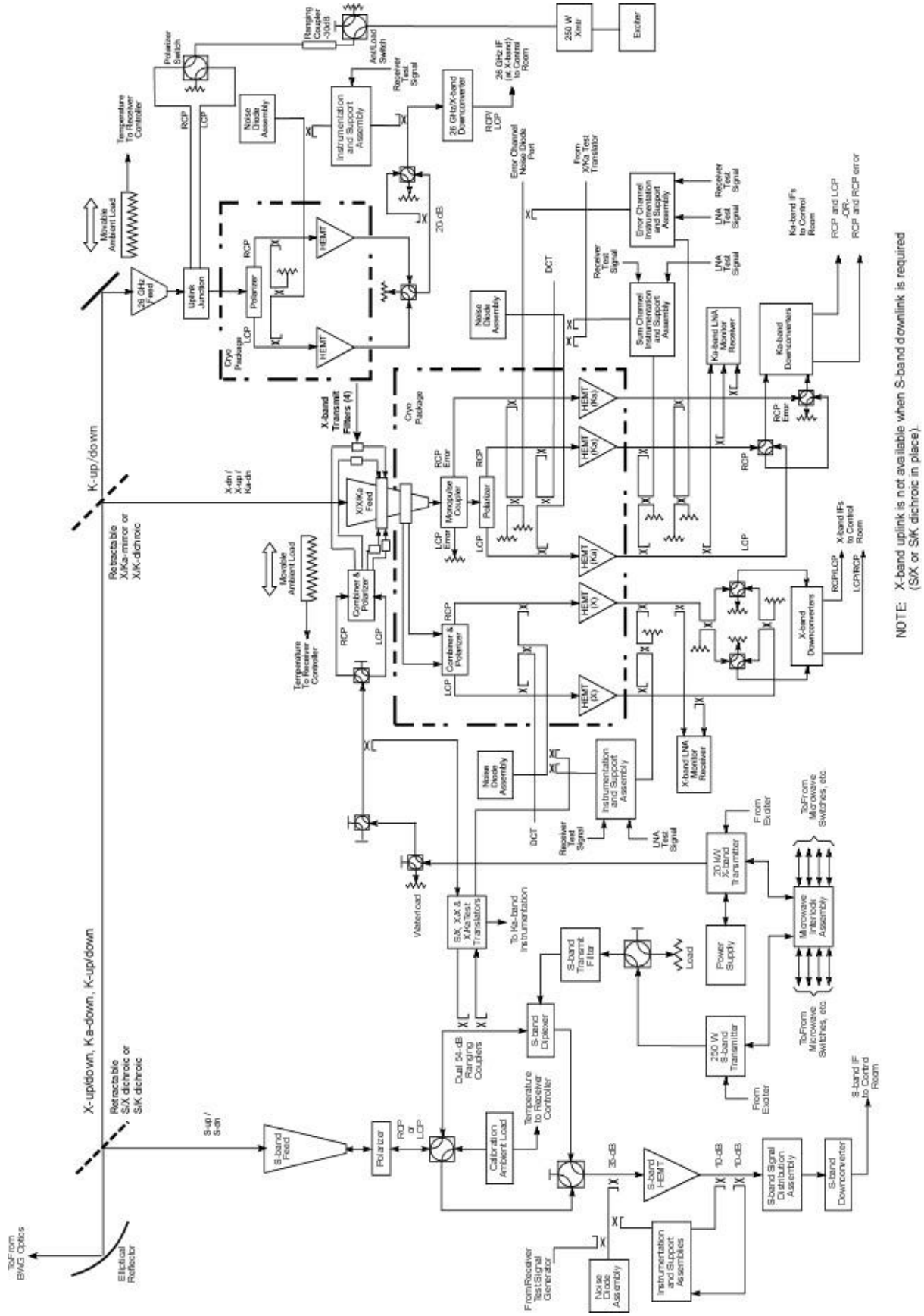

Figure 8. Functional Block Diagram of the DSS-36 Antenna.

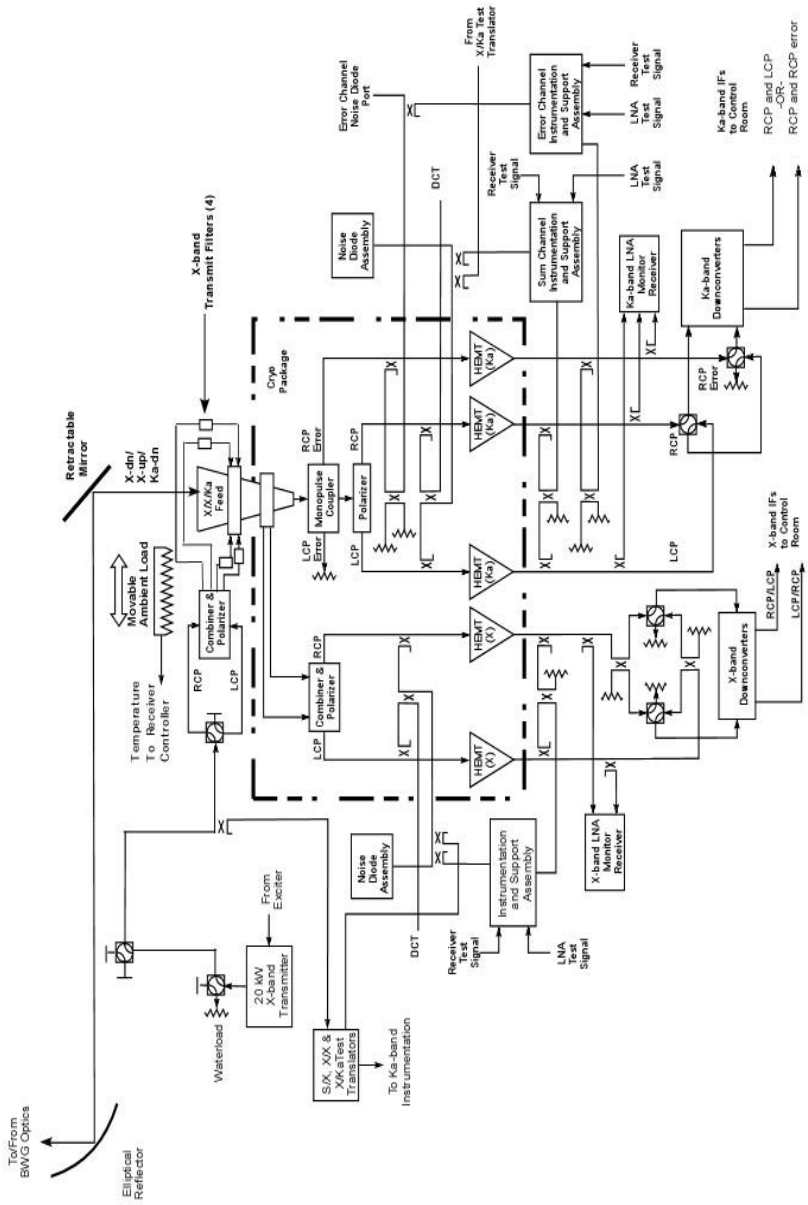

Figure 9. Functional Block Diagram of the DSS-53 Antenna.

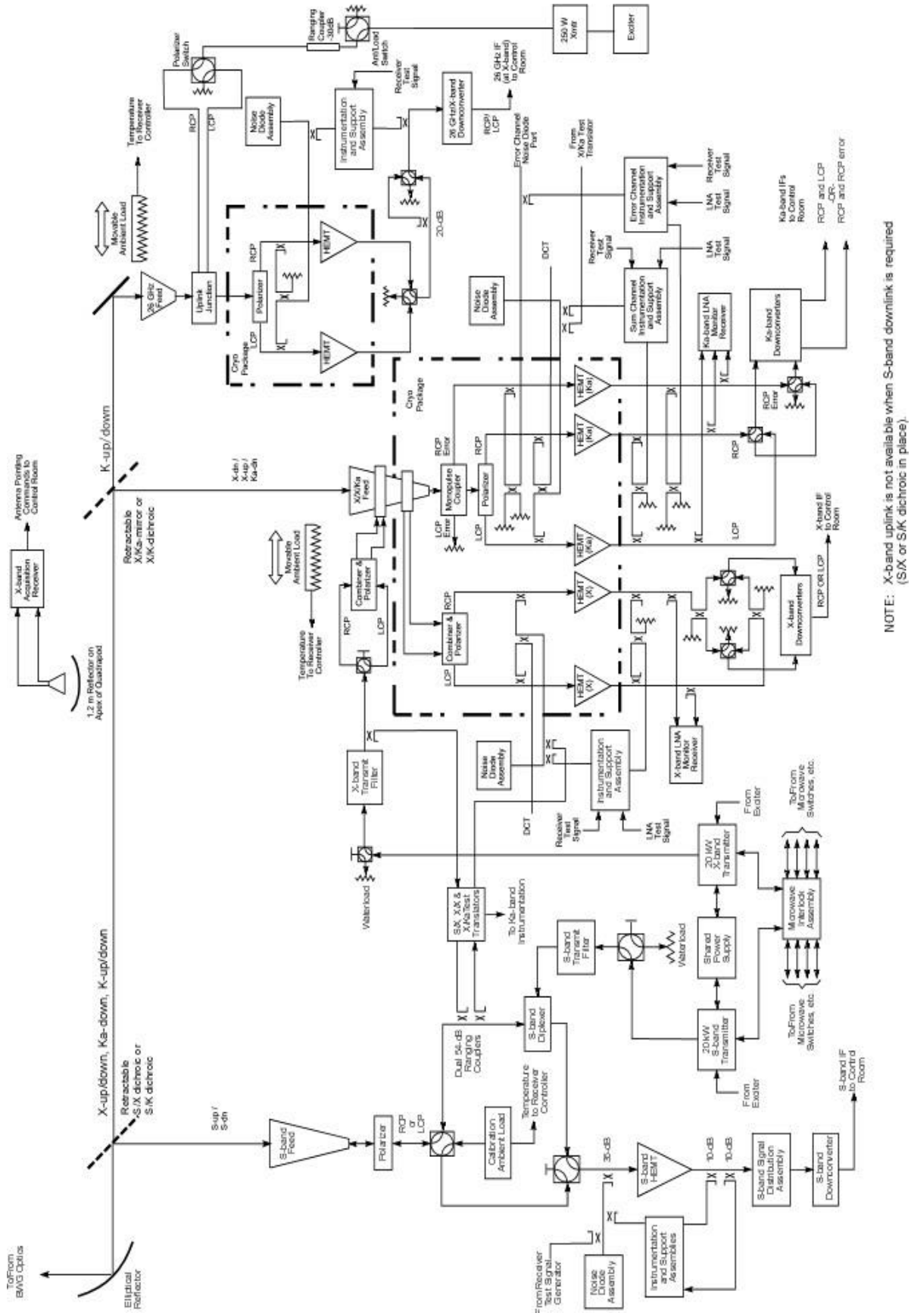

Figure 10. Functional Block Diagram of the DSS-54 Antenna.

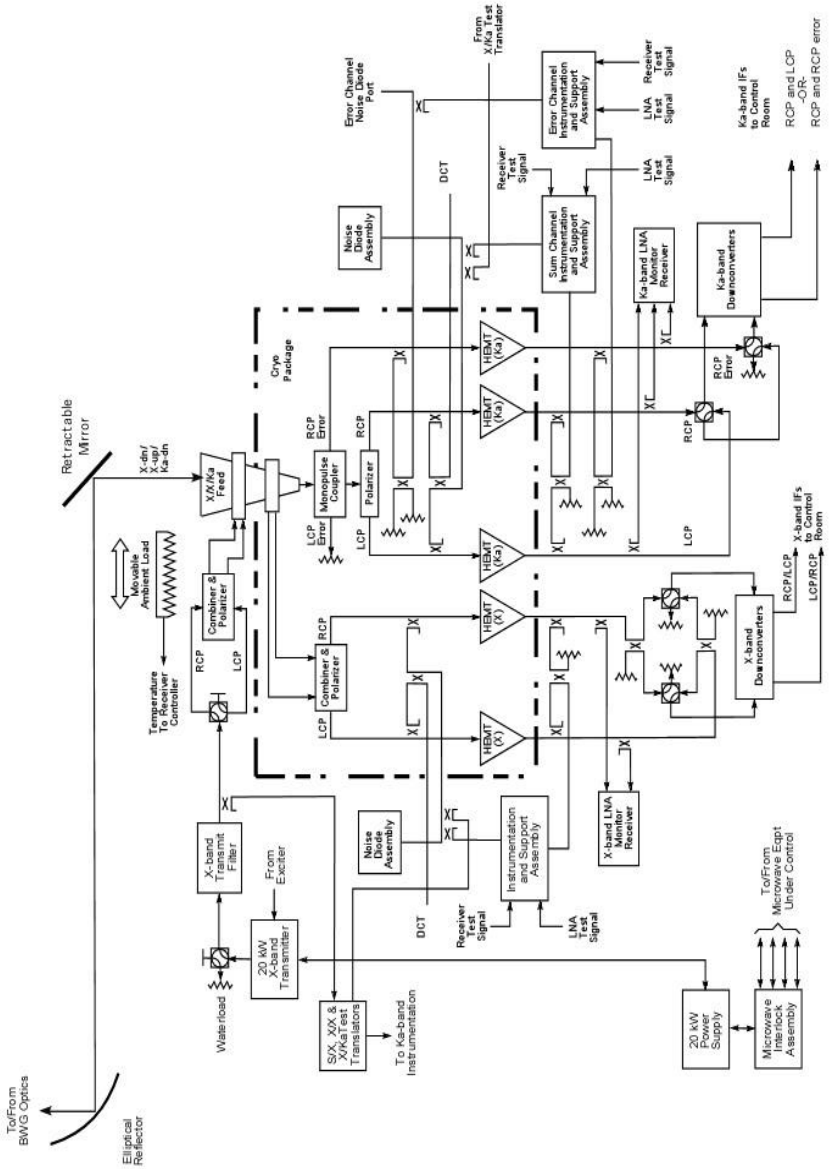

Figure 11. Functional Block Diagram of the DSS-55 Antenna.

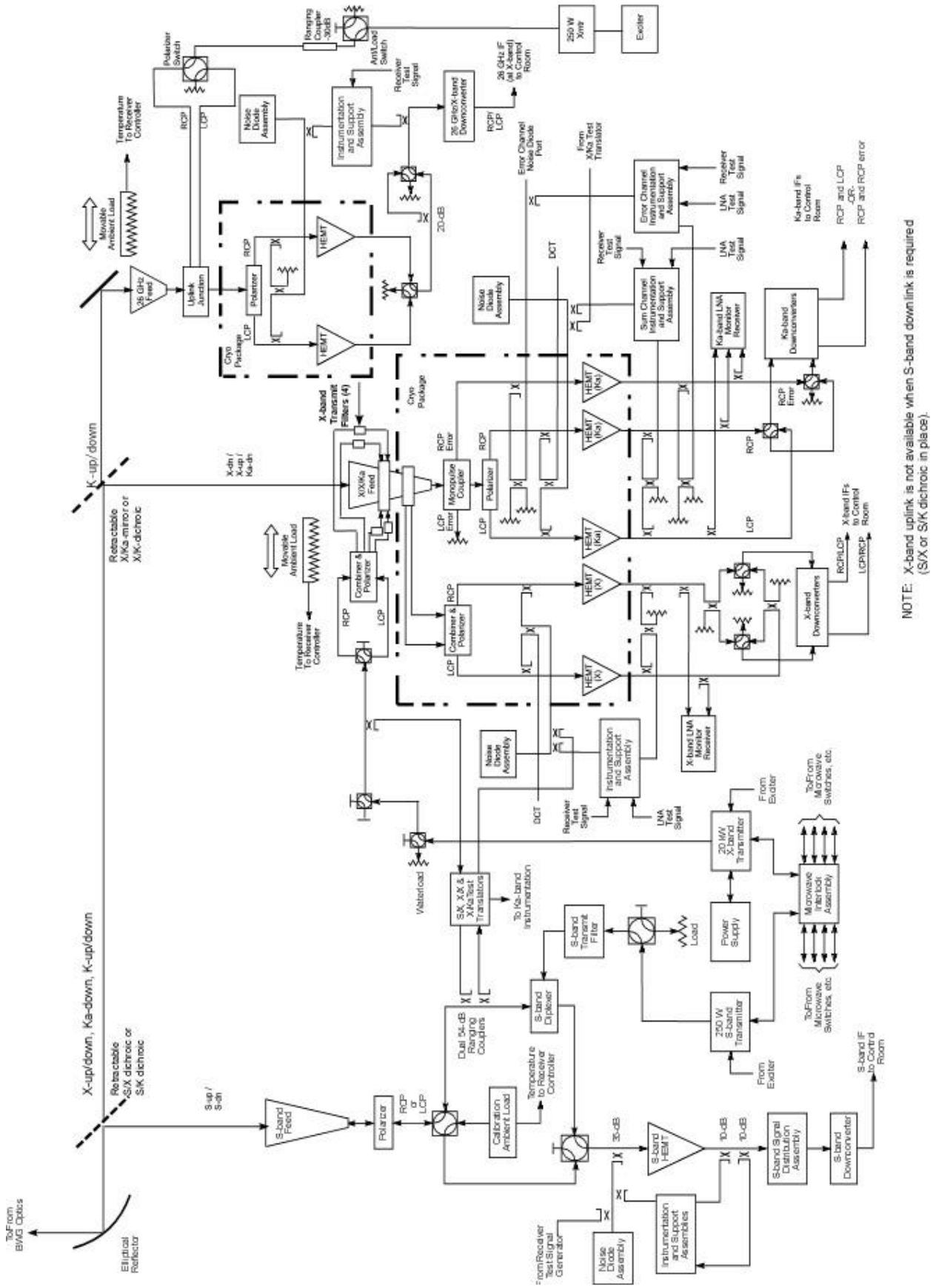

Figure 12. Functional Block Diagram of the DSS-56 Antenna.

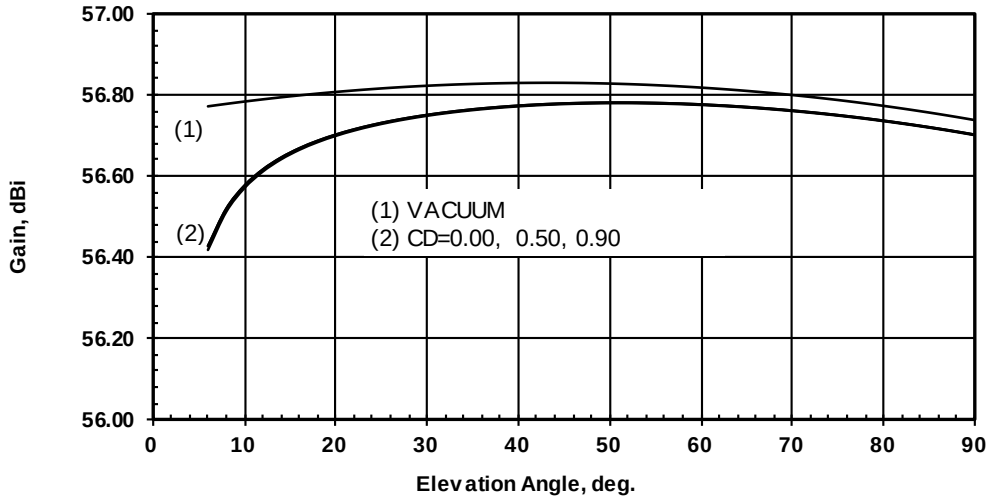

Figure 13. DSS-34 (Canberra) S-Band Receive Gain versus Elevation Angle, S/X-Mode (S/X Dichroic In Place), 2.3 GHz

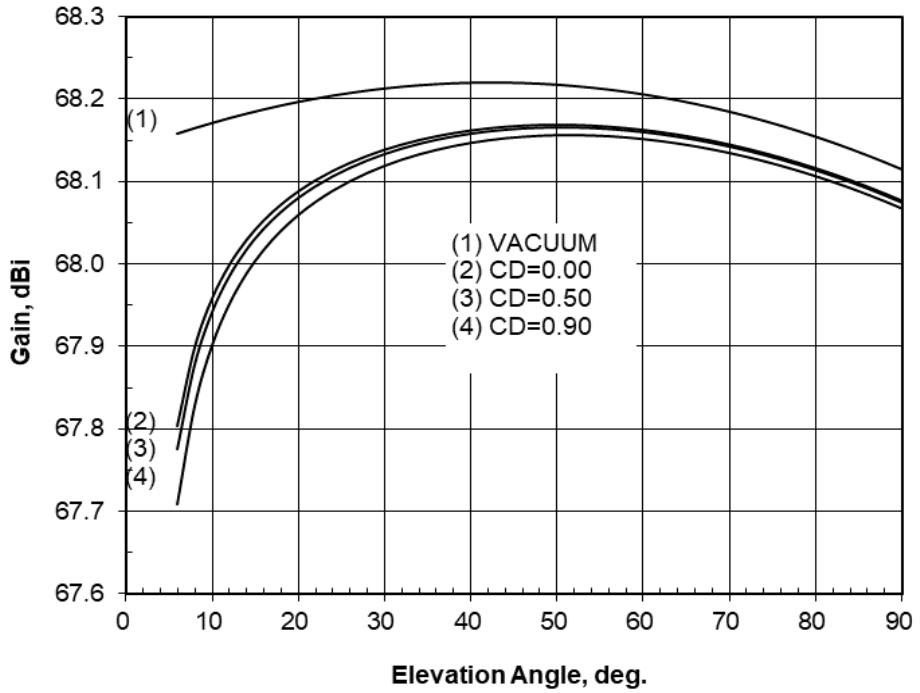

Figure 14. DSS-25 (Goldstone) X-Band Receive Gain versus Elevation Angle, X/Ka-Mode, 8.4 GHz

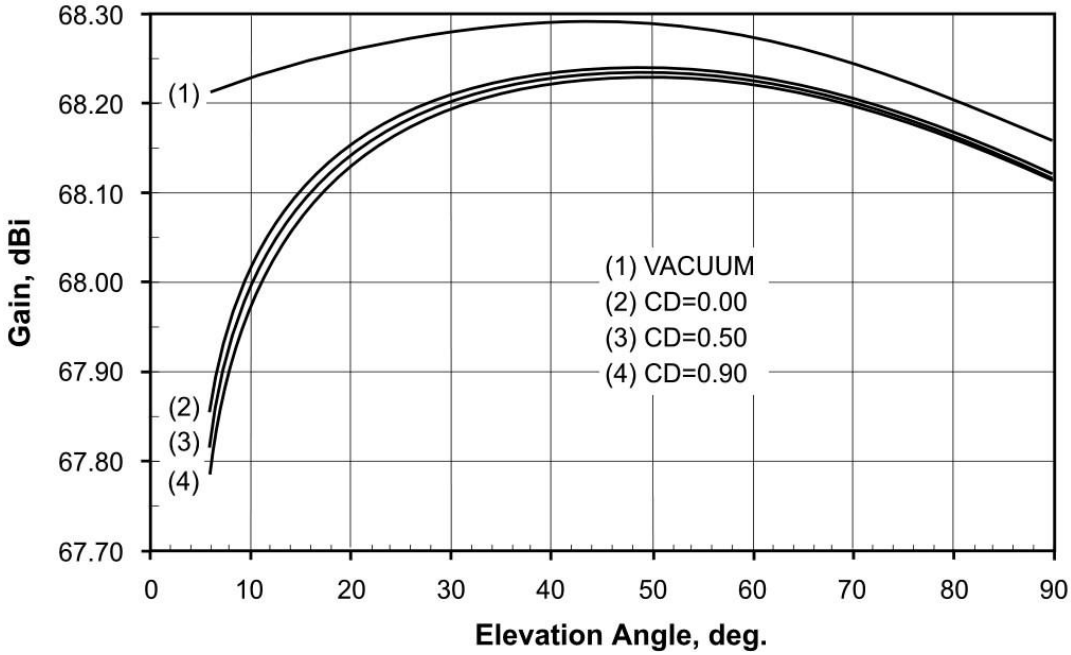

Figure 15. DSS-26 (Goldstone) X-Band Receive Gain versus Elevation Angle, X/Ka-Mode, 8.4 GHz

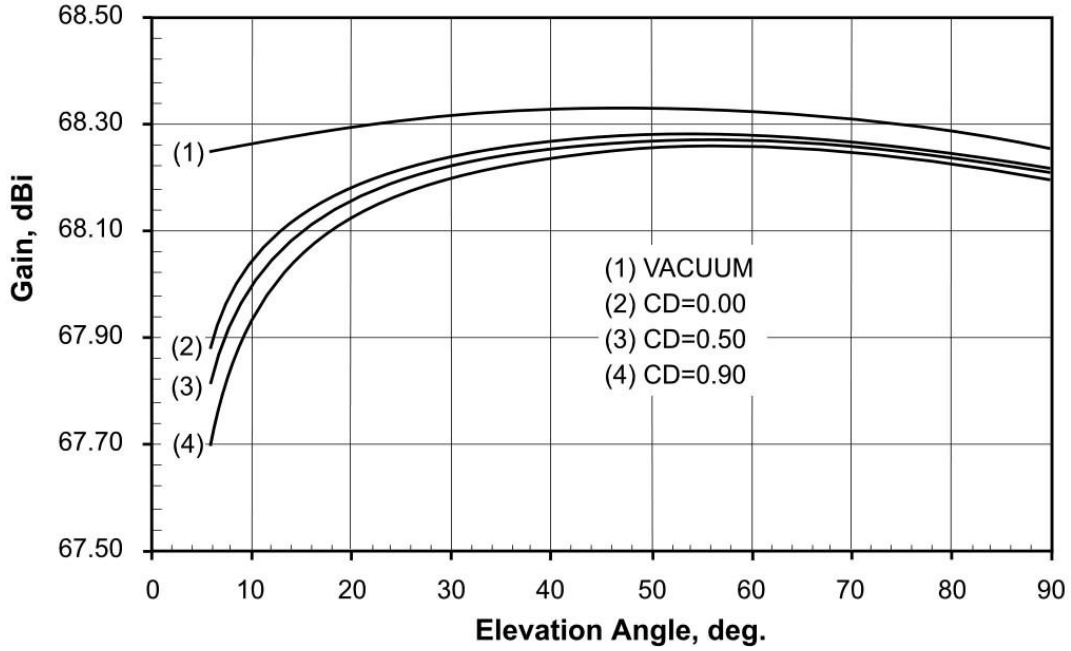

Figure 16. DSS-34 (Canberra) X-Band Receive Gain versus Elevation Angle, X/Ka-Mode (S/X Dichroic Retracted), 8.4 GHz

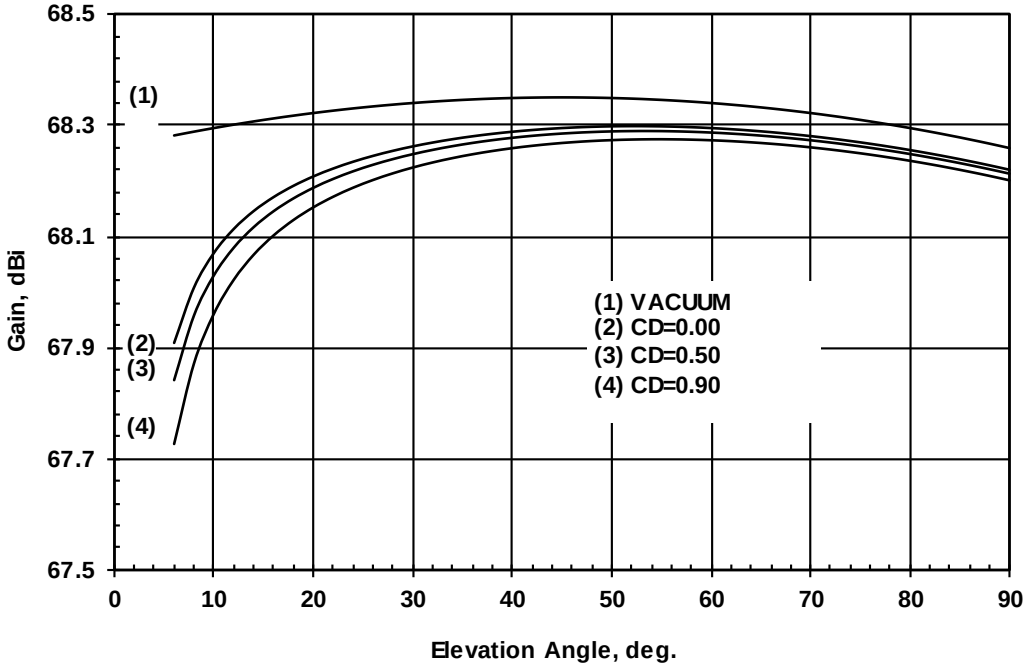

Figure 17. DSS-35 (Canberra) X-Band Receive Gain versus Elevation Angle, X/Ka-Mode, 8.4 GHz

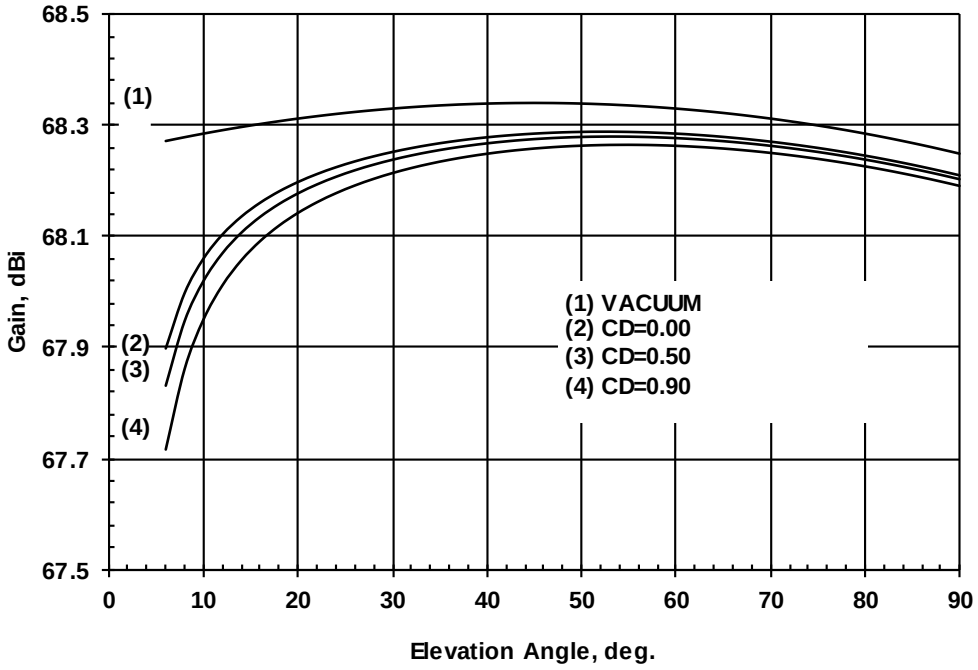

Figure 18. DSS-36 (Canberra) X-band Receive Gain versus Elevation Angle, X/Ka-Mode, 8.4 GHz

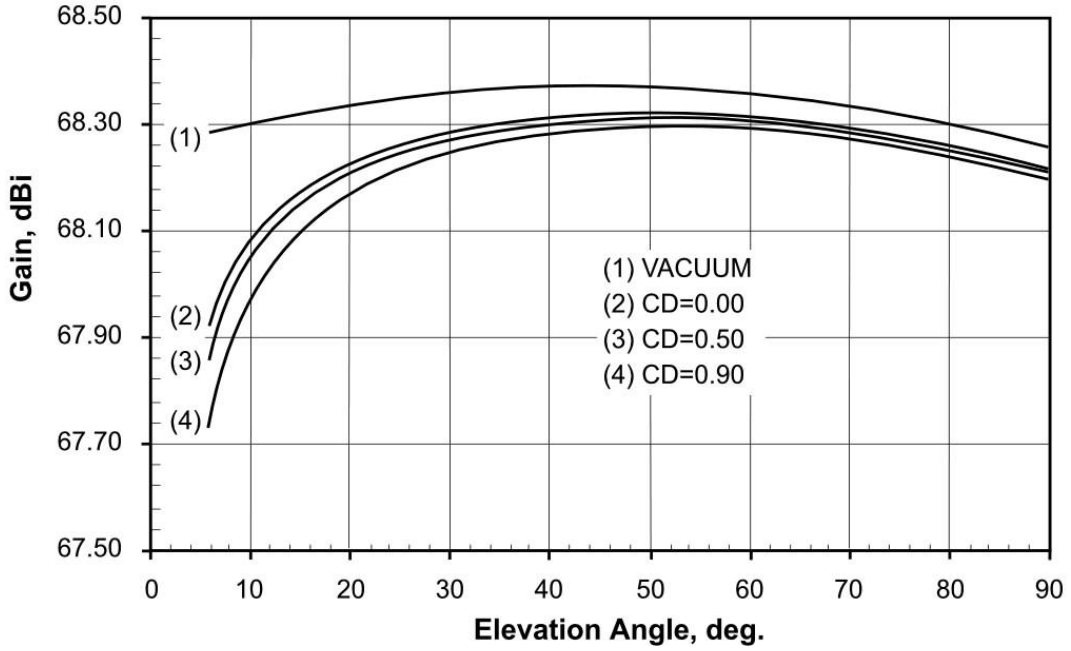

Figure 19. DSS-54 (Madrid) X-Band Receive Gain versus Elevation Angle, X/Ka-Mode (S/X Dichroic Retracted), 8.4 GHz

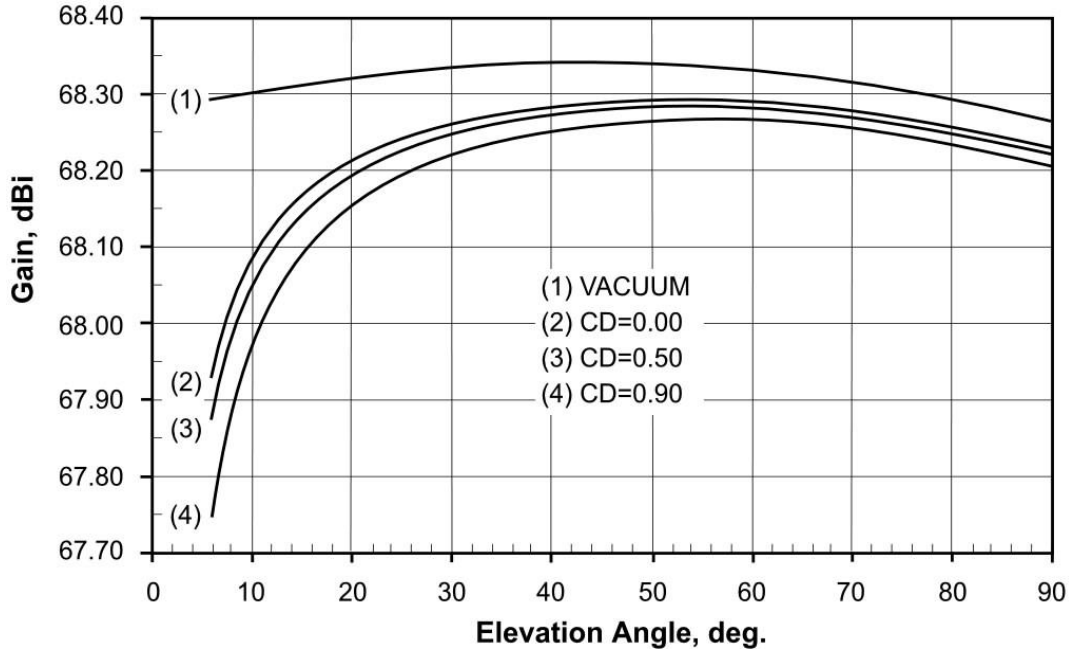

Figure 20. DSS-55 (Madrid) X-Band Receive Gain versus Elevation Angle, X/Ka Mode, 8.4 GHz

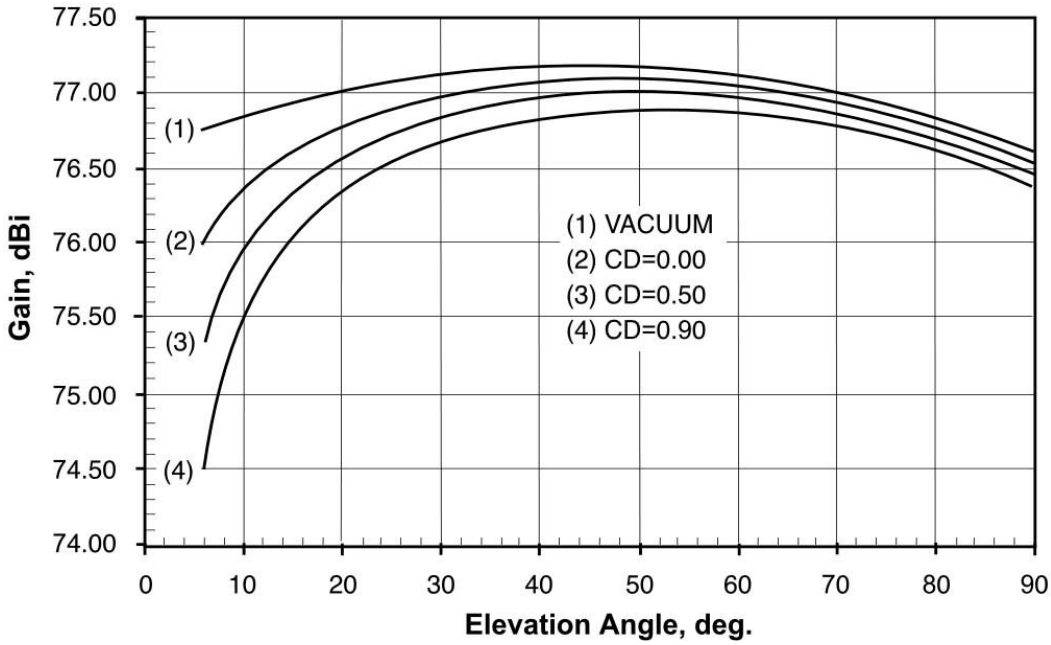

Figure 21. DSS-24 (Goldstone) K-Band Receive Gain versus Elevation Angle, K-Only Mode (S/K Dichroic Retracted), 26 GHz

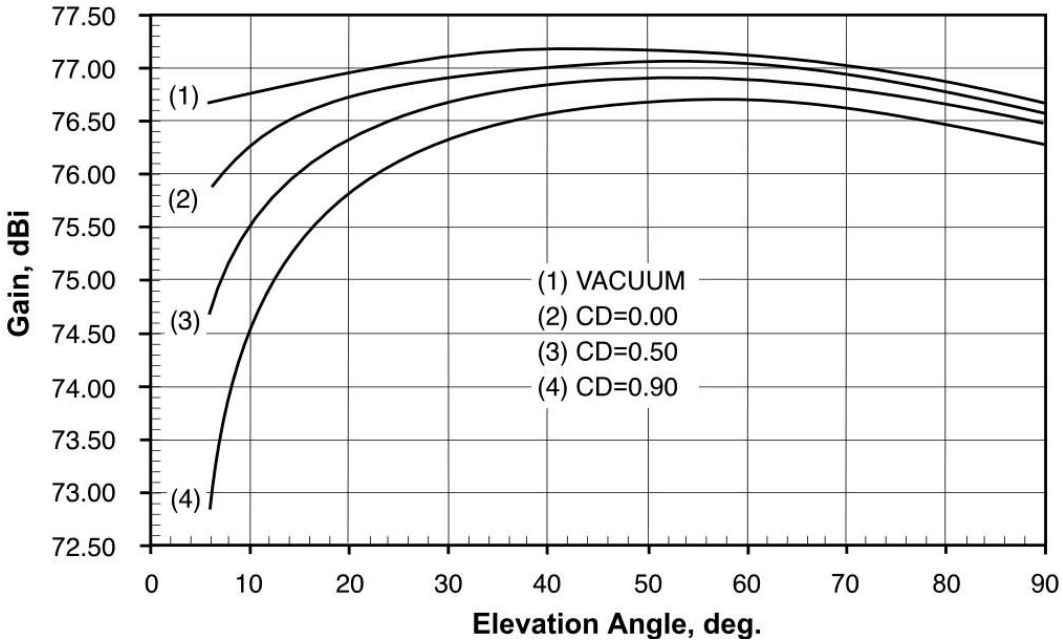

Figure 22. DSS-34 (Canberra) K-Band Receive Gain versus Elevation Angle, K-Only Mode (S/K Dichroic Retracted), 26 GHz

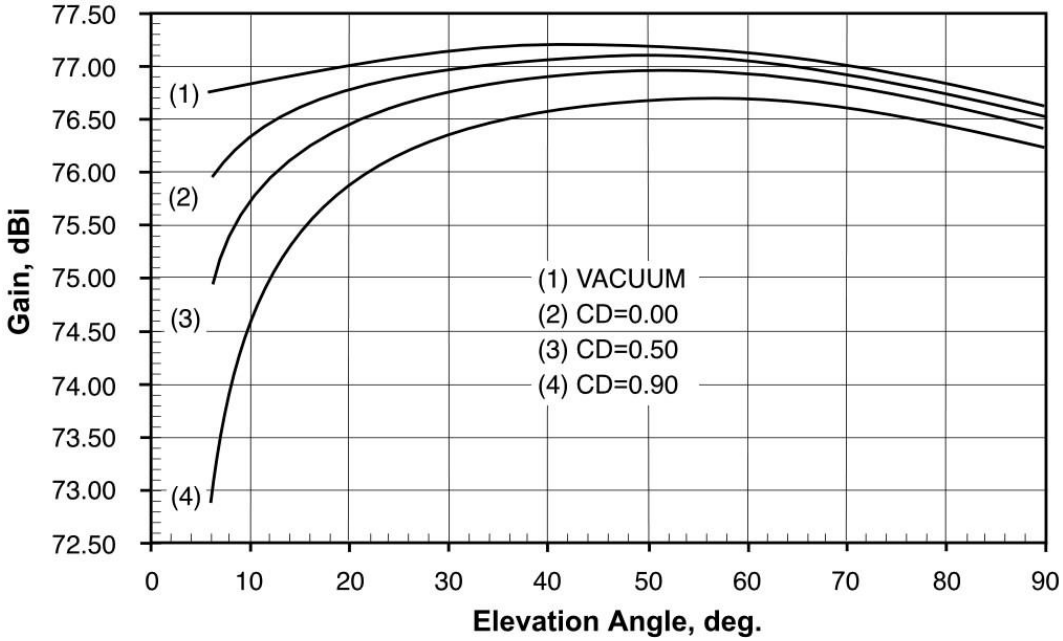

Figure 23. DSS-54 (Madrid) K-Band Receive Gain versus Elevation Angle, K-Only Mode (S/K Dichroic Retracted), 26 GHz

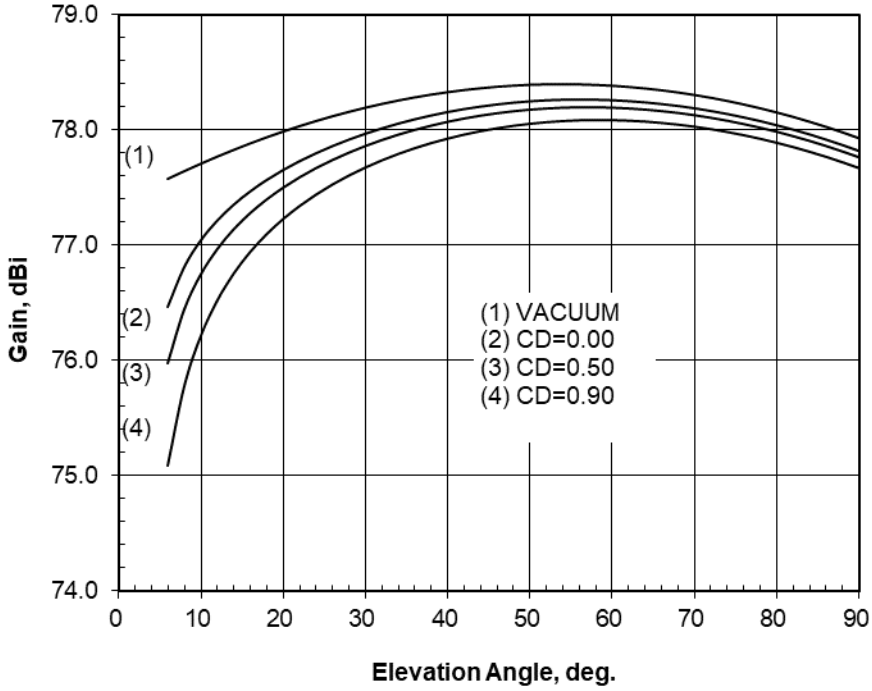

Figure 24. DSS-25 (Goldstone) Ka-Band Receive Gain versus Elevation Angle, X/Ka-Mode, 32 GHz

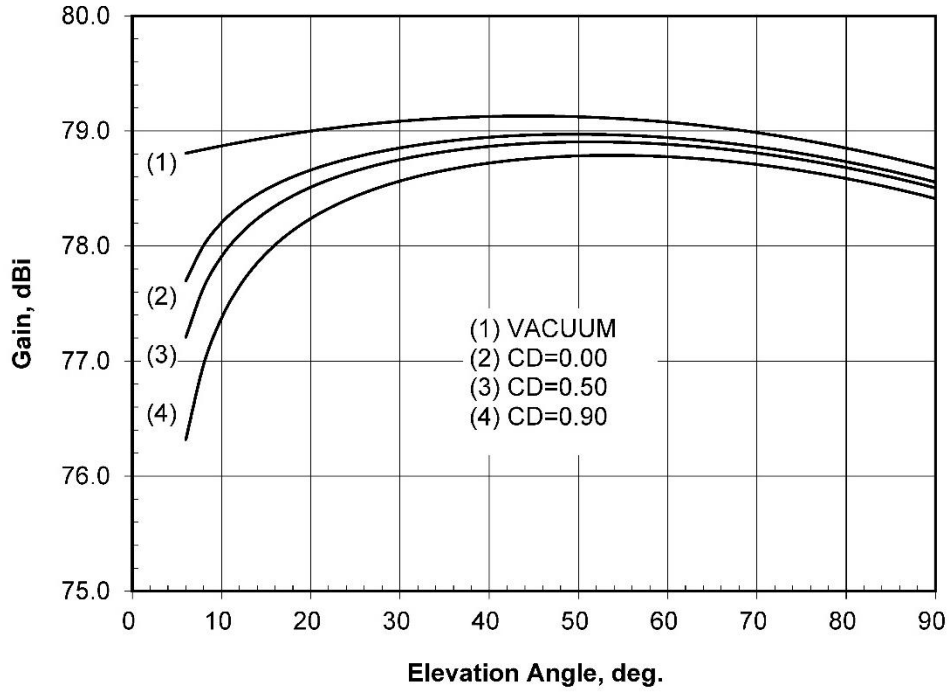

Figure 25. DSS-26 (Goldstone) Ka-Band Receive Gain versus Elevation Angle, X/Ka-Mode, 32 GHz

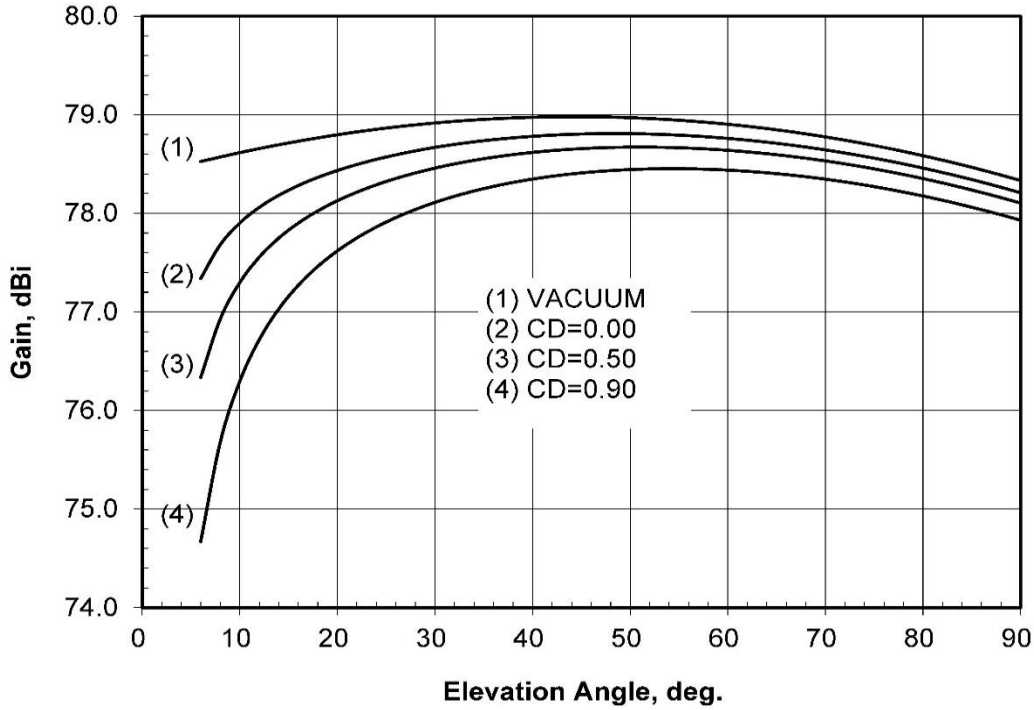

Figure 26. DSS-34 (Canberra) Ka-Band Receive Gain versus Elevation Angle, X/Ka-Mode, 32 GHz

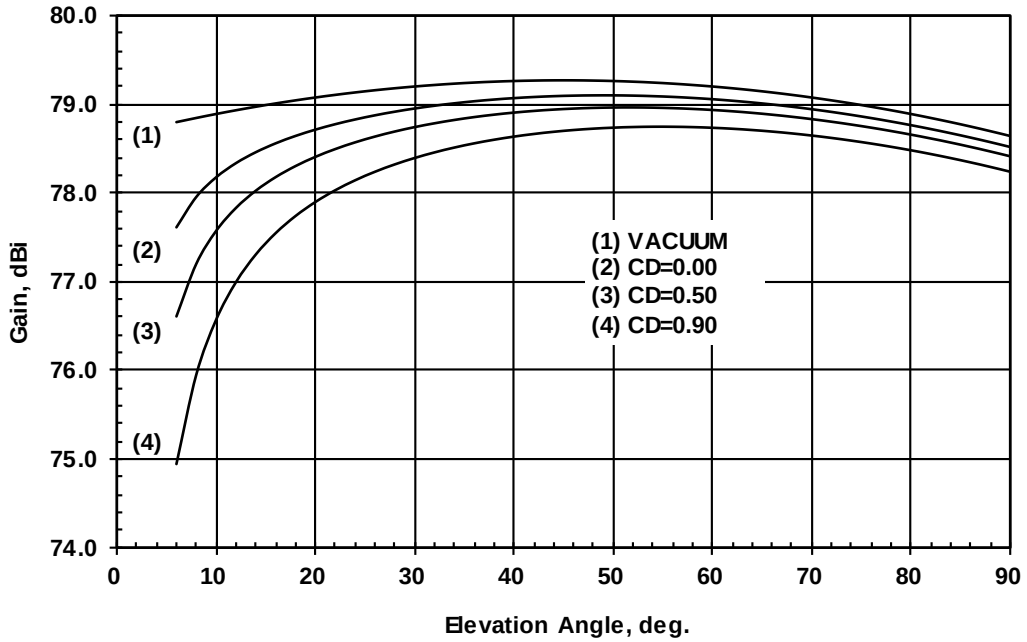

Figure 27. DSS-35 (Canberra) Ka-Band Receive Gain versus Elevation Angle, X/Ka-Mode, 32 GHz

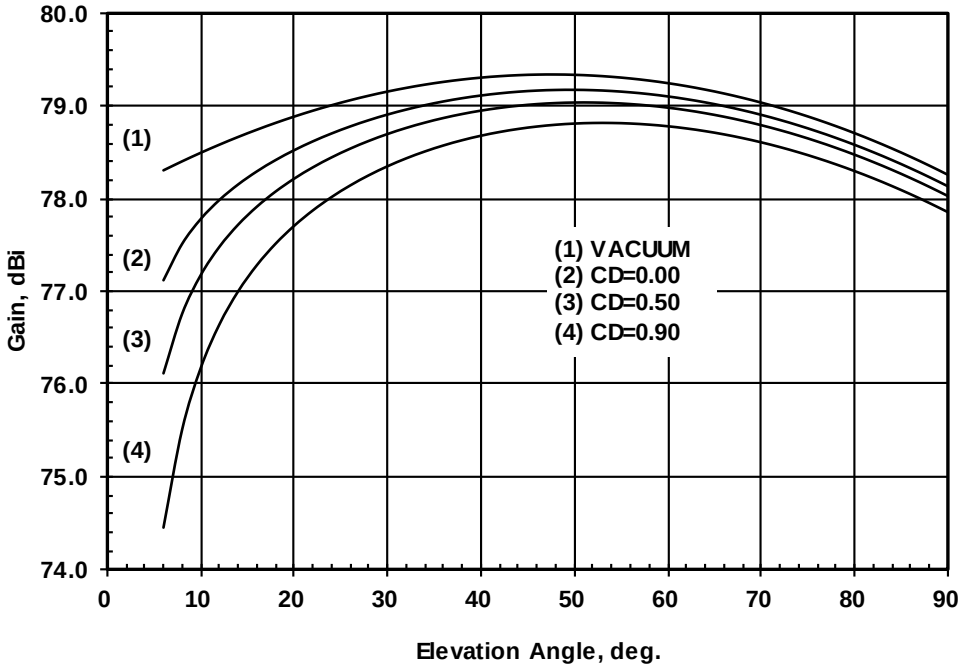

Figure 28. DSS-36 (Canberra) Ka-Band Receive Gain versus Elevation Angle, X/Ka-Mode, 32 GHz

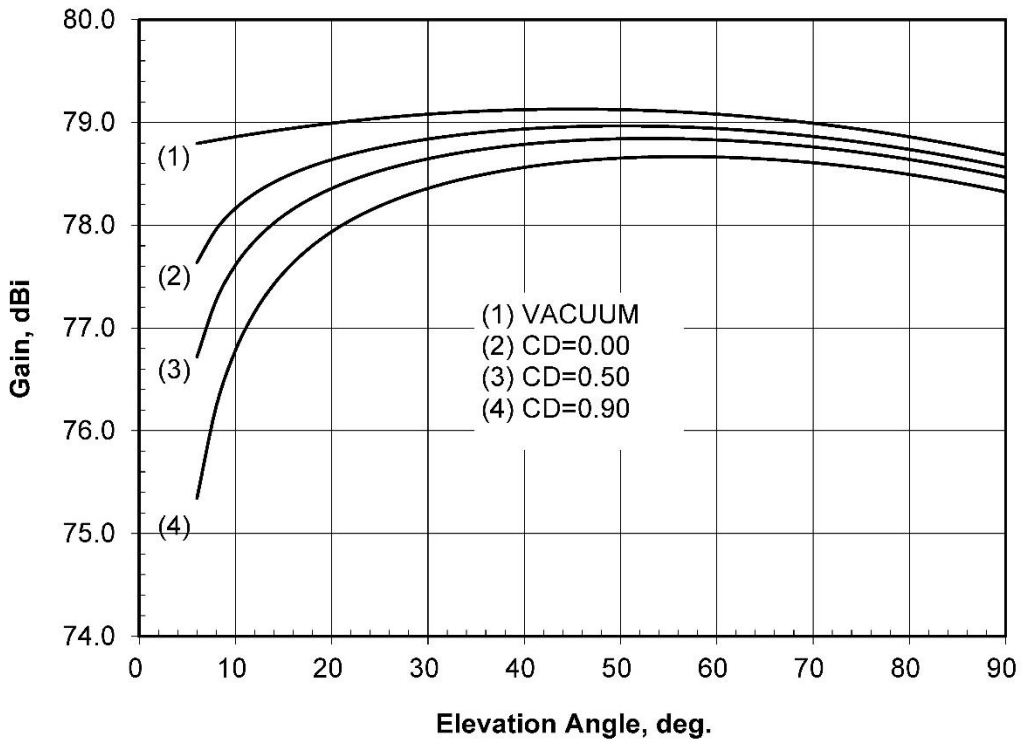

Figure 29. DSS-55 (Madrid) Ka-Band Receive Gain versus Elevation Angle,X/Ka-Mode, 32 GHz

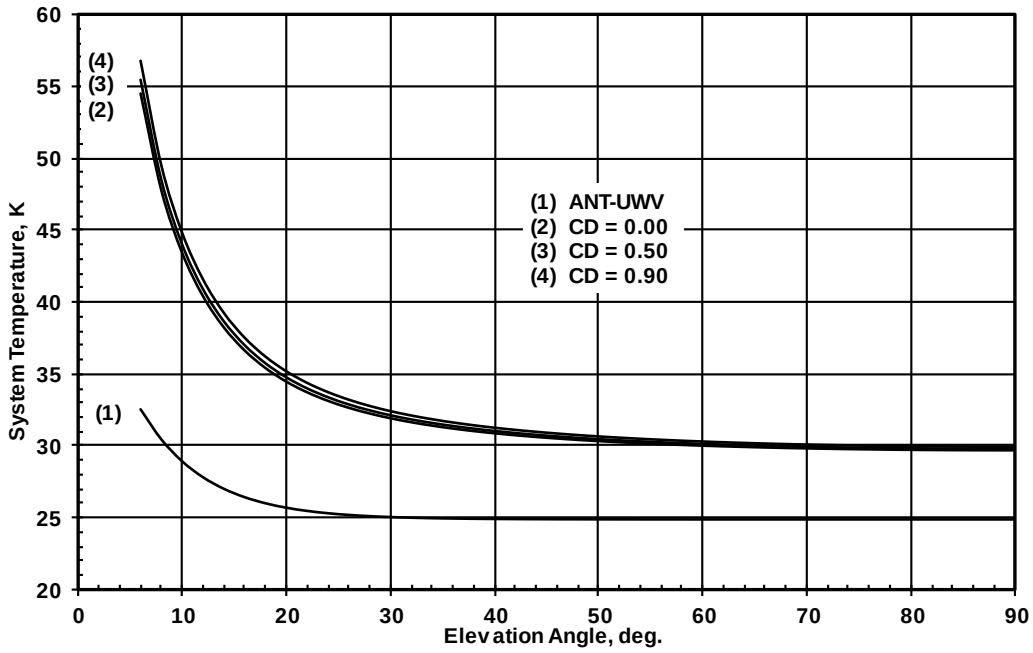

Figure 30. DSS-34 (Canberra) S-Band System Temperature versus Elevation Angle, S/X-Mode (S/X Dichroic In Place), Non-Diplexed Path, 2.3 GHz

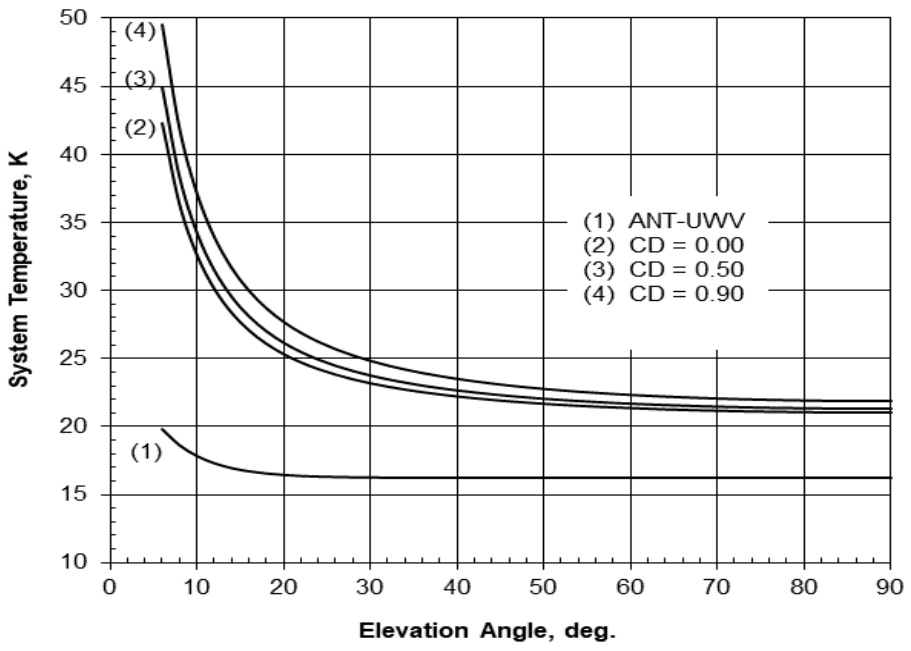

Figure 31. DSS-25 (Goldstone) X-Band RCP System Temperature versus Elevation Angle, X/Ka-Mode, 8.4 GHz

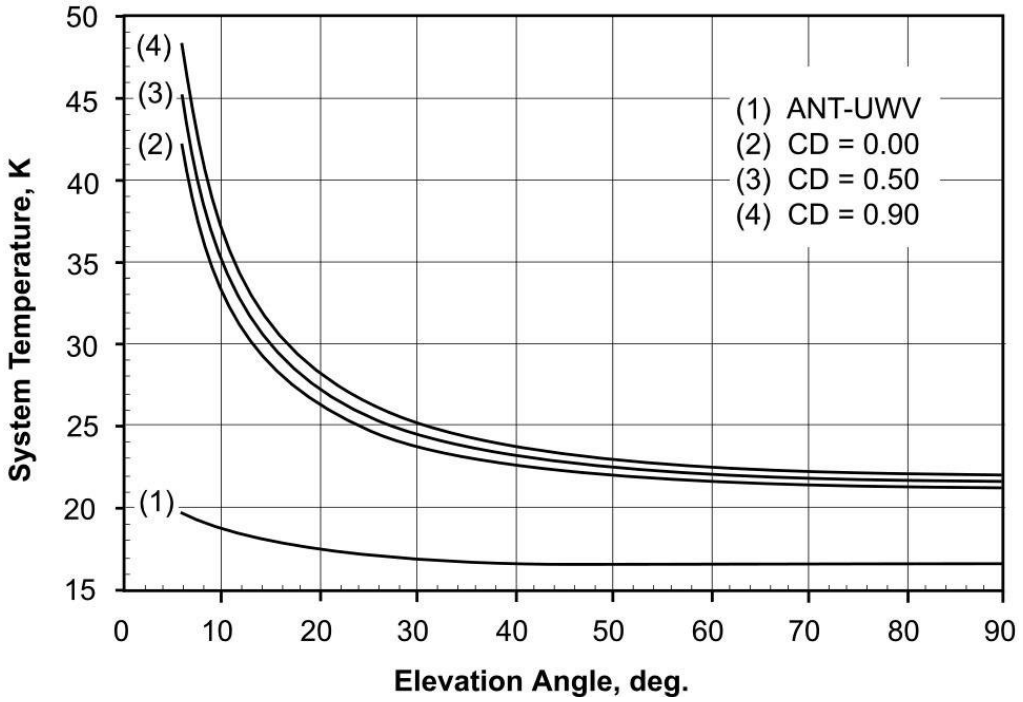

Figure 32. DSS-26 (Goldstone) X-Band RCP System Temperature versus Elevation Angle, X/Ka-Mode, 8.4 GHz

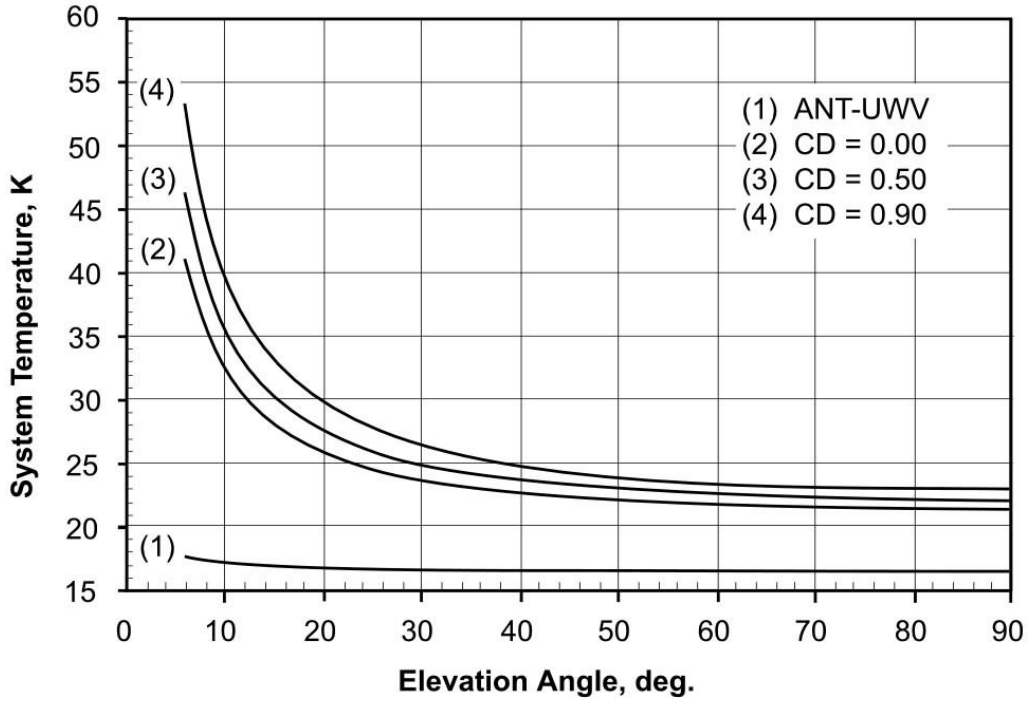

Figure 33. DSS-34 (Canberra) X-Band RCP System Temperature versus Elevation Angle, X/Ka-Mode (S/X Dichroic Retracted), 8.4 GHz

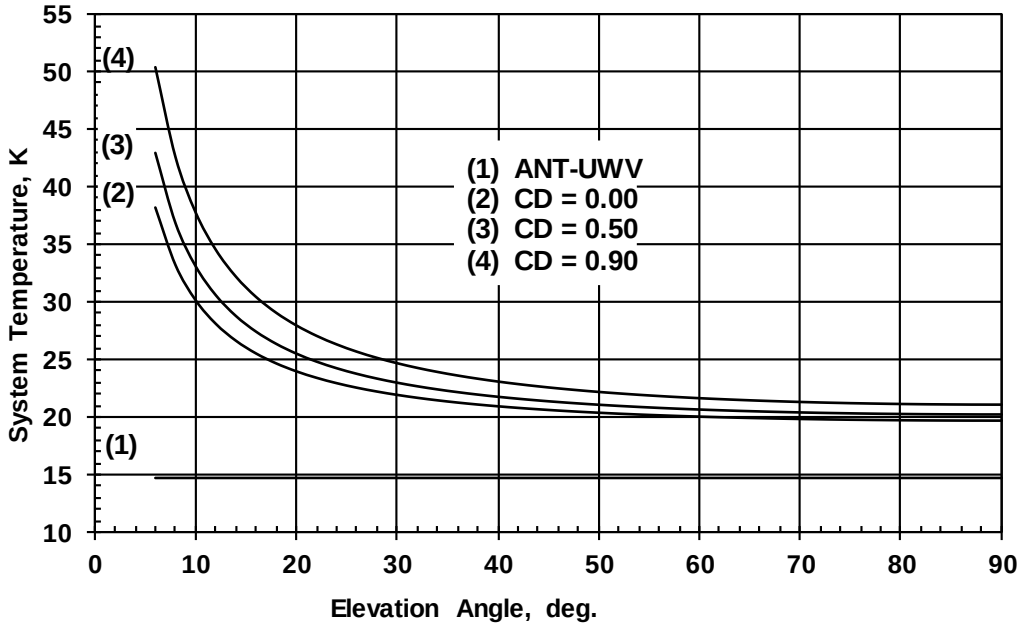

Figure 34. DSS-35 (Canberra) X-Band RCP System Temperature versus Elevation Angle, X/Ka-Mode, 8.4 GHz

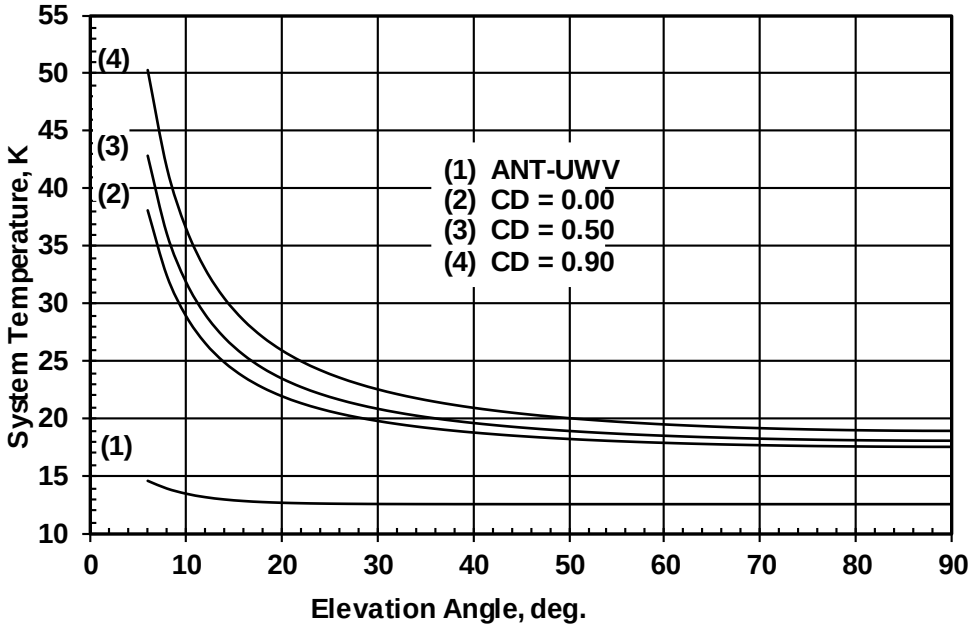

Figure 35. DSS-36 (Canberra) X-Band RCP System Temperature versus Elevation Angle, X/Ka-Mode, 8.4 GHz

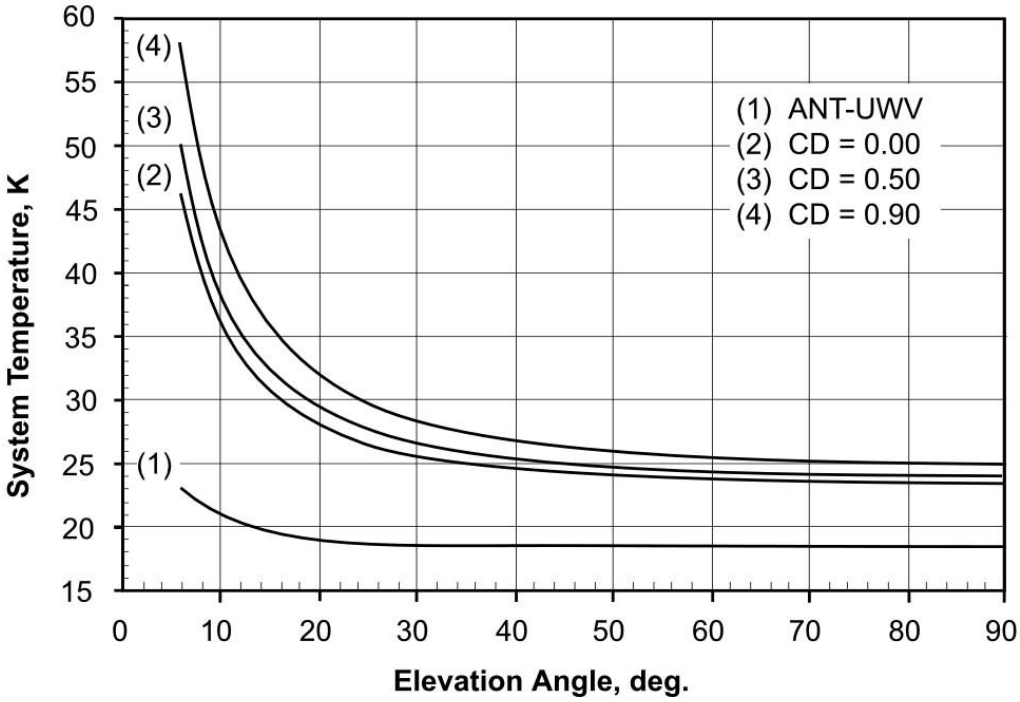

Figure 36. DSS-54 (Madrid) X-Band RCP System Temperature versus Elevation Angle, X/Ka-Mode (S/X Dichroic Retracted), 8.4 GHz

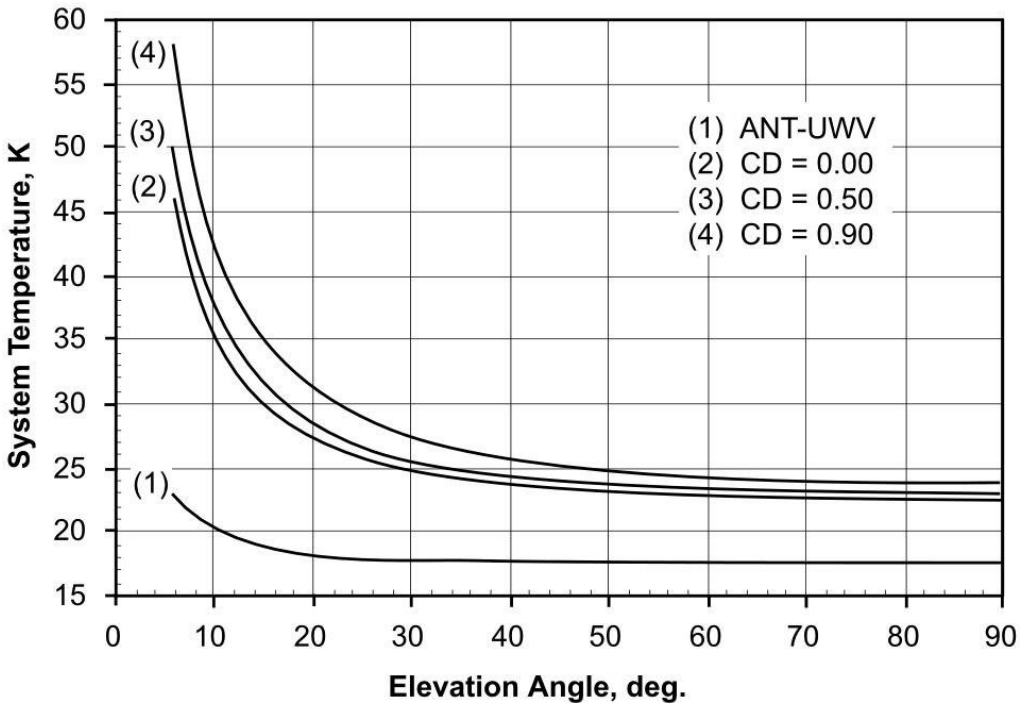

Figure 37. DSS-55 (Madrid) X-Band RCP System Temperature versus Elevation Angle, X/Ka-Mode, 8.4 GHz

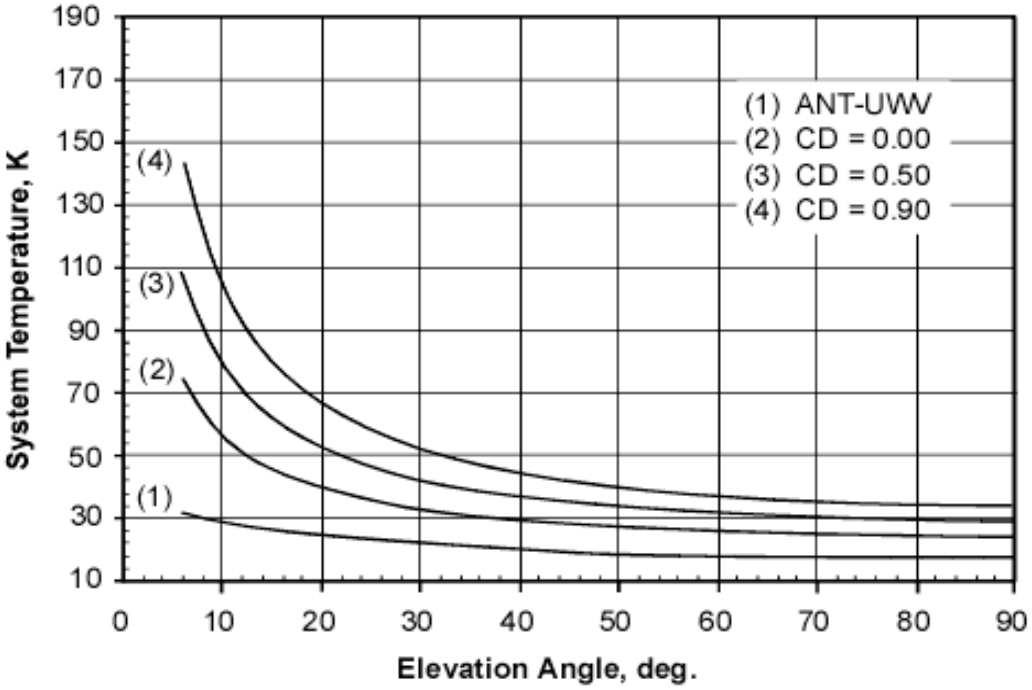

Figure 38. DSS-24 (Goldstone) K-Band RCP System Temperature versus Elevation Angle, K-only Mode (S/K Dichroic Retracted), 26 GHz

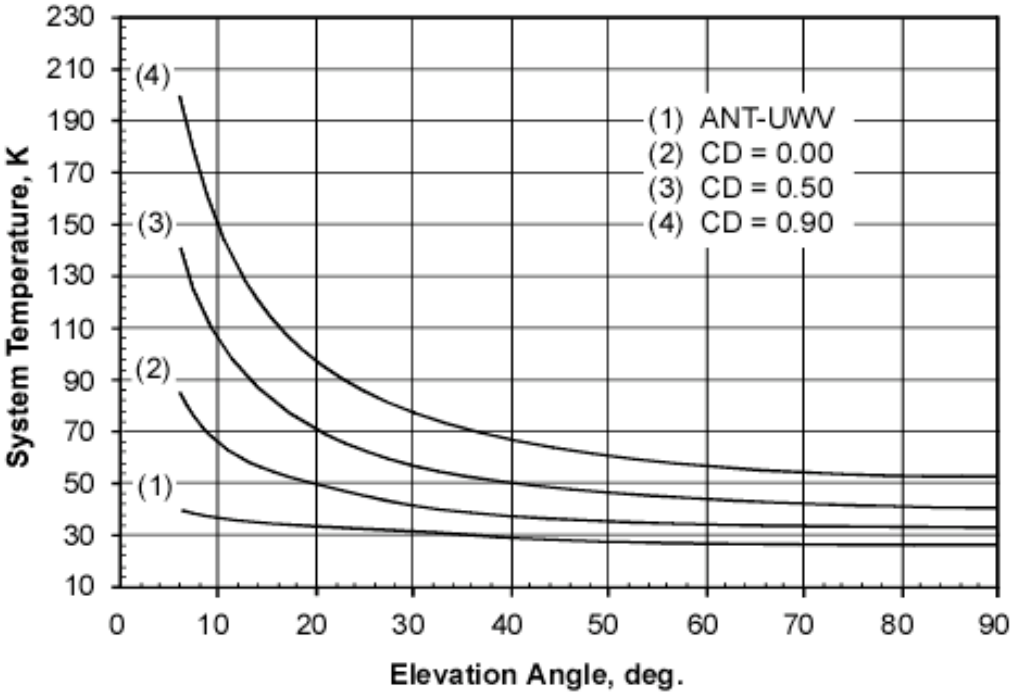

Figure 39. DSS-34 (Canberra) K-Band RCP System Temperature versus Elevation Angle, K-only Mode (S/K Dichroic Retracted), 26 GHz

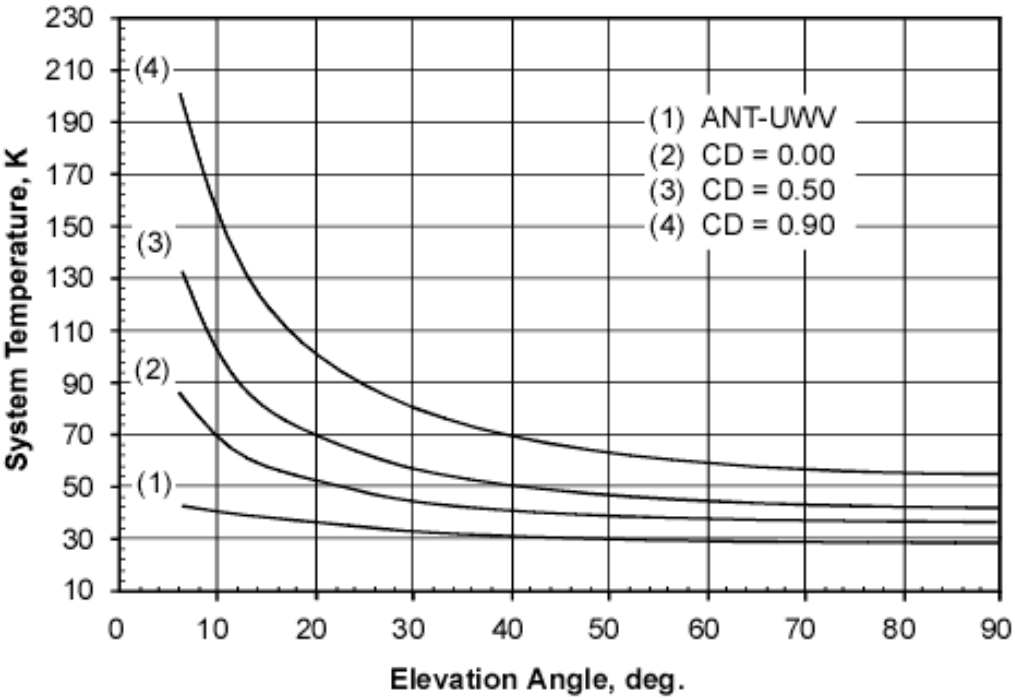

Figure 40. DSS-54 (Madrid) K-Band RCP System Temperature versus Elevation Angle, K-only Mode (S/K Dichroic Retracted), 26 GHz

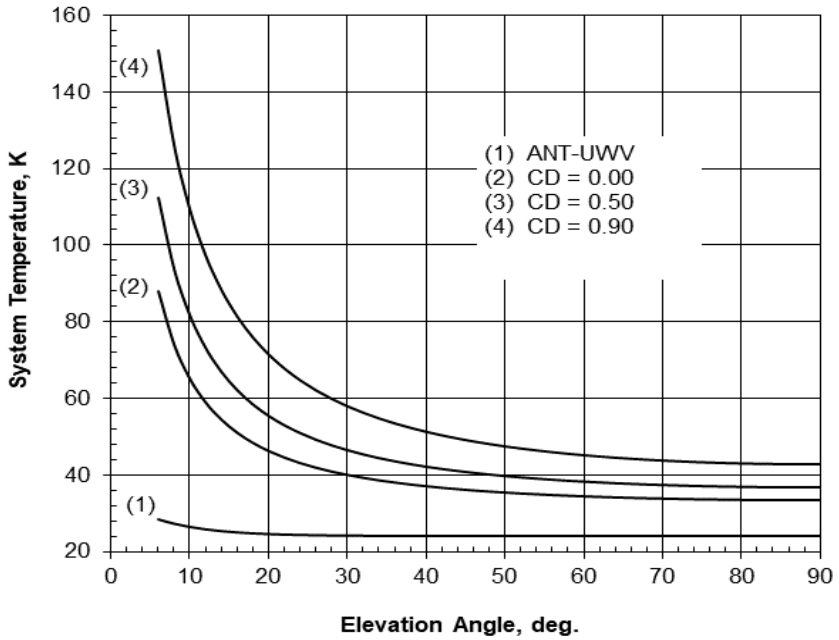

Figure 41. DSS-25 (Goldstone) Ka-Band RCP System Temperature versus Elevation Angle, X/Ka-Mode, 32 GHz

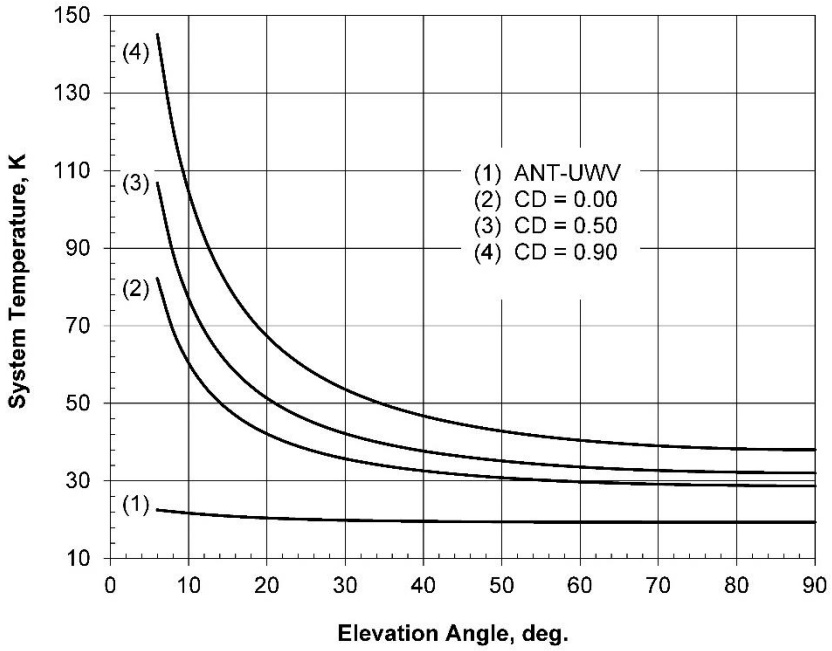

Figure 42. DSS-26 (Goldstone) Ka-Band RCP System Temperature versus Elevation Angle, X/Ka-Mode, 32 GHz

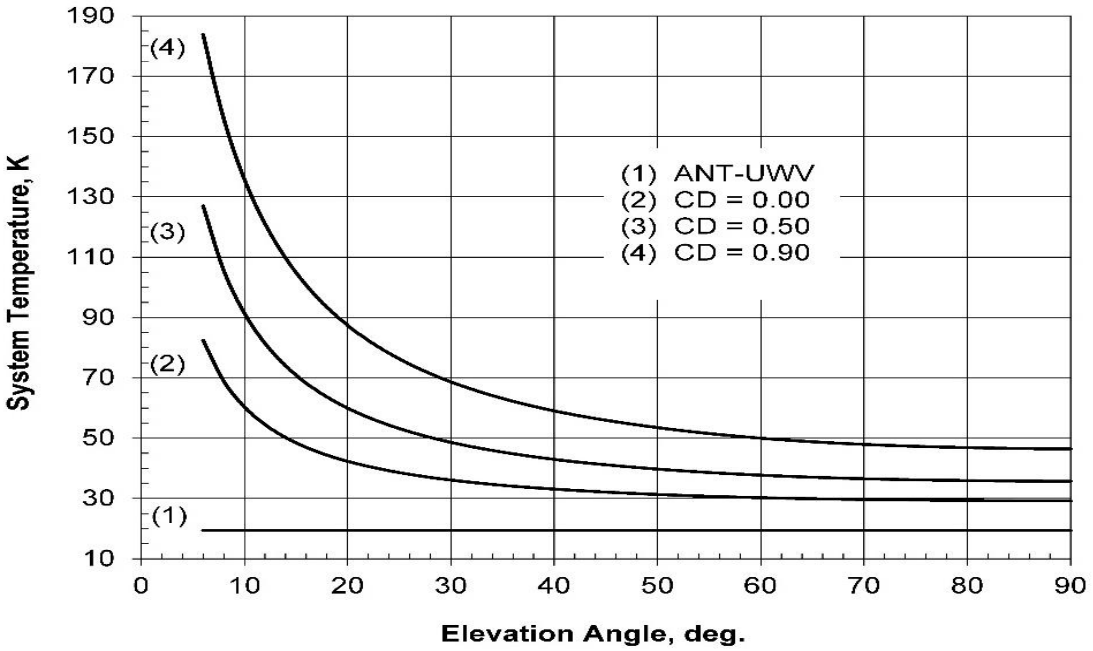

Figure 43. DSS-34 (Canberra) Ka-Band RCP System Temperature versus Elevation Angle, X/Ka-Mode, 32 GHz

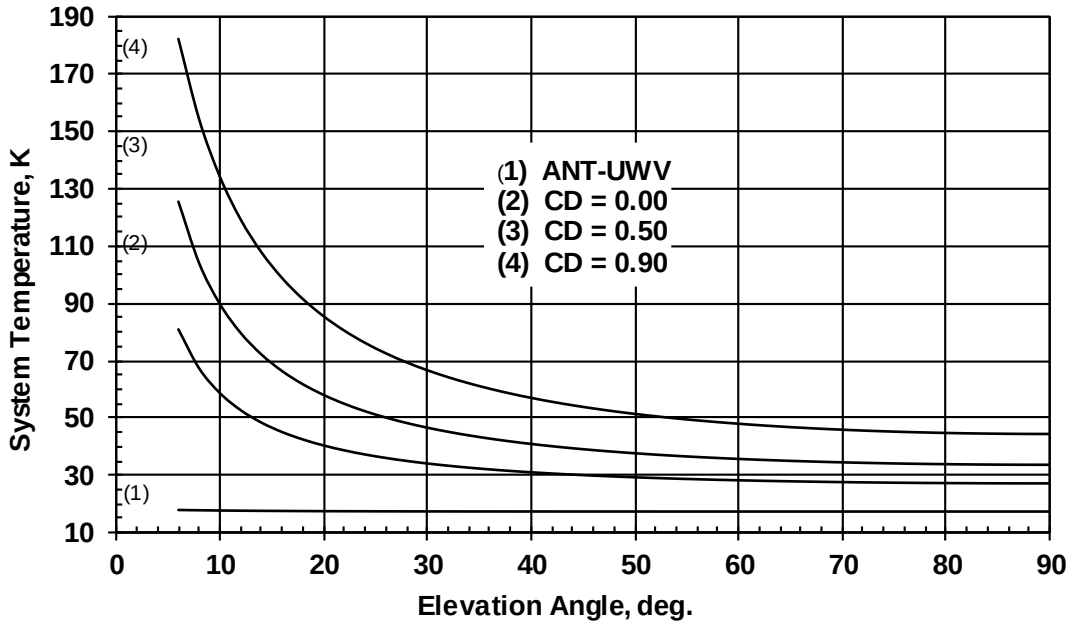

Figure 44. DSS-35 (Canberra) Ka-Band RCP System Temperature versus Elevation Angle, X/Ka-Mode, 32 GHz

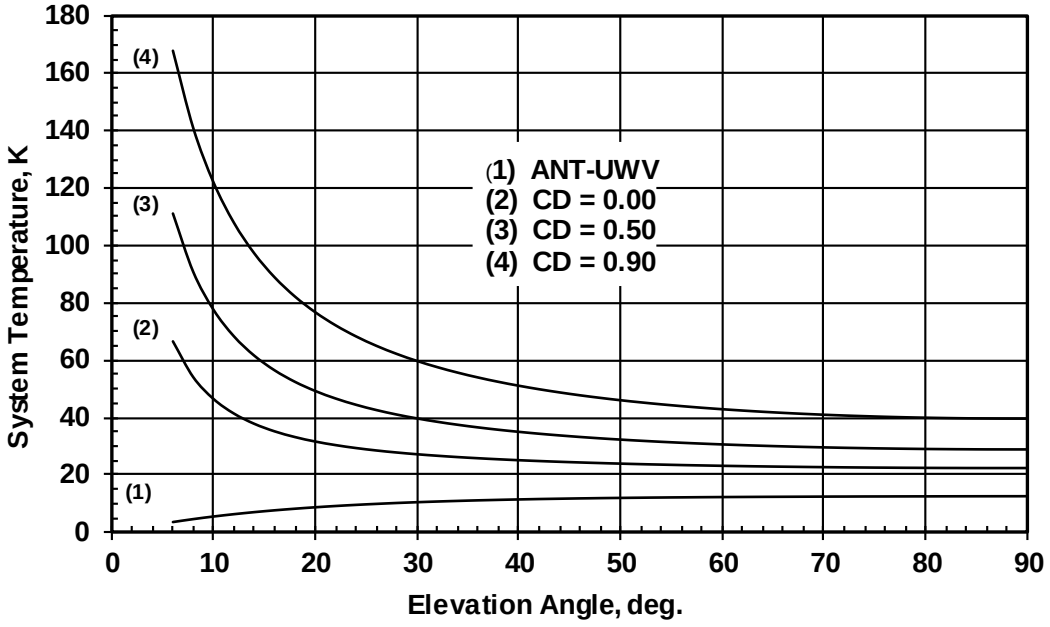

Figure 45. DSS-36 (Canberra) Ka-Band RCP System Temperature versus Elevation Angle, X/Ka-Mode, 32 GHz

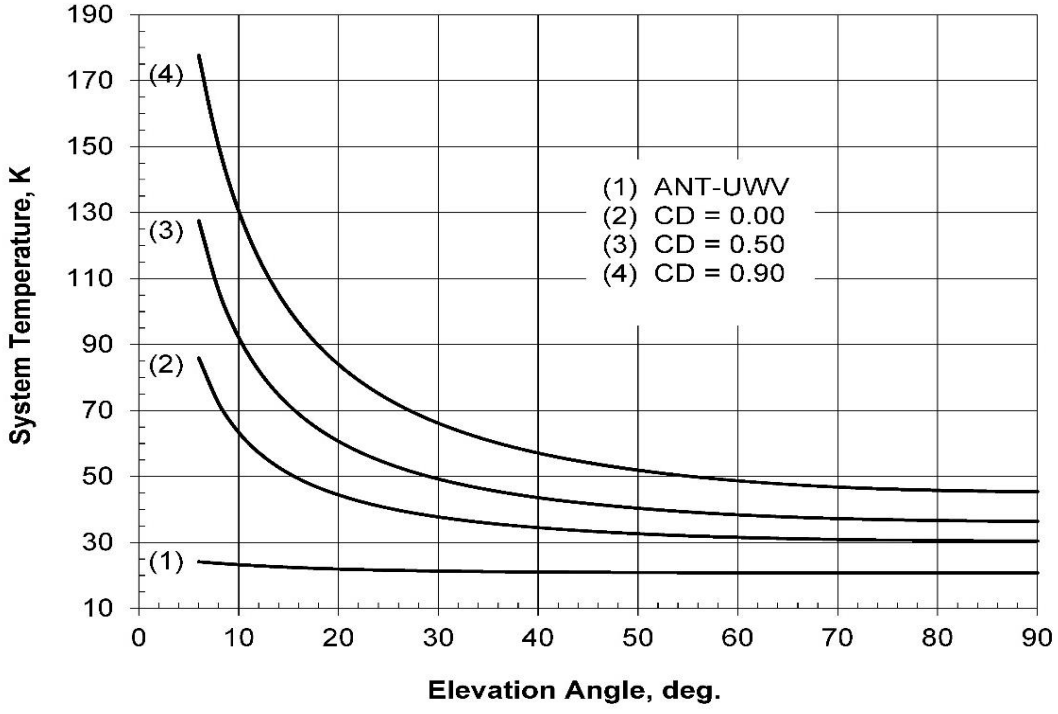

Figure 46. DSS-55 (Madrid) Ka-Band RCP System Temperature versus Elevation Angle, X/Ka-Mode, 32 GHz

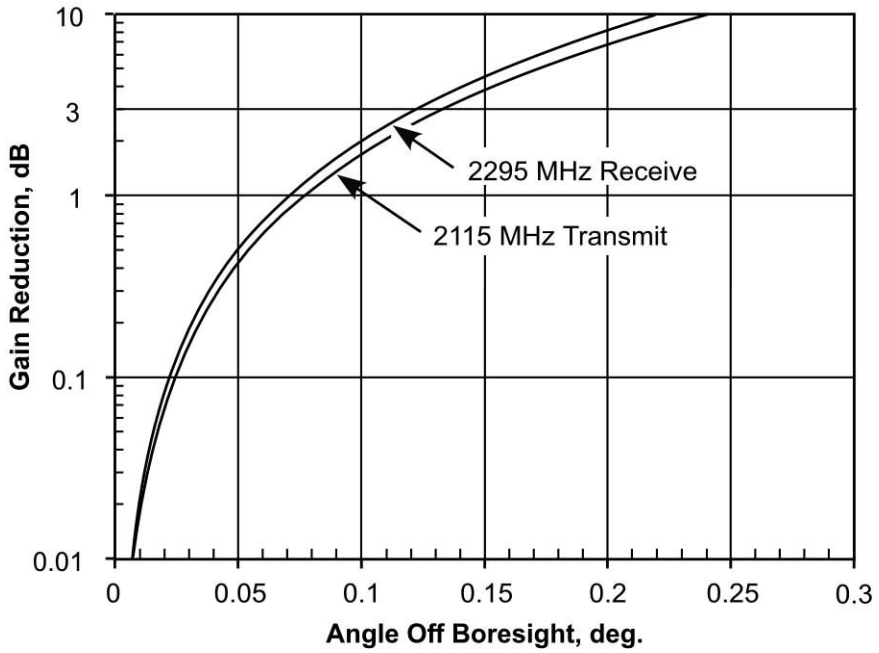

Figure 47. S-Band Gain Reduction versus Angle off Boresight

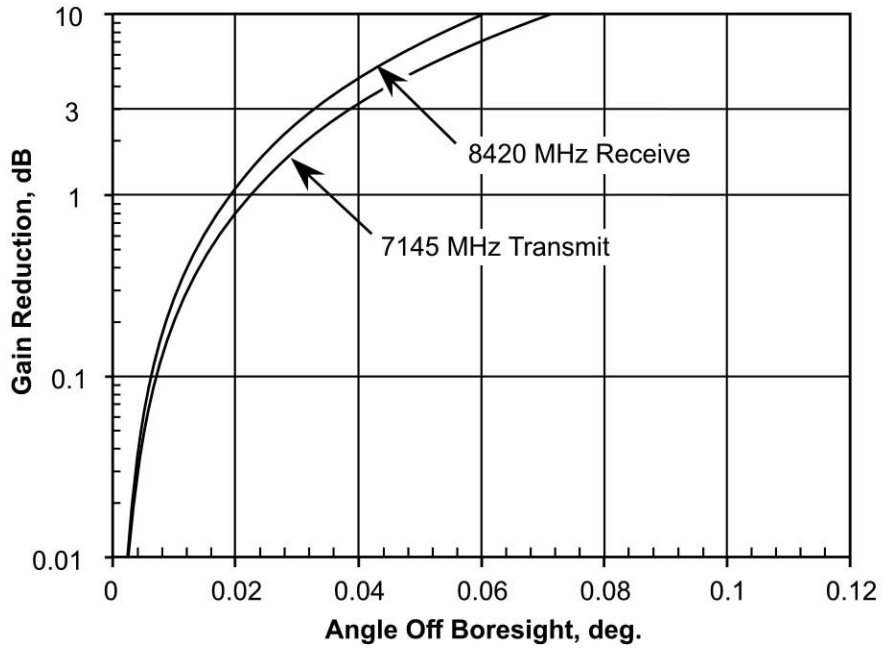

Figure 48. X-Band Gain Reduction versus Angle off Boresight

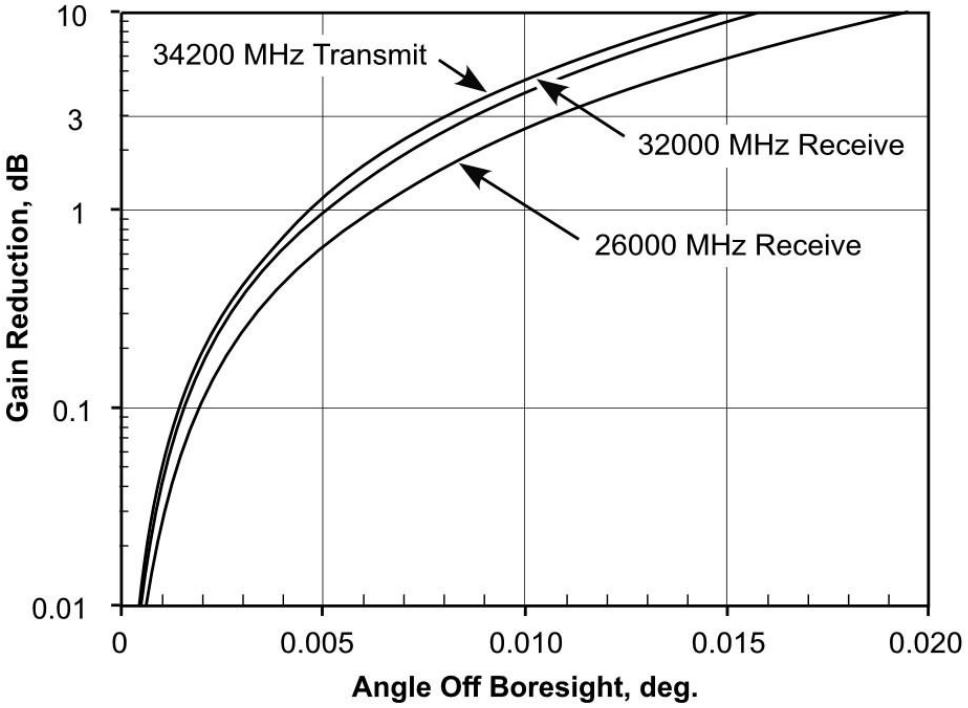

Figure 49. K- and Ka-Band Gain Reduction versus Angle off Boresight

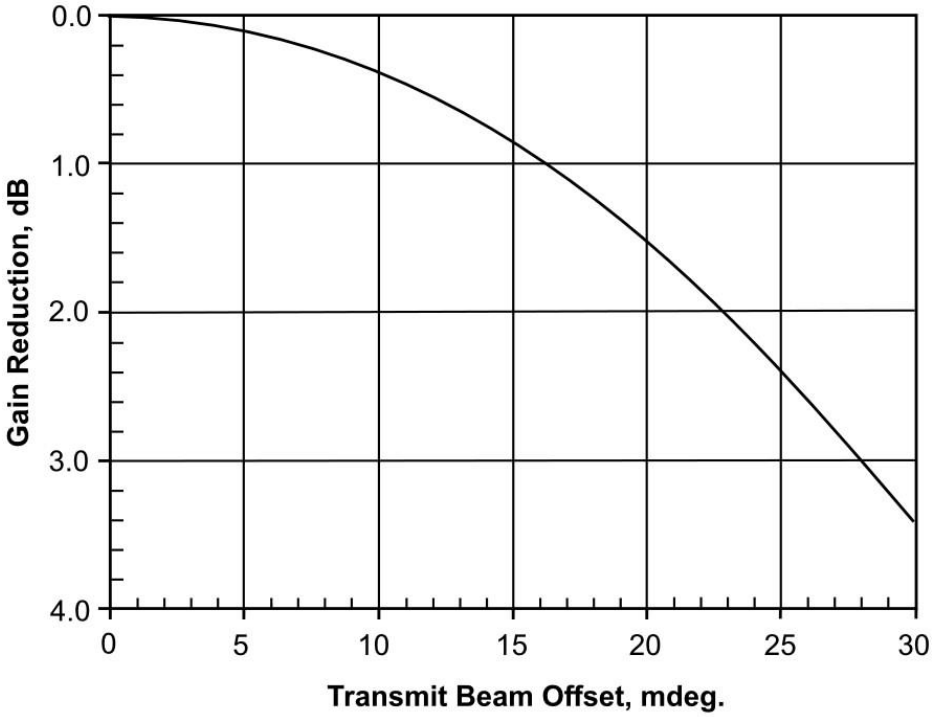

Figure 50. Ka-Band Transmit Gain Reduction Due to Aberration Correction

Appendix A
Equations for Modeling

A.1 Equations for Gain Versus Elevation Angle

The following equation can be used to generate S-, X-, K-, and Ka-band transmit and receive gain versus elevation angle curves. Examples of these curves for selected stations and configurations are shown in Figures 13–29. See paragraph 2.1.1.1 for frequency effect modeling and module 105 for atmospheric attenuation at weather conditions other than 0%, 50%, and 90% cumulative distribution.

$$G(\theta) = G_0 - G_1(\theta - \gamma)^2 - \frac{A_{zen}}{\sin\theta}, \quad \text{dBi} \tag{A-1}$$

where

θ	=	antenna elevation angle (deg.) $6 \leq \theta \leq 90$
G_0, G_1, γ	=	parameters from Table A-1 through Table A-4
A_{zen}	=	zenith atmospheric attenuation, dB, from this module, Table A-5 (Module 105, Rev. E), or from Tables 10 through 21 in module 105

A.2 Equations for System Temperature Versus Elevation Angle

The following equation can be used to generate S-, X, and Ka-band system temperature versus elevation angle curves. Examples of these curves are shown in Figures 30-46. See module 105 for atmospheric attenuation at weather conditions other than 0%, 50%, and 90% cumulative distribution.

System operating noise temperature:

$$T_{op}(\theta) = T_{AMW} + T_{sky}, \quad \text{K} \tag{A2}$$

Antenna-Microwave noise contribution:

$$T_{AMW} = T_1 + T_2 e^{-a\theta}, \quad \text{K} \tag{A3}$$

Sky noise contribution:

$$T_{sky} = T_{atm}(\theta) + T'_{CMB}(\theta), \quad \text{K} \tag{A4}$$

Atmospheric attenuation:

$$A(\theta) = \frac{A_{zen}}{\sin(\theta)}, \quad \text{dB} \tag{A5}$$

Atmospheric loss factor:

$$L(\theta) = 10^{\frac{A(\theta)}{10}}, \text{ dimensionless, } >1.0 \tag{A6}$$

Atmosphere mean physical temperature:

$$T_p = 255 + 25 \times CD, \quad \text{K} \tag{A7}$$

Atmospheric noise contribution:

$$T_{atm}(\theta) = T_p\left[1 - \frac{1}{L(\theta)}\right], \quad \text{K} \tag{A8}$$

Effective cosmic background noise:

$$T'_{CMB}(\theta) = \frac{T_{CMB}}{L(\theta)}, \quad \text{K} \tag{A9}$$

where

θ	=	antenna elevation angle (deg.), $6 \le \theta \le 90$
T_1, T_2, a	=	antenna-microwave noise temperature parameters from Tables A-1 through A-4
A_{zen}	=	zenith atmospheric attenuation, dB, from this module, Table A-5 (Module 105, Rev. E), or from Tables 10–21 in Module 105 as a function of frequency, station, and cumulative distribution (CD)
CD	=	cumulative distribution, $0 \le CD \le 0.99$, used to select A_{zen} from Table A-5 or from Tables 10–21 in Module 105
T_{CMB}	=	2.725 K, cosmic microwave background noise temperature

A.3 Equation for Gain Reduction Versus Pointing Error

The following equation can be used to generate gain reduction versus pointing error curves examples of which are depicted in Figures 47–49.

$$\Delta G(\theta) = 10\log\left(e^{\frac{2.773\theta^2}{HPBW^2}}\right), \quad \text{dB} \tag{A-3}$$

where

θ = pointing error, deg

$HPBW$ = half-power beamwidth (from Tables 2–7)

A.4 Equation for Transmit Aberration Gain Reduction

The following equation can be used to generate the Ka-band transmit gain reduction curve depicted in Figure 50.

$$\Delta G(\phi) = -0.0038\phi^2, \quad \text{dB} \tag{A-4}$$

where

ϕ = transmit beam offset, mdeg

Table A-1. S-Band Vacuum Gain and Antenna-Microwave Noise Temperature Parameters, Referenced to Feedhorn Aperture

Station and Configuration	Vacuum Gain Parameters				Antenna-Microwave Noise Temperature Parameters			Figures
	G_0 Transmit	G_0 Receive	G_1	γ	T_1	T_2	a	
DSS-24 (Goldstone)								
S/X or S/K, HEMT-1, RCP or LCP, Non-Diplexed	-	56.87	0.000032	90.0	26.04	5.2	0.05	
S/X or S/K, HEMT-1, RCP or LCP, Diplexed	56.20	56.87	0.000032	90.0	33.41	5.6	0.05	
DSS-26 (Goldstone)								
S/X or S/K, HEMT-1, RCP or LCP, Non-Diplexed	-	56.56	0.000033	63.9	17.6	14	0.11	
S/X or S/K, HEMT-1, RCP or LCP, Diplexed, Near-Earth Band	55.89	56.56	0.000033	63.9	23.4	14	0.11	N/A for deep space
DSS-34 (Canberra)								
S/X or S/K, HEMT-1, RCP or LCP, Non-Diplexed	-	56.83	0.000042	43.19	24.88	20.0	0.16	Figure 13 Figure 30
S/X or S/K, HEMT-1, RCP or LCP, Diplexed	56.16	56.83	0.000042	43.19	34.46	20.0	0.16	
DSS-36 (Canberra)								
S/X or S/K, HEMT-1, RCP or LCP, Non-Diplexed	-	56.63	0.000042	45.00	21.57	28.0	0.20	
S/X or S/K, HEMT-1, RCP or LCP, Diplexed, Near-Earth Band	55.96	56.63	0.000042	45.00	30.43	28.0	0.20	N/A for deep space
DSS-54 (Madrid)								
S/X or S/K, HEMT-1, RCP or LCP, Non-Diplexed	-	56.83	0.000042	45.00	25.72	12.0	0.08	
S/X or S/K, HEMT-1, RCP or LCP, Diplexed	56.16	56.83	0.000042	45.00	35.34	12.0	0.08	N/A for deep space
DSS-56 (Madrid)								
S/X or S/K, HEMT-1, RCP or LCP, Non-Diplexed	-	56.76	0.000037	40.92	20.63	20.0	0.15	
S/X or S/K, HEMT-1, RCP or LCP, Diplexed	56.09	56.76	0.000037	40.92	27.33	20.0	0.15	N/A for deep space

NOTES:

Figures referenced are typically for highest performance configuration for each stated antenna. See Sections 2.1.1.2 and 2.1.2.

Values in above table are for S-band deep-space uplink (transmit) and downlink (receive) frequencies.

Nominal S-band deep-space uplink frequency is 2115 MHz.
Nominal S-band deep-space downlink frequency is 2295 MHz.
Nominal S-band near-earth uplink frequency is 2067.5 MHz.
Nominal S-band near-earth downlink frequency is 2245 MHz.

For near-earth uplink G_0 gain, reduce above G_0 transmit gains by 0.19 dB.
For near-earth downlink G_0 gain, reduce above G_0 receive gains by 0.19 dB.

DSS-26, DSS-36, and DSS-56 not available for S-band deep-space uplink due to low transmit power (250 W). DSS-54 and DSS-56 not available for S-band deep-space uplink due to frequency restriction.

Table A-2. X-Band Vacuum Gain and Antenna-Microwave Noise Temperature Parameters, Referenced to Feedhorn Aperture

Station and Configuration	Vacuum Gain Parameters				Antenna-Microwave Noise Temperature Parameters			Figures
	G_0 Transmit	G_0 Receive	G_1	γ	T_1	T_2	a	
DSS-23 (Goldstone)								
X/Ka, HEMT-1, RCP, Diplexed	TBD	TBD			TBD			
X/Ka, HEMT-2, LCP, Diplexed	TBD	TBD			TBD			
DSS-24 (Goldstone)								
X-Only, MASER-1, RCP or LCP, Non-Diplexed	-	68.24	0.000027	51.50	21.28	1.5	0.11	
X-Only, MASER-1, RCP or LCP, Diplexed	66.88	68.24	0.000027	51.50	30.39	2.9	0.11	
S/X, MASER-1, RCP or LCP, Non-Diplexed	-	68.19	0.000027	51.50	22.72	1.5	0.11	
S/X, MASER-1, RCP or LCP, Diplexed	N/A	68.19	0.000027	51.50	31.89	2.9	0.11	
DSS-25 (Goldstone)								
X/Ka, HEMT-1, RCP, Diplexed	66.86	68.22	0.000047	42.44	16.2	12.0	0.2	Figure 14 Figure 31
X/Ka, HEMT-2, LCP, Diplexed	66.86	68.22	0.000047	42.44	16.0	12.0	0.2	
DSS-26 (Goldstone)								
X/Ka, HEMT-1, RCP, Diplexed	66.93	68.29	0.000059	42.46	16.29	5.2	0.08	Figure 15 Figure 32
X/Ka, HEMT-2, LCP, Diplexed	66.93	68.29	0.000059	42.46	15.43	5.2	0.08	
S/X, HEMT-1, RCP, Diplexed	N/A	68.24	0.000059	42.46	18.01	5.2	0.08	
S/X, HEMT-2, LCP, Diplexed	N/A	68.24	0.000059	42.46	17.15	5.2	0.08	
DSS-33 (Canberra)								
X/Ka, HEMT-1, RCP, Diplexed	TBD	TBD			TBD			
X/Ka, HEMT-2, LCP, Diplexed	TBD	TBD			TBD			

Table A-2. X-Band Vacuum Gain and Antenna-Microwave Noise Temperature Parameters, Referenced to Feedhorn Aperture (continued)

Station and Configuration	Vacuum Gain Parameters				Antenna-Microwave Noise Temperature Parameters			Figures
	G_0 Transmit	G_0 Receive	G_1	γ	T_1	T_2	a	
DSS-34 (Canberra)								
X/Ka, HEMT-1, RCP, Diplexed	66.97	68.33	0.000045	48.64	16.28	5.0	0.15	Figure 16 Figure 33
X/Ka, HEMT-2, LCP, Diplexed	66.97	68.33	0.000045	48.64	16.71	5.0	0.15	
S/X, HEMT-1, RCP, Diplexed	N/A	68.28	0.000045	48.64	17.99	5.0	0.15	
S/X, HEMT-2, LCP, Diplexed	N/A	68.28	0.000045	48.64	18.43	5.0	0.15	
DSS-35 (Canberra)								
X/Ka, HEMT-1, RCP, Diplexed	66.99	68.35	0.000045	45.00	14.7	0.0	0.00	Figure 17 Figure 34
X/Ka, HEMT-2, LCP, Diplexed	66.99	68.35	0.000045	45.00	15.0	0.0	0.00	
DSS-36 (Canberra)								
X/Ka, HEMT-1, RCP, Diplexed	66.98	68.34	0.000045	45.00	12.59	15.0	0.20	Figure 18 Figure 35
X/Ka, HEMT-2, LCP Diplexed	66.98	68.34	0.000045	45.00	13.95	12.0	0.20	
S/X, HEMT-1, RCP, Diplexed	N/A	68.29	0.000045	45.00	14.31	15.0	0.20	
S/X, HEMT-2, LCP, Diplexed	N/A	68.29	0.000045	45.00	15.67	12.0	0.20	
DSS-53 (Madrid)								
X/Ka, HEMT-1, RCP, Diplexed	66.89	68.25	0.000046	43.0	13.1	20.0	0.4	
X/Ka, HEMT-2, LCP, Diplexed	66.89	68.25	0.000046	43.0	13.2	20.0	0.4	
DSS-54 (Madrid)								
X/Ka, HEMT-1, RCP, Diplexed	67.01	68.37	0.000058	45.25	18.31	11.0	0.15	Figure 19 Figure 36
X/Ka, HEMT-2, LCP, Diplexed	67.01	68.37	0.000058	45.25	18.31	11.0	0.15	
S/X, HEMT-1, RCP, Diplexed	N/A	68.32	0.000058	45.25	20.03	11.0	0.15	
S/X, HEMT-2, LCP, Diplexed	N/A	68.32	0.000058	45.25	20.03	11.0	0.15	
DSS-55 (Madrid)								
X/Ka, HEMT-1, RCP, Diplexed	66.98	68.34	0.000035	43.55	17.42	13.2	0.15	Figure 20 Figure 37
X/Ka, HEMT-2, LCP, Diplexed	66.98	68.34	0.000035	43.55	17.82	13.2	0.15	

Table A-2. X-Band Vacuum Gain and Antenna-Microwave Noise Temperature Parameters, Referenced to Feedhorn Aperture (continued)

Station and Configuration	Vacuum Gain Parameters				Antenna-Microwave Noise Temperature Parameters			Figures
	G_0 Transmit	G_0 Receive	G_1	γ	T_1	T_2	a	
DSS-56 (Madrid)								
X/Ka, HEMT-1, RCP, Diplexed	66.75	68.11	0.000054	49.94	14.47	-0.9	0.05	
X/Ka, HEMT-2, LCP, Diplexed	66.75	68.11	0.000054	49.94	13.96	-0.9	0.05	
S/X, HEMT-1, RCP, Diplexed	N/A	68.06	0.000054	49.94	16.19	-0.9	0.05	
S/X, HEMT-2, LCP, Diplexed	N/A	68.06	0.000054	49.94	15.68	-0.9	0.05	

NOTES:

Figures referenced are typically for highest performance configuration for each stated antenna. See Sections 2.1.1.2 and 2.1.2.

Values in above table are for X-band deep-space uplink (transmit) and downlink (receive) frequencies.

Nominal X-band deep-space uplink frequency is 7167.5 MHz.
Nominal X-band deep-space downlink frequency is 8425 MHz.
Nominal X-band near-earth uplink frequency is 7212.5 MHz.
Nominal X-band near-earth downlink frequency is 8475 MHz.

For near-earth uplink G_0 gain, increase above G_0 transmit gains by 0.05 dB.
For near-earth downlink G_0 gain, increase above G_0 receive gains by 0.05 dB.
For low-gain mode add +20 K to T_1 values (X-band).

X-band uplink not available in S/X mode, with S/X dichroic extended.

Table A-3. K-Band Vacuum Gain and Antenna-Microwave Noise Temperature Parameters, Referenced to Feedhorn Aperture

Station and Configuration	Vacuum Gain Parameters			Antenna-Microwave Noise Temperature Parameters			Figures
	G_0 Receive	G_1		T_1	T_2	*a*	
DSS-24 (Goldstone)							
K-only, HEMT-1, RCP, 25.5 GHz, Non-Diplexed	77.03	0.00029	45.0	19.6	19.6	0.05	
K-only, HEMT-2, LCP, 25.5 GHz, Non-Diplexed	77.03	0.00029	45.0	27.1	19.6	0.05	
S/K, HEMT-1, RCP, 25.5 GHz, Non-Diplexed	76.99	0.00029	45.0	30.3	20.4	0.065	
S/K, HEMT-2, LCP, 25.5 GHz, Non-Diplexed	76.99	0.00029	45.0	37.8	20.4	0.065	
K-only, HEMT-1, RCP, 26.0 GHz, Non-Diplexed	77.20	0.00029	45.0	17.5	19.6	0.05	Figure 21 Figure 38
K-only, HEMT-2, LCP, 26.0 GHz, Non-Diplexed	77.20	0.00029	45.0	23.5	19.6	0.05	
S/K, HEMT-1, RCP, 26.0 GHz, Non-Diplexed	77.16	0.00029	45.0	23.5	20.4	0.065	
S/K, HEMT-2, LCP, 26.0 GHz, Non-Diplexed	77.16	0.00029	45.0	29.5	20.4	0.065	
K-only, HEMT-1, RCP, 27.0 GHz, Non-Diplexed	77.53	0.00029	45.0	20.8	19.6	0.05	
K-only, HEMT-2, LCP, 27.0 GHz, Non-Diplexed	77.53	0.00029	45.0	25.4	19.6	0.05	
S/K, HEMT-1, RCP, 27.0 GHz, Non-Diplexed	77.49	0.00029	45.0	30.5	20.4	0.065	
S/K, HEMT-2, LCP, 27.0 GHz, Non-Diplexed	77.49	0.00029	45.0	35.1	20.4	0.065	
DSS-26 (Goldstone)							
K-only, HEMT-1, RCP, 26.0 GHz, Diplexed	77.38	0.00094	45.0	31.8	-1.3	0.05	
K-only, HEMT-2, LCP, 26.0 GHz, Diplexed	77.38	0.00094	45.0	30.8	-1.3	0.05	
S/K, HEMT-1, RCP, 26.0 GHz, Diplexed	77.34	0.00094	45.0	40.4	-1.3	0.05	
S/K, HEMT-2, LCP, 26.0 GHz, Diplexed	77.34	0.00094	45.0	39.4	-1.3	0.05	

Table A-3. K-Band Vacuum Gain and Antenna-Microwave Noise Temperature Parameters, Referenced to Feedhorn Aperture (continued)

Station and Configuration	Vacuum Gain Parameters			Antenna-Microwave Noise Temperature Parameters			Figures
	G_0 Receive	G_1	γ	T_1	T_2	a	
DSS-34 (Canberra)							
K-only, HEMT-1, RCP, 25.5 GHz, Non-Diplexed	77.02	0.00029	48.0	24.9	19.6	0.05	
K-only, HEMT-2, LCP, 25.5 GHz, Non-Diplexed	77.02	0.00029	48.0	26.3	19.6	0.05	
S/K, HEMT-1, RCP, 25.5 GHz, Non-Diplexed	76.98	0.00029	48.0	35.6	20.4	0.065	
S/K, HEMT-2, LCP, 25.5 GHz, Non-Diplexed	76.98	0.00029	48.0	37.0	20.4	0.065	
K-only, HEMT-1, RCP, 26.0 GHz, Non-Diplexed	77.19	0.00029	48.0	25.3	19.6	0.05	Figure 22 Figure 39
K-only, HEMT-2, LCP, 26.0 GHz, Non-Diplexed	77.19	0.00029	48.0	25.4	19.6	0.05	
S/K, HEMT-1, RCP, 26.0 GHz, Non-Diplexed	77.15	0.00029	48.0	31.3	20.4	0.065	
S/K, HEMT-2, LCP, 26.0 GHz, Non-Diplexed	77.15	0.00029	48.0	31.4	20.4	0.065	
K-only, HEMT-1, RCP, 27.0 GHz, Non-Diplexed	77.52	0.00029	48.0	23.7	19.6	0.05	
K-only, HEMT-2, LCP, 27.0 GHz, Non-Diplexed	77.52	0.00029	48.0	24.5	19.6	0.05	
S/K, HEMT-1, RCP, 27.0 GHz, Non-Diplexed	77.48	0.00029	48.0	33.4	20.4	0.065	
S/K, HEMT-2, LCP, 27.0 GHz, Non-Diplexed	77.48	0.00029	48.0	34.2	20.4	0.065	
DSS-36 (Canberra)							
K-only, HEMT-1, RCP, 26.0 GHz, Non-Diplexed	TBD			TBD			
K-only, HEMT-2, LCP, 26.0 GHz, Non-Diplexed	TBD			TBD			

Table A-3. K-Band Vacuum Gain and Antenna-Microwave Noise Temperature Parameters, Referenced to Feedhorn Aperture (continued)

Station and Configuration	Vacuum Gain Parameters			Antenna-Microwave Noise Temperature Parameters			Figures
	G_0 Receive	G_1	γ	T_1	T_2	a	
S/K, HEMT-1, RCP, 26.0 GHz, Non-Diplexed	TBD			TBD			
S/K, HEMT-2, LCP, 26.0 GHz, Non-Diplexed	TBD			TBD			
DSS-54 (Madrid)							
K-only, HEMT-1, RCP, 25.5 GHz, Non-Diplexed	77.02	0.00029	45.0	28.2	19.6	0.05	
K-only, HEMT-2, LCP, 25.5 GHz, Non-Diplexed	77.02	0.00029	45.0	30.7	19.6	0.05	
S/K, HEMT-1, RCP, 25.5 GHz, Non-Diplexed	76.98	0.00029	45.0	38.9	20.4	0.065	
S/K, HEMT-2, LCP, 25.5 GHz, Non-Diplexed	76.98	0.00029	45.0	41.4	20.4	0.065	
K-only, HEMT-1, RCP, 26.0 GHz, Non-Diplexed	77.19	0.00029	45.0	28.1	19.6	0.05	Figure 23 Figure 40
K-only, HEMT-2, LCP, 26.0 GHz, Non-Diplexed	77.19	0.00029	45.0	29.0	19.6	0.05	
S/K, HEMT-1, RCP, 26.0 GHz, Non-Diplexed	77.15	0.00029	45.0	34.1	20.4	0.065	
S/K, HEMT-2, LCP, 26.0 GHz, Non-Diplexed	77.15	0.00029	45.0	35.0	20.4	0.065	
K-only, HEMT-1, RCP, 27.0 GHz, Non-Diplexed	77.52	0.00029	45.0	26.7	19.6	0.05	
K-only, HEMT-2, LCP, 27.0 GHz, Non-Diplexed	77.52	0.00029	45.0	26.6	19.6	0.05	
S/K, HEMT-1, RCP, 27.0 GHz, Non-Diplexed	77.48	0.00029	45.0	36.4	20.4	0.065	
S/K, HEMT-2, LCP, 27.0 GHz, Non-Diplexed	77.48	0.00029	45.0	36.3	20.4	0.065	
DSS-56 (Madrid)							
K-only, HEMT-1, RCP, 26.15 GHz, Non-Diplexed	77.57	0.00066	34.37	33.8	28.5	0.075	
K-only, HEMT-2, LCP, 26.15 GHz, Non-Diplexed	77.57	0.00066	34.37	33.8	28.5	0.075	

Table A-3. K-Band Vacuum Gain and Antenna-Microwave Noise Temperature Parameters, Referenced to Feedhorn Aperture (continued)

Station and Configuration	Vacuum Gain Parameters			Antenna-Microwave Noise Temperature Parameters			Figures
	G_0 Receive	G_1	γ	T_1	T_2	a	
S/K, HEMT-1, RCP, 26.15 GHz, Non-Diplexed	77.53	0.00066	34.37	39.8	28.5	0.075	
S/K, HEMT-2, LCP, 26.15 GHz, Non-Diplexed	77.53	0.00066	34.37	39.8	28.5	0.075	

NOTES:

Figures referenced are typically for highest performance configuration for each stated antenna. See Sections 2.1.1.2 and 2.1.2.

Values in above table are for K-band near-earth downlink (receive) frequencies.

Nominal K-band near-earth downlink frequency is 26250 MHz.

Nominal K-band near-earth uplink frequency is 22850 MHz.

For K-band uplink, $G_{0,transmit} = G_{0,receive} - 1.1$ dB.

For low-gain mode add +180 K to T_1 values (K-band).

See Section 3 and Table 1 for future K-band uplink and downlink implementation dates.

Table A-4. Ka-Band Vacuum Gain and Antenna-Microwave Noise Temperature Parameters, Referenced to Feedhorn Aperture

Station and Configuration	Vacuum Gain Parameters				Antenna-Microwave Noise Temperature Parameters			Figures
	G_0 Transmit	G_0 Receive	G_1	γ	T_1	T_2	a	
DSS-23 (Goldstone)								
X/Ka, HEMT-1, RCP, Non-Diplexed	-	TBD			TBD			
X/Ka, HEMT-2, RCP-error, Non-Diplexed	-	-	-	-	TBD			
X/Ka, HEMT-3, LCP, Non-Diplexed	-	TBD			TBD			
DSS-25 (Goldstone)								
X/Ka, HEMT-1, RCP, Diplexed	79.03	78.40	0.00036	53.83	24.2	10.0	0.15	Figure 24 Figure 41
X/Ka, HEMT-2, RCP-error, Diplexed	-	-	-	-	25.7	10.0	0.15	
X/Ka, HEMT-3, LCP, Diplexed	79.03	78.40	0.00036	53.83	23.0	10.0	0.15	
DSS-26 (Goldstone)								
X/Ka, HEMT-1, RCP, Non-Diplexed	-	79.13	0.00022	44.38	19.35	5.0	0.075	Figure 25 Figure 42
X/Ka, HEMT-2, RCP-error, Non-Diplexed	-	-	-	-	24.54	5.0	0.075	
X/Ka, HEMT-3, LCP, Non-Diplexed	-	79.13	0.00022	44.38	20.76	5.0	0.075	
DSS-33 (Canberra)								
X/Ka, HEMT-1, RCP, Non-Diplexed	-	TBD			TBD			
X/Ka, HEMT-2, RCP-error, Non-Diplexed	-	-	-	-	TBD			
X/Ka, HEMT-3, LCP, Non-Diplexed	-	TBD			TBD			
DSS-34 (Canberra)								
X/Ka, HEMT-1, RCP, Non-Diplexed	-	78.98	0.00031	44.30	19.38	0.0	0.000	Figure 26 Figure 43
X/Ka, HEMT-2, RCP-error, Non-Diplexed	-	-	-	-	23.25	0.0	0.000	
X/Ka, HEMT-3, LCP, Non-Diplexed	-	78.98	0.00031	44.30	19.61	0.0	0.000	
DSS-35 (Canberra)								
X/Ka, HEMT-1, RCP, Diplexed (8/2026)	TBD	79.27	0.00031	45.00	17.3	1.0	0.1	Figure 27 Figure 44
X/Ka, HEMT-2, RCP-error, Diplexed (8/2026)	-	-	-	-	not measured			
X/Ka, HEMT-3, LCP, Diplexed (8/2026)	TBD	79.27	0.00031	45.00	17.2	1.0	0.1	

Table A-4. Ka-Band Vacuum Gain and Antenna-Microwave Noise Temperature Parameters, Referenced to Feedhorn Aperture (continued)

Station and Configuration	Vacuum Gain Parameters				Antenna-Microwave Noise Temperature Parameters			Figures
	G_0 Transmit	G_0 Receive	G_1	γ	T_1	T_2	a	
DSS-36 (Canberra)								
X/Ka, HEMT-1, RCP, Non-Diplexed	-	79.34	0.00060	47.52	12.54	-13.0	0.060	Figure 28 Figure 45
X/Ka, HEMT-2, RCP-error, Non-Diplexed	-	-	-	-	Not measured			
X/Ka, HEMT-3, LCP, Non-Diplexed	-	79.34	0.00060	47.52	12.18	-12.8	0.060	
DSS-53 (Madrid)								
X/Ka, HEMT-1, RCP, Non-Diplexed	-	78.90	0.00078	45.00	13.0	0.0	0.0	
X/Ka, HEMT-2, RCP-error, Non-Diplexed	-	-	-	-	18.0	0.0	0.0	
X/Ka, HEMT-3, LCP, Non-Diplexed	-	78.90	0.00078	45.00	13.4	0.0	0.0	
DSS-54 (Madrid)								
X/Ka, HEMT-1, RCP, Non-Diplexed	-	78.38	0.00020	45.00	21.80	0.0	0.000	
X/Ka, HEMT-2, RCP-error, Non-Diplexed	-	-	-	-	25.00	0.0	0.000	
X/Ka, HEMT-3, LCP, Non-Diplexed	-	78.38	0.00020	45.00	21.80	0.0	0.000	
DSS-55 (Madrid)								
X/Ka, HEMT-1, RCP, Diplexed (5/2027)	TBD	79.13	0.00022	45.00	20.79	5.3	0.076	Figure 29 Figure 46
X/Ka, HEMT-2, RCP-error, Diplexed (5/2027)	-	-	-	-	21.97	5.3	0.076	
X/Ka, HEMT-3, LCP, Diplexed (5/2027)	TBD	79.13	0.00022	45.00	19.82	5.3	0.076	
DSS-56 (Madrid)								
X/Ka, HEMT-1, RCP, Non-Diplexed	-	79.01	0.0011	43.24	16.5	-5.0	0.2	
X/Ka, HEMT-2, RCP-error, Non-Diplexed	-	-	-	-	Not measured			
X/Ka, HEMT-3, LCP, Non-Diplexed	-	79.01	0.0011	43.24	17.0	-5.0	0.2	

NOTES:

Figures referenced are typically for highest performance configuration for each stated antenna. See Sections 2.1.1.2 and 2.1.2.

Values in above table are for Ka-band deep-space uplink (transmit) and downlink (receive) frequencies.

Nominal Ka-band deep-space uplink frequency is 34450 MHz.
Nominal Ka-band deep-space downlink frequency is 32050 MHz.

For low-gain mode add +70 K to T_1 values (Ka-band).

Noise temperatures for DSS-35 and DSS-36 RCP-error channels were not measured.

Table A-5. S-, X-, K-, and Ka-Band Zenith Atmospheric Attenuation (A_{zen})

Station	A_{zen}, dB (Module 105, Rev. D, 9/2009)			
	Cumulative Distribution = 0.00	Cumulative Distribution = 0.25	Cumulative Distribution = 0.50	Cumulative Distribution = 0.90
S-Band				
Goldstone	0.033	0.033	0.034	0.034
Canberra	0.036	0.036	0.036	0.037
Madrid	0.035	0.035	0.035	0.036
X-Band				
Goldstone	0.037	0.039	0.040	0.047
Canberra	0.039	0.044	0.046	0.058
Madrid	0.038	0.042	0.045	0.055
K-Band				
Goldstone	0.078	0.125	0.150	0.232
Canberra	0.083	0.176	0.212	0.387
Madrid	0.082	0.153	0.186	0.385
Ka-Band				
Goldstone	0.116	0.149	0.167	0.260
Canberra	0.124	0.195	0.229	0.403
Madrid	0.121	0.181	0.217	0.361

NOTE: Table values from earlier Module 105, Rev. D, 9/2009 (immediately above), have been used to generate the curves in Figures 13-46. Latest module 105, Rev. E, values are given below.

Station	A_{zen}, dB (Module 105, Rev. E, 10/2015)			
	Cumulative Distribution = 0.00	Cumulative Distribution = 0.25	Cumulative Distribution = 0.50	Cumulative Distribution = 0.90
S-Band				
Goldstone	0.033	0.033	0.034	0.034
Canberra	0.036	0.036	0.036	0.037
Madrid	0.035	0.035	0.035	0.036
X-Band				
Goldstone	0.037	0.039	0.040	0.045
Canberra	0.039	0.045	0.047	0.057
Madrid	0.038	0.043	0.045	0.058

K-Band				
Goldstone	0.078	0.125	0.150	0.232
Canberra	0.083	0.176	0.212	0.387
Madrid	0.082	0.153	0.186	0.385
Ka-Band				
Goldstone	0.116	0.150	0.171	0.239
Canberra	0.124	0.208	0.238	0.384
Madrid	0.121	0.192	0.221	0.407

NOTE: Table A-5 values from latest Module 105, Rev. E, 10/2015 (immediately above), should be used with the equations in Appendix A.

Deep Space Network

105
Atmospheric and Environmental Effects

Document Owner:		Approved by:	
Signature Provided	09/15/2015	Signature Provided	07/07/2015
Stephen D. Slobin Antenna System Engineer	Date	Timothy T. Pham Communications Systems Chief Engineer	Date
Prepared by:		Released by:	
Signature Provided	09/15/2015	Signature Provided	10/22/2015
Stephen D. Slobin Antenna System Engineer	Date	C. Chang DSN Document Release Authority	Date

DSN No. **810-005, 105, Rev. E**
Issue Date: October 22, 2015
JPL D-19379; CL#15-4732

Jet Propulsion Laboratory
California Institute of Technology

Users must ensure that they are using the current version in DSN Telecommunications Link Design Handbook website:
http://deepspace.jpl.nasa.gov/dsndocs/810-005/

Review Acknowledgment

By signing below, the signatories acknowledge that they have reviewed this document and provided comments, if any, to the signatories on the Cover Page.

Signature Provided	09/11/2015	Signature Not Provided	
Jeff Berner DSN Project Chief Engineer	Date	David Rochblatt Antenna System Engineer	Date

Change Log

Rev	Issue Date	Affected Paragraphs	Change Summary
Initial	11/30/2000	All	All
A	12/15/2002	All	Provides monthly weather statistics for all stations and frequency bands
B	5/26/2006	Sec. 2.1, 2.4	Revised weather models, provides new methods for calculating system operating noise temperature and planetary noise effects
C	8/1/2009	Various	Revised weather models and added models for 26 GHz. Removed references to the 26-m subnet which has been decommissioned
D	9/15/2009	Page 18	Corrected the order and labels for Equations (10) and (11)
E	10/22/2015	Sec. 2.1 Sec. 2.4.1 Sec. 2.4.3 Tables 1-18 Figures 1-9 Figure 10 Figure 11 Figure 20	Updated to describe new WVR data 2009-2013. Solar flux calculations updated using Fig. 11. Fig. 20 parameters explained. Updated to include 2009-2013 AWVR data for Goldstone and Madrid. New, added Canberra and Madrid sites. Updated to 2015. Caption updated to describe parameters.

Contents

Paragraph **Page**

Illustrations

Figure **Page**

Tables

Table **Page**

1 Introduction

1.1 Purpose

This module provides sufficient information concerning atmospheric, environmental, and extraterrestrial effects to enable a flight project to design a telecommunications link at the L-band (1.7 GHz), S-band (2.3 GHz), X-band (8.4 GHz), K-band (26 GHz), and Ka-band (32 GHz) frequencies used by the DSN.

1.2 Scope

Statistics of atmospheric attenuation and noise temperature at each tracking antenna site are presented for those microwave frequencies used by the DSN. In this module, the values of attenuation and noise temperature increase are given relative to a no-atmosphere (vacuum) condition thus this presentation is compatible for use with the vacuum gain and antenna-microwave noise temperature presentations of antenna performance given in modules 101 for 70-m antennas, 103 for 34-m high-efficiency (HEF) antennas, and 104 for 34-m beam-waveguide (BWG) antennas.

Statistics of wind speed at Goldstone are given. These are used both to determine the statistics of antenna gain reduction due to wind loading and also to ascertain the percentage of time an antenna will be unusable due to excessive wind speed.

Extraterrestrial effects are primarily the increased system noise temperature due to hot body noise from the Sun, Moon, planets, and galactic radio sources. These effects are significant only when the antenna beam is in the vicinity of these noise sources during tracking of spacecraft.

Charged-particle effects are given in module 106, Solar Corona and Solar Wind Effects.

2 General Information

2.1 Atmospheric Attenuation and Noise Temperature

The principal weather-related effects on telecommunications link performance are the atmospheric attenuation and noise temperature resulting from oxygen, water vapor, clouds, and rain. The two effects are related and higher atmospheric attenuation produces a higher noise contribution. Also, atmospheric effects generally increase with increasing frequency, except in the vicinity of the water vapor line at 22.235 GHz (20-25 GHz), and the oxygen band from about

55-65 GHz. K- and Ka-band effects are larger than X-band effects, which in turn are larger than S-band and L-band effects.

In the 810-005 antenna performance modules (modules 101, 103, and 104), *effective antenna gain* (vacuum gain minus atmospheric attenuation) is presented in the figures for various atmospheric attenuation values. Strictly speaking, the gain of an antenna is not a function of atmospheric attenuation; however for stand-alone use, the effective gain, including atmospheric loss, is a useful concept, and the equations for gain in the appendices of those modules include a term for atmospheric attenuation. Similarly, the *antenna-microwave noise temperature,* T_{AMW} (due to spillover, LNA contribution, waveguide loss, etc.), is also not a function of atmosphere. However, the system operating noise temperature, T_{op}, as presented in the appendices of the antenna performance modules, includes a term for sky noise, T_{SKY}, which is a combination of atmospheric noise and effective cosmic microwave background noise. Thus the system operating noise temperature $T_{op} = T_{AMW} + T_{SKY}$.

Design control tables (DCTs) used for telecommunications link design typically carry separate entries for atmospheric attenuation of the received and transmitted signals and the atmospheric noise contribution to the system noise temperature as a function of elevation angle and weather condition. It is important in those DCTs that the antenna gain and antenna-microwave noise temperature values reflect the vacuum performance of the antenna by itself, so as to prevent double-bookkeeping of the atmospheric attenuation and noise temperature contributions.

Four atmospheric models are presented here. The first covers L-band (1.7 GHz) and S-band (2.3 GHz). The second and third cover X-band (8.4 GHz) and Ka-band (32.0 GHz). The fourth, which is presented in a slightly different format in the tables, covers K-band (25.5 GHz to 27.0 GHz). Atmospheric noise temperature and attenuation statistics are provided in the form of cumulative distributions (CDs) for each effect. For example, a cumulative distribution of 0.90 ("90% weather") means that 90% of the time a particular weather effect (noise temperature or attenuation) is less than or equal to a given value. Conversely, that particular effect is exceeded 10% of the time. Qualitatively, the weather conditions associated with selected cumulative distributions are described as follows:

CD	=	0.00	clear dry, lowest weather effect
CD	=	0.25	average clear weather
CD	=	0.50	clear humid, or very light clouds
CD	=	0.90	very cloudy, no rain
CD	>	0.95	very cloudy, with rain

By their very natures, clouds and rain are poorly modeled, and the water vapor radiometer data used here are sparse for the larger rain-related weather effects, which are exceeded only 5% of the time.

The Ka-band model presented here is based on actual water vapor radiometer measurements of zenith sky brightness temperature at 31.4 GHz at all three DSN sites

(Goldstone, Canberra, and Madrid). Sky brightness temperature is a combination of the atmosphere noise temperature and the attenuated cosmic background noise. These models contain 202 months of Goldstone data covering the period October 1993 through December 2013, 112 months of Canberra data covering the period June 1999 through January 2009 (no new data were collected since 2009), and 248 months of Madrid data covering the period September 1990 through December 2013. There were missing months of data from each station. Note also that different numbers of months of data went into the model for each of the separate months (for example, there may have been 20 Februaries, but only 18 Marches). It is felt that because of the large amount of Madrid data (more than 20 years), the results will fairly accurately represent true long-term statistics. The 17 years of Goldstone data will also give a moderately accurate long-term model. The 9 years of Canberra data will probably give a reasonably accurate long-term model, and future updates, if any, of the Canberra model may show relatively large changes in the distributions, particularly at high CD levels (greater than 0.95). Atmosphere noise temperature can be deduced from the sky brightness temperature using an assumption about the mean effective radiating temperature of the atmosphere. Cumulative distributions of atmosphere noise temperature at 31.4 GHz for each of the 12 months were calculated, then increased by a small amount (0.3 – 3 K, a function of frequency and noise temperature) to create a model for 32 GHz. Year-average models for each station and frequency were generated from a weighted average of the monthly statistics.

L/S-band and X-band attenuation statistics were created from the Ka-band (32 GHz) statistics by subtracting out the 0% CD baseline (calculated for nominal temperatures and pressures, with 0% relative humidity), frequency-squaring to the appropriate frequency (for example, $[8.42/32]^2$) and then adding in the 0% CD baseline at the new frequency. Note that the 0% CD baselines for the DSN sites differ because of different heights above sea level. Noise temperature statistics were then derived from the frequency-modeled attenuation statistics.

Noise temperature statistics for zenith were created from the atmospheric attenuation statistics by methods given in Sections 2.1.1 and 2.1.3 below. The year-average noise temperature statistics were calculated from the year-average attenuation values.

For K-band statistics, a somewhat different method was used, rather than the frequency-squared technique described above. It was necessary to do this because atmosphere effects in the 26 GHz region, are on the high side of the 22 GHz water vapor line, where attenuation and noise temperature values are *increasing* with decreasing frequency. For this reason, the frequency-squaring technique would give inaccurate results. A series of "humid" and "wet" (liquid water cloud) atmosphere models were postulated that would give the existing Ka-band noise temperature values for each CD value and each station. Then, using these atmospheres, the attenuation and noise temperature were calculated for 25.5, 26.0, 26.5, and 27.0 GHz for the range of CD values at each frequency. The technique and results are described more completely in JPL Publication 09–14 (*Atmosphere Attenuation and Noise Temperature Models at DSN Antenna Locations for 1–45 GHz*, by Anil Kantak and Stephen Slobin, March 2009). K-band statistics have not been updated from the original 2009 calculations, but addition of new data is expected to result in only small changes in the statistics.

It should be noted that although the noise temperature statistics are the best qualitative measures for comparison of different locations and different frequencies, especially when dealing with low-noise systems (where the atmospheric noise is a large part of the total system noise temperature), the basic database for the calculation of atmospheric effects is actually the attenuation statistics. Given a station location, frequency, and CD of interest, the attenuation database value is extracted, modeled to the elevation angle of interest (Section 2.1.2), and then the appropriate atmospheric noise temperature is calculated (Section 2.1.3). Monthly, year-average, and maximum and minimum monthly zenith noise temperature statistics are given in Tables 1 through 9. Similarly, the attenuation statistics are given in Tables 10 through 18. Monthly, maximum, and minimum values are not available for K-band (Tables 19–21). In module 105, Rev. D (2009), the year-average values are based on the cumulative distributions of the 31.4 GHz measured noise temperatures for the entire data set for all the years of data. In this module, Rev. E (2015), the year-average values are weighted (by number of days) averages of the cumulative distributions of the twelve individual months. The differences between Rev. D and Rev. E statistics are small (1-2 K) at Ka-band at the highest CD levels, except for the particular case of Madrid at the 0.97-0.99 CD levels, where the differences range from 3-9 K. This large change is not presently explainable.

The atmospheric models thus generated for a particular complex (for example, Goldstone) should be used for all antennas at that complex (for example, DSS-14, DSS-15, DSS-24, etc.), regardless of the small altitude differences among the antennas.

Zenith atmospheric noise temperature statistics for the three DSN sites at L- and S-band are provided in Tables 1 through 3. Tables 4 through 6 provide similar statistics for X-band, and Tables 7 through 9 cover Ka-band. The tables include the cumulative distributions for each month, the maximum and minimum monthly value for each CD level, and the weighted year-average for that CD level. These noise temperature statistics should be used only in a qualitative sense to describe the relative levels of atmospheric noise contributions for different locations and cumulative distributions. They should not be used for elevation modeling, as this is properly performed using the calculated attenuation at a given elevation angle as a starting point and following the process that is described below.

When a nominal antenna zenith T_{op} (operating system noise temperature) is stated, it is considered to include the CD = 25% (average clear sky) value for the appropriate frequency and location.

Tables 10 through 18 provide similar presentations for zenith atmospheric attenuation. The tolerances of atmospheric noise temperature and attenuation, as given in Tables 1 through 18, should be considered to be 5% of the stated values at zenith, or 5% of the values calculated for elevation angles other than zenith. (see Section 2.1.5, below).

Tables 19–21 present year-average K-band zenith attenuation and noise temperature values for the three stations over the frequency range 25.5–27.0 GHz.

Figures 1, 2, and 3 show the L/S-band noise temperature statistics for Goldstone, Canberra, and Madrid respectively. Figures 4, 5, and 6 show X-band statistics for the three complexes. Figures 7, 8, and 9 provide the Ka-band statistics. On each figure, the year-average

cumulative distribution, the minimum envelope value, and the maximum envelope values are given for all the individual months at each CD value stated in Tables 1 through 9. Curves of zenith attenuation are not given, although using a rule-of-thumb that a medium with 1 dB attenuation at a physical temperature of about 20 C radiates a noise temperature of approximately 60 K, the noise temperature curves can be used to make rough estimates of the zenith attenuation at the various frequencies. This relationship is nearly linear over the range from 0 to 1 dB.

For other frequencies near to the L-, S-, X-, and Ka-bands (within about 5% of the nominal frequencies), the weather-effects models presented here should be used without modification. These models should definitely not be used to infer statistics in the vicinity of the 22.235 GHz water vapor line (20-25 GHz) or the 60 GHz oxygen band, (55-65 GHz).

2.1.1 Calculation of Atmosphere Mean Effective Radiating Temperature

The mean effective radiating temperature of the atmosphere is modeled to be a function of the cumulative distribution of weather effects. This reflects the assumption that those effects that are of larger value (for example, high noise temperature) occur closer to the surface (for example, rain, low moist clouds) and hence are at a higher average physical temperature than those that have a lesser effect (a clear sky with low humidity). The mean effective radiating temperature, T_M , is modeled as

$$T_M = 255 + 25 \times CD, \text{ K} \tag{1}$$

where

CD = cumulative distribution of weather effect ($0.0 \le CD \le 0.99$).

Note that the maximum value of T_M thus becomes nearly 280 K, or about 7 C.

2.1.2 Elevation Angle Modeling

Only the attenuation should be modeled as a function of elevation angle. The atmospheric noise temperature contribution at any elevation angle can be calculated from the modeled attenuation at that elevation angle. Elevation angle modeling can be performed using either a flat-Earth or a round-Earth model. A flat-Earth model is used here, wherein the attenuation increases with decreasing elevation angle:

$$A(\theta) = A_{zen} \times AM = \frac{A_{zen}}{\sin(\theta)}, \text{ dB} \tag{2}$$

where

θ = elevation angle of antenna beam

A_{zen} = zenith atmospheric attenuation (dB), as given Tables 10 through 18 of this module

AM = number of air masses $\left(\frac{1}{\sin(\theta)} = 1.0 \text{ at zenith} \right)$

The flat-Earth approximation produces a slightly higher attenuation then would be obtained with a round-Earth model for low elevation angles but is valid to within 1% to 3% at a 6-deg elevation angle, depending on the frequency and the amount of water vapor in the atmosphere. Note that in a telecom link design tool, if the atmosphere attenuation is carried as a separate line item, it should NOT also be included in the "effective" antenna gain (antenna gain minus atmosphere attenuation).

2.1.3 Calculation of Noise Temperature From Attenuation

An attenuating atmosphere creates a noise temperature contribution to ground antenna system temperature. The atmospheric noise temperature at any elevation angle (θ) is calculated from the attenuation by

$$T_{atm}(\theta) = T_M [1 - 1/L(\theta)], \text{ K} \tag{3}$$

where

T_M = atmosphere mean effective radiating temperature (K), calculated above

$L(\theta)$ = loss factor of atmosphere = $10^{\left[\frac{A(\theta)}{10}\right]}$

$A(\theta)$ = atmospheric attenuation at any elevation angle (dB), calculated above

Note that typical values of L range from about 1.01 to 2.0 (A = 0.04 dB to 3 dB)

2.1.4 Cosmic Background Adjustment

The noise temperature contribution of the cosmic microwave background is reduced by atmospheric attenuation. For all DSN frequencies the cosmic background noise temperature before atmospheric attenuation is

$$T_{CMB} = 2.725 \text{ K} \tag{4}$$

With atmosphere attenuation, the effective cosmic background becomes

$$T'_{CMB}(\theta) = \frac{T_{CMB}}{L(\theta)}, \text{ K} \tag{5}$$

where

T_{CMB} = cosmic microwave background noise (K) without atmosphere

$L(\theta)$ = loss factor of atmosphere at the elevation angle of interest, as calculated from Section 2.1.3.

The antenna modules (101, 103, and 104) present a system operating noise temperature, T_{op}, consisting of two parts – an *antenna-microwave* component, T_{AMW}, for the contribution of the antenna and microwave hardware, and a *sky* component, T_{sky} , which consists of the atmosphere noise plus the cosmic microwave background noise, attenuated by the atmosphere loss. The T_1 and T_2 coefficients associated with T_{AMW}, are given in the Appendices of the antenna modules, and the appropriate equation to use is also stated. Thus, for these modules, the system operating noise temperature with atmosphere and with attenuated cosmic contribution becomes

$$T_{op}(\theta) = T_{AMW} + T_{sky} = \left[T_1 + T_2 e^{-a\theta}\right] + \left[T_{atm}(\theta) + T'_{CMB}(\theta)\right] \tag{6}$$

where

T_1, T_2 and a are coefficients from the telecommunications interface modules

T_{atm} is the atmosphere noise term, given above

T'_{CMB} is the attenuated cosmic noise, given above

2.1.5 Example of Use of Attenuation Statistics to Calculate Atmospheric Noise Temperature, $T_{atm}(CD, \theta)$, and $T_{op}(CD, \theta)$

The following example will show a typical calculation of atmospheric attenuation and noise temperature for a particular situation. The parameters for the example are

DSS-34, Canberra

Ka-band (32 GHz)

90% year-average weather (CD = 0.90)

20-deg elevation angle (2.924 air masses)

From Table 17, the year-average zenith attenuation for CD = 0.90 is given as

A_{zen} = 0.384 dB

The attenuation at 20-deg elevation is

A(90%, 20°) = 0.384/sin(20) = 1.123 dB

Note that in a telecom link design tool, if the atmosphere attenuation is carried as a separate line item, it should NOT also be included in the *effective antenna gain* (antenna gain minus atmosphere attenuation).

The loss factor L at 20-deg elevation is

$L(90\%, 20°) = 10^{1.123/10} = 1.295$

The atmosphere mean effective radiating temperature is

$$T_M = 255 + 25\times0.90 = 277.5 \text{ K}$$

The atmospheric noise temperature at 20-deg elevation is

$$T_{atm}(90\%, 20°) = 277.5\ [1-1/(1.295)] = 63.214 \text{ K}$$

The effective cosmic background temperature at 20-deg elevation is

$$T'_{CMB} = 2.725/1.295 = 2.104 \text{ K}$$

The system operating noise temperature at 20-deg elevation is

$$T_{op}(90\%, 20°) = T_{AMW}(20°) + 63.214 + 2.104 = T_{AMW}(20°) + 65.318 \text{ K}$$

where

$T_{AMW}(\theta)$ is obtained from revisions of the telecommunications interface modules published after May, 2006.

2.1.6 Best/Worst Month Ranges of Atmospheric Noise Temperature and Attenuation

The absolute accuracy of the 31.4-GHz water vapor radiometer measurements used to create the noise temperature statistics is thought to be a few tenths K to 2 K at zenith. The month-to-month variation of average noise temperature at any CD varies much more than this at all values of cumulative distribution greater than about 10%. A particular month might be the “worst” at the 90% CD level, but merely “moderate” at lower CD levels. An example is a winter month that has a large amount of rain, but when not raining has low humidity and low noise temperature contribution. At this time, there are insufficient data to characterize “best” and “worst” months individually; however, tolerances on the mean statistics as given in Tables 1 through 18 can give the user a feeling of what yearly variations in atmospheric effects may be expected.

Inspection of Tables 1 through 18 and Figures 1 through 9 will show that fictitious "best month" and "worst month" statistics can be generated from the values giving the minimum and maximum envelope values of noise temperature and attenuation, without regard to the variability among the months as a function of CD. At high values of CD, the adverse (maximum envelope) yearly tolerances can be as high as 40% of the year-average value of an effect. It should be noted that adverse tolerances for both noise temperature and attenuation give INCREASES from the values in Tables 1 through 18. An adverse VALUE is a mean PLUS the adverse tolerance. For mission planning purposes, with no need to create a model for a specific month, it may be sufficient to use the year-average value at a particular CD, and use the maximum/minimum envelope values to define very conservative (large) adverse/favorable

tolerances, with a triangular distribution. For specific-month planning purposes, it may be sufficient to use the values given in Tables 1 through 18, with ±5% tolerances (triangular distribution) as stated above. A very conservative approach (acknowledging that any individual month in the future can be well outside the historical range of available data) would be to use the "maximum" envelope as the model for a possible "bad" month. Note also that for particular months characterized by "bad weather", year-to-year variation of noise temperature and attenuation statistics can be quite large.

2.2 Rainfall Statistics

To assist the user in determining which months may have large rainfall-related atmospheric noise temperature and attenuation increases, rainfall data are presented for the three DSN antenna locations. Months with large average rainfall amounts may not necessarily correspond to months with large noise temperature and attenuation values. Comparison with Tables 1 through 18 should be made.

Table 22 presents the monthly and year-average rainfall amounts for the three DSN antenna locations. The Goldstone data (1973–2000) were taken at the administration center, located near the middle of the Goldstone antenna complex. Some antennas may be located as much as 10 miles from this location. The Canberra data (1966–2002) were taken at the Tidbinbilla Nature Reserve, located about 3 miles southwest of the antenna site. The Madrid data (1961–1990) are the averages of the rainfall at two locations: Avila, about 20 miles northwest of the antenna site, and Madrid (Quatro Vientos) about 20 miles east of the antenna site. Although these averages may not exactly reflect the rainfall at the antenna site, the relative monthly amounts are probably correct.

2.3 Wind Loading

The effect of wind loading must be modeled probabilistically, since wind velocity varies randomly over time and space. Figure 10 shows the wind speed exceedance percentages for the three DSN antenna sites. These data were taken during a six month period, January thru June, 2011, and represent the average wind speed during spacecraft tracks made on the 70-meter antennas. The wind load on a particular antenna is dependent on the design of that antenna. Consequently, information about wind-load effect on antenna gain is listed in the appropriate antenna module.

It is seen in Figure 10 that Goldstone is the windiest of the three DSN sites. For example, at Goldstone, 5% of the time a wind speed of 40 km/h is exceeded, whereas at Canberra and Madrid, for the same percentage of time, the wind speed is only 15-18 km/h. These wind speed statistics are averages over an entire spacecraft track, whereas average wind speeds over shorter periods of time (5 minutes to 1 hour, for example) will be significantly higher. A rough estimate, based on Goldstone measurements, indicates that the short-term wind speeds can be double or more the speeds shown in Figure 10, for the same percentage of time.

DSN 70-meter and 34-meter antennas are stowed (pointed vertically) when the short-term wind speeds exceed 80.5 km/h (50 mi/h) under no-snow/ice conditions. It is seen

from Figure 10 that it is unlikely that any DSN antenna will need to be stowed for more than a few hours a year.

2.4 Hot Body Noise

2.4.1 Solar Noise

The increase in system noise when tracking a spacecraft angularly near the Sun depends on the intensity of solar radiation at the received frequency and on the position of the Sun relative to the antenna gain pattern. The subreflector support structure (typically a quadripod, but a tripod at the DSS-13 BWG antenna) introduces non-uniformities in the sidelobe structure. Increases in noise temperature are typically greater in directions at right angles to the planes established by the subreflector support legs and the center of the reflector surface. Thus, a quadripod-type antenna will have four regions of increased noise temperature, and a tripod-type antenna will have six. With an azimuth-elevation (AZ–EL) or X/Y mounted antenna, the plane containing the Sun–Earth–Probe (SEP) angle will rotate through the sidelobes during a tracking pass. This causes the solar noise to fluctuate during a track even if the SEP angle is constant.

A large number of measurements were made at Goldstone from 1987 to 1996 to determine the system noise temperature effects of tracking near the Sun (within about five deg from the center of the solar disk). These measurements were made at S-band on the 26-m antennas (now decommissioned) and at S-, X-, and Ka-bands on the 34-meter antennas.

Figure 11 shows the 10.7-cm (2800-MHz) solar radio flux during the period of January 2000 through December 2018 covering the end of solar cycle 23 and all of solar cycle 24, including predicted values. The flux is measured in solar flux units (SFU) where one SFU = 1×10^{-22} W/m^2/Hz. Updated solar flux predictions can be found at the National Oceanic and Atmospheric Administration (NOAA) Space Weather Prediction Center web site http://www.swpc.noaa.gov/products/solar-cycle-progression (Solar Cycle Progression Plots). Solar flux predictions can be used to model S- and X-band solar noise temperature contributions using the ratio of predicted solar flux to the solar flux that existed at the time the antenna noise temperatures were measured.

The general characteristic of the 11-year cycle of 2800-MHz solar flux is a rapid rise to a peak approximately 4–5 years after the minimum, followed by a 7–6 year gradual decrease. From cycle to cycle, the peak flux can vary by as much as a factor of two. The 10.7-cm flux varied during solar cycle 23 from a minimum of about 70 SFU during 1996 to a maximum of about 220 ± 15 SFU in late 2001. Note that the peak of solar cycle 24 was about 150 ± 20 SFU during 2014, about 30% lower than in 2001

Figure 12 shows X-band system noise temperature increases as measured at the Goldstone DSS-15 HEF antenna. These measurements show the increased effect for the Sun located (offset) at right angles to the quadripod legs. The quadripod legs are arranged in an “X” configuration, with 90-deg spacing. The measurements were made in November 1987 (near the beginning of the solar cycle) with a measured 2800-MHz flux value of 101 SFU and an 8800-

MHz flux value of 259 SFU. The following expression may be used as an upper limit of X-band solar noise contribution at DSS-15 as shown in Figure 12.

$$T_{sun} = 800e^{-2.0\theta}, \text{K} \tag{8}$$

where

θ = offset angle between center of beam and center of solar disk, deg

Figure 13 shows S-band (2295 MHz) solar noise contribution for a 34-meter diameter antenna. This curve is based on measurements made on the Goldstone DSS-16 26-meter diameter antenna on December 20, 1989, and the angular offset values were modeled by the ratio of antenna beamwidths. This antenna has since been decomissioned. The reported 2800-MHz solar flux at the time of the experiment was 194 SFU; at 8800 MHz it was 290 SFU. Note that compared to the November 1987 flux (Figure 12), the 2800-MHz flux has nearly doubled, but the 8800-MHz flux has only increased about 12 percent. The S-band solar noise contribution shown in Figure 13 can be modeled as

$$T_{sun} = 1400e^{-1.8\theta}, \text{K} \tag{9}$$

where

θ = offset angle between center of beam and center of solar disk, deg

This equation undoubtedly underestimates the solar noise contribution at offset angles less than 1 degree by hundreds of K.

Figures 14 and 15 are contour plots of the DSS-12, 34-m HA–DEC total system noise temperature versus declination and cross-declination antenna pointing offsets. Although DSS-12 has been decommissioned since the measurements were made, the figures are included because they are representative of the effects of the quadripod on solar noise at other antennas. The quadripod legs are arranged in a "+" configuration with 90-deg spacing, hence the peaks at right angles to the legs.

Figure 14 is a contour plot of total S-band system noise temperature versus declination and cross-declination antenna pointing offsets at DSS-12.The contour interval is 50 K. These measurements were made on January 12, 1990. On this day the reported 2800-MHz solar flux was 173 SFU.

Figure 15 is a contour plot of total X-band system noise temperature versus declination and cross-declination antenna pointing offsets at DSS-12. The contour interval, measurement date, and flux values are identical with those in Figure 14. The reported 8800-MHz solar flux was 272 SFU.

Figures 16 and 17 show the X-band (8.4-GHz) and Ka-band (32-GHz) solar noise contributions at the DSS-13, 34-m research and development beam waveguide antenna as a function of offset angle from the center of the sun. These data were taken during mid-March, 1996, when the 10.7-cm solar flux was about 70 SFU (the minimum at the end of solar cycle 22 and at the beginning of solar cycle 23) and should be considered as representative of what is expected at the operational DSN beam waveguide antennas.

The following expressions give an approximate upper envelope for the noise contributions shown in Figures 16 and 17 as a function of offset angle

$$T_{sun} = \left| \begin{array}{l} 5000e^{-6.6\theta},\ 0.35 < \theta \le 0.75\,\text{deg} \\ 100e^{-1.4\theta},\ \theta > 0.75\,\text{deg} \end{array} \right., \text{ at X-band.} \tag{10}$$

$$T_{sun} = \left| \begin{array}{l} 1400e^{-5.1\theta},\ 0.35 < \theta \le 0.75\,\text{deg} \\ 86e^{-1.4\theta},\ \theta > 0.75\,\text{deg} \end{array} \right., \text{ at Ka-band} \tag{11}$$

At offset angles less than 0.35 deg (0.08 deg from the edge of the solar disk), solar noise contributions are likely to be in excess of 300 K at both frequencies. At offsets greater than 4.0 degrees, the solar contribution is negligible.

All noise contribution expressions given above should be compared with values shown in the corresponding figures to assess their validity. Note that these expressions should be considered valid only for the flux values given at the time of measurement. For predictive purposes, Figure 11 may be used to obtain future predicted 2800-MHz solar flux, and the noise contributions at S- and X-band can be modeled as described below.

During the 11-year solar cycle, the S-band flux varies by a factor of 3 (reference Figure 11) while the corresponding X-band flux varies by a factor of 2. For cycle 23, when the S-band range is expected to be from 70 SFU to as much as 210 SFU, the X-band range is predicted to be from about 200 SFU to about 400 SFU. The predicted X-band flux can be derived from the predicted S-band flux by the following expression.

$$\text{FLUX,X} = 200 + \frac{200(\text{FLUX,S} - 70)}{140} \tag{12}$$

For example, in April 2016 the mean S-band flux is predicted to be 100 SFU (from Figure 11). The mean predicted X-band flux would be 243 SFU.

The predicted solar noise contribution can be calculated based on measured noise contributions described above. For example, using the equation provided for Figure 12 (Equation 8) and the predicted X-band solar flux in April 2016 (243 SFU), the predicted X-band solar noise contribution for a 2-degree offset angle using the 34-m HEF antenna would be

$$T_{sun} = (243/259) \times 800\, e^{-2.0\times 2.0} = 13.75 \text{ K} \tag{13}$$

At Ka-band, the solar flux varies little over the solar cycle and the relationship between noise temperature increase and offset angle depicted in Figure 17 can be used at all times.

Figure 18 shows examples of measured S-band system noise temperature made with a 64-m antenna tracking Pioneer 8 (November 1968, near the solar maximum) and Helios (April 1975, near the solar minimum). For all practical purposes, these curves may be used to predict S-band performance for the DSN 70-m antennas. The "maximum" and "minimum" curves for each month show the solar "clock angle" effect due to sidelobes at right angles to the quadripod legs.

Figure 19 shows a theoretical curve of X-band 70-m antenna noise temperature as a function of SEP angle. This curve is generated based on an assumed X-band blackbody disk temperature of 23,000 K, representing an "average" value during the solar cycle. An expression giving quiet Sun brightness temperature, T_b (K), as a function of wavelength (mm) has been found to be

$$T_b = 5672\lambda^{0.24517}, \quad \text{K} \tag{14}$$

For S-band (2.3 GHz), T_b = 18700 K. For X-band (8.5 GHz) T_b = 13600 K. For Ka-band (32 GHz) T_b = 9750 K. The active Sun may be expected to have an X-band brightness temperature of as much as two to four times as high as the 13600 K calculated above. Other studies give the X-band solar disk temperature minimum, average, and maximum values over the solar cycle as 14,000 K, 22,000 K, and 30,000 K, respectively. At Ka-band these values are 7500 K, 10,000 K, and 12,500 K.

2.4.2 Lunar Noise

For an antenna pointed near the Moon, a noise temperature determination similar to that made for the Sun should be carried out. The blackbody disk temperature of the Moon is about 240 K at X- and Ka-bands, somewhat lower at S-band (220 K), and its apparent diameter is almost exactly that of the Sun's (approximately 0.5 deg). Figures 12 through 19 may be used for lunar calculations, with the noise temperature values scaled by 240/23000. Figures 13, 14, 15, and 18 include clear-sky system noise temperatures, which must be subtracted out before scaling in order to determine the lunar noise temperature increase. Nevertheless, at offset angles greater than 2 deg, the lunar noise contribution is negligible. For rough calculations using antenna patterns with half-power beamwidths less than about 20% of the lunar diameter (all DSN antennas at X- and Ka-bands and the 70-m antennas at S-band), more than 90% of the antenna power is on the lunar disk when centered on the moon. In this case, the maximum noise temperature seen is roughly

$$T_{moon} = T_b \times 0.90 \times \eta_{ant}, \text{ K} \tag{15}$$

where

T_b = 240 K

η_{ant} = antenna efficiency ≈ 0.70 for most large antennas

Thus, the peak noise contribution from the moon for any DSN antenna except the 34-m BWG antenna at S-band will be approximately 150 K. Measurements on the DSS-13 34-m beam waveguide antenna (S-band half-power beamwidth ≈ 0.25 deg) yield a noise temperature increase due to the moon of about 136 K, which is nearly constant over the lunar monthly cycle. Measurements at new moon yield a noise contribution of 188K at X-band, and 156 K at Ka-band. Peak noise temperatures about 3-4 days after full moon at X-band and Ka-band were in the range of about 190-200 K.

2.4.3 Planetary Noise

The increase in system noise temperature when tracking near a planet can be calculated by the formula

$$T_{pl} = \left(\frac{T_k G d^2}{16 R^2}\right) e^{-2.77\left(\theta/\theta_0\right)^2}, \text{ K} \tag{16}$$

where

T_k = blackbody disk temperature of the planet, K

d = planet diameter, km

R = distance to planet, km

θ = angular distance from planet center to antenna beam center

θ_0 = antenna half-power beamwidth (full beamwidth at half power)

G = antenna gain ratio $\left\lfloor 10^{\left(G(\text{dBi})/10\right)} \right\rfloor$ including atmospheric attenuation.

An alternative method for calculating the noise contribution for a planetary disk somewhat smaller than the antenna beamwidth is presented in JPL document D-33697 (*System Noise Temperature Increase from the Sun, Moon, or Planet Blackbody Disk Temperature*, by Anil Kantak and Stephen Slobin, December 1, 2005). Figure 20 shows an excerpt from that document (Figure 8), that indicates the percentage of total antenna power on a planetary disk, for ratios of half-power beamwidth to disk angular diameter in the range 1.75 to 5.0. For other half-power beamwidth/diameter ratios, that document should be consulted.

For a particular case (Venus on February 1, 2006, as seen from the DSS-13 34-m beam waveguide antenna at X-band), the following calculation is made:

planet diameter (d) = 12,104 km

planet disk temperature (T_k) = 634 K at X-band (Table 23)

range from earth (R) = 0.318 AU = 47,572,800 km

disk angular diameter $\left(\tan^{-1}\left[\frac{d}{R}\right]\right)$ = 0.0146 degrees

half-power beamwidth (θ_0) = 0.066 degrees

beamwidth/diameter = 4.521

power ratio from Figure 20 = 0.034

antenna efficiency (η) = 0.673 without atmospheric loss at 39 deg. elevation

= 0.663 with clear sky atmospheric loss at 39 deg. elevation

The noise temperature calculated for the Figure 20 example is

$T_{venus} = 634 \times 0.034 \times 0.663 = 14.29$ K

Using Equation 16 above, the numerical gain of the DSS-13 antenna is first calculated using an efficiency of 0.663 (includes clear sky atmosphere loss),

$$G = \eta\left(\frac{\pi D}{\lambda}\right)^2 = 5,966,230 \tag{17}$$

where

D = antenna diameter = 34 m

λ = wavelength = 0.0356 m at 8420 MHz (X-band)

therefore

$$T_{venus} = \left(\frac{634 \times 5,966,230 \times 12,104^2}{16 \times 47,572,800^2}\right) = 15.30 \text{ K}$$

The measured noise temperature increase from Venus was 16.18 K, so Equation (16) gives an estimate about 5.4% low, and the Figure 20 method gives an estimate about 8.8% low.

Table 23 presents all the parameters needed for calculation of planetary noise contributions. Also given are the maximum values of expected X-band and Ka-band noise contributions for the mean minimum distance from Earth, with the antenna beam pointed at the center of the planet (θ=0). Corresponding S-band noise temperature increases will be approximately 1/13 as large as the X-band increases because of the lower antenna gain (wider beamwidth) at the lower frequency.

In the case of Jupiter, there is a significant and variable non-thermal component of the noise temperature. Thus the effective blackbody disk temperature at S-band appears to be much higher than at X-band. The S-band noise temperature increase will be approximately 1/6 the X-band values for average Jupiter emission; it will be about 1/3 the X-band values for maximum Jupiter emission. Except for Venus at inferior conjunction and Jupiter at opposition (minimum distances), the noise contribution from the planets at S-band is negligible.

The expression (Equation 16) for T_{pl} assumes that the angular extent of the radiating source is small compared to the antenna beamwidth. This approximation is adequate at X-band except for Venus near inferior conjunction (apparent diameter = 0.018 deg) using a 70-m antenna at X-band (beamwidth = 0.032 deg). At Ka-band with a 34-m antenna (beamwidth = 0.0174 deg), the approximation is not adequate for Venus near inferior conjunction and may not be adequate for Mars near oppositione 14 ? (apparent diameter = 0.005 deg). The expression also assumes that the antenna main beam has a Gaussian shape, with circular symmetry. Antenna gains and half-power beamwidths are given in modules 101, 103, and 104.

2.4.4 Galactic Noise

The center of the Milky Way galaxy is located near –30 degrees declination, 17 h 40 min right ascension. It is possible for a spacecraft with a declination of –30 deg to be in the vicinity of the galactic center, and an increase of system noise temperature would then be observed. A declination of –30 degrees is not typically achieved by spacecraft moving in the plane of the ecliptic, but there are some circumstances (for example, a flight out of the ecliptic) where this location may be observed. Galactic noise temperature contributions at frequencies above 10 GHz are typically insignificant. At S-band, looking directly at the galactic center, a noise temperature increase of about 10 K would be observed. A map of the galactic noise distribution can be seen in chapter 8 of the classic reference J. D. Kraus, *Radio Astronomy*, Cygnus-Quasar Books, Powell, Ohio, 1986.

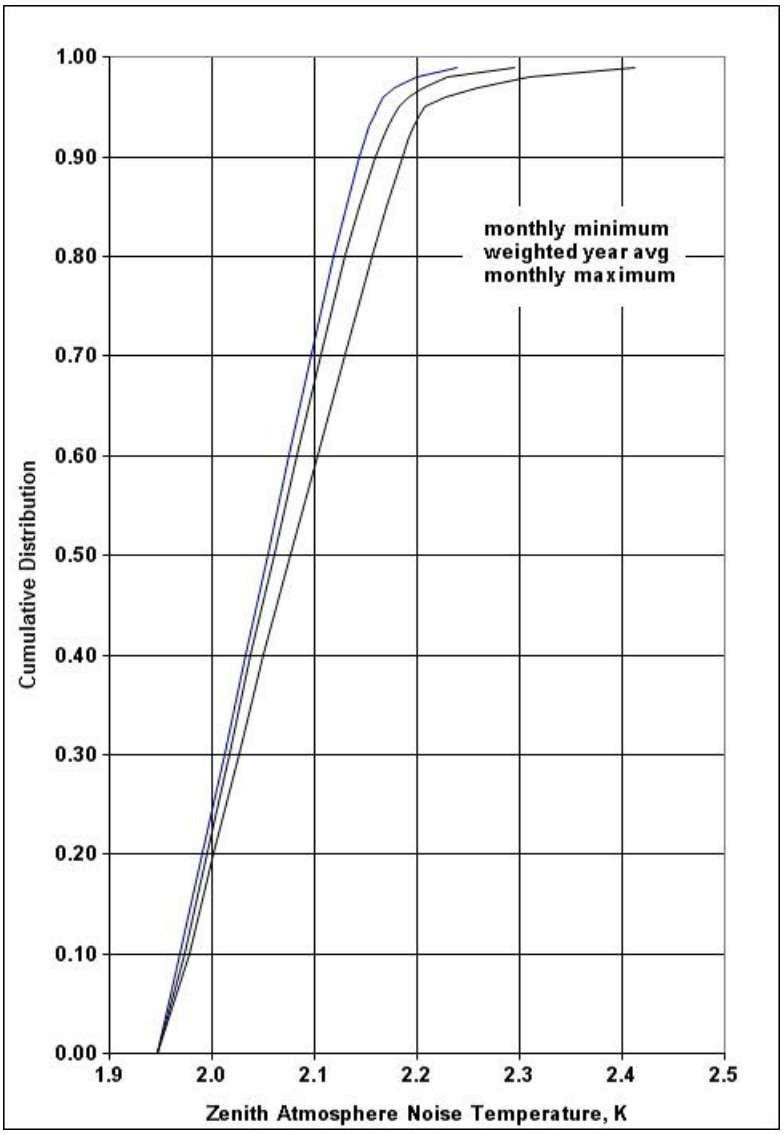

Figure 1. Cumulative Distributions of Zenith Atmospheric Noise Temperature at L-Band and S-Band, Goldstone DSCC

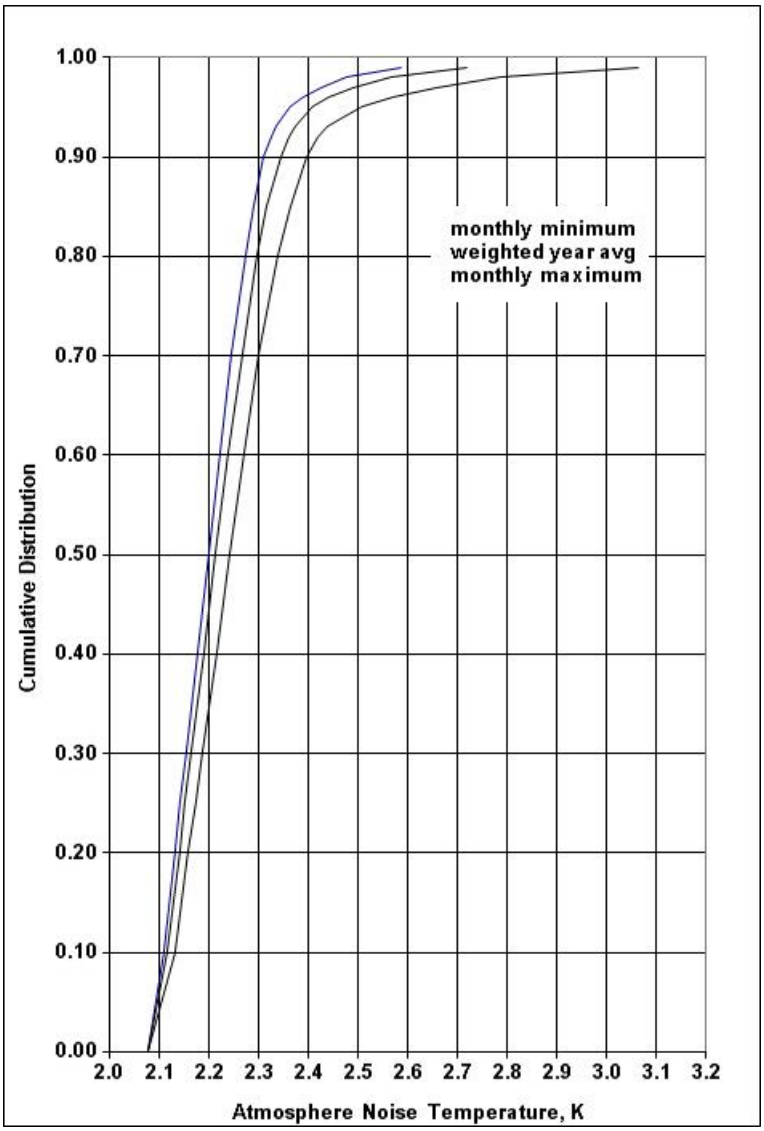

Figure 2. Cumulative Distributions of Zenith Atmospheric Noise Temperature at L-Band and S-Band, Canberra DSCC

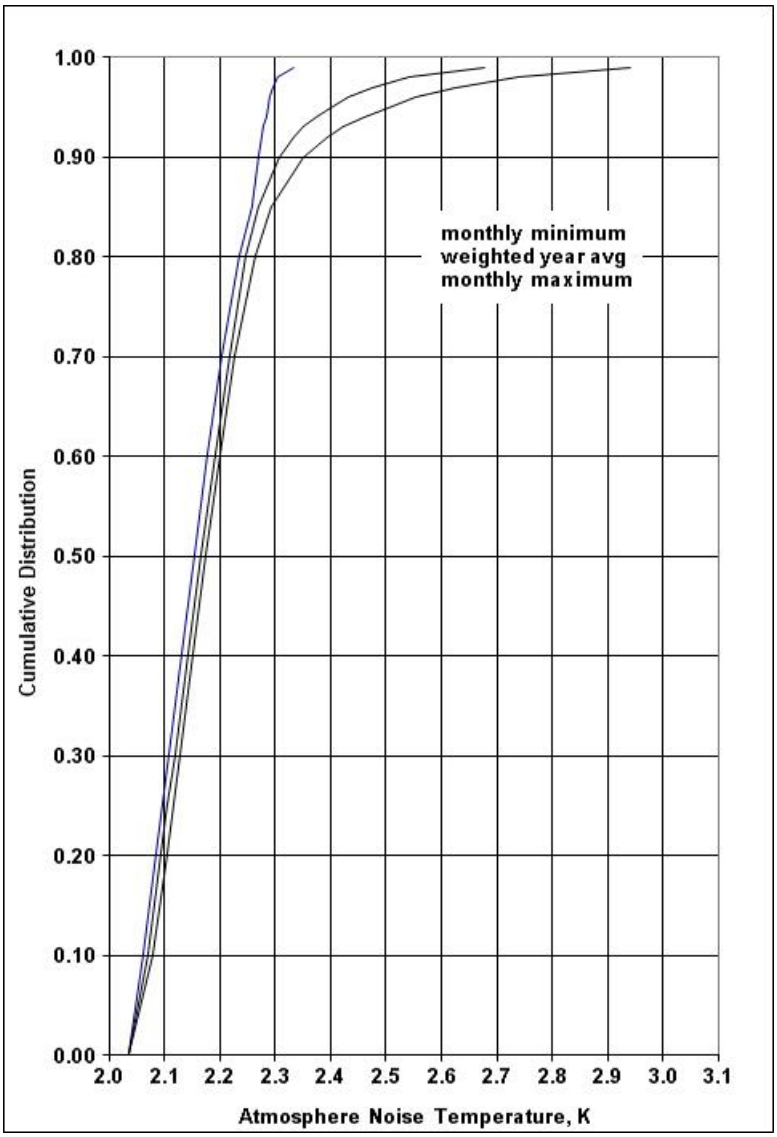

Figure 3. Cumulative Distributions of Zenith Atmospheric Noise Temperature at L-Band and S-Band, Madrid DSCC

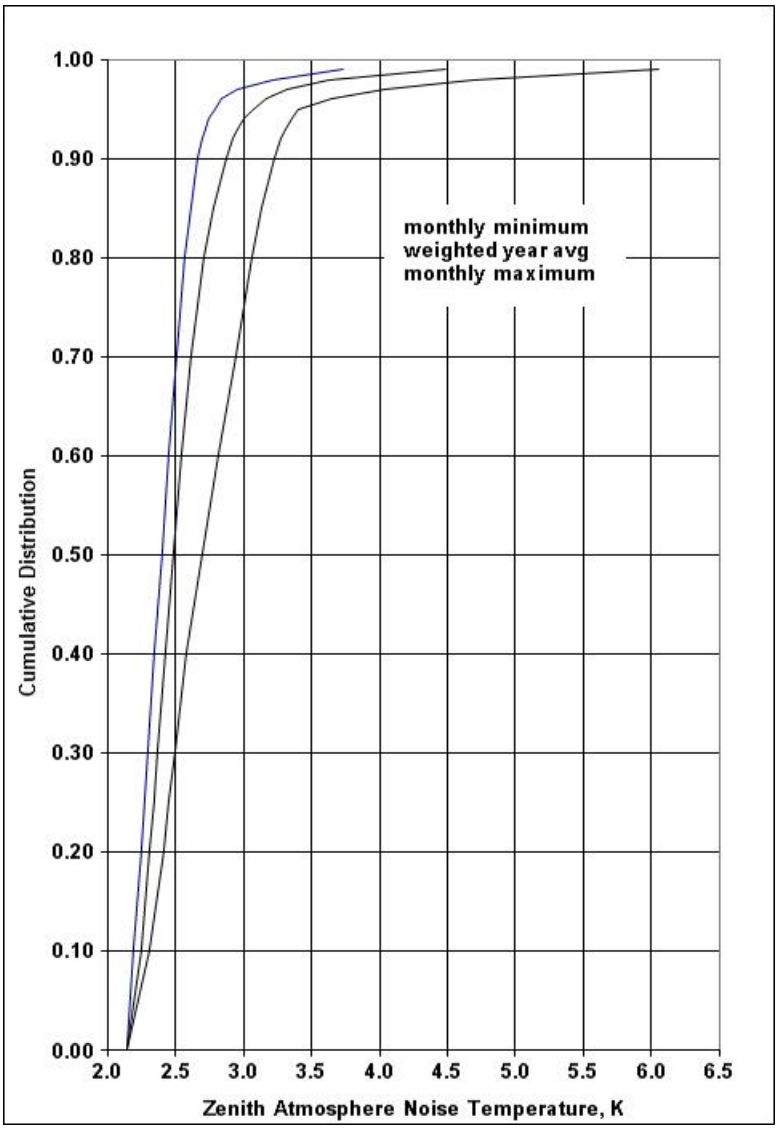

Figure 4. Cumulative Distributions of Zenith Atmospheric Noise Temperature at X-Band, Goldstone DSCC

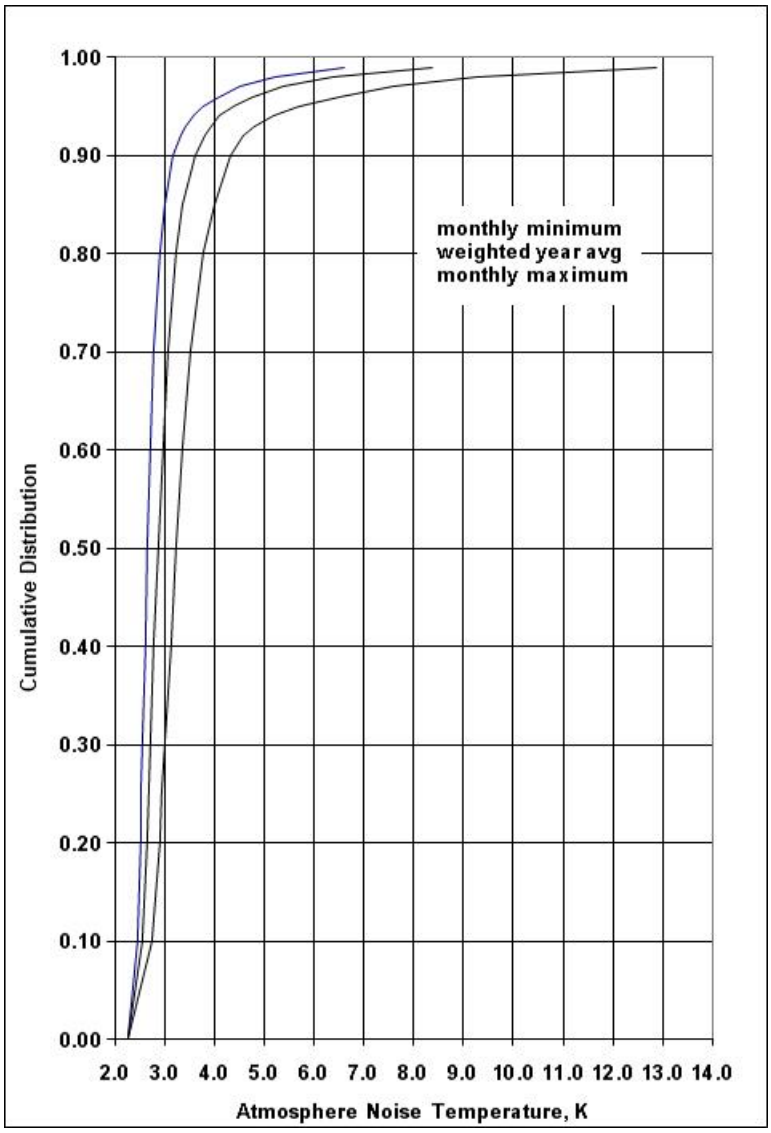

Figure 5. Cumulative Distributions of Zenith Atmospheric Noise Temperature at X-Band, Canberra DSCC

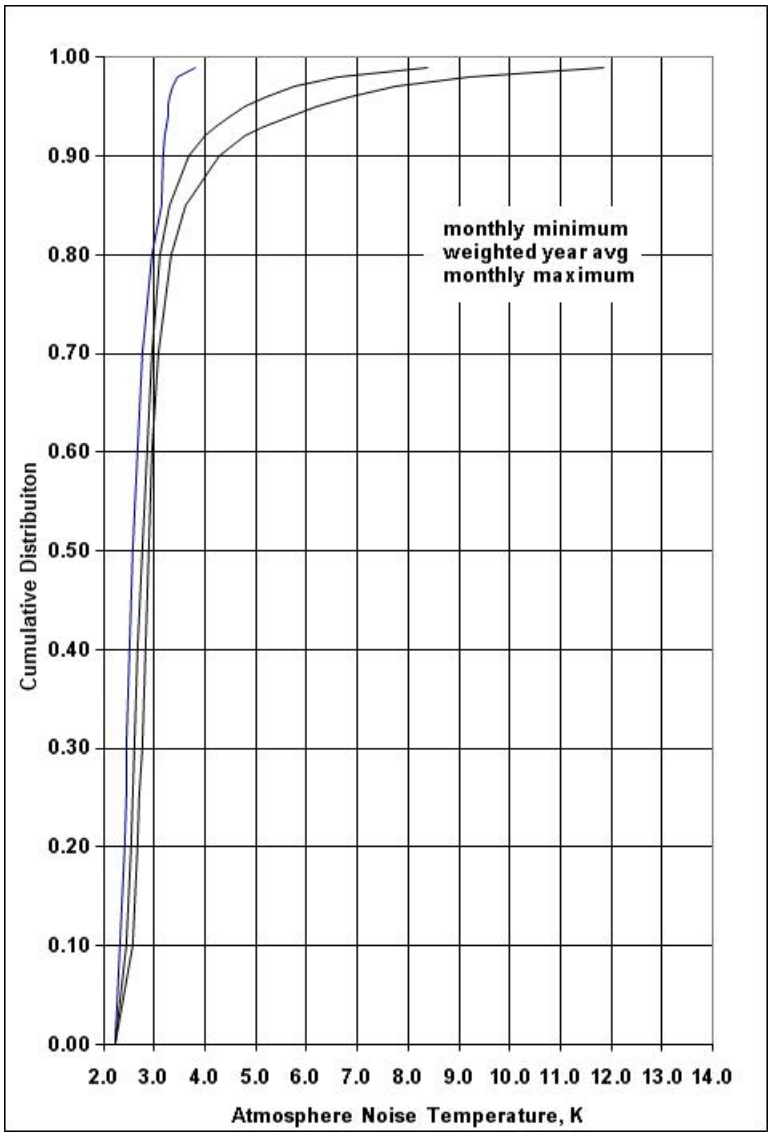

Figure 6. Cumulative Distributions of Zenith Atmospheric Noise Temperature at X-Band, Madrid DSCC

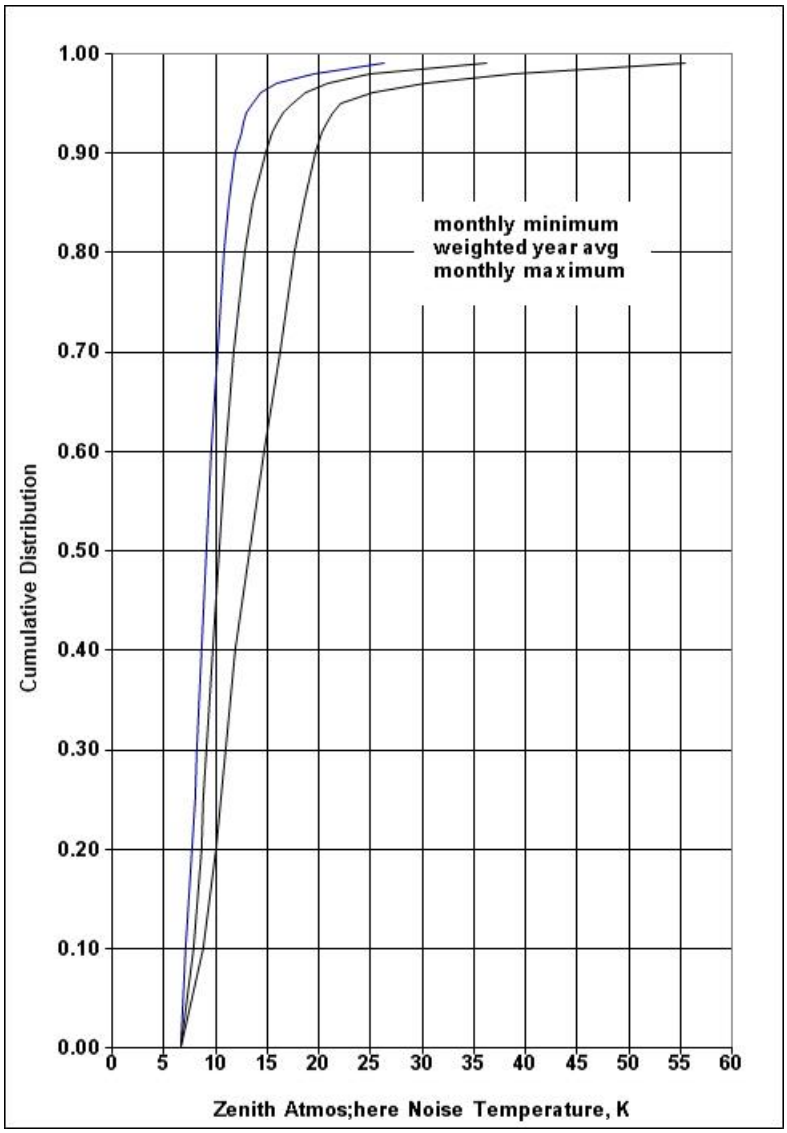

Figure 7. Cumulative Distributions of Zenith Atmospheric Noise Temperature at Ka-Band, Goldstone DSCC

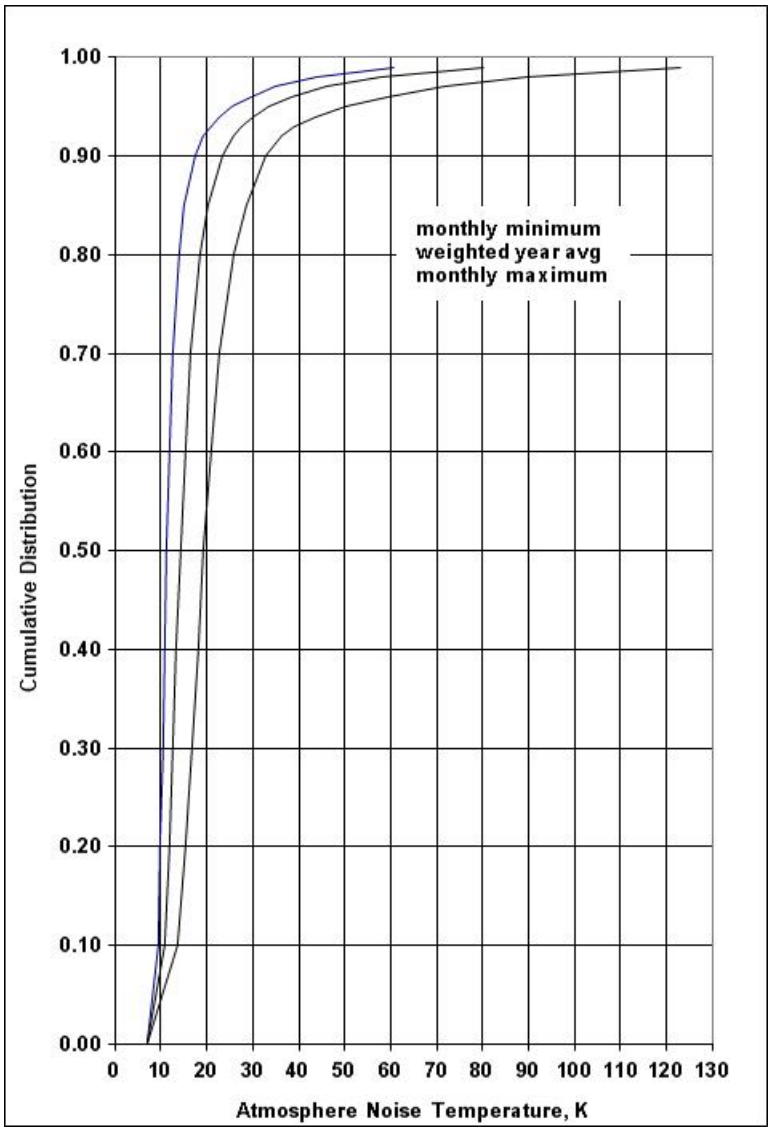

Figure 8. Cumulative Distributions of Zenith Atmospheric Noise Temperature at Ka-Band, Canberra DSCC

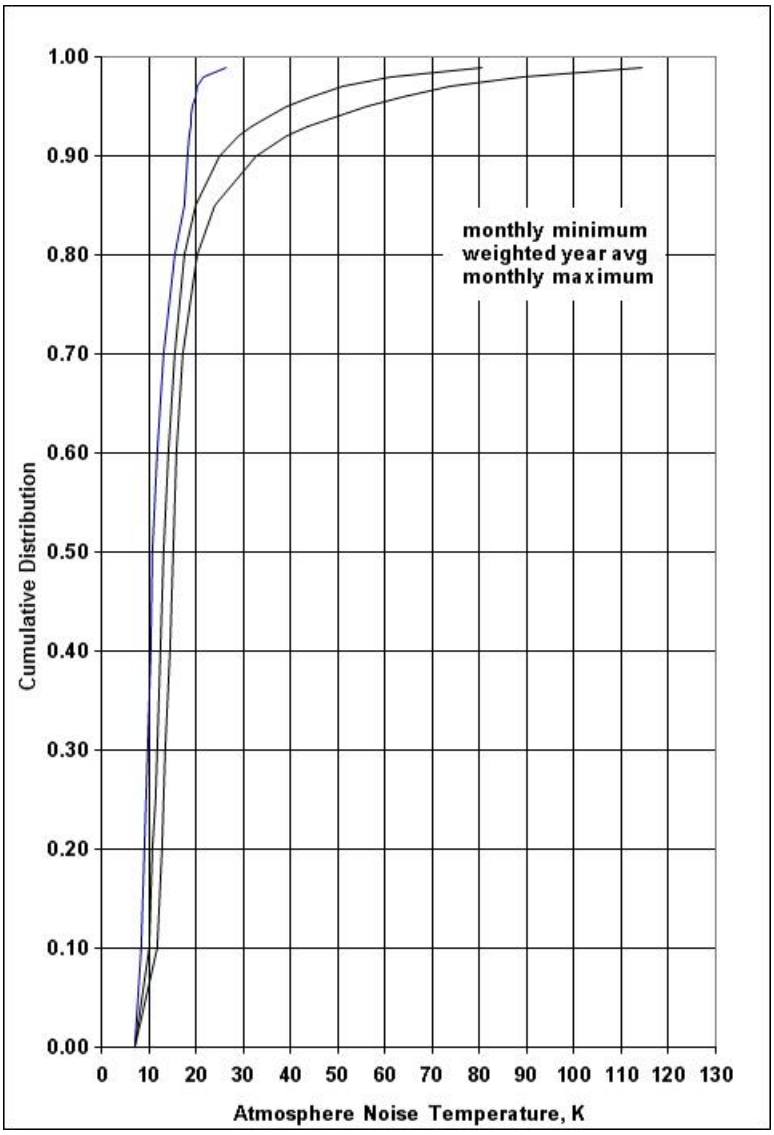

Figure 9. Cumulative Distributions of Zenith Atmospheric Noise Temperature at Ka-Band, Madrid DSCC

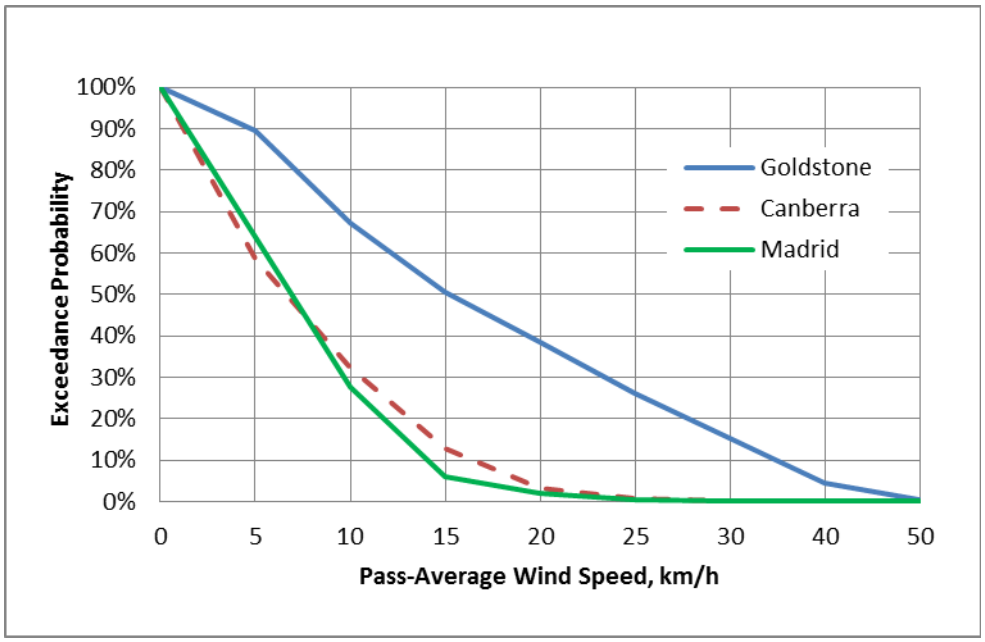

Figure 10. Pass-Average Wind Speed Exceedance Probabilities for the Three DSN Antenna Complexes

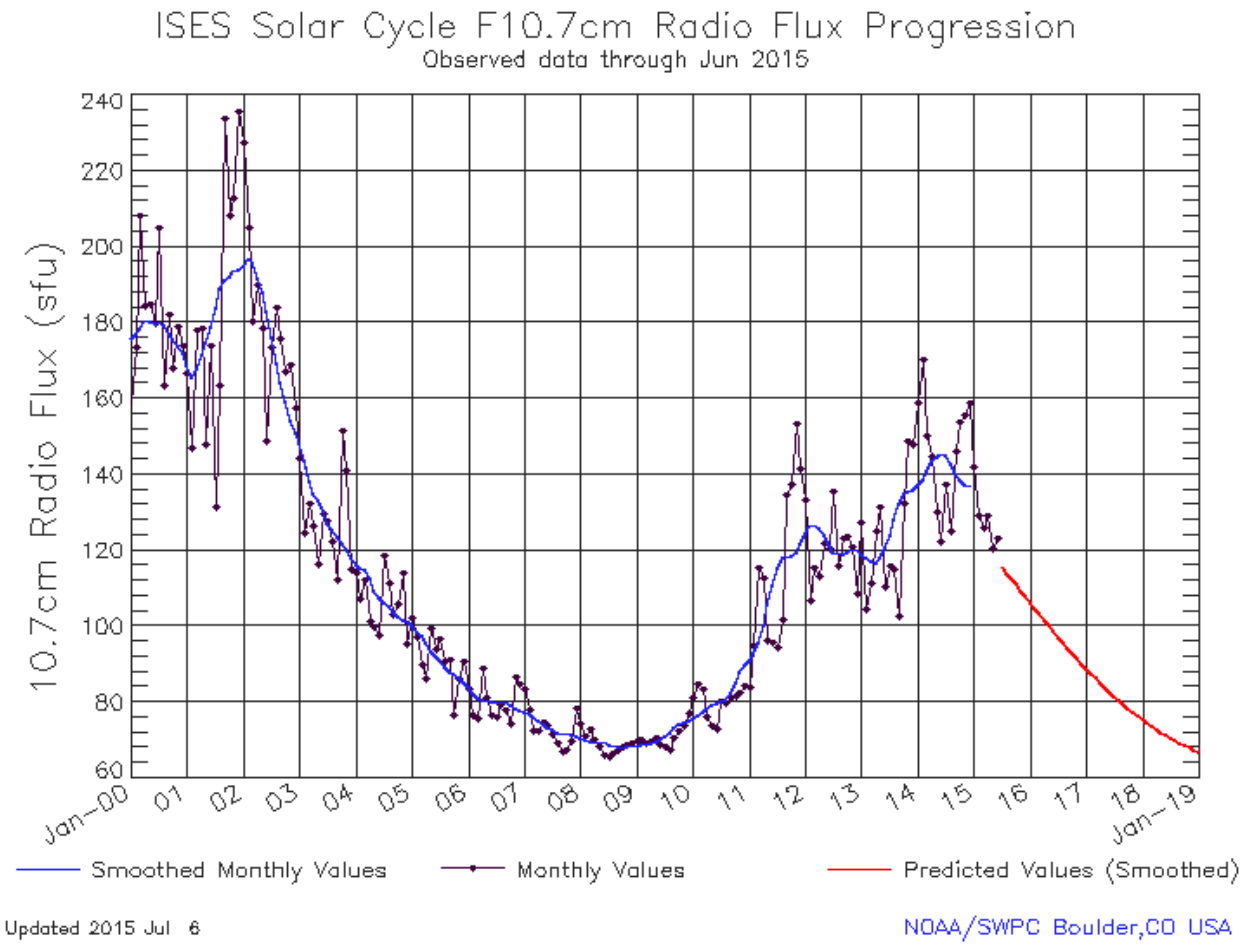

Figure 11. Solar Radio Flux at 2800 MHz (10.7 cm wavelength) from 2000 through 2018 (Covering the end of Solar Cycle 23 and all of Solar Cycle 24, including prediction)

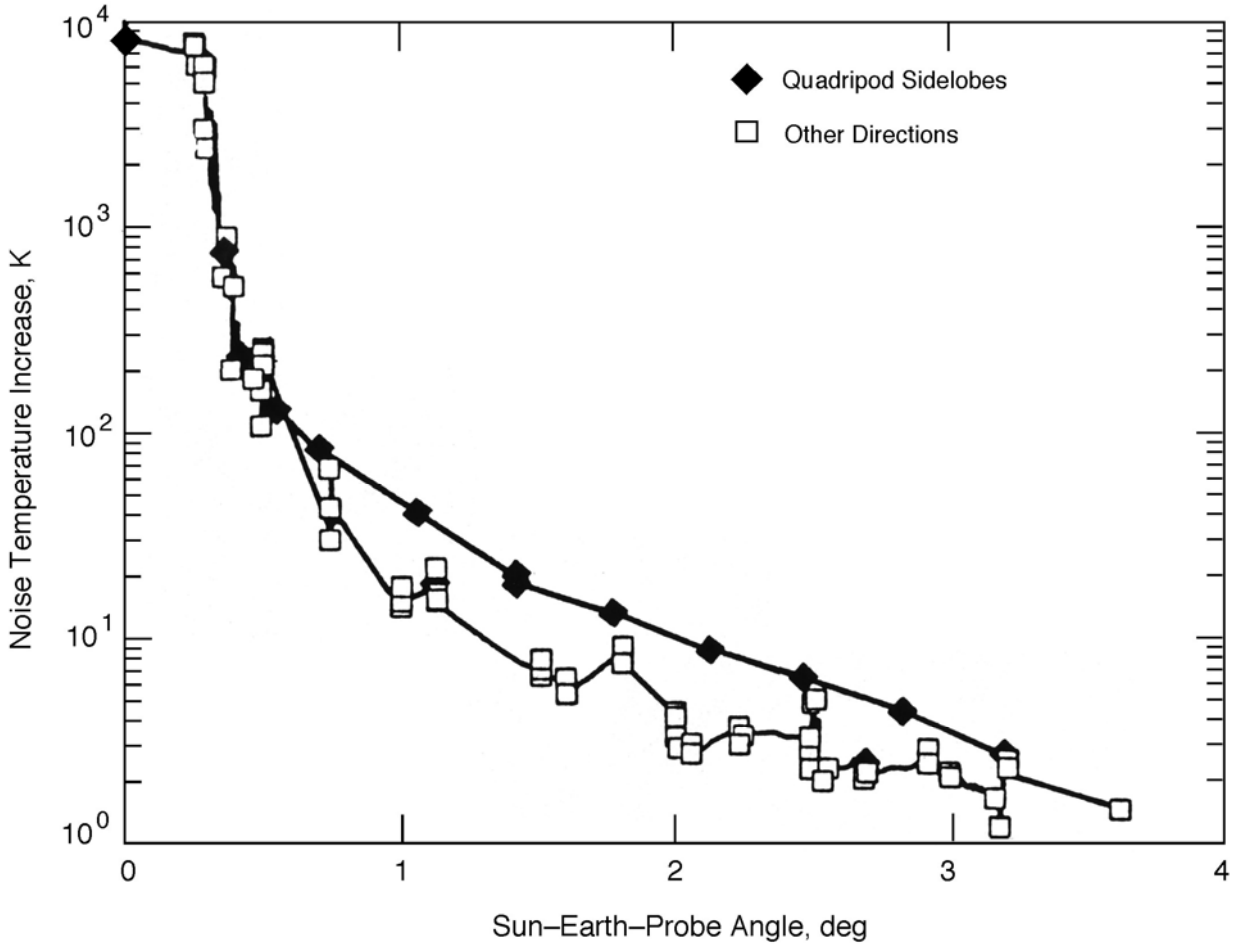

Figure 12. DSS-15 HEF Antenna X-Band System Noise Temperature Increases Due to the Sun at Various Offset Angles, Showing Larger Increases Perpendicular to Quadripod Directions

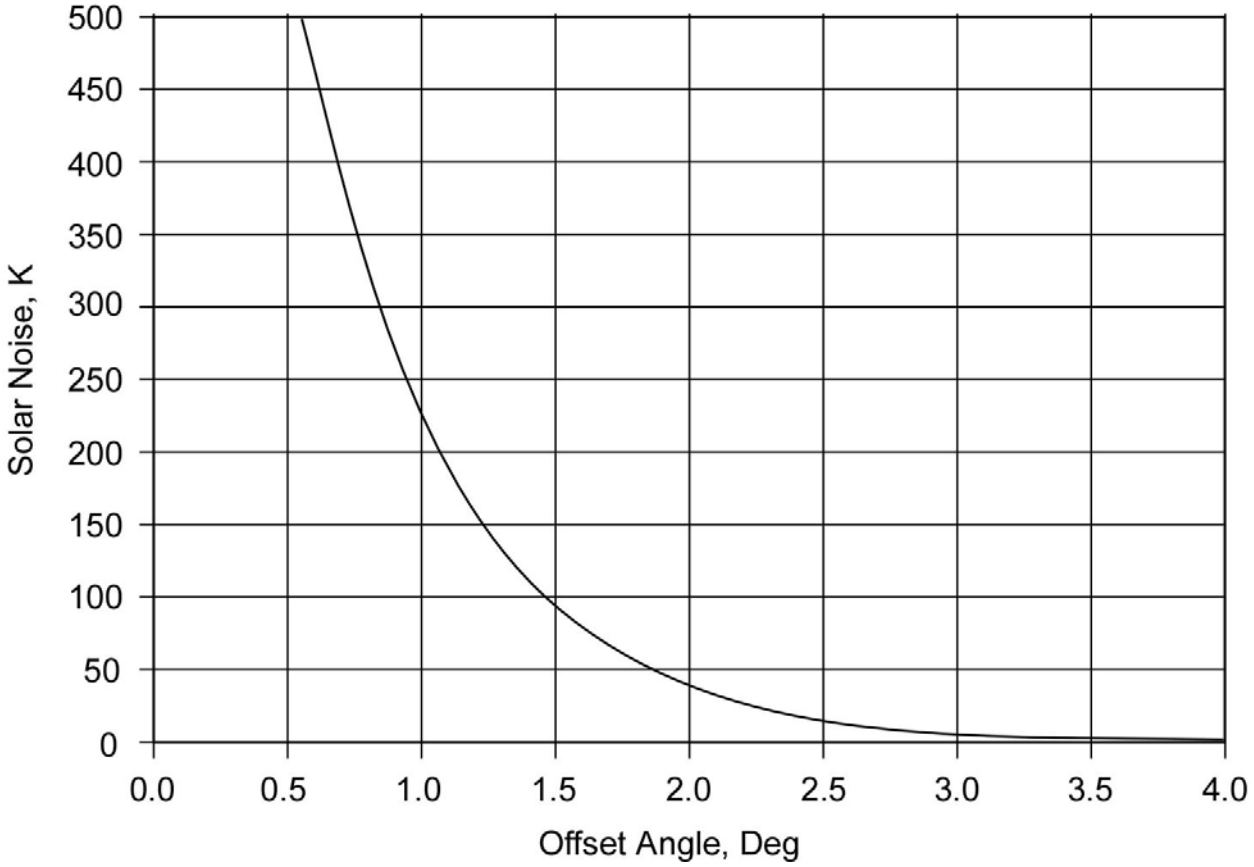

Figure 13. Solar Noise Contribution for a 34-Meter Antenna at S-band at Various Offset Angles from the Sun

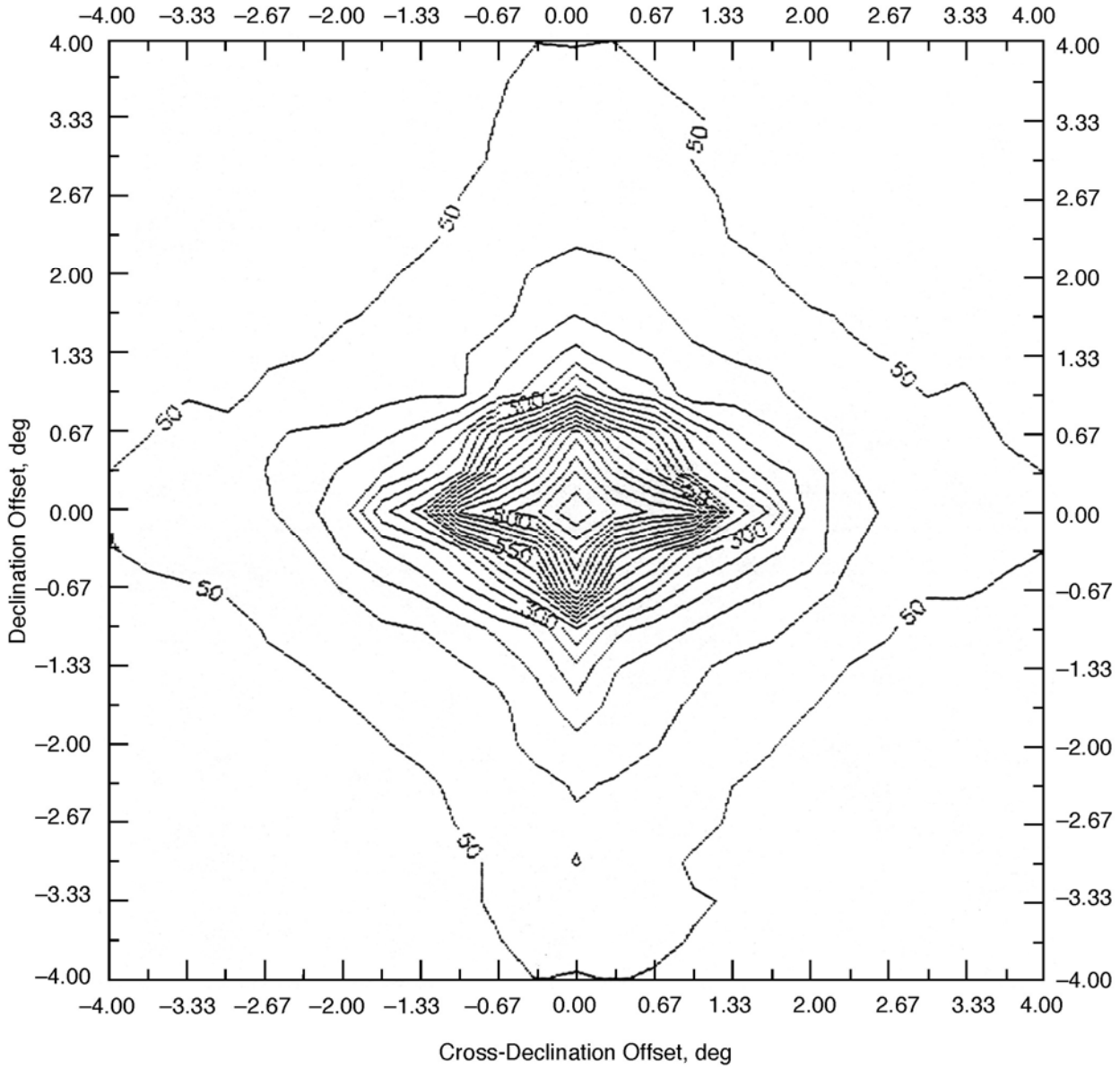

Figure 14. DSS-12 S-Band Total System Noise Temperature at Various Declination and Cross-Declination Offsets from the Sun

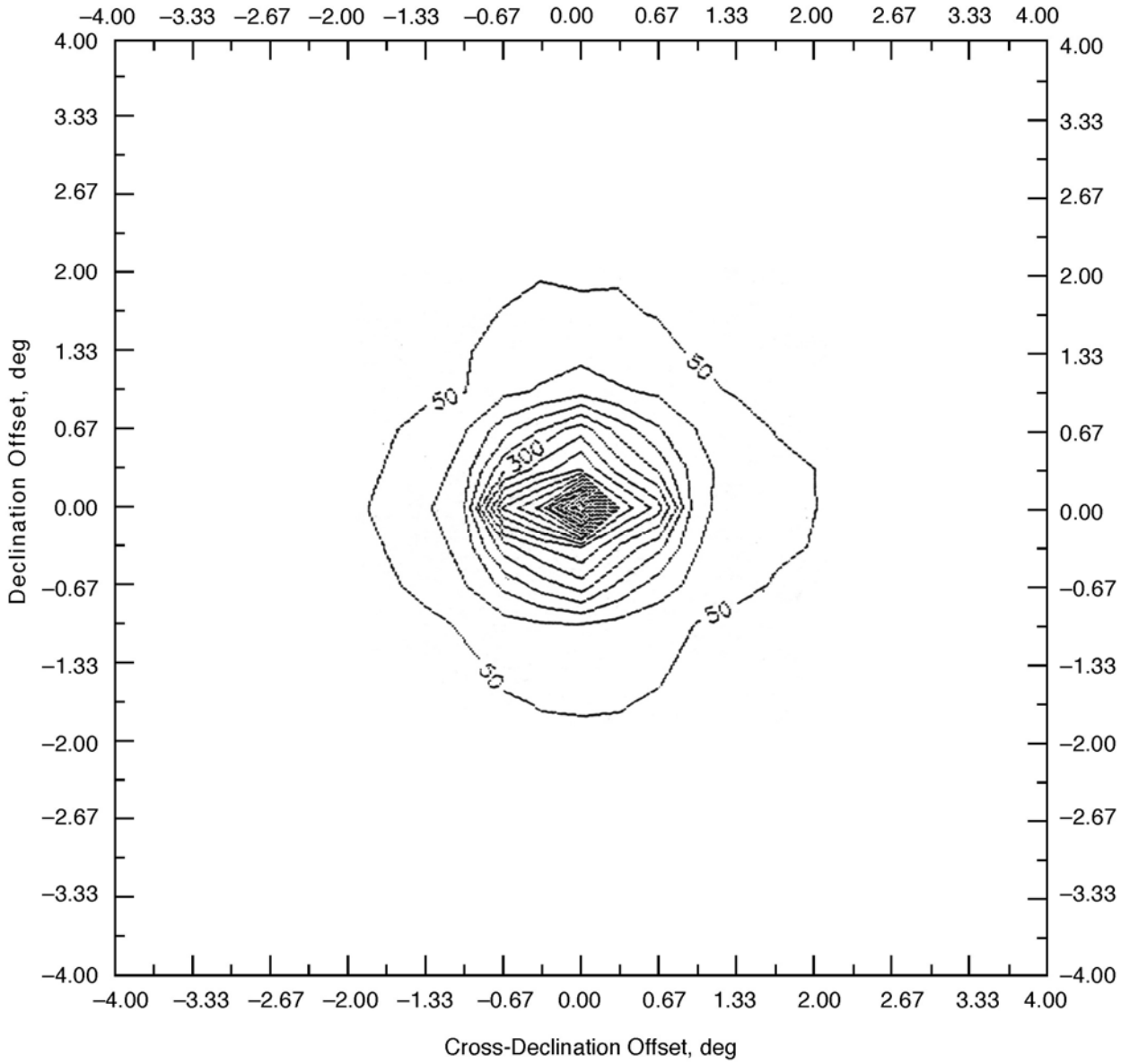

Figure 15. DSS-12 X-Band Total System Noise Temperature at Various Declination and Cross-Declination Offsets from the Sun

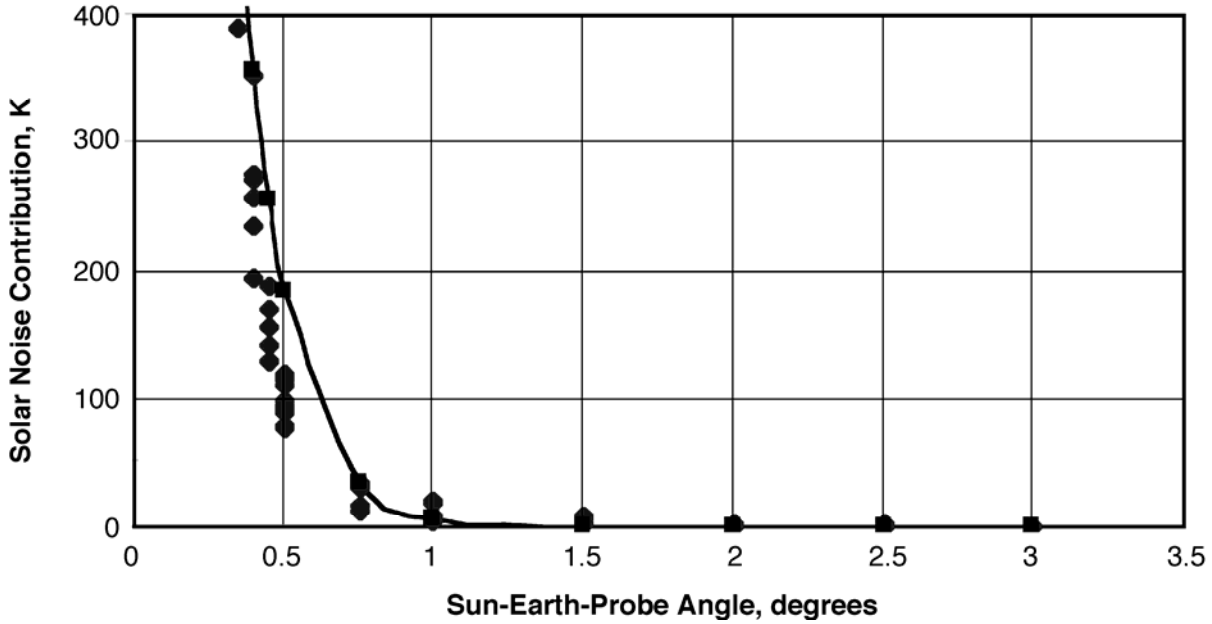

Figure 16. DSS-13 Beam-Waveguide Antenna X-Band Noise Temperature Increase Versus Offset Angle, March 1996

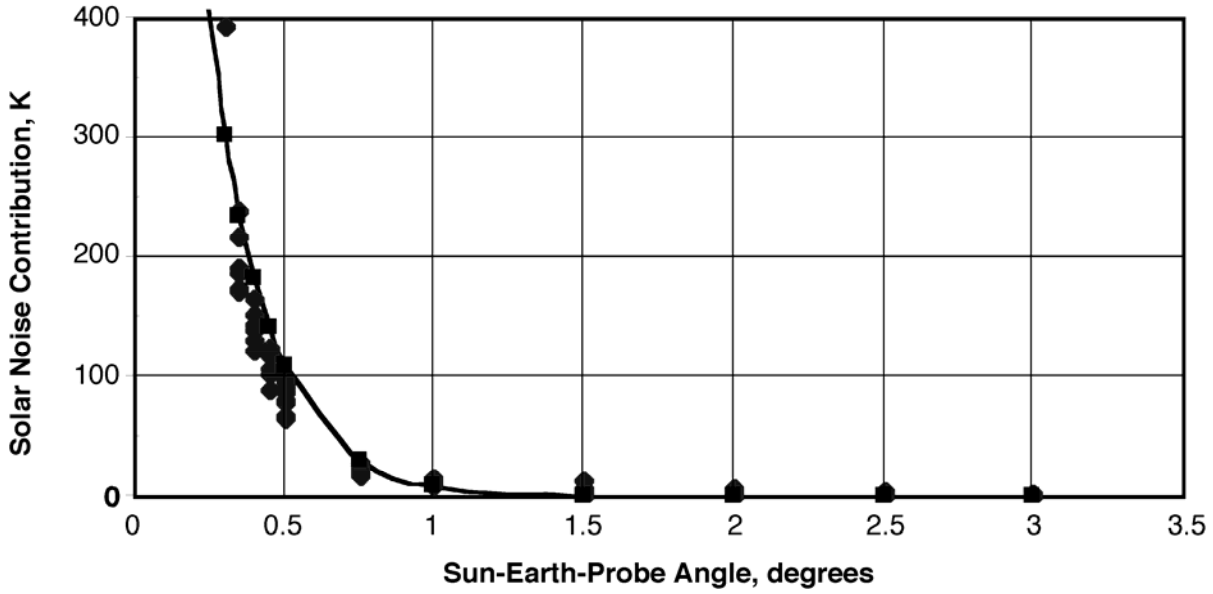

Figure 17. DSS-13 Beam-Waveguide Antenna Ka-Band Noise Temperature Increase Versus Offset Angle, March 1996

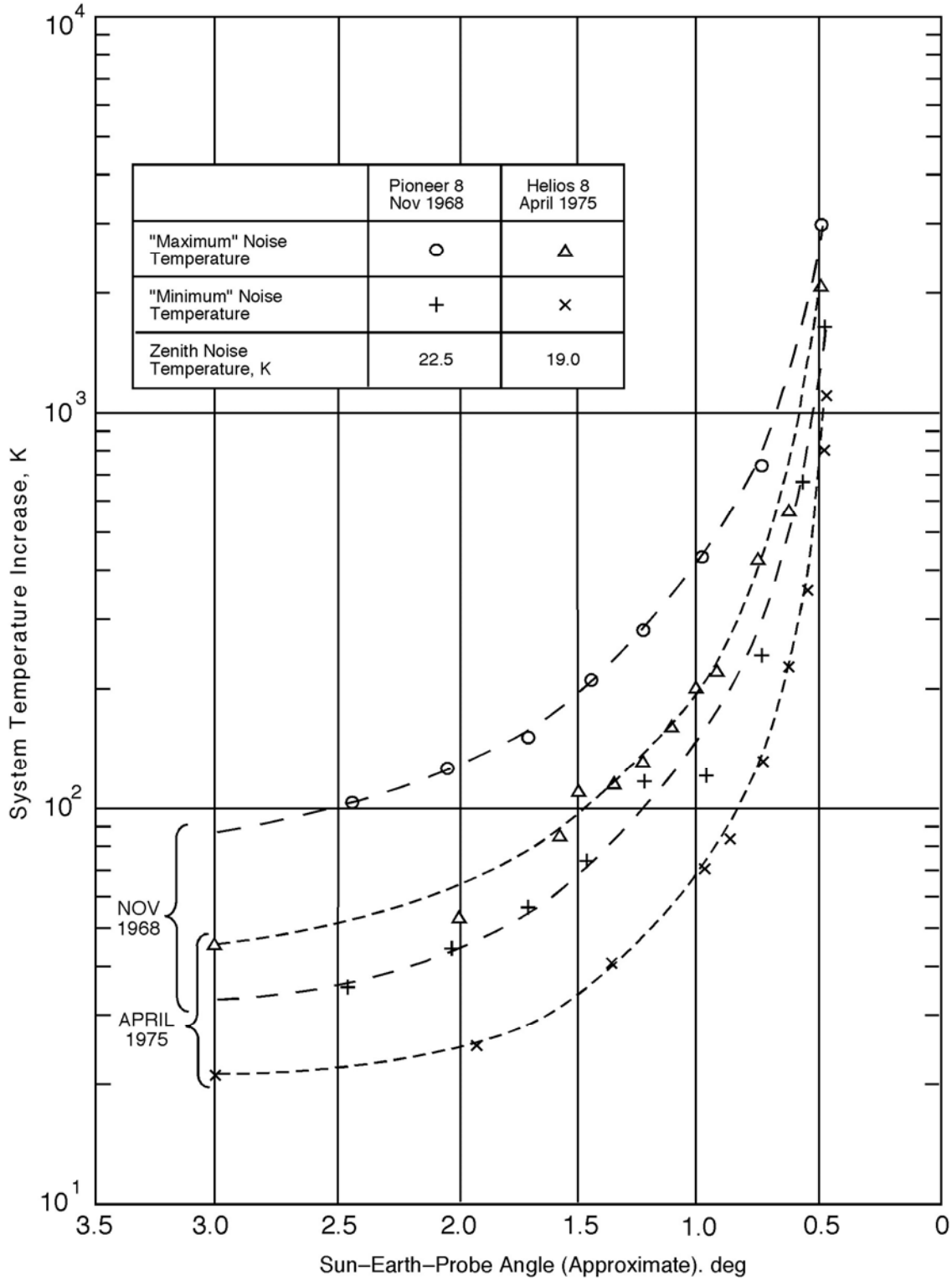

Figure 18. Total S-Band System Noise Temperature for 70-m Antennas Tracking Spacecraft Near the Sun (Derived from 64-m Measurements)

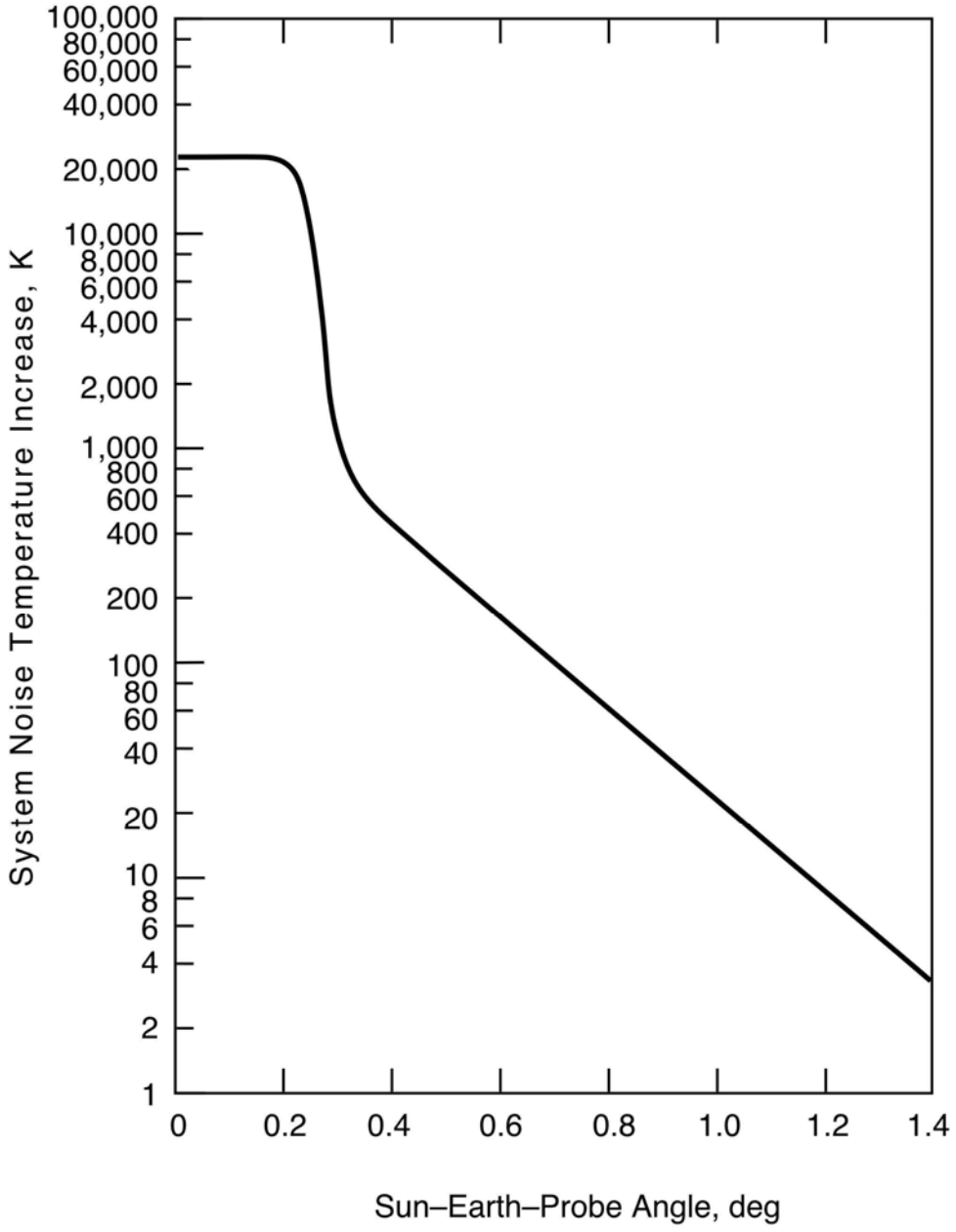

Figure 19. X-Band Noise Temperature Increase for 70-m Antennas as a Function of Sun-Earth-Probe Angle, Nominal Sun, 23,000 K Disk Temperature

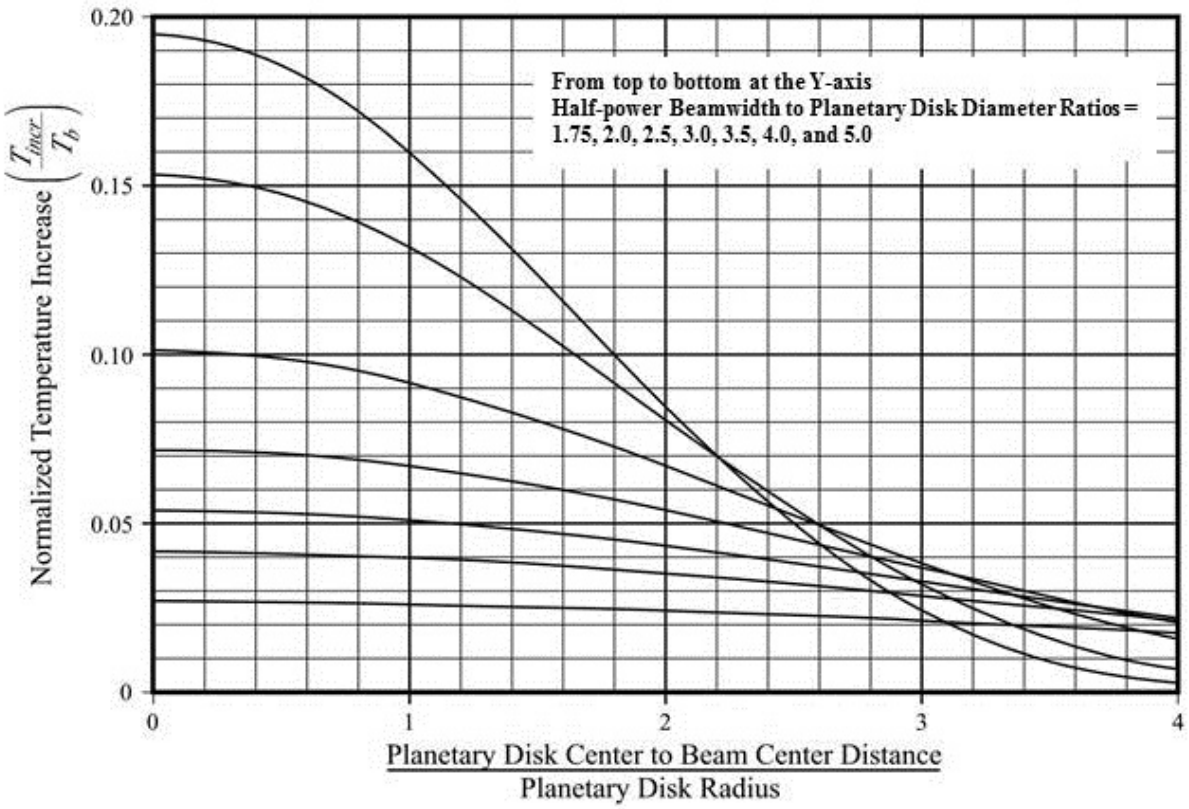

Figure 20. Normalized Temperature Increase for Half-Power Beamwidth to Planetary Disk Diameter Ratios of 1.75, 2.0, 2.5, 3.0, 3.5, 4.0, and 5.0 (top-to-bottom at the left side)

Table 1. Cumulative Distributions of Zenith Atmospheric Noise Temperature at L- and S-Bands for Goldstone DSCC, K

CD	January	February	March	April	May	June
0.00	1.948	1.948	1.948	1.948	1.948	1.948
0.10	1.970	1.971	1.972	1.973	1.974	1.974
0.20	1.992	1.992	1.993	1.994	1.996	1.996
0.25	2.002	2.003	2.004	2.004	2.007	2.007
0.30	2.013	2.013	2.014	2.015	2.017	2.017
0.40	2.034	2.034	2.035	2.036	2.038	2.039
0.50	2.055	2.055	2.056	2.057	2.059	2.061
0.60	2.076	2.076	2.076	2.078	2.081	2.083
0.70	2.098	2.098	2.098	2.099	2.103	2.106
0.80	2.121	2.122	2.120	2.121	2.126	2.131
0.85	2.134	2.137	2.132	2.133	2.139	2.145
0.90	2.150	2.157	2.144	2.145	2.153	2.159
0.92	2.158	2.171	2.151	2.151	2.159	2.166
0.93	2.163	2.181	2.154	2.154	2.163	2.169
0.94	2.170	2.193	2.158	2.158	2.167	2.173
0.95	2.178	2.206	2.163	2.162	2.172	2.177
0.96	2.192	2.229	2.171	2.168	2.178	2.182
0.97	2.213	2.259	2.183	2.179	2.189	2.189
0.98	2.248	2.310	2.207	2.204	2.207	2.200
0.99	2.331	2.414	2.281	2.277	2.260	2.240

Table 1 (Cont'd). Cumulative Distributions of Zenith Atmospheric Noise Temperature at L- and S-Bands for Goldstone DSCC, K

CD	July	August	September	October	November	December	Minimum	Year Average	Maximum
0.00	1.948	1.948	1.948	1.948	1.948	1.948	1.948	1.948	1.948
0.10	1.978	1.976	1.976	1.974	1.972	1.969	1.969	1.973	1.978
0.20	2.003	2.000	1.998	1.996	1.993	1.991	1.991	1.995	2.003
0.25	2.015	2.012	2.009	2.007	2.004	2.002	2.002	2.006	2.015
0.30	2.027	2.023	2.020	2.018	2.015	2.012	2.012	2.017	2.027
0.40	2.050	2.047	2.042	2.040	2.036	2.033	2.033	2.039	2.050
0.50	2.076	2.072	2.064	2.061	2.057	2.054	2.054	2.061	2.076
0.60	2.103	2.098	2.087	2.082	2.079	2.076	2.076	2.083	2.103
0.70	2.130	2.124	2.112	2.105	2.101	2.098	2.098	2.106	2.130
0.80	2.157	2.151	2.141	2.130	2.125	2.123	2.120	2.131	2.157
0.85	2.171	2.166	2.157	2.143	2.138	2.137	2.132	2.144	2.171
0.90	2.186	2.182	2.175	2.158	2.154	2.153	2.144	2.160	2.186
0.92	2.193	2.189	2.182	2.165	2.162	2.162	2.151	2.167	2.193
0.93	2.198	2.193	2.186	2.169	2.166	2.167	2.154	2.172	2.198
0.94	2.203	2.197	2.190	2.173	2.171	2.174	2.158	2.177	2.203
0.95	2.209	2.202	2.194	2.179	2.177	2.186	2.162	2.184	2.209
0.96	2.216	2.208	2.199	2.185	2.184	2.203	2.168	2.193	2.229
0.97	2.225	2.215	2.205	2.193	2.198	2.229	2.179	2.206	2.259
0.98	2.245	2.226	2.217	2.208	2.230	2.274	2.200	2.231	2.310
0.99	2.299	2.251	2.255	2.261	2.316	2.393	2.240	2.297	2.414

Table 2. Cumulative Distributions of Zenith Atmospheric Noise Temperature at L- and S-Bands for Canberra DSCC, K

CD	January	February	March	April	May	June
0.00	2.076	2.076	2.076	2.076	2.076	2.076
0.10	2.121	2.131	2.122	2.115	2.113	2.109
0.20	2.149	2.159	2.149	2.141	2.137	2.132
0.25	2.162	2.173	2.161	2.153	2.148	2.144
0.30	2.175	2.187	2.174	2.165	2.160	2.155
0.40	2.202	2.214	2.200	2.189	2.183	2.178
0.50	2.228	2.242	2.226	2.213	2.205	2.202
0.60	2.256	2.269	2.254	2.238	2.229	2.227
0.70	2.286	2.299	2.282	2.264	2.253	2.254
0.80	2.321	2.337	2.314	2.292	2.282	2.284
0.85	2.342	2.363	2.333	2.308	2.299	2.301
0.90	2.368	2.397	2.359	2.329	2.325	2.328
0.92	2.385	2.421	2.371	2.342	2.341	2.346
0.93	2.396	2.439	2.378	2.350	2.351	2.359
0.94	2.409	2.469	2.388	2.361	2.363	2.376
0.95	2.427	2.510	2.402	2.377	2.378	2.404
0.96	2.452	2.571	2.424	2.400	2.398	2.443
0.97	2.504	2.657	2.458	2.429	2.427	2.494
0.98	2.606	2.785	2.520	2.480	2.479	2.567
0.99	2.787	3.064	2.657	2.591	2.590	2.693

Table 2 (Cont'd). Cumulative Distributions of Zenith Atmospheric Noise Temperature at L- and S-Bands for Canberra DSCC, K

CD	July	August	September	October	November	December	Minimum	Year Average	Maximum
0.00	2.076	2.076	2.076	2.076	2.076	2.076	2.076	2.076	2.076
0.10	2.108	2.108	2.110	2.111	2.118	2.117	2.108	2.115	2.131
0.20	2.132	2.131	2.134	2.136	2.143	2.144	2.131	2.140	2.159
0.25	2.143	2.142	2.146	2.147	2.156	2.157	2.142	2.153	2.173
0.30	2.154	2.153	2.158	2.159	2.168	2.170	2.153	2.165	2.187
0.40	2.177	2.176	2.181	2.183	2.194	2.195	2.176	2.189	2.214
0.50	2.199	2.198	2.204	2.206	2.219	2.221	2.198	2.213	2.242
0.60	2.223	2.221	2.228	2.230	2.247	2.249	2.221	2.239	2.269
0.70	2.248	2.246	2.253	2.256	2.277	2.277	2.246	2.266	2.299
0.80	2.276	2.272	2.281	2.287	2.313	2.312	2.272	2.297	2.337
0.85	2.293	2.288	2.298	2.307	2.336	2.333	2.288	2.316	2.363
0.90	2.317	2.311	2.323	2.335	2.375	2.366	2.311	2.344	2.397
0.92	2.331	2.325	2.340	2.353	2.402	2.386	2.325	2.361	2.421
0.93	2.341	2.336	2.351	2.365	2.423	2.398	2.336	2.373	2.439
0.94	2.354	2.348	2.364	2.381	2.447	2.417	2.348	2.389	2.469
0.95	2.370	2.366	2.383	2.402	2.478	2.444	2.366	2.410	2.510
0.96	2.393	2.391	2.413	2.431	2.528	2.483	2.391	2.442	2.571
0.97	2.424	2.433	2.458	2.471	2.601	2.550	2.424	2.489	2.657
0.98	2.481	2.506	2.521	2.541	2.705	2.655	2.479	2.566	2.785
0.99	2.585	2.637	2.681	2.704	2.893	2.857	2.585	2.720	3.064

Table 3. Cumulative Distributions of Zenith Atmospheric Noise Temperature at L- and S-Bands for Madrid DSCC, K

CD	January	February	March	April	May	June
0.00	2.035	2.035	2.035	2.035	2.035	2.035
0.10	2.061	2.061	2.065	2.069	2.074	2.077
0.20	2.085	2.085	2.089	2.092	2.099	2.103
0.25	2.097	2.096	2.100	2.104	2.111	2.115
0.30	2.109	2.107	2.112	2.116	2.123	2.127
0.40	2.132	2.130	2.135	2.139	2.146	2.151
0.50	2.156	2.153	2.158	2.163	2.170	2.174
0.60	2.182	2.178	2.182	2.187	2.194	2.198
0.70	2.211	2.204	2.208	2.212	2.219	2.223
0.80	2.245	2.237	2.242	2.242	2.247	2.249
0.85	2.272	2.261	2.267	2.266	2.265	2.263
0.90	2.321	2.310	2.316	2.311	2.299	2.279
0.92	2.358	2.348	2.351	2.340	2.325	2.288
0.93	2.384	2.375	2.372	2.359	2.343	2.293
0.94	2.416	2.406	2.399	2.385	2.365	2.301
0.95	2.456	2.444	2.431	2.416	2.395	2.312
0.96	2.507	2.488	2.475	2.455	2.434	2.329
0.97	2.567	2.545	2.533	2.510	2.489	2.358
0.98	2.643	2.634	2.614	2.592	2.568	2.419
0.99	2.776	2.848	2.744	2.737	2.730	2.560

Table 3 (Cont'd). Cumulative Distributions of Zenith Atmospheric Noise Temperature at L- and S-Bands for Madrid DSCC, K

CD	July	August	September	October	November	December	Minimum	Year Average	Maximum
0.00	2.035	2.035	2.035	2.035	2.035	2.035	2.035	2.035	2.035
0.10	2.079	2.079	2.076	2.071	2.065	2.062	2.061	2.070	2.079
0.20	2.103	2.105	2.102	2.097	2.090	2.086	2.085	2.095	2.105
0.25	2.115	2.117	2.114	2.110	2.101	2.098	2.096	2.107	2.117
0.30	2.127	2.129	2.126	2.122	2.113	2.110	2.107	2.118	2.129
0.40	2.150	2.152	2.151	2.147	2.137	2.134	2.130	2.142	2.152
0.50	2.174	2.175	2.175	2.173	2.162	2.159	2.153	2.166	2.175
0.60	2.197	2.199	2.200	2.199	2.188	2.186	2.178	2.191	2.200
0.70	2.221	2.223	2.224	2.227	2.217	2.215	2.204	2.217	2.227
0.80	2.245	2.248	2.250	2.263	2.252	2.255	2.237	2.248	2.263
0.85	2.258	2.261	2.265	2.293	2.280	2.285	2.258	2.270	2.293
0.90	2.271	2.275	2.282	2.353	2.339	2.342	2.271	2.308	2.353
0.92	2.277	2.281	2.293	2.395	2.384	2.381	2.277	2.335	2.395
0.93	2.280	2.285	2.300	2.424	2.414	2.408	2.280	2.352	2.424
0.94	2.283	2.289	2.310	2.461	2.447	2.440	2.283	2.374	2.461
0.95	2.287	2.293	2.323	2.505	2.484	2.479	2.287	2.400	2.505
0.96	2.292	2.299	2.342	2.555	2.530	2.525	2.292	2.433	2.555
0.97	2.296	2.307	2.371	2.625	2.585	2.586	2.296	2.477	2.625
0.98	2.305	2.327	2.433	2.738	2.663	2.665	2.305	2.543	2.738
0.99	2.334	2.393	2.589	2.942	2.809	2.820	2.334	2.678	2.942

Table 4. Cumulative Distributions of Zenith Atmospheric Noise Temperature at X-Band for Goldstone DSCC, K

CD	January	February	March	April	May	June
0.00	2.140	2.140	2.140	2.140	2.140	2.140
0.10	2.200	2.213	2.229	2.238	2.256	2.251
0.20	2.259	2.265	2.277	2.288	2.317	2.316
0.25	2.283	2.289	2.300	2.313	2.341	2.342
0.30	2.307	2.312	2.324	2.337	2.364	2.368
0.40	2.354	2.359	2.367	2.380	2.411	2.420
0.50	2.402	2.404	2.410	2.424	2.462	2.479
0.60	2.450	2.450	2.452	2.471	2.513	2.542
0.70	2.510	2.514	2.508	2.522	2.576	2.615
0.80	2.583	2.600	2.566	2.583	2.656	2.720
0.85	2.638	2.674	2.610	2.622	2.707	2.788
0.90	2.743	2.832	2.661	2.674	2.778	2.862
0.92	2.799	2.968	2.701	2.706	2.814	2.899
0.93	2.846	3.077	2.721	2.721	2.841	2.923
0.94	2.906	3.226	2.753	2.745	2.869	2.946
0.95	3.001	3.365	2.797	2.784	2.910	2.977
0.96	3.156	3.651	2.872	2.843	2.977	3.021
0.97	3.415	4.039	3.017	2.961	3.091	3.091
0.98	3.865	4.691	3.319	3.270	3.316	3.218
0.99	4.954	6.052	4.285	4.230	3.994	3.729

Table 4 (Cont'd). Cumulative Distributions of Zenith Atmospheric Noise Temperature at X-Band for Goldstone DSCC, K

CD	July	August	September	October	November	December	Minimum	Year Average	Maximum
0.00	2.140	2.140	2.140	2.140	2.140	2.140	2.140	2.140	2.140
0.10	2.308	2.288	2.286	2.256	2.227	2.190	2.190	2.245	2.308
0.20	2.408	2.372	2.348	2.322	2.279	2.252	2.252	2.309	2.408
0.25	2.453	2.410	2.376	2.350	2.305	2.276	2.276	2.337	2.453
0.30	2.495	2.447	2.404	2.377	2.332	2.300	2.300	2.364	2.495
0.40	2.577	2.529	2.464	2.431	2.382	2.348	2.348	2.419	2.577
0.50	2.690	2.632	2.528	2.482	2.433	2.396	2.396	2.479	2.690
0.60	2.817	2.740	2.604	2.535	2.491	2.444	2.444	2.543	2.817
0.70	2.938	2.857	2.697	2.604	2.553	2.511	2.508	2.618	2.938
0.80	3.060	2.986	2.846	2.699	2.633	2.604	2.566	2.712	3.060
0.85	3.132	3.065	2.953	2.762	2.697	2.677	2.610	2.777	3.132
0.90	3.221	3.165	3.071	2.846	2.786	2.783	2.661	2.868	3.221
0.92	3.268	3.216	3.124	2.891	2.845	2.849	2.701	2.923	3.268
0.93	3.308	3.243	3.150	2.924	2.880	2.894	2.721	2.960	3.308
0.94	3.352	3.275	3.177	2.956	2.929	2.971	2.745	3.007	3.352
0.95	3.409	3.321	3.211	3.004	2.985	3.098	2.784	3.070	3.409
0.96	3.477	3.376	3.252	3.060	3.055	3.301	2.843	3.167	3.651
0.97	3.585	3.450	3.316	3.145	3.218	3.626	2.961	3.324	4.039
0.98	3.822	3.575	3.449	3.330	3.619	4.210	3.218	3.631	4.691
0.99	4.525	3.879	3.928	4.009	4.752	5.773	3.729	4.490	6.052

Table 5. Cumulative Distributions of Zenith Atmospheric Noise Temperature at X-Band for Canberra DSCC, K

CD	January	February	March	April	May	June
0.00	2.280	2.280	2.280	2.280	2.280	2.280
0.10	2.636	2.764	2.648	2.555	2.526	2.478
0.20	2.757	2.899	2.758	2.652	2.594	2.536
0.25	2.810	2.960	2.802	2.690	2.624	2.564
0.30	2.860	3.023	2.847	2.723	2.652	2.590
0.40	2.963	3.136	2.937	2.788	2.708	2.650
0.50	3.068	3.250	3.044	2.861	2.764	2.718
0.60	3.188	3.372	3.162	2.953	2.823	2.807
0.70	3.344	3.525	3.295	3.053	2.903	2.916
0.80	3.562	3.781	3.475	3.177	3.036	3.060
0.85	3.715	4.006	3.603	3.265	3.148	3.170
0.90	3.948	4.335	3.816	3.425	3.363	3.405
0.92	4.125	4.594	3.933	3.543	3.529	3.603
0.93	4.245	4.818	4.004	3.626	3.641	3.741
0.94	4.391	5.193	4.108	3.753	3.774	3.948
0.95	4.603	5.718	4.273	3.942	3.949	4.293
0.96	4.912	6.504	4.542	4.225	4.191	4.797
0.97	5.581	7.617	4.974	4.582	4.552	5.454
0.98	6.908	9.280	5.764	5.239	5.219	6.391
0.99	9.274	12.890	7.563	6.695	6.680	8.041

Table 5 (Cont'd). Cumulative Distributions of Zenith Atmospheric Noise Temperature at X-Band for Canberra DSCC, K

CD	July	August	September	October	November	December	Minimum	Year Average	Maximum
0.00	2.280	2.280	2.280	2.280	2.280	2.280	2.280	2.280	2.280
0.10	2.466	2.460	2.491	2.502	2.592	2.583	2.460	2.557	2.764
0.20	2.525	2.516	2.562	2.580	2.682	2.692	2.516	2.644	2.899
0.25	2.552	2.541	2.593	2.613	2.725	2.739	2.541	2.682	2.960
0.30	2.577	2.566	2.624	2.646	2.768	2.785	2.566	2.720	3.023
0.40	2.627	2.618	2.682	2.709	2.856	2.878	2.618	2.794	3.136
0.50	2.684	2.669	2.746	2.776	2.948	2.979	2.669	2.873	3.250
0.60	2.753	2.726	2.817	2.847	3.065	3.094	2.726	2.964	3.372
0.70	2.839	2.802	2.905	2.941	3.222	3.224	2.802	3.077	3.525
0.80	2.957	2.912	3.031	3.103	3.455	3.437	2.912	3.244	3.781
0.85	3.057	3.001	3.135	3.244	3.644	3.604	3.001	3.377	4.006
0.90	3.258	3.173	3.340	3.502	4.036	3.914	3.173	3.619	4.335
0.92	3.398	3.319	3.514	3.688	4.346	4.130	3.319	3.802	4.594
0.93	3.508	3.433	3.639	3.832	4.597	4.274	3.433	3.936	4.818
0.94	3.651	3.576	3.795	4.016	4.897	4.491	3.576	4.120	5.193
0.95	3.847	3.786	4.024	4.266	5.281	4.834	3.786	4.384	5.718
0.96	4.125	4.105	4.395	4.630	5.926	5.328	4.105	4.782	6.504
0.97	4.517	4.640	4.968	5.149	6.873	6.194	4.517	5.388	7.617
0.98	5.255	5.590	5.778	6.053	8.225	7.560	5.219	6.382	9.280
0.99	6.614	7.298	7.886	8.183	10.667	10.197	6.614	8.392	12.890

Table 6. Cumulative Distributions of Zenith Atmospheric Noise Temperature at X-Band for Madrid DSCC, K

CD	January	February	March	April	May	June
0.00	2.239	2.239	2.239	2.239	2.239	2.239
0.10	2.346	2.343	2.398	2.442	2.521	2.556
0.20	2.422	2.413	2.469	2.514	2.603	2.657
0.25	2.456	2.442	2.499	2.548	2.641	2.700
0.30	2.490	2.472	2.529	2.582	2.678	2.737
0.40	2.557	2.533	2.591	2.651	2.749	2.809
0.50	2.634	2.597	2.659	2.726	2.819	2.879
0.60	2.731	2.676	2.737	2.802	2.894	2.956
0.70	2.872	2.783	2.845	2.892	2.983	3.043
0.80	3.089	2.976	3.044	3.052	3.115	3.143
0.85	3.334	3.182	3.266	3.247	3.239	3.205
0.90	3.866	3.710	3.798	3.724	3.562	3.299
0.92	4.310	4.174	4.209	4.071	3.870	3.366
0.93	4.630	4.510	4.474	4.303	4.083	3.418
0.94	5.036	4.898	4.808	4.614	4.358	3.500
0.95	5.543	5.381	5.215	5.010	4.730	3.617
0.96	6.196	5.938	5.768	5.502	5.231	3.817
0.97	6.973	6.678	6.514	6.216	5.929	4.181
0.98	7.945	7.824	7.570	7.279	6.960	4.974
0.99	9.679	10.615	9.254	9.168	9.065	6.832

Table 6 (Cont'd). Cumulative Distributions of Zenith Atmospheric Noise Temperature at X-Band for Madrid DSCC, K

CD	July	August	September	October	November	December	Minimum	Year Average	Maximum
0.00	2.239	2.239	2.239	2.239	2.239	2.239	2.239	2.239	2.239
0.10	2.579	2.588	2.548	2.473	2.393	2.358	2.343	2.463	2.588
0.20	2.660	2.683	2.644	2.584	2.477	2.436	2.413	2.547	2.683
0.25	2.697	2.721	2.685	2.629	2.512	2.472	2.442	2.584	2.721
0.30	2.732	2.757	2.727	2.672	2.547	2.508	2.472	2.620	2.757
0.40	2.800	2.827	2.810	2.759	2.623	2.582	2.533	2.692	2.827
0.50	2.868	2.894	2.891	2.856	2.712	2.675	2.597	2.768	2.894
0.60	2.937	2.966	2.974	2.965	2.820	2.785	2.676	2.854	2.974
0.70	3.009	3.042	3.060	3.091	2.956	2.939	2.783	2.960	3.091
0.80	3.090	3.129	3.163	3.335	3.186	3.218	2.976	3.129	3.335
0.85	3.138	3.179	3.234	3.613	3.432	3.503	3.138	3.298	3.613
0.90	3.187	3.246	3.340	4.286	4.106	4.149	3.187	3.687	4.286
0.92	3.224	3.278	3.441	4.802	4.653	4.615	3.224	3.994	4.802
0.93	3.243	3.304	3.513	5.161	5.028	4.954	3.243	4.208	5.161
0.94	3.262	3.330	3.621	5.628	5.452	5.355	3.262	4.472	5.628
0.95	3.288	3.363	3.769	6.197	5.913	5.852	3.288	4.798	6.197
0.96	3.322	3.416	3.998	6.833	6.507	6.441	3.322	5.210	6.833
0.97	3.362	3.509	4.366	7.739	7.210	7.221	3.362	5.770	7.739
0.98	3.454	3.741	5.158	9.197	8.207	8.237	3.454	6.628	9.197
0.99	3.817	4.611	7.207	11.847	10.108	10.252	3.817	8.390	11.847

Table 7. Cumulative Distributions of Zenith Atmospheric Noise Temperature at Ka-Band for Goldstone DSCC, K

CD	January	February	March	April	May	June
0.00	6.693	6.693	6.693	6.693	6.693	6.693
0.10	7.308	7.500	7.723	7.845	8.106	8.037
0.20	7.913	8.002	8.164	8.325	8.735	8.722
0.25	8.135	8.219	8.385	8.565	8.952	8.971
0.30	8.358	8.436	8.606	8.779	9.169	9.221
0.40	8.801	8.859	8.984	9.163	9.601	9.721
0.50	9.242	9.272	9.350	9.546	10.077	10.323
0.60	9.681	9.684	9.718	9.984	10.569	10.974
0.70	10.297	10.351	10.265	10.468	11.228	11.763
0.80	11.101	11.328	10.854	11.094	12.108	13.012
0.85	11.750	12.248	11.365	11.525	12.711	13.836
0.90	13.096	14.334	11.962	12.136	13.592	14.750
0.92	13.835	16.166	12.474	12.533	14.042	15.221
0.93	14.458	17.643	12.730	12.731	14.397	15.520
0.94	15.262	19.651	13.147	13.037	14.751	15.819
0.95	16.548	21.502	13.744	13.562	15.302	16.226
0.96	18.649	25.319	14.753	14.345	16.200	16.803
0.97	22.138	30.415	16.732	15.953	17.735	17.739
0.98	28.112	38.775	20.815	20.156	20.775	19.451
0.99	42.063	55.416	33.563	32.862	29.789	26.298

Table 7 (Cont'd). Cumulative Distributions of Zenith Atmospheric Noise Temperature at Ka-Band for Goldstone DSCC, K

CD	July	August	September	October	November	December	Minimum	Year Average	Maximum
0.00	6.693	6.693	6.693	6.693	6.693	6.693	6.693	6.693	6.693
0.10	8.837	8.560	8.533	8.101	7.688	7.170	7.170	7.953	8.837
0.20	10.007	9.500	9.170	8.803	8.199	7.816	7.816	8.618	10.007
0.25	10.526	9.926	9.452	9.078	8.454	8.039	8.039	8.897	10.526
0.30	11.004	10.325	9.734	9.351	8.708	8.262	8.262	9.169	11.004
0.40	11.921	11.244	10.336	9.878	9.195	8.708	8.708	9.708	11.921
0.50	13.269	12.464	11.001	10.357	9.682	9.159	9.159	10.322	13.269
0.60	14.797	13.737	11.843	10.872	10.267	9.609	9.609	10.990	14.797
0.70	16.243	15.122	12.911	11.611	10.907	10.314	10.265	11.804	16.243
0.80	17.692	16.683	14.755	12.708	11.794	11.393	10.854	12.891	17.692
0.85	18.559	17.644	16.113	13.475	12.578	12.291	11.365	13.688	18.559
0.90	19.662	18.909	17.619	14.524	13.702	13.649	11.962	14.836	19.662
0.92	20.257	19.555	18.305	15.106	14.465	14.525	12.474	15.541	20.257
0.93	20.787	19.906	18.642	15.533	14.926	15.117	12.730	16.028	20.787
0.94	21.350	20.308	18.978	15.961	15.589	16.161	13.037	16.655	21.350
0.95	22.096	20.913	19.417	16.591	16.328	17.879	13.562	17.492	22.096
0.96	22.996	21.636	19.954	17.341	17.277	20.617	14.345	18.796	25.319
0.97	24.419	22.609	20.802	18.480	19.470	24.965	15.953	20.913	30.415
0.98	27.543	24.261	22.578	20.970	24.846	32.618	19.451	25.012	38.775
0.99	36.643	28.273	28.925	29.979	39.527	52.090	26.298	36.199	55.416

Table 8. Cumulative Distributions of Zenith Atmospheric Noise Temperature at Ka-Band for Canberra DSCC, K

CD	January	February	March	April	May	June
0.00	7.173	7.173	7.173	7.173	7.173	7.173
0.10	11.932	13.702	12.103	10.806	10.396	9.720
0.20	13.379	15.336	13.382	11.911	11.104	10.290
0.25	13.982	16.057	13.874	12.326	11.398	10.559
0.30	14.559	16.792	14.377	12.666	11.677	10.812
0.40	15.737	18.113	15.383	13.329	12.210	11.408
0.50	16.946	19.422	16.616	14.093	12.748	12.116
0.60	18.347	20.852	17.995	15.125	13.339	13.105
0.70	20.233	22.675	19.571	16.273	14.200	14.386
0.80	22.953	25.872	21.783	17.734	15.807	16.130
0.85	24.876	28.734	23.384	18.818	17.227	17.525
0.90	27.860	32.908	26.109	20.880	20.040	20.608
0.92	30.141	36.204	27.619	22.419	22.231	23.232
0.93	31.676	39.029	28.526	23.518	23.714	25.054
0.94	33.554	43.699	29.867	25.184	25.461	27.771
0.95	36.251	50.110	32.005	27.665	27.765	32.256
0.96	40.158	59.425	35.457	31.358	30.918	38.704
0.97	48.413	72.023	40.908	35.950	35.556	46.862
0.98	64.059	89.600	50.625	44.197	43.945	58.075
0.99	89.543	123.144	71.405	61.596	61.418	76.624

Table 8 (Cont'd). Cumulative Distributions of Zenith Atmospheric Noise Temperature at Ka-Band for Canberra DSCC, K

CD	July	August	September	October	November	December	Minimum	Year Average	Maximum
0.00	7.173	7.173	7.173	7.173	7.173	7.173	7.173	7.173	7.173
0.10	9.555	9.472	9.906	10.060	11.313	11.195	9.472	10.830	13.702
0.20	10.145	10.017	10.657	10.909	12.326	12.471	10.017	11.807	15.336
0.25	10.397	10.244	10.967	11.253	12.810	13.004	10.244	12.217	16.057
0.30	10.629	10.478	11.277	11.596	13.281	13.518	10.478	12.615	16.792
0.40	11.081	10.952	11.858	12.231	14.262	14.574	10.952	13.401	18.113
0.50	11.645	11.422	12.497	12.913	15.301	15.726	11.422	14.258	19.422
0.60	12.357	11.988	13.247	13.671	16.672	17.071	11.988	15.282	20.852
0.70	13.321	12.794	14.232	14.733	18.582	18.608	12.794	16.598	22.675
0.80	14.712	14.084	15.728	16.716	21.507	21.263	14.084	18.648	25.872
0.85	15.978	15.200	17.040	18.539	23.932	23.397	15.200	20.338	28.734
0.90	18.603	17.451	19.727	21.919	29.017	27.403	17.451	23.487	32.908
0.92	20.460	19.389	22.033	24.364	33.008	30.198	19.389	25.876	36.204
0.93	21.930	20.920	23.686	26.255	36.212	32.052	20.920	27.639	39.029
0.94	23.828	22.814	25.744	28.663	40.003	34.837	22.814	30.026	43.699
0.95	26.411	25.598	28.746	31.913	44.777	39.182	25.598	33.440	50.110
0.96	30.047	29.793	33.562	36.578	52.598	45.334	29.793	38.509	59.425
0.97	35.105	36.687	40.838	43.102	63.667	55.774	35.105	46.053	72.023
0.98	44.401	48.510	50.787	54.088	78.616	71.380	43.945	57.975	89.600
0.99	60.655	68.451	74.946	78.153	103.207	98.705	60.655	80.378	123.144

Table 9. Cumulative Distributions of Zenith Atmospheric Noise Temperature at Ka-Band for Madrid DSCC, K

CD	January	February	March	April	May	June
0.00	7.031	7.031	7.031	7.031	7.031	7.031
0.10	8.300	8.262	9.033	9.661	10.764	11.252
0.20	9.137	9.007	9.787	10.420	11.666	12.419
0.25	9.493	9.301	10.089	10.785	12.080	12.902
0.30	9.848	9.593	10.390	11.144	12.476	13.291
0.40	10.557	10.215	11.029	11.869	13.232	14.057
0.50	11.390	10.876	11.732	12.666	13.956	14.785
0.60	12.509	11.738	12.592	13.489	14.763	15.622
0.70	14.229	12.989	13.846	14.503	15.755	16.577
0.80	16.979	15.427	16.363	16.477	17.335	17.717
0.85	20.213	18.143	19.284	19.023	18.917	18.459
0.90	27.220	25.147	26.311	25.336	23.167	19.623
0.92	32.975	31.210	31.671	29.869	27.220	20.487
0.93	37.060	35.530	35.068	32.869	30.003	21.160
0.94	42.163	40.434	39.302	36.839	33.556	22.240
0.95	48.391	46.414	44.372	41.816	38.288	23.793
0.96	56.207	53.142	51.106	47.873	44.545	26.440
0.97	65.184	61.807	59.915	56.422	53.017	31.205
0.98	75.953	74.643	71.858	68.618	65.028	41.312
0.99	93.935	103.023	89.670	88.796	87.744	63.550

Table 9 (Cont'd). Cumulative Distributions of Zenith Atmospheric Noise Temperature at Ka-Band for Madrid DSCC, K

CD	July	August	September	October	November	December	Minimum	Year Average	Maximum
0.00	7.031	7.031	7.031	7.031	7.031	7.031	7.031	7.031	7.031
0.10	11.572	11.694	11.135	10.089	8.961	8.477	8.262	9.943	11.694
0.20	12.464	12.787	12.235	11.398	9.911	9.328	9.007	10.890	12.787
0.25	12.859	13.192	12.690	11.916	10.283	9.719	9.301	11.286	13.192
0.30	13.218	13.578	13.149	12.391	10.655	10.101	9.593	11.664	13.578
0.40	13.935	14.301	14.067	13.363	11.473	10.900	10.215	12.428	14.301
0.50	14.635	14.993	14.962	14.468	12.475	11.957	10.876	13.254	14.993
0.60	15.357	15.750	15.862	15.736	13.743	13.259	11.738	14.215	15.862
0.70	16.113	16.567	16.812	17.238	15.390	15.147	12.989	15.445	17.238
0.80	16.992	17.534	17.990	20.336	18.305	18.739	15.427	17.531	20.336
0.85	17.532	18.099	18.844	23.965	21.530	22.486	17.532	19.723	23.965
0.90	18.087	18.894	20.174	32.702	30.372	30.922	18.087	24.840	32.702
0.92	18.548	19.289	21.498	39.260	37.374	36.886	18.548	28.863	39.260
0.93	18.783	19.617	22.449	43.732	42.082	41.154	18.783	31.627	43.732
0.94	19.019	19.944	23.865	49.447	47.302	46.109	19.019	35.018	49.447
0.95	19.354	20.371	25.822	56.235	52.865	52.129	19.354	39.152	56.235
0.96	19.796	21.068	28.829	63.607	59.843	59.077	19.796	44.293	63.607
0.97	20.310	22.303	33.598	73.716	67.857	67.983	20.310	51.106	73.716
0.98	21.536	25.386	43.607	89.091	78.773	79.093	21.536	61.221	89.091
0.99	26.371	36.703	67.808	114.358	98.160	99.556	26.371	80.711	114.358

Table 10. Cumulative Distributions of Zenith Atmospheric Attenuation at L- and S-Bands for Goldstone DSCC, dB

CD	January	February	March	April	May	June
0.00	0.033	0.033	0.033	0.033	0.033	0.033
0.10	0.033	0.033	0.033	0.033	0.033	0.033
0.20	0.033	0.033	0.033	0.033	0.033	0.033
0.25	0.033	0.033	0.033	0.033	0.033	0.033
0.30	0.033	0.033	0.033	0.033	0.034	0.034
0.40	0.033	0.033	0.033	0.033	0.034	0.034
0.50	0.033	0.033	0.034	0.034	0.034	0.034
0.60	0.034	0.034	0.034	0.034	0.034	0.034
0.70	0.034	0.034	0.034	0.034	0.034	0.034
0.80	0.034	0.034	0.034	0.034	0.034	0.034
0.85	0.034	0.034	0.034	0.034	0.034	0.034
0.90	0.034	0.034	0.034	0.034	0.034	0.034
0.92	0.034	0.034	0.034	0.034	0.034	0.034
0.93	0.034	0.034	0.034	0.034	0.034	0.034
0.94	0.034	0.034	0.034	0.034	0.034	0.034
0.95	0.034	0.034	0.034	0.034	0.034	0.034
0.96	0.034	0.035	0.034	0.034	0.034	0.034
0.97	0.035	0.035	0.034	0.034	0.034	0.034
0.98	0.035	0.036	0.034	0.034	0.034	0.034
0.99	0.036	0.038	0.036	0.035	0.035	0.035

Table 10 (Cont'd). Cumulative Distributions of Zenith Atmospheric Attenuation at L- and S-Bands for Goldstone DSCC, dB

CD	July	August	September	October	November	December	Minimum	Year Average	Maximum
0.00	0.033	0.033	0.033	0.033	0.033	0.033	0.033	0.033	0.033
0.10	0.033	0.033	0.033	0.033	0.033	0.033	0.033	0.033	0.033
0.20	0.034	0.034	0.034	0.033	0.033	0.033	0.033	0.033	0.034
0.25	0.034	0.034	0.034	0.033	0.033	0.033	0.033	0.033	0.034
0.30	0.034	0.034	0.034	0.034	0.033	0.033	0.033	0.034	0.034
0.40	0.034	0.034	0.034	0.034	0.033	0.033	0.033	0.034	0.034
0.50	0.034	0.034	0.034	0.034	0.034	0.033	0.033	0.034	0.034
0.60	0.034	0.034	0.034	0.034	0.034	0.034	0.034	0.034	0.034
0.70	0.034	0.034	0.034	0.034	0.034	0.034	0.034	0.034	0.034
0.80	0.034	0.034	0.034	0.034	0.034	0.034	0.034	0.034	0.034
0.85	0.034	0.034	0.034	0.034	0.034	0.034	0.034	0.034	0.034
0.90	0.034	0.034	0.034	0.034	0.034	0.034	0.034	0.034	0.034
0.92	0.034	0.034	0.034	0.034	0.034	0.034	0.034	0.034	0.034
0.93	0.034	0.034	0.034	0.034	0.034	0.034	0.034	0.034	0.034
0.94	0.034	0.034	0.034	0.034	0.034	0.034	0.034	0.034	0.034
0.95	0.035	0.034	0.034	0.034	0.034	0.034	0.034	0.034	0.035
0.96	0.035	0.035	0.034	0.034	0.034	0.034	0.034	0.034	0.035
0.97	0.035	0.035	0.034	0.034	0.034	0.035	0.034	0.034	0.035
0.98	0.035	0.035	0.035	0.034	0.035	0.035	0.034	0.035	0.036
0.99	0.036	0.035	0.035	0.035	0.036	0.037	0.035	0.036	0.038

Table 11. Cumulative Distributions of Zenith Atmospheric Attenuation at L- and S-Bands for Canberra DSCC, dB

CD	January	February	March	April	May	June
0.00	0.036	0.036	0.036	0.036	0.036	0.036
0.10	0.036	0.036	0.036	0.036	0.036	0.036
0.20	0.036	0.036	0.036	0.036	0.036	0.036
0.25	0.036	0.036	0.036	0.036	0.036	0.036
0.30	0.036	0.036	0.036	0.036	0.036	0.036
0.40	0.036	0.036	0.036	0.036	0.036	0.036
0.50	0.036	0.037	0.036	0.036	0.036	0.036
0.60	0.036	0.037	0.036	0.036	0.036	0.036
0.70	0.037	0.037	0.037	0.036	0.036	0.036
0.80	0.037	0.037	0.037	0.036	0.036	0.036
0.85	0.037	0.037	0.037	0.036	0.036	0.036
0.90	0.037	0.038	0.037	0.037	0.037	0.037
0.92	0.037	0.038	0.037	0.037	0.037	0.037
0.93	0.038	0.038	0.037	0.037	0.037	0.037
0.94	0.038	0.039	0.037	0.037	0.037	0.037
0.95	0.038	0.039	0.038	0.037	0.037	0.038
0.96	0.038	0.040	0.038	0.038	0.037	0.038
0.97	0.039	0.042	0.038	0.038	0.038	0.039
0.98	0.041	0.043	0.039	0.039	0.039	0.040
0.99	0.043	0.048	0.041	0.040	0.040	0.042

Table 11 (Cont'd). Cumulative Distributions of Zenith Atmospheric Attenuation at L- and S-Bands for Canberra DSCC, dB

CD	July	August	September	October	November	December	Minimum	Year Average	Maximum
0.00	0.036	0.036	0.036	0.036	0.036	0.036	0.036	0.036	0.036
0.10	0.036	0.036	0.036	0.036	0.036	0.036	0.036	0.036	0.036
0.20	0.036	0.036	0.036	0.036	0.036	0.036	0.036	0.036	0.036
0.25	0.036	0.036	0.036	0.036	0.036	0.036	0.036	0.036	0.036
0.30	0.036	0.036	0.036	0.036	0.036	0.036	0.036	0.036	0.036
0.40	0.036	0.036	0.036	0.036	0.036	0.036	0.036	0.036	0.036
0.50	0.036	0.036	0.036	0.036	0.036	0.036	0.036	0.036	0.037
0.60	0.036	0.036	0.036	0.036	0.036	0.036	0.036	0.036	0.037
0.70	0.036	0.036	0.036	0.036	0.036	0.036	0.036	0.036	0.037
0.80	0.036	0.036	0.036	0.036	0.037	0.037	0.036	0.036	0.037
0.85	0.036	0.036	0.036	0.036	0.037	0.037	0.036	0.037	0.037
0.90	0.036	0.036	0.037	0.037	0.037	0.037	0.036	0.037	0.038
0.92	0.037	0.036	0.037	0.037	0.038	0.037	0.036	0.037	0.038
0.93	0.037	0.037	0.037	0.037	0.038	0.038	0.037	0.037	0.038
0.94	0.037	0.037	0.037	0.037	0.038	0.038	0.037	0.037	0.039
0.95	0.037	0.037	0.037	0.038	0.039	0.038	0.037	0.038	0.039
0.96	0.037	0.037	0.038	0.038	0.040	0.039	0.037	0.038	0.040
0.97	0.038	0.038	0.038	0.039	0.041	0.040	0.038	0.039	0.042
0.98	0.039	0.039	0.039	0.040	0.042	0.041	0.039	0.040	0.043
0.99	0.040	0.041	0.042	0.042	0.045	0.045	0.040	0.042	0.048

Table 12. Cumulative Distributions of Zenith Atmospheric Attenuation at L- and S-Bands for Madrid DSCC, dB

CD	January	February	March	April	May	June
0.00	0.035	0.035	0.035	0.035	0.035	0.035
0.10	0.035	0.035	0.035	0.035	0.035	0.035
0.20	0.035	0.035	0.035	0.035	0.035	0.035
0.25	0.035	0.035	0.035	0.035	0.035	0.035
0.30	0.035	0.035	0.035	0.035	0.035	0.035
0.40	0.035	0.035	0.035	0.035	0.035	0.035
0.50	0.035	0.035	0.035	0.035	0.035	0.035
0.60	0.035	0.035	0.035	0.035	0.035	0.036
0.70	0.035	0.035	0.035	0.035	0.036	0.036
0.80	0.036	0.035	0.036	0.036	0.036	0.036
0.85	0.036	0.036	0.036	0.036	0.036	0.036
0.90	0.036	0.036	0.036	0.036	0.036	0.036
0.92	0.037	0.037	0.037	0.037	0.036	0.036
0.93	0.037	0.037	0.037	0.037	0.037	0.036
0.94	0.038	0.038	0.038	0.037	0.037	0.036
0.95	0.038	0.038	0.038	0.038	0.037	0.036
0.96	0.039	0.039	0.039	0.038	0.038	0.036
0.97	0.040	0.040	0.040	0.039	0.039	0.037
0.98	0.041	0.041	0.041	0.040	0.040	0.038
0.99	0.043	0.044	0.043	0.043	0.043	0.040

Table 12 (Cont'd). Cumulative Distributions of Zenith Atmospheric Attenuation at L- and S-Bands for Madrid DSCC, dB

CD	July	August	September	October	November	December	Minimum	Year Average	Maximum
0.00	0.035	0.035	0.035	0.035	0.035	0.035	0.035	0.035	0.035
0.10	0.035	0.035	0.035	0.035	0.035	0.035	0.035	0.035	0.035
0.20	0.035	0.035	0.035	0.035	0.035	0.035	0.035	0.035	0.035
0.25	0.035	0.035	0.035	0.035	0.035	0.035	0.035	0.035	0.035
0.30	0.035	0.035	0.035	0.035	0.035	0.035	0.035	0.035	0.035
0.40	0.035	0.035	0.035	0.035	0.035	0.035	0.035	0.035	0.035
0.50	0.035	0.035	0.035	0.035	0.035	0.035	0.035	0.035	0.035
0.60	0.035	0.036	0.036	0.036	0.035	0.035	0.035	0.035	0.036
0.70	0.036	0.036	0.036	0.036	0.035	0.035	0.035	0.035	0.036
0.80	0.036	0.036	0.036	0.036	0.036	0.036	0.035	0.036	0.036
0.85	0.036	0.036	0.036	0.036	0.036	0.036	0.036	0.036	0.036
0.90	0.036	0.036	0.036	0.037	0.037	0.037	0.036	0.036	0.037
0.92	0.036	0.036	0.036	0.038	0.037	0.037	0.036	0.037	0.038
0.93	0.036	0.036	0.036	0.038	0.038	0.038	0.036	0.037	0.038
0.94	0.036	0.036	0.036	0.039	0.038	0.038	0.036	0.037	0.039
0.95	0.036	0.036	0.036	0.039	0.039	0.039	0.036	0.038	0.039
0.96	0.036	0.036	0.037	0.040	0.040	0.039	0.036	0.038	0.040
0.97	0.036	0.036	0.037	0.041	0.040	0.040	0.036	0.039	0.041
0.98	0.036	0.036	0.038	0.043	0.042	0.042	0.036	0.040	0.043
0.99	0.036	0.037	0.040	0.046	0.044	0.044	0.036	0.042	0.046

Table 13. Cumulative Distributions of Zenith Atmospheric Attenuation at X-Band for Goldstone DSCC, dB

CD	January	February	March	April	May	June
0.00	0.037	0.037	0.037	0.037	0.037	0.037
0.10	0.037	0.037	0.038	0.038	0.038	0.038
0.20	0.038	0.038	0.038	0.038	0.039	0.039
0.25	0.038	0.038	0.038	0.039	0.039	0.039
0.30	0.038	0.038	0.039	0.039	0.039	0.039
0.40	0.039	0.039	0.039	0.039	0.040	0.040
0.50	0.039	0.039	0.039	0.040	0.040	0.040
0.60	0.040	0.040	0.040	0.040	0.041	0.041
0.70	0.040	0.040	0.040	0.040	0.041	0.042
0.80	0.041	0.041	0.041	0.041	0.042	0.043
0.85	0.042	0.042	0.041	0.041	0.043	0.044
0.90	0.043	0.045	0.042	0.042	0.044	0.045
0.92	0.044	0.047	0.042	0.042	0.044	0.046
0.93	0.045	0.048	0.043	0.043	0.045	0.046
0.94	0.046	0.051	0.043	0.043	0.045	0.046
0.95	0.047	0.053	0.044	0.044	0.046	0.047
0.96	0.049	0.057	0.045	0.044	0.047	0.047
0.97	0.053	0.063	0.047	0.046	0.048	0.048
0.98	0.060	0.074	0.052	0.051	0.052	0.050
0.99	0.078	0.095	0.067	0.066	0.062	0.058

Table 13 (Cont'd). Cumulative Distributions of Zenith Atmospheric Attenuation at X-Band for Goldstone DSCC, dB

CD	July	August	September	October	November	December	Minimum	Year Average	Maximum
0.00	0.037	0.037	0.037	0.037	0.037	0.037	0.037	0.037	0.037
0.10	0.039	0.039	0.039	0.038	0.038	0.037	0.037	0.038	0.039
0.20	0.040	0.040	0.039	0.039	0.038	0.038	0.038	0.039	0.040
0.25	0.041	0.040	0.040	0.039	0.038	0.038	0.038	0.039	0.041
0.30	0.041	0.041	0.040	0.040	0.039	0.038	0.038	0.039	0.041
0.40	0.042	0.042	0.041	0.040	0.039	0.039	0.039	0.040	0.042
0.50	0.044	0.043	0.041	0.040	0.040	0.039	0.039	0.040	0.044
0.60	0.046	0.044	0.042	0.041	0.040	0.039	0.039	0.041	0.046
0.70	0.047	0.046	0.043	0.042	0.041	0.040	0.040	0.042	0.047
0.80	0.049	0.047	0.045	0.043	0.042	0.041	0.041	0.043	0.049
0.85	0.050	0.048	0.047	0.044	0.043	0.042	0.041	0.044	0.050
0.90	0.051	0.050	0.048	0.045	0.044	0.044	0.042	0.045	0.051
0.92	0.051	0.051	0.049	0.045	0.045	0.045	0.042	0.046	0.051
0.93	0.052	0.051	0.049	0.046	0.045	0.045	0.043	0.046	0.052
0.94	0.053	0.051	0.050	0.046	0.046	0.047	0.043	0.047	0.053
0.95	0.053	0.052	0.050	0.047	0.047	0.049	0.044	0.048	0.053
0.96	0.054	0.053	0.051	0.048	0.048	0.052	0.044	0.050	0.057
0.97	0.056	0.054	0.052	0.049	0.050	0.057	0.046	0.052	0.063
0.98	0.060	0.056	0.054	0.052	0.057	0.066	0.050	0.057	0.074
0.99	0.071	0.061	0.061	0.063	0.074	0.091	0.058	0.070	0.095

Table 14. Cumulative Distributions of Zenith Atmospheric Attenuation at X-Band for Canberra DSCC, dB

CD	January	February	March	April	May	June
0.00	0.039	0.039	0.039	0.039	0.039	0.039
0.10	0.045	0.047	0.045	0.043	0.043	0.042
0.20	0.046	0.049	0.046	0.045	0.044	0.043
0.25	0.047	0.049	0.047	0.045	0.044	0.043
0.30	0.048	0.050	0.047	0.045	0.044	0.043
0.40	0.049	0.052	0.048	0.046	0.045	0.044
0.50	0.050	0.053	0.050	0.047	0.045	0.044
0.60	0.052	0.055	0.051	0.048	0.046	0.045
0.70	0.054	0.057	0.053	0.049	0.047	0.047
0.80	0.057	0.060	0.055	0.050	0.048	0.049
0.85	0.059	0.063	0.057	0.052	0.050	0.050
0.90	0.062	0.068	0.060	0.054	0.053	0.054
0.92	0.065	0.072	0.062	0.056	0.055	0.057
0.93	0.067	0.076	0.063	0.057	0.057	0.059
0.94	0.069	0.082	0.065	0.059	0.059	0.062
0.95	0.072	0.090	0.067	0.062	0.062	0.067
0.96	0.077	0.102	0.071	0.066	0.066	0.075
0.97	0.088	0.120	0.078	0.072	0.071	0.086
0.98	0.109	0.147	0.091	0.082	0.082	0.100
0.99	0.146	0.205	0.119	0.105	0.105	0.127

Table 14 (Cont'd). Cumulative Distributions of Zenith Atmospheric Attenuation at X-Band for Canberra DSCC, dB

CD	July	August	September	October	November	December	Minimum	Year Average	Maximum
0.00	0.039	0.039	0.039	0.039	0.039	0.039	0.039	0.039	0.039
0.10	0.042	0.042	0.042	0.042	0.044	0.044	0.042	0.043	0.047
0.20	0.042	0.042	0.043	0.043	0.045	0.045	0.042	0.044	0.049
0.25	0.043	0.042	0.043	0.044	0.046	0.046	0.042	0.045	0.049
0.30	0.043	0.043	0.044	0.044	0.046	0.046	0.043	0.045	0.050
0.40	0.043	0.043	0.044	0.045	0.047	0.047	0.043	0.046	0.052
0.50	0.044	0.044	0.045	0.045	0.048	0.049	0.044	0.047	0.053
0.60	0.045	0.044	0.046	0.046	0.050	0.050	0.044	0.048	0.055
0.70	0.045	0.045	0.047	0.047	0.052	0.052	0.045	0.049	0.057
0.80	0.047	0.046	0.048	0.049	0.055	0.055	0.046	0.052	0.060
0.85	0.048	0.047	0.050	0.051	0.058	0.057	0.047	0.053	0.063
0.90	0.051	0.050	0.053	0.055	0.064	0.062	0.050	0.057	0.068
0.92	0.053	0.052	0.055	0.058	0.068	0.065	0.052	0.060	0.072
0.93	0.055	0.054	0.057	0.060	0.072	0.067	0.054	0.062	0.076
0.94	0.057	0.056	0.060	0.063	0.077	0.071	0.056	0.065	0.082
0.95	0.060	0.059	0.063	0.067	0.083	0.076	0.059	0.069	0.090
0.96	0.065	0.064	0.069	0.073	0.093	0.084	0.064	0.075	0.102
0.97	0.071	0.073	0.078	0.081	0.108	0.097	0.071	0.085	0.120
0.98	0.082	0.088	0.091	0.095	0.130	0.119	0.082	0.100	0.147
0.99	0.104	0.115	0.124	0.129	0.169	0.161	0.104	0.132	0.205

Table 15. Cumulative Distributions of Zenith Atmospheric Attenuation at X-Band for Madrid DSCC, dB

CD	January	February	March	April	May	June
0.00	0.038	0.038	0.038	0.038	0.038	0.038
0.10	0.040	0.040	0.041	0.041	0.043	0.043
0.20	0.041	0.040	0.041	0.042	0.044	0.045
0.25	0.041	0.041	0.042	0.043	0.044	0.045
0.30	0.041	0.041	0.042	0.043	0.045	0.046
0.40	0.042	0.042	0.043	0.044	0.045	0.046
0.50	0.043	0.042	0.043	0.044	0.046	0.047
0.60	0.044	0.043	0.044	0.045	0.047	0.048
0.70	0.046	0.045	0.046	0.046	0.048	0.049
0.80	0.049	0.047	0.048	0.048	0.049	0.050
0.85	0.053	0.050	0.052	0.051	0.051	0.051
0.90	0.061	0.058	0.060	0.059	0.056	0.052
0.92	0.068	0.066	0.066	0.064	0.061	0.053
0.93	0.073	0.071	0.070	0.068	0.064	0.054
0.94	0.079	0.077	0.076	0.073	0.068	0.055
0.95	0.087	0.085	0.082	0.079	0.074	0.057
0.96	0.098	0.093	0.091	0.086	0.082	0.060
0.97	0.110	0.105	0.103	0.098	0.093	0.066
0.98	0.125	0.123	0.119	0.115	0.110	0.078
0.99	0.153	0.168	0.146	0.145	0.143	0.107

Table 15 (Cont'd). Cumulative Distributions of Zenith Atmospheric Attenuation at X-Band for Madrid DSCC, dB

CD	July	August	September	October	November	December	Minimum	Year Average	Maximum
0.00	0.038	0.038	0.038	0.038	0.038	0.038	0.038	0.038	0.038
0.10	0.044	0.044	0.043	0.042	0.041	0.040	0.040	0.042	0.044
0.20	0.045	0.045	0.044	0.043	0.042	0.041	0.040	0.043	0.045
0.25	0.045	0.045	0.045	0.044	0.042	0.041	0.041	0.043	0.045
0.30	0.045	0.046	0.045	0.044	0.042	0.042	0.041	0.044	0.046
0.40	0.046	0.047	0.046	0.045	0.043	0.043	0.042	0.044	0.047
0.50	0.047	0.047	0.047	0.047	0.044	0.044	0.042	0.045	0.047
0.60	0.048	0.048	0.048	0.048	0.046	0.045	0.043	0.046	0.048
0.70	0.048	0.049	0.049	0.050	0.047	0.047	0.045	0.047	0.050
0.80	0.049	0.050	0.050	0.053	0.051	0.051	0.047	0.050	0.053
0.85	0.050	0.050	0.051	0.057	0.054	0.055	0.050	0.052	0.057
0.90	0.050	0.051	0.053	0.068	0.065	0.065	0.050	0.058	0.068
0.92	0.051	0.052	0.054	0.076	0.073	0.073	0.051	0.063	0.076
0.93	0.051	0.052	0.055	0.081	0.079	0.078	0.051	0.066	0.081
0.94	0.051	0.052	0.057	0.089	0.086	0.084	0.051	0.070	0.089
0.95	0.052	0.053	0.059	0.098	0.093	0.092	0.052	0.075	0.098
0.96	0.052	0.054	0.063	0.108	0.102	0.101	0.052	0.082	0.108
0.97	0.053	0.055	0.068	0.122	0.114	0.114	0.053	0.091	0.122
0.98	0.054	0.059	0.081	0.145	0.129	0.130	0.054	0.104	0.145
0.99	0.060	0.072	0.113	0.188	0.160	0.162	0.060	0.132	0.188

Table 16. Cumulative Distributions of Zenith Atmospheric Attenuation at Ka-Band for Goldstone DSCC, dB

CD	January	February	March	April	May	June
0.00	0.116	0.116	0.116	0.116	0.116	0.116
0.10	0.125	0.128	0.132	0.134	0.139	0.138
0.20	0.134	0.136	0.139	0.141	0.148	0.148
0.25	0.137	0.139	0.142	0.145	0.151	0.152
0.30	0.141	0.142	0.145	0.148	0.154	0.155
0.40	0.147	0.148	0.150	0.153	0.160	0.162
0.50	0.153	0.153	0.155	0.158	0.167	0.171
0.60	0.159	0.159	0.159	0.164	0.173	0.180
0.70	0.167	0.168	0.167	0.170	0.183	0.192
0.80	0.179	0.183	0.175	0.179	0.196	0.211
0.85	0.189	0.197	0.182	0.185	0.205	0.223
0.90	0.210	0.230	0.191	0.194	0.218	0.237
0.92	0.222	0.260	0.199	0.200	0.225	0.245
0.93	0.232	0.284	0.203	0.203	0.231	0.249
0.94	0.245	0.318	0.210	0.208	0.236	0.254
0.95	0.266	0.349	0.220	0.217	0.245	0.260
0.96	0.300	0.413	0.236	0.229	0.260	0.270
0.97	0.359	0.501	0.268	0.255	0.285	0.285
0.98	0.460	0.649	0.336	0.325	0.335	0.313
0.99	0.708	0.959	0.555	0.543	0.489	0.429

Table 16 (Cont'd). Cumulative Distributions of Zenith Atmospheric Attenuation at Ka-Band for Goldstone DSCC, dB

CD	July	August	September	October	November	December	Minimum	Year Average	Maximum
0.00	0.116	0.116	0.116	0.116	0.116	0.116	0.116	0.116	0.116
0.10	0.152	0.147	0.146	0.139	0.132	0.123	0.123	0.136	0.152
0.20	0.170	0.162	0.156	0.150	0.139	0.133	0.133	0.146	0.170
0.25	0.179	0.168	0.160	0.154	0.143	0.136	0.136	0.150	0.179
0.30	0.186	0.174	0.164	0.158	0.147	0.139	0.139	0.154	0.186
0.40	0.200	0.188	0.173	0.165	0.153	0.145	0.145	0.162	0.200
0.50	0.221	0.207	0.182	0.171	0.160	0.151	0.151	0.171	0.221
0.60	0.245	0.227	0.195	0.178	0.168	0.157	0.157	0.180	0.245
0.70	0.267	0.248	0.211	0.189	0.177	0.168	0.167	0.192	0.267
0.80	0.289	0.272	0.239	0.205	0.190	0.184	0.175	0.209	0.289
0.85	0.302	0.287	0.261	0.217	0.202	0.198	0.182	0.221	0.302
0.90	0.319	0.306	0.285	0.233	0.220	0.219	0.191	0.239	0.319
0.92	0.329	0.317	0.296	0.243	0.232	0.233	0.199	0.250	0.329
0.93	0.337	0.322	0.301	0.249	0.239	0.243	0.203	0.258	0.337
0.94	0.346	0.329	0.307	0.256	0.250	0.260	0.208	0.268	0.346
0.95	0.359	0.339	0.314	0.267	0.262	0.288	0.217	0.281	0.359
0.96	0.374	0.351	0.322	0.279	0.278	0.333	0.229	0.303	0.413
0.97	0.397	0.367	0.336	0.297	0.314	0.407	0.255	0.338	0.501
0.98	0.451	0.394	0.366	0.339	0.404	0.539	0.313	0.407	0.649
0.99	0.610	0.463	0.474	0.492	0.662	0.895	0.429	0.602	0.959

Table 17. Cumulative Distributions of Zenith Atmospheric Attenuation at Ka-Band for Canberra DSCC, dB

CD	January	February	March	April	May	June
0.00	0.124	0.124	0.124	0.124	0.124	0.124
0.10	0.206	0.237	0.209	0.186	0.179	0.167
0.20	0.229	0.264	0.229	0.204	0.190	0.175
0.25	0.239	0.275	0.237	0.210	0.194	0.179
0.30	0.248	0.287	0.245	0.215	0.198	0.183
0.40	0.266	0.307	0.260	0.224	0.205	0.191
0.50	0.284	0.327	0.279	0.235	0.212	0.201
0.60	0.306	0.349	0.300	0.250	0.220	0.216
0.70	0.335	0.377	0.324	0.267	0.232	0.236
0.80	0.379	0.429	0.358	0.290	0.257	0.263
0.85	0.410	0.477	0.384	0.306	0.280	0.285
0.90	0.459	0.548	0.429	0.340	0.326	0.335
0.92	0.498	0.606	0.454	0.365	0.362	0.379
0.93	0.525	0.656	0.470	0.384	0.387	0.410
0.94	0.558	0.741	0.493	0.412	0.416	0.456
0.95	0.605	0.861	0.530	0.454	0.456	0.534
0.96	0.675	1.040	0.590	0.518	0.510	0.649
0.97	0.827	1.295	0.688	0.599	0.591	0.798
0.98	1.131	1.679	0.868	0.748	0.743	1.012
0.99	1.675	2.520	1.280	1.080	1.077	1.390

Table 17 (Cont'd). Cumulative Distributions of Zenith Atmospheric Attenuation at Ka-Band for Canberra DSCC, dB

CD	July	August	September	October	November	December	Minimum	Year Average	Maximum
0.00	0.124	0.124	0.124	0.124	0.124	0.124	0.124	0.124	0.124
0.10	0.164	0.163	0.170	0.173	0.195	0.193	0.163	0.187	0.237
0.20	0.173	0.171	0.182	0.186	0.211	0.213	0.171	0.202	0.264
0.25	0.176	0.174	0.186	0.191	0.218	0.222	0.174	0.208	0.275
0.30	0.180	0.177	0.191	0.196	0.225	0.230	0.177	0.214	0.287
0.40	0.186	0.183	0.199	0.205	0.240	0.246	0.183	0.225	0.307
0.50	0.193	0.190	0.208	0.215	0.256	0.263	0.190	0.238	0.327
0.60	0.203	0.197	0.218	0.226	0.277	0.284	0.197	0.253	0.349
0.70	0.218	0.209	0.233	0.241	0.307	0.307	0.209	0.273	0.377
0.80	0.239	0.228	0.256	0.272	0.354	0.349	0.228	0.305	0.429
0.85	0.259	0.246	0.277	0.302	0.394	0.384	0.246	0.332	0.477
0.90	0.301	0.282	0.320	0.357	0.480	0.452	0.282	0.384	0.548
0.92	0.332	0.314	0.359	0.398	0.549	0.499	0.314	0.424	0.606
0.93	0.357	0.339	0.386	0.430	0.606	0.532	0.339	0.454	0.656
0.94	0.388	0.371	0.421	0.472	0.673	0.580	0.371	0.495	0.741
0.95	0.432	0.418	0.473	0.528	0.760	0.658	0.418	0.555	0.861
0.96	0.495	0.490	0.557	0.610	0.907	0.770	0.490	0.645	1.040
0.97	0.583	0.612	0.687	0.728	1.124	0.968	0.583	0.783	1.295
0.98	0.751	0.828	0.871	0.934	1.434	1.281	0.743	1.010	1.679
0.99	1.061	1.219	1.354	1.423	1.999	1.890	1.061	1.471	2.520

Table 18. Cumulative Distributions of Zenith Atmospheric Attenuation at Ka-Band for Madrid DSCC, dB

CD	January	February	March	April	May	June
0.00	0.121	0.121	0.121	0.121	0.121	0.121
0.10	0.142	0.142	0.155	0.166	0.185	0.194
0.20	0.155	0.153	0.167	0.178	0.199	0.213
0.25	0.161	0.157	0.171	0.183	0.206	0.220
0.30	0.166	0.162	0.175	0.188	0.211	0.226
0.40	0.177	0.171	0.185	0.199	0.222	0.237
0.50	0.189	0.180	0.195	0.211	0.233	0.247
0.60	0.206	0.193	0.207	0.223	0.244	0.259
0.70	0.233	0.212	0.226	0.238	0.259	0.273
0.80	0.277	0.251	0.266	0.268	0.283	0.289
0.85	0.330	0.295	0.314	0.310	0.308	0.300
0.90	0.448	0.413	0.433	0.416	0.379	0.319
0.92	0.548	0.517	0.525	0.494	0.448	0.332
0.93	0.621	0.593	0.585	0.546	0.496	0.344
0.94	0.713	0.681	0.661	0.616	0.558	0.361
0.95	0.828	0.791	0.753	0.706	0.642	0.387
0.96	0.977	0.918	0.879	0.818	0.755	0.432
0.97	1.154	1.086	1.049	0.980	0.914	0.515
0.98	1.377	1.349	1.291	1.223	1.150	0.695
0.99	1.777	1.995	1.678	1.658	1.635	1.119

Table 18 (Cont'd). Cumulative Distributions of Zenith Atmospheric Attenuation at Ka-Band for Madrid DSCC, dB

CD	July	August	September	October	November	December	Minimum	Year Average	Maximum
0.00	0.121	0.121	0.121	0.121	0.121	0.121	0.121	0.121	0.121
0.10	0.200	0.202	0.192	0.174	0.154	0.145	0.142	0.171	0.202
0.20	0.213	0.219	0.209	0.195	0.169	0.159	0.153	0.186	0.219
0.25	0.219	0.225	0.216	0.203	0.174	0.165	0.157	0.192	0.225
0.30	0.224	0.231	0.223	0.210	0.180	0.170	0.162	0.197	0.231
0.40	0.235	0.241	0.237	0.225	0.192	0.182	0.171	0.209	0.241
0.50	0.244	0.250	0.250	0.241	0.207	0.199	0.180	0.221	0.250
0.60	0.254	0.261	0.263	0.261	0.227	0.219	0.193	0.235	0.263
0.70	0.265	0.272	0.277	0.284	0.252	0.248	0.212	0.253	0.284
0.80	0.277	0.286	0.294	0.334	0.299	0.306	0.251	0.286	0.334
0.85	0.285	0.294	0.307	0.394	0.352	0.369	0.285	0.322	0.394
0.90	0.293	0.306	0.328	0.545	0.503	0.513	0.293	0.407	0.545
0.92	0.300	0.312	0.350	0.661	0.627	0.618	0.300	0.476	0.661
0.93	0.304	0.318	0.365	0.743	0.712	0.695	0.304	0.524	0.743
0.94	0.307	0.323	0.389	0.849	0.808	0.786	0.307	0.584	0.849
0.95	0.313	0.330	0.422	0.979	0.913	0.899	0.313	0.657	0.979
0.96	0.320	0.341	0.474	1.124	1.048	1.033	0.320	0.751	1.124
0.97	0.328	0.361	0.557	1.331	1.209	1.212	0.328	0.878	1.331
0.98	0.348	0.414	0.737	1.667	1.438	1.445	0.348	1.074	1.667
0.99	0.430	0.611	1.206	2.283	1.877	1.910	0.430	1.478	2.283

Table 19. Cumulative Distributions of Year-Average Zenith Atmospheric Attenuation and Noise Temperature at K-Band for Goldstone DSCC

CD	25.5 GHz		26.0 GHz		26.5 GHz		27.0 GHz	
	A_{zen}, dB	T_{zen}, K	A_{zen}, dB	T_{zen}, K	A_{zen}, dB	T_{zen}, K	A_{zen}, dB	T_{zen}, K
0.00	0.076	4.382	0.078	4.513	0.080	4.650	0.083	4.794
0.10	0.110	6.485	0.109	6.417	0.109	6.406	0.110	6.441
0.20	0.122	7.215	0.120	7.099	0.120	7.053	0.120	7.063
0.25	0.127	7.534	0.125	7.396	0.124	7.336	0.124	7.335
0.30	0.132	7.840	0.130	7.682	0.129	7.607	0.129	7.596
0.40	0.142	8.476	0.139	8.276	0.138	8.169	0.137	8.137
0.50	0.154	9.192	0.150	8.944	0.148	8.804	0.147	8.747
0.60	0.168	10.058	0.163	9.753	0.160	9.571	0.159	9.486
0.70	0.185	11.099	0.179	10.725	0.175	10.495	0.173	10.375
0.80	0.206	12.405	0.199	11.947	0.194	11.656	0.192	11.493
0.85	0.221	13.292	0.212	12.780	0.207	12.449	0.204	12.259
0.90	0.242	14.567	0.232	13.977	0.226	13.590	0.222	13.360
0.92	0.255	15.407	0.245	14.766	0.238	14.343	0.234	14.088
0.93	0.266	16.019	0.254	15.342	0.247	14.893	0.243	14.619
0.94	0.279	16.803	0.267	16.082	0.259	15.600	0.254	15.303
0.95	0.297	17.890	0.284	17.107	0.275	16.580	0.270	16.252
0.96	0.324	19.479	0.309	18.608	0.299	18.017	0.293	17.644
0.97	0.367	22.000	0.350	20.994	0.338	20.306	0.331	19.864
0.98	0.454	27.036	0.432	25.779	0.417	24.905	0.407	24.333
0.99	0.656	38.214	0.623	36.480	0.600	35.254	0.585	34.430

Table 20. Cumulative Distributions of Year-Average Zenith Atmospheric Attenuation and NoiseTemperature at K-Band for Canberra DSCC

CD	25.5 GHz		26.0 GHz		26.5 GHz		27.0 GHz	
	A_{zen}, dB	T_{zen}, K	A_{zen}, dB	T_{zen}, K	A_{zen}, dB	T_{zen}, K	A_{zen}, dB	T_{zen}, K
0.00	0.081	4.698	0.083	4.838	0.086	4.985	0.088	5.140
0.10	0.155	9.190	0.151	8.995	0.150	8.896	0.150	8.872
0.20	0.173	10.316	0.169	10.052	0.166	9.904	0.166	9.845
0.25	0.181	10.788	0.176	10.496	0.173	10.327	0.172	10.253
0.30	0.188	11.239	0.183	10.919	0.180	10.729	0.178	10.641
0.40	0.203	12.146	0.197	11.769	0.193	11.539	0.191	11.422
0.50	0.219	13.145	0.212	12.707	0.207	12.432	0.205	12.284
0.60	0.239	14.370	0.230	13.858	0.225	13.530	0.222	13.344
0.70	0.265	15.966	0.255	15.361	0.249	14.965	0.245	14.731
0.80	0.306	18.412	0.293	17.670	0.285	17.173	0.280	16.868
0.85	0.340	20.455	0.325	19.602	0.316	19.025	0.310	18.664
0.90	0.406	24.298	0.387	23.251	0.375	22.532	0.367	22.070
0.92	0.457	27.241	0.436	26.056	0.421	25.234	0.412	24.699
0.93	0.493	29.322	0.470	28.042	0.455	27.151	0.444	26.567
0.94	0.542	32.073	0.516	30.675	0.499	29.695	0.488	29.049
0.95	0.573	33.834	0.548	32.443	0.530	31.479	0.519	30.854
0.96	0.654	38.219	0.632	37.027	0.618	36.259	0.610	35.827
0.97	0.749	43.310	0.731	42.333	0.720	41.775	0.716	41.552
0.98	0.903	51.276	0.890	50.634	0.886	50.405	0.888	50.504
0.99	1.214	66.608	1.213	66.572	1.221	66.932	1.236	67.606

Table 21. Cumulative Distributions of Year-Average Zenith Atmospheric Attenuation and Noise Temperature at K-Band for Madrid DSCC

CD	25.5 GHz		26.0 GHz		26.5 GHz		27.0 GHz	
	A_{zen}, dB	T_{zen}, K	A_{zen}, dB	T_{zen}, K	A_{zen}, dB	T_{zen}, K	A_{zen}, dB	T_{zen}, K
0.00	0.079	4.605	0.082	4.742	0.084	4.886	0.087	5.037
0.10	0.132	7.815	0.130	7.690	0.129	7.641	0.130	7.650
0.20	0.149	8.865	0.146	8.674	0.145	8.578	0.144	8.554
0.25	0.156	9.294	0.153	9.076	0.151	8.959	0.150	8.922
0.30	0.163	9.706	0.159	9.462	0.157	9.327	0.156	9.276
0.40	0.177	10.563	0.172	10.265	0.169	10.089	0.168	10.011
0.50	0.191	11.472	0.186	11.117	0.182	10.901	0.181	10.793
0.60	0.208	12.530	0.202	12.108	0.197	11.844	0.195	11.703
0.70	0.230	13.871	0.222	13.368	0.217	13.044	0.214	12.861
0.80	0.268	16.138	0.257	15.501	0.250	15.081	0.246	14.830
0.85	0.307	18.490	0.294	17.722	0.286	17.207	0.280	16.889
0.90	0.404	24.150	0.385	23.090	0.373	22.361	0.365	21.892
0.92	0.484	28.753	0.461	27.477	0.445	26.589	0.435	26.007
0.93	0.507	30.114	0.485	28.863	0.470	28.001	0.460	27.447
0.94	0.585	34.408	0.561	33.085	0.545	32.187	0.535	31.626
0.95	0.639	37.366	0.616	36.140	0.602	35.341	0.594	34.881
0.96	0.704	40.842	0.683	39.757	0.671	39.097	0.666	38.775
0.97	0.785	45.123	0.768	44.228	0.759	43.754	0.757	43.615
0.98	0.906	51.374	0.893	50.733	0.889	50.508	0.892	50.613
0.99	1.136	62.772	1.132	62.589	1.137	62.809	1.149	63.349

Table 22. Monthly and Year-Average Rainfall Amounts at the DSN Antenna Locations

Month	Goldstone		Canberra		Madrid	
	inches	mm	inches	mm	inches	mm
January	1.02	25.9	3.61	91.7	1.48	37.5
February	1.18	30.0	2.74	69.7	1.38	35.0
March	0.90	22.9	2.90	73.6	1.10	28.0
April	0.20	5.1	2.85	72.4	1.87	47.5
May	0.19	4.8	2.94	74.8	1.56	39.5
June	0.04	1.0	2.70	68.7	1.26	32.0
July	0.35	8.9	3.36	85.3	0.57	14.5
August	0.59	15.0	3.90	99.0	0.59	15.0
September	0.39	9.9	3.73	94.7	1.16	29.5
October	0.15	3.8	3.70	94.0	1.54	39.0
November	0.23	5.8	3.50	88.8	2.01	51.0
December	0.57	14.5	2.42	61.4	1.75	44.5
Year Average	5.81	147.6	38.67	982.1	16.26	413.0

Table 23. Parameters for X-Band Planetary Noise Calculation, plus X-Band, K-band, and Ka-Band Noise Temperatures at Mean Minimum Distance from Earth

Planet	Diameter (km)		Mean Distance from Earth (10^6 km)		Mean Distance from Sun		Blackbody Disk Temp (K)	T_{planet} at Mean Minimum Distance (K)			
								X-Band		K-Band	Ka-Band
								70-m (74.4 dBi gain)	34-m (68.3 dBi gain)	34-m (77.2 dBi gain)	34-m (78.8 dBi gain)
	polar	equatorial	min.	max.	(10^6 km)	AU					
Mercury		4880	91.7	207.5	57.9	0.387	625	3.05	0.75	5.81	8.39
Venus		12104	41.4	257.8	108.2	0.723	634 (X-band) 497 (K-band) 472 (Ka-band)	93.29 – –	22.90 – –	– 139.35 –	– – 191.28
Earth		12757	–	–	149.6	1.000	250–300 [1]	–	–	–	–
Mars		6794	78.3	377.5	227.9	1.523	180	2.33	0.57	4.45	6.43
Jupiter	134102	142984	628.7	927.9	778.3	5.203	152	13.53	3.32	25.79	37.27
Saturn	108728	120536	1279.8	1579.0	1429.4	9.555	155	2.37	0.58	4.51	6.52
Uranus		51118	2721.4	3020.6	2871.0	19.191	160	0.10	0.02	0.19	0.27
Neptune		49532	4354.4	4653.6	4504.0	30.107	160	0.04	0.01	0.07	0.10
Pluto		2274	5763.9	6063.1	5913.5	39.529	160	0.00	0.00	0.00	0.00

Note:

1. Ocean (250 K) and Land (300 K)

DSN Telecommunications Link
Design Handbook

106, Rev. B
Solar Corona and Solar Wind Effects

Released September 30, 2010

Document Owner:

9/20/10

Christian M. Ho — Date
Sr. Engineer

Approved by:

9/20/10

Timothy T. Pham — Date
DSN Chief System Engineer

Released by:

Signature on file at DSN Library 9/30/2010
DSN Document Release — Date

Change Log

Rev	Issue Date	Affected Paragraphs	Change Summary
Initial	8/10/2005	All	Initial Release
A	10/21/2005	2.1.1, 2.1.3	Corrected units of Equation 4, Added attribution for Figures 2 and 4.
B	9/30/2010	All	Replaced DSMS with DSN. Eliminated the Rev. E designation for the document series.

Note to Readers

The 810-005 document series has been structured so that each document module can be independently revised without affecting others in the series. Hence, the Revision E previously designated at the 810-005 level has become unnecessary and eliminated. This module is one of the many in the 810-005 series; each may be published or changed, starting as an initial issue that has no revision letter. When a module is updated, a change letter is appended to the module number in the header and a summary of the changes is entered in the module's change log.

Contents

Illustrations

1 Introduction

1.1 Purpose

This module describes the effects of the solar corona and solar wind on Deep Space Network (DSN) telecommunications links. This will enable a telecommunications engineer to predict radio metric and radio science data performance of a signal at S, X and Ka bands when passing through the solar corona and solar wind.

1.2 Scope

This module discusses the effects of the solar corona and solar wind on DSN telecommunications links. The telecommunications performance in the absence of these effects and in the absence of weather effects is described in the telecommunications interfaces module for each antenna type (modules 101, 102, 103, and 104). Weather effects are discussed in module 105, Atmospheric and Environmental Effects. Module 105 also provides information on the effect of solar radiation on the operating system noise temperature of the antennas.

2 General Information

The solar corona and solar wind are the result of high density and strongly turbulent ionized gases (plasma) being ejected from the Sun. These ionized particles stream from the Sun at speeds on the order of 400 km/s and form the solar wind. The solar wind is not uniform and is accompanied by significant fluctuations in the solar magnetic field. Solar wind plasma density decreases with radial distance and becomes largely homogeneous when the distance from the Sun exceeds 4 solar radii. Within 4 solar radii, turbulence and irregularities are much greater and the plasma must be considered inhomogeneous. When radio frequency (RF) waves pass through these regions, the signals suffer severe degradation of their amplitude, frequency and phase.

Estimation of solar effects is complicated by the solar cycle that places an overlay of solar event frequency on top of the normal solar activity. Such events include coronal mass ejections, and an increase in the number of streamers. During the low periods of the solar cycle, events are less frequent and generally confined to the Sun’s equatorial region. During periods of high solar activity, events are much more frequent and may occur at any place on the Sun’s surface. Disentangling solar latitude dependence and solar activity dependence in each conjunction data set is difficult. In addition, many times the spacecraft ingress and egress scintillation profile curves are asymmetric and take on a different character depending on solar conditions. A chart predicting solar activity is shown in module 105.

Figure 1 illustrates the regions of the Sun and geometric relationships used in this module. The closest distance between the signal path and the Sun is *a*, the Solar Elongation

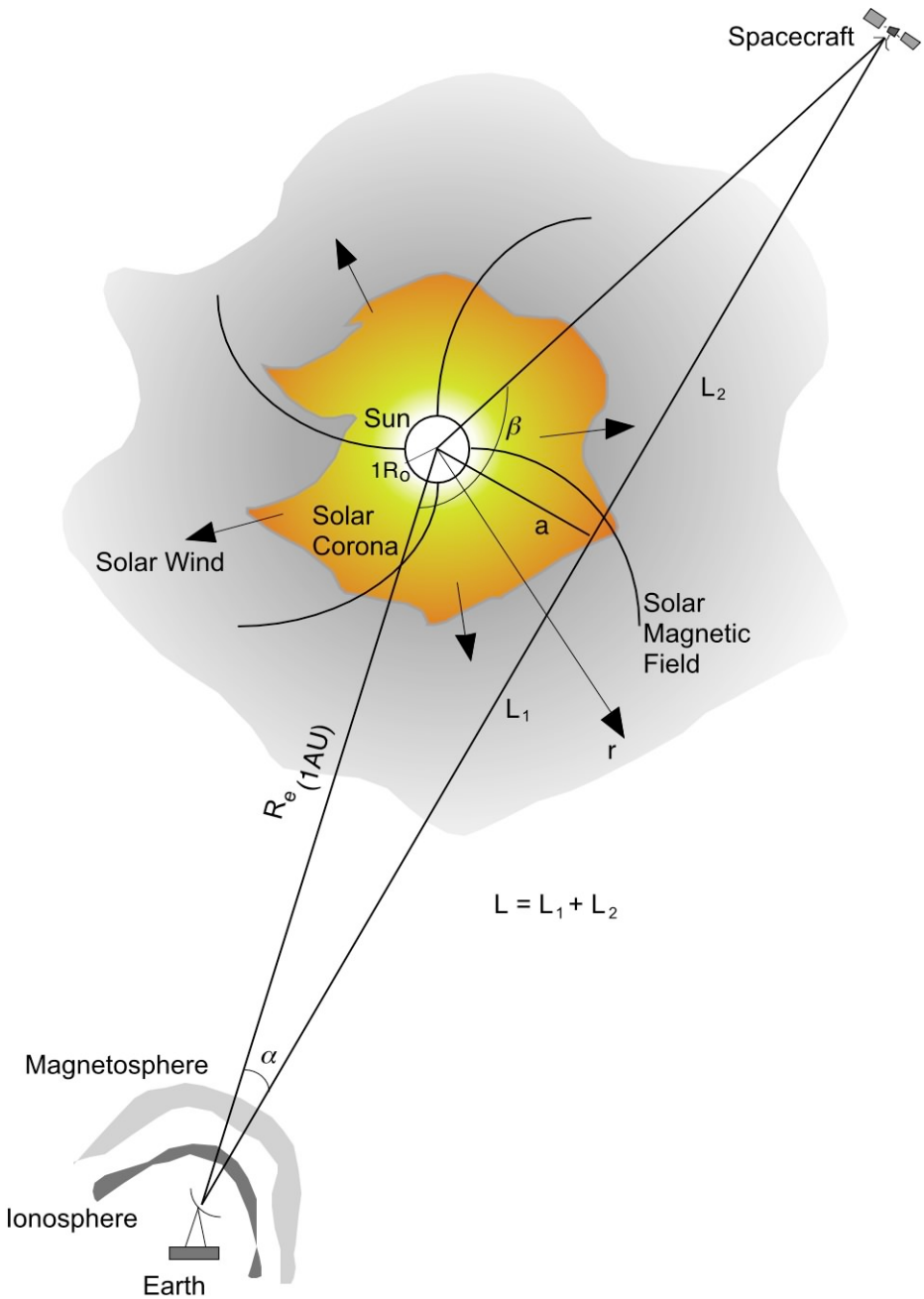

Figure 1. Geometric Relationships for Calculating Solar Effects

Angle or Sun-Earth-probe (SEP) angle is α (1 solar radius in $a = 0.25°$ in α), the spacecraft-Sun-Earth angle is β, and the signal path length between spacecraft and the Earth station is L. The figure also shows the Earth's ionosphere and magnetosphere that have a relatively low plasma density.

2.1 Effects in Homogeneous Region of the Solar Wind

As a plasma medium, the homogeneous region of the solar wind has the following basic effects on radio wave signals.

2.1.1 Group Delay

Group delay is the extra time delay due to the presence of an ionized medium in the propagation path. It is a function only of the slant total electron contents (*STEC*) along the path and the radio-wave frequency. It is defined as

$$\Delta T = \frac{1.3446 \times 10^{-19}}{f^2} \times \int_{L_{S/C}} N_e dl \tag{1}$$

where

ΔT	=	the group delay (μs)
f	=	the radio-wave frequency (GHz)
$\int_{L_{S/C}} N_e dl$		the *STEC* along the entire path, *L*, from earth station to spacecraft (see Figure 1).

N_e is solar wind electron density, a function only of radial distance. At low heliospheric latitude and equatorial regions, it can be modeled as [1]:

$$N_e(a) = 2.21 \times 10^{14} \left(\frac{a}{R_0}\right)^{-6} + 1.55 \times 10^{12} \left(\frac{a}{R_0}\right)^{-2.3} \tag{2}$$

where

R_o	=	solar radius (6.96×10^8 m)
a	=	radial distance, m.

This model is one of several postulated for $N_e(a)$, the primary difference between the models being the exponent of the second term. For example, the Muhleman-Anderson model [2] uses an exponent ranging from –2.04 to –2.08.

Finally, the integration along the ray path is a function of angles α and β that uniquely define the path, L (see Figure 1).

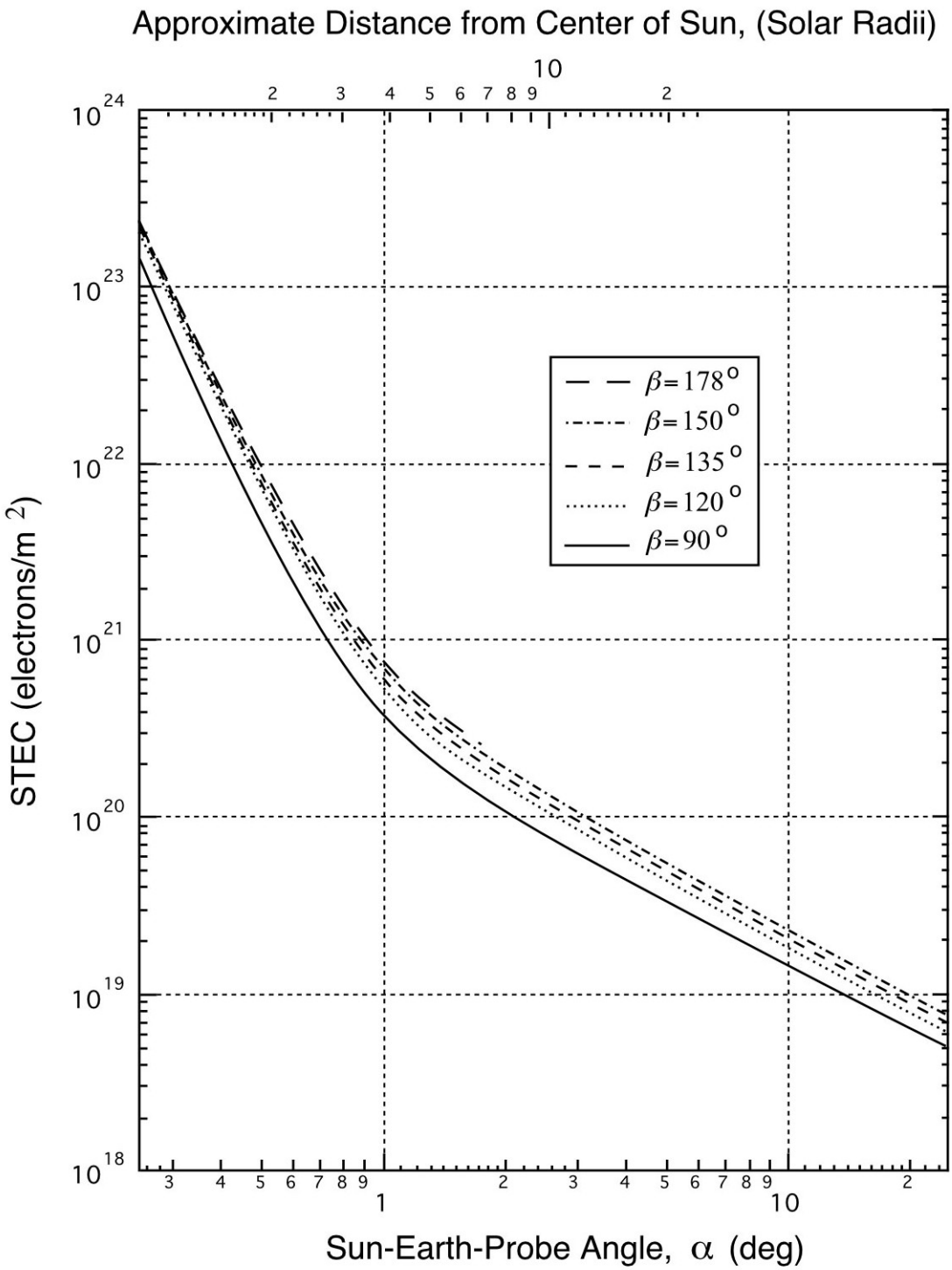

Figure 2. Slant Total Electron Content (STEC) as a Function of Sun-Earth-Probe and Earth-Sun-Probe Angles.

Figure 2 can be used to determine the approximate value of *STEC* as a function of Sun-Earth-Probe Angle, α, or distance from the center of the sun in solar radii, for values of β between 90° and 178°. For example, if a ray path passes near the Sun such that α and β are 1.5° and 150°, the *STEC* will be approximately 3×10^{20} electrons/m^2. Substituting this value in equation (1) provides a ΔT = 7.5 μs for an S band (2.3 GHz) signal and 0.6 μs for an X band (8.42 GHz) signal. Figure 3 illustrates this model as applied to an S-band Uplink and X-band downlink signal along with data from the Viking [2] and Ulysses [3] missions that used these frequencies for their telecommunications links.

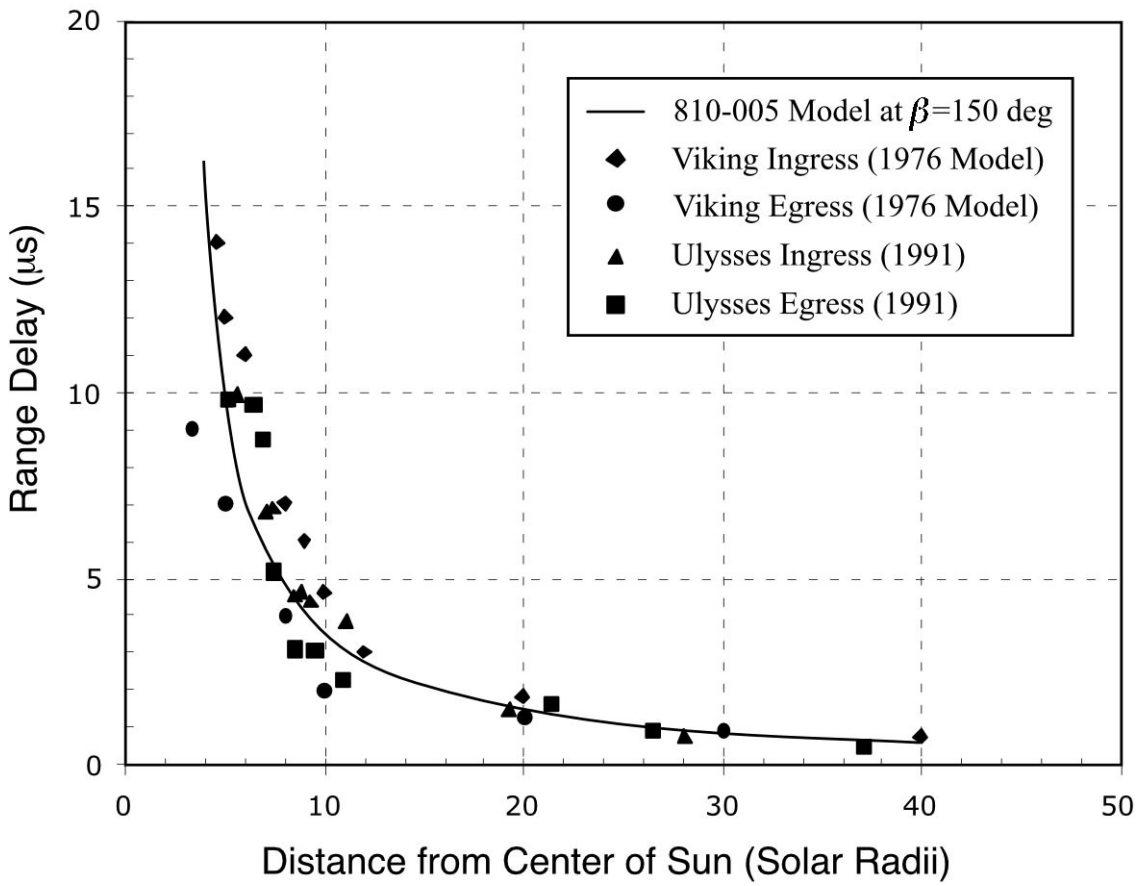

Figure 3. Comparison of Model with Representative Data from Several Solar Occultations.

2.1.2 Dispersion

Because group velocity is a function of the radio signal frequency, a dispersive phenomenon will occur when a broad band of frequency signals pass through the solar wind.

Differentiating the group delay ΔT in (1) and scaling to appropriate units yields the following relation

$$\frac{\Delta T}{\Delta f} = \frac{2.69 \times 10^{-19}}{f^3} \int_{L_{S/C}} N_e dl = \frac{2.69 \times 10^{-19}}{f^3} \times STEC . \tag{3}$$

where

$$\frac{\Delta T}{\Delta f} = \text{dispersion (ns/MHz)}$$

Using the *STEC* value derived above for an SEP angle of 1.5° and $\beta = 150°$, we find $\Delta T/\Delta f = 0.135$ ns/MHz for X band frequencies.

2.1.3 Faraday Rotation

An RF wave traversing the solar corona at an angle θ_B with respect to the Sun's magnetic field B (quasi-longitudinal) will rotate its polarization plane. The total rotation ϕ in radians is proportional to the product of the electron density and the magnetic field component along the path from the probe to the observer and is given to a very good approximation by

$$\phi = \frac{2.36 \times 10^{-17}}{f^2} \int_{L_{S/C}} N_e \vec{B} \cos\theta_B dl \text{ , rad} \tag{4}$$

where

f = signal frequency, MHz

B = magnetic field magnitude, nT

N_e = solar wind electron density, m^{-3}.

Thus, a large Faraday rotation could result from either a high electron density or a large net longitudinal field component. On the other hand, high electron densities and strong magnetic fields could produce no net Faraday rotation if the field orientations are such as to cancel out in the integral.

The observed Faraday rotation is due to the effects of both the solar corona and the plasma in the Earth's ionosphere however, the ionospheric contribution is usually negligible when the ray path passes within 10 solar radii of the sun. An example of S-band Faraday rotation as measured from two Earth stations during the second of two solar occultations by the Helios-1 spacecraft is shown in Figure 4 [4].

The change in polarization angle due to Faraday rotation can be measured at stations that are capable of receiving simultaneous RCP and LCP signals provided the spacecraft radiates significant energy in each circular polarization (or employs a linearly polarized signal). The 70-m stations presently have the capability for simultaneous RCP and LCP reception at S- and X-bands, and several of the BWG stations have this capability at X-band.

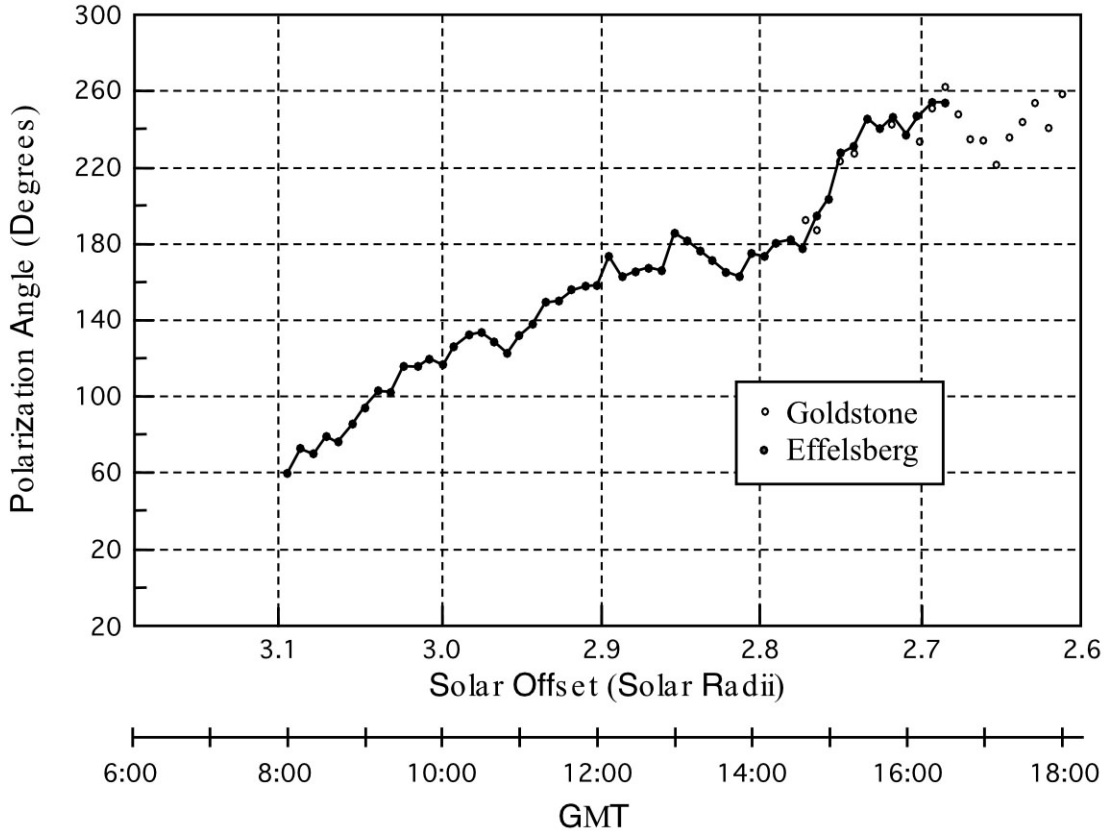

Figure 4. S-band Coronal Faraday Rotation (Helios-1 Spacecraft, Day 241, 1975).

The polarization angle is related to the phases of the received signals by

$$\alpha_{s,x} = \frac{\phi_{s,x}^{RCP} - \phi_{s,x}^{LCP}}{2} \tag{5}$$

where

$\phi_{s,x}$ = polarization angle at the received frequency

$\phi_{s,x}^{RCP}$ and $\phi_{s,x}^{LCP}$ are the phases of the S- or X-band RCP and LCP components.

The factor of one-half is necessary because Faraday rotation has equal but opposite effects on the phase of each circular polarization. That is, if it retards the phase of the RCP signal, it will advance the phase of the LCP signal and vice-versa.

2.1.4 Absorption

The absorption effect of solar wind plasma in the microwave bands, L_a, is very small and is given by

$$L_a = \frac{1.15 \times 10^{-21}}{f^2} \int_{L_{S/C}} N_e v dl \text{, dB} \tag{6}$$

where

N_e = solar wind electron density, m^{-3}

v = plasma collision frequency, Hz, (a function of temperature)

f = signal frequency, GHz

For a 2.3 GHz signal and a path length of 3×10^8 km, the total absorption will be only 0.01 dB and is negligible.

2.2 Solar Effects in Inhomogeneous Plasma

The solar corona and near-sun solar wind are an inhomogeneous plasma medium because of strong turbulence and irregularities–especially within 4 solar radii. In addition to the effects mentioned in Section 2.1, radio signals will experience intensity scintillations, spectral broadening, and phase scintillations. The first two of these are discussed below. Phase scintillation will be discussed in a later revision of this module.

2.2.1 Intensity Scintillation

RF signals passing through solar corona are scattered by turbulence within the Fresnel Zone of the signal. The Fresnel Zone size can be approximated by $\sqrt{\lambda L_1}$, where L_1 is the distance to the irregularity, usually assumed to be 1 AU. Irregularities within this region are classified as *small-scale* irregularities. Rapid amplitude changes around the average signal level will occur due to wave ray path changes and phase shifting as different portions of the wave front are affected to differing degrees. This is observed as instantaneous degradations to the received signal to noise ratio (SNR). The intensity scintillations can be described using a scintillation index, *m*, that is defined as the RMS of the signal intensity fluctuations divided by their mean intensity. As the intensity of the scintillations increase, their RMS value approaches the mean and the index becomes saturated at 1.

The scintillation index can be calculated from a measurement time series of signal strength, as the ratio of the RMS of the received power fluctuations relative to the mean power, over the observation interval. This parameter is only sensitive to characterizing the strength of small-scale charged particle density irregularities. In the regime of *weak scintillation*, ($0 < m < 0.5$), the RMS of the fluctuations is small relative to the mean intensity. In the regime of strong scintillation, the RMS of the fluctuations will be comparable to the mean intensity. As the SEP angle decreases, the scintillation index for a point source will increase until saturation occurs,

and then there will not be any further increase in m as the SEP angle decreases. Saturation is usually reached at an SEP angle ~1.2° for X-band and ~0.6° for Ka-band. However, the time scale of the fluctuations may become shorter as the SEP angle decreases further in the regime of saturation.

For spacecraft telemetry, frame errors have been observed to significantly increase when the scintillation index reaches values of 0.3 and above [5]. When the scintillation index is less than 0.3, few frame errors have been observed provided sufficient margin was available in both the carrier and data channels. This transition point where telemetry frame errors significantly increase occurs near 2.3° for X-band and is expected to occur near ~1° for Ka-band [5]. Flight projects and design engineers can use such information in the planning of solar conjunction operational scenarios.

2.2.1.1 Measurements

Figures 5 and 6 illustrate the values of the X-band and Ka-band scintillation indices that were measured from solar conjunction experiments of interplanetary spacecraft missions along with solid lines depicting the theoretical model curves described in Reference [6]. The missions included Mars Global Surveyor (MGS) in 1998 [7], Stardust in 2000 (X-band only), Cassini in 2000 [8], Deep Space 1 in 2000 [9], and Cassini in 2001 The Ka-band data for the 2001 Cassini conjunction are broken into two subsets with one representing the egress on day 158 and the second representing the data from all other tracks in 2001.

2.2.1.2 Data Reduction Technique

Most of the X-band data points from the MGS 1998 conjunction were from Block V Receiver (BVR) closed-loop data while most of the data points (X-band and Ka-band) from the other conjunctions were estimated using a software phase-locked-loop (PLL) program run on open-loop receiver sampled data recorded during the passes. The PLL algorithm used on the open-loop data samples acquired during strong scintillation or saturation results in lost fluctuation information due to the filtering effects of the PLL when the signal SNR gets too low during the deep fading. This results in depressed estimates of scintillation index. Therefore, the X-band scintillation data points with SEP < 1° were evaluated using an alternative approach. The histogram of the open-loop amplitude samples were fit to a Rician distribution function, solving for the Rician mean and sigma parameters, as well as a scale factor. These were then converted to scintillation index using appropriate formulation [10]. This approach appears to be very reasonable, as the resulting scintillation index values lie near unity, as expected in this region of small solar impact distance.

2.2.1.3 Discussion of the X-band Scintillation Measurements

The scintillation index is reduced when the signal traverses regions of less dense and less turbulent plasma, such as coronal holes. Most of the MGS 1998 X-band ingress points lie below the theoretical model in Figure 5 as the spacecraft signal was propagating through a coronal hole. The MGS 1998 egress measurements lie above and below the theoretical model, with the data points lying above the model appearing to be correlated with solar activity [7].

A significant increase in X-band scintillation index was observed during a Cassini solar conjunction pass in May 2000. This event occurred during a pass conducted at an SEP angle of 1.8° during egress, while in the X-band weak scintillation realm ($m < 1$). Hence, density-induced changes were detectable in which m increased from its background level of $m \sim 0.4$ up to $m \sim 0.8$. Two data points from this pass are plotted in Figure 5. This change in X-band scintillation index during a single pass is consistent with the overall scatter of all the measurements about the model for SEP < 2°, suggesting that such variability may contribute to the scatter seen in other measurements.

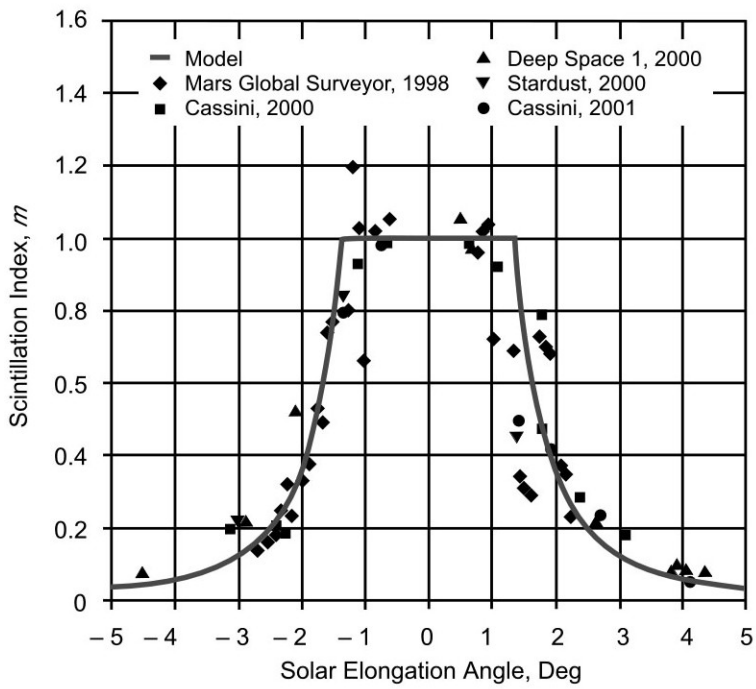

Figure 5. X-band Scintillation Index vs. Solar Elongation Angle.

The solar maximum scintillation observations of the Cassini 2000, Cassini 2001 and DS1 2000 solar conjunctions tend to be elevated with respect to the MGS 1998 data points, except during the solar events or streamer transits during egress.

2.2.1.4 Discussion of the Ka-band Scintillation Measurements

The Ka-band scintillation measurements provide a reasonably good match to the theoretical model as seen in Figure 6. In addition to there being less scintillation at Ka-band relative to X-band for the same SEP angle, there is also less variability in the Ka-band scintillation index measurements, although it is cautioned to keep in mind that the Ka-band data set lacks a sufficient number of measurements. The Ka-band curve appears to transition from weak scintillation to saturation near 0.6°.

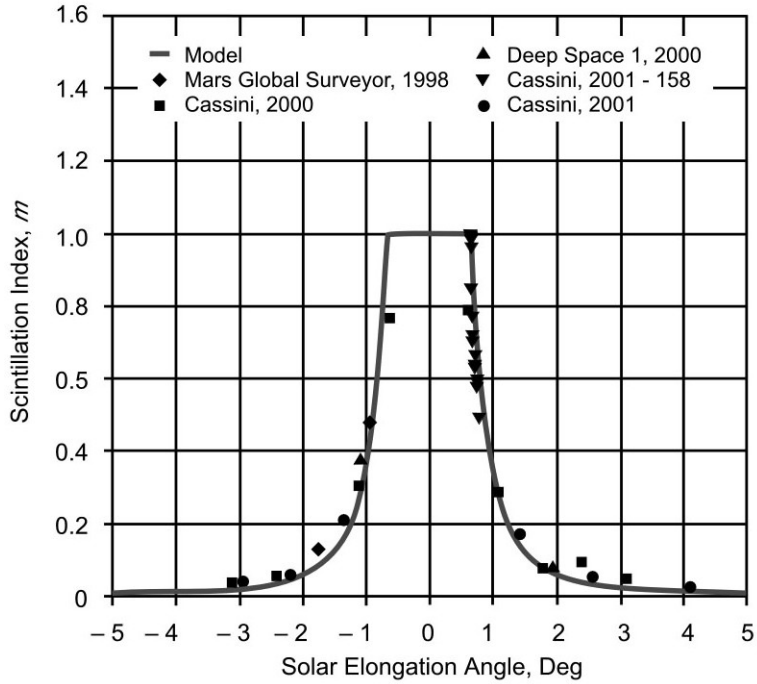

Figure 6. Ka-band Scintillation Index vs. Solar Elongation Angle.

A very few Ka-band data points were available from the MGS 1998 solar conjunction so the Ka-band data set is not as comprehensive as the X-band set. Changes in Ka-band scintillation index during the Cassini May 2000 solar conjunction were difficult to measure as the spacecraft was using thrusters to maintain pointing [8]. This caused signal amplitude excursions of as much as 20 dB with time scales on the order of 40 minutes. To minimize these effects for the Cassini May 2000 solar conjunction passes, the scintillation index for Ka-band was computed only during a short period of relatively constant signal strength – where dead-banding effects were minimal. The Cassini June 2001 solar conjunction used reaction wheel attitude control that provided excellent received signal strength stability.

2.2.1.5 Scintillation Model

A complex model based on theoretical considerations has been developed and is presented in Reference [6]. A simplified, exponential/polynomial approximation to this theoretical model is provided as equation (7) and is shown as the solid curve in Figures 5 and 6.

$$m = \begin{cases} \exp\left[-a_1(|\theta| - \theta_t)\right] + a_2 + a_3(|\theta| - \theta_t) + a_4(|\theta| - \theta_t)^2, & (|\theta| - \theta_t) \geq 0 \\ 1, \quad (|\theta| - \theta_t) < 0 \end{cases} \tag{7}$$

In this model, a_1, a_2, a_3, and a_4 are solve-for coefficients, θ is the actual SEP angle, and θ_t is near the SEP angle at which the scintillation index transitions to saturation ($m = 1$)

For X-band, the best-fit coefficients using the exponential model in (7) fit to the data with $\theta_t = 1.35°$ and $|\theta_t| < 5°$. were:

$a_1 = 2.0$

$a_2 = 0.14$

$a_3 = -0.03$

$a_4 = 0.0$

For Ka-band, the best-fit coefficients using the exponential model of (7) were:

$a_1 = 4.0$

$a_2 = 0.07$

$a_3 = -0.25$

$a_4 = 0.002$

where $\theta_t = 0.68°$ and $|\theta_t| < 5°$.

2.2.2 Spectral Broadening

Spectral broadening of the received carrier signal occurs due to Doppler shifting of the charged-particle refractive index (or density) irregularities as they are carried over the signal path by the solar wind. It is dependent on both electron density fluctuations and solar wind velocity, whereas the scintillation index only depends on the electron density fluctuations. Spectral broadening is observed when the signal path passes close enough to the Sun such that the broadening exceeds the line width of the spacecraft oscillator. Oscillator line widths are typically <0.02 Hz for ultra-stable oscillators (USOs) and <3 Hz for auxiliary oscillators. The broadened bandwidth, *B*, can be observed with the Radio Science Receiver (see module 209) and is defined as the bandwidth in which half of the carrier power resides.

Spectral broadening is not normally of concern in designing a telemetry link because it does not become significant until the SEP angle becomes so small that the telemetry performance has already become degraded due to intensity scintillation effects. However, it is of concern to a telecommunications engineer to determine an adequate value for the ground receiver carrier tracking loop bandwidth. If the broadening is excessive, the tracking loop bandwidth will need to be widened in order to capture all of the frequency fluctuations but not so wide that receiver lock might be lost due to excessive thermal noise.

For Ka-band, *B* is below 1 Hz for SEP angles greater then 0.7 degrees. Since Ka-band ground tracking loop bandwidths are usually set from 5 to 10 Hz, spectral broadening is not an issue considering that PSK telemetry is expected to degrade somewhere between 0.7 and 1.0 degrees SEP angle due to increased intensity scintillation destroying phase knowledge. Below 0.7 degrees, Ka-band *B* has been known to reach values of approximately 2 Hz at an SEP angle near 0.6 degrees.

For X-band, *B* usually lies below 2 Hz for SEP angles greater than 1 degree and below 1 Hz for SEP angles greater than 2 degrees. As is the case with Ka-band, telemetry will become degraded before an SEP of 2 degrees is reached and spectral broadening becomes an issue. Below 1 degree, X-band *B* has been known to reach 14 Hz at an SEP angle near 0.6 degrees.

2.3 Communications Strategies

Standard downlink BPSK link design and coding strategies can be used to achieve successful X-band data return at SEP angles down to at least 2.3 degrees and similar success should be achievable at Ka-band down to an SEP angle of 1 degree. Solar effects are significantly reduced at Ka-band. The Ka-band carrier experiences 15 percent less amplitude scintillation and 20 percent less spectral broadening than the X-band carrier at the same SEP angle. The presence of solar events, the sub-solar latitude, and the phase of the solar cycle should also be considered in any strategy.

The use of one-way referenced links instead of two-way or three-way coherent links will result in links free of additional phase effects from the uplink signal. Any phase disturbance received by the spacecraft will be turned around by the spacecraft transponder and appear on the downlink (multiplied by the transponder ratio). The downlink will also incur its own phase scintillation as well as amplitude scintillation. For example, a Ka-band downlink using the spacecraft's Ultra-Stable Oscillator (USO) as the signal source will have significantly fewer solar effects than if the Ka-band downlink signal was referenced to the normal X-band uplink signal.

In regions of strong scintillations where conventional telemetry is likely to fail, it may be possible to provide notification of critical spacecraft events by the use of frequency semaphores with reasonable duration for integration and appropriate spacing in frequency. Non-coherent frequency-shift keying (FSK), although not presently supported by the DSN, may provide improved data return provided adequate link margin is available.

Appendix A
References

1 Berman, A. L. and Wackley, J. A., "Doppler Noise Considered as a Function of the Signal Path Integration of Electron Density," Deep Space Network Progress Report 42-33, March–April 1976," Jet Propulsion Laboratory, Pasadena, California, June 15, 1976

2 Muhleman, D, and Andeson, J., "Solar Wind Electron Densities from Viking Dual-frequency Radio Measurements," Astrophysical Journal, 247, 1093–1101, August 1, 1981

3 Bird, M., Volland, H., Patzold, M., Edenhofer, P., Asmar, S., and Brenkle, J., "The Coronal Electron Density Distribution Determined from Dual-frequency Ranging Measurement During the 1991 Solar Conjunction of the Ulysses Spacecraft," The Astrophysical Journal, 426, 373–381, May 1, 1994

4 Volland, H., Bird, M. K., Levy, G. S., Stelzreid, C. T., and Seidel B. L., "Helios-1 Faraday Rotation Experiment: Results and Interpretations of the Solar Occultations in 1975," Journal of Geophys. Research, 42, 659–672, 1977

5 Morabito, D. D., and Hastrup, R., "Communicating with Mars During Periods of Solar Conjunction" Proceedings of the 2002 IEEE Aerospace Conference, Big Sky, Montana, March 9-16, 2002.

6 Morabito, D.D. "Solar Corona Amplitude Scintillation Modeling and Comparison to Measurements at X-band and Ka-band. Interplanetary Network Directorate Progress Report 42-153, January–March 2003, pp. 1–14, May 15, 2003.

7 Morabito, D. D., Shambayati, S., Butman, S., Fort, D., and Finley, S., "The 1998 Mars Global Surveyor Solar Corona Experiment", The Telecommunications and Mission Operations Progress Report 42-142, April–May 2000, Jet Propulsion Laboratory, Pasadena, California, August 15, 2000.

8 Morabito, D. D., Shambayati, S., Finley, S., Fort, D, "The Cassini May 2000 Solar Conjunction," IEEE Transactions on Antennas and Propagation, Volume 51, No. 2, Februaty 2003, pp. 201–219.

9 Morabito, D. D., Shambayati, S., Finley, S., Fort, D, Taylor, J. and Moyd, K., "Ka-band and X-band Observations of the Solar Corona Acquired During Solar Conjunctions of Interplanetary Spacecraft", Proceedings of the 7th Ka-band Utilization Conference, September 26, 2001, Santa Margherita Ligure, Italy. IIC - Istituto Internazionale delle Communicazioni, Via Perinace - Villa Piaggio, 16125 Genova, Italy.

10 Feria, Y. Belongie, M. McPheeters, T. and Tan, H., "Solar Scintillation Effects on Telecommunication Links at Ka-band and X-band," The Telecommunications and Data Acquisition Progress Report 42-129, vol. January–March 1997. Jet Propulsion Laboratory, Pasadena, California, May 15, 1997.

Deep Space Network

107
X-Band Radio Source Catalog

Document Owner:		Approved by:	
Signature provided	03/18/2021	Signature provided	11/18/2021
Christopher S. Jacobs DSN Reference Frame Calibration Task Lead	Date	Timothy Pham DSN Communications Systems Chief Engineer	Date
Prepared by:		**Released by:**	
Signature provided	03/25/2021	Signature provided	04/02/2021
Peter Kroger Deep Space Tracking Systems Group	Date	Christine Chang DSN Document Release Authority	Date

DSN No. **810-005, 107, Rev. E**
Issue Date: April 02, 2021
JPL D-19379; CL#21-1500

Jet Propulsion Laboratory
California Institute of Technology

Users must ensure that they are using the current version in DSN Telecommunications Link Design Handbook website:
https://deepspace.jpl.nasa.gov/dsndocs/810-005/

Review Acknowledgment

By signing below, the signatories acknowledge that they have reviewed this document and provided comments, if any, to the signatories on the Cover Page.

Signature provided	03/25/2021	Signature not provided	
Jeff Berner DSN Project Chief Engineer	Date	Alina Bedrossian DSN Science System Engineer	Date

Document Change Log

Rev	Issue Date	Prepared By	Paragraphs Affected	Change Summary
–	5/26/2006	Robert Sniffin	All	Initial Release
A	4/21/2011	Peter Kroger Christine Chang	Section 2 Section 2.1 Figure 1 Section 2.2 Sections 2.2.1-2.2.11 Table 1 Reference	• Updated radio source catalog entries, description, and references • Removed option for radio source file in tab-delimited format (catalog-delimited.txt).
B	04/08/2013	Andrew Romero-Wolf Peter Kroger	Section 2 Section 2.1 Figure 1 Section 2.2 Sections 2.2.1-2.2.11 Table 3	• Updated radio source map to include 21 new sources and updated observations. • Updated radio source catalogue table to include new sources and astrometric positions determined from 1.2 million new observations. • Added tables summarizing the agreement of the DDOR-2012 catalog in rotational alignment and position differences of the source catalog to International Celestial Reference Frame-2. • The analysis now includes weekly nutation estimates. Delay modelling was made more robust by cleaning up anomalies in the surface meteorology data.
C	12/15/2014	Ojars Sovers A. Romero-Wolf Peter Kroger Chris Jacobs		• Update catalog to include another 1.3 years of data and new sources for a total of 3746.
D	03/10/2015	Peter Kroger Chris Jacobs	Table 3	• Restore sign of RA-Dec correlation in Table 3
E	04/02/2021	Peter Kroger	Table 3	Correct source name indices

Contents

Paragraph **Page**

Figures

Figure **Page**

Tables

Table **Page**

1 Introduction

1.1 Purpose

This module provides an X-band catalog of the angular positions of astronomical radio sources that establish the celestial reference frame used for interplanetary spacecraft navigation using Delta-Differential-One-way Ranging (ΔDOR). The catalog may also be useful for other applications requiring the precise location of radio sources such as antenna pointing calibration.

1.2 Scope

The discussion in this module is limited to describing the contents of the source catalog and providing a listing of the catalog – both within the module and as a link to a computer−readable versions. The equipment used to collect the data from which the catalog is derived is discussed in module 211 of this handbook. The capabilities of the DSN for performing ΔDOR are contained in module 210.

2 General Information

The angular positions of a set of extragalactic radio sources serve as fiducial points for ΔDOR observations performed by the DSN. This set of point positions is commonly referred to as a *catalog*. The catalog described in this module comprises 3746 sources that have been observed in a frequency range--typically 8200-8600 MHz--that includes as a subset the X−band deep space allocation (International Telecommunications Union Category B) of 8,400 – 8,450 MHz. A distribution of the radio sources in the catalog is illustrated by Figure 1.

2.1 Catalog Development

The data used to develop the source catalog included delay and delay rate observables obtained from S−band and X−band Very Long Baseline Interferometry (VLBI) data acquired with the DSN VLBI subsystem. The catalog is essentially an X-band catalog with the S-band data being used only in order to calibrate plasma delays due to the Earth's ionosphere and the Solar plasma. We also included data acquired from other organizations observing at the same frequencies. The angular positions of the radio sources are estimated by a monolithic least−squares fit to these VLBI observables. A total of 7.45 million delay and delay rate observations, collected between October 28, 1978 and April 29, 2014, were used to estimate the final source positions. Details of the physical modeling required by this procedure are given in [1].

We estimated 947111 parameters including radio source positions, station locations, station clocks, wet troposphere delays, and troposphere gradients. A "no net rotation" constraint was placed on the radio source positions relative to International Celestial Reference Frame 2 (ICRF2) [2] using the subset of 295 "defining" sources. Kinematic station positions were estimated daily for each site relative to International Terrestrial Reference Frame 08 (ITRF08) a priori values and rates [3]. Station clocks were estimated using a linear model for the offset and rate parameters. Wet zenith

troposphere delays were estimated at intervals ranging from 20 minutes to one hour based on the Vienna Mapping Function 1 (VMF1) [4]. Troposphere gradients were estimated approximately once per day relative to a priori values with 100 mm uncertainties using the following formula from Steigenberger [5]:

$$G_{NS}(\text{mm}) = -0.5\sin(2\phi)$$

where G_{NS} is the troposphere gradient in the North−South direction and ϕ is the antenna geodetic latitude. The Kalman Earth Orientation Function (KEOF) COMB2010 Universal Time and Polar Motion (UTPM) solution [6] was used to fix Earth orientation and polar motion (EOP) values. Earth precession and nutation models are taken from MHB2000 [7]. Constant offsets for ecliptic longitude and obliquity nutation model parameters [1] were estimated at approximately weekly intervals to account for deficiencies in the MHB2000 a priori model.

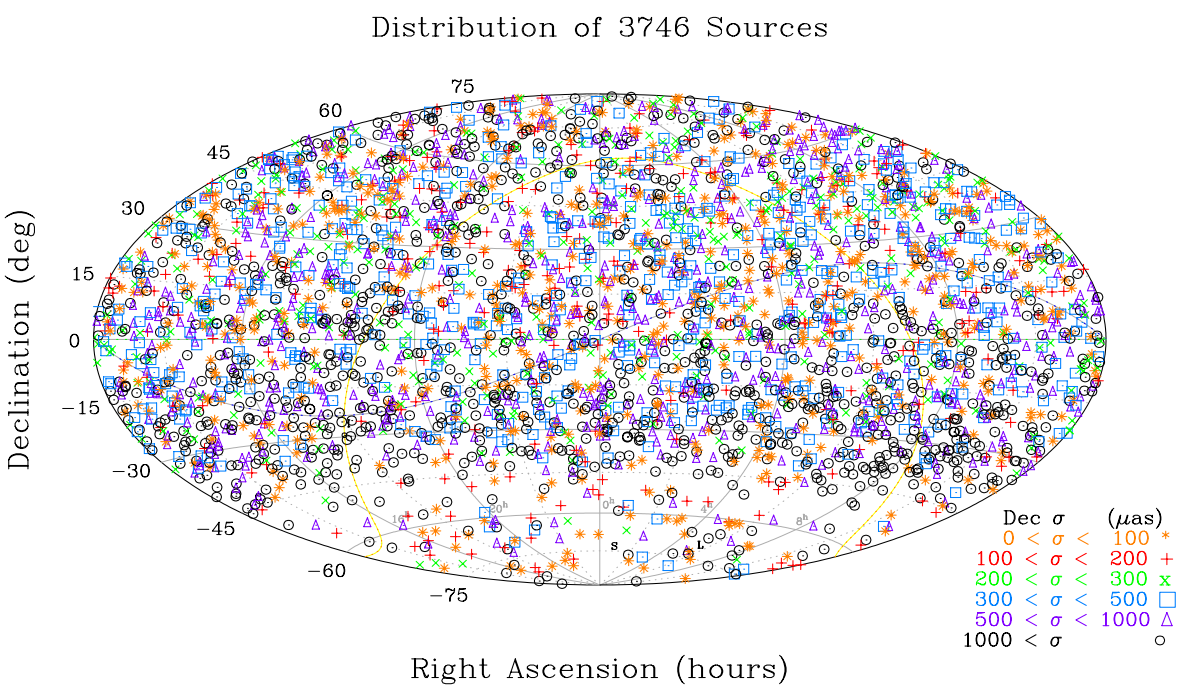

Figure 1. DDOR-2014-X Catalog

DDOR-2014-X catalog: distribution of 3746 radio sources in right ascension and declination. Color coding indicates 1-σ declination formal uncertainties according to the legend. Note that 1.0 nano-radian equals 206 µas. About 2200 of the sources are from surveys using 1-2 sessions per source. These sources typically have ~mas (5 nrad) precision.

We compare the rotational alignments and position differences to the ICRF2 catalog Limiting comparison to 295 ICRF2 defining sources yields rotational alignments with 4 μas uncertainty and Weighted Root Mean Square (WRMS) differences of 58 μas in the quantity right ascension (RA) cos(dec) and 95 μas in declination (DEC).

Table 1. Rotational Alignment Between X-band Catalogs: DDOR-2014-X vs. ICRF2

	295 ICRF2 Defining		3382 ICRF2 Overlapping	
Rotation Axis	Rotation Value (μas)	Rotation Error (μas)	Rotation Value (μas)	Rotation Error (μas)
X	-1.18	4.45	-0.35	3.62
Y	0.16	4.48	0.33	3.60
Z	1.49	3.92	0.65	2.99

Table 2. Position Scatter Between DDOR-2014-X and ICRF2 Catalogues

	295 ICRF2 Defining		3382 ICRF2 Overlapping	
Differenced Data	Weighted Mean (μas)	Weighted RMS (μas)	Weighted Mean (μas)	Weighted RMS (μas)
RA cos(Dec)	-0.34	58.17	-0.61	106.88
Dec	-46.79	95.18	-43.21	143.96

Broadening the comparison to include all 3382 common sources yields rotational alignment at the 3 μas level and WRMS differences of 107 μas in RA cos(dec) and 143 μas in declination (DEC). For purposes of solution traceability, we note that the source positions were extracted from a solution internally labelled all78-14VCSxbs_nut.srf file using the “catout” utility to produce the file “all78-14VCSxbs_nut.cat_iers.”

Figure 2 shows Declination differences between the DDOR-2104-X catalog and the 295 ICRF2 Defining sources. Note the largest shift is in the region from -5 to -30 degrees declination which covers much of the southern ecliptic. The source of this zonal shift is not completely understood, but is thought to be due in part to the 5 years of data added to DDOR-2014-X since ICRF2 was created. During this time, several southern stations were added to regular observing programs. So it is hoped that the new data is producing a more accurate catalog in the southern ecliptic. We note that reasonable alternate solutions show zonal shifts of similar shape but of about ½ the magnitude. Thus the magnitude of these zonal shifts has some uncertainty.

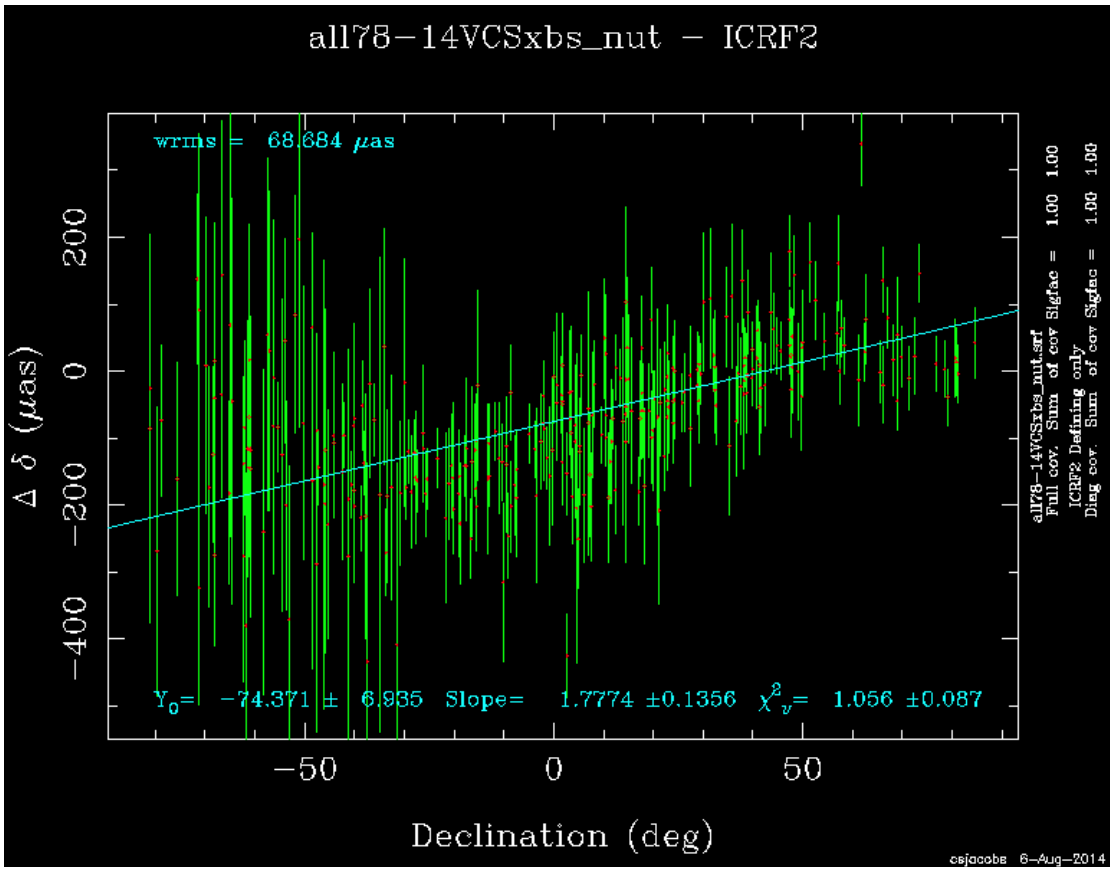

Figure 2. Declination Differences for DDOR-2014-X – ICRF2 Defining sources.

While scatter for sources with small separations is small, there is a zonal shift reaching a maximum of about -3/4 nrad (150 µas) in the declination band from about -5 to -30 deg.

2.2 Catalog Format

The catalog uses the J2000 reference frame and is rotationally aligned with ICRF2 [2,8] at the 4 µas level in all components. In addition to the presentation in Table 3 the catalog is available for download as a fixed-width file at:

http://deepspace.jpl.nasa.gov/dsndocs/810-005/107/catalog-fixed.txt

Lines of the fixed−width file are terminated with ASCII Character 10 (Unix convention). The fixed−width file may be read with the following FORTRAN format statement,

FORMAT (1X, A8, 1X, A12, 1X, I4, 1X, 2(1X,I2), 2X, F11.8, 1X, A1, I2, 1X, I2, 1X, F10.7, Fll.8, F10.7, F8.4, 2F8.1, I6, 2F6.2, F5.1).

2.2.1 B1950 Name (characters 2 through 9)

This is the source name based on its position at the Besselian epoch B1950.0 which is one of the two standard epochs that have been used in the last 30 years for reporting source positions (the other being the Julian epoch J2000.0). The name is related to the position of the source but is most useful for searching historical databases for information about the source. The name is constructed

as follows. The first two digits represent hours of right RA, the next two digits minutes of RA, the fifth place is used to specify the sign of the declination, places 6−7 give degrees of declination, and the last digit gives the first digit of the fractional part of degrees of declination. Thus the first name entry in the catalog, 2357-326, is interpreted as a right ascension of 23 hours and 57 (time) minutes and a declination of negative 32.6 degrees at the B1950.0 epoch. Note that because the catalog positions are given for epoch J2000 and many of the names (e.g. 2357-326) are based on a B1950 position, the catalog names do not start at zero right ascension whereas the actual positions do.

2.2.2 Common Name (characters 11 through 22)

This is the name most commonly used in the literature for the source and is also the name used by the DSN for Delta−DOR measurement scheduling. Often, there is a short prefix that indicates the organization or radio observatory that first documented the source in a survey. The remainder of the name may be related to the source position or an arbitrary sequence number. Some of the prefixes and naming conventions include [9]:

- 3C *nnn* – From the Third Cambridge Catalog. The *nnn* is the numerical designation assigned by the catalog. This survey, originally conducted at 159 MHz, identified many of the stronger sources used in VLBI. Unfortunately, many of these stronger sources are also less point-like making them less desirable for the highest accuracy astrometric measurements.
- 4C *zz.nn* – From the Fourth Cambridge Catalog. The *zz* corresponds to the declination "zone." The *nn* is a sequential number within the zone. There are no sequential numbers greater than 99.
- B2 *RRrrSDDa* – Most likely from the Second Bologna Survey. The *RRrr* is hours and minutes of right ascension, *S* is the sign of declination and *DD* is degrees of declination. The meaning of a (an alpha character) is unknown.
- CTA *nn* and CTD *nn* – From the California Institute of Technology "A" or "D" surveys where *nn* is the numerical designation assigned by the catalog.
- DW *RRrrSDDd* – From the Dwingelo Radio Observatory (Netherlands) catalog. The *RRrr* is hours and minutes of right ascension, *S* is the sign of declination, *DD* is degrees of declination, and *d* (if present) is the first digit of the fractional part of declination.
- GC *RRrrSDDd* – Most likely names taken from the "General Catalog of 33342 (optical) Stars." The *RRrrSDDd* are as described before.
- HR *nnnn* – Most likely names taken from the "Harvard Revised (optical) Catalog" where *nnn* is the numerical designation assigned by the catalog.
- M *nn* – Most likely names taken from the "Messier Catalog of Galaxies" where *nn* is the numerical designation assigned by the catalog.
- NRAO *nnn* – From the National Radio Observatory catalog where *nnn* is the numerical designation assigned by the catalog.
- O_ *nnn*– From the Ohio State Survey where the second letter indicates the hour of right ascension (two letters are skipped from the alphabet) and *nnn* is a numerical designation assigned by the catalog.

- P *RRrrSDDd* – From the Parkes Radio Observatory (southern Australia) survey. The *RRrrSDDd* are as described before.
- VRO *DD.RR.rr* – From the Vermillion River Observatory (University of Illinois) catalog. The *DD* is degrees declination and *RR* is hours right ascension. The *rr* is unknown but may be either minutes or fractional hours of right ascension.

2.2.3 ID Number (characters 24 through 27)

A unique number, presently in the range of 1 to 4044, is assigned to each radio source for use by programs that identify sources by number instead of name. The correspondence between source name and number will not change when the catalog is updated. This catalog can be used to establish a unique correspondence between the B1950 or Common Name and ID number. If a source in this catalog is deleted from future revisions of the catalog delivery, its number will be retired. When new sources are added, they will be assigned unique numbers starting with 4045.

2.2.4 Angular Positions (characters 29 through 65)

Angular positions are specified by a pair of angular coordinates: RA and DEC. Note that while right ascension used to be defined as the angular distance along the celestial equator from the intersection of the equator and the ecliptic, this is no longer true once one becomes concerned with accuracy levels < 100 milliarcseconds (500 nrad).

Since 1 January 1998, right ascension, and most importantly the origin of RA, have been defined by conventional agreement as to the value of the RA of extragalactic radio sources. In practice this means that the axes implicitly defined by a set of source positions must agree with the ICRF2 [2] to within the formal uncertainty of the ICRF2 axes or approximately 10 μas (1 standard deviation). Thus, the orientation of the celestial frame axes may vary in future realizations by roughly that amount.

2.2.4.1 Right Ascension (characters 29 through 47)

Right ascension is presented in the form " *hh mm SS.ssssssss*" where the first sub field gives hours of RA followed by (time) minutes of RA and (time) seconds of RA to eight decimal places.

2.2.4.2 Declination (characters 49 through 65)

Declination is presented in the form "*Sdd mm SS.sssssss*" where first sub−field, S or column 49, gives the sign of declination (a blank is allowed and should be interpreted as a positive declination). The remaining subfields give angular declination in degrees, minutes, and seconds to seven decimal places.

Note that a minus sign applies to the whole declination (*dd mm SS.sssssss*). For example, a declination of –00 00 00.*sssssss* should be read as minus 0.*sssssss* arcseconds of declination. This means that users desiring decimal representations of declination must first convert from degrees, minutes, seconds format to decimal format before applying the relevant sign. To simplify this conversion, the sign is in a fixed position in the fixed−width file.

2.2.5 Right Ascension Error (characters 66 through 76)

This field provides the formal one standard deviation right ascension uncertainty in units of seconds of time.

2.2.6 Declination Error (characters 77 through 86)

This field provides the formal one standard deviation declination uncertainty in units of arcseconds of angle.

2.2.7 Correlation of Right Ascension and Declination (characters 87 through 94)

This field provides the formal correlation of right ascension and declination. The quantity may range from –1.0 to +1.0 and a blank in front of the value should be interpreted as indicating a positive correlation. Values near zero indicate that the principal axes of the error ellipse are close to the RA−Dec axes. The large number of negative correlations is, in part, due to the large influence of the California to Australia baseline (typically between DSS−15 and DSS−45) on determination of declination.

2.2.8 Observation Epochs (characters 95 through 110)

Epochs are referred to Modified Julian Day (MJD) and are typically on the order of 50000 days.

2.2.8.1 Initial (characters 95 through 102)

The earliest epoch of the first observation.

2.2.8.2 Last (characters 103 through 110)

The termination epoch of the most recent observation.

2.2.9 Number of Sessions (characters 111 through 116)

The number of sessions, where a session is defined as a continuous data collection period, may be used as a rough indicator of the robustness of the position determination. Any position based on less than 3 sessions should be considered provisional.

2.2.10 Correlated Flux Density (characters 117 through 128)

This is an estimate of the average correlated flux density for observations of the radio source using DSN baselines Goldstone−Madrid and Goldstone−Canberra. Average correlated flux density values are reported for each baseline when available. This value, in Janskys (Jy), is computed from the measured signal−to−noise ratio (SNR) using the formula:

$$S(Jy) \approx \frac{SNR}{150}$$

The SNR is determined during the cross−correlation and fringe−fitting of actual radio source observations. If no recent observations of a radio source on DSN baselines are available, no value

is provided for correlated flux. Independent values for the correlated flux density are reported for the California−Madrid and the California−Canberra DSN baselines.

2.2.10.1 Correlated Flux Density Madrid Baseline (characters 117 through 122)

This is the correlated flux density for quasars observed on the Goldstone-Madrid (10-60) baseline. Flux densities on this baseline are available for 643 of the sources in Table 3.

2.2.10.2 Correlated Flux Density Canberra Baseline (characters 123 through 128)

This is the correlated flux density for quasars observed using the Goldstone-Canberra (10-40) baseline. Flux densities on this baseline are available for 608 of the sources in Table 3

2.2.11 Structure Index (characters 129 through 133)

The structure index is determined through the following relationship between the radio source structure index and the median value of the VLBI structure delay corrections [2]:

$$\mathrm{SI} = 1 + 2\log\left(\tau_{median}\right)$$

where SI is the structure index, and τ_{median} is the median value of the structure delay corrections (ps). A value for τ_{median} in the range of 0 to 40 ps is typical for a source that is point−like. A value in the range of 40 to 60 ps is typical for a source that has significant structure. The source structure itself may contribute an error of this magnitude to the delay error budget. Values of the delay scatter greater than 60 ps are typical for sources with large, extended, and possibly variable structure. Estimates of the structure index are available for 693 of the sources in Table 3.

Table 3. X-Band Radio Source Catalog: DDOR-2014-X

Source Name		ID No.	Right Ascension			Declination			RA Error (s)	Dec. Error (arcsec)	RA–Dec Corr.	Observation Epoch MJD		No. Obs.	Source Flux (Jy)		Str Index
B1950	Common		H	M	S	D	M	S				First	Last		10-60	10-40	
2357-326	2357-326	2274	00	00	20.39995646	-32	21	1.2341485	.00003605	.0010074	-0.1568	52305.9	52306.0	1			
2358+406	2358+406	2275	00	00	53.08158877	+40	54	1.7931619	.00015359	.0020370	-0.1702	50242.6	50242.7	1			
2358-161	2358-161	2276	00	01	5.32873051	-15	51	7.0756294	.00003475	.0009841	-0.7390	50631.3	50631.5	1			
2358+605	2358+605	2277	00	01	7.09962657	+60	51	22.8028338	.00030531	.0034085	-0.0996	52306.1	52306.1	1			
2358+189	2358+189	984	00	01	8.62156972	+19	14	33.8016881	.00000403	.0000745	-0.0439	50085.0	56664.1	97			
2359-221	2359-221	2278	00	02	11.98151630	-21	53	9.8647879	.00013558	.0033386	0.7251	54818.1	55483.3	2			
0000-199	0000-199	2279	00	03	15.94944558	-19	41	50.4043557	.00017952	.0071919	-0.8263	54088.0	54088.0	1			
0000-197	0000-197	2280	00	03	18.67501429	-19	27	22.3553356	.00003463	.0009540	-0.2104	50631.3	50687.5	2			
0000+212	0000+212	2281	00	03	19.35001932	+21	29	44.5078137	.00003320	.0009546	-0.4215	50085.0	50155.9	2			
0001+478	0001+478	2282	00	03	46.03098500	+48	07	4.2008098	.02167613	.1323638	-0.9936	50305.5	50305.5	1			
0001-120	0001-120	1309	00	04	4.91500315	-11	48	58.3857125	.00001196	.0004032	0.0268	50575.6	53133.7	3			
0001+459	0001+459	2283	00	04	16.12765771	+46	15	17.9701176	.00002779	.0005847	0.1118	50305.4	50305.5	1			
0002-478	0002-478	706	00	04	35.65549073	-47	36	19.6040785	.00001147	.0002013	0.4295	49330.5	56504.1	33			
0002+200	0002+200	985	00	04	35.75829598	+20	19	42.3173063	.00001456	.0002752	0.0946	52408.7	52983.4	3			
0002+541	0002+541	2284	00	05	4.36339833	+54	28	24.9248304	.00004002	.0003804	0.1936	49576.3	56393.6	2	0.22		
0002-170	0002-170	2285	00	05	17.93378034	-16	48	4.6787946	.00002823	.0009044	-0.5072	50631.3	50631.5	1			
0002+051	0002+051	2286	00	05	20.21554656	+05	24	10.8005007	.00013213	.0021387	-0.1058	49914.4	49914.5	1			
0003+380	GC 0003+38	1	00	05	57.17538923	+38	20	15.1490655	.00000525	.0000755	-0.1421	48719.9	56766.4	43	0.30	0.40	3.4
0003-302	0003-302	2287	00	06	1.12320481	-29	55	50.0966280	.00020176	.0056806	0.8648	52408.7	52409.6	1			
0003+340	0003+340	4121	00	06	7.38258280	+34	22	20.4058169	.00001848	.0004735	0.1091	55915.9	55916.2	1			
0003-066	0003-066	696	00	06	13.89288879	-06	23	35.3354137	.00000340	.0000537	-0.0569	48196.3	56776.1	1143	1.07	1.01	3.1
0003+123	0003+123	2288	00	06	23.05611993	+12	35	53.0973123	.00005770	.0010507	0.2592	54111.9	54112.1	1			
0004+240	0004+240	2289	00	06	48.78939742	+24	22	36.3929012	.00007456	.0013617	0.2432	50085.0	50155.9	2			
0005+568	0005+568	2290	00	07	48.46855993	+57	06	10.4391862	.00030458	.0032354	0.4617	49576.3	49576.5	1			
0005-239	0005-239	2291	00	08	0.36965705	-23	39	18.1508447	.00002570	.0007460	-0.7253	50631.3	54643.3	3			
0005+114	0005+114	2292	00	08	0.83833663	+11	44	0.7746711	.00005794	.0010698	-0.1352	52408.8	52409.7	1			
0005-262	0005-262	2293	00	08	26.25253369	-25	59	11.5391634	.00003832	.0012580	0.4295	50631.3	50687.5	2			
0005+683	0005+683	2294	00	08	33.47270295	+68	37	22.0480250	.00039129	.0014544	-0.2464	49826.7	54112.1	2			
0006-363	0006-363	2295	00	08	33.66108528	-36	01	25.0414158	.00012222	.0056954	0.4183	53552.5	55656.8	2			
0006+061	0006+061	2296	00	09	3.93184876	+06	28	21.2400688	.00000950	.0002627	0.0784	52408.7	56701.0	2	0.12	0.12	
0006+397	0006+397	2297	00	09	4.17357962	+40	01	46.7048409	.00003069	.0006426	-0.3266	50242.6	50242.7	1			
0007-325	0007-325	1310	00	09	35.55782459	-32	16	36.9309139	.00004656	.0011018	-0.7501	54965.6	54965.6	1			
0007+439	0007+439	2298	00	10	30.04645093	+44	12	42.5044093	.00002932	.0008687	0.2691	54087.1	54088.0	1			
0007+106	III ZW 2	986	00	10	31.00591022	+10	58	29.5041940	.00000382	.0000623	-0.0981	51427.3	56633.0	77			0.9
0007+171	GC 0007+17	6	00	10	33.99061349	+17	24	18.7612505	.00000534	.0000946	-0.1808	44203.1	55244.5	48	0.17	0.11	3.7
0008-311	0008-311	4046	00	10	34.90967756	-30	54	15.3008586	.00004795	.0017185	0.5297	55965.9	55965.9	1			
0008-307	0008-307	2299	00	10	35.74237629	-30	27	47.4164553	.00014542	.0043050	0.7871	52305.9	52306.0	1			
0008-300	0008-300	2300	00	10	45.17732291	-29	45	13.1769533	.00005091	.0027023	-0.3993	54087.1	55783.9	2			
0008-421	P 0008-42	707	00	10	52.51757282	-41	53	10.7751151	.00024803	.0084664	0.1635	49329.5	52408.7	4			
0008-222	0008-222	2301	00	10	53.64998229	-21	57	4.2198778	.00001116	.0003758	-0.2445	50631.3	50687.5	2			
0008-264	P 0008-264	7	00	11	1.24673888	-26	12	33.3771100	.00000503	.0000782	-0.1116	44227.2	56772.3	101	0.27	0.43	1.6
0008+704	0008+704	2302	00	11	31.90286621	+70	45	31.6257354	.00004723	.0003901	0.0561	49826.7	49826.8	1			
0009+081	0009+081	1253	00	11	35.26963568	+08	23	55.5859353	.00001015	.0003003	-0.5144	49914.4	53946.3	5	0.30	0.20	
0009-148	0009-148	2303	00	11	40.45587914	-14	34	4.6337440	.00005171	.0014628	0.2835	54111.9	54112.0	1			
0009+467	0009+467	1311	00	12	29.30290370	+47	04	34.7396084	.00004557	.0009570	-0.3786	53572.4	53572.5	1			
0009+655	0009+655	1312	00	12	37.67098190	+65	51	10.8235107	.00060065	.0039228	0.0430	53152.5	53152.6	1			
0010+336	0010+336	2304	00	12	47.38219160	+33	53	38.4715703	.00002447	.0005676	-0.3647	53502.7	53503.6	1			

Source Name		ID No.	Right Ascension			Declination			RA Error (s)	Dec. Error (arcsec)	RA–Dec Corr.	Observation Epoch MJD		No. Obs.	Source Flux (Jy)		Str Index
B1950	Common		H	M	S	D	M	S				First	Last		10-60	10-40	
0010-401	0010-401	2305	00	12	59.90983622	-39	54	26.0565928	.00002346	.0006945	0.0455	52305.9	52408.7	2		0.34	
0010+463	0010+463	2306	00	13	16.48890344	+46	36	8.6700639	.00011205	.0012306	-0.6158	50305.4	50305.5	1			
0010-155	0010-155	2307	00	13	20.70184953	-15	13	47.7851932	.00007605	.0026889	-0.3449	54088.0	54088.0	1			
0010+405	0010+405	708	00	13	31.13020510	+40	51	37.1441236	.00000449	.0000717	-0.0971	49098.7	56770.2	41	0.46	0.22	2.6
0011-046	0011-046	2308	00	13	54.13095961	-04	23	52.2942352	.00001347	.0004608	-0.3044	50575.6	50575.7	1			
0011+189	0011+189	2309	00	13	56.37611938	+19	10	41.9153347	.00002685	.0008436	0.0989	50085.0	50155.9	2			
0012+610	0012+610	2310	00	14	48.79217884	+61	17	43.5419936	.00010381	.0007699	0.4979	52409.5	52409.5	1			
0012-184	0012-184	2311	00	15	2.49205282	-18	12	50.8830094	.00001341	.0004489	0.2693	50631.5	50687.5	2			
0012+319	0012+319	1313	00	15	6.14739998	+32	16	13.3095745	.00001484	.0003715	-0.1111	53523.5	53523.7	1			
0013-184	0013-184	2312	00	15	34.32453186	-18	07	25.5836728	.00011751	.0034063	-0.6328	54111.9	54112.0	1		0.07	
0013-005	P 0013-00	666	00	16	11.08855702	-00	15	12.4454597	.00000426	.0000852	-0.3184	47381.3	56633.0	149	0.29	0.21	2.2
0014+813	0014+813	709	00	17	8.47492144	+81	35	8.1365453	.00000468	.0000506	-0.0193	48352.9	56749.7	1054	0.62		2.5
0015-054	0015-054	1314	00	17	35.81721775	-05	12	41.7684217	.00003078	.0009923	-0.3919	53561.5	53561.6	1			
0015+529	0015+529	2313	00	17	51.75984025	+53	12	19.1221047	.00005308	.0006253	-0.3065	49576.3	49576.5	1			
0015-280	0015-280	1315	00	17	59.00587101	-27	48	21.5819511	.00015839	.0047832	0.6664	53572.5	53572.5	1			
0017+200	0017+200	987	00	19	37.85450358	+20	21	45.6445467	.00000436	.0000627	0.0086	50085.0	56776.6	36	0.47	0.47	2.2
0017+257	0017+257	988	00	19	39.78060417	+26	02	52.2774883	.00001250	.0002820	0.1559	50219.6	56749.7	2	0.35	0.31	
0017-307	0017-307	2314	00	19	42.67533197	-30	31	19.3493403	.00002439	.0007349	-0.0500	52305.9	52306.0	1			
0016+731	0016+731	710	00	19	45.78636585	+73	27	30.0175849	.00000377	.0000506	-0.0558	47282.8	56782.2	559	1.02		2.1
0018+715	0018+715	2315	00	21	2.81375935	+71	50	20.7711697	.00021511	.0016542	-0.5398	49826.7	49826.8	1			
0018+729	0018+729	2316	00	21	27.37444360	+73	12	41.9305695	.00045481	.0014902	0.2603	49826.7	54112.1	2			
0019+451	J0022+4525	989	00	22	6.61134013	+45	25	33.8601149	.00001955	.0003840	0.0239	50305.4	50305.5	1			
0019-000	P 0019-00	2317	00	22	25.42589260	+00	14	56.1620523	.00010108	.0030940	-0.1344	50575.6	50575.7	1			
0019+058	P 0019+058	11	00	22	32.44121407	+06	08	4.2688950	.00000381	.0000646	-0.0438	45151.6	56772.0	238	0.45	0.41	1.4
0020+446	0020+446	2318	00	23	35.44248144	+44	56	35.7576954	.00003875	.0009348	0.4379	50305.4	50305.5	1			
0021-084	0021-084	1316	00	24	0.67271253	-08	11	10.0492032	.00006993	.0021739	-0.2797	53152.6	53523.7	2			
0021+464	0021+464	2319	00	24	21.53761443	+46	44	6.2280054	.00003744	.0011117	0.1749	50305.4	50305.5	1			
0021+243	0021+243	990	00	24	27.33054510	+24	39	26.2294581	.00001440	.0002833	-0.0762	52408.7	53307.0	11			
0022-423	0022-423	711	00	24	42.98985797	-42	02	3.9486439	.00010397	.0032768	-0.6902	50324.2	53131.7	4			
0022-044	0022-044	2320	00	24	45.98323157	-04	12	1.5488411	.00001842	.0005735	-0.3261	50575.8	50575.8	1			
0022-227	0022-227	2321	00	25	24.24741942	-22	27	47.5971822	.00001633	.0006767	0.1549	54087.1	54088.0	1			
0022+390	0022+390	2322	00	25	26.15767491	+39	19	35.4392518	.00001347	.0002880	-0.3994	50242.6	50242.7	1			
0023-263	0023-263	2323	00	25	49.15627665	-26	02	12.6164082	.00009023	.0025697	0.4363	52408.7	52409.6	1			
0024+348	OB 338	2324	00	26	41.72456862	+35	08	42.2761800	.00021939	.0045028	-0.6121	50219.6	50219.7	1			
0024-114	0024-114	1317	00	26	51.44301710	-11	12	52.4253777	.00006653	.0016896	0.2792	53552.5	53552.6	1			
0024+597	J0027+5958	991	00	27	3.28652880	+59	58	52.9602294	.00025975	.0016556	0.2090	49576.3	49576.5	1			
0024+092	0024+092	2325	00	27	5.79364909	+09	29	57.7633847	.00004828	.0008770	0.3344	52305.9	52306.1	1			
0024+224	0024+224	1318	00	27	15.37155862	+22	41	58.0687185	.00003606	.0005646	-0.0522	50085.0	54664.5	3			
0025+197	0025+197	992	00	28	29.81848453	+20	00	26.7441083	.00000486	.0000943	-0.0072	50085.0	56758.7	50			
0026-015	0026-015	1319	00	29	0.98602578	-01	13	41.7605093	.00004804	.0009233	0.3542	53125.6	53125.7	1			
0026+048	0026+048	2326	00	29	3.59228362	+05	09	34.8684108	.00015757	.0023459	-0.5056	49913.7	49914.6	1			
0026+346	OB 343	2327	00	29	14.24243458	+34	56	32.2472716	.00022529	.0031191	0.3464	50219.6	50219.7	1			
0027+056	0027+056A	1320	00	29	45.89630604	+05	54	40.7124442	.00001569	.0002579	-0.1084	49913.7	54643.7	2			
0027+703	0027+703	2328	00	30	14.41299067	+70	37	40.0606479	.00003841	.0003410	0.0148	49826.7	49826.8	1			
0027-426	0027-426	1321	00	30	17.49259240	-42	24	46.4821966	.00004210	.0014355	0.4363	54942.8	54943.7	1			
0027-024	0027-024	1322	00	30	31.82375327	-02	11	56.1335213	.00001482	.0004887	-0.2319	53125.6	53133.7	2			
0028-396	0028-396	2329	00	31	24.33155258	-39	22	49.3689939	.00017685	.0062847	-0.7751	52306.0	56162.4	3			
0029-147	0029-147	1323	00	31	56.41190522	-14	26	19.3464083	.00006725	.0018548	-0.6663	53125.7	53133.7	2			
0030+196	0030+196	2330	00	32	38.23770766	+19	53	54.9223025	.06249659	.8077359	-0.9976	50155.9	50155.9	1			
0032+276	0032+276	2331	00	34	43.48619949	+27	54	25.7208946	.00002057	.0005451	-0.2692	50219.6	50219.7	1			

Source Name		ID No.	Right Ascension			Declination			RA Error (s)	Dec. Error (arcsec)	RA–Dec Corr.	Observation Epoch MJD		No. Obs.	Source Flux (Jy)		Str Index
B1950	Common		H	M	S	D	M	S				First	Last		10-60	10-40	
0032+612	0032+612	1324	00	35	25.31061069	+61	30	30.7614847	.00005249	.0004253	0.1774	52620.0	53552.6	2			
0033+143	0033+143	2332	00	35	44.08793859	+14	38	1.9718774	.00002343	.0007517	0.0913	54112.0	54112.1	1			
0033-088	0033-088	2333	00	35	46.25037599	-08	35	54.0426629	.00001669	.0004978	-0.1728	53523.6	55657.7	2			
0033+142	0033+142	2334	00	36	35.10909654	+14	34	3.6200625	.00003117	.0007834	-0.2013	52408.8	52409.6	1			
0034-220	0034-220	2335	00	37	14.82589267	-21	45	24.7147000	.00003828	.0011312	-0.4520	54087.1	55784.6	2			
0034+108	J0037+1109	993	00	37	26.04141189	+11	09	50.9214553	.00002073	.0005989	-0.3162	49913.7	49914.6	1			
0034+078	0034+078	1325	00	37	32.19717447	+08	08	13.0575465	.00001878	.0005413	-0.2955	53561.5	53561.6	1			
0035+367	0035+367	2336	00	37	46.14325996	+36	59	10.8849547	.00027334	.0026175	0.7334	50242.6	50242.7	1			
0035+238	0035+238	2337	00	37	58.29981978	+24	07	11.8712484	.00017114	.0055871	-0.6073	54292.5	54292.6	1			
0035-252	0035-252	1326	00	38	14.73550322	-24	59	2.2353323	.00000432	.0000691	-0.0321	50631.5	56638.3	113			
0035+121	0035+121	2338	00	38	18.01631413	+12	27	31.2562434	.00057961	.0172445	-0.9820	50085.0	50156.0	2			
0035-024	0035-024	1327	00	38	20.52936563	-02	07	40.5469261	.00002111	.0005895	-0.3186	54124.8	54125.1	1			
0035-037	0035-037	1328	00	38	20.79433232	-03	29	58.9625776	.00001752	.0005931	-0.4008	53572.5	53572.5	1			
0035+413	0035+413	712	00	38	24.84358722	+41	37	6.0002779	.00000447	.0000660	-0.0031	49421.9	56692.3	38	0.21	0.26	2.8
0035+503	0035+503	2339	00	38	28.41354045	+50	35	25.8333230	.00009964	.0006398	-0.2283	50305.4	54112.1	2			
0036-216	0036-216	2340	00	38	29.95471856	-21	20	4.0235127	.00015643	.0033926	0.4232	50631.5	50687.5	2			
0036-099	0036-099	2341	00	39	6.29164933	-09	42	46.8875177	.00003551	.0016422	-0.1182	54088.0	54088.0	1			
0036-191	0036-191	2342	00	39	16.92441762	-18	54	5.6196185	.00033495	.0099328	0.7507	53560.6	53560.6	1			
0037+139	0037+139	994	00	39	39.61959225	+14	11	57.5569607	.00001545	.0004483	-0.2257	50085.0	53193.7	4			
0037+487	0037+487	2343	00	39	46.99884393	+49	00	33.1753616	.00002353	.0004608	0.2470	50305.4	50305.5	1			
0037-593	0037-593	2344	00	40	7.84828076	-59	03	52.7641973	.00068983	.0027513	-0.3350	52886.7	53138.2	3			
0037-329	0037-329	2345	00	40	17.54076240	-32	43	27.8253606	.00008889	.0022003	-0.2666	52305.9	52306.0	1			
0038-326	0038-326	2346	00	40	30.65489203	-32	25	20.3293074	.00012120	.0035915	-0.5894	52305.9	55776.5	2			
0038-020	0038-020	2347	00	40	57.61160304	-01	46	32.0265913	.00001343	.0004401	-0.4418	50575.8	56498.6	2	0.23	0.35	
0038+133	0038+133	2348	00	41	17.21095213	+13	39	27.5272543	.00011406	.0019115	-0.3078	54111.9	54112.1	1			
0039+230	0039+230	713	00	42	4.54517431	+23	20	1.0619112	.00000594	.0001312	-0.0839	50085.0	56638.6	25	0.29	0.16	4.2
0039+568	0039+568	1207	00	42	19.45169116	+57	08	36.5860843	.00001069	.0001766	0.4571	49576.4	56691.2	36	0.60		
0040+098	0040+098	2349	00	42	44.37174993	+10	09	49.2085276	.00004201	.0009977	0.4703	49913.7	49914.6	1			
0042+186	0042+186	1329	00	44	42.22789816	+18	55	5.0344788	.00004791	.0018406	0.4786	53125.6	53125.8	1			
0041+677	0041+677	1330	00	44	50.75958378	+68	03	2.6860017	.00005285	.0004432	-0.1263	53560.4	53560.6	1			
0043-392	0043-392	1331	00	45	30.50902847	-39	00	2.9317386	.00020640	.0103734	0.3666	52408.7	54853.0	2			
0043+246	0043+246	1208	00	46	7.82573422	+24	56	32.5245729	.00000944	.0002371	-0.0137	53125.6	53306.2	2			
0043-268	0043-268	1332	00	46	13.77618977	-26	31	54.4534036	.00002613	.0008578	-0.2936	54852.9	54853.0	1			
0044+387	0044+387	2350	00	46	47.57830020	+39	00	47.1483277	.00003315	.0006368	-0.2813	50242.6	50242.7	1			
0044+566	J0047+5657	995	00	47	0.42880225	+56	57	42.3952004	.00002808	.0004087	0.0717	49576.4	49576.5	1	0.30		
0045+243	0045+243	2351	00	47	43.87134752	+24	35	15.9952194	.00003911	.0011985	-0.7859	50085.0	50156.0	2			
0046+316	NGC 0262	996	00	48	47.14148274	+31	57	25.0847350	.00000518	.0000992	-0.1162	50219.6	55299.1	17	0.34	0.16	3.1
0046+063	0046+063	1333	00	48	58.72316004	+06	40	6.4752924	.00004300	.0013166	0.3871	53125.6	53133.7	2			
0046-315	0046-315	2352	00	49	22.90080472	-31	16	27.3225840	.00010966	.0031832	-0.5873	52305.9	55776.5	2			
0046+511	0046+511	2353	00	49	37.99120266	+51	28	13.6920256	.00001522	.0001910	-0.0613	49576.4	56547.5	6			
0047+023	J0049+0237	997	00	49	43.23593899	+02	37	3.7784795	.00000795	.0001875	-0.1755	49913.7	56700.9	21	0.16	0.19	
0047-579	P 0047-579	714	00	49	59.47306617	-57	38	27.3399572	.00001589	.0001697	0.2922	47626.2	55284.9	26			
0047-051	0047-051	2354	00	50	21.53482732	-04	52	20.5954869	.00004140	.0013033	-0.4750	50575.8	50575.9	1			
0048-097	P 0048-09	19	00	50	41.31738637	-09	29	5.2103813	.00000339	.0000524	-0.0555	46609.4	56758.6	1420	0.75	0.67	1.1
0048-071	P 0048-071	2355	00	51	8.20981858	-06	50	2.2290620	.00001261	.0004137	-0.3628	50575.8	50575.9	1			
0048-427	0048-427	998	00	51	9.50182479	-42	26	33.2933987	.00000761	.0000984	-0.0703	52306.0	56701.0	69			
0048+447	0048+447	2356	00	51	36.47368223	+44	59	35.9585863	.00008005	.0007511	0.2997	50305.4	50305.5	1			
0049+437	0049+437	2357	00	52	27.82588631	+44	02	54.5159335	.00002477	.0004149	-0.1201	50242.6	50305.5	2			
0046+861	0046+861	1334	00	52	32.85647817	+86	27	44.2520255	.00041421	.0002388	-0.6101	53572.4	55168.3	2			
0050-287	0050-287B	2358	00	52	52.55643376	-28	25	54.1865484	.00010439	.0029743	-0.6493	53572.5	55776.5	2			

Source Name		ID No.	Right Ascension			Declination			RA Error (s)	Dec. Error (arcsec)	RA–Dec Corr.	Observation Epoch MJD		No. Obs.	Source Flux (Jy)		Str Index
B1950	Common		H	M	S	D	M	S				First	Last		10-60	10-40	
0051-077	0051-077	1335	00	53	36.51568717	-07	27	29.6185640	.00011666	.0032614	-0.2460	53560.6	53560.6	1			
0051+291	0051+291	4047	00	53	44.32348400	+29	25	7.1007130	.00002117	.0003869	0.3587	56463.5	56463.7	1			
0051+679	J0054+6811	999	00	54	17.62158134	+68	11	11.1767726	.00015059	.0011129	-0.0967	49826.7	49826.8	1	0.13		
0051+706	0051+706	2359	00	54	17.68493448	+70	53	56.6181250	.00009107	.0008365	0.2695	49826.7	49826.8	1			
0052-201	0052-201	1336	00	54	32.94844348	-19	53	1.0041184	.00002820	.0009294	-0.2411	53523.6	53561.6	2			
0052-125	0052-125	1337	00	55	11.78257855	-12	17	57.0973081	.00001133	.0003917	-0.2194	53552.5	53552.6	1			
0054+161	0054+161	1254	00	56	55.29432868	+16	25	13.3408768	.00000503	.0000905	-0.0156	50155.9	56762.4	79	0.58	0.40	1.2
0054-006	0054-006	2360	00	57	17.00229640	-00	24	33.1751969	.00020550	.0037713	0.3976	53572.5	53572.6	1			
0055+300	DW 0055+30	1000	00	57	48.88334488	+30	21	8.8119751	.00000663	.0001183	-0.4369	50219.6	53575.7	7	0.20	0.30	3.6
0055-328	0055-328	2361	00	58	2.23032532	-32	34	20.7476138	.00008327	.0033203	-0.4639	52305.9	52306.0	1			
0055-059	0055-059	1338	00	58	5.06631590	-05	39	52.2783282	.00000431	.0000827	-0.0769	50575.8	56763.2	73			
0055-340	0055-340	4048	00	58	15.64182642	-33	47	57.4908099	.00004972	.0019484	0.2692	56204.2	56204.3	1			
0055+329	0055+329	1339	00	58	32.06904341	+33	11	17.2143343	.00002355	.0006842	-0.2535	53560.5	53560.6	1			
0055+060	0055+060	1340	00	58	33.80457542	+06	20	6.0729003	.00001573	.0013981	-0.4321	53125.7	56577.2	7	0.16	0.14	
0056-572	0056-572	715	00	58	46.58116192	-56	59	11.4708004	.00006650	.0007370	0.3823	47626.3	52941.3	6			
0056-001	P 0056-00	24	00	59	5.51495440	+00	06	51.6206929	.00001392	.0003749	-0.1384	48975.9	53068.7	8			4.3
0056+579	0056+579	2362	00	59	52.20902349	+58	12	23.6833563	.00006628	.0004784	0.3089	52305.8	52306.1	1			
0057-338	0057-338A	2363	01	00	9.39261704	-33	37	31.8997129	.00114035	.0250688	0.9648	52306.0	54440.2	2			
0057+334	0057+334	1341	01	00	38.29071930	+33	45	6.1217874	.00002813	.0007360	-0.1740	53561.5	53561.6	1			
0057+678	0057+678	2364	01	00	51.66359971	+68	08	20.5352749	.00027795	.0015707	0.1546	49826.7	49826.8	1			
0058+498	0058+498	2365	01	01	16.99752520	+50	04	44.9895737	.00010501	.0009468	-0.6049	50305.4	54088.0	2			
0059-287	0059-287	2366	01	01	52.38979467	-28	31	20.4190619	.00032016	.0083550	0.6119	50687.4	50687.5	1			
0059+163	0059+163	1342	01	01	57.71954595	+16	39	40.9540179	.00003841	.0024172	-0.4534	50085.0	53133.8	4			
0059+581	0059+581	716	01	02	45.76238261	+58	24	11.1366386	.00000338	.0000503	-0.0094	48719.9	56782.2	1416	1.49		1.6
0100-270	0100-270	2367	01	02	56.35401197	-26	46	36.5170143	.00020100	.0073956	0.1373	54112.0	54112.0	1			
0102-245	0102-245	2368	01	04	58.20537867	-24	16	28.4455263	.00001660	.0005671	-0.3165	50631.5	50687.5	2			
0102+511	0102+511	1343	01	05	29.55825970	+51	25	46.5812039	.00029240	.0015565	-0.5074	50305.4	54314.7	2			
0102+480	0102+480	1209	01	05	49.92816285	+48	19	3.1929023	.00000700	.0001431	-0.0191	50305.4	56782.1	96	0.34	0.33	
0103+337	0103+337	2369	01	06	0.29337481	+34	02	2.9888611	.00004701	.0011099	0.5306	50219.6	50219.8	1			
0103+253	0103+253	2370	01	06	10.96904884	+25	39	30.4940857	.00005958	.0017215	-0.8432	50219.6	50219.8	1			
0103-021	0103-021	2371	01	06	22.99426146	-01	55	38.4149841	.00003160	.0007880	0.1028	50575.8	50575.9	1			
0104-275	0104-275	2372	01	06	26.08207181	-27	18	11.8253677	.00001449	.0005018	-0.2274	50687.4	54664.3	2			
0103+127	0103+127	1344	01	06	33.35650252	+13	00	2.6051848	.00003083	.0009152	-0.5187	50155.9	54314.7	2			
0104-035	0104-035	1345	01	06	43.22871228	-03	15	36.2956715	.00001535	.0004996	-0.0945	53572.5	53572.6	1			
0104-408	P 0104-408	25	01	06	45.10796953	-40	34	19.9603990	.00000366	.0000561	-0.0339	43809.2	56748.9	1055		1.09	1.3
0104+195	0104+195	2373	01	06	52.63125040	+19	51	2.5622073	.00001766	.0005302	-0.5728	53502.8	53503.7	1			
0105+129	0105+129	2374	01	07	45.96188267	+13	12	5.1912843	.00002497	.0007608	-0.4367	54087.2	54088.0	1			
0105+259	0105+259	2375	01	07	47.88628409	+26	11	8.6721789	.00006962	.0024101	-0.7064	50219.6	50219.8	1			
0105-008	0105-008	2376	01	08	26.84265089	-00	37	24.1654059	.00006180	.0011983	0.5318	50575.8	50575.9	1			
0106+013	P 0106+01	27	01	08	38.77110632	+01	35	0.3171803	.00000342	.0000530	-0.0518	43809.3	56709.7	1178	1.22	1.00	3.2
0107-610	0107-610	1255	01	09	15.47521319	-60	49	48.4600873	.00001351	.0001509	0.1032	52780.1	56537.9	32			
0106+315	0106+315	4049	01	09	27.88714919	+31	49	56.0482771	.00003772	.0007129	0.2971	56301.9	56302.1	1			
0106+612	0106+612	2377	01	09	46.34439731	+61	33	30.4557181	.00005704	.0001929	-0.2342	52305.8	52306.2	1			
0106+678	0106+678	2378	01	10	12.87344037	+68	05	41.2186562	.00023159	.0015269	0.0588	49826.7	49826.8	1			
0107-045	0107-045	2379	01	10	30.90279644	-04	15	31.0268130	.00002783	.0010064	-0.4883	54112.0	54112.1	1			
0108-170	0108-170	2380	01	10	35.51122661	-16	48	27.7015943	.00032486	.0078278	0.5750	53152.6	53152.7	1			
0108-079	P 0108-079	2381	01	10	50.02098667	-07	41	41.1146369	.00001423	.0004672	-0.2216	50575.8	50575.9	1			
0107+562	0107+562	2382	01	10	57.55131612	+56	32	16.9748821	.00374630	.2013390	0.7731	52409.5	52409.5	1			
0108+388	GC 0108+38	29	01	11	37.31676292	+39	06	28.1036731	.00003135	.0004452	0.0748	49098.7	53129.7	5			
0109-135	0109-135	1346	01	11	56.85796607	-13	17	1.1983067	.00002460	.0008496	-0.5123	53561.5	53561.6	1			

Source Name		ID No.	Right Ascension			Declination			RA Error (s)	Dec. Error (arcsec)	RA–Dec Corr.	Observation Epoch MJD		No. Obs.	Source Flux (Jy)		Str Index
B1950	Common		H	M	S	D	M	S				First	Last		10-60	10-40	
0109+224	GC 0109+22	30	01	12	5.82471998	+22	44	38.7863217	.00000375	.0000641	-0.0150	49735.9	56772.7	149	0.53	0.37	2.0
0109+351	0109+351	2383	01	12	12.94440007	+35	22	19.3362842	.00000869	.0001520	0.0786	50242.6	56701.1	2	0.58	0.32	
0110-668	0110-668	2384	01	12	18.91294251	-66	34	45.1879734	.00003371	.0003289	0.4895	53222.9	56111.9	15			
0110+318	0110+318	2385	01	12	50.33305763	+32	08	17.4330836	.00001487	.0004005	-0.0606	50219.6	50219.8	1			
0110-361	0110-361	2386	01	13	15.85639203	-35	51	48.3672773	.00002377	.0005604	-0.1754	55112.2	55112.3	1			
0110+495	0110+495	717	01	13	27.00680913	+49	48	24.0431360	.00000458	.0000704	-0.0654	49421.9	56782.1	82	0.28		
0111+021	P 0111+021	32	01	13	43.14494994	+02	22	17.3162766	.00000404	.0000721	-0.3149	44227.2	56702.6	333	0.21	0.42	3.4
0111+131	0111+131	1347	01	13	54.51036173	+13	24	52.4777578	.00004852	.0007819	-0.0689	50155.9	54314.7	2			
0112-245	0112-245	1348	01	14	57.32743018	-24	19	44.7470043	.00410525	.1540599	-0.8162	54818.1	54818.1	1			
0112-017	P 0112-017	33	01	15	17.09996126	-01	27	4.5774031	.00000689	.0001553	-0.6012	47254.9	53946.4	95	0.28	0.30	4.2
0113-283	0113-283	1349	01	15	23.88363896	-28	04	55.2241188	.00002370	.0004599	-0.1907	50687.4	54643.3	2			
0113-310	0113-310	1350	01	15	46.50555364	-30	49	19.4010215	.00004174	.0011853	-0.6491	53125.7	53125.7	1			
0113-118	P 0113-118	34	01	16	12.52201532	-11	36	15.4344868	.00000549	.0001206	-0.5558	43809.4	56633.0	90	0.38	0.57	3.4
0113+241	0113+241	2387	01	16	38.06769599	+24	22	53.7237303	.00008531	.0016737	-0.1708	50085.0	50156.0	2			
0114-211	0114-211	1351	01	16	51.45376183	-20	52	8.0433084	.01456193	.3533937	-0.9987	52408.8	56498.5	3			
0114+140	0114+140	1001	01	17	25.20315838	+14	18	12.4190378	.00008924	.0014208	-0.8603	50085.0	53771.1	3		0.32	
0115-214	0115-214	1352	01	17	48.78013489	-21	11	6.6331932	.00000448	.0000645	0.0291	50631.5	56772.3	226	0.21	0.39	2.5
0116-219	0116-219	1353	01	18	57.26217954	-21	41	30.1402188	.00000556	.0000979	0.0051	50631.5	56699.6	32			
0116+082	0116+082	2388	01	19	1.27436057	+08	29	54.6927031	.00006587	.0017787	-0.3912	52408.7	52408.8	1			
0116+319	OC 328	718	01	19	35.00335846	+32	10	50.0545082	.00040285	.0045109	-0.2548	48975.9	54440.2	3			
0117-171	0117-171	1354	01	19	43.64592236	-16	54	8.9727032	.00003842	.0012905	0.6602	53552.5	53552.6	1			
0118-272	P 0118-272	37	01	20	31.66338583	-27	01	24.6526601	.00001046	.0002175	-0.3202	49960.7	54362.1	18		0.14	5.0
0118-283	0118-283	2389	01	21	0.74188575	-28	06	22.1773195	.00020151	.0059920	0.6929	53502.7	53502.8	1			
0119+115	P 0119+11	38	01	21	41.59504361	+11	49	50.4130296	.00000338	.0000527	-0.0507	47255.0	56744.7	1061	1.38	0.78	2.3
0119+041	GC 0119+04	667	01	21	56.86169816	+04	22	24.7343034	.00000341	.0000536	-0.1043	45476.6	56748.7	1136	0.36	0.37	2.9
0119-011	0119-011	2390	01	22	17.46999048	-00	56	15.6980979	.00003065	.0012722	-0.7152	54112.0	54112.1	1			
0119+247	0119+247	1210	01	22	38.81599483	+25	02	31.7929190	.00001057	.0003084	-0.0011	50219.6	53658.5	3	0.32	0.20	
0119+296	0119+296	1355	01	22	45.43001765	+29	54	12.6429871	.00001652	.0004204	-0.1433	53125.6	53133.8	2			
0120+304	0120+304	1356	01	23	2.28145371	+30	44	6.9170346	.00002998	.0009393	0.0021	53572.5	53572.6	1			
0121-040	0121-040	2391	01	23	35.77965312	-03	48	38.9253149	.01178595	.8923805	0.9990	54087.2	54087.2	1			
0120+259	0120+259	2392	01	23	43.04520508	+26	15	22.4263741	.00001807	.0005710	-0.2225	50219.6	50219.8	1			
0121-096	0121-096	1357	01	23	46.38463913	-09	23	3.3343264	.00009570	.0031300	0.4764	53560.6	53560.6	1			
0122-345	0122-345A	1358	01	24	21.45934259	-34	16	21.4529970	.00004417	.0013773	-0.2945	52306.0	53125.7	2			
0121+560	0121+560	2393	01	24	25.82701810	+56	18	51.9172965	.00008489	.0010453	0.3210	49576.4	54482.5	2			
0122+278	0122+278	2394	01	24	55.87922238	+28	05	11.3911601	.00002294	.0006679	-0.0315	50219.6	50219.8	1			
0122-514	0122-514	2395	01	24	57.39148338	-51	13	16.1677005	.00001760	.0002428	0.3048	53382.5	55784.1	10			
0122+470	0122+470	2396	01	25	7.70675439	+47	18	3.0848456	.00007845	.0010618	0.1507	50305.4	50305.5	1			
0122-260	0122-260	1359	01	25	18.83746058	-25	49	4.3896921	.00002361	.0008583	-0.2278	53561.6	53561.6	1			
0122-003	0122-003	1256	01	25	28.84384560	-00	05	55.9325775	.00001023	.0003117	-0.3635	50575.8	53946.4	5	0.29	0.21	
0122+705	0122+705	2397	01	26	7.84363055	+70	46	52.3856813	.00026539	.0029337	-0.6580	49826.7	49826.8	1			
0123-226	0123-226	1360	01	26	15.00160739	-22	22	33.6017192	.00002956	.0008988	-0.6623	53125.7	53125.8	1			
0124-155	0124-155	1361	01	26	33.89074299	-15	18	34.1165309	.00001966	.0006396	-0.0061	54657.5	54657.6	1			
0123+257	P 0123+25	40	01	26	42.79263886	+25	59	1.3001543	.00000461	.0000905	-0.0940	48377.8	56638.6	27	0.62	0.27	3.0
0123+731	0123+731	2398	01	27	4.71632772	+73	23	12.6751059	.00019432	.0008732	-0.4600	53572.4	56638.2	2			
0125+487	0125+487	2399	01	28	8.06339082	+49	01	5.9859149	.00003099	.0005543	0.4625	50305.4	50305.5	1			
0125+628	0125+628	1257	01	28	30.56515498	+63	06	29.8820963	.00006869	.0002499	-0.2296	53977.8	53978.6	1			
0127+145	0127+145	2400	01	29	55.34717135	+14	46	47.8358804	.00002149	.0005462	-0.2964	50085.0	54481.9	3			
0127+084	0127+084	719	01	30	27.63443052	+08	42	46.1722429	.00000941	.0003072	-0.2482	49913.7	55483.4	3	0.11	0.11	
0128+383	0128+383	1362	01	31	26.71351517	+38	34	39.2208673	.00005180	.0012752	-0.0432	53560.6	53560.8	1			
0129+220	0129+220	2401	01	32	3.07878699	+22	16	50.3354525	.00002303	.0005336	-0.1263	54112.0	54112.2	1			

Source Name		ID No.	Right Ascension			Declination			RA Error (s)	Dec. Error (arcsec)	RA–Dec Corr.	Observation Epoch MJD		No. Obs.	Source Flux (Jy)		Str Index
B1950	Common		H	M	S	D	M	S				First	Last		10-60	10-40	
0129+560	0129+560	2402	01	32	20.44727773	+56	20	40.3705257	.00004738	.0005898	0.3025	49576.4	49576.5	1			
0130-171	P 0130-17	43	01	32	43.48746495	-16	54	48.5219824	.00000698	.0001051	-0.1067	50631.5	55728.7	31	0.65	0.43	4.0
0129+431	0129+431	2403	01	32	44.12679312	+43	25	32.6609021	.00002659	.0005425	-0.2301	50242.6	50242.7	1			
0130-447	0130-447	2404	01	33	0.86363826	-44	30	43.5803463	.00012092	.0069060	-0.2057	53133.7	55168.2	2			
0131-522	P 0131-522	720	01	33	5.76253210	-52	00	3.9456372	.00000922	.0001226	0.2188	48388.3	56770.2	49			
0131-001	0131-001	2405	01	34	12.70420479	+00	03	45.1348020	.00009687	.0019117	-0.0833	50575.8	50575.9	1			
0132-389	0132-389A	2406	01	34	32.03008834	-38	43	33.3828555	.00003983	.0011471	-0.2496	52306.0	52408.7	2			
0132-097	P 0132-097	2407	01	34	35.66620075	-09	31	2.8827638	.00018591	.0028734	0.8684	52408.7	54440.2	2			
0130+691	0130+691	2408	01	34	40.75979453	+69	25	10.8963770	.00087437	.0032047	0.6389	49826.7	49826.8	1			
0133-204	P 0133-203	2409	01	35	37.50940158	-20	08	45.8620388	.00000971	.0002997	-0.1572	50631.5	50687.5	2			
0133+476	DA 55	44	01	36	58.59480804	+47	51	29.1000959	.00000337	.0000505	-0.0253	43873.4	56782.1	1496	2.03	1.71	2.0
0134+311	0134+311	1363	01	37	8.73363582	+31	22	35.8554689	.00000379	.0000630	0.0974	50219.6	56776.4	233			
0134+215	0134+215	1364	01	37	15.62497750	+21	45	44.2700091	.00006907	.0009692	0.4791	53561.5	53561.6	1			
0135-247	0135-247	721	01	37	38.34644440	-24	30	53.8855174	.00000589	.0001178	-0.0568	49789.9	55168.5	25	0.28	0.43	3.2
0134+329	3C 48	2410	01	37	41.30015319	+33	09	35.1329628	.00029024	.0077462	0.1177	50459.8	50460.2	1			
0135-274	0135-274	1365	01	38	9.81822679	-27	11	27.9353719	.00002494	.0008744	0.1734	53572.5	53572.6	1			
0136-059	0136-059	2411	01	38	51.85126704	-05	40	8.2426549	.00001386	.0003935	0.2159	50575.8	56393.7	4			
0136-231	0136-231	2412	01	38	57.46564891	-22	54	47.3306620	.00001452	.0005257	-0.0409	50631.5	50687.5	2			
0136+176	0136+176	1366	01	39	41.97920007	+17	53	7.5494136	.00002847	.0005755	-0.1464	50085.0	54664.5	3			
0137+012	0137+012	1367	01	39	57.30579072	+01	31	46.1385505	.00001786	.0004507	-0.2409	54314.4	56568.0	5			
0137-158	0137-158	1368	01	40	4.43518365	-15	32	55.6804407	.00001516	.0005680	-0.1199	53561.6	53561.6	1			
0137+467	0137+467	2413	01	40	43.07276386	+46	58	28.4880935	.00037950	.0026816	-0.2773	50305.4	54314.7	2			
0137+635	0137+635	2414	01	40	43.07801580	+63	46	6.8917506	.00021937	.0006430	0.1624	52305.9	52305.9	1			
0137+434	0137+434	2415	01	40	54.66442099	+43	42	45.2071709	.00003886	.0005304	-0.1443	54087.2	54088.0	1			
0138-097	0138-097	722	01	41	25.83216061	-09	28	43.6743291	.00000474	.0000880	-0.0425	49960.5	56772.3	42	0.25	0.29	
0139-022	0139-022	1369	01	41	33.79015244	-02	02	21.5536753	.00001907	.0006620	-0.3685	53572.5	53572.6	1			
0140+412	0140+412	2416	01	43	3.18454704	+41	29	20.4456239	.00001745	.0003831	-0.1834	50242.6	50242.7	1			
0140-322	0140-322	2417	01	43	10.13155598	-32	00	56.6512806	.00002829	.0009330	-0.3993	52306.0	52306.0	1			
0140+120	0140+120	1370	01	43	31.09226609	+12	15	42.9341907	.00010393	.0011676	0.1828	53125.7	53133.8	2			
0140+490	0140+490	2418	01	43	46.87984069	+49	15	41.5862289	.00056300	.0062618	0.0538	50305.4	50305.5	1			
0141+268	0141+268	1371	01	44	33.55390450	+27	05	3.1173316	.00008293	.0011684	0.0170	53560.6	53560.8	1			
0142-398	0142-398	2419	01	44	54.09377156	-39	38	10.5284125	.00013608	.0041190	-0.7584	52408.8	56162.5	2			
0142-278	P 0142-278	2420	01	45	3.39461816	-27	33	34.3292581	.00001557	.0004856	-0.1731	50687.4	50687.5	1			
0141+579	0141+579	2421	01	45	14.36947844	+58	10	49.2745267	.11114028	.6375960	-0.9920	49576.5	49576.5	1			
0143+230	0143+230	2422	01	45	52.90628638	+23	19	19.2972079	.00003105	.0007767	-0.5526	50085.0	50156.0	2			
0144+209	0144+209	2423	01	46	58.78390435	+21	10	24.3813848	.00009577	.0017706	-0.9001	50085.0	54440.2	3			
0144+487	0144+487	2424	01	47	37.77513427	+48	59	37.5105251	.00034761	.0037109	0.1591	50305.4	50305.5	1			
0144+584	J0147+58	1003	01	47	46.54084377	+58	40	44.9709523	.00002398	.0001812	-0.0106	49576.4	56701.1	6			
0145+386	0145+386	2425	01	48	24.37757449	+38	54	5.2198748	.00002834	.0004832	-0.3462	50242.6	50242.7	1			
0145+420	0145+420	4050	01	48	44.57636947	+42	15	19.4046346	.00001713	.0004389	0.2015	55965.9	55966.1	1			
0146+056	0146+056	668	01	49	22.37088101	+05	55	53.5685553	.00000456	.0000953	-0.3529	47254.9	56638.6	97	0.50	0.51	3.3
0147+187	0147+187	2426	01	49	49.71895084	+18	57	20.6109653	.00002540	.0005702	-0.0057	50085.1	50156.0	2			
0147-076	0147-076	1004	01	50	2.69554571	-07	25	48.4993280	.00210459	.0266100	0.7956	53067.8	53523.6	2			
0147+265	J0150+26	4051	01	50	2.80492264	+26	46	28.0842514	.00004210	.0007080	0.3076	56748.7	56749.0	1			
0148-177	0148-177	2427	01	51	6.08335076	-17	32	44.7183940	.00000908	.0002991	-0.1888	50631.5	56547.4	2	0.24	0.26	
0148+250	0148+250	1372	01	51	6.23387457	+25	17	28.6623913	.00005238	.0019812	-0.6107	53561.5	53561.6	1			
0149-348	0149-348	2428	01	51	23.48911318	-34	35	13.8769332	.00003462	.0011640	-0.1201	52306.0	52306.1	1			
0148+274	GC 0148+27	52	01	51	27.14618563	+27	44	41.7935885	.00000672	.0001143	-0.1933	48719.9	55306.7	21	0.28	0.30	3.8
0148+546	0148+546	1005	01	51	36.29573618	+54	54	37.5711131	.02307624	.1274241	-0.9960	49576.4	49576.4	1			
0149-175	0149-175	2429	01	51	48.04939623	-17	19	55.0540522	.00002770	.0008973	0.5787	53572.5	55371.7	2			

Source Name		ID No.	Right Ascension			Declination			RA Error (s)	Dec. Error (arcsec)	RA–Dec Corr.	Observation Epoch MJD		No. Obs.	Source Flux (Jy)		Str Index
B1950	Common		H	M	S	D	M	S				First	Last		10-60	10-40	
0149+370	0149+370	2430	01	52	12.21994451	+37	16	5.6666486	.00001689	.0003724	-0.2334	50242.6	50242.8	1			
0149+218	P 0149+21	53	01	52	18.05904374	+22	07	7.6997580	.00000378	.0000652	-0.2157	47301.6	56741.6	163	0.80	0.48	2.9
0150-144	0150-144	1373	01	52	32.01246378	-14	12	39.3940421	.00004165	.0011867	-0.5117	50631.5	54664.3	2			
0150-299	0150-299	1374	01	52	33.69286516	-29	42	47.9289581	.00010771	.0047554	0.0838	53560.5	53560.6	1			
0149+335	0149+335	2431	01	52	34.57645670	+33	50	33.1586385	.00002573	.0005508	-0.2531	50219.6	50219.8	1			
0150+000	0150+000	1375	01	52	43.14999992	+00	20	39.7107710	.00004996	.0016310	-0.4826	53125.8	53133.7	2			
0150-193	0150-193	2432	01	53	1.51120011	-19	06	56.6881546	.00008215	.0030108	-0.7177	54087.1	54087.2	1			
0150-334	P 0150-334	54	01	53	10.12173455	-33	10	25.8617867	.00001844	.0001760	-0.3726	48756.3	55728.7	25		0.15	4.5
0149+710	0149+710	2433	01	53	25.85095868	+71	15	6.4627078	.00031223	.0012974	-0.2055	49826.7	49826.8	1			
0151+081	0151+081	1376	01	54	2.77009876	+08	23	51.0725373	.00011711	.0026580	-0.0532	53133.7	53133.8	1			
0151+474	0151+474	723	01	54	56.28988921	+47	43	26.5395456	.00000458	.0000690	0.0449	49749.9	56782.1	126	0.39	0.32	2.2
0152+043	0152+043	1006	01	55	3.72555203	+04	38	30.3473478	.00007217	.0017665	-0.1364	49913.7	49914.6	1			
0153-410	P 0153-410	2434	01	55	37.05938130	-40	48	42.3583873	.00021427	.0123124	0.3399	52408.7	52408.8	1			
0153+222	0153+222	2435	01	55	58.93536254	+22	30	11.8657613	.00003984	.0008175	0.2525	50085.1	50156.0	2			
0153+389	0153+389	1377	01	56	31.41013174	+39	14	30.9238062	.00001810	.0003786	0.1149	53125.7	53125.8	1			
0155-549	0155-549	2436	01	56	49.71184876	-54	39	48.5000366	.00145511	.0125498	-0.9414	54722.9	54723.8	1			
0154-000	0154-000	1378	01	57	10.53490987	+00	11	24.4838224	.00001891	.0006604	-0.4374	53572.5	53572.6	1			
0153+744	0153+744	1007	01	57	34.96491386	+74	42	43.2298140	.00004934	.0002099	-0.0227	49826.7	55306.7	15	0.16		5.0
0155+211	0155+211	2437	01	58	0.10795103	+21	24	42.7877009	.00003801	.0006801	-0.2949	54087.2	54088.0	1			
0156-144	0156-144	2438	01	58	43.71963497	-14	13	7.1187155	.00002613	.0007385	0.2818	50631.5	50631.7	1			
0156+128	0156+128	2439	01	58	56.27379194	+13	07	2.7410356	.00003262	.0012387	-0.3328	50085.1	50156.0	2			
0158+031	0158+031	1379	02	00	40.81650056	+03	22	49.5072110	.00001501	.0005323	-0.2857	53560.5	53560.6	1			
0158-159	0158-159	2440	02	00	51.14885429	-15	42	36.8647487	.00002709	.0007834	-0.3687	53572.5	55916.2	2			
0158-141	0158-141	1380	02	00	58.31711421	-13	56	17.9802209	.00014164	.0055877	-0.1152	53561.6	53561.6	1			
0159+034	0159+034A	2441	02	01	51.50874825	+03	43	9.2597261	.00003393	.0011970	-0.3086	49913.7	49914.6	1			
0159-117	0159-117	1381	02	01	57.17938984	-11	32	33.4366751	.00001913	.0005951	-0.6619	54186.8	54187.0	1			
0159-062	0159-062	1382	02	02	6.86465687	-05	59	0.1201690	.00005427	.0018469	-0.6341	52620.0	52620.3	1			
0202-765	0202-765	2442	02	02	13.69538040	-76	20	3.0557379	.00325833	.0065631	0.0304	48110.1	48110.9	1			
0159-200	0159-200	1383	02	02	13.84771562	-19	48	19.4900348	.00003956	.0015346	0.2506	53560.5	53560.6	1			
0159+418	J0202+4205	1008	02	02	43.65332422	+42	05	16.3323975	.00001688	.0003436	-0.1737	50242.6	50242.8	1			
0157+808	0157+808	2443	02	03	7.87143865	+81	06	13.2100360	.00027602	.0005227	-0.4928	54439.8	54439.9	1			
0159+723	0159+723	724	02	03	33.38496082	+72	32	53.6673157	.00000673	.0000569	0.1110	48352.9	56782.2	141	0.23		1.9
0201+113	P 0201+113	57	02	03	46.65706058	+11	34	45.4094244	.00000346	.0000548	-0.1782	45432.7	56762.7	800	0.45	0.36	3.1
0200+539	0200+539	2445	02	03	46.65707578	+54	11	57.6250421	.00029891	.0034330	-0.6395	49576.4	49576.5	1			
0201+398	0201+398	4052	02	04	5.19476268	+40	05	3.5152438	.00003608	.0004672	0.1180	55965.9	55966.1	1			
0202-337	0202-337	1384	02	04	28.66416026	-33	28	50.4557903	.00009646	.0033626	0.7354	53125.8	53125.8	1			
0201+088	0201+088	2446	02	04	34.75911519	+09	03	49.2593629	.00033693	.0027677	0.1362	49913.7	49914.6	1			
0202+149	P 0202+14	58	02	04	50.41389642	+15	14	11.0435673	.00000339	.0000520	-0.0985	44203.1	56728.7	943	0.57	0.56	3.1
0201+438	0201+438	2447	02	04	54.78909921	+44	03	6.9044150	.00007492	.0007126	0.1185	50242.6	50305.5	2			
0201+365	0201+365	2448	02	04	55.59601953	+36	49	17.9967405	.00001720	.0004212	-0.1042	50242.6	50242.8	1			
0202-172	P 0202-17	60	02	04	57.67434499	-17	01	19.8406171	.00000542	.0001137	-0.0549	49750.0	55042.7	25	0.82	0.55	3.2
0202+319	DW 0202+31	59	02	05	4.92536454	+32	12	30.0954773	.00000359	.0000537	-0.0305	48196.4	56772.8	195	1.55	1.28	1.8
0202+145	0202+145	1385	02	05	13.11723883	+14	44	32.3863157	.00001388	.0004672	-0.1899	53561.6	53561.6	1			
0202+240	0202+240	1386	02	05	21.32274742	+24	16	32.8511482	.00003306	.0007042	-0.0296	53125.7	53133.8	2			
0203-349	0203-349	2449	02	05	55.50972602	-34	44	9.1841959	.00032186	.0132935	0.6631	52306.0	52306.1	1			
0204-224	0204-224	2450	02	06	20.07355702	-22	12	19.6567223	.00001700	.0005877	-0.2345	50631.5	50687.5	2			
0203-120	0203-120	2451	02	06	26.08474794	-11	50	39.7249449	.00001020	.0003593	0.0721	54112.1	56204.4	2	0.16	0.19	
0203+625	0203+625	2452	02	07	3.01672111	+62	46	12.0674250	.00001993	.0001414	0.2186	52305.9	56498.7	4			
0205-391	0205-391	2453	02	07	15.60903900	-38	57	3.0849592	.00435536	.0955394	0.9522	52408.8	52408.8	1			
0205-242	0205-242	2454	02	07	33.39946934	-24	02	2.1814868	.00096622	.0533660	0.8118	54087.1	54087.2	1			

Source Name		ID No.	Right Ascension			Declination			RA Error (s)	Dec. Error (arcsec)	RA–Dec Corr.	Observation Epoch MJD		No. Obs.	Source Flux (Jy)		Str Index
B1950	Common		H	M	S	D	M	S				First	Last		10-60	10-40	
0204+316	0204+316	2455	02	07	34.98961901	+31	52	6.4633834	.00001644	.0004675	-0.0744	50219.7	50219.8	1			
0206-689	0206-689	2456	02	07	50.93164362	-68	37	55.1632496	.00006740	.0008445	0.1276	54722.9	54723.8	1			
0206-270	0206-270	1387	02	08	22.35590595	-26	50	18.8786995	.00001655	.0006770	-0.0273	53152.7	53152.7	1			
0205-010	0205-010	2457	02	08	26.34591441	-00	47	44.2939773	.00001475	.0004210	-0.2466	50575.8	50575.9	1			
0206-178	0206-178	1388	02	08	34.94336165	-17	39	34.6818199	.00002226	.0009688	-0.0309	54818.1	54818.2	1			
0206+293	0206+293	2458	02	09	8.64446742	+29	32	45.7435407	.00008709	.0016511	0.5139	50219.7	50219.8	1			
0206-048	0206-048	1389	02	09	30.76662300	-04	38	26.1407700	.00021112	.0062517	-0.9036	52480.3	52480.7	1			
0205+643	0205+643	2459	02	09	35.98812100	+64	37	25.7703007	.00007747	.0005062	0.4923	52408.9	52409.6	1			
0206+136	0206+136	1390	02	09	35.99832910	+13	52	0.7518973	.00000582	.0001268	0.0169	50085.1	56751.7	30	0.33		
0205+722	0205+722	2460	02	09	51.79040639	+72	29	26.6696239	.00005168	.0002132	0.4956	52409.0	52409.6	1			
0207-078	0207-078	1391	02	10	16.52887721	-07	37	20.6938526	.00026981	.0047353	0.2966	52480.4	53552.6	2			
0207-149	0207-149	2461	02	10	23.18040191	-14	44	59.0199444	.00004279	.0013331	-0.3795	53502.7	53502.8	1			
0208-512	P 0208-512	725	02	10	46.20042740	-51	01	1.8918852	.00000464	.0000614	0.0514	47304.8	56638.7	403			
0208+106	0208+106	2462	02	11	13.17738092	+10	51	34.7992042	.00002645	.0006658	-0.1513	49913.7	49914.6	1			
0209+168	0209+168	1392	02	11	48.77886336	+17	07	22.7217332	.00004183	.0006637	-0.6765	50085.2	54314.7	3			
0209-162	0209-162	1393	02	11	49.76131935	-15	58	18.8378026	.00008263	.0027587	-0.3098	53572.5	53572.6	1			
0210-180	0210-180	1394	02	12	22.64360790	-17	46	14.3408086	.00003786	.0011634	-0.4386	54657.5	54657.6	1			
0210+225	0210+225	2463	02	12	52.83488188	+22	44	52.2530583	.00005213	.0010804	-0.0010	53125.7	55776.6	2			
0210+119	0210+119	2464	02	13	5.18307741	+12	13	10.9092103	.00004319	.0015586	-0.6931	54112.1	54112.2	1			
0210+181	0210+181	2465	02	13	10.52929741	+18	20	25.4476517	.00003257	.0008828	-0.2082	50085.1	50156.0	2			
0210-075	0210-075	1395	02	13	16.67051650	-07	19	32.4665879	.00027346	.0078614	-0.2227	52480.4	52480.7	1			
0210+366	0210+366	2466	02	13	48.19191617	+36	52	34.0069694	.00002709	.0005970	-0.4973	54087.2	54088.0	1			
0159+870	0159+870	1396	02	13	57.84590317	+87	17	28.7262434	.00078332	.0004376	-0.0489	53125.5	53125.8	1			
0212-620	0212-620	4053	02	14	16.20442475	-61	49	33.6596550	.00015400	.0006763	0.1282	56007.1	56313.8	3			
0210+515	0210+515	2467	02	14	17.93408652	+51	44	51.9445797	.00054901	.0032693	0.6018	54112.0	54112.1	1			
0211+171	0211+171	1397	02	14	44.91285696	+17	22	49.5121097	.00002740	.0007116	-0.2143	54277.7	56568.1	5			
0212-039	0212-039	1398	02	15	11.50646687	-03	43	7.8893275	.00024820	.0071486	-0.2488	52480.3	52480.7	1			
0213-026	0213-026	2468	02	15	42.01730278	-02	22	56.7528716	.00001076	.0003182	0.0895	50575.8	56748.9	2	0.35	0.20	
0213+051	0213+051	2469	02	15	55.01075066	+05	24	25.5544166	.00001564	.0005056	0.0260	54087.1	54087.2	1			
0214-522	0214-522	2470	02	16	3.19795408	-52	00	12.4783099	.00063799	.0026276	-0.3810	52886.7	53138.2	3			
0213-015	0213-015	1399	02	16	5.66382982	-01	18	3.3985914	.00016343	.0066698	-0.3698	52542.9	52543.5	1			
0213-013	0213-013	1400	02	16	12.21201872	-01	05	18.8300352	.00015065	.0060823	-0.2433	52543.1	52543.5	1			
0213+443	0213+443	2471	02	16	17.17158790	+44	37	43.3896415	.00018889	.0056045	0.0798	50305.4	50305.5	1			
0214-105	0214-105	2472	02	16	38.87599515	-10	17	3.0034379	.00009135	.0037937	-0.6682	54112.1	54112.2	1			
0214-330	0214-330	2473	02	16	48.18538625	-32	47	40.8503870	.00002355	.0008451	-0.3116	52306.0	52306.1	1			
0214-085	0214-085	2474	02	17	2.66231149	-08	20	52.3516609	.00001873	.0006267	-0.3668	50575.8	50575.9	1			
0214+083	0214+083	2475	02	17	17.12497058	+08	37	3.8980382	.00002169	.0006236	-0.0864	53125.7	53125.8	1			
0212+735	0212+735	669	02	17	30.81339303	+73	49	32.6217757	.00000428	.0000511	-0.0438	44927.9	56594.6	784	1.01		3.1
0215+015	0215+015	726	02	17	48.95475539	+01	44	49.6990239	.00000348	.0000533	-0.0155	49913.7	56758.7	166	0.92	0.71	1.4
0215-015	0215-015	1402	02	17	54.99944183	-01	21	50.7267619	.00008870	.0064652	-0.4697	52543.1	52543.5	1			
0215-167	0215-167	2476	02	17	57.24947307	-16	31	10.4741460	.00001619	.0006665	-0.1322	50631.5	50631.7	1			
0216+011	P 0216+011	2477	02	19	7.02450818	+01	20	59.8661908	.00001295	.0004359	-0.3378	49913.7	54482.7	2			
0217-189	0217-189	2478	02	19	21.16175230	-18	42	38.7476173	.00001208	.0004423	-0.0663	50631.5	50687.5	2			
0216+472	0216+472	1403	02	19	23.35996095	+47	27	40.0081451	.00003200	.0004884	-0.0404	53561.5	53561.7	1			
0216+478	0216+478	2479	02	19	26.67603266	+48	06	38.8605188	.00002671	.0002811	-0.0450	53133.7	55657.0	2			
0217+166	0217+166	2480	02	20	0.75882713	+16	52	28.5887673	.00009280	.0019085	-0.7840	50085.2	50156.1	2			
0218-133	0218-133	2481	02	20	28.21749760	-13	05	19.0693400	.00005454	.0011733	0.4311	50575.8	50575.9	1			
0218-220	0218-220	2482	02	20	35.15014023	-21	51	12.0801675	.00001915	.0006973	-0.4161	50631.5	50687.5	2			
0217+324	0217+324	2483	02	20	48.05306145	+32	41	6.4639393	.00002163	.0004910	0.4753	50219.7	50219.8	1			
0218+095	0218+095	4054	02	20	53.80226915	+09	45	35.1751071	.00013593	.0037506	-0.4303	56392.8	56392.9	1			

Source Name		ID No.	Right Ascension			Declination			RA Error (s)	Dec. Error (arcsec)	RA–Dec Corr.	Observation Epoch MJD		No. Obs.	Source Flux (Jy)		Str Index
B1950	Common		H	M	S	D	M	S				First	Last		10-60	10-40	
0218+357	GC 0218+35	727	02	21	5.46680529	+35	56	13.7371902	.00003430	.0005610	0.2199	48931.2	52408.8	3	0.12		
0219-164	0219-164	2484	02	22	0.72498748	-16	15	16.5478015	.00001867	.0005384	-0.2043	50631.5	50631.7	1			
0219+428	0219+428	728	02	22	39.61149734	+43	02	7.7989939	.00000490	.0000763	-0.0894	48649.9	56192.1	110	0.54	0.21	3.1
0220-349	P 0220-349	729	02	22	56.40164598	-34	41	28.7300821	.00000624	.0001301	-0.0282	49790.2	56638.7	29		0.29	3.2
0220+427	0220+427	2485	02	23	11.41128566	+42	59	31.3850520	.00003597	.0003749	0.3458	53067.8	53068.7	1			
0220-023	0220-023	1404	02	23	13.04045957	-02	05	7.9320078	.00004013	.0012024	-0.4186	52620.0	52620.3	1			
0219+628	0219+628	4055	02	23	29.60698706	+63	07	17.3051264	.00015944	.0007707	-0.1531	56204.2	56204.5	1			
0221-171	0221-171	1405	02	23	43.76370674	-16	56	37.7005395	.00005581	.0017011	-0.6025	53125.7	53133.8	2			
0221+067	GC 0221+06	67	02	24	28.42819484	+06	59	23.3414823	.00000390	.0000688	-0.3108	47255.0	56674.3	153	0.43	0.47	2.4
0222-234	0222-234	1406	02	25	2.82147521	-23	12	48.4856126	.00003710	.0010576	-0.1548	54657.5	54657.6	1			
0222+185	0222+185	1009	02	25	4.66883994	+18	46	48.7668608	.00002825	.0008130	-0.2804	50085.1	50156.1	2	0.19	0.40	
0222+296	0222+296	1407	02	25	19.19529469	+29	55	12.1292169	.00002926	.0008129	-0.2275	53560.5	53560.6	1			
0223+113	0223+113	1408	02	25	41.90987824	+11	34	25.4644951	.00001480	.0004595	0.0566	53572.5	53572.6	1			
0223+341	0223+341	2486	02	26	10.33319921	+34	21	30.2862008	.00001689	.0004331	0.2232	50219.7	50219.8	1			
0224-189	0224-189	1409	02	26	47.62836402	-18	43	39.2346181	.00009592	.0028017	-0.8085	54657.5	54657.7	1			
0225-306	0225-306	2487	02	27	40.53667522	-30	26	3.6299303	.00002280	.0007937	-0.3886	52306.0	52306.1	1			
0224+498	0224+498	1410	02	28	0.46573820	+50	05	59.0097043	.00003892	.0004245	-0.1510	53552.5	53552.7	1			
0225+419	0225+419	1411	02	28	12.46715896	+42	12	3.4449317	.00008395	.0009225	0.0498	53561.5	53561.7	1			
0226-559	0226-559	2488	02	28	21.59837692	-55	46	3.2793991	.00004619	.0008586	0.2962	54722.9	54723.8	1			
0224+540	0224+540	2489	02	28	25.69171097	+54	19	8.1335963	.00058529	.0046795	0.8398	53502.8	53503.7	1			
0226-375	0226-375	2490	02	28	33.73376087	-37	19	56.3531183	.00007654	.0034379	0.2083	52306.0	55847.4	3			
0224+671	DW 0224+67	68	02	28	50.05149177	+67	21	3.0293431	.00000487	.0000573	-0.0609	44089.1	56782.2	251	0.81		3.3
0226-038	0226-038	2491	02	28	53.21124449	-03	37	37.1257123	.00001377	.0004179	-0.1582	50575.8	50575.9	1			
0227-369	0227-369	1412	02	29	28.44905819	-36	43	56.8222268	.00000739	.0001080	-0.1142	52306.0	56701.0	49			
0230-790	0230-790	730	02	29	34.94665269	-78	47	45.6018718	.00001697	.0000720	-0.0334	47626.3	56637.7	57			
0227+403	0227+403	1010	02	30	45.71081256	+40	32	53.0680406	.00001601	.0003745	-0.0395	50242.6	54482.7	2			
0228-163	0228-163	1413	02	31	5.03526782	-16	06	49.0177858	.00008873	.0019283	0.4380	53572.5	53572.6	1			
0229+131	P 0229+13	69	02	31	45.89405673	+13	22	54.7162559	.00000338	.0000517	-0.0536	45814.0	56770.7	1866	0.73	0.59	2.4
0229-398	0229-398	2492	02	31	51.81631179	-39	35	47.2627938	.00003050	.0008647	0.1128	52306.0	52408.8	2		0.10	
0229+230	0229+230	1414	02	32	20.75648823	+23	17	56.8591250	.00002061	.0005053	-0.3234	50085.1	54482.7	3			
0229+262	0229+262	2493	02	32	27.62326445	+26	28	38.5903568	.00001170	.0003548	-0.0177	50219.7	50219.8	1			
0230-288	0230-288	2494	02	32	36.74094971	-28	39	26.3098796	.00002656	.0009487	-0.0248	54112.1	55616.0	2			
0230+344	0230+344	1415	02	33	20.42003494	+34	42	53.9890629	.00007506	.0010413	-0.0459	53560.5	53560.6	1			
0231+045	0231+045	1416	02	34	7.15543449	+04	46	43.0920679	.00005358	.0012171	-0.2730	53561.6	53561.6	1			
0234-301	0234-301	1417	02	36	31.16941036	-29	53	55.5402936	.00000909	.0001621	-0.0333	53125.8	56748.9	23			
0235-618	0235-618	1011	02	36	53.24575807	-61	36	15.1835418	.00001714	.0001427	0.3328	52850.7	56504.3	21			
0234+052	0234+052	2495	02	37	14.03813621	+05	26	49.9698809	.00031437	.0046083	0.0084	49914.5	49914.6	1			
0235-266	0235-266	2496	02	37	16.76168469	-26	23	53.1482948	.00009765	.0043980	0.3145	52408.7	52408.8	1			
0234+285	CTD 20	71	02	37	52.40567840	+28	48	8.9900016	.00000340	.0000517	-0.0969	44203.0	56749.7	748	1.77	1.43	2.6
0234+469	0234+469	1418	02	38	16.50326606	+47	12	18.5514428	.00006848	.0008565	0.2114	53133.7	53133.8	1			
0235+164	GC 0235+16	72	02	38	38.93010742	+16	36	59.2745097	.00000337	.0000513	-0.0180	44203.2	56701.7	897	1.24	1.00	1.8
0237-027	P 0237-027	73	02	39	45.47227166	-02	34	40.9145081	.00000364	.0000604	-0.0712	49253.4	56772.8	241	0.65	0.51	2.0
0237+040	GC 0237+04	74	02	39	51.26304817	+04	16	21.4117685	.00000476	.0001132	-0.3900	47381.4	56737.6	86	0.38	0.37	2.4
0236+420	0236+420	1419	02	40	5.25262503	+42	16	22.5197943	.00003024	.0006505	-0.0675	53572.5	53572.6	1			
0237-233	P 0237-23	75	02	40	8.17441470	-23	09	15.7300070	.00003611	.0004880	-0.1867	44227.2	55728.7	49	0.13		5.6
0236+610	0236+610	731	02	40	31.66432909	+61	13	45.5938440	.00013903	.0008638	-0.5482	49847.9	53313.7	15			
0237+185	0237+185	2497	02	40	42.81626730	+18	48	0.0541317	.00003862	.0006908	-0.0232	50085.1	50156.1	2			
0238-052	0238-052	1420	02	40	56.17270575	-05	04	42.2024736	.00013125	.0022883	0.2056	53560.5	53560.6	1			
0238-084	P 0238-084	76	02	41	4.79849948	-08	15	20.7518644	.00000491	.0001007	0.0507	48355.7	56763.7	333	0.15	0.12	4.4
0239+175	0239+175	1421	02	42	24.26827055	+17	42	58.8489631	.00000582	.0001297	-0.1465	50085.1	56498.7	30			

Source Name		ID No.	Right Ascension			Declination			RA Error (s)	Dec. Error (arcsec)	RA–Dec Corr.	Observation Epoch MJD		No. Obs.	Source Flux (Jy)		Str Index
B1950	Common		H	M	S	D	M	S				First	Last		10-60	10-40	
0239+108	OD 166	77	02	42	29.17085248	+11	01	0.7279416	.00000402	.0000730	-0.3270	45151.8	56600.5	180	0.49	0.55	3.0
0240-217	P 0240-217	2498	02	42	35.90986216	-21	32	25.9352631	.00001638	.0005604	0.0706	50631.5	50687.5	2			
0240-060	0240-060	2499	02	43	12.46947758	-05	50	55.2959395	.00001238	.0003803	-0.1899	50575.8	50575.9	1			
0238+711	0238+711	1012	02	43	30.89131270	+71	20	17.9038869	.00005153	.0003877	-0.0463	49826.7	54088.1	3	0.21		
0242+131	0242+131	1422	02	44	45.69332857	+13	20	7.2212608	.00001940	.0005571	-0.2065	53561.6	53561.7	1			
0241+622	0241+622	732	02	44	57.69665828	+62	28	6.5155251	.00005530	.0003309	-0.0056	49930.6	56638.3	8			2.9
0242+238	0242+238	2500	02	45	16.85598139	+24	05	35.1701021	.00019432	.0029395	0.7131	50085.1	50156.1	2			
0242-113	0242-113	2501	02	45	24.95218762	-11	07	16.8126435	.00006240	.0016977	-0.5833	54112.1	54112.2	1			
0244-452	0244-452	2502	02	45	54.11076042	-44	59	39.6096324	.00006896	.0019184	-0.7963	54489.1	54489.1	1			
0243+354	J0246+35	2503	02	46	21.07627804	+35	36	37.9982245	.00001750	.0004099	-0.3972	54087.1	54087.2	1			
0244-297	0244-297	2504	02	46	21.46129215	-29	35	5.9216721	.00015256	.0046647	0.1151	50687.4	50687.5	1			
0244-128	0244-128	2505	02	46	58.46980998	-12	36	30.7976793	.00002180	.0007303	-0.4807	50575.8	50575.9	1			
0244+327	0244+327	1423	02	47	41.23226207	+32	54	31.8362165	.00001594	.0003797	-0.0544	53572.5	53572.6	1			
0245-167	0245-167	2506	02	48	7.73222009	-16	31	46.3860636	.00000953	.0003072	0.0866	50631.5	56701.1	2	0.18	0.21	
0245+043	0245+043	1424	02	48	14.82816234	+04	34	40.8581738	.00006908	.0033338	-0.3137	53560.5	53560.6	1			
0246+061	0246+061	1425	02	49	18.01610628	+06	19	51.9479075	.00001130	.0002197	-0.0538	49913.7	54643.5	2			
0248-266	0248-266	1426	02	50	35.56931854	-26	27	42.5188442	.00008404	.0031448	-0.5297	53133.8	53133.8	1	0.19	0.15	
0248+430	0248+430A	1211	02	51	34.53673338	+43	15	15.8294376	.00000772	.0001208	-0.1205	48719.9	55264.7	22	0.26	0.18	4.3
0248+560	0248+560	1212	02	51	54.62812753	+56	16	19.5233919	.00002422	.0002969	-0.1930	52408.8	53306.5	2			
0250-225	0250-225	2507	02	52	47.95365983	-22	19	25.4658421	.00001542	.0005216	0.0413	50631.5	50687.5	2			
0249+383	0249+383	2508	02	53	8.88808808	+38	35	24.9985318	.00001270	.0003095	-0.1426	50242.6	50242.8	1			
0252-549	P 0252-549	734	02	53	29.18041445	-54	41	51.4359465	.00001453	.0001721	0.4042	47626.3	54706.3	23			
0250+320	0250+320	1427	02	53	33.65014359	+32	17	20.8917481	.00001736	.0003433	0.1899	53523.6	55916.3	2	0.20	0.17	
0250+178	GC 0250+17	79	02	53	34.88224195	+18	05	42.5248161	.00001427	.0004605	-0.0371	48977.4	54142.9	17	0.18	0.10	
0250+508	0250+508	2509	02	53	57.60787866	+51	02	56.4555558	.00003278	.0004441	0.3737	49576.4	50305.5	2			
0251+235	0251+235	1428	02	54	24.71813805	+23	43	26.4744897	.00001257	.0003709	-0.1041	53560.6	53560.6	1			
0251+393	0251+393	1013	02	54	42.63207274	+39	31	34.7106879	.00001625	.0003517	0.0019	50242.6	50242.8	1		0.09	
0253-218	0253-218	2510	02	56	12.83892778	-21	37	29.1451229	.00001811	.0007720	-0.2199	50631.6	50687.5	2			
0253+133	0253+133	2511	02	56	34.98465893	+13	34	35.3456064	.00002789	.0010716	-0.5730	50085.1	50156.1	2			
0254-334	0254-334A	2512	02	56	42.60273735	-33	15	21.2772116	.00001525	.0003752	0.0091	52306.0	54362.2	8			
0252+657	0252+657	2513	02	57	1.34299406	+65	56	35.4268808	.00009648	.0008734	0.1149	49826.7	49826.8	1			
0255-124	0255-124	2514	02	57	41.00461779	-12	12	1.3794627	.00004494	.0013230	0.4780	53502.8	53502.8	1			
0254+185	0254+185	2515	02	57	45.62871081	+18	47	5.3569885	.00011487	.0034468	-0.7193	50085.2	50156.1	2			
0251+785	0251+785	2516	02	57	52.57018206	+78	43	47.0584760	.00017427	.0003305	-0.4037	49826.7	50688.3	2			
0254+434	0254+434	1429	02	57	59.07776129	+43	38	37.6745410	.00003142	.0004963	-0.1096	53552.6	53552.7	1			
0256-393	0256-393	2517	02	58	14.04486468	-39	09	40.6836401	.00003427	.0009276	0.3352	52306.1	52408.8	2			
0256-256	0256-256	1430	02	58	16.79547006	-25	29	58.7916883	.00005759	.0019710	-0.8555	53561.6	53561.6	1			
0256+054	0256+054	2518	02	58	50.52633472	+05	41	8.0390082	.00006319	.0017016	-0.3092	49914.5	49914.6	1			
0255+288	0255+288	2519	02	58	55.18115147	+29	00	1.6070093	.00005702	.0010885	-0.5375	53125.8	56498.7	3			
0256+075	OD 094.7	81	02	59	27.07662986	+07	47	39.6430006	.00000428	.0000890	-0.2185	45151.9	56707.0	107	0.33	0.23	3.1
0256-005	0256-005	2520	02	59	28.51616003	-00	19	59.9753809	.00000370	.0000581	0.0178	50575.8	56776.0	124	0.58	0.70	2.5
0256+192	0256+192	1432	02	59	29.65593799	+19	25	44.3271591	.00001303	.0003431	0.1010	53523.6	56749.0	2	0.15	0.18	
0256+423	0256+424	2521	02	59	37.69444119	+42	35	49.8115654	.00006662	.0006680	0.1941	50242.6	54112.2	2			
0257-057	0257-057	1433	03	00	1.30002792	-05	31	20.3608378	.00002762	.0006317	-0.4661	53152.7	53152.8	1			
0258-184	0258-184	2522	03	01	6.71658976	-18	12	17.7763946	.00151517	.0266003	0.8808	53561.6	53561.7	1			
0259-316	0259-316	1434	03	01	16.24428964	-31	26	15.7880920	.00003672	.0011883	0.0436	53125.8	53125.8	1			
0258-170	0258-170	1435	03	01	16.62300394	-16	52	45.0885233	.00036548	.0091933	0.6193	53560.6	53560.6	1			
0258+011	0258+011	1436	03	01	23.60693432	+01	18	35.9969618	.00002898	.0010041	-0.2576	49913.7	54664.4	2			
0258+058	0258+058	2523	03	01	33.71391182	+06	02	27.2824029	.00002034	.0006027	-0.1400	49913.7	49914.6	1			
0258+533	0258+533	1014	03	02	22.73529644	+53	31	46.4832244	.00016031	.0014287	0.2901	49576.4	49576.6	1	0.25		

Source Name		ID No.	Right Ascension			Declination			RA Error (s)	Dec. Error (arcsec)	RA–Dec Corr.	Observation Epoch MJD		No. Obs.	Source Flux (Jy)		Str Index
B1950	Common		H	M	S	D	M	S				First	Last		10-60	10-40	
0259+121	0259+121	670	03	02	30.54674463	+12	18	56.7511106	.00001695	.0004811	-0.3252	46709.6	53666.2	18			3.9
0301-243	0301-243	1437	03	03	26.50294190	-24	07	11.4249020	.00006635	.0017640	-0.5364	54657.6	54657.7	1			
0300+470	OE 400	82	03	03	35.24222555	+47	16	16.2755164	.00000359	.0000527	-0.0877	43808.6	56782.2	654	0.77	0.70	2.5
0302-623	P 0302-623	735	03	03	50.63140282	-62	11	25.5500099	.00001393	.0001035	0.1595	48387.5	56638.5	39			
0259+681	0259+681	2524	03	04	22.00383111	+68	21	37.4746159	.00004496	.0003311	0.3405	49826.7	49826.8	1			
0302-437	0302-437	1438	03	04	29.20213928	-43	33	16.0329536	.00008820	.0035686	0.7774	55042.5	55042.6	1			
0301+336	0301+336	2525	03	04	41.36245426	+33	48	43.5306159	.00001575	.0003722	0.0636	50219.7	50219.8	1			
0302+173	0302+173	2526	03	05	10.22422162	+17	34	59.0923206	.00003147	.0011333	-0.2872	50085.1	50156.1	2			
0303+051	0303+051	2527	03	05	48.19159990	+05	23	31.5280517	.00006282	.0014770	0.4156	49913.7	49914.6	1			
0302+625	0302+625	736	03	06	42.65955818	+62	43	2.0242408	.00000547	.0000632	0.0610	48613.2	56782.2	168	0.20		2.7
0305+237	0305+237	2528	03	08	11.78774654	+23	55	13.5478243	.02261688	.0093451	0.0627	53133.7	53133.7	1			
0305+039	0305+039	1015	03	08	26.22380333	+04	06	39.3008156	.00000495	.0000942	0.0108	50919.0	55334.1	17			
0307-362	0307-362	2529	03	09	2.51078738	-36	04	3.7529386	.00005073	.0017608	-0.0018	53502.8	55656.9	2			
0306+102	0306+102	671	03	09	3.62349733	+10	29	16.3409851	.00000448	.0000800	-0.2231	47255.0	56713.6	109	0.68	0.59	2.8
0306+274	0306+274	4056	03	09	22.09675793	+27	38	54.3609860	.00002104	.0006372	0.0025	56638.1	56638.3	1			
0306-061	0306-061	4057	03	09	23.28886630	-05	59	20.4512011	.00002841	.0012557	0.2776	55966.0	55966.1	1			
0308-611	0308-611	737	03	09	56.09916027	-60	58	39.0562672	.00000514	.0000614	0.1369	47625.6	56772.7	231			
0307-085	0307-085	1439	03	10	2.04908338	-08	23	39.2983162	.00018035	.0036165	0.8169	53152.7	53152.8	1			
0307+380	0307+380	1258	03	10	49.87992767	+38	14	53.8378373	.00000357	.0000546	0.0111	50242.6	56776.1	162	0.76	0.28	0.0
0312-770	0312-770	738	03	11	55.25020326	-76	51	50.8482657	.00016742	.0004810	0.6144	48110.1	53129.5	6			
0310+013	0310+013	2530	03	12	43.60323790	+01	33	17.5647025	.00001347	.0004659	-0.3242	49913.7	49914.6	1			
0309+411	0309+411	672	03	13	1.96212023	+41	20	1.1835037	.00000426	.0000643	-0.1271	46611.0	56701.3	136	0.36	0.39	2.1
0310+022	0310+022	1440	03	13	13.40546458	+02	28	35.3063456	.00001290	.0004416	-0.1414	53572.5	53572.6	1			
0312+100	0312+100	2531	03	15	21.13981738	+10	12	43.0837738	.00002026	.0003899	-0.2695	54278.5	56568.1	5			
0313-171	0313-171	2532	03	15	27.67839972	-16	56	29.7108172	.00009790	.0020319	0.2551	50631.6	50631.7	1			
0315-282	0315-282	2533	03	17	33.69720231	-28	03	18.5782213	.05297435	.3196406	-0.9969	54818.1	54818.1	1			
0314+565	0314+565	2534	03	17	54.94283137	+56	43	57.7913377	.00008138	.0008099	-0.0880	52408.8	52408.9	1			
0316-444	0316-444	4058	03	17	57.67944922	-44	14	17.1624692	.00006277	.0023044	-0.0737	56035.8	56638.2	4			
0315-006	0315-006	1441	03	18	14.42728566	-00	29	48.9330800	.00020436	.0026027	0.0103	53560.6	53560.6	1			
0316+162	0316+162	2535	03	18	57.80258716	+16	28	32.6987650	.00004408	.0008497	-0.0846	50085.1	50156.1	2			
0316-164	0316-164	1442	03	19	5.52804816	-16	13	47.0445617	.00005057	.0017274	-0.6411	54657.6	54657.7	1			
0314+696	0314+696	2536	03	19	22.07100766	+69	49	25.6184952	.00012201	.0006235	-0.5909	49826.7	54088.1	2			
0316+413	3C 84	87	03	19	48.16011958	+41	30	42.1044096	.00000722	.0001285	-0.0147	44088.7	56492.1	110	1.05	0.53	4.4
0317+188	P 0317+188	88	03	19	51.25672309	+19	01	31.2909170	.00000463	.0000859	-0.2904	48942.4	54886.6	97	0.30	0.23	3.0
0318-172	0318-172	1443	03	20	19.10752213	-17	02	39.1300723	.00008068	.0023200	-0.3584	54657.6	54657.7	1			
0318-388	0318-388	2537	03	20	46.40484004	-38	37	28.5134741	.00039736	.0195233	0.5708	52306.1	52408.8	2			
0319-315	0319-315	2538	03	21	28.74026172	-31	22	56.3360291	.00007374	.0029869	0.4334	52306.0	52306.1	1			
0318+438	0318+438	2539	03	21	36.86837940	+43	59	22.4816381	.00013065	.0014385	0.1798	50242.7	50242.8	1			
0319+121	P 0319+12	89	03	21	53.10350796	+12	21	13.9536951	.00000575	.0001299	-0.2455	49790.1	54713.6	24			
0319-056	0319-056	2540	03	21	59.87035825	-05	26	12.4290208	.00002335	.0006879	-0.0796	53152.7	53502.8	2			
0319-133	0319-133	4059	03	22	15.14714630	-13	12	58.1060590	.00003938	.0015239	-0.5186	56162.5	56162.6	1			
0317+659	0317+659	2541	03	22	27.22879160	+66	10	28.3003469	.00004452	.0003594	-0.2984	49826.7	54112.2	2			
0319+396	0319+396	1444	03	22	51.83003787	+39	48	2.2593269	.00001700	.0002696	0.1859	53561.6	56638.3	5			
0320+015	0320+015	2542	03	23	9.87231791	+01	45	50.5074642	.00002329	.0007306	-0.0692	49913.7	49914.6	1			
0320+045	0320+045	2543	03	23	14.72281544	+04	46	12.5755637	.00005506	.0021522	-0.3197	54087.1	54087.2	1			
0322-230	0322-230	2544	03	24	17.55321710	-22	54	17.9251607	.00002066	.0007458	-0.2224	53552.6	55538.3	2			
0321+340	0321+340	2545	03	24	41.16133410	+34	10	45.8573346	.00001689	.0004118	0.1500	50219.7	50219.8	1			
0322-294	0322-294	2546	03	24	44.29547456	-29	18	21.2211002	.00009170	.0038378	-0.5612	53502.8	53502.8	1			
0323-244	0323-244	2547	03	25	13.34466111	-24	15	48.0524275	.00001446	.0005057	-0.0155	50631.6	50687.5	2			
0321+467	0321+467	2548	03	25	20.30385980	+46	55	6.6351649	.00007809	.0011606	0.4355	50305.4	50305.5	1			

Source Name		ID No.	Right Ascension			Declination			RA Error (s)	Dec. Error (arcsec)	RA–Dec Corr.	Observation Epoch MJD		No. Obs.	Source Flux (Jy)		Str Index
B1950	Common		H	M	S	D	M	S				First	Last		10-60	10-40	
0322+222	0322+222	1017	03	25	36.81435515	+22	24	0.3655590	.00000348	.0000535	-0.0151	50085.1	56776.6	306	0.54	0.49	1.8
0324-379	0324-379	4060	03	26	3.00038304	-37	46	9.1880423	.00013005	.0055360	0.6479	56392.8	56392.9	1			
0325-182	0325-182	1445	03	27	43.34159996	-18	03	42.0229525	.00005946	.0024163	-0.4980	54657.6	54657.7	1			
	UGC02748	1018	03	27	54.19499096	+02	33	41.9827000	.00003388	.0009543	0.1338	53067.9	53067.9	1			
0325+005	0325+005	2549	03	27	59.21553001	+00	44	22.7271299	.00006405	.0011780	0.1294	49913.7	49914.6	1			
0325-222	0325-222	2550	03	27	59.92402811	-22	02	6.3958763	.00002146	.0007301	0.0146	50631.6	50687.5	2			
0325+256	0325+256	2551	03	28	44.34856387	+25	52	8.3982019	.00011532	.0018004	0.2490	54112.1	54112.2	1			
0325+395	0325+395	2552	03	28	50.31208172	+39	40	44.5665792	.00005386	.0009333	-0.7439	50242.7	56568.5	6			
0326+349	0326+349	2553	03	29	15.35489072	+35	10	5.9912685	.00001286	.0003216	0.1618	50219.7	50219.8	1			
0327-241	P 0327-241	2554	03	29	54.07556303	-23	57	8.7732593	.00001084	.0003663	-0.0569	50631.6	50687.5	2			
0326+277	0326+277	673	03	29	57.66942908	+27	56	15.4991405	.00000861	.0001311	-0.3937	46610.9	54643.6	35	0.19	0.11	4.3
0327+467	0327+467	2555	03	30	32.62733590	+46	56	23.2927705	.00001356	.0001812	0.0456	50305.4	56547.6	5			
0327+364	0327+364	2556	03	30	34.76570696	+36	39	41.0336294	.00026992	.0036054	0.0057	50242.7	50242.8	1			
0329-404	0329-404	1446	03	30	51.10394680	-40	14	16.6001996	.00005612	.0023387	0.3482	55042.5	55042.6	1			
0329-255	0329-255	1447	03	31	8.92058615	-25	24	43.2655003	.00003287	.0012953	-0.4170	53572.6	53572.6	1			
0329-110	0329-110	2557	03	31	50.75660110	-10	51	55.5034531	.00002604	.0009632	-0.4046	50575.8	50575.9	1			
0329+654	0329+654	2558	03	33	56.73723144	+65	36	56.1829988	.00034559	.0014415	0.6803	49826.9	55776.4	2			
0331+022	0331+022	739	03	34	9.94762037	+02	26	9.6486303	.00017531	.0027942	0.2102	50553.9	50800.1	3			
0332-403	P 0332-403	93	03	34	13.65449278	-40	08	25.3980206	.00000374	.0000565	-0.0506	43809.4	56776.5	287		1.18	2.3
0332-375	0332-375	1448	03	34	15.42497180	-37	25	43.0672335	.00005159	.0026165	-0.5921	54942.8	54942.9	1			
0332+078	0332+078	1449	03	34	53.31667923	+08	00	14.4190722	.00000534	.0001084	0.1037	49913.7	56748.5	82		0.18	
0334-546	0334-546	740	03	35	53.92484537	-54	30	25.1147986	.00001380	.0001713	0.3818	48388.3	56504.2	34			
0333-073	0333-073	1450	03	35	57.05518663	-07	09	55.8556328	.00014540	.0039872	-0.2655	53560.6	53560.7	1			
0333+321	NRAO 140	94	03	36	30.10760973	+32	18	29.3422230	.00000422	.0000688	-0.1135	43808.7	55236.7	134	0.67	0.85	3.7
0334-131	0334-131	2559	03	36	35.03581787	-13	02	4.6605887	.00001201	.0004152	-0.0438	50575.8	56749.0	2	0.30	0.30	
0334-207	0334-207	2560	03	36	45.61145431	-20	36	37.1726049	.00009469	.0027636	-0.5963	54087.2	54087.2	1			
0334+004	HR 1099	741	03	36	47.30305235	+00	35	16.6214083	.01280045	.0605703	0.9188	49987.3	50002.4	2			
0335-364	0335-364	742	03	36	54.02353169	-36	16	6.2241199	.00002131	.0004575	0.0677	50918.9	53079.9	9			
0334+014	0334+014	743	03	37	17.10811434	+01	37	22.7507433	.00035135	.0058516	0.7920	49177.6	53502.9	3			
0335-122	0335-122	2561	03	37	55.45157340	-12	04	4.5432527	.00018459	.0045393	0.2726	50575.8	54482.7	2			
0336-017	0336-017	1451	03	39	0.98625034	-01	33	17.6066900	.00007343	.0014097	0.3209	54187.0	54187.0	1			
0335+599	0335+599	2562	03	39	9.39287375	+60	08	56.9745352	.00028649	.0028233	0.4979	49576.5	49576.6	1			
0336-019	CTA 26	95	03	39	30.93778705	-01	46	35.8041788	.00000337	.0000516	-0.0125	44203.1	56762.6	1562	0.95	0.97	3.0
0336+539	0336+539	4061	03	40	6.49058358	+54	05	38.7759081	.00063712	.0043686	0.4486	56302.0	56302.2	1			
0336+473	0336+473	2563	03	40	10.78884178	+47	32	27.3150425	.00002405	.0005069	0.2063	50305.4	50305.5	1			
0338-030	0338-030	2564	03	40	32.59570678	-02	54	54.2304713	.00002416	.0008713	-0.3363	54112.1	54112.2	1			
0338-214	P 0338-214	744	03	40	35.60786341	-21	19	31.1721401	.00000456	.0000861	-0.0553	49973.1	56751.6	126	0.28		3.4
0337+337	0337+337	2565	03	41	9.97368961	+33	52	21.6456549	.00003714	.0006576	0.7051	50219.7	50219.8	1			
0338+480	0338+480	2566	03	42	10.35266957	+48	09	46.9410231	.00008580	.0015560	-0.5263	50305.4	50305.6	1			
0340-140	0340-140	2567	03	42	44.98789272	-13	54	51.6603092	.00002877	.0009671	0.1312	53561.6	55847.5	2			
0341-256	0341-256	2568	03	43	19.52400525	-25	30	17.4034007	.00007519	.0027554	-0.2036	50631.6	50687.5	2			
0340+362	J0343+3622	1019	03	43	28.95241183	+36	22	12.4296412	.00000508	.0000841	0.0314	50242.7	56720.0	67	0.29	0.23	2.5
0341+158	0341+158	745	03	44	23.17215955	+15	59	43.3691507	.00000611	.0001578	-0.1655	47381.4	56707.0	70	0.24	0.13	2.5
0339+683	0339+683	1452	03	44	41.44124978	+68	27	47.8111002	.00004433	.0003880	-0.3202	53572.5	53572.7	1	0.12		
0342+147	0342+147	674	03	45	6.41654204	+14	53	49.5581893	.00000452	.0000867	-0.1935	46337.6	56707.0	91	0.35	0.25	2.9
0342+538	0342+538	2569	03	46	34.50413351	+54	00	59.1092114	.00001135	.0001179	0.1113	52408.8	56701.2	5			
0344+199	0344+199	2570	03	47	29.55916261	+20	04	53.0438741	.00002962	.0009740	0.0567	50085.2	55856.2	4	0.09	0.08	
0344+558	0344+558	1453	03	47	56.81208462	+55	57	31.5785131	.00003074	.0002848	0.0756	53523.6	53523.9	1			
0344+235	0344+235	2571	03	47	57.11177215	+23	39	55.3222714	.00010316	.0025553	-0.8227	50085.1	50156.1	2			
0346-279	0346-279	1259	03	48	38.14457393	-27	49	13.5657126	.00000504	.0000687	-0.1816	50687.4	56758.6	112		0.58	2.3

Source Name		ID No.	Right Ascension			Declination			RA Error (s)	Dec. Error (arcsec)	RA–Dec Corr.	Observation Epoch MJD		No. Obs.	Source Flux (Jy)		Str Index
B1950	Common		H	M	S	D	M	S				First	Last		10-60	10-40	
0346-163	0346-163	2572	03	48	39.27073074	-16	10	17.7524591	.00001412	.0005033	-0.0890	50631.6	50631.7	1			
0345+416	0345+416	1454	03	48	45.12239240	+41	49	14.6759931	.00005641	.0007838	-0.3165	53152.7	53152.8	1			
0345+460	0345+460	1213	03	49	18.74157489	+46	09	59.6579301	.00000387	.0000575	-0.0319	50305.4	56762.6	173	0.28	0.30	3.1
0346+209	0346+209	2573	03	49	45.23011308	+21	04	45.9661945	.00014509	.0033728	-0.4281	50085.1	50156.1	2			
0347-211	0347-211	1455	03	49	57.82667566	-21	02	47.7415932	.00000526	.0000835	-0.0452	50631.6	56763.6	69			
0346+514	0346+514	2574	03	50	25.05153305	+51	38	38.7346364	.00010477	.0011613	-0.3998	52408.8	52408.9	1			
0348-326	0348-326	2575	03	50	43.31623719	-32	32	59.4284994	.00013570	.0046149	0.8917	52306.1	52306.1	1			
0348+049	0348+049	2576	03	50	54.20315939	+05	06	21.1875587	.00050286	.0036923	-0.3416	49913.7	49914.6	1			
0348-120	0348-120	2577	03	51	10.97693022	-11	53	22.6647503	.00003262	.0012070	-0.4653	50575.8	50575.9	1			
0348-031	0348-031	4122	03	51	15.36690664	-03	01	17.8021025	.00004327	.0012339	0.1672	55916.1	55916.3	1			
0350-253	0350-253	1456	03	52	11.05238818	-25	14	50.2686599	.00001741	.0006173	-0.3779	53560.6	53560.7	1			
0349+662	0349+662	2578	03	54	3.69926325	+66	21	26.1253512	.00011309	.0005767	0.4346	54087.3	54088.1	1			
0351+045	0351+045	2579	03	54	24.12890425	+04	41	7.2637576	.00004792	.0015792	-0.6268	49913.7	49914.6	1			
0352-164	0352-164	2580	03	54	25.02808144	-16	16	22.4470777	.00008651	.0025518	-0.5530	53502.8	53502.9	1			
0350+465	0350+465	1260	03	54	30.01164895	+46	43	18.7504654	.00001375	.0002342	0.0099	50305.6	53946.5	5	0.46	0.36	
0346+800	0346+800A	1214	03	54	46.12598426	+80	09	28.8477214	.00006232	.0003025	0.0248	50688.1	56701.5	2	0.18		
0355-669	0355-669	1261	03	55	47.88346221	-66	45	33.8172266	.00003175	.0001602	0.5432	52860.2	55784.6	24			
0353+289	0353+289	2581	03	56	8.46195237	+29	03	42.3212221	.00004141	.0013391	0.1930	50219.7	50219.8	1			
0352+605	0352+605	1021	03	56	25.19874794	+60	43	57.9797498	.00002414	.0001819	-0.0555	49576.5	56498.4	4	0.11		
0354+231	0354+231	1022	03	57	21.60988648	+23	19	53.8256483	.00001205	.0003123	-0.1400	50085.1	56659.2	13	0.39	0.37	
0355-483	0355-483	746	03	57	21.91794267	-48	12	15.1590232	.00014402	.0044991	0.8460	49330.7	52884.0	3			
0355-079	0355-079	2582	03	57	43.29326473	-07	51	14.5677453	.00002002	.0006798	-0.4528	50575.8	50575.9	1			
0355+055	0355+055	1023	03	57	46.12569597	+05	42	31.2579774	.00005966	.0009955	0.0811	49913.7	54664.4	2			
0354+559	0354+559	1215	03	58	30.18818851	+56	06	44.4604908	.00002401	.0002309	-0.0360	52408.8	53306.6	2			
0354+599	0354+599	2583	03	59	2.63993762	+60	05	22.0689402	.00004539	.0005126	0.0863	49576.5	49576.6	1			
0356-033	0356-033	2584	03	59	23.21125082	-03	10	34.0669190	.00238469	.0499686	-0.9793	53552.6	56393.0	2			
0356+278	0356+278	1457	03	59	27.93557451	+27	58	24.0474059	.00001496	.0004705	0.0649	53561.6	53561.7	1			
0355+508	NRAO 150	99	03	59	29.74728134	+50	57	50.1615976	.00000549	.0000749	-0.0794	44088.8	56772.2	130	2.34		2.0
0357-263	0357-263	2585	03	59	33.68178015	-26	15	31.3273347	.00012903	.0042213	-0.2977	50631.6	54643.4	3			
0356+322	0356+322	2586	03	59	44.91292151	+32	20	47.1558847	.00001280	.0002975	0.2544	50219.7	50219.8	1			
0357+057	0357+057	2587	04	00	11.73536335	+05	50	43.1229684	.00002752	.0007256	0.1152	49913.7	49914.6	1			
0358-162	0358-162	1458	04	01	6.63674466	-16	06	39.0122113	.00001977	.0007871	-0.1431	53572.6	53572.7	1			
0358+040	0358+040	1262	04	01	19.91294898	+04	13	34.4073946	.00001726	.0003409	-0.2286	53607.3	53608.5	1	0.37	0.34	1.4
0359-294	0359-294	2588	04	01	21.48366225	-29	21	26.8308353	.00018634	.0042813	0.6744	50687.4	50687.5	1			
0358+210	J0401+2110	1024	04	01	45.16607438	+21	10	28.5868266	.00000422	.0000811	-0.0640	50085.1	56636.8	77	0.23	0.21	0.8
0359-151	0359-151	1459	04	02	16.78727761	-14	58	20.9952966	.00004830	.0014377	-0.4482	53560.6	53560.7	1			
0400-319	P 0400-319	101	04	02	21.26599708	-31	47	25.9454497	.00000631	.0001057	-0.1866	49329.7	56728.5	58		0.49	3.0
0400+258	CTD 26	100	04	03	5.58607252	+26	00	1.5026456	.00000429	.0000727	-0.1766	44947.5	56684.1	106	0.70	0.50	3.0
0402-362	P 0402-362	102	04	03	53.74990238	-36	05	1.9131820	.00000372	.0000619	0.0845	43873.2	56749.1	680		0.90	2.4
0403-132	P 0403-13	103	04	05	34.00339140	-13	08	13.6908704	.00000400	.0000836	-0.1780	50459.3	56707.0	109	0.79	0.69	0.6
0402+379	0402+379	2589	04	05	49.26234579	+38	03	32.2352718	.00009215	.0009384	0.2594	50242.7	50242.8	1			
0403-179	0403-179	1460	04	06	12.24453126	-17	49	57.9275708	.00002157	.0007325	-0.1037	50631.6	54664.4	3			
0403+064	0403+064	2590	04	06	34.30728524	+06	37	14.9914527	.00018948	.0028951	-0.2039	49913.7	49914.6	1			
0404-240	0404-240	1461	04	06	39.34013041	-23	55	3.7856838	.00002904	.0011062	0.0034	54657.6	54657.7	1			
0405-385	P 0405-385	104	04	06	59.03533942	-38	26	28.0424095	.00000434	.0000705	-0.0861	49330.7	56755.6	310		0.54	2.3
0404+075	0404+075	2591	04	07	29.08671975	+07	42	7.4719698	.00002117	.0005711	0.4725	52408.8	52408.9	1			
0405-331	0405-331	2592	04	07	33.91372867	-33	03	46.3579422	.00001619	.0005774	0.0222	52306.1	56267.2	2		0.25	
0405-123	P 0405-12	105	04	07	48.43098651	-12	11	36.6595278	.00000436	.0001041	-0.0460	50209.6	56699.0	84	0.49	0.21	3.1
0402+682	0402+682	2593	04	07	49.16549802	+68	21	31.6351849	.00095924	.0037629	-0.5907	49826.8	49827.0	1			
0405-015	0405-015	4062	04	08	18.53414866	-01	22	34.8947670	.00002825	.0008476	0.2122	55966.0	55966.2	1			

Source Name		ID No.	Right Ascension			Declination			RA Error (s)	Dec. Error (arcsec)	RA–Dec Corr.	Observation Epoch MJD		No. Obs.	Source Flux (Jy)		Str Index
B1950	Common		H	M	S	D	M	S				First	Last		10-60	10-40	
0405+304	0405+305	748	04	08	20.37758807	+30	32	30.4904741	.00001907	.0004677	0.4034	49032.8	54142.9	22	0.08		1.8
0407-658	0407-658	747	04	08	20.37468767	-65	45	9.0753074	.00514857	.0217268	-0.1325	50258.9	50259.5	1			
0406-056	0406-056	2594	04	08	59.64995910	-05	29	40.5388572	.00001694	.0005961	-0.1929	50575.8	53502.9	2			
0406-127	0406-127	749	04	09	5.76972855	-12	38	48.1438251	.00000466	.0001047	-0.2595	46797.3	56770.2	117	0.32	0.26	3.1
0406+121	GC 0406+12	107	04	09	22.00870653	+12	17	39.8477139	.00000451	.0000845	-0.3277	44203.1	56707.0	108	0.27	0.19	2.9
0406+065	0406+065	1462	04	09	25.84774317	+06	40	35.1026504	.00003075	.0007800	-0.3037	53561.6	53561.7	1			
0407-170	0407-170	2595	04	09	37.33404923	-16	55	35.5314215	.00024745	.0064919	-0.5770	50631.6	50631.7	1			
0407-199	0407-199	2596	04	09	40.54919813	-19	48	1.7824748	.00005541	.0020352	0.6354	54112.1	55371.7	2			
0403+768	4C 76.03	2597	04	10	45.61079236	+76	56	45.3109470	.00014680	.0008526	-0.1965	52408.8	52408.9	1			
0409-280	0409-280	2598	04	11	25.23210165	-27	58	20.8114910	.00002202	.0007732	-0.3444	55413.6	55413.6	1			
0408+085	0408+085	4063	04	11	33.85754322	+08	43	11.4166311	.00002911	.0006145	0.6479	56748.9	56749.0	1			
0409+000	0409+000	2599	04	12	33.45637795	+00	10	48.4917040	.00013104	.0050695	0.1041	49913.7	49914.6	1			
0409+045	0409+045	2600	04	12	38.18707673	+04	38	6.0359238	.00008957	.0020517	0.5721	49913.7	49914.6	1			
0409+229	P 0409+22	109	04	12	43.66686945	+23	05	5.4527237	.00000576	.0001124	-0.1300	50085.1	54664.6	26	0.17	0.22	3.4
0409+188	0409+188	2601	04	12	45.94418633	+18	56	37.0766328	.00003175	.0006689	0.4981	50085.1	50156.1	2			
0411-063	0411-063	2602	04	13	28.23950673	-06	15	1.4867542	.00019917	.0061034	-0.6047	53152.7	53152.8	1			
0409+527	0409+527	1463	04	13	37.08641459	+52	50	52.9446496	.00003869	.0006260	0.2823	53572.6	53572.7	1			
0410+110	0410+110	1464	04	13	40.34099543	+11	12	14.7860271	.00001053	.0002603	-0.2172	54314.5	56568.7	5			
0411+341	0411+341	2603	04	14	37.25575185	+34	18	51.2065058	.00002457	.0006311	-0.0016	50218.8	50218.9	1			
0411+054	0411+054	2604	04	14	37.76784206	+05	34	42.3421559	.00023314	.0067073	-0.3218	49913.7	54314.6	2			
0412+447	J0415+4452	1025	04	15	56.52652629	+44	52	49.6835417	.00002291	.0003716	-0.1739	50305.6	53613.4	2	0.34		
0413-210	0413-210	2605	04	16	4.35973486	-20	56	27.5183080	.00001099	.0003667	-0.1972	50631.6	50687.5	2			
0414-341	0414-341	2606	04	16	10.05432511	-34	03	3.9591259	.00044991	.0091146	0.5594	52306.1	52306.2	1			
0414-337	0414-337	2607	04	16	20.51036578	-33	39	32.3668328	.00031110	.0120699	0.8429	52306.1	52306.2	1			
0414-189	P 0414-189	112	04	16	36.54444980	-18	51	8.3402569	.00000422	.0000676	-0.0205	49790.0	56644.7	99	0.39	0.31	1.8
0414+548	0414+548	2608	04	18	19.52227150	+54	57	15.2741231	.01148297	.0069834	-0.7776	49576.5	49576.5	1			
0415+379	3C 111	1026	04	18	21.27721043	+38	01	35.8001615	.00001075	.0001510	0.2512	51464.1	52408.9	5	0.53	0.51	
0416-216	0416-216	2609	04	19	0.41814383	-21	32	35.6756142	.00031778	.0078612	0.8633	54112.2	54112.2	1			
0415+572	0415+572	2610	04	19	19.41299126	+57	22	59.9857462	.00014372	.0013383	0.5171	49576.5	49576.6	1			
0415+398	0415+398	1465	04	19	22.54951707	+39	55	28.9775466	.00000472	.0000694	0.0363	50242.7	56755.0	73	0.23	0.21	1.6
0417-302	0417-302	2611	04	19	47.20496206	-30	10	23.8506305	.00014213	.0039401	-0.1492	52306.1	55483.4	3			
0418-151	0418-151	2612	04	20	18.39334711	-15	01	26.5766854	.00001638	.0005974	-0.1607	50631.6	50631.7	1			
0418+437	0418+437	1466	04	21	51.77491309	+43	52	10.4294830	.00004852	.0007373	-0.1650	53560.6	53560.7	1			
0419+308	0419+308	2614	04	22	21.22391378	+30	58	9.7146053	.00018468	.0020219	0.7251	54087.2	54087.3	1			
0418+532	0418+532	1467	04	22	44.39890220	+53	24	26.2632260	.00003460	.0004927	0.2864	49576.5	54482.6	2			
0420-206	0420-206	2615	04	22	48.46166436	-20	34	56.0092429	.00114899	.0285579	0.2592	53561.6	53561.7	1			
0420+022	0420+022	1263	04	22	52.21465152	+02	19	26.9307652	.00000370	.0000582	0.0216	49913.7	56750.7	89	0.86	0.41	
0420+210	0420+210	1468	04	23	1.98840921	+21	08	2.1270584	.00002103	.0003863	0.1369	52479.8	52480.7	1			
0420-014	P 0420-01	116	04	23	15.80072492	-01	20	33.0655342	.00000342	.0000530	-0.0710	43873.3	56776.7	928	2.23	2.22	2.5
0420+417	VRO 41.04.01	115	04	23	56.00979228	+41	50	2.7129330	.00000501	.0000772	-0.0222	44203.1	56707.0	76	0.82	0.81	3.3
0421+019	0421+019	2616	04	24	8.56202688	+02	04	24.9647758	.00001431	.0004875	-0.1957	49913.7	49914.6	1			
0421+145	0421+145	2617	04	24	23.49066781	+14	42	16.6827936	.00005493	.0008395	-0.1044	50085.2	54440.4	3			
0422-389	0422-389	1469	04	24	33.71640908	-38	48	41.6218571	.00023159	.0108673	-0.0564	54964.8	54964.9	1			
0422-380	0422-380	750	04	24	42.24370891	-37	56	20.7843315	.00000589	.0001040	0.0221	48387.4	56701.2	59		0.62	4.1
0422+004	P 0422+00	118	04	24	46.84206444	+00	36	6.3293189	.00000397	.0000751	-0.0570	50254.8	56758.8	72	0.76	0.41	2.0
0422+079	0422+079	1470	04	24	57.60285919	+08	05	17.3267555	.00001040	.0003482	-0.0903	53572.6	53572.7	1			
0423-163	0423-163	2618	04	25	53.57252775	-16	12	40.2504406	.00028406	.0067911	0.6168	50631.6	50631.7	1			
0423+297	0423+297	2619	04	26	30.22612880	+29	52	22.9332851	.00004113	.0008557	-0.1225	54112.1	54112.2	1			
0423+051	P 0423+051	120	04	26	36.60409902	+05	18	19.8723021	.00000774	.0002108	0.0144	49254.4	54937.4	14			
0421+683	0421+683	1027	04	26	50.07012227	+68	25	52.9292816	.00004116	.0002203	-0.3871	49827.0	55916.4	2	0.10		

Source Name		ID No.	Right Ascension			Declination			RA Error (s)	Dec. Error (arcsec)	RA–Dec Corr.	Observation Epoch MJD		No. Obs.	Source Flux (Jy)		Str Index
B1950	Common		H	M	S	D	M	S				First	Last		10-60	10-40	
0423+233	GC 0423+23	119	04	26	55.73479179	+23	27	39.6337635	.00001754	.0005174	-0.4240	50085.2	53087.6	9			
0423+237	0423+237	1471	04	26	55.96944071	+23	50	26.5926338	.00039484	.0091132	-0.4133	50155.9	54313.8	2			
0425-071	0425-071	1472	04	27	26.15924207	-07	00	31.2634281	.00001019	.0003229	-0.1790	53502.8	53560.7	2			
0424+414	0424+414	2620	04	27	46.04553422	+41	33	1.0992798	.00001296	.0002468	0.2500	50242.7	50242.8	1			
0425+048	P 0425+048	121	04	27	47.57052260	+04	57	8.3257515	.00001008	.0002055	-0.7158	46609.5	53854.1	39	0.18	0.15	3.2
0424+328	0424+328	2621	04	28	5.80873176	+32	59	52.0437351	.00002419	.0005520	-0.4198	50218.8	50218.9	1			
0425+174	0425+174	1473	04	28	35.63367856	+17	32	23.5877868	.00002073	.0003880	-0.1966	50085.2	54643.5	3			
0426-380	P 0426-380	122	04	28	40.42427344	-37	56	19.5805451	.00000919	.0001304	-0.2111	50258.8	55168.6	16		1.02	4.1
0424+670	0424+670	2622	04	29	5.97572102	+67	10	16.8672778	.10013334	.9605288	-0.9904	49826.9	49826.9	1			
0426+332	0426+332	1474	04	29	52.72113417	+33	19	1.8582863	.00002335	.0004124	-0.2726	53523.7	53523.9	1			
0426+273	0426+273	751	04	29	52.96076608	+27	24	37.8762076	.00000404	.0000750	-0.0254	50218.8	56751.5	91	0.57	0.44	2.6
0428+205	0428+205	2623	04	31	3.76136011	+20	37	34.2644152	.00007831	.0014676	-0.1257	52306.1	52306.2	1			
0428-042	0428-042	1475	04	31	28.08855636	-04	06	27.3192307	.00005000	.0013111	-0.1305	53552.6	53552.8	1			
0429+174	0429+174	1028	04	31	57.37925670	+17	31	35.7753552	.00004180	.0011589	-0.6379	50085.2	50156.1	2		0.20	
0431-512	P 0431-512	2624	04	32	21.17819551	-51	09	25.1878590	.00023882	.0033113	0.8842	48749.4	52941.0	3			
0430-163	0430-163	2625	04	32	29.08228760	-16	14	5.6689493	.00001909	.0006493	-0.5011	53502.8	53502.9	1			
0429+415	3C 119	2626	04	32	36.50261902	+41	38	28.4489703	.00001928	.0004191	0.0648	50242.7	50242.8	1			
0430-332	0430-332	2627	04	32	44.56426536	-33	09	11.9326352	.00005524	.0021976	0.5082	52306.1	55847.5	2		0.10	
0430+052	3C 120	125	04	33	11.09552986	+05	21	15.6192092	.00000441	.0000915	-0.0181	43808.6	56679.6	118	0.38	0.25	4.3
0432-606	0432-606	2628	04	33	34.10843149	-60	30	13.7694546	.00004438	.0008073	0.3836	54722.9	54723.1	1			
0430+289	0430+289	752	04	33	37.82986132	+29	05	55.4769895	.00000381	.0000628	0.0031	50042.9	56758.3	141	0.25	0.23	
0432-148	0432-148	2629	04	34	19.02509341	-14	42	55.3577660	.00001775	.0006130	-0.2425	50631.6	50631.7	1			
0432+254	0432+254	2630	04	35	34.58296939	+25	32	59.6977129	.00008700	.0024649	0.4509	50218.8	50218.9	1			
0434-188	P 0434-188	126	04	37	1.48273484	-18	44	48.6136092	.00000413	.0000802	-0.4885	44227.3	56751.6	381	0.26	0.40	3.3
0433+295	0433+295	2631	04	37	4.37533451	+29	40	13.8184903	.00003084	.0004444	-0.0198	52408.9	55657.1	2			
0435-300	0435-300	1476	04	37	36.56868726	-29	54	4.1182416	.00002149	.0007015	-0.2044	53523.8	53523.8	1			
0434+299	0434+299	2632	04	38	4.94831117	+30	04	45.5177114	.00001595	.0004543	-0.3161	50218.8	50218.9	1			
0436-129	0436-129	1477	04	38	35.02100664	-12	51	3.3590386	.00000487	.0000965	0.0481	50575.8	56749.1	71	0.24	0.17	
0436-089	0436-089	2633	04	38	37.87657963	-08	48	21.5084397	.00021012	.0029611	0.3272	50575.8	50576.0	1			
0436-203	0436-203	2634	04	38	50.48944007	-20	12	26.3929091	.00015918	.0044583	-0.6833	50631.6	50687.6	2			
0435+217	0435+217	1478	04	38	55.88495305	+21	53	10.3070094	.00002129	.0005572	-0.0565	53560.6	53560.7	1			
0437-454	P 0437-454	753	04	39	0.85467623	-45	22	22.5630958	.00000777	.0001109	0.1433	49329.7	56772.1	42		0.09	2.2
0436+052	0436+052	1479	04	39	2.26218459	+05	20	43.6739846	.00003529	.0007539	0.1110	53133.8	53133.9	1			
0436+306	0436+306	2635	04	39	17.77455956	+30	45	7.5520412	.00002129	.0006196	-0.2636	50218.8	50218.9	1			
0437-303	0437-303	2636	04	39	53.20156975	-30	17	45.6227427	.00021783	.0063216	0.9043	52408.8	52408.9	1			
0436+426	J0440+4244	1029	04	40	7.87161354	+42	44	40.2579183	.00001598	.0003197	0.2015	50242.7	50242.8	1			
0438-436	P 0438-43	127	04	40	17.17996766	-43	33	8.6039527	.00000851	.0001265	0.0172	43809.4	56741.7	74		0.21	
0437+145	0437+145	1480	04	40	21.13936012	+14	37	56.9517779	.00005873	.0012277	0.0156	53125.8	53125.9	1			
0437+273	0437+273	2637	04	40	27.73946460	+27	28	40.6813731	.00008654	.0019584	-0.3115	50218.8	50218.9	1			
0439-337	P 0439-337	2638	04	41	33.76803532	-33	40	3.9171474	.00007106	.0016218	-0.2769	52306.1	52306.2	1			
0440-285	0440-285	2639	04	42	37.65719518	-28	25	30.8364586	.00002140	.0007779	-0.0347	50687.6	50687.7	1			
0440-003	NRAO 190	129	04	42	38.66073489	-00	17	43.4206413	.00000429	.0001044	-0.2454	43873.3	56695.7	77	0.58	0.41	2.9
0440+345	0440+345	675	04	43	31.63519856	+34	41	6.6641022	.00000461	.0000744	-0.0902	46757.5	56737.8	65	0.17	0.16	2.8
0441+106	P 0441+106	2640	04	44	12.46602679	+10	42	47.2655622	.00013192	.0046666	-0.7891	49913.7	49914.6	1			
0442+071	0442+071	2641	04	45	1.42875735	+07	15	53.9128261	.00005431	.0017592	-0.6611	49913.7	49914.6	1			
0438+785	0438+785	4064	04	45	46.30643552	+78	38	58.1322649	.00740624	.0248135	0.8335	56392.9	56392.9	1			
0442+389	0442+389	1481	04	46	11.49404243	+39	00	17.1000244	.00000664	.0001185	0.3326	50242.7	56751.3	42	0.19	0.09	2.4
0445-221	0445-221	2642	04	47	37.28141582	-22	03	36.8216888	.00010071	.0023651	0.1613	52408.8	55616.1	2			
0446-212	0446-212	1482	04	48	17.38173137	-21	09	44.8304728	.00009120	.0020905	0.5875	53560.6	53560.7	1			
0443+592	0443+592	2643	04	48	20.48032765	+59	21	49.7107960	.01917113	.6943364	0.9833	53125.7	53125.7	1			

Source Name		ID No.	Right Ascension			Declination			RA Error (s)	Dec. Error (arcsec)	RA–Dec Corr.	Observation Epoch MJD		No. Obs.	Source Flux (Jy)		Str Index
B1950	Common		H	M	S	D	M	S				First	Last		10-60	10-40	
0445+097	0445+097	1483	04	48	21.73841135	+09	50	51.4607859	.00002194	.0005245	0.0628	53523.7	53523.9	1			
0446-265	0446-265	2644	04	48	23.96384892	-26	26	14.8389773	.00005503	.0024181	-0.1723	54112.2	55518.4	2			
0445+364	0445+364	2645	04	48	35.16160030	+36	29	31.4160169	.00002828	.0005761	0.5165	50242.7	50242.8	1			
0450-743	0450-743	754	04	48	48.55782458	-74	17	31.2478895	.00112112	.0031736	0.8305	48589.5	52884.1	3			
0446-096	0446-096	2646	04	48	49.46978718	-09	35	31.5066775	.00013543	.0090610	-0.5120	53572.6	53572.7	1			
0446+113	0446+113	2647	04	48	50.41216592	+11	27	54.3681024	.00007746	.0019361	-0.7295	49913.7	49914.6	1			
0446+112	P 0446+11	131	04	49	7.67110226	+11	21	28.5963214	.00000351	.0000539	-0.0373	47255.1	56758.7	275	0.89	0.93	2.4
0446+178	0446+178	1484	04	49	12.51167651	+17	54	31.5968352	.00009298	.0016986	-0.2644	53133.8	53133.9	1			
0444+634	0444+634	755	04	49	23.31057069	+63	32	9.4340136	.00000796	.0000729	-0.0903	49422.0	53946.9	11	0.40		2.0
0448-392	P 0448-392	2648	04	49	42.25472669	-39	11	9.4716376	.00003012	.0009006	-0.1228	52306.1	52408.9	2			
0447-010	0447-010	1485	04	49	42.90597232	-00	57	22.3526755	.00003233	.0009558	-0.5911	53561.6	53561.7	1			
0454-810	P 0454-81	756	04	50	5.44023880	-81	01	2.2313491	.00002008	.0000691	0.0110	47625.6	56637.7	48			
0446+462	0446+462	2649	04	50	30.80177665	+46	20	59.7966689	.00016035	.0016044	0.1299	55412.8	55413.5	1			
0448-187	0448-187	2650	04	50	35.90964015	-18	37	0.4079885	.00001436	.0004957	-0.1474	50631.6	50687.7	2			
0447+408	0447+408	2651	04	50	43.67960399	+40	56	13.9676823	.00003226	.0004998	0.4529	52408.7	52408.8	1			
0447+227	0447+227	1486	04	50	51.94471202	+22	49	5.8989084	.00001676	.0004228	-0.2058	53551.8	53552.6	1	0.09	0.11	
0446+595	0446+595	1264	04	51	18.72177466	+59	35	32.1835494	.00001540	.0001300	0.1130	53767.8	56701.3	2	0.13		
0449+125	0449+125	4123	04	52	42.60116390	+12	36	24.5901505	.00003681	.0006264	-0.2224	55775.7	55776.5	1			
0450+013	0450+013	1487	04	53	2.23862790	+01	28	35.6284799	.00001424	.0003606	0.2553	53125.8	56204.6	2	0.25	0.20	
0451-282	P 0451-28	132	04	53	14.64679783	-28	07	37.3267001	.00000507	.0000872	-0.2761	44227.3	56671.6	60		0.41	3.3
0452+068	0452+068	2652	04	55	20.71265448	+06	55	38.8749820	.00004847	.0011941	-0.2944	53560.6	56162.7	2			
0454-463	P 0454-46	757	04	55	50.77253057	-46	15	58.6797965	.00001311	.0001894	0.1682	49015.2	56776.2	18			
0454-220	0454-220	1488	04	56	8.92352881	-21	59	9.3940377	.00010201	.0020940	-0.2113	54657.6	54657.7	1			
0454+039	0454+039	2653	04	56	47.17473658	+04	00	52.9466117	.00003090	.0011553	0.4898	49913.7	49914.6	1			
0454-234	0454-234	758	04	57	3.17922779	-23	24	52.0202731	.00000340	.0000527	-0.0537	46844.9	56776.7	1843	1.01	1.39	1.9
0454+066	0454+066	2654	04	57	7.70995252	+06	45	7.2603263	.00002285	.0006447	0.1784	49913.7	49914.6	1			
0454-088	0454-088	2655	04	57	20.21285375	-08	49	5.4857233	.00006635	.0014392	0.2426	50575.8	50576.0	1			
0455-183	0455-183	1489	04	57	54.32520658	-18	19	16.0732714	.00004479	.0017541	0.2337	53561.7	53561.7	1			
0456+060	0456+060	1490	04	58	48.77157433	+06	08	3.8604009	.00002178	.0008879	-0.2669	54124.9	54125.7	1			
0454+550	0454+550	1030	04	58	54.83994065	+55	08	42.0576037	.00012012	.0011628	0.5538	49576.5	49576.6	1	0.20		
0456+310	0456+310	2656	04	59	33.03371370	+31	06	34.2874493	.00002557	.0006831	-0.0493	50218.9	50219.0	1			
0457+024	P 0457+024	136	04	59	52.05066363	+02	29	31.1766729	.00000884	.0001444	0.0756	49098.8	55118.6	51	0.30		4.2
0456+428	0456+428	2657	05	00	27.47287051	+42	53	30.8551369	.00018128	.0015181	-0.6520	52408.8	52409.0	1			
0458-020	P 0458-02	137	05	01	12.80988186	-01	59	14.2563327	.00000337	.0000520	-0.1098	47415.5	56772.7	1683	0.88	0.85	2.6
0458+138	P 0458+138	138	05	01	45.27082982	+13	56	7.2203415	.00000578	.0001351	0.0338	46757.4	56627.2	55	0.17	0.08	2.9
0456+714	0456+714	1491	05	01	45.77991645	+71	28	33.9634517	.00006351	.0003914	-0.0821	53133.7	53133.9	1			
0459-139	0459-139	1492	05	01	59.94482792	-13	55	4.8246345	.00009429	.0023914	0.2520	53552.7	53552.8	1			
0459+060	GC 0459+06	139	05	02	15.44594158	+06	09	7.4943955	.00001292	.0002684	-0.6389	47379.5	53771.3	29	0.18	0.24	3.5
0459+387	0459+387	2658	05	02	32.49293059	+38	49	54.9414548	.00011175	.0010086	-0.3663	52408.9	52409.0	1			
0459+135	P 0459+135	1031	05	02	33.21951435	+13	38	10.9588403	.00000798	.0002361	0.0495	50085.2	53542.8	6	0.19	0.19	
0459+415	0459+415	2659	05	02	37.98819598	+41	39	19.3480614	.00001913	.0002990	-0.4285	52408.9	52409.0	1			
0500-357	0500-357	2660	05	02	44.36653064	-35	41	14.7908986	.00041394	.0215699	0.7732	52306.2	53125.9	3			
0459+252	0459+252	1493	05	02	58.47475585	+25	16	25.2756415	.00001620	.0003770	0.0279	54124.9	56498.6	2	0.18	0.21	3.0
0500+019	0500+019	141	05	03	21.19718285	+02	03	4.6764606	.00001244	.0002793	-0.4070	47255.1	52403.1	17	0.10	0.11	4.3
0501-215	0501-215	2661	05	03	48.08956231	-21	28	31.3344804	.00017865	.0091410	-0.2175	52408.8	52408.9	1			
0500+443	0500+443	2662	05	03	50.22393803	+44	24	39.3815198	.00002859	.0003914	-0.3707	52408.9	52409.0	1			
0501-067	0501-067	2663	05	03	56.05016167	-06	38	3.5193617	.00108955	.0277467	-0.9635	53572.6	53572.7	1			
0500+339	0500+339	2664	05	03	56.78503902	+34	03	28.1153113	.00031415	.0023728	0.2971	50218.9	50219.0	1			
0503-608	P 0503-608	759	05	04	1.70112925	-60	49	52.5394518	.00003330	.0002284	0.4328	48110.0	54706.3	17			
0502-152	0502-152	1494	05	04	28.79717186	-15	12	26.8505783	.00005663	.0016106	-0.3756	54853.1	54853.2	1			

Source Name		ID No.	Right Ascension			Declination			RA Error (s)	Dec. Error (arcsec)	RA–Dec Corr.	Observation Epoch MJD		No. Obs.	Source Flux (Jy)		Str Index
B1950	Common		H	M	S	D	M	S				First	Last		10-60	10-40	
0502+049	P 0502+049	142	05	05	23.18472404	+04	59	42.7243653	.00000427	.0000787	-0.1803	47379.5	56684.1	95	0.40	0.32	3.4
0503-043	0503-043	2665	05	05	51.23832999	-04	19	26.6178644	.00009348	.0034039	0.0787	54112.2	54112.2	1			
0503-163	0503-163	1495	05	05	57.16065621	-16	15	58.0075849	.00007492	.0023845	-0.8017	53560.6	53560.7	1			
0503+216	0503+216	1496	05	06	34.03335663	+21	41	0.1597781	.00002082	.0005740	-0.1507	53561.6	53561.8	1			
0506-612	P 0506-61	760	05	06	43.98875006	-61	09	40.9939396	.00001178	.0000972	0.0462	48110.1	56741.7	84			
0504-099	0504-099	2666	05	06	53.04674798	-09	50	42.1717205	.05470580	.9941439	-0.9980	54087.3	54087.3	1			
0503+466	0503+466	2667	05	07	23.65882976	+46	45	42.3386614	.00002639	.0005160	-0.2157	50305.6	50305.7	1			
0503+608	0503+608	2668	05	08	27.25942335	+60	56	27.3366813	.00007193	.0004833	0.0279	53503.0	56749.2	2			
0454+844	0454+844	676	05	08	42.36350322	+84	32	4.5440565	.00001499	.0000550	-0.0577	45301.0	56463.7	335	0.19		2.9
0505+354	0505+354	2669	05	09	5.84612778	+35	28	17.2863872	.00002710	.0006221	0.0270	50242.7	50242.8	1			
0506+056	0506+056	1265	05	09	25.96448317	+05	41	35.3333472	.00000900	.0002509	0.0837	49913.7	56701.2	3	0.49	0.29	
0506+101	P 0506+101	677	05	09	27.45706560	+10	11	44.6000879	.00000380	.0000711	-0.1585	46757.4	56770.4	153	0.33	0.37	1.3
0507+179	P 0507+17	678	05	10	2.36913125	+18	00	41.5815931	.00000440	.0000723	-0.2392	46336.5	56701.4	109	0.60	0.57	2.9
0508-317	0508-317	1497	05	10	46.34090195	-31	42	53.9294443	.00002091	.0007641	-0.2594	53523.8	53523.8	1			
0508+138	0508+138	1033	05	11	38.31968904	+13	57	19.1936733	.00000684	.0002058	-0.0907	50085.2	56707.0	34	0.26	0.17	
0508+264	0508+264	2670	05	11	50.37151126	+26	31	54.8662045	.00003393	.0011756	0.1986	54112.2	54112.3	1			
0509+011	0509+011	2671	05	11	57.61254497	+01	10	49.4338298	.00012020	.0032326	-0.4119	49913.7	49914.6	1			
0509+205	J0512+20	2672	05	12	39.07523422	+20	37	42.8040305	.00002144	.0006042	0.0441	53560.7	56162.7	2			
0509+152	P 0509+152	2673	05	12	41.01286852	+15	17	23.4795456	.00004319	.0006590	0.4468	50085.2	50156.1	2			
0509+293	0509+293	1498	05	12	42.20586730	+29	27	3.6107872	.00004651	.0008145	0.4337	53561.6	53561.8	1			
0509+406	0509+406	2674	05	12	52.54281217	+40	41	43.6205213	.00001519	.0001964	-0.4379	52408.9	52409.0	1			
0511+009	0511+009	2675	05	13	40.03254092	+01	00	21.6537040	.00002328	.0007373	-0.0946	49913.7	49914.6	1			
0511-203	0511-203	2676	05	13	42.85847553	-20	16	11.4911160	.00007338	.0033116	-0.3410	54087.3	54087.3	1			
0511-220	P 0511-220	143	05	13	49.11432362	-21	59	16.0921246	.00000995	.0001987	-0.6796	46797.4	53854.1	39	0.28	0.65	2.8
0512-205	0512-205	1499	05	14	17.34744969	-20	29	20.5111238	.00003093	.0008325	-0.7204	53552.7	53552.8	1			
0510+559	0510+559	2677	05	14	18.69965182	+56	02	11.0539736	.00017517	.0010825	0.1447	49576.5	54664.2	2	0.21		
0515-674	0515-674	2678	05	15	37.53673440	-67	21	27.8400586	.00461711	.0161873	0.6055	48589.5	48589.8	1			
0514-459	0514-459	1500	05	15	45.25021134	-45	56	43.1958984	.00006144	.0024899	0.4863	54942.9	54943.0	1			
0514-161	0514-161	2679	05	16	15.92934601	-16	03	7.6346403	.00002798	.0008008	-0.0800	50631.6	54482.0	2			
0517-726	0517-726	761	05	16	37.71901557	-72	37	7.4661263	.00024800	.0008520	0.8235	48589.5	53143.5	5			
0513+276	0513+276	1501	05	16	40.47721370	+27	43	10.2774384	.00005888	.0009531	0.3932	53125.8	53126.0	1			
0516-621	0516-621	762	05	16	44.92618524	-62	07	5.3892892	.00001075	.0000994	0.0804	48589.5	56709.6	36			
0514+109	0514+109	2680	05	16	46.64627681	+10	57	54.7867489	.00002045	.0007050	0.1609	49913.7	54482.6	2			
0514+074	0514+074	2681	05	16	56.36469255	+07	32	53.2507329	.00002460	.0006453	-0.1497	53561.7	55616.2	2			
0514-156	0514-156	2682	05	16	57.18539059	-15	37	10.3678280	.00003362	.0012207	0.3931	53572.6	55966.2	2			
0515-179	0515-179	1502	05	17	24.04696564	-17	56	24.1479328	.00008814	.0025890	-0.4500	53561.7	53561.7	1			
0515-053	0515-053	1503	05	17	28.11016203	-05	20	40.8414335	.00002061	.0007526	0.1124	53523.8	53560.7	2			
0513+455	0513+455	2683	05	17	28.89947835	+45	37	4.8649900	.00003021	.0004079	0.0003	50305.6	50305.7	1			
0515+067	P 0515+067	2684	05	17	51.34416267	+06	48	3.2102841	.00002209	.0006203	-0.2040	49913.7	49914.6	1			
0515+208	0515+208	1034	05	18	3.82451592	+20	54	52.4974207	.00000436	.0000867	-0.0662	50085.2	56734.7	62	0.24	0.26	
0514+330	0514+330	1035	05	18	5.14244455	+33	06	13.3649265	.00002584	.0005647	-0.5292	50218.9	50219.0	1			
0516-249	0516-249	2685	05	18	6.05152968	-24	55	1.9108250	.00042615	.0080324	0.3459	54112.2	54112.2	1			
0514+474	0514+474	2686	05	18	12.08982827	+47	30	55.5283215	.00004819	.0006145	-0.3033	50305.6	50305.7	1			
0516+087	0516+087	1504	05	19	10.81112964	+08	48	56.7349145	.00000998	.0003449	-0.0216	53133.8	53133.9	1			
0518+165	3C 138	145	05	21	9.88595015	+16	38	22.0515047	.00001206	.0001929	-0.0896	49254.4	55306.7	15		0.15	4.1
0519-176	0519-176	1505	05	21	23.55741458	-17	37	30.1850362	.00005788	.0021202	-0.4954	53560.6	53560.7	1			
0518+211	0518+211	2687	05	21	45.96584722	+21	12	51.4516746	.00003293	.0007183	-0.3274	50085.3	50156.2	2			
0519+011	0519+011	2688	05	22	17.46745290	+01	13	31.1857634	.00002251	.0006631	0.0471	49913.7	49914.6	1			
0522-611	P 0522-611	763	05	22	34.42549569	-61	07	57.1335942	.00001766	.0001527	0.3039	47625.5	56538.3	24			
0520-165	0520-165	1506	05	22	44.65497238	-16	27	52.4049704	.00001980	.0007437	0.0591	53561.7	53561.8	1	0.09	0.10	

Source Name		ID No.	Right Ascension			Declination			RA Error (s)	Dec. Error (arcsec)	RA–Dec Corr.	Observation Epoch MJD		No. Obs.	Source Flux (Jy)		Str Index
B1950	Common		H	M	S	D	M	S				First	Last		10-60	10-40	
0519+142	0519+142	1507	05	22	45.14658845	+14	15	29.2838993	.00016025	.0015992	0.0096	50156.0	54314.7	2			
0521-403	0521-403	2689	05	22	54.11513966	-40	20	30.9402947	.00002892	.0005764	0.1182	55112.4	55112.5	1			
0521-365	P 0521-36	146	05	22	57.98464010	-36	27	30.8513189	.00000549	.0000979	0.0592	48110.0	56638.7	151		0.99	3.6
0518+600	0518+600	2690	05	23	11.00797200	+60	07	45.7158741	.00004328	.0004811	-0.1273	53126.1	56638.5	3			
0521-262	0521-262	2691	05	23	18.46955779	-26	14	9.5543199	.00002469	.0007345	-0.0578	50631.6	56439.4	5			
0520+411	0520+411	2692	05	23	55.78024693	+41	13	50.8101468	.00003026	.0004847	0.1461	50242.7	50242.8	1			
0518+705	0518+705	1036	05	24	13.43337003	+70	34	52.9057661	.00008012	.0004757	0.0118	54087.1	54087.3	1			
0522-283	0522-283	2693	05	24	54.63029879	-28	18	41.6188569	.00002747	.0011227	-0.1140	54112.2	54112.3	1			
0523-236	0523-236	1508	05	25	6.50588663	-23	38	10.8063348	.00002925	.0006804	-0.5298	53552.7	53552.8	1			
0524-460	P 0524-460	764	05	25	31.40016085	-45	57	54.6850627	.00001452	.0001897	0.1129	49749.9	56504.2	27			
0524-485	0524-485	2694	05	26	16.67132098	-48	30	36.7917117	.00001217	.0001838	0.3002	53223.1	56538.1	23			
0524-237	0524-237	1509	05	26	48.38542697	-23	42	55.8591365	.00007142	.0022015	0.5529	54656.8	54657.7	1			
0525-231	0525-231	1510	05	27	18.60819712	-23	07	36.9985626	.00003132	.0010238	0.3536	54656.8	54657.7	1			
0525-100	0525-100	4065	05	27	24.06071718	-10	02	57.2700265	.00006602	.0015699	0.0433	56204.4	56204.6	1			
0524+034	J0527+0331	1037	05	27	32.70544287	+03	31	31.5166109	.00000419	.0000826	-0.0963	49913.7	56758.7	79	0.38	0.38	1.1
0528-654	HD36705	2695	05	28	44.78766773	-65	26	56.1367568	.00236291	.0092610	0.6359	48589.4	48589.8	1			
0530-727	P 0530-728	765	05	29	30.04219919	-72	45	28.5074210	.00002042	.0001125	0.0230	47625.5	56555.2	53			
0527-053	0527-053	1511	05	29	53.53347546	-05	19	41.6175520	.00003488	.0009270	0.1332	53561.7	55847.6	2	0.12	0.13	
0527-253	0527-253	1512	05	29	57.06739627	-25	15	58.9325776	.00001683	.0003661	-0.3888	54818.2	54818.3	1			
0521+793	0521+793	4066	05	30	7.08262831	+79	20	53.6667951	.11350325	.0650201	0.9486	56392.9	56392.9	1			
0528-250	0528-250	147	05	30	7.96278869	-25	03	29.8993546	.00000671	.0001705	-0.2302	48643.8	56734.4	22			
0526+373	0526+373	2696	05	30	12.54928312	+37	23	32.6194889	.00004260	.0006689	-0.0773	52409.0	52409.0	1			
0528+134	P 0528+134	148	05	30	56.41674752	+13	31	55.1495017	.00000336	.0000512	-0.0149	44203.1	56749.7	2000	1.29	0.84	2.6
0530-388	0530-388	2697	05	32	2.06164987	-38	48	54.3285865	.00018679	.0084300	-0.9147	53523.8	53523.9	1			
0529-031	0529-031	1513	05	32	7.51924953	-03	07	7.0382917	.00002165	.0005965	0.4385	53502.8	53572.7	2			
0529+075	OG 050	766	05	32	38.99845049	+07	32	43.3451634	.00014447	.0026213	0.1349	48976.1	54643.4	4			
0531-397	0531-397	2698	05	32	57.18561113	-39	41	9.0281578	.00010592	.0040413	-0.8003	52306.2	55483.5	3			
0529+483	J0533+4822	1038	05	33	15.86578777	+48	22	52.8078043	.00000349	.0000518	0.0055	50305.6	56776.7	213	0.81	0.53	
0530+421	0530+421	1039	05	33	56.48496761	+42	10	54.4213410	.00003415	.0006955	0.2158	50242.7	50242.8	1			
0532-378	0532-378	1514	05	34	17.48657664	-37	47	25.5925304	.00002624	.0006927	-0.2105	54853.2	54853.2	1			
0534-611	0534-611	767	05	34	35.77247317	-61	06	7.0730454	.00001708	.0001493	0.1111	48589.5	56504.5	24			
0531+194	0531+194	2699	05	34	44.51702701	+19	27	21.4692096	.00424082	.0327591	-0.8696	52409.0	56036.1	2			
0532+506	0532+506	1216	05	36	20.23191871	+50	38	26.2516006	.00001370	.0001938	0.1018	49576.5	53306.6	3			
0534-201	0534-201	2700	05	36	22.30101097	-20	05	31.3924675	.00012984	.0045189	0.6585	52408.9	53125.9	2			
0534-340	0534-340	1040	05	36	28.43237145	-34	01	11.4683794	.00000706	.0001153	0.1521	52306.1	56639.6	57		0.30	
0533+097	0533+097	2701	05	36	31.97789148	+09	44	20.6290432	.00532074	.0925086	-0.9795	53561.7	53561.8	1			
0533+446	0533+446	2702	05	37	30.06063148	+44	41	3.5397090	.00004631	.0006245	0.0260	50305.6	50305.7	1			
0537-441	P 0537-441	149	05	38	50.36155487	-44	05	8.9390246	.00000358	.0000545	-0.0251	43809.4	56762.7	929		1.68	2.7
0534+510	0534+510	1515	05	38	54.79522776	+51	07	23.4069086	.00001922	.0003911	0.2484	53572.6	53572.7	1			
0537-158	P 0537-158	768	05	39	32.01012965	-15	50	30.3208604	.00000783	.0002452	-0.2093	46806.4	56707.0	43	0.28	0.08	3.4
0536+145	0536+145	679	05	39	42.36598717	+14	33	45.5616859	.00000373	.0000612	-0.1058	46609.6	56717.1	212	0.34	0.29	1.4
0537-286	0537-286	769	05	39	54.28147323	-28	39	55.9479932	.00000414	.0000657	-0.0415	48573.4	56744.8	154		0.64	0.8
0537+251	0537+251	2703	05	40	14.34274895	+25	07	55.3488615	.00003889	.0009923	-0.3259	50218.9	50219.0	1			
0535+677	0535+677	2704	05	41	13.39703075	+67	45	23.2725233	.00035246	.0025955	0.2394	49826.8	49827.0	1			
0537+558	0537+558	2705	05	41	14.75774815	+55	50	43.5707089	.00005147	.0008151	-0.6415	54112.1	54112.3	1			
0537+531	0537+531	1217	05	41	16.17405727	+53	12	24.8348938	.00002098	.0003418	0.2946	49576.5	53645.8	8	0.10		
0539-057	P 0539-057	770	05	41	38.08337346	-05	41	49.4285097	.00000613	.0001368	-0.1196	49176.9	55545.7	24	0.68	0.43	2.8
0538+474	0538+474	2706	05	41	49.24549236	+47	29	7.6108337	.00002329	.0003718	0.1102	50305.6	50305.7	1			
0543-735	0542-735	2707	05	41	50.77536058	-73	32	15.3478935	.00104792	.0026210	0.0501	52886.7	53138.3	3			
0540-270	0540-270	2708	05	42	12.71442329	-26	58	42.6093424	.00072160	.0645365	-0.9607	54818.2	54818.3	1			

Source Name		ID No.	Right Ascension			Declination			RA Error (s)	Dec. Error (arcsec)	RA–Dec Corr.	Observation Epoch MJD		No. Obs.	Source Flux (Jy)		Str Index
B1950	Common		H	M	S	D	M	S				First	Last		10-60	10-40	
0538+498	3C 147	151	05	42	36.13789714	+49	51	7.2338534	.00001063	.0001358	0.0235	50459.4	55042.4	16	0.23		4.4
0540-092	0540-092	2709	05	42	55.87744283	-09	13	31.0069449	.00004258	.0009953	0.1580	53502.8	53502.9	1			
0532+826	0532+826	1516	05	43	38.84718474	+82	38	28.7643367	.00028235	.0010653	0.0799	53560.9	53561.7	1			
0540+456	0540+456	2710	05	44	1.16614859	+45	41	2.7926999	.00014129	.0015695	-0.2664	50305.6	50305.7	1			
0542-227	0542-227	1517	05	44	7.56709678	-22	41	9.9827576	.00001214	.0004207	-0.3425	53523.8	53560.7	2			
0540+529	0540+529	1518	05	44	14.07590055	+52	58	6.5089664	.00032540	.0037695	0.0950	54087.2	55041.8	2			
0542+112	0542+112	2711	05	44	52.19968094	+11	18	49.9251065	.00013084	.0020096	-0.1326	49913.8	56547.6	2			
0544+123	0544+123	2712	05	47	6.27628911	+12	23	46.2448331	.00002971	.0005825	-0.0482	54112.2	54112.3	1			
0544+273	0544+273	680	05	47	34.14892452	+27	21	56.8425591	.00000373	.0000622	-0.0453	46609.6	56776.1	167	0.37	0.30	2.1
0547-278	0547-278	1519	05	49	32.34717636	-27	52	38.8578689	.00009228	.0030555	-0.8104	53561.7	53561.8	1			
0546+308	0546+308	1520	05	49	54.18067886	+30	54	47.6009034	.00020919	.0022038	0.1173	53551.8	53552.7	1			
0549-575	0549-575	2713	05	50	9.58018131	-57	32	24.3964767	.00001366	.0001703	0.2534	53223.1	56702.6	24			
0547+234	0547+234	1041	05	50	47.39089118	+23	26	48.1769235	.00000958	.0002023	-0.0922	52306.1	56152.4	32	0.23	0.14	2.0
0548+084	0548+084	1521	05	51	11.22933398	+08	29	11.2221633	.00005446	.0011057	0.3744	53523.8	53572.7	2	0.16	0.12	
0549-191	0549-191	1522	05	51	55.26031926	-19	09	20.9704141	.00006138	.0017157	0.0607	53560.7	53560.7	1			
0548+378	J0552+3754	1042	05	52	17.93692077	+37	54	25.2823895	.00000579	.0000898	0.0831	50242.7	56701.0	52	0.42	0.33	1.8
0549+192	0549+192	1043	05	52	25.88501006	+19	13	40.2680600	.00002499	.0005688	-0.5482	52306.1	53946.6	8	0.10	0.09	
0550+032	P 0550+032	1044	05	52	50.10150005	+03	13	27.2427008	.00004002	.0008542	-0.1718	49913.7	49914.6	1	0.80	0.30	
0546+726	0546+726	2714	05	52	52.99981155	+72	40	45.1130708	.00065384	.0022787	-0.7037	52408.9	52409.1	1			
0551-086	0551-086	1523	05	53	41.89161834	-08	40	1.9043085	.00023495	.0050711	-0.6607	53561.7	53561.8	1			
0548+689	0548+689	2715	05	54	0.80743169	+68	57	54.4454922	.00052341	.0041850	0.5022	49826.8	54087.4	2			
0550+356	0550+356	2716	05	54	9.52926668	+35	41	31.4009948	.00007540	.0014969	-0.7284	54112.2	54112.3	1			
0552+398	DA 193	152	05	55	30.80561195	+39	48	49.1649980	.00000336	.0000504	0.0340	43808.6	56770.7	2233	1.71	0.95	2.5
0552+393	0552+393	4124	05	55	56.61769565	+39	22	7.7984491	.00001270	.0001961	0.0723	55538.2	55538.5	1			
0554+242	0554+242	771	05	57	4.71358252	+24	13	55.2988096	.00000494	.0001070	0.1037	50065.1	56317.2	56	0.32	0.13	2.9
0554+343	0554+343	2717	05	58	0.08860351	+34	18	48.3873699	.00001896	.0003789	0.2561	53502.8	53503.0	1			
0555-132	0555-132	2718	05	58	2.54671598	-13	17	41.1960829	.00001143	.0003722	-0.3096	50575.8	50576.0	1			
0556-009	0556-009	1524	05	58	44.39167071	-00	55	6.9160012	.00025015	.0091753	0.6214	53523.8	53523.9	1			
0555+378	0555+378	2719	05	59	0.45212382	+37	49	55.5198300	.00003105	.0006700	-0.6337	50241.8	50241.9	1			
0557-454	0557-454	2720	05	59	11.54441240	-45	29	40.3062602	.00003783	.0012339	0.2104	55413.6	55413.7	1			
0554+580	0554+580	2721	05	59	13.39422099	+58	04	3.4467679	.00012270	.0009613	0.4841	49576.5	49576.6	1			
0556+238	0556+238	681	05	59	32.03313272	+23	53	53.9267721	.00000344	.0000543	-0.0208	46610.9	56772.4	643	0.43	0.29	1.3
0557-182	0557-182	2722	05	59	46.40352391	-18	17	47.5701009	.00002938	.0011478	-0.3934	53560.7	55916.4	2			
0557-001	0557-001	2723	06	00	3.50693446	-00	05	59.1234794	.00969387	.1813424	-0.9883	53551.8	53561.8	2			
0558-396	0558-396	2724	06	00	31.41748769	-39	37	2.1970104	.00002694	.0010308	0.3184	54489.2	54489.2	1			
0559+422	0559+422	2725	06	02	58.94406660	+42	12	10.0092078	.00001529	.0003281	-0.4195	50241.8	50241.9	1			
0600+177	0600+177	682	06	03	9.13026049	+17	42	16.8105266	.00000464	.0000828	-0.3607	46336.4	56713.7	96	0.20	0.24	2.8
0600+063	0600+063	2726	06	03	14.35547708	+06	22	27.9496548	.00021696	.0037509	0.8236	53502.8	53503.0	1			
0600+219	0600+219	1266	06	03	51.55700268	+21	59	37.6990057	.00001351	.0003745	-0.2267	52408.9	54076.7	3			
0600+299	0600+299	2727	06	03	55.85193645	+29	57	5.3586820	.00006802	.0013344	0.0301	50218.9	50219.0	1			
0601-172	0601-172	2728	06	03	57.73244922	-17	16	28.2185108	.00001234	.0003648	-0.0911	50631.8	54643.5	2			
0602-424	0602-424	2729	06	04	25.17469046	-42	25	30.0959384	.00005425	.0017176	-0.5660	52306.2	52408.9	2		0.34	
0600+442	0600+442	2730	06	04	35.62874068	+44	13	58.5493733	.00011499	.0011135	-0.6242	50305.6	50305.7	1			
0602+109	0602+109	2731	06	04	49.36966354	+10	55	40.3732338	.00020394	.0019051	0.0166	49913.7	49914.6	1			
0601+245	0601+245	1045	06	04	55.12137853	+24	29	55.0364654	.00000565	.0001253	-0.1322	52409.0	56717.1	63	0.30	0.16	3.1
0603-353	0603-353	2732	06	05	6.46514399	-35	22	17.4660612	.00004324	.0014948	-0.3673	52306.2	52408.9	2			
0602+096	0602+096	2733	06	05	10.11311126	+09	39	13.6129195	.00004824	.0014095	-0.0490	49913.8	49913.9	1			
0601+578	0601+578	2734	06	05	42.22782422	+57	53	16.3552406	.00049200	.0027781	0.3937	49576.6	49576.6	1			
0602+405	0602+405	772	06	05	50.85537939	+40	30	8.1034928	.00000880	.0001444	-0.0590	50241.8	53613.4	7	0.69	0.38	
0604-074	0604-074	1525	06	06	43.54633408	-07	24	30.2316078	.00000726	.0002099	0.1110	53560.7	56701.3	5			

Source Name		ID No.	Right Ascension			Declination			RA Error (s)	Dec. Error (arcsec)	RA–Dec Corr.	Observation Epoch MJD		No. Obs.	Source Flux (Jy)		Str Index
B1950	Common		H	M	S	D	M	S				First	Last		10-60	10-40	
0604-004	0604-004	2735	06	06	57.44358992	-00	24	57.4645163	.00001912	.0005525	0.0567	53551.8	56204.6	2			
0605-247	0605-247	4067	06	07	16.33661641	-24	47	40.9675418	.00145187	.0372197	-0.9963	56162.6	56162.6	1			
0603+476	0603+476	2736	06	07	23.25498545	+47	39	46.9420610	.00001691	.0002683	0.0509	50305.6	50305.7	1			
0602+673	0602+673	773	06	07	52.67160716	+67	20	55.4100455	.00000354	.0000507	-0.0828	49750.0	56770.7	629	0.29		3.5
0605-085	P 0605-08	158	06	07	59.69923424	-08	34	49.9782063	.00000430	.0000815	-0.2765	43808.7	56638.7	111	0.61	1.12	3.4
0605-153	0605-153	2737	06	08	1.53193057	-15	20	36.9783486	.00004584	.0015626	0.3173	54112.3	54112.3	1			
0606-387	0606-387	2738	06	08	11.46162193	-38	47	26.5823347	.00057275	.0303846	0.7560	53523.9	53523.9	1			
0606-272	0606-272	2739	06	08	45.23687810	-27	17	10.8324627	.00005225	.0015130	-0.5038	53502.9	53503.0	1			
0606-223	P 0606-223	1526	06	08	59.68684694	-22	20	20.9566723	.00000411	.0000606	0.0136	50631.8	56770.6	160	0.49	0.53	2.9
0607-157	P 0607-15	160	06	09	40.94953605	-15	42	40.6727052	.00000341	.0000524	-0.0162	43873.3	56637.8	649	1.56	2.01	2.2
0608-187	0608-187	2740	06	10	17.88609466	-18	47	40.0922453	.00002826	.0010803	-0.0077	53551.8	55966.2	2			
0602+780	0602+780	2741	06	10	24.27931523	+78	01	36.1934017	.00034677	.0019039	0.1224	54087.2	54087.4	1			
0608-230	0608-230	1527	06	10	38.78737229	-23	01	45.8381632	.00016403	.0048636	-0.5849	53560.7	53560.7	1			
0604+728	0604+728	1528	06	10	48.87199264	+72	48	53.1859303	.00022556	.0007752	0.0360	49826.8	54664.7	2			
0609-119	0609-119	1529	06	11	35.06516368	-11	55	45.8294984	.00013960	.0032054	-0.2094	53561.7	53561.8	1			
0609-284	0609-284	1530	06	11	51.36535285	-28	27	59.8528379	.00003224	.0011682	0.4524	54818.3	54818.3	1			
0607+624	0607+624	2742	06	12	10.32506775	+62	25	34.0123716	.00025151	.0016792	0.5198	54112.1	54112.3	1			
0610-436	0610-436	2743	06	12	28.60523001	-43	37	48.4130952	.00035067	.0297309	-0.2429	52306.2	52408.9	2			
0610-316	0610-316	2744	06	12	29.66423508	-31	38	58.1836431	.00017387	.0108234	-0.2418	53133.9	53133.9	1			
0609+413	0609+413	2745	06	12	51.18523276	+41	22	37.4083141	.00001195	.0002647	-0.3876	50241.8	50241.9	1			
0610+171	0610+171	1046	06	13	36.36005188	+17	08	24.9456548	.00002515	.0007545	0.2367	52409.0	52758.6	2			
0610+260	3C 154	774	06	13	50.13917851	+26	04	36.7199061	.00000876	.0001502	-0.1809	50065.1	54142.9	22	0.15	0.17	
0611+131	0611+131	683	06	13	57.69275171	+13	06	45.4009020	.00000442	.0001055	-0.1498	47379.6	56717.1	68	0.30	0.13	2.2
0612-255	0612-255	1531	06	14	17.21085623	-25	36	53.5254320	.00001912	.0006964	-0.3287	53560.7	53560.7	1			
0609+607	0609+607	775	06	14	23.86617684	+60	46	21.7559844	.00000769	.0000804	-0.1452	49576.5	55138.6	20	0.21		3.3
0610+510	0610+510	1047	06	14	49.15928133	+51	02	13.1192645	.00004539	.0009529	-0.1422	50305.6	50305.7	1	0.12		
0611+483	0611+483	2746	06	15	4.05333046	+48	19	4.7296676	.00002343	.0003904	0.3078	50305.6	50305.7	1			
0613-030	0613-030	1532	06	16	7.94136102	-03	06	48.8532735	.00003905	.0013659	0.2409	53522.9	53523.8	1			
0614-349	P 0614-349	1048	06	16	35.98065055	-34	56	16.5484711	.00061247	.0167660	-0.0946	53068.0	53503.0	2			
0614-106	0614-106	1533	06	16	41.80760104	-10	41	8.4532091	.00005376	.0012310	-0.2049	53551.8	53552.7	1			
0614-219	0614-219	1534	06	17	2.04271881	-22	00	28.1717391	.00001996	.0006733	-0.5303	53551.8	53552.8	1			
0613+570	J0617+5701	1049	06	17	16.92256381	+57	01	16.4232881	.00000640	.0000693	-0.0365	49576.5	56751.7	57	0.19		
0615-365	P 0615-365	1535	06	17	32.32868056	-36	34	14.8571081	.00115506	.0235357	-0.8199	52306.2	54943.1	3			
0615-172	0615-172	1536	06	17	33.41831615	-17	15	25.0888066	.00026285	.0044017	0.6867	53572.7	53572.7	1			
0610+782	0610+782	1537	06	17	56.93292804	+78	16	7.3942902	.00018509	.0003517	0.3741	53523.0	53523.7	1			
0614+463	0614+463	1538	06	18	8.20367668	+46	20	16.2124382	.00002381	.0004789	0.2337	53560.6	53560.8	1			
0614+421	0614+421	2747	06	18	8.61994660	+42	07	59.8461130	.00003545	.0007602	-0.7004	54087.2	54087.4	1			
0616-244	0616-244	2748	06	18	22.65525150	-24	26	37.9465114	.00005475	.0014842	-0.5625	55370.8	55371.7	1			
0621-787	0621-787	2749	06	18	30.15865742	-78	43	2.1417852	.00011561	.0006253	0.3307	54723.0	54723.4	1			
0616-116	0616-116	1539	06	19	4.10256706	-11	40	54.8893128	.00002444	.0007608	0.3096	53152.8	53152.9	1			
0616+076	0616+076	1540	06	19	9.97102200	+07	36	41.2204242	.00019174	.0015726	0.4205	53125.9	53125.9	1			
0617+210	0617+210	2750	06	20	19.52839319	+21	02	29.5470840	.00001752	.0004735	-0.3686	50085.2	56638.5	5			
0618-284	0618-284	2751	06	20	29.35874871	-28	27	36.0847890	.00002543	.0009080	0.4010	53502.9	53503.0	1			
0618-252	0618-252	2752	06	20	32.11697448	-25	15	17.4852765	.00001214	.0004322	-0.1421	50631.8	50687.7	2			
0618-061	0618-061	2753	06	21	10.35787925	-06	09	54.2867486	.01606545	.2350221	0.9955	53523.8	53523.8	1			
0614+761	0614+761	2754	06	21	18.79290099	+76	05	4.5581420	.00229232	.0039837	-0.3332	49826.8	49827.0	1			
0620-194	0620-194	2755	06	22	28.53704603	-19	27	18.1763161	.00009382	.0044931	-0.7326	54112.2	54112.3	1			
0619+334	0619+334	1541	06	22	52.22195455	+33	26	10.4101022	.00002868	.0007099	-0.3012	53572.7	53572.8	1			
0620-011	0620-011	1542	06	22	57.94230038	-01	09	27.1205329	.00011970	.0050876	0.2624	53152.8	53552.7	2			
0620+227	0620+227	2756	06	23	17.81358561	+22	41	35.7746801	.00009789	.0019166	0.3322	50085.4	56547.7	3			

Source Name		ID No.	Right Ascension			Declination			RA Error (s)	Dec. Error (arcsec)	RA–Dec Corr.	Observation Epoch MJD		No. Obs.	Source Flux (Jy)		Str Index
B1950	Common		H	M	S	D	M	S				First	Last		10-60	10-40	
0618+588	0618+588	2757	06	23	21.77921894	+58	49	1.8777070	.00017202	.0011637	0.2729	49576.5	49576.6	1			
0620+385	0620+385	1543	06	23	28.93955821	+38	30	49.8085919	.00001769	.0004334	0.0747	53560.6	53560.8	1			
0622-441	P 0622-441	2758	06	23	31.78563433	-44	13	2.5469089	.00062291	.0315743	0.5553	52306.2	52408.9	2			
0620+459	0620+459	2759	06	23	56.51179279	+45	54	39.5097245	.00012817	.0012060	0.4962	50305.6	50305.7	1			
0621-010	0621-010	2760	06	24	1.68516585	-01	03	28.1209317	.00030422	.0150838	0.7879	53502.9	53503.0	1			
0620+389	0620+389	776	06	24	19.02128077	+38	56	48.7361413	.00000534	.0000824	-0.1467	49391.0	55334.5	21	0.31	0.28	2.5
0621+446	0621+446	2761	06	25	18.26538736	+44	40	1.6261945	.00001769	.0003293	0.1170	50305.6	56498.6	2	0.22	0.22	
0622+147	0622+147	2762	06	25	45.92223355	+14	40	19.7522461	.00006818	.0014520	-0.2445	52409.0	52409.0	1			
0615+820	0615+820	777	06	26	3.00620005	+82	02	25.5677796	.00002304	.0000683	-0.0458	48352.9	55118.6	64	0.26		3.5
0625-354	0625-354	2763	06	27	6.72937821	-35	29	15.3398772	.00001906	.0007291	-0.2325	54489.2	54489.3	1			
0625+034	0625+034	1050	06	27	38.50434988	+03	24	54.6623530	.15631142	.3963320	-0.9999	53133.9	53133.9	1			
0628-671	0628-671	2764	06	28	39.60782703	-67	12	47.4062942	.00008083	.0008740	0.4836	54723.0	54723.4	1			
0626-280	0626-280	1544	06	28	43.27902616	-28	05	19.3831908	.00002294	.0007692	-0.4227	53551.8	53561.8	2			
0625+286	0625+286	1545	06	28	50.31893404	+28	35	50.4293642	.00012520	.0015686	0.4868	53522.9	53523.8	1			
0628-627	0628-627	2765	06	28	57.48728704	-62	48	44.7464347	.00078997	.0023207	0.1664	52886.7	53138.2	3			
0627-199	P 0627-199	1546	06	29	23.76186339	-19	59	19.7235559	.00000400	.0000674	0.0416	50631.8	56749.7	92			
0627-050	0627-050	2766	06	29	55.03095377	-05	05	0.0720465	.00012679	.0027480	0.1209	53502.9	53503.0	1			
0627+176	0627+176	2767	06	30	7.25850761	+17	38	12.9313971	.00001657	.0004975	-0.1353	50085.2	50156.2	2			
0628-133	0628-133	1547	06	30	53.90309222	-13	23	34.4933799	.00002986	.0008355	-0.1574	53152.8	53152.9	1			
0628+203	0628+203	2768	06	31	1.06254816	+20	20	59.2105451	.00002055	.0006719	-0.1737	50085.2	50156.2	2	0.17	0.17	
0629-418	0629-418	778	06	31	11.99802031	-41	54	26.9464894	.00001260	.0002975	0.1777	47625.6	54706.2	32		0.19	
0629-141	0629-141	1548	06	31	20.22617801	-14	10	31.7429343	.00001282	.0004435	-0.2905	53522.9	53523.8	1			
0627+532	0627+532	2769	06	31	34.68595148	+53	11	27.7566469	.00036993	.0018062	0.7772	49576.5	49576.6	1			
0629-128	0629-128	2770	06	32	1.64488987	-12	50	32.7821372	.00008260	.0033421	-0.2675	54087.3	54087.3	1			
0630-261	0630-261	2771	06	32	6.50175620	-26	14	14.0323818	.00003429	.0011391	-0.1051	53551.9	54440.5	2			
0629+320	0629+320	1051	06	32	30.78278679	+32	00	53.6331150	.00016466	.0017022	0.0144	50218.9	50219.0	1			
0629+160	0629+160	779	06	32	43.13554096	+15	59	57.6201417	.00001439	.0004240	-0.0040	50085.2	54125.2	5			
0631-223	0631-223	1549	06	33	26.75334785	-22	23	22.3537686	.00001311	.0004490	-0.1327	53133.9	53134.0	1			
0630+367	0630+367	2772	06	33	34.41183159	+36	42	49.7434975	.00003001	.0004259	0.1506	53572.7	55616.3	2			
0630+497	0630+497	2773	06	33	52.20666201	+49	43	45.9242907	.00006096	.0008210	0.2646	50305.6	50305.7	1			
0632-235	0632-235	1550	06	34	59.00099968	-23	35	11.9573088	.00000465	.0000759	-0.0032	53502.9	56763.7	64			
0632-183	0632-183	1551	06	35	11.01296819	-18	21	26.2450308	.00025612	.0074973	-0.8820	54600.9	54601.0	1			
0633-26B	0633-26B	1552	06	35	19.41632736	-26	20	55.7148499	.00005445	.0023069	-0.0173	54559.0	54559.1	1			
0633-263	0633-263	1553	06	35	20.90914603	-26	20	39.8663082	.00003842	.0014738	0.0439	53560.7	54559.1	3			
0634-584	0634-584	2774	06	35	40.82992128	-58	27	10.2766600	.00005636	.0009937	0.4951	54723.0	54723.2	1			
0637-752	P 0637-75	780	06	35	46.50790041	-75	16	16.8153809	.00000887	.0000589	-0.0015	47625.5	56667.7	271			
0633-211	0633-211	1554	06	36	0.60166321	-21	13	12.2004146	.00001679	.0006306	-0.2346	53561.7	53561.8	1			
0632+502	0632+502	2775	06	36	11.01656191	+50	09	59.6276088	.00007755	.0006866	-0.5100	49576.6	54112.3	3			
0634-057	0634-057	1555	06	36	48.32950010	-05	47	7.5456899	.00001215	.0004115	-0.2825	53522.9	53523.8	1			
0634-108	0634-108	2776	06	37	7.79697227	-10	52	48.8798957	.01515906	.2479884	0.9984	53152.8	53152.8	1			
0635-296	0635-296	2777	06	37	8.86019202	-29	42	38.7616090	.00051771	.0287736	0.6078	54112.2	54112.3	1			
0627+814	0627+814	2778	06	37	43.37762953	+81	25	27.6946472	.00099749	.0010897	0.5993	53560.9	55112.2	2			
0635-355	0635-355	2779	06	37	46.40854426	-35	36	48.3777365	.00023107	.0083434	0.7016	52306.2	56393.1	3			
0634+150	0634+150	1052	06	37	51.05228775	+14	58	57.2852138	.00004737	.0013760	-0.6236	50085.2	50156.1	2			
0634+334	0634+334	4125	06	37	55.94044857	+33	22	6.2511619	.00004605	.0006499	0.1505	55775.8	55776.6	1			
0633+595	0633+596	2780	06	38	2.87194763	+59	33	22.2138618	.00002194	.0001396	0.1100	49576.5	56701.3	2	0.32		
0637-337	P 0637-337	167	06	39	20.90462475	-33	46	0.1132874	.00001669	.0002941	-0.0345	51115.5	54362.3	9			
0633+734	0633+734	2781	06	39	21.96120127	+73	24	58.0406792	.00005618	.0003283	0.4649	49826.8	49827.0	1			
0637-216	0637-216	2782	06	39	28.72565687	-21	41	57.8050769	.00004517	.0016792	0.2766	53560.7	55847.6	2			
0639+098	0639+098	2783	06	41	45.19704298	+09	47	4.3411809	.00060635	.0088066	-0.8930	53502.9	55518.5	2			

Source Name		ID No.	Right Ascension			Declination			RA Error (s)	Dec. Error (arcsec)	RA–Dec Corr.	Observation Epoch MJD		No. Obs.	Source Flux (Jy)		Str Index
B1950	Common		H	M	S	D	M	S				First	Last		10-60	10-40	
0639-032	0639-032	1267	06	41	51.13293520	-03	20	48.5824699	.00000815	.0002634	-0.1742	52409.0	53946.6	4	0.34	0.27	
0636+680	0636+680	781	06	42	4.25740369	+67	58	35.6207838	.00000946	.0000727	-0.1431	48572.9	56776.6	45	0.14		1.7
0603+882	0603+882	1556	06	42	6.13718547	+88	11	55.0165334	.00306059	.0017808	0.1031	53560.9	53561.7	1	0.18		
0639+115	0639+115	2784	06	42	25.01603895	+11	28	32.9075453	.00010651	.0018412	0.4408	53523.0	56267.5	2			
0638+528	0638+528	1557	06	42	27.82186173	+52	47	59.2735506	.00003462	.0005726	0.0373	53572.6	53572.8	1			
0639+352	0639+352	1558	06	42	58.13961892	+35	09	18.3789777	.00001497	.0003129	0.0354	53561.7	55916.4	2	0.12	0.09	
0641-248	0641-248	2785	06	43	7.46891322	-24	51	21.3121085	.00003288	.0011102	-0.1038	54087.3	54087.3	1			
0640+074	0640+074	2786	06	43	22.07328333	+07	24	52.4460462	.00011065	.0021106	0.5922	53502.9	53503.0	1			
0640+090	0640+090	1559	06	43	26.44502834	+08	57	38.0131088	.00020631	.0025115	-0.1766	53133.9	53523.8	2			
0641-135	0641-135	2787	06	43	32.36174279	-13	35	49.8789211	.00001499	.0005241	-0.0039	53502.9	53503.0	1			
0641+126	0641+126	4068	06	43	59.85551824	+12	38	18.1068183	.00002777	.0006689	-0.0487	56749.0	56749.2	1			
0642-349	P 0642-349	2788	06	44	25.28100455	-34	59	41.9497357	.00003642	.0014821	-0.1888	52306.2	52306.3	1			
0641+292	0641+292	2789	06	44	44.81576275	+29	11	4.0172204	.00015472	.0017623	-0.4354	54112.2	54112.3	1			
0641+392	0641+393	1560	06	44	53.70960143	+39	14	47.5338966	.00000392	.0000606	0.1352	50241.8	56776.7	137	0.22	0.11	2.6
0642+214	3C 166	169	06	45	24.09951520	+21	21	51.2015050	.00000949	.0001726	-0.5159	46659.0	56699.0	42	0.33	0.18	3.8
0643+057	0643+057	1561	06	45	47.27647820	+05	41	22.3886119	.00009768	.0026492	0.4140	53551.9	53552.7	1			
0643+307	0643+307	2790	06	46	15.23806271	+30	41	23.6315065	.00007242	.0011561	0.1044	50218.9	50219.0	1			
0644-390	0644-390	2791	06	46	30.92044183	-39	03	39.1307742	.00020328	.0103233	0.4706	53133.9	53503.0	2			
0642+449	OH 471	171	06	46	32.02599518	+44	51	16.5901610	.00000337	.0000505	0.0197	48572.8	56772.8	1129	1.59	1.15	1.5
0645-160	0645-160	1562	06	47	29.96690578	-16	05	27.3596362	.00002208	.0007806	-0.5527	53522.9	53523.8	1			
0646-306	P 0646-306	173	06	48	14.09646314	-30	44	19.6598655	.00000553	.0000932	-0.2040	49030.2	56701.3	62		0.50	2.7
0646-176	0646-176	1563	06	48	28.49853031	-17	44	5.4398109	.00001705	.0005280	-0.3591	53551.9	53552.8	1			
0645+209	0645+209	1564	06	48	32.71379904	+20	53	8.9206101	.00005305	.0007698	0.2004	54313.8	54314.6	1			
0644+491	0644+491	2792	06	48	47.11858105	+49	07	20.7296339	.00043789	.0040194	0.4503	50305.6	50305.8	1			
0647-475	P 0647-475	1565	06	48	48.44998147	-47	34	27.1541241	.00129803	.0965247	-0.5979	54943.0	56462.9	2			
0647-410	0647-410	2793	06	49	14.11090080	-41	08	53.0173173	.00036876	.0175535	-0.6966	55413.7	55413.7	1			
0648-165	0648-165	782	06	50	24.58185956	-16	37	39.7254430	.00000354	.0000543	-0.0138	50048.6	56776.7	246	1.19	0.94	1.8
0647-018	0647-018	1566	06	50	25.69824297	-01	52	22.1643865	.00008621	.0024097	-0.1508	53125.9	53126.0	1			
0646+600	0646+600	1218	06	50	31.25431572	+60	01	44.5558047	.00003197	.0003829	0.5926	49576.5	53211.1	6	0.37		
0648-287	0648-287	2794	06	50	32.92729326	-28	49	17.8501166	.00023147	.0056956	-0.2394	54600.9	54600.9	1			
0647+040	0647+040	1567	06	50	38.13416027	+03	58	8.4406385	.00004441	.0010245	0.1081	53551.9	53552.8	1			
0648-086	0648-086	2795	06	50	45.17526208	-08	40	0.1816810	.00005047	.0014202	0.0354	53502.9	53503.0	1			
0646+563	0646+563	1568	06	50	48.19063340	+56	16	34.4910085	.00004692	.0007259	0.0660	53561.7	53561.8	1			
0649-209	0649-209	1268	06	51	58.12006012	-21	01	11.9152935	.00003371	.0009391	-0.8851	53719.1	53719.5	1			
0650-063	0650-063	1569	06	53	0.59757564	-06	25	32.7016214	.00002146	.0007388	-0.6952	53551.9	53552.8	1			
0650+052	0650+052	1570	06	53	27.48391935	+05	08	51.0634328	.00024953	.0033409	0.7940	53523.0	53523.9	1			
0651-194	0651-194	2796	06	53	57.80562812	-19	29	39.6775292	.00001415	.0005023	-0.2165	53502.9	53503.0	1			
0650+371	0650+371	783	06	53	58.28281310	+37	05	40.6066750	.00000577	.0000970	-0.2560	48348.3	56674.3	124	0.44	0.24	3.2
0650+507	0650+507	1571	06	54	22.09318036	+50	42	23.8731873	.00002178	.0003439	0.0973	53572.6	53572.8	1			
0650+453	0650+453	2797	06	54	23.71367926	+45	14	23.5458904	.00002061	.0003987	0.2566	50305.6	50305.8	1			
0651+410	0651+410	784	06	55	10.02472393	+41	00	10.1601586	.00000895	.0001773	-0.2034	50241.9	53575.0	8		0.11	
0653-242	0653-242	1572	06	55	48.76816354	-24	16	20.7965055	.00013171	.0052370	-0.1269	53152.9	53153.0	1			
0653-033	OH-090	1573	06	56	11.12059230	-03	23	6.7821974	.00000893	.0002765	-0.0412	53133.9	53134.0	1			
0653+322	0653+322	2798	06	56	40.88919233	+32	09	32.5479442	.00003109	.0006810	-0.1976	54112.2	54112.3	1			
0654+033	0654+033	2799	06	56	59.18018268	+03	15	53.4570824	.00094496	.0308927	0.9010	53153.0	53153.0	1			
0654+244	0654+244	1053	06	57	5.67553857	+24	23	55.3939621	.00001442	.0003456	-0.2338	50085.2	54482.2	10	0.11	0.13	3.5
0652+577	0652+577	2800	06	57	12.50917312	+57	41	56.7834633	.01339331	.0518309	0.9940	49576.7	49576.7	1			
0656-062	0656-062	2801	06	59	3.25213387	-06	21	10.5952116	.00008912	.0018766	-0.0530	53125.9	55616.3	2			
0656+082	0656+082	785	06	59	17.99603270	+08	13	30.9532812	.00000353	.0000631	-0.2640	49913.8	56770.6	606	0.36	0.37	2.9
0657-276	0657-276	1574	06	59	49.91699710	-27	45	18.5134141	.00002947	.0010146	0.0756	53560.7	53560.8	1			

Source Name		ID No.	Right Ascension			Declination			RA Error (s)	Dec. Error (arcsec)	RA–Dec Corr.	Observation Epoch MJD		No. Obs.	Source Flux (Jy)		Str Index
B1950	Common		H	M	S	D	M	S				First	Last		10-60	10-40	
0657+172	0657+172	684	07	00	1.52553850	+17	09	21.7013093	.00000344	.0000530	-0.0739	46336.4	56772.7	390	0.77	0.75	2.2
0655+696	0655+696	2802	07	01	6.61644110	+69	36	29.4156311	.00050230	.0020508	-0.1534	49826.8	49827.0	1			
0700-465	0700-465	4069	07	01	34.54641160	-46	34	36.5791717	.00110920	.0431643	0.5356	56162.6	56162.7	1			
0659+268	0659+268	2803	07	02	31.79088489	+26	44	11.0273023	.00000865	.0002296	-0.0018	50218.9	54087.4	2			
0645+858	0645+858	2804	07	02	32.81906794	+85	49	52.4769508	.00290844	.0028744	-0.8454	50688.1	50688.3	1			
0700-101	0700-101	1575	07	02	35.75682444	-10	15	6.4172094	.00001927	.0005729	0.0626	53125.9	53126.0	1			
0700-286	0700-286	2805	07	02	40.40269089	-28	41	50.0497452	.00003710	.0016406	-0.6284	53503.0	53503.0	1			
0700-197	0700-197	1576	07	02	42.90066576	-19	51	22.0356135	.00000521	.0000832	-0.0481	53551.9	56751.2	76	0.32	0.62	
0658+548	0658+548	1577	07	02	46.26271196	+54	44	35.7337831	.00015044	.0018275	0.4058	53125.8	53126.1	1			
0700-007	0700-007	1578	07	03	19.08661416	-00	51	3.1575336	.00000887	.0002826	-0.0235	53133.9	53134.0	1			
0701-130	0701-130	1579	07	04	6.23630703	-13	07	22.3162865	.00014998	.0036495	0.2016	53561.7	53561.8	1			
0700+470	0700+470	2806	07	04	9.55828594	+47	00	56.0397481	.00006066	.0009946	-0.5454	50305.6	50305.8	1			
0702+400	0702+400	2807	07	05	44.52231746	+39	58	32.0229040	.00003374	.0004571	-0.3393	54112.3	55657.2	2			
0704-231	0704-231	1580	07	06	33.51816066	-23	11	37.8412044	.00016589	.0054074	-0.2397	54942.9	56498.7	2			
0705-412	0705-412	2808	07	06	43.05954630	-41	22	23.7947186	.00019528	.0145442	-0.2745	55112.5	55112.5	1			
0702+612	0702+612	2809	07	07	0.61578239	+61	10	11.6080983	.00022672	.0013443	0.7784	49576.6	49576.7	1			
0705+025	0705+025	2810	07	07	45.88985127	+02	27	5.1991621	.03019877	.0406882	0.9998	53552.8	53552.8	1			
0705-142	0705-142	2811	07	08	3.37548619	-14	21	15.8169133	.00006442	.0016160	0.0091	52408.9	52409.0	1			
0705+350	0705+350	2812	07	08	24.44773311	+34	55	42.1172366	.00016482	.0048838	-0.8208	54087.3	54087.4	1			
0705+377	0705+377	1581	07	09	9.22253271	+37	37	53.1813726	.00002503	.0004385	0.3809	53572.7	53572.8	1			
0707-028	0707-028	1582	07	09	45.05461232	-02	55	17.4965912	.00001650	.0005525	0.0330	53560.7	53560.8	1			
0709-387	0709-387	2813	07	10	43.63633325	-38	50	37.0352899	.00015722	.0050408	0.8608	52306.2	52409.0	2			
0707+424	0707+424	2814	07	10	44.32633031	+42	20	55.0425799	.00021505	.0018454	-0.5634	50241.9	50242.0	1			
0707+476	0707+476	786	07	10	46.10487693	+47	32	11.1427368	.00000466	.0000707	0.0274	50254.8	56770.4	131	0.35	0.24	2.5
0708-204	0708-204	2815	07	10	46.62251217	-20	33	23.9439446	.00034070	.0078242	0.1484	53561.8	53561.8	1			
0709-015	0709-015	4126	07	11	51.39887426	-01	37	57.3980699	.00002378	.0006969	0.0763	55916.3	55916.4	1			
0708+506	0708+506	1583	07	12	43.68356590	+50	33	22.7073176	.00001472	.0002013	0.2701	53560.7	56749.2	2	0.30		
0709+509	0709+509	1055	07	13	12.89633319	+50	53	43.8913184	.00007485	.0011411	-0.2090	50305.6	50305.8	1	0.08		
0710+439	OI 417	177	07	13	38.16408312	+43	49	17.2052190	.00003215	.0005139	-0.1300	48352.9	55271.4	39	0.23	0.09	5.7
0710+196	0710+196	1219	07	13	55.67916263	+19	35	0.4091189	.00001266	.0003502	-0.2473	53125.9	53306.4	2			
0711+356	0711+356	787	07	14	24.81746596	+35	34	39.7961404	.00001465	.0002914	-0.2376	49254.5	56664.4	14			4.6
0708+742	0708+742	2816	07	14	36.12498498	+74	08	10.1440304	.00005629	.0002400	0.2677	54087.2	54087.4	1			
0713-092	0713-092	2817	07	15	33.39349875	-09	21	54.2697399	.00020767	.0064362	0.3540	53133.9	53134.0	1			
0714+457	0714+457	1584	07	17	51.85241238	+45	38	3.2609418	.00000381	.0000565	-0.0315	50305.6	56748.1	111			
0713+669	0713+669	1585	07	18	5.63192569	+66	51	53.3290567	.00003348	.0002703	0.0018	54942.8	54943.1	1			
0716-181	0716-181	1586	07	18	14.15806019	-18	13	4.0542095	.00003054	.0009192	0.4488	53551.9	53552.8	1			
0716+332	0716+332	1587	07	19	19.41965812	+33	07	9.7086144	.00001188	.0002839	0.1173	53125.9	55966.3	2	0.30	0.29	
0717-198	0717-198	2818	07	19	24.37357431	-19	55	20.5086813	.01237854	.5838336	-0.9997	52408.9	52408.9	1			
0717-393	0717-393	2819	07	19	39.27860306	-39	28	48.6927492	.00015346	.0096945	-0.0508	55112.5	55112.6	1			
0716+477	0716+477	1269	07	20	21.49777030	+47	37	44.1249084	.00001367	.0001645	-0.0799	50305.6	56701.3	3	0.31	0.21	
0718+157	0718+157	1588	07	21	2.41362147	+15	40	42.9712047	.00004283	.0013184	-0.3618	53561.7	53561.8	1			
0718-154	0718-154	1589	07	21	13.49135770	-15	30	41.0060684	.00006202	.0019844	-0.3433	54656.8	54656.9	1			
0718+042	0718+042	2820	07	21	23.91000871	+04	06	44.2136538	.00002713	.0008189	0.0968	49913.8	49913.9	1			
0719-353	0719-353	2821	07	21	46.70874605	-35	28	16.7951526	.05690376	.8465725	0.9997	52408.9	52408.9	1			
0716+714	0716+714	788	07	21	53.44846254	+71	20	36.3634139	.00000370	.0000507	0.0087	47415.5	56770.4	483	1.12		1.9
0718+374	0718+374	2822	07	22	1.25968355	+37	22	28.6330238	.00003291	.0005716	-0.2925	50241.9	50242.0	1			
0720-305	0720-305	2823	07	22	27.69724733	-30	38	4.5797184	.00125343	.0280485	0.8789	52306.2	52306.3	1			
0721-071	0721-071	1270	07	24	17.29264141	-07	15	20.3529205	.00001069	.0003672	-0.3070	52306.2	53946.6	4	0.41	0.26	
0722+032	0722+032	2824	07	24	48.40893627	+03	08	25.0887507	.00005851	.0019754	-0.1462	49913.8	49913.8	1			
0722+145	P 0722+145	685	07	25	16.80776350	+14	25	13.7466365	.00000396	.0000678	-0.1330	47253.2	56701.7	86	0.48	0.61	2.7

Source Name		ID No.	Right Ascension			Declination			RA Error (s)	Dec. Error (arcsec)	RA–Dec Corr.	Observation Epoch MJD		No. Obs.	Source Flux (Jy)		Str Index
B1950	Common		H	M	S	D	M	S				First	Last		10-60	10-40	
0723-265	0723-265	1590	07	25	24.41312689	-26	40	32.6801737	.00002082	.0007632	-0.4522	53503.0	53572.8	2			
0723-189	0723-189	1591	07	25	50.16557146	-19	04	19.0741145	.00000810	.0002814	0.0096	53125.9	56547.7	5			
0723-008	DW 0723-00	180	07	25	50.63995645	-00	54	56.5442838	.00000561	.0001039	-0.4560	44203.2	55728.1	69	0.66	1.29	3.3
0718+792	0718+793	789	07	26	11.73523189	+79	11	31.0161688	.00000484	.0000506	0.0387	49421.9	56770.4	1062	0.34		2.5
0723+219	0723+219	1592	07	26	14.26073557	+21	53	20.1140038	.00000476	.0000793	-0.0128	53133.9	56751.7	55			
0723+067	0723+067	1593	07	26	36.36411664	+06	36	42.8520179	.00004191	.0011992	-0.0201	53560.7	53560.8	1			
0725-381	0725-381	2825	07	27	0.13024103	-38	13	11.4004644	.00029546	.0142819	-0.1121	55412.8	55413.7	1			
0723+488	0723+488	2826	07	27	3.10059129	+48	44	10.1269241	.00001922	.0003632	0.1186	50305.6	50305.8	1			
0723+679	3C 179	1594	07	28	10.89560545	+67	48	47.0330186	.00004776	.0002033	-0.1899	53523.0	53523.7	1			
0725+219	0725+219	1056	07	28	20.60829838	+21	53	6.3902818	.00000572	.0001381	-0.1867	50085.2	56691.2	46	0.24	0.16	2.1
0726-224	0726-224	2827	07	28	29.79849124	-22	31	36.7085704	.00011081	.0034364	0.1418	53133.9	56302.3	2			
0724+571	0724+571	1220	07	28	49.63164275	+57	01	24.3746776	.00002482	.0003948	0.0657	49576.6	53525.8	7	0.14		
0727-365	0727-365	2828	07	29	5.41199172	-36	39	45.2578343	.00066268	.0146999	-0.6656	54291.7	54291.8	1			
0726-132	0726-132	1595	07	29	17.81766389	-13	20	2.2717679	.00003315	.0009144	-0.0173	53126.0	53126.0	1			
0728-345	0728-345	2829	07	29	57.36526126	-34	39	19.5958926	.00020668	.0089490	0.6425	52306.2	52306.3	1			
0727-115	P 0727-11	182	07	30	19.11247295	-11	41	12.6006023	.00000336	.0000516	-0.0465	43808.7	56770.7	2316	2.16	2.33	2.0
0727-025	0727-025	2830	07	30	25.87759994	-02	41	24.9043432	.00001468	.0004701	0.0291	50575.8	50576.0	1			
0728-054	0728-054	2831	07	30	28.43653300	-05	35	46.9011549	.00012335	.0036042	-0.0100	54112.3	54112.4	1			
0728-320	0728-320	2832	07	30	38.29832272	-32	08	20.1778824	.00006522	.0023897	0.1930	52306.2	52306.3	1			
0727+409	0727+409	1596	07	30	51.34658438	+40	49	50.8266498	.00003357	.0004784	-0.4411	50241.9	54664.7	2			
0728-235	0728-235	1597	07	31	6.66798745	-23	41	47.8694735	.00002218	.0006655	-0.3214	53133.9	53134.0	1			
0729-222	0729-222	1598	07	31	31.50839013	-22	24	20.8668519	.00004155	.0012064	0.2651	53126.0	53126.0	1			
0728+249	J0731+2451	1057	07	31	33.74546793	+24	51	58.5987518	.00001033	.0002960	0.0501	50085.2	56706.9	18	0.14	0.08	2.3
0729+146	0729+146	1599	07	31	58.99697056	+14	33	36.4928825	.00004261	.0009354	-0.2722	53561.8	53561.8	1			
0729+019	0729+019	1600	07	32	22.78867952	+01	50	35.3842196	.00001293	.0004109	0.2370	53133.9	53134.0	1			
0729+259	0729+259	1601	07	32	56.27526112	+25	48	38.7954600	.00000485	.0000924	0.1257	50218.9	56762.6	40			
0730+504	0730+504	1221	07	33	52.52057927	+50	22	9.0622316	.00000637	.0001178	0.3657	49576.6	56770.4	89	0.37		
0731+050	J0733+0456	1058	07	33	57.45989050	+04	56	14.4966818	.00001338	.0003605	0.0249	49913.8	56749.2	2	0.25	0.34	
0731+479	0731+479	2833	07	35	2.31168461	+47	50	8.4274685	.00002132	.0003474	0.2063	50305.6	50305.8	1			
0733-174	P 0733-17	188	07	35	45.81248148	-17	35	48.5027862	.00002063	.0003473	0.1421	49267.4	55545.7	26			4.9
0733+016	0733+016	2834	07	35	58.63464818	+01	30	3.6380220	.00015856	.0020379	0.5007	49913.8	49913.9	1			
0732+237	0732+237	2835	07	35	59.92635212	+23	41	2.8294289	.00815408	.0931284	-0.9455	50156.1	50156.2	1			
0733+300	GC 0733+30	2836	07	36	13.66109480	+29	54	22.1848983	.00001996	.0006776	-0.1970	50218.9	50219.0	1			
0734-044	0734-044	2837	07	36	33.62709206	-04	33	11.8611662	.00034400	.0088689	-0.0261	53560.7	53560.8	1			
0733+261	0733+261	2838	07	36	58.07373714	+26	04	49.9453847	.00002402	.0006232	0.1100	50218.9	50219.0	1			
0734-072	0734-072	1602	07	37	7.13306867	-07	20	38.0395191	.00011210	.0019647	0.2576	53561.8	53561.8	1			
0733+597	0733+597	2839	07	37	30.08699837	+59	41	3.1939846	.00003623	.0008071	-0.3418	49576.6	54087.4	2			
0736-397	0736-397	2840	07	37	55.84052213	-39	54	34.0469473	.00079654	.0265647	-0.6775	53134.0	53134.0	1			
0733+646	0733+646	2841	07	37	58.98054805	+64	30	43.3441810	.00041863	.0018242	-0.2450	49826.8	49827.0	1			
0735+178	P 0735+17	190	07	38	7.39374622	+17	42	18.9982015	.00000360	.0000565	0.0063	43808.7	55138.6	432	0.38	0.39	3.4
0736-332	P 0736-332	790	07	38	16.94872717	-33	22	12.7853692	.00015602	.0063362	0.4230	50258.9	53126.0	2			
0738-674	0738-674	791	07	38	56.49623470	-67	35	50.8261245	.00002381	.0001561	0.3288	47625.6	55784.2	22			
0736-063	0736-063	2842	07	38	57.17553264	-06	26	58.0560679	.00001921	.0005596	0.0442	50576.0	50576.1	1			
0732+755	0732+755	2843	07	39	13.19536646	+75	27	47.7103915	.00097732	.0038574	0.1124	49826.8	49827.0	1			
0736+017	P 0736+01	192	07	39	18.03389896	+01	37	4.6177218	.00000388	.0000643	-0.1963	47253.2	56762.7	132	0.70	0.88	2.3
0738-246	0738-246	1603	07	40	14.71665916	-24	44	36.6838279	.00003732	.0012652	0.4987	53126.0	53126.0	1			
0737+289	0737+289	1604	07	40	33.54387535	+28	52	47.2468513	.00004607	.0010722	-0.1515	53572.7	53572.8	1			
0735+674	0735+674	2844	07	40	53.39828713	+67	19	8.2292581	.00081706	.0087762	0.8599	49827.0	49827.1	1			
0738+313	OI 363	193	07	41	10.70330407	+31	12	0.2294536	.00000609	.0001133	-0.1132	43808.7	56716.7	65	1.02	0.36	4.1
0738+272	0738+272	2845	07	41	25.73283165	+27	06	45.3910842	.00002917	.0006969	0.0322	50218.9	50219.0	1			

Source Name		ID No.	Right Ascension			Declination			RA Error (s)	Dec. Error (arcsec)	RA–Dec Corr.	Observation Epoch MJD		No. Obs.	Source Flux (Jy)		Str Index
B1950	Common		H	M	S	D	M	S				First	Last		10-60	10-40	
0739-266	0739-266	1605	07	41	55.68132066	-26	47	30.4909670	.00008135	.0036401	-0.0750	53134.0	53134.0	1			
0738+491	0738+491	792	07	42	2.74894725	+49	00	15.6089324	.00000404	.0000582	0.0053	49750.1	56770.6	80	0.54		1.4
0738+548	0738+548	2846	07	42	39.79069511	+54	44	24.6668622	.00003943	.0005413	0.4005	49576.6	49576.8	1			
0740-383	0740-383	2847	07	42	42.00512201	-38	29	3.9065793	.00048318	.0181360	0.8185	52306.3	53551.9	3			
0740+173	0740+173	2848	07	43	5.10679376	+17	14	24.4129818	.00002387	.0008662	-0.5005	50085.2	50156.2	2			
0739+398	0739+398A	2849	07	43	9.88654821	+39	41	30.7804240	.00001847	.0004653	-0.3311	50241.9	50242.0	1			
0743-673	0743-673	2850	07	43	31.61160307	-67	26	25.5464114	.00002530	.0001238	0.0265	48110.1	54670.5	26			
0741-444	0741-444	1606	07	43	32.75811072	-44	34	5.1394920	.00017477	.0130909	0.4118	54853.3	54853.3	1			
0741-379	0741-379	1607	07	43	44.82057601	-38	03	56.4116299	.00018054	.0089158	0.7573	52306.3	53523.0	3			
0740+235	0740+235	2851	07	43	44.97231518	+23	28	39.0035385	.00034812	.0033307	0.5643	50156.0	50156.2	1			
0741-045	0741-045	2852	07	43	52.40666644	-04	40	20.5304178	.00002070	.0006864	-0.2052	53503.0	53503.0	1			
0744-691	0744-691	2853	07	44	20.39350160	-69	19	7.1561503	.00116118	.0029613	0.4070	52886.8	53138.3	3			
0741-063	0741-063	1608	07	44	21.65635966	-06	29	35.9135052	.00002713	.0009090	-0.1939	54187.0	54187.2	1			
0741+214	0741+214	1222	07	44	47.27714910	+21	20	0.4361093	.00038778	.0085120	0.9740	53550.8	53600.7	2			
0742+103	DW 0742+10	196	07	45	33.05952150	+10	11	12.6923888	.00000408	.0000805	-0.1139	43808.7	56637.8	228	0.34	0.35	3.9
0742+318	0742+318	2854	07	45	41.67150355	+31	42	56.6168038	.00002478	.0006393	-0.4329	50218.9	50219.0	1			
0743-006	P 0743-006	197	07	45	54.08232043	-00	44	17.5400117	.00000381	.0000730	-0.2423	48352.9	56749.7	159	0.71	0.65	1.9
0742+333	0742+333	1609	07	45	59.32402555	+33	13	34.1357661	.00004913	.0011718	0.1925	53560.7	53560.8	1			
0744-158	0744-158	2855	07	46	18.23602828	-15	55	34.7462366	.00004369	.0011858	-0.5901	52306.2	52306.3	1			
0743+259	GC 0743+25	198	07	46	25.87417933	+25	49	2.1347075	.00000340	.0000516	-0.0325	47253.2	56699.0	681	0.42	0.29	2.1
0743+277	0743+277	1059	07	46	40.43231068	+27	34	59.0470968	.00000384	.0000621	-0.0844	50218.9	56758.1	114	0.36	0.37	1.5
0740+767	0740+767	2856	07	47	14.60754714	+76	39	17.2714890	.00008591	.0003977	0.4522	49826.9	49827.1	1			
0745-330	P 0745-330	2857	07	47	19.68319818	-33	10	46.9727538	.00003968	.0012808	0.6456	52306.2	52306.3	1			
0745-291	0745-291	2858	07	47	41.88959351	-29	19	2.0752709	.00007750	.0031424	0.6458	53126.0	55616.2	2			
0745-165	0745-165	1610	07	48	3.08385430	-16	39	50.2552767	.00001411	.0004808	-0.3870	53551.8	53551.9	1			
0745+241	B2 0745+24	200	07	48	36.10928041	+24	00	24.1099525	.00000381	.0000619	-0.1263	45432.0	56709.6	235	0.61	0.56	2.5
0746-167	0746-167	2859	07	48	48.67854811	-16	50	27.4009090	.00003841	.0011926	0.6640	52409.0	52409.0	1			
0743+744	0743+744	2860	07	49	22.45666920	+74	20	41.5925702	.00009206	.0006555	0.4919	49826.9	49827.1	1			
0746+110	0746+110	2861	07	49	27.38550504	+10	57	33.1281650	.00019210	.0040460	0.5211	54087.3	54087.4	1			
0747+185	0747+185	1611	07	50	0.32994829	+18	23	11.4071867	.00000533	.0000984	-0.0770	50085.2	56734.7	43			
0746+503	0746+503	2862	07	50	8.34284104	+50	15	6.8111404	.00010675	.0009351	0.1916	49576.7	54112.4	3			
0746+483	0746+483	1223	07	50	20.43631893	+48	14	53.5564184	.00001594	.0002621	-0.0319	50305.6	53946.8	10	0.32	0.21	2.7
0747+104	0747+104	4127	07	50	32.87800958	+10	21	26.7684608	.00002557	.0005696	-0.3727	55775.9	55776.7	1			
0742+792	0742+792	2863	07	50	43.26540717	+79	09	17.0025184	.00024509	.0009484	0.4933	49826.9	54087.4	3			
0748-069	0748-069	2864	07	50	47.14840508	-07	06	4.0270013	.00006520	.0015755	0.0308	53503.0	53503.1	1			
0748+126	P 0748+126	202	07	50	52.04572908	+12	31	4.8281807	.00000341	.0000516	0.0035	44203.3	56776.7	366	1.21	1.08	2.1
0740+828	0740+828	2865	07	50	57.75551196	+82	41	58.0318739	.00009925	.0003606	0.2376	50688.2	50688.3	1			
0748+019	0748+019	1612	07	51	2.28154635	+01	52	15.7605984	.00006841	.0017283	-0.1788	53572.7	53572.8	1			
0749-333	0749-333	2866	07	51	5.47043462	-33	31	35.9993760	.00020113	.0069132	0.6792	52306.2	52306.3	1			
0748-006	0748-006	2867	07	51	10.20519148	-00	46	51.0510027	.00005916	.0019344	-0.4588	54112.3	56393.2	2			
0746+688	0746+688	1613	07	51	45.98469073	+68	40	26.8330678	.00030765	.0011771	0.5681	53559.8	53560.7	1			
0748+333	0748+333	2868	07	51	53.67322457	+33	13	19.8184559	.00001727	.0004722	-0.0694	50218.9	50219.0	1			
0749+376	0749+376	2869	07	52	40.90788779	+37	30	24.3116866	.00002959	.0006326	-0.4621	50241.9	50242.0	1			
0749+540	0749+540	793	07	53	1.38456684	+53	52	59.6371155	.00000342	.0000507	0.0804	48353.1	56770.4	830	0.57		2.7
0749+426	0749+426	2870	07	53	3.33749688	+42	31	30.7651320	.00002295	.0004555	-0.1741	50241.9	50242.0	1			
0752-116	0752-116	1614	07	54	26.45641654	-11	47	16.9484178	.00001016	.0003314	-0.0743	53133.9	53134.0	1			
0751+485	0751+485	2871	07	54	45.67045947	+48	23	50.7481897	.00003393	.0005265	0.2792	50305.7	50305.8	1			
0750+633	0750+633	1615	07	55	21.64085862	+63	12	35.7149681	.00003284	.0003382	0.0601	54942.9	54943.2	1			
0753-425	0753-425	2872	07	55	23.17238655	-42	39	58.2905191	.00045447	.0100288	-0.8517	55370.8	56462.9	2			
0754-155	0754-155	2873	07	56	50.69894954	-15	42	5.4368921	.00001186	.0004227	-0.4027	53503.0	53503.1	1			

Source Name		ID No.	Right Ascension			Declination			RA Error (s)	Dec. Error (arcsec)	RA–Dec Corr.	Observation Epoch MJD		No. Obs.	Source Flux (Jy)		Str Index
B1950	Common		H	M	S	D	M	S				First	Last		10-60	10-40	
0752+639	0752+639	2874	07	56	54.61043707	+63	47	59.0369154	.00006279	.0008554	0.1226	49826.9	49827.1	1			
0753+519	0753+519	2875	07	56	59.54318887	+51	51	0.2376077	.00002645	.0003495	0.3033	49576.6	54087.4	2			
0754+100	P 0754+100	206	07	57	6.64294853	+09	56	34.8522078	.00000373	.0000747	-0.2219	47253.2	56717.1	165	0.78	0.58	3.1
0755+117	0755+117	2876	07	58	7.65791054	+11	36	46.0479169	.00001778	.0004195	-0.0070	49913.8	55657.2	2			
0755+379	3C 189	1616	07	58	28.10815536	+37	47	11.8075514	.00003141	.0004623	-0.4073	51245.9	52409.1	2			
0758-229	0758-229	1617	08	00	12.79091273	-23	02	50.5346454	.00006448	.0022852	0.1483	53523.0	53523.9	1			
0758-398	0758-398	1618	08	00	24.26964899	-39	59	17.5947535	.00016566	.0086973	0.6817	52306.3	53551.9	4			
0757+441	0757+441	1619	08	01	8.27616623	+44	01	10.1561414	.00002055	.0004119	0.0836	53572.7	53572.8	1			
0759-334	0759-334	2877	08	01	25.95241695	-33	36	19.8948925	.00012816	.0045513	0.7044	52306.2	53126.0	2			
0759-283	0759-283	1620	08	01	46.49394460	-28	31	6.8749135	.00008398	.0035473	0.0393	53126.0	53126.0	1			
0758+594	0758+594	2878	08	02	24.59272187	+59	21	34.7952467	.00011540	.0013153	0.6986	49576.6	54112.4	2			
0800-380	0800-380	4070	08	02	27.60467472	-38	10	53.0634249	.00027280	.0099589	0.4060	56161.8	56162.6	1			
0759+252	0759+252	2879	08	02	41.58740928	+25	09	10.8977695	.00005690	.0012673	0.7094	50218.9	50218.9	1			
0759+183	J0802+1809	1060	08	02	48.03196507	+18	09	49.2492230	.00000398	.0000729	-0.0795	50085.2	56770.6	113	0.34	0.33	2.4
0801-079	0801-079	1621	08	03	39.30692591	-08	05	21.3901863	.00006560	.0014903	0.1419	53559.9	53560.7	1			
0759+641	0759+641	2880	08	03	52.15956231	+64	03	14.3697134	.00061141	.0054922	-0.8205	49826.9	49827.1	1			
0801+044	0801+044	2881	08	03	56.44437500	+04	21	2.7410644	.00007314	.0027282	-0.5878	49913.8	49913.9	1			
0802-170	0802-170	2882	08	04	33.71906930	-17	12	3.7833790	.00699474	.1633337	0.9982	53560.9	53560.9	1			
0802-276	P 0802-276	2883	08	04	51.45117798	-27	49	11.3209363	.00003430	.0010149	0.0713	50687.6	53382.7	2			
0802+115	0802+115	1622	08	05	8.50566175	+11	21	57.1907554	.00004892	.0013114	-0.6276	53572.7	53572.8	1			
0802-010	0802-010	2884	08	05	12.88847606	-01	11	13.7954614	.00001104	.0003725	-0.2358	50576.0	50576.1	1			
0800+618	0800+618	1623	08	05	18.17955117	+61	44	23.7006357	.00000371	.0000519	-0.0265	52409.1	56772.8	178			
0802+212	0802+212	2885	08	05	38.53424007	+21	06	51.5926321	.00002649	.0006492	-0.2785	50084.5	50156.2	2			
0803-047	0803-047	4071	08	06	8.78558204	-04	54	11.3386348	.00015361	.0043591	-0.0954	56105.8	56106.0	1			
0804-267	P 0804-267	2886	08	06	12.72258035	-26	52	33.3084980	.00001800	.0006175	0.0541	50631.8	50687.7	2			
0804-172	0804-172	1624	08	06	24.96565037	-17	24	44.3353242	.00011231	.0029248	-0.1498	53560.9	53561.8	1			
0804-290	0804-290	1625	08	06	33.44522084	-29	11	34.8923429	.00008955	.0034550	0.2645	53134.0	53134.0	1			
0803+452	0803+452	2887	08	06	33.47250480	+45	04	32.2719065	.00003819	.0004977	0.5689	50305.7	50305.8	1			
0806-710	0806-710	2888	08	06	34.06230497	-71	12	15.9664061	.03742907	.2168232	0.9892	52886.8	52886.8	1			
0804-351	0804-351	2889	08	06	44.76634978	-35	19	41.4558426	.00009273	.0042303	0.7013	52306.3	56749.1	3			
0803+514	0803+514	2890	08	07	1.01355171	+51	17	38.6763545	.00003502	.0004686	0.5075	49576.6	50305.8	2			
0804-153	0804-153	1626	08	07	5.30897346	-15	31	25.3809461	.00001459	.0004771	-0.4049	54559.0	54559.2	1			
0804-055	0804-055	2891	08	07	9.61759371	-05	41	13.9149222	.00001856	.0006692	-0.2408	50576.0	50576.1	1			
0805-119	0805-119	2892	08	07	35.99891244	-12	07	43.7145792	.00004538	.0015139	-0.1011	50576.0	50576.1	1			
0804+140	0804+140	1627	08	07	38.50486631	+13	52	17.3619844	.00001472	.0005247	-0.2631	53125.9	53126.0	1			
0805+046	0805+046	794	08	07	57.53856600	+04	32	34.5307965	.00000682	.0001632	-0.1132	49913.8	56596.0	25	0.17		
0805-077	P 0805-07	210	08	08	15.53603376	-07	51	9.8863682	.00000471	.0001009	-0.4493	46797.4	56674.2	88	0.68	0.76	3.3
0802+733	0802+733	2893	08	08	16.49154361	+73	15	11.9905790	.00011471	.0007690	-0.0498	49826.9	49827.1	1			
0805+269	0805+269	2894	08	08	36.76494501	+26	46	36.7387977	.00010310	.0021115	0.0057	50218.9	50218.9	1			
0804+499	OJ 508	795	08	08	39.66628510	+49	50	36.5304381	.00000340	.0000506	-0.0456	48377.9	56770.4	1028	0.54		1.8
0805+410	0805+410	796	08	08	56.65204035	+40	52	44.8889220	.00000344	.0000521	0.0478	48720.0	56772.4	651	0.56	0.44	2.1
0806-153	0806-153	1628	08	09	7.39182231	-15	32	46.8742637	.00005789	.0014885	0.0383	54559.0	54559.2	1			
0806+524	0806+524	1629	08	09	49.18706357	+52	18	58.2528719	.00018834	.0015942	0.5376	53559.8	53560.7	1			
0807+103	0807+103	2895	08	10	26.42388982	+10	10	40.9995099	.00003557	.0008246	0.0235	53560.9	55966.3	2			
0807+417	0807+417	2896	08	10	58.99426608	+41	34	2.8060509	.00004345	.0008093	-0.5581	50241.9	50242.0	1			
0806+573	0806+573	2897	08	11	0.60920841	+57	14	12.4957243	.00019714	.0010629	0.4022	49576.6	49576.8	1			
0809-493	P 0809-492	2898	08	11	8.80242096	-49	29	43.5109581	.00113229	.0055712	0.5572	52877.8	56462.9	2			
0808+019	P 0808+019	211	08	11	26.70731334	+01	46	52.2202112	.00000346	.0000539	-0.0291	48352.9	56717.1	477	0.61	0.57	1.6
0810-180	0810-180	2899	08	12	28.51593233	-18	10	42.8128508	.00002209	.0007301	0.2807	50631.8	50631.9	1			
0810+258	0810+258	2900	08	13	3.83406998	+25	42	11.0318647	.00002898	.0006695	0.5448	50218.9	50218.9	1			

Source Name		ID No.	Right Ascension			Declination			RA Error (s)	Dec. Error (arcsec)	RA–Dec Corr.	Observation Epoch MJD		No. Obs.	Source Flux (Jy)		Str Index
B1950	Common		H	M	S	D	M	S				First	Last		10-60	10-40	
0810+247	0810+247	2901	08	13	47.13768139	+24	35	59.1497203	.00007295	.0011612	-0.5334	50084.5	50156.2	2			
0811-179	0811-179	2902	08	14	7.90079931	-18	06	26.0545182	.00003574	.0012539	0.1900	53572.7	55616.3	2			
0812-252	0812-252	2903	08	14	55.12993237	-25	21	43.9249682	.00016074	.0031143	0.3277	50631.8	50687.7	2			
0812+020	0812+020	1630	08	15	22.96080770	+01	54	59.4813770	.00001414	.0003117	-0.2949	54124.9	56568.7	5			
0812+367	0812+367	797	08	15	25.94485931	+36	35	15.1488164	.00000444	.0000745	0.0420	50241.9	56755.6	40	0.45	0.24	2.8
0812+100	0812+100	2904	08	15	29.47302827	+09	54	40.7000654	.00003917	.0010761	0.1708	53134.0	56302.4	2			
0814-241	0814-241	1631	08	16	40.41235539	-24	21	6.5701527	.00001919	.0006477	-0.4518	53126.0	53126.1	1			
0814+240	0814+240	1632	08	17	10.54780148	+23	52	23.9523989	.00007394	.0010578	-0.2646	53559.9	53560.8	1			
0814-029	0814-029	2905	08	17	27.48601795	-03	07	37.3129743	.00014857	.0028783	0.6145	50576.0	50576.1	1			
0814+326	0814+326	2906	08	17	28.54227788	+32	27	2.9259391	.00006107	.0011510	0.5391	50218.9	50218.9	1			
0813+557	0813+557	1633	08	17	41.01991568	+55	37	33.2828540	.00002540	.0002488	-0.1174	53133.9	53134.1	1			
0815-094	0815-094	1634	08	17	49.74953882	-09	33	30.5284862	.00003468	.0012673	-0.6258	53560.9	53561.8	1			
0815-294	0815-294	2907	08	17	58.85024258	-29	36	31.4214009	.00003382	.0011075	0.1363	53503.0	53503.1	1			
0814+425	OJ 425	214	08	18	15.99960686	+42	22	45.4148929	.00000400	.0000592	-0.0950	43808.8	56776.7	305	0.88	0.68	2.3
0816+054	0816+054	1635	08	18	56.23684456	+05	17	37.2655247	.00000904	.0002976	-0.2308	53126.0	53916.0	2			
0815+326	0815+326	2908	08	19	2.32858495	+32	26	37.2158344	.00003975	.0008792	0.5480	50218.9	50218.9	1			
0816+279	0816+279	1636	08	19	18.85572439	+27	47	30.6886508	.00002863	.0007494	-0.2378	53572.7	53572.8	1			
0817-063	0817-063	1637	08	19	36.64761417	-06	30	48.1707165	.00010071	.0037986	0.2222	53522.9	54112.3	2			
0818-128	P 0818-128	216	08	20	57.44761005	-12	58	59.1691855	.00000644	.0001080	-0.0850	49482.1	55257.6	47	0.11	0.08	3.5
0820-578	0820-578	2909	08	21	20.52747744	-58	00	18.7514147	.00005680	.0010401	0.4922	54723.1	54723.2	1			
0819-032	0819-032	2910	08	21	40.03746647	-03	23	12.5343364	.00006641	.0022011	-0.3101	50576.0	50576.1	1			
0819+408	0819+408	2911	08	22	57.55595164	+40	41	49.7667422	.00001625	.0003748	0.1009	50241.9	50242.0	1			
0820+225	0820+225	2912	08	23	24.75917110	+22	23	3.2885191	.00002740	.0008075	0.3541	50084.5	50156.2	2			
0820+296	0820+296	2913	08	23	41.13195775	+29	28	28.1992665	.00005085	.0011278	0.1312	50218.9	50218.9	1			
0821-094	0821-094	1638	08	23	52.02320837	-09	39	25.9066109	.00016655	.0047298	-0.0636	53551.9	53552.0	1			
0821-182	0821-182	1639	08	24	4.06603805	-18	27	40.8397927	.00002878	.0010281	-0.0374	53559.9	53560.8	1			
0821+248	0821+248	1061	08	24	33.00929048	+24	38	43.1160690	.00000912	.0002987	-0.3539	50084.5	56754.1	30	0.20	0.13	1.7
0820+560	0820+560	702	08	24	47.23635067	+55	52	42.6694029	.00000484	.0000580	-0.0161	47282.9	55773.2	62	0.24		3.2
0822-243	0822-243	1640	08	24	49.26024888	-24	28	52.5570201	.00013803	.0054220	0.0960	53560.9	53561.8	1			
0822-152	0822-152	2914	08	24	51.62146998	-15	27	45.9157402	.00002637	.0007138	0.0247	54087.3	55168.5	2			
0821+394	0821+394	798	08	24	55.48385386	+39	16	41.9040695	.00000422	.0000642	-0.0707	49268.4	56758.5	50	0.82	0.66	2.4
0822+086	0822+086	1641	08	25	4.77639881	+08	31	11.0919008	.00007615	.0013611	-0.2141	53572.7	53572.8	1			
0822+137	J0825+1332	799	08	25	11.89094319	+13	32	32.5386233	.00000564	.0002337	-0.1878	50084.5	56717.1	40	0.24	0.13	
0823-500	0823-500	800	08	25	26.86949165	-50	10	38.4926279	.00099532	.0107100	-0.8725	50259.2	53568.5	2			
0821+621	0821+621	801	08	25	38.61217665	+61	57	28.5794287	.00001028	.0000803	0.0802	49422.0	53613.0	14	0.13		
0823+033	P 0823+033	221	08	25	50.33835465	+03	09	24.5200010	.00000338	.0000530	-0.0412	44200.7	56758.4	1161	0.71	0.70	2.7
0823-321	0823-321	1642	08	25	51.37262896	-32	18	23.2334730	.00005082	.0018523	-0.3139	53153.0	53153.0	1			
0823-223	P 0823-223	2915	08	26	1.57293827	-22	30	27.2032950	.00000895	.0002715	-0.3358	50631.8	56561.0	7		0.30	
0824+355	0824+355	1062	08	27	38.58822961	+35	25	5.0773422	.00001485	.0003252	-0.0763	50241.9	50242.0	1		0.11	
0824+524	0824+524	2916	08	27	53.69811261	+52	17	58.2962103	.00021510	.0014088	0.0496	49576.6	49576.8	1			
0826-373	0826-373	802	08	28	4.78023193	-37	31	6.2812200	.00000621	.0001181	0.0976	48110.0	56601.1	44		0.32	4.2
0826+180	0826+180	1643	08	29	4.82877185	+17	54	15.8625873	.00030855	.0035473	-0.7217	54087.3	54965.1	2			
0827+243	B2 0827+24	224	08	30	52.08619027	+24	10	59.8203600	.00000373	.0000589	-0.1347	44200.7	56772.6	171	0.74	0.84	2.4
0828-222	0828-222	1644	08	31	9.14861916	-22	28	26.7857829	.00059209	.0326703	-0.9060	53572.8	54278.0	2			
0829+046	MA 0829+04	226	08	31	48.87695398	+04	29	39.0858320	.00000467	.0000888	-0.0268	49913.8	55327.7	34	0.21	0.23	3.0
0829+089	0829+089	4128	08	31	55.09150940	+08	47	43.6516288	.00002224	.0006387	0.3184	55847.5	55916.5	2			
0829+187	0829+187	2917	08	32	16.04025731	+18	32	12.1338950	.00003166	.0007557	-0.0387	50084.5	50156.2	2			
0828+493	OJ 448	225	08	32	23.21670790	+49	13	21.0381589	.00000635	.0000834	0.0668	48352.9	56766.5	60	0.16		2.3
0829+108	0829+108	2918	08	32	38.47715805	+10	40	19.6544257	.00006508	.0019090	-0.4048	49913.8	49913.9	1			
0830+160	0830+160	1645	08	32	49.39710110	+15	54	8.6233432	.00002512	.0007169	-0.2300	53559.9	53560.8	1			

Source Name		ID No.	Right Ascension			Declination			RA Error (s)	Dec. Error (arcsec)	RA–Dec Corr.	Observation Epoch MJD		No. Obs.	Source Flux (Jy)		Str Index
B1950	Common		H	M	S	D	M	S				First	Last		10-60	10-40	
0830+115	0830+115	2919	08	33	14.36667861	+11	23	36.2351241	.00003023	.0008231	0.3732	49913.8	49913.9	1			
0830+040	0830+040	2920	08	33	18.91302561	+03	50	32.3504114	.00003669	.0012264	-0.1441	49913.8	49913.9	1			
0831-445	0831-445	803	08	33	22.33356940	-44	41	38.9098889	.01728449	.2054513	-0.9855	49330.9	49330.9	1			
0830+425	0830+425	2921	08	33	53.88536706	+42	24	1.8503703	.00002749	.0004981	0.0883	50241.9	50242.0	1			
0830+605	0830+605	2922	08	34	17.54591577	+60	19	47.0669499	.00008975	.0011224	0.3892	49576.6	49576.8	1			
0832-225	0832-225	4072	08	34	44.19793878	-22	41	12.8133833	.00013743	.0053662	-0.2618	56497.9	56498.7	1			
0831+557	4C 55.16	228	08	34	54.90400746	+55	34	21.0703511	.00009108	.0007497	-0.0136	48975.7	55180.7	17			5.1
0830+687	0830+687	4129	08	35	47.60876465	+68	35	11.4900701	.00017181	.0006094	-0.0677	55776.0	55776.6	1			
0833+218	0833+218	2923	08	36	16.21692805	+21	39	3.5780215	.00009582	.0016046	-0.6911	54087.3	54087.5	1			
0833+276	0833+276	2924	08	36	22.88866266	+27	28	52.5336107	.00001745	.0004480	0.0852	50218.9	50219.0	1			
0833+416	0833+416	2925	08	36	36.89265658	+41	25	54.7121870	.00002301	.0006232	-0.0639	50241.9	50242.0	1			
0834-201	P 0834-20	804	08	36	39.21524474	-20	16	59.5042557	.00000440	.0000780	0.0574	49425.7	56776.6	70	0.83	0.75	2.3
0834-223	0834-223	2926	08	36	50.76881064	-22	33	10.0878952	.00010751	.0026927	-0.0047	50631.8	50687.7	2			
0835-339	0835-339	1271	08	37	0.31666510	-34	09	14.8587777	.00002829	.0006342	0.2598	53977.8	53978.7	1			
0833+585	0833+585	805	08	37	22.40966774	+58	25	1.8449421	.00000734	.0000747	0.0212	48353.2	55327.5	58	0.54		3.3
0834+250	OJ 259	1063	08	37	40.24568712	+24	54	23.1215490	.00000533	.0001097	-0.2652	50218.9	56749.2	30	0.36	0.35	2.8
0836-384	0836-384	4073	08	38	11.01515265	-38	36	49.6582757	.00010156	.0037770	0.0671	56204.6	56204.7	1			
0836+290	0836+290	1064	08	39	15.82767733	+28	50	38.8028833	.00001332	.0004547	-0.2108	53067.9	54142.1	6	0.14	0.07	
0836+182	0836+182	1646	08	39	30.72138362	+18	02	47.1423425	.00001961	.0004368	-0.5976	50084.5	52543.5	5			
0837+035	P 0837+035	2927	08	39	49.19582308	+03	19	53.8586306	.00002236	.0006015	-0.3168	49913.8	49913.9	1			
0837+012	0837+012	2928	08	39	49.61100693	+01	04	26.7361816	.00001807	.0005611	0.0194	49913.8	49913.9	1			
0836+426	0836+426	2929	08	39	56.56134495	+42	27	55.8154259	.00002387	.0004851	0.0927	50241.9	50242.0	1			
0838+133	0838+133A	1272	08	40	47.58842211	+13	12	23.5636368	.00000731	.0002012	-0.3282	52409.1	53820.1	4	0.39	0.41	
0837+448	0837+448	4074	08	40	51.28893549	+44	39	59.2924457	.00007029	.0008581	0.3482	56267.3	56267.6	1			
0836+710	4C 71.07	231	08	41	24.36527146	+70	53	42.1730381	.00000602	.0000568	0.0485	44202.9	55166.6	94	1.17		3.6
0842-754	0842-754	2930	08	41	27.03379988	-75	40	27.8749586	.00315071	.0114846	-0.1484	48110.1	48110.9	1			
0839-314	0839-314	1647	08	41	32.60257209	-31	36	35.6873940	.00013399	.0043654	0.7604	53153.0	53153.0	1			
0839+187	GC 0839+18	234	08	42	5.09417143	+18	35	40.9904863	.00000627	.0001497	0.0495	48976.2	56637.9	34	0.16	0.19	4.3
0839+458	0839+458	2931	08	43	7.09423847	+45	37	42.8979373	.00050098	.0102961	0.3218	50305.7	50305.8	1			
0840+424	0840+424	2932	08	43	31.63738248	+42	15	29.5258606	.00016947	.0029898	0.2088	50241.9	50242.0	1			
0839+687	0839+687	2933	08	43	49.10151177	+68	33	17.1547603	.00005437	.0004152	0.1477	49826.9	54087.4	2			
0841+386	0841+386	2934	08	44	29.09781461	+38	30	55.7102567	.00001729	.0004382	-0.1542	50241.9	50242.0	1			
0842-375	0842-375	2935	08	44	52.32117668	-37	42	9.3829181	.00027667	.0135947	0.7804	52306.3	52409.1	2			
0843-336	0843-336	1648	08	45	8.14434044	-33	47	41.0610832	.00007743	.0028965	-0.7746	54964.9	54965.1	1			
0842+048	0842+048	2936	08	45	17.14377078	+04	39	47.3545153	.00021889	.0026004	0.5476	49913.8	49913.9	1			
0843-371	0843-371	2937	08	45	42.49653920	-37	18	55.0022824	.00046057	.0178609	0.4084	52409.1	55483.6	2			
0843-259	0843-259	2938	08	46	0.73385854	-26	10	54.1553754	.00025033	.0055792	-0.0477	50631.8	50687.7	2			
0844-342	0844-342	2939	08	46	10.89370213	-34	24	33.5821422	.00021024	.0073721	0.7866	52306.3	52306.4	1			
0844-259	0844-259	2940	08	46	56.61656294	-26	07	50.6594031	.00012550	.0037374	0.7462	53503.0	53503.1	1			
0844-177	0844-177	1649	08	47	11.17021243	-17	54	50.1387172	.00013390	.0036801	0.4861	53523.0	53560.8	2			
0844+387	0844+387	1650	08	47	15.16919709	+38	31	9.9842594	.00009352	.0011251	-0.0466	53551.8	53552.0	1			
0843+575	0843+575	2941	08	47	28.05982091	+57	23	38.3325091	.00098486	.0081740	0.8467	49576.6	49576.8	1			
0844+463	0844+463	2942	08	47	34.29850700	+46	09	28.0053024	.00002160	.0003646	0.2463	50305.7	50305.8	1			
0845-068	0845-068	2943	08	47	56.73723797	-07	03	16.9025171	.00001359	.0004723	-0.2165	53503.0	53503.1	1			
0845-051	0845-051	1651	08	47	58.72492904	-05	20	33.9001976	.00000781	.0002396	-0.1053	53133.9	56701.4	2	0.17	0.21	
0847-354	0847-354	2944	08	49	45.62349315	-35	41	1.2786883	.00002362	.0007538	-0.1200	52306.3	52409.1	2		0.27	
0846+513	0846+513	1652	08	49	57.97686274	+51	08	29.0239984	.00002189	.0003586	0.2436	53560.9	53561.8	1			
0847-120	0847-120	1653	08	50	9.63563060	-12	13	35.3760884	.00000394	.0000664	0.0298	53134.0	56637.6	130	0.34	0.43	
0847+379	0847+379	1065	08	50	24.72978393	+37	47	9.4778663	.00001828	.0004277	-0.1463	50241.9	50242.0	1			
0848-304	0848-304	2945	08	50	33.68170247	-30	39	34.3470603	.00037566	.0090454	-0.0918	52306.3	56638.4	2			

Source Name		ID No.	Right Ascension			Declination			RA Error (s)	Dec. Error (arcsec)	RA–Dec Corr.	Observation Epoch MJD		No. Obs.	Source Flux (Jy)		Str Index
B1950	Common		H	M	S	D	M	S				First	Last		10-60	10-40	
0848+089	0848+089	2946	08	51	28.42529412	+08	45	15.3109018	.00002852	.0005877	0.1985	49913.8	55657.2	2			
0849+287	0849+287	1654	08	52	5.16955008	+28	33	59.7311739	.00001713	.0004783	-0.3300	53125.1	53126.0	1			
0850-152	0850-152	2947	08	52	30.84719052	-15	28	8.4766131	.00004654	.0013887	-0.2865	53572.8	53572.8	1			
0851-382	0851-382	2948	08	52	59.93280503	-38	24	20.4023427	.75622826	1.5593300	1.0000	52409.	52409.	1			
0850-016	0850-016	2949	08	53	1.33035021	-01	50	48.1385874	.01341497	.2188028	-0.9963	53552.0	53552.0	1			
0851+071	0851+071	1224	08	53	48.19003004	+06	54	47.2362633	.00005600	.0014247	0.5357	49913.8	49913.9	1			
0852-254	0852-254	1655	08	54	32.17990710	-25	40	20.8435370	.00006999	.0025443	0.1061	53523.0	53523.0	1			
0851+075	0851+075	1656	08	54	35.03643501	+07	20	24.1250107	.00002393	.0006447	0.0176	53559.9	53560.8	1			
0850+581	0850+581	808	08	54	41.99639609	+57	57	29.9391499	.00000655	.0000794	-0.0646	48720.0	56770.3	89	0.18		3.2
0847+807	0847+807	2950	08	54	48.59874083	+80	34	22.3819854	.00009026	.0004566	0.1606	54087.4	54087.5	1			
0851+202	OJ 287	236	08	54	48.87492726	+20	06	30.6408446	.00000335	.0000507	0.0103	43808.7	56776.7	2281	1.78	1.67	2.6
0850+625	0850+625	2951	08	54	50.57625135	+62	18	50.1908081	.00016200	.0013656	-0.0790	49826.9	49827.1	1			
0855-716	0855-716	2952	08	55	11.76993935	-71	49	6.4574311	.00007471	.0004575	0.1152	54723.1	54723.5	1			
0854-108	0854-108	1657	08	56	41.80415119	-11	05	14.4303210	.00000406	.0000650	-0.0722	53551.9	56763.7	126	0.24	0.31	
0851+719	0851+719	1658	08	56	54.86911606	+71	46	23.9015977	.00096400	.0023371	-0.3628	53560.9	53561.7	1			
0854+213	0854+213	1659	08	56	57.24476683	+21	11	43.6582430	.00000635	.0001324	-0.0143	50084.5	52009.4	4			
0855-196	0855-196	2953	08	58	5.36321476	-19	50	36.9356647	.00001149	.0004044	0.1654	50631.8	50687.7	2			
0855+143	3C 212	2954	08	58	41.44703008	+14	09	44.7618026	.00001237	.0002930	-0.1799	55111.8	55112.5	1			
0855+142	0855+142	1660	08	58	41.60032783	+14	05	40.3716089	.00007376	.0029586	-0.4699	53523.1	53523.1	1			
0857-329	0857-329	2955	08	59	20.81292447	-33	09	24.7209821	.00012906	.0059356	0.0878	52306.3	55112.6	2			
0857+413	0857+413	1661	09	00	21.43383961	+41	08	22.9897368	.00002223	.0004730	-0.2785	53572.7	53572.9	1			
0858-125	0858-125	1662	09	00	39.76563615	-12	42	32.6220248	.00021157	.0059056	-0.1793	53559.9	53560.8	1			
0858-279	0858-279	2956	09	00	40.03874066	-28	08	20.3521988	.00006059	.0016929	0.0201	50687.6	54643.7	2			
0858-313	0858-313	2957	09	00	44.29435971	-31	31	28.5780662	.00003868	.0013016	0.3334	52306.3	55657.1	2			
0858+050	0858+050	1663	09	01	11.86429055	+04	48	58.8331252	.00002178	.0006172	-0.4020	53560.9	53561.8	1			
0859-068	0859-068	2958	09	01	44.24375060	-07	02	16.1026638	.01278500	.2344880	-0.9910	53552.0	53552.0	1			
0859-140	P 0859-14	240	09	02	16.83091832	-14	15	30.8754309	.00000485	.0000879	-0.3616	43808.7	56637.9	124	0.26	0.50	3.8
0858+542	0858+542	1664	09	02	19.28741328	+54	02	57.2554676	.00006673	.0008376	0.0685	53572.8	53572.9	1			
0859+433	0859+433	2959	09	02	30.91996002	+43	10	14.1656440	.00001541	.0003403	-0.0746	50241.9	50242.0	1			
0900-171	0900-171	1665	09	03	0.01978431	-17	21	5.2324990	.00002691	.0008174	-0.3823	53559.8	53559.9	1			
0859+470	OJ 499	239	09	03	3.99010171	+46	51	4.1374232	.00000441	.0000675	-0.0416	43808.9	56782.1	238	0.51	0.29	3.1
0901-310	0901-310	1666	09	03	37.93483062	-31	17	39.1298552	.00014749	.0066138	0.5079	52409.0	53523.0	2			
0859+681	0859+681	1667	09	03	53.15504749	+67	57	22.6859039	.00002990	.0002535	0.3103	49826.9	54664.7	2			
0900+520	0900+520	2960	09	03	58.57441410	+51	51	0.6618866	.00022753	.0022066	0.5743	49576.8	49576.9	1			
0900+428	0900+428	2961	09	04	15.62848783	+42	38	4.7644625	.00002438	.0004686	-0.2644	50241.9	50242.0	1			
0902-309	0902-309	2962	09	04	20.51593609	-31	11	25.6649266	.00004248	.0016527	-0.1904	52409.0	56204.6	2			
0902-350	0902-350	2963	09	04	42.37878669	-35	14	24.3499955	.00002410	.0009279	0.0873	55370.8	55370.9	1			
0902-256	0902-256	2964	09	04	52.18599993	-25	52	51.7585855	.00004838	.0012216	0.1462	50631.8	50687.8	2			
0903-573	0903-573	2965	09	04	53.17915879	-57	35	5.7847133	.00054210	.0021940	0.3171	52886.8	53138.5	3			
0902+490	0902+490A	2966	09	05	27.46386851	+48	50	49.9649671	.00001738	.0002954	0.1180	50305.7	50305.8	1			
0902+290	0902+290	1067	09	05	41.76989068	+28	49	28.3015498	.00005638	.0008801	0.5215	50218.9	50219.0	1		0.07	
0902+468	0902+468	2967	09	06	15.53965190	+46	36	19.0254769	.00010664	.0019808	-0.3951	50305.7	50305.8	1			
0904-201	0904-201	1668	09	06	51.30535105	-20	19	54.8051481	.00001290	.0004405	-0.1811	53551.9	53552.0	1			
0903+684	0903+684	2968	09	07	52.94636688	+68	15	44.9206092	.00018982	.0011388	0.3360	49826.9	49827.1	1			
0905-202	0905-202	2969	09	07	54.04047667	-20	26	49.4750621	.00001983	.0008026	-0.4254	53503.1	53503.1	1			
0905+420	0905+420	2970	09	08	35.86340003	+41	50	46.2044323	.00004925	.0007806	0.1445	54112.3	56106.1	2			
0906+163	0906+163	1068	09	08	55.92535236	+16	09	54.7636264	.00003456	.0007689	-0.7746	50084.5	53820.1	5	0.17	0.13	
0906+015	P 0906+01	244	09	09	10.09160002	+01	21	35.6178046	.00000543	.0001349	-0.4821	48352.9	56691.2	69	0.82	0.65	3.1
0906+087	0906+087	1669	09	09	12.15751061	+08	35	41.0982529	.00003092	.0007547	-0.4205	53523.0	53561.8	2			
0906-048	0906-048	1670	09	09	17.00384047	-05	00	52.8971598	.00010948	.0031661	-0.2635	54313.8	54313.9	1			

Source Name		ID No.	Right Ascension			Declination			RA Error (s)	Dec. Error (arcsec)	RA–Dec Corr.	Observation Epoch MJD		No. Obs.	Source Flux (Jy)		Str Index
B1950	Common		H	M	S	D	M	S				First	Last		10-60	10-40	
0906+430	0906+430	1671	09	09	33.49711708	+42	53	46.4817599	.00001270	.0001875	0.2507	53133.9	53134.1	1			
0907+022	0907+022	1672	09	09	39.84790449	+02	00	5.2668838	.00004156	.0004186	0.0460	49913.8	54643.7	2			
0907-023	0907-023	1673	09	09	44.92413808	-02	31	30.3550906	.00013825	.0036140	0.5103	53559.8	53559.9	1			
0907-179	0907-179	1674	09	09	45.25918025	-18	08	33.9443550	.00012441	.0048357	-0.7157	53560.9	53561.8	1			
0908-052	0908-052	2971	09	10	51.00187636	-05	26	29.1931726	.00005919	.0017173	0.0434	53152.9	56393.2	2			
0908+201	0908+201	2972	09	11	33.45959562	+19	58	14.0905646	.00020991	.0023348	-0.1902	50084.5	50156.3	2			
0908+340	0908+340	2973	09	11	47.76148567	+33	49	16.7941518	.00004827	.0017365	0.4025	50218.9	50219.0	1			
0910-414	0910-414	1675	09	12	12.75084668	-41	37	16.1444823	.00011373	.0048957	0.8372	54943.1	54943.1	1			
0909+222	0909+222	1676	09	12	24.78461216	+22	05	6.2479151	.00002707	.0005711	-0.2768	53125.1	53126.0	1			
0910-276	0910-276	2974	09	12	31.58688460	-27	52	17.2267934	.00063082	.0125053	0.3760	53559.8	53559.9	1			
0909+445	0909+445	2975	09	12	51.12936924	+44	22	4.6446699	.00069629	.0042531	-0.6234	53572.8	53572.9	1			
0910+442	0910+442	2976	09	13	53.36560741	+44	02	57.2010629	.00010030	.0016100	-0.5484	54087.3	54087.5	1			
0912-273	0912-273	2977	09	14	16.58609086	-27	33	16.6699394	.00052992	.0187930	-0.7724	53560.9	56638.5	2			
0912-330	0912-330	2978	09	14	36.72104279	-33	14	52.4157750	.00006277	.0024707	0.2328	55168.4	55168.5	1			
0912+029	P 0912+029	245	09	14	37.91343512	+02	45	59.2465141	.00000347	.0000550	0.0230	47253.3	56770.6	380	0.60	0.44	2.3
0911+354	0911+354	2979	09	14	39.42353380	+35	12	4.5914732	.00003368	.0006979	0.2479	50241.9	50242.0	1			
0912-204	0912-204	4075	09	14	59.69591955	-20	38	57.6262378	.00018249	.0085048	-0.8756	56638.4	56638.5	1			
0913-042	0913-042	1677	09	15	37.67766398	-04	29	16.2972048	.00017003	.0023770	0.2974	53551.9	53572.9	2			
0913-302	0913-302	4076	09	15	40.89579712	-30	29	49.4229565	.00055504	.0145822	-0.2482	56638.4	56638.5	1			
0913+003	0913+003	2980	09	15	51.69517650	+00	07	13.3090447	.00006264	.0016523	-0.3385	54112.4	54112.4	1			
0912+297	B2 0912+29	246	09	15	52.40163576	+29	33	24.0427495	.00001158	.0002431	-0.1039	49176.9	56568.5	20	0.09		2.5
0913+079	0913+079	2981	09	15	52.96821844	+07	45	39.6955355	.00005791	.0013933	-0.3790	53134.1	55518.6	2			
0913+391	0913+391	2982	09	16	48.90456414	+38	54	28.1463443	.00001519	.0003210	0.0683	50241.9	50242.0	1			
0915-213	0915-213	2983	09	17	27.01630783	-21	31	34.4634510	.00001518	.0005422	-0.2169	50631.8	50687.8	2			
0915-135	0915-135	1678	09	17	39.00067913	-13	45	42.2377214	.00001604	.0005471	-0.4338	53503.1	53559.9	2			
0913+657	0913+657	2984	09	17	55.56823530	+65	30	15.1254236	.00030084	.0018919	0.3673	54440.3	55916.6	2			
0915-118	0915-118	1679	09	18	5.66850958	-12	05	43.8050868	.00004188	.0012749	0.8095	54853.3	54853.4	1			
0916-074	0916-074	1680	09	19	1.96265198	-07	39	5.1096598	.00006853	.0018370	-0.0582	53152.9	53153.1	1			
0916+336	0916+336	2985	09	19	8.78712333	+33	24	41.9433893	.00001277	.0003404	0.2833	50218.9	55966.4	2	0.16	0.14	
0913+786	0913+786	2986	09	19	52.55956522	+78	25	26.5578658	.00023426	.0009065	0.7473	49826.9	50688.3	2			
0918-363	0918-363	2987	09	20	26.20110992	-36	31	47.5151005	.00006138	.0020421	-0.6411	52306.3	52409.1	2			
0918-297	0918-297	2988	09	20	43.19377609	-29	56	30.2935682	.00001865	.0007731	-0.2307	54489.3	54489.4	1			
0917+449	0917+449	810	09	20	58.45848435	+44	41	53.9851292	.00000472	.0000734	-0.0718	47940.5	56766.5	120	0.76	0.65	3.1
0916+718	0916+718	1681	09	21	23.94511344	+71	36	12.4016615	.00007386	.0004093	-0.3265	53125.1	53125.9	1			
0919-260	0919-260	811	09	21	29.35385015	-26	18	43.3863109	.00000371	.0000700	-0.1089	47736.7	56758.7	317		0.51	2.7
0918+140	0918+140	2989	09	21	31.37387984	+13	50	48.4043734	.00110930	.1967678	0.8354	50156.3	56302.5	2			
0917+624	0917+624	698	09	21	36.23106329	+62	15	52.1803430	.00000430	.0000540	-0.1528	48720.0	55823.3	132	0.65		3.1
0919-052	0919-052	1682	09	22	23.67288647	-05	29	7.1843181	.00001789	.0006321	-0.4275	53523.0	53523.1	1			
0920-397	P 0920-39	249	09	22	46.41826873	-39	59	35.0684273	.00000413	.0000775	-0.1393	46797.4	56751.7	395		0.26	2.5
0920+390	0920+390	812	09	23	14.45293368	+38	49	39.9101294	.00000384	.0000580	0.0437	49736.1	56734.6	154			
0920+416	0920+416	2990	09	23	31.30495296	+41	25	27.4392574	.00001534	.0003298	-0.0269	50241.9	50242.0	1			
0921-213	0921-213	2991	09	23	38.88517883	-21	35	47.1274444	.00003296	.0009800	0.2913	50631.8	50687.8	2			
0920+313	0920+313	1683	09	23	47.94862395	+31	07	54.1417988	.00011132	.0016674	-0.5637	53560.9	53561.8	1			
0920+284	0920+284	2992	09	23	51.52343344	+28	15	25.0220018	.00003050	.0007009	0.1686	50218.9	50219.0	1			
0921+454	0921+454	1684	09	24	44.99434809	+45	11	57.9172987	.00012498	.0009436	0.1041	53572.8	53572.9	1			
0922+005	P 0922+005	2993	09	25	7.81503343	+00	19	13.9343600	.00002194	.0007512	0.2634	49913.8	49913.9	1			
0922-202	0922-202	2994	09	25	11.94736549	-20	27	35.6083961	.00012511	.0038450	0.2692	52409.1	52409.1	1			
0922+316	0922+316	2995	09	25	43.65024855	+31	27	10.8046367	.00009245	.0024512	0.2773	50218.9	50219.0	1			
0923+171	0923+171	2996	09	25	49.96439045	+16	58	12.2040192	.00002450	.0005242	-0.3691	53559.8	56463.1	2			
0922+364	0922+364	1685	09	25	51.85137823	+36	12	35.6741272	.00002190	.0004405	-0.0393	53560.9	53561.8	1			

Source Name		ID No.	Right Ascension			Declination			RA Error (s)	Dec. Error (arcsec)	RA–Dec Corr.	Observation Epoch MJD		No. Obs.	Source Flux (Jy)		Str Index
B1950	Common		H	M	S	D	M	S				First	Last		10-60	10-40	
0922+407	0922+407	2997	09	26	0.42684969	+40	29	49.6724504	.00001176	.0002792	-0.0061	50241.9	50242.0	1			
0923+392	4C 39.25	251	09	27	3.01393353	+39	02	20.8518493	.00000336	.0000505	-0.0206	43808.8	56717.1	2079	1.79	1.06	2.8
0923+575	0923+575	1686	09	27	6.05353938	+57	17	45.3439794	.00011475	.0012121	0.0978	53134.0	53134.1	1			
0925-203	P 0925-203	686	09	27	51.82431992	-20	34	51.2325443	.00000375	.0000576	-0.1150	46797.5	56770.5	354	0.56	0.77	2.2
0925+449	0925+449	2998	09	28	24.13710995	+44	46	4.7996540	.00003557	.0005578	0.2641	50305.7	50305.8	1			
0926-039	0926-039	1687	09	28	33.46943503	-04	09	8.8488854	.00005056	.0020406	-0.7152	53125.1	53126.0	1			
0926-306	0926-306	2999	09	28	33.98818533	-30	49	44.0035682	.00013413	.0041261	0.6906	52306.3	52306.4	1			
0926-181	0926-181	3000	09	29	2.26150680	-18	20	45.7609735	.00005397	.0024446	-0.2423	54087.4	54087.5	1			
0925+504	0925+504	1225	09	29	15.44019199	+50	13	35.9898883	.00001224	.0001734	0.0505	49576.7	53306.7	3			
0916+864	0916+864	1069	09	29	43.05601255	+86	12	21.2770003	.00246579	.0052070	-0.0555	50688.2	50688.3	1	0.16		
0927-378	0927-378	3001	09	29	57.50800147	-38	01	48.1701786	.00003845	.0009982	0.5007	52306.3	52409.1	2			
0936-853	0936-853	813	09	30	32.57051441	-85	33	59.6834693	.00933203	.0119529	-0.0152	49329.1	49331.0	1			
0927+469	0927+469	1688	09	30	35.08071983	+46	44	8.6555173	.00014375	.0015909	0.3654	50305.7	54314.7	2			
0928+008	0928+008	3002	09	30	52.25354114	+00	34	58.9416260	.00002215	.0009378	-0.5427	49913.8	54482.5	2			
0925+745	0925+745	3003	09	30	53.78264586	+74	20	5.9106145	.00036806	.0015993	-0.3387	49826.9	49827.1	1			
0927+352	0927+352	3004	09	30	55.27909978	+35	03	37.6082673	.00001231	.0003018	-0.0251	50241.9	50242.0	1			
0928-100	0928-100	3005	09	31	2.71243226	-10	13	25.0238185	.00003229	.0010945	0.1997	53560.9	56106.0	2			
0928+144	0928+144	3006	09	31	5.34243907	+14	14	16.5189973	.00002233	.0006619	-0.4851	50084.5	53916.0	3	0.18	0.17	
0928+280	0928+280	3007	09	31	51.78402443	+27	50	50.5993659	.00004210	.0007605	-0.3751	54112.3	56106.1	2			
0930-200	0930-200	1689	09	32	19.58651189	-20	16	37.2062736	.00010468	.0034516	-0.0953	53560.9	53561.9	1			
0930-338	0930-338	1690	09	32	36.49499147	-34	05	58.4859896	.00019320	.0112371	-0.5494	53126.1	53126.1	1			
0929+533	0929+533	3008	09	32	41.15081307	+53	06	33.8008967	.00003863	.0005489	-0.0339	49576.7	49576.9	1			
0928+653	0928+653	1691	09	32	54.57750751	+65	07	41.2959207	.00009068	.0011180	-0.4587	53560.0	53560.7	1			
0930-080	0930-080	1692	09	33	17.09540199	-08	19	10.8513325	.00002027	.0008199	-0.2396	53559.8	53559.9	1			
0931-114	0931-114	3009	09	33	34.45351405	-11	39	25.4756516	.00002417	.0007448	-0.4432	50576.0	50576.1	1			
0930+396	0930+396	1693	09	34	6.67006297	+39	26	32.1344738	.00009354	.0020307	0.3841	53561.0	53561.8	1			
0930+493	0930+493	3010	09	34	15.76227209	+49	08	21.7307519	.00003932	.0005332	0.4988	50305.7	50305.8	1			
0932+075	0932+075	3011	09	35	1.07591864	+07	19	18.6101558	.00003456	.0007846	0.2066	49913.8	55847.7	2			
0933-333	0933-333	3012	09	35	9.22984986	-33	32	37.7085333	.00010301	.0050179	0.3775	52409.1	52409.1	1			
0932-281	0932-281	3013	09	35	11.50188210	-28	20	31.4713823	.00288209	.0623420	0.1415	50687.6	50687.8	1			
0932+094	J0935+0915	1070	09	35	13.64139983	+09	15	7.8327767	.00004242	.0011714	-0.2285	49913.8	49913.9	1		0.20	
0932-194	0932-194	3014	09	35	15.61532943	-19	39	8.7706963	.00057607	.0125095	-0.8045	53559.8	53559.9	1			
0932+243	0932+243	4077	09	35	23.27351908	+24	05	12.3227789	.00003063	.0012935	0.2324	56161.9	56162.7	1			
0932+197	0932+197	1694	09	35	29.21942557	+19	29	35.0662137	.00006963	.0022585	-0.7223	53572.8	53572.9	1			
0932+367	0932+367	1695	09	35	31.83993097	+36	33	17.5666876	.00003551	.0006752	0.1326	53134.0	53134.1	1			
0933+503	J0937+5008	1072	09	37	12.32734758	+50	08	52.0972249	.00002183	.0003508	-0.3466	49576.7	50305.9	2	0.26		
0936-069	0936-069	1696	09	38	56.10426215	-07	08	0.6185839	.00001380	.0004382	-0.1424	53572.8	56497.9	2	0.19	0.20	
0936-172	0936-172	1697	09	39	19.19505063	-17	31	35.7782349	.00011958	.0038091	-0.4224	53153.0	53153.1	1			
0936+419	0936+419	3015	09	39	49.61584639	+41	41	54.1910505	.00002146	.0004672	-0.1797	50241.9	50242.0	1			
0937+262	0937+262A	1226	09	40	14.72279807	+26	03	29.9457343	.00001319	.0003489	0.0597	50218.9	53306.5	2			
0938-133	0938-133	1698	09	41	2.54947885	-13	35	50.9848346	.00000891	.0002880	-0.3285	53559.9	56701.4	2	0.17	0.22	
0938+119	0938+119	3016	09	41	13.55890335	+11	45	32.3389858	.00027888	.0025824	0.6970	54291.8	54292.0	1			
0938+277	0938+277	1699	09	41	48.11604513	+27	28	38.8157955	.00002802	.0006108	-0.1847	53125.1	53126.0	1			
0939-077	0939-077	3017	09	42	21.46142031	-07	59	53.2047771	.00001986	.0007324	-0.5561	53503.1	53503.1	1			
0939+620	0939+620	3018	09	43	14.50279916	+61	50	33.3486261	.00017495	.0012066	-0.0305	54440.4	54440.6	1			
0940+172	0940+172	3019	09	43	17.22396502	+17	02	18.9627074	.00003494	.0011514	-0.5313	50084.5	50156.3	2			
0940+364	0940+364	1700	09	43	19.15348740	+36	14	52.0726972	.00002572	.0005958	-0.0833	53561.0	53561.8	1			
0941-080	P 0941-080	3020	09	43	36.94432144	-08	19	30.8122967	.00024238	.0051368	-0.2184	50576.0	50576.2	1			
0941+206	0941+206	3021	09	43	48.09841386	+20	28	9.9612121	.00010250	.0030325	-0.5919	54087.4	54087.5	1			
0941+522	0941+522	3022	09	44	52.15525923	+52	02	34.2173306	.00001965	.0002134	-0.0441	49576.7	56749.3	2	0.25		

Source Name		ID No.	Right Ascension			Declination			RA Error (s)	Dec. Error (arcsec)	RA–Dec Corr.	Observation Epoch MJD		No. Obs.	Source Flux (Jy)		Str Index
B1950	Common		H	M	S	D	M	S				First	Last		10-60	10-40	
0942+358	0942+358	3023	09	45	38.12071540	+35	34	55.0885737	.00000834	.0001372	-0.0150	50241.9	50854.4	2			
0942+468	0942+468	3024	09	45	42.09267330	+46	36	50.5961141	.00005002	.0006957	0.1219	50305.8	50305.9	1			
0943-016	0943-016	1701	09	45	44.03723482	-01	53	3.9548021	.00002677	.0010070	0.0482	53551.9	53552.0	1			
0942+505	0942+505	1702	09	46	16.04500873	+50	20	9.3480033	.00005355	.0010812	-0.0396	53559.9	53560.8	1			
0943+105	0943+105	1703	09	46	35.06995789	+10	17	6.1343783	.00000537	.0001312	-0.0430	49913.8	56701.5	29			
0944-201	0944-201	3025	09	46	50.21157782	-20	20	44.4505994	.00037302	.0077487	0.1227	53153.0	53153.1	1			
0943+593	0943+593	1704	09	47	4.86494716	+59	07	41.4759204	.00005699	.0008848	-0.5502	53561.0	53561.8	1			
0945-321	0945-321	3026	09	48	9.51254191	-32	23	47.4406206	.00007356	.0020856	0.1929	52306.3	52306.4	1			
0945-287	0945-287	3027	09	48	11.54328479	-29	01	44.1516463	.00011319	.0038471	0.6162	53503.1	56106.0	2			
0945+408	0945+408	814	09	48	55.33814713	+40	39	44.5870076	.00000455	.0000698	-0.0968	50003.5	56600.9	34	0.59	0.55	3.6
0947+064	0947+064	1705	09	50	3.46748633	+06	15	3.8165503	.00004830	.0015514	-0.1934	53134.0	53134.1	1			
0949+510	0949+510	3028	09	52	27.30826260	+50	48	50.6504530	.00003847	.0006279	-0.0837	53573.0	55847.5	2			
0950-246	0950-246	3029	09	52	31.67918903	-24	53	51.6646174	.05264319	.5522402	-0.9996	53153.0	53153.0	1			
0949+354	0949+354	815	09	52	32.02616745	+35	12	52.4029472	.00000504	.0000932	-0.0005	50241.9	56498.7	31		0.15	2.6
0951+175	0951+175	3030	09	53	59.23132339	+17	20	56.6542640	.00002957	.0007919	-0.1531	53559.8	56463.1	2			
0951+268	0951+268	1706	09	54	39.79653520	+26	39	24.5432748	.00000631	.0001551	-0.0034	50218.9	56667.8	31			
0950+748	0950+748	3031	09	54	47.44201531	+74	35	57.1453858	.00046947	.0013346	0.1526	49826.9	49827.1	1			
0952+179	AO 0952+17	255	09	54	56.82361282	+17	43	31.2222352	.00000441	.0000827	-0.1650	44200.7	56347.3	83	0.39	0.18	3.0
0951+488	0951+488	1707	09	55	5.00119695	+48	38	19.0422262	.00008651	.0009427	-0.0665	53561.0	53561.8	1			
0952-185	0952-185	3032	09	55	14.74315619	-18	45	33.6650479	.18674390	.4428042	-1.0000	53153.1	53153.1	1			
0951+692	M 81 nucl	816	09	55	24.77473316	+69	01	13.7016945	.00015229	.0010927	0.2496	49247.5	49267.7	2			
0951+693	M 81	817	09	55	33.17306483	+69	03	55.0609198	.00001398	.0000786	0.2573	49247.5	55112.7	61			
0952+581	0952+581	818	09	56	22.63442307	+57	53	55.9041939	.00009123	.0006867	-0.0527	49576.7	50974.7	2			
0953+254	OK 290	256	09	56	49.87537857	+25	15	16.0498986	.00000347	.0000531	0.1001	44446.6	56754.2	844	0.44	0.31	3.2
0954-135	0954-135	1708	09	57	18.18308112	-13	50	1.1763485	.00001404	.0004674	-0.3255	53523.0	53572.9	2			
0954+556	4C 55.17	819	09	57	38.18441153	+55	22	57.7679362	.00013501	.0013133	0.2447	49576.7	50989.8	3			
0955+476	0955+476	820	09	58	19.67164008	+47	25	7.8424724	.00000337	.0000504	-0.0096	48720.0	56775.2	1515	0.90	0.63	1.2
0955+326	3C 232	259	09	58	20.94963254	+32	24	2.2095066	.00000385	.0000632	-0.0700	50218.9	56748.7	92	0.61	0.37	2.8
0956-359	0956-359	1709	09	58	30.89417110	-36	12	40.7869795	.00041130	.0177341	0.7990	53523.0	53523.1	1			
0955+509	0955+509	3033	09	58	37.80940272	+50	39	57.4834784	.00001928	.0003012	-0.1840	49576.7	54112.4	3			
0956-409	0956-409	3034	09	58	38.29597493	-41	10	33.1765806	.00017157	.0066101	0.7489	52306.4	52409.1	2			
0954+658	0954+658	821	09	58	47.24510305	+65	33	54.8180573	.00000422	.0000537	-0.0405	47917.7	56770.4	324	0.73		2.6
0957-082	0957-082	3035	09	59	57.64765719	-08	28	26.0458529	.00007782	.0034471	-0.3933	54087.4	54087.5	1			
0958-314	0958-314	1710	10	00	40.83679038	-31	39	52.3748241	.00011880	.0053605	-0.0638	53134.1	53134.1	1			
0958+294	0958+294	3036	10	01	10.20565502	+29	11	37.5359820	.00001806	.0004513	0.2533	50218.9	50219.0	1			
0958+346	0958+346	1711	10	01	11.94921028	+34	24	50.4592666	.00000606	.0001043	0.1572	50218.9	56755.4	32			
0959+105	0959+105	3037	10	01	57.73496448	+10	15	49.7046561	.00005344	.0026915	-0.3757	49913.9	49913.9	1			
0959-443	P 0959-443	822	10	01	59.90833544	-44	38	0.6007316	.00010829	.0020968	-0.6211	50765.8	52409.1	3		0.34	
0959+127	0959+127	3038	10	02	30.53662186	+12	32	9.5475929	.00001636	.0005828	0.0549	53559.9	56036.3	2			
1000+125	1000+125	3039	10	02	52.84523110	+12	16	14.5851828	.00002104	.0004364	0.1587	49913.9	55657.3	2			
1001+329	1001+329	3040	10	03	57.56467209	+32	44	3.5421391	.00006596	.0014002	0.5523	50218.9	50219.1	1			
1003+351	3C 236	1712	10	06	1.75026777	+34	54	10.4006306	.00003276	.0006433	-0.0384	54313.8	54314.0	1			
1005-739	1005-739	3041	10	06	4.14468816	-74	09	44.0899991	.00157800	.0038903	0.2435	52886.9	53138.5	3			
1004-500	1004-500	823	10	06	14.00930305	-50	18	13.4707542	.00000895	.0001140	0.1995	52067.3	56716.2	69			
1004+054	1004+054	3042	10	06	37.61073780	+05	09	53.9788682	.00002718	.0007568	-0.2862	54112.4	55413.0	2			
1004-217	1004-217	1713	10	06	46.41368250	-21	59	20.4099874	.00000933	.0002017	-0.0279	50631.8	56387.6	24			
1004-018	P 1004-018	3043	10	07	4.34990697	-02	07	10.9178580	.00001266	.0003852	-0.0576	50576.0	50576.2	1			
1004-125	1004-125	3044	10	07	15.22773434	-12	47	45.9957008	.00002288	.0008758	-0.2826	53503.1	53503.2	1			
1005-333	1005-333	1714	10	07	31.38747340	-33	33	6.7166002	.00002661	.0008389	-0.2678	53125.1	55847.6	2		0.28	
1004+141	GC 1004+14	261	10	07	41.49808317	+13	56	29.6007905	.00000383	.0000650	-0.2142	44200.7	55168.6	292	0.24	0.22	3.5

Source Name		ID No.	Right Ascension			Declination			RA Error (s)	Dec. Error (arcsec)	RA–Dec Corr.	Observation Epoch MJD		No. Obs.	Source Flux (Jy)		Str Index
B1950	Common		H	M	S	D	M	S				First	Last		10-60	10-40	
1005+066	1005+066	1273	10	08	0.81615831	+06	21	21.2161271	.00000791	.0002147	-0.1338	49913.9	56701.4	3	0.42	0.36	
1006-093	1006-093	3045	10	08	43.86530288	-09	33	23.3575553	.00002916	.0009328	-0.0425	50576.0	50576.2	1			
1007+066	1007+066	3046	10	09	49.80822956	+06	22	0.9852937	.00011954	.0025547	-0.1842	53572.8	53572.9	1			
1003+830	1003+830	3047	10	10	15.78305117	+82	50	14.3840292	.00020284	.0003655	0.6948	50688.2	50688.3	1			
1008+082	1008+082	3048	10	10	47.23311710	+08	03	5.5045911	.00907464	.0064227	-0.0758	53559.9	53559.9	1			
1008-017	1008-017	3049	10	10	51.66665650	-02	00	19.5736078	.00001583	.0005638	-0.4734	50576.0	50576.2	1			
1007+337	J1010+3330	1074	10	10	51.82902368	+33	30	17.7605426	.00002109	.0005407	-0.2653	50219.1	50219.2	1			
1008-285	1008-285	1715	10	11	5.51732950	-28	47	40.4158541	.00002601	.0008987	-0.2573	53559.9	53559.9	1			
1008+013	1008+013	1716	10	11	15.63923701	+01	06	42.5137919	.00006198	.0027114	-0.8347	53561.0	53561.9	1			
1009-041	1009-041	3050	10	11	30.23997429	-04	23	27.7066827	.00006250	.0012860	0.3333	53572.8	55413.0	3			
1009+234	1009+234	1717	10	12	16.38973413	+23	12	14.6101796	.00001168	.0003350	0.0123	53134.0	53134.1	1			
1010-374	1010-374	1718	10	12	24.07552105	-37	40	5.8862095	.00089233	.0326108	0.9277	53523.1	53523.1	1			
1010-255	1010-255	1719	10	13	13.10509027	-25	46	54.6933148	.00002731	.0009182	-0.1036	53125.1	53125.1	1			
1010+495	1010+495	3051	10	13	29.93217684	+49	18	40.9860319	.00070559	.0235759	-0.7237	50305.8	54314.7	2			
1010+350	1010+350	3052	10	13	49.61404864	+34	45	50.7840284	.00001092	.0002694	0.0728	50241.9	50242.0	1			
1011+250	1011+250	824	10	13	53.42876221	+24	49	16.4404218	.00000455	.0000791	-0.1401	48353.1	56782.1	101	0.41	0.15	3.2
1012+232	1012+232	264	10	14	47.06546248	+23	01	16.5708108	.00000393	.0000647	-0.1251	47253.4	56751.6	79	0.31	0.41	2.8
1012-448	1012-448	1075	10	14	50.35496042	-45	08	41.1541283	.00001420	.0002783	0.3411	52306.4	55784.3	18			
1011+496	1011+496	3053	10	15	4.13986046	+49	26	0.7043931	.00006223	.0008581	-0.4202	50305.8	50305.9	1			
1013+127	1013+127	2	10	15	44.02338961	+12	27	7.0703994	.00000730	.0001774	0.0123	49913.9	56770.2	23	0.30	0.41	1.1
1013+014	1013+014	1720	10	15	57.05514965	+01	09	13.7477199	.00004373	.0009836	0.2200	53561.0	53561.9	1			
1013+054	1013+054	1721	10	16	3.13647375	+05	13	2.3413274	.00000385	.0000681	0.0019	49913.9	56749.0	72	0.75	0.66	
1013+208	OL 224	1076	10	16	44.32210159	+20	37	47.3056082	.00000851	.0002122	0.0845	50084.5	54643.7	6	0.15	0.07	3.7
1014+615	1014+615	825	10	17	25.88757287	+61	16	27.4966524	.00000713	.0000677	0.0489	49422.1	56749.6	39	0.24		
1015-314	1015-314	3054	10	18	9.26754875	-31	44	14.0902213	.00049963	.0140993	-0.5637	52306.3	56302.4	2			
1015+359	1015+359	1722	10	18	10.98809912	+35	42	39.4409396	.00000396	.0000660	0.1039	50241.9	56762.7	81			
1015+057	J1018+0530	1077	10	18	27.84828297	+05	30	29.9620243	.00000394	.0000624	0.0380	49913.9	56758.5	89	0.23	0.24	
1016-311	1016-311	1078	10	18	28.75348944	-31	23	53.8495623	.00001035	.0001769	-0.1099	52306.3	55545.7	17		0.34	
1016-268	1016-268	4078	10	19	8.48297533	-27	08	55.6650275	.00003010	.0012015	-0.1528	56204.6	56204.7	1			
1016+635	1016+635	3055	10	19	50.87680477	+63	20	1.6263238	.00004776	.0003028	0.4415	49827.0	54087.6	2			
1017+436	1017+436	1723	10	20	27.20305580	+43	20	56.3387610	.00004921	.0006118	0.3388	53559.8	53560.0	1			
1018+348	1018+348	3056	10	21	17.47469887	+34	37	21.6649469	.00001553	.0003666	-0.4272	50219.1	50219.2	1			
1019+416	1019+416	1724	10	22	2.02352343	+41	26	5.3724141	.00002350	.0003406	0.0331	54187.3	55966.4	2	0.11	0.10	
1019+429	1019+429	3057	10	22	13.13234113	+42	39	25.6126432	.00002140	.0004338	0.0656	50241.9	50242.0	1			
1019+309	1019+309	3058	10	22	30.29841684	+30	41	5.1166794	.00003871	.0008168	-0.5517	52306.4	52306.5	1			
1020-103	P 1020-103	3059	10	22	32.82343260	-10	37	44.0895407	.02648792	.3896672	0.9978	50576.0	50576.0	1			
1020+191	1020+191	3060	10	22	55.15677190	+18	53	34.2631899	.00016373	.0030705	0.8220	50084.5	54482.3	3			
1020-097	1020-097	1725	10	22	57.51769470	-09	58	22.5939160	.00015996	.0042441	-0.7562	53572.8	53572.9	1			
1020+400	1020+400	826	10	23	11.56566243	+39	48	15.3854051	.00000495	.0000821	-0.2130	50003.5	55320.6	21	0.34	0.39	3.1
1022-665	1022-665	1274	10	23	43.53319099	-66	46	48.7177879	.00001679	.0001178	0.2680	52780.6	56737.1	34			
1021-323	1021-323	1726	10	24	0.42386720	-32	34	16.0586127	.00004815	.0015014	-0.1186	53134.1	53134.1	1			
1021-006	P 1021-00	273	10	24	29.58664505	-00	52	55.4971894	.00001961	.0004291	0.5383	48664.2	56741.7	11	0.10		4.6
1022+194	GC 1022+19	274	10	24	44.80959518	+19	12	20.4155658	.00000386	.0000678	-0.1123	47379.8	56775.1	115	0.32	0.25	2.6
1022+237	1022+237	1727	10	24	53.63733289	+23	32	33.9636590	.00001823	.0004329	-0.2736	53523.0	56498.0	2	0.17	0.15	
1023-049	1023-049	1728	10	25	45.42295403	-05	09	54.1325970	.00008311	.0024026	-0.4745	53559.9	53559.9	1			
1023+131	1023+131	1079	10	25	56.28537067	+12	53	49.0219652	.00000473	.0000904	-0.1323	50084.5	56196.5	67	0.23	0.47	
1024+483	1024+483	3061	10	27	13.07991412	+48	03	13.5350365	.00003865	.0006048	-0.6444	50305.8	50305.9	1			
1023+747	1023+747	1729	10	27	24.14687097	+74	28	26.0980623	.00009862	.0005982	0.0699	53561.0	53561.8	1			
1025+031	1025+031	3062	10	28	20.40128670	+02	55	22.4721848	.00002186	.0008229	-0.5221	49913.9	49914.0	1			
1025+242	1025+242	1730	10	28	21.25995494	+24	01	21.7729147	.00004933	.0017343	-0.0345	53572.8	53573.0	1			

Source Name		ID No.	Right Ascension			Declination			RA Error (s)	Dec. Error (arcsec)	RA–Dec Corr.	Observation Epoch MJD		No. Obs.	Source Flux (Jy)		Str Index
B1950	Common		H	M	S	D	M	S				First	Last		10-60	10-40	
1026-084	1026-084	1731	10	28	38.79632349	-08	44	38.5324671	.00010769	.0032770	-0.2907	51169.5	54482.2	2		0.09	
1026+055	1026+055	3063	10	29	21.83063894	+05	19	38.7814896	.00007794	.0012806	0.0109	54087.4	54087.5	1			
1027-186	1027-186	1732	10	29	33.09770959	-18	52	50.2890196	.00000731	.0001300	-0.1891	50631.8	56750.9	62			
1027+749	1027+749	3064	10	31	22.02403637	+74	41	58.3458128	.00024254	.0014800	0.5931	49827.0	49827.2	1			
1028+605	1028+605	3065	10	31	44.75626393	+60	20	30.3640243	.00023426	.0012471	0.1360	49576.7	49576.9	1			
1029-222	1029-222	3066	10	31	52.31211694	-22	28	24.9746980	.00012294	.0034996	0.6113	50631.8	50687.8	2			
1029-041	1029-041	1733	10	31	55.00186027	-04	23	52.8694496	.00003212	.0009962	0.7249	53560.9	53561.0	1			
1029-137	1029-137	1734	10	32	6.22650267	-14	00	19.4717053	.00025763	.0051059	0.4377	53572.8	53572.9	1			
1030+415	1030+415	827	10	33	3.70787184	+41	16	6.2329259	.00000393	.0000582	-0.0455	50242.1	56776.7	48	0.68	0.37	0.6
1030-357	1030-357	1735	10	33	7.66080868	-36	01	56.8101525	.00018477	.0062750	0.9138	53125.1	53125.1	1			
1030+398	1030+398	3067	10	33	22.06100648	+39	35	51.0834705	.00001496	.0003112	0.4172	50241.9	50242.1	1			
1030+074	1030+074	828	10	33	34.02429515	+07	11	26.1475490	.00000568	.0000961	0.0433	51722.9	56653.7	75	0.33		
1030+611	1030+611	3068	10	33	51.42897068	+60	51	7.3341817	.00007623	.0011068	-0.3057	49576.7	49576.9	1			
1032-199	P 1032-199	829	10	35	2.15531148	-20	11	34.3596263	.00000459	.0000827	-0.1480	48776.1	56638.6	50	0.16	0.41	3.2
1032+509	1032+509	3069	10	35	6.01945175	+50	40	6.1012077	.00004237	.0006413	-0.5542	49576.7	54087.5	3			
1031+567	OL 553	277	10	35	7.03992561	+56	28	46.7959150	.00003609	.0003308	0.4093	49328.2	53059.7	4			
1032+382	1032+382	4079	10	35	51.16713094	+37	56	41.7130115	.00008380	.0011643	-0.3613	56393.1	56393.3	1			
1033+223	1033+223	3070	10	36	32.98065947	+22	03	12.2061067	.00006875	.0010699	-0.0790	50084.5	50156.3	2			
1034-058	1034-058	3071	10	36	47.57298023	-06	05	41.1835492	.00001898	.0005656	0.1127	50576.0	50576.2	1			
1034-374	1034-374	1736	10	36	53.43959472	-37	44	15.0658891	.00000978	.0001403	-0.0770	53222.4	56573.8	24			
1034-293	P 1034-293	278	10	37	16.07973773	-29	34	2.8135088	.00000349	.0000541	-0.1308	44200.6	56770.5	1570		1.06	2.4
1035+046	1035+046	1737	10	37	39.33954029	+04	24	1.7458843	.00002956	.0008665	0.3658	53559.9	53560.0	1			
1035-281	1035-281	3072	10	37	42.45749597	-28	23	4.1112209	.00010367	.0025163	-0.8324	50687.6	50687.8	1			
1034+288	1034+288	3073	10	37	43.83527234	+28	34	59.4602371	.00002992	.0006585	-0.1482	50219.1	50219.2	1			
1036-431	1036-431	1738	10	38	14.69601561	-43	25	45.9049539	.00025933	.0087724	0.9495	53134.1	53134.1	1			
1035+430	1035+430	1739	10	38	18.19054891	+42	44	42.7606020	.00004524	.0005865	-0.3672	53561.0	53561.8	1			
1036-529	1036-529	4080	10	38	40.65717751	-53	11	43.2698758	.00005952	.0006221	0.3845	56007.1	56314.0	3			
1036+054	1036+054	1740	10	38	46.77989254	+05	12	29.0871734	.00000671	.0001851	-0.1144	49913.9	53551.9	4	1.55	1.12	
1036-154	1036-154	3074	10	39	6.70511083	-15	41	6.6915617	.00001817	.0006040	-0.2631	50631.8	50631.9	1			
1038+064	OL 064.5	279	10	41	17.16249692	+06	10	16.9236281	.00000401	.0000828	-0.2407	44203.4	56754.1	158	0.88	0.85	3.5
1038+212	1038+212	1741	10	41	27.10285586	+21	01	41.4633629	.00026366	.0027471	0.5214	53572.8	53572.9	1			
1038+528	1038+52A	830	10	41	46.78163432	+52	33	28.2314227	.00000438	.0000627	-0.0044	48524.7	56766.5	264	0.38		2.8
1038+529	1038+52B	831	10	41	48.89762163	+52	33	55.6080585	.00018342	.0011347	-0.3854	48650.3	53411.0	7			
1040+123	3C 245	281	10	42	44.60524307	+12	03	31.2635936	.00000972	.0001705	-0.2160	44200.8	54937.7	40	0.14	0.13	3.9
1040+244	J1043+2408	1080	10	43	9.03577463	+24	08	35.4093930	.00000357	.0000555	0.0098	50219.1	56776.6	132	0.53	0.31	1.6
1041+536	1041+536	3075	10	44	10.67299394	+53	22	20.5413136	.00003515	.0006220	-0.1011	49576.7	49576.9	1			
1039+811	1039+811	832	10	44	23.06253426	+80	54	39.4430412	.00000975	.0000546	0.0089	48353.0	56772.8	114	0.65		2.3
1042+071	P 1042+071	687	10	44	55.91124349	+06	55	38.2625777	.00000433	.0000993	-0.2710	47253.4	56754.7	96	0.23	0.28	2.5
1042+178	1042+178	3076	10	45	14.35978674	+17	35	48.0840700	.00001153	.0003222	-0.5931	50084.5	53503.2	3			
1043-291	1043-291	3077	10	45	40.62568642	-29	27	26.3358549	.00009775	.0037943	0.3301	50687.6	50687.8	1			
1043+066	1043+066A	1275	10	45	52.73330703	+06	24	36.4517230	.00002104	.0006365	-0.6582	49913.9	53575.1	2	0.26	0.17	
1043+541	1043+541	3078	10	46	24.03835981	+53	54	26.2356778	.00014197	.0012070	0.4842	49576.7	49576.9	1			
1044-128	1044-128	3079	10	47	3.93090338	-13	08	32.4157474	.00004143	.0011932	0.1042	50576.0	50576.2	1			
1044+007	1044+007	3080	10	47	6.86403110	+00	29	37.0828176	.00003072	.0007574	-0.1708	53559.9	55916.6	2			
1045-620	1045-620	3081	10	47	42.95227156	-62	17	14.6344831	.00006288	.0021504	-0.3629	52872.2	52872.3	1			
1045-188	1045-188	833	10	48	6.62060532	-19	09	35.7268074	.00000387	.0000749	-0.1016	50459.4	56691.2	124	0.66	0.86	3.0
1045+011	1045+011	3082	10	48	7.74458140	+00	55	43.4822517	.00005970	.0014839	-0.5312	49913.9	49914.0	1			
1045+019	1045+019	3083	10	48	22.86782105	+01	41	48.1126097	.00022969	.0041628	0.7094	49913.9	49914.0	1			
1044+719	1044+719	688	10	48	27.61991405	+71	43	35.9384153	.00000354	.0000504	-0.0956	46925.4	56770.4	958	0.94		2.2
1046-409	1046-409	3084	10	48	38.27115181	-41	14	0.1161175	.00002026	.0005048	-0.0488	54489.4	56568.2	6		0.12	

Source Name		ID No.	Right Ascension			Declination			RA Error (s)	Dec. Error (arcsec)	RA–Dec Corr.	Observation Epoch MJD		No. Obs.	Source Flux (Jy)		Str Index
B1950	Common		H	M	S	D	M	S				First	Last		10-60	10-40	
1046-222	1046-222	1742	10	49	21.86915217	-22	31	7.5090071	.00007020	.0029629	-0.8394	54656.9	54657.0	1			
1047+147	J1049+14	1743	10	49	46.32762010	+14	29	38.5739320	.00003342	.0005691	-0.5559	54112.4	54559.3	2			
1048-526	1048-526	3085	10	50	38.02845237	-52	49	48.3281808	.00003986	.0010124	0.3643	54723.2	54723.3	1			
1049-726	1049-726	3086	10	50	45.24979019	-72	54	32.3105911	.00007480	.0004975	0.2731	54723.2	54723.4	1			
1048+347	1048+347	3087	10	50	58.12294679	+34	30	10.9406608	.00007513	.0012304	-0.5206	50219.1	50219.2	1			
1048+207	1048+207	1744	10	51	1.37428128	+20	27	19.9705963	.00001312	.0003875	-0.0217	53125.2	53126.1	1			
1048-313	P 1048-313	284	10	51	4.77752676	-31	38	14.3076847	.00001257	.0001388	-0.2854	50048.7	55728.2	22		0.23	4.3
1048+470	1048+470	3088	10	51	15.89544161	+46	44	17.3705217	.00030251	.0015831	-0.5223	50305.9	50306.0	1			
1049-650	1049-650	3089	10	51	23.52178538	-65	18	8.6248393	.00075152	.0030139	0.1293	52886.9	53138.6	3			
1049+215	P 1049+21	834	10	51	48.78907895	+21	19	52.3137676	.00000444	.0000791	-0.0756	50085.4	56547.5	68	0.33	0.25	3.0
1051+397	J1054+39	3090	10	54	32.42215027	+39	28	12.3819830	.00005527	.0006589	0.0486	54087.4	54087.6	1			
1053+704	1053+704	835	10	56	53.61749571	+70	11	45.9156519	.00000420	.0000519	-0.0022	49125.0	56741.5	184	0.50		1.8
1054+004	1054+004	1745	10	57	15.75361613	+00	12	3.5746284	.01106223	.0616253	0.1292	54278.1	54278.1	1			
1054-234	1054-234	3091	10	57	24.42134813	-23	42	1.7108080	.00016626	.0043704	0.8631	50631.9	50687.8	2			
1055-248	1055-248	3092	10	57	54.13366860	-25	09	29.0634716	.00002080	.0007913	0.1258	50631.8	50687.8	2			
1055-242	P 1055-242	3093	10	57	55.40903197	-24	33	48.8629746	.00030168	.0067166	0.0039	50631.8	56749.3	4			
1055-301	1055-301	1746	10	58	0.42742737	-30	24	55.0275177	.00001485	.0002612	-0.0781	53125.1	54362.5	9			
1055+433	1055+433	3094	10	58	2.92079514	+43	04	41.5053716	.00002350	.0003890	-0.5717	50242.1	50242.2	1			
1055-028	1055-028	1747	10	58	11.01071504	-03	09	27.2545339	.00004590	.0011164	-0.4199	53134.1	53134.2	1			
1053+815	1053+815	836	10	58	11.53535861	+81	14	32.6751776	.00000526	.0000509	0.0204	48720.0	56744.2	601	0.60		2.3
1055+201	1055+201	1748	10	58	17.90082828	+19	51	50.8699090	.00001319	.0003351	-0.1627	50084.5	54664.7	3			
1055+018	P 1055+01	287	10	58	29.60520412	+01	33	58.8237334	.00000356	.0000609	-0.2815	44200.7	56754.1	438	2.04	2.20	2.8
1055+567	1055+567	3095	10	58	37.72744823	+56	28	11.2068512	.00040678	.0015500	0.4041	49576.7	49576.9	1			
1057-797	P 1057-79	837	10	58	43.30974512	-80	03	54.1597450	.00000858	.0000540	0.0087	47625.6	56763.7	486			
1056-113	1056-113	3096	10	59	12.42638361	-11	34	22.7779220	.00001937	.0007333	-0.0390	50576.0	50576.2	1			
1056+212	J1059+2057	1081	10	59	39.04268435	+20	57	21.9558872	.00000865	.0001350	0.0048	50084.5	55776.1	17		0.15	1.9
1058+393	1058+393	3097	11	01	30.06956708	+39	04	32.6333356	.00002548	.0004896	-0.5361	50242.1	50242.2	1			
1058+726	1058+726	3098	11	01	48.80538145	+72	25	37.1181948	.00005166	.0004276	0.3821	49827.1	49827.2	1			
1058+629	1058+629	3099	11	01	53.45082054	+62	41	50.6058436	.00006068	.0008090	0.4791	49827.1	49827.2	1			
1059+229	1059+229	1749	11	02	3.14444768	+22	41	56.1260821	.00004140	.0008680	-0.5153	53560.9	53561.0	1			
1059-438	1059-438	1750	11	02	4.83609317	-44	04	22.8385364	.00003026	.0010119	0.1597	54853.4	54853.4	1			
1059+282	1059+282	1751	11	02	14.28845897	+27	57	8.6895538	.00000486	.0000903	-0.0965	50219.1	56772.4	51			
1059+599	1059+599A	3100	11	02	42.76282824	+59	41	19.5847424	.00007416	.0005611	0.4108	49576.7	54112.5	2			
1100+122	1100+122	1752	11	03	3.52983839	+11	58	16.6242046	.00000848	.0002434	-0.0418	53125.2	55974.0	17			
1100+305	J1103+3014	1082	11	03	13.30189460	+30	14	42.7023580	.00001851	.0004425	-0.5846	50219.1	53659.0	2	0.24	0.15	
1100+223	P 1100+223	3101	11	03	23.06767182	+22	03	37.7199429	.00003620	.0007506	-0.3232	50084.5	50156.3	2			
1101-325	P 1101-325	290	11	03	31.52641254	-32	51	16.6938150	.00001661	.0002243	-0.1946	52067.2	54362.5	13			
1101-536	1101-536	838	11	03	52.22167174	-53	57	0.6965838	.00001137	.0001547	0.3277	47625.6	56504.5	36			
1100+798	1100+798	3102	11	04	5.55883956	+79	32	52.9543550	.00238748	.0028492	0.8924	49827.1	50688.3	2			
1101+384	B2 1101+38	291	11	04	27.31394150	+38	12	31.7990500	.00000351	.0000535	-0.1180	49965.8	56782.2	562	0.34	0.24	2.3
1102-242	1102-242	3103	11	04	46.17644899	-24	31	25.8005126	.00001383	.0004467	-0.2097	50631.8	50687.8	2	0.23	0.19	
1101+609	1101+609	3104	11	04	53.69461975	+60	38	55.3148396	.00006126	.0008234	-0.1223	49576.8	54087.6	2			
1102-392	1102-392	1753	11	05	11.08134998	-39	28	42.1556632	.00021303	.0109272	0.6836	53153.1	53552.0	2			
1103+023	1103+023	1754	11	05	38.99286548	+02	02	57.4762777	.00011892	.0025064	-0.3592	53134.1	53134.2	1			
1103+284	1103+284	1755	11	06	7.26170628	+28	12	47.0650194	.00001853	.0004796	0.1178	53559.9	53560.0	1			
1104-445	P 1104-445	293	11	07	8.69412570	-44	49	7.6185032	.00000596	.0000824	-0.1440	43808.7	56776.7	268		0.48	
1105-680	P 1105-680	839	11	07	12.69507374	-68	20	50.7278835	.00003505	.0002524	0.5699	48387.6	55784.5	18			
1104+167	1104+167	3105	11	07	15.04743333	+16	28	2.2448121	.00002667	.0009961	-0.6412	50084.5	50156.3	2			
1104+525	1104+525	3106	11	07	25.82780281	+52	19	31.6363824	.00002850	.0004939	-0.5505	53503.1	53503.2	1			
1104+728	1104+728	840	11	07	41.72255805	+72	32	36.0049778	.00003396	.0001608	-0.2363	49827.1	56568.5	13			

Source Name		ID No.	Right Ascension			Declination			RA Error (s)	Dec. Error (arcsec)	RA–Dec Corr.	Observation Epoch MJD		No. Obs.	Source Flux (Jy)		Str Index
B1950	Common		H	M	S	D	M	S				First	Last		10-60	10-40	
1105+437	1105+437	1083	11	08	23.47692807	+43	30	53.6571323	.00002048	.0003528	-0.4966	50242.1	50242.2	1		0.15	
1106+084	1106+084	3107	11	08	37.49883524	+08	11	1.5844122	.00001290	.0004481	-0.5289	53572.9	55538.6	2			
1106+023	1106+023	3108	11	08	45.48840321	+02	02	40.9044032	.00002051	.0005586	0.2214	53523.0	56749.3	2			
1106+380	1106+380	3109	11	09	28.85382047	+37	44	31.1046465	.00005830	.0011057	0.6197	52306.4	52306.5	1			
1107-187	1107-187	3110	11	10	0.40689892	-18	58	48.7445791	.00007164	.0019172	-0.3360	50631.8	50687.8	2			
1107+607	1107+607	3111	11	10	13.08807659	+60	28	42.5665265	.00011838	.0014875	0.5260	49576.7	49576.9	1			
1107+485	1107+485	3112	11	10	36.32374910	+48	17	52.4494705	.00024433	.0051719	0.4427	50305.9	54314.6	2			
1107+443	1107+443	3113	11	10	46.34580890	+44	03	25.9251258	.00002086	.0003373	-0.4612	50242.1	50306.0	2			
1108+527	1108+527	4081	11	11	5.88214012	+52	27	48.9992684	.00012535	.0011901	-0.4361	56393.1	56393.3	1			
1108+201	1108+201	3114	11	11	20.06575265	+19	55	35.9999333	.00020922	.0024196	-0.6693	50084.5	50156.3	2			
1109-567	1109-567	3115	11	12	7.27004154	-57	03	39.7460296	.00126726	.0033262	-0.1644	52676.5	52947.9	3			
1109+076	1109+076	1756	11	12	9.55852653	+07	24	49.1183049	.00001526	.0004948	0.0074	53559.9	53560.0	1	0.09	0.09	
1109+350	1109+350	1757	11	12	38.76915467	+34	46	39.1096857	.00002662	.0005780	-0.3770	53560.9	53561.0	1			
1110-217	P 1110-217	3116	11	12	49.84870362	-21	58	29.3523204	.00009167	.0024422	-0.3164	50631.8	50687.8	2			
1110-355	1110-355	3117	11	13	1.48172727	-35	49	48.2677822	.00024920	.0174127	0.2146	53134.1	53134.1	1			
1111+149	GC 1111+14	296	11	13	58.69508672	+14	42	26.9526321	.00000392	.0000744	-0.1949	44200.9	56775.1	169	0.26	0.23	2.5
1112-080	1112-080	3118	11	14	32.55064890	-08	16	39.0023051	.00001412	.0004695	-0.0596	50576.0	50576.2	1			
1113-307	1113-307	3119	11	15	58.81409406	-30	59	27.4251714	.00048223	.0125935	0.7716	53503.2	53503.2	1			
1113+087	J1116+0829	1084	11	16	9.97336007	+08	29	22.0323194	.00002707	.0007996	-0.4554	49913.9	49914.0	1	0.11	0.27	
1115-122	1115-122	3120	11	18	17.14137542	-12	32	54.2629227	.00001146	.0003580	-0.0419	50576.0	56547.7	2	0.40	0.73	
1115-306	1115-306	3121	11	18	20.61019157	-30	54	58.5232984	.00040320	.0169921	0.9457	52306.4	52306.5	1			
1116-462	1116-462	841	11	18	26.95765152	-46	34	15.0012498	.00002020	.0002537	0.1709	48110.0	54706.4	24			
1116+128	P 1116+12	297	11	18	57.30143528	+12	34	41.7180375	.00000430	.0000820	-0.1728	44250.6	56637.9	76	0.61	0.35	3.3
1116+603	1116+603	3122	11	19	14.34543185	+60	04	57.2047523	.00015358	.0010468	0.1535	49576.7	54087.6	2			
1116+227	1116+227	3123	11	19	30.31809205	+22	26	49.3681184	.00098956	.0196058	-0.9081	53560.0	56638.7	2			
1117+044	1117+044	3124	11	19	42.82420254	+04	10	27.9272665	.00002184	.0006110	0.0754	49913.9	49914.0	1			
1117-248	1117-248	3125	11	20	9.11967961	-25	08	7.6233784	.00090199	.0205394	-0.8095	50631.8	55538.6	3			
1117-124	1117-124	3126	11	20	12.08052247	-12	43	37.8305725	.00001813	.0006619	0.0805	50576.0	50576.2	1			
1117-270	1117-270	3127	11	20	16.19178290	-27	19	6.3662107	.00001817	.0004315	-0.1128	50687.7	54664.7	2			
1117+146	1117+146	1085	11	20	27.80625486	+14	20	54.9924002	.00030510	.0034921	-0.6667	50084.5	54440.6	4			
1118+073	1118+073	3128	11	20	38.44391224	+07	04	47.1753928	.00030509	.0051551	0.8790	49913.9	49914.0	1			
1118-140	1118-140	3129	11	20	55.56365003	-14	20	29.9244489	.00001782	.0005773	-0.0396	50631.8	50631.9	1			
1118-056	1118-056	3130	11	21	25.10805509	-05	53	56.4409800	.00001139	.0003786	0.0418	50576.0	50576.2	1			
1119-069	1119-069	1758	11	21	42.12294505	-07	11	6.3422962	.00001012	.0003425	-0.1439	53572.0	56701.4	2	0.17	0.18	
1119-044	1119-044	1759	11	21	43.11428649	-04	42	36.1544809	.00032417	.0088863	0.7874	53560.9	53561.0	1			
1119-252	1119-252	3131	11	22	5.74321898	-25	32	33.8315998	.00002232	.0007324	-0.2575	50631.8	50687.8	2			
1119+183	1119+183	1086	11	22	29.71147699	+18	05	26.3431554	.00000703	.0001551	0.0127	50084.5	54125.7	4			3.8
1120-274	1120-274	1760	11	22	56.41007995	-27	42	48.4574693	.00017301	.0063281	0.7236	53559.9	53560.0	1			
1121-147	1121-147	1761	11	24	2.56568599	-15	01	58.9503899	.00009585	.0022240	0.5263	53572.0	53572.9	1			
1121+238	J1124+2336	1087	11	24	2.70587561	+23	36	45.8702371	.00001990	.0002951	-0.3001	50084.5	53286.4	8		0.16	
1121+234	1121+234	3132	11	24	31.58826890	+23	07	55.9526383	.00001708	.0004331	-0.1189	54112.4	54112.6	1			
1123+264	P 1123+26	299	11	25	53.71192231	+26	10	19.9786528	.00000379	.0000588	-0.1480	44200.8	56782.1	302	0.52	0.54	2.4
1123+203	1123+203	3133	11	25	58.74195607	+20	05	54.3370883	.00003683	.0006433	0.0507	50084.5	50156.3	2			
1124-382	1124-382	1762	11	26	44.13297146	-38	28	44.0581176	.00017259	.0088437	0.6009	53125.2	53552.0	2			
1124+067	1124+067	1763	11	26	53.14592085	+06	25	56.9408746	.00005485	.0010483	-0.1182	53559.9	53560.0	1			
1124-056	1124-056	3134	11	26	57.52325697	-05	55	52.7859378	.00007923	.0017602	-0.2804	53560.9	55371.1	2			
1124+455	1124+455	3135	11	26	57.65499583	+45	16	6.2826418	.00003281	.0010621	-0.3061	50305.9	50306.0	1			
1124-186	P 1124-186	300	11	27	4.39244976	-18	57	17.4418153	.00000339	.0000523	-0.0286	47681.9	56776.7	1239	1.17	1.27	1.5
1124-073	1124-073	3136	11	27	12.43626973	-07	35	12.1649065	.00001035	.0003379	0.0320	50576.1	50576.2	1			
1125+062	1125+062	1764	11	27	36.52553886	+05	55	32.0591944	.00001079	.0003145	-0.0126	53125.1	53916.1	2			

Source Name		ID No.	Right Ascension			Declination			RA Error (s)	Dec. Error (arcsec)	RA–Dec Corr.	Observation Epoch MJD		No. Obs.	Source Flux (Jy)		Str Index
B1950	Common		H	M	S	D	M	S				First	Last		10-60	10-40	
1124+571	1124+571	1765	11	27	40.13511483	+56	50	14.7950319	.00004776	.0004638	0.1479	49576.7	54643.6	2			
1125+366	1125+366	1766	11	27	58.87081889	+36	20	28.3512686	.00001163	.0002238	-0.1792	50242.1	56316.8	14			
1125+596	1125+596	842	11	28	13.34065388	+59	25	14.7983280	.00001391	.0001215	0.0862	49422.2	53612.9	5	0.59		
1125+213	1125+213	3137	11	28	35.54142298	+21	02	37.3591946	.00017457	.0025706	-0.1878	50084.5	50156.3	2			
1126+109	1126+109	4130	11	28	45.54956502	+10	39	6.9797270	.00006038	.0011219	0.2443	55775.8	55776.0	1			
1127-443	1127-443	3138	11	29	31.72199550	-44	35	49.9384482	.00006078	.0019007	0.3365	54723.2	54723.4	1			
1127-368	1127-368	3139	11	29	55.78376683	-37	07	57.3686117	.00042273	.0174208	0.7288	53503.2	53503.2	1			
1127-358	1127-358	3140	11	30	4.41672162	-36	08	4.0833223	.00005175	.0019463	0.2895	52409.2	56204.7	2			
1127-145	P 1127-14	301	11	30	7.05257710	-14	49	27.3883109	.00000817	.0001434	-0.2359	43808.7	55545.7	68	0.22	0.73	4.3
1128+090	1128+090	1767	11	30	35.95153480	+08	46	43.1070970	.00001401	.0004106	0.1417	53134.1	53134.2	1			
1128+308	1128+308	3141	11	30	42.42917106	+30	31	35.3878778	.00001969	.0004914	-0.1072	50219.1	50219.2	1			
1128+385	GC 1128+38	302	11	30	53.28261083	+38	15	18.5470012	.00000337	.0000508	-0.0398	44283.3	56763.7	1033	0.97	0.76	2.0
1128-047	P 1128-047	303	11	31	30.51674542	-05	00	19.6583286	.00001139	.0003774	-0.0846	49099.2	53185.7	4	0.10	0.23	3.3
1129-161	1129-161	3142	11	31	36.74790051	-16	28	33.4365630	.00003515	.0011684	0.2440	53560.0	55966.5	2			
1129-580	1129-580	1088	11	31	43.28801127	-58	18	53.4434038	.00001862	.0001974	0.4239	52940.8	55784.3	18			
1130-741	1130-741	3143	11	32	19.11006268	-74	25	9.0233847	.00014189	.0006900	0.6090	54723.2	54723.4	1			
1130+005	1130+005	1304	11	33	3.03005019	+00	15	48.9795378	.00002414	.0005758	-0.1834	53560.9	53561.0	1			
1130+009	P 1130+009	304	11	33	20.05578763	+00	40	52.8372701	.00000402	.0000862	-0.1726	44203.4	56754.1	124	0.33	0.22	2.4
1131-088	1131-088	3144	11	33	35.99346056	-09	05	23.4133583	.00483771	.1035869	-0.9997	53572.9	56161.9	2			
1131+730	1131+730	3145	11	34	11.40775449	+72	49	20.0524634	.00019863	.0019115	0.6765	49827.1	54482.7	2			
1132-306	1132-306	1768	11	35	20.77703583	-30	56	29.9264227	.00040425	.0170657	0.8261	53523.1	53523.1	1			
1133-041	1133-041	1769	11	35	58.23496934	-04	28	27.8868424	.00001189	.0003908	-0.1861	53559.9	53560.0	1			
1134-739	1133-739	3146	11	36	9.65960851	-74	15	45.2747402	.00160103	.0037233	0.0678	52886.9	53138.6	3			
1133-032	1133-032	1305	11	36	24.57692778	-03	30	29.4966550	.00000388	.0000711	-0.0345	50576.1	56772.3	114			
1133+704	1133+704	1089	11	36	26.40839752	+70	09	27.3070687	.00005493	.0002529	0.3178	49827.2	54087.6	4			
1133+344	1133+344	1770	11	36	27.34395900	+34	07	39.4841892	.00002852	.0004923	-0.0103	53560.9	53561.0	1			
1135+480	1135+480	3147	11	38	21.13817600	+47	45	15.3968695	.00004619	.0008843	0.0822	50305.9	50306.0	1			
1136+408	1136+408	3148	11	39	2.73423444	+40	32	54.8413593	.00002590	.0004504	-0.3510	50242.1	50242.2	1			
1136-135	1136-135	3149	11	39	10.70257095	-13	50	43.6396580	.00004215	.0013289	-0.0092	50576.1	50576.2	1			
1136-156	1136-156	3150	11	39	29.57605698	-15	52	51.6536446	.00002168	.0007464	0.4646	50631.8	50632.0	1			
1136+771	1136+771	3151	11	39	51.53869577	+76	54	32.3464339	.00008717	.0005260	0.4176	49827.1	49827.2	1			
1137+660	1137+660A	1771	11	39	57.02550591	+65	47	49.4834310	.00026473	.0017563	0.1928	55041.8	55042.1	1			
1137-272	1137-272	3152	11	40	10.59774945	-27	30	40.6822362	.00032540	.0154112	0.6994	53572.0	53572.9	1			
1138-277	1138-277	3153	11	40	51.36925461	-28	00	38.7296198	.00003284	.0012016	0.5371	53560.0	56463.0	2			
1138+644	1138+644	3154	11	41	12.22821254	+64	10	5.5052774	.00015602	.0013283	-0.1684	49827.1	49827.2	1			
1138-120	1138-120	3155	11	41	24.20178460	-12	16	38.5426716	.01033205	.2259329	0.9985	53561.0	53561.0	1			
1139+160	1139+160	1772	11	42	7.73593584	+15	47	54.1792687	.00006017	.0016526	-0.4990	53572.0	53572.9	1			
1140+188	1140+188	3156	11	43	26.06964492	+18	34	38.3615557	.00003901	.0011472	0.0563	50084.5	50156.3	2			
1140+668	1140+668	3157	11	43	41.60307421	+66	33	31.2286880	.00012889	.0012069	0.3954	49827.1	49827.2	1	0.12		
1141+011	1141+011	1773	11	44	8.71371873	+00	54	36.3351655	.00006683	.0015596	-0.1322	53559.9	53560.0	1			
1142+198	1142+198	1090	11	45	5.00905282	+19	36	22.7410405	.00001622	.0003770	0.4319	51246.2	53153.2	6		0.12	
1142+052	1142+052	1091	11	45	21.31520672	+04	55	26.6893284	.00009183	.0020594	0.7311	49913.9	54643.7	3			
1142-225	1142-225	3158	11	45	22.04678533	-22	50	31.3436876	.00002384	.0007168	-0.2975	50631.8	54482.2	3			
1143+446	1143+446	3159	11	45	38.51854254	+44	20	21.9137994	.00006507	.0004996	-0.1220	50305.9	56036.4	2			
1143-696	1143-696	3160	11	45	53.62416924	-69	54	1.7977839	.00002500	.0001670	0.4269	52872.3	56716.0	18			
1143-245	P 1143-245	306	11	46	8.10331930	-24	47	32.8965824	.00000617	.0001149	-0.0831	50209.9	55728.2	28		0.21	3.5
1143-287	1143-287	1774	11	46	26.18856332	-28	59	18.5048236	.00001127	.0001896	-0.1603	50687.7	55545.7	13		0.28	
1143+590	1143+590	1775	11	46	26.91157265	+58	48	34.2631542	.00005066	.0004377	0.1407	49576.0	54664.7	2			
1143-332	1143-332	1776	11	46	28.45175158	-33	28	42.6324034	.00001480	.0004555	-0.1808	54313.8	56568.7	6		0.11	2.8
1144+542	GC 1144+54	3161	11	46	44.20421693	+53	56	43.0823331	.00006943	.0016595	-0.0912	49576.0	49576.9	1			

Source Name		ID No.	Right Ascension			Declination			RA Error (s)	Dec. Error (arcsec)	RA–Dec Corr.	Observation Epoch MJD		No. Obs.	Source Flux (Jy)		Str Index
B1950	Common		H	M	S	D	M	S				First	Last		10-60	10-40	
1144+402	1144+402	699	11	46	58.29791377	+39	58	34.3045056	.00000347	.0000520	-0.0358	45940.8	56772.6	333	0.72	0.63	1.5
1144-379	P 1144-379	309	11	47	1.37070607	-38	12	11.0235572	.00000354	.0000544	-0.0575	43808.7	56770.6	1009		1.40	2.2
1144+352	1144+352	843	11	47	22.13054468	+35	01	7.5225977	.00003356	.0004786	-0.3053	50242.1	51184.5	3			
1145-071	1145-071	689	11	47	51.55403037	-07	24	41.1412352	.00000354	.0000617	-0.1815	47379.8	56748.2	204	0.38	0.49	2.8
1145+268	1145+268	1777	11	47	59.76390657	+26	35	42.3323393	.00000420	.0000740	-0.0089	50219.1	56751.6	93			
1145-005	1145-005	1778	11	48	7.19179275	-00	46	45.6731795	.00016043	.0047871	-0.7442	53559.9	53560.0	1			
1146+189	1146+189	3162	11	48	37.77678643	+18	40	8.9691655	.00007984	.0009189	0.4740	50084.5	50156.3	2			
1146+596	1146+596	844	11	48	50.35824311	+59	24	56.3819790	.00004101	.0004060	-0.6374	49576.0	51787.2	6			4.1
1146-037	1146-037	3163	11	48	55.88479458	-04	04	9.5632979	.00001919	.0005743	-0.1117	50576.1	50576.2	1			
1146+531	1146+531	1227	11	48	56.56907601	+52	54	25.3229302	.00001611	.0002935	-0.2553	53107.1	56023.6	16	0.32		
1146+286	1146+286	1779	11	49	8.90554784	+28	24	34.8939141	.00002840	.0005205	0.0472	53560.9	53561.0	1			
1146+362	J1149+35	3164	11	49	33.97567356	+35	59	8.0948842	.00002779	.0006918	-0.2944	54112.4	54112.5	1			
1147+438	1147+438	3165	11	50	16.60269386	+43	32	5.9055177	.00011447	.0019926	-0.1840	50242.1	50242.2	1			
1147+245	B2 1147+24	845	11	50	19.21217386	+24	17	53.8353211	.00000410	.0000717	-0.0730	48720.2	56762.6	82	0.27	0.27	2.6
1147-063	1147-063	3166	11	50	23.98670652	-06	40	26.5711910	.00001321	.0004595	-0.5104	53503.1	56111.5	2			
1147-192	1147-192	1780	11	50	31.52711454	-19	30	49.5485079	.00001251	.0004465	-0.0901	54559.2	54559.3	1			
1147+067	1147+067	1781	11	50	32.72906204	+06	30	29.4195561	.00003047	.0007906	-0.1356	53572.0	53572.9	1			
1148-001	P 1148-00	312	11	50	43.87076488	-00	23	54.2051550	.00001179	.0003401	-0.2365	43808.9	54184.5	36	0.21	0.17	4.6
1148-171	1148-171	3167	11	51	3.20366906	-17	23	59.8433663	.00002543	.0008586	-0.1529	50631.8	50632.0	1			
1148-671	P 1148-671	846	11	51	13.42649141	-67	28	11.0936690	.00003084	.0002933	0.2835	49014.8	54670.4	17			
1149-084	1149-084	1306	11	52	17.20951043	-08	41	3.3139139	.00000361	.0000561	-0.0146	50576.1	56770.7	206			
1149+499	1149+499	1228	11	52	32.87106369	+49	39	38.7678795	.00000974	.0001750	-0.3163	52409.1	56591.0	28	0.30		
1150+334	1150+334	1782	11	52	51.91010632	+33	07	18.7653874	.00002998	.0010548	-0.0797	53559.9	53560.0	1			
1150-050	1150-050	1783	11	52	55.49160033	-05	19	48.5367912	.00010621	.0022411	-0.0212	53560.9	53561.0	1			
1150+812	1150+812	847	11	53	12.49918859	+80	58	29.1545999	.00000982	.0000551	0.0695	47282.8	55042.7	104	0.68		3.2
1150+095	1150+095	3168	11	53	12.55211375	+09	14	2.2781717	.00004165	.0012039	-0.0856	49913.9	49914.1	1			
1150-108	1150-108	3169	11	53	22.31373408	-11	05	12.5873978	.00002796	.0009271	-0.0120	50576.1	50576.2	1			
1150+497	4C 49.22	848	11	53	24.46663994	+49	31	8.8302386	.00000463	.0000699	0.0610	49252.9	56591.0	152	0.57		3.2
1151+102	1151+102	3170	11	53	48.52735876	+09	55	54.8885334	.00003014	.0010791	-0.6235	49913.9	49914.1	1			
1151+408	1151+408	3171	11	53	54.65898094	+40	36	52.6188388	.00002190	.0003590	-0.3619	50242.1	50242.2	1			
1151+598	1151+598	4082	11	54	1.36623407	+59	34	54.1993296	.00006391	.0010314	-0.1580	56302.3	56302.7	1			
1151-324	1151-324	3172	11	54	6.16641470	-32	42	42.9814379	.00002995	.0009373	-0.5575	52306.4	52306.5	1			
1151+126	1151+126	4131	11	54	10.40735159	+12	25	9.7528059	.00004097	.0008626	-0.2780	55775.8	55776.0	1			
1151-348	1151-348	3173	11	54	21.78714353	-35	05	29.0741566	.00010903	.0046437	0.5499	52306.4	52409.2	2			
1152-308	1152-308	3174	11	55	3.15769961	-31	07	58.7273486	.00002618	.0008800	-0.2618	52306.4	52409.2	2			
1152+462	1152+462	3175	11	55	11.00919925	+45	55	39.6255527	.00026681	.0050573	-0.3811	50305.9	50306.0	1			
1153-119	1153-119	3176	11	55	36.81941698	-12	16	35.5025153	.00012390	.0030579	-0.1346	50576.1	50576.2	1			
1153-100	1153-100	3177	11	55	45.55142159	-10	17	52.2471498	.00019497	.0048774	0.3280	53572.0	53572.9	1			
1154+069	1154+069	3178	11	57	0.65243736	+06	41	12.5922580	.00003257	.0011688	-0.5108	54112.4	54112.5	1			
1155+169	1155+169	1092	11	57	34.83625556	+16	38	59.6500994	.00001047	.0002067	0.1293	50084.5	52779.7	4		0.08	
1155+251	GC 1155+25	849	11	58	25.78754100	+24	50	17.9639904	.00002117	.0004076	-0.0930	48975.7	54937.7	13			4.7
1155+486	1155+486	3179	11	58	26.76952238	+48	25	16.2292937	.00002141	.0004112	-0.1529	50305.9	50306.0	1			
1156-221	P 1156-221	3180	11	59	11.26725946	-22	28	36.9016963	.00002151	.0007288	0.2785	50631.8	50687.9	2			
1156+101	1156+101	3181	11	59	11.86747488	+09	54	46.9758578	.00007692	.0025155	0.1188	53559.9	55483.7	2			
1156-094	P 1156-094	318	11	59	12.71171352	-09	40	52.0492745	.00001418	.0002728	-0.6310	46797.6	53066.0	29	0.18	0.14	3.6
1156-663	1156-663	3182	11	59	18.30545606	-66	35	39.4270750	.00002212	.0001792	0.3078	52872.3	56538.4	22			
1156-214	1156-214	1784	11	59	21.43254674	-21	42	44.9131851	.00001251	.0004504	-0.1360	54559.2	54559.3	1			
1156+295	GC 1156+29	319	11	59	31.83391073	+29	14	43.8268846	.00000337	.0000510	-0.0553	47305.1	56770.7	1176	1.45	0.93	2.5
1157-215	P 1157-215	3183	11	59	51.90611803	-21	48	53.7080338	.00001315	.0004167	-0.2851	50631.8	50687.8	2			
1157+532	1157+532	3184	12	00	11.38428995	+53	00	46.8773623	.00002963	.0004493	-0.1539	53561.1	54087.6	2			

Source Name		ID No.	Right Ascension			Declination			RA Error (s)	Dec. Error (arcsec)	RA–Dec Corr.	Observation Epoch MJD		No. Obs.	Source Flux (Jy)		Str Index
B1950	Common		H	M	S	D	M	S				First	Last		10-60	10-40	
1158+007	1158+007	1786	12	01	23.25077307	+00	28	28.3160362	.00001224	.0004047	-0.2569	53572.0	55916.6	2	0.18	0.20	
1159+148	1159+148	1787	12	01	44.26886326	+14	31	36.4497814	.00000858	.0002279	-0.0445	53559.9	53916.1	2			
1200-051	1200-051	1307	12	02	34.22487262	-05	28	2.4902983	.00001113	.0003707	0.0326	50576.1	50576.2	1			
1200+068	1200+068	1788	12	03	1.01256563	+06	34	41.5382054	.00008548	.0007304	0.0892	49913.9	54664.6	2			
1200+608	1200+608	3185	12	03	3.50713237	+60	31	19.1626907	.00007506	.0010780	0.1843	54087.4	54087.6	1			
1200+045	1200+045	1789	12	03	21.93497346	+04	14	19.0935716	.00005599	.0008830	-0.0756	54125.4	54125.5	1			
1200+483	1200+483	1229	12	03	29.85302250	+48	03	13.6261204	.00000753	.0001684	-0.0858	52409.1	56754.2	54	0.39	0.34	
1200+468	1200+468	3186	12	03	31.79784830	+46	32	55.5582872	.00112755	.0133430	0.4016	50305.9	54314.6	2			
1202-262	P 1203-26	3187	12	05	33.21233654	-26	34	4.4649322	.00001950	.0006706	-0.5907	50631.8	50687.9	2			
1204+399	1204+399	1790	12	06	37.05336632	+39	41	3.7473749	.00001645	.0002851	-0.3125	50242.1	54664.7	2			
1204+057	1204+057	3188	12	06	58.02671734	+05	29	52.2482165	.00006856	.0025335	0.4856	49913.9	49914.1	1			
1204+124	J1207+1211	850	12	07	12.62452627	+12	11	45.8465846	.00001716	.0003022	0.1150	49913.9	53575.1	5		0.10	
1204+281	1204+281	3189	12	07	27.90046308	+27	54	58.8502392	.00001313	.0003605	-0.1947	50219.1	50219.2	1			
1204-267	1204-267	1791	12	07	28.35237275	-27	03	10.0877169	.00014678	.0038583	-0.5588	53561.0	53561.0	1			
1205-008	1205-008	1792	12	07	41.67761362	-01	06	36.6902114	.00000753	.0003400	-0.1288	53134.1	56782.1	19	0.14	0.10	
1205-140	1205-140	3190	12	08	23.36193454	-14	21	43.9170839	.09106679	.2342167	-0.9999	53560.0	53560.0	1			
1205+545	1205+545	3191	12	08	27.49940486	+54	13	19.5179864	.00023750	.0016055	-0.1742	49576.0	49576.9	1			
1205+011	1205+011	3192	12	08	33.65421039	+00	54	21.9252753	.00018694	.0045609	-0.2831	53572.0	53572.9	1			
1206+549	1206+549	3193	12	08	54.25631470	+54	41	58.1641841	.00004795	.0008096	0.1613	49576.0	49576.9	1			
1206-238	1206-238	1793	12	09	2.44510971	-24	06	20.7589513	.00001261	.0003157	0.0720	50632.0	54643.7	3			
1206-202	1206-202	3194	12	09	14.61097840	-20	32	38.9899896	.00001360	.0004543	-0.0153	50631.8	50687.9	2			
1206+416	1206+415	3195	12	09	22.78802664	+41	19	41.3699434	.00002477	.0004002	-0.3695	50242.1	50242.2	1			
1206-399	1206-399	3196	12	09	35.24364590	-40	16	13.1003129	.00006280	.0020181	0.4593	53134.2	53134.2	1			
1207-319	1207-319	1276	12	09	40.04464262	-32	14	53.1072928	.00001191	.0003470	-0.0451	52306.4	53771.4	3		0.19	
1207+260	1207+260	3197	12	09	45.09511185	+25	47	3.7304153	.00001583	.0004389	-0.2190	50219.1	50219.2	1			
1207-120	1207-120	3198	12	10	4.16444938	-12	17	44.9400137	.00026434	.0030586	0.7685	54112.5	54112.5	1			
1208+186	1208+186	3199	12	11	6.68829169	+18	20	34.2829541	.00004037	.0006377	0.2365	50084.5	50156.3	2			
1209-191	1209-191	3200	12	11	57.73867466	-19	26	7.6583796	.00013852	.0025826	0.4682	50632.0	50687.9	2			
1209-220	1209-220	3201	12	12	3.69760768	-22	21	51.5128318	.00001739	.0005720	-0.4926	50632.0	50687.9	2			
1210+197	1210+197	1794	12	12	56.09591467	+19	25	47.0161657	.00006435	.0003701	0.0863	50084.5	54643.7	3			
1210-097	1210-097	3202	12	13	22.94288362	-10	03	25.2672487	.00001965	.0007246	-0.0559	50576.1	50576.2	1			
1210-246	1210-246	3203	12	13	29.68554082	-24	53	13.1729697	.00021756	.0120276	0.9466	53561.0	55966.5	2			
1210+134	1210+134	3204	12	13	32.17037119	+13	07	20.9036889	.00024910	.0127811	-0.6559	50084.5	50085.5	1			
1211-167	1211-167	3205	12	13	43.76781363	-16	58	56.7664537	.00010163	.0036623	-0.5415	54087.5	56463.1	2			
1211+334	1211+334	3206	12	14	4.11579353	+33	09	45.5955606	.00002844	.0005441	-0.0878	50219.1	50219.2	1			
1212+087	1212+087	3207	12	14	59.91318668	+08	29	22.5177821	.00009324	.0016954	0.3436	49913.9	54482.4	2			
1212+171	J1215+1654	1093	12	15	3.97913590	+16	54	37.9568294	.00000431	.0000757	0.0127	50084.5	56638.7	69	0.21	0.14	2.2
1213-172	P 1213-17	326	12	15	46.75175813	-17	31	45.4030910	.00000400	.0000698	-0.1532	49867.9	56716.5	64	0.52	0.84	2.2
1213+350	4C 35.28	851	12	15	55.60104764	+34	48	15.2208298	.00000635	.0001104	-0.1145	48975.8	55194.7	22	0.30	0.09	3.3
1213+097	1213+097	4083	12	16	6.21573285	+09	29	9.5251851	.02147478	.2390691	-0.7495	56302.6	56302.6	1			
1213-102	1213-102	3208	12	16	24.40258276	-10	33	15.6193849	.00001414	.0005120	-0.0976	50576.1	50576.2	1			
1214+588	1214+588	3209	12	17	11.01861140	+58	35	26.2479976	.00004297	.0005254	-0.0672	49576.0	49576.9	1			
1215+303	B2 1215+30	328	12	17	52.08196500	+30	07	0.6360230	.00000478	.0000870	-0.0620	50219.1	56724.4	71	0.26	0.21	2.5
1215-002	1215-002	3210	12	17	58.72904866	-00	29	46.2996472	.00001876	.0005652	0.0770	50576.1	55847.7	2	0.19	0.22	
1215-457	1215-457	852	12	18	6.25249719	-46	00	28.9970095	.00148992	.0161192	-0.6993	49329.0	56498.0	2			
1215+113	1215+113	1795	12	18	26.09229304	+11	05	5.2619142	.00001042	.0003118	0.1185	53125.1	53125.2	1			
1216-010	1216-010	3211	12	18	34.92982358	-01	19	54.3412678	.00001407	.0004645	0.1587	50576.1	50576.2	1			
1216+179	1216+179	4084	12	18	46.60446776	+17	38	17.2678451	.00002831	.0007071	-0.0832	56393.2	56393.4	1			
1216-217	1216-217	3212	12	18	58.76212756	-21	59	46.1588815	.03217811	.1532105	0.9866	53572.9	53572.9	1			
1216+487	1216+487	853	12	19	6.41474508	+48	29	56.1647858	.00000576	.0000751	0.0011	48378.1	56136.3	40	0.33		3.1

Source Name		ID No.	Right Ascension			Declination			RA Error (s)	Dec. Error (arcsec)	RA–Dec Corr.	Observation Epoch MJD		No. Obs.	Source Flux (Jy)		Str Index
B1950	Common		H	M	S	D	M	S				First	Last		10-60	10-40	
1216+061	1216+061	1095	12	19	23.21607674	+05	49	29.6998787	.00002598	.0004480	0.1311	53067.9	54125.4	2			
1217+662	1217+662	1796	12	19	35.79396941	+66	00	31.8444564	.00036797	.0017143	0.4880	53559.8	53560.1	1			
1217+713	1217+713	1096	12	20	3.62839424	+71	05	31.1335605	.00004815	.0002988	-0.0006	49827.1	53134.3	3	0.11		
1217+295	NGC 4278	3213	12	20	6.82686889	+29	16	50.6311711	.04951718	.3282160	-0.9989	53134.1	53134.1	1			
1217+348	1217+348	3214	12	20	8.29414533	+34	31	21.7433298	.00002802	.0006661	-0.6224	50219.1	50219.2	1			
1217+023	P 1217+02	332	12	20	11.88455927	+02	03	42.2248751	.00002527	.0002873	0.0506	49913.9	53108.6	5		0.08	
1218+339	1218+339	3215	12	20	33.86470511	+33	43	11.9921562	.00888713	.1333890	0.4420	54278.1	54278.1	1			
1218+384	1218+384	3216	12	20	59.22931989	+38	08	55.7068549	.00002181	.0004228	-0.5270	50242.1	50242.2	1			
1218-024	1218-024	3217	12	21	23.94118515	-02	41	49.6084541	.00001564	.0004951	0.1728	50576.1	50576.2	1			
1218+444	1218+444	3218	12	21	27.04466580	+44	11	29.6717604	.00002057	.0004465	0.0582	50305.9	50306.0	1			
1219+285	ON 231	335	12	21	31.69051617	+28	13	58.5001846	.00000694	.0001151	-0.3600	44446.8	55180.6	58	0.19	0.17	3.8
1219-164	1219-164	3219	12	22	16.09900191	-16	45	54.8777427	.00025465	.0067094	0.7373	54112.5	54112.6	1			
1219+044	P 1219+04	336	12	22	22.54962090	+04	13	15.7760992	.00000339	.0000531	-0.1111	48378.1	56782.1	968	0.81	0.64	1.9
1221+464	1221+464	3220	12	23	39.33665988	+46	11	18.6021044	.00002892	.0003191	0.0658	50305.9	56267.5	2			
1221+809	1221+809	854	12	23	40.49374008	+80	40	4.3404589	.00001261	.0000591	0.0329	48975.8	56762.7	47	0.29		2.6
1221+071	1221+071	3221	12	23	54.62414551	+06	50	2.5764947	.00038013	.0063797	0.6759	49913.9	49914.0	1			
1221+484	1221+484	4085	12	23	58.23064384	+48	12	57.6642797	.00004085	.0005532	0.0295	56267.5	56267.7	1			
1222+438	1222+438	3222	12	24	51.50534822	+43	35	19.2868468	.00003259	.0007394	-0.1545	50242.1	50242.2	1			
1222+037	P 1222+037	337	12	24	52.42194141	+03	30	50.2926637	.00000859	.0001991	-0.3975	44200.8	54184.5	104	0.29	0.31	4.5
1222+216	P 1222+21	1230	12	24	54.45840040	+21	22	46.3887712	.00000583	.0001403	-0.1496	50084.6	53552.1	5	1.19	0.95	
1222+131	3C 272.1	1797	12	25	3.74333480	+12	53	13.1394089	.00000604	.0001845	-0.0151	50988.9	55112.7	11			
1223+395	1223+395	3223	12	25	50.56908695	+39	14	22.6864994	.00002140	.0004962	-0.2458	50242.1	50242.2	1			
1223-188	1223-188	1798	12	26	35.27695746	-19	04	38.5335048	.00001329	.0004901	-0.3804	54559.2	54601.2	2			
1224-132	1224-132	1799	12	26	54.41871501	-13	28	38.9839119	.00003323	.0011080	-0.3295	53552.0	53552.1	1			
1224+439	1224+439	3224	12	26	57.90456357	+43	40	58.4419983	.00035261	.0096046	-0.7971	53561.0	53561.1	1			
1224-443	1224-443	3225	12	27	26.68278866	-44	36	38.3478514	.00008861	.0024140	-0.6315	53125.2	53125.2	1			
1225+498	1225+498	1800	12	27	55.72470400	+49	32	56.0461255	.00002005	.0004829	-0.0909	53572.0	53572.9	1			
1225+368	ON 363	3226	12	27	58.72550829	+36	35	11.8268674	.00006803	.0010659	-0.5954	50242.1	50242.2	1			
1225+028	1225+028	1801	12	28	19.25662392	+02	32	29.3965769	.00002189	.0006837	-0.1378	53560.0	53560.0	1			
1225+317	1225+317A	3227	12	28	24.96599301	+31	28	37.6293255	.00001475	.0004251	-0.2313	50219.1	50219.3	1			
1224-854	1224-854	3228	12	28	34.77463355	-85	42	55.9518758	.20847146	.2495402	-0.9900	54723.2	54723.2	1			
1226-028	1226-028	855	12	28	36.91730872	-03	04	39.3116801	.00001522	.0004559	-0.3299	50653.9	54184.4	11	0.12	0.13	
1226+373	1226+373	856	12	28	47.42367068	+37	06	12.0958604	.00000377	.0000593	-0.0017	48378.1	56758.6	123			
1226+492	1226+492	3229	12	28	51.76787398	+48	58	1.2920018	.00005578	.0012039	0.3882	50305.9	50306.0	1			
1226+638	1226+638	3230	12	29	6.02599205	+63	35	0.9801917	.00037930	.0036462	0.0284	49827.1	49827.2	1			
1226+023	3C 273	341	12	29	6.69974236	+02	03	8.5982028	.00000384	.0000733	-0.3027	43808.8	54976.8	536			
1227+274	1227+274	3231	12	29	34.24794968	+27	11	56.3779614	.00002191	.0004821	-0.2297	53561.0	56036.4	2			
1227+587	1227+587	3232	12	30	7.05725020	+58	30	7.7641786	.00013021	.0021801	0.4908	49576.0	49576.9	1			
1227+255	1227+255	1097	12	30	14.08935144	+25	18	7.1365771	.00001266	.0002687	-0.4181	50219.1	56701.6	2	0.30	0.32	
1228-310	1228-310	1802	12	30	44.93264337	-31	21	23.3113688	.00008398	.0057745	-0.3329	52306.4	53134.2	3			
1228+126	3C 274	342	12	30	49.42338206	+12	23	28.0437044	.00000341	.0000524	-0.0961	44200.8	56772.6	1271	0.25		3.6
1228-113	1228-113	3233	12	30	55.55593834	-11	39	9.7956767	.00004452	.0014154	-0.5337	50576.1	50576.2	1			
1228-352	1228-352	3234	12	31	16.54218207	-35	33	18.9231495	.00029870	.0133694	-0.1629	53503.2	56161.9	2			
1228+045	1228+045	3235	12	31	27.58580192	+04	18	1.8897695	.00010151	.0014825	0.1397	49913.9	49914.1	1			
1229-123	1229-123	3236	12	31	50.26248262	-12	36	37.0773287	.02948465	.0892676	0.9682	53560.0	53560.0	1			
1229-021	1229-021	3237	12	32	0.01601299	-02	24	4.7945054	.00001193	.0003663	0.0612	50576.1	50576.2	1			
1229-099	1229-099	1803	12	32	15.85986651	-10	15	25.1684456	.00009349	.0024343	-0.1478	53561.0	53561.1	1			
1230+486	1230+486	3238	12	32	34.78761968	+48	21	32.9403367	.00004487	.0007476	0.1935	50305.9	50306.0	1			
1231+811	1231+811	3239	12	33	12.89308144	+80	54	33.9712506	.00010612	.0003826	-0.3494	54112.4	54112.6	1			
1230-101	1230-101	3240	12	33	13.16487440	-10	25	18.4383897	.00002537	.0008327	0.4370	50576.1	50576.2	1			

Source Name		ID No.	Right Ascension			Declination			RA Error (s)	Dec. Error (arcsec)	RA–Dec Corr.	Observation Epoch MJD		No. Obs.	Source Flux (Jy)		Str Index
B1950	Common		H	M	S	D	M	S				First	Last		10-60	10-40	
1231+481	1231+481	3241	12	34	13.33078220	+47	53	51.2356043	.00004771	.0008321	0.0978	50305.9	50306.0	1			
1232-338	1232-338	3242	12	34	46.12015492	-34	08	59.0538299	.00002506	.0008843	-0.0242	55111.8	55112.7	1			
1232+366	1232+366	3243	12	35	5.80645223	+36	21	19.3211433	.00003047	.0004911	-0.3647	50242.1	54482.5	2			
1234-504	1234-504	857	12	37	15.23914073	-50	46	23.1770833	.00256622	.0086133	-0.8042	50048.9	52941.1	2			
1235+196	1235+196	3244	12	37	36.42036702	+19	24	40.6198876	.00001238	.0004121	-0.1146	50084.6	50156.3	2			
1235+208	1235+208	1804	12	37	56.59089227	+20	34	18.8500687	.00005833	.0009274	0.5680	53560.0	53560.1	1			
1235+076	1235+076	3245	12	38	2.44564471	+07	23	21.8176202	.00002067	.0005740	-0.0273	49914.0	49914.2	1			
1236-381	1236-381	3246	12	38	52.73158755	-38	25	56.9984262	.00025450	.0126086	0.1662	52306.5	53125.2	3			
1236+077	P 1236+077	344	12	39	24.58832736	+07	30	17.1890668	.00000411	.0000707	0.0106	48378.3	56749.5	45	0.39	0.70	2.8
1236+049	1236+049	3247	12	39	32.75567730	+04	43	5.2343170	.00001913	.0006244	-0.2229	49914.0	49914.2	1			
1237-101	P 1237-10	345	12	39	43.06147618	-10	23	28.6925179	.00000427	.0000808	-0.0672	49960.0	55229.7	40	0.28	0.25	4.3
1236-684	P 1236-684	858	12	39	46.65141584	-68	45	30.8926013	.00004921	.0003378	-0.3543	50181.7	54706.7	13			
1237-113	M 104	346	12	39	59.43185813	-11	37	22.9961997	.00006324	.0028803	-0.8319	50002.7	53552.1	8			
1238+702	1238+702	3248	12	40	34.70031029	+69	58	30.6099933	.00007482	.0005971	-0.2421	49827.2	54087.6	2			
1238-110	1238-110	3249	12	40	37.32848504	-11	21	25.7950278	.05409824	.0011455	0.9999	53572.9	53572.9	1			
1238+243	1238+243	3250	12	40	47.98501588	+24	05	14.1513087	.00016181	.0027479	-0.3477	50219.1	50219.3	1			
1239+552	1239+552	3251	12	41	27.70387075	+54	58	19.0575097	.00086116	.0107728	0.8623	54439.8	54440.7	1			
1239+606	1239+606	859	12	41	29.59054595	+60	20	41.3225198	.00005253	.0004124	-0.4255	49576.0	54112.6	5			
1239+376	1239+376A	1232	12	42	9.81238176	+37	20	5.6927747	.00001391	.0002372	-0.1736	50242.1	52990.9	9			
1240+381	1240+381	861	12	42	51.36906479	+37	51	0.0253798	.00000487	.0000741	-0.0914	49750.4	56650.2	36	0.16	0.18	2.8
1240-294	1240-294	1805	12	43	10.66193027	-29	43	22.5044708	.00001767	.0005559	-0.1404	53125.2	53125.2	1			
1241+735	1241+735	3252	12	43	11.21713610	+73	15	59.2500341	.00010501	.0004781	-0.4292	53560.9	56204.5	2			
1241+749	1241+749	3253	12	43	45.03359130	+74	42	37.1142959	.00045130	.0023611	0.2391	49827.1	49827.2	1			
1241+166	1241+166	1806	12	43	57.64917551	+16	22	53.3944456	.00004331	.0021472	0.1224	54313.9	54314.1	1			
1241+176	1241+176	1277	12	44	10.82492131	+17	21	4.5063341	.00025898	.0053954	-0.9429	53719.5	55413.1	3			
1241-262	1241-262	1807	12	44	14.64192402	-26	33	24.9995094	.00003399	.0012087	0.0660	53560.0	53560.0	1			
1242+410	1242+410	3254	12	44	49.18716260	+40	48	6.1528269	.00027530	.0054302	0.9112	50242.1	50242.3	1			
1243-160	1243-160	1808	12	45	53.74227810	-16	16	45.7050257	.00000573	.0001109	0.0454	50632.0	56744.6	58			
1243-412	1243-412	3255	12	45	57.70320305	-41	28	44.0976830	.29529761	.6366224	1.0000	54292.0	54292.0	1			
1243-072	1243-072	690	12	46	4.23211008	-07	30	46.5747361	.00000387	.0000678	-0.1469	47253.5	56782.1	138	0.62	0.59	2.1
1244-255	P 1244-255	350	12	46	46.80203641	-25	47	49.2889729	.00000388	.0000622	-0.1856	44200.7	56772.4	269	0.56	0.84	0.2
1245+710	1245+710	3256	12	47	7.55341187	+70	46	45.1230758	.00066376	.0027638	0.2152	54112.4	54112.6	1			
1245+676	1245+676	3257	12	47	33.32957568	+67	23	16.4503806	.00021315	.0014830	-0.1902	49827.2	54087.6	2			
1245-235	1245-235	3258	12	47	59.35117733	-23	48	59.2808391	.00015896	.0037491	0.4955	50632.0	50687.9	2			
1246+586	1246+586	3259	12	48	18.78463158	+58	20	28.7172620	.00006487	.0010498	0.3188	49576.0	49576.9	1			
1245-062	1245-062	1308	12	48	22.97565533	-06	32	9.8180411	.00000663	.0002635	-0.0028	50576.1	56782.1	19	0.21	0.16	
1245-197	P 1245-197	3260	12	48	23.89814841	-19	59	18.5894887	.00005874	.0013581	0.6143	50632.0	50688.0	2			
1245-457	1245-454	3261	12	48	28.49512507	-45	59	47.1800883	.00001501	.0002681	0.3508	53138.3	54670.6	12			
1246+489	1246+489	3262	12	48	50.94798650	+48	39	53.1526024	.00062372	.0128645	0.6982	50305.9	54314.1	2			
1246+285	1246+285	1809	12	49	18.40927510	+28	17	43.6147320	.00003348	.0006628	-0.3694	53125.1	53125.3	1			
1247+022	1247+022	1810	12	50	6.84191373	+01	58	4.1445510	.00028176	.0052061	0.8052	53134.1	53134.2	1			
1247+166	1247+166	1811	12	50	9.22709044	+16	21	21.4619824	.00013609	.0019025	0.0051	53560.0	53560.1	1			
1247-442	1247-442	3263	12	50	22.80484481	-44	32	3.4816919	.00003704	.0011191	-0.0970	55168.6	55168.6	1			
1247+139	1247+139	3264	12	50	28.21804811	+13	43	40.3846666	.00001042	.0003344	-0.0381	53572.0	55371.2	2			
1247+025	1247+025	1812	12	50	32.58077876	+02	16	32.1728017	.00001178	.0004024	-0.2052	53561.0	53561.1	1			
1248-170	1248-170	1813	12	51	14.47512821	-17	17	13.1599057	.00002122	.0007401	-0.5209	53561.0	53561.1	1			
1248-350	1248-350	3265	12	51	39.22514929	-35	18	39.5695091	.00025091	.0160001	0.3452	53134.2	53134.2	1			
1250-330	1250-330	1814	12	52	58.39738464	-33	19	59.5614878	.00002160	.0006896	-0.3282	53125.2	53125.2	1			
1250+293	1250+293	4086	12	53	6.40901610	+29	05	13.8842964	.00016023	.0044127	-0.0991	56393.2	56393.4	1			
1250+532	1250+532	3266	12	53	11.92032334	+53	01	11.7375156	.00024307	.0017151	0.6808	49576.9	49576.9	1			

Source Name		ID No.	Right Ascension			Declination			RA Error (s)	Dec. Error (arcsec)	RA–Dec Corr.	Observation Epoch MJD		No. Obs.	Source Flux (Jy)		Str Index
B1950	Common		H	M	S	D	M	S				First	Last		10-60	10-40	
1251-407	1251-407	3267	12	53	59.53349207	-40	59	30.7051435	.00034628	.0241951	0.1695	52306.5	53134.2	3			
1252+458	J1254+4536	1098	12	54	28.82867120	+45	36	4.3260758	.00003665	.0008231	0.2455	50305.9	50306.0	1			
1251-130	1251-130	1815	12	54	31.46819732	-13	17	16.2146280	.00005061	.0020980	0.4469	53560.0	53560.1	1			
1251-197	1251-197	3268	12	54	37.25558526	-20	00	56.4070172	.00001735	.0005054	-0.3300	54489.4	56546.9	3			
1252+119	P 1252+11	351	12	54	38.25559439	+11	41	5.8950749	.00000441	.0000795	-0.1637	48353.1	56776.7	81	0.42	0.39	2.9
1252+028	1252+028	1816	12	54	45.46653260	+02	33	28.9621949	.00006307	.0015881	0.2937	53572.0	53573.0	1			
1252-441	1252-441	3269	12	54	57.51336936	-44	24	56.6006637	.00043782	.0318614	-0.4134	53125.2	53125.2	1			
1252+092	1252+092	3270	12	54	58.95766826	+08	59	47.5504422	.00006035	.0020460	-0.7155	54087.5	54087.6	1			
1251-713	P 1251-71	862	12	54	59.92147961	-71	38	18.4365316	.00001987	.0001116	0.2455	47625.8	56741.0	34			
1253+185	J1255+1817	1099	12	55	31.75994551	+18	17	50.9111902	.00001989	.0005658	0.4177	50084.6	50156.3	2			
1253-055	3C 279	352	12	56	11.16655988	-05	47	21.5247870	.00000432	.0000939	-0.1706	43808.9	56681.6	194	2.72	2.84	4.1
1254+571	1254+571	863	12	56	14.23396786	+56	52	25.2379384	.00002474	.0003884	-0.2944	51245.7	53515.2	9	0.13		
1253-216	1253-216	1817	12	56	25.51111867	-21	55	21.1471509	.00026216	.0068370	-0.5901	53561.0	53561.0	1			
1256+802	1256+802	3271	12	57	31.72641656	+79	58	2.5069546	.00076840	.0014035	-0.1385	50688.2	55168.4	2			
1255+327	1255+327	3272	12	57	57.23185475	+32	29	29.3261023	.00001277	.0003600	-0.4543	50219.1	50219.3	1			
1255-316	1255-316	864	12	57	59.06082100	-31	55	16.8517908	.00000382	.0000608	0.0908	48748.7	56776.6	692		0.23	3.2
1255-177	1255-177	1818	12	58	38.30170720	-18	00	3.1245167	.00000499	.0000838	0.0172	50632.0	56770.7	81			
1256-220	1256-220	1278	12	58	54.47877948	-22	19	31.1255170	.00000714	.0002219	-0.2672	50632.0	53820.2	5	0.42	0.30	
1256-229	1256-229	3273	12	59	8.46203425	-23	10	38.6547550	.00001143	.0003828	-0.2541	50632.0	50688.0	2			
1256-243	1256-243	3274	12	59	12.62560009	-24	36	5.5040284	.00003780	.0012106	0.2070	50632.0	50688.0	2			
1257+519	1257+519	3275	12	59	31.17401805	+51	40	56.2607766	.00002774	.0003886	-0.2294	49576.0	54112.6	2			
1257+123	1257+123	3276	13	00	1.93886449	+12	06	22.1186841	.00005753	.0012258	-0.3028	49914.0	49914.2	1			
1257+145	P 1257+145	356	13	00	20.91881525	+14	17	18.5315992	.00000641	.0001201	0.1285	48811.9	55293.7	31		0.21	2.1
1258+287	1258+287	3277	13	00	28.52992803	+28	30	10.1886774	.00003123	.0005174	0.2425	53125.1	53125.2	1			
1258+087	1258+087	3278	13	00	36.43874869	+08	28	2.8636683	.00002948	.0009286	-0.3667	53503.2	53503.3	1			
1258+145	1258+145	3279	13	00	41.03699297	+14	17	29.4145750	.00002454	.0006226	-0.0385	53560.0	56106.1	2			
1258+507	1258+507	3280	13	00	41.24704992	+50	29	36.7653636	.00003056	.0006362	-0.2061	49576.0	50306.0	2			
1257-326	1257-326	1819	13	00	42.42599749	-32	53	12.1135557	.00003908	.0014819	-0.1552	52306.5	53411.6	3			
1259+468	1259+468	1820	13	01	32.60629373	+46	34	2.9397831	.00003684	.0006800	0.1642	53561.0	53561.1	1			
1300+485	1300+485	3281	13	02	17.19607971	+48	19	17.5744409	.00001616	.0002165	-0.0323	50305.9	56749.5	2	0.14	0.08	
1300+693	1300+693	3282	13	02	37.92470618	+69	02	51.6011447	.00034793	.0036300	0.4854	49827.2	49827.2	1			
1300+580	1300+580	865	13	02	52.46527374	+57	48	37.6093823	.00000341	.0000505	-0.0061	49422.2	56782.1	968	0.49		1.3
1300-105	1300-105	3283	13	03	13.86792909	-10	51	17.1293994	.00001050	.0003164	0.1173	50575.3	56463.2	4			
1302-034	1302-034	3284	13	04	43.64221139	-03	46	2.5517223	.00001952	.0005948	-0.0449	50575.3	50575.3	1			
1302+641	1302+641	3285	13	04	47.37007508	+63	53	47.4316993	.00234213	.0882086	0.4794	53125.1	53134.3	2			
1302-208	1302-208	1821	13	04	59.06930254	-21	06	42.4589347	.00005651	.0016430	-0.0168	54965.1	54965.2	1			
1304+791	1304+791	3286	13	05	0.01395863	+78	54	35.7964979	.00020380	.0002746	0.1583	49827.2	50688.3	2			
1302-285	1302-285	3287	13	05	8.46859740	-28	50	42.0272544	.00005882	.0019485	0.3657	50687.9	50688.0	1			
1302-312	1302-312	3288	13	05	31.07332345	-31	32	52.2095871	.00136739	.0406592	0.6709	52306.5	52306.5	1			
1302-102	P 1302-102	359	13	05	33.01502367	-10	33	19.4281979	.00000450	.0001024	-0.3157	47379.8	56782.1	146	0.34	0.26	3.3
1303+557	1303+557	3289	13	06	3.35107333	+55	29	43.8606030	.00027316	.0021111	0.3699	49576.0	49576.9	1			
1303-170	1303-170	3290	13	06	32.66050970	-17	18	58.3896025	.00002002	.0007749	-0.0245	50632.0	50632.2	1			
1304-318	1304-318	3291	13	07	15.17883546	-32	07	58.6412364	.00002786	.0009149	0.4219	55482.8	55482.8	1			
1305+502	1305+502	3292	13	08	7.92424637	+49	57	53.4697656	.00005108	.0007140	0.4735	50305.9	50306.0	1			
1305+042	1305+042	1822	13	08	15.55306598	+04	01	9.3516424	.00002514	.0008876	-0.6983	53125.2	53125.3	1			
1306+360	1306+360	1823	13	08	23.70913267	+35	46	37.1640807	.00000425	.0000704	-0.0422	52409.1	56498.7	50	0.39	0.35	1.6
1305-247	1305-247	3293	13	08	32.72735419	-24	58	32.4082084	.00007382	.0026831	-0.8199	54112.5	54112.6	1			
1303-827	1303-827	3294	13	08	38.19583283	-82	59	34.7950028	.00280616	.0060145	0.2706	52886.9	53138.6	3			
1307+562	1307+562	3295	13	09	9.75440437	+55	57	38.1963050	.00004544	.0009949	-0.1294	49576.0	49576.9	1			
1307+121	1307+121	866	13	09	33.93244463	+11	54	24.5531035	.00000512	.0000925	0.1258	49099.2	53690.0	87	0.18	0.12	3.6

Source Name		ID No.	Right Ascension			Declination			RA Error (s)	Dec. Error (arcsec)	RA–Dec Corr.	Observation Epoch MJD		No. Obs.	Source Flux (Jy)		Str Index
B1950	Common		H	M	S	D	M	S				First	Last		10-60	10-40	
1306-395	1306-395	1824	13	09	48.48837870	-39	48	33.0872887	.00002945	.0011382	-0.1564	53523.2	55916.6	2		0.20	
1307+010	1307+010	1100	13	10	28.50431051	+00	44	8.8841961	.00004482	.0008695	-0.2359	49914.1	55776.1	2	0.14		
1308+326	B2 1308+32	361	13	10	28.66385083	+32	20	43.7829086	.00000337	.0000508	-0.0987	44200.9	56724.4	1528	1.07	1.16	3.3
1308+471	1308+471	3296	13	10	53.59159134	+46	53	52.2182140	.00009799	.0017029	0.3844	50305.9	50306.0	1			
1308+328	1308+328	867	13	10	59.40272753	+32	33	34.4495822	.00000356	.0000538	-0.0103	50219.1	56772.6	147	0.43	0.31	2.7
1308+554	1308+554	1279	13	11	3.21079864	+55	13	54.3226707	.00000658	.0000857	-0.0595	49576.0	56547.6	33	0.17		2.1
1308+145	1308+145	3297	13	11	7.82433210	+14	17	46.6481382	.00006294	.0013455	-0.3804	50084.6	50156.3	2			
1308+172	1308+172	3298	13	11	23.82011123	+16	58	44.1896085	.00012171	.0039929	-0.8564	50084.6	50156.3	2			
1309+257	1309+257	1825	13	12	14.28882676	+25	31	13.1764529	.00012138	.0022624	-0.3751	53134.1	53134.3	1			
1310+487	1310+487	3299	13	12	43.35369476	+48	28	30.9408409	.00005415	.0007292	-0.0006	50305.9	50306.0	1			
1310-041	1310-041	3300	13	12	50.90122154	-04	24	49.8921328	.00000669	.0003241	-0.1357	50575.3	56782.1	18	0.22	0.26	
1310-271	1310-271	3301	13	13	1.42140253	-27	22	58.8474174	.00024233	.0082853	-0.1572	50632.0	50688.0	2			
1311+678	1311+678	3302	13	13	27.98585632	+67	35	50.3812077	.00084101	.0044707	-0.3884	52409.1	52409.3	1			
1311+552	1311+552	3303	13	13	37.85312016	+54	58	23.8993262	.00010873	.0010137	-0.0931	49576.0	54087.6	2			
1312+533	1312+533	3304	13	14	43.83055573	+53	06	27.7306587	.00007023	.0012979	0.1083	49576.0	49576.9	1			
1312+126	1312+126	1826	13	15	1.85285753	+12	20	52.6384862	.00006974	.0021493	-0.8212	53561.0	53561.1	1			
1312+289	1312+289	1827	13	15	13.49151600	+28	40	53.6692234	.00002376	.0005159	0.1115	53125.1	53125.3	1			
1313-333	OP-322	363	13	16	7.98594635	-33	38	59.1727761	.00000380	.0000644	-0.2230	43808.8	56671.2	348		0.86	2.7
1313+200	1313+200	3305	13	16	24.56803860	+19	47	4.4605644	.00020820	.0023210	-0.0092	50084.6	54482.4	3			
1314-202	1314-202	1828	13	17	26.14897193	-20	31	38.1320467	.00013924	.0062312	-0.8126	53134.2	53134.2	1			
1315+346	OP 326	364	13	17	36.49418185	+34	25	15.9326228	.00000532	.0000930	-0.0800	47946.2	56691.2	69	0.26	0.15	3.5
1314-134	1314-134	3306	13	17	36.53769476	-13	45	32.6518576	.00002922	.0008854	0.4821	50575.3	50575.4	1			
1315+415	1315+415	1829	13	17	39.19382394	+41	15	45.6185084	.00021703	.0034510	0.5316	53560.0	53560.1	1			
1315+047	1315+047	4087	13	18	29.64220640	+04	30	10.0112198	.00001798	.0006780	-0.2585	56161.9	56162.0	1			
1315-058	1315-058	3307	13	18	33.70942601	-06	07	23.8202911	.00001261	.0004719	-0.2737	54112.5	54112.6	1			
1316-120	1316-120	3308	13	19	12.07204173	-12	17	32.1287098	.00002003	.0005882	0.3139	50575.3	50575.4	1			
1319-126	NGC 5077	3309	13	19	31.66962157	-12	39	25.0749954	.00001896	.0006894	-0.4574	53503.2	53503.3	1			
1317-005	1317-005	1830	13	19	38.76620837	-00	49	39.9380397	.00001866	.0007382	0.2907	53552.0	53552.1	1			
1317+520	1317+520	1831	13	19	46.19807172	+51	48	5.7779001	.00007154	.0005673	-0.1176	49576.0	54664.7	2			
1317+019	1317+019	3310	13	20	26.79487177	+01	40	36.8116151	.00001913	.0004006	0.2509	49914.0	54643.0	2			
1318+508	1318+508	3311	13	20	42.20805415	+50	36	7.7990523	.00057358	.0023164	-0.5056	49576.1	54112.6	3			
1318+225	1318+225	1101	13	21	11.20255636	+22	16	12.1082287	.00000832	.0001818	0.0246	50084.6	53362.1	28		0.07	
1318-434	1318-434	1832	13	21	12.84449495	-43	42	16.8623307	.00030321	.0185533	0.2355	55042.0	55042.0	1			
1318-263	1318-263	3312	13	21	14.03691479	-26	36	10.4670698	.00003572	.0016542	-0.6655	50632.0	54664.7	3			
1322+835	1322+835	3313	13	21	45.60896627	+83	16	13.4236209	.00008029	.0001996	-0.0983	50688.2	56498.4	4			
1319+220	1319+220	3314	13	22	11.40358521	+21	48	12.2790182	.00002092	.0004532	-0.2886	54087.5	54087.7	1			
1319+270	1319+270	3315	13	22	14.97080024	+26	45	46.3193132	.00480605	.0614543	-0.9156	50219.1	50219.3	1			
1319-093	1319-093	3316	13	22	36.91261498	-09	37	37.7998117	.00000618	.0002910	-0.0691	50575.3	56782.1	15	0.71	0.64	
1320+394	1320+394	1833	13	22	55.66443485	+39	12	7.9516027	.00003881	.0007680	0.4282	53560.0	53560.1	1			
1320-385	1320-385	1834	13	23	4.14838057	-38	49	0.6922161	.00024410	.0165551	0.1073	53153.2	53153.2	1			
1320-446	P 1320-446	868	13	23	4.24688937	-44	52	33.8569173	.00035603	.0096751	0.0574	49329.0	52409.2	4			
1320-338	1320-338	3317	13	23	17.13878800	-34	07	12.3503596	.00004916	.0014535	-0.3464	53134.2	56638.7	2			
1320-303	1320-303	1835	13	23	19.46731158	-30	38	6.6656304	.00001633	.0005822	0.0100	54943.2	54943.3	1			
1323+799	1323+799	1836	13	23	51.56973810	+79	42	51.8470112	.00012288	.0002169	0.1596	50688.2	54664.6	2			
1321-323	1321-323	3318	13	24	11.86079594	-32	35	35.5903426	.00014579	.0040802	0.8894	52306.5	52409.3	2			
1321+410	1321+410	3319	13	24	12.09560667	+40	48	11.7631204	.00003084	.0005699	-0.1860	50242.1	50242.3	1			
1321-105	1321-105	3320	13	24	25.79309527	-10	49	23.1340262	.00000830	.0003200	0.0041	50575.3	56701.6	2	0.48	0.45	
1322+479	1322+479	3321	13	24	29.34245477	+47	43	20.6235817	.00006399	.0009179	-0.1973	50305.9	50306.0	1			
1322+366	NGC 5141	3322	13	24	51.44093442	+36	22	42.7654005	.00031265	.0076314	0.5820	53134.1	53134.3	1			
1322-078	1322-078	3323	13	25	9.61553074	-08	04	48.3902433	.00003857	.0011660	-0.4302	54112.5	54112.6	1			

Source Name		ID No.	Right Ascension			Declination			RA Error (s)	Dec. Error (arcsec)	RA–Dec Corr.	Observation Epoch MJD		No. Obs.	Source Flux (Jy)		Str Index
B1950	Common		H	M	S	D	M	S				First	Last		10-60	10-40	
1322-110	1322-110	3324	13	25	13.21960353	-11	17	39.0824603	.00002539	.0010927	-0.3928	54087.6	54087.7	1			
1322-427	P 1322-42	869	13	25	27.61520072	-43	01	8.8054738	.00004636	.0009826	0.6477	48110.0	52409.2	6			
1323+321	1323+321	870	13	26	16.51167402	+31	54	9.5197844	.00017090	.0023522	-0.1549	48975.8	50219.3	4			4.6
1323-527	1323-527	3325	13	26	49.22916814	-52	56	23.6327503	.00003769	.0008725	0.4613	54723.3	54723.4	1			
1324+574	1324+574	3326	13	26	50.57254580	+57	12	6.7504227	.00044907	.0051934	-0.6393	49576.0	49577.0	1			
1324-047	1324-047	3327	13	26	54.59927978	-05	00	59.2865011	.07716167	.6109859	1.0000	53572.1	53572.1	1			
1324+224	1324+224	704	13	27	0.86131055	+22	10	50.1628462	.00000339	.0000514	-0.0515	48428.4	56770.7	440	0.98	0.73	0.3
1325+437	1325+436	3328	13	27	20.97901302	+43	26	27.9891058	.00002520	.0004334	0.0690	50242.1	50242.3	1			
1325+504	1325+504	3329	13	27	25.12365858	+50	08	49.1724925	.00004360	.0008675	0.1541	49576.0	54112.6	3			
1325-133	1325-133	4088	13	27	42.02372042	-13	36	0.1621825	.00002999	.0010651	0.2110	55966.4	55966.5	1			
1325+126	1325+126	1837	13	27	54.68300085	+12	23	9.1781743	.00000783	.0002064	-0.1607	53523.2	56749.5	2	0.21	0.30	
1325-558	1325-558	1102	13	29	1.14489996	-56	08	2.6657519	.00001465	.0001832	0.4025	52676.6	56604.4	33			
1327+504	1327+504	1838	13	29	5.80271279	+50	09	26.4009657	.00000667	.0000798	-0.1910	49576.0	56749.6	35			
1327+321	1327+321A	1839	13	29	52.86491768	+31	54	11.0547472	.00000527	.0000974	-0.1553	50219.1	53770.8	5			
1326-697	1326-698	3330	13	30	11.07684370	-70	03	13.0777255	.00006110	.0003537	0.2330	54723.3	54723.7	1			
1327-311	1327-311	3331	13	30	19.08406486	-31	22	59.1353457	.00001847	.0006475	-0.4067	52306.5	52409.3	2			
1328+254	3C 287	1840	13	30	37.69029243	+25	09	10.8762199	.00018111	.0022641	-0.3573	52409.2	54187.5	2			
1328+522	1328+522	3332	13	30	42.60508462	+52	02	15.4960494	.01239303	.0700404	0.9933	49577.0	49577.0	1			
1328+307	3C 286	370	13	31	8.28807656	+30	30	32.9598432	.00013690	.0022366	0.3479	49253.8	53185.6	7			5.7
1328-263	1328-263	3333	13	31	11.69294047	-26	39	9.6147856	.00011415	.0048060	-0.6703	53503.2	53503.3	1			
1328-034	1328-034	1841	13	31	29.16142412	-03	41	14.1134708	.00003366	.0008482	0.0419	53552.0	53552.1	1			
1329+063	1329+063	1103	13	31	53.89715309	+06	08	23.3917481	.00004016	.0008210	0.1298	53125.2	53125.3	1		0.12	
1329-049	1329-049	3334	13	32	4.46466605	-05	09	43.3056775	.00001481	.0004194	0.2087	50575.3	56463.2	2	0.60	0.48	
1330+300	1330+300	3335	13	32	20.56711826	+29	49	45.5964039	.04973303	.0362618	-0.9985	53561.0	53561.0	1			
1329-137	1329-137	3336	13	32	30.92817605	-14	02	13.1865755	.00005159	.0014119	-0.0815	53560.0	56106.1	2			
1329-126	1329-126	1842	13	32	39.25155203	-12	56	15.3422004	.00005599	.0017782	0.3731	53572.0	53572.1	1			
1330+476	1330+476	871	13	32	45.24641497	+47	22	22.6677345	.00000758	.0000866	0.0674	50305.9	56761.9	10		0.12	0.8
1330+022	1330+022	1843	13	32	53.27053704	+02	00	45.6992584	.00000731	.0001927	-0.3815	54187.3	56770.7	6			
1330+071	1330+071	1844	13	33	4.99696664	+06	52	31.9708193	.00002200	.0006013	-0.0273	53134.2	53134.3	1			
1330+276	1330+276	3337	13	33	7.49072994	+27	25	18.3831937	.00001503	.0004392	-0.3226	50219.1	50219.3	1			
1331+170	1331+170	1104	13	33	35.78263392	+16	49	4.0149248	.00000954	.0001825	0.2807	50084.6	54643.7	4			
1330-236	1330-236	3338	13	33	38.92594352	-23	56	25.5803508	.00011297	.0055400	-0.3358	54087.6	54087.7	1			
1331-195	1331-195	3339	13	33	45.17564493	-19	50	42.3452784	.00006165	.0020477	-0.1772	50632.0	50688.0	2			
1331-115	1331-115	3340	13	34	4.19076921	-11	50	14.2711491	.00002340	.0006739	0.3522	50575.3	50575.4	1			
1332+031	1332+031	3341	13	35	11.90483794	+02	53	9.5072625	.00005282	.0012454	-0.0883	53125.2	56106.2	2			
1333+459	1333+459	3342	13	35	21.96227359	+45	42	38.2314227	.00002564	.0004188	-0.0017	50305.9	50306.0	1			
1333+589	1333+589	3343	13	35	25.92839599	+58	44	0.2923105	.00004364	.0004872	-0.3506	49576.0	49577.0	1			
1333-049	1333-049	3344	13	35	56.47671981	-05	11	41.6592852	.00002282	.0006598	0.3109	50575.3	50575.4	1			
1333-082	1333-082	3345	13	36	8.25981546	-08	29	51.7972160	.00000920	.0004738	-0.0607	50575.3	56748.2	11	0.34	0.09	
1333-152	1333-152	1845	13	36	34.08915082	-15	29	48.0708979	.00001183	.0003880	-0.0853	54559.3	56560.9	5			
1333-186	1333-186	1846	13	36	34.39329679	-18	52	41.6744036	.00003053	.0009709	0.1472	53560.0	53560.1	1			
1333-337	1333-337	3346	13	36	39.03253945	-33	57	57.0739465	.00002405	.0005065	-0.4664	54489.6	56638.7	5			
1335+658	1335+658	1847	13	37	16.05969118	+65	32	46.3166871	.00003105	.0002157	0.0349	54943.1	54943.4	1			
1334-127	DW 1335-12	376	13	37	39.78277782	-12	57	24.6934188	.00000337	.0000520	-0.0648	43816.8	56782.1	1929	2.24	2.45	2.3
1335+552	1335+552	1848	13	37	49.64221706	+55	01	2.1180012	.00004882	.0004045	0.1115	49576.0	54643.6	2			
1336-237	1336-237	3347	13	39	1.74638534	-24	01	14.0065417	.00001038	.0003522	-0.2348	50632.0	50688.0	2			
1336-260	P 1336-260	3348	13	39	19.89077553	-26	20	30.4962328	.00001311	.0003725	-0.0519	50632.0	54643.7	3			
1337+637	1337+637	3349	13	39	23.78304910	+63	28	58.4249949	.00015698	.0011998	0.4045	49827.2	49827.3	1			
1337-013	1337-013	3350	13	40	4.61505471	-01	37	46.5435018	.00003415	.0009579	0.5768	50575.3	50575.4	1			
1337-033	1337-033	1849	13	40	13.30450921	-03	35	20.8055937	.00022816	.0028404	-0.4740	54125.3	54125.4	1			

Source Name		ID No.	Right Ascension			Declination			RA Error (s)	Dec. Error (arcsec)	RA–Dec Corr.	Observation Epoch MJD		No. Obs.	Source Flux (Jy)		Str Index
B1950	Common		H	M	S	D	M	S				First	Last		10-60	10-40	
1338+381	1338+381	872	13	40	22.95179488	+37	54	43.8339193	.00001388	.0002656	-0.2421	48942.0	55801.0	36	0.08	0.07	3.8
1338+362	1338+362	3351	13	40	36.00996741	+36	00	26.7382918	.00024967	.0036581	0.6855	54112.5	54112.7	1			
1339+696	1339+696	3352	13	40	48.03465088	+69	23	22.5102974	.02546544	.4520616	-0.9727	49827.2	49827.2	1			
1338+285	1338+285	3353	13	41	15.28275990	+28	16	5.0771583	.00002257	.0006623	-0.5373	50219.1	50219.3	1			
1339-206	1339-206	3354	13	42	4.73952030	-20	51	29.5417967	.00001666	.0005510	-0.2386	50632.0	50688.0	2			
1339+274	1339+274	3355	13	42	8.37669072	+27	09	30.6174303	.00001401	.0003646	-0.1399	50219.2	50219.3	1			
1339-287	1339-287	1850	13	42	15.34563587	-29	00	41.8317527	.00001231	.0002990	-0.1030	50687.9	56498.1	11			
1341+691	1341+691	3356	13	43	0.55333280	+68	55	17.1602424	.00029333	.0045060	0.3815	49827.2	54087.7	2			
1340-175	1340-175	3357	13	43	37.41427786	-17	47	55.4448045	.00003302	.0009736	0.0529	50632.0	50632.2	1			
1342+662	GC 1342+662	691	13	43	45.95958132	+66	02	25.7452377	.00000400	.0000522	0.0266	45301.1	56744.2	253	0.34		1.9
1342+663	GC 1342+663	382	13	44	8.67963954	+66	06	11.6438648	.00000530	.0000568	0.0395	44263.7	56723.6	222	0.26		2.8
1341-171	1341-171	1851	13	44	14.40246127	-17	23	40.3950719	.00000893	.0002926	-0.0539	53572.0	56749.4	2	0.29	0.33	
1343+451	1343+451	1852	13	45	33.17246742	+44	52	59.5730268	.00001783	.0003404	0.0186	53561.0	53561.1	1			
1343+386	1343+386	3358	13	45	36.94235931	+38	23	12.4610190	.00009699	.0037964	0.0282	54112.5	56302.7	2			
1343+073	1343+073	1853	13	45	49.31476359	+07	06	31.1214598	.00004807	.0012661	0.2024	53560.0	53560.1	1			
1343-300	1343-300	3359	13	45	51.51990508	-30	15	4.5941742	.00013348	.0038252	0.5899	52306.5	52306.6	1			
1343-601	1343-601	3360	13	46	49.04335334	-60	24	29.3539967	.00048262	.0018742	-0.0546	52887.1	53138.7	3			
1344+188	1344+188	3361	13	47	23.49018394	+18	35	37.5735330	.00001169	.0003364	0.1252	50084.6	50156.3	2			
1345+061	1345+061	3362	13	47	31.44472984	+05	52	33.8045360	.00003589	.0008839	0.3051	53134.2	56203.9	2			
1345+125	P 1345+12	383	13	47	33.36163614	+12	17	24.2407858	.00004267	.0015167	0.0170	48975.7	53612.8	6	0.18	0.12	5.4
1344-375	1344-375	1854	13	47	40.42895776	-37	50	36.6189197	.00004898	.0014625	-0.0001	53153.2	53153.2	1			
1345+289	1345+289	4089	13	48	4.34910275	+28	40	25.3660338	.00005210	.0012265	-0.2083	56393.2	56393.4	1			
1346-109	1346-109	3363	13	49	3.15104793	-11	09	59.3107738	.16266840	.9817112	-1.0000	53560.0	53560.0	1			
1346-306	1346-306	1855	13	49	20.39851866	-30	56	24.1955641	.00003545	.0012423	0.3434	54965.2	54965.2	1			
1346-113	1346-113	3364	13	49	31.44325999	-11	32	53.8294273	.00002450	.0007321	0.2816	50575.3	50575.4	1			
1347+539	1347+539	873	13	49	34.65661660	+53	41	17.0401812	.00000696	.0000818	-0.0954	48720.2	55349.5	23	0.27		3.0
1347-218	1347-218	3365	13	50	14.09005245	-22	04	41.0762160	.00004990	.0014299	0.2636	50632.0	50688.0	2			
1347+099	1347+099	3366	13	50	22.13603749	+09	40	10.6554484	.00010552	.0015935	0.4015	49914.0	49914.2	1			
1347-163	1347-163	3367	13	50	36.14392929	-16	34	49.5139548	.00002040	.0007434	0.3031	53561.0	56267.7	2			
1349+617	1349+617	3368	13	50	38.18070385	+61	32	48.5744933	.02721773	.2615708	-0.9940	49576.1	49576.1	1			
1348+237	1348+237	1856	13	50	45.65839589	+23	31	45.1593425	.00005106	.0007407	0.0116	53125.2	53125.3	1			
1348+308	1348+308	1857	13	50	52.73621944	+30	34	53.5905485	.00000544	.0000962	0.0336	50219.2	56463.1	43			
1348+087	1348+087	1858	13	51	16.91907553	+08	30	39.9034946	.00000768	.0002276	-0.0551	53125.2	56749.5	2	0.22	0.13	
1348-289	1348-289	1859	13	51	46.83881215	-29	12	17.6506314	.00004666	.0013382	-0.8575	53125.2	53125.3	1			
1349-145	1349-145	3369	13	51	52.64960829	-14	49	14.5552110	.00001717	.0007048	-0.2109	50632.0	50632.2	1			
1349-275	1349-275	1860	13	52	28.04620994	-27	45	7.1294952	.00013660	.0053810	-0.5831	53572.0	53572.1	1			
1349-439	P 1349-439	387	13	52	56.53494042	-44	12	40.3876181	.00001066	.0001109	-0.4005	44265.5	56538.5	72		0.22	2.2
1352+757	1352+757	3370	13	53	23.16806670	+75	32	57.7350452	.00019966	.0008291	0.5318	49827.2	49827.3	1			
1351+021	1351+021	1861	13	53	51.58447728	+01	51	53.8939256	.00015337	.0040976	0.7453	53560.0	53560.1	1			
1351-018	P 1351-018	388	13	54	6.89532276	-02	06	3.1904809	.00000341	.0000571	0.0068	48572.8	56782.2	1010	0.52	0.12	2.3
1352-104	P 1352-104	389	13	54	46.51868725	-10	41	2.6561544	.00000475	.0000807	0.0422	50456.4	56649.7	82		0.39	2.6
1352-632	1352-632	3371	13	55	46.61210257	-63	26	42.5705852	.00063377	.0034594	-0.2805	52941.0	55784.5	2			
1353-341	P 1353-341	3372	13	56	5.38663200	-34	21	10.8602772	.00006265	.0019268	-0.5845	52306.5	52306.6	1			
1353-171	1353-171	1862	13	56	6.95303990	-17	24	31.8208812	.00022861	.0066398	-0.0471	53572.0	53572.1	1			
1354+247	1354+247	4090	13	56	40.38050163	+24	31	0.2005724	.00029528	.0079530	-0.9445	56393.2	56393.4	1			
1354-107	1354-107	1863	13	56	46.83189025	-11	01	29.2220100	.00030249	.0038834	0.7441	53561.0	53561.1	1			
1354+195	P 1354+19	392	13	57	4.43665049	+19	19	7.3724330	.00000448	.0000768	-0.3939	44200.9	55271.7	208	0.62	0.79	3.7
1354-174	P 1354-174	390	13	57	6.07419012	-17	44	1.9049582	.00001029	.0001441	-0.1188	50456.4	55545.0	29	0.07		
1354-152	OP-192	391	13	57	11.24497741	-15	27	28.7869248	.00000373	.0000622	-0.1649	47253.4	56782.1	306	0.58	0.60	1.7
1355+441	1355+441	3373	13	57	40.59226160	+43	53	59.7687189	.00005497	.0005127	-0.0963	52409.1	52409.3	1			

Source Name		ID No.	Right Ascension			Declination			RA Error (s)	Dec. Error (arcsec)	RA–Dec Corr.	Observation Epoch MJD		No. Obs.	Source Flux (Jy)		Str Index
B1950	Common		H	M	S	D	M	S				First	Last		10-60	10-40	
1357+769	1357+769	874	13	57	55.37152959	+76	43	21.0510632	.00000361	.0000503	-0.0169	49341.7	56776.7	1300	0.75		0.7
1355+115	1355+115	1864	13	58	22.41964692	+11	19	32.9192121	.00003584	.0009334	-0.1688	53560.0	53560.1	1			
1356+478	1356+478	1865	13	58	40.66638330	+47	37	58.3108678	.00005394	.0006824	0.0324	53561.0	53561.1	1			
1355-416	P 1355-41	394	13	59	0.18447844	-41	52	52.6369867	.00056819	.0028321	-0.8303	48110.1	54076.7	6			
1357+559	1357+559	3374	13	59	5.72830109	+55	44	29.2957209	.03356495	.2062889	0.9971	53572.1	53572.1	1			
1356+022	1356+022	1866	13	59	27.14932572	+01	59	54.5640244	.00001730	.0006516	-0.6241	49914.0	54482.6	2			
1357+404	1357+404	3375	13	59	38.09427775	+40	11	38.2504447	.00001461	.0003385	-0.2215	50242.1	50242.3	1			
1357-187	1357-187	1867	14	00	3.86602619	-18	58	11.0868596	.00001395	.0004975	-0.2637	53523.2	53523.2	1			
1358+624	1358+624	3376	14	00	28.64862597	+62	10	38.5888043	.00014794	.0013412	-0.5451	52409.2	52409.3	1			
1358+046	1358+046	3377	14	00	48.44918279	+04	25	30.9573972	.02183004	.2728712	0.9983	53560.0	53560.0	1			
1358-090	1358-090	3378	14	01	5.33184950	-09	16	31.5723474	.00002094	.0007075	-0.2888	50575.3	50575.4	1			
1358-298	1358-298	1868	14	01	34.93941485	-30	04	36.8694711	.00009766	.0031313	0.5398	53125.2	53125.2	1			
1400+588	1400+588	3379	14	01	45.70005984	+58	35	42.2646310	.00023492	.0019578	-0.3590	53561.2	54087.7	2			
1359-281	1359-281	3380	14	02	2.40169332	-28	22	25.1433942	.00002957	.0011562	-0.2197	50687.9	50688.0	1			
1400+162	1400+162	3381	14	02	44.51358570	+15	59	56.6759043	.00070688	.0060260	-0.2083	53572.0	53572.0	1			
1400-184	1400-184	3382	14	02	48.50453661	-18	40	47.4902444	.00001501	.0005840	0.1405	54112.6	54112.6	1			
1402+660	1402+660	3383	14	04	5.27905704	+65	51	37.5835832	.00011924	.0010235	-0.3550	52409.2	52409.3	1			
1401+000	1401+000	3384	14	04	12.12398670	-00	13	25.0912472	.00001436	.0004175	-0.0461	50575.3	50575.4	1			
1402+077	1402+077	1869	14	04	32.99232110	+07	28	46.9643711	.00002916	.0007771	0.5591	53560.0	53560.1	1			
1402-012	P 1402-012	397	14	04	45.89547922	-01	30	21.9470661	.00000851	.0001168	-0.1856	48664.4	55544.9	26		0.24	
1402+044	P 1402+044	398	14	05	1.11981763	+04	15	35.8189400	.00000484	.0001059	-0.1888	48887.8	56638.2	49		0.19	3.0
1403+411	1403+411	1870	14	05	7.79546817	+40	56	57.8311885	.00001215	.0002239	-0.0466	53125.2	53125.3	1			
1402-144	1402-144	3385	14	05	32.86737332	-14	40	18.2964057	.00002209	.0009489	-0.2984	50575.3	50575.4	1	0.13	0.08	
1403-085	DW 1403-08	3386	14	06	0.70185329	-08	48	6.8799659	.00001819	.0005535	-0.3313	50575.3	50575.4	1			
1406+787	1406+787	3387	14	06	36.56689770	+78	28	10.4063975	.00023294	.0004968	-0.3613	49827.2	50688.3	2			
1404+347	1404+347	3388	14	06	53.84725617	+34	33	37.3064023	.00001742	.0005090	-0.3134	50219.2	50219.3	1			
1404+286	OQ 208	400	14	07	0.39441466	+28	27	14.6901958	.00000340	.0000520	-0.1122	44341.1	56657.2	1394	0.29	0.18	3.6
1406+767	1406+767	3389	14	07	1.98932754	+76	28	13.4246053	.00582792	.2736611	-0.4632	49827.3	49827.3	1			
1404-267	1404-267	3390	14	07	29.76219916	-27	01	4.2918147	.00011256	.0031564	0.1931	50632.1	50688.0	2			
1404-342	1404-342	3391	14	07	54.91684877	-34	31	28.2730869	.00016730	.0055423	0.3449	54489.5	54489.6	1			
1406+564	1406+564	1105	14	08	12.94626298	+56	13	32.4843855	.00003482	.0004209	-0.6660	49576.0	54482.7	2			
1407+691	1407+691	3392	14	08	19.07541530	+68	54	50.8269914	.00036693	.0023560	0.1080	49827.2	49827.3	1			
1405-287	1405-287	3393	14	08	49.61370683	-29	00	23.6076045	.00002322	.0008036	0.1207	50687.9	50688.0	1			
1406-076	P 1406-076	402	14	08	56.48119624	-07	52	26.6665893	.00000377	.0000651	-0.1682	47379.9	56782.2	167	0.58	0.72	2.3
1406-230	1406-230	3394	14	09	11.97617108	-23	15	49.6115041	.00009325	.0030273	-0.2430	50632.1	50688.0	2			
1406-267	1406-267	1871	14	09	50.16978568	-26	57	36.9802599	.00000507	.0001105	0.1226	50632.1	56763.1	92		0.28	
1407+022	1407+022	1872	14	10	4.65596070	+02	03	6.9127730	.00000977	.0003287	-0.1272	53134.2	53134.3	1			
1408+077	1408+077	3395	14	10	35.07536440	+07	31	21.4898228	.00007659	.0016902	-0.5847	49914.0	49914.2	1			
1409+373	1409+373	1873	14	11	14.51613363	+37	05	35.6235960	.00002877	.0006175	-0.4621	53572.0	53572.1	1			
1409+218	1409+218	875	14	11	54.86222627	+21	34	23.4374022	.00000916	.0002447	-0.3700	50459.5	53131.5	4		0.11	2.5
1410+138	1410+138	3396	14	12	36.37265503	+13	34	38.1526669	.00002722	.0007416	-0.4633	50084.6	50156.3	2			
1412+461	1412+461	3397	14	14	14.85260667	+45	54	48.7183437	.00059476	.0100831	-0.2738	50305.9	54314.1	2			
1412-279	1412-279	3398	14	15	4.48619716	-28	09	54.4311130	.00002285	.0008512	-0.0967	53572.0	55916.7	2			
1412+087	1412+087	3399	14	15	9.91842694	+08	32	5.3691704	.00003187	.0006665	-0.5493	54112.6	55413.1	2			
1412-097	1412-097	3400	14	15	20.83391214	-09	55	58.3309114	.00002353	.0007490	0.2198	53561.1	55846.9	2			
1412-368	1412-368	1106	14	15	26.01632717	-37	05	26.9702281	.00001493	.0002371	-0.2407	52306.6	55545.1	19			
1413+373	1413+373	3401	14	15	28.46678861	+37	06	21.1623185	.00003060	.0005129	-0.2806	50242.1	50242.3	1			
1413+135	P 1413+135	404	14	15	58.81750927	+13	20	23.7128570	.00000403	.0000741	-0.1494	48353.2	56751.6	74	0.44	0.35	1.9
1413+349	OQ 323	405	14	16	4.18624375	+34	44	36.4274195	.00001544	.0003911	0.1004	50219.2	51687.5	2			
1413-168	1413-168	1874	14	16	34.36977292	-17	05	45.7350427	.00003551	.0011998	-0.2581	53560.0	53560.1	1			

Source Name		ID No.	Right Ascension			Declination			RA Error (s)	Dec. Error (arcsec)	RA–Dec Corr.	Observation Epoch MJD		No. Obs.	Source Flux (Jy)		Str Index
B1950	Common		H	M	S	D	M	S				First	Last		10-60	10-40	
1415+463	1415+463	3402	14	17	8.16134856	+46	07	5.4481472	.00004551	.0005120	0.1186	50305.9	50306.0	1			
1415-349	J1418-35	1875	14	18	58.91694685	-35	09	42.5075800	.00003160	.0009453	-0.1636	53134.2	53134.2	1			
1416+067	1416+067	876	14	19	8.18019516	+06	28	34.8034847	.00001443	.0002524	-0.1971	49176.9	54440.7	10	0.08	0.07	3.1
1418+546	GC 1418+54	408	14	19	46.59739890	+54	23	14.7872331	.00000345	.0000509	-0.0677	44282.8	56782.1	903	0.45		3.0
1417+385	1417+385	877	14	19	46.61376002	+38	21	48.4751137	.00000345	.0000518	-0.0246	49750.4	56772.7	385	1.14	0.36	1.9
1417-192	1417-192	3403	14	19	49.73876890	-19	28	25.2672279	.00001132	.0003725	-0.1120	50632.1	50688.0	2			
1417+273	1417+273	878	14	19	59.29706798	+27	06	25.5528442	.00000502	.0000826	-0.0031	50219.2	55112.7	18			
1417+375	1417+375	1876	14	20	0.34105795	+37	21	34.6595670	.00002560	.0003693	0.1108	53134.1	53134.3	1			
1418-065	1418-065	3404	14	21	7.75558313	-06	43	56.3560897	.00004455	.0010714	0.5833	50575.3	50575.4	1			
1419+469	1419+469	1107	14	21	23.07301605	+46	45	47.9869461	.00004654	.0006152	0.0429	50305.9	50306.0	1			
1418-192	1418-192	1877	14	21	36.95802295	-19	31	18.8461925	.00006827	.0040674	-0.9127	54601.3	54601.3	1			
1420+326	1420+326	879	14	22	30.37896015	+32	23	10.4401087	.00000978	.0001816	-0.1209	50209.9	53136.6	6			
1419-229	1419-229	4091	14	22	37.10634830	-23	08	30.1364437	.00005014	.0017428	-0.4326	56498.0	56498.1	1			
1421+482	1421+482	3405	14	23	6.15673130	+48	02	10.8459458	.00009832	.0009658	0.0425	50305.9	50306.0	1			
1421+511	1421+511	3406	14	23	14.18654580	+50	55	37.2833675	.00015037	.0023440	-0.5740	50305.9	50306.0	1			
1421+122	1421+122	3407	14	23	30.10122025	+11	59	51.2405334	.00028652	.0029889	-0.4685	49914.1	54314.2	2			
1420-220	1420-220	3408	14	23	40.81027437	-22	18	17.5148598	.00009053	.0025499	0.2672	53503.2	53503.3	1			
1418-782	1417-782	3409	14	23	43.55155992	-78	29	34.8999966	.00182186	.0045214	0.2301	52887.0	53138.6	3			
1421+048	1421+048	4092	14	24	9.50093940	+04	34	52.0823631	.00003687	.0008684	-0.3322	56161.9	56162.1	1			
1421-138	1421-138	1878	14	24	16.03501690	-14	07	2.9968029	.00011114	.0024665	0.2816	53560.0	53560.2	1			
1422+473	1422+473	3410	14	24	37.07980756	+47	05	56.6982005	.00006628	.0012232	-0.0578	50305.9	50306.0	1			
1422+231	1422+231	3411	14	24	38.10362692	+22	56	0.9013526	.00091399	.0141136	0.9904	53125.3	53561.2	2			
1420-724	1420-725	3412	14	24	52.23818095	-72	41	17.0949280	.00007660	.0003896	0.1819	54723.3	54723.8	1			
1420-679	1420-679	3413	14	24	55.55737135	-68	07	58.0945595	.00002160	.0002007	0.3298	52872.4	56713.4	18			
1422-249	1422-249	1879	14	25	23.03739369	-25	13	6.9707455	.00002535	.0007859	-0.3862	53134.2	53134.3	1			
1423+146	1423+146	1109	14	25	49.01801112	+14	24	56.9017993	.00000516	.0001156	-0.1098	50084.6	56574.2	31		0.23	
1424+366	1424+366	880	14	26	37.08748877	+36	25	9.5737197	.00000532	.0000822	0.0146	50242.1	56687.2	50	0.19	0.14	2.6
1424+240	1424+240	881	14	27	0.39177542	+23	48	0.0375261	.00000640	.0001590	-0.0730	50084.6	56754.1	43	0.16	0.14	2.1
1425+267	1425+267	1233	14	27	35.60764555	+26	32	14.5379407	.00448374	.1177446	0.9918	53313.7	53313.7	1			
1424-328	1424-328	1880	14	27	41.36110596	-33	05	31.5066912	.00002573	.0014667	-0.0725	53125.3	54087.7	2			
1424-418	P 1424-41	409	14	27	56.29756245	-42	06	19.4376937	.00000360	.0000550	-0.0274	47305.3	56776.7	812		1.42	2.5
1427+543	1427+543	882	14	29	21.87880303	+54	06	11.1227633	.00002029	.0002054	-0.3789	49576.0	51471.5	6			
1427+109	P 1427+109	3414	14	30	9.73879194	+10	43	26.8620885	.00001292	.0003966	0.0662	49914.0	49914.2	1			
1428+422	1428+422	883	14	30	23.74160876	+42	04	36.4909604	.00000994	.0001437	0.1333	50242.1	54664.7	13			
1428+370	1428+370	1881	14	30	40.58369404	+36	49	3.8888833	.00000579	.0000932	0.0732	53134.1	56498.3	27			
1429+400	1429+400	3415	14	31	20.53840675	+39	52	41.5300372	.00001918	.0005402	-0.2584	50242.2	50242.3	1			
1430+365	1430+365	1882	14	32	39.82958656	+36	18	7.9320104	.00010321	.0009286	-0.4623	51687.0	51687.4	1			
1430-178	OQ-151	412	14	32	57.69062744	-18	01	35.2489726	.00001351	.0002154	-0.8008	44227.7	54664.7	49	0.08	0.29	3.9
1430-155	P 1430-155	3416	14	33	21.45930810	-15	48	44.6874999	.00001075	.0003495	-0.1544	50632.1	50632.2	1			
1432+422	1432+422	3417	14	34	5.69448205	+42	03	15.9915384	.00001520	.0003430	-0.2027	50242.2	50242.3	1			
1431-115	1431-115	3418	14	34	21.13590420	-11	46	19.5121038	.00003126	.0011709	-0.6894	53503.2	53503.3	1			
1432+200	1432+200	884	14	34	39.79335700	+19	52	0.7357336	.00000412	.0000741	0.0702	50084.6	56498.0	66			
1433+304	1433+304	885	14	35	35.40216872	+30	12	24.5193476	.00002454	.0003222	0.2892	50002.9	52809.0	5			
1433-040	1433-040	1883	14	35	39.90457818	-04	14	55.2991267	.00016956	.0042712	0.3132	53153.2	53153.2	1			
1436+763	1436+763	3419	14	35	47.10038056	+76	05	25.8315709	.00118718	.0054869	0.1671	49827.2	54112.7	2			
1434+235	P 1434+235	1110	14	36	40.98108533	+23	21	3.2599769	.00000830	.0001985	-0.2312	50084.6	54482.7	6	0.32	0.18	
1435+638	1435+638	886	14	36	45.80215071	+63	36	37.8664143	.00001153	.0000981	0.0897	49827.2	55271.7	18	0.52		4.2
1435-218	P 1435-218	887	14	38	9.46939664	-22	04	54.7482886	.00000547	.0001125	-0.3112	48161.8	56782.2	61	0.27	0.32	4.5
1436+445	1436+445	3420	14	38	28.50447506	+44	18	12.0718269	.00004647	.0007297	0.0480	50305.9	50306.1	1			
1437+624	1437+624	3421	14	38	44.78301351	+62	11	54.4367292	.00013047	.0009838	-0.6525	52409.2	52409.3	1			

Source Name		ID No.	Right Ascension			Declination			RA Error (s)	Dec. Error (arcsec)	RA–Dec Corr.	Observation Epoch MJD		No. Obs.	Source Flux (Jy)		Str Index
B1950	Common		H	M	S	D	M	S				First	Last		10-60	10-40	
1436+373	1436+373	1884	14	38	53.61097717	+37	10	35.4167220	.00001244	.0002213	-0.1184	50242.2	51687.3	2		0.16	
1436+214	1436+214	1885	14	39	8.90235532	+21	14	50.8223987	.00009444	.0014016	0.2910	53560.1	53560.2	1			
1437+331	1437+331	1886	14	39	23.65437537	+32	53	54.8245616	.00021318	.0013263	-0.4497	51687.1	51687.5	1			
1438+501	1438+501	3422	14	39	46.97622710	+49	58	5.4551451	.00002156	.0003761	-0.0912	50305.9	50306.1	1			
1437-153	1437-153	3423	14	39	56.87205619	-15	31	50.5554653	.00001183	.0003956	-0.1452	50632.1	56498.1	2	0.21	0.17	
1437+061	1437+061	3424	14	40	17.98506775	+05	56	34.0902256	.00004485	.0010121	-0.1764	54112.5	55413.1	2			
1438+385	1438+385	3425	14	40	22.33609488	+38	20	13.6163413	.00001202	.0002907	-0.1701	50242.2	50242.3	1			
1438+016	1438+016	1887	14	40	33.64696285	+01	27	5.2103287	.00004767	.0013015	-0.3120	53523.2	53523.3	1			
1438+021	1438+021	1888	14	40	59.49587931	+01	57	44.1512144	.00001613	.0005177	-0.0681	53561.1	53561.2	1			
1438-328	1438-328	1889	14	41	19.89353512	-33	03	24.3986643	.00003050	.0009316	0.0804	53134.3	53134.3	1			
1438-347	1438-347	1890	14	41	23.97014397	-34	56	45.9450897	.00022562	.0114442	-0.6065	53125.3	53125.3	1			
1438-151	1438-151	1891	14	41	45.41724139	-15	23	36.2655880	.00004150	.0014759	-0.2883	53560.0	53560.2	1			
1440+635	1440+635	3426	14	41	58.66921379	+63	18	33.4365718	.00061243	.0048657	0.8537	49827.2	49827.3	1			
1439+327	1439+327	3427	14	42	0.13896569	+32	34	20.3014987	.00002459	.0006312	-0.1341	50219.2	50219.3	1			
1441+522	1441+522B	1892	14	43	2.76060354	+52	01	37.2988863	.00006673	.0008750	-0.0129	53767.8	53768.5	1			
1441+252	1441+252	1893	14	43	56.89218753	+25	01	44.4906879	.00000449	.0000765	0.0333	52409.3	56475.6	46			
1442+637	1442+637	1894	14	43	58.60077130	+63	32	26.3650655	.00003542	.0002899	0.1366	49827.2	54664.7	2			
1442+031	1442+031	4093	14	44	31.76668436	+02	57	53.5155877	.00003027	.0010260	0.0554	56749.5	56749.5	1			
1442+101	OQ 172	420	14	45	16.46524640	+09	58	36.0728515	.00000624	.0000979	0.0968	48572.8	55320.7	34		0.14	3.6
1442-245	1442-245	3428	14	45	44.21148152	-24	45	41.5932893	.00002484	.0008515	0.0381	55413.0	55413.1	1			
1443-162	1443-162	692	14	45	53.37628777	-16	29	1.6190478	.00000602	.0000934	-0.4139	47379.9	56782.2	69	0.28	0.36	2.8
1444+175	1444+175	1111	14	46	35.34629380	+17	21	7.5812023	.00000651	.0001681	-0.1459	50084.6	53946.0	9	0.57	0.47	
1445-161	P 1445-16	421	14	48	15.05414615	-16	20	24.5490842	.00000760	.0001339	-0.6693	47379.9	54802.0	66	0.12	0.24	3.5
1448+762	1448+762	888	14	48	28.77902761	+76	01	11.5972767	.00000808	.0000561	-0.0242	49827.2	56770.6	45	0.46		2.7
1446+042	1446+042	3429	14	48	50.36107734	+04	02	19.8921771	.00016527	.0030115	0.6540	49914.0	49914.2	1			
1446-111	1446-111	3430	14	48	51.16009835	-11	22	15.7379378	.00007116	.0023848	0.6766	50575.3	50575.4	1			
1446-005	1446-005	3431	14	49	16.59033735	-00	45	19.2299099	.00004119	.0010651	-0.2735	53503.2	53503.3	1			
1448+093	1448+093	3432	14	50	31.16894691	+09	10	27.9551586	.00002189	.0006879	-0.3754	49914.0	49914.2	1			
1448-232	1448-232	1895	14	51	2.50975389	-23	29	31.1044164	.00031659	.0145679	-0.7753	53572.1	53572.1	1			
1449+139	1449+139	1896	14	51	31.49102273	+13	43	24.0007858	.00011310	.0013109	0.1918	50084.8	53134.3	3			
1449-012	1449-012	3433	14	51	47.41230043	-01	27	35.3079824	.00001633	.0005287	-0.5053	50575.3	50575.4	1			
1450+641	1450+641A	3434	14	51	57.36250675	+63	57	19.1999389	.00029255	.0019313	-0.5227	54087.5	54087.7	1			
1450+455	1450+455	3435	14	52	24.67423690	+45	22	23.6696971	.00017513	.0027931	-0.7657	50305.9	50306.1	1			
1448-648	1448-648	3436	14	52	39.67920111	-65	02	3.4332890	.00003381	.0002296	0.2598	52887.0	56504.7	14			
1451+352	1451+352	1897	14	53	18.54529001	+35	05	39.3640282	.00005002	.0013880	-0.0114	53572.0	53572.1	1			
1450-251	1450-251	1898	14	53	44.21893413	-25	22	47.5033809	.00003644	.0012055	-0.4926	53560.1	53560.2	1			
1451+106	1451+106	1899	14	53	44.24111302	+10	25	57.5634517	.00002969	.0007499	0.0308	53561.1	53561.2	1			
1451+270	1451+270	4094	14	53	53.60063965	+26	48	33.4099374	.00001020	.0002610	-0.3374	50219.2	53575.3	4	0.37	0.39	
1451+094	1451+094	3438	14	53	59.73209869	+09	15	43.3292362	.00001722	.0004267	-0.0983	53560.2	55657.5	2			
1450-338	1450-338	3439	14	54	2.47338085	-34	00	57.2134112	.00010934	.0045009	0.4985	52306.5	52409.3	2			
1452+166	1452+166	1900	14	54	20.85505776	+16	24	24.3709364	.00001212	.0004124	-0.1304	53523.2	53523.3	1			
1451-375	P 1451-375	423	14	54	27.40975845	-37	47	33.1449603	.00000420	.0000701	-0.0009	48110.1	56772.5	287		0.45	3.0
1452+301	1452+301	3440	14	54	32.29790551	+29	55	58.0566120	.00002524	.0008500	0.0685	53561.1	55371.3	2			
1451-400	1451-400	889	14	54	32.91235685	-40	12	32.5143182	.00000730	.0001396	0.0377	49330.2	56574.2	57		0.20	
1451-248	1451-248	3441	14	54	46.69901749	-25	05	12.4918331	.00013366	.0052643	-0.6177	50632.1	50688.0	2			
1452-168	1452-168	3442	14	55	2.81065603	-17	00	13.9534379	.00009985	.0024568	0.0798	50632.1	50632.2	1			
1453+217	1453+217	1901	14	55	31.84631811	+21	31	39.1757178	.00001915	.0004738	0.0349	53125.2	53125.3	1			
1454+447	1454+447	3443	14	55	54.13577205	+44	31	37.6549632	.00005502	.0009168	-0.2734	50305.9	50306.1	1			
1454+510	1454+510	3444	14	56	8.11974046	+50	48	36.3003414	.00022021	.0015951	0.3953	49576.1	50306.2	2			
1454-354	1454-354	1902	14	57	26.71170955	-35	39	9.9715016	.00001209	.0002163	0.1018	53134.3	55545.0	14			

Source Name		ID No.	Right Ascension			Declination			RA Error (s)	Dec. Error (arcsec)	RA–Dec Corr.	Observation Epoch MJD		No. Obs.	Source Flux (Jy)		Str Index
B1950	Common		H	M	S	D	M	S				First	Last		10-60	10-40	
1455+080	1455+080	3445	14	57	38.12870719	+07	49	54.7150316	.00001995	.0005795	-0.0424	49914.0	49914.2	1			
1455+247	1455+247	1903	14	57	43.42526568	+24	35	7.7233697	.00033839	.0087442	0.0608	53340.9	53341.6	1			
1455+098	1455+098	1904	14	57	52.53165977	+09	38	16.5486775	.00017330	.0039351	-0.4330	53572.1	53572.1	1			
1456+375	1456+375	3446	14	58	44.79443237	+37	20	21.6229213	.00002785	.0006429	-0.2644	50242.2	50242.3	1			
1456+044	1456+044	1112	14	58	59.35620912	+04	16	13.8204979	.00000469	.0000874	-0.0542	49914.0	56758.8	78	0.34	0.37	
1458+718	3C 309.1	426	14	59	7.58392410	+71	40	19.8664458	.00000795	.0000641	-0.0707	49268.0	56751.7	32	0.21		4.0
1456-367	1456-367	3447	14	59	15.76376192	-36	55	47.9382261	.00006586	.0019806	-0.3137	52306.6	52409.3	2			
1457+449	1457+449	1905	14	59	35.45807433	+44	42	7.9195291	.00002572	.0005864	0.2898	53560.1	53560.1	1			
1458+088	1458+088	3448	15	00	34.00377761	+08	39	41.8058178	.00010522	.0025779	0.1822	54112.7	55966.6	2			
1459+480	1459+480	890	15	00	48.65421793	+47	51	15.5381907	.00000486	.0000671	-0.0176	49252.9	56776.5	64	0.23	0.15	2.6
1457-237	1457-237	1906	15	00	51.88927488	-23	58	20.1906767	.00010256	.0061604	-0.2645	53572.1	53572.1	1			
1458-391	1458-391	3449	15	01	34.75785554	-39	18	39.4397367	.00011864	.0036248	0.8161	52306.6	52409.3	2			
1459-149	1459-149	1907	15	02	25.01743587	-15	08	52.5193458	.00003514	.0013114	-0.2575	53560.1	53560.2	1			
1500+094	1500+094	3450	15	03	0.89951570	+09	17	58.9830543	.00003150	.0006347	0.2152	54087.6	54087.7	1			
1500+045	1500+045	1908	15	03	28.88772023	+04	19	48.9912541	.00002073	.0007134	-0.5060	53561.1	53561.2	1			
1502+330	1502+330	3451	15	04	7.52536772	+32	49	21.1825432	.00006593	.0010209	0.1605	50219.2	50219.3	1			
1502+106	OR 103	428	15	04	24.97978115	+10	29	39.1985506	.00000353	.0000581	-0.2167	43809.0	56754.2	519	0.95	0.89	2.9
1502+291	1502+291	3452	15	04	26.69653922	+28	54	30.5424353	.00003592	.0010898	0.1634	50219.2	50219.3	1			
1501-343	1501-343	1909	15	05	2.37034490	-34	32	56.8201785	.00001563	.0004230	-0.1956	54818.6	54818.7	1			
1502+036	P 1502+036	429	15	05	6.47715506	+03	26	30.8125708	.00000360	.0000575	-0.0417	49914.0	56772.7	175	0.47	0.50	1.7
1503-091	1503-091	3453	15	06	3.03497390	-09	19	12.0548317	.00014779	.0038549	0.2034	50575.3	50575.4	1			
1504+377	1504+377	891	15	06	9.52996555	+37	30	51.1324827	.00000433	.0000676	-0.0205	47940.7	56770.4	119	0.32	0.19	2.0
1510+835	1510+835	3454	15	06	24.71427252	+83	19	28.0370896	.00059753	.0008491	-0.3758	50688.2	50688.3	1			
1505+497	1505+497	3455	15	06	44.11436406	+49	33	55.8039698	.00003711	.0005342	-0.5460	50306.1	50306.2	1			
1505+428	1505+428	1236	15	06	53.04185918	+42	39	23.0353691	.00000975	.0001741	-0.0594	50242.2	53946.8	8	0.27	0.17	3.4
1504-166	P 1504-167	431	15	07	4.78695776	-16	52	30.2672214	.00000436	.0000787	-0.3640	45154.0	56638.3	159	0.58	0.52	3.5
1505+514	1505+514	3456	15	07	11.61558910	+51	17	16.8629338	.00003825	.0005129	-0.0625	49576.1	54112.7	3			
1504+127	1504+127	1910	15	07	21.75810898	+12	36	29.0759630	.00002439	.0007675	-0.2891	53560.1	53560.2	1			
1505+044	1505+044	3457	15	07	59.73243389	+04	15	11.9853497	.00001243	.0004237	-0.1250	52306.5	52306.6	1			
1505-156	1505-156	1911	15	08	35.70156765	-15	48	31.5319946	.00001487	.0005649	-0.3722	53561.1	53561.2	1		0.07	
1505-496	1505-496	1113	15	08	38.94457079	-49	53	2.3112136	.00041356	.0025325	-0.5562	52676.6	53165.6	4			
1505-304	1505-304	1912	15	08	52.99313262	-30	36	29.4301843	.00007795	.0021889	-0.8159	53125.3	55784.4	2			
1506+163	1506+163	1913	15	09	10.11183457	+16	11	27.7356055	.00002168	.0007696	-0.4182	53125.2	53125.3	1			
1506-074	1506-074	1914	15	09	20.55344875	-07	35	48.1772728	.00008216	.0016613	0.3562	53572.1	53572.1	1			
1508+572	1508+572	892	15	10	2.92236806	+57	02	43.3760689	.00000596	.0000706	0.1651	49576.1	56772.5	53	0.21		
1508-111	1508-111	4132	15	10	44.43370867	-11	21	39.7040039	.00005301	.0018899	-0.4753	55776.0	55776.1	1			
1508-055	1508-055	893	15	10	53.59142133	-05	43	7.4175864	.00000455	.0000835	-0.0451	50575.3	55313.7	21	0.33	0.40	3.0
1508+223	1508+223	3458	15	11	5.58493166	+22	08	6.6377206	.03128306	.3038564	-0.9944	54087.7	54087.7	1			
1509+054	1509+054	3459	15	11	41.26654570	+05	18	9.2600713	.00001235	.0003563	-0.1711	52306.5	52306.6	1			
1508-325	1508-325	1915	15	11	50.40275758	-32	42	57.7901319	.00010873	.0043821	-0.0814	54943.3	54943.4	1			
1509+022	1509+022	1282	15	12	15.74175696	+02	03	16.9785611	.00003642	.0009592	-0.8159	53768.5	53768.6	1			
1510-089	P 1510-08	433	15	12	50.53292914	-09	05	59.8298329	.00000374	.0000660	-0.2752	43808.9	56782.2	394	1.29	1.47	2.9
1508-656	1508-656	3460	15	12	51.55085547	-65	53	2.2234316	.00110525	.0041393	0.2863	52887.1	53138.7	3			
1510-319	1510-319	3461	15	13	21.77727575	-32	09	32.6958988	.00003265	.0009676	-0.2541	55482.8	55482.9	1			
1510-421	1510-421	1916	15	13	30.62277582	-42	21	56.0484841	.00038536	.0207851	0.1481	55042.0	55042.1	1			
1511+238	1511+238	3462	15	13	40.18558817	+23	38	35.2003245	.00006017	.0008225	-0.2125	50084.6	50155.6	2			
1511-100	P 1511-100	434	15	13	44.89342217	-10	12	0.2648067	.00000462	.0000911	-0.3621	47254.5	56706.7	65	0.59	0.65	2.6
1511-210	P 1511-210	3463	15	13	56.97012422	-21	14	57.5070986	.00000951	.0003269	-0.0766	50632.1	50688.0	2	0.22	0.23	
1512+030	1512+030	1917	15	14	34.73446379	+02	52	48.5080364	.00002237	.0006652	0.1740	53560.1	53560.2	1			
1511-476	1511-476	1114	15	14	40.02457032	-47	48	29.8579211	.00001579	.0003170	0.3892	52676.6	54706.6	12			

Source Name		ID No.	Right Ascension			Declination			RA Error (s)	Dec. Error (arcsec)	RA–Dec Corr.	Observation Epoch MJD		No. Obs.	Source Flux (Jy)		Str Index
B1950	Common		H	M	S	D	M	S				First	Last		10-60	10-40	
1511-360	1511-360	3464	15	14	40.87384039	-36	17	4.8848813	.00012654	.0045813	-0.4916	55167.8	55168.6	1			
1511-558	1511-558	4095	15	15	12.67274871	-55	59	32.8378794	.00014153	.0009540	-0.0944	56007.1	56439.8	3			
1514+004	1514+004	1283	15	16	40.21905785	+00	15	1.9088756	.00000645	.0001974	-0.2896	49914.0	53945.9	6	0.49	0.51	
1514+197	GC 1514+19	437	15	16	56.79616389	+19	32	12.9920958	.00000409	.0000711	-0.0624	50084.6	56709.4	71	0.62	0.64	2.0
1514-241	P 1514-24	438	15	17	41.81313102	-24	22	19.4761235	.00000358	.0000641	-0.2173	47254.5	56638.3	303	0.71	0.50	3.5
1517-116	1517-116	1918	15	19	44.78403390	-11	51	44.5277625	.00002104	.0007650	0.1471	53560.1	53560.2	1			
1518+162	1518+162	4096	15	20	37.06113155	+16	01	26.6310566	.00006724	.0012180	-0.2963	56463.1	56463.3	1			
1522+791	1522+791	3465	15	21	2.79780184	+78	58	30.2603971	.00035840	.0006324	-0.5355	49827.3	50688.3	2			
1518+046	1518+046	3466	15	21	14.41937495	+04	30	21.6603926	.00023831	.0053059	0.5231	49914.0	49914.2	1			
1519+181	1519+181	3467	15	21	17.57899338	+17	56	1.0688047	.00007873	.0012854	-0.2698	54112.6	56463.3	2			
1518+045	1518+045	1115	15	21	22.54357614	+04	20	30.1327203	.00020994	.0071276	0.9214	49914.0	49914.1	1			
1520+437	1520+437	1919	15	21	49.61387549	+43	36	39.2682449	.00000373	.0000561	0.0325	50242.2	56749.6	176			
1520+319	1520+319	1920	15	22	9.99172878	+31	44	14.3819291	.00000374	.0000567	0.0273	50219.2	56776.1	155			
1519-294	1519-294	1921	15	22	25.48633975	-29	36	25.2308694	.00000901	.0001324	-0.0289	50687.9	56769.8	35			
1519-273	P 1519-273	440	15	22	37.67598839	-27	30	10.7855796	.00000352	.0000539	-0.0267	44200.9	56776.7	779		1.09	1.8
1521-300	1521-300	1922	15	24	33.41450751	-30	12	21.3399865	.00014683	.0048030	0.9261	53134.3	53134.3	1			
1522+155	1522+155	1116	15	24	41.61148095	+15	21	21.0505345	.00000893	.0002634	-0.1791	50084.6	53333.2	48			
1522+113	1522+113	3468	15	25	2.93403808	+11	07	44.0604988	.00013231	.0036941	-0.1830	49914.0	49914.2	1			
1523-042	1523-042	1923	15	26	15.01470455	-04	25	10.0582025	.00008008	.0019358	0.5280	53561.1	53561.2	1			
1526+670	J1526+6650	1117	15	26	42.87420892	+66	50	54.6417671	.00004393	.0002802	0.4973	49827.2	54643.4	5	0.19		
1524-136	P 1524-13	3469	15	26	59.44073630	-13	51	0.1650511	.00017442	.0042766	-0.2239	50575.3	50575.4	1			
1525+314	1525+314	3470	15	27	18.73703987	+31	15	24.3862259	.00006947	.0010097	0.1379	50219.2	50219.3	1			
1526+384	1526+384	4097	15	28	37.00614752	+38	16	5.9026190	.00006265	.0009310	-0.2477	56498.0	56498.2	1			
1526-189	1526-189	3471	15	29	40.14153286	-19	04	54.5847642	.00114797	.0172894	0.3287	53152.3	53152.3	1			
1528+381	1528+381	3472	15	30	16.25225745	+37	58	31.1666612	.00008402	.0016230	-0.1831	54112.5	54112.7	1			
1531+722	1531+722	3473	15	31	33.57840404	+72	06	41.2271833	.00011762	.0004927	0.4172	49827.2	49827.4	1			
1529+346	1529+346	3474	15	31	39.14597624	+34	30	3.8209761	.00035796	.0030817	0.0173	53523.2	53523.2	1			
1529-271	1529-271	1924	15	32	2.57168445	-27	16	37.9191242	.00003093	.0009973	-0.5037	53560.1	53560.2	1			
1532+680	1532+680	3475	15	32	43.34185987	+67	55	14.0082127	.00037143	.0029197	0.8297	49827.4	54087.8	2			
1529-131	1529-131	1925	15	32	45.37472524	-13	19	10.0866786	.00002237	.0005963	-0.0533	53572.1	53572.2	1			
1530+239	1530+239	1926	15	32	46.34519074	+23	44	5.2681429	.00001162	.0002694	0.0391	53125.2	53125.4	1			
1530-041	1530-041	1927	15	33	14.20533633	-04	21	16.6290305	.00004203	.0015188	0.0553	53523.2	53523.3	1			
1531-379	1531-379	3476	15	34	21.62258243	-38	05	6.2779898	.00898541	.3036621	0.9934	53153.2	53153.2	1			
1531-225	1531-225	3477	15	34	22.80136444	-22	43	57.6261212	.00011068	.0030444	0.7585	53153.2	56638.7	2			
1531-221	1531-221	1928	15	34	23.52794321	-22	18	54.3406750	.00009078	.0030189	-0.3633	53552.1	53561.2	2			
1532+016	P 1532+01	442	15	34	52.45367760	+01	31	4.2064619	.00000618	.0001172	-0.1507	47253.5	56638.2	57	0.23	0.46	4.1
1531-352	1531-352	3478	15	34	54.68748715	-35	26	23.4969075	.00001915	.0007000	0.3143	54489.6	54489.6	1			
1533+487	1533+487	3479	15	35	14.65337436	+48	36	59.6949758	.00019537	.0011648	-0.4571	50306.1	50306.2	1			
1533+200	1533+200	1929	15	35	16.53386996	+19	54	50.9050197	.00014099	.0021552	0.0531	53134.2	53134.3	1			
1534+501	1534+501	3480	15	35	52.03896687	+49	57	39.0795487	.00005788	.0008193	-0.6441	50306.1	50306.2	1			
1541+835	1541+835	1930	15	35	56.12670921	+83	26	15.2470922	.00040798	.0007948	-0.6427	53560.1	53560.3	1			
1534+387	1534+387	1118	15	36	13.84617772	+38	33	28.6057518	.00002447	.0004662	-0.1076	53523.2	53523.3	1			
1533-316	1533-316	3481	15	36	54.49811667	-31	51	15.1289589	.00007169	.0025982	-0.8197	53125.3	53503.3	2			
1534-152	1534-152	1931	15	37	41.57312981	-15	27	12.5005463	.00001217	.0004338	-0.4456	53523.2	53560.2	2	0.16	0.16	
1533-652	1533-653	3482	15	38	11.91526452	-65	25	51.1951231	.00011742	.0014347	0.6888	54723.4	54723.8	1			
1535+004	P 1535+004	1932	15	38	15.95309575	+00	19	5.3242717	.00002417	.0007901	-0.2538	49914.0	54482.7	2			
1535-036	1535-036	3483	15	38	20.35160747	-03	46	14.3124531	.00028332	.0054923	0.7025	53152.3	53153.2	1			
1536+057	1536+057	1933	15	39	5.20651949	+05	34	38.4378176	.00029363	.0058985	0.7925	53561.1	53561.2	1			
1536+046	1536+046	1934	15	39	10.10496561	+04	30	51.2298698	.00001547	.0004644	-0.0951	53125.3	53125.4	1			
1537+312	1537+312	1935	15	39	16.17438558	+31	04	7.6742278	.00004616	.0007143	-0.2219	53572.0	53572.2	1			

Source Name		ID No.	Right Ascension			Declination			RA Error (s)	Dec. Error (arcsec)	RA–Dec Corr.	Observation Epoch MJD		No. Obs.	Source Flux (Jy)		Str Index
B1950	Common		H	M	S	D	M	S				First	Last		10-60	10-40	
1537+162	1537+162	3484	15	39	25.09905424	+16	04	0.3401626	.00002371	.0006012	0.0423	50084.6	50155.6	2			
1537+279	1537+279	1119	15	39	39.13710681	+27	44	38.2143319	.00003793	.0011624	-0.2990	50219.2	50219.3	1			
1537-082	1537-082	1936	15	40	3.15240152	-08	23	25.5041308	.00016029	.0030822	0.0942	53560.1	53560.2	1			
1537-389	1537-389	3485	15	40	34.55095887	-39	06	17.7359943	.00019891	.0086622	-0.6627	53552.2	56162.1	2			
1538+149	GC 1538+14	444	15	40	49.49151529	+14	47	45.8847253	.00000391	.0000651	-0.1407	48102.9	56782.1	140	0.56	0.70	2.4
1539-111	1539-111	1937	15	42	0.03426583	-11	18	52.9042754	.00009735	.0023393	-0.0206	53561.1	53561.2	1			
1539-093	1539-093	3486	15	42	7.46471561	-09	27	43.2461202	.03928302	.4002447	-0.9842	50575.4	50575.4	1			
1542+616	1542+616	3487	15	42	56.94370513	+61	29	55.3455557	.00036507	.0018917	-0.7700	53503.2	53503.4	1			
1540-077	P 1540-077	3488	15	43	1.68720085	-07	57	6.6339717	.00004572	.0008407	0.5993	50575.3	56547.1	5			
1541+050	1541+050	1938	15	43	33.92576403	+04	52	19.3194495	.00002655	.0009327	0.1608	49914.1	54314.2	2			
1542+328	1542+328	3489	15	44	5.65662488	+32	40	48.3207054	.00002846	.0005980	-0.5236	50219.3	50219.4	1			
1541-230	1541-230	1939	15	44	14.17794405	-23	12	1.3489293	.00016247	.0054590	0.8472	53572.1	53572.1	1			
1542+042	1542+042	3490	15	44	59.42731399	+04	07	46.3563753	.00008666	.0022089	-0.2730	49914.0	49914.2	1			
1543+517	1543+517	3491	15	45	2.82369377	+51	35	0.8730762	.00001742	.0003265	-0.2899	49576.1	50306.2	2			
1543+480	1543+480	3492	15	45	8.52982817	+47	51	54.6641476	.00003884	.0006112	-0.4305	50306.1	50306.2	1			
1544+541	1544+541	1940	15	45	43.82575579	+54	00	42.7600643	.00009309	.0014104	-0.0889	53560.1	53560.2	1			
1543+005	DW 1543+00	3493	15	46	9.53146232	+00	26	24.6139302	.00001526	.0004845	0.0054	49914.0	49914.2	1			
1544-095	1544-095	1941	15	47	41.28569886	-09	43	33.0009040	.00007136	.0018656	-0.3321	53561.1	53561.2	1			
1545+210	1545+210	4098	15	47	43.53782789	+20	52	16.6162303	.00008066	.0019472	0.3482	56301.8	56302.5	1			
1545-120	1545-120	3494	15	48	12.93938553	-12	13	31.3216033	.00014476	.0025536	0.6632	50575.3	50575.4	1			
1547+507	1547+507	894	15	49	17.46854919	+50	38	5.7882919	.00000537	.0000753	0.0155	49576.1	56052.7	30	0.59		3.3
1546+027	P 1546+027	446	15	49	29.43684436	+02	37	1.1632678	.00000344	.0000530	-0.0299	48353.3	56770.7	288	1.26	0.89	2.7
1547-054	1547-054	1942	15	50	29.84746971	-05	38	11.0171347	.00010796	.0021319	0.2655	53572.1	53572.2	1			
1548+056	DW 1548+05	448	15	50	35.26924146	+05	27	10.4484215	.00000364	.0000619	-0.1403	45888.3	56679.6	288	1.43	0.66	2.9
1548+114	1548+114	1943	15	50	43.59477613	+11	20	47.4554314	.00002475	.0008226	-0.5482	53134.2	53134.4	1			
1540-828	P 1540-82	895	15	50	59.14237560	-82	58	6.8576373	.00581834	.0196432	-0.2918	49329.2	49329.4	1			
1548-177	1548-177	1944	15	51	14.59828484	-17	55	2.3301350	.00016799	.0051104	-0.3527	53152.3	53153.2	1			
1550+582	1550+582	3495	15	51	58.20787155	+58	06	44.4537279	.00009798	.0015263	-0.1986	49576.1	49577.0	1			
1549+089	1549+089	1945	15	52	3.26162339	+08	50	47.3353460	.00003477	.0009460	-0.3484	53560.1	53560.2	1			
1549-242	1549-242	4099	15	52	5.52191998	-24	25	20.7923867	.00003441	.0011901	0.0125	56393.3	56393.4	1			
1550-242	1550-242	3496	15	53	31.62781252	-24	22	6.0360066	.00000863	.0002051	-0.0952	50632.1	56498.1	22	0.08	0.29	
1551+130	1551+130	3497	15	53	32.69787394	+12	56	51.7163982	.00002125	.0007002	-0.0088	50084.7	50155.6	2			
1550-269	P 1550-269	3498	15	54	2.46977824	-27	04	40.2335302	.00001853	.0004629	0.1816	50632.1	54664.7	3			
1551-416	1551-416	4142	15	55	18.11799889	-41	50	31.7030881	.00012789	.0070842	0.6472	55616.5	55616.5	1			
1552-033	1552-033	3499	15	55	30.74815114	-03	26	49.5196761	.00001669	.0005465	0.0211	50575.3	50575.4	1			
1553+113	1553+113	3500	15	55	43.04401248	+11	11	24.3655993	.00002384	.0007149	-0.0263	49914.0	49914.2	1			
1556+744	1556+744	3501	15	56	3.00463814	+74	20	57.9906827	.01311614	.1389930	-0.9872	49827.3	49827.3	1			
1554+185	1554+185	3502	15	56	54.81663255	+18	25	13.5741344	.00023821	.0032272	0.1344	53572.1	53572.2	1			
1549-790	P 1549-79	896	15	56	58.86980709	-79	14	4.2815883	.00004843	.0001466	0.3149	47625.8	55784.5	26			
1555+001	DW 1555+00	452	15	57	51.43397036	-00	01	50.4137152	.00000369	.0000643	-0.3012	43808.9	56745.3	402	0.49	0.51	1.8
1555+030	1555+030	1946	15	57	52.76340479	+02	53	27.8823949	.00011090	.0044661	-0.4723	53560.2	53560.2	1			
1555-140	P 1555-140	453	15	58	21.94809304	-14	09	59.0518914	.00002835	.0005459	-0.5498	45474.5	51168.7	13			4.0
1557+565	1557+565	1947	15	58	48.28889589	+56	25	14.1191801	.00003816	.0003645	0.0136	53125.2	53125.4	1			
1554-643	1554-643	1284	15	58	50.28432550	-64	32	29.6374512	.00002166	.0002001	0.1693	52860.5	56504.7	17			
1558+595	1558+595	3503	15	59	1.70197767	+59	24	21.8347184	.00006950	.0006181	0.1558	53561.1	55657.6	2			
1557+032	1557+032	897	15	59	30.97261400	+03	04	48.2568521	.00000460	.0000867	-0.0586	49736.4	56699.3	46			
1556-245	1556-245	1948	15	59	41.40908012	-24	42	38.8322607	.00001047	.0001465	-0.2143	50632.1	55728.4	18			
1557-053	1557-053	3504	15	59	49.64225371	-05	31	22.5665683	.00001573	.0004827	-0.0215	53572.1	55916.6	2			
1558-072	1558-072	1949	16	00	56.47653217	-07	22	5.2248643	.00006066	.0022414	0.7491	53152.3	53153.2	1			
1600+432	1600+43A	3505	16	01	40.44388840	+43	16	47.7567840	.00018580	.0046330	0.6082	50560.1	50560.3	1			

Source Name		ID No.	Right Ascension			Declination			RA Error (s)	Dec. Error (arcsec)	RA–Dec Corr.	Observation Epoch MJD		No. Obs.	Source Flux (Jy)		Str Index
B1950	Common		H	M	S	D	M	S				First	Last		10-60	10-40	
1600+431	1600+43B	3506	16	01	40.51538827	+43	16	46.4780223	.00277044	.0347823	0.9926	50560.3	50560.3	1			
1559+140	1559+140	1950	16	01	54.53722652	+13	57	10.7641123	.00010657	.0025760	0.0202	53560.1	53560.2	1			
1600+335	B2 1600+33	455	16	02	7.26346105	+33	26	53.0723598	.00000480	.0000838	-0.1099	48102.9	56119.2	48	0.28	0.18	4.0
1600+244	1600+244	3507	16	02	13.83839461	+24	18	37.7944637	.00006168	.0009905	-0.1410	54087.7	54087.8	1			
1600-294	1600-294	1951	16	03	16.57144220	-29	33	55.4247692	.00001890	.0005815	-0.0579	54559.4	54601.3	2			
1603+699	1603+699	4100	16	03	18.62161535	+69	45	57.4418052	.00018333	.0014590	-0.6901	56301.9	56302.4	1			
1600-099	1600-099	1952	16	03	18.77827284	-10	07	21.2958909	.00002049	.0006929	-0.5264	53152.3	53153.2	1			
1601+173	1601+173	1285	16	03	32.08362682	+17	11	55.3082252	.08220396	.7567606	0.9999	53928.4	54075.9	2			
1601+160	1601+160	3508	16	03	38.06239325	+15	54	2.3592217	.00002338	.0006158	-0.0698	50155.4	56393.5	2			
1601+112	1601+112	1953	16	03	41.93125488	+11	05	48.6790574	.00000611	.0001136	0.2110	49914.1	56772.7	32			
1600-489	1600-489	3509	16	03	50.68391919	-49	04	5.5115063	.01306752	.0843894	0.9953	52676.7	52947.9	2			
1602+576	1602+576	3510	16	03	55.93157027	+57	30	54.4122643	.00018784	.0017706	-0.6256	49576.1	49576.3	1			
1601-222	1601-222	3511	16	04	1.47171711	-22	23	40.9880322	.00003714	.0012560	0.5586	50632.1	50688.0	2			
1600-445	1600-445	3512	16	04	31.02090459	-44	41	31.9718736	.00011102	.0017365	0.8832	52675.9	54440.7	6		0.12	
1603+573	1603+573	1237	16	04	37.35461296	+57	14	36.6608375	.00002563	.0001983	0.1177	49576.1	53306.1	3			
1602+195	1602+195	1954	16	04	49.99377587	+19	26	20.9417206	.00005825	.0012265	0.1247	53561.1	53561.2	1			
1602-115	1602-115	1955	16	05	17.53165301	-11	39	26.8311814	.00000436	.0000915	-0.0374	53552.1	56763.1	99	0.37	0.33	
1603+301	1603+301	3513	16	05	33.04804806	+30	01	29.7015869	.00004135	.0008168	-0.6480	50219.3	50219.4	1			
1604+554	1604+554	4101	16	06	7.61743289	+55	21	35.4201046	.00090524	.0070469	-0.3155	56266.9	56267.6	1			
1604+315	1604+315	3514	16	06	8.51838449	+31	24	46.4577214	.00001751	.0004100	-0.4850	50219.3	50219.4	1			
1604+183	1604+183A	1956	16	06	16.02785333	+18	14	59.8173055	.00003162	.0010800	-0.6786	53572.1	53572.2	1			
1605+542	1605+542	4102	16	06	23.56582004	+54	05	55.7629897	.00025457	.0014329	-0.4797	56266.9	56267.6	1			
1604+274	1604+274	3515	16	06	58.30033565	+27	17	5.5829609	.00003281	.0007722	-0.7567	50219.3	50219.4	1			
1604+159	1604+159	3516	16	07	6.43044254	+15	51	34.4849749	.00001804	.0004801	-0.0206	50084.6	50155.6	2			
1604-333	P 1604-333	457	16	07	34.76233801	-33	31	8.9134964	.00000890	.0001109	-0.6010	48393.3	56638.7	68		0.20	2.8
1605-162	1605-162	3517	16	08	7.02130994	-16	25	0.0718971	.00012287	.0056392	-0.2532	54087.7	54087.8	1			
1607+563	1607+563	3518	16	08	20.75220465	+56	13	56.3701762	.00024542	.0040551	-0.8022	49576.1	49576.3	1			
1606+403	1606+403	3519	16	08	22.15771708	+40	12	17.8327718	.00003578	.0006118	-0.4235	53503.3	53503.4	1			
1606+106	P 1606+10	458	16	08	46.20318619	+10	29	7.7757317	.00000336	.0000510	-0.0491	48102.9	56782.1	1555	0.51	0.60	2.5
1607+268	CTD 93	459	16	09	13.32075948	+26	41	29.0355441	.00002846	.0005311	-0.0347	44090.9	53659.1	8		0.07	4.4
1606-219	1606-219	1957	16	09	34.93278042	-22	05	46.6096268	.00021772	.0064050	-0.4160	53561.2	53561.2	1			
1606-056	1606-056	3520	16	09	38.74961893	-05	47	24.5726286	.00008598	.0030633	-0.5520	53560.2	56302.6	2			
1606-398	1606-398	1121	16	10	21.87912853	-39	58	58.3298381	.00001853	.0004082	0.0156	52306.6	54362.7	16		0.35	
1608+243	J1610+2414	1122	16	10	42.02677623	+24	14	49.0116384	.00000546	.0000965	-0.0798	50219.3	56749.5	45			
1613+782	1613+782	4103	16	10	50.60475739	+78	09	0.5418610	.00012373	.0002834	0.5904	56748.8	56749.3	1			
1609+190	1609+190	3521	16	11	49.04754317	+18	56	38.1069723	.00001459	.0003896	-0.2025	50084.6	50155.6	2			
1611+343	DA 406	460	16	13	41.06424344	+34	12	47.9089402	.00000336	.0000507	-0.0586	43809.1	56775.1	1428	1.83	1.30	3.2
1613+216	1613+216	3522	16	15	31.09339289	+21	30	11.0840316	.00053425	.0063627	0.7808	50084.6	50155.6	2			
1614+466	1614+466	1958	16	16	3.76673222	+46	32	25.2400139	.00002594	.0005381	-0.0152	53560.1	53560.2	1			
1611-710	1611-710	3523	16	16	30.64150626	-71	08	31.4544498	.00003481	.0002009	0.3301	52887.1	56504.6	15			
1614+051	P 1614+051	461	16	16	37.55681259	+04	59	32.7365006	.00000382	.0000690	-0.2446	46659.3	56745.3	231	0.57	0.52	3.0
1613-350	1613-350	1959	16	16	43.00525691	-35	09	41.8407847	.00003121	.0009146	-0.2772	54965.3	54965.4	1			
1615+364	1615+364	3524	16	16	55.58005087	+36	21	34.5015880	.00009633	.0009279	0.2514	50242.2	50242.3	1			
1614-112	1614-112	1960	16	17	5.99490315	-11	22	38.6190709	.00009402	.0030957	0.2419	53572.1	53572.2	1			
1614+042	1614+042	3525	16	17	13.58894951	+04	08	41.6981578	.00029159	.0032126	-0.1107	53561.1	56302.6	2			
1613-586	1613-586	4104	16	17	17.89126422	-58	48	7.8587503	.00018114	.0012731	0.3734	56007.5	56314.0	3			
1614-255	1614-255	1961	16	17	20.57093282	-25	37	23.6571701	.00002987	.0010221	-0.0347	54559.4	54559.4	1			
1614-195	1614-195	1962	16	17	27.09306783	-19	41	32.0154367	.00003038	.0010711	-0.0550	53152.3	55847.0	2	0.10	0.15	
1610-771	P 1610-77	900	16	17	49.27643565	-77	17	18.4676274	.00001204	.0000655	0.0256	47625.9	56638.7	210			
1615+029	P 1615+029	1963	16	17	49.90811346	+02	46	43.1048318	.00000616	.0001427	0.0627	49914.1	56740.9	54			

Source Name		ID No.	Right Ascension			Declination			RA Error (s)	Dec. Error (arcsec)	RA–Dec Corr.	Observation Epoch MJD		No. Obs.	Source Flux (Jy)		Str Index
B1950	Common		H	M	S	D	M	S				First	Last		10-60	10-40	
1616+063	DW 1616+06	464	16	19	3.68767549	+06	13	2.2429311	.00000475	.0000976	-0.1730	49914.1	56751.7	61	0.10	0.11	2.8
1617+229	1617+229	1123	16	19	14.82459821	+22	47	47.8510353	.00000363	.0000578	-0.1284	50084.6	56770.7	179	0.26	0.36	2.2
1616-181	1616-181	1964	16	19	16.68111300	-18	17	21.7000044	.00004254	.0014437	-0.4747	53560.2	53560.2	1			
1619+491	1619+491	1965	16	20	31.22519097	+49	01	53.2570511	.00001992	.0004204	-0.1976	50306.1	54643.7	2			
1618-399	1618-399	1966	16	21	59.68936570	-40	03	34.4752388	.00026678	.0152165	-0.2875	55042.1	55042.1	1			
1620+145	1620+145	1967	16	22	33.99577894	+14	26	20.5971338	.00002150	.0004713	0.2715	53134.2	53134.4	1			
1622+665	1622+665	3526	16	23	4.52166082	+66	24	1.0792615	.00008437	.0008325	0.2360	49826.5	49827.4	1			
1621+392	1621+392	3527	16	23	7.62238241	+39	09	32.4112180	.00001816	.0004063	-0.0885	50242.2	50242.3	1			
1621+078	1621+078	3528	16	23	58.25191619	+07	41	30.5501555	.00001613	.0004160	0.1244	49914.1	55371.3	2			
1621+058	1621+058	1968	16	24	7.73388004	+05	43	24.2450029	.00001253	.0003983	-0.0141	53125.3	53125.4	1			
1619-680	P 1619-680	901	16	24	18.43696747	-68	09	12.4965148	.00001630	.0001208	0.1741	47625.8	56770.7	33			
1621-351	1621-351	1969	16	24	22.45182857	-35	16	31.2046946	.00005654	.0026531	-0.7701	54943.4	54943.4	1			
1623+578	1623+578	1124	16	24	24.80755983	+57	41	16.2810454	.00000603	.0000643	-0.0224	49576.1	56751.4	140	0.31		
1623+569	1623+569	3529	16	24	32.17956046	+56	52	28.0020577	.00007413	.0016803	0.1309	49576.1	49576.3	1			
1621-067	1621-067	3530	16	24	32.92674095	-06	49	49.6273808	.00001576	.0004489	0.1523	50575.3	56638.7	5			
1621-321	1621-321	3531	16	24	59.61947454	-32	13	24.4439130	.00004844	.0017778	-0.0842	55413.1	55413.1	1			
1622-253	P 1622-253	465	16	25	46.89164131	-25	27	38.3269581	.00000342	.0000531	-0.0341	47737.0	56758.2	1688	0.63	1.01	2.0
1622-310	1622-310	1970	16	25	55.50394611	-31	08	8.5794120	.00001672	.0005208	0.0038	54965.3	55111.9	2			
1624+416	1624+416	902	16	25	57.66971238	+41	34	40.6293301	.00000552	.0000822	-0.0931	47940.8	55264.6	60	0.16	0.17	3.7
1622-297	P 1622-29	466	16	26	6.02083634	-29	51	26.9712469	.00000539	.0000853	-0.3747	47254.6	56601.3	97		1.00	3.8
1625+582	1625+582	3532	16	26	37.23658455	+58	09	17.6676639	.00004788	.0007864	-0.3119	49576.1	54087.8	2			
1626+229	1626+229	3533	16	28	15.23995449	+22	47	57.3108909	.00026482	.0075296	-0.6838	50084.6	50155.6	2			
1627+476	1627+476	3534	16	28	37.50435817	+47	34	10.4148217	.00049671	.0056273	0.6032	50306.1	54314.3	2			
1625-141	1625-141	3535	16	28	46.61979412	-14	15	41.8869662	.00004249	.0012205	-0.4119	50575.3	50575.5	1			
1626-005	1626-005	1971	16	28	48.46773438	-00	41	39.7037122	.00006045	.0015466	0.1924	53523.2	53572.2	2			
1624-617	1624-617	1126	16	28	54.68980169	-61	52	36.3982645	.00001614	.0001510	0.1257	52780.7	56723.4	23			
1626-172	1626-172	3536	16	29	16.76016861	-17	20	43.0906176	.01066347	.3964775	0.9995	53560.2	53560.2	1			
1629+680	1629+680	3537	16	29	51.83811797	+67	57	14.9785683	.00019992	.0041099	-0.1420	49827.3	54112.8	3			
1628+216	1628+216A	3538	16	30	11.23088972	+21	31	34.3112826	.00027908	.0051518	0.8339	50853.8	50853.8	1			
1628+071	1628+071	1972	16	30	41.81713422	+07	01	9.1066166	.00012867	.0020114	0.0870	53561.2	53561.2	1			
1629+495	1629+495	3539	16	31	16.53988922	+49	27	39.5159485	.00002832	.0005001	-0.2787	50306.1	50306.2	1			
1637+826	1637+826	903	16	32	31.96989626	+82	32	16.3999350	.00001331	.0000546	-0.1813	50687.3	56741.3	176	0.26		3.7
1630-107	1630-107	1973	16	32	50.10970411	-10	52	31.9964819	.00018417	.0046393	-0.5814	53561.2	53561.3	1			
1630-004	1630-004	1974	16	32	57.68132874	-00	33	21.0751900	.00005871	.0025148	-0.3046	53560.2	53560.2	1			
1630-258	1630-258	1975	16	33	28.89072802	-25	57	35.4765354	.00012822	.0044152	0.3179	53572.1	53572.2	1			
1632+321	1632+321	1976	16	34	12.78980353	+32	03	35.4249039	.00001789	.0005023	0.1373	53125.3	53125.4	1			
1631-208	1631-208	1977	16	34	30.32372783	-20	58	25.9391414	.00003947	.0012267	0.6667	53552.2	53552.2	1			
1634+628	3C 343	3540	16	34	33.84473910	+62	45	35.3079255	.04343001	.5736110	-0.9972	52409.3	52409.3	1			
1633+382	GC 1633+38	468	16	35	15.49297361	+38	08	4.5006135	.00000365	.0000561	-0.0632	44202.8	56010.2	368	1.44	0.94	3.4
1634+600	1634+600	3541	16	35	37.64877507	+59	55	15.0773126	.00002802	.0004191	-0.2292	54112.6	54112.7	1			
1634+604	1634+604	3542	16	35	37.65479181	+60	19	56.7492593	.00016211	.0019854	0.5596	49576.2	54087.8	2			
1633+186	1633+186	3543	16	35	39.19324145	+18	31	3.3784659	.03210182	.3019991	-0.9921	54087.8	54087.8	1			
1633-131	1633-131	1978	16	36	15.86093454	-13	15	32.6931417	.00007599	.0018491	0.1815	53560.2	53560.2	1			
1634+213	J1636+2112	1127	16	36	38.18343912	+21	12	55.5947404	.00001477	.0002842	-0.0676	50084.6	53020.2	5		0.09	
1633-409	1633-409	1979	16	36	55.37516954	-41	02	0.5011074	.00020004	.0077912	-0.1273	54852.8	54853.6	1			
1634-330	1634-330	1980	16	37	36.53601163	-33	09	4.8379174	.00013645	.0069453	-0.3494	53152.3	53152.3	1			
1636+473	1636+473	904	16	37	45.13055609	+47	17	33.8312814	.00000388	.0000573	-0.0477	50306.1	56772.7	205	0.53	0.27	2.5
1637+574	P 1637+574	905	16	38	13.45629576	+57	20	23.9790737	.00000397	.0000554	0.0218	45140.9	56754.1	408	0.92		2.5
1635-035	1635-035	3544	16	38	19.25202424	-03	40	5.0871346	.00000890	.0002390	0.0416	50575.3	56701.7	5			
1637+626	3C 343.1	3545	16	38	28.23738295	+62	34	43.8603417	.04562978	.5741919	-0.9971	52409.3	52409.3	1			

Source Name		ID No.	Right Ascension			Declination			RA Error (s)	Dec. Error (arcsec)	RA–Dec Corr.	Observation Epoch MJD		No. Obs.	Source Flux (Jy)		Str Index
B1950	Common		H	M	S	D	M	S				First	Last		10-60	10-40	
1635-141	1635-141	3546	16	38	45.28498799	-14	15	50.2371832	.00004991	.0013878	-0.5831	50575.3	50575.5	1			
1654+866	1654+866	3547	16	39	25.02103311	+86	31	53.1247844	.00497810	.0037523	-0.7444	52409.3	52409.4	1			
1638+540	1638+540	3548	16	39	39.84295225	+53	57	47.1196647	.00012537	.0016467	0.5588	49576.1	49576.3	1			
1637+166	1637+166	3549	16	39	42.13711344	+16	32	21.7599507	.00036200	.0053630	-0.9574	53561.2	56267.7	2			
1637-001	1637-001	1981	16	40	10.58617341	-00	11	47.5450024	.00004068	.0010707	0.0122	53560.2	53560.2	1			
1638+398	NRAO 512	472	16	40	29.63277123	+39	46	46.0284949	.00000337	.0000507	-0.0589	43873.9	56776.7	943	0.70	0.55	1.6
1637-373	1637-373	3550	16	40	41.08722882	-37	27	27.5285090	.00030464	.0131240	0.2261	53152.3	56267.7	2			
1638+124	1638+124	3551	16	40	47.93883131	+12	20	2.0787920	.00002441	.0006130	-0.2928	49914.1	49914.3	1			
1638+118	1638+118	3552	16	40	58.89435270	+11	44	4.2237557	.00158267	.0115402	-0.0989	53572.1	53572.2	1			
1639+230	1639+230	906	16	41	25.22756471	+22	57	4.0327891	.00000359	.0000562	-0.0445	50084.6	56776.3	194		0.22	1.3
1639-062	1639-062	1982	16	42	2.17771627	-06	21	23.6950437	.00000355	.0000538	0.0187	53125.3	56776.7	161	0.87	1.07	2.3
1639-200	1639-200	1983	16	42	5.29097344	-20	07	24.8510804	.00026561	.0134623	-0.9251	54601.3	54601.4	1	0.09	0.07	1.8
1642+690	1642+690	907	16	42	7.84851022	+68	56	39.7564543	.00000413	.0000522	0.0126	44089.1	56671.7	208	1.16		3.0
1640+254	1640+254	3553	16	42	40.41183941	+25	23	7.6821125	.00001680	.0004426	-0.3709	50219.4	50219.5	1			
1633-810	1633-810	3554	16	42	57.34553742	-81	08	35.0702536	.00006195	.0001877	0.2501	52860.5	56538.6	21			
1641+399	3C 345	473	16	42	58.80996787	+39	48	36.9939626	.00000377	.0000582	-0.2274	44088.9	56728.6	520	1.67	2.01	4.1
1639-287	1639-287	3555	16	42	59.37310834	-28	49	57.9428389	.00011774	.0044349	-0.5711	53561.2	56393.4	2			
1640-231	1640-231	1286	16	43	33.39057718	-23	16	7.8594570	.00028740	.0093597	0.8445	53992.0	53992.1	1			
1637-771	1637-771	3556	16	44	16.12108896	-77	15	48.8115169	.00147291	.0043426	0.1631	52887.1	53138.5	3			
1641+074	1641+074	1128	16	44	16.32973074	+07	20	33.7576464	.00011987	.0045934	-0.6861	49914.1	49914.3	1			
1641-179	1641-179	1984	16	44	35.74671767	-18	04	32.4588174	.00015085	.0052270	-0.3303	53152.3	53152.3	1			
1642-076	1642-076	4133	16	44	52.05853671	-07	43	43.1789943	.00003542	.0009833	-0.6476	55776.1	55776.2	1			
1642+183	1642+183	1129	16	44	52.43239807	+18	13	17.2383695	.00004445	.0015645	-0.7523	50084.6	50155.6	2			
1642+256	1642+256	3557	16	44	59.06084282	+25	36	30.5880933	.00005262	.0008553	-0.5324	50219.4	50219.5	1			
1645+635	1645+635	3558	16	45	58.55270333	+63	30	10.9227763	.00009478	.0009137	0.4212	49826.5	49827.4	1			
1647+744	1647+744	3559	16	46	15.17245479	+74	19	11.0827930	.00160470	.0129049	0.6108	53523.2	56749.3	3			
1645+410	1645+410	3560	16	46	56.85870077	+40	59	17.1721774	.00000994	.0002232	0.1494	50242.2	50242.3	1			
1645+271	1645+271	1985	16	47	33.59838190	+27	05	58.2921597	.00007097	.0010744	0.3895	50219.4	54314.4	2			
1646+499	1646+499	3561	16	47	34.91195506	+49	50	0.5874660	.00009658	.0012232	-0.5280	50306.1	50306.2	1			
1645+174	1645+174	3562	16	47	41.83918896	+17	20	11.8424794	.00026804	.0042913	0.0181	54314.1	54314.3	1			
1645+224	J1648+2224	1130	16	48	1.53553818	+22	24	33.1480471	.00001890	.0003523	0.1817	50084.6	52975.3	4			
1646+411	1646+411	3563	16	48	29.25797259	+41	04	5.5536894	.00003345	.0004830	-0.6526	50242.3	50242.4	1			
1645-329	1645-329	3564	16	48	42.35108572	-33	01	48.9312626	.00001172	.0003969	-0.0763	54489.6	54489.7	1			
1645-262	1645-262	3565	16	49	4.31531233	-26	20	8.6119831	.00005163	.0020216	0.1538	53560.2	56302.7	2			
1646+042	1646+042	1131	16	49	27.67945381	+04	12	3.9866188	.00004619	.0013066	-0.6994	49914.1	49914.3	1			
1651+747	1651+747	1986	16	49	40.95346783	+74	42	44.6197005	.00028077	.0012826	0.3034	53552.1	53552.3	1			
1647+065	1647+065	3566	16	49	50.49136869	+06	26	53.4486048	.00010003	.0013132	0.3715	49914.1	49914.3	1			
1646-506	1646-506	3567	16	50	16.62717974	-50	44	48.2107110	.00038388	.0024427	0.9266	52676.7	52948.1	3			
1648+084	1648+084	1987	16	50	37.56271036	+08	24	52.2307001	.00001692	.0004419	-0.1642	49914.1	54314.7	2			
1647-296	P 1647-296	477	16	50	39.54412368	-29	43	46.9548573	.00000995	.0001140	-0.6497	48345.6	55728.4	53		0.39	2.3
1648+015	P 1648+015	3568	16	51	3.66235917	+01	29	23.4578286	.00001675	.0005507	-0.4321	49914.1	49914.3	1			
1649+216	1649+216	3569	16	51	37.84413127	+21	35	24.6535546	.00003288	.0007253	0.3722	53561.2	56547.2	2			
1649+063	1649+063	3570	16	52	1.40008549	+06	18	55.3537090	.00004587	.0013424	-0.4357	49914.1	49914.3	1			
1651+391	1651+391	1988	16	52	58.50958368	+39	02	49.8222685	.00000379	.0000573	-0.0409	50242.3	56706.6	50			
1651+312	1651+312	1132	16	53	29.91065020	+31	07	56.8726487	.00001399	.0003259	-0.3584	50219.4	53659.1	2		0.19	
1650-157	1650-157	1989	16	53	34.20642367	-15	51	29.8882228	.00001826	.0005571	0.1002	54853.6	54853.7	1			
1652+398	DA 426	479	16	53	52.21668456	+39	45	36.6089839	.00000384	.0000574	-0.0895	48196.2	56744.5	314	0.52	0.34	3.4
1653+426	J1655+42	1990	16	55	18.79497900	+42	33	39.8235720	.00001924	.0004817	-0.1893	53572.1	53572.2	1			
1653-329	1653-329	3571	16	56	16.86095809	-33	02	10.7995633	.00011889	.0043449	-0.6830	55413.1	55413.1	1			
1654+185	1654+185	3572	16	56	34.08907443	+18	26	26.3472347	.00005220	.0010212	0.2107	50084.6	50155.6	2			

Source Name		ID No.	Right Ascension			Declination			RA Error (s)	Dec. Error (arcsec)	RA–Dec Corr.	Observation Epoch MJD		No. Obs.	Source Flux (Jy)		Str Index
B1950	Common		H	M	S	D	M	S				First	Last		10-60	10-40	
1655+534	1655+534	3573	16	56	39.62412584	+53	21	48.7720566	.00003223	.0004420	-0.0581	54087.6	54087.8	1			
1656+602	1656+602	1991	16	56	48.24495084	+60	12	16.4348773	.00003287	.0003913	-0.1433	53560.1	53560.3	1			
1654-020	1654-020	3574	16	56	56.11815597	-02	06	49.5200415	.00003138	.0008656	-0.1222	50575.3	50575.5	1			
1656+571	1656+571	1238	16	57	20.70895267	+57	05	53.5039224	.00001375	.0001751	0.0449	49576.1	54428.8	35	0.38		
1654-199	1654-199	1992	16	57	33.33472183	-20	04	34.9821171	.00003603	.0010504	-0.1529	53503.3	53561.2	2			
1656+482	1656+482	3575	16	57	46.87894140	+48	08	33.0414948	.00001739	.0003127	-0.1969	50306.1	50306.2	1			
1656+348	1656+348	908	16	58	1.41919343	+34	43	28.4019813	.00000937	.0001286	0.0013	49254.0	55306.7	16		0.13	3.1
1656+477	1656+477	909	16	58	2.77959764	+47	37	49.2309762	.00000617	.0000910	-0.0642	50306.1	56707.0	40	0.49	0.15	4.0
1655+077	OS 092	480	16	58	9.01146435	+07	41	27.5404334	.00000424	.0000763	-0.3034	46338.2	56638.3	99	0.69	0.96	3.2
1656+053	DW 1656+05	481	16	58	33.44733697	+05	15	16.4438785	.00000444	.0000810	-0.1747	44200.9	56599.8	91	0.34	0.38	3.2
1656-075	1656-075	1993	16	58	44.06198896	-07	39	17.6942068	.00000456	.0000940	0.0961	52306.6	56679.2	90	0.46	0.24	
1657+265	B2 1657+26	1133	16	59	24.14944818	+26	29	36.9432300	.00001463	.0003664	-0.2113	50219.4	56498.3	3	0.32	0.34	
1657+022	1657+022	1994	16	59	44.99720870	+02	13	7.0433827	.00005264	.0020712	-0.7074	53572.1	53572.2	1			
1700+685	1700+685	3576	17	00	9.29289588	+68	30	6.9600348	.00006041	.0003175	0.0251	49826.5	54112.5	2			
1657+054	1657+054	1995	17	00	23.95598578	+05	22	44.0948893	.00001052	.0003421	-0.0826	53134.3	53134.4	1			
1657-261	P 1657-261	484	17	00	53.15406005	-26	10	51.7254602	.00000382	.0000602	-0.2295	45356.7	56776.4	306	0.60	0.62	2.1
1658+037	1658+037	3577	17	01	21.37818903	+03	38	51.1739913	.00002289	.0008400	-0.4731	54087.7	54087.8	1			
1659+399	1659+399	1996	17	01	24.63481489	+39	54	37.0916581	.00000518	.0000840	0.0421	53523.2	56499.8	32			
1658-189	1658-189	1997	17	01	26.89421026	-19	03	31.5757563	.00004978	.0019622	-0.0530	53560.2	53560.3	1			
1657-562	1657-562	1287	17	01	44.85809023	-56	21	55.9020342	.00001132	.0001648	0.3094	52675.8	56643.7	38			
1700+151	1700+151	3578	17	02	21.71813823	+15	02	6.0817613	.00014005	.0025736	0.5340	50084.7	50155.6	2			
1700+320	1700+320	4105	17	02	32.61019808	+31	57	52.3527621	.00024337	.0139136	-0.4270	56463.1	56463.4	1			
1659-621	1659-621	3579	17	03	36.54122050	-62	12	40.0084450	.00001412	.0001335	0.4419	52779.7	56763.2	31			
1701-132	1701-132	1998	17	04	5.08676264	-13	16	34.2335464	.00022859	.0033076	0.2818	53152.3	53152.3	1			
1701+016	1701+016	1999	17	04	7.48912353	+01	34	8.4742937	.00007840	.0013556	-0.0091	53561.2	53561.3	1			
1704+512	1704+512	3580	17	05	26.41352832	+51	09	35.3988345	.00007149	.0019314	-0.0060	50306.1	54112.8	2			
1704+122	1704+122	2000	17	06	20.49752064	+12	08	59.7947452	.00004617	.0009047	0.2917	53560.2	53560.3	1			
1704+099	1704+099	2001	17	06	36.72732915	+09	53	59.6371070	.00003834	.0009833	-0.2231	53572.1	53572.2	1			
1705+456	1705+456	910	17	07	17.75340821	+45	36	10.5529528	.00000679	.0000908	0.0371	49268.0	55342.6	18			
1704-141	1704-141	3581	17	07	20.39056544	-14	15	23.1275860	.00002902	.0007360	-0.4739	53503.3	53503.4	1			
1705+018	P 1705+018	485	17	07	34.41526919	+01	48	45.6992937	.00000368	.0000600	0.0596	49271.7	56762.0	138	0.62	0.31	2.6
1705+135	1705+135	1134	17	07	45.63727460	+13	31	5.2326192	.00001035	.0002795	-0.0086	50084.6	53212.9	6			
1705+188	1705+188	2002	17	07	53.74751365	+18	46	39.0205111	.00003169	.0008885	-0.6787	53561.2	53561.3	1			
1706+338	1706+338	3582	17	08	1.25144191	+33	46	46.3769604	.00002834	.0007006	-0.0108	54087.7	54087.8	1			
1706+006	1706+006	3583	17	08	44.64748910	+00	35	9.5140710	.00013728	.0042358	-0.8098	49914.1	49914.3	1			
1705-353	1705-353	3584	17	09	18.66628461	-35	25	22.1936281	.00021106	.0074309	-0.2396	54489.6	54489.7	1			
1706-174	OT-111	486	17	09	34.34539095	-17	28	53.3650861	.00000463	.0000827	-0.4715	45356.7	56758.3	224	0.25	0.33	2.4
1708+433	1708+433	2003	17	09	41.08658716	+43	18	44.5328418	.00001110	.0001784	-0.1662	54075.9	54076.6	1			
1707-038	1707-038	3585	17	10	17.20540138	-03	55	50.1286150	.00001767	.0005036	0.1336	50575.3	50575.5	1			
1708-250	1708-250	3586	17	11	27.78869148	-25	11	5.2888602	.11482701	.0834446	-0.9998	53560.2	53560.2	1			
1710+542	1710+542	2004	17	11	40.50475984	+54	11	45.1348202	.00002255	.0004435	-0.3359	53572.2	53572.2	1			
1708-335	1708-335	3587	17	11	48.99351394	-33	38	41.0568796	.00019230	.0085819	-0.0751	53552.2	56106.2	2			
1709-182	1709-182	2005	17	12	31.69732304	-18	20	2.7680547	.00007788	.0036612	-0.2461	53561.2	53561.3	1			
1710-269	1710-269	3588	17	13	31.27559629	-26	58	52.5275048	.00001235	.0004124	-0.1846	50632.1	50688.0	2	0.22	0.21	
1712+493	1712+493	3589	17	13	35.14760419	+49	16	32.5369118	.00003965	.0005829	-0.2156	50306.1	50306.3	1			
1710-323	1710-323	3590	17	13	50.79022880	-32	26	12.2091408	.00003789	.0013323	-0.1138	54489.6	54489.7	1			
1711-208	1711-208	2006	17	14	32.51300597	-20	53	54.2905784	.00007996	.0027832	-0.0102	53523.3	53523.4	1			
1711-209	1711-209	2007	17	14	40.26187795	-21	00	41.3562565	.00010241	.0022255	0.3989	54853.6	54853.7	1			
1712-059	1712-059	3591	17	14	56.57371095	-05	58	20.5942475	.00001466	.0004750	-0.5441	53503.3	53503.4	1			
1714+219	1714+219	3592	17	16	11.19070447	+21	52	13.6671849	.00009333	.0010404	-0.3398	50084.6	50155.6	2			

Source Name		ID No.	Right Ascension			Declination			RA Error (s)	Dec. Error (arcsec)	RA–Dec Corr.	Observation Epoch MJD		No. Obs.	Source Flux (Jy)		Str Index
B1950	Common		H	M	S	D	M	S				First	Last		10-60	10-40	
1716+686	1716+686	3593	17	16	13.93803271	+68	36	38.7448332	.00003562	.0003542	0.2706	49826.5	49827.4	1			
1713-048	1713-048	2008	17	16	26.48808941	-04	52	11.9456927	.00001660	.0006215	-0.2871	53552.2	53552.3	1			
1714+193	1714+193	2009	17	17	1.16594481	+19	17	40.6555081	.00001741	.0004995	-0.3531	53561.2	53561.3	1			
1714-336	1714-336	3594	17	17	36.02903212	-33	42	8.8245641	.00022925	.0059912	-0.1508	53134.4	53503.4	2			
1714-397	1714-397	3595	17	17	38.59961825	-39	48	52.6442577	.00089452	.0282719	0.2716	53523.3	56547.1	2			
1715-112	1715-112	2010	17	18	14.94821536	-11	20	44.9696726	.00018011	.0056162	0.0504	53152.3	53152.4	1			
1715-287	1715-287	2011	17	18	49.37973005	-28	50	41.0983551	.00016715	.0047632	0.7141	53572.2	53572.2	1			
1716-142	1716-142	2012	17	19	2.01996808	-14	20	19.0103401	.00002049	.0007490	-0.5201	53552.2	53552.3	1			
1716+070	1716+070	2013	17	19	10.93338124	+06	58	15.7464020	.00001039	.0003418	-0.1550	53125.3	53125.4	1			
1717+178	GC 1717+17	489	17	19	13.04847895	+17	45	6.4373369	.00000385	.0000679	-0.0841	44203.6	56770.4	115	0.49	0.28	2.8
1718+481	1718+481	2014	17	19	38.24952922	+48	04	12.2488646	.00008687	.0010615	0.0004	53560.1	53560.3	1			
1717+083	1717+083	3596	17	19	52.20620618	+08	17	3.5541403	.00001106	.0003767	0.0087	49914.1	49914.3	1			
1718+384	1718+384	3597	17	20	10.33481825	+38	25	56.1648500	.00003904	.0007297	-0.3235	54111.8	54112.7	1			
1718-084	1718-084	3598	17	20	59.68630937	-08	32	17.3290388	.00037522	.0165314	-0.7515	53152.3	53152.3	1			
1719+357	1719+357	3599	17	21	9.49103100	+35	42	16.0636193	.00002466	.0006567	-0.3757	50242.3	50242.4	1			
1718-259	1718-259	3600	17	21	55.97913994	-25	58	40.6920147	.00006940	.0020577	0.0807	54601.3	55847.0	2	0.07	0.09	
1719-050	1719-050	3601	17	22	3.53851420	-05	03	25.0065279	.00002094	.0006099	-0.3504	53503.3	53503.4	1			
1721+589	1721+589	1239	17	22	36.72655663	+58	56	22.2606986	.00003254	.0002490	-0.0188	49576.1	53306.1	4			
1722+611	1722+611	2015	17	22	40.05936341	+61	05	59.7874359	.00002172	.0002252	-0.4853	49576.1	54087.9	4			
1720+282	1720+282	3602	17	22	42.16158047	+28	15	0.0765056	.00001736	.0004666	-0.2402	50219.4	50219.5	1			
1720+102	1720+102	2016	17	22	44.58279047	+10	13	35.7731577	.00001482	.0003969	0.0366	53134.3	53134.4	1			
1720+250	1720+250	3603	17	22	52.98990802	+24	58	34.6921010	.00010871	.0034015	0.2570	50219.4	50219.5	1			
1723+658	1723+658	2017	17	23	14.13812974	+65	47	46.1785337	.00014227	.0014067	-0.3630	53560.1	53560.3	1			
1721+343	1721+343	3604	17	23	20.79591675	+34	17	57.9650842	.00004515	.0009451	-0.3712	54124.9	54125.5	1			
1722+526	1722+526	2019	17	23	39.74627566	+52	36	48.3956763	.00008404	.0008207	-0.0747	49576.1	54664.5	2			
1718-649	P 1718-649	911	17	23	41.02932373	-65	00	36.6104731	.00002659	.0002407	0.2255	48110.1	54670.7	17			
1726+769	1726+769	3605	17	23	59.44517064	+76	53	11.5519523	.00007166	.0003569	0.5153	49826.5	49827.4	1			
1722+401	1722+401	3606	17	24	5.42883709	+40	04	36.4568700	.00001881	.0003379	-0.5671	50242.3	54482.3	2			
1722+330	1722+330	2020	17	24	14.19783000	+33	03	3.9392370	.00000586	.0001128	-0.0821	50219.4	56748.6	37			
1724+609	1724+609	3607	17	24	41.41503222	+60	55	55.7279272	.00015767	.0010723	-0.5198	49576.1	54112.8	2			
1721-146	1721-146	2021	17	24	46.96653883	-14	43	59.7611233	.00002111	.0005711	-0.4238	53552.2	53552.3	1			
1723+051	1723+051	2022	17	26	24.78347924	+05	04	42.6745752	.00008258	.0018115	0.1488	53560.2	53560.3	1			
1724+322	1724+322	2023	17	26	35.12467111	+32	13	23.0222315	.00001620	.0004298	-0.3659	53572.2	53572.2	1			
1724+066	1724+066	2024	17	26	44.94527916	+06	39	18.5098871	.00001617	.0005130	-0.2888	53561.2	53561.3	1			
1723-229	1723-229	3608	17	26	58.90450953	-22	58	1.5476024	.00004179	.0014166	-0.0025	53503.4	53503.4	1			
1726+552	1726+552	3609	17	27	23.46924458	+55	10	53.5370524	.00007984	.0011718	-0.4998	49576.1	49576.3	1			
1726+455	1726+455	912	17	27	27.65080653	+45	30	39.7313758	.00000342	.0000509	-0.0076	48720.4	56758.7	929	0.64	0.46	2.2
1725+123	J1728+1215	913	17	28	7.05121569	+12	15	39.4854689	.00000481	.0000989	-0.0138	49914.1	56749.6	49	0.34	0.24	2.5
1727+502	1727+502	914	17	28	18.62402595	+50	13	10.4700395	.00001529	.0002233	0.1237	49176.9	56627.2	24	0.07		
1725+044	P 1725+044	493	17	28	24.95272669	+04	27	4.9136793	.00000446	.0000855	-0.1660	49177.0	56770.4	65	0.46	0.29	3.2
1726-038	1726-038	3610	17	28	50.23514584	-03	50	50.4351646	.00004014	.0009859	0.6423	50575.3	50575.5	1			
1727+386	1727+386	2025	17	28	59.14138109	+38	38	26.4480041	.00002181	.0004256	0.2668	53134.3	53134.4	1			
1726-269	1726-269	3611	17	29	8.21641077	-26	57	50.7407959	.00011910	.0043266	-0.1021	54087.8	54087.8	1			
1727-052	1727-052	3612	17	30	33.07598382	-05	15	8.0737091	.00020238	.0045828	0.2502	54111.8	54112.7	1			
1728+004	1728+004	2026	17	30	34.99948470	+00	24	38.6905651	.00005087	.0022050	-0.5353	53125.3	53125.4	1			
1730-130	NRAO 530	495	17	33	2.70578762	-13	04	49.5482551	.00000364	.0000612	-0.2413	43809.0	56702.3	430	1.71	1.34	2.5
1729-373	1729-373	3613	17	33	15.19310077	-37	22	32.3930630	.00007489	.0041064	0.5209	52306.7	52409.4	2			
1725-795	1725-795	3614	17	33	40.70019611	-79	35	55.7169614	.00004812	.0001802	0.2265	52887.1	56504.7	14			
1732+389	1732+389	700	17	34	20.57854080	+38	57	51.4431634	.00000375	.0000576	-0.0203	48196.2	56775.2	201	0.51	0.53	1.7
1732+094	GC 1732+09	3615	17	34	58.37698423	+09	26	58.2603528	.00003142	.0007219	-0.1633	49914.1	49914.3	1			

Source Name		ID No.	Right Ascension			Declination			RA Error (s)	Dec. Error (arcsec)	RA–Dec Corr.	Observation Epoch MJD		No. Obs.	Source Flux (Jy)		Str Index
B1950	Common		H	M	S	D	M	S				First	Last		10-60	10-40	
1732+081	1732+081	2027	17	35	10.44551836	+08	08	31.0633684	.00002465	.0007382	0.2827	53560.2	53560.3	1			
1732-059	1732-059	2028	17	35	26.78448689	-05	59	50.2151543	.00008567	.0025353	-0.1796	53561.2	53561.3	1			
1734+363	1734+363	915	17	35	48.08662691	+36	16	45.6114588	.00000894	.0001241	0.1263	50242.4	53770.9	7	0.33	0.17	
1734+508	1734+508	916	17	35	49.00517766	+50	49	11.5662209	.00001036	.0001948	-0.0910	49576.1	55221.1	22	0.35		
1734+065	1734+065	4134	17	36	28.58370910	+06	31	47.5272837	.00003288	.0006356	-0.4111	55776.1	55776.3	1			
1734-228	1734-228	3616	17	37	2.03320935	-22	51	55.3935674	.00036522	.0088432	0.5904	54111.8	54112.7	1			
1734+063	P 1734+063	3617	17	37	13.72902429	+06	21	3.5723904	.00001056	.0003452	-0.2016	49914.1	54482.7	2			
1733-565	1733-565	917	17	37	35.77065329	-56	34	3.1546186	.00044074	.0024196	0.8379	48388.0	52878.4	5			
1735-150	1735-150	2029	17	38	11.63555788	-15	03	0.5971102	.00003693	.0011769	-0.6837	53572.2	53572.3	1			
1736+324	J1738+3224	1135	17	38	40.50181970	+32	24	9.0257101	.00000725	.0001685	-0.1184	50219.4	56170.6	10			
1738+499	1738+499	918	17	39	27.39049693	+49	55	3.3684846	.00000494	.0000685	-0.0008	49422.4	56748.1	38	0.20		2.3
1737+339	1737+339	3618	17	39	35.36253024	+33	58	8.1938893	.00002202	.0004680	-0.4400	50219.4	50219.5	1			
1738+476	OT 465	498	17	39	57.12907546	+47	37	58.3615819	.00000444	.0000649	0.0363	43809.2	56775.1	156	0.46	0.19	2.7
1737-081	1737-081	2030	17	40	1.56619958	-08	11	14.7823118	.00000968	.0003185	0.1428	53523.3	56498.3	4			
1737+222	1737+222	3619	17	40	5.86285819	+22	11	0.9733046	.00002817	.0009026	-0.1762	50084.7	50155.6	2			
1738+451	1738+451	3620	17	40	6.37261399	+45	06	50.3710266	.00001829	.0003314	-0.5492	50306.1	50306.3	1			
1738+197	1738+197	3621	17	40	26.97048967	+19	43	19.6799122	.00005496	.0010711	0.0160	54087.8	54087.9	1			
1739+522	4C 51.37	919	17	40	36.97784906	+52	11	43.4074818	.00000338	.0000504	-0.0315	47283.3	56775.1	1455	0.78		1.5
1738+032	1738+032	2031	17	40	37.19901040	+03	11	47.8389557	.00010187	.0013805	-0.1605	53503.3	53560.3	2			
1739+438	1739+438	3622	17	40	48.95053577	+43	48	16.1508421	.00003311	.0005357	-0.5456	50242.4	50242.5	1			
1740+478	1740+478	3623	17	41	34.82194826	+47	51	32.5366853	.00005680	.0007012	-0.4340	50306.1	50306.3	1			
1739-152	1739-152	2032	17	42	11.66286236	-15	17	29.1598159	.00003294	.0012207	-0.2742	53552.2	53561.3	2	0.09	0.08	
1740-190	1740-190	3624	17	42	59.54919129	-19	03	8.5594670	.00002960	.0010608	0.4343	53503.4	55966.7	2			
1740+134	1740+134	3625	17	43	3.00386947	+13	26	36.3012992	.02220350	.0096471	0.1136	53134.3	53134.3	1			
1740-169	1740-169	3626	17	43	6.21830719	-16	58	15.9674380	.00003029	.0010504	-0.0374	53152.4	56106.3	2			
1740-309	1740-309	3627	17	43	17.87447519	-30	58	18.1594778	.00901313	.3072780	-0.9813	52306.7	52409.4	2			
1742+378	1742+378	3628	17	43	47.64631500	+37	47	53.8302920	.00002286	.0004550	-0.5364	50242.4	50242.5	1			
1741+279	1741+279	4106	17	43	56.43739287	+27	52	50.3489196	.00003080	.0005398	-0.3151	56463.2	56463.4	1			
1741+196	1741+196	2033	17	43	57.83259927	+19	35	9.0176974	.00013389	.0013266	0.2253	53572.1	53572.3	1			
1741-038	P 1741-038	500	17	43	58.85613405	-03	50	4.6167605	.00000335	.0000513	-0.0114	43809.0	56776.7	2397	1.82	1.55	1.9
1742+402	1742+402	3629	17	44	25.09588877	+40	14	48.1409788	.00024287	.0019692	-0.0367	50242.4	50242.5	1			
1742-088	1742-088	3630	17	44	47.60186660	-08	49	14.3316501	.00003663	.0011224	-0.0425	54111.8	56637.9	2			
1744+557	1744+557	1136	17	44	56.60706265	+55	42	17.1611966	.00000918	.0000926	0.2463	51283.9	54943.4	14			
1742+228	1742+228	1137	17	45	4.66884016	+22	52	48.0772876	.00002337	.0006507	0.2736	50084.7	50155.6	2			
1742-078	1742-078	1288	17	45	27.10493874	-07	53	3.9476530	.00000943	.0003203	0.1674	52306.6	53946.0	4	0.48	0.14	
1743+173	GC 1743+17	501	17	45	35.20817169	+17	20	1.4236180	.00000407	.0000779	-0.2543	48103.0	56770.4	138	0.38	0.20	2.6
1745+670	1745+670	2034	17	45	54.35683425	+67	03	49.2975812	.00049848	.0022285	0.4037	49827.3	54314.3	2			
1743+182	1743+182	3631	17	45	55.92741621	+18	14	50.4198821	.00003374	.0012737	0.0262	50084.7	50155.6	2			
1745+624	1745+624	920	17	46	14.03413799	+62	26	54.7384202	.00000361	.0000512	0.0800	48915.8	55182.7	779	0.30		1.7
1744+260	1744+260	2035	17	46	48.27890775	+26	03	20.3541375	.00002098	.0005552	-0.2542	53560.2	53560.3	1			
1746+470	1746+470	921	17	47	26.64727957	+46	58	50.9264027	.00000454	.0000654	0.0115	49422.4	56782.1	102	0.29	0.26	1.1
1746+340	1746+340	3632	17	48	5.81968462	+34	04	1.1804054	.00001779	.0005199	-0.3446	50219.4	50219.5	1			
1745+085	1745+085	3633	17	48	6.26040190	+08	32	19.2864417	.00003415	.0014193	-0.6216	54087.8	54087.9	1			
1749+701	1749+701	502	17	48	32.84033439	+70	05	50.7688325	.00000947	.0000705	-0.0399	44202.8	55299.6	44	0.27		3.0
1747+433	1747+433	3634	17	49	0.36039999	+43	21	51.2869709	.00002005	.0003646	-0.4525	50242.4	50242.5	1			
1746+197	1746+197	3635	17	49	5.47372501	+19	44	8.8398862	.00004622	.0011074	0.4430	50084.7	50155.6	2			
1749+096	OT 081	503	17	51	32.81857303	+09	39	0.7283891	.00000335	.0000510	-0.0229	44446.1	56772.7	1921	2.33	1.91	1.3
1749+293	1749+293	2036	17	51	42.68397682	+29	20	50.2022572	.00001763	.0003788	-0.1314	53125.3	53125.5	1			
1748-253	1748-253	922	17	51	51.26255064	-25	24	0.0646765	.00009170	.0023945	0.2951	48110.2	52409.4	4			
1753+731	1753+731	2037	17	52	11.69246600	+73	11	20.5450770	.00012717	.0007401	0.2923	53560.1	53560.3	1			

Source Name		ID No.	Right Ascension			Declination			RA Error (s)	Dec. Error (arcsec)	RA–Dec Corr.	Observation Epoch MJD		No. Obs.	Source Flux (Jy)		Str Index
B1950	Common		H	M	S	D	M	S				First	Last		10-60	10-40	
1749+062	1749+062	2038	17	52	14.66871925	+06	11	48.1552658	.00001842	.0006634	-0.2294	53572.2	53572.2	1			
1749-299	1749-299	3636	17	52	33.10804622	-29	56	44.9171787	.00036018	.0089056	0.1242	53552.2	56547.1	2			
1749-101	1749-101	3637	17	52	36.97411519	-10	11	44.7311512	.00006453	.0017044	-0.2453	50575.3	50575.5	1			
1750+175	1750+175	3638	17	52	46.00288065	+17	34	20.3501932	.00001388	.0004471	0.0293	50084.7	50155.6	2			
1750-187	1750-187	3639	17	53	9.08867213	-18	43	38.5230331	.00001969	.0006990	0.0680	53503.4	55616.7	3	0.08		
1751+441	1751+441	923	17	53	22.64789280	+44	09	45.6863219	.00000576	.0000780	-0.0410	50242.4	55168.7	20	0.17	0.17	3.2
1751+288	GC 1751+28	504	17	53	42.47364638	+28	48	4.9388875	.00000360	.0000553	-0.0475	48103.2	56776.7	127	1.06	0.76	2.3
1753+648	1753+648	3640	17	54	7.58978130	+64	52	2.6318306	.00027211	.0031732	-0.1705	49826.5	49827.4	1			
1751+050	1751+050	3641	17	54	17.52500466	+04	59	39.6148021	.00094438	.0118524	0.2673	53134.3	53134.4	1			
1752-225	1752-225	2039	17	55	26.28494912	-22	32	10.6191929	.00019132	.0039023	-0.1833	53134.4	53134.4	1			
1753+204	1753+204	1138	17	55	35.52094848	+20	23	57.1369519	.00003983	.0013096	-0.7058	50084.7	54643.7	3			
1755+626	1755+626	3642	17	55	48.43891542	+62	36	44.1293505	.00183023	.0084256	0.4444	55371.1	56036.6	2			
1753+049	1753+049	4107	17	55	51.15203599	+04	54	52.5736022	.00020200	.0023882	-0.0300	56162.0	56162.2	1			
1753+183	1753+183	3643	17	55	59.78224552	+18	20	17.6681519	.00024215	.0038880	0.8822	52305.8	52409.5	2			
1755+578	1755+578	3644	17	56	3.62828527	+57	48	47.9977242	.00015520	.0016662	0.3665	49576.1	54643.7	2			
1753-144	1753-144	2040	17	56	25.86252659	-14	27	9.5617588	.00007002	.0020214	0.0847	54087.8	55042.2	2			
1754+159	1754+159	1140	17	56	33.72560739	+15	53	43.8328202	.00001023	.0003396	-0.2424	50084.8	53761.4	12			
1754+155	1754+155	1141	17	56	53.10214109	+15	35	20.8264747	.00000380	.0000600	0.0668	52305.8	56464.6	167	0.25	0.21	2.1
1753-418	1753-418	3645	17	57	15.67137323	-41	49	18.6825696	.00009735	.0043681	0.7218	55167.8	55167.8	1			
1759+756	1759+756	4108	17	57	46.35889873	+75	39	16.1797397	.00016637	.0014951	-0.1906	56301.9	56302.4	1			
1755+055	1755+055	2041	17	57	58.82500912	+05	31	48.0228138	.00012688	.0054382	0.0509	53125.4	53125.5	1			
1756+061	1756+061	2042	17	58	34.11761363	+06	10	32.9695869	.00004684	.0017259	-0.7373	53572.2	53572.2	1			
1756+237	P 1756+237	1142	17	59	0.35808248	+23	43	46.9535445	.00001569	.0003216	0.2046	50084.7	53613.0	5	0.32	0.13	
1758+388	1758+388	924	18	00	24.76536251	+38	48	30.6975014	.00000390	.0000604	0.0053	49749.8	56763.7	93	0.79	0.63	2.2
1803+784	1803+784	693	18	00	45.68391713	+78	28	4.0184547	.00000376	.0000503	0.0106	45459.6	56751.8	1757	1.38		2.5
1758+046	1758+046	2043	18	01	4.24178176	+04	38	18.2042522	.00002639	.0008419	-0.0294	53134.3	53134.4	1			
1800+440	1800+440	925	18	01	32.31481994	+44	04	21.9003865	.00000369	.0000561	0.0281	50242.4	56782.1	150	0.71	0.33	2.2
1801+459	1801+459	3646	18	02	25.14266497	+45	57	34.6351450	.00013855	.0014773	0.1993	50306.1	50306.3	1			
1759-396	1759-396	2044	18	02	42.68005482	-39	40	7.9081396	.00000472	.0000714	-0.0012	52306.7	56770.0	264		0.73	2.4
1800-045	1800-045	3647	18	03	9.42759094	-04	33	2.8008329	.00011438	.0029982	0.1528	53503.3	55537.9	2			
1758-651	P 1758-651	926	18	03	23.49665201	-65	07	36.7613900	.00001188	.0000929	0.2024	48756.8	56758.3	51			
1801+036	1801+036	4143	18	03	56.28253054	+03	41	7.6072365	.00001415	.0003786	0.0687	55616.5	55616.7	1			
1801+010	1801+010	3648	18	04	15.98459112	+01	01	32.4080428	.00006817	.0014818	-0.0287	49914.1	54643.0	2			
1801-077	1801-077	3649	18	04	31.07364005	-07	47	19.6184612	.00193449	.0146458	0.0449	53523.3	53523.3	1			
1802-046	1802-046	3650	18	05	31.11563358	-04	38	9.7230040	.00016283	.0039306	-0.1133	53125.4	55966.6	2			
1802-141	1802-141	3651	18	05	31.19984300	-14	08	45.4305941	.24977334	.1474719	1.0000	53552.3	53552.3	1			
1803+172	1803+172	2045	18	05	47.43634830	+17	14	55.9211691	.00001686	.0004877	-0.1513	53560.2	53560.3	1			
1805+616	1805+616	3652	18	06	19.94584347	+61	41	18.3295587	.00020833	.0010946	0.0092	49576.2	49827.4	2			
1807+698	3C 371	512	18	06	50.68064994	+69	49	28.1085892	.00000353	.0000504	0.0184	44202.8	56744.8	1007	0.58		3.2
1805+310	1805+310	2046	18	07	31.75813655	+31	06	21.5779680	.00007716	.0019141	-0.6315	53572.2	53572.3	1			
1805+220	1805+220	2047	18	07	38.80615488	+22	04	56.4108666	.00002514	.0005087	-0.1998	53561.2	53561.3	1			
1804-251	1804-251	2048	18	07	40.68790270	-25	06	25.9427479	.00014900	.0036840	0.1160	53134.4	53134.4	1			
1806+456	1806+456	927	18	08	21.88588955	+45	42	20.8665183	.00000388	.0000571	-0.0500	49422.5	56772.7	132		0.25	0.0
1807+279	J1809+2758	1143	18	09	11.97860763	+27	58	11.7996915	.00001206	.0003594	-0.1650	50219.4	50219.5	1			
1806-458	P 1806-458	509	18	09	57.87173269	-45	52	41.0140367	.00001439	.0001714	-0.2138	52067.3	56637.9	37			
1809+568	1809+568	3653	18	10	3.31916389	+56	49	22.9681600	.00008915	.0011111	-0.5978	49576.1	49576.3	1			
1809+170	1809+170	1240	18	11	43.18347658	+17	04	57.2575902	.00001028	.0002762	0.0740	53134.3	53305.9	2			
1809-286	1809-286	3654	18	12	40.19227018	-28	36	26.9416994	.00005527	.0019541	0.2628	53503.4	53503.5	1			
1810-068	1810-068	3655	18	12	50.94172941	-06	48	23.8473996	.01389822	.2753391	-0.9957	50575.3	50575.5	1			
1812+560	1812+560	3656	18	12	57.66947670	+56	03	49.2000482	.00002381	.0002575	-0.2066	49576.2	54087.9	2			

Source Name		ID No.	Right Ascension			Declination			RA Error (s)	Dec. Error (arcsec)	RA–Dec Corr.	Observation Epoch MJD		No. Obs.	Source Flux (Jy)		Str Index
B1950	Common		H	M	S	D	M	S				First	Last		10-60	10-40	
1811+430	1811+430	3657	18	13	14.68941282	+43	04	15.6764642	.00002355	.0003687	-0.3698	50242.4	50242.5	1			
1811+062	1811+062	3658	18	13	33.41164201	+06	15	42.0339920	.00005268	.0015929	-0.5814	49914.1	49914.3	1			
1811+298	1811+298	3659	18	13	37.26680951	+29	52	37.8710864	.00001829	.0004784	-0.4288	50219.4	50219.5	1			
1812+412	1812+412	2049	18	14	22.70618740	+41	13	5.6086161	.00001559	.0002655	-0.4261	50242.4	54643.7	2			
1813+163	1813+163	4135	18	15	14.85448772	+16	23	46.2955496	.00003042	.0005759	-0.3862	55776.1	55776.3	1			
1815+614	1815+614	3660	18	15	36.79197852	+61	27	11.6472803	.00059756	.0031748	0.4258	49576.1	49827.4	2			
1814+349	1814+349	3661	18	16	23.90082847	+34	57	45.7490826	.00026048	.0038444	-0.0883	50219.4	50219.5	1			
1815+531	1815+531	3662	18	16	57.07081028	+53	07	44.4992358	.00004224	.0005118	-0.3778	49576.1	54112.6	2			
1815-111	1815-111	3663	18	18	19.31360199	-11	08	48.3186092	.00018568	.0026507	0.3125	53125.4	55537.9	2			
1817+502	1817+502	3664	18	18	30.51924814	+50	17	19.7438544	.00003871	.0005216	-0.2412	49576.2	50306.3	2			
1816-029	1816-029	3665	18	19	17.40883328	-02	58	7.8690018	.00003233	.0005493	0.3768	50575.5	56498.3	4			
1817+387	1817+387	2050	18	19	26.54736812	+38	45	1.7863984	.00001019	.0001897	-0.0576	53134.3	56701.5	2	0.26	0.11	
1814-637	P 1814-63	928	18	19	35.00271493	-63	45	48.2037145	.00021826	.0034238	-0.6105	49329.2	53108.4	2			
1817+157	1817+157	3666	18	19	38.28932792	+15	43	44.7275767	.00003647	.0006297	0.0425	54087.8	55112.1	2			
1815-553	P 1815-554	929	18	19	45.39952011	-55	21	20.7454609	.00001018	.0000732	-0.0733	47626.0	56639.5	262			
1817-254	1817-254	664	18	20	57.84869608	-25	28	12.5842581	.00000841	.0002587	-0.2728	47407.2	53134.4	15	0.18	0.16	3.5
1818-050	1818-050	3667	18	21	11.80952136	-05	02	20.0873224	.00004079	.0011897	0.1283	53503.4	53503.5	1			
1822+682	1822+682	3668	18	21	59.49178140	+68	18	43.0092377	.00009526	.0005435	0.5998	49826.5	54087.9	2			
1820+397	1820+397	3669	18	21	59.70062622	+39	45	59.6564036	.00013102	.0020826	-0.5381	50242.4	50242.5	1			
1819+159	1819+159	1144	18	22	9.96896586	+16	00	14.8439958	.00002792	.0007656	0.2863	50084.7	50155.7	2			
1826+796	1826+796	930	18	23	14.10871996	+79	38	49.0024603	.00005928	.0001574	0.3250	48353.1	53613.4	19	0.21		4.4
1820-274	1820-274	2051	18	23	19.65174574	-27	26	26.3798898	.00131268	.0362553	-0.8916	50631.3	56302.7	3			
1823+689	1823+689	2052	18	23	32.85391398	+68	57	52.6126480	.00000682	.0000637	0.0748	49826.5	56772.6	71			
1821+107	P 1821+10	513	18	24	2.85525545	+10	44	23.7739848	.00000422	.0000896	-0.3211	44202.8	56770.4	132	0.62	0.31	3.2
1821+114	1821+114	2053	18	24	3.94796536	+11	27	37.6996008	.00008841	.0026994	-0.6185	53572.2	53572.3	1			
1823+568	1823+568	931	18	24	7.06837657	+56	51	1.4908954	.00000383	.0000538	-0.0126	47620.3	56782.1	384	0.77		2.5
1822+033	1822+033	2054	18	24	32.06597694	+03	22	5.9424485	.00019795	.0042985	-0.5714	54314.2	54314.3	1			
1822+012	1822+012	1145	18	24	48.14342677	+01	19	34.2020606	.00000768	.0002409	-0.2325	53134.4	56749.6	4	0.26	0.20	
1822-173	1822-173	3670	18	25	36.53228508	-17	18	49.8476862	.00002935	.0008202	0.1817	51732.1	55518.1	3			
1822-076	1822-076	3671	18	25	37.60953788	-07	37	30.0133264	.00002196	.0004930	0.2285	52305.8	55518.0	3			
1824+578	1824+578	2055	18	25	41.59870777	+57	53	5.9578116	.00015367	.0013018	0.3408	53560.2	53560.3	1			
1822-368	1822-368	2056	18	26	8.13488634	-36	50	49.7260082	.00004043	.0012803	0.0119	53152.4	53152.4	1			
1824+185	1824+185	3672	18	26	17.71068841	+18	31	52.8932178	.00027596	.0039455	-0.0335	50084.7	50155.7	2			
1823-294	1823-294	2057	18	26	20.59910607	-29	24	24.9522785	.00003795	.0011711	0.3904	53503.4	53561.3	2			
1823+017	1823+017	2058	18	26	25.06119622	+01	49	40.1193045	.00001039	.0003225	-0.1173	53552.2	53552.3	1			
1825+344	1825+344	3673	18	26	59.98285835	+34	31	14.1198249	.00002021	.0004756	-0.3670	50219.4	50219.5	1			
1823-455	1823-455	3674	18	27	10.23811634	-45	33	9.9636906	.00006677	.0019673	-0.3049	52306.7	52306.7	1			
1825+266	1825+266	3675	18	27	20.13461218	+26	38	24.1510714	.00003934	.0010055	0.1952	54111.8	54112.7	1			
1825-041	1825-041	3676	18	27	45.04052694	-04	05	44.5764909	.00002325	.0006430	0.1318	50575.5	56547.2	5			
1825+269	1825+269	3677	18	27	55.42496184	+26	58	5.9180262	.00003883	.0010458	-0.7313	50219.4	50219.5	1			
1827+645	1827+645	3678	18	28	9.85761472	+64	34	16.0335210	.00020623	.0015696	0.5146	49826.5	49827.4	1			
1825-214	1825-214	2059	18	28	19.48690413	-21	23	38.7709968	.00014389	.0034661	-0.1890	54657.2	54657.3	1			
1825-055	1825-055	1289	18	28	40.15340833	-05	30	50.8654207	.00014362	.0036980	-0.3523	53991.9	56393.6	2			
1824-582	1824-582	3679	18	29	12.40236091	-58	13	55.1619285	.00002040	.0001774	0.4434	53222.6	56504.7	16			
1826+052	1826+052	3680	18	29	21.27914996	+05	18	12.8498988	.05425868	.7322705	-0.9986	53572.3	53572.3	1			
1826-391	1826-391	3681	18	29	28.90280284	-39	04	0.3644131	.00050650	.0302376	-0.3489	53152.4	53152.4	1			
1828+487	3C 380	2060	18	29	31.78095422	+48	44	46.1609145	.00001193	.0002632	-0.2327	53552.2	53552.4	1			
1828+399	1828+399	3682	18	29	56.52021002	+39	57	34.7031541	.00002676	.0004382	-0.5004	50242.4	50242.5	1			
1826-447	1826-447	3683	18	30	0.86975323	-44	41	11.6767089	.00012111	.0032978	-0.0180	55167.8	55167.9	1			
1827+062	1827+062	3684	18	30	5.93986731	+06	19	15.9525551	.00002508	.0007927	-0.5832	49914.1	49914.3	1			

Source Name		ID No.	Right Ascension			Declination			RA Error (s)	Dec. Error (arcsec)	RA–Dec Corr.	Observation Epoch MJD		No. Obs.	Source Flux (Jy)		Str Index
B1950	Common		H	M	S	D	M	S				First	Last		10-60	10-40	
1827-272	1827-272	1290	18	31	0.04484560	-27	14	6.1812446	.00003218	.0017689	-0.1579	53767.8	53768.6	1			
1829+290	1829+290	3685	18	31	14.85922067	+29	07	10.2934330	.00021081	.0028030	-0.0365	50219.4	50219.5	1			
1829+219	1829+219	3686	18	31	18.89180892	+22	00	12.3350101	.00040555	.0034250	-0.7842	50155.5	53503.5	2			
1829-207	1829-207	1241	18	32	11.04653098	-20	39	48.2040517	.00004354	.0008672	0.6383	50631.3	53551.5	3	0.07		4.8
1829-106	1829-106	663	18	32	20.83398038	-10	35	11.1674533	.00196013	.0271871	-0.9185	51732.1	55537.9	3			
1832+687	1832+687	3687	18	32	35.52237222	+68	48	7.1484898	.00114192	.0036972	-0.5616	55482.8	55538.6	2			
1830+012	1830+012	2061	18	32	40.09375823	+01	18	16.4731249	.00006211	.0020253	-0.3319	53125.4	53125.5	1			
1830+074	1830+074	3688	18	32	41.98909205	+07	31	55.1245031	.00004153	.0018136	-0.7936	49914.1	49914.3	1			
1830+139	1830+139	1146	18	32	43.47108243	+13	57	44.4007067	.00001215	.0003871	-0.3653	50084.7	53770.9	6	0.24	0.13	
1830+285	GC 1830+28	516	18	32	50.18562277	+28	33	35.9552667	.00000556	.0001014	-0.2641	50219.4	55112.7	20			
1830+011	LANA	2062	18	33	7.76086498	+01	15	35.3012168	.00004061	.0012141	-0.6239	53523.3	53523.4	1			
1830-211	1830-21B	932	18	33	39.88514132	-21	03	40.5806961	.00040671	.0056297	0.9278	49177.2	50688.1	3			
1831-030	1831-030	2063	18	34	14.07465787	-03	01	19.6272311	.00002844	.0005641	0.0458	53134.4	55518.0	2			
1831+050	1831+050	2064	18	34	27.31152755	+05	06	3.9655620	.00013972	.0021775	-0.0515	53560.2	53560.3	1			
1828-733	1828-733	3689	18	34	53.19783764	-73	15	14.3345489	.00022466	.0010380	-0.2504	54722.9	54723.7	1			
1833+326	1833+326	3690	18	35	3.38963120	+32	41	46.8568011	.00004429	.0006203	0.0051	50219.4	50219.5	1			
1832-113	1832-113	4136	18	35	19.57593912	-11	15	59.3143105	.00031059	.0052226	0.4082	55537.8	55538.0	1			
1834+612	1834+612	3691	18	35	19.67526656	+61	19	40.0138108	.00006587	.0008680	-0.1101	49576.2	49576.4	1			
1829-718	P 1829-718	933	18	35	37.21189692	-71	49	58.2318000	.01715436	.1003374	0.1060	50259.0	50259.1	1			
1833+240	1833+240	2065	18	35	46.27250833	+24	07	50.8298703	.00001477	.0004242	-0.1749	53552.3	53561.4	2			
1831-693	1831-693	3692	18	37	5.56390985	-69	17	33.3304087	.00016088	.0013346	0.3626	54722.9	54723.8	1			
1831-711	P 1831-711	934	18	37	28.71493325	-71	08	43.5549111	.00002453	.0001756	0.1578	47626.0	56538.7	15			
1835+064	1835+064	3693	18	38	22.91199200	+06	28	8.7092717	.00015914	.0064577	-0.1701	49914.1	49914.3	1			
1835-345	1835-345	2066	18	38	28.49698130	-34	27	41.7550685	.00012871	.0056222	-0.7279	53523.4	53523.4	1			
1836+040	1836+040	3694	18	38	48.82902620	+04	04	24.6694998	.00017931	.0026673	-0.3206	49914.1	49914.3	1			
1836+094	1836+094	2067	18	38	54.83524497	+09	27	27.8966844	.00002642	.0011339	-0.6024	53125.4	53125.5	1			
1837+409	1837+409	3695	18	39	5.80336872	+41	00	59.0917145	.00030923	.0054506	0.2096	54111.8	54112.7	1			
1839+389	1839+389	1147	18	40	57.15423224	+39	00	45.7242840	.00001570	.0002846	-0.3541	50242.4	54664.7	2			
1839+548	1839+548	3696	18	40	57.37670213	+54	52	15.9102708	.00004258	.0005816	0.1298	49576.2	54087.9	3	0.13		
1845+797	3C 390.3	519	18	42	8.98990458	+79	46	17.1283963	.00004010	.0001190	-0.3628	44202.9	54936.8	60	0.20		3.9
1842+681	1842+681	935	18	42	33.64169817	+68	09	25.2278020	.00000578	.0000579	-0.0544	49422.0	56762.7	40	0.82		1.9
1841+447	1841+447	2068	18	43	7.91744466	+44	49	51.5226900	.00014732	.0012974	-0.1856	53125.3	53125.5	1			
1841+131	1841+131	3697	18	44	7.26249449	+13	12	28.0398996	.00009625	.0022963	-0.6871	50084.7	50155.7	2			
1841+116	1841+116	3698	18	44	18.05166888	+11	40	23.7675274	.06256736	.1349903	-0.9992	53561.3	53561.3	1			
1842-134	1842-134	3699	18	44	50.30407115	-13	24	45.2795631	.03249903	.3464792	-0.9999	53152.4	53152.4	1			
1843+400	1843+400	1148	18	45	11.13152513	+40	07	51.5791485	.00008462	.0008442	0.7862	53067.8	53068.5	1			
1843+356	1843+356	3700	18	45	35.10884401	+35	41	16.7264426	.00002304	.0004735	-0.0915	50242.4	50242.5	1			
1842-220	1842-220	3701	18	45	39.90284181	-22	00	36.5796913	.00005416	.0018686	-0.0709	53552.3	55847.1	2			
1842-289	1842-289	2069	18	45	51.36828697	-28	52	40.2761545	.00001107	.0003774	-0.0021	53152.4	56749.6	2		0.18	
1843-001	1843-001	3702	18	46	3.78234488	-00	03	38.2530053	.00011454	.0030991	0.4653	55413.1	55413.3	1			
1843-069	1843-069	2070	18	46	6.30039209	-06	51	27.7469222	.00027229	.0030973	-0.1090	53134.4	53134.5	1			
1844+081	J1847+0810	1150	18	47	12.66038705	+08	10	35.3876855	.00002892	.0007575	0.2333	49914.1	49914.2	1			
1846+322	1846+322	2071	18	48	22.08857934	+32	19	2.6037501	.00000346	.0000523	-0.0083	50219.4	56772.7	300			
1846+326	1846+326	3703	18	48	34.36117450	+32	44	0.1394456	.00001928	.0004151	-0.3378	50219.4	50219.5	1			
1845-273	1845-273	2072	18	48	47.50413664	-27	18	18.0717319	.00002043	.0008183	-0.3831	54601.4	56393.5	2		0.27	0.0
1849+670	1849+670	697	18	49	16.07228831	+67	05	41.6803784	.00000413	.0000526	-0.0159	49826.5	56770.7	343	1.16		1.5
1847+303	1847+303	3704	18	49	20.10341465	+30	24	14.2371594	.00001704	.0005555	-0.2007	50219.4	50219.5	1			
1849+499	1849+499	3705	18	50	22.23121128	+49	59	21.2594839	.01592474	.3434159	0.9910	50306.3	50306.3	1			
1848+283	1848+283	1242	18	50	27.58984934	+28	25	13.1550700	.00001537	.0003394	-0.6639	50219.5	54482.3	8	0.27	0.41	
1849+005	1849+005	3706	18	51	46.72559138	+00	35	32.3204184	.05631245	.8783502	-0.9997	52409.5	52409.5	1			

Source Name		ID No.	Right Ascension			Declination			RA Error (s)	Dec. Error (arcsec)	RA–Dec Corr.	Observation Epoch MJD		No. Obs.	Source Flux (Jy)		Str Index
B1950	Common		H	M	S	D	M	S				First	Last		10-60	10-40	
1851+609	1851+609	3707	18	51	52.36088313	+61	00	38.7790794	.00047002	.0019803	0.5500	49576.3	54112.6	2			
1851+488	J1852+4855	1151	18	52	28.54780056	+48	55	47.4815160	.00001966	.0002571	0.0909	50306.2	54482.7	2	0.40		
1850+402	1850+402	3708	18	52	30.37252168	+40	19	6.6082274	.00001847	.0003643	-0.2237	50242.4	50242.5	1			
1850+143	1850+143	3709	18	52	50.58042350	+14	26	39.7024736	.00004933	.0018403	-0.8171	54087.8	54087.9	1			
1849-365	1849-365	2073	18	53	17.92014795	-36	28	42.1773786	.00011480	.0074364	-0.1084	52306.7	53134.4	3			
1851+331	1851+331	2074	18	53	26.78725125	+33	10	56.1328950	.00004529	.0010148	-0.5180	53561.3	53561.4	1			
1851+236	1851+236	2075	18	53	27.62798141	+23	44	35.5311066	.00004257	.0016262	-0.6035	53523.3	53523.5	1			
1851-157	1851-157	2076	18	54	4.33206298	-15	39	13.1999614	.00002904	.0009339	0.3194	53552.3	53572.3	2			
1851-162	1851-162	2077	18	54	16.46663305	-16	11	38.6175131	.00013255	.0032108	0.6805	55042.2	55042.3	1			
1856+737	1856+736	936	18	54	57.29991715	+73	51	19.9069997	.00001396	.0000829	0.0537	49268.1	55333.8	21	0.32		
1853+376	1853+376	3710	18	55	27.70679908	+37	42	56.9662884	.00003526	.0009601	-0.7222	50242.4	50242.5	1			
1853+027	1853+027	3711	18	55	35.43643720	+02	51	19.5607791	.00009020	.0018703	0.1515	52306.7	55616.6	3			
1852-275	1852-275	3712	18	55	36.31387433	-27	27	9.0179571	.09449280	.5940877	-0.9996	53152.4	53152.4	1			
1853-122	1853-122	3713	18	55	54.44542996	-12	09	57.9674559	.00001683	.0005997	0.0156	53503.4	56637.9	5			
1853-179	1853-179	3714	18	55	56.37866968	-17	54	42.9348352	.00005475	.0014263	-0.0393	53152.3	56266.9	2			
1854+061	1854+061	3715	18	56	31.83884711	+06	10	16.7626343	.00018922	.0039722	0.5073	52305.8	52409.5	2			
1853-226	1853-226	3716	18	56	36.46401862	-22	36	16.7132703	.07379718	.5513249	0.9999	53523.4	53523.4	1			
1852-534	1852-534	3717	18	57	0.45152662	-53	25	0.3419766	.00116060	.0240997	0.4219	50989.4	50989.6	1			
1855+163	1855+163	3718	18	57	25.59557057	+16	24	55.8373007	.00006541	.0024446	0.7629	54111.9	54112.7	1			
1855+031	1855+031	1291	18	58	2.35283098	+03	13	16.2956064	.00011838	.0021664	-0.2289	53978.0	55616.6	2			
1855-252	1855-252	3719	18	58	19.07776552	-25	10	50.7142992	.00006099	.0020848	-0.0211	53152.4	55847.0	2			
1856-252	1856-252	2078	18	59	5.03812719	-25	09	47.1080478	.00003274	.0011168	-0.1375	54817.8	54817.9	1			
1858+273	1858+273	3720	19	00	34.67742557	+27	22	30.9175965	.00010175	.0021420	0.0303	50219.5	50219.5	1			
1858+269	1858+269	3721	19	00	48.51392979	+27	01	57.5712770	.00004605	.0010982	-0.6016	50219.5	50219.5	1			
1858-255	1858-255	3722	19	01	32.12635092	-25	28	14.2283794	.00002712	.0010483	-0.1061	53503.5	55657.6	2			
1901+319	3C 395	521	19	02	55.93889893	+31	59	41.7017526	.00000506	.0000775	-0.1415	48103.1	55159.5	50	0.30	0.38	3.9
1902+556	1902+556	3723	19	03	11.60703798	+55	40	38.4494435	.00072242	.0081351	0.7992	49576.2	54087.9	2			
1901+016	1901+016	2079	19	03	53.06292201	+01	45	26.3122497	.00051943	.0064371	-0.7752	54075.9	54076.2	1			
1901+155	1901+155	1152	19	04	14.36113263	+15	36	38.4513331	.00001887	.0006176	-0.0928	50084.7	53314.8	16			
1902-119	1902-119	3724	19	05	28.58789488	-11	53	32.4158022	.00009411	.0020318	0.7373	53503.4	54112.7	2			
1903+196	1903+196	2080	19	05	36.47208680	+19	43	8.0454592	.00001507	.0004695	-0.3366	53552.3	53552.4	1	0.14	0.14	4.6
1903+097	1903+097	4109	19	05	39.89899018	+09	52	8.4093837	.00012297	.0021957	-0.2481	56637.8	56637.9	1			
1904+013	1904+013	1153	19	07	11.99619701	+01	27	8.9621001	.00003060	.0006241	0.1176	49914.1	55518.0	3			
1905+222	1905+222	2081	19	08	6.21082997	+22	22	34.1476658	.00000836	.0001750	0.1732	53561.3	56701.6	5			
1905-297	1905-297	2082	19	08	29.43320786	-29	42	16.9426604	.00004506	.0019138	-0.0324	54559.5	54559.6	1			
1905-252	1905-252	3725	19	08	48.46281334	-25	09	28.6558198	.16413285	.8066207	1.0000	53152.4	53152.4	1			
1907+425	1907+425	3726	19	08	49.54919409	+42	35	29.1535022	.02646417	.9297944	-0.9926	53125.4	53125.4	1			
1906-217	1906-217	2083	19	09	45.15460275	-21	39	35.4012292	.00004168	.0011549	-0.4826	54087.9	54965.5	2			
1908+484	1908+484	2084	19	09	46.56271001	+48	34	31.8204735	.00002442	.0002233	-0.0268	50306.2	56568.3	7			
1908+230	1908+230	2085	19	10	45.12719357	+23	05	58.6111322	.00004121	.0012031	-0.2698	50155.5	53134.5	2			
1907-224	1907-224	2086	19	10	57.55718923	-22	23	29.3214532	.00004310	.0016442	0.2527	55042.2	55042.3	1			
1908-201	OV-213	522	19	11	9.65289121	-20	06	55.1091941	.00000345	.0000573	-0.1224	45356.9	56770.4	887	1.01	0.73	2.5
1909+268	1909+268	3727	19	11	35.07735283	+26	58	13.7631849	.00002947	.0006884	-0.5670	50219.5	50219.5	1			
1908-211	1908-211	2087	19	11	53.93740581	-21	02	43.8021001	.00003371	.0012282	-0.7500	53125.5	53125.5	1			
1909-194	1909-194	2088	19	11	56.51917332	-19	21	50.9637507	.00012543	.0030690	0.3610	53572.2	53572.3	1			
1909+161	J1911+1611	1154	19	11	58.25740513	+16	11	46.8652709	.00000366	.0000597	0.0549	50084.7	56775.9	182			
1909-081	1909-081	2089	19	12	7.12880064	-08	04	21.9027351	.00003072	.0008463	0.0831	53152.3	53152.5	1			
1909-151	1909-151	2090	19	12	11.93963202	-15	04	57.5429454	.00001826	.0006021	-0.2382	53523.4	53523.5	1			
1910+375	1910+375	1155	19	12	25.12359005	+37	40	36.6450238	.00001620	.0003712	-0.4179	50242.4	50242.5	1		0.15	
1903-802	P 1904-80	937	19	12	40.01909095	-80	10	5.9466459	.00005151	.0001402	0.1464	47626.0	55229.1	21			

Source Name		ID No.	Right Ascension			Declination			RA Error (s)	Dec. Error (arcsec)	RA–Dec Corr.	Observation Epoch MJD		No. Obs.	Source Flux (Jy)		Str Index
B1950	Common		H	M	S	D	M	S				First	Last		10-60	10-40	
1910+052	1910+052	3728	19	12	54.25764997	+05	18	0.4214131	.00003027	.0004449	0.0185	50919.4	55538.0	4			
1910-365	1910-365	4110	19	13	20.88947975	-36	30	19.4292747	.00009090	.0034264	-0.0424	56301.8	56301.8	1			
1911-019	1911-019	3729	19	13	39.13105793	-01	51	47.0427969	.02327816	.0610856	0.9762	53134.4	53134.4	1			
1911+165	1911+165A	3730	19	14	14.50123349	+16	36	38.1787548	.05920797	.3003353	-0.9993	52306.7	52306.7	1			
1911+013	1911+013	3731	19	14	14.52622894	+01	24	26.8277801	.15188460	.2298488	-0.9999	53560.3	53560.3	1			
1915+657	1915+657	3732	19	15	23.81913619	+65	48	46.3847241	.00017052	.0018862	-0.0595	49826.5	49827.4	1			
1913-272	1913-272	2091	19	16	19.86275572	-27	08	32.2610946	.00001316	.0005163	-0.0789	54852.8	54853.7	1			
1914-154	1914-154	2092	19	16	52.51100734	-15	19	0.0715845	.00001271	.0004562	-0.3121	53503.4	53561.4	2	0.14	0.13	
1914-212	1914-212	3733	19	17	8.64444633	-21	10	30.7833493	.00036272	.0114475	0.1595	53560.3	53560.4	1			
1914-194	1914-194	2093	19	17	44.81929600	-19	21	31.6095018	.00002036	.0008060	-0.4654	53572.3	53572.3	1			
1917+552	J1918+5520	1156	19	18	10.75003329	+55	20	38.6096154	.00005231	.0005647	-0.5152	49576.2	49576.4	1	0.53		
1917+495	1917+495	2094	19	18	45.57959657	+49	37	56.0340834	.00003391	.0006063	-0.3467	53561.3	53561.4	1			
1916+062	1916+062	3734	19	19	17.35220415	+06	19	42.7335553	.00961616	.1905342	-0.9990	52306.7	56637.8	2			
1917-248	1917-248	3735	19	20	14.43095829	-24	45	5.8004605	.00003142	.0010761	-0.2895	53572.3	55371.3	2			
1918+267	1918+267	1157	19	20	29.10816159	+26	51	48.0018475	.00003877	.0015960	-0.1943	54111.9	54112.7	1			
1917-386	1917-386	3736	19	20	43.00948190	-38	31	6.0577771	.00012195	.0036225	0.6376	53503.5	55966.7	2			
1918-026	1918-026	2095	19	20	43.26220274	-02	36	11.6060347	.00001096	.0003504	-0.1009	53552.3	56498.4	4			
1919+434	1919+434	3737	19	21	9.93471419	+43	33	41.8376709	.00011669	.0011275	-0.3569	54087.8	54087.9	1			
1920+450	1920+450	3738	19	21	54.20527970	+45	06	26.8866502	.00057004	.0032441	-0.3383	50306.2	50306.3	1			
1919+086	1919+086	2096	19	22	18.63375822	+08	41	57.3714940	.00011777	.0038325	-0.6147	50700.1	50700.1	1			
1920+154	1920+154	3739	19	22	34.69900777	+15	30	10.0334405	.00023707	.0022272	0.1272	50084.7	50155.7	2			
1918-634	1918-634	3740	19	23	24.60601451	-63	20	45.7660599	.00005632	.0005250	0.1870	54722.9	54723.8	1			
1922+478	1922+478	3741	19	23	27.22977405	+47	54	16.8171624	.00003977	.0007321	0.2330	50306.2	50306.3	1			
1920-211	OV-235	665	19	23	32.18981769	-21	04	33.3332217	.00000384	.0000624	-0.2376	46709.1	56772.7	273	0.80	0.76	2.5
1922+333	1922+333	3742	19	24	17.48218382	+33	29	29.7456256	.00036510	.0027895	0.2998	52305.8	52306.6	1			
1922+155	1922+155	2097	19	24	39.45587584	+15	40	43.9413875	.00000701	.0001602	-0.0543	50084.8	50654.5	3	0.24	0.17	2.3
1921-293	OV-236	524	19	24	51.05595243	-29	14	30.1211716	.00000346	.0000551	0.0185	43809.0	56763.7	1197		3.09	2.8
1922-341	1922-341	2098	19	25	17.02025665	-34	01	1.5374254	.00003741	.0011916	-0.1346	53125.5	53125.5	1			
1922-224	1922-224	2099	19	25	39.79016891	-22	19	35.1124531	.00001224	.0001941	0.1005	53523.4	56512.2	3			
1923+123	1923+123	2100	19	25	40.81708231	+12	27	38.0869590	.00002569	.0007684	0.1672	53134.4	53134.5	1			
1923+210	OV 239.7	526	19	25	59.60535909	+21	06	26.1620219	.00000347	.0000520	0.0646	46367.8	56749.7	828	0.75	0.74	3.3
1924+507	1924+507	3743	19	26	6.32163773	+50	52	57.0177080	.00002975	.0004566	0.1214	49576.2	50306.3	2			
1923-101	1923-101	2101	19	26	26.96695409	-10	05	51.9593562	.00019536	.0047787	0.7263	53560.3	53560.4	1			
1928+770	1928+770	2102	19	26	31.19095180	+77	06	31.4977842	.00030713	.0011074	-0.2253	53572.2	53572.4	1			
1926+611	1926+611	3744	19	27	30.44257132	+61	17	32.8789571	.00004753	.0004078	-0.3611	49576.2	49576.4	1			
1928+738	1928+738	701	19	27	48.49516065	+73	58	1.5699035	.00000808	.0000595	-0.0095	44772.1	55847.7	172	1.19		3.9
1925-206	1925-206	2103	19	28	9.18334304	-20	35	43.7845846	.00001143	.0003400	-0.3446	54559.5	54601.5	2			
1926+440	1926+440	2104	19	28	21.35157202	+44	12	1.8545634	.00013053	.0028092	0.4117	50306.2	53125.5	2			
1926+087	1926+087	938	19	28	40.85549722	+08	48	48.4126926	.00000806	.0002293	-0.2391	50065.0	54937.0	13			
1926+233	1926+233	3745	19	29	4.57595579	+23	25	29.2781893	.00006990	.0008848	-0.0254	50084.7	50155.7	2			
1926+050	1926+050	3746	19	29	19.94806208	+05	07	57.5899310	.00013867	.0038108	-0.3901	49914.3	49914.4	1			
1927+256	1927+256	3747	19	29	44.91811747	+25	43	16.2455677	.00001062	.0002406	0.3195	50219.5	56547.3	5			
1927+090	1927+090	3748	19	29	47.86322763	+09	10	3.6434882	.00016872	.0033865	-0.6570	53561.3	55483.1	2			
1925-610	1925-610	939	19	30	6.16009352	-60	56	9.1842964	.00001474	.0001381	0.1547	47626.0	56638.6	32			
1928+154	1928+154	1159	19	30	52.76699794	+15	32	34.4274174	.00000868	.0001914	0.1206	52305.8	53613.0	3	0.42	0.27	
1929+312	1929+312	3749	19	31	8.67383703	+31	22	33.3962492	.00010891	.0016554	-0.3930	50219.5	50219.5	1			
1929+226	1929+226	940	19	31	24.91678201	+22	43	31.2586138	.00000388	.0000670	-0.1218	48613.6	56758.8	161	0.30	0.28	2.5
1929-295	1929-295	2105	19	32	35.45376035	-29	28	42.0479278	.00002083	.0007665	-0.2891	53552.3	53552.4	1			
1929-457	1929-457	3750	19	32	44.88776364	-45	36	37.9288987	.00001636	.0002811	0.2287	53222.6	54669.9	11			
1931+149	1931+149	3751	19	33	21.80501757	+15	04	46.4003563	.00005782	.0018866	-0.1392	52305.8	52306.7	1			

Source Name		ID No.	Right Ascension			Declination			RA Error (s)	Dec. Error (arcsec)	RA–Dec Corr.	Observation Epoch MJD		No. Obs.	Source Flux (Jy)		Str Index
B1950	Common		H	M	S	D	M	S				First	Last		10-60	10-40	
1928-698	1928-698	3752	19	33	31.15982028	-69	42	58.9146744	.00012964	.0005465	-0.2596	53222.7	53569.0	2			
1933+655	J1933+6540	1160	19	33	57.33725564	+65	40	16.8283989	.00003778	.0004707	0.2199	49826.5	49827.4	1			
1932+106	1932+106	941	19	34	35.02550873	+10	43	40.3662211	.00017387	.0068169	-0.3247	51168.9	51169.7	1			
1934+615	1934+615	2106	19	34	40.68334424	+61	38	41.6234635	.00004783	.0004814	-0.1722	53572.2	53572.4	1			
1931-243	1931-243	2107	19	34	52.84873713	-24	16	24.3611353	.00008216	.0024118	-0.1421	53152.4	53152.5	1			
1932+204	1932+204	942	19	35	10.47290942	+20	31	54.1541181	.00000543	.0001101	-0.0455	48916.1	56568.7	24	0.22	0.13	2.1
1939+813	1939+813	3753	19	35	22.72236143	+81	30	14.5541725	.00032744	.0004340	-0.5454	50687.3	50687.4	1			
1932-161	1932-161	3754	19	35	35.79528578	-16	02	32.3720319	.00004915	.0014191	-0.1403	54111.8	54111.8	1			
1936+714	1936+714	2108	19	36	3.56081914	+71	31	31.7847237	.00004107	.0002777	0.2207	49826.5	54664.6	3			
1934+365	1934+365	3755	19	36	27.81664204	+36	42	34.9808445	.00006036	.0007913	0.0325	50242.4	50242.5	1			
1934+226	1934+226	3756	19	36	29.30469629	+22	46	25.8561812	.00009119	.0011925	0.5108	52306.6	55483.2	2			
1933-400	P 1933-400	528	19	37	16.21735610	-39	58	1.5531911	.00000751	.0000939	-0.4919	44228.0	56574.3	94		0.60	
1934-065	1934-065	3757	19	37	19.99229130	-06	27	28.0851570	.00003883	.0011264	-0.0010	53503.6	55847.1	2			
1935+360	1935+360	2109	19	37	31.43662992	+36	07	35.8415110	.00001129	.0001977	-0.0228	53134.4	56701.6	2	0.15	0.16	
1935-179	1935-179	2110	19	38	4.95831549	-17	49	20.3891348	.00002977	.0011168	-0.6805	53560.3	53560.4	1			
1936+046	1936+046	3758	19	38	30.66955024	+04	48	11.6138316	.00001469	.0004018	-0.1781	49914.3	56463.4	2	0.16	0.29	
1936+095	1936+095	3759	19	38	43.61050354	+09	42	20.0122921	.00994056	.2096576	-0.9979	54087.9	55167.8	2			
1934-638	P 1934-63	943	19	39	25.02773793	-63	42	45.6051531	.00410432	.0410676	0.6903	50181.6	50182.4	1			
1936-155	P 1936-15	529	19	39	26.65774887	-15	25	43.0585211	.00000377	.0000640	-0.2129	47301.3	56770.5	207	0.57	0.59	2.1
1937+381	1937+381	2111	19	39	33.56694443	+38	17	35.3892598	.00009381	.0008157	0.4231	53125.4	53125.5	1			
1938+371	1938+371	3760	19	39	51.80642388	+37	13	30.4868841	.00005656	.0006674	-0.2920	50242.4	50242.5	1			
1937-101	P 1937-101	530	19	39	57.25657418	-10	02	41.5205298	.00000608	.0001391	-0.0554	48110.4	55112.4	26			
1935-692	1935-692	944	19	40	25.52816203	-69	07	56.9716668	.00001581	.0001171	0.0735	47626.0	56638.7	38			
1939+429	1939+429	2112	19	40	49.32005070	+43	04	24.6580737	.00007385	.0008428	0.3053	53572.2	53572.3	1			
1938-302	1938-302	3761	19	41	10.24275425	-30	07	20.4280106	.00038502	.0097236	0.8410	53503.5	53503.5	1			
1936-623	P 1936-623	3762	19	41	21.76866420	-62	11	21.0568871	.00006637	.0008541	-0.5337	52941.0	54670.1	7			
1942+722	1942+722	2113	19	41	26.98411623	+72	21	42.2182193	.00053712	.0054322	0.3077	53560.2	53560.5	1			
1939-053	1939-053	2114	19	41	47.00857387	-05	11	32.3828835	.00002652	.0009176	-0.5806	53523.4	53523.5	1			
1939-316	1939-316	2115	19	42	40.91400897	-31	30	14.6084490	.00003811	.0014323	-0.6317	53523.4	53523.5	1			
1941+413	1941+413	2116	19	42	58.63811636	+41	29	23.0600345	.00001122	.0002457	0.1167	53133.5	53134.4	1			
1943+546	1943+546	1244	19	44	31.51232273	+54	48	7.0635386	.00011637	.0009920	0.4445	49576.2	53167.2	2	0.12		
1942+097	1942+097	3763	19	45	15.92279035	+09	52	59.5627307	.00002926	.0012139	0.1107	49914.3	49914.4	1			
1942-020	1942-020	2117	19	45	22.82079104	-01	53	21.8309583	.00001178	.0004087	-0.3355	53552.3	53561.4	2			
1946+708	1946+708	3764	19	45	53.51997301	+70	55	48.7319637	.00033071	.0017506	0.3429	49826.5	49827.4	1			
1942-313	1942-313	2118	19	45	59.36937068	-31	11	38.3569648	.00002243	.0007217	-0.3662	54943.5	54943.6	1			
1943+228	1943+228	945	19	46	6.25140594	+23	00	4.4139955	.00001822	.0004365	-0.2711	48797.2	52620.1	4			
1944+126	1944+126	3765	19	47	19.52673520	+12	48	55.4208280	.00006226	.0010792	0.1228	50084.7	50155.7	2			
1945-011	1945-011	3766	19	47	43.78374290	-01	03	24.5279436	.00002197	.0007243	-0.6282	53503.4	53503.6	1			
1946+358	1946+358	3767	19	48	4.52010321	+35	56	20.6706869	.00008432	.0012369	-0.0576	50242.4	50242.5	1			
1945-325	1945-325	4137	19	48	25.24917471	-32	28	6.4498624	.00008510	.0031424	0.7466	55616.7	55616.7	1			
1946+396	1946+396	3768	19	48	35.77023554	+39	43	52.0681916	.00014116	.0014900	0.0564	54087.9	54088.0	1			
1947+242	1947+242	3769	19	49	33.14262079	+24	21	18.2450647	.00037467	.0035826	0.6398	52305.8	52306.7	1			
1950+727	1950+727	3770	19	49	35.23113415	+72	52	42.9679071	.00034466	.0034310	-0.1894	49826.5	49827.4	1			
1948+505	1948+505	2119	19	49	43.49229166	+50	41	31.9729042	.00002798	.0004866	0.2435	49576.2	54664.7	3			
1946-200	1946-200	3771	19	49	53.42017764	-19	57	13.3303028	.00000886	.0003021	0.0910	50631.3	50688.2	2	0.25	0.23	
1947+079	1947+079	946	19	50	5.53973224	+08	07	13.9847094	.00002931	.0005874	-0.6594	48103.1	52306.7	24		0.09	5.1
1946-582	1946-582	3772	19	50	37.40167091	-58	04	39.7487305	.00004261	.0006722	0.3945	54722.9	54723.8	1			
1948-047	1948-047	3773	19	50	44.05507775	-04	36	11.8400681	.00012039	.0022760	-0.1442	50575.5	50575.6	1			
1950+573	1950+573	3774	19	51	6.98247970	+57	27	17.1764840	.00029472	.0020934	0.4986	49576.2	49576.4	1			
1949+014	1949+014	2120	19	51	36.01847615	+01	34	42.7142285	.00001109	.0003265	-0.0188	53125.4	53125.5	1	0.18	0.14	

Source Name		ID No.	Right Ascension			Declination			RA Error (s)	Dec. Error (arcsec)	RA–Dec Corr.	Observation Epoch MJD		No. Obs.	Source Flux (Jy)		Str Index
B1950	Common		H	M	S	D	M	S				First	Last		10-60	10-40	
1949-052	1949-052	2121	19	51	47.46845999	-05	09	43.9622051	.00001117	.0003590	-0.0052	53523.4	56749.7	2	0.14	0.13	
1950+253	1950+253	3775	19	52	48.29395668	+25	26	53.4844629	.00001563	.0003618	0.0406	52409.4	52409.6	1			
1951+355	1951+355	947	19	53	30.87574864	+35	37	59.3594733	.00001537	.0002874	0.3665	49177.1	53131.6	7			
1951-115	1951-115	2122	19	54	41.15572250	-11	23	22.6416995	.00001191	.0004088	-0.2100	53523.4	53523.5	1			
1950-613	P 1950-613	948	19	55	10.77047527	-61	15	19.1389395	.00012756	.0011092	0.4005	49329.4	56111.8	4			
1952+138	J1955+1358	949	19	55	11.57140968	+13	58	16.2410326	.00001623	.0004833	-0.1209	50084.7	53946.1	5	0.26	0.11	
1954+513	1954+513	950	19	55	42.73825370	+51	31	48.5462846	.00000429	.0000609	-0.0520	47612.7	56782.2	160	0.53		2.6
1954+282	1954+282	1245	19	56	46.04047365	+28	20	57.9772110	.00001119	.0002634	-0.1036	52409.4	53306.4	2			
1953-325	P 1953-325	3776	19	56	59.45528506	-32	25	46.0080012	.00001556	.0005074	-0.1898	52305.8	56204.1	2		0.43	
1955+343	1955+343	3777	19	57	34.45469820	+34	27	54.6334229	.00152774	.0410697	0.7279	54292.2	54292.5	1			
1955+335	1955+335	951	19	57	40.54992400	+33	38	27.9432680	.00004038	.0004221	0.0583	49403.5	52711.5	4			
1954-388	P 1954-388	533	19	57	59.81927689	-38	45	6.3559766	.00000361	.0000557	-0.0628	49014.8	56776.7	786		1.00	2.6
1957+386	1957+386	2123	19	59	22.03919879	+38	46	54.1657134	.00005590	.0007692	0.1008	53572.3	53572.4	1			
1957+406	3C 405	1162	19	59	28.35633622	+40	44	2.0959473	.00009856	.0010176	0.0500	53067.9	53068.5	1			
1959+650	1959+650	3778	19	59	59.85215726	+65	08	54.6529986	.00019327	.0019629	0.1911	49826.5	49827.4	1			
1957-135	1957-135	2124	20	00	42.14511885	-13	25	33.5329671	.00001199	.0004036	-0.1258	53552.3	53552.4	1			
1958-179	OV-198	534	20	00	57.09044337	-17	48	57.6726839	.00000342	.0000529	-0.0138	43809.1	56776.7	1177	1.09	1.21	1.5
1958+103	1958+103	3779	20	01	10.64346530	+10	27	58.1161359	.00013492	.0020444	-0.4930	49914.3	49914.4	1			
1959+437	1959+437	3780	20	01	12.87371687	+43	52	52.8384130	.00060889	.0068088	0.2603	50242.4	50242.5	1			
1959+241	1959+241	2125	20	01	53.77800066	+24	16	39.9905206	.00002762	.0006921	0.3402	53561.3	53561.4	1			
1959+067	1959+067	3781	20	02	9.57487451	+06	51	15.3918270	.00007813	.0016544	0.4657	54111.8	54111.9	1			
2000+472	2000+472	1246	20	02	10.41825445	+47	25	28.7739027	.00000351	.0000518	-0.0238	50306.2	56758.7	287	0.45	0.45	2.1
2000+148	2000+148	2126	20	02	41.99923555	+15	01	14.5738807	.00000441	.0000935	-0.1320	50084.7	56701.7	44			
1959-169	1959-169	3782	20	02	43.08826114	-16	49	22.7069633	.00009928	.0030793	-0.5129	54087.9	54087.9	1			
2001+449	2001+449	2127	20	02	52.09615828	+45	06	8.3274912	.00001704	.0002675	-0.0725	50306.2	53523.5	2			
2000-330	P 2000-330	535	20	03	24.11632722	-32	51	45.1329009	.00000764	.0001465	-0.2070	48579.8	55334.7	28		0.25	4.1
2000-045	2000-045	3783	20	03	24.97542897	-04	21	38.4290246	.00015697	.0065616	0.1813	53560.3	53560.4	1			
2001+304	2001+304	3784	20	03	30.24406002	+30	34	30.7885967	.00001073	.0002994	0.0680	52409.4	52409.5	1			
2003+662	2003+662	3785	20	03	54.50964068	+66	25	56.3759751	.00036440	.0016800	0.2588	49826.5	54112.7	2			
2005+737	2005+737	4111	20	04	17.12176758	+73	55	6.0094894	.00012373	.0002886	-0.0240	55966.0	55966.5	1			
2002-185	2002-185	3786	20	05	17.29314996	-18	22	3.3231337	.00001707	.0008388	-0.1684	50631.3	50688.2	2			
2007+777	2007+777	952	20	05	30.99851794	+77	52	43.2475477	.00000760	.0000539	-0.0369	48377.8	55293.5	162	0.59		3.4
2004+443	2004+443	3787	20	05	52.08826874	+44	28	55.1231338	.00054603	.0063431	0.2566	50306.2	53552.4	2			
2002-375	2002-375	2128	20	05	55.07090460	-37	23	41.4782859	.00000900	.0001870	0.0188	52305.8	56749.7	20			
2002-233	2002-233	2129	20	05	56.59556389	-23	10	27.0097427	.00002953	.0009164	-0.2645	53152.4	53152.5	1			
2005+642	2005+642	953	20	06	17.69457911	+64	24	45.4180046	.00002269	.0001677	0.1039	49422.0	53946.6	9	0.34		
2004-125	2004-125	2130	20	06	48.34304263	-12	22	55.3044720	.00015170	.0059183	0.6089	53561.3	53561.4	1			
2007+747	2007+747	3788	20	07	4.38948725	+74	52	25.3988957	.00171998	.0011780	0.2404	54087.1	54087.8	1			
2004+064	2004+064	1163	20	07	11.91530469	+06	36	44.5954188	.00007933	.0018431	0.2255	49914.3	49914.4	1			
2007+659	2007+659	3789	20	07	28.77107245	+66	07	22.5356423	.00003156	.0002331	0.3428	49826.5	56749.4	2	0.32		
2005+403	2005+403	954	20	07	44.94486188	+40	29	48.6039733	.00009943	.0012406	0.4647	48665.8	54643.7	4			3.6
2005+372	2005+372	3790	20	07	45.39796082	+37	22	2.2991823	.00054964	.0067410	-0.7887	52409.4	55112.2	2			
2004-447	2004-447	3791	20	07	55.18447863	-44	34	44.2792512	.00005903	.0017130	0.0940	52305.8	52409.5	2			
2005-044	2005-044	1292	20	08	24.42920093	-04	18	29.3024380	.00012278	.0028831	0.4059	53767.8	53768.7	1			
2005-283	2005-283	3792	20	09	0.73596574	-28	12	25.8887120	.08411726	.3663993	-0.9998	53560.4	53560.4	1			
2005-489	P 2005-489	955	20	09	25.39069442	-48	49	53.7217929	.00003448	.0002719	0.6563	47626.2	56716.2	59			
2010+723	2010+723	3793	20	09	52.30387604	+72	29	19.3511067	.00004405	.0002953	0.2690	49826.5	49827.4	1			
2007+073	2007+073	4138	20	09	55.50742060	+07	27	13.6670377	.00001782	.0005701	0.1340	55915.8	55916.0	1			
2009+611	2009+611	3794	20	10	49.28859532	+61	16	15.1572006	.00005280	.0006143	-0.3032	49576.2	49576.4	1			
2008+332	2008+332	3795	20	10	49.72332019	+33	22	13.8100879	.00009390	.0012893	0.0391	52409.5	52409.6	1			

Source Name		ID No.	Right Ascension			Declination			RA Error (s)	Dec. Error (arcsec)	RA–Dec Corr.	Observation Epoch MJD		No. Obs.	Source Flux (Jy)		Str Index
B1950	Common		H	M	S	D	M	S				First	Last		10-60	10-40	
2008-068	OW-015	537	20	11	14.21584322	-06	44	3.5556674	.00000944	.0002211	-0.5312	48345.7	55545.1	38	0.07		4.1
2008-159	P 2008-159	536	20	11	15.71092967	-15	46	40.2537820	.00000351	.0000545	-0.0370	47254.6	56772.7	478	1.27	0.69	1.6
2010+463	2010+463	3796	20	12	5.63739335	+46	28	55.7775360	.00010568	.0011738	-0.7200	50306.2	50306.3	1			
2013+508	2013+508	2131	20	14	28.59024260	+50	59	9.5276238	.00021715	.0017230	-0.2679	50305.3	54314.3	2			
2014+657	2014+657	3797	20	14	32.04689699	+65	53	55.9492302	.00809229	.9611577	0.2239	49827.4	49827.4	1			
2012-017	2012-017	3798	20	15	15.15797574	-01	37	32.5606169	.00001642	.0005242	-0.0449	50575.5	50575.6	1			
2013+527	2013+527	3799	20	15	19.16832042	+52	53	59.7199120	.00015722	.0015077	0.6157	49576.2	49576.4	1			
2013+370	2013+370	3800	20	15	28.72978853	+37	10	59.5147505	.00001885	.0003274	-0.0038	52305.8	52305.9	1			
2013+340	2013+340	3801	20	15	28.83184685	+34	10	39.4091923	.00006898	.0008738	-0.0262	50219.5	50219.5	1			
2014+463	2014+463	4112	20	15	39.98585034	+46	28	50.8695067	.00057250	.0121029	-0.7272	56106.2	56106.5	1			
2015+657	2015+657	3802	20	15	55.36870143	+65	54	52.6591259	.00004279	.0003630	0.4190	49826.5	49827.4	1			
2013+163	2013+163	1164	20	16	13.86003226	+16	32	34.1128898	.00000416	.0000748	-0.0088	50084.7	56770.1	113	0.34	0.32	1.4
2014+358	2014+358	3803	20	16	45.61882518	+36	00	33.3744235	.00010531	.0017757	0.4902	52409.4	52409.5	1			
2013-273	2013-273	3804	20	16	46.41557032	-27	08	48.1884944	.00037174	.0164332	0.3603	53561.3	53561.4	1			
2017+745	2017+743	956	20	17	13.07934017	+74	40	48.0000050	.00000895	.0000614	-0.0449	48353.1	56754.1	110	0.31		0.0
2014-254	2014-254	2132	20	17	53.00201540	-25	14	50.0835382	.00010721	.0033749	-0.4296	53152.4	53152.5	1			
2015+083	J2018+0831	1165	20	18	11.31195384	+08	31	54.5472123	.00001414	.0004754	-0.3223	49914.3	49914.4	1			
2015-113	2015-113	2133	20	18	28.01424030	-11	09	55.4980281	.00002347	.0007104	-0.0401	53152.4	53152.5	1			
2018+295	2018+295	3805	20	20	6.56356373	+29	42	14.1494695	.00013251	.0040067	-0.2245	52409.4	52409.6	1			
2018+282	2018+282	3806	20	20	45.87129387	+28	26	59.1913055	.00059515	.0061427	-0.6096	50219.5	54314.6	2			
2019+050	2019+050	3807	20	21	35.28121161	+05	15	4.7780712	.00001702	.0005599	-0.3133	49914.3	49914.4	1			
2021+614	OW 637	539	20	22	6.68172646	+61	36	58.8044939	.00000866	.0000830	0.0809	46336.9	55257.6	45	0.76		4.8
2023+760	2023+760	3808	20	22	35.57595133	+76	11	26.1718537	.00014729	.0008186	0.7304	49826.5	49827.4	1			
2019-408	2019-408	3809	20	22	52.00367057	-40	38	22.0403626	.15170460	.1197241	0.9995	53134.5	53134.5	1			
2020-122	2020-122	3810	20	22	55.15433473	-12	04	4.7531208	.00006170	.0017100	0.6124	53561.3	56204.2	2			
2021+317	2021+317	957	20	23	19.01734907	+31	53	2.3059779	.00000554	.0000935	-0.1282	48353.4	56495.1	54	0.29	0.22	3.3
2021+222	2021+222	3811	20	23	23.16021462	+22	23	52.5256824	.00002922	.0010263	-0.5751	50084.7	50155.7	2	0.08	0.08	
2020-015	2020-015	2134	20	23	32.81638108	-01	23	42.1532963	.00006108	.0016196	-0.3632	53560.3	53560.4	1			
2022+542	2022+542	1247	20	23	55.84402125	+54	27	35.8290343	.00000677	.0001449	0.1235	49576.2	56782.2	104	0.36		
2021+003	2021+003	1166	20	24	22.71504908	+00	27	53.1013563	.00002469	.0007478	-0.3547	53561.3	53561.4	1	0.10		
2021-330	2021-330	2135	20	24	35.57648835	-32	53	35.9125742	.00003820	.0012794	0.3735	53125.5	53125.5	1			
2022+274	2022+274	1167	20	24	51.23121186	+27	36	1.6986053	.00003665	.0005552	-0.4374	50219.5	55776.4	2			
2022+171	J2024+1718	1168	20	24	56.56344693	+17	18	13.1974607	.00000757	.0002137	-0.1135	50084.7	54481.8	12	0.35	0.28	
2022+031	2022+031A	2136	20	25	9.63214688	+03	16	44.5045151	.00001592	.0002826	0.0632	49914.3	54643.2	2			
2023+335	2023+336	703	20	25	10.84210004	+33	43	0.2143880	.00001186	.0001537	-0.2236	49177.1	52830.6	6	0.10		3.4
2023+503	2023+503	3812	20	25	24.97245692	+50	28	39.5364351	.00005834	.0004513	-0.5973	49576.2	50305.4	2			
2022-077	2022-077	3813	20	25	40.66040922	-07	35	52.6890731	.00001022	.0003250	-0.2486	50575.5	56547.3	2	0.55	0.81	
2022-289	2022-289	2137	20	25	53.61284922	-28	45	48.6969674	.00001725	.0006197	-0.1639	53523.5	53560.4	2			
2025-086	2025-086	2138	20	27	52.60106329	-08	31	55.8772858	.00001641	.0005178	-0.4257	53552.3	53552.4	1			
2027+464	2027+464	1169	20	29	18.93647737	+46	36	2.2501635	.00037476	.0057029	-0.2728	50305.3	50305.4	1			
2025-538	2025-538	3814	20	29	35.05517984	-53	39	7.2924827	.00010012	.0032741	-0.0687	54723.6	54723.8	1			
2028+492	2028+492	3815	20	29	39.89763467	+49	26	21.9942334	.05233860	.3250043	-0.9962	53561.4	53561.4	1			
2027-035	2027-035	3816	20	30	7.47481196	-03	25	12.5479940	.00087997	.0072261	0.9268	54439.9	54440.0	1			
2027-065	2027-065	3817	20	30	15.13900816	-06	22	14.9339994	.00001654	.0005357	0.0813	54087.9	54088.0	1			
2027-052	2027-052	2139	20	30	22.42836452	-05	03	12.7745743	.00003197	.0009069	-0.6043	53560.3	53560.4	1			
2028+368	2028+368	3818	20	30	31.26197354	+37	00	36.0700729	.00394815	.0437112	-0.8912	53572.3	53572.4	1			
2027-308	2027-308	3819	20	30	57.93375024	-30	39	24.3457007	.00035655	.0135952	0.0321	53134.5	53134.5	1			
2028-264	2028-264	3820	20	31	4.22838447	-26	15	33.4386574	.26902418	.1991443	1.0000	53572.3	53572.3	1			
2029+024	2029+022	1293	20	31	47.25111710	+02	39	37.2838509	.00000662	.0001846	-0.1222	53767.8	56749.6	6	0.14	0.17	0.4
2030+547	OW 551	543	20	31	47.95854902	+54	55	3.1395046	.00000834	.0001158	-0.1138	44203.0	55229.7	74	0.26		4.1

Source Name		ID No.	Right Ascension			Declination			RA Error (s)	Dec. Error (arcsec)	RA–Dec Corr.	Observation Epoch MJD		No. Obs.	Source Flux (Jy)		Str Index
B1950	Common		H	M	S	D	M	S				First	Last		10-60	10-40	
2029+121	P 2029+121	542	20	31	54.99426708	+12	19	41.3401366	.00000378	.0000657	-0.0591	44202.8	56770.4	147	0.79	0.60	2.7
2031+216	2031+216	3821	20	33	32.03141111	+21	46	22.4096479	.00010693	.0010413	0.0019	50084.8	50155.7	2			
2032+281	2032+281	2140	20	34	28.28383274	+28	20	39.9867966	.00022538	.0030921	-0.7231	53523.4	53523.5	1			
2032+117	2032+117	3822	20	34	37.10983778	+11	54	31.3833776	.00010628	.0015795	0.0578	49914.3	49914.4	1			
2032-168	2032-168	3823	20	34	54.46444831	-16	40	26.6113576	.00007127	.0020511	-0.0397	53503.6	53503.6	1			
2032+107	2032+107	3824	20	35	22.33330267	+10	56	6.7884120	.00000971	.0002834	-0.1087	49914.3	49914.4	1			
2034+581	2034+581	3825	20	35	23.75213293	+58	21	18.7465914	.00023524	.0015500	-0.1199	49576.2	49576.4	1			
2033+187	2033+187	3826	20	35	33.98351696	+18	57	5.4582534	.00011213	.0017715	0.1668	52306.7	56106.5	2			
2030-689	2030-689	3827	20	35	48.87646868	-68	46	33.8409136	.00004672	.0002475	-0.1659	53222.7	54578.0	8			
2033-286	2033-286	2141	20	36	37.77490434	-28	30	26.5321273	.00002294	.0007681	-0.2333	55042.2	55042.3	1			
2034-066	2034-066	2142	20	36	40.70895341	-06	29	3.8474996	.00001140	.0003648	-0.2640	53523.4	53523.5	1			
2033-219	2033-219	2143	20	36	51.17273220	-21	46	36.7495519	.00001732	.0005571	-0.2561	53552.4	56498.4	2	0.17	0.15	
2034+222	2034+222	4113	20	36	56.91268901	+22	27	59.2904159	.00002612	.0006667	-0.1888	56393.5	56393.7	1			
2034-155	2034-155	2144	20	37	27.93729465	-15	22	0.5006077	.00015059	.0037829	-0.1221	53572.3	53572.3	1			
2034-248	2034-248	2145	20	37	56.67496215	-24	38	32.5605215	.00002823	.0009967	-0.2140	53560.4	53560.4	1			
2037+511	3C 418	545	20	38	37.03473624	+51	19	12.6626609	.00000341	.0000507	-0.0054	45495.3	56776.7	1328	1.10		3.3
2036-034	2036-034	3828	20	39	9.98488717	-03	17	14.4174244	.00002454	.0007334	0.1539	53561.3	55657.7	2			
2037+216	2037+216	3829	20	39	34.80821857	+21	52	9.6851087	.00011876	.0040181	-0.6740	50084.8	50155.7	2			
2037-253	P 2037-253	546	20	40	8.77292038	-25	07	46.6635239	.00001023	.0001365	-0.3193	50077.8	55728.6	35			3.3
2036-387	2036-387	3830	20	40	14.16127868	-38	36	50.0188470	.36812814	.5352651	1.0000	53523.5	53523.5	1			
2037-172	2037-172	2146	20	40	27.73356185	-17	07	3.1055294	.00006307	.0019075	-0.2619	53560.4	53560.4	1			
2039+037	2039+037	3831	20	42	14.50183370	+03	56	13.9389270	.00004693	.0008960	-0.0029	54087.9	55112.2	2			
2043+749	2043+749	4114	20	42	37.30798226	+75	08	2.4451560	.00017814	.0006285	-0.5569	56302.1	56302.6	1			
2039-231	2039-231	2147	20	42	54.25407748	-22	55	59.9011945	.00002278	.0006478	0.3043	53552.4	53552.4	1			
2040-225	2040-225	2148	20	42	57.27637355	-22	23	26.9148383	.00017213	.0050840	0.4351	53572.3	53572.4	1			
2040+127	2040+127	3832	20	43	10.20913182	+12	55	13.5701720	.00004467	.0015350	-0.6640	50084.8	50155.7	2			
2041+342	2041+342	3833	20	43	34.45323413	+34	23	16.9943198	.00039097	.0040050	-0.1548	53560.3	53560.4	1			
2042-098	2042-098	2149	20	44	42.67522345	-09	40	38.7247238	.00005566	.0024266	-0.4465	53152.5	53152.5	1			
2043+156	2043+156	2150	20	45	45.49406592	+15	47	27.3408081	.00001035	.0002384	0.0208	53561.3	56701.7	5			
2044-027	2044-027	3834	20	47	10.36659908	-02	36	22.1469968	.00010793	.0033563	-0.1273	52305.9	52306.7	1			
2044-168	P 2044-168	3835	20	47	19.66702778	-16	39	5.8432769	.00001906	.0006161	-0.2381	50631.3	54643.1	2			
2044-188	2044-188	3836	20	47	37.65524542	-18	41	41.3519988	.00002746	.0013163	0.2962	54111.8	54111.9	1			
2044-290	2044-290	3837	20	47	37.73549359	-28	50	2.6682085	.12375428	.8736681	-0.9997	53561.4	53561.4	1			
2046+535	2046+535	3838	20	47	53.79592033	+53	43	32.3980849	.00025214	.0017897	0.2481	49576.2	49576.4	1			
2046+429	2046+429	1294	20	48	19.52624970	+43	10	42.0630943	.00094706	.0125774	-0.2304	52409.4	56393.5	3			
2045-405	2045-405	3839	20	49	10.01505167	-40	20	31.1360134	.00003680	.0009233	-0.3307	55167.9	55168.0	1			
2047+098	2047+098	3840	20	49	45.86498016	+10	03	14.3981038	.00001650	.0005095	-0.2467	49914.3	49914.4	1			
2048+361	2048+361	3841	20	50	2.28437462	+36	19	52.5016129	.00014681	.0020246	0.1453	50242.4	50242.5	1			
2047+039	2047+039	3842	20	50	6.24058947	+04	07	48.8897108	.00001922	.0006079	-0.4968	49914.3	49914.4	1			
2047-266	2047-266	2151	20	50	24.69382845	-26	28	18.0572231	.00001047	.0003770	-0.1096	53561.4	56701.7	2	0.25	0.28	
2048+312	2048+312	1248	20	50	51.13147247	+31	27	27.3739594	.00002220	.0002441	0.0636	50219.6	55118.4	16	0.11	0.09	3.0
2051+745	2051+745	958	20	51	33.73458773	+74	41	40.4980695	.00003241	.0001097	-0.3588	48353.1	54937.0	45	0.12		
2049+175	2049+175	3843	20	51	35.58292388	+17	43	36.9004118	.00002122	.0004586	0.0033	50084.8	50155.7	2			
2050+161	2050+161	3844	20	52	43.61987495	+16	19	48.8278142	.00001974	.0005581	0.1485	50084.8	50155.7	2			
2050+364	B2 2050+36	3845	20	52	52.05497580	+36	35	35.3002259	.00001219	.0003633	-0.1146	50242.4	50242.5	1			
2051+350	2051+350	3846	20	53	2.54767793	+35	15	21.9280194	.00022793	.0072218	-0.3620	53560.3	53560.4	1			
2050+226	2050+226	1170	20	53	9.36401063	+22	48	1.4864352	.00002954	.0005710	0.5165	53125.5	53133.6	2			
2051-204	2051-204	2152	20	54	22.07243700	-20	16	16.8188619	.00001351	.0004267	-0.0179	53152.4	56701.7	2	0.08	0.11	
2054+611	2054+611	1171	20	55	38.83831217	+61	22	0.6390974	.00007462	.0009997	-0.3131	49576.2	49826.7	2	0.30		
2053-044	2053-044	3847	20	55	50.25798844	-04	16	47.0810215	.00001172	.0003562	-0.0393	50575.5	56463.5	4			

Source Name		ID No.	Right Ascension			Declination			RA Error (s)	Dec. Error (arcsec)	RA–Dec Corr.	Observation Epoch MJD		No. Obs.	Source Flux (Jy)		Str Index
B1950	Common		H	M	S	D	M	S				First	Last		10-60	10-40	
2053-127	2053-127	2153	20	55	51.19934239	-12	34	44.2388255	.00013892	.0028267	0.5551	53152.4	53152.6	1			
2052-474	P 2052-47	959	20	56	16.35981130	-47	14	47.6277889	.00000441	.0000603	-0.1715	48388.0	56763.7	462			
2053-323	2053-323	2154	20	56	25.07023884	-32	08	47.8006911	.00003403	.0012243	-0.4229	53125.5	53125.5	1			
2054-377	2054-377	960	20	57	41.60344641	-37	34	2.9905368	.00001876	.0004486	-0.1458	49960.6	53770.8	9		0.36	3.1
2056-369	2056-369	3848	20	59	41.59691028	-36	45	54.6108170	.00007945	.0038370	-0.4217	54601.5	54601.6	1			
2058+260	2058+260	2155	21	00	39.10013173	+26	15	37.0250523	.00016481	.0017506	-0.1912	53133.6	53134.4	1			
2059+560	2059+560	3849	21	00	54.97394321	+56	12	36.6627618	.00081065	.0121081	-0.6473	54112.0	54112.0	1			
2058-297	P 2058-297	2156	21	01	1.65998166	-29	33	27.8364178	.00001191	.0002397	0.0729	50688.1	55545.2	14			
2059+034	P 2059+034	553	21	01	38.83415978	+03	41	31.3207708	.00000347	.0000539	0.0651	49914.3	56772.7	405	0.67	0.49	2.1
2058-425	2058-425	961	21	01	59.11389160	-42	19	16.1505248	.00020154	.0087886	0.0935	49329.4	52409.5	3			
2100+468	2100+468	962	21	02	17.05606847	+47	02	16.2534489	.00003102	.0005154	-0.0152	49177.3	53666.0	6	0.13	0.10	
2101+600	2101+600	3850	21	02	40.21924002	+60	15	9.8361819	.00011762	.0005686	-0.1574	49576.4	54087.8	2			
2102+677	2102+677	3851	21	02	43.78720357	+67	58	19.6972397	.01357152	.0332363	0.8658	49826.5	49826.6	1			
2059-334	2059-334	2157	21	02	45.88598083	-33	13	16.1787210	.00015583	.0074060	0.1214	53133.5	53133.5	1			
2102+003	2102+003	2158	21	05	7.71546442	+00	33	25.0071898	.00006941	.0015107	0.2878	53560.4	53560.4	1			
2059-786	2059-786	963	21	05	44.96143855	-78	25	34.5471902	.00004562	.0001488	0.1295	47626.3	54706.7	19			
2103+213	2103+213	2159	21	06	10.81819474	+21	35	35.9967156	.00001117	.0003308	-0.2332	50084.8	53134.5	3	0.14	0.15	
2103+023	2103+023	2160	21	06	28.14881425	+02	31	37.8007095	.00002609	.0008599	-0.1505	53561.3	53561.4	1			
2102-659	2102-659	1172	21	06	59.72192082	-65	47	43.5857458	.00005648	.0004987	0.0036	52860.7	55784.4	11			
2104-173	2104-173	2161	21	07	27.02165652	-17	08	10.3580094	.00006631	.0025259	0.1291	53523.5	53523.5	1			
2105-293	2105-293	3852	21	08	7.40051089	-29	11	17.1826273	.00088705	.0413355	0.8296	53572.3	53572.4	1			
2105-250	2105-250	2162	21	08	12.32005464	-24	52	33.3222822	.00014104	.0042724	0.2190	53152.5	53152.5	1			
2105-212	2105-212	3853	21	08	29.39937243	-21	01	39.5170506	.00201437	.0243946	0.0936	53152.5	53152.5	1			
2106+143	J2108+1430	964	21	08	41.03214822	+14	30	27.0124216	.00000516	.0001141	0.1012	50084.8	56762.2	24	0.30	0.25	2.6
2111+801	2111+801	4115	21	09	19.16446871	+80	21	11.2279044	.00045853	.0019733	-0.0212	56301.9	56302.4	1			
2107+353	2107+353	3854	21	09	31.87871285	+35	32	57.5974498	.00000947	.0002409	-0.0882	50242.4	50242.5	1			
2106-413	P 2106-413	554	21	09	33.18859615	-41	10	20.6055089	.00000726	.0000984	-0.2574	47626.2	56574.4	68		0.49	
2107-105	2107-105	3855	21	10	0.97900725	-10	20	57.3197105	.00001626	.0004519	-0.3354	50575.5	55784.6	2			
2107-016	2107-016	2163	21	10	22.61910656	-01	26	58.2421245	.00003736	.0009406	0.1290	53152.6	53152.6	1			
2111+400	2111+400	2164	21	13	29.48635089	+40	12	51.3874795	.00007701	.0010187	-0.2747	53152.4	53152.5	1			
2112+283	2112+283	3856	21	14	58.33363149	+28	32	57.1967760	.00001069	.0002587	-0.2537	50219.6	56498.4	4			
2112-144	2112-144	2165	21	15	18.43556974	-14	16	43.3718721	.00001372	.0003911	-0.0723	53552.4	56547.3	2	0.12	0.17	
2113+293	B2 2113+29B	555	21	15	29.41345674	+29	33	38.3669623	.00000339	.0000520	0.0054	44202.9	56776.4	922	0.48	0.28	2.8
2109-811	2109-811	965	21	16	30.84585375	-80	53	55.2231138	.00006910	.0001360	-0.0820	48756.3	54706.7	23			
2114+053	2114+053	3857	21	16	36.63486308	+05	36	17.0449650	.00001357	.0004811	-0.0292	54111.8	54111.9	1			
2114+048	2114+048	3858	21	17	20.75708815	+05	03	4.1129702	.00002131	.0007210	-0.3489	49914.3	49914.4	1			
2116+543	2116+543	2166	21	17	56.48464143	+54	31	32.5045520	.00027935	.0028030	0.3323	53572.3	53572.5	1			
2115-305	2115-305	1295	21	18	10.59828813	-30	19	11.6340828	.00084362	.0270924	-0.9048	52305.8	53642.1	2			
2116-068	2116-068	3859	21	18	43.24215908	-06	36	17.9986123	.00002688	.0007668	0.2457	53503.5	55847.2	2	0.09	0.08	
2119+709	2119+709	1173	21	19	54.16457605	+71	10	36.1074682	.00069382	.0045583	0.4141	49826.5	49826.7	1			
2118+443	2118+443	3860	21	20	31.77394439	+44	34	34.2630561	.00033471	.0020454	-0.2236	50305.3	56638.1	2			
2118+053	2118+053	2167	21	20	41.18232800	+05	33	45.0079725	.00001566	.0004787	-0.1056	53133.6	53134.5	1			
2119+664	2119+664	3861	21	20	46.20155379	+66	42	20.2309189	.00052159	.0029041	0.7400	49826.5	54112.7	2			
2118-037	2118-037	2168	21	20	48.47359211	-03	30	28.9301945	.00006153	.0016310	0.0754	53561.4	53561.5	1			
2118+188	2118+188	1174	21	21	0.60658252	+19	01	28.2814930	.00007861	.0018841	-0.6373	50084.9	50155.8	2			
2117-614	2117-614	1175	21	21	4.07416240	-61	11	24.6248182	.00003220	.0002805	0.5188	52860.7	55784.7	14			
2118-372	2118-372	2169	21	21	13.19381055	-37	03	8.9029932	.00003084	.0009571	-0.4560	53125.6	53125.6	1			
2117-642	2117-642	3862	21	21	55.02270876	-64	04	30.0410232	.00131363	.0045621	-0.2367	52886.7	53138.7	2			
2121+547	2121+547	1176	21	23	5.31346017	+55	00	27.3252837	.00002728	.0003256	-0.7297	49576.3	53133.6	3	0.18		
2120+099	2120+099	2170	21	23	13.35861149	+10	07	54.9446448	.00003956	.0012644	-0.4542	49914.3	50700.2	2			

Source Name		ID No.	Right Ascension			Declination			RA Error (s)	Dec. Error (arcsec)	RA–Dec Corr.	Observation Epoch MJD		No. Obs.	Source Flux (Jy)		Str Index
B1950	Common		H	M	S	D	M	S				First	Last		10-60	10-40	
2121+460	2121+460	1177	21	23	31.82845176	+46	14	22.9605045	.00002310	.0002677	0.1849	50305.3	56498.5	4			
2121+053	OX 036	557	21	23	44.51740125	+05	35	22.0929769	.00000341	.0000528	-0.0362	44946.9	56692.7	961	0.47	0.62	3.0
2120-309	2120-309	2171	21	23	48.59956371	-30	46	5.4392272	.00002196	.0006668	-0.0199	54965.5	54965.5	1			
1438-390	2121-199	4116	21	24	44.64018778	-19	41	43.3749958	.00002480	.0007265	0.1842	56036.5	56036.7	1			
2122-148	2122-148	2172	21	24	55.34977863	-14	38	13.3186575	.00015760	.0032000	0.6754	53561.4	53561.5	1			
2123+244	2123+244	3863	21	25	26.17040237	+24	42	3.5786755	.00017306	.0052649	0.3101	53125.5	53133.6	2			
2124+641	2124+641	3864	21	25	27.44711722	+64	23	39.3538716	.00005048	.0006516	-0.2645	49826.5	49826.7	1			
2122+044	2122+044	3865	21	25	29.25542977	+04	41	35.5215032	.00001507	.0005110	-0.1453	49914.3	49914.4	1			
2122-238	2122-238	2173	21	25	52.12226877	-23	38	11.7407107	.00002172	.0007892	-0.1760	54965.5	54965.6	1			
2123-463	2123-463	3866	21	26	30.70425283	-46	05	47.8921916	.00001269	.0002156	0.1331	53222.7	56769.9	21			
2123-015	2123-015	3867	21	26	32.75747019	-01	19	32.4060110	.00002088	.0007137	-0.4056	50575.5	50575.6	1			
2126-158	P 2126-15	559	21	29	12.17589654	-15	38	41.0414842	.00000355	.0000618	-0.0369	48196.1	56772.3	785	0.72	0.30	2.4
2126-185	P 2126-185	3868	21	29	21.41910410	-18	21	22.7900950	.00001398	.0004581	-0.0529	50631.3	50688.2	2			
2127+085	2127+085	3869	21	30	16.24974599	+08	43	55.9274285	.00000915	.0002733	0.0400	52409.5	52409.6	1			
2127-096	2127-096	2174	21	30	19.08826194	-09	27	37.4353399	.00000428	.0000764	0.0420	50575.5	56733.9	88			
2128+048	P 2127+04	562	21	30	32.87739322	+05	02	17.4740755	.00001747	.0004057	-0.0968	48205.9	53666.0	16	0.07		
2128-123	P 2128-12	563	21	31	35.26174781	-12	07	4.7962648	.00000366	.0000657	-0.0133	47254.7	56638.6	818	0.78	0.55	4.2
2136+824	2136+824	2175	21	33	34.07954968	+82	39	6.0535632	.00027050	.0005641	-0.7698	50687.3	54482.6	2			
2131+145	2131+145	4139	21	33	37.38927753	+14	43	46.4639682	.00003029	.0007446	-0.1537	55776.2	55776.5	1			
2130-425	2130-425	3870	21	34	1.17273333	-42	18	43.2326903	.00037020	.0257480	0.1488	53133.6	53133.6	1			
2131-021	P 2131-021	564	21	34	10.30959767	-01	53	17.2388758	.00000384	.0000665	-0.3146	47254.8	56744.8	189	0.72	0.82	2.8
2131-340	2131-340	3871	21	34	50.82449420	-33	51	14.7513553	.00002344	.0007723	-0.0869	55413.3	55413.4	1			
2134+428	2134+428	2176	21	36	24.00630317	+43	01	42.4734524	.00013955	.0012441	-0.1482	53572.3	53572.5	1			
2134+004	P 2134+004	565	21	36	38.58633278	+00	41	54.2131022	.00000375	.0000676	-0.2713	43809.2	56638.5	683	0.75	1.55	3.5
2135+508	2135+508	1249	21	37	0.98616399	+51	01	36.1293481	.00002150	.0001780	-0.0973	52306.0	53679.9	7	0.24		
2135+347	2135+347	2177	21	37	44.10284837	+34	55	42.0932912	.00013489	.0062789	-0.1062	53133.6	53134.4	1			
2135-209	2135-209	3872	21	37	50.00792740	-20	42	31.6665897	.00026164	.0046639	0.3564	52305.8	52305.9	1			
2135-248	P 2135-248	3873	21	38	37.18110659	-24	39	54.4659325	.00001685	.0005289	-0.1005	50631.3	50688.2	2			
2135-184	2135-184	3874	21	38	41.92685842	-18	10	44.3757789	.00030344	.0069489	-0.3993	50631.3	56638.0	5			
2136-190	2136-190	2178	21	38	47.44909327	-18	49	30.6692300	.00021171	.0052753	0.0941	53560.4	53560.5	1			
2136+141	OX 161	567	21	39	1.30927122	+14	23	35.9921463	.00000338	.0000514	-0.0785	48196.2	56679.7	847	0.61	1.09	2.8
2136-251	OX-260	3875	21	39	13.22892061	-24	54	15.0662342	.00003641	.0010765	0.0530	55371.4	55371.5	1			
2137+130	2137+130	2179	21	39	38.14036186	+13	16	13.0517419	.00012158	.0021787	0.1382	53561.4	53561.5	1			
2137+011	2137+011	3876	21	39	42.50889622	+01	22	27.1671834	.00008021	.0017470	-0.1702	49914.3	49914.4	1			
2138+389	2138+389	3877	21	40	16.94710495	+39	11	44.8548132	.00008095	.0015242	-0.0833	50242.5	50242.5	1			
2137-196	2137-196	2180	21	40	46.86016225	-19	23	56.0436177	.00011054	.0032429	-0.8192	53572.3	53572.4	1			
2138-283	2138-283	3878	21	40	56.52484942	-28	04	59.9574689	.00023081	.0084840	0.7390	53503.6	53503.6	1			
2138-377	2138-377	2181	21	41	52.44897948	-37	29	12.9913655	.00002147	.0003363	0.0035	53125.6	54741.6	14			
2139-260	2139-260	3879	21	42	15.92575467	-25	51	26.5971154	.00045912	.0135149	0.3306	53523.5	53523.5	1			
2139-249	2139-249	3880	21	42	30.95903978	-24	44	38.8322318	.00001047	.0003872	0.0212	54111.9	56749.7	2	0.20	0.37	
2140-048	P 2140-048	3881	21	42	36.90168862	-04	37	43.5123779	.00001430	.0004395	-0.2951	50575.5	56638.1	5			
2139-232	2139-232	2182	21	42	41.94582927	-23	03	38.4822460	.00022336	.0077700	0.8522	53560.4	53560.5	1			
2141+175	2141+175	1250	21	43	35.54456805	+17	43	48.7874970	.00000355	.0000539	0.0312	53125.5	56751.8	129			
2141+333	2141+333	2183	21	43	50.13573247	+33	37	10.8167605	.00015053	.0014094	0.1796	53561.3	53561.5	1			
2141-334	2141-334	2184	21	44	51.18569743	-33	12	55.0988090	.00002144	.0006800	-0.1478	53133.6	53133.6	1			
2142+110	2142+110	2185	21	45	18.77506543	+11	15	27.3121714	.00000576	.0001393	-0.0836	49914.3	56547.3	32		0.10	2.7
2143-156	OX-173	570	21	46	22.97933052	-15	25	43.8856532	.00000418	.0000716	-0.1008	44202.9	56766.5	204	0.37	0.31	3.1
2144+568	2144+568	3882	21	46	25.93629427	+57	03	24.6873395	.00129554	.0110808	-0.3497	53125.6	56638.1	3			
2144+042	2144+042	2186	21	46	55.19199952	+04	27	25.4775642	.00001477	.0004817	-0.3081	53560.4	53560.4	1			
2144+092	OX 074	571	21	47	10.16297190	+09	29	46.6722137	.00000396	.0000750	-0.0070	48196.2	56770.4	116	0.52	0.45	3.4

Source Name		ID No.	Right Ascension			Declination			RA Error (s)	Dec. Error (arcsec)	RA–Dec Corr.	Observation Epoch MJD		No. Obs.	Source Flux (Jy)		Str Index
B1950	Common		H	M	S	D	M	S				First	Last		10-60	10-40	
2142-758	2142-758	966	21	47	12.73059350	-75	36	13.2249782	.00002642	.0001089	0.1427	47626.1	56681.7	30			
2144-362	2144-362	3883	21	47	31.12589470	-36	01	51.2722644	.00009376	.0035531	0.2742	53125.6	56301.9	2			
2145+082	2145+082	2187	21	47	55.21939884	+08	30	11.8963823	.00001856	.0007217	-0.4818	49914.3	56568.7	6			
2145+067	P 2145+06	572	21	48	5.45867299	+06	57	38.6041553	.00000336	.0000515	-0.0736	43809.2	56766.5	1410	1.83	2.44	2.8
2146+608	2146+608	3884	21	48	16.04228434	+61	07	5.7936726	.00003303	.0003580	0.3695	52409.4	52409.5	1			
2145-176	2145-176	3885	21	48	36.80084675	-17	23	44.0139979	.00001147	.0003871	-0.0753	50631.3	50631.4	1			
2147+077	2147+077	2188	21	49	35.26384348	+07	56	25.3482574	.00006210	.0015830	-0.0141	49914.3	50700.2	2			
2147-186	2147-186	4117	21	50	1.73567920	-18	22	26.1618661	.00002767	.0008870	0.1962	56036.6	56036.7	1			
2147+145	P 2147+14	3886	21	50	23.60711566	+14	49	47.8946007	.00019009	.0046453	-0.2830	52409.5	52409.6	1			
2147-284	2147-284	3887	21	50	53.08795527	-28	12	41.8147100	.00002114	.0008217	0.0320	54111.9	54111.9	1			
2148-279	2148-279	3888	21	51	21.90509876	-27	42	23.0094142	.00001701	.0006870	0.2705	54088.0	54088.0	1			
2149+069	2149+069	3889	21	51	31.42929823	+07	09	26.7834608	.00001610	.0004140	-0.1823	49914.3	49914.4	1			
2149+056	OX 082	577	21	51	37.87549377	+05	52	12.9544983	.00000366	.0000641	-0.2382	44202.9	56763.4	484	0.30	0.29	2.6
2149-307	P 2149-306	575	21	51	55.52398014	-30	27	53.6980771	.00000540	.0001147	-0.1967	48388.0	56638.6	29		0.94	
2146-783	2146-783	967	21	52	3.15458560	-78	07	6.6392587	.00006098	.0002102	0.5124	47626.3	55784.7	23			
2150+173	2150+173	968	21	52	24.81940297	+17	34	37.7949995	.00000401	.0000717	-0.1282	48196.2	56758.8	75	0.30	0.36	2.8
2151-118	2151-118	4140	21	53	50.24224155	-11	36	14.1109497	.00001589	.0005429	-0.1045	55915.9	55916.0	1			
2151+431	2151+431	2189	21	53	50.95914539	+43	22	54.5009004	.00002962	.0004049	-0.1971	53133.6	53134.4	1			
2151-152	2151-152	2190	21	54	7.43868814	-15	01	31.4722414	.00006554	.0020926	0.6966	53561.4	53561.5	1			
2152+172	2152+172A	3890	21	54	40.90047728	+17	27	50.7938183	.00003329	.0007472	0.6195	50084.8	50155.8	2			
2152+226	J2155+2250	1178	21	55	6.45851180	+22	50	22.2812031	.00001292	.0002276	-0.1987	50084.8	53658.4	6		0.08	4.5
2153+190	2153+190	2191	21	55	34.43686526	+19	14	48.4868209	.00009150	.0019863	-0.4433	53572.3	53572.4	1			
2153-119	2153-119	2192	21	55	50.71846402	-11	39	47.9784810	.00024128	.0040425	-0.1913	53560.4	53560.5	1			
2153-008	2153-008	3891	21	56	14.75791824	-00	37	4.5943575	.00001076	.0003471	-0.1708	50575.5	50575.7	1			
2153-204	2153-204	3892	21	56	33.75584961	-20	12	30.8945010	.00002975	.0011938	-0.0610	53560.4	56463.5	2			
2154-037	2154-037	3893	21	56	50.14547609	-03	33	27.7368772	.01259666	.2189444	-0.9931	53572.4	53572.4	1			
2159+833	2159+833	3894	21	56	57.31618500	+83	37	14.7226161	.00116795	.0012262	-0.7809	50687.3	50687.4	1			
2152-699	2152-699	969	21	57	5.98062129	-69	41	23.6851446	.00018102	.0011412	0.8395	48110.0	52948.0	5			
2154+100	2154+100	3895	21	57	12.86045058	+10	14	24.7982977	.00002619	.0007488	-0.1263	49914.3	49914.4	1			
2155+312	2155+312	1179	21	57	28.82389198	+31	27	1.3516791	.00000436	.0000690	-0.0165	50219.6	56770.2	67	0.29	0.29	1.3
2154-183	2154-183A	3896	21	57	29.12375180	-18	07	2.8659841	.00011624	.0028827	0.2260	50631.3	50631.4	1			
2155-152	OX-192	579	21	58	6.28190694	-15	01	9.3281216	.00000542	.0001093	-0.3970	43809.2	56540.1	126	0.45	0.87	3.7
2155-304	P 2155-304	970	21	58	52.06512115	-30	13	32.1182145	.00000881	.0001259	-0.1473	50210.3	56701.7	29		0.12	2.1
2156-013	2156-013	2193	21	59	34.27573818	-01	05	54.8922894	.00020307	.0029982	0.3186	53561.4	53561.5	1			
2157-255	2157-255	2194	21	59	50.79223992	-25	16	52.1760604	.00001125	.0004075	-0.0120	54852.8	54852.9	1			
2157+102	2157+102	3897	22	00	7.93336868	+10	30	7.9238608	.00108271	.0236284	0.7704	53134.5	53134.5	1			
2157+213	2157+213	3898	22	00	14.19773258	+21	37	57.0417168	.00030456	.0035438	0.7609	50084.9	50155.8	2			
2157-375	2157-375	3899	22	00	16.96647406	-37	16	57.0517131	.00013182	.0050431	-0.6681	53503.6	56162.3	2			
2158-167	2158-167	2195	22	00	54.87887807	-16	32	32.7016901	.00006057	.0019857	-0.7795	53125.5	53125.6	1			
2158+029	2158+029	3900	22	01	27.50871826	+03	12	15.1630146	.00001949	.0005743	-0.1519	49914.3	49914.4	1			
2159+505	2159+505	2196	22	01	43.53724885	+50	48	56.3891001	.00002337	.0002522	-0.5139	49576.3	54643.5	3			
2200+420	VRO 42.22.01	581	22	02	43.29137719	+42	16	39.9799745	.00000343	.0000515	-0.0865	43809.4	56766.5	859	1.69	1.04	3.5
2200-238	2200-238	3901	22	02	55.99949092	-23	35	10.2455837	.00001412	.0004346	-0.3468	50631.3	50688.2	2			
2201+676	2201+676	3902	22	03	12.62280193	+67	50	47.6731791	.00006340	.0004042	-0.5964	49826.6	54087.8	2			
2201+315	B2 2201+31A	582	22	03	14.97579439	+31	45	38.2700532	.00000349	.0000528	0.0271	45491.7	56770.4	807	1.30	0.51	3.2
2201+171	2201+171	1180	22	03	26.89368281	+17	25	48.2478651	.00000745	.0001854	-0.2007	50084.9	54482.7	9	0.81	0.52	
2202+716	2202+716	3903	22	03	30.47741130	+71	51	8.5573379	.04794342	.0769455	0.9827	49826.7	49826.7	1			
2201+098	2201+098	3904	22	03	30.95266105	+10	07	42.5859185	.00027188	.0023438	-0.0249	49914.3	49914.4	1			
2202+363	2202+363	3905	22	04	21.10047560	+36	32	37.0913855	.00011029	.0015223	-0.5827	50242.5	50242.5	1			
2203+292	2203+292	2197	22	05	46.50638398	+29	26	55.1324234	.00001520	.0002891	0.1311	53561.4	56547.4	5			

Source Name		ID No.	Right Ascension			Declination			RA Error (s)	Dec. Error (arcsec)	RA–Dec Corr.	Observation Epoch MJD		No. Obs.	Source Flux (Jy)		Str Index
B1950	Common		H	M	S	D	M	S				First	Last		10-60	10-40	
2205+743	2205+743	2198	22	05	47.39413329	+74	36	21.0471960	.01337358	.0534368	-0.9651	54278.5	54278.7	1			
2203-188	P 2203-18	3906	22	06	10.41637402	-18	35	38.7524779	.00030500	.0064701	-0.4462	50631.3	54187.7	3			
2203-215	2203-215	2199	22	06	41.38227118	-21	19	40.5133218	.00005337	.0014314	0.7045	53133.6	53133.6	1			
2204-007	2204-007	3907	22	06	43.28261799	-00	31	2.4959308	.00001682	.0004549	0.3786	55371.4	55371.5	1			
2204-540	P 2204-54	971	22	07	43.73328267	-53	46	33.8199226	.00000705	.0001064	0.1841	48110.0	56653.1	56			
2205+166	2205+166	1181	22	07	52.86569235	+16	52	17.8155084	.00000780	.0002073	0.2005	50084.8	56639.1	22			
2206+650	2206+650	3908	22	08	3.11035565	+65	19	38.7905231	.00034500	.0020018	0.5930	49826.6	54482.7	2			
2207+741	2207+741	2200	22	08	23.95449026	+74	23	38.3422403	.00043366	.0032348	-0.0294	53560.3	53560.5	1			
2205-636	2205-636	3909	22	08	47.24158999	-63	25	47.4886594	.00009313	.0011138	0.5208	52860.8	52872.8	2			
2207+374	2207+374	2201	22	09	21.42505541	+37	42	18.2267044	.00005696	.0009880	0.1957	50242.5	54664.7	2			
2207+517	2207+517	1182	22	09	21.48682293	+51	58	1.8340166	.00016203	.0016263	0.4814	49576.3	49576.5	1	0.07		
2207+356	2207+356	3910	22	09	45.33433286	+35	56	1.1292504	.00001778	.0005216	-0.4156	50242.5	54482.5	2			
2207+087	2207+087	3911	22	10	6.05026758	+08	57	29.5621734	.00010565	.0023077	0.5287	54111.9	54112.0	1			
2208+199	2208+199	3912	22	10	51.65245230	+20	13	24.0558351	.00001878	.0006894	0.0762	53561.4	56638.2	2			
2208-137	2208-137	2202	22	11	24.09945506	-13	28	9.7238963	.00000536	.0001009	-0.1076	50575.5	56639.7	51	0.25	0.15	
2208-373	2208-373	2203	22	11	50.52613937	-37	07	4.9842336	.00034076	.0208625	-0.1356	53152.5	53152.5	1			
2209+184	2209+184	2204	22	11	53.88890178	+18	41	49.8622803	.00002399	.0006022	0.0891	53572.3	53572.5	1			
2209+080	2209+080	2205	22	12	1.58933188	+08	19	16.5096740	.00003508	.0015232	-0.0880	53523.5	53523.6	1			
2209+236	P 2209+236	588	22	12	5.96631493	+23	55	40.5437827	.00000343	.0000522	-0.0112	49848.0	56755.5	336	0.98	0.58	1.9
2209+328	2209+328	3913	22	12	7.97728562	+33	08	34.5193733	.00005695	.0009114	-0.0279	50219.6	50219.7	1			
2210+016	2210+016	3914	22	12	37.96798895	+01	52	51.2661012	.00278550	.0480269	-0.9843	52408.7	52408.7	1			
2210+277	2210+277	3915	22	12	39.10337740	+27	59	38.4532346	.00021454	.0047119	0.5630	54111.9	54112.0	1			
2210+065	J2212+0646	1183	22	12	50.83928252	+06	46	8.7410215	.00001761	.0005844	0.0405	49914.3	49914.4	1			
2211+587	2211+587	3916	22	12	51.14677526	+59	00	47.3931823	.01215686	.0040616	-0.0667	53552.4	53552.4	1			
2210-257	P 2210-25	705	22	13	2.49798043	-25	29	30.0806931	.00000749	.0001371	-0.1727	49960.4	54362.0	25	0.27	0.24	3.1
2210+361	2210+361	3917	22	13	10.22238193	+36	23	55.1831600	.00004596	.0008788	-0.1523	53561.4	56302.0	2			
2211+069	2211+069	3918	22	14	8.86159160	+07	11	42.3935621	.00002307	.0008186	-0.3900	49914.3	49914.4	1			
2211-388	P 2211-388	972	22	14	38.56983843	-38	35	45.0038052	.00016221	.0065039	0.3509	50258.6	52409.6	4			
2211-256	2211-256	3919	22	14	46.40221314	-25	21	16.0734304	.00004651	.0021529	0.0205	53572.4	55538.0	2			
2212-299	2212-299	3920	22	15	16.03452032	-29	44	23.3335208	.00004355	.0019248	0.6600	50688.1	54664.0	2			
2214+350	GC 2214+35	590	22	16	20.00990428	+35	18	14.1800419	.00000352	.0000532	0.0167	49749.8	56776.5	261	0.39	0.40	1.9
2214+307	2214+307	3921	22	16	42.71044500	+31	02	35.3642795	.00002598	.0004884	-0.2704	50219.6	50219.7	1			
2214+241	2214+241	1184	22	17	0.82118362	+24	21	45.9581299	.00000975	.0002353	-0.3225	50219.6	53946.1	7	0.56	0.30	
2214-192	2214-192	2206	22	17	2.16572500	-19	02	3.8246222	.00002537	.0007659	-0.1868	53133.5	53133.6	1			
2215+316	2215+316	3922	22	17	17.57637449	+31	56	49.9950718	.00001635	.0004112	-0.3255	50219.6	50219.7	1			
2215+020	2215+020	2207	22	17	48.23793733	+02	20	10.7121967	.00000866	.0002300	-0.1435	49914.4	56498.4	16			
2215+150	2215+150	2208	22	18	10.91390506	+15	20	35.7173824	.00000365	.0000573	0.0105	53560.4	56776.7	77			
2215-508	2215-508	3923	22	18	19.02527711	-50	38	41.7310225	.00056414	.0024428	-0.0855	52886.7	53138.7	3			
2216-007	2216-007	4118	22	18	36.68208049	-00	28	53.0561263	.01232676	.2074584	-0.9909	56267.1	56267.1	1			
2216-038	P 2216-03	592	22	18	52.03772804	-03	35	36.8794111	.00000367	.0000661	-0.0722	45139.2	56766.5	418	0.70	0.81	3.3
2216+178	J2219+1806	1185	22	19	14.09248991	+18	06	35.5806032	.00000803	.0002184	0.0858	50084.9	56638.2	17			
2216-275	2216-275	3924	22	19	35.32031727	-27	19	3.2935981	.00030438	.0060037	0.1648	54088.0	54088.0	1			
2217+214	2217+214	3925	22	19	38.52160726	+21	41	12.5601604	.00002000	.0004090	-0.0012	53572.3	55657.6	2			
2217+210	2217+210	3926	22	19	44.17524451	+21	20	53.2043298	.00035771	.0188864	0.3978	53561.5	53561.5	1			
2217-011	2217-011	3927	22	19	47.28245375	-00	51	32.5560557	.00003254	.0011946	-0.4612	54111.9	54112.0	1			
2217+259	2217+259	3928	22	19	49.74112673	+26	13	27.9445226	.00010946	.0045538	-0.0282	50219.6	50219.7	1			
2220+134	2220+134	2209	22	22	45.16318376	+13	44	54.4485773	.00002726	.0008283	-0.0568	53560.4	53560.5	1			
2220+119	2220+119	3929	22	22	52.98900423	+12	13	49.8086336	.00004847	.0010647	-0.3138	49914.4	49914.5	1			
2220-119	2220-119	3930	22	22	56.00532282	-11	44	26.3704788	.00033248	.0084517	0.6197	53503.6	53503.7	1			
2220-351	2220-351	2210	22	23	5.93057166	-34	55	47.1776125	.00001099	.0002609	0.1680	53222.8	56734.1	24			

Source Name		ID No.	Right Ascension			Declination			RA Error (s)	Dec. Error (arcsec)	RA–Dec Corr.	Observation Epoch MJD		No. Obs.	Source Flux (Jy)		Str Index
B1950	Common		H	M	S	D	M	S				First	Last		10-60	10-40	
2221+625	2221+625	1186	22	23	18.09661696	+62	49	33.8055160	.00013695	.0013410	-0.0445	53133.6	54087.9	2			
2220-318	2220-318	2211	22	23	21.63166079	-31	37	2.1098896	.00002237	.0007205	0.1293	54852.8	54852.9	1			
2221-116	2221-116	3931	22	24	7.96268094	-11	26	21.1060741	.00001588	.0004863	-0.0327	50575.5	50575.7	1			
2222+600	2222+600	3932	22	24	37.02469530	+60	16	15.5988318	.00041533	.0037749	-0.1665	52409.4	55776.5	2			
2221-387	2221-387	3933	22	24	43.96136260	-38	31	33.0311589	.00003247	.0010554	-0.5105	55168.0	55168.1	1			
2223+210	2223+210	1187	22	25	38.04713256	+21	18	6.4151098	.00000760	.0001493	0.0122	50084.9	53771.1	5	0.51	0.38	
2223-114	2223-114	3934	22	25	43.71839280	-11	13	40.6973114	.00001182	.0003948	-0.1413	50575.5	56749.6	2	0.08	0.08	
2223-052	3C 446	594	22	25	47.25929425	-04	57	1.3908513	.00000338	.0000519	-0.0516	45151.6	56766.5	1005	1.70	1.93	2.3
2224+006	J2226+0052	1188	22	26	46.53702147	+00	52	11.3312855	.00001469	.0004520	-0.4139	49914.4	53771.0	2	0.27	0.22	
2226+772	2226+772	3935	22	27	21.66389035	+77	33	19.0318975	.04185194	.1733541	-0.9796	53152.5	53152.6	1			
2225+247	2225+247	4119	22	28	1.54173308	+25	03	3.0404910	.00006719	.0013350	0.3241	55965.8	55966.0	1			
2226+440	2226+440	3936	22	28	50.46307813	+44	19	8.4435187	.00018705	.0015359	-0.5325	50305.4	50305.5	1			
2226-081	2226-081	3937	22	28	52.63380219	-07	53	46.3583709	.07150604	.8081661	0.9998	53572.5	53572.5	1			
2227-088	P 2227-08	596	22	29	40.08433882	-08	32	54.4355965	.00000351	.0000542	-0.0766	47254.8	56776.4	314	1.33	1.10	1.6
2227+009	2227+009	2212	22	29	51.80193944	+01	14	56.7230708	.00006220	.0011165	0.2264	53125.6	53125.7	1			
2227-136	2227-136	2213	22	30	15.30603013	-13	25	42.9010912	.00003266	.0011615	-0.4472	53560.4	53560.4	1			
2229+695	2229+695	694	22	30	36.46975647	+69	46	28.0769169	.00000366	.0000507	-0.0234	46337.1	56782.1	416	0.51		2.6
2227-399	P 2227-399	597	22	30	40.27857028	-39	42	52.0666263	.00001962	.0005834	-0.0259	49790.1	53658.3	5		0.11	3.8
2227-445	2227-445	3938	22	30	56.44293117	-44	16	29.8924229	.00003542	.0010398	-0.2326	55371.4	55371.5	1			
2228-146	2228-146	2214	22	31	39.62620900	-14	22	22.9724828	.00005298	.0020159	0.2884	53561.4	53561.5	1			
2229-172	2229-172	2215	22	32	22.56457164	-16	59	1.8917017	.00003017	.0003837	-0.0179	50631.3	54643.2	2			
2230+114	CTA 102	599	22	32	36.40890501	+11	43	50.9040054	.00000433	.0000791	-0.1780	43809.4	56638.5	230	1.46	1.89	4.2
2231+425	2231+425	3939	22	33	32.40650879	+42	45	39.9246507	.00004278	.0008168	0.1383	50242.5	50242.5	1			
2231+098	2231+098	3940	22	33	58.45032803	+10	08	52.1155593	.00010066	.0018577	-0.0760	49914.4	49914.5	1			
2232-211	2232-211	3941	22	34	57.44032431	-20	55	3.2378767	.00006529	.0016469	-0.7039	50631.3	50688.2	2			
2232-488	P 2232-488	973	22	35	13.23658072	-48	35	58.7944349	.00000887	.0001279	0.0364	48757.0	56776.2	49			
2233-186	2233-186	2216	22	35	56.17042141	-18	26	12.5558404	.00005493	.0022131	-0.6178	54088.0	55042.4	2			
2233-173	2233-173	3942	22	36	9.52275453	-17	06	21.9728449	.00001510	.0004887	-0.1808	50631.3	50631.4	1			
2234+282	GC 2234+28	601	22	36	22.47085070	+28	28	57.4132191	.00000338	.0000512	0.0437	44202.9	56770.4	1538	0.53	0.56	2.4
2233-234	2233-234	2217	22	36	26.23868698	-23	09	26.5975260	.00001878	.0006795	-0.2113	53572.4	56463.5	2	0.07	0.13	
2233-148	P 2233-148	600	22	36	34.08714864	-14	33	22.1894593	.00000999	.0001658	-0.7847	48196.2	54184.9	62	0.22	0.33	3.3
2235+731	2235+731	974	22	36	38.59703156	+73	22	52.6623671	.00001241	.0000738	0.2136	49826.6	55342.6	107	0.07		3.2
2234+420	J2237+42	3943	22	37	4.20975126	+42	16	48.2622930	.00002524	.0004657	0.0389	54111.8	54112.0	1			
2234-253	2234-253	2218	22	37	18.35536246	-25	06	32.5177780	.00023068	.0071034	0.4150	53560.4	53560.4	1			
2235+071	2235+071	2219	22	38	10.39570496	+07	24	13.9857579	.00001408	.0004181	-0.1859	53561.4	53561.5	1			
2235+275	2235+275	2220	22	38	12.87362478	+27	49	52.7736434	.00002349	.0004589	-0.2510	53572.3	53572.5	1			
2236+678	2236+678	2221	22	38	15.02922593	+68	04	59.7623959	.00004663	.0002124	-0.2023	49826.7	56701.6	7			
2236+124	2236+124	3944	22	38	34.60485132	+12	42	50.7819998	.00002575	.0007476	-0.4405	50084.9	50155.8	2			
2236-572	2236-572	3945	22	39	12.07589915	-57	01	0.8393661	.00001455	.0001674	0.1492	53222.8	56636.7	21			
2236-221	2236-221	3946	22	39	23.71688937	-21	53	15.4387796	.00003051	.0009970	0.0232	53560.4	55916.0	2			
2238+512	2238+512	3947	22	40	19.87840368	+51	33	11.7964252	.00006412	.0007177	-0.5088	49576.3	50305.5	2			
2238+410	2238+410	1189	22	41	7.20523419	+41	20	11.6185113	.00002260	.0006285	-0.1403	50242.5	50242.5	1		0.07	
2238-362	2238-362	2222	22	41	48.31140233	-35	59	47.7795785	.00003263	.0012518	0.0390	54942.8	54943.7	1			
2239+096	2239+096	1296	22	41	49.71730865	+09	53	52.4447444	.00001016	.0001482	0.2075	49914.4	56568.7	9	0.28	0.23	
2239-631	2239-631	3948	22	43	7.83927682	-62	50	57.3227325	.00003807	.0004188	0.3210	53222.8	54578.2	9			
2240-064	2240-064	4120	22	43	8.76078313	-06	09	2.5679618	.00002793	.0009137	-0.3029	56463.4	56463.6	1			
2240-260	2240-260	3949	22	43	26.40878302	-25	44	30.6875067	.00001750	.0005269	-0.3774	50631.3	50688.2	2			
2241+406	2241+406	3950	22	44	12.73110362	+40	57	13.6213411	.00004132	.0007187	-0.3601	50242.5	50242.5	1			
2242+257	2242+257	2223	22	44	35.14735434	+26	00	20.7027995	.00009540	.0010993	-0.6027	53572.4	53572.5	1			
2242+031	2242+031	3951	22	45	28.28473917	+03	24	8.8637141	.00001444	.0004340	0.0199	49914.4	49914.5	1			

Source Name		ID No.	Right Ascension			Declination			RA Error (s)	Dec. Error (arcsec)	RA–Dec Corr.	Observation Epoch MJD		No. Obs.	Source Flux (Jy)		Str Index
B1950	Common		H	M	S	D	M	S				First	Last		10-60	10-40	
2243-081	2243-081	2224	22	45	49.00380237	-07	55	19.3816406	.00002656	.0008547	-0.4155	53560.4	53560.5	1			
2243+047	2243+047	2225	22	45	53.65411825	+05	00	56.9621457	.00000518	.0001023	0.0785	49914.4	56770.0	47			
2243-123	OY-172.6	605	22	46	18.23197408	-12	06	51.2777289	.00000342	.0000557	-0.0823	43809.2	56638.5	1066	1.09	0.74	3.8
2244-372	2244-372	1190	22	47	3.91732235	-36	57	46.3039807	.00000922	.0001185	-0.2512	52676.0	56706.1	34		0.52	
2244-002	2244-002	3952	22	47	30.19597841	+00	00	6.4629261	.00001019	.0003376	-0.3385	50575.6	50575.7	1			
2245+471	2245+471	2226	22	47	51.81694466	+47	23	7.7688623	.00020524	.0029578	0.3631	53133.5	53133.6	1			
2245-091	2245-091	2227	22	47	52.19292084	-08	50	22.0818500	.00014827	.0040929	0.2299	53561.4	53561.5	1			
2245-128	2245-128	3953	22	47	52.64103639	-12	37	19.7214906	.00001794	.0005771	0.0507	50575.6	55847.3	2	0.36	0.58	
2245+029	P 2245+029	3954	22	47	58.68207040	+03	10	42.3533802	.00002052	.0005870	-0.0720	49914.4	49914.5	1			
2245-059	2245-059	3955	22	48	0.08053663	-05	41	18.2181735	.00003624	.0012490	-0.7622	50575.6	50575.7	1			
2246+370	2246+370	1191	22	48	37.91047437	+37	18	12.4621339	.00001896	.0005262	-0.1408	50242.5	50242.5	1			
2245-328	P 2245-328	608	22	48	38.68573220	-32	35	52.1881266	.00000872	.0001064	-0.5477	43809.2	56615.4	76		0.52	2.8
2246+208	2246+208	1192	22	49	0.56672854	+21	07	2.8357232	.00000992	.0002674	0.2260	50084.9	52975.3	4			
2246-309	2246-309	2228	22	49	19.04183199	-30	39	12.6317427	.00003190	.0009351	-0.6630	53125.6	53125.6	1			
2247+132	2247+132	3956	22	49	44.94685740	+13	31	9.4793714	.00033450	.0043867	-0.4249	50084.9	50155.8	2			
2247+113	2247+113	3957	22	49	54.58600266	+11	36	30.8457520	.00008729	.0016981	0.1711	52408.7	52409.4	1			
2247-131	2247-131	3958	22	49	59.61250900	-12	51	16.8250345	.00007672	.0037016	-0.5685	50575.6	50575.7	1			
2248+555	J2250+5550	1193	22	50	42.85102658	+55	50	14.5814190	.00004734	.0006081	-0.2023	49576.3	49576.5	1			
2247-283	2247-283	3959	22	50	44.49237688	-28	06	39.3301993	.00001601	.0007228	0.1627	54088.0	54088.0	1			
2249-210	2249-210	2229	22	52	28.68049540	-20	47	31.5380780	.00009546	.0034141	-0.0654	53560.4	53560.5	1			
2251+704	2251+704	3960	22	52	48.16028284	+70	43	15.8241457	.00122261	.0019980	0.3300	49826.6	49826.6	1			
2250+190	2250+190	975	22	53	7.36917494	+19	42	34.6286484	.00000380	.0000650	-0.0352	50084.9	56701.7	87	0.47	0.33	2.3
2250+323	2250+323	2230	22	53	12.49981545	+32	36	4.3260868	.00002995	.0006562	-0.2721	53561.5	53561.6	1			
2250+023	2250+023	2231	22	53	21.10447752	+02	36	13.0411457	.00009600	.0020917	0.0470	53560.4	53560.5	1			
2251+158	3C 454.3	611	22	53	57.74794281	+16	08	53.5609052	.00000358	.0000589	-0.1969	43809.3	56686.5	561	1.23	1.47	3.7
2251+006	2251+006	3961	22	54	4.40615363	+00	54	20.9528680	.00004589	.0011012	-0.3381	49914.4	49914.5	1			
2251+244	2251+244	3962	22	54	9.34191035	+24	45	23.4222240	.00001760	.0005377	-0.1928	50219.6	50219.7	1			
2251+134	2251+134	2232	22	54	21.01622476	+13	41	48.6756904	.00000939	.0002721	-0.1575	53133.7	53134.5	1			
2252+618	2252+618	3963	22	54	25.29278955	+62	09	38.7188297	.00050272	.0029872	-0.2884	52409.4	55538.2	2			
2252-090	P 2252-089	614	22	55	4.23979881	-08	44	4.0216485	.00000624	.0001133	-0.4439	47393.4	55545.3	56	0.16	0.20	
2253+417	GC 2253+41	615	22	55	36.70784840	+42	02	52.5326411	.00000548	.0000880	-0.1238	44263.8	56770.4	127	0.62	0.46	3.6
2253-278	2253-278	3964	22	56	0.15574151	-27	35	56.1196566	.00004604	.0017721	0.5742	50631.3	50688.2	2			
2253+227	2253+227	3965	22	56	10.67515600	+23	01	45.1811637	.00006327	.0013317	0.2521	54111.9	55966.0	2			
2254-204	2254-204	3966	22	56	41.20771211	-20	11	40.5092416	.00001375	.0004349	-0.1972	50631.3	50688.2	2			
2254-367	2254-367	3967	22	57	10.60678007	-36	27	43.9966692	.00011532	.0026070	-0.4408	52305.9	53138.1	4			
2254+074	GC 2254+07	617	22	57	17.30312167	+07	43	12.3024116	.00000416	.0000836	-0.0793	47409.2	56653.6	92	0.33	0.23	2.2
2254+024	P 2254+024	616	22	57	17.56309679	+02	43	17.5116545	.00000496	.0001053	-0.4182	47254.8	56192.1	69	0.31	0.32	1.0
2255+570	2255+570	3968	22	57	22.04596021	+57	20	30.1938324	.00026159	.0049536	-0.4602	52409.4	52409.5	1			
2255+416	2255+416	3969	22	57	22.07287343	+41	54	16.5302119	.00003012	.0009471	-0.3867	50242.5	50242.5	1			
2255-282	P 2255-282	619	22	58	5.96288162	-27	58	21.2568638	.00000349	.0000550	0.2311	47415.3	56776.2	1421		1.59	1.9
2256+017	2256+017	3970	22	58	57.75255375	+02	03	42.2896029	.00015521	.0032684	-0.7594	49914.4	49914.5	1			
2256+570	2256+570	2233	22	58	57.94117903	+57	19	6.4636323	.00006005	.0004082	0.2970	53125.5	53125.7	1			
2256-084	2256-084	2234	22	59	0.68884827	-08	11	3.0457700	.00001847	.0006640	-0.3358	53572.4	56204.3	2		0.08	
2256-296	2256-296	3971	22	59	29.93350558	-29	20	43.7989476	.00002226	.0007002	0.0514	52409.6	52409.6	1			
2257+103	2257+103	2235	23	00	18.31253972	+10	37	54.0833829	.00002429	.0008315	-0.5121	53560.5	53560.5	1			
2257-270	2257-270	3972	23	00	25.50071910	-26	44	22.7807173	.00002729	.0009841	-0.3038	50631.3	50688.2	2			
2258+033	2258+033	3973	23	00	40.88577763	+03	37	10.8391250	.00003863	.0011059	0.1615	49914.4	49914.5	1			
2258+166	2258+166	1194	23	00	42.99114198	+16	55	14.3913172	.00001564	.0002640	-0.0002	52408.7	52765.6	3			
2258-022	2258-022	3974	23	01	7.97846401	-01	58	4.5859412	.00000939	.0002982	-0.2225	50575.6	50575.7	1			
2259+568	2259+568	3975	23	01	26.62694384	+57	06	25.5091007	.00047313	.0034300	-0.0480	49826.6	49826.7	1			

Source Name		ID No.	Right Ascension			Declination			RA Error (s)	Dec. Error (arcsec)	RA–Dec Corr.	Observation Epoch MJD		No. Obs.	Source Flux (Jy)		Str Index
B1950	Common		H	M	S	D	M	S				First	Last		10-60	10-40	
2259+371	2259+371	3976	23	01	27.73737546	+37	26	49.2424161	.00001962	.0006680	-0.2234	50242.6	50242.6	1			
2259+058	2259+058	2236	23	01	53.46117734	+06	09	12.8210432	.00002071	.0004887	-0.2946	49914.4	54643.6	2			
2259-375	2259-375	3977	23	02	23.88887698	-37	18	6.8318259	.00053395	.0094240	-0.1343	49329.4	56638.0	4			
2300+638	2300+638	1195	23	02	41.31501281	+64	05	52.8490038	.00002740	.0003015	0.0188	49826.6	54087.9	3			
2300-189	2300-189	3978	23	03	2.97599011	-18	41	25.8222455	.00001927	.0006849	0.4802	50631.3	50688.3	2			
2300+386	2300+386	3979	23	03	4.06581357	+38	53	48.3657633	.00002266	.0006712	-0.2820	50242.6	50242.6	1			
2300-307	P 2300-307	3980	23	03	5.82080139	-30	30	11.4712803	.00015205	.0038717	0.3653	48110.5	52305.9	2			
2300+142	2300+142	3981	23	03	9.95278570	+14	31	41.3538705	.00002420	.0006713	0.0379	54111.9	54112.0	1			
2300-683	2300-683	3982	23	03	43.56460707	-68	07	37.4432453	.00000857	.0000724	-0.0341	52970.6	56687.7	103			
2301-103	2301-103	3983	23	03	57.91951514	-10	02	19.2152456	.00006752	.0026906	0.3416	53561.5	56638.1	2			
2301+060	2301+060	3984	23	04	28.29128908	+06	20	8.3076219	.00002811	.0010686	-0.4633	49914.4	54482.5	2			
2302+232	2302+232	1196	23	04	36.43640354	+23	31	7.6109163	.00000840	.0002201	-0.2433	50084.9	53362.1	21			
2304+824	2304+824	2237	23	05	17.53967683	+82	42	49.1563789	.00026428	.0009682	0.1087	53560.3	53560.5	1			
2303-052	2303-052	3985	23	06	15.31708964	-04	59	48.2850598	.00001953	.0006124	-0.2223	50575.6	50575.7	1			
2304+377	2304+377	3986	23	07	0.99503844	+38	02	42.2302389	.00030707	.0038472	-0.1683	50242.6	54314.4	2			
2304+322	2304+322	3987	23	07	15.91256847	+32	30	31.9365948	.00002196	.0004377	-0.4856	50219.6	50219.7	1			
2305+145	2305+145	3988	23	07	34.00170736	+14	50	17.9759618	.00012606	.0018635	0.6282	50084.9	56302.0	2			
2304-230	2304-230	3989	23	07	38.65483961	-22	47	52.9949686	.00001872	.0005753	0.0149	50631.3	50688.3	2			
2305+198	2305+198	3990	23	08	11.63648906	+20	08	42.1946947	.00005343	.0009541	0.0088	50084.9	50155.9	2			
2306+095	2306+095	2238	23	08	44.17162252	+09	46	26.1112292	.00001446	.0004726	0.0008	53125.6	53125.6	1	0.22	0.19	
2306-312	2306-312	2239	23	09	14.33140087	-30	59	12.5842244	.00001490	.0003339	-0.0895	53125.6	54362.1	11			
2307+680	2307+680	3991	23	09	26.66606015	+68	20	10.7564582	.00006682	.0003635	-0.0403	49826.6	54087.9	2			
2307+106	2307+106	2240	23	10	28.51773727	+10	55	30.6966614	.00000398	.0000715	-0.0298	49914.4	56758.4	104			
2308+341	2308+341	3992	23	11	5.32879976	+34	25	10.9050844	.00001185	.0002640	-0.2326	52408.7	52409.6	1			
2309+454	J2311+4543	1197	23	11	47.40897236	+45	43	56.0166395	.00000418	.0000620	-0.0705	50305.4	56776.3	181	0.36	0.42	
2310+724	2310+724	3993	23	12	19.69785983	+72	41	26.9172874	.00007394	.0005351	0.0711	49826.6	49826.7	1			
2310+385	2310+385	3994	23	12	58.79401910	+38	47	42.6604176	.00006023	.0008267	0.3658	50242.6	50242.6	1			
2311-477	2311-477	3995	23	13	51.89993145	-47	29	11.7222722	.00059708	.0027228	0.2509	52886.8	53138.7	2			
2311-373	2311-373	3996	23	13	59.70823318	-37	04	46.2181120	.00003636	.0016047	0.3772	55112.1	55112.2	1			
2311-452	P 2311-452	625	23	14	9.38274628	-44	55	49.2375201	.00005563	.0012486	-0.3678	49329.4	52948.4	5		0.09	
2312-319	P 2312-319	626	23	14	48.50057920	-31	38	39.5265103	.00000819	.0001455	-0.2103	48110.5	55728.7	29		0.39	3.1
2313-182	2313-182	3997	23	15	48.13584562	-18	00	40.2217667	.00358598	.0603360	0.8505	50631.3	50631.4	1			
2316+862	2316+862	1198	23	15	49.81955563	+86	31	43.5958204	.00091166	.0006978	0.3109	53560.3	53560.5	1			
2313-439	2313-439	3998	23	16	21.09979715	-43	37	46.9041614	.00023722	.0152852	0.2411	52305.9	52409.6	2			
2314-340	2314-340	1297	23	16	43.38634689	-33	49	12.4854166	.00003187	.0003502	-0.2443	52305.9	55545.5	14			
2314-409	2314-409	3999	23	16	46.91988351	-40	41	21.0865826	.00003133	.0004571	-0.2847	54601.6	56568.7	5			
2314-182	2314-182	4000	23	17	25.25229728	-17	56	18.0705125	.00267168	.5909523	0.9379	54111.9	54111.9	1			
2315+287	2315+287	2241	23	17	41.56200961	+29	02	22.7694552	.00007561	.0009054	-0.4365	53561.5	53561.6	1			
2315-404	2315-404	4001	23	18	6.86207077	-40	10	6.2199981	.00013353	.0066974	-0.8335	53503.7	53503.7	1			
2315-172	2315-172	2242	23	18	11.36140877	-16	59	29.1878822	.00001922	.0006537	-0.0291	53552.5	53572.5	2	0.09	0.08	
2316+238	2316+238	4002	23	18	33.96785154	+24	04	39.7494620	.00001060	.0002543	0.0002	54111.9	56638.2	5	0.08	0.10	
2318+049	GC 2318+04	627	23	20	44.85659791	+05	13	49.9524444	.00000343	.0000528	-0.1085	47254.8	56776.5	938	0.65	0.64	2.6
2318+182	2318+182	2243	23	20	46.77597532	+18	29	25.7753524	.00002975	.0008255	0.2565	53560.5	53560.5	1			
2318-087	2318-087	4003	23	21	18.25023763	-08	27	21.5215877	.00002206	.0006683	0.1282	50575.6	55784.6	2			
2319+317	2319+317	2244	23	21	54.95599199	+32	04	7.6225488	.00000369	.0000569	0.0295	53125.6	56776.5	158			
2319+272	B2 2319+27	629	23	21	59.86222881	+27	32	46.4436192	.00000451	.0000809	-0.0728	48103.2	56638.6	75	0.46	0.30	3.1
2320+689	2320+689	2245	23	22	9.04525615	+69	11	3.4168589	.00006778	.0004774	-0.1409	53125.6	53133.7	2			
2319+444	J2322+4445	1199	23	22	20.35808728	+44	45	42.3536082	.00000467	.0000732	0.0408	50305.4	56749.7	53			
2320+506	2320+506	977	23	22	25.98218648	+50	57	51.9636971	.00000484	.0000725	0.0862	48719.9	56691.3	134	0.37		3.6
2319+184	2319+184	1200	23	22	28.56882765	+18	43	24.8986574	.00002808	.0005728	0.4446	50084.9	50155.9	2			

Source Name		ID No.	Right Ascension			Declination			RA Error (s)	Dec. Error (arcsec)	RA–Dec Corr.	Observation Epoch MJD		No. Obs.	Source Flux (Jy)		Str Index
B1950	Common		H	M	S	D	M	S				First	Last		10-60	10-40	
2320+079	2320+079	4004	23	22	36.08941313	+08	12	1.5916409	.00003687	.0008247	-0.2946	49914.5	49914.5	1			
2320-021	2320-021	4005	23	23	4.62986976	-01	50	48.1130463	.00004094	.0009544	0.2256	50575.6	50575.7	1			
2320-035	P 2320-035	633	23	23	31.95375897	-03	17	5.0239760	.00000467	.0000928	-0.5209	44202.9	56633.0	186	0.69	0.68	3.2
2321-065	2321-065	2246	23	23	39.11375721	-06	17	59.2401473	.00002209	.0007621	0.2908	53561.5	55784.6	2			
2321-164	2321-164	2247	23	23	44.63149040	-16	12	52.1250390	.00010831	.0024023	0.2169	53572.4	53572.5	1			
2321-375	2321-375	1201	23	24	7.11180488	-37	14	22.4556708	.00001367	.0001925	-0.0441	52305.9	54362.0	14			
2321-215	2321-215	4006	23	24	28.05632534	-21	19	0.4959749	.00005788	.0016299	0.2120	53560.5	55615.9	2			
2322-411	2322-411	4007	23	25	3.37941644	-40	51	30.0988516	.00064445	.0157412	0.4337	52409.6	55168.1	2			
2322+396	2322+396	2248	23	25	17.86983881	+39	57	36.5078890	.00004922	.0006739	-0.3359	55042.3	55042.6	1			
2323+478	2323+478	4008	23	25	44.91239811	+48	06	25.2877307	.00053170	.0033622	-0.8213	50305.4	50305.5	1			
2323+009	2323+009	4009	23	26	25.64383360	+01	12	8.6894346	.00025313	.0056537	-0.8319	49914.4	49914.5	1			
2324-023	2324-023	1298	23	26	53.77684191	-02	02	13.7817186	.00027956	.0017028	0.4676	53767.8	53768.6	1			
2325+799	2325+799	2249	23	27	6.42551007	+80	12	58.9346226	.00011268	.0004377	-0.4392	53572.4	53572.6	1			
2324+151	2324+151	4010	23	27	21.96605716	+15	24	37.3110662	.00001296	.0003566	-0.1178	50084.9	56498.5	5			
2325+093	2325+093	1299	23	27	33.58056003	+09	40	9.4627834	.00000628	.0001086	-0.0448	49914.4	56749.7	13	0.81	0.72	
2325+152	2325+152	2250	23	27	35.98491514	+15	33	9.5745498	.00003126	.0007918	-0.1772	53561.5	53561.6	1			
2325-150	P 2325-150	634	23	27	47.96426637	-14	47	55.7514615	.00000614	.0001506	-0.1307	49960.4	54362.1	16	0.24	0.21	2.5
2325+764	2325+764	2251	23	27	52.82253226	+76	43	8.6432965	.00030314	.0018946	0.3019	53523.5	53523.6	1			
2325+192	2325+192	2252	23	28	24.87479464	+19	29	58.0298355	.00018787	.0022663	0.6162	53560.4	53560.5	1			
2326+082	2326+082	4011	23	29	5.78674864	+08	34	15.8536787	.00003583	.0012349	-0.4208	49914.4	49914.6	1			
2326-477	P 2326-477	978	23	29	17.70434850	-47	30	19.1149287	.00000840	.0001315	0.2258	47304.8	56713.5	46			
2327+335	J2330+3348	1202	23	30	13.73766843	+33	48	36.4712422	.00001158	.0002911	-0.2781	50219.6	50219.7	1			
2327-376	2327-376	4012	23	30	35.79573641	-37	24	37.9620566	.00002398	.0008800	-0.4136	55168.0	55168.1	1			
2327-459	2327-459	4013	23	30	37.68051717	-45	39	58.1043306	.00026365	.0093522	0.7084	52305.9	52305.9	1			
2328+107	P 2328+10	636	23	30	40.85226428	+11	00	18.7095193	.00000881	.0001786	-0.5956	48196.3	54184.9	34	0.45	0.43	3.9
2328+316	2328+316	4014	23	30	46.15998116	+31	55	33.5073742	.00002157	.0005448	-0.1896	50219.6	50219.7	1			
2329-162	P 2329-16	638	23	31	38.65244356	-15	56	57.0097822	.00000510	.0001056	-0.1041	50258.6	56638.6	34	0.13	0.12	3.7
2329+451	2329+451	4015	23	31	48.97150087	+45	22	48.9390204	.05707382	.2402795	-0.9844	50305.5	50305.5	1			
2329-384	P 2329-384	639	23	31	59.47615375	-38	11	47.6505976	.00000916	.0001574	-0.1299	48110.5	56749.7	25			
2329-415	2329-415	4016	23	32	19.04827020	-41	18	37.5826867	.00002981	.0005015	-0.0449	54601.6	56568.7	5			
2330+083	P 2330+083	4017	23	32	57.59623862	+08	38	10.4264614	.00004864	.0009396	-0.1683	49914.4	49914.6	1			
2330+387	2330+387	4018	23	33	2.53340766	+39	01	12.0488441	.00003638	.0008496	-0.0875	50242.6	50242.7	1			
2330-017	2330-017	4019	23	33	16.68837152	-01	31	7.3867095	.00002263	.0007160	0.2374	50575.6	50575.7	1			
2331-240	2331-240	979	23	33	55.23781705	-23	43	40.6581273	.00000808	.0001361	-0.6331	48196.2	54184.9	54	0.22	0.59	3.5
2331+073	2331+073	4020	23	34	12.82815701	+07	36	27.5511448	.00000706	.0002036	0.0956	49914.4	54111.9	3			
2332-293	2332-293	4021	23	35	18.72710805	-29	07	16.6104663	.00006972	.0036030	0.2978	50688.3	50688.3	1			
2332-017	2332-017	4022	23	35	20.41206246	-01	31	9.5919434	.00002682	.0006185	0.2797	50575.6	50575.7	1			
2333-528	P 2333-528	980	23	36	12.14453892	-52	36	21.9507710	.00010621	.0012635	0.2996	48110.3	56111.7	5			
2333-415	2333-415	1300	23	36	33.98507218	-41	15	21.9842041	.00001060	.0001813	-0.1140	53222.8	56574.5	31			
2335-181	2335-181	4023	23	37	56.62777216	-17	52	20.4108810	.00002941	.0011396	-0.0768	50631.3	54482.7	2			
2335-027	P 2335-027	644	23	37	57.33907120	-02	30	57.6293280	.00000388	.0000670	-0.0602	47381.3	56763.3	217	0.38	0.31	3.0
2335+267	NGC 7720	2253	23	38	29.38323148	+27	01	53.2583208	.00005386	.0007210	-0.3004	53067.8	53068.7	1			
2336+598	2336+598	4024	23	39	21.12520398	+60	10	11.8493657	.00002430	.0001952	-0.1548	52408.7	56393.6	4			
2336+024	2336+024	2254	23	39	29.71054951	+02	44	5.3553842	.00015697	.0055087	-0.5524	53152.5	53152.6	1			
2337-234	2337-234	2255	23	39	53.57723949	-23	10	39.2257847	.00019443	.0071880	0.6175	53561.5	53561.5	1			
2337-334	P 2337-334	4025	23	39	54.53520918	-33	10	16.8819843	.00005264	.0018073	-0.7219	52305.9	52306.0	1			
2337-011	2337-011	2256	23	40	23.67011794	-00	53	26.9998955	.00019701	.0035942	0.4697	53572.4	53572.5	1			
2337+264	GC 2337+26	647	23	40	29.02947938	+26	41	56.8045337	.00001544	.0002907	-0.0235	49177.2	51927.3	9			
2338+330	2338+330	2257	23	40	57.29949275	+33	19	2.6216592	.00001903	.0003488	0.2361	53133.6	53133.7	1			
2338+000	2338+000	4026	23	41	6.90983412	+00	18	33.3371826	.00005064	.0011459	0.2038	49914.6	55847.3	2			

Source Name		ID No.	Right Ascension			Declination			RA Error (s)	Dec. Error (arcsec)	RA–Dec Corr.	Observation Epoch MJD		No. Obs.	Source Flux (Jy)		Str Index
B1950	Common		H	M	S	D	M	S				First	Last		10-60	10-40	
2338+191	2338+191	2258	23	41	18.79617648	+19	28	5.4863825	.00003766	.0005992	-0.4268	50084.9	54643.5	3			
2338-295	2338-295	4141	23	41	29.76237351	-29	19	15.0387299	.00003279	.0011853	0.0053	55916.0	55916.0	1			
2340-226	2340-226	2259	23	42	47.98368755	-22	23	40.2021841	.00017241	.0053189	0.0902	53561.5	53561.5	1			
2340+233	J2343+2339	1203	23	43	12.38702736	+23	39	45.6476146	.00001534	.0003462	-0.0604	50084.9	53020.0	4			
2341+154	2341+154	4027	23	43	42.74911590	+15	43	2.9786728	.00004927	.0015881	-0.2667	53502.7	53572.4	2			
2341+697	2341+697	2260	23	43	43.73432037	+70	03	19.4068558	.00009729	.0008415	-0.5794	53560.3	54087.9	2			
2342+821	2342+821	4028	23	44	3.77160301	+82	26	40.4005368	.00275156	.0034186	0.0285	52408.9	52409.4	1			
2341+295	2341+295	4029	23	44	22.55207126	+29	52	20.6990589	.00065572	.0041959	0.1638	53523.5	53523.6	1			
2342-161	2342-161	2261	23	45	12.46231348	-15	55	7.8344572	.00001286	.0004416	-0.2313	53552.5	53552.5	1			
2344+092	P 2344+09	649	23	46	36.83854829	+09	30	45.5147403	.00000572	.0001177	-0.2427	48196.3	56633.0	43	0.31	0.27	3.4
2344+068	2344+068	4030	23	46	39.93322129	+07	05	6.8451039	.00060199	.0044250	-0.1748	49914.4	49914.6	1			
2344+299	2344+299	1204	23	46	46.25077571	+30	11	59.2494000	.00007455	.0014608	-0.4747	53502.7	53503.6	1			
2344+514	2344+514	4031	23	47	4.83675832	+51	42	17.8811935	.00011786	.0011104	-0.5896	53572.5	54112.1	2			
2344-192	2344-192	4032	23	47	8.62669350	-18	56	18.8578765	.00004800	.0014310	0.1139	50631.3	50688.3	2			
2344-514	2344-514	4033	23	47	19.86409093	-51	10	36.0652857	.00001399	.0002224	0.3757	53222.9	56504.0	15			
2344+429	2344+429	2262	23	47	22.87425064	+43	10	53.2189502	.00003029	.0004115	-0.3508	50242.6	54643.1	2			
2345+270	2345+270	2263	23	47	35.17488456	+27	19	1.4936367	.00001903	.0005035	-0.3653	53561.5	53561.6	1			
2345-167	P 2345-16	651	23	48	2.60852123	-16	31	12.0223367	.00000546	.0000998	-0.5754	43809.2	56600.7	201	0.61	1.02	3.8
2345-047	2345-047	2264	23	48	11.75773504	-04	25	56.3818956	.00001130	.0003758	-0.0953	53523.6	53560.5	2			
2346+385	2346+385	4034	23	49	20.82653491	+38	49	17.5584776	.00001018	.0001955	-0.0847	50242.6	56749.7	2	0.41	0.35	
2346+052	J2349+0534	1205	23	49	21.05151068	+05	34	39.8724477	.00001286	.0004069	-0.0082	49914.4	53152.6	2			
2347+108	2347+108	4035	23	50	2.03086978	+11	06	36.7040108	.00007455	.0018442	0.1280	49914.4	49914.6	1			
2347+079	2347+079	2265	23	50	10.07933604	+08	12	55.2782439	.00018065	.0027035	0.0429	53561.5	53561.6	1			
2348-432	2348-432	4036	23	51	34.94588184	-42	59	33.4877845	.00005497	.0016271	0.1977	55112.2	55112.2	1			
2349-223	2349-223	2266	23	51	46.00682256	-22	03	9.6597887	.00002923	.0009806	-0.0475	53572.5	53572.5	1			
2349-014	2349-014	2267	23	51	56.12274772	-01	09	13.3159743	.00057679	.0122823	-0.2322	54292.4	54292.6	1			
2350+395	2350+395	2268	23	52	48.90729309	+39	47	56.2237419	.00002622	.0006082	-0.1983	53560.5	53560.5	1			
2350+704	2350+704	4037	23	52	52.85422711	+70	44	48.3267107	.00072575	.0046354	0.8206	49826.6	49826.7	1			
2350-280	2350-280	2269	23	53	11.45916792	-27	43	25.6208396	.00492756	.1937187	0.6592	54818.0	54818.0	1			
2351+550	J2353+5518	1206	23	53	42.29977491	+55	18	40.6673792	.00004993	.0007042	0.0405	49826.6	49826.7	1			
2351-309	2351-309	4038	23	53	47.45885761	-30	37	48.5031507	.00001364	.0002207	-0.1875	53125.7	55545.4	14			
2351-006	2351-006	4039	23	54	9.17589247	-00	19	47.9557586	.00001733	.0005099	0.2874	50575.6	50575.7	1			
2351+456	2351+456	981	23	54	21.68023119	+45	53	4.2365438	.00000464	.0000689	0.0549	47941.2	56347.2	66	0.26	0.30	3.4
2351-154	2351-154	695	23	54	30.19517627	-15	13	11.2130421	.00000460	.0000903	-0.3491	47381.3	56763.5	118	0.39	0.50	2.5
2352-217	2352-217	2270	23	55	2.14654143	-21	25	36.7823215	.00004533	.0013685	0.5651	53552.5	53552.6	1			
2352+495	DA 611	656	23	55	9.45816096	+49	50	8.3391482	.00002203	.0002449	-0.3218	44203.0	51246.5	3			
2353-686	P 2353-68	982	23	56	0.68141439	-68	20	3.4718329	.00001501	.0001032	0.0720	48387.5	56763.7	41			
2353+816	2353+816	1252	23	56	22.79382009	+81	52	52.2552541	.00003955	.0000993	-0.1413	50687.3	56568.6	11	0.46		2.7
2354-251	2354-251	2271	23	57	23.85097053	-24	51	3.1640626	.00013991	.0047430	0.5827	53561.5	53561.5	1			
2354-021	2354-021	4040	23	57	25.13794350	-01	52	15.5092773	.00000883	.0002600	-0.1289	50575.6	56701.0	2	0.15	0.09	
2354-117	2354-117	4041	23	57	31.19756205	-11	25	39.1764171	.00000989	.0003421	-0.0957	50575.6	50575.7	1			
2355-534	P 2355-534	983	23	57	53.26606012	-53	11	13.6897268	.00001607	.0001984	0.1806	47626.2	56611.8	26			
2355-106	P 2355-106	658	23	58	10.88240351	-10	20	8.6114568	.00000354	.0000559	-0.1007	46337.1	56772.7	480	0.51	0.60	0.7
2355-291	2355-291	4042	23	58	16.97160320	-28	53	34.1044979	.00003047	.0009827	-0.1605	53560.5	56463.6	2			
2355+042	2355+042	2272	23	58	28.84694651	+04	30	24.8345154	.00003379	.0010696	0.3332	53572.4	53572.5	1			
2356+196	P 2356+196	4043	23	58	46.08513412	+19	55	20.3021633	.00001335	.0003728	0.1099	50084.9	54482.5	3			
2356+390	2356+390	4044	23	58	59.85518922	+39	22	28.3057732	.00002368	.0004717	-0.2596	50242.6	50242.7	1			
2356+385	GC 2356+38	660	23	59	33.18080185	+38	50	42.3182891	.00000346	.0000525	-0.0403	50242.6	56751.7	939	0.57		1.9
2357-318	2357-318	2273	23	59	35.49153947	-31	33	43.8246598	.00000504	.0000978	-0.1617	52408.7	56734.5	113		0.29	

3 References

1. Sovers, O. J., J. L. Fanselow, and C. S. Jacobs, "Astrometry and Geodesy with Radio Inteferometry: Experiments, Models, Results," *Reviews of Modern Physics, Vol. 70, No. 4*, The American Physical Society, October, 1998. http://link.aps.org/doi/10.1103/RevModPhys.70.1393
2. Ma, C., E.F. Arias, G. Bianco, D. A. Boboltz, S.L. Bolotin, P. Charlot, G. Engelhardt, A.L. Fey, R.A. Gaume, A.−M. Gontier, R. Heinkelmann, C.S. Jacobs, S. Kurdubov, S.B. Lambert, Z.M. Malkin, A. Nothnagel, L. Petrov, E. Skurikhina, J. Sokolova, J. Souchay, O.J. Sovers, V. Tesmer, O.A. Titov, G. Wang, V. Zharov C. Barache, S. Boeckmann, A. Collioud, J.M. Gipson, D. Gordon, S.O. Lytvyn, D.S. MacMillan, R. Ojha, "IERS Technical Note No. 35: The Second Realization of the ICRF by VLBI," IERS, Bundesamt fur Kartographie und Geodasie, BKG, Frankfurt am Main, A. Fey, D. Gordon, and C.S. Jacobs, Eds. Germany, Oct. 2009. http://www.iers.org/nn_11216/IERS/EN/Publications/TechnicalNotes/tn35.html
3. Altamimi, Z., X. Collileux, and L. Metivier (2011). ITRF2008: an improved solution of the international terrestrial reference frame. *Journal of Geodesy*, doi: 10.1007/s00190−011−0444−4. https://link.springer.com/article/10.1007/s00190-011-0444-4
4. Boehm, J., B. Werl, H. Schuh, "Troposphere mapping functions for GPS and very long baseline interferometry from European Centre for Medium−Range Weather Forecasts operational analysis data", *J. Geophys. Res*., 111, B02406, Feb. 2006. https://agupubs.onlinelibrary.wiley.com/doi/full/10.1029/2005JB003629
5. Steigenberger, P, V. Tessmer, J. Boehm, "A priori gradients in the analysis of GPS and VLBI observations", IERS Workshop on Conventions, Paris, September 20−21 2007.http://www.bipm.org/utils/en/events/iers/Steigenberger.pdf
6. Ratcliff, J.T. and R.S. Gross, "Combinations of Earth Orientation Measurements: SPACE2010, COMB2010, and POLE2010," *JPL Publication 11−15*, Jet Propulsion Laboratory, Pasadena, CA, 2010.
7. Matthews, P.M., T.A. Herring, and B.A. Buffet, "Modeling of Nutation and Precession: New nutation series for Nonrigid Earth and Insights into the Earth's Interior," *J. Geophys. Res.* 107, no. B4, 10.1029/2001JB000390, Apr. 2002. www.agu.org/journals/jb/jb0204/2001JB000390/
8. IAU General Assembly XXVII, Resolution B3, Rio de Janeiro, Brazil, 13 August 2009. http://www.iau.org/static/resolutions/IAU2009_English.pdf
9. Kesteven, M. J. L. and A. H. Bridle, "Index of extragalactic radio−source catalogues", *J. Royal Astronomical Society of Canada*, Vol. 71, Feb. 1977, p. 21−39. http://articles.adsabs.harvard.edu//full/1977JRASC..71...21K/0000027.000.html
10. W. Schlüter, D. Behrend, "The International VLBI Service for Geodesy and Astrometry (IVS): current capabilities and future prospects", Journal of Geodesy, Vol. 81, Nos. 6–8, pp. 379–387, June 2007. doi: 10.1007/s00190-006-0131-z.

4 Acknowledgements

Production of the radio source catalog requires the efforts and cooperation of a large number of people. This includes the support staffs at the DSN and the antennas of the International VLBI Service [10] who ensure that the data are collected, the correlation and fringe fitting staffs, and the analysts who have developed the models and software to convert the delay and delay rate observations to produce final estimates of the source positions, and finally the authors of this document. Among these we would like to particularly acknowledge JPL employees Christine Chang, Christopher Jacobs, Christina King, Peter Kroger, Gabor Lanyi, Charles Naudet, Andrew Romero-Wolf, Ojars Sovers, and Alan Steppe.

The research was carried out at the Jet Propulsion Laboratory, California Institute of Technology, under a contract with the National Aeronautics and Space Administration (80NM0018D0004).

Deep Space Network

108
Ka-Band Radio Source Catalog

Document Owner:

Signature Provided 10/21/2020

Christopher S. Jacobs Date
DSN Reference Frame Calibration Task Lead
Califronia Institute of Technology,
Jet Propulsion Laboratory

Approved by:

Signature Provided 10/20/2020

Timothy T. Pham Date
DSN Communication System Chief Engineer

Prepared by:

Signature Provided 10/21/2020

Christopher S. Jacobs Date
DSN Reference Frame Calibration Task Lead

Released by:

Signature Provided 11/12/2020

DSN Release Authority Date
Christine Chang

DSN No. **810-005, 108**
Issue Date: November 12, 2020
JPL D-19379; CL#20-5791

Jet Propulsion Laboratory
California Institute of Technology

Users must ensure that they are using the current version in DSN Telecommunications Link Design Handbook website:
http://deepspace.jpl.nasa.gov/dsndocs/810-005/

Review Acknowledgment

By signing below, the signatories acknowledge that they have reviewed this document and provided comments, if any, to the signatories on the Cover Page.

Signature Provided	10/19/2020	Signature Provided	10/21/2020
Jeff Berner DSN Project Chief Engineer	Date	Alina Bedrossian Science System Engineer	Date

Signature Provided	10/21/2020
Peter Kroger DeltaDOR team	Date

Document Change Log

Rev	Issue Date	Prepared By	Paragraphs Affected	Change Summary
initial	11/12/2020	Christopher S. Jacobs, Peter Kroger, Christopher Volk	All (formatting) (Fluxes)	Initial Release of Ka-band catalog 810-005 module 108 was modeled after the X-band catalog document 810-005 module 107

Table of Contents

Illustrations

Figure **Page**

Tables

Table **Page**

1 Introduction

1.1 Purpose

This module provides a Ka-band (32 GHz) catalog of the angular positions of naturally occurring extra-galactic radio sources which establish a celestial reference frame to be used for interplanetary spacecraft navigation using Delta−Differential One−way Ranging (ΔDOR, Border, 2006) at Ka-band. The catalog is also useful for other applications requiring the precise location of radio sources most notably station locations as well as antenna pointing calibration, antenna arraying, and imaging.

This initial formal release of the Ka-band catalog is driven by the maturing of ΔDOR operations at Ka-band. Ka-band ΔDOR was first demonstrated in 2005 (Shambayati et al, 2006) with the Mars Reconaissance Orbiter (MRO). Today all three space agencies that are engaged in ΔDOR cross-support have Ka-band missions: the National Aeronautics and Space Administration's (NASA) Parker Solar Probe, the European Space Agency's (ESA) Bepi-Columbo, and Japanese Aerospace Exploration Agency's (JAXA) Hayabusa-2. All three of these missions are leveraging Ka-band's superior performance very close to the Sun where Ka-band cuts through solar plasma better than X-band or S-band. Ka-band ΔDOR has come of age.

1.2 Scope

The discussion in this module is limited to describing the contents of the Ka-band source catalog, assessing the accuracy of the positions, and providing a listing of that catalog both within the module and with a link to computer readable versions. The equipment used to collect the data from which the catalog is derived is discussed in module 211 of this handbook. The capabilities of the Deep Space Network (DSN) for performing ΔDOR are contained in module 210.

2 General Information

The angular positions of a set of extragalactic radio sources serve as fiducial points for ΔDOR observations performed by the DSN. This set of point positions is commonly referred to as a *catalog*. The catalog described in this module consists of 680 sources which have been observed in a frequency range that includes the Ka-band deep space allocation specified by the International Telecommunications Union of 31,800 – 32,300 MHz (Hunter, 1979; de Groot 1987). The angular distribution of the radio sources in the catalog is illustrated in Figure 1.

2.1 Desired Accuracy

The DSN goal for Ka-band calls for 0.5 nanoradian (100 µas) accuracy including both random and systematic errors. A stability of 0.05 nrad/year (10 µas/yr) is an implied goal in order to give the

catalog a reasonable lifetime. Note that in the field of astrometry typical units are microarcseconds (µas) where 1.0 nrad = 206 µas. The required spatial density is a source within 6 degrees.

2.2 Catalog Observations and Estimation Strategy

The data used to develop the source catalog were obtained from Ka−band Very Long Baseline Interferometry (VLBI) data with complementary X-band data used to calbrate the Earth's ionosphere and solar plasma. The data were first acquired with the DSN VLBI Subsystem's Mark4 Data Acquisition Terminal recording at 112 Mbps, then from about 2008, the Mark5A at 112 to 448 Mbps and since about 2013 with the DSN VLBI Processor (DVP) at 2048 Mbps. Starting in late 2012, ESA's Deep Space Antenna 3 (DSA 03) located at Malargüe, Argentina was added to the program using the Portable Radio Science Receiver (PRSR) which was upgraded to the Portable Open Loop Receiver (POLR) in 2019. The addition of DSA 03 enabled, for the first time, full sky coverage at Ka-band and in particular coverage of the southern polar cap from declination -45 to -90 degrees.

The angular positions of the radio sources are estimated by a monolithic least−squares fit to the VLBI observables: group delay and phase delay rate. A total of 110,551 delay and delay rate observations were collected in 206 single baseline observing sessions from April 2005 to March 2020 and then correlated. Of these processed observations, 88,173 were used in the final solution to estimate the final source positions. The weighted RMS (wRMS) delay scatter was 43.58 psec; phase delay rate wRMS scatter was 103.85 fsec/sec. About 11,300 parameters were adjusted most of which were to calibrate troposphere changes and instrumental delays. The majority of the 20.2% of the obserations that were not used were deleted because no signal was detected (SNR < 6.5) due to poor pointing at Ka-band and to a lesser extent due to antenna mechanical problems, recorder problems or inherently weak sources. Because the radio catalog monitors about 730 targets per observing day, one must use blind pointing. Time limitations prevent the use of conscan or monopulse techniques for real time pointing refinement. Accordingly, pointing errors due to thermal distortions of the DSN antennas and beamwaveguide mirror misalignments are not corrected. As a result, more than half the data are either not detected or are SNR limited.

Details of the physical modeling required by this procedure are given in (Sovers, Fanselow, & Jacobs, 1998). Estimated parameters included radio source positions, station locations & velocities, station clocks, wet troposphere delays, and troposphere gradients.

NNR: A 3-dimensional "No-Net-Rotation" constraint (Jacobs et al, 2010) was placed on the radio source positions relative to International Celestial Reference Frame 3 (ICRF3) (Charlot, Jacobs, et al, 2020) using a subset of 173 of the 303 defining sources.

TRF: The terrestrial Reference Frame (TRF) estimated station locations for DSS 34, DSS 54, DSS 55, and DSA 03 as linear functions over the time range of the data set with the Goldstone stations DSS 25 and 26 fixed from 2005 until July 2019 in order to provide a No-Net-Translation (NNT) constraint on the terrestrial reference frame. After the July 2019 Ridgecrest earthquake, the positions of DSS 25 and DSS 26 had to be estimated relative to the overseas stations. A priori

station locations and velocities were expressed in the ITRF-1993 system. Similarly, the velocities of the Goldstone stations DSS 25 and DSS 26 were fixed to their apriori ITRF-1993 values in order to provide a No-Net-Velocity (NNV) constraint.

EOP: A No-Net-Rotation constraint was enforced by fixing the earth orientation (UT1-UTC and Polar Motion) to JPL's "Space" series as determined by the JPL Kalman Earth Orientation Function (KEOF) (Ratclif & Gross, 2019). Earth precession and nutation models are taken from MHB-2000 (Mathews, Herring & Buffet, 2002). Time linear corrections to nutations in ecliptic longitude & obliquity, plus a 4 parameter correction to the Free Core Nutation (FCN) with period 431 days were estimated using the MODEST software package (Sovers, Fanselow, Jacobs, 1998).

Station clocks were estimated using a time linear model (offset and rate parameters). Hydrostatic a.k.a. "dry" troposphere delays were fixed to an apriori model based on measured surface pressures (Davis et al, 1985). Wet zenith troposphere delays were estimated at intervals of approximately once per 20 scans (~40 minutes) and then mapped to the elevation of the observation using the Vienna Mapping Function 1 (VMF1) mapping function (Boehm et al, 2006). A mean troposphere gradient was estimated once per station.

2.3 Results

The Ka-band celestial reference frame ("radio catalog") that resulted from the above described data and parameter estimation strategy is listed in Table 3. We are calling this catalog DDOR-2020a-Ka to indicate that it is the first Ka-band catalog constructed for DDOR users in 2020. Figure 1 shows the distribution of sources over the sky using a Hammer-Aitoff equal area plot. There are 680 sources total with fairly uniform spatial density. Median precison is < 100 μas (0.5 nrad). The ecliptic plane is marked as a blue-grey dashed line. The galactic plane is marked by a light yellow-orange line. We note that the southern most part of the ecliptic plane crosses the galactic plane very near the galactic center (α = 17h 45m, δ = -29). This is the most difficult part of the sky to observe because of the scattering by the inter-stellar media (ISM).

Figure 1. Ka-band radio source distribution in Right Ascension & Declination

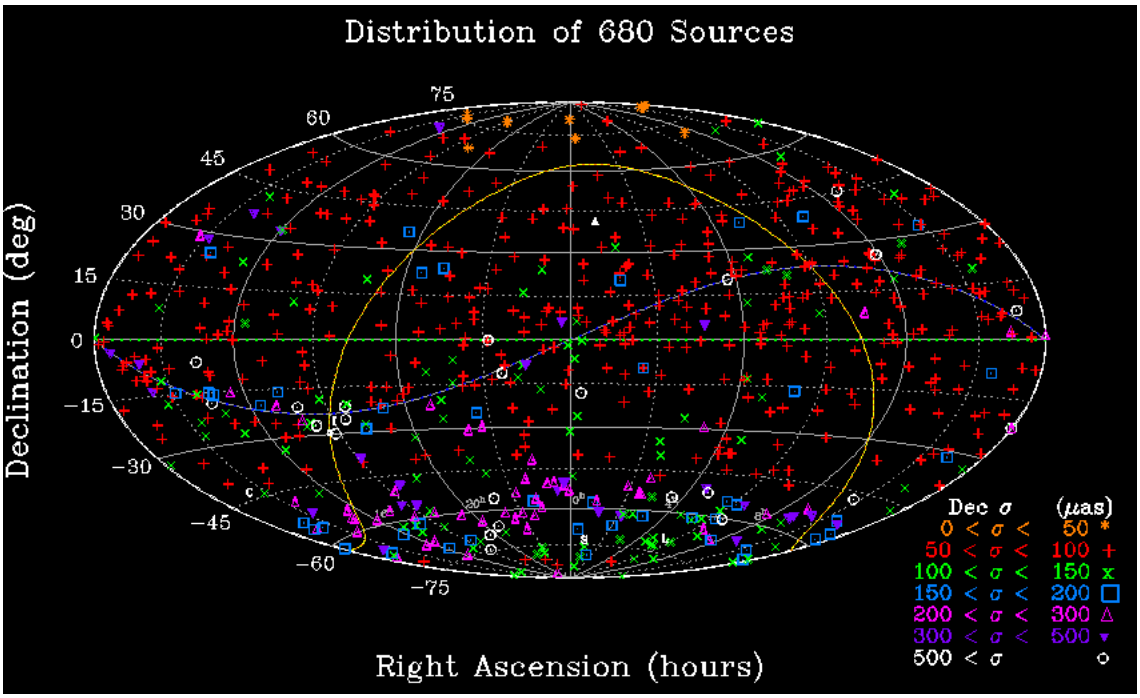

We compare the rotational alignments and position differences to the ICRF3-SX catalog. Limiting comparison to our 173 (of 303) ICRF3-SX defining sources yields rotational alignments with ~15 µas uncertainty and weighted Root Mean Square (wRMS) differences of 172 µas in Right Ascension (RA or α cosδ) and 149 µas in declination (δ). The differences are dominated by spatially correlated systematic errors (zonal errors).

Table 1. Rotational Alignment Between DDOR-2020a-Ka and ICRF3-SX Catalogues

	173 ICRF3-SX Defining		550 ICRF3-SX Overlapping	
Rotation Axis	Rotation Value (µas)	Rotation Error (µas)	Rotation Value (µas)	Rotation Error (µas)
X	-20.5	9.7	11.0	9.4
Y	-7.9	10.2	-5.4	10.4
Z	-1.1	7.9	27.8	5.5

Table 2. Differenced Positions Between DDOR-2020a-Ka and ICRF3-SX Catalogues

	173 ICRF3 Defining		550 ICRF3- Overlapping	
Differenced Data	Weighted Mean (µas)	Weighted RMS (µas)	Weighted Mean (µas)	Weighted RMS (µas)
RA cos(Dec)	28	172	-4	152
Dec	-132	149	-137	162

Broadening the comparison to include all common sources and after removing 60 outliers of more than 5-sigma, we have 550 common sources. The rotational alignment is better than 30 µas and wRMS differences about the mean of 152 µas in RA cos(dec) and 162 µas in declination (Dec). The Z-rotation is likely biased by the zonal defomations and in particular the quarupole 2,0 term that effects RA.

Source positions were extracted from the MODEST binary output file, "xka.srf," using the “catout” utility and the resulting file, xka.cat_iers, is available from JPL’s Service Preparation Subsystem (SPS) portal.

2.4 Systematic Errors

The celestial frame presented in this document has precision (random measurement error) within the 0.5 nrad goal. However at present, systematic errors consume the entire near term error budget of 1.0 nrad and twice the long term goal of 0.5 nrad leaving the accuracy considerably worse than the precision.

Specifically, the fact that about 85% of the data comes from just two DSN baselines (Goldstone to Tidbinbilla and Goldstone to Madrid) means that the solution is very susceptible to systematic distortion. For example, the solution has difficulty separating tropospheric effects such as average tropospheric gradients from the celestial frame. Because the Goldstone to Tidbinbilla baseline with 10,400 km length is close to an earth diameter, it has anti-correlated elevation angles, that is, on average, high elevation at Goldstone implies low elevation at Tidbinbilla and vice-versa. This prevents the solution from cleanly separating the celestial frame from tropsophere effects. As a result, we see a large quadrupole error in RA:

quadrupole 2, 0 term: $\Delta\alpha \cos(\delta) = (197 +- 21)$ µas $\sin(2\delta)$

The $\sin(2\delta)$ dependence means that northern RAs and southern RAs are based in opposite directions.

The lack of a direct north-south baseline means that declination depend largely on the angled Goldstone-Tidbinbilla baseline which is observed more than 10 times more often than the nearly orthogonal Goldstone-Malargüe baseline which is needed to determine balanced declinations. The resulting geometric weakness is reflected in the uncertainties when estimating a 3-D dipole difference between catalogs: Dipole X and Y have ~15 µas uncertainties whereas dipole-Z has almost 60 µas uncertainty. While the estimated diole-X is not statistically significant, the factor of four (4) larger uncertainty quantifies how weak the declinations are.

Dipole-Z: $\Delta\delta = (-46 +- 57)$ µas $\cos(\delta)$

The process for correcting these errors has been demonstrated. We have Goldstone to Malargüe data. All that is needed is to get more observations on Goldstone to Malargüe to correct the order of magntiude imbalance in observations. In the near future, there may be help from JAXA’s new 54-meter Misasa, Japan station via the Japan to Tidbinbilla, Australia baseline.

2.5 Galactic acceleration

The Solar system orbits the galactic center with roughly a 200 million year period. Just as with the Earth's orbit about the Sun, our orbit around the galactic center creates an aberration effect. Because our orbit is so slow, we absorb most of this nearly constant aberration effect into the reported source positions. However, our acceleration towards the galactic center creates a small, but measureable, change in aberration amounting to 5 μas/year times a projection factor depending on the RA and Dec of the source. The latest International Astronmical Union (IAU) standard (ICRF3, Charlot, Jacobs, et al, 2020) models this drift relative to epoch J2015.0.

For applications with epochs either far from 2015.0 or requiring the highest accuracies, this effect must be considered. For more detailed discussion we refer the reader to MacMillan et al (2019).

2.6 Catalog Format

The catalog uses the J2000 reference epoch and is rotationally aligned with the ICRF3-SX (Charlot, Jacobs et al, 2020) at the ~20 μas level in all components. In addition to the presentation in Table 1, the catalog is available for download as a fixed−width file at:

https://deepspace.jpl.nasa.gov/dsndocs/810-005/108/Ka-catalog-fixed.txt

Lines of the fixed−width file are terminated with ASCII Character 10 (Unix convention). The fixed−width file may be read with the following FORTRAN format statement,

FORMAT (1X, A8, 1X, A12, 1X, I4, 1X, 2(1X,I2), 2X, F11.8, 1X, A1, I2, 1X, I2, 1X, F10.7, Fll.8, F10.7, F8.4, 2F8.1, I6, 2F6.2, F5.1).

2.6.1 B1950 Name (characters 2 through 9)

This is the source name based on its position at the Besselian epoch B1950.0 which is one of the two standard epochs that have been used in the last 40 years for reporting source positions (the other being the Julian epoch J2000.0). The name is related to the position of the source, but is most useful for searching historical databases for information about the source. The name is constructed as follows. The first two digits represent hours of right RA, the next two digits minutes of RA, the fifth place is used to specify the sign of the declination, places 6−7 give degrees of declination, and the last digit gives the first digit of the fractional part of degrees of declination. Thus the first entry in the catalog, 0002-478, is interpreted as a right ascension of zero hours and 2 minutes (of time) and a declination of negative 48.8 degrees at the B1950.0 epoch.

2.6.2 Common Name (characters 11 through 22)

This is the name most commonly used in the literature for the source and is also the name used by the DSN for Delta−DOR measurement scheduling. Often, there is a short prefix that indicates the organization or radio observatory that first documented the source in a survey. The remainder of the name may be related to the source position or an arbitrary sequence number. Some of the prefixes and naming conventions include (Kesteven & Bridle, 1977):

- 3C *nnn* – From the Third Cambridge Catalog. The *nnn* is the numerical designation assigned by the catalog. This survey, originally conducted at 159 MHz, identified many

of the stronger sources used in VLBI. Unfortunately, many of these stronger sources are also less point-like making them less desirable for the highest accuracy astrometric measurements.

- 4C *zz.nn* – From the Fourth Cambridge Catalog. The *zz* corresponds to the declination "zone." The *nn* is a sequential number within the zone. There are no sequential numbers greater than 99.
- B2 *RRrrSDDa* – Most likely from the Second Bologna Survey. The *RRrr* is hours and minutes of right ascension, *S* is the sign of declination and *DD* is degrees of declination. The meaning of a (an alpha character) is unknown.
- CTA *nn* and CTD *nn* – From the California Institute of Technology "A" or "D" surveys where *nn* is the numerical designation assigned by the catalog.
- DW *RRrrSDDd* – From the Dwingelo Radio Observatory (Netherlands) catalog. The *RRrr* is hours and minutes of right ascension, *S* is the sign of declination, *DD* is degrees of declination, and *d* (if present) is the first digit of the fractional part of declination.
- GC *RRrrSDDd* – Most likely names taken from the "General Catalog of 33342 (optical) Stars." The *RRrrSDDd* are as described before.
- HR *nnnn* – Most likely names taken from the "Harvard Revised (optical) Catalog" where *nnn* is the numerical designation assigned by the catalog.
- M *nn* – Most likely names taken from the "Messier Catalog of Galaxies" where *nn* is the numerical designation assigned by the catalog.
- NRAO *nnn* – From the National Radio Observatory catalog where *nnn* is the numerical designation assigned by the catalog.
- O_ *nnn*– From the Ohio State Survey where the second letter indicates the hour of right ascension (two letters are skipped from the alphabet) and *nnn* is a numerical designation assigned by the catalog.
- P *RRrrSDDd* – From the Parkes Radio Observatory (southern Australia) survey. The *RRrrSDDd* are as described before.
- VRO *DD.RR.rr* – From the Vermillion River Observatory (University of Illinois) catalog. The *DD* is degrees declination and *RR* is hours right ascension. The *rr* is unknown but may be either minutes or fractional hours of right ascension.

2.6.3 ID Number (characters 24 through 27)

A unique number, presently in the range of 1 to 4272, is assigned to each radio source for use by programs that identify sources by number instead of name. The correspondence between source name and number will not change when the catalog is updated---except to correct errors. This catalog can be used to establish a unique correspondence between the B1950 or Common Name and ID number. If a source in this catalog is deleted from future revisions of the catalog delivery, its number will be retired. When new sources are added, they will be assigned unique numbers starting with 4273.

2.6.4 Angular Positions (characters 29 through 65)

Background: When the IAU's fundamental reference frame transitioned from the optically based catalog of galactic stars, FK5 (Fricke et al, 1988), to the catalog of extragalactic Active Galactic

Nuclei (AGNs) on 1 January 1998 (IAU, 1998; Ma et al 1998), right ascension, and most importantly the origin of RA, transitioned by conventional agreement to values based on the RA of the extragalactic radio sources. In practice at the time of this documents prepration, this means that the axes implicitly defined by a set of source positions must agree with the ICRF3-SX (Charlot, Jacobs et al, 2020) to within the formal uncertainty of the ICRF3-SX axes or approximately 10 μas (1 standard deviation). Thus, the orientation of the celestial frame axes may vary in future realizations by roughly that amount.

Angular positions are specified by a pair of angular coordinates: RA and DEC. Note that while in the pre-ICRF era (pre-1998) right ascension used to be defined as the angular distance along the celestial equator from the intersection of the equator and the ecliptic, since 01 Jan 1998 this is no longer strictly true. The ICRF-1 (Ma et al, 1998) was aligned to the FK5 optical frame within the errors of the FK5 to better than 100 milli-arcseconds. Thus, once one becomes concerned with accuracy levels < 100 milliarcseconds (500 nrad) as we are in this document, the differences between the old equator and ecliptic system and the new extra-glactic system are significant and must be accounted for.

The Ka-band coordinates reported in this module 108 are consistent with the new extagalactic ICRF-1 system (Ma et al, 1998) defined by the IAU as of 01 Jan 1998 (IAU, 1997) and refined with the release of the ICRF-2 (IAU, 2009; Ma et al, 2009) and ICRF-3 (IAU, 2018; Charlot, Jacobs et al, 2020).

2.6.4.1 Right Ascension (characters 29 through 47)

Right ascension is presented in the form " *hh mm SS.ssssssss*" where the first sub field gives hours of RA, followed by (time) minutes of RA, and (time) seconds of RA to eight decimal places.

2.6.4.2 Declination (characters 49 through 65)

Declination is presented in the form "*Sdd mm SS.sssssss*" where first sub−field, S or column 49, gives the sign of declination (a blank is allowed and should be interpreted as a positive declination). The remaining subfields give angular declination in degrees, minutes, and seconds to seven decimal places.

Warning regarding sign convention: Note that a minus sign applies to the whole declination (*dd mm SS.sssssss*). For example, a declination of –00 00 00.*sssssss* should be read as minus 0.*sssssss* arcseconds of declination. This means that users desiring decimal representations of declination must first convert from degrees, minutes, seconds format to decimal format before applying the relevant sign. To simplify this conversion, the sign is in a fixed position in the fixed−width file.

2.6.5 Right Ascension Error (characters 66 through 76)

This field provides the formal one standard deviation right ascension uncertainty in units of seconds of time.

2.6.6 Declination Error (characters 77 through 86)

This field provides the formal one standard deviation declination uncertainty in units of arcseconds of angle.

2.6.7 Correlation of Right Ascension and Declination (characters 87 through 94)

This field provides the formal correlation of right ascension and declination. The quantity may range from –1.0 to +1.0 and a blank in front of the value should be interpreted as indicating a positive correlation. Values near zero indicate that the principal axes of the error ellipse are close to the RA−Dec axes. The large number of negative correlations is, in part, due to the large influence of the California to Australia baseline (typically between DSS−25,26 and DSS−34) on determination of declination.

2.6.8 Observation Epochs (characters 95 through 110)

Epochs are referred to Modified Julian Day (MJD) and are typically on the order of 50000 days.

The relation with Julian Date is given by

MJD = 2400000.5 –JD

or

MJD(t=J2000) = 51543

2.6.8.1 Initial (characters 95 through 102)

The earliest epoch of the first observation.

2.6.8.2 Last (characters 103 through 110)

The termination epoch of the most recent observation.

2.6.9 Number of Sessions (characters 111 through 116)

The number of sessions, where a session is defined as a continuous data collection period, may be used as a rough indicator of the robustness of the position determination. Any position based on less than 3 sessions should be considered provisional.

2.6.10 Correlated Flux Density (characters 117 through 128)

The correlated flux density reported is an estimate of the median correlated flux density for observations of the radio source using DSN baselines Goldstone−Madrid and Goldstone−Canberra. These median correlated flux density values are reported for each baseline when available. This value, in Janskys (Jy = 1.e-26 watts/m^2/Hz), is computed from the measured signal−to−noise ratio (SNR) ouput by the quasar fringe fitting program using the following formula.

$$Flux = SNR * \frac{1}{K_l} * \frac{2k}{10^{-26}} * \frac{4\pi}{\lambda^2} * \frac{1}{\sqrt{\left(\frac{G}{T}\right)_1 \left(\frac{G}{T}\right)_2}} * \frac{1}{\sqrt{DT_{QU}}}$$

Where K_L is the system loss factor (1.0), k is the Stefan-Boltzman constant (1.38x10^{-23} J/K), λ is the wavelength of the signal, G/T is the antenna gain over system temperature parameter for antenna 1 and 2, D is the total sampling rate, and T_{QU} is the quasar integration time. Most of these parameters are recording in the output of the Cfit fringe fitting program, but the G/T values for

each antenna are estimated using the elevation angles and the appropriate equations from the 810-005 module 101-G for the 70m antennas (Slobin, 2019), module 103-C for the 34m HEF antennas (Slobin, 2014), and module 104-L 34m BWG antennas (Slobin, 2019).

Loss factor, K_L, is for the moment set to unity. As a result various losses are absorbed into the report flux densities in Table 3. Of particular concern is the loss from pointing errors which may be in the range of 5 to 10 milli-degrees or 1 to 4 dB (Slobin, module 104-L, fig. 49). The beam waveguide antenna design and calibration does not account for antenna deformation due to thermal changes in the structure. These may be as large a 1 milli-degree per deg C. Given that pointing calibrations are done at night, one might expect up to 10 milli-deg pointing errors (4 dB) during the heat of the day. Mirror mislaignment is another concern. For example, in the first half of 2017, DSS 55 had large mirror misalignments that greatly reduced the Ka-band signal levels.

The fluxe densities presented here are intended to guide DDOR source selection by providing meaningful realtive fluxes. However, the absolute flux scale has not been determined and may be in error by a factor of 2 to 4. The absolute scale could be determined to about 20% if needed and if sufficent resources were to be allocated to the task.

The SNR is determined during the cross−correlation and fringe fitting of actual radio source observations. Only DDOR, TEMPO, and CAT M&E observations from the last 5 years (2015-2020) were used in computing the median SNR which went into the flux calculation. If no observations of a radio source on DSN baselines since 2015 are available, no value is provided for correlated flux. Note that only 3 sources, all of which are near the galactic center (α=17h 45m, δ= -29 deg), have not been detected since 2015.0.

Independent values for the correlated flux density are reported for the California−Madrid and the California−Canberra DSN baselines. These columns necessarily represent only a subset of the sources since each baseline can access only about 2/3 of the sky. Also note that the format defined for this document does not include baselines to the ESA antennas at Malargüe, Argentina. As a result, sources below declination -45 deg which are observable only on the Tidbinbilla, Australia to Argentina baseline are not tabulated, but these fluxes do exist and can be provided upon request.

As an example, a typical DSN observation may use the following parameter values: G/T = 64.5 dB-K (typical 34m BWG performance), D = 704 Msamples/sec (11 channels of 32 MHz complex bandwidth), and T = 60 seconds. If the minimum accceptable detection is for SNR > 6.5, the weakest quasars that can be detected in these observations are on the order of 5 mJy.

2.6.10.1 Correlated Flux Density Madrid Baseline (characters 117 through 122)

This is the realtive correlated flux density for quasars observed on the Goldstone-Madrid (10-60) baseline. Flux densities on this baseline are available for 438 of 680 of the sources in Table 1. The absolute flux density scale is likely uncertain by a factor of 2 to 4.

2.6.10.2 Correlated Flux Density Canberra Baseline (characters 123 through 128)

This is the relative correlated flux density for quasars observed using the Goldstone-Canberra (10-40) baseline. Flux densities on this baseline are available for 462 of 680 of the sources in Table 1. The absolute flux density scale is likely uncertain by a factor of 2 to 4.

2.6.11 Structure Index (characters 129 through 133)

The structure index is determined through the following relationship between the radio source structure index and the median value of the VLBI structure group delay corrections (Ma et al, 2009):

$$\mathrm{SI} = 1 + 2\log(\tau_{median})$$

where SI is the structure index, and τ_{median} is the median value of the structure delay corrections in picoseconds (ps). A value for τ_{median} in the range of 0 to 40 ps is typical for a source that is point−like. A value in the range of 40 to 60 ps is typical for a source that has significant structure. The source structure itself may contribute an error of this magnitude to the delay error budget. Values of the delay scatter greater than 60 ps are typical for sources with large, extended, and possibly variable structure.

Table 3 presents K-band (24 GHz)---not Ka-band (32 GHz)---estimates of the structure index for a fraction of the sources because no maps at Ka-band exist with which to make Ka-band structure index estimates.

The actual Ka-band τ_{median} values are likely a factor of 1.5 smaller (better) than the K-band proxy measurements of τ_{median} tablualted below. In fact, one of the key benefits of observing at Ka-band should be the reduction in source structure.

The K-band (24 GHz) estimates of the structure index for a few hundred sources are from Charlot et al (2010). De Witt et al (2020, in prep.) are preparing to publish K-band images of over 700 sources which should enable better proxy structure indices to be calculated for the next release of this module.

Table 3. Ka-Band Radio Source Catalog: DDOR_2020a-Ka

Source Name		ID No.	Right Ascension			Declination			RA Error (s)	Dec. Error (arcsec)	RA–Dec Corr.	Observation Epoch MJD		No. Obs.	Source Flux (Jy)		K Struct Index
B1950	Common		H	M	S	D	M	S				First	Last		10-60	10-40	
0002-478	0002-478	706	00	04	35.65546157	-47	36	19.6046298	0.00001248	0.0001342	-0.4744	56297.6	58810.2	29		0.09	
0002+541	0002+541	2284	00	05	4.36335936	+54	28	24.9241233	0.00000740	0.0000990	0.2360	55304.5	58874.6	43	0.04		
0003+380	GC 0003+38	1	00	05	57.17539933	+38	20	15.1489523	0.00000430	0.0000719	-0.2596	53561.7	58937.1	114	0.09	0.11	
0003-066	0003-066	696	00	06	13.89286699	-06	23	35.3350922	0.00000547	0.0001147	-0.5643	53561.6	58937.0	120	0.38	0.27	
0006+061	0006+061	2296	00	09	3.93183234	+06	28	21.2400466	0.00000547	0.0001068	-0.6119	53651.5	58938.0	105	0.02	0.03	1.51
0007+106	III ZW 2	986	00	10	31.00589912	+10	58	29.5044219	0.00000346	0.0000798	-0.4790	53694.3	58938.0	144	0.07	0.12	1.15
0008-264	P 0008-264	7	00	11	1.24672037	-26	12	33.3773903	0.00000757	0.0001089	-0.6807	53561.7	58937.9	83	0.15	0.10	
0009+081	0009+081	1253	00	11	35.26959838	+08	23	55.5861777	0.00000447	0.0000944	-0.5484	53694.3	58938.0	98	0.04	0.06	2.14
0010-401	0010-401	2305	00	12	59.90980804	-39	54	26.0560627	0.00000912	0.0001020	-0.5356	55451.4	58937.9	71		0.07	
0013-184	0013-184	2312	00	15	34.32452131	-18	07	25.5852007	0.00006340	0.0008559	-0.9802	56746.9	58839.2	28		0.02	
0013-005	P 0013-00	666	00	16	11.08854117	-00	15	12.4453015	0.00000474	0.0001032	-0.6470	53561.7	58937.9	96	0.07	0.06	
0017+200	0017+200	987	00	19	37.85450011	+20	21	45.6444550	0.00000371	0.0000769	-0.4231	53609.5	58937.9	130	0.13	0.15	2.1
0017+257	0017+257	988	00	19	39.78060744	+26	02	52.2769820	0.00000414	0.0000857	-0.4483	55304.6	58937.9	99	0.09	0.05	
0016+731	0016+731	710	00	19	45.78639981	+73	27	30.0175400	0.00001099	0.0000461	0.0930	53568.0	58874.5	81	0.37		0.87
0019+058	P 0019+058	11	00	22	32.44120798	+06	08	4.2687902	0.00000359	0.0000823	-0.4987	53561.7	58895.2	139	0.08	0.10	1.4
0021-686	0021-686	4144	00	24	6.72292449	-68	20	54.5874650	0.00002821	0.0001563	-0.1121	56297.6	58643.9	15			
0038-020	0038-020	2347	00	40	57.61155924	-01	46	32.0258365	0.00000446	0.0000934	-0.6069	53609.6	58937.0	111	0.06	0.11	1.68
0044-846	0044-846	4145	00	44	26.68913098	-84	22	39.9875867	0.00007451	0.0001279	0.1249	56297.5	58643.9	15			
0044+030	0044+030	4146	00	47	5.91872592	+03	19	54.7856439	0.00000401	0.0000941	-0.5622	56892.5	58895.2	72	0.10	0.08	
0046+316	NGC 0262	996	00	48	47.14149773	+31	57	25.0847844	0.00000399	0.0000795	-0.3363	53687.1	58937.1	125	0.10	0.04	1.65
0047+023	J0049+0237	997	00	49	43.23593371	+02	37	3.7785348	0.00000366	0.0000851	-0.5161	55262.7	58895.2	110	0.10	0.10	
0047-579	P 0047-579	714	00	49	59.47303069	-57	38	27.3400805	0.00001634	0.0001934	-0.0647	56275.6	58643.9	15			
0048-097	P 0048-09	19	00	50	41.31735959	-09	29	5.2104361	0.00000392	0.0000855	-0.5018	53561.6	58937.0	148	0.07	0.08	
0054+161	0054+161	1254	00	56	55.29433059	+16	25	13.3408701	0.00000345	0.0000783	-0.4116	53609.5	58937.9	134	0.11	0.09	0.81
0055+060	0055+060	1340	00	58	33.80456871	+06	20	6.0734535	0.00000362	0.0000844	-0.4926	55262.7	58937.0	114	0.11	0.06	
0056-572	0056-572	715	00	58	46.58113436	-56	59	11.4702457	0.00001190	0.0002116	-0.2485	56297.7	58643.8	15			
0101-804	0101-804	4147	01	02	14.91173561	-80	12	39.4310762	0.00005570	0.0001185	0.0571	56297.5	58643.9	13			
0100-760	0100-760	4148	01	02	18.66007412	-75	46	51.7307496	0.00002630	0.0001168	-0.1375	56275.7	58643.8	17			
0059+581	0059+581	716	01	02	45.76240562	+58	24	11.1364321	0.00000579	0.0000549	0.1539	53568.0	58874.7	83	0.56		0.55
0104-408	P 0104-408	25	01	06	45.10794604	-40	34	19.9608603	0.00000746	0.0000914	-0.4630	53561.5	58937.9	100		0.38	1.86
0106+013	P 0106+01	27	01	08	38.77110178	+01	35	0.3170942	0.00000298	0.0000756	-0.3721	53561.6	58938.0	139	0.44	0.39	
0107-610	0107-610	1255	01	09	15.47517783	-60	49	48.4598105	0.00002119	0.0003656	-0.2775	56394.8	58643.9	10			
0106+315	0106+315	4049	01	09	27.88718695	+31	49	56.0492429	0.00000564	0.0001366	-0.3573	56892.7	58937.1	63	0.04	0.02	
0109+224	GC 0109+22	30	01	12	5.82471996	+22	44	38.7862866	0.00000356	0.0000754	-0.3891	53644.3	58937.1	136	0.14	0.14	1.29
0109+200	0109+200	4149	01	12	10.19081418	+20	20	21.7640844	0.00000751	0.0001551	-0.6120	56738.7	58895.1	53	0.02	0.02	
0109+351	0109+351	2383	01	12	12.94440756	+35	22	19.3362535	0.00000438	0.0000822	-0.3458	55304.6	58937.1	103	0.07	0.05	
0110+495	0110+495	717	01	13	27.00682390	+49	48	24.0431670	0.00000495	0.0000757	0.1689	53568.4	58874.7	71	0.16		1.85
0111+021	P 0111+021	32	01	13	43.14494010	+02	22	17.3161839	0.00000436	0.0000897	-0.6254	53561.6	58937.9	132	0.05	0.12	2.34
0112-017	P 0112-017	33	01	15	17.09989768	-01	27	4.5771740	0.00000391	0.0000847	-0.5519	53561.7	58938.0	117	0.10	0.14	
0113-118	P 0113-118	34	01	16	12.52200868	-11	36	15.4347745	0.00000378	0.0000836	-0.4812	53561.6	58937.9	123	0.27	0.31	
0115-214	0115-214	1352	01	17	48.78010739	-21	11	6.6333271	0.00000521	0.0000912	-0.5281	55178.2	58937.9	90	0.05	0.12	
0119+115	P 0119+11	38	01	21	41.59504004	+11	49	50.4127543	0.00000330	0.0000778	-0.4311	53561.7	58937.9	140	0.13	0.09	
0119+041	GC 0119+04	667	01	21	56.86169306	+04	22	24.7340819	0.00000359	0.0000802	-0.5089	53561.7	58937.1	139	0.08	0.16	2.63
0119+247	0119+247	1210	01	22	38.81598971	+25	02	31.7924487	0.00000451	0.0000908	-0.4798	53644.2	58937.1	97	0.05	0.03	2.41
0122-003	0122-003	1256	01	25	28.84383312	-00	05	55.9315212	0.00000405	0.0000931	-0.5816	53609.6	58937.0	114	0.09	0.09	2.85
0123+257	P 0123+25	40	01	26	42.79264315	+25	59	1.3000968	0.00000367	0.0000773	-0.3691	53644.3	58937.1	122	0.21	0.12	
0127+084	0127+084	719	01	30	27.63443257	+08	42	46.1717540	0.00000392	0.0000867	-0.5307	55262.7	58937.1	98	0.08	0.06	0.9

Source Name		ID No.	Right Ascension			Declination			RA Error (s)	Dec. Error (arcsec)	RA–Dec Corr.	Observation Epoch MJD		No. Obs.	Source Flux (Jy)		K Struct Index
B1950	Common		H	M	S	D	M	S				First	Last		10-60	10-40	
0131-795	0131-795	4150	01	31	48.82274948	-79	16	17.4854900	0.00005351	0.0001736	0.1760	56275.7	58643.4	17			
0133+476	DA 55	44	01	36	58.59483132	+47	51	29.1000041	0.00000435	0.0000701	0.1115	53568.3	58874.1	82	0.47		
0138-097	0138-097	722	01	41	25.83215062	-09	28	43.6743122	0.00000353	0.0000801	-0.4249	53644.2	58937.0	143	0.19	0.14	2.38
0139-097	J0141-0930	4151	01	41	37.93973951	-09	30	1.7863903	0.00001005	0.0001676	-0.7714	56510.4	58937.0	61	0.02	0.02	
0146+056	0146+056	668	01	49	22.37095332	+05	55	53.5680378	0.00000453	0.0000956	-0.5273	54967.6	58937.1	93	0.03	0.03	
0148-177	0148-177	2427	01	51	6.08334334	-17	32	44.7184790	0.00000486	0.0000938	-0.5371	55178.2	58937.9	100	0.05	0.06	
0149+218	P 0149+21	53	01	52	18.05904450	+22	07	7.6997027	0.00000329	0.0000706	-0.3513	53561.7	58937.1	150	0.27	0.25	
0152-513	0152-513	4152	01	54	19.69616630	-51	07	51.7280163	0.00001717	0.0003015	-0.0171	56394.7	58643.8	13			
0159-668	0159-668	4153	02	01	7.74395563	-66	38	12.6666527	0.00002179	0.0001610	0.1276	56275.7	58643.4	15			
0201+113	P 0201+113	57	02	03	46.65705136	+11	34	45.4093512	0.00000421	0.0000919	-0.5261	53561.7	58937.1	112	0.07	0.05	
0202+149	P 0202+14	58	02	04	50.41390675	+15	14	11.0431089	0.00000350	0.0000758	-0.4462	53561.8	58937.1	143	0.15	0.13	
0202+319	DW 0202+31	59	02	05	4.92537742	+32	12	30.0952957	0.00000347	0.0000677	-0.2369	53561.8	58937.1	154	0.28	0.18	0.39
0203-120	0203-120	2451	02	06	26.08472159	-11	50	39.7249360	0.00000410	0.0000868	-0.4852	55262.8	58937.0	111	0.08	0.09	
0206-625	0206-625	4154	02	08	1.17102399	-62	16	35.5342662	0.00006099	0.0003218	0.1139	56395.6	58643.8	11			
0212-620	0212-620	4053	02	14	16.20425795	-61	49	33.6595753	0.00001384	0.0001526	-0.1765	56297.7	58643.9	16			
0213-026	0213-026	2468	02	15	42.01728995	-02	22	56.7527618	0.00000427	0.0000989	-0.4763	53728.0	58937.0	103	0.05	0.03	2.45
0219+428	0219+428	728	02	22	39.61151114	+43	02	7.7986790	0.00000453	0.0000699	-0.1266	53561.8	58937.1	117	0.10	0.10	
0220-349	P 0220-349	729	02	22	56.40162145	-34	41	28.7306175	0.00001075	0.0001127	-0.6682	53609.5	58937.9	76		0.06	3.1
0221-540	0221-540	4155	02	23	30.87476807	-53	47	39.9013463	0.00001459	0.0002073	-0.0014	56394.8	58643.7	14			
0221+067	GC 0221+06	67	02	24	28.42819762	+06	59	23.3413928	0.00000324	0.0000728	-0.4247	53561.8	58937.1	144	0.15	0.33	2.14
0224+671	DW 0224+67	68	02	28	50.05151036	+67	21	3.0292481	0.00000846	0.0000535	0.1705	53568.3	58874.5	77	0.21		2.61
0227-542	0227-542	4156	02	29	12.78529469	-54	03	24.0349468	0.00001729	0.0002177	0.1841	56394.8	58643.9	14			
0229-479	0229-479	4157	02	31	11.80401034	-47	46	11.5836076	0.00001038	0.0002676	0.1677	56394.8	58643.9	13			
0229+131	P 0229+13	69	02	31	45.89404008	+13	22	54.7159992	0.00000318	0.0000718	-0.4139	53561.7	58937.1	151	0.16	0.13	
0229-398	0229-398	2492	02	31	51.81628107	-39	35	47.2635768	0.00001172	0.0001319	-0.5216	56313.1	58860.2	58		0.03	
0235-618	0235-618	1011	02	36	53.24571052	-61	36	15.1835695	0.00001452	0.0001482	0.1734	56275.6	58643.5	17			
0234+285	CTD 20	71	02	37	52.40568769	+28	48	8.9897831	0.00000321	0.0000664	-0.2777	53561.8	58937.1	162	0.58	0.18	2.56
0235+164	GC 0235+16	72	02	38	38.93011197	+16	36	59.2744350	0.00000310	0.0000701	-0.3831	53561.7	58937.1	153	0.41	0.30	1.13
0237-027	P 0237-027	73	02	39	45.47227286	-02	34	40.9146904	0.00000378	0.0000842	-0.5383	53561.7	58937.0	152	0.05	0.19	1.7
0237+040	GC 0237+04	74	02	39	51.26304639	+04	16	21.4115438	0.00000335	0.0000768	-0.4834	53561.7	58937.1	143	0.12	0.17	
0239+108	OD 166	77	02	42	29.17084955	+11	01	0.7277746	0.00000355	0.0000781	-0.4742	53561.8	58937.1	135	0.07	0.08	1.94
0244-470	0244-470	4158	02	46	0.11793730	-46	51	17.2333144	0.00000821	0.0000978	-0.2424	56297.7	58860.2	47		0.13	
0245-167	0245-167	2506	02	48	7.73221893	-16	31	46.3860237	0.00000481	0.0000972	-0.5579	55451.5	58937.0	103	0.08	0.06	
0248-266	0248-266	1426	02	50	35.56918112	-26	27	42.5159663	0.00000815	0.0001185	-0.6546	56031.9	58937.0	70		0.03	
0252-549	P 0252-549	734	02	53	29.18037592	-54	41	51.4363733	0.00000980	0.0001341	0.2872	56275.7	58643.9	17			
0250+320	0250+320	1427	02	53	33.65015652	+32	17	20.8919645	0.00000392	0.0000747	-0.3159	53644.3	58937.1	136	0.13	0.08	0.56
0256-005	0256-005	2520	02	59	28.51616314	-00	19	59.9756957	0.00000431	0.0000989	-0.6063	55304.7	58937.1	96	0.07	0.04	
0256+192	0256+192	1432	02	59	29.65594699	+19	25	44.3274980	0.00000404	0.0000812	-0.4885	53603.5	58937.1	121	0.07	0.08	1.46
0301-721	0301-721	4159	03	01	38.44578198	-71	56	34.3997007	0.00002594	0.0001069	-0.0594	56297.7	58643.9	16			
0300+470	OE 400	82	03	03	35.24224138	+47	16	16.2754615	0.00000451	0.0000650	0.0404	53644.2	58895.3	103	0.33	0.37	1.86
0302-623	P 0302-623	735	03	03	50.63134990	-62	11	25.5506006	0.00002171	0.0001798	0.2632	56275.6	58643.4	14			
0303+051	0303+051	2527	03	05	48.19160066	+05	23	31.5268616	0.00002371	0.0005002	-0.7418	56802.0	58873.9	20	0.01	0.01	
0306+102	0306+102	671	03	09	3.62350034	+10	29	16.3407275	0.00000308	0.0000713	-0.4167	53561.7	58937.1	149	0.42	0.37	1.92
0309+411	0309+411	672	03	13	1.96214453	+41	20	1.1832126	0.00000446	0.0000658	-0.2370	54001.6	58937.1	129	0.08	0.28	2.24
0322-294	0322-294	2546	03	24	44.29538825	-29	18	21.2181531	0.00002392	0.0002707	-0.9356	57985.5	58937.0	16		0.08	
0322+222	0322+222	1017	03	25	36.81436155	+22	24	0.3654321	0.00000351	0.0000716	-0.4130	53561.8	58937.1	135	0.29	0.29	1.01
0326+277	0326+277	673	03	29	57.66940239	+27	56	15.4993466	0.00000495	0.0000868	-0.5233	54450.0	58937.1	94	0.04	0.07	
0332-403	P 0332-403	93	03	34	13.65446339	-40	08	25.3983950	0.00000642	0.0000856	-0.3573	53561.6	58937.9	87		0.22	
0332+078	0332+078	1449	03	34	53.31669458	+08	00	14.4188573	0.00000419	0.0000843	-0.5548	55304.8	58937.2	113	0.05	0.06	
0334-546	0334-546	740	03	35	53.92481667	-54	30	25.1151007	0.00004777	0.0009482	0.2741	57272.7	58643.9	5			

Source Name		ID No.	Right Ascension			Declination			RA Error (s)	Dec. Error (arcsec)	RA–Dec Corr.	Observation Epoch MJD		No. Obs.	Source Flux (Jy)		K Struct Index
B1950	Common		H	M	S	D	M	S				First	Last		10-60	10-40	
0333+321	NRAO 140	94	03	36	30.10761408	+32	18	29.3420263	0.00000393	0.0000699	-0.3629	53644.2	58937.1	136	0.23	0.26	1.85
0334-131	0334-131	2559	03	36	35.03580596	-13	02	4.6599907	0.00000488	0.0000937	-0.5318	55227.9	58937.0	102	0.05	0.05	
0336-019	CTA 26	95	03	39	30.93778443	-01	46	35.8043042	0.00000309	0.0000725	-0.4068	53561.7	58937.1	161	0.31	0.33	2.67
0340+362	J0343+3622	1019	03	43	28.95242002	+36	22	12.4295319	0.00000535	0.0000932	-0.2874	53644.2	58937.1	97	0.03	0.03	1.19
0339+683	0339+683	1452	03	44	41.44123389	+68	27	47.8100967	0.00001322	0.0000632	-0.0756	56053.3	58874.2	43	0.04		
0342+147	0342+147	674	03	45	6.41652851	+14	53	49.5580505	0.00000412	0.0000797	-0.5408	53561.8	58937.1	121	0.04	0.08	
0344+199	0344+199	2570	03	47	29.63783493	+20	04	52.0964605	0.00367871	0.0414527	-0.9981	58895.3	58895.3	1		0.02	
0346-279	0346-279	1259	03	48	38.14454707	-27	49	13.5660595	0.00000513	0.0000862	-0.4419	53609.7	58937.0	98		0.38	2.15
0345+460	0345+460	1213	03	49	18.74159454	+46	09	59.6577441	0.00000539	0.0000741	-0.1659	53644.3	58874.2	102	0.06	0.09	1.96
0350+465	0350+465	1260	03	54	30.01167679	+46	43	18.7497920	0.00000505	0.0000769	0.0800	53644.2	58874.2	102	0.06	0.06	1.75
0346+800	0346+800A	1214	03	54	46.12605518	+80	09	28.8473450	0.00002266	0.0000620	-0.0507	55304.7	58874.5	51	0.04		
0354+231	0354+231	1022	03	57	21.60989896	+23	19	53.8251776	0.00000365	0.0000735	-0.4235	53644.3	58937.1	132	0.15	0.16	0.87
0358+040	0358+040	1262	04	01	19.91297328	+04	13	34.4069431	0.00000317	0.0000731	-0.4315	53609.6	58937.2	150	0.19	0.17	0.56
0358+210	J0401+2110	1024	04	01	45.16609103	+21	10	28.5867176	0.00000445	0.0000905	-0.5147	53561.8	58937.1	115	0.05	0.04	1.07
0400+258	CTD 26	100	04	03	5.58609368	+26	00	1.5025808	0.00000467	0.0000888	-0.4374	53644.3	58937.1	117	0.04	0.04	1.96
0402-362	P 0402-362	102	04	03	53.74987985	-36	05	1.9135850	0.00000517	0.0000833	-0.3267	53561.7	58937.0	95		0.46	0
0403-132	P 0403-13	103	04	05	34.00337938	-13	08	13.6910559	0.00000382	0.0000825	-0.4492	53561.7	58937.0	110	0.19	0.13	
0405-385	P 0405-385	104	04	06	59.03532675	-38	26	28.0425146	0.00000612	0.0000857	-0.3420	53609.6	58937.0	92		0.19	2.2
0405-331	0405-331	2592	04	07	33.91371201	-33	03	46.3583648	0.00000756	0.0001022	-0.5652	53609.6	58937.0	81		0.06	1.16
0405-123	P 0405-12	105	04	07	48.43097367	-12	11	36.6595566	0.00000398	0.0000857	-0.4601	54966.7	58937.2	106	0.13	0.06	
0406-127	0406-127	749	04	09	5.76971491	-12	38	48.1439350	0.00000674	0.0001273	-0.5816	53561.9	58937.2	84	0.04	0.03	
0406+121	GC 0406+12	107	04	09	22.00870493	+12	17	39.8476878	0.00000572	0.0001040	-0.6497	53561.8	58937.2	111	0.02	0.03	1.98
0409+229	P 0409+22	109	04	12	43.66688534	+23	05	5.4522237	0.00000490	0.0000890	-0.5791	55304.7	58895.3	102	0.04	0.06	
0414-189	P 0414-189	112	04	16	36.54443575	-18	51	8.3403888	0.00000458	0.0000858	-0.4704	55228.0	58937.0	95	0.06	0.09	
0415+398	0415+398	1465	04	19	22.54953709	+39	55	28.9775296	0.00000488	0.0000756	-0.3520	53644.3	58937.3	111	0.06	0.09	2.08
0420+022	0420+022	1263	04	22	52.21465201	+02	19	26.9305986	0.00000382	0.0000809	-0.5278	53609.7	58937.1	142	0.04	0.06	
0420-014	P 0420-01	116	04	23	15.80071895	-01	20	33.0658128	0.00000289	0.0000699	-0.3688	53561.8	58937.0	168	0.76	0.49	
0420+417	VRO 41.04.01	115	04	23	56.00981742	+41	50	2.7129955	0.00000437	0.0000640	-0.1466	53561.0	58937.3	119	0.21	0.20	
0422-380	0422-380	750	04	24	42.24368116	-37	56	20.7848082	0.00000577	0.0000848	-0.3461	53609.6	58937.0	93		0.17	2.88
0422+004	P 0422+00	118	04	24	46.84205557	+00	36	6.3292229	0.00000344	0.0000856	-0.4382	53568.6	58937.2	151	0.10	0.04	
0425+048	P 0425+048	121	04	27	47.57053896	+04	57	8.3252206	0.00000364	0.0000790	-0.4761	53561.9	58937.1	134	0.08	0.07	1.72
0426-380	P 0426-380	122	04	28	40.42424822	-37	56	19.5811386	0.00000502	0.0000824	-0.3016	53609.5	58937.0	94		0.73	1.64
0427-502	0427-502	4160	04	28	42.63217427	-50	05	34.2949475	0.00001501	0.0003999	0.1059	56394.5	58643.9	12			
0426+273	0426+273	751	04	29	52.96078156	+27	24	37.8762080	0.00000570	0.0001318	-0.4551	53561.8	58937.3	91	0.02	0.02	0.92
0430-332	0430-332	2627	04	32	44.56421102	-33	09	11.9313408	0.00001066	0.0001315	-0.6546	55451.5	58937.0	61		0.03	
0430+052	3C 120	125	04	33	11.09557155	+05	21	15.6194398	0.00000326	0.0000723	-0.4380	53609.7	58937.2	146	0.21	0.20	2.89
0432-606	0432-606	2628	04	33	34.10841962	-60	30	13.7695448	0.00001424	0.0001506	-0.0653	56394.8	58643.4	15			
0434-188	P 0434-188	126	04	37	1.48273814	-18	44	48.6141068	0.00000623	0.0001090	-0.6432	55738.9	58895.3	81	0.05	0.07	
0437-719	0437-719	4161	04	37	4.37834517	-71	48	20.1650852	0.00003091	0.0001350	0.3329	56297.7	58644.0	13			
0436-129	0436-129	1477	04	38	35.02099607	-12	51	3.3592429	0.00000392	0.0000836	-0.4527	55228.0	58937.2	112	0.12	0.08	
0438-436	P 0438-43	127	04	40	17.17997229	-43	33	8.6049246	0.00000662	0.0000855	-0.2835	55793.7	58937.0	76		0.17	
0441-699	0441-699	4162	04	40	47.75740634	-69	52	18.0867053	0.00001986	0.0001189	0.0237	56297.7	58643.8	15			
0440-520	0440-520	4163	04	41	58.27715876	-51	54	54.1695433	0.00002849	0.0007127	-0.1993	56394.5	58643.8	9			
0442+389	0442+389	1481	04	46	11.49405138	+39	00	17.0997751	0.00000712	0.0001836	0.0207	55304.7	58937.3	53	0.03	0.02	
0446+112	P 0446+11	131	04	49	7.67110701	+11	21	28.5961527	0.00000312	0.0000688	-0.4075	53561.8	58937.2	150	0.22	0.23	
0454-810	P 0454-81	756	04	50	5.44016698	-81	01	2.2315987	0.00003158	0.0000705	-0.0223	56275.6	58644.0	17			
0447+227	0447+227	1486	04	50	51.94468297	+22	49	5.8984514	0.00000881	0.0001404	-0.7566	56087.9	58895.4	75	0.02	0.03	
0446+595	0446+595	1264	04	51	18.72181723	+59	35	32.1834655	0.00000906	0.0000899	0.1556	55227.1	58874.2	44	0.04		
0450+013	0450+013	1487	04	53	2.23860934	+01	28	35.6286456	0.00000388	0.0000872	-0.4886	53644.3	58937.2	133	0.05	0.04	0.81
0454-234	0454-234	758	04	57	3.17920754	-23	24	52.0205323	0.00000398	0.0000800	-0.3853	53561.8	58937.2	119	0.19	0.51	1.88

Source Name		ID No.	Right Ascension			Declination			RA Error (s)	Dec. Error (arcsec)	RA–Dec Corr.	Observation Epoch MJD		No. Obs.	Source Flux (Jy)		K Struct Index
B1950	Common		H	M	S	D	M	S				First	Last		10-60	10-40	
0458-020	P 0458-02	137	05	01	12.80988523	-01	59	14.2566604	0.00000307	0.0000716	-0.3883	53687.2	58937.1	158	0.48	0.42	
0459+135	P 0459+135	1031	05	02	33.21952678	+13	38	10.9588467	0.00000431	0.0000819	-0.5430	53852.1	58937.2	92	0.04	0.05	1.83
0459+252	0459+252	1493	05	02	58.47477521	+25	16	25.2755639	0.00000391	0.0000748	-0.4317	55262.8	58937.3	107	0.11	0.10	
0502+049	P 0502+049	142	05	05	23.18472173	+04	59	42.7243673	0.00000325	0.0000729	-0.4388	53561.9	58937.2	146	0.19	0.25	2.11
0507-611	0507-611	4164	05	07	54.67067741	-61	04	43.1159066	0.00001519	0.0001918	0.0128	56395.6	58643.9	15			
0506+056	0506+056	1265	05	09	25.96446844	+05	41	35.3335855	0.00000355	0.0000812	-0.4526	53603.5	58937.2	132	0.13	0.05	1.96
0506+101	P 0506+101	677	05	09	27.45706800	+10	11	44.6000129	0.00000377	0.0000781	-0.5350	53560.9	58937.2	127	0.08	0.07	
0507+179	P 0507+17	678	05	10	2.36913236	+18	00	41.5814660	0.00000312	0.0000666	-0.3788	53561.9	58937.3	156	0.64	0.55	
0508+138	0508+138	1033	05	11	38.31966670	+13	57	19.1933279	0.00000515	0.0001007	-0.5477	53561.8	58937.3	108	0.03	0.02	
0511-220	P 0511-220	143	05	13	49.11430386	-21	59	16.0922671	0.00000488	0.0000893	-0.5362	53561.8	58937.2	105	0.07	0.16	1.8
0510+559	0510+559	2677	05	14	18.69963124	+56	02	11.0528688	0.00000692	0.0000831	0.1136	55304.7	58874.2	50	0.05		
0517-726	0517-726	761	05	16	37.71908671	-72	37	7.4657055	0.00002647	0.0001215	0.0162	56297.7	58643.8	14			
0516-621	0516-621	762	05	16	44.92613213	-62	07	5.3897019	0.00001623	0.0001345	-0.1087	56297.7	58643.9	16			
0515+208	0515+208	1034	05	18	3.82452152	+20	54	52.4972850	0.00000488	0.0001035	-0.5389	55304.7	58937.3	89	0.03	0.04	
0520-165	0520-165	1506	05	22	44.65492859	-16	27	52.4062292	0.00000896	0.0001734	-0.6597	56801.9	58937.2	51	0.04	0.02	
0524+034	J0527+0331	1037	05	27	32.70543972	+03	31	31.5164182	0.00000307	0.0000718	-0.4273	53609.7	58937.2	150	0.21	0.18	0.82
0530-727	P 0530-728	765	05	29	30.04215887	-72	45	28.5076270	0.00001831	0.0001047	-0.0849	56297.5	58643.9	16			
0527-053	0527-053	1511	05	29	53.53350128	-05	19	41.6175937	0.00000389	0.0000864	-0.4965	55263.0	58937.2	116	0.07	0.05	
0528+134	P 0528+134	148	05	30	56.41674390	+13	31	55.1493189	0.00000307	0.0000675	-0.4045	53561.0	58937.2	157	0.24	0.23	2.37
0529+483	J0533+4822	1038	05	33	15.86580235	+48	22	52.8076765	0.00000508	0.0000867	0.0930	55059.0	58874.5	54	0.14		
0534-611	0534-611	767	05	34	35.77245528	-61	06	7.0732952	0.00001795	0.0001533	0.1729	56394.5	58643.8	13			
0534-340	0534-340	1040	05	36	28.43234428	-34	01	11.4687862	0.00000598	0.0000887	-0.4616	53609.6	58937.0	93		0.11	1.41
0537-441	P 0537-441	149	05	38	50.36154162	-44	05	8.9396960	0.00001017	0.0001025	-0.4571	53561.8	58937.0	93		0.21	2.33
0536+145	0536+145	679	05	39	42.36599636	+14	33	45.5614785	0.00000336	0.0000722	-0.4257	53561.8	58937.1	124	0.13	0.10	
0539-543	0539-543	4165	05	40	45.84804042	-54	18	22.0959566	0.00001032	0.0001927	0.2472	56394.5	58643.8	14			
0544+273	0544+273	680	05	47	34.14893436	+27	21	56.8424973	0.00000373	0.0000785	-0.4056	53603.4	58937.3	133	0.10	0.07	0.79
0549-575	0549-575	2713	05	50	9.58017993	-57	32	24.3965970	0.00001351	0.0001488	-0.0314	56394.7	58643.8	14			
0547+234	0547+234	1041	05	50	47.39090549	+23	26	48.1770327	0.00000440	0.0001000	-0.3742	53840.9	58937.3	96	0.03	0.03	1.88
0548+084	0548+084	1521	05	51	11.22934396	+08	29	11.2218705	0.00000480	0.0001151	-0.5626	55304.8	58937.2	92	0.05	0.02	
0552+398	DA 193	152	05	55	30.80562048	+39	48	49.1650602	0.00000370	0.0000588	-0.1748	53561.0	58937.3	151	0.28	0.28	2.29
0556+238	0556+238	681	05	59	32.03313591	+23	53	53.9264309	0.00000419	0.0000927	-0.3862	53644.3	58937.3	112	0.06	0.04	1.21
0601-706	0601-706	4166	06	01	11.24774293	-70	36	8.7923992	0.00001927	0.0001134	0.1291	56297.7	58643.5	15			
0600+177	0600+177	682	06	03	9.13027111	+17	42	16.8103247	0.00000516	0.0000946	-0.6343	55227.0	58937.3	100	0.03	0.04	
0602-424	0602-424	2729	06	04	25.17463789	-42	25	30.0936994	0.00000657	0.0000896	-0.3787	55451.7	58937.0	81		0.12	
0601+245	0601+245	1045	06	04	55.12143805	+24	29	55.0365991	0.00000481	0.0000893	-0.4300	53840.9	58937.3	100	0.04	0.04	2.46
0607-605	0607-605	4167	06	07	55.08668929	-60	31	51.9927606	0.00001741	0.0001587	0.1623	56275.6	58643.9	14			
0605-085	P 0605-08	158	06	07	59.69922681	-08	34	49.9784757	0.00000320	0.0000736	-0.4054	53561.0	58937.2	136	0.29	0.41	
0607-549	0607-549	4168	06	08	49.05958489	-54	56	42.8838536	0.00001220	0.0001811	-0.0052	56394.5	58643.8	15			
0606-223	P 0606-223	1526	06	08	59.68683046	-22	20	20.9569149	0.00000502	0.0000862	-0.4434	55451.7	58937.2	87	0.12	0.06	
0607-157	P 0607-15	160	06	09	40.94951614	-15	42	40.6727999	0.00000352	0.0000766	-0.4090	53560.9	58937.2	138	0.29	0.21	
0611+131	0611+131	683	06	13	57.69275716	+13	06	45.4006454	0.00000355	0.0000824	-0.4826	53840.9	58937.2	117	0.19	0.06	1.7
0621-787	0621-787	2749	06	18	30.15877938	-78	43	2.1412304	0.00004301	0.0001076	0.0525	56275.7	58643.9	17			
0622-645	0622-645	4169	06	23	7.69631013	-64	36	20.7229722	0.00003388	0.0003080	0.7751	56297.5	58643.4	14			
0621+446	0621+446	2761	06	25	18.26539467	+44	40	1.6261319	0.00000509	0.0000702	-0.1682	55451.8	58937.3	100	0.08	0.07	1.64
0624-603	0624-603	4170	06	25	24.28948454	-60	20	29.5081297	0.00006950	0.0008616	-0.1781	56522.0	57229.8	2			
0624-546	0624-546	4171	06	25	52.23068757	-54	38	50.7070077	0.00002037	0.0004579	-0.0079	56395.6	58643.9	13			
0628+203	0628+203	2768	06	31	1.06256675	+20	20	59.2108162	0.00000388	0.0000799	-0.3956	55304.8	58937.3	98	0.08	0.06	
0629-418	0629-418	778	06	31	11.99804887	-41	54	26.9478713	0.00000776	0.0000933	-0.4858	55451.7	58937.0	81		0.14	
0633+595	0633+596	2780	06	38	2.87196343	+59	33	22.2139094	0.00000764	0.0000816	0.2297	54820.1	58874.1	57	0.05		
0639-032	0639-032	1267	06	41	51.13293821	-03	20	48.5824774	0.00000322	0.0000729	-0.4125	53609.7	58937.2	141	0.22	0.28	1.78

Source Name		ID No.	Right Ascension			Declination			RA Error (s)	Dec. Error (arcsec)	RA–Dec Corr.	Observation Epoch MJD		No. Obs.	Source Flux (Jy)		K Struct Index
B1950	Common		H	M	S	D	M	S				First	Last		10-60	10-40	
0603+882	0603+882	1556	06	42	6.13545060	+88	11	55.0155390	0.00011856	0.0000583	-0.1127	56053.3	58874.2	48	0.04		
0639+352	0639+352	1558	06	42	58.13962236	+35	09	18.3788290	0.00000452	0.0000870	-0.3590	55304.8	58937.3	100	0.05	0.04	2.83
0644-671	0644-671	4172	06	44	28.04404943	-67	12	57.3585977	0.00002384	0.0001462	-0.0607	56275.7	58643.4	14			
0641+392	0641+393	1560	06	44	53.70958702	+39	14	47.5334910	0.00000782	0.0001574	-0.0527	55059.5	58937.3	64	0.02	0.02	
0642+449	OH 471	171	06	46	32.02600956	+44	51	16.5900166	0.00000423	0.0000582	-0.1094	53561.1	58937.3	140	0.23	0.25	2.34
0646-306	P 0646-306	173	06	48	14.09644774	-30	44	19.6601968	0.00000525	0.0000842	-0.4139	53609.7	58937.2	91		0.13	2.82
0648-165	0648-165	782	06	50	24.58183574	-16	37	39.7255212	0.00000360	0.0000767	-0.3545	53560.9	58937.2	137	0.27	0.09	2.06
0654+244	0654+244	1053	06	57	5.67552605	+24	23	55.3938278	0.00000396	0.0000758	-0.4521	53840.8	58937.3	121	0.07	0.09	1.89
0656+082	0656+082	785	06	59	17.99601620	+08	13	30.9536034	0.00001310	0.0002223	-0.7917	55647.9	58937.3	46	0.02	0.02	
0657+172	0657+172	684	07	00	1.52554597	+17	09	21.7012162	0.00000336	0.0000715	-0.4480	53561.1	58937.3	129	0.12	0.12	
0700-465	0700-465	4069	07	01	34.54670729	-46	34	36.6271659	0.00000786	0.0000955	-0.4132	56297.5	58860.3	49		0.18	
0700-197	0700-197	1576	07	02	42.90065693	-19	51	22.0357288	0.00000382	0.0000780	-0.3725	55451.7	58937.2	106	0.28	0.30	
0707+476	0707+476	786	07	10	46.10489799	+47	32	11.1424823	0.00000493	0.0000754	0.0323	53644.3	58874.3	86	0.10	0.09	1.9
0708+506	0708+506	1583	07	12	43.68361156	+50	33	22.7070623	0.00000555	0.0000813	0.0397	55304.8	58874.0	49	0.11		
0716+332	0716+332	1587	07	19	19.41969306	+33	07	9.7083317	0.00000394	0.0000715	-0.3358	55304.8	58937.3	111	0.12	0.09	
0716+477	0716+477	1269	07	20	21.49777656	+47	37	44.1248476	0.00000634	0.0001009	-0.0289	54170.1	58874.0	61	0.04	0.06	1.63
0716+714	0716+714	788	07	21	53.44847989	+71	20	36.3633665	0.00000909	0.0000461	0.0738	55059.0	58874.5	57	0.65		
0721-071	0721-071	1270	07	24	17.29262901	-07	15	20.3522496	0.00000332	0.0000761	-0.3714	53609.8	58937.2	149	0.15	0.09	1.36
0722+145	P 0722+145	685	07	25	16.80777438	+14	25	13.7463996	0.00000343	0.0000692	-0.4631	53560.9	58937.3	141	0.14	0.18	1.29
0723-008	DW 0723-00	180	07	25	50.63997929	-00	54	56.5448559	0.00000343	0.0000785	-0.5624	53560.9	58937.3	122	0.25	0.69	
0725+219	0725+219	1056	07	28	20.60830323	+21	53	6.3901602	0.00000364	0.0000748	-0.4332	54128.1	58937.3	119	0.12	0.11	1.97
0727-115	P 0727-11	182	07	30	19.11246609	-11	41	12.6007203	0.00000307	0.0000717	-0.3310	53560.9	58937.2	161	0.50	0.20	
0731+050	J0733+0456	1058	07	33	57.45990075	+04	56	14.4963945	0.00000322	0.0000706	-0.4086	55263.0	58937.3	123	0.20	0.14	
0736-770	0736-770	4173	07	34	43.41984545	-77	11	13.4847663	0.00004831	0.0001402	0.0119	56297.6	58643.9	14			
0735+178	P 0735+17	190	07	38	7.39375852	+17	42	18.9980402	0.00000413	0.0000777	-0.5548	53561.0	58937.3	138	0.04	0.07	
0738-674	0738-674	791	07	38	56.49623648	-67	35	50.8263534	0.00003064	0.0002753	0.3393	56395.7	58643.1	11			
0736+017	P 0736+01	192	07	39	18.03390252	+01	37	4.6175804	0.00000302	0.0000683	-0.3840	53561.0	58937.3	156	0.32	0.46	
0742-562	0742-562	4174	07	43	20.48510848	-56	19	32.9585716	0.00001424	0.0002938	0.4012	56394.5	58644.0	13			
0743-673	0743-673	2850	07	43	31.61176276	-67	26	25.5468353	0.00004590	0.0001962	0.1833	56297.6	58643.3	10			
0742+263	0742+263	4175	07	45	5.92252073	+26	14	9.7707426	0.00000450	0.0001001	-0.5524	56746.4	58937.3	69	0.06	0.05	
0743-006	P 0743-006	197	07	45	54.08227779	-00	44	17.5407371	0.00000378	0.0000945	-0.5349	53852.1	58937.3	110	0.10	0.05	3.16
0743+259	GC 0743+25	198	07	46	25.87418727	+25	49	2.1345976	0.00000387	0.0000774	-0.4642	53561.0	58937.3	120	0.07	0.08	
0745+241	B2 0745+24	200	07	48	36.10929137	+24	00	24.1098615	0.00000339	0.0000684	-0.3826	53561.0	58937.3	147	0.16	0.16	1.97
0746+483	0746+483	1223	07	50	20.43636079	+48	14	53.5566477	0.00000529	0.0000948	0.0631	53644.5	58874.3	72	0.07		2.31
0748+126	P 0748+126	202	07	50	52.04573859	+12	31	4.8280995	0.00000306	0.0000666	-0.3836	53561.1	58937.3	150	0.23	0.23	1.69
0749+540	0749+540	793	07	53	1.38459321	+53	52	59.6368411	0.00000543	0.0000788	0.0418	53568.2	58874.7	74	0.11		1.92
0752+258	0752+258	4176	07	55	37.03268889	+25	42	39.0230548	0.00003675	0.0007897	-0.7450	56892.9	57440.2	7	0.01	0.02	
0754+100	P 0754+100	206	07	57	6.64296009	+09	56	34.8520925	0.00000310	0.0000723	-0.4297	53561.0	58937.4	152	0.27	0.11	2.41
0759+183	J0802+1809	1060	08	02	48.03197892	+18	09	49.2492534	0.00000576	0.0001216	-0.5268	53561.1	58937.2	94	0.03	0.03	1.72
0805-077	P 0805-07	210	08	08	15.53602770	-07	51	9.8865962	0.00000304	0.0000699	-0.3151	53561.0	58937.2	159	0.40	0.29	
0804+499	OJ 508	795	08	08	39.66631454	+49	50	36.5302304	0.00000488	0.0000791	0.0377	53603.4	58874.7	79	0.12		0.7
0805+410	0805+410	796	08	08	56.65206466	+40	52	44.8889782	0.00000404	0.0000616	-0.1974	53561.1	58937.3	134	0.20	0.30	1.18
0808+019	P 0808+019	211	08	11	26.70731122	+01	46	52.2200262	0.00000304	0.0000683	-0.4150	53560.9	58937.3	158	0.32	0.36	0.95
0812+367	0812+367	797	08	15	25.94487377	+36	35	15.1486716	0.00000425	0.0000734	-0.3626	53644.5	58937.3	119	0.10	0.09	2.74
0814+425	OJ 425	214	08	18	15.99962599	+42	22	45.4149473	0.00000412	0.0000630	-0.2022	53561.1	58895.5	138	0.11	0.14	1.49
0820+560	0820+560	702	08	24	47.23635929	+55	52	42.6694233	0.00000605	0.0000721	0.0504	53644.5	58874.7	69	0.08		2.31
0821+394	0821+394	798	08	24	55.48386982	+39	16	41.9040084	0.00000410	0.0000646	-0.3032	53799.0	58937.3	134	0.13	0.14	0.92
0823+033	P 0823+033	221	08	25	50.33835744	+03	09	24.5199121	0.00000291	0.0000662	-0.3642	53561.0	58937.3	168	0.31	0.23	1.59
0827+243	B2 0827+24	224	08	30	52.08619864	+24	10	59.8202812	0.00000335	0.0000673	-0.3982	53561.0	58937.3	151	0.15	0.23	1.76
0834-201	P 0834-20	804	08	36	39.21524080	-20	16	59.5045304	0.00000408	0.0000781	-0.3816	53609.8	58937.2	118	0.12	0.12	

Source Name		ID No.	Right Ascension			Declination			RA Error (s)	Dec. Error (arcsec)	RA–Dec Corr.	Observation Epoch MJD		No. Obs.	Source Flux (Jy)		K Struct Index
B1950	Common		H	M	S	D	M	S				First	Last		10-60	10-40	
0834+250	OJ 259	1063	08	37	40.24569386	+24	54	23.1215303	0.00000422	0.0000797	-0.5325	53561.1	58937.3	123	0.06	0.11	1.95
0838+133	0838+133A	1272	08	40	47.58841961	+13	12	23.5637669	0.00000321	0.0000681	-0.3859	53609.9	58937.2	144	0.12	0.15	
0839+187	GC 0839+18	234	08	42	5.09416288	+18	35	40.9896135	0.00000411	0.0000977	-0.4627	54449.3	58937.3	111	0.05	0.03	1.48
0838+456	0838+456	4177	08	42	15.35179180	+45	25	44.1818261	0.00003659	0.0020294	0.5489	56907.5	57600.7	8	0.01		
0841-607	0841-607	4178	08	42	26.56107452	-60	53	50.4019259	0.00001330	0.0001321	0.2696	56297.7	58643.4	14			
0843-547	0843-547	4179	08	45	2.48269838	-54	58	8.5400453	0.00001517	0.0003558	-0.0529	56275.6	58643.5	14			
0844-652	0844-652	4180	08	45	11.33502254	-65	27	23.1624951	0.00005056	0.0003704	0.0070	56521.9	57851.2	6			
0844-557	0844-557	4181	08	45	49.67977079	-55	55	26.7419664	0.00001498	0.0003097	-0.2472	56394.7	58643.6	15			
0845-051	0845-051	1651	08	47	58.72492092	-05	20	33.9002583	0.00000453	0.0000900	-0.5460	55451.9	58937.4	109	0.05	0.05	
0847-354	0847-354	2944	08	49	45.62346954	-35	41	1.2788264	0.00000646	0.0000881	-0.4638	55178.5	58937.2	86		0.13	
0847-120	0847-120	1653	08	50	9.63562793	-12	13	35.3762550	0.00000349	0.0000738	-0.3492	55304.9	58937.4	118	0.17	0.19	
0850-522	0850-522	4182	08	51	55.84912168	-52	28	12.7798495	0.00001415	0.0002719	-0.5504	56275.6	58643.9	15			
0851-577	0851-577	4183	08	52	38.72588107	-57	55	29.8092825	0.00001269	0.0001412	-0.1963	56297.7	58643.9	15			
0850+284	0850+284	4184	08	53	17.82844821	+28	13	49.9975767	0.00000587	0.0001395	-0.5621	56313.3	58874.2	63	0.03	0.03	
0850+581	0850+581	808	08	54	41.99638768	+57	57	29.9396821	0.00000819	0.0001180	-0.0761	54128.1	58874.6	49	0.03		1.83
0851+202	OJ 287	236	08	54	48.87493101	+20	06	30.6407604	0.00000289	0.0000609	-0.3420	53561.0	58937.3	162	0.76	1.31	
0854-108	0854-108	1657	08	56	41.80415039	-11	05	14.4305041	0.00000423	0.0000802	-0.4166	55451.8	58937.4	106	0.07	0.09	
0859-140	P 0859-14	240	09	02	16.83090700	-14	15	30.8758256	0.00000507	0.0000894	-0.6064	54961.2	58937.4	114	0.03	0.12	
0859+470	OJ 499	239	09	03	3.99011560	+46	51	4.1373099	0.00000455	0.0000699	-0.0407	53561.2	58895.5	98	0.14	0.13	
0901+697	J0906+6930	4185	09	06	30.74875309	+69	30	30.8285274	0.00002912	0.0001485	0.1147	56234.4	58453.2	18	0.01		
0906+163	0906+163	1068	09	08	55.92534899	+16	09	54.7636540	0.00000451	0.0000976	-0.4991	55227.2	58937.3	111	0.03	0.03	1.15
0906+015	P 0906+01	244	09	09	10.09160391	+01	21	35.6173241	0.00000320	0.0000714	-0.3837	53561.0	58937.2	136	0.13	0.13	
0912+029	P 0912+029	245	09	14	37.91343922	+02	45	59.2460503	0.00000328	0.0000726	-0.4197	53561.0	58937.2	144	0.10	0.11	1.6
0916+336	0916+336	2985	09	19	8.78715344	+33	24	41.9433106	0.00000570	0.0001030	-0.5429	55304.9	58874.3	95	0.03	0.04	
0918-534	0918-534	4186	09	19	44.03956485	-53	40	6.4466981	0.00004149	0.0004304	0.3196	56297.5	58643.5	7			
0917+449	0917+449	810	09	20	58.45851157	+44	41	53.9848165	0.00000436	0.0000580	-0.1521	53561.2	58874.3	117	0.62	0.69	
0917+624	0917+624	698	09	21	36.23112250	+62	15	52.1801529	0.00000677	0.0000535	-0.0288	53568.3	58874.5	80	0.19		2.14
0925-203	P 0925-203	686	09	27	51.82431771	-20	34	51.2329211	0.00000436	0.0000822	-0.4468	54855.5	58937.4	109	0.15	0.12	
0928+144	0928+144	3006	09	31	5.34243108	+14	14	16.5185188	0.00000435	0.0000900	-0.5913	55262.1	58937.3	107	0.04	0.06	
0933+503	J0937+5008	1072	09	37	12.32736210	+50	08	52.0975630	0.00000517	0.0000786	0.0844	55262.2	58874.7	48	0.21		
0936-069	0936-069	1696	09	38	56.10426864	-07	08	0.6189234	0.00000452	0.0000879	-0.5291	54820.3	58937.4	116	0.04	0.06	
0938-133	0938-133	1698	09	41	2.54946903	-13	35	50.9852200	0.00000496	0.0000928	-0.5679	54820.3	58937.4	112	0.05	0.06	
0941+522	0941+522	3022	09	44	52.15529725	+52	02	34.2170769	0.00000549	0.0000778	0.1230	55227.1	58874.0	52	0.12		
0944-469	0944-469	4187	09	46	51.33623580	-47	07	59.2357933	0.00015605	0.0008969	-0.7248	56899.8	57110.2	3		0.02	
0945+408	0945+408	814	09	48	55.33815486	+40	39	44.5869750	0.00000442	0.0000668	-0.2332	54016.5	58895.5	128	0.07	0.09	2.81
0950+326	0950+326	4188	09	53	27.95659898	+32	25	51.5207581	0.00000701	0.0001815	-0.2219	56102.3	58895.5	52	0.02	0.02	
0953+254	OK 290	256	09	56	49.87540177	+25	15	16.0499244	0.00000321	0.0000639	-0.3454	53561.1	58937.3	155	0.24	0.17	2.23
0955+476	0955+476	820	09	58	19.67168001	+47	25	7.8423257	0.00000497	0.0000690	-0.0486	53603.5	58874.1	103	0.08	0.16	2.45
0955+326	3C 232	259	09	58	20.94964872	+32	24	2.2094729	0.00000392	0.0000697	-0.4288	53840.9	58874.3	134	0.09	0.13	2.13
1005-333	1005-333	1714	10	07	31.38742668	-33	33	6.7167908	0.00000610	0.0000895	-0.4765	55451.8	58937.2	85		0.11	
1004+141	GC 1004+14	261	10	07	41.49809242	+13	56	29.6007489	0.00000429	0.0000856	-0.5952	53561.1	58937.3	113	0.04	0.08	
1005+066	1005+066	1273	10	08	0.81616011	+06	21	21.2157291	0.00000364	0.0000817	-0.5328	53609.9	58937.3	145	0.04	0.05	1.82
1012+232	1012+232	264	10	14	47.06547400	+23	01	16.5705826	0.00000355	0.0000692	-0.4202	53644.5	58895.4	141	0.07	0.09	2.66
1013+127	1013+127	2	10	15	44.02339435	+12	27	7.0700754	0.00000382	0.0000808	-0.5058	55262.1	58937.5	109	0.06	0.08	
1015+057	J1018+0530	1077	10	18	27.84829502	+05	30	29.9617313	0.00000444	0.0000931	-0.4763	55262.1	58937.3	100	0.04	0.03	
1016-311	1016-311	1078	10	18	28.75347485	-31	23	53.8500909	0.00000548	0.0000866	-0.4515	53651.7	58937.2	91		0.20	2.3
1019+416	1019+416	1724	10	22	2.02352731	+41	26	5.3725545	0.00000704	0.0001464	-0.0349	53686.5	58874.2	79	0.02	0.02	
1020+400	1020+400	826	10	23	11.56569813	+39	48	15.3852333	0.00000436	0.0000677	-0.3748	53610.1	58895.6	132	0.07	0.15	2.33
1020+292	1020+292	4189	10	23	24.04615855	+28	56	50.9881034	0.00000442	0.0000854	-0.4141	56031.5	58895.6	98	0.04	0.04	
1022-665	1022-665	1274	10	23	43.53317742	-66	46	48.7175915	0.00002015	0.0001725	0.0685	56297.5	58643.5	15			

Source Name		ID No.	Right Ascension			Declination			RA Error (s)	Dec. Error (arcsec)	RA–Dec Corr.	Observation Epoch MJD		No. Obs.	Source Flux (Jy)		K Struct Index
B1950	Common		H	M	S	D	M	S				First	Last		10-60	10-40	
1022+194	GC 1022+19	274	10	24	44.80960390	+19	12	20.4156724	0.00000494	0.0001119	-0.3181	54121.3	58895.4	96	0.02	0.02	1.31
1022+237	1022+237	1727	10	24	53.63729478	+23	32	33.9635114	0.00000406	0.0000821	-0.4169	53644.6	58874.4	130	0.05	0.04	1.64
1023+131	1023+131	1079	10	25	56.28538095	+12	53	49.0217291	0.00000388	0.0000796	-0.5475	55262.1	58937.5	110	0.08	0.11	
1026-084	1026-084	1731	10	28	38.79646237	-08	44	38.5360731	0.00001146	0.0001906	-0.7627	56312.4	58810.6	48	0.02	0.02	
1032-199	P 1032-199	829	10	35	2.15532268	-20	11	34.3595921	0.00000467	0.0000892	-0.4487	53651.8	58937.4	110	0.09	0.05	2.44
1034-293	P 1034-293	278	10	37	16.07973569	-29	34	2.8138398	0.00000495	0.0000827	-0.4340	53561.0	58937.4	99		0.39	1.96
1036-529	1036-529	4080	10	38	40.65715595	-53	11	43.2704976	0.00001089	0.0001654	-0.2872	56275.6	58643.6	16			
1038+064	OL 064.5	279	10	41	17.16249977	+06	10	16.9237409	0.00000313	0.0000722	-0.4349	53561.1	58937.3	130	0.28	0.17	
1039+811	1039+811	832	10	44	23.06262524	+80	54	39.4430796	0.00001892	0.0000457	0.0850	53568.7	58874.7	78	0.21		2.04
1042+071	P 1042+071	687	10	44	55.91124942	+06	55	38.2624505	0.00000374	0.0000835	-0.5240	53561.1	58937.5	126	0.05	0.07	
1045-188	1045-188	833	10	48	6.62060415	-19	09	35.7273154	0.00000405	0.0000795	-0.4184	53561.1	58895.5	133	0.14	0.17	1.95
1046-409	1046-409	3084	10	48	38.27112537	-41	14	0.1158896	0.00001052	0.0001046	-0.5733	55793.9	58937.2	71		0.07	
1048-313	P 1048-313	284	10	51	4.77751368	-31	38	14.3080398	0.00001664	0.0001764	-0.8775	53609.9	58937.4	62		0.04	3.06
1049-534	1049-534	4190	10	51	9.09986194	-53	44	46.5437738	0.00002024	0.0003815	-0.3463	56297.5	58643.6	12			
1049+215	P 1049+21	834	10	51	48.78908756	+21	19	52.3136242	0.00000379	0.0000762	-0.4010	53561.1	58895.6	127	0.06	0.03	
1052+023	1052+023	4191	10	55	17.27242382	+02	05	44.9020046	0.00001015	0.0002314	-0.6801	56893.1	58937.3	49	0.02	0.02	
1053+704	1053+704	835	10	56	53.61753325	+70	11	45.9156616	0.00000989	0.0000531	0.1305	55262.2	58874.5	48	0.19		
1053+815	1053+815	836	10	58	11.53538221	+81	14	32.6751566	0.00001944	0.0000453	0.0461	53567.8	58874.5	84	0.18		0.93
1055+018	P 1055+01	287	10	58	29.60521402	+01	33	58.8234582	0.00000283	0.0000655	-0.3829	53561.0	58937.5	164	0.58	1.45	
1059-631	1059-631	4192	11	01	54.37844990	-63	25	22.5999300	0.00001764	0.0001351	0.0801	56275.7	58644.0	16			
1101+384	B2 1101+38	291	11	04	27.31396496	+38	12	31.7988551	0.00000412	0.0000694	-0.3058	53561.1	58937.6	140	0.08	0.08	1.53
1102-242	1102-242	3103	11	04	46.17642332	-24	31	25.7999514	0.00000643	0.0000980	-0.6048	55451.8	58895.4	80	0.06	0.09	
1109+076	1109+076	1756	11	12	9.55849234	+07	24	49.1176843	0.00004466	0.0007336	-0.9125	56417.9	58362.9	13		0.01	
1111+149	GC 1111+14	296	11	13	58.69509206	+14	42	26.9525368	0.00000415	0.0000898	-0.5505	53561.1	58937.4	119	0.04	0.03	
1115-122	1115-122	3120	11	18	17.14137356	-12	32	54.2621379	0.00000430	0.0000857	-0.5572	55178.6	58937.4	106	0.11	0.22	
1116+128	P 1116+12	297	11	18	57.30144103	+12	34	41.7178680	0.00000310	0.0000707	-0.3943	53561.1	58937.5	133	0.18	0.12	
1119-069	1119-069	1758	11	21	42.12293529	-07	11	6.3420238	0.00000507	0.0001029	-0.6405	55262.2	58937.5	104	0.04	0.05	
1123+264	P 1123+26	299	11	25	53.71193584	+26	10	19.9785717	0.00000384	0.0000744	-0.3767	53561.2	58895.6	118	0.06	0.05	
1124-186	P 1124-186	300	11	27	4.39244026	-18	57	17.4420248	0.00000377	0.0000801	-0.4178	53561.0	58937.4	136	0.38	0.25	1.32
1128+385	GC 1128+38	302	11	30	53.28262847	+38	15	18.5467876	0.00000398	0.0000649	-0.2896	53561.3	58874.2	139	0.19	0.21	1.93
1129-580	1129-580	1088	11	31	43.28807033	-58	18	53.4427688	0.00001676	0.0001566	-0.2260	56275.6	58643.1	14			
1129-558	1129-558	4193	11	32	16.41468682	-56	06	44.7350040	0.00001614	0.0001732	0.0348	56297.5	58643.6	14			
1130+106	1130+106	4194	11	32	59.48879894	+10	23	42.2133421	0.00000464	0.0000982	-0.6337	56738.1	58937.5	75	0.03	0.05	
1130+009	P 1130+009	304	11	33	20.05579428	+00	40	52.8369852	0.00000361	0.0000852	-0.4581	53561.2	58937.5	120	0.06	0.06	
1133-681	1133-681	4195	11	36	2.09814996	-68	27	5.8226896	0.00002736	0.0001557	0.1588	56275.7	58643.4	16			
1136-466	1136-466	4196	11	38	55.55906798	-46	53	42.2605515	0.00001650	0.0001390	-0.5226	56297.5	58810.6	38		0.03	
1140+668	1140+668	3157	11	43	41.60336679	+66	33	31.2295985	0.00001553	0.0001221	0.0550	56738.2	58874.7	39	0.02		
1143-696	1143-696	3160	11	45	53.62413627	-69	54	1.7977602	0.00002422	0.0001335	0.0927	56275.7	58643.4	15			
1143-287	1143-287	1774	11	46	26.18858243	-28	59	18.5052819	0.00000586	0.0000914	-0.5199	55793.9	58937.4	81		0.13	
1143-332	1143-332	1776	11	46	28.45175757	-33	28	42.6327697	0.00000838	0.0001099	-0.6077	55863.7	58937.4	71		0.04	
1144+402	1144+402	699	11	46	58.29792943	+39	58	34.3044651	0.00000373	0.0000580	-0.2024	53561.3	58937.6	147	0.37	0.43	1.09
1144-379	P 1144-379	309	11	47	1.37069746	-38	12	11.0240215	0.00000645	0.0000872	-0.4200	53561.0	58937.4	90		0.17	2.06
1145-676	1145-676	4197	11	47	33.39950224	-67	53	41.7699127	0.00001895	0.0001134	-0.1604	56297.5	58643.5	15			
1145-071	1145-071	689	11	47	51.55403930	-07	24	41.1414232	0.00000374	0.0000778	-0.4801	53561.1	58937.3	126	0.08	0.17	
1147+245	B2 1147+24	845	11	50	19.21219084	+24	17	53.8350408	0.00000354	0.0000735	-0.4144	53561.2	58937.6	137	0.10	0.09	2.18
1150-834	1150-834	4198	11	52	53.22191394	-83	44	9.4406240	0.00008792	0.0001433	0.0087	56275.7	58643.8	17			
1150+812	1150+812	847	11	53	12.49926436	+80	58	29.1545534	0.00002041	0.0000458	0.1411	53798.7	58874.2	70	0.20		3.18
1150+497	4C 49.22	848	11	53	24.46666203	+49	31	8.8301105	0.00000483	0.0000705	-0.0010	53568.1	58874.5	74	0.20		2.33
1156-215	J1159-2150	4199	11	59	10.78555162	-21	50	4.6767294	0.00020901	0.0025205	-0.9854	56893.0	58601.3	7		0.01	
1156-214	1156-214	1784	11	59	21.43252539	-21	42	44.9134664	0.00000859	0.0001260	-0.6490	56711.3	58839.6	37	0.09	0.11	

Source Name		ID No.	Right Ascension			Declination			RA Error (s)	Dec. Error (arcsec)	RA–Dec Corr.	Observation Epoch MJD		No. Obs.	Source Flux (Jy)		K Struct Index
B1950	Common		H	M	S	D	M	S				First	Last		10-60	10-40	
1156+295	GC 1156+29	319	11	59	31.83392619	+29	14	43.8266450	0.00000341	0.0000645	-0.3750	53561.1	58937.6	157	0.47	0.48	1.23
1157+014	1157+014	4200	11	59	44.82785329	+01	12	6.9836639	0.00001639	0.0003072	-0.8150	56746.4	58937.4	29	0.02	0.02	
1157-215	1157-215	4201	11	59	51.90595020	-21	48	53.7055380	0.00001659	0.0002110	-0.8798	56088.2	58839.6	41	0.05	0.05	
1158+007	1158+007	1786	12	01	23.25078139	+00	28	28.3155375	0.00000614	0.0001178	-0.7147	55738.2	58937.5	92	0.02	0.03	
1204-613	1204-613	4202	12	06	51.49646456	-61	38	56.7597746	0.00002409	0.0001989	0.0010	56297.5	58643.6	13			
1205-008	1205-008	1792	12	07	41.67761640	-01	06	36.6902877	0.00000336	0.0000747	-0.4186	55262.2	58937.5	116	0.07	0.11	
1207-319	1207-319	1276	12	09	40.04460968	-32	14	53.1078795	0.00001020	0.0001318	-0.7366	53651.9	58937.4	69		0.05	2.01
1213-172	P 1213-17	326	12	15	46.75175379	-17	31	45.4034061	0.00000480	0.0000858	-0.5405	53693.8	58937.4	110	0.08	0.14	
1215+303	B2 1215+30	328	12	17	52.08198330	+30	07	0.6358474	0.00000391	0.0000737	-0.4047	54961.3	58937.6	115	0.09	0.09	
1215-002	1215-002	3210	12	17	58.72904472	-00	29	46.2999746	0.00000366	0.0000858	-0.5599	55262.2	58937.4	99	0.12	0.17	
1219+044	P 1219+04	336	12	22	22.54962749	+04	13	15.7758755	0.00000296	0.0000682	-0.4084	53561.2	58937.5	136	0.28	0.31	
1222+037	P 1222+037	337	12	24	52.42194493	+03	30	50.2924528	0.00000309	0.0000705	-0.4061	53561.1	58937.5	129	0.34	0.34	
1221-829	1221-829	4203	12	24	54.38254141	-83	13	10.1017829	0.00007179	0.0001502	-0.1781	56275.7	58644.0	17			
1222+216	P 1222+21	1230	12	24	54.45842212	+21	22	46.3884149	0.00000358	0.0000717	-0.3326	55304.2	58937.6	109	0.06	0.05	
1226-028	1226-028	855	12	28	36.91729095	-03	04	39.3122446	0.00001885	0.0004632	-0.6555	55227.3	57565.3	17	0.02	0.01	
1227+255	1227+255	1097	12	30	14.08935918	+25	18	7.1361482	0.00000368	0.0000705	-0.3737	55304.2	58937.6	105	0.09	0.10	
1236+077	P 1236+077	344	12	39	24.58833091	+07	30	17.1888965	0.00000326	0.0000723	-0.4549	53610.0	58937.6	150	0.06	0.17	
1240-679	1240-679	4204	12	43	45.22001917	-68	11	3.4326828	0.00003738	0.0002371	-0.3710	56297.5	58643.4	12			
1243-072	1243-072	690	12	46	4.23210470	-07	30	46.5748428	0.00000307	0.0000724	-0.3417	53610.0	58937.5	148	0.20	0.10	1.33
1244-255	P 1244-255	350	12	46	46.80202077	-25	47	49.2892318	0.00000493	0.0000838	-0.4609	53561.1	58937.4	89	0.71	0.58	
1245-062	1245-062	1308	12	48	22.97565941	-06	32	9.8183809	0.00000374	0.0000864	-0.4361	55730.9	58937.5	114	0.06	0.06	
1249-673	1249-673	4205	12	52	43.21203096	-67	37	38.7467002	0.00002248	0.0001452	0.2948	56275.7	58643.4	16			
1252+119	P 1252+11	351	12	54	38.25562808	+11	41	5.8947804	0.00000323	0.0000705	-0.3937	54961.3	58937.6	118	0.10	0.12	
1251-713	P 1251-71	862	12	54	59.92151948	-71	38	18.4365884	0.00002119	0.0001020	0.0663	56275.7	58643.4	17			
1253-055	3C 279	352	12	56	11.16657619	-05	47	21.5253673	0.00000290	0.0000680	-0.3001	55969.6	58937.5	113	3.25	1.01	
1256-220	1256-220	1278	12	58	54.47876769	-22	19	31.1252263	0.00000435	0.0000848	-0.4161	53757.4	58937.5	100	0.22	0.16	1.92
1300+485	1300+485	3281	13	02	17.19609192	+48	19	17.5745006	0.00000589	0.0001000	-0.1053	55227.2	58874.5	55	0.05		
1300-554	1300-554	4206	13	03	49.21590529	-55	40	31.6080979	0.00001469	0.0001551	-0.2486	56297.5	58643.1	13			
1302-102	P 1302-102	359	13	05	33.01501339	-10	33	19.4285690	0.00000325	0.0000739	-0.3375	53610.0	58937.5	146	0.32	0.19	2.34
1304-668	1304-668	4207	13	08	17.37545732	-67	07	5.2305267	0.00002183	0.0001643	-0.0168	56297.5	58643.9	15			
1306+360	1306+360	1823	13	08	23.70914970	+35	46	37.1639757	0.00000396	0.0000663	-0.3213	55262.2	58937.6	103	0.34	0.22	
1306-395	1306-395	1824	13	09	48.48831043	-39	48	33.0862503	0.00000901	0.0001021	-0.5730	55738.2	58937.4	76		0.08	
1308+326	B2 1308+32	361	13	10	28.66387494	+32	20	43.7826827	0.00000343	0.0000620	-0.3644	53561.2	58937.6	152	0.18	0.19	1.85
1307-556	1307-556	4208	13	10	43.35556974	-55	52	11.5295797	0.00001229	0.0002169	-0.2832	56395.5	58643.8	13			
1308+554	1308+554	1279	13	11	3.21082395	+55	13	54.3223296	0.00000751	0.0000966	0.0599	53727.5	58874.5	63	0.03		0.8
1310-041	1310-041	3300	13	12	50.90122621	-04	24	49.8922013	0.00000342	0.0000767	-0.4223	55647.2	58937.6	115	0.09	0.10	
1312-533	1312-533	4209	13	15	4.18111785	-53	34	35.8746196	0.00001261	0.0001995	-0.4383	56297.5	58643.4	14			
1313-333	OP-322	363	13	16	7.98592592	-33	38	59.1730621	0.00000561	0.0000852	-0.4369	53561.1	58937.4	91		0.42	2.36
1315+346	OP 326	364	13	17	36.49419533	+34	25	15.9324645	0.00000385	0.0000717	-0.2919	53561.2	58937.6	119	0.16	0.08	
1315-058	J1318-0607	4210	13	18	33.70947739	-06	07	23.8211019	0.00002599	0.0004022	-0.9535	58069.8	58937.5	21	0.01	0.04	
1319-093	1319-093	3316	13	22	36.91262504	-09	37	37.8005024	0.00000333	0.0000769	-0.4102	55647.2	58937.5	117	0.08	0.07	
1319-652	1319-652	4211	13	22	53.88803002	-65	32	19.8920392	0.00003073	0.0004079	-0.2393	56297.6	58643.4	10			
1321-105	1321-105	3320	13	24	25.79310443	-10	49	23.1345797	0.00000339	0.0000767	-0.3802	55730.9	58937.6	116	0.20	0.19	
1324+224	1324+224	704	13	27	0.86132674	+22	10	50.1626199	0.00000315	0.0000667	-0.4124	53561.2	58937.6	151	0.17	0.16	1.36
1346-109	J1327-1336	4212	13	27	42.02367394	-13	36	0.1604279	0.00002239	0.0003156	-0.9280	57299.9	58937.5	32	0.02	0.03	
1325+126	1325+126	1837	13	27	54.68300867	+12	23	9.1779725	0.00000406	0.0000835	-0.5041	55304.2	58937.6	103	0.05	0.05	
1325-558	1325-558	1102	13	29	1.14488877	-56	08	2.6659143	0.00001294	0.0001660	-0.2785	56297.5	58643.5	13			
1329-049	1329-049	3334	13	32	4.46468206	-05	09	43.3062569	0.00000318	0.0000753	-0.3967	55730.9	58937.6	117	0.16	0.14	
1333-082	1333-082	3345	13	36	8.25982593	-08	29	51.7983426	0.00000344	0.0000968	-0.4147	55647.3	58937.5	108	0.14	0.04	
1334-127	DW 1335-12	376	13	37	39.78277100	-12	57	24.6935739	0.00000301	0.0000714	-0.3072	53561.2	58937.5	164	1.40	0.65	1.27

Source Name		ID No.	Right Ascension			Declination			RA Error (s)	Dec. Error (arcsec)	RA–Dec Corr.	Observation Epoch MJD		No. Obs.	Source Flux (Jy)		K Struct Index
B1950	Common		H	M	S	D	M	S				First	Last		10-60	10-40	
1342+663	GC 1342+663	382	13	44	8.67960510	+66	06	11.6436553	0.00000929	0.0000582	0.0728	55227.2	58874.0	52	0.06		
1341-171	1341-171	1851	13	44	14.40244615	-17	23	40.3961315	0.00000588	0.0001080	-0.6063	55738.3	58937.5	97	0.06	0.04	
1345+289	1345+289	4089	13	48	4.34910484	+28	40	25.3666186	0.00000953	0.0002494	-0.4447	56907.7	58937.6	38	0.02	0.02	
1346-109	J1349-1110	4213	13	49	3.19303911	-11	10	0.8193133	0.00000622	0.0001496	-0.5567	57299.9	58937.5	52	0.04	0.02	
1348+087	1348+087	1858	13	51	16.91906782	+08	30	39.9032157	0.00000343	0.0001042	-0.4029	55227.3	58895.6	104	0.12	0.03	
1349-439	P 1349-439	387	13	52	56.53493649	-44	12	40.3881547	0.00001004	0.0001083	-0.5304	55738.2	58810.8	67		0.04	
1351-018	P 1351-018	388	13	54	6.89532485	-02	06	3.1906720	0.00000373	0.0000879	-0.4452	53561.3	58937.6	129	0.04	0.03	
1354+195	P 1354+19	392	13	57	4.43665493	+19	19	7.3724099	0.00000314	0.0000677	-0.3775	53561.2	58937.6	132	0.23	0.24	
1354-152	OP-192	391	13	57	11.24498085	-15	27	28.7871711	0.00000372	0.0000811	-0.4061	53686.6	58895.5	135	0.13	0.10	0.91
1357+769	1357+769	874	13	57	55.37155018	+76	43	21.0510322	0.00001563	0.0000502	0.1102	53567.8	58874.5	81	0.05		0.34
1402-144	1402-144	3385	14	05	32.86733364	-14	40	18.2965890	0.00000902	0.0001769	-0.7122	56088.3	58874.4	67	0.03	0.02	
1404+286	OQ 208	400	14	07	0.39436770	+28	27	14.6885017	0.00002778	0.0004437	-0.5404	56102.4	57327.5	9	0.02	0.03	
1406-076	P 1406-076	402	14	08	56.48119812	-07	52	26.6668125	0.00000315	0.0000750	-0.3876	53561.2	58937.6	144	0.17	0.26	1.64
1406-267	1406-267	1871	14	09	50.16976168	-26	57	36.9811890	0.00000983	0.0001292	-0.7137	53652.0	58937.5	64		0.04	2.33
1413+135	P 1413+135	404	14	15	58.81752124	+13	20	23.7127842	0.00000356	0.0000732	-0.4972	53561.2	58937.6	125	0.09	0.21	
1414-596	1414-596	4214	14	17	41.63601507	-59	50	37.6089177	0.00002683	0.0002102	-0.5782	56297.5	58643.5	14			
1416-516	1416-516	4215	14	19	35.24524852	-51	54	58.5700877	0.00001455	0.0003406	-0.1062	56297.6	58643.4	12			
1418+546	GC 1418+54	408	14	19	46.59742332	+54	23	14.7871478	0.00000563	0.0000657	-0.1697	53841.1	58874.5	72	0.07		2.6
1418-481	1418-481	4216	14	21	38.64649250	-48	20	22.7969691	0.00001135	0.0002936	-0.5147	56297.6	58643.4	13			
1419-229	1419-229	4091	14	22	37.10634788	-23	08	30.1362250	0.00001095	0.0001511	-0.8024	57299.9	58937.5	37	0.06	0.09	
1424+240	1424+240	881	14	27	0.39179028	+23	48	0.0374014	0.00000388	0.0000858	-0.4443	55227.4	58937.6	103	0.07	0.04	
1424-418	P 1424-41	409	14	27	56.29753776	-42	06	19.4380426	0.00000690	0.0000876	-0.3932	54855.5	58937.4	75		0.61	
1428+422	1428+422	883	14	30	23.74165309	+42	04	36.4914028	0.00000844	0.0001361	-0.1836	57985.2	58937.6	28	0.04	0.03	
1429+249	1429+249	4217	14	31	25.88471993	+24	42	20.7047784	0.00000918	0.0001755	-0.6539	57300.1	58937.6	42	0.02	0.02	
1424-834	1424-834	4218	14	33	28.43284145	-83	41	8.7106584	0.00007077	0.0001095	0.1202	56275.7	58643.9	18			
1435-218	P 1435-218	887	14	38	9.46939162	-22	04	54.7488370	0.00000563	0.0000931	-0.5312	53652.0	58895.7	97	0.10	0.10	1.72
1437+374	1437+374	4219	14	39	20.57787304	+37	12	2.8362129	0.00001964	0.0003989	-0.7150	56893.2	58846.6	29	0.01	0.02	
1437-153	1437-153	3423	14	39	56.87205401	-15	31	50.5552553	0.00000489	0.0000985	-0.5431	53610.1	58895.7	119	0.06	0.05	1.32
1438-151	J1441-1523	4220	14	41	45.41724893	-15	23	36.2656586	0.00000732	0.0001309	-0.7305	56053.1	58895.7	78	0.03	0.03	
1445-161	P 1445-16	421	14	48	15.05414025	-16	20	24.5492923	0.00000487	0.0000964	-0.5636	54961.4	58895.7	103	0.04	0.08	
1448+762	1448+762	888	14	48	28.77914823	+76	01	11.5973585	0.00001398	0.0000494	-0.0669	55227.3	58874.6	53	0.17		
1451+270	1451+270B	4221	14	53	53.60066004	+26	48	33.4096306	0.00000399	0.0000816	-0.4796	55304.2	58937.6	104	0.07	0.04	
1451-375	P 1451-375	423	14	54	27.40974214	-37	47	33.1449766	0.00000800	0.0000943	-0.4847	53651.9	58937.4	78		0.12	1.83
1454-060	1454-060	4222	14	56	41.39253448	-06	17	43.2022419	0.00004352	0.0008376	-0.8095	56893.1	58741.1	7	0.01	0.01	
1458+718	3C 309.1	426	14	59	7.58397559	+71	40	19.8667587	0.00005499	0.0003938	-0.2018	56011.3	56234.7	4			
1456-179	J1459-1810	4223	14	59	28.76315543	-18	10	45.1865241	0.00005415	0.0008326	-0.9665	57299.9	58741.1	17	0.02	0.02	
1459+480	1459+480	890	15	00	48.65424547	+47	51	15.5381126	0.00000544	0.0000972	0.1097	53727.5	58874.6	72	0.04		1.94
1459-149	1459-149	1907	15	02	25.01742416	-15	08	52.5197354	0.00001104	0.0002059	-0.7093	58028.0	58937.5	26	0.03	0.03	
1502+106	OR 103	428	15	04	24.97978723	+10	29	39.1983334	0.00000292	0.0000685	-0.4214	53561.2	58937.5	153	0.68	0.67	2.15
1502+036	P 1502+036	429	15	05	6.47717001	+03	26	30.8123155	0.00000338	0.0000771	-0.5032	53610.1	58937.6	144	0.12	0.14	1.54
1504+377	1504+377	891	15	06	9.52998982	+37	30	51.1323966	0.00000400	0.0000686	-0.2844	53644.6	58937.6	129	0.18	0.08	2.34
1505+428	1505+428	1236	15	06	53.04186528	+42	39	23.0354951	0.00000423	0.0000631	-0.2417	53609.3	58937.6	139	0.17	0.12	2.22
1505-156	1505-156	1911	15	08	35.70161221	-15	48	31.5322747	0.00001260	0.0001979	-0.8404	55969.6	58937.5	62	0.03	0.02	
1510-089	P 1510-08	433	15	12	50.53293360	-09	05	59.8300866	0.00000317	0.0000753	-0.3940	53561.2	58937.5	136	0.75	0.70	
1509-564	1509-564	4224	15	12	55.81934038	-56	40	30.6429789	0.00001875	0.0002233	-0.4363	56297.6	58643.5	13			
1511-100	P 1511-100	434	15	13	44.89343105	-10	12	0.2652560	0.00000350	0.0000795	-0.4481	53610.1	58937.5	146	0.17	0.16	2.08
1511-210	P 1511-210	3463	15	13	56.97011435	-21	14	57.5073585	0.00000822	0.0001284	-0.7179	55738.3	58895.6	67	0.07	0.05	
1511-558	1511-558	4095	15	15	12.67285338	-55	59	32.8384635	0.00001707	0.0002134	-0.5688	56297.6	58643.8	12			
1514+004	1514+004	1283	15	16	40.21906259	+00	15	1.9088003	0.00000339	0.0000783	-0.4986	53610.1	58937.5	143	0.15	0.20	2.35
1514+197	GC 1514+19	437	15	16	56.79617471	+19	32	12.9918514	0.00000319	0.0000705	-0.4351	53610.3	58937.6	141	0.14	0.13	1.62

Source Name		ID No.	Right Ascension			Declination			RA Error (s)	Dec. Error (arcsec)	RA–Dec Corr.	Observation Epoch MJD		No. Obs.	Source Flux (Jy)		K Struct Index
B1950	Common		H	M	S	D	M	S				First	Last		10-60	10-40	
1514-241	P 1514-24	438	15	17	41.81312602	-24	22	19.4764120	0.00000487	0.0000873	-0.4551	53610.0	58937.4	107	0.35	0.41	
1519-273	P 1519-273	440	15	22	37.67597488	-27	30	10.7857944	0.00000677	0.0001044	-0.6277	53651.9	58937.5	84		0.09	1.11
1528-684	1528-684	4225	15	33	34.48846258	-68	37	19.6523296	0.00003770	0.0002233	-0.0147	56297.5	58643.5	14			
1530-536	1530-536	4226	15	34	20.66067823	-53	51	13.4230095	0.00001445	0.0002291	-0.6018	56297.6	58643.5	13			
1532+016	P 1532+01	442	15	34	52.45367735	+01	31	4.2062956	0.00000365	0.0000809	-0.5189	53561.3	58937.7	128	0.06	0.09	
1532-473	1532-473	4227	15	35	52.24146806	-47	30	22.9775736	0.00001273	0.0001464	-0.5867	56394.5	58810.8	26		0.18	
1535+231	1535+231	4228	15	37	14.50087138	+23	00	40.5110923	0.00000467	0.0001143	-0.4409	56738.2	58874.6	70	0.04	0.02	
1534-152	1534-152	1931	15	37	41.57308823	-15	27	12.4989274	0.00001454	0.0002540	-0.8156	56102.3	58874.5	40	0.03	0.02	
1538+477	1538+477	4229	15	39	34.81039161	+47	35	31.2641596	0.00000544	0.0000972	-0.1154	56907.8	58874.6	43	0.08	0.06	
1538+149	GC 1538+14	444	15	40	49.49153116	+14	47	45.8845451	0.00000344	0.0000769	-0.5034	53561.3	58937.7	119	0.10	0.12	
1544-638	1544-638	4230	15	48	30.39620045	-64	01	34.8004002	0.00001846	0.0001670	-0.0095	56297.6	58643.4	16			
1546+027	P 1546+027	446	15	49	29.43685171	+02	37	1.1631412	0.00000300	0.0000733	-0.4229	53561.3	58937.6	150	0.60	0.66	1.64
1548+056	DW 1548+05	448	15	50	35.26924885	+05	27	10.4478522	0.00000307	0.0000739	-0.4555	53603.9	58937.7	147	0.30	0.19	2.95
1550-242	1550-242	3496	15	53	31.62780619	-24	22	6.0363232	0.00000502	0.0000910	-0.4507	55451.1	58937.5	92	0.20	0.36	
1555+001	DW 1555+00	452	15	57	51.43398771	-00	01	50.4141951	0.00000361	0.0000841	-0.5621	53561.3	58937.5	120	0.06	0.11	
1556+335	1556+335	4231	15	58	55.18629467	+33	23	18.6064088	0.00000890	0.0004240	-0.1204	56738.2	58874.6	32	0.02	0.01	
1556-580	1556-580	4232	16	00	12.37742984	-58	11	2.9688013	0.00002253	0.0002330	-0.5603	56297.6	58643.8	16			
1600+335	B2 1600+33	455	16	02	7.26352144	+33	26	53.0741145	0.00000498	0.0001055	-0.3668	54961.6	58937.7	93	0.04	0.03	
1602-115	1602-115	1955	16	05	17.53165208	-11	39	26.8313458	0.00000378	0.0000859	-0.4897	55059.0	58937.6	116	0.19	0.14	
1604-333	P 1604-333	457	16	07	34.76231577	-33	31	8.9136991	0.00000961	0.0001149	-0.6861	54855.7	58937.5	71		0.10	
1606+106	P 1606+10	458	16	08	46.20319262	+10	29	7.7755675	0.00000311	0.0000739	-0.4351	53561.3	58937.7	140	0.20	0.14	
1606-398	1606-398	1121	16	10	21.87908286	-39	58	58.3294698	0.00000847	0.0001001	-0.5444	55738.3	58937.5	69		0.15	
1606-742	1606-742	4233	16	12	33.88503185	-74	23	40.1432986	0.00003729	0.0002156	0.2242	56297.7	58643.4	14			
1611+343	DA 406	460	16	13	41.06425811	+34	12	47.9086730	0.00000348	0.0000658	-0.3046	53561.4	58937.6	152	0.30	0.15	2.29
1611-710	1611-710	3523	16	16	30.64151245	-71	08	31.4541112	0.00003394	0.0001803	-0.3787	56297.7	58643.8	15			
1614+051	P 1614+051	461	16	16	37.55681921	+04	59	32.7361754	0.00000559	0.0001099	-0.6754	53561.3	58937.6	95	0.02	0.03	
1614-195	1614-195	1962	16	17	27.09307145	-19	41	32.0150324	0.00001364	0.0001892	-0.8757	55738.3	58937.5	65	0.03	0.03	
1617+229	1617+229	1123	16	19	14.82460569	+22	47	47.8510618	0.00000400	0.0000830	-0.5246	53644.8	58937.7	136	0.05	0.06	2.13
1619-680	P 1619-680	901	16	24	18.43699315	-68	09	12.4966056	0.00004437	0.0002736	-0.2922	56297.5	58643.5	12			
1622-253	P 1622-253	465	16	25	46.89163384	-25	27	38.3271599	0.00000584	0.0000956	-0.5517	53610.1	58937.6	96	0.13	0.15	1.26
1622-297	P 1622-29	466	16	26	6.02082830	-29	51	26.9716330	0.00000678	0.0000995	-0.5871	53610.1	58937.6	81		0.29	
1624-617	1624-617	1126	16	28	54.68976426	-61	52	36.3979771	0.00001828	0.0001358	-0.2636	56297.6	58643.4	16			
1636+473	1636+473	904	16	37	45.13057986	+47	17	33.8310366	0.00000437	0.0000638	-0.1809	53561.5	58895.9	102	0.22	0.17	
1637+574	P 1637+574	905	16	38	13.45632957	+57	20	23.9789056	0.00000548	0.0000588	-0.0911	53568.0	58874.6	81	0.22		1.96
1638+398	NRAO 512	472	16	40	29.63279676	+39	46	46.0282645	0.00000400	0.0000669	-0.3362	53561.4	58937.7	138	0.09	0.13	1.88
1639-062	1639-062	1982	16	42	2.17771542	-06	21	23.6952503	0.00000332	0.0000796	-0.3993	55227.5	58937.7	119	0.16	0.19	
1639-200	1639-200	1983	16	42	5.29085688	-20	07	24.8494646	0.00001737	0.0002570	-0.8747	56340.6	58852.6	39	0.03	0.02	
1642+690	1642+690	907	16	42	7.84856536	+68	56	39.7561745	0.00000885	0.0000536	-0.0454	55227.2	58874.6	55	0.21		
1642-645	1642-645	4234	16	47	37.74138361	-64	38	0.2692176	0.00001699	0.0001328	0.0088	56297.7	58643.9	16			
1647-296	P 1647-296	477	16	50	39.54409355	-29	43	46.9548846	0.00000650	0.0000983	-0.5280	53561.3	58937.7	84		0.17	
1650-157	1650-157	1989	16	53	34.20640734	-15	51	29.8880012	0.00000964	0.0001745	-0.7822	57299.2	58937.7	49	0.03	0.03	
1652+398	DA 426	479	16	53	52.21671218	+39	45	36.6086180	0.00000436	0.0000767	-0.3164	53561.5	58937.7	120	0.05	0.06	2.55
1655+077	OS 092	480	16	58	9.01146467	+07	41	27.5403815	0.00000300	0.0000721	-0.4721	53561.3	58937.7	134	0.23	0.37	
1657+265	B2 1657+26	1133	16	59	24.14946945	+26	29	36.9428996	0.00000393	0.0000816	-0.4309	55304.2	58937.7	105	0.06	0.05	
1657-261	P 1657-261	484	17	00	53.15404312	-26	10	51.7256238	0.00000564	0.0000943	-0.5249	53610.1	58937.5	89		0.30	1.48
1657-562	1657-562	1287	17	01	44.85806370	-56	21	55.9010007	0.00001813	0.0003055	-0.4079	56297.8	58643.5	14			
1659-621	1659-621	3579	17	03	36.54116485	-62	12	40.0085649	0.00001226	0.0001110	-0.1264	56297.6	58643.5	16			
1705+018	P 1705+018	485	17	07	34.41527327	+01	48	45.6990832	0.00000325	0.0000805	-0.4382	53644.8	58937.7	139	0.08	0.09	1.15
1708-250	J1711-2509	4235	17	11	23.10222922	-25	09	1.5628517	0.00001477	0.0002167	-0.8542	58027.1	58937.7	20	0.08	0.10	
1710-269	1710-269	3588	17	13	31.27558310	-26	58	52.5268450	0.00001163	0.0001505	-0.7661	54526.6	58937.6	50		0.08	3.34

Source Name		ID No.	Right Ascension			Declination			RA Error (s)	Dec. Error (arcsec)	RA–Dec Corr.	Observation Epoch MJD		No. Obs.	Source Flux (Jy)		K Struct Index
B1950	Common		H	M	S	D	M	S				First	Last		10-60	10-40	
1711-208	1711-208	2006	17	14	32.51319684	-20	53	54.2929473	0.00029076	0.0039601	-0.9852	56697.8	58601.5	4		0.01	
1717+178	GC 1717+17	489	17	19	13.04849600	+17	45	6.4370987	0.00000333	0.0000758	-0.4688	53561.4	58937.6	137	0.18	0.13	2.22
1717-618	1717-618	4236	17	21	39.01655460	-61	54	43.0182873	0.00002137	0.0001661	-0.1672	56297.6	58643.5	14			
1718-259	1718-259	3600	17	21	55.97912834	-25	58	40.6932977	0.00001077	0.0001460	-0.7611	55451.2	58895.8	54	0.16	0.09	
1722+119	1722+119	4237	17	25	4.34090070	+11	52	15.4714874	0.00000575	0.0001283	-0.6362	56738.4	58937.6	72	0.02	0.02	
1719-729	1719-729	4238	17	26	1.11240885	-72	59	59.9921357	0.00003807	0.0001093	-0.0239	56297.7	58643.5	15			
1726+455	1726+455	912	17	27	27.65083800	+45	30	39.7312059	0.00000427	0.0000603	-0.1536	53561.5	58896.0	131	0.13	0.12	1.09
1726-269	1726-269	3611	17	29	8.22389661	-26	57	50.6797367	0.00334888	0.0283390	0.9988	56710.6	56710.6	1		0.01	
1730-130	NRAO 530	495	17	33	2.70578367	-13	04	49.5484608	0.00000327	0.0000789	-0.3751	53561.3	58937.7	157	0.71	0.44	2.11
1732+389	1732+389	700	17	34	20.57856452	+38	57	51.4429543	0.00000361	0.0000616	-0.2701	53561.4	58937.8	154	0.38	0.30	1.87
1732-593	1732-593	4239	17	37	19.67254214	-59	21	41.8919394	0.00001981	0.0002597	0.2112	56394.7	58643.6	12			
1738+476	OT 465	498	17	39	57.12910302	+47	37	58.3614588	0.00000482	0.0000846	0.1665	53568.1	58874.7	73	0.07		1.97
1739-152	1739-152	2032	17	42	11.66283863	-15	17	29.1586747	0.00000487	0.0000990	-0.5655	55304.3	58937.7	98	0.10	0.07	
1741-038	P 1741-038	500	17	43	58.85613443	-03	50	4.6170282	0.00000305	0.0000750	-0.4257	53561.3	58937.7	159	0.86	0.39	2.11
1742-078	1742-078	1288	17	45	27.10494418	-07	53	3.9483709	0.00000395	0.0000909	-0.5107	53609.3	58937.7	132	0.07	0.06	2.48
1743+173	GC 1743+17	501	17	45	35.20818972	+17	20	1.4234151	0.00000361	0.0000841	-0.4933	54961.6	58937.7	100	0.08	0.06	
1745+624	1745+624	920	17	46	14.03414507	+62	26	54.7382116	0.00001045	0.0000945	-0.0218	55227.4	58853.1	48	0.02		
1743-548	1743-548	4240	17	47	24.43509750	-54	50	21.5766901	0.00002050	0.0003223	0.0824	56395.5	58643.9	13			
1746+469	1746+470	921	17	47	26.64730530	+46	58	50.9261572	0.00000468	0.0000691	-0.0761	53727.6	58937.8	111	0.07	0.08	
1749+701	1749+701	502	17	48	32.84037463	+70	05	50.7687776	0.00000932	0.0000536	-0.1144	54016.0	58874.7	64	0.15		3.27
1749+096	OT 081	503	17	51	32.81858263	+09	39	0.7281517	0.00000274	0.0000676	-0.3974	53561.4	58937.6	165	1.15	0.94	1.11
1749-299	1749-299	3636	17	52	33.10597696	-29	56	44.8816295	0.00446013	0.0735474	-0.9998	56956.1	56956.1	1		0.02	
1750-187	1750-187	3639	17	53	9.08862061	-18	43	38.5232143	0.00000811	0.0001492	-0.7069	56340.7	58937.7	61	0.05	0.03	
1751+288	GC 1751+28	504	17	53	42.47366093	+28	48	4.9387656	0.00000335	0.0000720	-0.3564	53604.1	58937.8	152	0.23	0.06	0.83
1754+155	1754+155	1141	17	56	53.10214792	+15	35	20.8261824	0.00000328	0.0000754	-0.4544	53609.3	58937.7	148	0.10	0.09	1.58
1803+784	1803+784	693	18	00	45.68395493	+78	28	4.0184731	0.00001423	0.0000431	-0.0187	53568.0	58874.6	82	0.55		2.16
1800+440	1800+440	925	18	01	32.31484485	+44	04	21.9002097	0.00000406	0.0000597	-0.1570	53561.5	58937.9	146	0.22	0.15	0.64
1759-396	1759-396	2044	18	02	42.68000019	-39	40	7.9084829	0.00000838	0.0000997	-0.5196	54366.1	58937.5	75		0.15	
1802-381	J1805-3805	4241	18	05	41.64819960	-38	05	44.5250755	0.00004406	0.0003709	-0.9548	57300.0	58937.5	23		0.05	
1803-642	1803-642	4242	18	07	54.03268179	-64	13	50.1143306	0.00001937	0.0001369	0.0697	56297.7	58643.9	17			
1804-502	1804-502	4243	18	08	13.83555296	-50	11	53.6119975	0.00001541	0.0002746	-0.0603	56394.6	58643.9	12			
1810-700	1810-700	4244	18	15	51.79964898	-70	01	38.6430011	0.00004074	0.0001649	-0.3006	56297.7	58644.0	14			
1810-745	1810-745	4245	18	16	40.07817538	-74	29	7.3459017	0.00020576	0.0016510	-0.6774	57823.2	58643.9	3			
1817+387	1817+387	2050	18	19	26.54738150	+38	45	1.7860543	0.00000438	0.0000837	-0.1693	53757.5	58896.0	102	0.04	0.04	1.66
1815-553	P 1815-554	929	18	19	45.39951119	-55	21	20.7462153	0.00001582	0.0003338	0.0249	56394.8	58643.9	11			
1817-254	1817-254	664	18	20	57.84862648	-25	28	12.5837330	0.00007830	0.0010649	-0.9786	56381.7	56697.9	4			1.83
1821+107	P 1821+10	513	18	24	2.85526449	+10	44	23.7739869	0.00000412	0.0000963	-0.5459	53561.4	58937.8	118	0.04	0.03	
1822+012	1822+012	1145	18	24	48.14343720	+01	19	34.2014233	0.00000440	0.0000956	-0.6066	55304.3	58937.8	104	0.05	0.05	
1825-214	1825-214	2059	18	28	19.48871533	-21	23	38.7870662	0.00244697	0.0247348	-0.9997	56956.0	56956.0	1		0.01	
1824-582	1824-582	3679	18	29	12.40233266	-58	13	55.1619342	0.00001244	0.0001454	-0.1629	56297.8	58643.5	17			
1827-481	1827-481	4246	18	31	41.45663237	-48	05	21.0091830	0.00001598	0.0003215	-0.0569	56394.6	58643.6	9			
1829-207	1829-207	1241	18	32	11.04654566	-20	39	48.2024561	0.00000696	0.0001194	-0.5365	54526.7	58895.7	51	0.07	0.07	2.7
1830-589	1830-589	4247	18	34	27.47227333	-58	56	36.2741508	0.00002658	0.0002606	0.0861	56297.7	58643.9	14			
1831-711	P 1831-711	934	18	37	28.71493233	-71	08	43.5546443	0.00001836	0.0001167	-0.0097	56275.6	58643.9	17			
1839+548	1839+548	3696	18	40	57.37673372	+54	52	15.9105136	0.00000664	0.0000930	0.2654	55304.3	58874.0	49	0.04		
1842-289	1842-289	2069	18	45	51.36825137	-28	52	40.2761717	0.00001480	0.0001889	-0.8416	54366.1	58937.7	53		0.04	
1845-273	1845-273	2072	18	48	47.50414952	-27	18	18.0725152	0.00001059	0.0001416	-0.7694	55451.2	58937.7	63		0.05	
1849+670	1849+670	697	18	49	16.07232727	+67	05	41.6803295	0.00000725	0.0000488	-0.0676	53568.1	58874.6	82	0.40		0.96
1851+488	J1852+4855	1151	18	52	28.54784423	+48	55	47.4812814	0.00000500	0.0000856	0.2228	55058.9	58874.5	55	0.09		
1901+319	3C 395	521	19	02	55.93889528	+31	59	41.7017520	0.00000409	0.0000773	-0.4076	53727.7	58937.8	121	0.07	0.09	

Source Name		ID No.	Right Ascension			Declination			RA Error (s)	Dec. Error (arcsec)	RA–Dec Corr.	Observation Epoch MJD		No. Obs.	Source Flux (Jy)		K Struct Index
B1950	Common		H	M	S	D	M	S				First	Last		10-60	10-40	
1903+196	1903+196	2080	19	05	36.47211123	+19	43	8.0448259	0.00000664	0.0001314	-0.6422	56417.3	58937.8	64	0.03	0.03	
1908-201	OV-213	522	19	11	9.65286762	-20	06	55.1091874	0.00000429	0.0000867	-0.4724	53561.3	58937.7	115	0.37	0.35	
1903-802	P 1904-80	937	19	12	40.01909254	-80	10	5.9467359	0.00003851	0.0000997	-0.0054	56275.6	58643.8	17			
1910-466	1910-466	4248	19	14	13.81402681	-46	31	31.9385498	0.00001751	0.0001381	-0.6503	56394.6	58643.6	34		0.08	
1914-154	1914-154	2092	19	16	52.51098550	-15	19	0.0717597	0.00000544	0.0001027	-0.6253	55304.4	58937.7	103	0.06	0.07	
1920-211	OV-235	665	19	23	32.18979107	-21	04	33.3332038	0.00000432	0.0000864	-0.4700	53561.3	58937.8	113	0.10	0.25	
1921-293	OV-236	524	19	24	51.05592879	-29	14	30.1212075	0.00000518	0.0000891	-0.4722	53561.3	58937.8	94		0.92	1.43
1922-224	1922-224	2099	19	25	39.79017868	-22	19	35.1130617	0.00001329	0.0002025	-0.8231	58027.1	58937.7	26	0.03	0.04	
1925-610	1925-610	939	19	30	6.16006350	-60	56	9.1849377	0.00002826	0.0002815	-0.5202	56394.5	58643.9	12			
1928+154	1928+154	1159	19	30	52.76699357	+15	32	34.4271886	0.00000332	0.0000786	-0.4489	53609.3	58937.8	144	0.15	0.07	1.45
1929+226	1929+226	940	19	31	24.91679294	+22	43	31.2583166	0.00000388	0.0000828	-0.4756	53561.5	58937.8	116	0.06	0.06	
1910-872	1910-872	4249	19	34	25.97427379	-87	11	59.4775694	0.00040991	0.0002785	-0.3800	56394.5	58643.8	9			
1933-400	P 1933-400	528	19	37	16.21732581	-39	58	1.5535358	0.00000771	0.0000962	-0.4414	53561.3	58937.7	75		0.13	
1935+360	1935+360	2109	19	37	31.43663720	+36	07	35.8418279	0.00000740	0.0001689	-0.3560	55451.3	58874.7	62	0.02	0.02	
1936+046	1936+046	3758	19	38	30.66955024	+04	48	11.6143164	0.00000391	0.0000868	-0.5773	55304.4	58937.8	109	0.06	0.10	
1936-155	P 1936-15	529	19	39	26.65773982	-15	25	43.0587136	0.00000444	0.0000918	-0.5429	53561.4	58937.8	131	0.07	0.14	
1935-692	1935-692	944	19	40	25.52826500	-69	07	56.9687210	0.00099362	0.0131147	0.9709	58643.6	58643.6	1			
1946-200	1946-200	3771	19	49	53.42018195	-19	57	13.3302302	0.00000514	0.0000993	-0.5294	53609.3	58937.8	94	0.11	0.06	2.78
1949-052	1949-052	2121	19	51	47.46845054	-05	09	43.9626997	0.00000355	0.0000847	-0.5062	54820.7	58937.8	120	0.19	0.15	
1953-325	P 1953-325	3776	19	56	59.45525551	-32	25	46.0073949	0.00000789	0.0001072	-0.6248	55451.2	58937.7	71		0.12	
1954-388	P 1954-388	533	19	57	59.81924860	-38	45	6.3564215	0.00000670	0.0000930	-0.4280	53609.3	58937.7	87		0.38	
1958-179	OV-198	534	20	00	57.09042320	-17	48	57.6728265	0.00000350	0.0000811	-0.3799	53561.4	58937.8	149	0.48	0.61	0.2
2000+472	2000+472	1246	20	02	10.41824687	+47	25	28.7738385	0.00000537	0.0000789	0.0071	53694.3	58874.7	88	0.05	0.08	2.04
1959-639	1959-639	4250	20	04	29.47801882	-63	47	23.3099534	0.00004365	0.0002944	0.0354	56394.5	58643.8	10			
2007+659	2007+659	3789	20	07	28.77113273	+66	07	22.5355323	0.00000827	0.0000605	0.0932	55304.4	58874.5	52	0.11		
2008-159	P 2008-159	536	20	11	15.71091507	-15	46	40.2538901	0.00000349	0.0000829	-0.3817	53561.4	58937.8	144	0.36	0.27	
2013+163	2013+163	1164	20	16	13.86003773	+16	32	34.1128647	0.00000346	0.0000784	-0.4519	53652.2	58937.9	139	0.08	0.10	1.18
2021+317	2021+317	957	20	23	19.01735840	+31	53	2.3061626	0.00000387	0.0000753	-0.3735	53609.5	58937.9	125	0.10	0.08	2.73
2021+222	2021+222	3811	20	23	23.16023380	+22	23	52.5253326	0.00000968	0.0001785	-0.6937	56102.6	58937.8	63	0.02	0.02	
2022-077	2022-077	3813	20	25	40.66039702	-07	35	52.6890508	0.00000345	0.0000840	-0.4674	55059.1	58937.8	123	0.26	0.28	
2029+024	2029+022	1293	20	31	47.25111255	+02	39	37.2834088	0.00000444	0.0000969	-0.6040	55262.5	58937.8	109	0.04	0.04	
2029+121	P 2029+121	542	20	31	54.99427374	+12	19	41.3398465	0.00000338	0.0000813	-0.4777	53561.5	58895.9	149	0.07	0.06	
2030-689	2030-689	3827	20	35	48.87638142	-68	46	33.8408302	0.00002575	0.0001488	0.1227	56275.7	58643.9	16			
2031-662	2031-662	4251	20	35	51.52201650	-66	02	7.5333088	0.00004867	0.0006633	-0.1723	56394.7	57957.3	6			
2033-219	2033-219	2143	20	36	51.17271190	-21	46	36.7508070	0.00001532	0.0002335	-0.8654	55178.0	58937.8	51	0.03	0.02	
2037+511	3C 418	545	20	38	37.03476564	+51	19	12.6625288	0.00000494	0.0000702	0.2416	53644.5	58874.6	78	0.46		
2036-109	J2039-1046	4252	20	39	0.71041333	-10	46	41.8630912	0.00000567	0.0001175	-0.6804	57299.2	58937.8	64	0.05	0.06	
2047-266	2047-266	2151	20	50	24.69382874	-26	28	18.0580303	0.00000743	0.0001124	-0.6363	55451.3	58937.8	71		0.04	
2048+312	2048+312	1248	20	50	51.13148389	+31	27	27.3737005	0.00000439	0.0001005	-0.3215	53798.6	58937.0	100	0.05	0.03	2.19
2051-204	2051-204	2152	20	54	22.07243970	-20	16	16.8197634	0.00000748	0.0001231	-0.7036	55451.3	58895.9	69	0.05	0.06	
2052+239	2052+239	4253	20	54	29.53309346	+24	07	33.7650371	0.00000944	0.0001819	-0.6777	56892.4	58937.8	57	0.02	0.02	
2054-377	2054-377	960	20	57	41.60345838	-37	34	2.9908249	0.00000857	0.0001007	-0.5470	53652.2	58937.7	82		0.14	1.16
2059+034	P 2059+034	553	21	01	38.83415350	+03	41	31.3206882	0.00000318	0.0000785	-0.4566	54961.6	58937.9	129	0.44	0.59	
2059-786	2059-786	963	21	05	44.96131770	-78	25	34.5472160	0.00004162	0.0001349	0.0084	56275.7	58643.4	14			
2103+213	2103+213	2159	21	06	10.81818648	+21	35	35.9963345	0.00000498	0.0001004	-0.5803	55451.3	58937.9	96	0.04	0.04	
2106+143	J2108+1430	964	21	08	41.03215250	+14	30	27.0124657	0.00000384	0.0000857	-0.5373	55227.6	58937.9	112	0.06	0.06	
2106-413	P 2106-413	554	21	09	33.18854223	-41	10	20.6059924	0.00001238	0.0001187	-0.6689	53609.3	58895.8	82		0.07	
2112-144	2112-144	2165	21	15	18.43554407	-14	16	43.3724098	0.00000621	0.0001144	-0.7198	55451.3	58937.8	89	0.05	0.06	
2113+293	B2 2113+29B	555	21	15	29.41346427	+29	33	38.3668083	0.00000348	0.0000783	-0.2951	53561.6	58937.9	140	0.22	0.09	
2112-556	2112-556	4254	21	16	29.81615564	-55	27	20.4449362	0.00003710	0.0005628	0.4282	56394.8	58643.5	11			

Source Name		ID No.	Right Ascension			Declination			RA Error (s)	Dec. Error (arcsec)	RA–Dec Corr.	Observation Epoch MJD		No. Obs.	Source Flux (Jy)		K Struct Index
B1950	Common		H	M	S	D	M	S				First	Last		10-60	10-40	
2109-811	2109-811	965	21	16	30.84562902	-80	53	55.2232464	0.00004454	0.0000957	-0.0106	56297.5	58643.9	17			
2116-068	2116-068	3859	21	18	43.24215325	-06	36	17.9992887	0.00000530	0.0001445	-0.5196	55451.3	58895.9	70	0.04	0.03	
2117-614	2117-614	1175	21	21	4.07416923	-61	11	24.6249797	0.00003741	0.0003017	0.5773	56394.8	58643.4	11			
2121+547	2121+547	1176	21	23	5.31346940	+55	00	27.3252703	0.00000643	0.0000767	-0.0151	55227.5	58874.5	53	0.06		
2121+053	OX 036	557	21	23	44.51741022	+05	35	22.0928134	0.00000338	0.0000785	-0.4958	53652.2	58937.9	142	0.18	0.32	
2120-309	2120-309	2171	21	23	48.59955140	-30	46	5.4396534	0.00002742	0.0003051	-0.9391	57299.2	58895.9	29		0.04	
2123-463	2123-463	3866	21	26	30.70421563	-46	05	47.8926864	0.00001389	0.0001166	-0.5246	56395.6	58810.1	45		0.07	
2126-158	P 2126-15	559	21	29	12.17586970	-15	38	41.0416476	0.00000459	0.0000947	-0.5269	53609.3	58937.8	101	0.12	0.11	
2128-123	P 2128-12	563	21	31	35.26176510	-12	07	4.7957463	0.00000362	0.0000846	-0.4351	53609.4	58937.8	139	0.18	0.13	
2131-021	P 2131-021	564	21	34	10.30959016	-01	53	17.2390258	0.00000318	0.0000773	-0.4501	53561.5	58937.9	154	0.25	0.23	
2132-638	2132-638	4255	21	36	22.07471572	-63	35	51.0381211	0.00002531	0.0002434	0.1345	56297.7	58643.8	14			
2134+004	P 2134+004	565	21	36	38.58638776	+00	41	54.2119641	0.00000328	0.0000794	-0.4720	53561.5	58937.9	128	0.18	0.22	
2136+141	OX 161	567	21	39	1.30926663	+14	23	35.9921069	0.00000354	0.0000812	-0.4983	53561.5	58937.9	143	0.10	0.11	
2139-249	2139-249	3880	21	42	30.95903663	-24	44	38.8325027	0.00001565	0.0001873	-0.8943	55451.3	58937.7	66	0.03	0.04	
2143-298	J2146-2935	4256	21	46	5.75216739	-29	35	11.4116760	0.00002383	0.0002661	-0.9268	57299.2	58895.9	31		0.04	
2143-156	OX-173	570	21	46	22.97931828	-15	25	43.8859234	0.00000390	0.0000859	-0.4609	54016.0	58937.9	122	0.15	0.22	1.63
2141-784	2141-784	4257	21	47	5.84077664	-78	12	21.9119352	0.00003261	0.0001159	-0.0831	56275.7	58643.8	18			
2144+092	OX 074	571	21	47	10.16296730	+09	29	46.6721472	0.00000337	0.0000800	-0.4885	53561.5	58937.8	132	0.09	0.11	
2145+067	P 2145+06	572	21	48	5.45866639	+06	57	38.6038989	0.00000290	0.0000727	-0.4128	53561.5	58937.8	161	0.48	0.41	
2146-682	2146-682	4258	21	50	13.39072567	-68	02	50.4079366	0.00006073	0.0002305	0.2441	56522.7	58643.9	8			
2150+173	2150+173	968	21	52	24.81939936	+17	34	37.7949995	0.00000388	0.0000987	-0.4225	53561.6	58938.0	119	0.08	0.03	2.37
2153-760	2153-760	4259	21	57	59.22497355	-75	49	53.6076279	0.00003389	0.0001435	-0.1792	56297.5	58643.9	15			
2154-838	2154-838	4260	22	02	19.23761238	-83	38	11.8286166	0.00006109	0.0001016	0.0652	56275.7	58643.8	17			
2200+420	VRO 42.22.01	581	22	02	43.29139307	+42	16	39.9798639	0.00000391	0.0000616	-0.0663	53561.6	58937.9	152	0.40	0.25	
2201+171	2201+171	1180	22	03	26.89368976	+17	25	48.2476240	0.00000323	0.0000782	-0.4146	53604.1	58937.9	150	0.30	0.22	1.73
2200-617	2200-617	4261	22	03	59.63793318	-61	30	22.0108200	0.00004875	0.0002848	-0.1701	56395.6	58643.9	10			
2204-007	2204-007	3907	22	06	43.28260069	-00	31	2.4952562	0.00000393	0.0000921	-0.5809	56088.6	58937.9	86	0.09	0.14	
2204-540	P 2204-54	971	22	07	43.73325587	-53	46	33.8206721	0.00001285	0.0002627	0.1270	56275.6	58643.6	15			
2205-002	J2207-0002	4262	22	07	55.24706766	-00	02	15.0858807	0.00004714	0.0009818	-0.7556	57299.3	58874.7	7	0.01	0.01	
2208-137	2208-137	2202	22	11	24.09943451	-13	28	9.7239788	0.00000394	0.0000912	-0.4836	55304.5	58937.9	107	0.13	0.08	
2209+236	P 2209+236	588	22	12	5.96632865	+23	55	40.5434846	0.00000380	0.0000801	-0.4161	53561.6	58937.9	139	0.07	0.08	
2214+350	GC 2214+35	590	22	16	20.00991906	+35	18	14.1800418	0.00000475	0.0000881	-0.3865	53757.7	58937.9	107	0.05	0.03	
2223-114	2223-114	3934	22	25	43.71841352	-11	13	40.6988831	0.00003818	0.0005912	-0.9372	55451.4	58839.1	26		0.01	
2223-052	3C 446	594	22	25	47.25929348	-04	57	1.3909492	0.00000340	0.0000786	-0.4458	53561.5	58937.9	133	0.09	0.31	
2227-088	P 2227-08	596	22	29	40.08432769	-08	32	54.4357664	0.00000327	0.0000795	-0.4337	53561.5	58937.9	155	0.59	0.68	
2229+695	2229+695	694	22	30	36.46972772	+69	46	28.0768275	0.00001138	0.0000575	0.0021	55059.0	58874.0	53	0.06		
2227-399	P 2227-399	597	22	30	40.27855670	-39	42	52.0673084	0.00000885	0.0001026	-0.5327	55451.3	58937.8	76		0.08	
2227-627	2227-627	4263	22	31	7.91977930	-62	31	19.3443230	0.00004933	0.0002856	0.2396	56394.5	58643.9	11			
2232-488	P 2232-488	973	22	35	13.23655417	-48	35	58.7951144	0.00001190	0.0002921	0.0389	56275.6	58643.7	13			
2234+282	GC 2234+28	601	22	36	22.47084283	+28	28	57.4128675	0.00000352	0.0000720	-0.3313	53561.7	58937.9	124	0.36	0.40	
2233-234	2233-234	2217	22	36	26.23869530	-23	09	26.5975768	0.00000596	0.0001011	-0.5653	55451.3	58937.8	80	0.12	0.06	
2233-148	P 2233-148	600	22	36	34.08713961	-14	33	22.1898091	0.00000377	0.0000830	-0.4300	53561.6	58937.9	118	0.13	0.26	
2236-572	2236-572	3945	22	39	12.07588172	-57	01	0.8399155	0.00001256	0.0001916	0.0044	56394.8	58643.8	15			
2239+096	2239+096	1296	22	41	49.71731197	+09	53	52.4448215	0.00000387	0.0000885	-0.4807	53694.2	58874.7	126	0.02	0.03	1.54
2243-563	2243-563	4264	22	46	16.79256365	-56	07	46.0053441	0.00001764	0.0002596	0.1220	56394.8	58643.8	13			
2244-372	2244-372	1190	22	47	3.91729449	-36	57	46.3043712	0.00000805	0.0000991	-0.5378	55451.3	58937.8	81		0.10	
2245-128	2245-128	3953	22	47	52.64102386	-12	37	19.7218069	0.00000780	0.0001255	-0.7699	55451.3	58937.9	81	0.02	0.05	
2245-328	P 2245-328	608	22	48	38.68571583	-32	35	52.1885678	0.00000638	0.0000947	-0.4969	53561.5	58937.8	80		0.13	
2251+158	3C 454.3	611	22	53	57.74796298	+16	08	53.5609751	0.00000604	0.0001182	-0.5920	54282.6	58937.9	105	1.24	0.92	
2251-419	J2254-4139	4265	22	54	36.69753852	-41	39	40.2553257	0.00003492	0.0002587	-0.9125	57299.3	58895.9	29		0.05	

Source Name		ID No.	Right Ascension			Declination			RA Error (s)	Dec. Error (arcsec)	RA–Dec Corr.	Observation Epoch MJD		No. Obs.	Source Flux (Jy)		K Struct Index
B1950	Common		H	M	S	D	M	S				First	Last		10-60	10-40	
2251-597	2251-597	4266	22	54	56.82957982	-59	26	0.6878488	0.00001859	0.0002066	-0.0048	56394.8	58643.8	15			
2252-090	P 2252-089	614	22	55	4.23979582	-08	44	4.0218946	0.00000604	0.0001184	-0.6042	55793.4	58937.9	80	0.02	0.03	
2253+417	GC 2253+41	615	22	55	36.70786474	+42	02	52.5325443	0.00000445	0.0000772	-0.0093	54960.9	58937.1	102	0.07	0.05	
2254+074	GC 2254+07	617	22	57	17.30312069	+07	43	12.3024039	0.00000374	0.0000843	-0.4621	53561.6	58937.0	121	0.05	0.05	
2254+024	P 2254+024	616	22	57	17.56308871	+02	43	17.5115753	0.00000375	0.0000892	-0.5136	53561.6	58938.0	125	0.08	0.07	
2255-282	P 2255-282	619	22	58	5.96286216	-27	58	21.2570742	0.00000536	0.0000898	-0.4813	53561.5	58937.9	96		0.61	
2256-084	2256-084	2234	22	59	0.68883879	-08	11	3.0461387	0.00002323	0.0003426	-0.9448	55451.4	58895.9	53	0.01	0.02	
2309+454	J2311+4543	1197	23	11	47.40899434	+45	43	56.0163557	0.00000474	0.0000734	0.0134	53694.4	58895.1	109	0.07	0.09	1.61
2312-505	2312-505	4267	23	15	44.33031897	-50	18	39.7045271	0.00001043	0.0002238	-0.0956	56297.6	58643.8	14			
2315-172	2315-172	2242	23	18	11.36137372	-16	59	29.1888746	0.00000808	0.0001334	-0.7464	56341.0	58937.9	76	0.03	0.04	
2316+238	2316+238	4002	23	18	33.96785970	+24	04	39.7491727	0.00000534	0.0001091	-0.5632	55451.5	58937.9	94	0.04	0.03	
2318+049	GC 2318+04	627	23	20	44.85659844	+05	13	49.9523636	0.00000353	0.0000803	-0.4882	53561.6	58937.0	146	0.10	0.14	
2319+272	B2 2319+27	629	23	21	59.86224084	+27	32	46.4436598	0.00000367	0.0000768	-0.3553	53561.6	58937.9	123	0.17	0.18	
2320-035	P 2320-035	633	23	23	31.95374643	-03	17	5.0240063	0.00000322	0.0000790	-0.4139	53561.5	58937.0	133	0.34	0.46	
2325+093	2325+093	1299	23	27	33.58055357	+09	40	9.4625456	0.00000313	0.0000752	-0.4070	53568.3	58938.0	156	0.30	0.36	0.73
2326-502	2326-502	4268	23	29	20.88174171	-49	55	40.6548922	0.00001317	0.0002665	0.1699	56297.6	58643.7	13			
2328+107	P 2328+10	636	23	30	40.85225639	+11	00	18.7094150	0.00000381	0.0000846	-0.5248	53561.6	58937.9	125	0.09	0.07	
2331-240	2331-240	979	23	33	55.23781892	-23	43	40.6585923	0.00000469	0.0000892	-0.4885	53561.5	58937.9	104	0.17	0.39	
2332-531	2332-531	4269	23	34	44.91671985	-52	51	19.6329323	0.00002230	0.0004769	-0.5271	56297.6	57851.3	11			
2335-027	P 2335-027	644	23	37	57.33906640	-02	30	57.6293962	0.00000338	0.0000798	-0.4428	53609.5	58937.0	148	0.13	0.10	
2344+092	P 2344+09	649	23	46	36.83855166	+09	30	45.5149488	0.00000365	0.0000832	-0.4920	53561.6	58938.0	131	0.18	0.14	
2344-514	2344-514	4033	23	47	19.86408080	-51	10	36.0652680	0.00001440	0.0002896	0.1883	56297.6	58643.7	15			
2345-500	2345-500	4270	23	47	43.68518995	-49	46	27.8752562	0.00001644	0.0003892	-0.2556	56297.6	58643.7	12			
2345+061	2345+061	4271	23	48	31.77065620	+06	24	59.7822213	0.00000847	0.0003321	-0.4698	56892.5	58847.0	39	0.02	0.01	
2346+385	2346+385	4034	23	49	20.82655619	+38	49	17.5583423	0.00000421	0.0000726	-0.2488	53609.6	58937.1	140	0.09	0.12	2.11
2346-498	2346-498	4272	23	49	25.37887558	-49	32	26.5482643	0.00002016	0.0003852	0.4085	56395.8	58643.8	11			
2351+456	2351+456	981	23	54	21.68026577	+45	53	4.2364760	0.00000545	0.0000747	-0.0694	54933.5	58937.1	99	0.04	0.07	
2351-154	2351-154	695	23	54	30.19515533	-15	13	11.2131458	0.00000525	0.0000972	-0.6087	53561.6	58937.9	111	0.05	0.10	
2353+816	2353+816	1252	23	56	22.79395035	+81	52	52.2552071	0.00002122	0.0000452	0.0199	53568.0	58874.5	80	0.12		1.34
2354-021	2354-021	4040	23	57	25.13792907	-01	52	15.5095807	0.00000605	0.0001222	-0.5733	55451.5	58937.0	80	0.03	0.03	
2355-534	P 2355-534	983	23	57	53.26603257	-53	11	13.6895950	0.00001280	0.0002267	-0.0222	56275.6	58643.8	15			
2355-106	P 2355-106	658	23	58	10.88237737	-10	20	8.6115608	0.00000362	0.0000822	-0.4353	53561.6	58937.0	144	0.08	0.15	
2357-318	2357-318	2273	23	59	35.49152971	-31	33	43.8248220	0.00000993	0.0001217	-0.7096	54366.3	58937.9	78		0.05	

3 References

1. Altamimi, et al, ITRF2014: a new Release of the Interantional Celestail Reference Frame modeling non-linear station locations. improved solution of the international terrestrial reference frame. *JGR: Solid Earth*, 2016. https://doi.org/10.1002/2016JB013098 https://agupubs.onlinelibrary.wiley.com/doi/full/10.1002/2016JB013098
2. Boehm, J., B. Werl, H. Schuh, "Troposphere mapping functions for GPS and very long baseline interferometry from European Centre for Medium−Range Weather Forecasts operational analysis data", *J. Geophys. Res*., 111, B02406, Feb. 2006. http://www.hg.tuwien.ac.at/~ecmwf1/boehm_etal_3rd.pdf
3. Border, J.S., A Global Approach to Delta Differenced One-way Range, Proc. 25th ISTS and 19th ISSFD, Kakzawa, Japan, 4-11 June 2006. https://issfd.org/ISSFD_2009/OrbitDeterminationI/Border.pdf
4. CCSDS, `DeltaDOR Technical Characteristics and Performance', "GreenBook", CCSDS 500.1-G-2, Nov 2019. https://public.ccsds.org/Pubs/500x1g2.pdf
5. Charlot et al, The Celestial Reference Frame at 24 and 43 GHz. II. Imaging, AJ, 139, 2010. https://iopscience.iop.org/article/10.1088/0004-6256/139/5/1713
6. Charlot, P., Jacobs, C.S., et al, The Third Realization of the International Celestial Reference Frame by Very Long Baseline Interferometry, A&A, accepted July 2020.
7. Davis, et al, Geodesy by Radio Interferometry: Effects of Atmospheric Modelling Errors on Estimates of Baseline Length, Radio Science 20, 6, 1593, 1985. https://ui.adsabs.harvard.edu/abs/1985RaSc...20.1593D/abstract
8. deGroot, N. F., `Ka-Band (32 GHz) Allocations for Deep Space,' NASA JPL TDA Progress Report, 42-88, pp. 104--109, 15 Feb. 1987. https://ipnpr.jpl.nasa.gov/progress_report/42-88/88N.PDF
9. de Witt, A., Jacobs, C.S, et al, `K-band Celestial Frame: Imaging Results,' AJ, 2021, in preparation.
10. Fricke, W.; Schwan, H.; Lederle, T.; Bastian, U.; Bien, R.; Burkhardt, G.; Du Mont, B.; Hering, R.; Jährling, R.; Jahreiß, H.; Röser, S.; Schwerdtfeger, H.-M.; Walter, H. G., `Fifth fundamental catalogue (FK5). Part 1: The basic fundamental stars,' Veröffentlichungen Astronomisches Rechen-Institut Heidelberg, Verlag G. Braun, Karlsruhe, No. 32, p. 1-106,1988. https://ui.adsabs.harvard.edu/abs/1988VeARI..32....1F/abstract
11. Hunter, J.A. et al, Orbiting Deep Space Relay Station Study: Final Report, JPL Publication 79-30, vol. III, Jet Propulsion Laboratory, Pasadena CA, 15 June 1979. http://hdl.handle.net/2060/19790020039
12. IAU General Assembly XXIII, Resolution B2-d, Kyoto, Japan, August 1997. http://iau.org/static/resolutions/IAU1997_French.pdf
13. IAU General Assembly XXVII, Resolution B3, on the Second Realization of the International Celestial Reference Fame, Rio de Janeiro, Brazil, 13 August 2009. https://www.iau.org/static/resolutions/IAU2009_English.pdf

14. IAU General Assembly XXX, Resolution B2, on the Third Realization of the International Celestial Reference Frame, Vienna, Austria, August 2018, https://www.iau.org/static/resolutions/IAU2018_ResolB2_English.pdf
15. Jacobs, C.S., M.B. Heflin, G.E. Lanyi, O.J. Sovers, and J.A. Steppe, `Rotational Alignment Altered by Source Position Correlations,' Proc. of IVS 2010 General Meeting, Hobart, Tasmania Australia, 8--11 Feb 2010, eds. D. Behrend and K. D. Baver, NASA/CP-2010-215864, Dec 2010. https://ui.adsabs.harvard.edu/abs/2010ivs..conf..305J/abstract
16. Kesteven, M.J.L. and A. H. Bridle, "Index of extragalactic radio−source catalogues", *J. Royal Astronomical Society of Canada*, Vol. 71, Feb. 1977, p. 21−39. http://articles.adsabs.harvard.edu/full/1977JRASC..71...21K
17. Ma, Arias, Eubanks, Fey, Gontier, Jacobs, Sovers, Archinal, Charlot, The [First] International Celestial Reference Frame as Realized by VLBI, AJ, 116, 1, 516, 1998. https://ui.adsabs.harvard.edu/abs/1998AJ....116..516M/abstract
18. Ma, C., E.F. Arias, G. Bianco, D. A. Boboltz, S.L. Bolotin, P. Charlot, G. Engelhardt, A.L. Fey, R.A. Gaume, A.−M. Gontier, R. Heinkelmann, C.S. Jacobs, S. Kurdubov, S.B. Lambert, Z.M. Malkin, A. Nothnagel, L. Petrov, E. Skurikhina, J. Sokolova, J. Souchay, O.J. Sovers, V. Tesmer, O.A. Titov, G. Wang, V. Zharov C. Barache, S. Boeckmann, A. Collioud, J.M. Gipson, D. Gordon, S.O. Lytvyn, D.S. MacMillan, R. Ojha, "IERS Technical Note No. 35: The Second Realization of the ICRF by VLBI," IERS, Bundesamt fur Kartographie und Geodasie, BKG, Frankfurt am Main, A. Fey, D. Gordon, and C.S. Jacobs, Eds. Germany, Oct. 2009. http://www.iers.org/nn_11216/IERS/EN/Publications/TechnicalNotes/tn35.html
19. MacMillan, D., et al, Galacto-centric Acceleration in VLBI Analysis: Findings of IVS working group 8, A&A, 630, 2019.

    https://doi.org/10.1051/0004-6361/201935379
20. Matthews, P.M., T.A. Herring, and B.A. Buffet, "Modeling of Nutation and Precession: New nutation series for Nonrigid Earth and Insights into the Earth's Interior," *J. Geophys. Res.* 107, no. B4, 10.1029/2001JB000390, Apr. 2002.

    https://ui.adsabs.harvard.edu/abs/2002JGRB..107.2068M/abstract
21. Ratcliff, J.T. and R.S. Gross, "Combinations of Earth Orientation Measurements: SPACE2018, COMB2018, and POLE2018," *JPL Publication 19−7*, Jet Propulsion Laboratory, Pasadena, CA, October 2019.

    https://keof.jpl.nasa.gov/combinations/SpaceCombPole_latest.pdf
22. Shambayati, Morabito, Border, Davarian, Lee, Mendoza, Britcliffe, Weinreb, Mars Reconaissance Orbiter Ka-band (32 GHz) Demonstration: Cruise Phase Operations, AIAA 2006-5786, Space Ops 2006 Conference, Rome, Italy, 19-23 June 2006. https://doi.org/10.2514/6.2006-5786
    https://arc.aiaa.org/doi/pdfplus/10.2514/6.2006-5786
23. Slobin, S.D., DSN 810-005 module 101-G, 70-m Subnet Telecommunications Interfaces, 2019 Sep 04.
    https://deepspace.jpl.nasa.gov/dsndocs/810-005/101/101G.pdf

24. Slobin, S.D., DSN 810-005 module 103-C, 34-m HEF subnet Telecommunications Interfaces, 2014 Aug 01. https://deepspace.jpl.nasa.gov/dsndocs/810-005/103/103C.pdf
25. Slobin, S.D., DSN 810-005 module 104-L, 34-m BWG Stations Telecommunications Interfaces, 2019 Oct 16. https://deepspace.jpl.nasa.gov/dsndocs/810-005/104/104L.pdf
26. Sovers, O. J., J. L. Fanselow, and C. S. Jacobs, "Astrometry and Geodesy with Radio Inteferometry: Experiments, Models, Results," *Reviews of Modern Physics, 70, 4*, October, 1998. http://link.aps.org/doi/10.1103/RevModPhys.70.1393

4 Acknowledgements

Production of the radio source catalog requires the efforts and cooperation of a large number of people. This includes the support staffs at the Deep Space Network who ensure that the data are collected especially Cristina Garcia-Miro, Shinji Horiuchi, and Larry Snedeker. Steve Lowe wrote the core of the VLBI scheduling and processing software: the S scheduler, SOFTC correlator, and FIT/CFIT fringe fitting. We also thank the correlation operators, and the analysts who have developed the models and software to convert the delay and delay rate observations to produce final estimates of the source positions, and finally the authors of this document. Among these we would like to particularly acknowledge Peter Kroger, Christopher Volk, Christine Chang, Christopher Jacobs, Gabor Lanyi, Charles Naudet, Ojars Sovers, and Alina Bedrossian.

The research was carried out at the Jet Propulsion Laboratory, California Institute of Technology, under a contract with the National Aeronautics and Space Administration (80NM0018D0004).

Deep Space Network

201
Frequency and Channel Assignments

Document Owner:		Approved by:	
Signature Provided	04/19/2022	Signature Provided	04/19/2022
Dong K. Shin DSN System Engineer	Date	Timothy Pham Communications Systems Chief Engineer	Date

Prepared by:		Released by:	
Signature Provided	04/19/2022	Signature Provided	05/04/2022
Dong K. Shin DSN System Engineer	Date	Christine Chang DSN Document Release Authority	Date

DSN No. **810-005, 201, Rev. F**
Issue Date: May 04, 2022
JPL D-19379; CL#22-2078

Jet Propulsion Laboratory
California Institute of Technology

Users must ensure that they are using the current version in DSN Telecommunications Link Design Handbook website:
https://deepspace.jpl.nasa.gov/dsndocs/810-005/

Review Acknowledgment

By signing below, the signatories acknowledge that they have reviewed this document and provided comments, if any, to the signatories on the Cover Page.

Signature Provided	03/24/2022	Signature Provided	03/22/2022
Jeff Berner DSN Project Chief Engineer	Date	Andrew O'Dea DSN TTC System Engineer	Date
Signature Provided	03/23/2022	Signature Provided	04/19/2022
Alina Bedrossian DSN OBD System Engineer	Date	Harvey Soldan Supervisor, DSN Systems Engineering	Date

Document Change Log

Rev	Issue Date	Prepared By	Affected Paragraphs	Change Summary
Initial	11/30/2000	Robert Sniffin	All	All
A	9/19/2008	Robert Sniffin	2.4, Tables 1 & 2	Adds 26 GHz assignment. Removes suggested turn-around ratios in Ka-band
B	12/15/2009	Andrew Kwok	Page 4	Removed references of the 26-m subnet stations for they have been decommissioned.
C	12/15/2014	Dong Shin	Page 6	Add a footnote for Deep Space S-band uplink restriction at Madrid tracking stations.
D	09/04/2020	Dong Shin	2, 2.2, 2.4, Table 1, 2, 3, 4, 6-1, 6-2, 6-3	Added K-band, updated Table 3 & 4 per SFCG recommendations, added Ka-band channels (Table 6-1, 6-2, 6-3) per SFCG recommendations
E	02/05/2021	Dong Shin	Table 1	Corrected K-band transponder turnaround ratio
F	05/4/2022	Dong Shin	2 Table 1	Added SFCG recommended publication for channel assignments. Updated K-band Doppler and range capability and implementation schedule

Contents

Tables

1 Introduction

1.1 Purpose and Scope

This module provides basic information about the frequencies that are available in the Deep Space Network (DSN) and presents the way certain of the DSN frequency allocations have been divided into channels. It does not specify which stations can or will support assigned frequencies. That information is contained in the appropriate Telecommunications Interfaces modules (101, 70-m Antenna Subnet Telecommunications Interfaces; 103, 34-m HEF Antenna Subnet Telecommunications Interfaces; or 104, 34-m BWG Stations Telecommunications Interfaces) of this handbook. It also does not include propagation characteristics of the frequencies. This information is provided in module 105 (Atmospheric and Environmental Effects) and module 106 (Solar Corona and Solar Wind Effects) of this handbook.

2 General Information

The DSN has developed channel plans to provide for orderly selection and assignment of frequencies for deep-space missions (Category B, greater than 2 million km from Earth) for the S-, X-, and Ka-bands in compliance with Space Frequency Coordination Group (SFCG) recommendations (SFCG Recommendation SFCG 7-1R6). These deep space channel plans are based on bandwidth and transponder turnaround-ratio considerations. The plans allow simultaneous phase coherent uplink (Earth-to-space) and downlink (space-to-Earth) transmissions where the uplink and downlinks are in the same or different bands. In accordance with SFCG Recommendation SFCG 13-3R3, there are no designated channel number/frequency assignments for K-Band.

Through international agreements, the International Telecommunications Union (ITU) allocates and regulates portions of the frequency spectrum for both commercial and government use. The primary objective of the ITU is to establish regulatory procedures for the coordinated use of frequencies by those agencies permitted to operate in the allocated bands. The ITU has allocated certain bands to deep space (Category B) research. In some cases, the deep space missions may be required to conditionally share a frequency band between multiple users in the same band.

The Consultative Committee for Space Data Systems (CCSDS) is an international organization for space agencies interested in mutually developing standard transmission and data handling techniques to support space research, including space science and applications. As a member of the CCSDS, NASA has submitted recommendations for various space systems applications.

The National Telecommunications and Information Administration (NTIA), an agency of the U.S. Department of Commerce, is the Executive Branch's principal authority on domestic and international telecommunications and information technology issues. During the planning phase of all missions using the DSN, the proposed operating frequencies and other operating parameters are reviewed by the NTIA for approval through the System Review process. The NTIA evaluations are based upon the technical and regulatory criteria for the efficient and coordinated use of the frequency spectrum by NASA missions.

2.1 Tracking Modes of Operation

The following paragraphs describe the various ways in which the telecommunications link can be configured for radio tracking. The source of the uplink signal and the choice of references for measuring the received frequency determine the mode of operation.

2.1.1 One-way

The spacecraft generates the downlink signal(s) from an onboard oscillator. The DSN compares the received frequency against a locally generated frequency.

2.1.2 Two-way

The DSN transmits a signal to the spacecraft. The spacecraft tracks the phase of the uplink signal and generates a phase coherent downlink signal. The DSN compares the received frequency with the same reference frequency from which the uplink was generated.

2.1.3 Three-way

The spacecraft is tracked by two stations—the uplink is transmitted from one antenna and the downlink is received at a different antenna. The most common application of this mode is during the handover between stations at two different Deep Space Communication Complexes (DSCCs). When three-way tracking is done within one DSCC, both uplink and downlink equipment share a common frequency reference. When three-way tracking is done across two DSCCs, higher noise performance is expected due to the use of two different frequency references.

2.1.4 Coherent Three-way

Coherent three-way tracking is three-way tracking when the transmitting and receiving stations share a common frequency reference. This is possible at all three DSN complexes as all antennas at a complex share the same frequency reference.

2.2 Spacecraft Transponder Turnaround Ratios

To measure two-way or three-way Doppler shift, the spacecraft must transmit a downlink signal that is phase coherent with the uplink signal. Table 1 provides the recommended spacecraft transponder turnaround ratios for various uplink and downlink frequency bands. The tracking equipment at the DSN 34-m and 70-m stations can accommodate other turnaround ratios but this support must be negotiated through the JPL Frequency Manager, see <https://deepspace.jpl.nasa.gov/about/commitments-office/>.

Table 1. Spacecraft Transponder Turnaround Ratios

Uplink	Downlink	Ratio (downlink/uplink)
S	S	240/221
S	X	880/221
S	Ka	3328/221, 3344/221, 3360/221
X	S	240/749
X	X	880/749
X	K_a	3328/749, 3344/749, 3360/749
K*	K	2720/2407, 2760/2407, 2816/2407**
K_a	K_a	3344/3599, 3360/3599

* K-band uplink implementation, at two 34-meter BWG antennas per complex, will start February 2022 and complete July 2024.

** Due to the difference between 600 MHz uplink and 1500 MHz downlink bandwidths, the coherency between uplink and downlink using these transponder ratios does not apply to the entire allocated bandwidth.

2.3 Frequency Bands Allocated by the International Telecommunication Union (ITU)

Frequency ranges have been allocated by the ITU for use in deep space and near-Earth research. These ranges are listed in Table 2.

Table 2. Allocated Frequency Bands

Band Designation	Deep Space Bands (for spacecraft outside 2 million km from Earth)		Near Earth Bands (for spacecraft within 2 million km from Earth)	
	Uplink (Earth to space)	Downlink (space to Earth)	Uplink (Earth to space)	Downlink (space to Earth)
S-band	2110–2120*	2290–2300	2025–2110	2200–2290
X-band	7145–7190	8400–8450	7190–7235	8450–8500
K-band (Near Earth)	N/A	N/A	22550-23150	25500–27000
Ka-band (Deep Space)	34200–34700	31800–32300	N/A	N/A

* Deep Space S-band is not available at Madrid tracking stations due to a conflict with IMT-2000 users, per agreement between NASA and Secretaria de Estado de Telecomunicaciones para la Sociedad de la Informacion (SETSI), January 2001”

2.4 Deep Space Frequency Channels

The DSN has divided the frequency ranges allocated for deep space use into channels for tracking support associated with a given transponder ratio. Note that the frequencies out of the allocated ranges for deep space research are not shown in the tables.

The S-band downlink center frequency ($F_{ch(14)}$ = 2295 MHz) is used to derive all entries in the tables using the expressions

$$F_{ch(n)} = (n\text{-}14)*(10/27) + 2295 \text{ MHz, rounded to the nearest Hertz}$$

where $F_{ch(n)}$ is the center frequency (in MHz) of channel *n* rounded to the nearest Hz, and the ratio 10/27 is the spacing (in MHz) between the centers of two adjacent channels.

Frequencies for other columns are derived by the procedure described below. The calculated downlink frequencies may differ by one or two Hertz between the tables because each table assumes an integer uplink frequency and precise turnaround ratios.

(1) The uplink frequency specified in the table is calculated from the expression

$$f_{ch(n)} = F_{ch(n)} \times TM/240, \text{ rounded to the nearest Hertz,}$$

where

$f_{ch(n)}$ is the frequency of uplink channel *n* being calculated;

Fch(*n*) is the frequency of channel *n* calculated for the S-band downlink column (including values for out-of-band channels);

TM is the Transmit Multiplier of the frequency band, that is, *TM* = 221 for S-uplink and 749 for X-uplink.

(2) The downlink frequencies specified in the table are calculated from the expression

$$F_{ch(n)} = f_{ch(n)} \times TR, \text{ rounded to the nearest Hertz,}$$

where

$F_{ch(n)}$ is the frequency of channel *n* for the downlink columns;

$f_{ch(n)}$ is the frequency of channel *n* in the uplink column;

TR is the Turnaround Ratio for the downlink frequency band provided in Table 1.

Because Ka-band has a wide bandwidth, channels are divided into three categories: channel L1 to L50 for a low-band as shown in Table 6-1, channel 1 to 42 for a mid-band as shown in Table 6-2, and channel H1 to H34 for a high-band as shown in Table 6-3.

Although the DSN is capable of supporting two-way and three-way tracking in S-and X-band where the downlink frequency is not at the frequency specified for the selected uplink channel, the use of non-standard turn-around rations is highly discouraged. Therefore, only channels 5 through 27 fully support coherent uplink and downlink for both frequency bands. Channel 28, for example, supports S- or X-band uplink with a coherent X-band downlink, but not with a coherent S-band downlink.

Channel selection is also highly dependent on bandwidth considerations. The channel plan was developed to accommodate both low-rate spacecraft operating within a single channel and higher-rate spacecraft requiring one or more adjacent channels on each side of the nominal operating channel. Before selecting operating frequencies or channels for a project, the telecommunication designer should consult the JPL Frequency Spectrum Management (see< https://deepspace.jpl.nasa.gov/about/commitments-office/>) to avoid frequency interference with other spacecraft, present or planned.

Table 3. Frequency and Channel Assignments for S-band Uplink and S/X-bands Downlink

Channel	S-band U/L (MHz)	S-band D/L (MHz)	X-band D/L (MHz)
1		2290.185185	
2		2290.555556	
3		2290.925926	8400.061729
4		2291.296296	8401.419752
5	2110.243056	2291.666667	8402.777779
6	2110.584105	2292.037037	8404.135802
7	2110.925154	2292.407407	8405.493825
8	2111.266204	2292.777778	8406.851853
9	2111.607253	2293.148148	8408.209877
10	2111.948303	2293.518519	8409.567903
11	2112.289352	2293.888889	8410.925927
12	2112.630401	2294.259259	8412.283950
13	2112.971451	2294.629630	8413.641977
14	2113.312500	2295.000000	8415.000000
15	2113.653549	2295.370370	8416.358023
16	2113.994599	2295.740741	8417.716050
17	2114.335648	2296.111111	8419.074073
18	2114.676697	2296.481481	8420.432097
19	2115.017747	2296.851852	8421.790123
20	2115.358796	2297.222222	8423.148147
21	2115.699846	2297.592593	8424.506175
22	2116.040895	2297.962963	8425.864198
23	2116.381944	2298.333333	8427.222221
24	2116.722994	2298.703704	8428.580248
25	2117.064043	2299.074074	8429.938271
26	2117.405092	2299.444444	8431.296295
27	2117.746142	2299.814815	8432.654321
28	2118.087191		8434.012345
29	2118.428241		8435.370372
30	2118.769290		8436.728395
31	2119.110339		8438.086418
32	2119.451389		8439.444446
33	2119.792438		8440.802469
34			8442.160493
35			8443.518520
36			8444.876543
37			8446.234570
38			8447.592593
39			8448.950616

Table 4. Frequency and Channel Assignments for X-band Uplink and S-/X-bands Downlink

Channel	X-band U/L (MHz)	S-band D/L (MHz)	X-band D/L (MHz)
1	7147.286265	2290.185185	
2	7148.442131	2290.555556	
3	7149.597994	2290.925926	8400.061729
4	7150.753857	2291.296296	8401.419752
5	7151.909723	2291.666667	8402.777779
6	7153.065586	2292.037037	8404.135802
7	7154.221449	2292.407407	8405.493825
8	7155.377316	2292.777778	8406.851853
9	7156.533179	2293.148148	8408.209877
10	7157.689045	2293.518519	8409.567903
11	7158.844908	2293.888889	8410.925927
12	7160.000771	2294.259259	8412.283950
13	7161.156637	2294.629630	8413.641977
14	7162.312500	2295.000000	8415.000000
15	7163.468363	2295.370370	8416.358023
16	7164.624229	2295.740741	8417.716050
17	7165.780092	2296.111111	8419.074073
18	7166.935955	2296.481481	8420.432097
19	7168.091821	2296.851852	8421.790123
20	7169.247684	2297.222222	8423.148147
21	7170.403551	2297.592593	8424.506175
22	7171.559414	2297.962963	8425.864198
23	7172.715277	2298.333333	8427.222221
24	7173.871143	2298.703704	8428.580248
25	7175.027006	2299.074074	8429.938271
26	7176.182869	2299.444444	8431.296295
27	7177.338735	2299.814815	8432.654321
28	7178.494598		8434.012345
29	7179.650464		8435.370372
30	7180.806327		8436.728395
31	7181.962190		8438.086418
32	7183.118057		8439.444446
33	7184.273920		8440.802469
34	7185.429783		8442.160493
35	7186.585649		8443.518520
36	7187.741512		8444.876543
37	7188.897378		8446.234570
38			8447.592593
39			8448.950616

Table 5. Frequency and Channel Assignments for X-band Uplink and Ka-band Downlink

Channel	X-band U/L (MHz)	Ka-band D/L (MHz), 3328/749	Ka-band D/L (MHz), 3344/749	Ka-band D/L (MHz), 3360/749
1	7147.286265		31909.913578	32062.592591
2	7148.442131		31915.074080	32067.777784
3	7149.597994		31920.234569	32072.962964
4	7150.753857		31925.395057	32078.148144
5	7151.909723		31930.555559	32083.333337
6	7153.065586		31935.716048	32088.518517
7	7154.221449		31940.876536	32093.703696
8	7155.377316		31946.037042	32098.888894
9	7156.533179		31951.197531	32104.074074
10	7157.689045	31803.456798	31956.358033	32109.259267
11	7158.844908	31808.592595	31961.518521	32114.444447
12	7160.000771	31813.728392	31966.679010	32119.629627
13	7161.156637	31818.864203	31971.839512	32124.814820
14	7162.312500	31824.000000	31977.000000	32130.000000
15	7163.468363	31829.135797	31982.160488	32135.185180
16	7164.624229	31834.271608	31987.320990	32140.370373
17	7165.780092	31839.407405	31992.481479	32145.555553
18	7166.935955	31844.543202	31997.641967	32150.740733
19	7168.091821	31849.679012	32002.802469	32155.925926
20	7169.247684	31854.814810	32007.962958	32161.111106
21	7170.403551	31859.950624	32013.123464	32166.296304
22	7171.559414	31865.086422	32018.283952	32171.481483
23	7172.715277	31870.222219	32023.444441	32176.666663
24	7173.871143	31875.358029	32028.604943	32181.851856
25	7175.027006	31880.493826	32033.765431	32187.037036
26	7176.182869	31885.629624	32038.925920	32192.222216
27	7177.338735	31890.765434	32044.086422	32197.407409
28	7178.494598	31895.901231	32049.246910	32202.592589
29	7179.650464	31901.037042	32054.407412	32207.777782
30	7180.806327	31906.172839	32059.567901	32212.962962
31	7181.962190	31911.308636	32064.728389	32218.148142
32	7183.118057	31916.444451	32069.888895	32223.333340
33	7184.273920	31921.580248	32075.049384	32228.518520
34	7185.429783	31926.716045	32080.209872	32233.703699
35	7186.585649	31931.851856	32085.370374	32238.888893
36	7187.741512	31936.987653	32090.530863	32244.074073
37	7188.897378	31942.123463	32095.691365	32249.259266
38		31947.259260	32100.851853	32254.444446
39		31952.395058	32106.012341	32259.629625
40		31957.530868	32111.172843	32264.814819
41		31962.666665	32116.333332	32269.999999
42		31967.802462	32121.493820	32275.185178

Table 6-1. Frequency and Channel Assignments for Ka-band Uplink and Ka-band Downlink (Channel L1 to L50)

Channel	Ka-band U/L (MHz)	Ka-band D/L (MHz), 3344/3599	Ka-band D/L (MHz), 3360/3599
L1			31803.333340
L2			31808.518520
L3			31813.703699
L4			31818.888893
L5			31824.074073
L6			31829.259266
L7			31834.444446
L8			31839.629625
L9			31844.814819
L10			31849.999999
L11			31855.185178
L12			31860.370376
L13			31865.555556
L14			31870.740736
L15			31875.925929
L16			31881.111109
L17			31886.296302
L18			31891.481482
L19			31896.666662
L20			31901.851855
L21			31907.037035
L22			31912.222215
L23			31917.407408
L24			31922.592592
L25			31927.777785
L26	34204.385033		31932.962965
L27	34209.939040		31938.148145
L28	34215.493061		31943.333338
L29	34221.047067		31948.518518
L30	34226.601074	31801.543204	31953.703698
L31	34232.155095	31806.703706	31958.888891
L32	34237.709102	31811.864194	31964.074071
L33	34243.263123	31817.024696	31969.259264
L34	34248.817129	31822.185185	31974.444444
L35	34254.371136	31827.345673	31979.629624
L36	34259.925162	31832.506180	31984.814822
L37	34265.479168	31837.666668	31990.000001
L38	34271.033175	31842.827157	31995.185181
L39	34276.587196	31847.987659	32000.370375
L40	34282.141202	31853.148147	32005.555554
L41	34287.695209	31858.308635	32010.740734
L42	34293.249230	31863.469137	32015.925927
L43	34298.803237	31868.629626	32021.111107
L44	34304.357258	31873.790128	32026.296301
L45	34309.911264	31878.950616	32031.481480
L46	34315.465271	31884.111105	32036.666660
L47	34321.019297	31889.271611	32041.851858
L48	34326.573303	31894.432099	32047.037038
L49	34332.127310	31899.592588	32052.222218
L50	34337.681331	31904.753090	32057.407411

Table 6-2. Frequency and Channel Assignments for Ka-band Uplink and Ka-band Downlink (Channel 1 to 42)

Channel	Ka-band U/L (MHz)	Ka-band D/L (MHz), 3344/3599	Ka-band D/L (MHz), 3360/3599
1	34343.235337	31909.913578	32062.592591
2	34348.789358	31915.074080	32067.777784
3	34354.343365	31920.234569	32072.962964
4	34359.897372	31925.395057	32078.148144
5	34365.451393	31930.555559	32083.333337
6	34371.005399	31935.716048	32088.518517
7	34376.559406	31940.876536	32093.703696
8	34382.113432	31946.037042	32098.888894
9	34387.667438	31951.197531	32104.074074
10	34393.221459	31956.358033	32109.259267
11	34398.775466	31961.518521	32114.444447
12	34404.329472	31966.679010	32119.629627
13	34409.883493	31971.839512	32124.814820
14	34415.437500	31977.000000	32130.000000
15	34420.991507	31982.160488	32135.185180
16	34426.545528	31987.320990	32140.370373
17	34432.099534	31992.481479	32145.555553
18	34437.653541	31997.641967	32150.740733
19	34443.207562	32002.802469	32155.925926
20	34448.761568	32007.962958	32161.111106
21	34454.315594	32013.123464	32166.296304
22	34459.869601	32018.283952	32171.481483
23	34465.423607	32023.444441	32176.666663
24	34470.977628	32028.604943	32181.851856
25	34476.531635	32033.765431	32187.037036
26	34482.085642	32038.925920	32192.222216
27	34487.639663	32044.086422	32197.407409
28	34493.193669	32049.246910	32202.592589
29	34498.747690	32054.407412	32207.777782
30	34504.301697	32059.567901	32212.962962
31	34509.855703	32064.728389	32218.148142
32	34515.409729	32069.888895	32223.333340
33	34520.963736	32075.049384	32228.518520
34	34526.517742	32080.209872	32233.703699
35	34532.071763	32085.370374	32238.888893
36	34537.625770	32090.530863	32244.074073
37	34543.179791	32095.691365	32249.259266
38	34548.733798	32100.851853	32254.444446
39	34554.287804	32106.012341	32259.629625
40	34559.841825	32111.172843	32264.814819
41	34565.395832	32116.333332	32269.999999
42	34570.949838	32121.493820	32275.185178

Table 6-3. Frequency and Channel Assignments for Ka-band Uplink and Ka-band Downlink (Channel H1 to H34)

Channel	Ka-band U/L (MHz)	Ka-band D/L (MHz), 3344/3599	Ka-band D/L (MHz), 3360/3599
H1	34576.503864	32126.654327	32280.370376
H2	34582.057871	32131.814815	32285.555556
H3	34587.611877	32136.975304	32290.740736
H4	34593.165898	32142.135806	32295.925929
H5	34598.719905	32147.296294	
H6	34604.273926	32152.456796	
H7	34609.827933	32157.617284	
H8	34615.381939	32162.777773	
H9	34620.935960	32167.938275	
H10	34626.489967	32173.098763	
H11	34632.043973	32178.259252	
H12	34637.597994	32183.419754	
H13	34643.152006	32188.580246	
H14	34648.706027	32193.740748	
H15	34654.260033	32198.901237	
H16	34659.814040	32204.061725	
H17	34665.368061	32209.222227	
H18	34670.922067	32214.382716	
H19	34676.476074	32219.543204	
H20	34682.030095	32224.703706	
H21	34687.584102	32229.864194	
H22	34693.138123	32235.024696	
H23	34698.692129	32240.185185	
H24		32245.345673	
H25		32250.506180	
H26		32255.666668	
H27		32260.827157	
H28		32265.987659	
H29		32271.148147	
H30		32276.308635	
H31		32281.469137	
H32		32286.629626	
H33		32291.790128	
H34		32296.950616	

Deep Space Network

202
Doppler Tracking

Document Owner:

Signature Provided	06/14/2022
Andrew O'Dea Telemetry, Tracking, and Command System Engineer	Date

Approved by:

Signature Provided	04/06/2022
Timothy T. Pham Communications Systems Chief Engineer	Date

Prepared By:

Signature Provided	06/07/2022
Peter Kinman Telecommunications Technical Consultant	Date

Released by:

Signature Provided	07/14/2022
Christine Chang DSN Document Release Authority	Date

DSN No. **810-005, 202, Rev. E**
Issue Date: July 19, 2022
JPL D-19379; CL# 22-3475

Jet Propulsion Laboratory
California Institute of Technology

Users must ensure that they are using the current version in DSN Telecommunications Link Design Handbook website:
http://deepspace.jpl.nasa.gov/dsndocs/810-005/

Review Acknowledgment

By signing below, the signatories acknowledge that they have reviewed this document and provided comments, if any, to the signatories on the Cover Page.

Signature Provided	06/07/2022	Signature Provided	04/12/2022
Jeff B. Berner DSN Project Chief Engineer	Date	Dong K. Shin DSN System Engineer	Date

Document Change Log

Rev	Issue Date	Prepared By	Affected Sections or Pages	Change Summary
Initial	11/30/2000	P. W. Kinman	All	New Module
A	12/15/2002	P. W. Kinman	Many	Added Discussion of one-way Doppler error and X-Up/S-Down Solar Phase Scintillation errors. Renumbered all equations.
B	9/30/2010	D. K. Shin	All	Replaced DSMS with DSN. Eliminated the Rev. E designation for the document series.
C	12/3/2018	P. W. Kinman	All	Title of module changed to "Doppler Tracking". Added new equation on data imbalance. Added new equations on uplink noise affecting coherent operation. Added new equations on the effect of phase noise. Equations on phase scintillation corrected. Added Appendix A, "Carrier-Loop Transfer Function," and Appendix B, "Glossary of Parameters". Figures 3, 4, 5, 11, 12, and 13 added. Several sections were rewritten for better clarity.
D	6/6/2021	P. W. Kinman	2.1.3, 2.1.4, 2.2.1	Equation (8) corrected for the case of OQPSK. Comments added on recommended minimum carrier loop signal-to-noise ratio. New Subsection 2.1.4 on carrier loop bandwidth. Figures 3, 4, and 5 corrected.
E	07/19/2022	P. W. Kinman	2.2.1.3, 2.2.2.3, 2.3.4.1.3, 2.3.4.2.3	Equation for one-way ${\sigma_{VS}}^2$ corrected [Eq. (19)]. Equations for C_{band} corrected [Eqs. (20) and (29) in 202D; now Eqs. (21) and (31) in 202E]. Figures 3, 4, and 5 of 202D corrected [Figures 3, 4, and 6 in 202E]. New Figure 5 added for one-way K-band σ_{VS}. Figures 6 through 12 corrected [Figures 7 through 13 in 202E]. New Figure 14 added for coherent K-up/K-down σ_{VS}. New general equation for C_{band} added [Eq. (20)].

Contents

Illustrations

Figure **Page**

Tables

Table **Page**

1. Introduction

1.1 Purpose

This module provides sufficient information for the telecommunications engineer to understand the capabilities and limitations of the equipment used for Doppler measurement at the Deep Space Network (DSN).

1.2 Scope

The scope of this module is limited to those features of the Low-Rate Downlink Channel at the 34-m High-efficiency (34-m HEF), 34-m Beam Waveguide (34-m BWG), and 70-m stations that relate to the measurement and reporting of the Doppler effect.

2. General Information

The relative motion of a transmitter and receiver causes the received carrier frequency to differ from that of the transmitter. This Doppler shift depends on the range rate—the rate-of-change of the distance separating transmitter and receiver. In the DSN a Doppler measurement consists of a set of carrier phase measurements. From these phase data, frequency may be calculated, since frequency is the rate-of-change of phase. Moreover, the calculated Doppler shift is related to the range rate. Doppler measurements are one of the most important radiometric data types used in orbit determination.

There are three types of Doppler measurement: one-way, two-way, and three-way. In all of these cases, the accumulating downlink carrier phase is measured and recorded.

With a one-way Doppler measurement, the spacecraft transmits a downlink carrier that is unrelated to any frequency source in the DSN and the downlink Doppler shift is determined. The frequency stability of the spacecraft oscillator used to generate the downlink carrier typically limits the performance of this Doppler measurement. Ultra-Stable Oscillators (USOs) are typically used for one-way Doppler measurement.

A two-way Doppler measurement employs an uplink from a Deep Space Station (DSS) and a downlink to that same station. The spacecraft's transponder tracks the arriving uplink carrier, whose frequency differs from that transmitted by the DSS by the uplink Doppler shift. The transponder produces a downlink carrier that is coherently related to the received uplink carrier. To be precise, the transmitted downlink carrier frequency equals the received uplink carrier frequency multiplied by a constant G, the transponding ratio. (The frequency multiplication is needed to achieve frequency separation between uplink and downlink carriers). The downlink carrier is received at the same DSS that transmitted the uplink carrier. The arriving downlink carrier experiences a two-way Doppler effect. The downlink carrier frequency is therefore different from that on the uplink because of the two-way Doppler effect and because of the transponding ratio.

Three-way Doppler measurement is similar to two-way measurement, except that the downlink carrier is received at a different DSS than that from which the uplink carrier was

transmitted. In a three-way measurement there are three nodes present: transmitting DSS, spacecraft, and receiving DSS.

A two-way or three-way Doppler measurement originates at a DSS. The uplink carrier frequency is synthesized within the exciter from a highly stable frequency reference provided by the Frequency and Timing Subsystem (FTS). Since this reference is typically more stable than the spacecraft-borne oscillator, a two-way or three-way Doppler measurement is more accurate than a one-way measurement.

For two-way and three-way Doppler measurements, it is necessary to account for the transponding ratio G. It is usual to define two-way Doppler as the transmitted uplink carrier frequency minus the ratio of the received downlink carrier frequency to the factor G. With this definition, the two-way Doppler would be zero if there were no relative motion between the DSS and the spacecraft. For a receding spacecraft that is typical of deep space exploration, two-way Doppler is a positive quantity.

The instrumentation of a Doppler measurement within a DSS is shown in diagrammatic form for a one-way measurement in Figure 1 and for a two-way measurement in Figure 2. In all Doppler measurements, the downlink carrier from the Low-Noise Amplifier (LNA) passes to the Downlink Tracking and Telemetry Subsystem (DTT), which resides in part in the antenna and in part in the Signal Processing Center (SPC). The Radio-frequency to Intermediate-frequency Downconverter (RID), which is located at the antenna, synthesizes a local oscillator from a frequency reference supplied by the FTS and then heterodynes this local oscillator with the downlink carrier. The Intermediate-Frequency (IF) signal that results is sent to the Signal Processing Center (SPC).

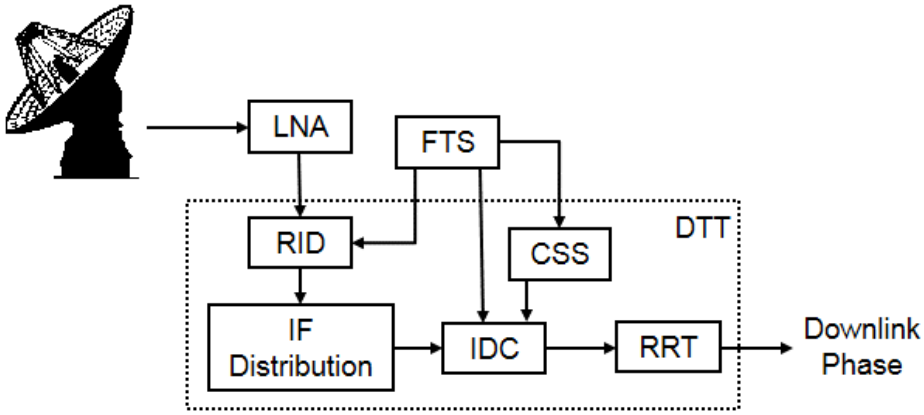

Figure 1. One-Way Doppler Measurement

In the SPC, the IF to Digital Converter (IDC) alters the frequency of the IF signal by a combination of up-conversion and down-conversion to a final analog frequency of approximately 200 MHz and then performs analog-to-digital conversion. The final analog stage of down-conversion uses a local oscillator supplied by the Channel-Select Synthesizer (CSS). The CSS is adjusted before the beginning of a pass to a frequency appropriate for the anticipated frequency range of the incoming downlink signal. During the pass, the frequency of the CSS

remains constant. The local oscillator frequencies of the CSS (and, indeed, of all local oscillators in the analog chain of down-conversion) are synthesized within the DTT from highly stable frequency references provided by the FTS. All analog stages of down-conversion are open-loop, and so the digital signal coming out of the IDC reflects the full Doppler shift.

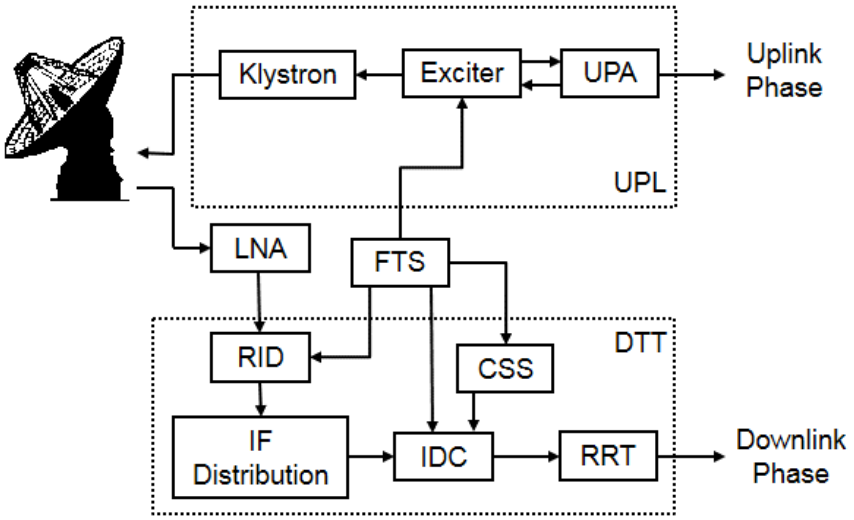

Figure 2. Two-Way Doppler Measurement

The Receiver, Ranging and Telemetry (RRT) processor accepts the signal from the IDC and extracts carrier phase with a digital phase-locked loop (Reference 1). The loop is configured to track the phase of a residual carrier, a suppressed carrier, or a QPSK (or Offset QPSK) signal. Since every analog local oscillator is held at constant frequency during a pass, the downlink carrier phase at sky frequency (that is, the phase that arrives at the DSS antenna) is easily computed from the local oscillator frequencies and the time-varying phase extracted by the digital phase-locked loop.

For a two-way or three-way Doppler measurement, the DSS exciter synthesizes the uplink carrier from a stable FTS frequency reference, as illustrated in Figure 2. The uplink carrier may be either constant or varied in accord with a tuning plan. In either case, the phase of the uplink carrier is recorded for use in the Doppler determination. The uplink phase counts are available from the Uplink Processor Assembly (UPA) at 1.0-second intervals.

The uplink and downlink carrier phase records must account for integer as well as fractional cycles. This is unlike many telecommunications applications where it is necessary to know the carrier phase only modulo one cycle. The reported data are uplink and downlink phase counts at sky frequency (but only downlink phase counts in the case of a one-way measurement). The downlink phase counts are available at 0.1-second intervals.

2.1 Carrier Loop Signal-to-Noise Ratio

The downlink carrier loop signal-to-noise ratio ρ_L must be known in order to calculate the Doppler measurement error and to calculate the variance of the phase error in the loop. The equation for ρ_L depends on the type of modulation on the downlink.

2.1.1 Residual Carrier

When the downlink carrier has a residual carrier and carrier synchronization is attained by tracking that residual carrier, ρ_L is

$$\rho_L = \left.\frac{P_C}{N_0}\right|_{D/L} \cdot \frac{1}{B_L} \tag{1}$$

where

$P_C/N_0|_{D/L}$ = downlink residual-carrier power to noise spectral density ratio, Hz

B_L = one-sided, noise-equivalent bandwidth of the downlink carrier loop, Hz

When non-return-to-zero (NRZ) telemetry symbols directly modulate the carrier (in the absence of a subcarrier), there is an additional loss to the carrier loop signal-to-noise ratio. This loss is due to the presence of data sidebands overlaying the residual carrier in the frequency domain and therefore increasing the effective noise level for carrier synchronization. In this case, ρ_L must be calculated as (Reference 2)

$$\rho_L = \left.\frac{P_C}{N_0}\right|_{D/L} \cdot \frac{1}{B_L} \cdot \frac{1}{1 + 2\,E_S/N_0} \tag{2}$$

where

E_S/N_0 = telemetry symbol energy to noise spectral density ratio

It is recommended that ρ_L meet the following constraint when the residual carrier is being tracked:

$$\rho_L \geq 10 \text{ dB}, \quad \text{residual carrier} \tag{3}$$

If ρ_L is larger than 10 dB for a residual-carrier loop, cycle slips should be rare, as long as there is no static phase error in the loop. Static phase error arises when there is an uncompensated Doppler rate for a 2nd order loop or an uncompensated Doppler acceleration for a 3rd order loop. Table 1 contains equations for calculating the static phase error in the presence of uncompensated Doppler dynamics. If a finite static phase error is present in the loop, the minimum required ρ_L might be larger than 10 dB. This can be accurately assessed through computer simulation or actual experimentation.

2.1.2 Suppressed-Carrier BPSK

A Costas loop is used to track a suppressed-carrier, binary phase-shift keyed (BPSK) carrier. For such a loop,

$$\rho_L = \left.\frac{P_T}{N_0}\right|_{D/L} \cdot \frac{S_L}{B_L} \tag{4}$$

where

$P_T/N_0|_{D/L}$ = downlink total signal power to noise spectral density ratio, Hz

S_L = squaring loss of the Costas loop (Reference 3),

$$S_L = \frac{2\frac{E_S}{N_0}}{1 + 2\frac{E_S}{N_0}} \tag{5}$$

It is recommended that ρ_L meet the following constraint for suppressed-carrier BPSK tracking:

$$\rho_L \geq 17 \text{ dB}, \quad \text{suppressed-carrier BPSK} \tag{6}$$

This recommended minimum ρ_L is larger than for residual-carrier tracking because with a Costas loop there is the risk of half-cycle slips as well as full cycle slips.

2.1.3 QPSK and Offset QPSK

When tracking a quadriphase-shift keyed (QPSK) carrier or an Offset QPSK (OQPSK) carrier, the loop signal to noise ratio is

$$\rho_L = \left.\frac{P_T}{N_0}\right|_{D/L} \cdot \frac{S_{LQ}}{B_L} \tag{7}$$

P_T is the *total* carrier power. For (O)QPSK this includes the power in *both* phases of the carrier. $P_T/N_0|_{D/L}$ is the ratio, on the downlink, of the total carrier power to the one-sided noise spectral density. As before, B_L is the one-sided, noise-equivalent loop bandwidth of the downlink carrier loop.

The squaring loss S_{LQ} for QPSK and OQPSK is given by (Reference 4)

$$S_{LQ} = \begin{cases} \dfrac{1}{1 + \dfrac{9}{4(E_S/N_0)} + \dfrac{3}{2(E_S/N_0)^2} + \dfrac{3}{16(E_S/N_0)^3}}, & \text{QPSK} \\ \dfrac{1}{4} \cdot \dfrac{1}{1 + \dfrac{9}{4(E_S/N_0)} + \dfrac{3}{2(E_S/N_0)^2} + \dfrac{3}{16(E_S/N_0)^3}}, & \text{OQPSK} \end{cases} \tag{8}$$

E_S/N_0 is the ratio of the energy per quaternary symbol to the one-sided noise spectral density in each arm of the Costas loop. The power in each arm of the Costas loop is $P_T/2$, and the quaternary symbol period is denoted here $2T_{S\,(\text{binary})}$. So E_S/N_0 is given by

$$\frac{E_S}{N_0} = \frac{(P_T/2) \cdot \left(2T_{S\,(\text{binary})}\right)}{N_0} \tag{9}$$

where

$T_{S\,(\text{binary})}$ = period of the binary symbol, s

The period $T_{S\,(\text{binary})}$ is the duration of a binary symbol at the input to the decoder or, equivalently, at the output of the receiver's demodulator (after the multiplexer in the QPSK or OQPSK demodulator).

E_S/N_0 also equals the ratio, at the decoder input, of the energy in one binary symbol to the one-sided noise spectral density.

$$\frac{E_S}{N_0} = \left.\frac{P_T}{N_0}\right|_{D/L} \cdot T_{S\,(\text{binary})} \tag{10}$$

Equations (9) and (10) are equivalent definitions for E_S/N_0.

As indicated in Equation (8), the squaring loss S_{LQ} is worse by a factor of $1/4$ for OQPSK than for QPSK. In comparing the performance of the OQPSK loop with that of the QPSK loop, with all fundamental parameters being equal, the OQPSK loop will have a ρ_L that is smaller by 6 dB. This is a result of the OQPSK carrier-tracking loop having an S-curve slope (at the operating point) that is one-half that for the QPSK loop. (The square of this slope is a factor in S_{LQ}.)

It is recommended that ρ_L meet the following constraint for QPSK and OQPSK:

$$\rho_L \geq 23,\ \text{dB} \qquad \text{QPSK and Offset QPSK} \tag{11}$$

With a QPSK or Offset QPSK loop there is a risk of quarter-cycle slips and half-cycle slips as well as full cycle slips. If ρ_L is larger than 23 dB, these quarter-, half-, and full-cycle slips should be rare, as long as there is no static phase error in the loop.

Static phase error arises when there is an uncompensated Doppler rate for a 2nd order loop or an uncompensated Doppler acceleration for a 3rd order loop. Table 1 contains equations for calculating the static phase error in the presence of uncompensated Doppler dynamics. If a finite static phase error is present in the loop, the minimum required ρ_L might be larger than 23 dB. This can be accurately assessed through computer simulation or actual experimentation.

Equation (11) might seem to suggest that an OQPSK loop has the same performance in the presence of thermal noise as does a QPSK loop. But this is not the case. For a common $P_T/N_0|_{D/L}$ and a common B_L, the OQPSK loop will have a ρ_L that is smaller by 6 dB than that for the QPSK loop. Equation (11) merely states that the minimum ρ_L, which must be calculated while accounting for S_{LQ}, is the same for both loops.

2.1.4 Carrier Loop Bandwidth

In this module, carrier loop bandwidth means the one-sided, noise-equivalent carrier loop bandwidth of the receiver. It is denoted B_L. There are limits on the carrier loop bandwidth. B_L can be no larger than 200 Hz. The lower limit on B_L is determined by the phase noise on the downlink. In addition, when operating in the suppressed-carrier mode, B_L should be no larger than $(1/20)$ times the binary symbol rate.

In general, the value selected for B_L should be small in order to maximize the carrier loop signal-to-noise ratio. On the other hand, B_L must be large enough that neither of the following variables becomes too large:

a) The static phase error due to uncompensated Doppler dynamics,

b) The contribution to carrier loop phase error variance due to phase noise on the downlink.

The best B_L to select will depend on circumstances. Sometimes it will be possible to select a B_L of about 1 Hz. A larger value for B_L is necessary when there is significant uncertainly in the downlink Doppler dynamics or when the Sun-Earth-probe angle is small (so that solar coronal phase scintillations are present on the downlink). When tracking a spinning spacecraft, it may be necessary to set the carrier loop bandwidth to a value that is somewhat larger than would otherwise be needed. The loop bandwidth must be large enough to track out the variation due to the spin.

2.2 Doppler Measurement Error

The performance of one-way Doppler measurements and two-way (or three-way) coherent Doppler measurements is addressed here. Models are given for the important contributors to measurement error. More information about Doppler performance is available in References 5 and 6.

The error in Doppler measurement is characterized here as a standard deviation σ_V, having velocity units (such as $\mathrm{mm/s}$), or as a variance ${\sigma_V}^2$ $(\mathrm{mm^2/s^2})$. Models are given here for measurement error in the case of two-way (or three-way) coherent Doppler measurement and in the case of one-way Doppler measurement.

A Doppler measurement error can also be characterized as a standard deviation of frequency σ_f. This standard deviation and σ_V are related as follows:

$$\sigma_f = \begin{cases} \dfrac{f_C}{c}\sigma_V, & \text{one} - \text{way} \\ \dfrac{2f_C}{c}\sigma_V, & \text{two} - \text{way or three} - \text{way} \end{cases} \tag{12}$$

where

σ_V = standard deviation of range rate, same units as c

f_C = downlink carrier frequency

c = speed of electromagnetic waves in vacuum

σ_f = standard deviation of frequency, same units as f_C

The factor of 2 in Equation (12) for two-way and three-way measurements is present because σ_V represents the error in the rate-of-change of the (one-way) range and σ_f represents the error in the *total* Doppler shift, including uplink as well as downlink.

The error variance ${\sigma_V}^2$ for a Doppler measurement can be modeled as

$$ {\sigma_V}^2 = {\sigma_{VN}}^2 + {\sigma_{VF}}^2 + {\sigma_{VS}}^2 \tag{13} $$

where

${\sigma_V}^2$ = variance of range rate (square of σ_V)

${\sigma_{VN}}^2$ = contribution to ${\sigma_V}^2$ from white (thermal) noise

${\sigma_{VF}}^2$ = contribution to ${\sigma_V}^2$ from phase noise of frequency sources

${\sigma_{VS}}^2$ = contribution to ${\sigma_V}^2$ from (solar) phase scintillation

When using BPSK with direct modulation of the carrier (that is, no subcarrier), a data imbalance (that is, an unequal number of logical ones and zeros) will cause a residual-carrier loop to experience an additional phase jitter. This phase jitter represents an additional error source for Doppler measurement, beyond those included in Equation (13). The standard deviation σ_{VI} of Doppler error due to telemetry data imbalance, when direct-modulation BPSK is employed, may be roughly modeled as follows:

$$ \sigma_{VI} \cong \begin{cases} \dfrac{c \cdot \theta_t \cdot I_{\text{data}} \cdot B_L}{\sqrt{24} \cdot \pi \cdot f_C}, & \text{one} - \text{way} \\ \dfrac{c \cdot \theta_t \cdot I_{\text{data}} \cdot B_L}{2\sqrt{24} \cdot \pi \cdot f_C}, & \text{two} - \text{way or three} - \text{way} \end{cases} \tag{14} $$

where

σ_{VI} = standard deviation of Doppler error due to telemetry data imbalance, same units as c

θ_t = telemetry modulation index, rad

I_{data} = data imbalance, $0 \le I_{\text{data}} \le 0.5$

Data imbalance I_{data} is defined as follows. In a large set of $n_0 + n_1$ binary-valued telemetry symbols, if n_0 is the number of logical zeros and n_1 is the number of logical ones, $I_{\text{data}} = |n_0 - n_1|/(n_0 + n_1)$. The case $I_{\text{data}} = 0$ represents a perfect balance (and therefore $\sigma_{VI} = 0$). The case $I_{\text{data}} = 0.5$ represents the case where $n_0 = 3n_1$ (or vice versa), a highly imbalanced situation. It is possible, of course, for I_{data} to be larger than 0.5 (as large as 1, for which all symbols are identical); but the model of Equation (14) is only valid in the range $0 \le I_{\text{data}} \le 0.5$.

Pseudo randomization of the telemetry data can be employed in the transponder. When this is done, there is no significant data imbalance and the Doppler error σ_{VI} is 0.

2.2.1 *One-Way Doppler Measurement Error*

One-way Doppler measurement is subject to the following error sources: white noise at the receiver, phase noise originating in the frequency source on the spacecraft, and phase scintillation acquired by the downlink carrier in passing through the solar corona.

2.2.1.1 *Downlink White (Thermal) Noise Contribution to $\sigma_V{}^2$, One-Way*

For a one-way Doppler measurement, all of the white (thermal) noise originates on the downlink. The contribution $\sigma_{VN}{}^2$ is modeled as

$$\sigma_{VN}{}^2 = 2 \cdot \left(\frac{c}{2\pi f_C T}\right)^2 \cdot \frac{1}{\rho_L}, \qquad \text{one-way} \tag{15}$$

where

T = integration time for Doppler measurement, s

The carrier loop signal-to-noise ratio ρ_L may be calculated from equations in Section 2.1.

2.2.1.2 *Phase Noise Contribution to $\sigma_V{}^2$, One-Way*

The frequency source of the downlink carrier introduces two kinds of error to a one-way Doppler measurement: an unknown bias and a random error. The bias is due to uncertainty in the transmitted frequency; this bias is not further discussed here. The random error is due to frequency instability of the frequency source. Frequency instability can be characterized either in terms of a fractional frequency deviation (the Allan deviation) or in terms of phase noise. If the phase noise of the source has been characterized, its contribution to $\sigma_V{}^2$ may be calculated as follows.

$$\sigma_{VF}{}^2 = \left(\frac{c}{\pi f_C T}\right)^2 \int_0^\infty S_{D/L}(f) \cdot \left|H_{D/L}(j2\pi f)\right|^2 \cdot \sin^2(\pi f T)\, df, \qquad \text{one-way} \tag{16}$$

where

$S_{D/L}(f)$ = one-sided power spectral density of downlink-carrier phase noise, rad^2/Hz

$H_{D/L}(j2\pi f)$ = frequency response of DTT receiver's carrier loop

The frequency response $H_{D/L}(j2\pi f)$ is related to the transfer function $H_{D/L}(s)$ of that loop by

$$H_{D/L}(j2\pi f) = H_{D/L}(s)\big|_{s=j2\pi f} \tag{17}$$

where s is the Laplace transform variable. The form of $H_{D/L}(s)$ depends on whether the DTT receiver is configured as a 2nd or 3rd order loop. Appendix A provides equations for $H_{D/L}(s)$.

The product $S_{D/L}(f) \cdot \left|H_{D/L}(j2\pi f)\right|^2$ appearing in Equation (16) represents that portion of the (one-sided) power spectral density of the phase noise that lies in the passband of $H_{D/L}(j2\pi f)$. This shows that $\sigma_{VF}{}^2$ depends, in general, on the carrier-loop bandwidth B_L.

In order to keep the phase error of the carrier loop small, B_L is normally selected to be large enough to pass almost all of the (low-pass) power spectral density $S_{D/L}(f)$. In this typical scenario, ${\sigma_{VF}}^2$ becomes insensitive to the exact value of B_L. The following approximation is then possible:

$$\sigma_{VF} \cong c\ \sigma_y(T), \qquad \text{one-way} \qquad (18)$$

where

$\sigma_y(T)$ = Allan deviation of the carrier's frequency source

Allan deviation is a dimensionless measure of the fractional frequency stability and is a function of the integration time T (Reference 7). When using Equation (18), the Allan deviation function should be evaluated at the Doppler measurement time T. When using the approximation of Equation (18), ${\sigma_{VF}}^2$ will, of course, be the square of the standard deviation σ_{VF}.

Equation (18) is an excellent approximation when the phase noise is predominantly white-in-frequency, for which $S_{D/L}(f) \propto 1/f^2$. Therefore, when the phase noise is predominantly white-in-frequency and B_L is large enough that the carrier-loop phase error is small, then Equation (18) is an excellent estimate of σ_{VF} for one-way Doppler measurement.

In general, there is also a contribution to ${\sigma_{VF}}^2$ from phase noise in the local oscillators of the DTT receiving chain. This contribution may be calculated using an equation similar to Equation (16), with $S_{D/L}(f)$ replaced by the one-sided power spectral density of the local oscillator phase noise. This contribution will depend, in general, on B_L. However, if B_L is large enough that the carrier-loop phase error is small, then the contribution may be approximated as the square of the σ_{VF} calculated by Equation (18), where the local oscillator's Allan deviation is used. At the stations, the local oscillators are derived from the FTS, where the Allan deviation of the local oscillators is typically very small compared with that for the frequency source, onboard the spacecraft, of the downlink carrier (for non-coherent operation). The contribution of the local oscillators in one-way Doppler measurement at a station is therefore typically negligible by comparison. However, at a test facility where there is no FTS, the phase noise of the local oscillators might be a significant contributor to ${\sigma_{VF}}^2$.

It is expected that atomic clocks will in the future be employed on spacecraft; when this occurs, ${\sigma_{VF}}^2$ will be calculated as the sum of two components: one from the onboard atomic clock and one from the DTT receiving-chain local oscillators.

2.2.1.3 Phase Scintillation Contribution to ${\sigma_V}^2$, One-Way

A microwave carrier passing through the solar corona experiences phase scintillation, which introduces a random error to the Doppler measurement. The contribution ${\sigma_{VS}}^2$ of phase scintillation to Doppler measurement error depends on the Sun-Earth-probe angle, the carrier frequency f_C, and the integration time T. A coarse approximation for ${\sigma_{VS}}^2$ is:

$$\sigma_{VS}{}^2 = \begin{cases} \dfrac{2.13\ C_{\text{band}}\ c^2}{f_C{}^2 T^{0.35} [\sin(\theta_{\text{SEP}})]^{2.45}}, & 0^\circ < \theta_{\text{SEP}} \leq 90^\circ \\ \dfrac{2.13\ C_{\text{band}}\ c^2}{f_C{}^2 T^{0.35}}, & 90^\circ < \theta_{\text{SEP}} \leq 180^\circ \end{cases} \qquad \text{one-way} \tag{19}$$

where

θ_{SEP} = Sun-Earth-probe angle ($0^\circ < \theta_{\text{SEP}} \leq 180^\circ$)

The standard deviation σ_{VS} (the square-root of the variance $\sigma_{VS}{}^2$) has the same dimensions as c. (The product $2.13\ C_{\text{band}}$ is not dimensionless; it has the same dimensions as $f_C{}^2 \cdot T^{0.35}$.)

The constant parameter C_{band} depends on the downlink band,

$$C_{\text{band}} = \begin{cases} 0.00001247 \left(\dfrac{\nu_{DS}}{\nu_D}\right)^2, & \text{non} - \text{coherent} \\ 0.00001247 \left(\dfrac{\nu_{DS}}{\nu_D}\right)^2 [G^4 + 1], & \text{coherent} \end{cases} \tag{20}$$

$$C_{\text{band}} = \begin{cases} 1.2 \times 10^{-5}, & \text{S} - \text{down} \\ 9.3 \times 10^{-7}, & \text{X} - \text{down} \\ 9.5 \times 10^{-8}, & \text{K} - \text{down} \\ 6.4 \times 10^{-8}, & \text{Ka} - \text{down} \end{cases} \qquad \text{one-way} \tag{21}$$

In Equation (19), $\sigma_{VS}{}^2$ is a continuous function of θ_{SEP} (when f_C and T are kept constant) for $0^\circ < \theta_{\text{SEP}} \leq 180^\circ$.

Throughout this module, the band designation K refers to the bands 22,550 to 23,150 MHz on the uplink and 25,500 to 27,000 MHz on the downlink. The band designation Ka refers to the bands 34,200 to 34,700 MHz on the uplink and 31,800 to 32,300 MHz on the downlink.

The approximation of Equation (19) is based on the work reported in Reference 8. This model is valid when tracking binary phase-shift keyed telemetry with either a residual or suppressed carrier or when tracking a QPSK (or Offset QPSK) signal. This model is the recommended estimate for all Sun-Earth-probe angles, even though this model was originally based on data for Sun-Earth-probe angles between 5° and 27°. More recent measurements suggest that the estimate is more generally applicable.

Figure 3 shows the standard deviation σ_{VS} (the square-root of the variance $\sigma_{VS}{}^2$) as a function of θ_{SEP} for one-way Doppler measurement with an S-band downlink. The vertical

axis is in units of mm/s. Figure 4 shows σ_{VS} for an X-band downlink. Figure 5 shows σ_{VS} for a K-band downlink. Figure 6 shows σ_{VS} for a Ka-band downlink. For all four of these figures, σ_{VS} depends on f_C. For Figures 3, 4, 5, and 6, the curves were calculated using a value for f_C of 2295 MHz, 8425 MHz, 26250 MHz and 32050 MHz, respectively. (Each of these frequencies corresponds to the center of the band.)

2.2.2 Two-Way and Three-Way Doppler Measurement Error

Two-way and three-way Doppler measurements are made with the spacecraft transponder in coherent mode. The most important error sources for coherent measurements are white noise on both the uplink and downlink and phase scintillation acquired by the uplink and downlink carriers in passing through the solar corona.

2.2.2.1 White (Thermal) Noise Contribution to $\sigma_V{}^2$, Two- and Three-Way

The white (thermal) noise contribution $\sigma_{VN}{}^2$ to two-way and three-way Doppler measurement error has two components:

$$\sigma_{VN}{}^2 = \sigma_{VNU}{}^2 + \sigma_{VND}{}^2 \tag{22}$$

where

$\sigma_{VNU}{}^2$ = contribution to $\sigma_{VN}{}^2$ from uplink white (thermal) noise

$\sigma_{VND}{}^2$ = contribution to $\sigma_{VN}{}^2$ from downlink white (thermal) noise

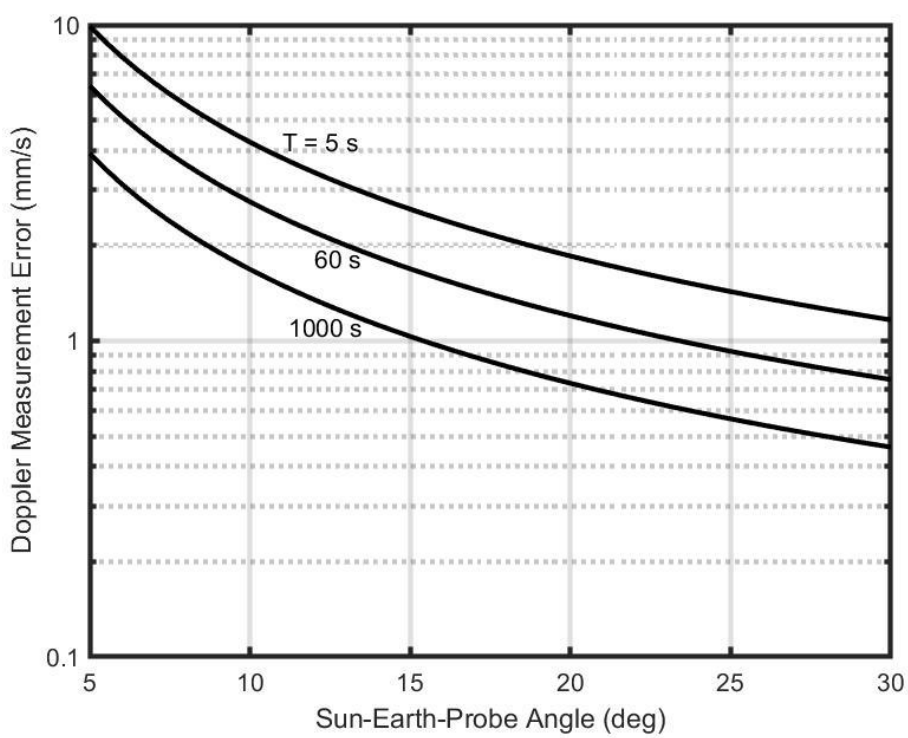

Figure 3. Doppler Measurement Error Due to Solar Phase Scintillation: S-Down

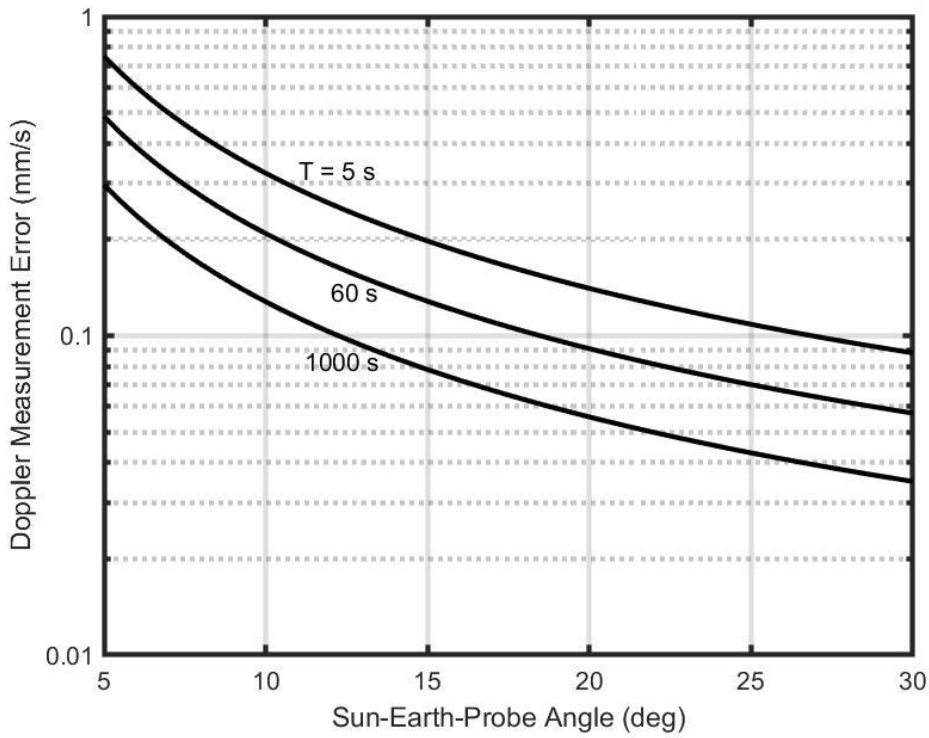

Figure 4: Doppler Measurement Error Due to Solar Phase Scintillation: X-Down

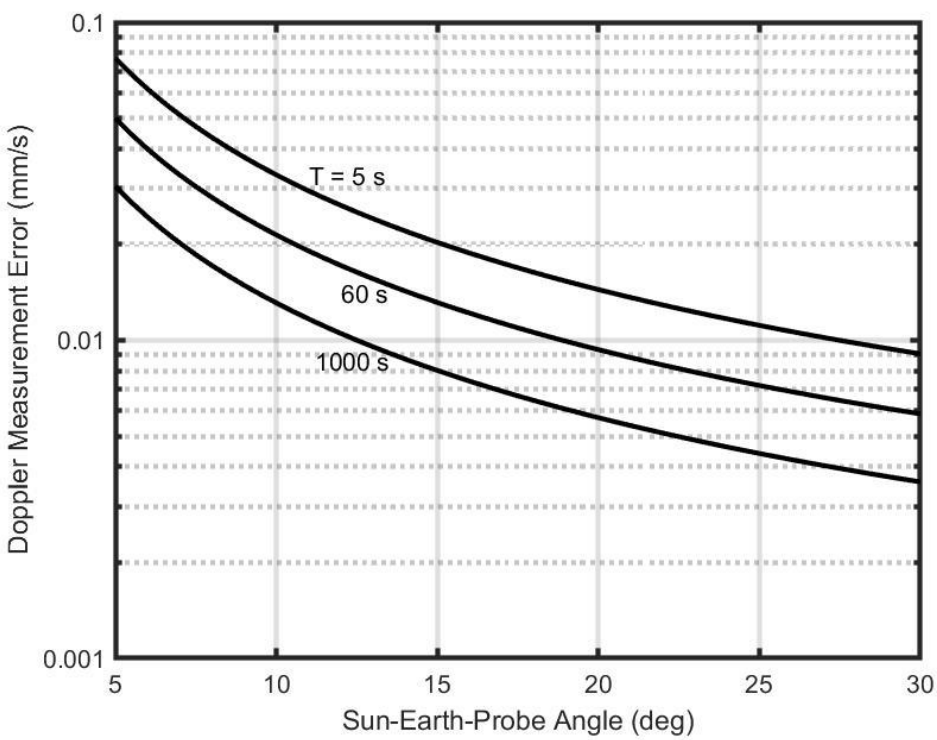

Figure 5. Doppler Measurement Error Due to Solar Phase Scintillation: K-Down

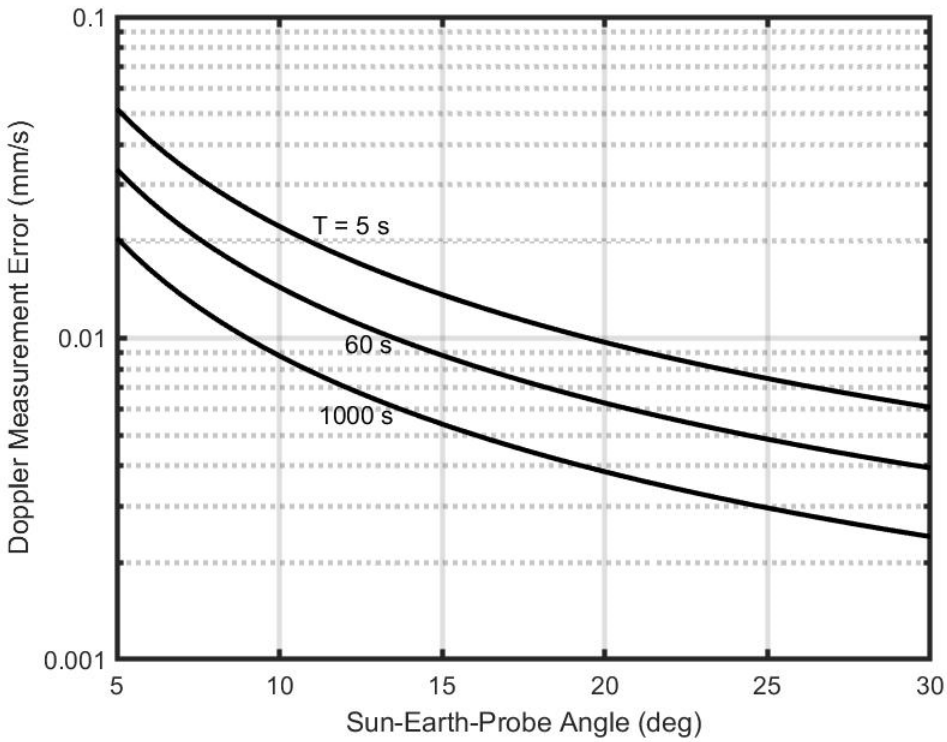

Figure 6. Doppler Measurement Error Due to Solar Phase Scintillation: Ka-Down

The variance ${\sigma_{VNU}}^2$ accounts for white (thermal) noise that originates on the uplink, is tracked by the transponder's carrier loop, is transponded to the downlink band, and is tracked by the downlink receiver. For two- or three-way coherent Doppler measurement, the contribution ${\sigma_{VNU}}^2$ of uplink white noise is modeled as

$$ {\sigma_{VNU}}^2 = \frac{1}{2} \cdot \left(\frac{c}{2\pi f_C T}\right)^2 \cdot \frac{G^2}{\rho_{TR} \cdot B_{TR}} \int_0^\infty \left|H_{U/L}(j2\pi f)\right|^2 \cdot \left|H_{D/L}(j2\pi f)\right|^2 df \tag{23} $$

where

G	=	transponding ratio
ρ_{TR}	=	signal-to-noise ratio in transponder's carrier loop
B_{TR}	=	noise-equivalent bandwidth of the transponder's carrier loop, Hz
$H_{U/L}(j2\pi f)$	=	frequency response of uplink (transponder) carrier loop

Here B_{TR} (Hz) is the noise-equivalent bandwidth of the transponder's carrier loop:

$$B_{TR} = \int_0^\infty \left|H_{U/L}(j2\pi f)\right|^2 df \tag{24}$$

ρ_{TR} is the signal-to-noise ratio in the transponder's carrier loop with bandwidth B_{TR}. It can be calculated from equations similar to those given in Section 2.1 but using uplink parameters, instead of downlink parameters. For example, when the uplink is residual carrier, ρ_{TR} is calculated as the uplink residual-carrier power to noise spectral density ratio divided by B_{TR}. If the uplink were suppressed carrier and tracked by a Costas loop, ρ_{TR} would equal the uplink total signal power to noise spectral density ratio times a squaring loss divided by B_{TR}.

In order to evaluate Equation (23), it is also necessary to know the frequency response $H_{U/L}(j2\pi f)$ of the transponder's carrier loop. Fortunately, there is an approximation for ${\sigma_{VNU}}^2$ that requires only the bandwidth B_{TR} of the transponder's carrier loop. This approximation is

$${\sigma_{VNU}}^2 \cong \begin{cases} \frac{1}{2}\cdot\left(\frac{c}{2\pi f_C T}\right)^2 \cdot \frac{G^2}{\rho_{TR}} \cdot \frac{B_L}{B_{TR}}, & B_L < B_{TR} \\ \frac{1}{2}\cdot\left(\frac{c}{2\pi f_C T}\right)^2 \cdot \frac{G^2}{\rho_{TR}}, & B_L \geq B_{TR} \end{cases} \tag{25}$$

Equation (25) can be understood with the following heuristic argument. In the case $B_L < B_{TR}$, only a fraction B_L/B_{TR} of the uplink noise that is tracked by the transponder's carrier loop is also tracked by the DTT carrier loop; in this case, therefore, ${\sigma_{VNU}}^2$ is proportional to B_L/B_{TR}. In the case $B_L \geq B_{TR}$, all of the uplink noise that is tracked by the transponder's loop is also tracked by the DTT receiver's loop; therefore, B_L/B_{TR} is replaced by 1. When $B_L$and B_L are comparable (that is, when neither $B_L \gg B_{TR}$ nor $B_L \ll B_{TR}$), the best accuracy is obtained for ${\sigma_{VNU}}^2$ by using Equation (23).

The variance ${\sigma_{VND}}^2$ accounts for white (thermal) noise that originates on the downlink and is tracked by the DTT receiver. The contribution ${\sigma_{VND}}^2$ is modeled as

$${\sigma_{VND}}^2 = \frac{1}{2}\cdot\left(\frac{c}{2\pi f_C T}\right)^2 \cdot \frac{1}{\rho_L}, \qquad \text{two-way and three-way} \tag{26}$$

where ρ_L is the downlink carrier loop signal-to-noise ratio. Section 2.1 has equations for calculating ρ_L.

Equation (26) for two-way and three-way Doppler measurement is different from Equation (15) for one-way Doppler measurement. This difference is due to the fact that σ_V is the error in the determination of the range-of-change of a (one-way) range, so there must be a scaling by a factor of $1/2$ for a two-way (or three-way) measurement. This factor of $1/2$ also appears in Equation (12). For the variance ${\sigma_{VND}}^2$, the factor becomes $1/4$.

2.2.2.2 Phase Noise Contribution to ${\sigma_V}^2$, Two- and Three-Way

When making two- and three-way Doppler measurements at the stations (as opposed to the making of measurements entirely within a test facility), the contribution ${\sigma_{VF}}^2$ may be modeled as:

$$\sigma_{VF}{}^2 = 2\left(\frac{c\ G}{2\pi f_C T}\right)^2 \int_0^\infty S_{U/L}(f) \cdot \left|H_{D/L}(j2\pi f)\right|^2 \cdot \sin^2(\pi f T)\ df, \tag{27}$$

two- and three-way coherent measurement at the stations

where

$S_{U/L}(f)$ = one-sided power spectral density of uplink-carrier phase noise, $\mathrm{rad}^2/\mathrm{Hz}$

Equation (27) accounts for both phase noise in the uplink frequency source and phase noise in the DTT receiving-chain local oscillators. For a three-way measurement, the uplink source phase noise is independent of the local-oscillator phase noise. For a two-way coherent measurement in deep space, the round-trip signal delay is large enough that local-oscillator phase noise is uncorrelated with the delayed uplink source phase noise, even though both originate with a common FTS. The factor of 2 at the front of the right-hand side of Equation (27) is present because the total contribution $\sigma_{VF}{}^2$ is twice as large as a contribution from either the uplink-source phase noise alone or the local-oscillator phase noise alone.

For two-way and three-way Doppler measurements, the uplink frequency source and the local oscillators in the DTT receiving chain are supplied by the FTS. The Allan deviation for the FTS frequency sources may be found in Module 304, "Frequency and Timing".

The contribution $\sigma_{VF}{}^2$ depends on the DTT receiver carrier-loop bandwidth B_L, since the frequency response $H_{D/L}(j2\pi f)$ of this loop depends on B_L. In order to keep the phase error of the carrier loop small, B_L is normally selected to be large enough to pass almost all of the (low-pass) power spectral density $G^2 \cdot S_{U/L}(f)$. In this typical scenario, $\sigma_{VF}{}^2$ becomes insensitive to the exact value of B_L. The following approximation is then possible:

$$\sigma_{VF} \cong \frac{c\ \sigma_y(T)}{\sqrt{2}}, \qquad \text{two- and three-way} \tag{28}$$

When using Equation (28), the Allan deviation function should be evaluated at the Doppler measurement time T. $\sigma_{VF}{}^2$ is the square of the standard deviation σ_{VF} given in Equation (28). When the phase noise is predominantly white-in-frequency, for which $S_{U/L}(f) \propto 1/f^2$, Equation (28) is an excellent approximation.

Equation (28) has a factor $1/\sqrt{2}$ that is absent in Equation (18). The two-way and three-way case accounts for both the uplink-source phase noise and the DTT receiver local-oscillator phase noise; this is a factor of 2 in $\sigma_{VF}{}^2$, or a factor of $\sqrt{2}$ in σ_{VF}. Moreover, σ_V is the error in the determination of the range-of-change of a (one-way) range, so there must be a scaling by a factor of $1/2$ for a two-way (or three-way) measurement.

Typically, $\sigma_{VF}{}^2$ is negligible for two-way and three-way Doppler measurement, owing to the excellent frequency stability of the frequency sources, which are derived at the stations from the FTS. It is possible, however, to cause $\sigma_{VF}{}^2$ to be significant during coherent operations by choosing a DTT receiver bandwidth B_L that is too small. However, if this is done, the DTT carrier loop will have a large phase error. In such a case, a poor $\sigma_{VF}{}^2$ might be the less concerning problem. Generally, for two-way or three-way coherent Doppler measurement with a

spacecraft, a B_L of at least 1 Hz should ensure that ${\sigma_{VF}}^2$ will be small. However, the phase error in the carrier loop might still be a problem, depending on the rate-of-change and the acceleration of the downlink carrier's frequency.

When testing a transponder at the Development and Test Facility (DTF-21) or the Compatibility Test Trailer (CTT-22), the frequency stability of the uplink carrier and local oscillators is substantially poorer than at the stations. For a two-way Doppler measurement at DTF-21 or CTT-22, ${\sigma_{VF}}^2$ might be significant. For this scenario, ${\sigma_{VF}}^2$ can be modeled as:

$$ {\sigma_{VF}}^2 = \left(\frac{c\ G}{2\pi f_C T}\right)^2 \int_0^\infty S_{U/L}(f) \cdot \left|1 - H_{U/L}(j2\pi f)\right|^2 \cdot \left|H_{D/L}(j2\pi f)\right|^2 \cdot \sin^2(\pi f T)\ df, \tag{29} $$

DTF-21 and CTT-22

Equation (29) reflects the fact that uplink-carrier phase noise will largely be canceled by phase noise in the local oscillators of the receiving chain but that this cancellation is imperfect when the transponder does not track all of the uplink-carrier phase noise. The term $S_{U/L}(f) \cdot \left|1 - H_{U/L}(j2\pi f)\right|^2$ represents that portion of the uplink-carrier phase noise that is not tracked by the transponder. When the transponder's carrier loop bandwidth is large enough that almost all of the uplink-carrier phase noise is tracked, the cancellation of downlink-carrier phase noise and receiving-chain local-oscillator phase noise will be nearly complete; and, under these circumstances, ${\sigma_{VF}}^2$ will be negligible.

2.2.2.3 Phase Scintillation Contribution to ${\sigma_V}^2$, Two- and Three-Way

The contribution ${\sigma_{VS}}^2$ of phase scintillation to Doppler measurement error may be approximated as follows.

$$ {\sigma_{VS}}^2 = \begin{cases} \dfrac{0.53\ C_{\text{band}}\ c^2}{{f_C}^2 T^{0.35} [\sin(\theta_{\text{SEP}})]^{2.45}}, & 0^\circ < \theta_{\text{SEP}} \le 90^\circ \\ \dfrac{0.53\ C_{\text{band}}\ c^2}{{f_C}^2 T^{0.35}}, & 90^\circ < \theta_{\text{SEP}} \le 180^\circ \end{cases} \quad \text{two- and three-way} \tag{30} $$

As before, θ_{SEP} is the Sun-Earth probe angle ($0^\circ < \theta_{\text{SEP}} \le 180^\circ$), T is the measurement integration time, f_C is the downlink carrier frequency, and c is the speed of electromagnetic waves in vacuum. The standard deviation σ_{VS} (the square-root of the variance ${\sigma_{VS}}^2$) has the same dimensions as c. (The product $0.53\ C_{\text{band}}$ is not dimensionless; it has the same dimensions as ${f_C}^2 \cdot T^{0.35}$.)

Equation (30) is applicable to two-way and three-way Doppler measurements. The parameter C_{band} is different for two-way (and three-way) Doppler measurement than for one-way Doppler measurement. The parameter C_{band} depends on the uplink/downlink band pairing.

$$C_{\text{band}} = \begin{cases} 3.0 \times 10^{-5}, & \text{S} - \text{up/S} - \text{down} \\ 2.3 \times 10^{-4}, & \text{S} - \text{up/X} - \text{down} \\ 1.3 \times 10^{-5}, & \text{X} - \text{up/S} - \text{down} \\ 2.7 \times 10^{-6}, & \text{X} - \text{up/X} - \text{down} \\ 2.6 \times 10^{-5}, & \text{X} - \text{up/Ka} - \text{down} \\ 9.3 \times 10^{-7}, & \text{Ka} - \text{up/X} - \text{down} \\ 1.1 \times 10^{-7}, & \text{Ka} - \text{up/Ka} - \text{down} \\ 2.6 \times 10^{-7}, & \text{K} - \text{up/K} - \text{down} \end{cases} \qquad \text{two- and three-way} \tag{31}$$

Throughout this module, the band designation K refers to the bands 22,550 to 23,150 MHz on the uplink and 25,500 to 27,000 MHz on the downlink. The band designation Ka refers to the bands 34,200 to 34,700 MHz on the uplink and 31,800 to 32,300 MHz on the downlink.

The approximation of Equation (30) is based on the work reported in Reference 8. This model is valid when tracking binary phase-shift keyed telemetry with either a residual or suppressed carrier or when tracking a QPSK (or Offset QPSK) signal. This model is the recommended estimate for all Sun-Earth-probe angles, even though this model was originally based on data for Sun-Earth-probe angles between 5° and 27°. More recent measurements suggest that the estimate is more generally applicable.

Figure 7 shows the standard deviation σ_{VS} (the square-root of the variance ${\sigma_{VS}}^2$) as a function of Sun-Earth-probe angle for two-way or three-way Doppler measurement with an S-band uplink and an S-band downlink. The vertical axis is in units of mm/s. The three curves in that figure correspond to measurement integration times of 5, 60, and 1000 seconds. Figure 8 shows σ_{VS} for an S-band uplink and an X-band downlink. Figure 9 shows σ_{VS} for an X-band uplink and an S-band downlink. Figure 10 shows σ_{VS} for an X-band uplink and an X-band downlink. Figure 11 shows σ_{VS} for an X-band uplink and a Ka-band downlink. Figure 12 shows σ_{VS} for a Ka-band uplink and an X-band downlink. Figure 13 shows σ_{VS} for a Ka-band uplink and a Ka-band downlink. Figure 14 shows σ_{VS} for a K-band uplink and a K-band downlink. In comparing these figures, it should be noted that the vertical scale is not the same for all of these figures.

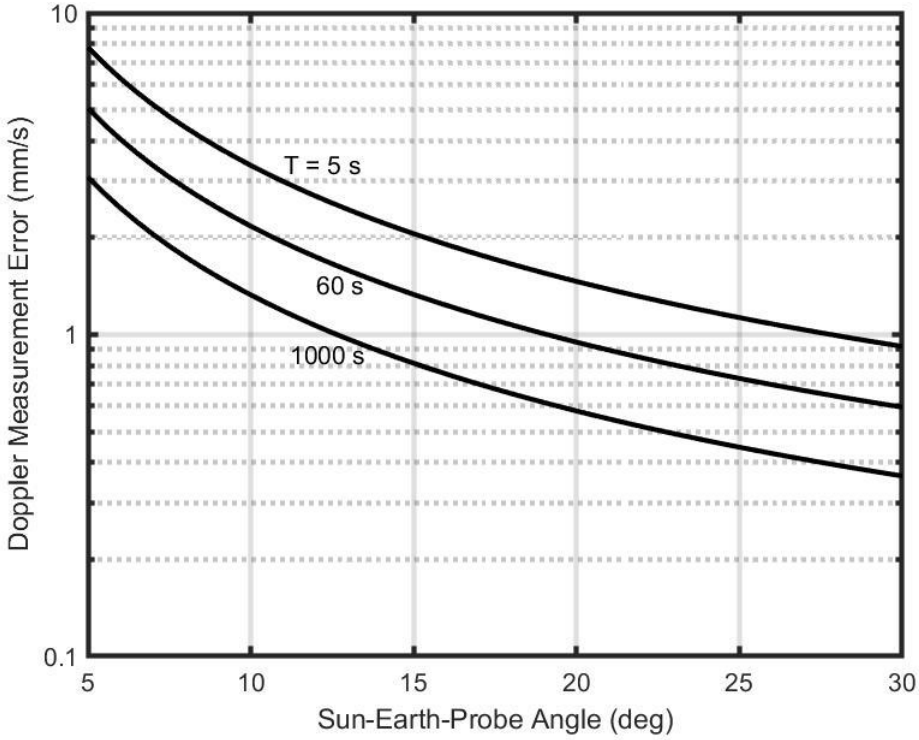

Figure 7. Doppler Measurement Error Due to Solar Phase Scintillation: S-Up/S-Down

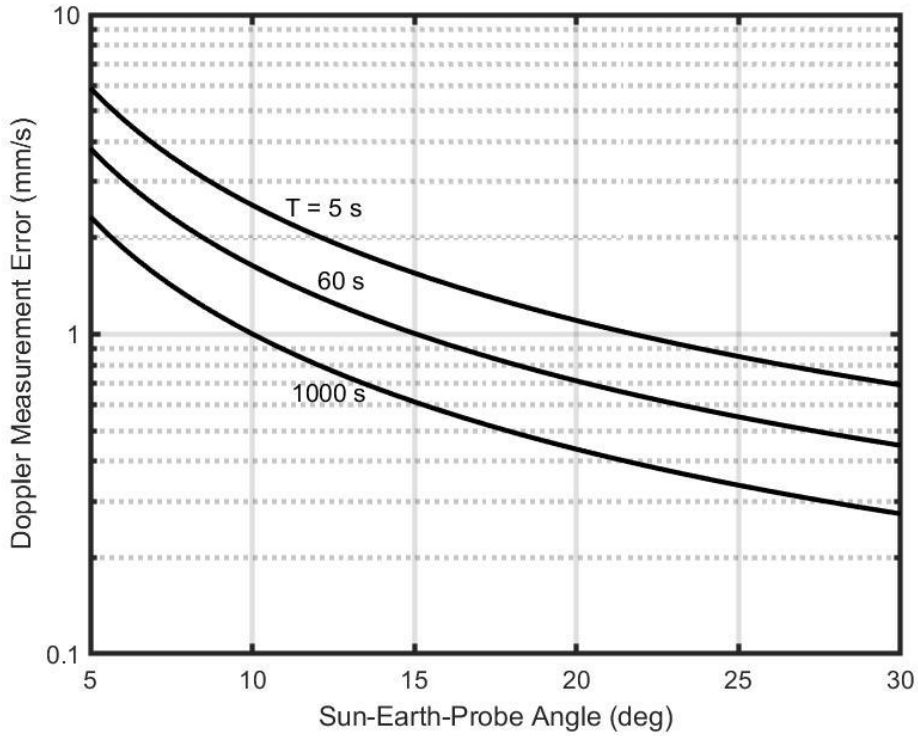

Figure 8. Doppler Measurement Error Due to Solar Phase Scintillation: S-Up/X-Down

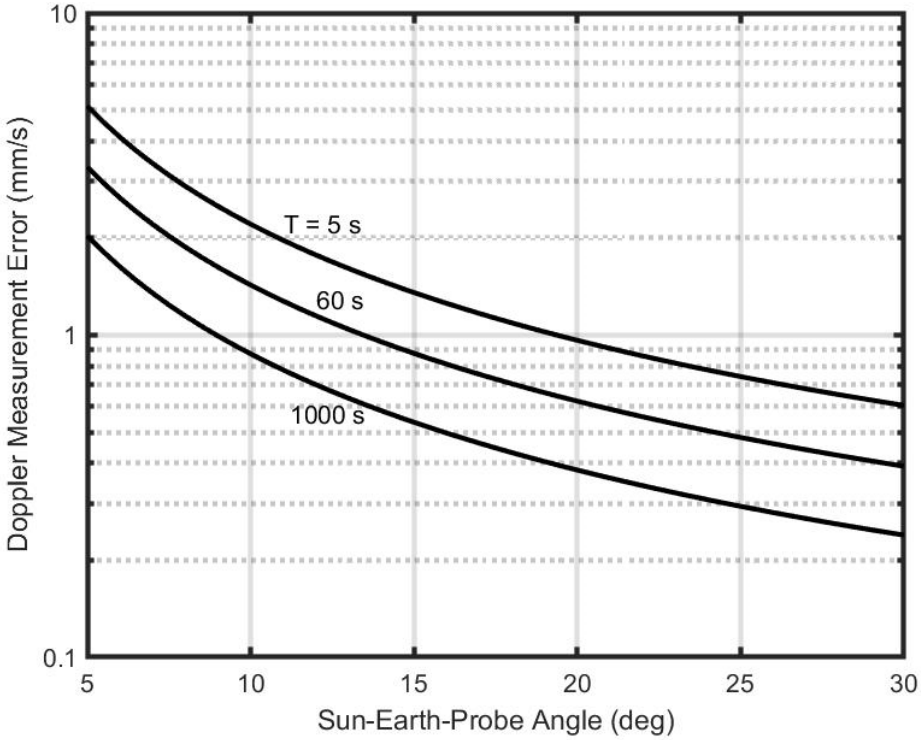

Figure 9. Doppler Measurement Error Due to Solar Phase Scintillation: X-Up/S-Down

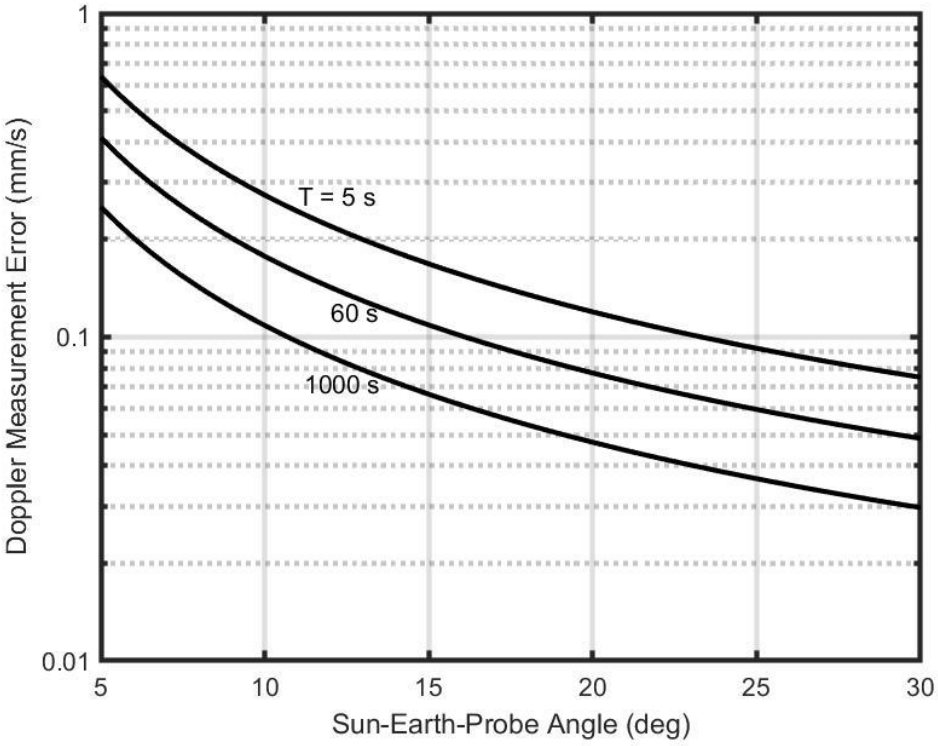

Figure 10. Doppler Measurement Error Due to Solar Phase Scintillation: X-Up/X-Down

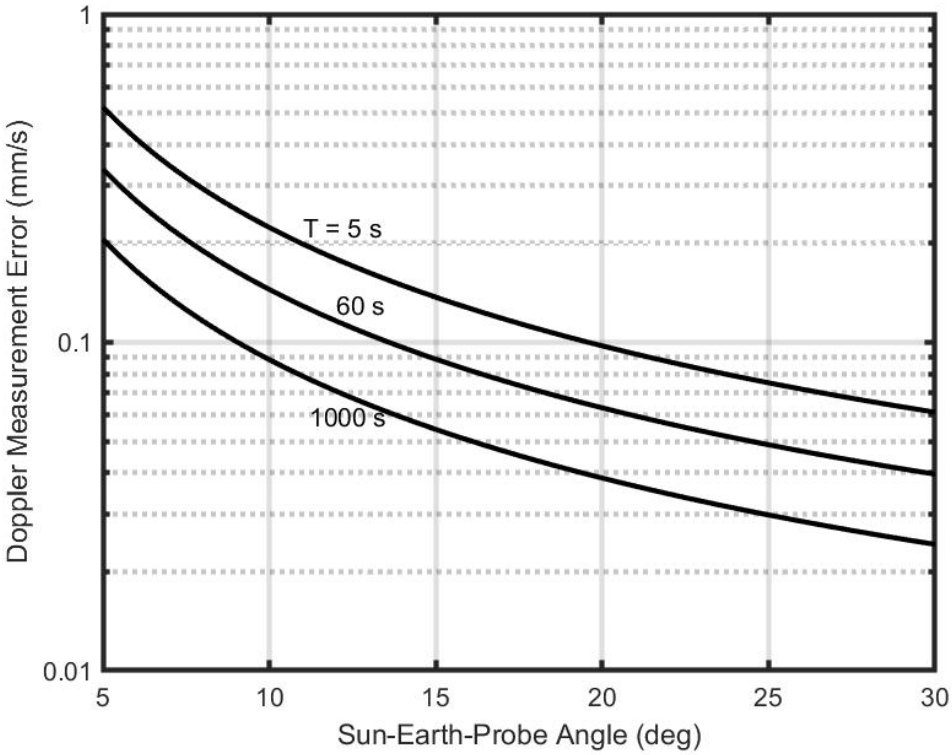

Figure 11. Doppler Measurement Error Due to Solar Phase Scintillation: X-Up/Ka-Down

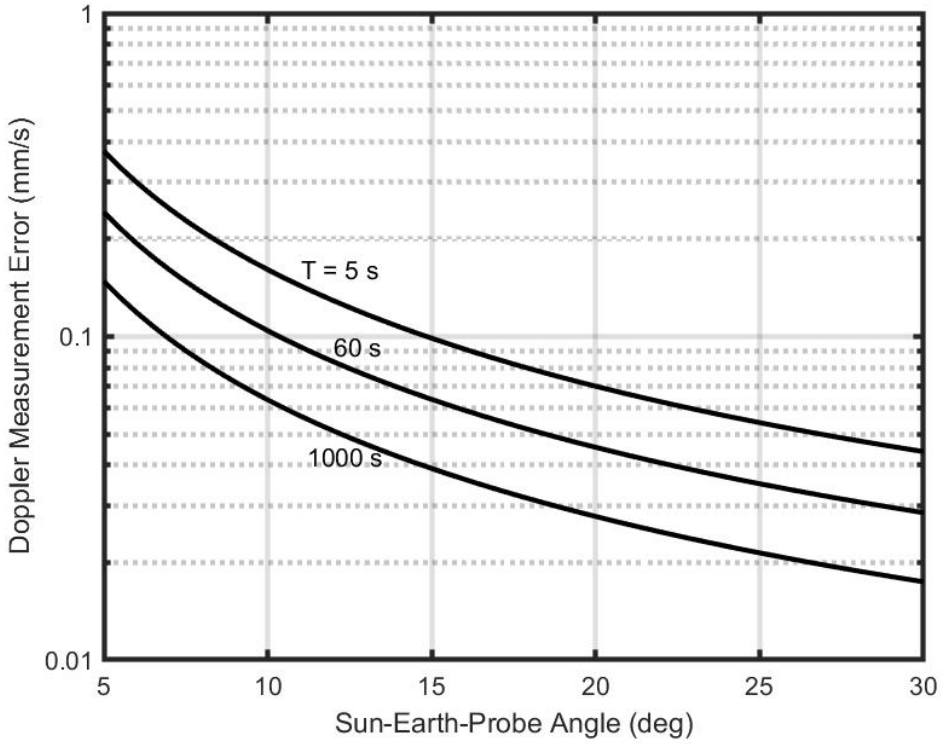

Figure 12. Doppler Measurement Error Due to Solar Phase Scintillation: Ka-Up/X-Down

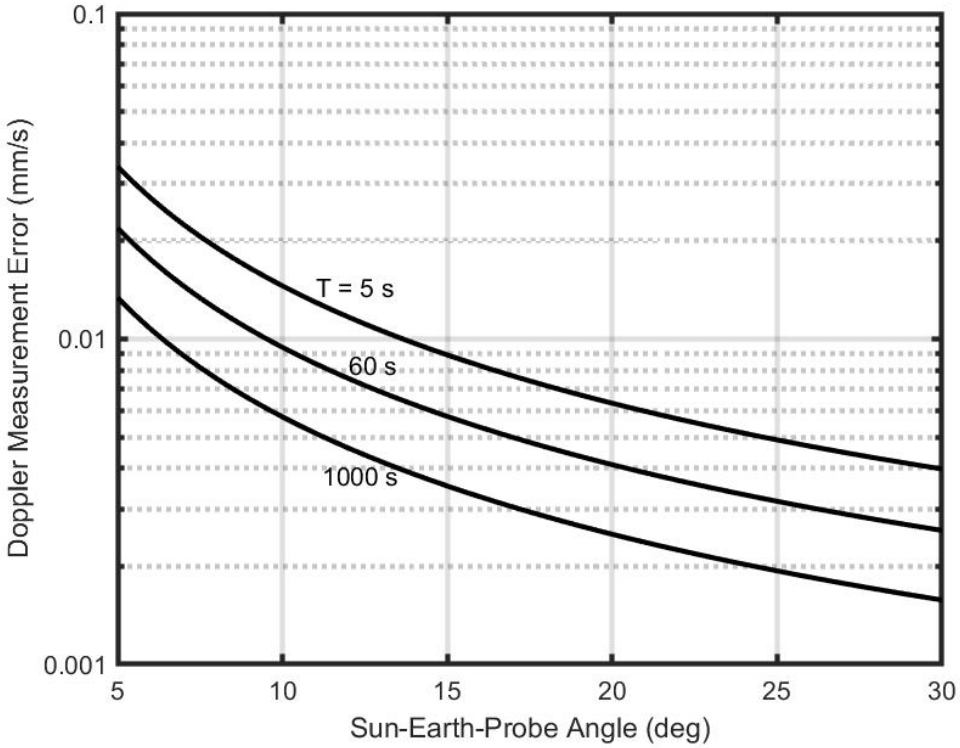

Figure 13. Doppler Measurement Error Due to Solar Phase Scintillations: Ka-Up/Ka-Down

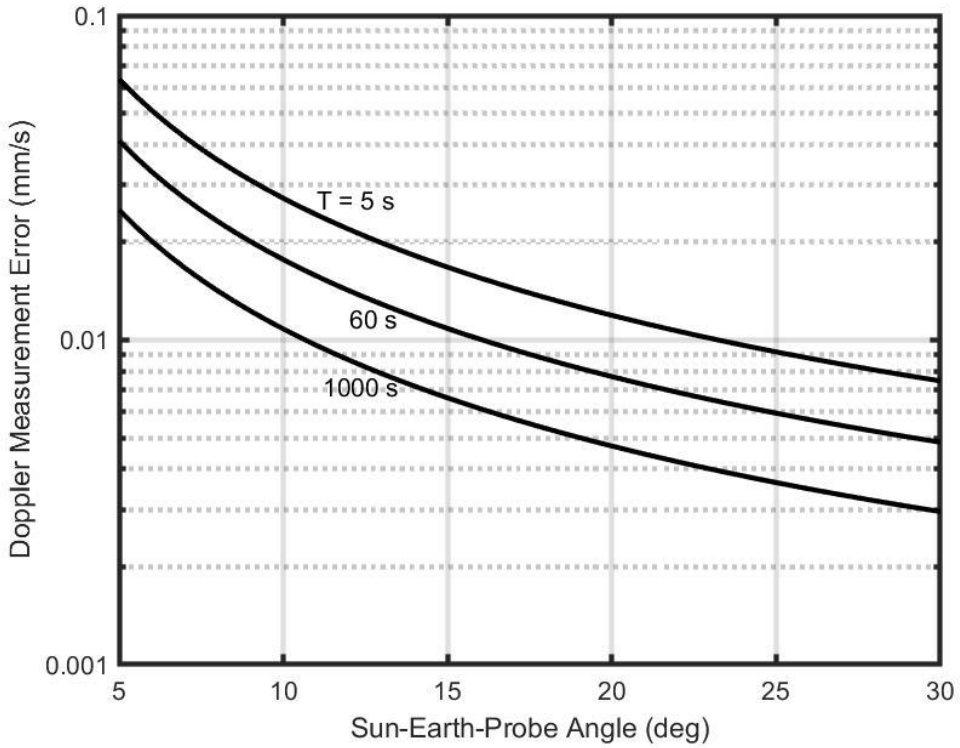

Figure 14. Doppler Measurement Error Due to Solar Phase Scintillations: K-Up/K-Down

2.3 Carrier Tracking

The DTT receiver can be configured to track phase-shift keyed telemetry with a residual carrier or a suppressed carrier or to track a QPSK or Offset QPSK signal. In order to achieve good telemetry performance and good Doppler measurement performance, it is important to characterize the phase error in the carrier loop.

2.3.1 Carrier Power Measurement

When the downlink is residual-carrier, an estimate of the downlink residual-carrier power P_C is available. When the downlink is suppressed-carrier, an estimate of the total downlink power P_T is available. This is done by first estimating $P_C/N_0|_{D/L}$ (with a modified version of the algorithm described in Reference 9) or $P_T/N_0|_{D/L}$ (with the split-symbol moments algorithm described in Reference 10). An estimate of the noise spectral density N_0 comes from continual measurements made by a noise-adding radiometer. This information is used to compute absolute power P_C or P_T. The results are reported once per second.

2.3.2 Carrier Loop Bandwidth

The one-sided, noise-equivalent, carrier loop bandwidth of the DTT receiver is denoted B_L. The user may choose to change B_L during a tracking pass, and this can be implemented without losing phase-lock, assuming the change is not too large. There are limits on the carrier loop bandwidth. For the DTT receiver, B_L can be no larger than 200 Hz. The lower limit on B_L is determined by the phase noise on the downlink. In addition, when operating in the suppressed-carrier mode, B_L is subject to the following constraint.

$$B_L \leq \frac{R_{SYM}}{20}, \text{ suppressed carrier} \tag{32}$$

where

R_{SYM} = telemetry symbol rate

In general, the value selected for B_L should be small in order to maximize the carrier loop signal-to-noise ratio. On the other hand, B_L must be large enough that neither of the following variables becomes too large: the static phase error due to Doppler dynamics and the contribution to carrier loop phase error variance from phase noise on the downlink. The best B_L to select will depend on circumstances. Often, it will be possible to select a B_L of about 1 Hz. A larger value for B_L is necessary when there is significant uncertainty in the downlink Doppler dynamics, when the downlink is one-way (or two-way non-coherent) and originates with a less stable frequency source, or when the Sun-Earth-probe angle is small (so that solar phase scintillations are present on the downlink).

When tracking a spinning spacecraft, it may be necessary to set the carrier loop bandwidth to a value that is somewhat larger than would otherwise be needed. The loop bandwidth must be large enough to track out the variation due to the spin. Also, the coherent AGC in the receiver must track out the amplitude variations.

The user may select either a 2nd order or 3rd order carrier loop. Both 2nd and 3rd order loops are perfect, meaning that the loop filter implements a true accumulation.

2.3.3 Static Phase Error in the Carrier Loop

The carrier loop, of either 2nd or 3rd order, has a very large tracking range; even a Doppler offset of several megahertz can be tracked. With a finite Doppler rate, however, there will be a static phase error in a 2nd order loop.

Table 1 shows the static phase error in the carrier loop that results from various Doppler dynamics for several different loops. These equations are based on the work reported in Reference 11. The Doppler dynamics are here defined by the parameters α and β.

α = Doppler Rate, Hz/s

β = Doppler Acceleration, $\mathrm{Hz/s^2}$

In the presence of a persistent Doppler acceleration, a 2nd order loop will periodically slip cycles. The equations of Table 1 are valid when tracking binary phase-shift keyed telemetry with either a residual or suppressed carrier or when tracking a QPSK or Offset QPSK signal. These equations are exactly the same as those appearing in Module 207.

Table 1. Static Phase Error (rad)

Loop	**Constant Range Rate** (Constant Doppler Offset)	**Constant Derivative of Range Rate** (Constant Doppler Rate)	**Constant Second Derivative of Range Rate** (Constant Doppler Acceleration)
2nd order, standard underdamped	0	$\frac{9\pi\alpha}{16{B_L}^2}$	$\left(\frac{9\pi\beta}{16{B_L}^2}\right)t - \frac{27\pi\beta}{64{B_L}^3}$
2nd order, supercritically damped	0	$\frac{25\pi\alpha}{32{B_L}^2}$	$\left(\frac{25\pi\beta}{32{B_L}^2}\right)t - \frac{125\pi\beta}{128{B_L}^3}$
3rd order, standard underdamped	0	0	$\frac{12167\pi\beta}{8000{B_L}^3}$
3rd order, supercritically damped	0	0	$\frac{35937\pi\beta}{16384{B_L}^3}$

2.3.4 Carrier Phase Error Variance

In order to ensure a strong phase lock, the phase error variance in the downlink carrier loop should be small. If this variance grows too large, both telemetry detection and Doppler measurement may suffer. This is, however, a second-order effect. For a baseline assessment of Doppler measurement error, the equations of Section 2.2 should be used.

In general, the carrier phase error variance ${\sigma_\phi}^2$ may be modeled as

$$ {\sigma_\phi}^2 = {\sigma_{\phi N}}^2 + {\sigma_{\phi F}}^2 + {\sigma_{\phi S}}^2 \tag{33} $$

where

${\sigma_\phi}^2$	=	carrier phase error variance, rad^2
${\sigma_{\phi N}}^2$	=	contribution to ${\sigma_\phi}^2$ from white (thermal) noise, rad^2
${\sigma_{\phi F}}^2$	=	contribution to ${\sigma_\phi}^2$from phase noise of frequency sources, rad^2
${\sigma_{\phi S}}^2$	=	contribution to ${\sigma_\phi}^2$from (solar) phase scintillation, rad^2

Equation (33) does *not* characterize Doppler measurement error; rather it characterizes the variance of the phase error in the DTT receiver's carrier loop. For characterizing the Doppler measurement error, Equation (13) should be used. The loop phase error is, however, relevant because if the phase error is large it has a second-order effect on the Doppler measurement.

The models for ${\sigma_{\phi N}}^2$, ${\sigma_{\phi F}}^2$, and ${\sigma_{\phi S}}^2$ depend on whether the transponder is in coherent or non-coherent mode.

It is recommended that the variance ${\sigma_\phi}^2$ of the downlink receiver's carrier loop not exceed the following limits:

$$ {\sigma_\phi}^2 \le \begin{cases} 0.1\ \text{rad}^2, & \text{residual carrier} \\ 0.02\ \text{rad}^2, & \text{suppressed carrier BPSK} \\ 0.005\ \text{rad}^2, & \text{QPSK or Offset QPSK} \end{cases} \tag{34} $$

The limits of Equation (34) are consistent with the limits on ρ_L given in Equations (3), (6) and (11) for the case where the only significant contributor to ${\sigma_\phi}^2$ is downlink thermal noise.

The recommended maximum variance ${\sigma_\phi}^2$ of Equation (34) is intended for the case of zero static phase error. If there is a significant static phase error, ${\sigma_\phi}^2$ should be smaller than the maximum given by Equation (34). As a rough guide, the maximum value of ${\sigma_\phi}^2$ (rad^2) in the presence of a static phase error ϕ_{SPE} (rad) should be less than the suggested maximum of Equation (34) by ${\phi_{\text{SPE}}}^2$.

2.3.4.1 Non-Coherent Operation

For non-coherent operation (such as one-way), the important contributors to ${\sigma_\phi}^2$ are: white noise at the receiver, phase noise originating in the frequency source on the spacecraft, and phase scintillation acquired by the downlink carrier in passing through the solar corona.

2.3.4.1.1 Downlink White (Thermal) Noise Contribution to ${\sigma_\phi}^2$, Non-Coherent

The variance ${\sigma_{\phi N}}^2$ accounts for white (thermal) noise.

$$ {\sigma_{\phi N}}^2 = \frac{1}{\rho_L}, \qquad \text{non-coherent} \tag{35} $$

where ρ_L is the downlink carrier loop signal-to-noise ratio. Section 2.1 has equations for calculating ρ_L.

2.3.4.1.2 Phase Noise Contribution to $\sigma_\phi{}^2$, Non-Coherent

The frequency source for the (non-coherent) downlink carrier has inherent phase noise. When this phase noise is characterized by the one-sided power spectral density $S_{D/L}(f)$, having units rad^2/Hz, $\sigma_{\phi F}{}^2$ is given by

$$\sigma_{\phi F}{}^2 = \int_0^\infty S_{D/L}(f) \cdot \left|1 - H_{D/L}(j2\pi f)\right|^2 df \tag{36}$$

$H_{D/L}(j2\pi f)$ is the frequency response of the downlink carrier loop and is given in Appendix A for 2nd order and 3rd order DTT carrier loops. This transfer function depends on the noise-equivalent loop bandwidth B_L.

The term $S_{D/L}(f) \cdot \left|1 - H_{D/L}(j2\pi f)\right|^2$ represents that portion of the downlink-carrier phase noise that is not tracked by the DTT carrier loop. Without evaluating the integral of Equation (36), it is possible to say that $\sigma_{\phi F}{}^2$ decreases with increasing B_L. When B_L is large enough that almost all of the downlink-carrier phase noise is tracked, $\sigma_{\phi F}{}^2$ will be negligible.

In general, there is also a contribution to $\sigma_{\phi F}{}^2$ from phase noise in the local oscillators of the DTT receiving chain. This contribution may be calculated using an equation similar to Equation (36), with $S_{D/L}(f)$ replaced by the one-sided power spectral density of the local oscillator phase noise. Since the local oscillators are derived from the FTS, this contribution has typically been very small compared with that for the frequency source, onboard the spacecraft, of the downlink carrier (for non-coherent operation). It is expected that atomic clocks will in the future be employed on spacecraft; when this occurs, $\sigma_{\phi F}{}^2$ will be calculated as the sum of two components: one from the onboard atomic clock and one from the DTT receiving-chain local oscillators.

2.3.4.1.3 Phase Scintillation Contribution to $\sigma_\phi{}^2$, Non-Coherent

The contribution $\sigma_{\phi S}{}^2$ may be approximated by

$$\sigma_{\phi S}{}^2 = \begin{cases} \dfrac{C_{\text{band}} \cdot C_{\text{loop}}}{[\sin(\theta_{\text{SEP}})]^{2.45} \cdot B_L{}^{1.65}}, & 0^\circ < \theta_{\text{SEP}} \le 90^\circ \\ \dfrac{C_{\text{band}} \cdot C_{\text{loop}}}{B_L{}^{1.65}}, & 90^\circ < \theta_{\text{SEP}} \le 180^\circ \end{cases} \tag{37}$$

θ_{SEP} is the Sun-Earth-probe angle ($0^\circ < \theta_{\text{SEP}} \le 180^\circ$). $\sigma_{\phi S}{}^2$ has the dimensions rad^2. (The product $C_{\text{band}} \cdot C_{\text{loop}}$ has the same dimensions as $B_L{}^{1.65}$.) The parameter C_{band} is constant for any given band and is given by Equation (21), which is repeated below for the reader's convenience.

$$C_{\text{band}} = \begin{cases} 1.2 \times 10^{-5}, & \text{S} - \text{down} \\ 9.3 \times 10^{-7}, & \text{X} - \text{down} \\ 9.5 \times 10^{-8}, & \text{K} - \text{down} \\ 6.4 \times 10^{-8}, & \text{Ka} - \text{down} \end{cases} \tag{21}$$

The parameter C_{loop} is constant for a given loop.

$$C_{\text{loop}} = \begin{cases} 5.9, & \text{standard underdamped } 2^{\text{nd}} \text{ order loop} \\ 5.0, & \text{supercritically damped } 2^{\text{nd}} \text{ order loop} \\ 8.3, & \text{standard underdamped } 3^{\text{rd}} \text{ order loop} \\ 6.7, & \text{supercritically damped } 3^{\text{rd}} \text{ order loop} \end{cases} \tag{38}$$

Equation (37) indicates that ${\sigma_{\phi S}}^2$ increases as θ_{SEP} decreases and as B_L decreases. Equation (21) indicates that ${\sigma_{\phi S}}^2$ increases with decreasing downlink carrier frequency.

2.3.4.2 Coherent Operation

The most important contributors to the carrier phase error variance ${\sigma_\phi}^2$ for coherent operation are white noise on both the uplink and downlink and phase scintillation acquired by the uplink and downlink carriers in passing through the solar corona.

2.3.4.2.1 White (Thermal) Noise Contribution to ${\sigma_\phi}^2$, Coherent

The white (thermal) noise contribution ${\sigma_{\phi N}}^2$ to carrier phase error variance ${\sigma_\phi}^2$ has two components:

$${\sigma_{\phi N}}^2 = {\sigma_{\phi NU}}^2 + {\sigma_{\phi ND}}^2 \tag{39}$$

where

${\sigma_{\phi NU}}^2$ = contribution to ${\sigma_{\phi N}}^2$ from uplink white (thermal) noise, rad^2

${\sigma_{\phi ND}}^2$ = contribution to ${\sigma_{\phi N}}^2$ from downlink white (thermal) noise, rad^2

For coherent operation, the contribution ${\sigma_{\phi NU}}^2$ of uplink white noise is modeled as

$${\sigma_{\phi NU}}^2 = \frac{G^2}{\rho_{TR} \cdot B_{TR}} \int_0^\infty \left|H_{U/L}(j2\pi f)\right|^2 \cdot \left|1 - H_{D/L}(j2\pi f)\right|^2 df \tag{40}$$

where

B_{TR} = transponder's carrier-loop bandwidth, Hz

Equation (40) accounts for noise that originates on the uplink, is tracked by the transponder's carrier loop, is transponded to the downlink band, and is *not* tracked by the DTT carrier loop. ${\sigma_{\phi NU}}^2$ generally increases as the DTT carrier-loop bandwidth B_L decreases. In the case where B_L is much smaller than the transponder's carrier-loop bandwidth B_{TR}, the following approximation is accurate:

$$\sigma_{\phi NU}{}^2 \cong \frac{G^2}{\rho_{TR}}, \qquad B_L \ll B_{TR} \tag{41}$$

Equation (41) is as an upper bound on $\sigma_{\phi NU}{}^2$. This upper bound is accurate when $B_L \ll B_{TR}$.

In general, when B_L is comparable with B_{TR} or larger than B_{TR}, the integral of Equation (40) must be evaluated in order to obtain an accurate value for $\sigma_{\phi NU}{}^2$. Both terms $\left|H_{U/L}(j2\pi f)\right|^2$ and $\left|1 - H_{D/L}(j2\pi f)\right|^2$, considered as functions of Fourier frequency, have relatively large transition bands. This is because they represent filters that are only of second or third order. These two functions of Fourier frequency are plotted in Figure 15 for a case where $B_L = B_{TR}$. In this case, there is considerable overlap between the functions. So it would clearly be a mistake for the case $B_L = B_{TR}$ to assume that $\sigma_{\phi NU}{}^2$ is zero (based on the simple notion that $\sigma_{\phi NU}{}^2$ represents uplink white noise that lies simultaneously inside B_{TR} and outside $B_L = B_{TR}$).

The variance $\sigma_{\phi ND}{}^2$ (rad^2) accounts for white (thermal) noise that originates on the downlink.

$$\sigma_{\phi ND}{}^2 = \frac{1}{\rho_L} \tag{42}$$

where ρ_L is the downlink carrier loop signal-to-noise ratio. Section 2.1 has equations for calculating ρ_L.

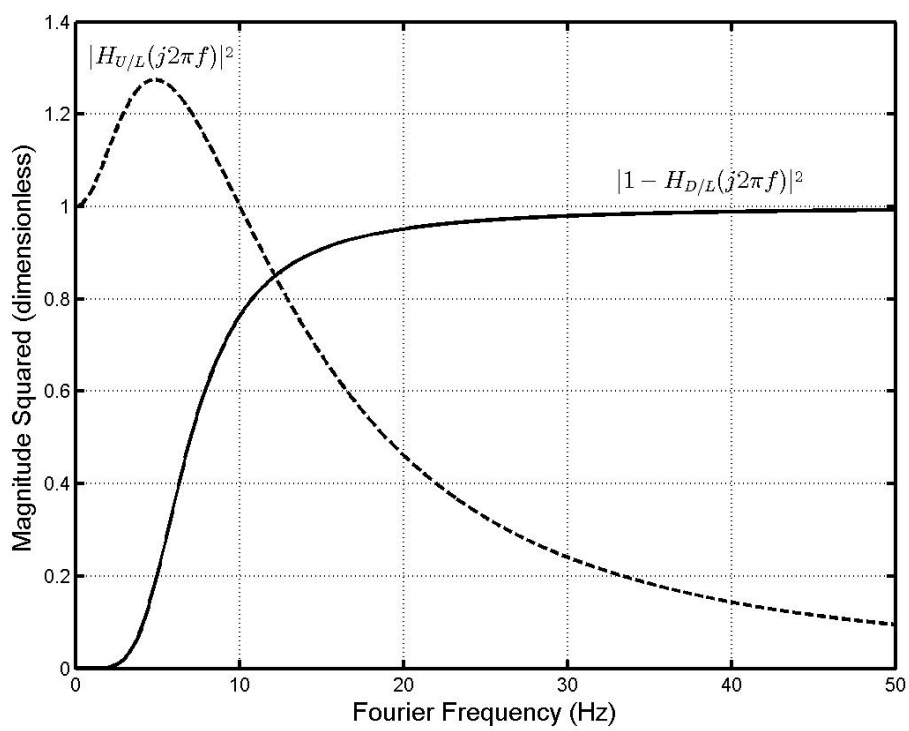

Figure 15. Terms Relating U/L White Noise to D/L Carrier Phase-Error Variance

2.3.4.2.2 Phase Noise Contribution to $\sigma_\phi{}^2$, Coherent

For coherent operations at the stations (but not at a test facility), the contribution $\sigma_{\phi F}{}^2$ may be modeled as:

$$\sigma_{\phi F}{}^2 = 2\,G^2 \int_0^\infty S_{U/L}(f) \cdot \left|1 - H_{D/L}(j2\pi f)\right|^2 df, \tag{43}$$

coherent operation at the stations

Equation (43) accounts for both phase noise in the uplink frequency source and phase noise in the DTT receiving-chain local oscillators. For a three-way measurement, the uplink source phase noise is independent of the local-oscillator phase noise. For a two-way coherent measurement in deep space, the round-trip signal delay is large enough that local-oscillator phase noise is uncorrelated with the delayed uplink source phase noise, even though both originate with a common FTS. The factor of 2 at the front of the right-hand side of Equation (43) is present because the total contribution $\sigma_{VF}{}^2$ is twice as large as a contribution from either the uplink-source phase noise alone or the local-oscillator phase noise alone.

The term $G^2 \cdot S_{U/L}(f) \cdot \left|1 - H_{D/L}(j2\pi f)\right|^2$ represents that portion of the downlink-carrier phase noise that is not tracked by the DTT carrier loop. Without evaluating the integral of Equation (43), it is possible to say that $\sigma_{\phi F}{}^2$ decreases with increasing B_L. When B_L is large enough that almost all of the downlink-carrier phase noise is tracked, $\sigma_{\phi F}{}^2$ will be negligible. A DTT carrier-loop bandwidth B_L of at least 1 Hz is adequate to ensure that $\sigma_{\phi F}{}^2$ is small while tracking a coherent downlink carrier. Of course, the rate-of-change and the acceleration of the downlink carrier's frequency causes a static phase error; therefore, B_L must be chosen large enough to ensure that this static phase error is not a problem.

At DTF-21 and CTT-22 the frequency stability of the uplink carrier and local oscillators is substantially poorer than at the stations; so, for coherent operation, $\sigma_{\phi F}{}^2$ might be significant. For this scenario, $\sigma_{\phi F}{}^2$ can be modeled as:

$$\sigma_{\phi F}{}^2 = G^2 \int_0^\infty S_{U/L}(f) \cdot \left|1 - H_{U/L}(j2\pi f)\right|^2 \cdot \left|1 - H_{D/L}(j2\pi f)\right|^2 df, \tag{44}$$

DTF-21 and CTT-22

Equation (44) reflects the fact that uplink-carrier phase noise will largely be canceled by phase noise in the local oscillators of the receiving chain but that this cancellation is imperfect when the transponder does not track all of the uplink-carrier phase noise. The product $S_{U/L}(f) \cdot \left|1 - H_{U/L}(j2\pi f)\right|^2 \cdot \left|1 - H_{D/L}(j2\pi f)\right|^2$ represents that portion of the uplink-carrier phase noise that is not tracked by the transponder and not tracked by the DTT receiver. When the transponder's carrier-loop bandwidth B_{TR} and the DTT carrier-loop bandwidth B_L are large,

${\sigma_{\phi F}}^2$ will be negligible. To the extent that B_{TR} and B_L are not sufficiently large, an estimate of ${\sigma_{\phi F}}^2$ requires a numerical evaluation of Equation (44).

2.3.4.2.3 Phase Scintillation Contribution to ${\sigma_\phi}^2$, Coherent

In two-way and three-way tracking, both the uplink and downlink carriers acquire phase scintillation when passing through the solar corona. During coherent operation, the uplink phase scintillation is transponded onto the downlink carrier.

The contribution ${\sigma_{\phi S}}^2$ of phase scintillation to downlink-carrier phase error variance may be approximated with Equation (37), which is repeated below for the reader's convenience.

$$ {\sigma_{\phi S}}^2 = \begin{cases} \dfrac{C_{\text{band}} \cdot C_{\text{loop}}}{[\sin(\theta_{\text{SEP}})]^{2.45} \cdot {B_L}^{1.65}}, & 0^\circ < \theta_{\text{SEP}} \leq 90^\circ \\ \dfrac{C_{\text{band}} \cdot C_{\text{loop}}}{{B_L}^{1.65}}, & 90^\circ < \theta_{\text{SEP}} \leq 180^\circ \end{cases} \tag{37} $$

θ_{SEP} is the Sun-Earth-probe angle ($0^\circ < \theta_{\text{SEP}} \leq 180^\circ$). ${\sigma_{\phi S}}^2$ has the dimensions rad^2. (The product $C_{\text{band}} \cdot C_{\text{loop}}$ has the same dimensions as ${B_L}^{1.65}$.) The parameter C_{band} is constant for any given band pairing and is given by Equation (31), which is repeated below for the reader's convenience.

$$ C_{\text{band}} = \begin{cases} 3.0 \times 10^{-5}, & \text{S} - \text{up/S} - \text{down} \\ 2.3 \times 10^{-4}, & \text{S} - \text{up/X} - \text{down} \\ 1.3 \times 10^{-5}, & \text{X} - \text{up/S} - \text{down} \\ 2.7 \times 10^{-6}, & \text{X} - \text{up/X} - \text{down} \\ 2.6 \times 10^{-5}, & \text{X} - \text{up/Ka} - \text{down} \\ 9.3 \times 10^{-7}, & \text{Ka} - \text{up/X} - \text{down} \\ 1.1 \times 10^{-7}, & \text{Ka} - \text{up/Ka} - \text{down} \\ 2.6 \times 10^{-7}, & \text{K} - \text{up/K} - \text{down} \end{cases} \tag{31} $$

The parameter C_{loop} is constant for a given loop and is given by Equation (38), which is repeated below for the reader's convenience.

$$ C_{\text{loop}} = \begin{cases} 5.9, & \text{standard underdamped } 2^{\text{nd}} \text{ order loop} \\ 5.0, & \text{supercritically damped } 2^{\text{nd}} \text{ order loop} \\ 8.3, & \text{standard underdamped } 3^{\text{rd}} \text{ order loop} \\ 6.7, & \text{supercritically damped } 3^{\text{rd}} \text{ order loop} \end{cases} \tag{38} $$

Equation (37) indicates that ${\sigma_{\phi S}}^2$ increases as θ_{SEP} decreases and as B_L decreases.

Appendix A: Carrier-Loop Transfer Function

The transfer function of the DTT receiver's carrier loop is characterized here. For a 2nd order loop, the transfer function is given by:

$$H_{D/L}(s) = \frac{K_1 s + K_2}{s^2 + K_1 s + K_2} \tag{45}$$

where s is the Laplace transform variable. The parameters K_1 and K_2 depend on whether the loop is standard underdamped or supercritically damped (Reference 11), as shown in Table 2.

Table 2. 2nd Order Loop Parameters

	K_1	K_2
standard underdamped	$\frac{8}{3}B_L$	$\frac{1}{2}{K_1}^2$
supercritically damped	$\frac{16}{5}B_L$	$\frac{1}{4}{K_1}^2$

B_L is the one-sided, noise-equivalent bandwidth of the carrier loop (Hz).

$$B_L = \int_0^\infty \left|H_{D/L}(j2\pi f)\right|^2 df \tag{46}$$

For a 3rd order loop, the transfer function is given by:

$$H_{D/L}(s) = \frac{K_1 s^2 + K_2 s + K_3}{s^3 + K_1 s^2 + K_2 s + K_3} \tag{47}$$

The parameters K_1, K_2 and K_3 depend on whether the loop is standard underdamped or supercritically damped (Reference 11), as shown in Table 3.

Table 3. 3rd Order Loop Parameters

	K_1	K_2	K_3
standard underdamped	$\frac{60}{23}B_L$	$\frac{4}{9}{K_1}^2$	$\frac{2}{27}{K_1}^3$
supercritically damped	$\frac{32}{11}B_L$	$\frac{1}{3}{K_1}^2$	$\frac{1}{27}{K_1}^3$

Appendix B: Glossary of Parameters

$P_C/N_0\|_{D/L}$	downlink residual-carrier power to noise spectral density ratio, Hz
$P_T/N_0\|_{D/L}$	downlink total signal power to noise spectral density ratio, Hz
E_S/N_0	telemetry symbol energy to noise spectral density ratio
ρ_{TR}	signal-to-noise ratio of transponder's carrier loop
ρ_L	signal-to-noise ratio of DTT receiver's carrier loop
B_{TR}	noise-equivalent bandwidth of transponder's carrier-loop bandwidth, Hz
B_L	noise-equivalent bandwidth of DTT receiver's carrier loop, Hz
$H_{U/L}(j2\pi f)$	frequency response of transponder's carrier loop
$H_{D/L}(j2\pi f)$	frequency response of DTT receiver's carrier loop
$S_{U/L}(f)$	one-sided power spectral density of uplink-carrier phase noise, $\mathrm{rad}^2/\mathrm{Hz}$
$S_{D/L}(f)$	one-sided power spectral density of downlink-carrier phase noise, $\mathrm{rad}^2/\mathrm{Hz}$
S_L	squaring loss of a (BPSK) Costas loop
S_{LQ}	squaring loss of a QPSK or OQPSK loop
T	integration time for Doppler measurement, s
$T_{S\,(\mathrm{binary})}$	period of the binary symbol, s
R_{SYM}	telemetry symbol rate, symbols per second
f_C	downlink carrier frequency, Hz
c	speed of electromagnetic waves in vacuum, mm/s
G	transponding ratio
α	Doppler Rate, Hz/s
β	Doppler Acceleration, $\mathrm{Hz/s}^2$
θ_{SEP}	Sun-Earth-probe angle ($0^\circ < \theta_{\mathrm{SEP}} \leq 180^\circ$)
θ_t	telemetry modulation index, rad
I_{data}	data imbalance, $0 \leq I_{\mathrm{data}} \leq 0.5$
σ_f	standard deviation of frequency, Hz
σ_{VI}	standard deviation of Doppler error due to telemetry data imbalance, mm/s

$\sigma_y(T)$	Allan deviation
${\sigma_V}^2$	variance of range rate, $\mathrm{mm}^2/\mathrm{s}^2$
${\sigma_{VN}}^2$	contribution to ${\sigma_V}^2$ from white (thermal) noise, $\mathrm{mm}^2/\mathrm{s}^2$
${\sigma_{VF}}^2$	contribution to ${\sigma_V}^2$ from phase noise of frequency sources, $\mathrm{mm}^2/\mathrm{s}^2$
${\sigma_{VS}}^2$	contribution to ${\sigma_V}^2$ from (solar) phase scintillation, $\mathrm{mm}^2/\mathrm{s}^2$
${\sigma_\phi}^2$	carrier phase error variance, rad^2
${\sigma_{\phi N}}^2$	contribution to ${\sigma_\phi}^2$ from white (thermal) noise, rad^2
${\sigma_{\phi F}}^2$	contribution to ${\sigma_\phi}^2$ from phase noise of frequency sources, rad^2
${\sigma_{\phi S}}^2$	contribution to ${\sigma_\phi}^2$ from (solar) phase scintillation, rad^2
${\sigma_{\phi NU}}^2$	contribution to ${\sigma_{\phi N}}^2$ from uplink white (thermal) noise, rad^2
${\sigma_{\phi ND}}^2$	contribution to ${\sigma_{\phi N}}^2$ from downlink white (thermal) noise, rad^2

References

1. J. B. Berner and K. M. Ware, "An Extremely Sensitive Digital Receiver for Deep Space Satellite Communications," *Eleventh Annual International Phoenix Conference on Computers and Communications*, pp. 577-584, Scottsdale, Arizona, April 1-3,1992.

2. J. Lesh, "Tracking Loop and Modulation Format Considerations for High Rate Telemetry," *DSN Progress Report 42-44*, Jet Propulsion Laboratory, Pasadena, CA, pp. 117-124, April 15, 1978.

3. M. K. Simon and W. C. Lindsey, "Optimum Performance of Suppressed Carrier Receivers with Costas Loop Tracking," *IEEE Transactions on Communications*, Vol. COM-25, No. 2, pp. 215-227, February 1977.

4. M. K. Simon, "Carrier Synchronization of Offset Quadrature Phase-Shift Keying," *TMO Progress Report 42-133*, Jet Propulsion Laboratory, Pasadena, CA, May 15, 1998.

5. C. L. Thornton and J. S. Border, *Radiometric Tracking Techniques for Deep-Space Navigation*, Monograph 1 of the *Deep-Space Communications and Navigation Series*, Jet Propulsion Laboratory, Pasadena, CA, 2000.

6. S. W. Asmar, J. W. Armstrong, L. Iess, and P. Tortora, "Spacecraft Doppler Tracking: Noise Budget and Accuracy Achievable in Precision Radio Science Observations," *Radio Science*, Vol. 40, RS2001, 2005.

7. J. A. Barnes, *et al.*, "Characterization of Frequency Stability," *IEEE Transactions on Instrumentation and Measurement*, Vol. IM-20, No. 2, pp. 105-120, May 1971.

8. R. Woo and J. W. Armstrong, "Spacecraft Radio Scattering Observations of the Power Spectrum of Electron Density Fluctuations in the Solar Wind," *Journal of Geophysical Research*, Vol. 84, No. A12, pp. 7288-7296, December 1, 1979.

9. A. Monk, "Carrier-to-Noise Power Estimation for the Block-V Receiver," *TDA Progress Report 42-106*, Jet Propulsion Laboratory, Pasadena, CA, pp. 353-363, August 15, 1991.

10. S. Dolinar, "Exact Closed-Form Expressions for the Performance of the Split-Symbol Moments Estimator of Signal-to-Noise Ratio," *TDA Progress Report 42-100*, pp. 174-179, Jet Propulsion Laboratory, Pasadena, CA, February 15, 1990.

11. S. A. Stephens and J. B. Thomas, "Controlled-Root Formulation for Digital Phase-Locked Loops," *IEEE Transactions on Aerospace and Electronic Systems*, Vol. 31, No. 1, pp. 78-95, January 1995.

Deep Space Network

203
Sequential Ranging

Document Owner:		Approved by:	
Signature Provided	06/20/2019	Signature Provided	06/13/2019
Andrew O'Dea Telemetry, Tracking, and Command System Engineer	Date	Timothy Pham Communications Systems Chief Engineer	Date
Prepared By:		**Released by:**	
Signature Provided	06/13/2019	Signature Provided	06/20/2019
Peter Kinman Telecommunications Technical Consultant	Date	Christine Chang DSN Document Release Authority	Date

DSN No. **810-005, 203, Rev. D**
Issue Date: July 17, 2019
JPL D-19379; CL# 19-4107

Jet Propulsion Laboratory
California Institute of Technology

Users must ensure that they are using the current version in DSN Telecommunications Link Design Handbook website:
https://deepspace.jpl.nasa.gov/dsndocs/810-005/

Review Acknowledgment

By signing below, the signatories acknowledge that they have reviewed this document and provided comments, if any, to the signatories on the Cover Page.

Signature Provided	06/13/2019	Signature Provided	06/18/2019
Jeff Berner DSN Project Chief Engineer	Date	Scott Bryant DSN Ranging Cognizant Development Engineer	Date

Document Change Log

Rev	Issue Date	Prepared By	Affected Sections or pages	Change Summary
Initial	1/15/2001	P. W. Kinman	All	New Module
A	2/20/2006	P. W. Kinman	Many	Revised to incorporate changes resulting from improvements in sequential ranging implementation.
B	4/2/2007	P. W. Kinman	2.6	Added new paragraph in section on “Range Measurement Performance” providing recommended range for P_r/N_0.
C	10/31/2009	P. W. Kinman	Page 5, 31, 40, A1 & A2	Removed references of the 26-m subnet stations for they have been decommissioned. Made editorial changes.
D	07/17/2019	P. W. Kinman	Many	Rewrote “Allocation of Link Power” section, including new models for downlink phase deviation for each of two types of ranging channels. Reorganized “Range Measurement Performance” section, including new curve fit and new interpolation for probability of acquisition. Removed square-wave models. Added glossary. Rewrote many paragraphs for improved clarity.

Contents

Illustrations

Figure **Page**

Tables

Table **Page**

1. Introduction

1.1 Purpose

This module describes capabilities of the Deep Space Network (DSN) for sequential ranging. These capabilities are available within the 70-m, the 34-m High Efficiency (HEF), and the 34-m Beam Waveguide (BWG) subnets.

1.2 Scope

The material contained in this module covers the sequential ranging system that may be utilized by both near-Earth and deep-space missions. This document describes those parameters and operational considerations that are independent of the particular antenna being used to provide the telecommunications link. For antenna-dependent parameters, refer to Module 101, 103, or 104 of this handbook. The other ranging scheme employed by the DSN is PN ranging, described in Module 214.

An overview of the ranging system is given in Section 2.1. The sequential ranging signal structure is explained in Section 2.2. The parameters to be specified for ranging operations are explained in Section 2.3. The distribution of link power is characterized in Section 2.4. The spectrum of an uplink carrier modulated by a sequential ranging signal is described in Section 2.5. The performance of sequential ranging is summarized in Section 2.6. In Section 2.7 the corrections required to determine the actual range to a spacecraft are described. In Section 2.8 the total error for a range measurement is discussed.

2. General Information

The ranging signal of interest in this module is a sequence of periodic signals; this signaling technique is called sequential ranging. A different signaling technique, PN ranging, is also supported by the DSN. The same instrumentation within the DSN supports both sequential ranging and PN ranging. However, there are performance differences between these two signaling techniques. This module only discusses sequential ranging. PN ranging is discussed in Module 214.

The range clock is coherently related to the carrier. The uplink carrier is often tuned during a tracking pass, in order to compensate for the Doppler effect on the uplink carrier, thereby reducing stress on the transponder's carrier-tracking loop. As the uplink carrier is tuned, the range-clock frequency varies proportionately.

In two-way ranging, one Deep Space Station (DSS) both transmits the uplink and receives the downlink. For two-way ranging, the user may calculate the round-trip light time (RTLT) from data provided by the DSN: phase measurements of the ranging signal and a record of the transmitted uplink carrier frequency.

Three-way ranging is also supported, for which one DSS transmits the uplink and a different DSS receives the downlink. As with two-way ranging, the DSN reports phase measurements of the ranging signal and a record of the uplink-carrier frequency. From these

data, the user may calculate the light time for the travel of the ranging signal from the uplink DSS, through the spacecraft, to the downlink DSS.

To put matters in perspective, the measurements discussed here are phase measurements and the resulting data permit the user to calculate time delays. Range cannot be calculated directly and accurately from the time delays because the range changes significantly over the course of the signal travel time. Similar measurement techniques employed in terrestrial applications, where the distances and measurement times are much smaller, typically permit the calculation of the range as the two-way time delay times the speed of an electromagnetic wave divided by 2. That has been the justification for using the term range measurement for this class of measurement technique. The two-way and three-way time delays calculated for deep-space missions are useful in the orbit determination process. These calculated delays assist in the improvement of trajectory models; and so, indirectly, the delays assist in the estimation of range as a function of time.

It is customary to quote range measurement error in units of meters. For two-way ranging, the range error is defined as the error in the two-way time delay times the speed of electromagnetic waves in vacuum divided by 2. (The division by two accounts for the fact that range is a one-way distance but the time delay is two-way.)

2.1 System Description

The DSN ranging system records the phase of the ranging signal that is transmitted and measures the phase of the ranging signal that returns. For two-way ranging, both recorded phase values (that of the uplink ranging signal and that of the downlink ranging signal) apply to a common instant in time, an epoch of the 1-pulse per second timing reference, which becomes the common time tag. From the difference between the uplink and downlink phases and from the history of the transmitted range-clock frequency (which can be calculated from the history of the uplink-carrier frequency), a user may compute the RTLT (Reference 1). This two-way time delay applies to a signal arriving at the DSS at the instant specified by the time tag.

The architecture for the DSN ranging system is shown in Figure 1. The ranging signal originates in the Uplink Subsystem (UPL). The returned signal is processed in the Downlink Tracking and Telemetry Subsystem (DTT). Both the UPL and the DTT are located at the Deep Space Communications Complex (DSCC).

The signal processing in the UPL may be summarized as follows. The Uplink Signal Generator (USG) synthesizes the range clock such that it is coherently related to the uplink carrier. The range-clock frequency equals a rational factor times the uplink carrier frequency. The USG generates the ranging signal, which is the range clock modified by additional signal structure that makes possible resolution of the phase ambiguity. A sample of the uplink phase, which is required for the delay measurement, is passed from the USG to the Uplink Processor Assembly (UPA). The USG modulates the uplink carrier with the ranging signal. The klystron supplies the final stage of power amplification for the uplink carrier.

The downlink carrier, after amplification within the Low-Noise Amplifier (LNA), passes to the DTT. Frequency down-conversion to an intermediate frequency (IF) takes place in the RF-to-IF Downconverter (RID). The IF signal is sent to an IF-to-Digital Converter (IDC). Demodulation of the IF carrier occurs in the Receiver, Ranging and Telemetry (RRT) processor.

Also within the RRT, the correlation of the received, baseband ranging signal with a local model produces a measurement of the downlink phase. This downlink phase is passed to the Downlink Channel Controller (DCC).

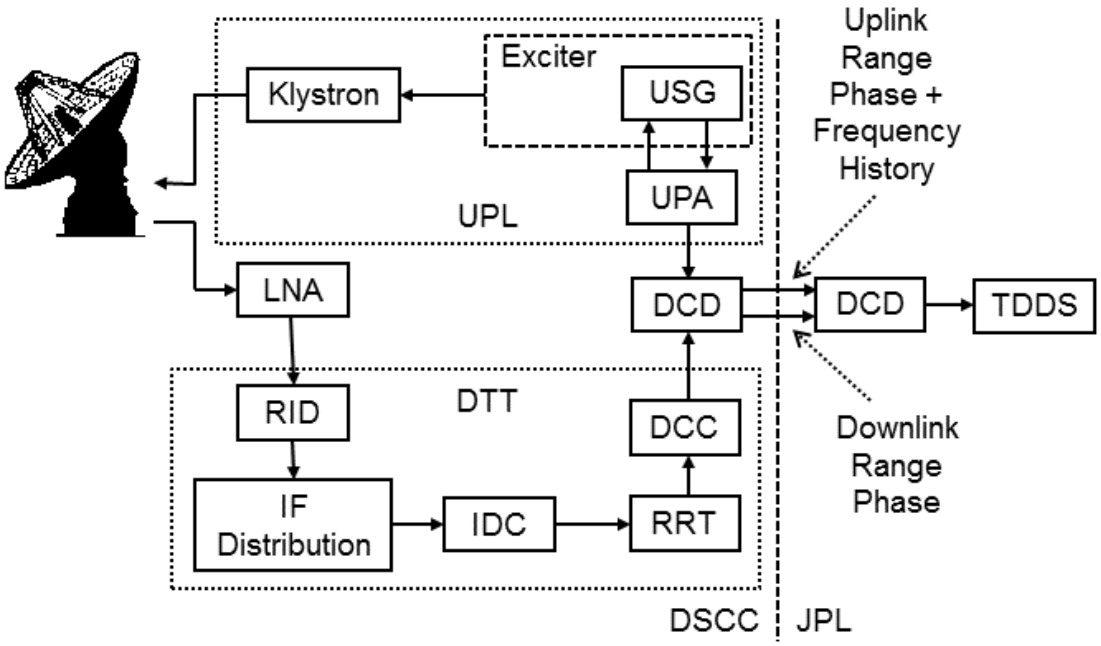

Figure 1. The DSN Ranging System Architecture

Uplink phase samples, each corresponding to an epoch of the 1-PPS (pulse per second) clock, are passed from the UPA, via the Data Capture and Delivery (DCD) software, to the Tracking Data Delivery Subsystem (TDDS), located in Pasadena. The DCC passes the downlink phase measurement and its time tag (an epoch of the 1-PPS clock), via the DCD, to the TDDS. A history of the uplink range clock's frequency is also needed for the calculation of the two-way time delay. Since the uplink range clock is coherently related to the uplink carrier, this necessary information can be derived from the history of the uplink carrier frequency, which is supplied by the UPA to the TDDS. All data required for the two-way delay calculation are archived by the TDDS for later use by a navigation team or other users.

The IDC, RRT, and DCC required for the processing of a downlink carrier are located within a Downlink Channel Processing Cabinet (DCPC). Each DCPC supports a single channel. For spacecraft with multiple channels (for example, X-band and Ka-band), or for multiple spacecraft within a single antenna beamwidth, multiple DCPCs will be assigned to that antenna.

The DSN uses the Range Unit (RU) to deliver the difference of the ranging signal's uplink phase and downlink phase. Since the range clock and the carrier are coherently related, it is permissible to define the RU in terms of carrier phase. For an S-band uplink, the RU is defined as two cycles of the carrier. For an X-band uplink, one RU is $(749/221)$ times two cycles of the carrier. For a Ka-band uplink, one RU is $(3599/221)$ times two cycles of the

carrier. Because the RU is defined with a factor (1 for an S-band uplink, $749/221$ for an X-band uplink, and $3599/221$ for a Ka-band uplink) that is proportional to frequency, the RU is proportional to time delay. (But the RU is a dimensionless unit.) One RU corresponds to approximately 0.94 ns of time delay.

A user may convert a two-way phase delay in RU into a two-way time delay as follows:

$$\text{Two-way Time Delay} = \begin{cases} \dfrac{2 \times RU}{f_S}, & \text{S-band uplink} \\ \dfrac{749}{221} \cdot \dfrac{2 \times RU}{f_X}, & \text{X-band uplink} \\ \dfrac{3599}{221} \cdot \dfrac{2 \times RU}{f_{Ka}}, & \text{Ka-band uplink} \end{cases} \tag{1}$$

where f_S is the frequency of an S-band uplink carrier, f_X is the frequency of an X-band uplink carrier, and f_{Ka} is the frequency of a Ka-band uplink carrier. For example, if the uplink carrier is in the X band with a frequency of 7.16 GHz and the two-way phase delay is reported as 6,500,000 RU, then the two-way time delay is 6,153,467 ns.

2.2 Sequential Ranging Signal Structure

The sequential ranging signal is a sequence of periodic signals. These periodic signals are all coherently related to each other and to the uplink carrier. The basis for these periodic ranging signals is a table of well-defined range components.

2.2.1 Range Components

The range components are periodic signals. Each component is assigned a number. A larger number represents a component with a smaller frequency (but a larger period). The components that are available, at least in theory, are ordered according to these component numbers. The frequency f_0 of component 0, which is never actually used in practice, is related to the uplink carrier frequency by

$$f_0 = \begin{cases} 2^{-7} \cdot f_S\,, & \text{S-band uplink} \\ 2^{-7} \cdot \dfrac{221}{749} \cdot f_X\,, & \text{X-band uplink} \\ 2^{-7} \cdot \dfrac{221}{3599} \cdot f_{Ka}\,, & \text{Ka-band uplink} \end{cases} \tag{2}$$

where f_S is the frequency of the S-band uplink carrier, f_X is the frequency of the X-band uplink carrier, and f_{Ka} is the frequency of the Ka-band uplink carrier. The frequency f_n of component n is related to f_0 by

$$f_n = 2^{-n} \cdot f_0 \tag{3}$$

Because the component frequencies are related to the uplink carrier frequency, the exact values of the component frequencies depend on the channel assignment and any uplink Doppler compensation that may be present. An example table of the transmitted range component frequencies is given in Table 1 for channel assignment 18, assuming the transmitted

uplink carrier is at its nominal channel frequency (no uplink Doppler compensation). The frequencies of Table 1 are rounded-off to the nearest millihertz. (In a typical measurement, the component frequencies are known to a better accuracy than 1 mHz. The intent of Table 1 is to give the reader a general idea of the component frequencies and how they vary with component number.) Even though Table 1 represents a particular case (nominal Channel 18), there are discernable features of this table that are also present in any table of range component frequencies. The frequency of component 4 is always approximately 1 MHz, and it is often called the "1 MHz component". Every component has a frequency that is exactly half of its immediate predecessor.

Whenever a periodic signal is used to measure signal delay, there is an ambiguity. The phase delay consists, in principle, of an integer number of cycles plus some fraction of a cycle. If only one periodic signal of frequency f_n is used in the measurement, only the fractional part of the phase delay (a fraction of one cycle) can be measured. The integer number of cycles in the delay cannot be known from the measurement itself. However, *a priori* knowledge of the approximate value of the delay may provide that information. The successful resolution of the ambiguity requires that the *a priori* estimate of the delay be correct to within 1 cycle of phase. In time units, the *a priori* estimate of the delay must be correct to within 1 period ($1/f_n$). Considering that the speed c of an electromagnetic wave in vacuum is 299,792,458 m/s and that the delay measurement is two-way, the *a priori* estimate of the range must be correct to within $c/(2\,f_n)$ if the ambiguity is to be resolved. This is the number entered in the third column of Table 1.

2.2.2 Range Clock

The first periodic signal in the ranging sequence is called the range clock. With component n_{RC} as the range clock, the frequency f_{RC} of the range clock is

$$f_{RC} = \begin{cases} (2^{-7-n_{RC}}) \cdot f_S\,, & \text{S-band uplink} \\ (2^{-7-n_{RC}}) \cdot \dfrac{221}{749} \cdot f_X\,, & \text{X-band uplink} \\ (2^{-7-n_{RC}}) \cdot \dfrac{221}{3599} \cdot f_{Ka}\,, & \text{Ka-band uplink} \end{cases} \tag{4}$$

This equation is consistent with Equations (2) and (3).

2.2.3 Ranging Sequence

The ranging signal consists of a sequence of range components. The first is the range clock. The second is the component having a component number equal to one plus that of the range clock. The third is the component having a component number equal to two plus that of the range clock, and so forth. For example, if the range clock is component 4, then the sequence is 4, 5, 6, etc.

All range components in a ranging sequence except the first (the range clock) are known as ambiguity-resolving components. The number of ambiguity-resolving components that should be used in the ranging sequence for any particular range measurement is determined by the required ambiguity-resolving capability for that measurement. The range components

always occur sequentially, in order of increasing component number, without skipping any, from the range clock to the last ambiguity-resolving component.

Table 1. Range Components for Channel 18 (Nominal)

Component Number	Frequency (Hz)	Ambiguity-Resolving Capability (km)
4	1,032,556.981	0.1452
5	516,278.490	0.2903
6	258,139.245	0.5807
7	129,069.623	1.1614
8	64,534.811	2.3227
9	32,267.406	4.6454
10	16,133.703	9.2909
11	80,66.851	18.5818
12	4,033.426	37.1635
13	2,016.713	74.3270
14	1,008.356	148.6540
15	504.178	297.3081
16	252.089	594.6161
17	126.045	1,189.2323
18	63.022	2,378.4645
19	31.511	4,756.9291
20	15.756	9,513.8581
21	7.878	19,027.7163
22	3.939	38,055.4326
23	1.969	76,110.8651
24	0.985	152,221.7303

In any given measurement, some ambiguity-resolving components will be multiplied by a higher-frequency component; this multiplication is called chopping. The purpose of chopping is to enforce spectral separation between the ranging signal and command on the uplink and between the ranging signal and telemetry on the downlink. The effect of the chopping is to modulate the lower frequency range components onto a ranging subcarrier. This ranging subcarrier is called the chop component. Often, the chop component is the range clock. Figure 2 shows an example of component 6 multiplied (chopped) by component 4. In this case, the chop component 4 has a frequency four times that of component 6, so there are two cycles of the chop component for each half-cycle of component 6. The user specifies at which point in the sequence the chopping should begin; all components after this point are multiplied by the chop component. The user also specifies the chop component. This chop component remains the same for the duration of the range measurement session.

The ranging sequence passes through the uplink ranging filter on its way to the phase modulator for the uplink carrier. This filter, implemented digitally in the USG, is low-pass with a default bandwidth of 1.2 MHz but is configurable for larger bandwidths. The purpose of the uplink ranging filter is to reduce the bandwidth of the modulated carrier for the sake of spectral efficiency. In Figure 2, the chop component (component 4, in this case) is shown as a sinewave; this is a good approximation when the uplink ranging filter passes the fundamental harmonic of the range clock but blocks the third and higher-order harmonics.

The purpose of ranging with a sequence is to get the advantages of both high-frequency and low-frequency range components. The accuracy of a range measurement improves when a higher-frequency range clock is used (see Section 2.6). All components that follow the range clock are present in order to resolve the phase ambiguity. The ambiguity-resolving capability of a ranging sequence equals the ambiguity-resolving capability of the lowest-frequency range component (see, for example, Table 1).

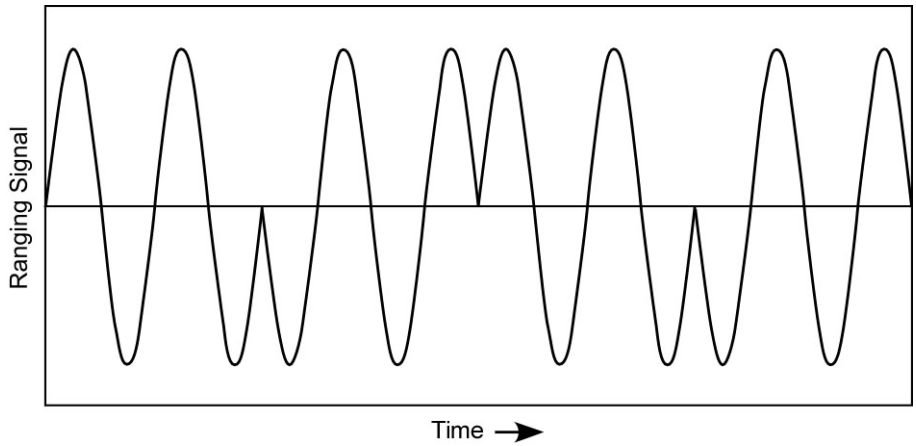

Figure 2. Component 6 Chopped by Sinewave Component 4

2.2.4 Sequence Timing

Three parameters control the timing of the transmitted sequence: the transmit time (XMIT), the integration time T_1 that is to be used for the range clock, and the integration time T_2 that is used to be used for each of the ambiguity-resolving components. XMIT is always selected to fall on an integer-second epoch, as determined by the uplink timing system. That is to say, this time, when expressed in seconds, has no fractional part. Each of the integration times T_1 and T_2 is an integer number of seconds.

2.2.4.1 Timing at the Exciter

At the exciter, the actual start time of the ranging sequence, which is also the start time of the range clock, is 1 second before the specified time XMIT. (The purpose of this slightly early start is to increase the probability that the range clock integration at the receiver does not begin before the range clock arrives at the receiver.) The range clock persists from the $(\mathrm{XMIT} - 1)$-second epoch up through the $(\mathrm{XMIT} + T_1 + 1)$-second epoch. The transition from the range clock to the first ambiguity-resolving component occurs sometime within the 1-second interval that immediately follows the $(\mathrm{XMIT} + T_1 + 1)$-second epoch. Hence, the range clock is present for $T_1 + 2$ seconds (plus a fraction of another second).

Once the first ambiguity-resolving component has started, a fraction of a second before the $(\mathrm{XMIT} + T_1 + 2)$-second epoch, it persists up through the $(\mathrm{XMIT} + T_1 + T_2 + 2)$-second epoch. The transition to the next ambiguity-resolving component occurs sometime within the 1-second interval that immediately follows the $(\mathrm{XMIT} + T_1 + T_2 + 2)$-second epoch. Hence, the first ambiguity-resolving component has a duration of at least T_2. The actual duration is typically about $T_2 + 1$ seconds: from a fraction of a second before the $(\mathrm{XMIT} + T_1 + 2)$-second epoch to a fraction of a second after the $(\mathrm{XMIT} + T_1 + T_2 + 2)$-second epoch, but no guarantee is made for a duration longer than T_2.

In general, the transition to the *n*-th ambiguity-resolving component occurs a fraction of a second before the $[\mathrm{XMIT} + T_1 + 2 + (n - 1) \cdot (T_2 + 1)]$-second epoch. The duration of the *n*-th ambiguity-resolving component is typically about $T_2 + 1$ seconds, but no guarantee is made for a duration longer than T_2.

Figure 3 shows an example of the sequence timing. In this example, the range clock is component 4 (C4) and the last component is 9 (C9). The range clock begins 1 second before XMIT. After XMIT, the range clock continues for an additional T_1 seconds (for the nominal measurement) plus 1 second (as a margin for error). During the next second there is a transition from the range clock to component 5 (C5). The transition itself occurs essentially instantaneously, but there is no programmatic guarantee of when within this second the actual transition occurs. There is another transition second following the planned T_2-second period for C5. The pattern established by C5 is repeated for components 6 through 9 (C6 through C9). Following a transition second that accommodates the transition from C9 back to C4 (in preparation for a second range measurement), the range clock is transmitted for 1 second (as a margin for error) plus T_1 seconds (for the nominal measurement), and so forth.

The phase is continuous throughout the ranging sequence, including at the transitions from one component to the next. This is essential for the correct resolution of the phase ambiguity.

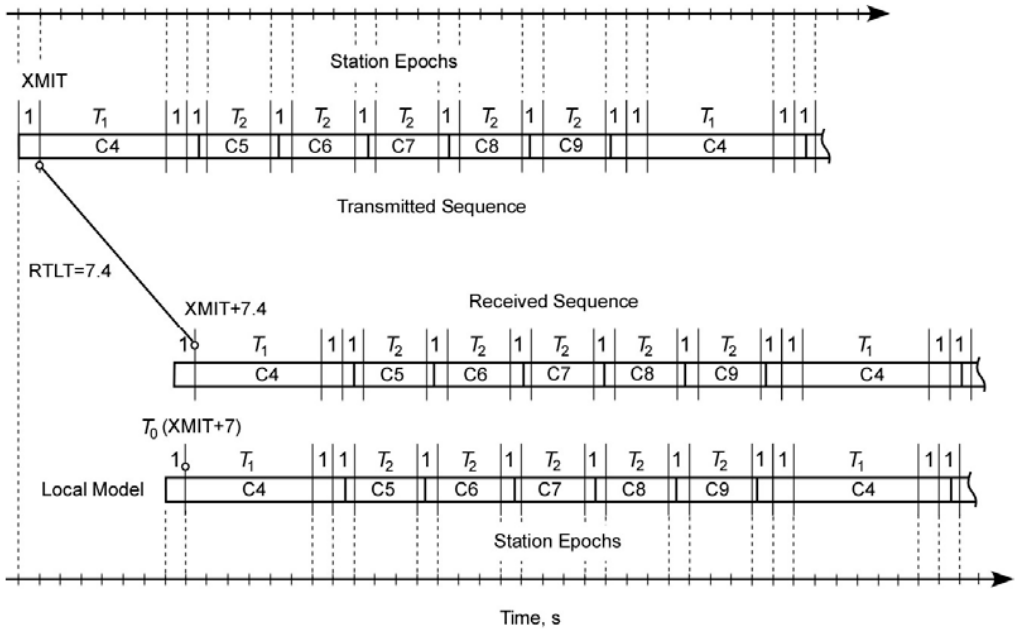

Figure 3. Example Timing Diagram

$T_1 = 6$ s, $T_2 = 3$ s, RTLT = 7.4 s

2.2.4.2 Timing at the Receiver

At the receiver, the estimated RTLT is an input parameter. Within the DTT this estimate is rounded-off to the nearest integer second. The rounded-off, estimated RTLT is added to XMIT to get the start time T_0 of the range-clock integration. The start time T_0, when expressed in seconds, has no fractional part. The range clock integration extends from the T_0 epoch to the $T_0 + T_1$ epoch, as marked by the timing system. The error introduced to T_0 by round-off is no larger than 0.5 second. Therefore, if the estimated RTLT is correct to within 0.5 second, T_0 is different from XMIT + RTLT by less than 1 second. That is why the range clock at the exciter begins 1 second before the specified sequence start time and ends $T_1 + 1$ seconds after the specified start time. The 1-second padding at the start and at the end of the range clock interval ensures that the range clock is present at the receiver during the entire range clock integration (as long as the estimated RTLT is correct to within 0.5 second).

The integration for the first ambiguity-resolving component begins at the $(T_0 + T_1 + 2)$-second epoch. Hence, there is 2-second interval that separates the range-clock integration from that of the first ambiguity-resolving component.

In general, the integration for the n-th ambiguity-resolving component begins at the $[T_0 + T_1 + 2 + (n-1) \cdot (T_2 + 1)]$-second epoch. There is a 1-second interval that separates the integrations of any two ambiguity-resolving components.

Figure 3 is an example of the timing. In this example, the RTLT (and the estimated RTLT) is 7.4 s. This value is rounded-off to 7 s within the DTT. In this case, T_0 is less than XMIT + RTLT by 0.4 s. Shown in Figure 3 is the received sequence as well as a local

model of that sequence, as computed from T_0. The local model is, in this case, 0.4 s in advance of the received sequence. The timing of the component integrations is determined by this local model. In this case, all integrations begin 0.4 s early.

Because T_0 does not, in general, exactly equal XMIT + RTLT, it will sometimes happen that the integration of each ambiguity-resolving component in a range measurement begins slightly before that component arrives or ends slightly after that component departs. In such cases, the effective integration time for each ambiguity-resolving component is slightly less than the design value T_2. The difference between the design value and the effective value of T_2 is typically a fraction of a second. Normally, this is not a problem. However, if the design value T_2 is only 1 or 2 seconds, the degradation in performance may be noticeable, as discussed in Subsection 2.6.5.1. As mentioned previously, this alignment problem does not affect the range-clock integration (as long as the estimated RTLT is correct to within 0.5 s), owing to the 1-s padding at the start and the end of the range clock interval.

2.2.4.3 Cycle Time

Typically, range measurements are done serially during a tracking pass. For each range measurement there is a ranging sequence of the type described above (a range clock followed by a set of ambiguity-resolving components). When the ranging sequence associated with one range measurement ends, another ranging sequence with exactly the same signal structure begins immediately. The cycle time is the repetition period of the range measurements. The cycle time is given by

$$\text{Cycle Time} = T_1 + 3 + (n_L - n_{RC}) \cdot (T_2 + 1) \qquad \text{seconds} \tag{5}$$

where n_L is the range component number of the last ambiguity-resolving component and n_{RC} is the range component number of the range clock. In light of the previous discussion of sequence timing, Equation (5) can be understood as follows. There is a period of time, $T_1 + 2$ seconds, during which the range clock is transmitted, followed by a 1-second interval that contains the transition from the range clock to the first ambiguity-resolving component. This is the $T_1 + 3$ seconds appearing in Equation (5). There are $(n_L - n_{RC})$ ambiguity-resolving components. Each of these ambiguity-resolving components has a guaranteed duration T_2, and associated with each ambiguity-resolving component is a 1-second interval that contains the transition to the next component.

The last component n_L should be chosen carefully if it is desirable to maximize the number of range data points in a tracking pass. For any given *a priori* range ambiguity, there is a minimum n_L that will resolve the ambiguity (see Table 1). Choosing an n_L larger than this will reduce the number of range data points that can be obtained in a tracking pass. Table 2 shows the number of range points that can be obtained per hour as a function of n_L for integration time $T_1 = 100$ s and for range clock component $n_{RC} = 4$.

Table 2. Range Points per Hour

$T_1 = 100$ s and $n_{RC} = 4$

n_L	Range Points per Hour	
	$T_2 = 5$ s	$T_2 = 20$ s
12	23.8	13.3
13	22.9	12.3
14	22.1	11.5
15	21.3	10.8
16	20.6	10.1
17	19.9	9.6
18	19.3	9.1
19	18.7	8.6
20	18.1	8.2
21	17.6	7.8
22	17.1	7.5
23	16.6	7.2
24	16.1	6.9

2.3 Parameters Specified for Ranging Operations

The following subsections present the parameters that are required in ranging operations.

2.3.1 Ranging Sequence Parameters

The ranging sequence is established by specifying the range clock component number, the last component number, the chop component number, the component number at which chopping begins, and the integration times T_1 and T_2.

The range clock component number determines the approximate frequency of the range clock. The exact frequency of the range clock is set by its relation to the uplink carrier frequency (see Section 2.2). The range clock is typically selected to be component 4, which corresponds to a range-clock having a frequency of approximately 1 MHz.

The last component number determines the ambiguity-resolving capability of the ranging sequence. Therefore, the proper selection of this number depends on *a priori* knowledge of the range. The approximate ambiguity-resolving capability of the different range components is given in Table 1. The exact ambiguity-resolving capability depends on the uplink frequency.

The purpose of chopping is to enforce spectral separation between the ranging sequence and the command signal on the uplink and between the ranging sequence and the telemetry signal on the downlink. Selection of the chop component and the component at which chopping begins should be made with this in mind.

There is a fundamental trade-off in the selection of the integration times T_1 and T_2. On the one hand, a large T_1 decreases the range measurement error due to thermal noise and a large T_2 increases the probability of range acquisition (see Section 2.6). On the other hand, large values for T_1 and T_2 increase the cycle time (see Section 2.2), decreasing the number of range measurements that can be made in a tracking pass. The selection of these integration times will depend on the available the ratio P_R/N_0 of the downlink ranging signal power to the noise spectral density (see Section 2.6).

2.3.2 Correlation Type

Either a sinewave or a squarewave may be used at the receiver as the local model of the range clock for the purpose of correlation. Normally, the user will select a local model that matches the form of the actual range clock. A small degradation in performance results if a local model is selected that does not match the form of the actual range clock.

2.3.3 Uplink Ranging Modulation Index

The uplink ranging modulation index is chosen to get a suitable distribution of power among the ranging and command sidebands and the residual carrier on the uplink (see Section 2.4). The uplink ranging modulation index also affects the distribution of power on the downlink carrier, because of the turn-around processing in the spacecraft transponder. The analysis appearing below employs an rms phase deviation of the uplink carrier. This rms phase deviation equals the peak modulation index divided by $\sqrt{2}$ for the case of a sinewave range clock.

2.3.4 Probability of Acquisition Tolerance

The tolerance plays a role in deciding whether to judge range acquisitions as “in lock” or “out of lock”. The ranging process does not use a phase-locked loop, so ranging lock status is estimated using the ranging probability of acquisition. For any given range acquisition, the ratio P_R/N_0 of the downlink ranging signal power to the noise spectral density is measured. From this measured P_R/N_0, an estimate of the probability of acquisition P_{acq} is calculated. Section 2.6 describes the calculation of the P_{acq} from P_R/N_0.

Tolerance may be selected over the range of 0.0% to 100.0%. The default value for tolerance is 99%. An acquisition lock status depends upon the following criteria:

$P_{\mathrm{acq}}(\%) \geq \mathrm{Tolerance}$ *results in* Acquisition declared “in lock”

$P_{\mathrm{acq}}(\%) < \mathrm{Tolerance}$ *results in* Acquisition declared “out of lock”

This procedure is explained for the example where the tolerance has the default value of 99%. For a given acquisition, P_R/N_0 is measured. From this measured value, the probability of acquisition P_{acq} is calculated; this number is the probability that the ambiguity is correctly resolved for this particular acquisition. Treating P_{acq} as a percentage, it is compared with the tolerance of 99%. If $P_{\mathrm{acq}}(\%)$ equals or exceeds 99%, the acquisition is declared "in lock". Otherwise, it is declared "out of lock". Note that the "out of lock" ranging data may be valid data, with a probability of $P_{\mathrm{acq}}(\%)$ of being correct.

2.4 Allocation of Link Power

The power allocation for a link is the distribution of power among the important link components: the residual carrier, the ranging sidebands, and the data (command or telemetry) sidebands. The following notation is used here for both the uplink and downlink:

P_C = power in residual carrier

P_R = usable power in ranging sidebands

P_D = usable power in data sidebands

P_T = total link power

P_C is the power in a single spectral line at the carrier frequency. When P_C is finite (greater than zero), carrier synchronization may be obtained at the receiver using a phase-locked loop that tracks this residual carrier. (Carrier synchronization may also be obtained with a Costas loop tracking the data sidebands, which are symmetrically located about the nominal carrier frequency.)

P_R is that portion of the power in the ranging sidebands that is used in the range measurement. At the beginning of the ranging sequence, when the range clock is present, P_R comprises two discrete spectral lines (one at f_{RC} Hz above and a second at f_{RC} Hz below the residual carrier) that correspond to the range clock's fundamental harmonic. Higher-order harmonics (beyond the fundamental harmonic) of the range clock are not used in a range measurement and are not included in P_R. For the components in the ranging sequence that come after the range clock, P_R comprises those discrete spectral lines, both above and below the residual carrier, that correspond to the fundamental harmonic of the component or of the chop component.

For the uplink, P_D is that portion of the power in the command sidebands that is employed in command detection in the transponder. In the most common signal design for a deep-space uplink, command data modulate a sinewave subcarrier and P_D only accounts for the power in the sidebands associated with the upper and lower fundamental harmonic of the subcarrier frequency. In the case of a sinewave subcarrier, the higher-order harmonics of the subcarrier frequency are not employed in command detection in the typical transponder and are not included in P_D.

For some missions, the command signal is bi-polar. An example of this is when the command symbols, represented as rectangular pulses, directly phase-modulate the uplink carrier. In this case, the uplink P_D accounts for all power in command sidebands, since the

command detection process in the typical transponder utilizes all command sidebands arising from a bi-polar command signal.

For the downlink, P_D is that portion of the power in the telemetry sidebands that is employed in telemetry detection at the station. Commonly, the telemetry signal is bi-polar; this happens when rectangular pulses (the telemetry symbols) directly phase-modulate the downlink carrier or when these symbols modulate a square-wave subcarrier that, in turn, phase-modulates the downlink carrier. In such cases, all of the power in the telemetry sidebands is employed in telemetry detection. This is a result of both the data and the subcarrier (if present) being bi-polar.

For some missions, the telemetry signal modulates a sinewave subcarrier and this composite signal phase-modulates the downlink carrier. In such a case, the downlink P_D is that portion of the power in the telemetry sidebands that is employed in telemetry detection at the station. Not included is the power in the higher-order harmonics of the subcarrier frequency.

P_T is not, in general, the sum of P_C, P_R, and P_D. In general, P_T is larger than that sum. There are multiple reasons for this. First, P_R does not account for power in the higher-order harmonics of a sinewave range clock. Second, when multiple signals (for example, a ranging signal and a telemetry signal) simultaneously phase-modulate a carrier, intermodulation products arise. These intermodulation products consume link power but do not contribute to either the range measurement or telemetry detection. Moreover, for the downlink, noise sidebands are present (in the case of turn-around ranging).

In calculating power allocations for a modulated carrier, it is necessary to characterize the level of the modulation. In this document, the root-mean-square (rms) phase deviation of the carrier will be used for this purpose. The following symbols are used in this module to represent rms phase deviation of the carrier:

uplink:	ϕ_r	=	rms phase deviation by ranging signal, rad rms
uplink:	ϕ_{cmd}	=	rms phase deviation by command signal, rad rms
downlink:	θ_{rs}	=	rms phase deviation by ranging signal (strong signal), rad rms
downlink:	θ_r	=	rms phase deviation by ranging signal, rad rms
downlink:	θ_{cmd}	=	rms phase deviation by feedthrough command signal, rad rms
downlink:	θ_n	=	rms phase deviation by noise, rad rms
downlink:	θ_{tlm}	=	rms phase deviation by telemetry signal, rad rms

On the uplink, ϕ_r and ϕ_{cmd} are parameters, constant for any given tracking pass. For a sinewave range clock, ϕ_r is related to the peak modulation index for uplink ranging by:

$$\phi_r = (\text{peak modulation index for uplink ranging, rad})/\sqrt{2} \tag{6}$$

When a sinewave subcarrier is used with command, ϕ_{cmd} is related to the peak modulation index for command by:

$$\phi_{cmd} = (\text{peak modulation index for command, rad})/\sqrt{2}, \quad \text{sinewave subcarrier} \tag{7}$$

However, for a bi-polar command signal, ϕ_{cmd} equals the peak modulation index for command.

A turn-around ranging channel is used for sequential ranging. Within this channel the uplink carrier is demodulated, and the baseband signal plus noise that is the result of this demodulation is presented to a filter. The filter output is applied to an automatic gain control (AGC) circuit. The signal plus noise that exits the turn-around ranging channel is phase-modulated onto the downlink carrier.

On the downlink, θ_{rs} is a constant parameter that is determined by the AGC in the turn-around ranging channel. θ_{rs} is the rms phase deviation of the downlink carrier by the ranging signal in a strong-signal scenario. In such a scenario, the noise in the transponder's ranging channel is negligible compared with the ranging signal and there is no command. This scenario occurs in a test facility before flight and in the early phase of flight when the ranging signal-to-noise ratio in the transponder's ranging channel is large. For a sinewave range clock, θ_{rs} is related to the peak modulation index (strong signal) by:

$$\theta_{rs} = (\text{strong-signal peak modulation index for downlink ranging, rad})/\sqrt{2} \qquad (8)$$

For an arbitrary signal-to-noise ratio in the transponder's ranging channel, the rms phase deviation by ranging signal on the downlink, denoted θ_r, is less than or equal to θ_{rs}. Thus, θ_r is a variable, depending on both the parameter θ_{rs} and the ranging signal-to-noise ratio in the ranging channel. θ_{rs} is the limiting value of θ_r, corresponding to the strong-signal case. If command is present on the uplink and that command passes through the transponder's ranging channel, then θ_r also depends on the command signal-to-noise ratio in the ranging channel.

Uplink noise passes through the ranging channel and is phase-modulated onto the downlink carrier. θ_n is the rms phase deviation by this ranging-channel noise. θ_n, like θ_r, is a variable that depends on both the parameter θ_{rs} and the ranging signal-to-noise ratio (and, possibly, also the command signal-to-noise ratio) in the ranging channel.

θ_{tlm} is the rms phase deviation of the downlink carrier due to telemetry. When the telemetry signal is bi-polar, the rms phase deviation and the peak modulation index for telemetry are identical. When a sinewave subcarrier is used with telemetry, θ_{tlm} is related to the peak modulation index for telemetry by:

$$\theta_{tlm} = (\text{peak modulation index for telemetry, rad})/\sqrt{2}, \quad \begin{matrix}\text{sinewave}\\ \text{subcarrier}\end{matrix} \qquad (9)$$

2.4.1 Uplink

The equations of this subsection represent the case where a ranging signal and a command signal are simultaneously present on the uplink carrier. The range clock is taken here to be a sinewave. The ratio of P_C to P_T, the carrier suppression, is

$$\left.\frac{P_C}{P_T}\right|_{\mathrm{U/L}} = J_0{}^2\left(\sqrt{2}\,\phi_r\right) \cdot S_{cmd}(\phi_{cmd}) \qquad (10)$$

The ratio of P_R to P_T is

$$\left.\frac{P_R}{P_T}\right|_{\mathrm{U/L}} = 2J_1{}^2\left(\sqrt{2}\,\phi_r\right) \cdot S_{cmd}(\phi_{cmd}) \tag{11}$$

The ratio of the fundamental command sideband power to P_T is

$$\left.\frac{P_D}{P_T}\right|_{\mathrm{U/L}} = J_0{}^2\left(\sqrt{2}\,\phi_r\right) \cdot M_{cmd}(\phi_{cmd}) \tag{12}$$

where $J_0(\cdot)$ and $J_1(\cdot)$ are Bessel functions of the first kind of order 0 and 1, respectively. These functions are plotted in Figure 4. When the argument x of $J_0(x)$ and $J_1(x)$ is small and positive, the following approximations may be used:

$$J_0(x) \cong 1, \qquad 0 \le x \ll 1 \tag{13}$$

$$J_1(x) \cong x/2, \qquad 0 \le x \ll 1 \tag{14}$$

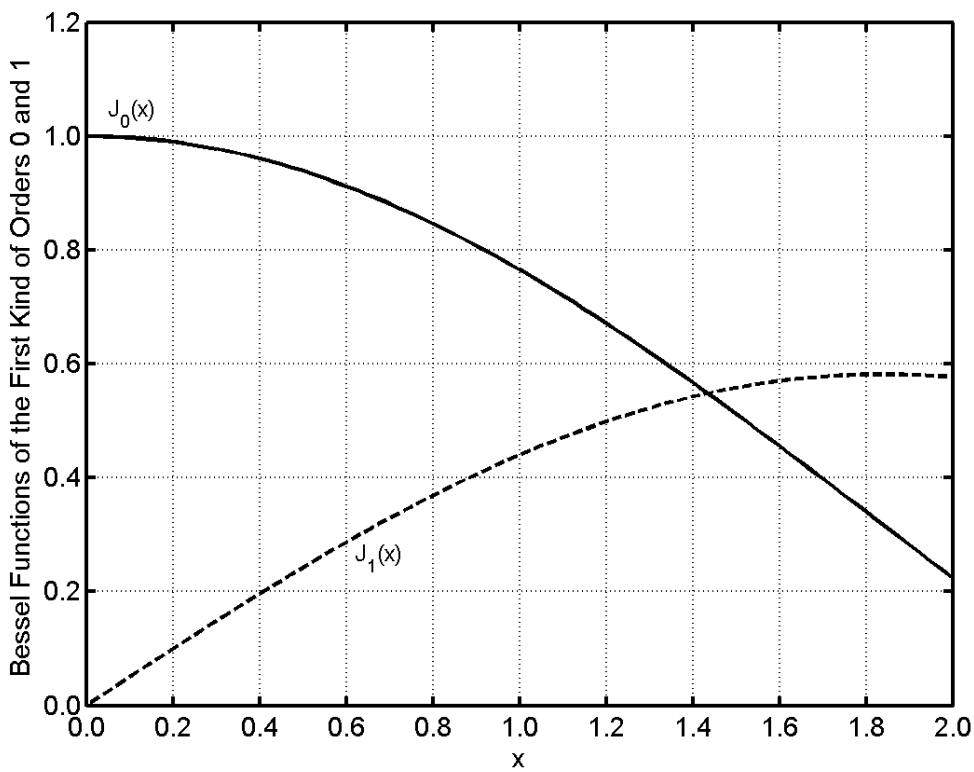

Figure 4. Bessel Functions of the First Kind of Order 0 and 1

The suppression factor $S_{cmd}(\phi_{cmd})$ in Equations (10) and (11) and the modulation factor $M_{cmd}(\phi_{cmd})$ in Equation (12) depend on whether the command signal is bi-polar or uses a sinewave subcarrier. These two factors are given by:

$$S_{cmd}(\phi_{cmd}) = \begin{cases} \cos^2(\phi_{cmd}), & \text{bi-polar} \\ {J_0}^2(\sqrt{2}\,\phi_{cmd}), & \text{sinewave subcarrier} \end{cases} \tag{15}$$

$$M_{cmd}(\phi_{cmd}) = \begin{cases} \sin^2(\phi_{cmd}), & \text{bi-polar} \\ 2{J_1}^2(\sqrt{2}\,\phi_{cmd}), & \text{sinewave subcarrier} \end{cases} \tag{16}$$

In the event that command is absent from the uplink, the factor $S_{cmd}(\phi_{cmd})$ in Equations (10) and (11) can be omitted, since $S_{cmd}(0) = 1$.

2.4.2 Downlink

A turn-around ranging channel demodulates the uplink carrier, filters the baseband signal, applies automatic gain control, and then re-modulates the baseband signal onto the downlink carrier. The AGC serves the important purpose of ensuring that the downlink carrier suppression is approximately constant, independent of received uplink signal level. The bandwidth B_R of the transponder's ranging channel must be larger (typically about 50% larger) than the range-clock frequency, in order to pass the ranging signal with minimal distortion. For example, B_R is typically about 1.5 MHz when the transponder is intended to accommodate a range clock of 1 MHz. Substantial thermal noise from the uplink also passes through this channel. In many deep space scenarios, the thermal noise dominates over the ranging signal in this wideband, turn-around channel. Moreover, command signal from the uplink may pass through this ranging channel. In general, then, noise and command signal as well as the desired ranging signal are modulated onto the downlink carrier whenever the ranging channel is active (Reference 2).

The equations of this subsection represent the case where a ranging signal, a (feedthrough) command signal and noise are simultaneously present in the ranging channel, so that all three of these components, plus telemetry, phase-modulate the downlink carrier. The range clock is taken here to be a sinewave. The ratio of P_C to P_T, the carrier suppression, is

$$\left.\frac{P_C}{P_T}\right|_{\mathrm{D/L}} = {J_0}^2(\sqrt{2}\,\theta_r) \cdot S_{fth}(\theta_{cmd}) \cdot e^{-{\theta_n}^2} \cdot S_{tlm}(\theta_{tlm}) \tag{17}$$

The ratio of P_R to P_T is

$$\left.\frac{P_R}{P_T}\right|_{\mathrm{D/L}} = 2{J_1}^2(\sqrt{2}\,\theta_r) \cdot S_{fth}(\theta_{cmd}) \cdot e^{-{\theta_n}^2} \cdot S_{tlm}(\theta_{tlm}) \tag{18}$$

The ratio of the telemetry sideband power to P_T is

$$\left.\frac{P_D}{P_T}\right|_{\mathrm{D/L}} = {J_0}^2(\sqrt{2}\,\theta_r) \cdot S_{fth}(\theta_{cmd}) \cdot e^{-{\theta_n}^2} \cdot M_{tlm}(\theta_{tlm}) \tag{19}$$

where $J_0(\cdot)$ and $J_1(\cdot)$ are Bessel functions of the first kind of order 0 and 1, respectively.

The command-feedthrough suppression factor $S_{fth}(\theta_{cmd})$ that appears in each of Equations (17), (18) and (19) depends on whether the command signal is bi-polar or uses a sinewave subcarrier. This factor is given by:

$$S_{fth}(\theta_{cmd}) = \begin{cases} \cos^2(\theta_{cmd}), & \text{bi-polar} \\ {J_0}^2(\sqrt{2}\,\theta_{cmd}), & \text{sinewave subcarrier} \end{cases} \tag{20}$$

In the event that command feedthrough is absent from the ranging channel, the factor $S_{fth}(\theta_{cmd})$ in each of Equations (17), (18) and (19) can be omitted, since $S_{fth}(0) = 1$.

The suppression factor $S_{tlm}(\phi_{tlm})$ in Equations (17) and (18) and the modulation factor $M_{tlm}(\phi_{tlm})$ in Equation (19) depend on whether the telemetry signal is bi-polar or uses a sinewave subcarrier. These two factors are given by:

$$S_{tlm}(\theta_{tlm}) = \begin{cases} \cos^2(\theta_{tlm}), & \text{bi-polar} \\ {J_0}^2(\sqrt{2}\,\theta_{tlm}), & \text{sinewave subcarrier} \end{cases} \tag{21}$$

$$M_{tlm}(\theta_{tlm}) = \begin{cases} \sin^2(\theta_{tlm}), & \text{bi-polar} \\ 2{J_1}^2(\sqrt{2}\,\theta_{tlm}), & \text{sinewave subcarrier} \end{cases} \tag{22}$$

For a turn-around ranging channel, the downlink rms phase deviations θ_r, θ_n, and (if command feedthrough is present) θ_{cmd} depend on the ranging signal-to-noise ratio ρ_r and (if command feedthrough is present) the command signal-to-noise ratio ρ_{cmd} in the ranging channel.

$$\rho_r = \left.\frac{P_R}{P_T}\right|_{\mathrm{U/L}} \cdot \left.\frac{P_T}{N_0}\right|_{\mathrm{U/L}} \cdot \frac{1}{B_R} \tag{23}$$

$$\rho_{cmd} = \left.\frac{P_D}{P_T}\right|_{\mathrm{U/L}} \cdot \left.\frac{P_T}{N_0}\right|_{\mathrm{U/L}} \cdot \frac{1}{B_R} \tag{24}$$

where

$P_T/N_0|_{\mathrm{U/L}}$ = uplink total power to noise spectral density ratio, Hz

B_R = noise-equivalent (one-sided) bandwidth of transponder's ranging channel, Hz

In some transponders with a turn-around ranging channel, the AGC is designed to keep constant the average of the absolute value of the voltage at the AGC output. In other transponders, the AGC is designed to keep constant the rms voltage at the AGC output. For both types of AGC, the downlink rms phase deviations θ_r, θ_n, and θ_{cmd} depend on ρ_r and ρ_{cmd} (as well as the parameter θ_{rs}). Turn-around ranging channels with both types of AGC are treated below.

2.4.2.1 AGC with Constant Average of Absolute Value of Voltage

When the transponder's ranging channel has an AGC that keeps constant the average of the absolute value of the channel voltage, there are no exact, analytical expressions for the rms phase deviations θ_r, θ_{cmd} and θ_n. However, these rms phase deviations may be obtained by computer simulation. Curve fits to the simulations appear below.

$$\theta_r = \frac{\theta_{rs}}{1 + \exp[\gamma - 0.79 \cdot \ln(\rho_r)]} \tag{25}$$

where

$$\gamma = \begin{cases} -1.2, & \rho_{cmd} = 0 \\ \ln[0.3 + 0.27 \cdot {\rho_{cmd}}^{0.88}], & \rho_{cmd} > 0 \end{cases} \tag{26}$$

Here $\exp(\cdot)$ and $\ln(\cdot)$ are the exponential function and natural logarithm, respectively. In the event that there is no command feedthrough, $\rho_{cmd} = 0$ and θ_r depends only on the constant parameter θ_{rs} and the ranging signal-to-noise ratio ρ_r. The asymptotes for Equation (25) are $\lim_{\rho_r \to 0} \theta_r = 0$ and $\lim_{\rho_r \to \infty} \theta_r = \theta_{rs}$.

A similar set of equations are valid (approximately) for θ_{cmd}

$$\theta_{cmd} = \frac{\theta_{rs}}{1 + \exp[\chi - 0.79 \cdot \ln(\rho_{cmd})]} \tag{27}$$

where

$$\chi = \ln[0.3 + 0.27 \cdot {\rho_r}^{0.88}] \tag{28}$$

The asymptotes for Equation (27) are $\lim_{\rho_{cmd} \to 0} \theta_{cmd} = 0$ and $\lim_{\rho_{cmd} \to \infty} \theta_{cmd} = \theta_{rs}$.

A curve-fit to the simulation data for θ_n as a function of ρ_r and ρ_{cmd} is:

$$\theta_n = \frac{\theta_{rs} \cdot \left(2/\sqrt{\pi}\right)}{1 + \exp[-0.87 + 0.81 \cdot \ln(\rho_{rss})]} \tag{29}$$

where ρ_{rss} is the root-sum-square of ρ_r and ρ_{cmd}:

$$\rho_{rss} = \sqrt{{\rho_r}^2 + {\rho_{cmd}}^2} \tag{30}$$

The asymptotes for this curve are $\lim_{\rho_{rss} \to 0} \theta_n = \theta_{rs} \cdot \left(2/\sqrt{\pi}\right)$ and $\lim_{\rho_{rss} \to \infty} \theta_n = 0$.

Since θ_r is directly proportional to the parameter θ_{rs}, the ratio θ_r/θ_{rs} may be plotted as a function of ρ_r (and ρ_r alone when $\rho_{cmd} = 0$). This appears in Figure 5 for the case of no command feedthrough: $\rho_{cmd} = 0$ and $\theta_{cmd} = 0$. The solid curve labeled AAV is valid for a turn-around ranging channel whose AGC keeps constant the average of the absolute voltage (AAV). Figure 5 shows that the ratio θ_r/θ_{rs} increases monotonically as a function of ρ_r with a limiting value of 1. (In other words, the strong-signal value of θ_r is θ_{rs}.) The AAV curve of Figure 5 comes from Equations (25) and (26) with $\rho_{cmd} = 0$.

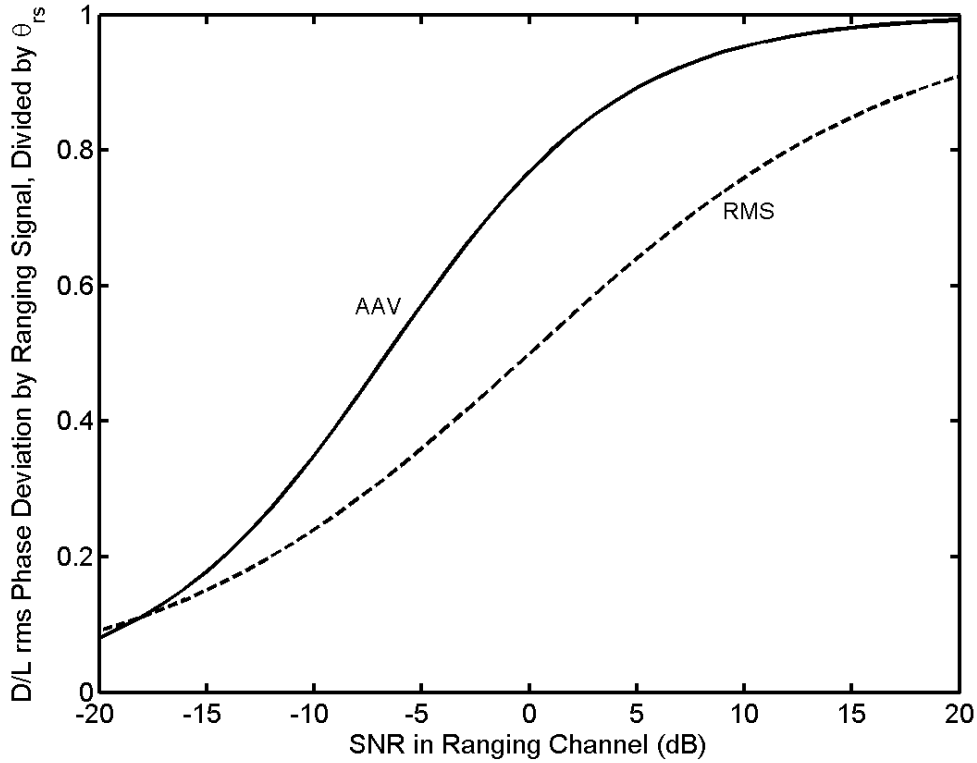

Figure 5. Downlink rms Phase Deviation by Ranging Signal (No Command Feedthrough)

The ratio θ_n/θ_{rs} may also be plotted as a function of ρ_r when $\rho_{cmd} = 0$. This appears in Figure 6. The solid curve labeled AAV is valid for a turn-around ranging channel whose AGC keeps constant the average of the absolute voltage (AAV). Figure 6 shows that the ratio θ_n/θ_{rs} decreases monotonically as a function of ρ_r. The AAV curve of Figure 6 comes from Equations (29) and (30) with $\rho_{cmd} = 0$.

2.4.2.2 AGC with Constant Root-Mean-Square Voltage

In some transponders, especially older designs, the ranging channel has an AGC that enforces a constant rms voltage at the AGC output. Since an unchanging rms voltage corresponds to an unchanging power, this type of AGC is also called a power-controlled AGC.

An AGC that enforces constant rms voltage (equivalently, constant power) at the AGC output is characterized by the following relationship among the rms phase deviations θ_r, θ_{cmd}, θ_n, and θ_{rs}.

$$\theta_r{}^2 + \theta_{cmd}{}^2 + \theta_n{}^2 = \theta_{rs}{}^2 \tag{31}$$

In other words, the total power in the turn-around ranging channel, which equals the ranging signal power plus the feedthrough command signal power plus the noise power in the channel bandwidth, equals a constant value. The rms phase deviations are given by

$$\theta_r = \theta_{rs} \cdot \sqrt{\frac{\rho_r}{1 + \rho_r + \rho_{cmd}}} \tag{32}$$

$$\theta_{cmd} = \theta_{rs} \cdot \sqrt{\frac{\rho_{cmd}}{1 + \rho_r + \rho_{cmd}}} \tag{33}$$

$$\theta_n = \frac{\theta_{rs}}{\sqrt{1 + \rho_r + \rho_{cmd}}} \tag{34}$$

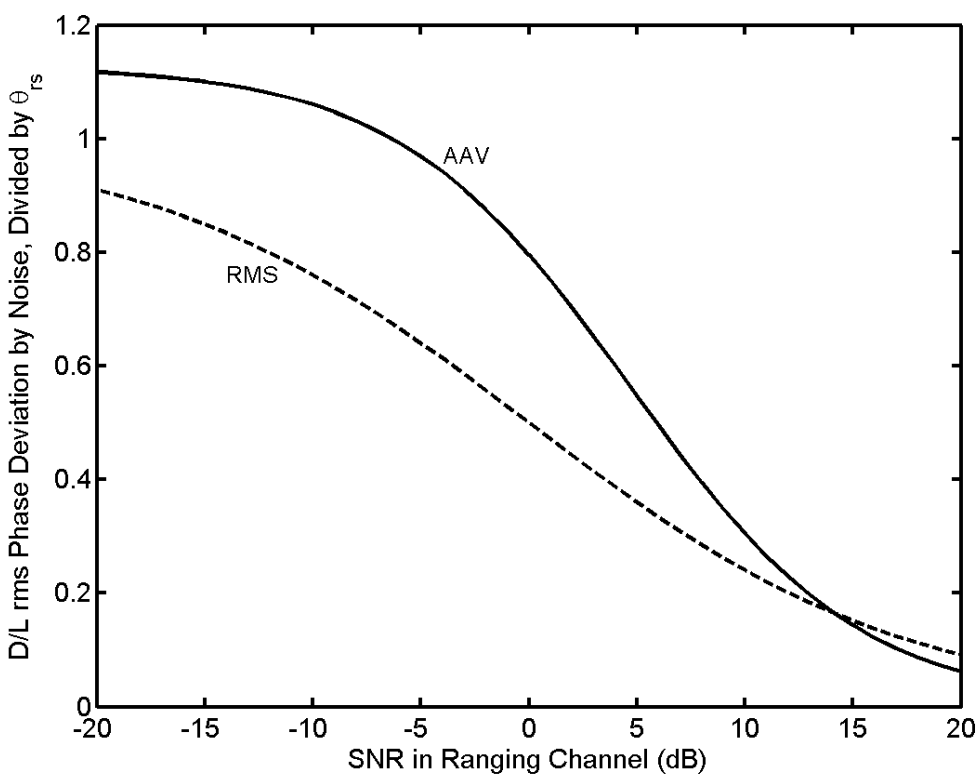

Figure 6. Downlink rms Phase Deviation by Noise (No Command Feedthrough)

The ratio θ_r/θ_{rs} is plotted as a function of ρ_r in Figure 5 for the case of no command feedthrough: $\rho_{cmd} = 0$ and $\theta_{cmd} = 0$. The dashed curve labeled RMS is valid for a turn-around ranging channel whose AGC enforces a constant rms voltage at the AGC output. The RMS curve of Figure 5 comes from Equation (32) with $\rho_{cmd} = 0$.

The ratio θ_n/θ_{rs} is plotted as a function of ρ_r in Figure 6 for the case of no command feedthrough: $\rho_{cmd} = 0$ and $\theta_{cmd} = 0$. The dashed curve labeled RMS is valid for a turn-around ranging channel whose AGC enforces a constant rms voltage at the AGC output. The RMS curve of Figure 6 comes from Equation (34) with $\rho_{cmd} = 0$.

2.4.2.3 Comparison of Two AGC Types

As explained above, there are two types of AGC that have been employed in transponders with turn-around ranging channels. These two AGCs differ in the quantity that is kept constant: either the average of the absolute voltage (AAV) or the root-mean-square (RMS).

Figure 7 plots $P_R/P_T|_{D/L}$ as a function of ρ_r for each of the two AGC types. For all curves in this figure, there is no telemetry and there is no command feedthrough. For each AGC type, there are two curves: one for $\theta_{rs} = 0.2$ rad rms and a second for $\theta_{rs} = 0.4$ rad rms. $P_R/P_T|_{D/L}$ was calculated using Equation (18). The phase deviations θ_r and θ_n needed within Equation (18) were calculated using the equations of Subsection 2.4.2.1 for the AAV curves and Subsection 2.4.2.2 for the RMS curves.

Figure 8 plots the carrier suppression $P_C/P_T|_{D/L}$ as a function of ρ_r for each of the two AGC types. For all curves in this figure, there is no telemetry and there is no command feedthrough. For each AGC type, there are two curves: one for $\theta_{rs} = 0.2$ rad rms and a second for $\theta_{rs} = 0.4$ rad rms. $P_C/P_T|_{D/L}$ was calculated using Equation (17). The phase deviations θ_r and θ_n needed within Equation (17) were calculated using the equations of Subsection 2.4.2.1 for the AAV curves and Subsection 2.4.2.2 for the RMS curves.

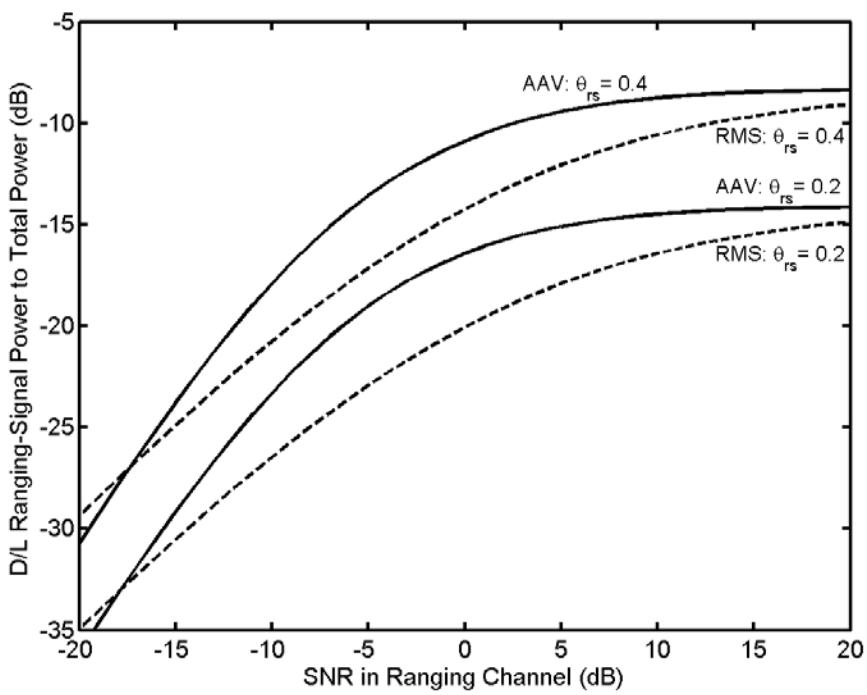

Figure 7. Downlink Ranging-Signal Power to Total Power (No Telemetry, No Command)

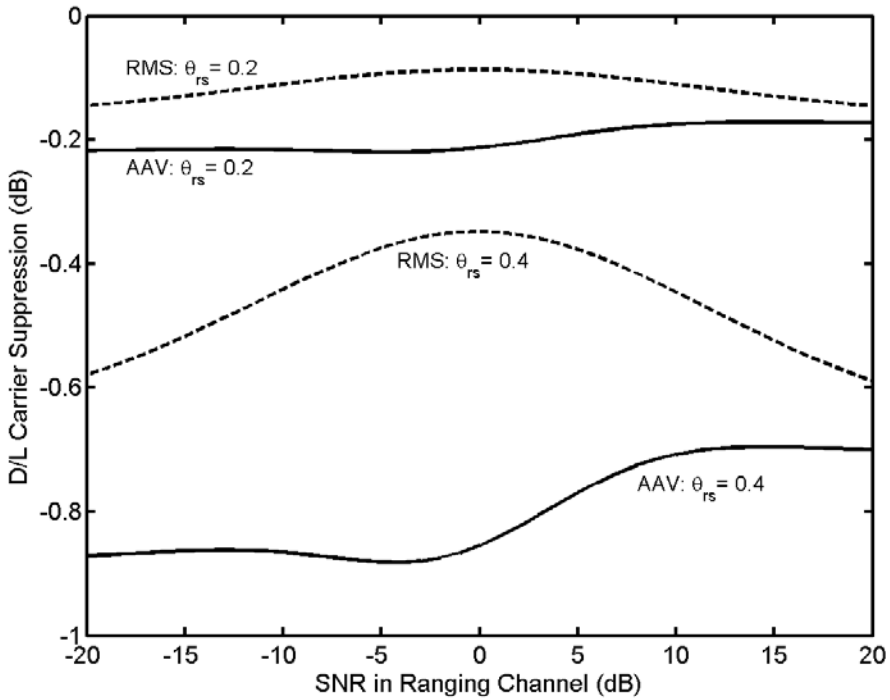

Figure 8. Downlink Carrier Suppression (No Telemetry, No Command)

2.5 Uplink Spectrum

The spectrum of the uplink carrier is of some concern because of the very large transmitter power used on the uplink for deep space missions. In the interest of spectral efficiency, the ranging signal is filtered prior to passing to the phase modulator for the uplink carrier. This is accomplished with the uplink ranging filter, which is digitally implemented within the USG. The uplink ranging filter is a low-pass filter with a configurable bandwidth. The default (and minimum) bandwidth is 1.2 MHz.

Below are some examples of the spectrum of an uplink carrier when ranging is present. It is assumed that ranging is the only signal that modulates the uplink carrier in all examples given here. In the more general case, where command and ranging are both present, the spectrum would be similar to that indicated below except that the ranging sidebands would be reduced by an extra suppression factor due to the presence of command and there would also be command sidebands and intermodulation products. In general, the calculation of the spectrum is quite complicated.

Since the ranging sequence consists of a set of periodic signals, the spectrum for every ranging component consists of a set of discrete spectral lines. The ratio of the power in any one discrete spectral line to the total uplink power is denoted here

$$\frac{P_k}{P_T} = \begin{cases} \text{fraction of uplink total power} \\ \text{in the discrete spectral line} \\ \text{with frequency } f_C + kf_R \end{cases} \tag{35}$$

where f_C is the uplink carrier frequency, k is an integer harmonic number, and f_R is the frequency of the range component that presently modulates the carrier. The spectrum is symmetric about the carrier: for every discrete spectral line at $f_C + kf_R$ there is another of equal power at $f_C - kf_R$. When ranging alone modulates the carrier, the ratios of Equation (35) are subject to the conservation-of-energy law:

$$\frac{P_0}{P_T} + 2\sum_{k=1}^{\infty} \frac{P_k}{P_T} = 1 \tag{36}$$

The first term in Equation (36), P_0/P_T, represents the ratio of the residual-carrier power to the total power P_T.

When the range component is a sinewave (such as the range clock, for example, when the third and higher-order harmonics have been blocked by the uplink ranging filter), the relative powers of the discrete spectral lines are given by

$$\frac{P_k}{P_T} = {J_k}^2\left(\sqrt{2}\,\phi_r\right) \tag{37}$$

ϕ_r is the rms phase deviation of the uplink carrier by the ranging signal. $J_k(\cdot)$ is the Bessel function of the first kind of order k. The spectrum defined by Equation (37) is illustrated in Figure 9 for the case of a range-clock frequency $f_{RC} = 1$ MHz and $\phi_r = 0.80$ rad rms, corresponding to 3 dB of carrier suppression.

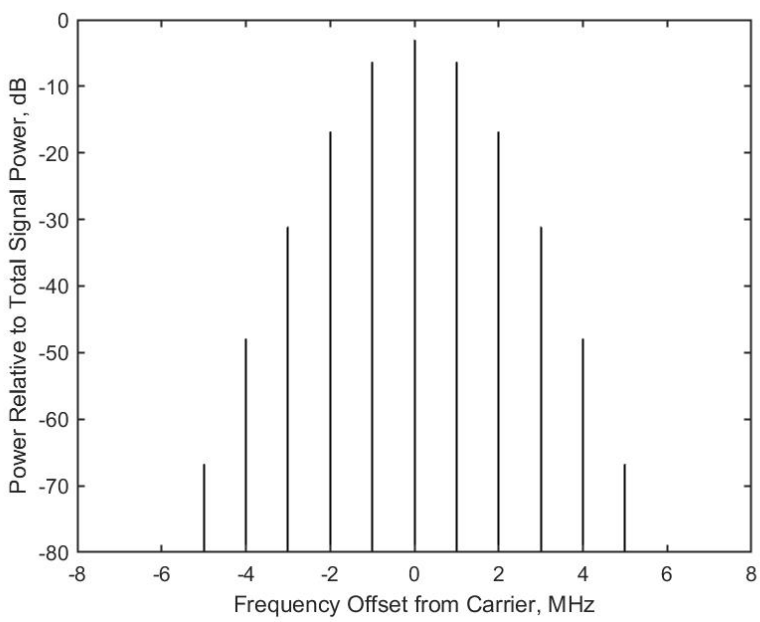

Figure 9. Spectrum: Sinewave Range Clock
$f_{RC} = 1$ MHz, $\phi_r = 0.80$ rad rms

During those periods when an ambiguity-resolving component is multiplied by a chop component, the spectrum of the uplink carrier consists of discrete spectral lines, as indicated in Equation (35). Figure 10 shows the spectrum of a 125-kHz component chopped by the range clock. In this example, $\phi_r = 0.80$ rad rms and the chop component, which is the range clock, is a sinewave and has a frequency $f_{RC} = 1$ MHz. The effect of the uplink ranging filter has been taken into account in Figure 10. The uplink spectrum would be much broader in the absence of the uplink ranging filter; the spectrum without filtering is shown in Figure 11.

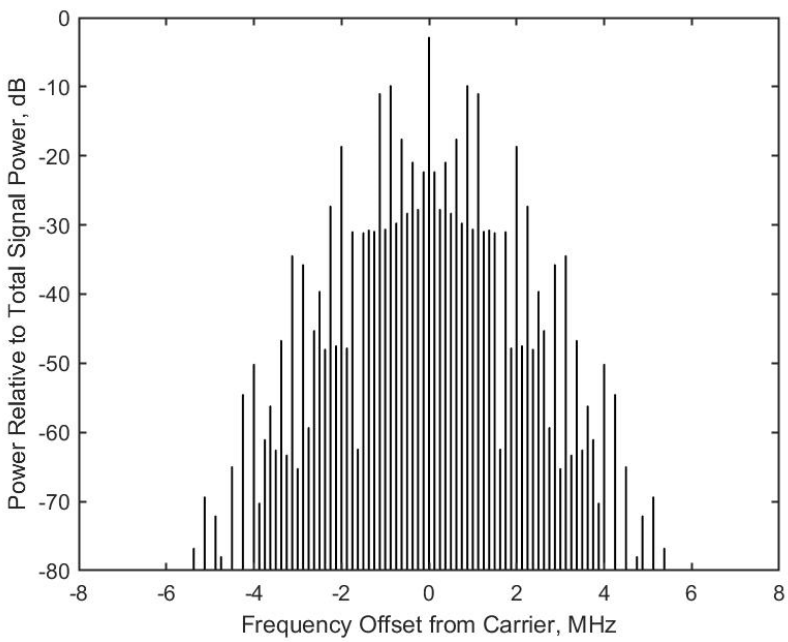

Figure 10. Spectrum: 125-kHz Component Chopped by Range Clock
$f_{RC} = 1$ MHz, $\phi_r = 0.80$ rad rms

2.6 Range Measurement Performance

Thermal noise has two effects on range measurements. First, there is a standard deviation of range measurement error due to thermal noise. Second, there is a probability of acquisition of the range measurement that is less than 100% due to the presence of thermal noise.

2.6.1 Range Measurement Error Due to Thermal Noise

The standard deviation σ_ρ of range measurement error, in meters rms, due to downlink thermal noise is given by

$$\sigma_\rho = \frac{c}{f_{RC} \cdot \sqrt{32\pi^2 \cdot T_1 \cdot (P_R/N_0)}} \tag{38}$$

where

c = speed of electromagnetic waves in vacuum, $299{,}792{,}458\ \mathrm{m/s}$

T_1 = integration time for range clock, s

f_{RC} = frequency of the range clock, Hz

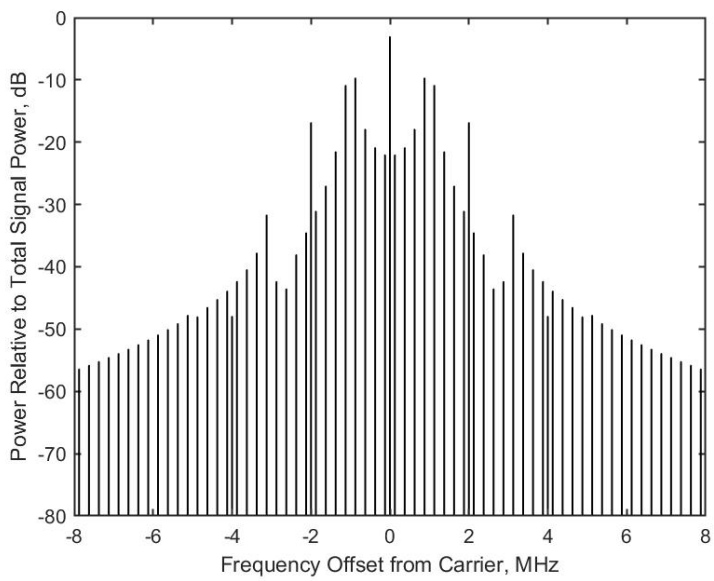

Figure 11. Unfiltered Spectrum: 125-kHz Component Chopped by Range Clock
$f_{RC} = 1$ MHz, $\phi_r = 0.80$ rad rms

Equation (38) is valid for the case of a sinewave range clock and a matching sinewave local model of the range clock at the RRT.

P_R/N_0, the ratio of the downlink ranging signal power to the noise spectral density, is given by

$$\frac{P_R}{N_0} = \frac{P_R}{P_T}\bigg|_{\mathrm{D/L}} \cdot \frac{P_T}{N_0}\bigg|_{\mathrm{D/L}} \tag{39}$$

where $P_T/N_0|_{\mathrm{D/L}}$ is the downlink total signal to noise spectral density ratio and where $P_R/P_T|_{\mathrm{D/L}}$ is the ratio of downlink ranging signal power to total power, which is given in Equation (18).

P_R is reduced by the effect of uplink noise and any command feedthrough. This can be understood by noting that $P_R/P_T|_{\mathrm{D/L}}$, as given in Equation (18), depends on the rms phase deviations θ_r, θ_{cmd}, and θ_n; and these rms phase deviations depend, in turn, on the ranging signal-to-noise ratio ρ_r in the transponder's ranging channel.

The standard deviation of range measurement error (m) due to thermal noise is plotted in Figure 12 against the product $T_1 \cdot (P_R/N_0)$, expressed in decibels: $10\log(T_1 \cdot P_R/N_0)$. These curves were calculated from Equation (38) for three different values of range-clock frequency: 250 kHz, 500 kHz, and 1 MHz.

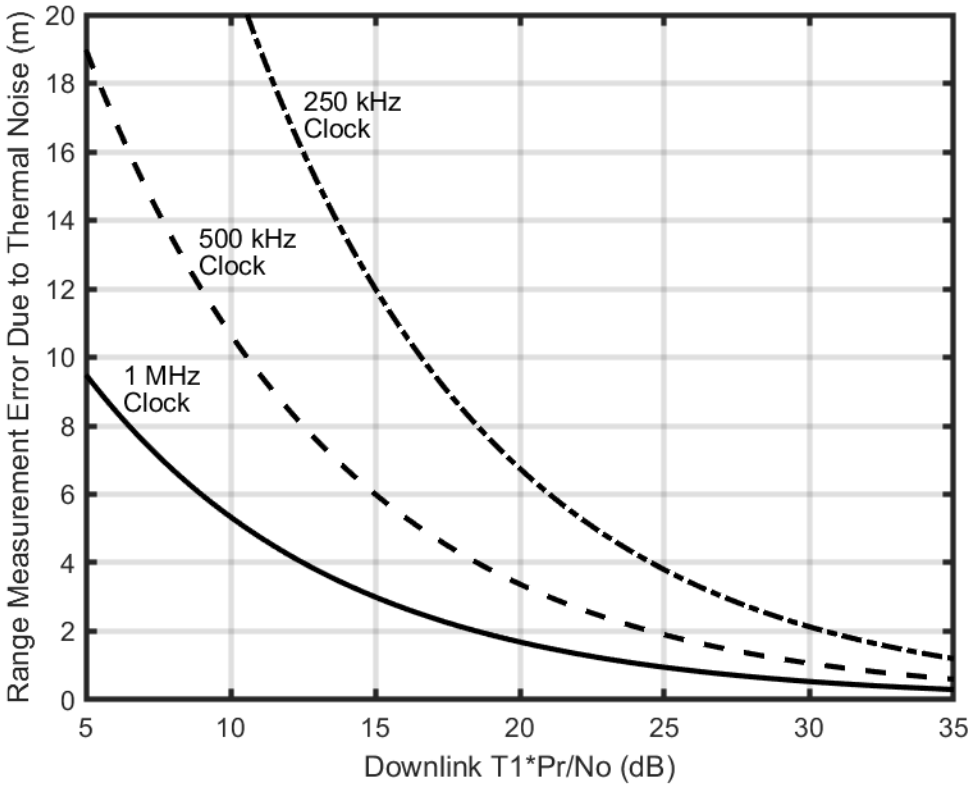

Figure 12. Range Measurement Error for Sinewave Range Clock

When σ_ρ has a specified value and an estimate is available for P_R/N_0, the required integration time T_1 can be found by a rewriting of Equation (38):

$$T_1 = \frac{c^2}{32\pi^2 \cdot {f_{RC}}^2 \cdot (P_R/N_0) \cdot {\sigma_\rho}^2} \tag{40}$$

The standard deviation of the two-way time delay σ_τ, in seconds, is related to σ_ρ, as given in Eq. (38), by

$$\sigma_\tau = \frac{2}{c} \cdot \sigma_\rho \tag{41}$$

The factor of 2 in Eq. (41) accounts for the fact that σ_ρ characterizes the error in the *one*-way range, while σ_τ characterizes the error in a *two*-way time delay. The standard deviation of the two-way phase delay σ_{RU}, as measured in range units, is related to σ_τ by

$$\sigma_{RU} = \begin{cases} \dfrac{f_S}{2} \cdot \sigma_\tau, & \text{S-band uplink} \\ \dfrac{221}{749} \cdot \dfrac{f_X}{2} \cdot \sigma_\tau, & \text{X-band uplink} \\ \dfrac{221}{3599} \cdot \dfrac{f_{Ka}}{2} \cdot \sigma_\tau, & \text{Ka-band uplink} \end{cases} \tag{42}$$

where f_S is the frequency of an S-band uplink carrier, f_X is the frequency of an X-band uplink carrier, and f_{Ka} is the frequency of a Ka-band uplink carrier.

2.6.2 Probability of Acquisition

A correct determination of the range can only happen if the ambiguity is correctly resolved. This is accomplished with a set of correlations within the RRT between the received baseband ranging signal and local models of the ambiguity-resolving components. A range measurement is successfully acquired when every ambiguity-resolving correlation is correctly determined. The probability of acquisition P_{acq} for the range measurement is

$$P_{\text{acq}} = \left[\frac{1}{2} + \frac{1}{2}\operatorname{erf}\left(\sqrt{T_2 \cdot P_R/N_0}\right)\right]^{N_C} \tag{43}$$

where T_2 is the integration time for each ambiguity-resolving component and N_C is the number of ambiguity-resolving components in the ranging sequence,

$$N_C = n_L - n_{RC} \tag{44}$$

This is the difference between the component number n_L of the last (smallest-frequency) component and the component number n_{RC} of the range clock. For example, if the range clock is component 4 (approximately 1 MHz) and the last component is 20, then $N_C = 16$. (In this case, the ranging sequence consists of the range clock followed by 16 ambiguity-resolving components.) The error function erf(·) is defined by

$$\operatorname{erf}(y) = \frac{2}{\sqrt{\pi}} \int_0^y e^{-t^2}\ dt \tag{45}$$

The value that Equation (43) gives for P_{acq} is, in general, greater than 0 and less than 1. P_{acq} is often characterized as a percentage (between 0% and 100%).

P_{acq} is plotted in Figure 13 as a function of the product $T_2 \cdot (P_R/N_0)$, in decibels: $10\log(T_2 \cdot P_R/N_0)$. The functional dependence is shown for three representative values of N_C: 10, 15, and 20. The curves in this figure were calculated from Equation (43).

It will often be necessary to work the problem in the reverse direction. For a specified P_{acq}, what is the required value for $T_2 \cdot P_R/N_0$? Of course, this question can be answered approximately by applying a graphical method to Figure 13. Table 3 provides a more accurate method; this table lists required values for $T_2 \cdot P_R/N_0$ (in decibels) as a function of $\log(P_{\text{acq}})/N_C$. Here log(·) is is the common logarithm (the base-10 logarithm). This table is based on Equation (43).

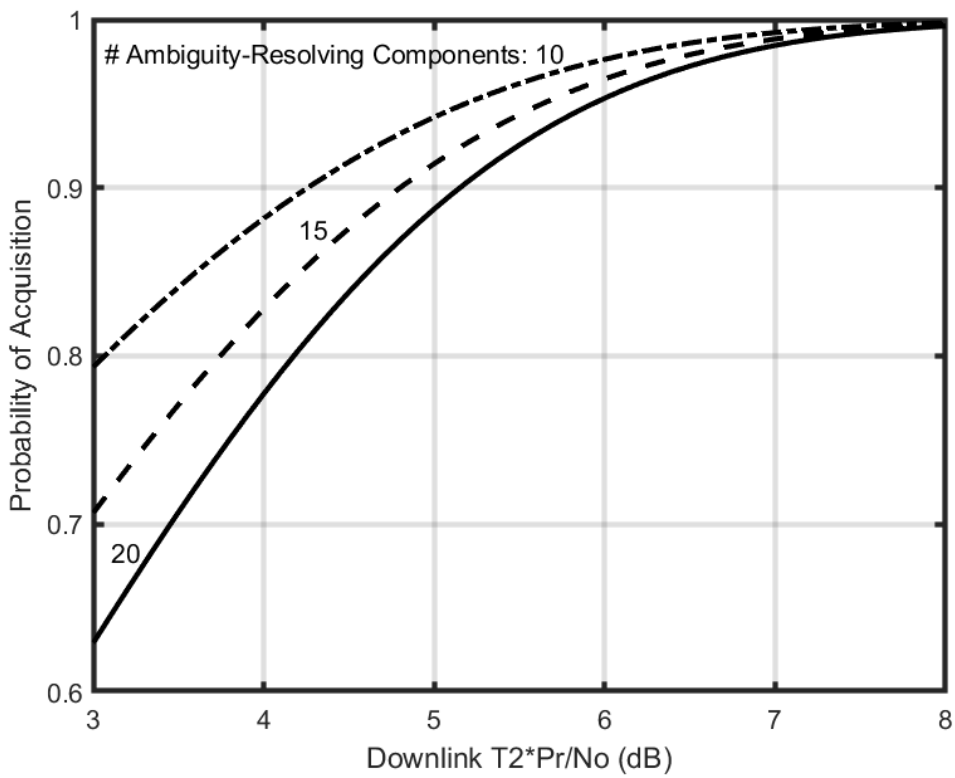

Figure 13. Probability of Acquisition

Here is an example of how Table 3 can be used. If the desired P_{acq} is 0.95 and N_C is 16, then $\log(P_{\text{acq}})/N_C = -0.00139$. From Table 3, the decibel values 5.3 dB and 6.1 dB are found for $\log(P_{\text{acq}})/N_C = -0.0020$ and $\log(P_{\text{acq}})/N_C = -0.0010$, respectively. An interpolation suggests that $T_2 \cdot P_R/N_0$ must be about 5.8 dB in order to acquire correctly with $P_{\text{acq}} = 0.95$ when $N_C = 16$.

In a computational environment where a special function like erf(·) is not available, it is useful to have an algebraic approximation to Equation (43). Here is such an approximation:

$$P_{\text{acq}} = \begin{cases} [c_3 Z^3 + c_2 Z^2 + c_1 Z + c_0]^{N_C}, & 0 \le Z \le 8.0 \\ 1.00, & Z > 8.0 \end{cases} \tag{46}$$

where Z is the product $T_2 \cdot (P_R/N_0)$ in units of decibels,

$$Z = 10 \log[T_2 \cdot (P_R/N_0)] \quad \text{dB} \tag{47}$$

The coefficients for the model of Equation (46) are given in Table 4. The Equation (46) model is not reliable for $Z < 0$ dB. For $Z > 8.0$ dB, it is approximately true that $P_{\text{acq}} = 1$.

Table 3. Interpolation Table
Required $T_2 \cdot P_R/N_0$ (in decibels) for Given $\log(P_{\text{acq}})/N_C$

$\frac{\log(P_{\text{acq}})}{N_C}$	$T_2 \cdot (P_R/N_0)$ dB
-0.0300	0.7
-0.0200	1.6
-0.0100	3.0
-0.0080	3.4
-0.0060	3.9
-0.0040	4.5
-0.0030	4.8
-0.0020	5.3
-0.0010	6.1
-0.0008	6.3
-0.0006	6.6
-0.0004	7.0
-0.0003	7.4
-0.0002	8.0

Table 4. Coefficients for Equation (46)

c_3	0.000158
c_2	-0.003843
c_1	0.031437
c_0	0.9131

The recommended range for P_R/N_0 is -20 dB-Hz to $+50$ dB-Hz. Range measurement performance has been validated down to -20 dB-Hz. At this low end of performance, however, the integration times are quite large. (For a given measurement accuracy,

the smaller P_R/N_0, the larger must be the integration times.) Although there is no upper limit on P_R/N_0, a value in excess of $+50$ dB-Hz is not needed. Moreover, two downlink estimators—that for the symbol signal-to-noise ratio and that for the system noise temperature—become inaccurate when P_R/N_0 is large (see Subsection 2.6.6).

2.6.3 Selection of Integration Times

Thermal noise sets lower limits on the integration times $T_1$and T_2. For a specified σ_ρ, a given f_{RC} and an estimated available P_R/N_0, a minimum required integration time T_1 may be calculated from Equation (40). For a specified P_{acq}, a N_C dictated by considerations of ambiguity resolution, and an estimated available P_R/N_0, a minimum required integration time T_2 may be found with the aid of Table 3.

If the RTLT changes by more than about 1 second during a tracking pass in which ranging is done, then the integration times $T_1$and T_2 should be increased beyond the values calculated from thermal-noise considerations. Subsection 2.6.5.2 offers guidance in this matter.

2.6.4 Three-Way Ranging

Three-way ranging may be done if the RTLT is too large for two-way ranging. One station transmits a ranging sequence to the spacecraft where it is received and re-transmitted. A second station receives the ranging sequence and performs the necessary correlations.

Three-way ranging yields less accurate results than two-way ranging. There are two reasons for this. First, the station delays cannot be accurately calibrated for three-way ranging. Second, the clock offset between the transmitter and receiver is imperfectly known.

Ideally, in order to get the best three-way ranging measurements, the transmitting station's one-way uplink delay and the receiving station's one-way downlink delay should be removed from the measured three-way delay. However, these one-way delays cannot be measured directly. Instead, the two-way station delay of each station is measured with the assumption that half of the delay is in the uplink equipment and the other half is in the downlink equipment. The two round-trip station delays are averaged, and this average is subtracted from the round-trip phase delay to the spacecraft. This average is only as accurate as the approximation that the delay is equally distributed between the uplink and downlink at both stations.

Three-way range measurement error is often dominated by a clock offset between the time reference at the transmitting and receiving stations. This clock offset can be as large as 9 μs (3σ), and there is an additional small uncertainty in the delay between the station clock and the exciter or receiver (see Module 304). The largest part of the clock offset can be determined and removed from the range measurement. However, the remaining (unmodeled) clock offset translates directly into an error in the three-way range measurement.

2.6.5 Ranging Anomalies Related to Sequence Timing

It has been observed that there can be problems with range measurements when the integration time T_2 is very short or when the RTLT changes during a single tracking pass by an amount comparable with T_2. These anomalies, along with suggested remedies, are discussed below.

2.6.5.1 Short Integration Time T_2

If a very short integration time such as 1 or 2 s is used for T_2, the effective integration time of each ambiguity-resolving component may be significantly less that the design value of T_2. This happens if the downlink integration interval for each ambiguity-resolving component does not completely overlap the received component being integrated (as discussed in Section 2.2). The difference between the design T_2 and the effective integration time will typically be a fraction of a second.

The user may suspect this problem when a very small T_2 is being used and the number of range blunder points is more than the Probability of Acquisition Tolerance should permit. The simplest solution is to increase the design T_2. It will often suffice to increase T_2 by just 1 s.

2.6.5.2 Changing RTLT

The effective integration time of each component (the range clock as well as the ambiguity-resolving components) is reduced for some range measurements if the RTLT varies significantly during a tracking pass. The estimated RTLT that is applied to ranging operations for a tracking pass is typically correct at the beginning of the pass. But if the actual RTLT moves away from this estimated value by a few seconds during the pass, a misalignment arises for range measurements occurring later in the pass. This causes the integration of any given component of measurements made later in the pass to slip so that there is not a complete overlap with the received component. The result can be an increase in the range measurement error and a decrease in the probability of range acquisition.

The preferred solution to the problem of a changing RTLT is to use larger values for the integration times, with due consideration for the variability of the RTLT. With this solution, the range measurements will not degrade significantly as the tracking pass proceeds. In the description of this solution, ΔRTLT represents the absolute value of the change in RTLT over the course of a ranging pass.

If ΔRTLT exceeds 1 s, the integration time T_1 should be increased by $\lceil \Delta\mathrm{RTLT} - 1 \rceil$, where $\lceil \cdot \rceil$ is the ceiling function (the smallest integer that is greater than or equal to its argument). Two examples are given here. If $1\ \mathrm{s} < \Delta\mathrm{RTLT} \leq 2\ \mathrm{s}$, T_1 should be increased by 1 s. If $2\ \mathrm{s} < \Delta\mathrm{RTLT} \leq 3\ \mathrm{s}$, T_1 should be increased by 2 s.

If ΔRTLT exceeds 0.5 s, the integration time T_2 should be increased by $\mathrm{round}(\Delta\mathrm{RTLT})$, where $\mathrm{round}(\cdot)$ indicates rounding to the nearest integer. Two examples are given here. If $0.5\ \mathrm{s} < \Delta\mathrm{RTLT} \leq 1.5\ \mathrm{s}$, T_2 should be increased by 1 s. If $1.5\ \mathrm{s} < \Delta\mathrm{RTLT} \leq 2.5\ \mathrm{s}$, T_2 should be increased by 2 s.

An alternative solution is to stop the downlink range measurements whenever the difference between the estimated RTLT and the actual RTLT exceeds some threshold and restart the downlink range measurements with an updated RTLT estimate. In order to maintain the quality of the range measurements while using the smallest possible integration times, it may be necessary to stop and restart the downlink range measurements multiple times during some tracking passes. This will be particularly true for missions having a fast-changing RTLT and small integration times. The first solution, discussed in the previous paragraph, will ordinarily be the preferred solution, due to its simplicity.

P_R/N_0, the ratio of the downlink ranging signal power to the noise spectral density, is estimated by the RRP during range measurements, and the estimate is included in the delivered data. An accurate estimate depends on having a value for RTLT that is correct to within about 1 s. When the RTLT changes, during a tracking pass, by more than about 1 s, P_R/N_0 is underestimated during the later part of the tracking pass. This effect is most noticeable for large values of P_R/N_0.

2.6.6 Interference Caused by Sequential Ranging

Sequential ranging has, on occasion, been a source of interference to conical-scan tracking and to the downlink signal power estimators. This interference is usually only an issue during early mission phase when signal-to-noise ratios are very high.

Perhaps the best-known case of such interference occurred with the Ulysses spacecraft. In that case, sequential ranging caused variations in the uplink carrier suppression, which was a problem for the conical-scan (conscan) pointing of the high-gain antenna on the Ulysses spacecraft. This is not a general problem because conscan is not used for pointing most spacecraft antennas. Furthermore, this problem for Ulysses occurred at a time when a squarewave was being used for the 1-MHz range clock. At present, a 1-MHz range clock is filtered and approximates a sinewave, and with a sinewave range clock the variation in carrier suppression is much reduced.

Sequential ranging has also, on occasion, caused variations in the downlink residual-carrier power, which can interfere with the conscan pointing of the DSS antenna (Reference 2). This only happens when the ranging signal-to-noise ratio is large, as occurs sometimes during the early phase of a mission.

It has been observed in the early phase of some missions, shortly after launch when the signal-to-noise ratios are large, that sequential ranging can cause variations in some of the downlink signal power estimators. In particular, the symbol signal-to-noise ratio estimate may be low when a strong ranging signal is present on the downlink. This is due to the fact that the ranging signal looks like noise to the estimator. The symbol signal-to-noise ratio estimate is used as an input by the algorithm that estimates the system noise temperature. When the symbol signal-to-noise ratio estimate is low, the system noise temperature estimate is high. Both estimates have been observed to be affected by the presence of a strong ranging signal.

2.7 Range Corrections

Range is defined to be the distance from the reference point on the DSS antenna to the reference point on the spacecraft antenna. The reference point of a DSS antenna is the intersection of the azimuth and elevation axes. When the two-way time delay is measured, the result includes more than just the two-way delay between the reference points of the DSS and spacecraft antennas. The measured two-way delay also includes station delay and spacecraft delay. These extra delays must be determined through calibration and then removed from the measured two-way time delay. The spacecraft delay is measured during DSN compatibility testing prior to launch. The station delay is determined in two parts: the DSS delay and the Z-correction.

A range measurement (that has not yet been corrected) provides the two-way delay through the station uplink path, starting from the USG, to and from the spacecraft, and through the station downlink path, ending in the RRT. Figure 14 illustrates the two-way signal path at the station. It is necessary to determine the uplink station delay for the path from the USG to the antenna reference point, to determine the downlink station delay for the path from the antenna reference point to the RRT, and to remove these delays from the measured two-way delay.

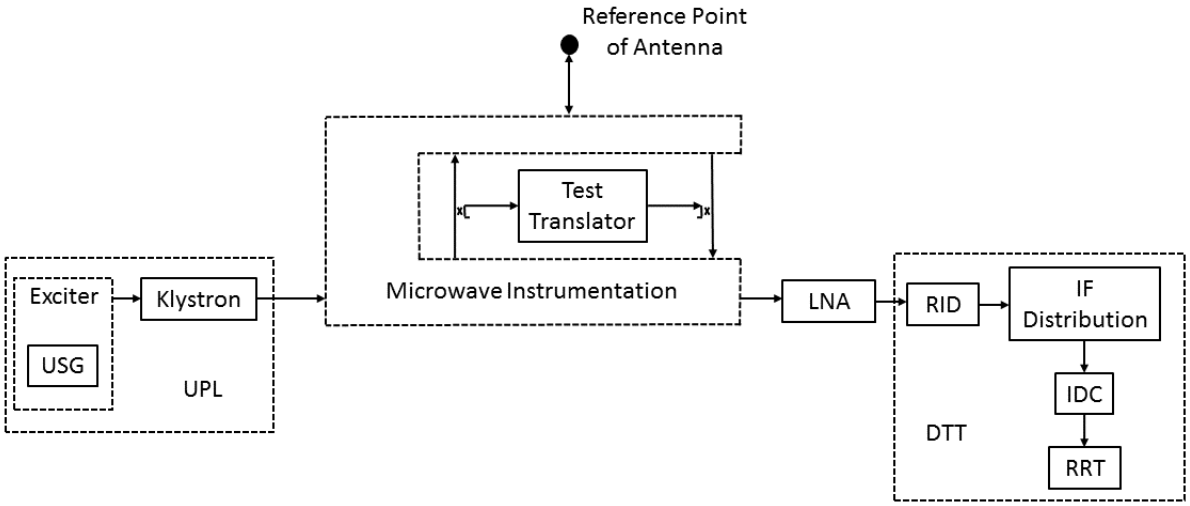

Figure 14. DSS Delay Calibration

2.7.1 DSS Delay

The DSS delay is obtained by a calibration that mimics an actual two-way range measurement, except that the signal path lies entirely within the station. A portion of the uplink carrier is diverted through a coupler to a test translator. The test translator shifts the carrier to the downlink frequency (while not altering the modulation) and feeds this frequency-shifted carrier to a coupler that places it on the downlink path within the station. The DSS delay contains most of the station delay. To be precise, the DSS delay comprises the delay from the USG to the ranging coupler on the uplink, the delay through the test translator (and its cables), and the delay from the ranging coupler on the downlink to the RRT.

Figure 14 is a somewhat abstract representation of the configuration. The microwave instrumentation shown in this figure is not an official subsystem, rather it is a conceptual grouping of microwave signal paths and microwave devices. On the uplink, the uplink carrier that is output from the klystron passes through the microwave instrumentation on its way to the reference point of the antenna. On the downlink, the downlink passes through the microwave instrumentation on its way to the LNA. Along the uplink path, a portion of the uplink carrier is coupled to the test translator. The portion of the carrier that has been frequency shifted to the downlink band inside the test translator is then coupled to the downlink path. The specific details of the microwave instrumentation are generally different at different DSSs and for different bands within a given DSS. Modules 101, 103 and 104 should be consulted for those details.

The DSS delay is station and configuration dependent. It should be measured for every ranging pass. This measurement is called precal for pre-track calibration and postcal for post-track calibration. The former is done at the beginning of a ranging pass; the latter is only needed when there is a change in equipment configuration during the track or precal was not performed due to a lack of time.

The DSS delay varies significantly as a function of carrier frequency. This is illustrated in Figure 15 for an X-band (uplink and downlink) calibration at DSS 63. The vertical axis on this plot is the DSS delay, labeled STDL in this plot. The difference between the largest and smallest delays over the 8400—8450 MHz band is about 18 ns in this case. On both the lower and upper ends of this band, the rise in station delay originates in the klystron on the uplink side of the station. The ripple in the station delay arises from impedance mismatches; every transmission line that has some mismatch at both ends will introduce ripple in the group delay.

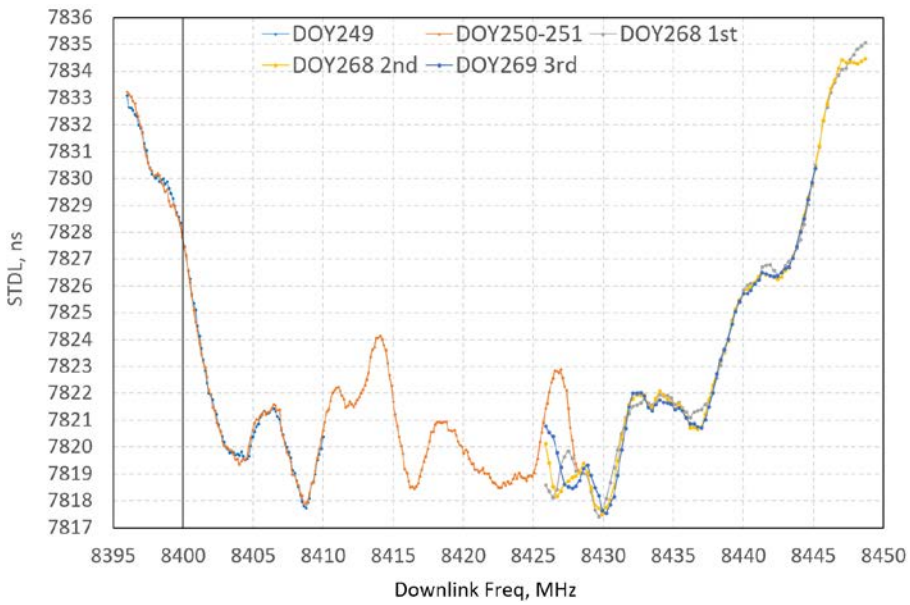

Figure 15. DSS Delay as a Function of Downlink Frequency

2.7.2 Z-Correction

The DSS delay itself must be corrected. This is accomplished with the Z-correction. The DSS delay includes the delay through the test translator (and its cables), but the test translator is not in the signal path of an actual range measurement. Moreover, the DSS delay does not include, but should include, the delays between the ranging couplers and the antenna reference point.

The Z-correction is defined as the delay through the test translator (and its cables) minus the uplink and downlink delays between the ranging couplers and the antenna reference point. The DSS delay minus the Z-correction therefore gives the delay between the USG and the antenna reference point plus the delay between the antenna reference point and the RRT. This is

exactly the quantity that must be subtracted from a range measurement in order to produce a two-way delay relative to the antenna reference point.

The test translator delay is measured by installing a zero delay device (ZDD) in place of the test translator. Since the ZDD delay is measured in the laboratory, the signal delay contributed by the test translator can be calculated to a known precision. This measurement is made approximately once each year or when there are hardware changes in this portion of the signal path. The delays between the ranging couplers and the antenna reference point are stable and need not be updated often; they are determined by a combination of calculation and measurement.

2.8 Total Error for Range Measurement

Several error sources contribute to the total error for a range measurement. For two-way range measurement, the two most important error sources are typically thermal noise and station calibration error. The error due to thermal noise is discussed in Section 2.6. The error in calibrating and removing the station delay is often the dominant error source for two-way ranging. For two-way range measurements in the X band, there is typically about 6 ns of station calibration error in the two-way delay, corresponding to a (one-way) range error of about 1 meter.

The error in calibrating and removing the spacecraft delay is stable for a given spacecraft and a given band pairing (for example, X band on the uplink and X band on the downlink). The orbit determination program can, given enough range measurements for this spacecraft and band pairing, solve for this error.

There are error contributions, usually small compared to the station calibration error, due to the passage of the uplink and downlink through the troposphere, ionosphere and solar corona (Reference 3). When the angle between the sun and the spacecraft, as seen from the station, is small and the spacecraft is beyond the sun, the error contribution from the solar corona can become the dominant contributor to error in the range measurement.

For three-way ranging (in which one station transmits the uplink and a second station receives the downlink), the total delay measurement error is larger than for two-way. There are two reasons for this. First, there is a clock offset between the transmitting and receiving stations. Second, the calibration of the station delays is more difficult to achieve accurately in this case.

Appendix: Glossary of Parameters

$P_T/N_0\|_{\mathrm{U/L}}$	ratio of uplink total power to noise spectral density, Hz
$P_C/P_T\|_{\mathrm{U/L}}$	ratio of uplink residual-carrier to total power
$P_R/P_T\|_{\mathrm{U/L}}$	ratio of uplink ranging-signal to total power
$P_D/P_T\|_{\mathrm{U/L}}$	ratio of uplink command-signal to total power
$P_T/N_0\|_{\mathrm{D/L}}$	ratio of downlink total power to noise spectral density, Hz
$P_C/P_T\|_{\mathrm{D/L}}$	ratio of downlink residual-carrier to total power
$P_R/P_T\|_{\mathrm{D/L}}$	ratio of downlink ranging-signal to total power
$P_D/P_T\|_{\mathrm{D/L}}$	ratio of downlink telemetry to total power
P_R/N_0	ratio of downlink ranging-signal power to noise spectral density, Hz
P_k/P_T	ratio of discrete spectral line power to total power
P_0/P_T	ratio of residual-carrier power to total power
Z	$T_2 \cdot (P_R/N_0)$ in decibels
ρ_ρ	ranging signal-to-noise ratio in transponder's ranging channel
ρ_{cmd}	command-feedthrough signal-to-noise ratio in transponder's ranging channel
B_R	noise-equivalent bandwidth of transponder's ranging channel, Hz
T_1	integration time for range clock, s
T_2	integration time for ambiguity-resolving component, s
f_n	frequency of range component n, Hz
f_{RC}	range-clock frequency, Hz
f_S	S-band carrier frequency, Hz
f_X	X-band carrier frequency, Hz
f_{Ka}	Ka-band carrier frequency, Hz
c	speed of electromagnetic waves in vacuum, m/s
n_{RC}	component number of range clock
n_L	component number of last ambiguity-resolving component
N_C	number of ambiguity-resolving components

ϕ_r	phase deviation of uplink carrier by ranging signal, rad rms
ϕ_{cmd}	phase deviation of uplink carrier by command signal, rad rms
θ_{rs}	phase deviation of downlink carrier by ranging signal (strong signal), rad rms
θ_r	phase deviation of downlink carrier by ranging signal, rad rms
θ_{cmd}	phase deviation of downlink carrier by command feedthrough, rad rms
θ_n	phase deviation of downlink carrier by noise, rad rms
θ_{tlm}	telemetry modulation index, rad
$S_{cmd}(\phi_{cmd})$	suppression factor on uplink due to command
$M_{cmd}(\phi_{cmd})$	modulation factor on uplink for command
$S_{fth}(\theta_{cmd})$	suppression factor on downlink due to command feedthrough
$S_{tlm}(\theta_{tlm})$	suppression factor on downlink due to telemetry
$M_{tlm}(\theta_{tlm})$	modulation factor on downlink for telemetry
P_{acq}	probability of acquisition
σ_ρ	standard deviation of range measurement error, m
σ_τ	standard deviation of two-way delay, s
σ_{RU}	standard deviation of the two-way phase delay, RU
$\Delta\mathrm{RTLT}$	change in RTLT over the course of a ranging pass, s

References

1. J. B. Berner, S. H. Bryant, and P. W. Kinman, “Range Measurement as Practiced in the Deep Space Network,” *Proceedings of the IEEE*, Vol. 95, No. 11, November 2007.
2. P. W. Kinman and J. B. Berner, “Two-Way Ranging During Early Mission Phase,” *2003 IEEE Aerospace Conference*, March 8-15, 2003, Big Sky, MT.
3. C. L. Thornton and J. S. Border, *Radiometric Tracking Techniques for Deep-Space Navigation*, Monograph 1 of the *Deep-Space Communications and Navigation Series*, Jet Propulsion Laboratory, Pasadena, CA, 2000.

Deep Space Network

205
Command Service

Document Owner:

Signature provided 12/13/2022

Michael Settember Date
Command Service System Engineer

Approved by:

Signature provided 11/01/2022

Timothy T. Pham Date
DSN Communications Systems
Chief Engineer

Released by:

Signature provided 03/23/2023

Christine Chang Date
DSN Document Release Authority

DSN No. **810-005, 205, Rev. G**
Issue Date: March 23, 2023
JPL D-19379; URS CL#23-1592

Jet Propulsion Laboratory
California Institute of Technology

Users must ensure that they are using the current version in DSN Telecommunications Link Design Handbook website::
https://deepspace.jpl.nasa.gov/dsndocs/810-005/

Review Acknowledgment

By signing below, the signatories acknowledge that they have reviewed this document and provided comments, if any, to the signatories on the Cover Page.

Signature provided	10/31/2022	Signature not provided	
Jeff Berner DSN Project Chief Engineer	Date	J. Andrew O'Dea Tracking, Telemetry, and Command System Engineer	Date

Document Change Log

Rev	Issue Date	Prepared By	Affected Sections or pages	Change Summary
Initial	1/15/2001	Robert Sniffin	All	Initial Release
A	12/15/2002	Robert Sniffin	All	Provides description and capabilities of new DSN command equipment.
B	12/15/2009	A. Kwok	All	Replaced DSMS with DSN. Removed references to the decommissioned 26-m subnet. Updated Table 1 and replaced previous Figure 3 with the current Figure 3, Figure 4, and Figure 5.
C	6/1/2010	A. Kwok	Page 18	Corrected an error in Equation (1). Eliminated the Rev. E designation for the document series.
D	12/15/2014	T. Cornish	Table 1	Updated to current data. Added restrictions on S-band uplink from MDSCC. Deleted Ka-band uplink from DSS-25. Deleted DSS-27. Added DSS-35, -36 20 kW and DSS-26 80 kW.
			3.12	Changed “output of the exciter” to “output of command modulator”.
			Was 4.1 is now 3.4	Added 128k and 256k data rates and removed statement about rates above 64k being unavailable due to exciter bandwidth restrictions (future Block 6 Exciter capabilities). Moved entire paragraph to 3.8, thus eliminating section 4 on “Proposed Capabilities”. Changed “will be implemented” to “is available, with some restrictions”. Added statement about CLTU size versus bit rate.
E	11/17/2016	T. Cornish	Table 1	Added DSS-36 S- and X-band. Deleted DSS-45.
			Section 2	Added 0239-Telecomm and CLTUF. Updated Figs. 3, 4, and 5.
			Appendix A	Updated references.
F	04/02/2021	M. Settember	Table 1	Added DSS-56 S/X-band and DSS-26 S-band Deleted DSS-15. Updated DSS-43 power level/EIRP per upgrades Removed Gain/ G/T column, not relevant to cmd. Updated EIRP column per subnet interface docs.
			Section 2 & 3 Figure 3	Removed FCLTU “Red book”, 0163 support
			Section 2 & 3.1	Removed emergency recording capability.

Rev	Issue Date	Prepared By	Affected Sections or pages	Change Summary
			Section 3.2 & 3.6	Clarified step tuning limitations applicable to 20kW S-band only.
			Appendix A	Added “2010 blue book” reference. Added missing referenced 820-013 modules.
G	03/23/2023	M. Settember	Table 1 & 3, Figures 1, 2, 4, 5 & 6, Section 3.2, 3.4, 3.9, 3.10 & 3.13	Added K-band and current Ka-band capability. Updated reference figures to reflect current RF power capabilities. Added new command modulation, data rate and encoding capabilities. Removed Mean-time between Command Aborts numbers.

Contents

Figures

Figure **Page**

Tables

Table **Page**

1 Introduction

1.1 Purpose

This module provides performance parameters for the elements of the Deep Space Network (DSN) that are exclusively used for sending commands to spacecraft. It is intended to assist the telecommunications engineer in designing an uplink (or forward space link) that is compatible with currently installed DSN equipment. It also contains brief descriptions of future enhancements that have been proposed for this equipment and capabilities that are being maintained for legacy customers using the previous generation of command equipment.

1.2 Scope

The discussion in this module is limited to command equipment used with the Deep Space Network (DSN) antennas. Detailed performance of equipment used for purposes in addition to command is covered elsewhere in 810-005. Information on antennas, exciters, and transmitters have been included as a convenience and should be verified against their primary source. In particular, the following modules should be considered:

101 70-m Subnet Telecommunications Interfaces,

103 34-m HEF Subnet Telecommunications Interfaces,

104 34-m BWG Stations Telecommunications Interfaces, and

301 Coverage and Geometry.

2 General Information

Each antenna in the DSN is capable of sending commands to one spacecraft at a time. Each Deep Space Communications Complex (DSCC) contains one 70-m and multiple 34-m antennas. There are two types of 34-m antennas. The first is the so-called high-efficiency (HEF) antennas that have their feed, low-noise amplifiers, and transmitter located on the tilting structure of the antenna. These antennas were named when a less-efficient 34-m antenna was in use by the DSN and the name has survived. The efficiency of all DSN 34-m antennas is now approximately the same. Note that only one HEF antenna remains in operation, located at Madrid DSCC. The HEF at Goldstone and Canberra DSCC have been decommissioned. The second type of 34-m antenna is the beam waveguide (BWG) antenna where the feeds, low noise amplifiers and transmitters are located in a room below the antenna structure and the radio frequency energy is transferred to and from the antenna surface by a series of mirrors and dichroics encased in a protective tube.

The capabilities of each antenna type and, in some cases, of the individual antennas are different and must be considered in designing a command link. Often, the selection of antenna for uplink will depend on the downlink frequencies it supports.

Table 1 lists the uplink and downlink frequency ranges for each antenna type and provides approximate ranges for uplink Effective Isotropic Radiated Power (EIRP). The modules referred to above should be consulted for exact values and other parameters. The telecommunications link designer is cautioned against making designs dependent on the 70-m antenna, as there is only one per complex and it subject to severe scheduling constraints.

Table 1. Capabilities of DSN 70-m and 34-m Antennas

Antenna Type	Complex/Site	DSS ID	Uplink Freq (MHz)	TXR Power (W)	EIRP (dBW)	Downlink Freq (MHz)
34M BWG	Goldstone, CA USA	DSS 24	S: 2025 - 2120	20,000	78.6 - 98.6	S: 2200 - 2300
		DSS 26	S: 2025 - 2110	250	71.9 - 78.9	S: 2200 - 2300
	Canberra, Australia	DSS 34	S: 2025 - 2120	20,000	78.6 - 98.6	S: 2200 - 2300
		DSS 36	S: 2025 - 2110	250	71.9 - 78.9	S: 2200 - 2300
	Madrid, Spain	DSS 54 [1]	S: 2025 - 2120	20,000	78.6 - 98.6	S: 2200 - 2300
		DSS 56	S: 2025 - 2110	250	71.9 - 78.9	S: 2200 - 2300
	Goldstone, CA USA	DSS 24, 25, 26	X: 7145 - 7235	20,000	89.4 - 109.4	X: 8400 - 8500
		DSS 26	X: 7145 - 7235	80,000	89.3 - 115.3	X: 8400 - 8500
	Canberra, Australia	DSS 34, 35, 36	X: 7145 - 7235	20,000	89.4 - 109.4	X: 8400 - 8500
	Madrid, Spain	DSS 54, 55, 56	X: 7145 - 7235	20,000	89.4 - 109.4	X: 8400 - 8500
	Goldstone, CA USA	DSS 26, 24[2]	K: 22550 - 23150	250	113.7 - 127.7	K: 25500 - 27000
	Canberra, Australia	DSS 36, 34[2]	K: 22550 - 23150	250	113.7 - 127.7	K: 25500 - 27000
	Madrid, Spain	DSS 56[2], 54[2]	K: 22550 - 23150	250	113.7 - 127.7	K: 25500 - 27000
	Goldstone, CA USA	DSS 25[3]	Ka: 34315 - 34415	300	125.8 - 133.6	Ka: 31800 - 32300
34M HEF	Madrid, Spain	DSS 65	S: 2025 - 2110	250	71.8 - 78.8	S: 2200 - 2300
	Madrid, Spain	DSS 65	X: 7145 - 7190	20,000	89.8 - 109.8	X: 8400 - 8500
70M	Goldstone, CA USA	DSS 14	S: 2110 - 2120	20,000	85.6 - 105.6	S: 2200 - 2300
	Canberra, Australia	DSS 43	S: 2110 - 2120	100,000	85.6 - 111.6	S: 2200 - 2300
	Madrid, Spain	DSS 63 [1]	S: 2110 - 2120	20,000	85.6 - 105.6	S: 2200 - 2300
	Goldstone, CA USA	DSS 14	X: 7145 - 7190	20,000	95.8 - 115.8	X: 8400 - 8500
	Canberra, Australia	DSS 43	X: 7145 - 7235	80,000	95.8 - 121.8	X: 8400 - 8500
	Madrid, Spain	DSS 63	X: 7145 - 7190	20,000	95.8 - 115.8	X: 8400 - 8500

Notes:
1) S-band uplink in the Deep Space frequency range of 2110-2120 MHz is not available from MDSCC except for Voyager support by special agreement with the Spanish Frequency Spectrum Regulator.
2) Near-earth K-band uplink capability planned to be deployed at 24 (2023), 56 (2024), 34 (2024), 54 (2026), dates subject to change.
3) Deep Space Ka-band uplink capability planned to be deployed at DSS 55 (2028}, 35 (2030), dates subject to change.

Figure 1 and Figure 2 illustrate the DSN command capabilities assuming a reference spacecraft employing a residual carrier uplink and having the characteristics specified in Table 2. These figures show that command range at low bit rates is limited by the spacecraft carrier tracking performance. At higher bit rates, the range is limited by available E_b/N_o.

Figure 1 is intended to show performance during a spacecraft emergency that forces the use of an omnidirectional antenna. The uplink modulation index has been intentionally lowered to 0.5 radians to direct more power to the carrier. Figure 2 assumes a more typical spacecraft configuration using a high-gain antenna and an uplink modulation index of 1.2 radians.

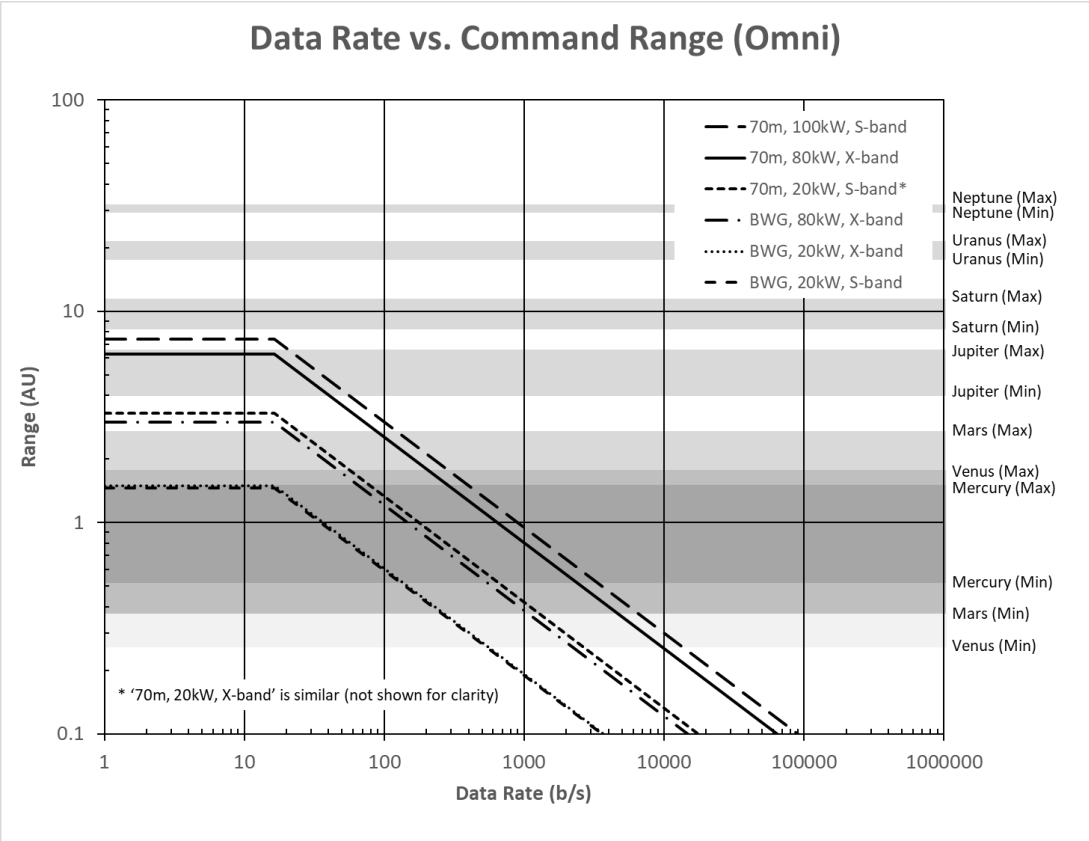

Figure 1. Maximum Command Range for a Reference Spacecraft with an Omni-directional Antenna and a 0.5 Radian Command Modulation Index.

Table 2. Reference Spacecraft Characteristics for Figure 1 and Figure 2

Parameter	Value
Antenna Gain including pointing loss Omnidirectional S-band Hi-gain X-band Hi-gain	 0 dB 30 dB 39.7 dB
Other RF losses	–1.8 dB
System Temperature	500 K
Carrier Loop Bandwidth	100 Hz
Required Carrier Margin	12 dB
Command Detection Losses	–1.5 dB
Required E_b/N_o	9.6 dB

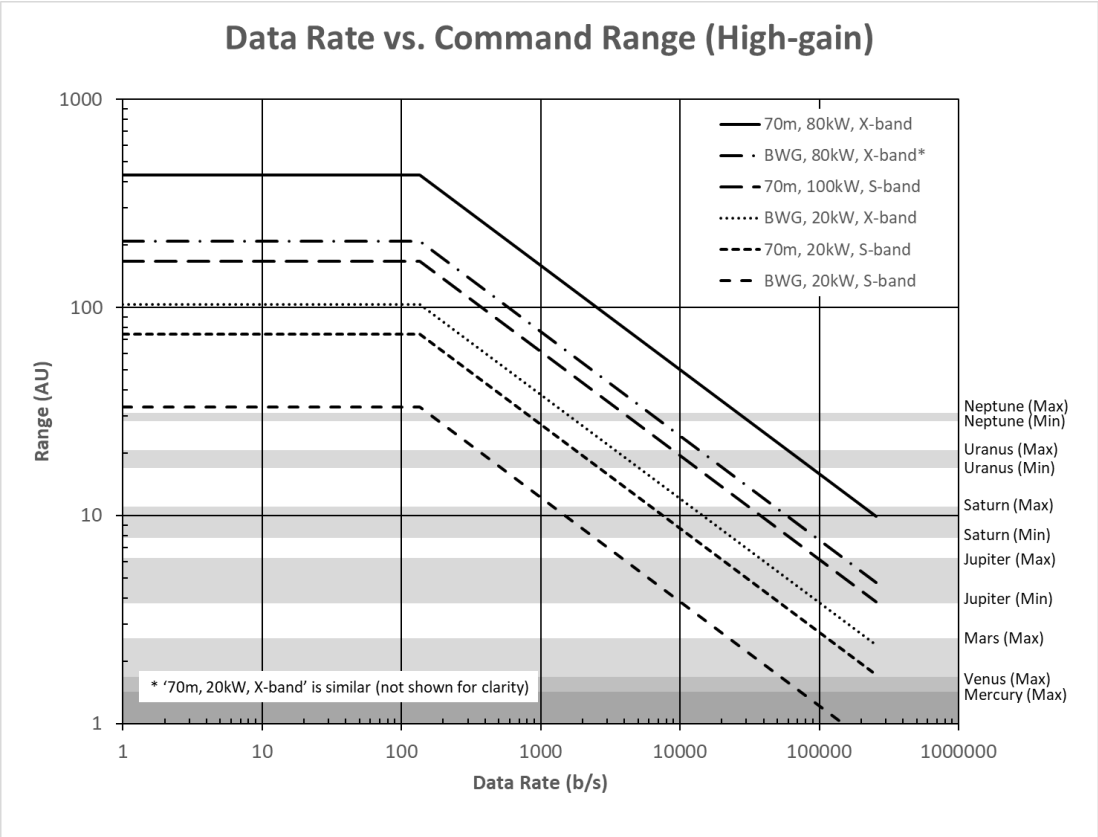

Figure 2. Maximum Command Range for a Reference Spacecraft with a High-gain Antenna and a 1.2 Radian Command Modulation Index.

Uplink data are delivered to the DSN using one of three services. The first is referred to as Stream Mode Command Radiation Service using the *Space Link Extension* (SLE) forward service, an implementation of the Consultative Committed for Space Data Systems (CCSDS) recommendation 912.1, Space Link Extension Forward Command Link Transmission Unit (CLTU) Service, and is described in DSN Document 820-013, module 0239-Telecomm, which describes the DSN implementation of Forward CLTU Service Specifications "2004 Blue Book", CCSDS 912.1-B-2-S, and "2010 Blue Book", CCSDS 912.1-B-3-S, and Enhanced Forward CLTU Service Specification "Orange Book", CCSDS 912.11-O-1. See the data flow diagram in Figure 3.

The SLE forward service is an online only service including service users providing command bits to be transferred to the spacecraft and ancillary information such as routing (e.g., antenna to be used for command service), ensuring the integrity of the Earth segment of the communications link, and providing the customer limited control of the command process as described in the aforementioned documents.

The second, File Mode Command Radiation Service, is provided by accessing a file of CLTUs from the Mission Operations Center (MOC) via DSN File Store where the individual CLTUs are extracted and passed on to the Ground Station for modulation onto the uplink carrier and radiation to the spacecraft. The file of CLTUs is referred to as a Spacecraft Command Message File (SCMF per DSN Document 820-013, module 0198-Telecomm-SCMF), or CLTU File (CLTUF per DSN Document 820-013, module 0241-Telecomm-CLTUF). See the data flow diagram in Figure 4. This service is an online or offline store and forward service that allows management of multiple stored command files.

The SCMF contains a layer of service provision parameters (window open/close times, allowable bit rates, modulation index, etc.) in addition to the CLTUs to be radiated. The CLTUF contains just a simple header and the CLTUs to be radiated.

In addition to the files containing the actual CLTUs, there are a number of other products that may optionally be exchanged between the service user and the DSN for scheduling and reporting:

1) Radiation List (Rad_List per DSN Document 820-013, module 0197-Telecomm-CMDRAD), which contains a list of SCMFs or CLTUFs to be radiated as a batch.

2) SCMF Radiation Report (Rad_SCMF per DSN Document 820-013, module 0191-Telecomm), which is a report of SCMFs and CLTUs radiated, including information such as bit-1 times, number of bits, etc.

3) CLTUF Radiation Report (Rad_CLTUF per DSN Document 820-013, module 0242-Telecomm), which is a report of CLTUFs and CLTUs radiated, including information such as bit-1 times, number of bits, etc.

The third, Command Delivery Service, uses the CCSDS File Delivery Protocol (CFDP) and is available for spacecraft that employ this protocol. It is described in DSN Document 820-013, module 0213-Telecomm-CFDP. The service is provided by accessing files from the MOC via DSN File Store where the files are converted CLTUs which are then passed to the Ground Station for modulation onto the uplink carrier and radiation to the spacecraft. See the data flow diagram in Figure 5. This is also an online or offline service that allows generalized uplink file transfer.

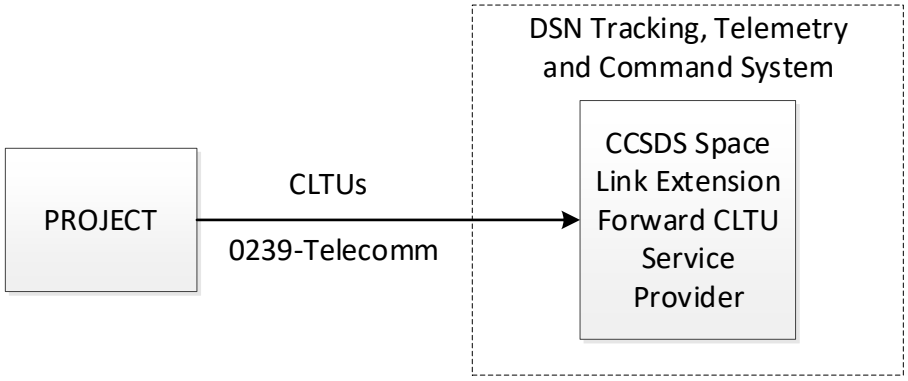

Figure 3. Space Link Extension (SLE) Forward Service Data Flow

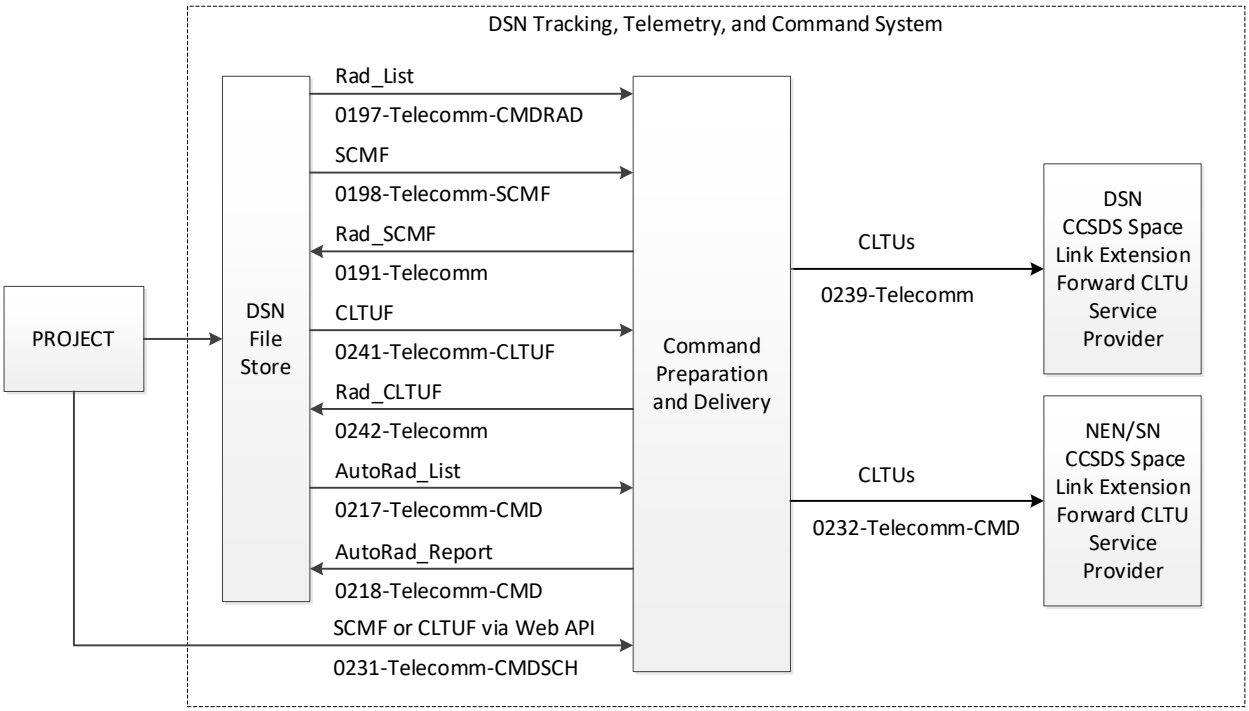

Figure 4. Command Radiation Service Data Flow – File Mode (SCMF or CLTUF)

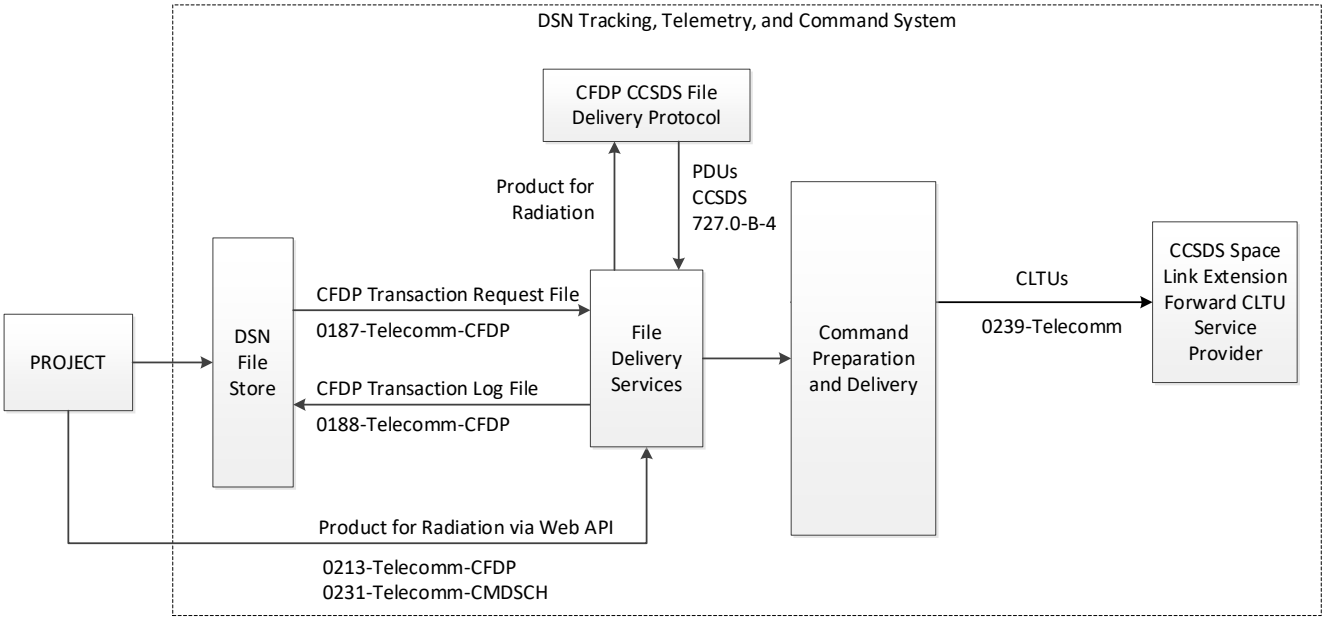

Figure 5. Command Delivery Service Data Flow – (CFDP)

When configured for Forward CLTU Service (CCSDS 912.1-B-2-S and CCSDS 912.1-B-3-S) the only function performed at the stations is the mechanism whereby command data are extracted from the delivery format and converted to an RF signal suitable for reception by a spacecraft. This means that all commands including prefix symbols and command data symbols must be generated at the appropriate MOC. If coding such as Bose-Chaudhuri-Hocquenghem (BCH) is required, it must be accomplished before the commands are delivered to the DSN. The DSN may perform checks for format compliance, but it will not interpret nor modify the contents of any command. Neither does it guarantees error free command delivery to the spacecraft. It is up to the project to provide its own error detection and correction schemes.

When configured for Enhanced Forward CLTU Service (Orange Book), the input stream to the DSN is in the form of Telecommand (TC) or Advanced Orbiter System (AOS) transfer frames. The DSN can optionally apply forward error correction block encoding, optionally randomize the frames, and optionally can attach sync markers to the frames. It will also insert user defined idle frames when no command data is present, and then radiate the frames in the form of CLTUs.

In addition to the interfaces by which command data are delivered to the DSN, a management interface is required for selecting the particular set of parameters appropriate for the spacecraft being supported. Details of this interface can be found in DSN Document 820-013 module 0211-Service_Mgmt-SEQ. A discussion of this interface is contained in DSN Document 810-007 Module 109, DSN Mission Interface Design Handbook, Service Management. (This document is still in development and not available at the time of this writing.)

3 Command Parameters

The following paragraphs provide a discussion of the principal command parameters. Parameters that are a function of antenna type performance capabilities are summarized in Table 1.

Parameters that are independent of antenna type are summarized in Table 3.

Table 3. Command Parameters

Parameter	Value	Remarks
RF Power Output	See Table 1	Also see modules 101, 103, and 104
Effective Isotropic Radiated Power (EIRP)	See Table 1	Also see modules 101, 103, and 104
Carrier Frequency	See Table 1	Also see modules 101, 103, and 104
Subcarrier Frequencies Sine wave Square wave	 999 Hz – 250075 Hz 100 Hz – 1000 Hz	The CCSDS recommends a 16 kHz sine wave subcarrier for all data rates up to and including 8 kbps. Direct carrier modulation is recommended above 8 kbps. Subcarrier Frequency Resolution is 0.1 Hz for Sine wave and Square wave Harmonic and Spurious Signals (Sine wave Subcarrier) are >45 dB below subcarrier amplitude (dB-V) Harmonic Response (Square wave Subcarrier) are < 6 dB attenuation of 7th harmonic (dB-V) Subcarrier Stability is $<1 \times 10^{-9}$ for all measurement times from 100 s through 12 h (derived from station frequency standard)
PCM Data Formats	NRZ-L, M, S Bi-ϕ-L, M, S QPSK, OQPSK	NRZ-L, M, S and Bi-ϕ-L, M, S are BPSK See Figure 4
Modulation Types	Residual carrier BPSK with or without subcarrier, Suppressed Carrier QPSK, OQPSK	Optional Square Root Raised Cosine (SRRC) Filter (α = 0.5) available for suppressed carrier modulations

Parameter	Value	Remarks
Modulation Index Range Sine wave Subcarrier Square wave Subcarrier No Subcarrier	 0.1 – 1.52 radians 0.1 – 1.40 radians 0.1 – 1.57 radians	 6 – 87 degrees 6 – 80 degrees 6 – 90 degrees Modulation Index Accuracy is ±10% of carrier suppression in dB Modulation Index Stability is ±3% of carrier suppression in dB over a 12-h period
Data Rates Sine wave Subcarrier Square wave Subcarrier No Subcarrier	 7.8 bps – 125037.5 bps 7.8 bps – 500 bps 8 kbps – 20 Mbps	Set by subcarrier frequency: Subcarrier Frequency/2^n, $1 \leq n \leq 11$ Max. encoded symbol rate is 40 Msps (assuming QPSK, OQPSK) Coherency to Subcarrier is ±6° offset between bit/symbol transitions and subcarrier zero crossings. Data Rate Stability is $<1 \times 10^{-9}$ for all measurement times from 100 s through 12 h (derived from subcarrier stability)
Inter-command modulation	None (Carrier only), carrier and command subcarrier, carrier, command subcarrier and idle pattern	
Available Encoding	RS and LDPC	
Reed Solomon (RS) Encoding Parameters	Redundancy (E) = 16 Bits / Symbol (J) = 8 Symbol /RS Codeword (n) = 255 Interleave Depth (I) = 1, 2, 3, 4, 5, or 8	CCSDS 131.0-B-3

Parameter	Value	Remarks
Low Density Parity Check (LDPC) Encoding Parameters	(r) = 1/2, (k) = 64 or 256 (r) = 1/2, (k) = 1024, 4096 or 16384 (r) = 2/3, (k) = 1024, 4096 or 16384 (r) = 4/5, (k) = 1024, 4096 or 16384 (r) = 7/8, (k) = 7136	CCSDS 231.0-B-3 CCSDS 131.0-B-3 (r)=Code Rate (k)= Block Length
Idle Pattern	8-bit repetitive or idle PDU	
Command Timing	0.1 s	0.1 s plus 1 – 8 bit times if idle pattern is present
Pre-track Calibration	20 minute 5 minute	With Transmitter warm-up or band change Transmitter already warmed-up
Availability	95% 98%	Nominal Mission critical events (with backup station allocation)

3.1 RF Power

RF power is produced by solid state or variable beam klystron amplifiers that permit saturated operation over a relatively wide power range. Refer to Table 1 for the power levels available at each antenna. Since DSN can support simultaneous command and ranging, carrier power is a function of both the data modulation index and ranging modulation index.

3.2 Carrier Frequency

The DSN considers establishment of carrier frequency to be a tracking function as opposed to a command function. Small frequency changes such as might be required for Doppler compensation will have little effect on the transmitter output. Larger frequency changes such as might be required to command two spacecraft within the same beamwidth may cause the transmitter output to vary by as much as 1-dB due to ripple across the klystron passband. Should this happen, the operator at the station will be warned that the transmitter should be re-calibrated. This warning may be ignored to no detriment other than the power output being as much as 1 dB from the requested value.

The S/X 20kW capable BWG's have two klystron amplifiers that share a common power supply and cooling system. Therefore, a change of band will require a minimum of 20-minutes to cool-down the klystron that is no longer needed and warm-up and calibrate the other klystron. Additionally, the S-band 20kW klystron at these stations is step-tunable to provide coverage over the entire uplink band. Changing from one band segment to another requires turning off the transmitter, changing the band segment, and re-calibrating at the new frequency.

K-band (Near-Earth) or Ka-band (Deep-Space) command link capability, where equipped, can be supported independent and simultaneous with an S-band or X-band command link on a common aperture (Deep Space Station).

3.3 Subcarriers

Both sine wave and square wave subcarriers are available. Subcarrier frequencies are initialized from an entry in the Forward Spacelink Carrier Profile (see interface 820-013 module 0211-Service_Mgmt-SEQ) but may be changed during a support activity providing no command waveform is being radiated. This technique can be used to provide a limited amount of subcarrier Doppler compensation recognizing that command modulation (including the subcarrier) must be removed when the subcarrier frequency is changed. Changing the subcarrier frequency will cause a corresponding change in data rate because these two items are coherent. See the discussion on data rate for details.

3.4 Direct Carrier Modulation

CCSDS Medium Rate Command Recommendation (CCSDS Recommendation 401.0-B, paragraph 2.2.7) is available, with some restrictions. NRZ bit rates and bi-phase symbol rates of 8000, 16000, 32000, 64000, 128000, and 256000 are supported. Carrier and data suppression for direct carrier modulation are calculated using the equations for square wave modulation (3) and (4).

Suppressed carrier modulation formats, similar to those used in telemetry (space to earth) links are available with some restrictions. DSN Command Service supports Binary Phase-shift keying

(BPSK), Quadrature Phase-shift Keying (QPSK) and Offset QPSK (OQPSK) formats at data rates up to 40 Mega-symbols per second. A Square-root-raised-cosine (SRRC) filter option (α = 0.5) is available and recommended to optimize bandwidth efficiency. Maximum data rates will be limited by operational RF band and allocated bandwidth.

3.5 Modulation Index

The modulation index is established by applying a variable-amplitude voltage to the phase modulator in the exciter. The amplitude of this voltage can be adjusted in 255 steps of approximately 0.0065 radians. The range of 0.1 radians through 1.52 radians occupies approximately 220 of these steps. The modulating voltage is calibrated periodically at the 3-dB carrier suppression point for both sine wave and square wave subcarriers. The calibration interval is selected to assure a carrier suppression within 10% of the specified value in dB at any time between calibrations. For example, a sine wave modulation index of 0.67 radians (38.5°) will produce a carrier suppression of 1.0 dB ± 0.1 dB. A sine wave modulation index of 1.13 radians (64.5°) will produce a carrier suppression of 3.0 dB ±0.3 dB.

The modulation index is initialized from an entry in the activity service table but may be changed during a support activity providing no command waveform is being radiated. Carrier power suppression and data power suppression as functions of modulation index angle are:

Sine-wave subcarrier:

$$\frac{P_C}{P_T}(\text{dB}) = 10\log\left[\text{J}_0^2(\theta_D)\right], \text{ dB} \tag{1}$$

$$\frac{P_D}{P_T}(\text{dB}) = 10\log\left[2\text{J}_1^2(\theta_D)\right], \text{ dB \{first upper and lower sidebands\}} \tag{2}$$

Square-wave subcarrier:

$$\frac{P_C}{P_T}(\text{dB}) = 10\log\left[\cos^2(\theta_D)\right], \text{ dB} \tag{3}$$

$$\frac{P_D}{P_T}(\text{dB}) = 10\log\left[\sin^2(\theta_D)\right], \text{ dB \{all sidebands\}} \tag{4}$$

where

θ_D	=	data modulation index, radians, peak
P_T	=	total power
P_C	=	carrier power
P_D	=	data power
J_0	=	zero-order Bessel function
J_1	=	first-order Bessel Function

3.6 Modulation Losses

The bandpass of all elements in the command path, with the exception of the S-band power amplifier at the 20kW capable BWG stations, is adequate to make modulation losses negligible over the frequency and power ranges specified in Table 1. The modulation losses at the S-band 20kW BWG stations are negligible provided the klystron frequency step is properly selected.

3.7 PCM Data Formats

The baseband signal is a pulse code modulated (PCM) waveform that is binary phase-shift keyed (BPSK) onto a subcarrier. That is, phase-shift keyed with a signaling level of ±90° and resulting in a fully suppressed subcarrier. The six supported PCM data formats are illustrated in Figure 4. The data format is established at the start of a support activity by an entry in the activity service table.

When configured for direct modulation, BPSK PCM types are modulated on the carrier based on the modulation index. When configured for QPSK or OQPSK data is modulated resulting in a fully suppressed carrier.

3.8 Subcarrier to Data Rate Ratios

Bit rates for NRZ modulation and symbol rates for bi-phase modulation are available over the range of 7.8 to 125,037.5 bps or sps. They are derived from the subcarrier frequency generator using a binary divider of 2^n where n can be from 1 to 11 depending on the combination of subcarrier frequency and data rate desired. Thus, a 7.8 bps data stream would require a sine wave subcarrier of no more than 8000 Hz and the lowest bit rate available for a 1000 Hz subcarrier would be 1.953125 bps. For a 16000 Hz subcarrier, the bit can be between 7.8125 and 8000 bps. For a 250075 Hz subcarrier, the bit can be between 122.1069 and 125037.5 bps.

The data rate entry in the activity service table is rounded to the nearest acceptable value depending on the subcarrier frequency selected divided by 2^n. If Doppler correction to the nominal subcarrier frequency and data rate are desired, it should be applied to the subcarrier frequency only. The data rate will be correspondingly Doppler compensated, since it is the subcarrier frequency divided by 2^n, and 2^n is a fixed integer. The data rate may be changed during a support activity providing no command waveform is being radiated.

BPSK

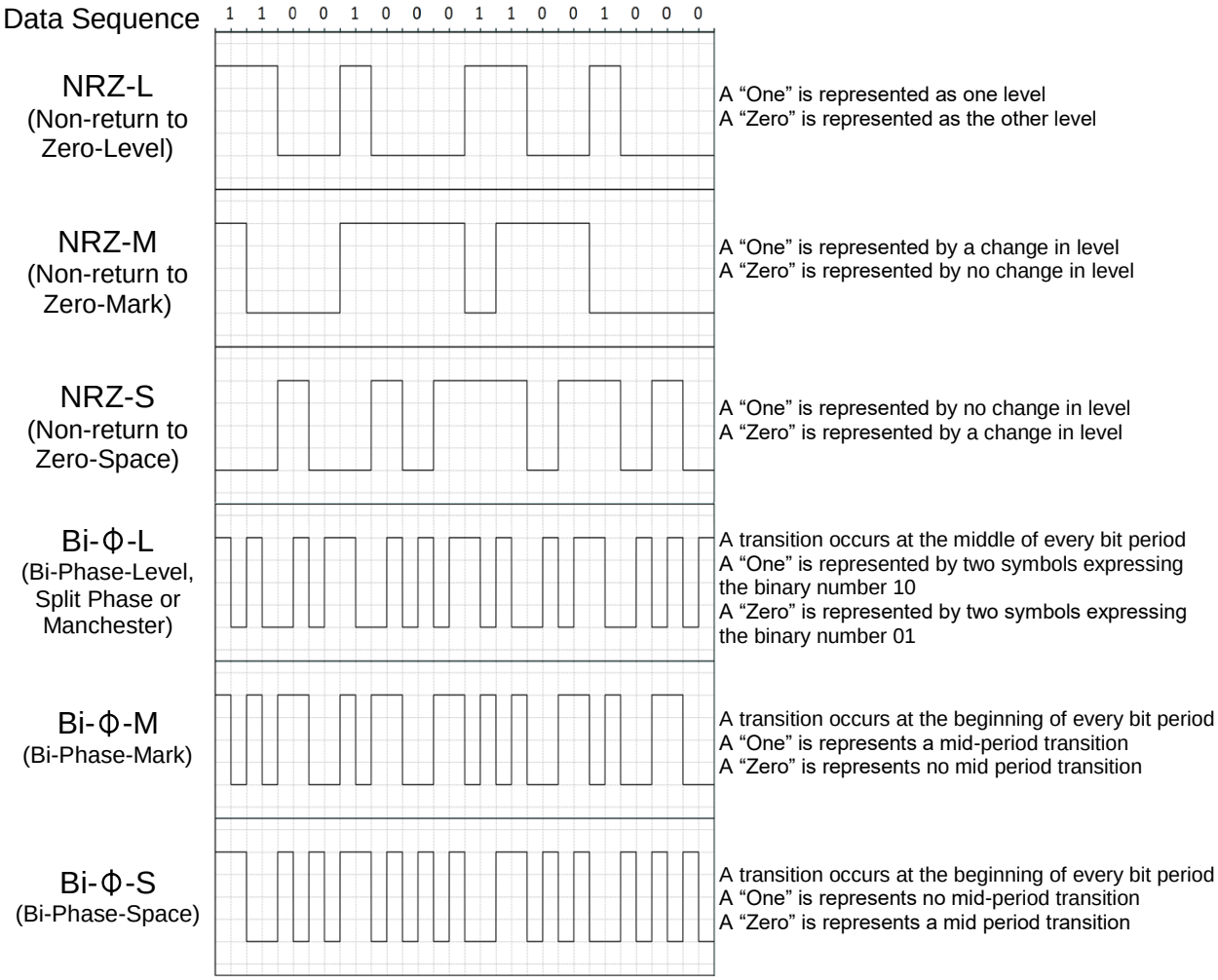

O/QPSK

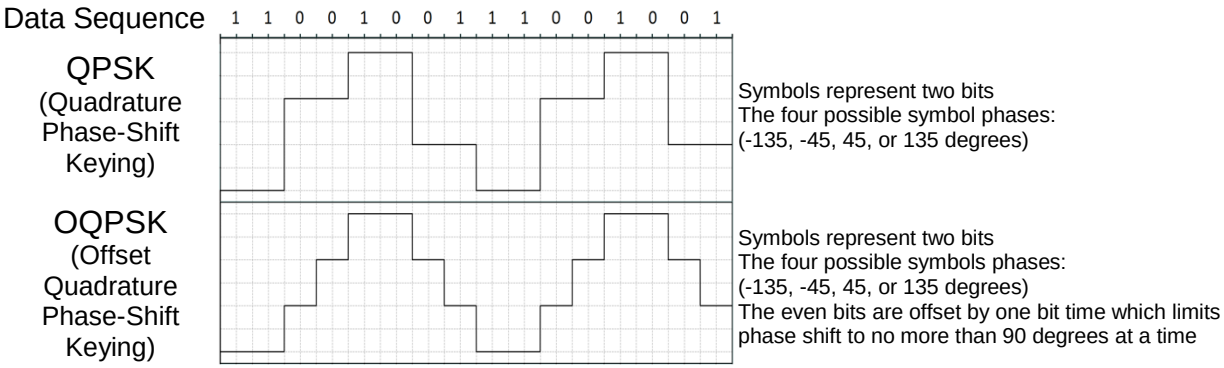

Figure 6. Command Data Formats

3.9 Encoding

DSN command can optionally apply error correction encoding to data formatted as TC or AOS transfer frames, per CDSCC 912.11-0-1. Command supports Reed-Solomon (RS) code capable of correcting up to 16 encoded symbol errors out of each 255 and Low-Density Parity-Check (LDPC) codes conforming to the code family specified in the CCSDS Recommended Standards 231.0-B-3 and 131.0-B-3.

Optional frame randomization and synchronization marker attachment of coded blocks is also available per CDSCC 912.11-0-1.

3.10 Idle Patterns

The DSN command equipment can be configured to operate in one of three modes during a command support activity whenever command data is not being radiated. The command mode is initialized from an entry in the activity service table but may be changed during a support activity providing no command waveform (subcarrier or subcarrier and data) is being radiated. The first of these is carrier only as might be used during a support activity not involving commands. In this mode, all command modulation is removed whenever command data are not being radiated. The second mode is subcarrier only in which a continuous, unmodulated subcarrier is transmitted to the spacecraft at the specified frequency and modulation index. The third mode is a repeating customer defined 8-bit idle pattern or idle Protocol Data Unit (PDU), with or without a subcarrier. The most common idle pattern is an alternating sequence of ones and zeros. If a sequence cannot be specified as an 8-bit pattern, it must be originated at the MOC or POCC as command bits.

When configured for Enhanced Forward CLTU Service (Orange Book), command will insert user defined idle PDU when no command data is present.

3.11 Command Timing

The customer may specify a first bit radiation time within the command data stream to an accuracy of 0.1 s. If an idle pattern has been specified, the actual first bit radiation time will be from 1 to 8 bit times later than the specified radiation time, since the transition between an idle pattern and command bits can only occur at 8-bit boundaries. Commands will be radiated upon receipt if no first bit radiation time is specified. If contiguous radiation of commands is desired, it is the customer’s responsibility to ensure that the commands are delivered at a rate sufficient to satisfy the radiation requirements while not overflowing the buffering capability of the command equipment. Further details can be found in 820-013 module 0239-Telecomm (SLE Command).

3.12 Command Verification

No test on data content is performed because there is no independent source of data available for comparison. The transmitter power level, waveguide configuration, presence of frequency and timing references, and software health are monitored. Failure of a monitored parameter will cause command radiation to abort.

3.13 Availability

The DSN Command System availability is 95 percent for nominal commanding and 98 percent for mission critical events, achieved by allocating back-up stations.

There is no history available from which an undetected command bit error rate can be determined but it is believed to be significantly less than 3 in 10^8 transmitted bits and may be as low as 1 in 10^{13} which is the error rate of the communications channel between the customer and the stations.

Appendix A
References

1 CCSDS 727.0-B-4, CCSDS file Delivery Protocol, Blue Book, January 2007.

2 CCSDS 401.0-B-25-S, Recommendations for Radio Frequency and Modulation Systems, February 2015.

3 CCSDS 912.1-B-2-S, Space Link Extension – Forward CLTU Service Specification, Silver Book, November 2004.

4 CCSDS 912.1-B-3-S, Space Link Extension – Forward CLTU Service Specification, Silver Book, July 2010.

5 CCSDS 912.11-O-1, Space Link Extension – Enhanced Forward CLTU Service Specification, Orange Book, July 2012.

6 810-007, Deep Space Mission System Mission Interface Design Handbook.

7 820-013 module 0188-Telecomm-CFPD, Transaction Log File Interface, Revision B, October 31, 2019.

8 820-013 module 0191-Telecomm, Radiated Spacecraft Command Message File (Rad_SCMF), Revision A, October 28, 2009.

9 820-013 module 0197-Telecomm-CMDRAD, Command Radiation List File Software Interface Specification, July 15, 2008.

10 820-013 module 0198-Telecomm-SCMF, Spacecraft Command Message File (SCMF) Interface, Revision C, November 26, 2012.

11 820-013 module 0211-Service_Mgmt-SEQ, Flight Project and the DSN Interface for Sequence of Events Generation, Revision C, January 4, 2022.

12 820-013 module 0213-Telecomm-CFDP, Deep Space Network (DSN) Interface for the CCSDS File Delivery Protocol (CFDP), Revision B, October 28, 2009.

13 820-013 module 0239-Telecomm, Space Link Extension Forward Link Service, Revision A, September 16, 2019.

14 820-013 module 0241-Telecomm-CLTUF, Command Link Transmission Unit File (CLTUF) Interface, December 15, 2015.

15 820-013 module 0242-Telecomm, Radiated Command Link Transmission Unit File (RAD_CLTUF) Interface, December 15, 2015.

16 CCSDS 131.0-B-3, TM Synchronization and Channel Coding Standard, Blue Book, September 2017.

17 CCSDS 231.0-B-3, TC Synchronization and Channel Coding Standard, Blue Book, September 2017

Deep Space Network

206
Telemetry General Information

Document Owner:		Approved by:	
Signature provided	09/13/2023	Signature provided	09/13/2023
Andrew O'Dea TT&C System Engineer	Date	Timothy Pham Communications Systems Chief Engineer	Date

Prepared by:		Released by:	
Signature provided	09/14/2023	Signature provided	10/09/2023
Scott Allen DSN Support System Engineer	Date	Christine Chang DSN Document Release Authority	Date

DSN No. **810-005, 206, Rev. E**
Issue Date: October 10, 2023
JPL D-19379; CL#23-5791

Jet Propulsion Laboratory
California Institute of Technology

Users must ensure that they are using the current version in DSN Telecommunications Link Design Handbook website:
https://deepspace.jpl.nasa.gov/dsndocs/810-005/

Review Acknowledgment

By signing below, the signatories acknowledge that they have reviewed this document and provided comments, if any, to the signatories on the Cover Page.

Signature provided	09/11/2023	Signature provided	08/23/2023
Jeff Berner DSN Project Chief Engineer	Date	Harvey Soldan DSN Systems Engineer	Date
Signature provided	09/13/2023	Signature provided	09/13/2023
Bo Cen DTT Telemetry Subsystem Engineer	Date	Stephen Slobin DSN Systems Engineer	Date
Signature not provided		Signature provided	09/19/2023
Robert Navarro Manager, TTC E2E Data Services Office	Date	Felicia Sanders Deputy Manager, TTC E2E Data Services Office	Date

Document Change Log

Rev	Issue Date	Prepared By	Affected Paragraphs	Change Summary
Initial	10/7/2004	L. Paal	All	All
Rev. A	9/19/2008	R. Sniffin	Many	Added 34-m and 70-m array information originally planned for inclusion in module 215. Deleted references to portions of AMMOS that are responsibility of projects and to the GDSCC 26-m antenna that has been decommissioned. Added Near-earth 26 GHz (K-band) support and revised proposed capabilities
Rev. B	10/31/2009	A. Kwok	Many	Removed all references related to the 26-m stations.
Rev. C	05/03/2017	S. Allen	Most of sections 2, 3 and 4; removal of section 5. Minor changes in section 1.	Update to reflect current and near future station changes, update Figure 1 and Table 2 to reflect station changes, update to reflect projected capabilities that are now implemented capabilities.
Rev. D	09/01/2021	S. Allen	ALL	Minor updates to reflect current and near future station changes. Update to Figure 1 to reflect station changes. Addition of LDPC rates. Addition of DSS-56 and DSS-53.
Rev. E	10/10/2023	S. Allen	Many	Update to Table 1, update to Table 2 Downlink Frequency Ranges, updated to Table 3 to reflect HRT specs, update to Figure 1, movement of Figures 2 and 3, as well as Table 6, to Section 3, update to Table 6, removal of long constraint length decoder (MCD3), other minor corrections.

Contents

Illustrations

Figure **Page**

Tables

Table **Page**

1 Introduction

1.1 Purpose

This module is intended to provide Deep Space Network (DSN) customers with an overview of DSN telemetry capability and to direct telecommunications designers with specific concerns to the appropriate portions of this handbook. This module also contains brief descriptions of future enhancements to telemetry capability that are in the design or early implementation phases and of capabilities that are being maintained for legacy customers using the previous generation of telemetry equipment.

1.2 Scope

This module describes the Telemetry Service as currently implemented in the DSN. It includes high-level definitions, equations, functional descriptions, and capabilities to provide the telecommunication designer with an introduction to the more detailed information in the other modules of this handbook. Some characteristics are extracted from these modules for the readers' convenience and information relating to telemetry reception that does not conveniently fit in the major divisions of this handbook is included. Schedules for proposed implementation or the removal of any legacy support are not included. All questions relating to schedule should be directed to the Customer Interface Management Office (910).

1.3 Relation to Other 810-005 Material

The information necessary to properly design a telemetry link is distributed across many modules of this handbook. The following paragraphs discuss these modules and describe the parameters contained in them that should be of interest to a telecommunications link designer.

1.3.1 Telecommunications Interface Modules

Modules 101, 103, and 104 contain the radio frequency (RF) characteristics of the Deep Space Network (DSN) antennas. These characteristics include the frequencies of operation, antenna gain, system noise temperature, beamwidth, and polarization capability. A block diagram of each antenna's microwave equipment is also included.

1.3.2 Environmental Effects

Module 105 provides the model for attenuation effects of the Earth's atmosphere on the telecommunications link. Statistics are provided from which a confidence level for link performance can be derived. Limited information on wind effects is provided as a guide for

estimating when the antennas may not be available. The module also includes information on solar, lunar, and planetary noise that will be experienced when the antenna beam is in their vicinity when tracking spacecraft.

Module 106 provides information on additional effects caused by the solar wind or corona when the antenna beam passes near the sun.

1.3.3 Receiver Performance

The telemetry receiver used in the 34-m and 70-m stations is described in module 207. This module provides information on the types of telemetry modulation that can be accommodated and recommendations on carrier loop bandwidth, subcarrier frequency, modulation index, and data rate for each modulation type. Also included is a discussion of system losses for each modulation type.

The 34-m and 70-m stations may make use of the open-loop Radio Science receiver to record an appropriate segment of the received spectrum for post-pass processing. The characteristics of this receiver are described in module 209, however the process of extracting telemetry from radio science receiver recordings is not a standard DSN Service and is not covered in this handbook.

1.3.4 Arraying

The 34-m antennas at each complex can be combined into an array with or without the co-located 70-m antenna. The capabilities of such an array are discussed in paragraph 2.3.4.

1.3.5 Telemetry Decoding

Telemetry decoding capability for the 34-m and 70-m stations is covered in module 208.

1.3.6 Other Factors

Although not of primary interest, the telemetry link designer may be interested in coverage limits presented in module 301 and antenna mechanical performance, including open-loop beam positioning, presented in module 302. Test support provided by the DSN may also be of interest and is described in module 305.

2 General Information

Telemetry service support is available from the three Deep Space Communication Complexes (DSCCs) located in Goldstone, California, USA (GDSCC), near Canberra, Australia (CDSCC), and near Madrid, Spain (MDSCC). Telemetry support is also available from the DSN development and test facility, DTF-21, near JPL, the Merritt Island Launch Area also known as MIL-71 at the Kennedy Space Center, and the transportable Compatibility Test Trailer, CTT-22. CCSDS (Consultative Committee for Space Data Communications) Space Link Extension (SLE)

data is available from JPL. All data types including SLE are routed by the Ground Networks Subsystem (GNW) to JPL before delivery to the users.

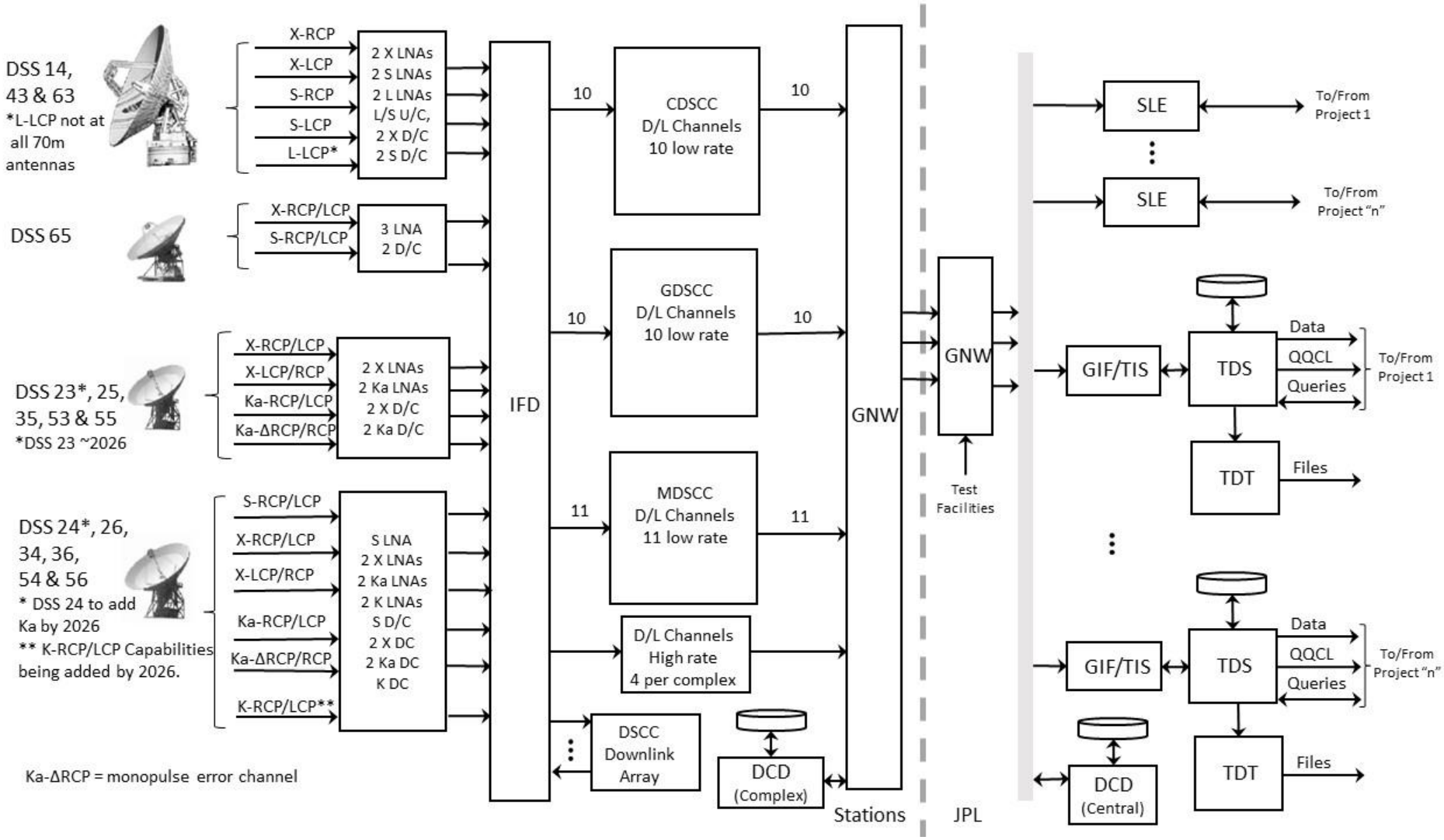

Figure 1. DSN Telemetry Equipment for Spacecraft Support

Figure 1 shows the DSN equipment used for telemetry service support. The items shown on the figure are discussed below.

In general, telemetry service support requires one antenna, at least one receiver, and telemetry processing equipment for each spacecraft. Additional receivers and telemetry processing equipment can be added for spacecraft with multiple downlinks or for redundancy. In addition, the DSN can track up to four spacecraft per antenna (MSPA) if they all are within the scheduled antenna's beamwidth.

Table 1 summarizes the DSN telemetry service support available from each complex.

Table 1. Telemetry Support Capability

Capability	Value	Remarks
Number of simultaneous spacecraft tracks per complex	GDSCC = 7 CDSCC = 7 MDSCC = 8	Based on the number of antennas plus three for MSPA
MSPA	Up to 2 antennas per complex configurable for MSPA concurrently	MSPA is presently limited to four spacecraft per antenna
Frequency bands supported	S, X, K[1], and Ka	Depends on antenna.
Polarization	Right-hand circular (RCP) or left-hand circular (LCP)	Simultaneous RCP and LCP is available on some antennas
Arraying	All 34-m and 70-m antennas within one complex	Uses full-spectrum combining. See paragraph 2.3.4

[1] K-band and 26 GHz are used interchangeably and refer to the near-earth 25.5 – 27.0 GHz band. They are distinct from Ka-band (also referred to as 32 GHz band), which refers to the deep space 31.8 – 32.3 GHz band.

2.1 Telemetry Services

Two distinct types of telemetry service are available. The first of these is the traditional return link from a spacecraft (Return Channel Frame Service, Return All Frame Service, …) that may carry engineering or science data as one of several forms of telemetry modulation including residual-carrier or suppressed-carrier binary-phase-shift keying (BPSK), quadrature-phase-shift keying (QPSK), or offset QPSK (OQPSK). The second is the Return Beacon Tone Service that is intended to monitor the high-level state of a spacecraft during periods when insufficient link margin prevents the reception of traditional telemetry.

2.2 Facilities and Equipment

2.2.1 Antennas

Each Deep Space Communications Complex contains one 70-m and three, four or five 34-m antennas. There are two types of 34-m antennas. The first is the high-efficiency (HEF) antennas that have their feed, low-noise amplifiers, and transmitter located on the tilting structure of the antenna. These antennas were the first antennas in the DSN to use dual shaped reflectors (main reflector and subreflector) instead of conventional paraboloid and hyperboloid shapes. The efficiency of all DSN 34-m antennas is now approximately the same. Note that the 34-m HEF antennas are being decommissioned and will not be available in the future. DSS-45 and DSS-15 have already been taken off-line. DSS-65 decommission is expected in the future (TBD). The second type of 34-m antenna is the beam waveguide (BWG) antenna where the feeds, low noise amplifiers and transmitters are located in a room below the antenna structure and the radio frequency energy is transferred to and from the antenna surface by a series of mirrors encased in a protective tube. All antennas that are designed to support both RCP and LCP. Antennas with two low noise amplifiers (LNAs) and downconverters in either S or X band can receive simultaneous RCP and LCP. Five of the six antennas that receive 32 GHz can receive LCP provided that autotrack (monopulse) capability is not required.

The capabilities of each antenna type and of the individual Beam Waveguide (BWG) antennas are different and must be considered in designing a return link. The selection of antenna will depend on the downlink frequencies it supports and the gain it can provide. Table 2 lists the uplink and downlink frequency ranges for each antenna type and the sensitivity, expressed as the ratio of antenna gain to system temperature, at the time this module was published. The modules referred to in Section 1.3.1 should be consulted for current values and other parameters. The telecommunications link designer is cautioned against making designs dependent on the 70-m antenna as there is only one per complex and it is subject to severe scheduling constraints.

Table 2. Frequencies Covered and Sensitivity of DSN Antennas for Telemetry

Antenna type	Downlink Frequency Ranges (MHz)	Sensitivity (G/T, dB) (See Note 1)	GDSCC	CDSCC	MDSCC
70-m	2200 – 2300 8200 – 8600	48.3 – 50.9 60.9 – 61.7	1	1	1
34-m HEF (Note 2)	2200 – 2300 8400 – 8500	39.1 – 39.8 53.2– 54.6	0	0	1
34-m BWG S/X/K/Ka (Notes 3 and 4)	2200 – 2300 8200 - 8600 25500 – 27000 31800 – 32300	40.6 – 42.2 51.3 – 55.2 58.2 – 60.2 60.1 – 62.5	4 (Note 5)	3	4

Notes:

1. Range covers best performing antenna with 90% weather (see module 105) at band center and 45-degrees elevation in highest sensitivity configuration (usually one band, downlink only) to worst performing antenna at band center and peak gain point in lowest sensitivity configuration (usually dual band downlink or backup LNA with uplink in one band). See appropriate telecommunications interface modules (101, 103 and 104) for complete performance envelope and module 105 for atmospheric effects. In the context of this document, G/T is defined as effective antenna gain divided by system noise temperature, including the effects of atmospheric attenuation and noise temperature contribution.
2. The 8200 – 8600 MHz (VLBI) band uses a wideband HEMT LNA with generally lower performance than the maser LNA that supports only the 8400 – 8500 MHz frequency range. DSS65, the only operational HEF, will be updated in 2024 to include the wideband HEMT and will support 8200 – 8600 Mhz at that time. See module 103.
3. S-Band capability is available at DSS-24, -26, -34, -36 -54 & -56. K-band capability is available at DSS-24, -26, -34, -36, -54 & -56 – NOTE: K-band implementation includes a special low G/T mode for high signal level conditions. Some X and Ka-band BWG antennas also allow for the same higher input signal power.
4. Wide range of K- and Ka-band performance results from much lower atmospheric contribution at GDSCC compared with that at CDSCC and MDSCC. Wide range of X-band performance results from use of partially-cooled X/X/Ka-band feeds at all BWG antennas except DSS-24, compared with the room-temperature feeds at DSS-24.
5. Includes DSS23 expected ~2026.

2.2.2 Telemetry Receivers

All DSN antennas employ a receiver architecture where one or both circular polarizations of the received spectrum are amplified by an LNA and translated to an intermediate frequency by a downconverter (D/C) before being routed to the control room where the desired signal is extracted. The antennas are designed to receive extremely weak signals and can be overloaded by signals in excess of –85 dBm. Antennas supporting K-band have a special low-gain mode that permits operation up to –50 dBm with degraded G/T. X and Ka-band BWG antennas also have a low-gain mode that allow for the same higher input signal power. Missions must be careful to not exceed these limits when designing for near-Earth operations.

Each S-, X-, K-, and Ka-band intermediate frequency from the 34-m and 70-m stations is made available to from one to four sets of receiving and telemetry processing equipment in the SPC. The additional receivers can be used to provide redundancy or reception for additional return links from the supported spacecraft. The following is a brief discussion of the DSN telemetry receivers. Their characteristics are summarized in Table 3.

Each receiver for the S-, X-, K-, and Ka- bands at the 34-m and 70-m antennas is contained in an assembly referred to as a *Downlink Channel.* The receiver utilizes a closed-loop digital super-heterodyne receiver with a selectable carrier tracking loop bandwidth to produce an 8-bit estimated symbol value as its output. Alternatively, these receivers can be used to detect the presence or absence of one of four subcarriers referred to as beacon tones. A complete discussion of the capabilities of this receiver is contained in module 207 of this handbook.

The receiver for K-band is part of a special Downlink Channel containing a wideband telemetry processor. The receiver is preceded by a fixed-frequency downconverter in the antenna and a step-tunable downconverter in the control room.

2.2.3 Telemetry Processing

Telemetry processing at the stations is available for both CCSDS and non-CCSDS (legacy) spacecraft. A summary of the capabilities for these stations is provided in Table 3.

At the stations, the digital symbol output of the telemetry receiver is time-tagged, subjected to optional decoding and frame synchronization, virtual channel extraction and formatting of the data for delivery to the customer. Decoding and frame synchronization are discussed in module 208 of this handbook.

Real-time data delivery may sometimes be limited to critical data. The remainder will be delivered non real-time within an agreed timeframe.

2.2.4 Ground Communications Network

The GNW uses communications circuits provided by the NASA Communications (NASCOM) infrastructures provided by the NASA Communications Program to connect the

stations to JPL Central. The communication lines are shared with all users. The bandwidth is scoped such that it would meet the latency requirements from various missions.

2.2.5 DSN Data Delivery

The DSN provides CCSDS SLE data delivery through the DSN central facility at JPL. Data delivery for additional telemetry functions such as packet extraction (for legacy missions) and CCSDS File Delivery Protocol (CFDP) file processing is also from the DSN central facility.

Table 3. 34-m and 70-m Telemetry Reception Characteristics

Parameter	**S-, X-, K (low rate) and Ka-band Characteristics**	**K-band (high rate) Characteristics**
Receiver Type	Digital	Digital
Closed-loop Carrier Loop Bandwidth (1 sided)	0.2 Hz – 100 Hz	0.1% of symbol rate
Carrier Tracking	Residual Carrier or Suppressed Carrier	Suppressed Carrier
Pre-digitization Bandwidth	66 MHz	400 MHz
Modulation Types	Residual Carrier BPSK with or without subcarrier, Suppressed Carrier BPSK, QPSK, OQPSK	Suppressed Carrier BPSK, QPSK, OQPSK
Subcarrier Frequencies	500 Hz – 2.0 MHz	Not Available
Subcarrier Data Rate (Residual Carrier)	4 s/s – 0.67 X f_subcarrier (s/s)	Not Available
Subcarrier Data Rate (Suppressed Carrier)	20 X loop B/W (s/s) – 0.67 X f_subcarrier (s/s)	Not Available
Direct Modulation (Residual Carrier)	10 ks/s – 26 Ms/s (NRZ) 100 s/s – 13 Ms/s (Bi-phase)	Not Available
Direct Modulation (Suppressed Carrier)	20 X loop B/W (s/s) – 26 Ms/s (NRZ) 20 X loop B/W (s/s) – 13 Ms/s (Bi-phase)) 40 ks/s – 26 Ms/s (QPSK or OQPSK)	1 Ms/s to 300 Ms/s
Beacon Mode	1 of 4 tones, SNR > 5 dB-Hz	Not Available
Data Formats	NRZ (-L, -M, -S) Bi-phase (-L, -M, -S)	NRZ (-L, -M, -S) Bi-phase -L
Available Decoding	Short and long Constraint Convolutional, Reed-	Short Constraint Convolutional, Reed-

Parameter	S-, X-, K (low rate) and Ka-band Characteristics	K-band (high rate) Characteristics
	Solomon, Concatenated Convolutional and Reed-Solomon, Turbo, LDPC	Solomon, Concatenated Convolutional and Reed-Solomon, LDPC
Short Constraint Convolutional Decoding	k=7, r=1/2 CCSDS or DSN Connection vector, Optional De-randomization and alternate symbol inversion 26.4 Ms/s (max)	k=7, r=1/2 CCSDS Connection vector, Optional De-randomization 300 Ms/s (max)
Frame Synchronization	CCSDS and non-CCSDS, 13.2 Mb/s (max)	CCSDS, 300 Ms/s (Max)
Reed-Solomon Decoding	RS (255, 223), Interleave = 1 – 8	RS (255, 223), Interleave = 1 – 8
Turbo Decoding Frame Size Code Rate and Data Rate	CCSDS Code Rates 1/2, 1/3 and 1/4 have a max rate of 1.6 Mb/s. Code Rate 1/6 has a max rate of 1.0 Mb/s. Frame sizes: 1784, 3568, 7136, 8920 Code rates: 1/2. 1/3, 1/4, and 1/6	Not Available
LDPC Decoding Frame Size Code Rate and Data Rate	CCSDS All frame sizes and Data rates limited to 5 Mb/s max Frame sizes: 1024, 4096, 16384 for Code Rates: 1/2, 2/3, and 4/5 Frame Size 7136, for code rate 7/8 (223/255)	CCSDS All frame sizes and Data rates limited to 150 Mb/s max Frame size: 16384 for Code Rates: ½, 2/3, and 4/5 Frame Size 7136, for code rate 7/8 (223/255)

2.3 Concepts Used in Estimating Telemetry Performance

The following concepts are important to understanding telemetry performance. A more detailed discussion of these concepts is contained in module 207 of this handbook.

2.3.1 Relative Power of Telemetry Signal Components

It is possible to share the available downlink power between more than one type of modulation when using residual carrier power modulation schemes. The functions $\alpha(\theta)$ and $\beta(\theta)$, as shown in Table 4, are used to describe the allocation of downlink power between two or more modulation types.

The equations below provide the component to total power relationships for any combination of the modulating signals identified as Channels 1 through 4 although it is rare that more than two types of modulation will be used. Power not accounted for by these equations is distributed as inter-modulation products and is not available to the communications process. The modulation indices, ϕ_N, for all equations must be in units of radians, peak, and the modulation index for the unused channels should be set to zero.

Table 4. Definition of $\alpha(\theta)$ and $\beta(\theta)$ for θ in radians, peak

Telemetry type	$\alpha(\theta)$	$\beta(\theta)$	Remarks
Square wave subcarrier or data only	$\cos(\theta)$	$\sin(\theta)$	$\beta(\theta)$ includes data power in all harmonics
Sine wave subcarrier	$J_0(\theta)$	$\sqrt{2}J_1(\theta)$	$\beta(\theta)$ only includes data power in fundamental harmonics

(1) Channel 1 data ($D1$) directly modulates the carrier with modulation index ϕ_1.

(2) Channel 2 data ($D2$) bi-phase modulates a square-wave or sine wave subcarrier that is used to modulate the carrier with modulation index ϕ_2.

(3) Channel 3 data ($D3$) bi-phase modulates a square wave or sine wave subcarrier that is used to modulate the carrier with modulation index ϕ_3.

(4) Channel 4 data ($D4$) is a square wave or sine wave ranging signal that directly modulates the carrier with modulation index ϕ_4.

The carrier suppression is

$$\frac{P_C}{P_T} = \left[\cos(\phi_1)\cdot \alpha(\phi_2)\cdot \alpha(\phi_3)\cdot \alpha(\phi_4)\right]^2 . \tag{1}$$

The ratio of the available data power to total power for each of the data streams is

$$\frac{P_{D1}}{P_T} = \left[\sin(\phi_1)\cdot \alpha(\phi_2)\cdot \alpha(\phi_3)\cdot \alpha(\phi_4)\right]^2, \tag{2}$$

$$\frac{P_{D2}}{P_T} = \left[\cos(\phi_1)\cdot \beta(\phi_2)\cdot \alpha(\phi_3)\cdot \alpha(\phi_4)\right]^2, \tag{3}$$

$$\frac{P_{D3}}{P_T} = \left[\cos(\phi_1)\cdot \alpha(\phi_2)\cdot \beta(\phi_3)\cdot \alpha(\phi_4)\right]^2, \tag{4}$$

$$\frac{P_{D4}}{P_T} = \left[\cos(\phi_1)\cdot \alpha(\phi_2)\cdot \alpha(\phi_3)\cdot \beta(\phi_4)\right]^2. \tag{5}$$

2.3.2 Definition of STB/N0 and STSY/N0 (dB)

Telemetry signal-to-noise ratios (SNRs) are expressed as bit SNR (represented as either ST_B/N_0 or E_B/N_0) or symbol SNR (represented as either ST_{SY}/N_0 or E_S/N_0). The distinction between symbols and bits is that when the telemetry data are encoded prior to transmission, channel bits (information bits plus overhead such as frame sync and parity bits) are the input to the encoder and symbols are the output. When coded data are processed after receipt on the ground, the telemetry stream consists of symbols until converted to bits again by the decoder at which time any overhead bits are discarded. The relationship between ST_{SY}/N_0 and ST_B/N_0 is:

$$ST_{SY}/N_0 = \frac{1}{r}\cdot ST_B/N_0 \tag{6}$$

where

S = the data power as defined in equations (1), (2), or (3);

T_B = the bit period,

T_{SY} = the symbol period,

N_0 = the one-sided noise spectral density,

r = the number of symbols per bit.

Some typical values for r include:

1 for uncoded data,

2 for rate 1/2 convolutionally, turbo, or LDPC coded data,

6 for rate 1/6 convolutionally coded or turbo coded data,

2.3.3 Carrier Loop SNR

The DSN Telemetry provides the user with an estimate of E_S/N_0. This can be used to calculate a value for Carrier Loop SNR that includes system losses. This provides both a way to validate link design and a way to determine the system loss in a controlled environment. The following equations provide the Carrier Loop SNR (ρ_L) where B_L is the one-sided carrier loop bandwidth.

$$\rho_L = \frac{E_S/N_0}{\tan^2\phi \cdot T_{SY} \cdot B_L} \quad \text{for square wave subcarrier and direct modulation.} \tag{7}$$

$$\rho_L = \frac{(E_S/N_0)\cdot \mathrm{J}_0^2(\phi)}{2\,\mathrm{J}_2^2(\phi)\cdot T_{SY} \cdot B_L} \quad \text{for sine wave subcarrier modulation.} \tag{8}$$

When using these relationships with more than one data stream modulating the carrier, care should be taken to use the values of E_S/N_0, T_{SY}, and ϕ that all pertain to the same data stream.

2.3.4 Arraying

The DSN Telemetry can combine the intermediate frequencies from the 70-m and 34-m antennas at each complex by full spectrum combining. The output of the Array Combiner appears to be another IF spectrum that can be selected by from one to four receivers.

Ideally, the combined telemetry SNR is:

$$\left(\frac{E_b}{N_0}\right)\sum = \sum_{i=1}^{n}\left(\frac{E_b}{N_0}\right)_i \tag{9}$$

where

$\left(\frac{E_b}{N_0}\right)$ = the telemetry SNR at the input of the ith receiver for the non-arrayed case

n = the number of streams combined.

The ratio of the array sum E_b/N_0 to the E_b/N_0 of the master antenna (usually the antenna with the highest individual E_b/N_0) is the array gain. The individual SNRs are proportional to the ratios of antenna sensitivity, G/T, at each of the contributing antennas. Table 5 is a tabulation of G/T ratios relative to a 34-m and 70-m antenna for individual antennas and for combinations of arrayed antennas. The antenna performance values used to calculate the values in this table are those of the average antenna for each antenna type listed in Table 2 at its peak gain elevation angle. Relative aperture will approach the ratio of the antenna areas at low

elevation angles where the high atmospheric temperature component becomes dominant over the LNA temperature.

The values in the table must be considered approximations as they do not take into consideration the particular antennas being arrayed, the effects of varying elevation, and the selected support configuration (polarization, diplexed vs. non-diplexed, etc.). The "Equivalent (dB)" column has been reduced by 0.3 dB to accommodate the typical combining loss.

Note: K-band arraying is not supported.

Table 5. Relative Telemetry Aperture

Practical Arrays [Best Antenna, Arrayed Antenna(s)]	G/T Ratio Relative to Reference Antenna	Equivalent (dB) Less Combining Loss
Relative to 34-m BWG Antenna		
S-band, 34-m BWG & 34-m HEF	1.66	1.90
X-band, 2 34-m (BWG or HEF)	2	2.71
X-band, 3 34-m (BWG or HEF)	3	4.47
X-band, 3 34-m BWG and HEF	4	5.72
Ka-band, 2 34-m BWG	2	2.71
Relative to 70-m Antenna		
S-band, 70-m, 34-m BWG	1.12	0.18
S-band, 70-m, 34-m BWG & 34-m HEF	1.23	0.60
X-band, 70-m, 1 34-m (BWG or HEF)	1.18	0.42
X-band, 70-m, 2 34-m (BWG or HEF)	1.36	1.03
X-band, 70-m, 3 34-m (BWG or HEF)	1.53	1.55
X-band, 70-m, 3 34-m BWG and HEF	1.70	2.01

3 Typical Performance

Figure 2 and Figure 3 provide the expected performance at X-band and Ka-band using a generic reference spacecraft having equal antenna size and transmitter power for the two bands of interest. These figures illustrate that, all other factors being the same, the performance of the 34-m BWG antennas at Ka-band is essentially the same as the 70-m antennas at X-band. It is also evident that the use of a spacecraft omni-directional antenna at X-band and Ka-band is not practical for reception using a BWG antenna. Table 6 presents a set of antenna performance parameters for "average" DSN 34m and 70m antennas, in this case DSS-34 and DSS-43 in Canberra. All parameters are given for 45-degree elevation angle and a CD = 0.50 weather condition. It should be noted that the G/T values for a 70m antenna at X-band and a 34m antenna at Ka-band are nearly the same, as stated above.

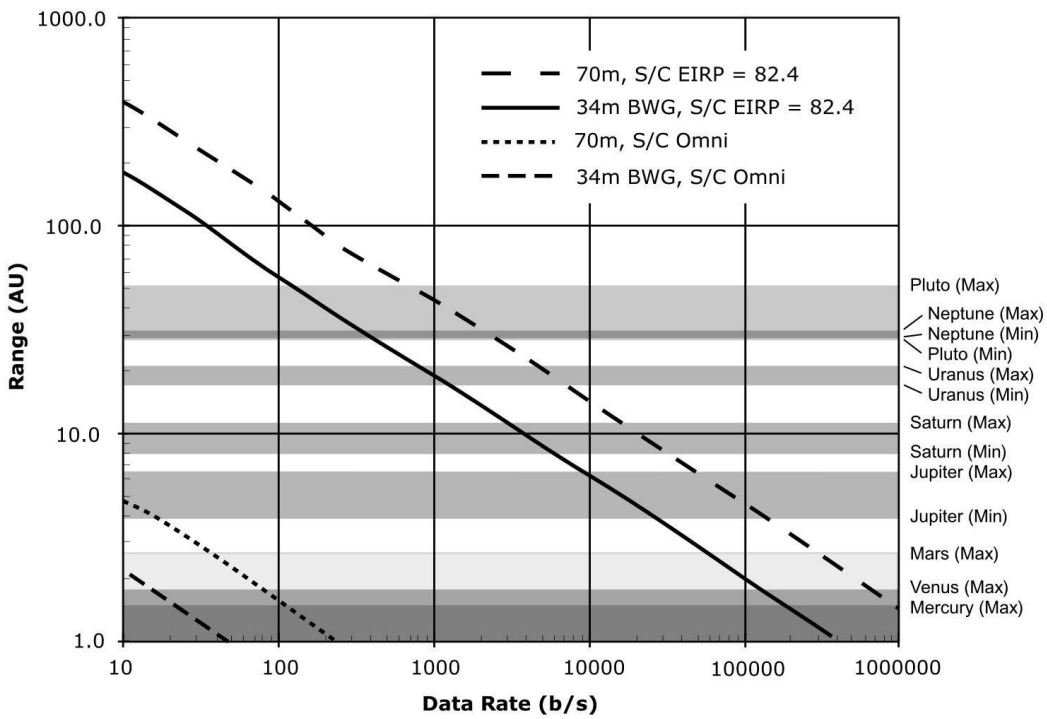

Figure 2. X-band Telemetry Performance with Reference Spacecraft

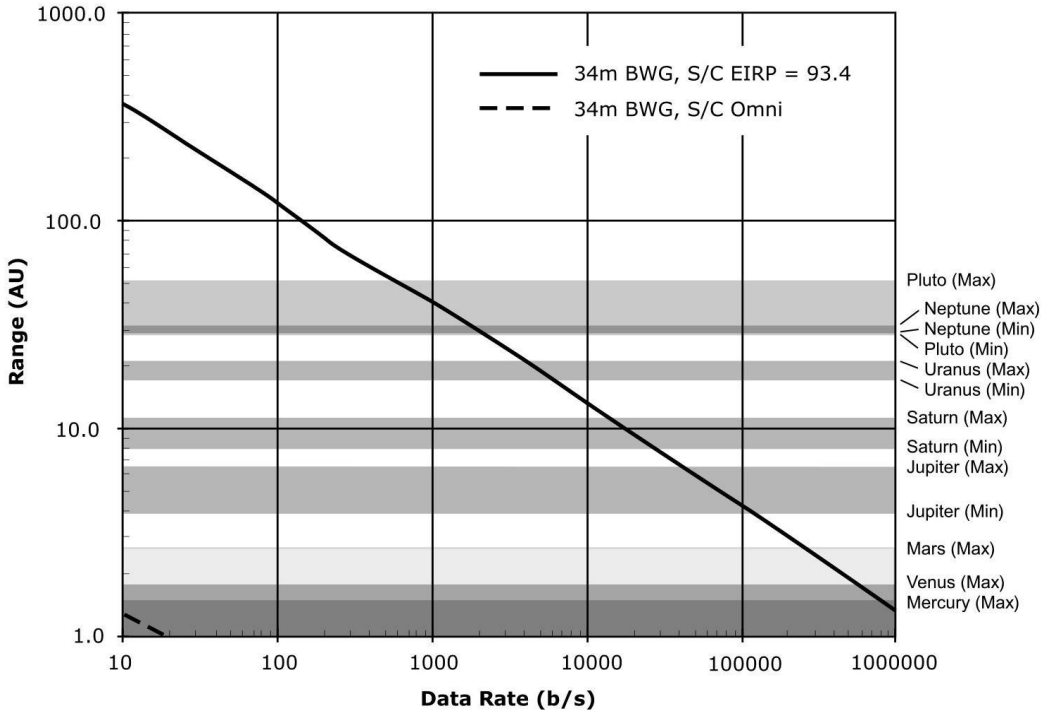

Figure 3. Ka-band Telemetry Performance with Reference Spacecraft

Table 6. Typical 34m BWG and 70m Antenna Parameters with CD=0.50 Weather, 45-degree Elevation Angle

	S-Band		**X-Band**		**K-Band**	**Ka-Band**
	34-m	**70-m**	**34-m**	**70-m**	**34-m**	**34-m**
Gain, dBi	56.8	63.5	68.3	74.5	76.9	78.6
Atmosphere loss, dB	0.051	0.051	0.066	0.066	0.300	0.337
T-op, K	30.7	19.4	23.0	19.1	48.3	41.9
G/T, dB	41.9	50.7	54.6	61.7	60.1	62.4

4 Recommendations for Mission Design

4.1 Operating Frequency

The DSN supports telemetry reception in the S-, X-, K-, and Ka-bands. The trend in deep space communications (Category B spacecraft) has been towards the higher frequencies. Near-Earth (Category A) spacecraft have used S-band exclusively but are adopting K-band for high data rate applications.

4.1.1 S-band (2.2 – 2.3 GHz)

S-band has been the frequency of choice for near-Earth spacecraft where link performance is relatively easy to obtain and the mass of spacecraft components is not as critical as with deep space spacecraft. Other advantages include the availability of low-cost spacecraft components and ground resources along with compatibility with the Goddard Spaceflight Center (GSFC)-managed Tracking and Data Relay Satellite System (TDRSS). The principal disadvantage of S-band for Category A spacecraft is that the total allocation bandwidth is 90 MHz. This creates a significant possibility of interference between spacecraft.

The principal advantage of S-band for deep space (Category B) spacecraft is low space loss that may be important for applications where there is little or no antenna gain at the transmitting (space) end of the link. Its disadvantages include larger spacecraft components, a limited channel bandwidth of 370 kHz, and significant link degradation when the link must pass near the sun. While it is possible to use more than one channel, the total deep space S-band allocation bandwidth is only 10 MHz.

Note that DSN S-band assets are limited, so scheduling may be challenging.

4.1.2 X-band (8.4 – 8.5 GHz)

X-band is presently the most heavily used allocation for deep space missions. It is the highest frequency band in which uplink is currently supported making it possible to have a single-band spacecraft with a moderately high telemetry rate. The standard telemetry channel bandwidth at X-band is 1.4 MHz and, while missions may use more than one channel, the total X-band allocation bandwidth is only 50 MHz and the use of bandwidth-efficient modulation is preferred over multiple channel use.

4.1.3 K-band (25.5 – 27.0 GHz)

K-band is available for high data-rate, Category A (near-Earth) missions in combination with S-band for command and engineering telemetry. It provides an advantage of approximately 20 dB over an S-band link with equivalent specifications. Its principal disadvantage is degradation from adverse weather but this can be ameliorated by a combination of on-board data storage, weather forecasting, and an adaptive downlink data rate strategy.

4.1.4 Ka-band (31.8 – 32.3 GHz)

Ka-band is recommended for high data-rate missions in combination with X-band for command and engineering or emergency telemetry. It has no defined channels as its total allocation of 500 MHz cannot be accommodated with a single turn-around ratio from S- or X-band uplinks. It provides an advantage of approximately 9 dB over X-band for spacecraft with equivalent specifications and is the least susceptible to solar effects. Its principal disadvantages are degradation from adverse weather, high space loss that precludes use of an omni-directional antenna for emergency transmission, and somewhat greater spacecraft pointing requirements. Adverse weather effects can be ameliorated by a combination of on-board data storage, weather forecasting, and an adaptive downlink data rate strategy.

4.2 Telemetry Modulation

The DSN supports a wide range of telemetry modulation schemes. Some advantages and disadvantages of the various schemes are discussed in the following paragraphs. Additional information can be found in Module 207.

4.2.1 Residual-Carrier BPSK

Residual carrier BPSK using a square wave subcarrier is the modulation scheme that has been most commonly employed for deep space telemetry. There are historical reasons for this but it remains a good choice in many applications. A residual carrier provides the ability to share downlink power to support additional functions such as two-way ranging and Delta-differential One-way Ranging (ΔDOR). The ability of a spacecraft to provide an un-modulated carrier is also useful for Radio Science investigations. Residual carrier tracking tolerates a lower carrier loop SNR before experiencing cycle slips and is not subject to the more damaging half-cycle slips that are possible with suppressed carrier tracking. The subcarrier keeps the data sidebands away from the residual carrier in the frequency domain so the carrier can be tracked without interference. Use of a subcarrier occupies more spectrum than direct modulation, but the occupied bandwidth is typically not an issue for low data-rate telemetry.

Sine wave subcarriers have been used for Category A (near Earth) missions where relatively high power and wide antenna beamwidths make spectrum conservation essential. The higher-order harmonics of a sine wave subcarrier fall off faster with the result being that less bandwidth is occupied than by a square wave subcarrier of the same frequency. The disadvantage of sine wave subcarriers is that the receiver can recover only the power in the fundamental harmonics. Data power transmitted in the higher-order harmonics is lost. This is contrasted to square wave subcarriers where all data power within the bandwidth of the receiver is recovered.

Direct carrier modulation is a good choice for medium and high-rate telemetry when other considerations require a residual carrier. The baseline performance of this scheme is the same as that when using a square wave subcarrier and spectral occupancy is no more than half that of the equivalent square wave subcarrier system.

4.2.2 Suppressed-Carrier BPSK

Suppressed-carrier BPSK provides approximately the same performance at high data rates as residual-carrier BPSK and improved performance at some medium data rates. The bandwidth occupancy is the same as residual-carrier BPSK without a subcarrier. Suppressed-carrier BPSK can result in half-cycle slips and telemetry inversion, which is subsequently handled in frame synchronization. The half-cycle slips can also invert the ranging, which can be handled by configuring for automated detection of ranging polarity.

4.2.3 QPSK and OQPSK

QPSK and Offset QPSK offer better bandwidth efficiency than BPSK. For a given binary symbol rate, a QPSK or OQPSK carrier occupies only half the bandwidth of a BPSK-modulated carrier (with no subcarrier). QPSK and OQPSK have the disadvantage that telemetry must be disabled in order to perform DSN ranging or ΔDOR.

The baseline telemetry performance of QPSK and OQPSK is the same as suppressed-carrier BPSK at high data rates. When shaped data pulses are used, there is some advantage to OQPSK, relative to QPSK, which accounts for the popularity of OQPSK in satellite communications; however, for unshaped data pulses, the performance and spectral occupancy of QPSK and OQSPK are the same. Note that for OQPSK modulation with shaped pulses (e.g., Gaussian Minimum-Shift Keying (GMSK) or Square Root Raised Cosine (SRRC) filtering), the DSN receivers can track the signal, but there are additional losses.

4.3 Symbol Formats

NRZ-L and biphase-L symbol formats are supported for all decoding schemes. Differentially encoded NRZ-M, NRZ-S, biphase-M and biphase-S formats are supported for uncoded and short constraint length convolutionally coded data (see below). The data is presented to downstream functions in NRZ-L format with differential decoding applied after convolutional decoding, if applicable.

4.4 Coding Schemes

Selection of coding scheme is independent of modulation scheme and involves the tradeoff of four considerations. These are coding gain, bandwidth, latency, and error floor. In general, coding gain increases with bandwidth and latency. More detailed information can be found in Module 208. The following coding schemes are supported by the DSN.

4.4.1 Uncoded

Uncoded data requires the least bandwidth and introduces the lowest latency. Its primary use is for transfer of extremely high data rates in bandwidth-limited situations when adequate link margin is available.

4.4.2 Reed-Solomon Code

The (255,223) Reed-Solomon (RS) code used by the DSN is capable of correcting up to 16 symbol errors out of each 255. The error-correcting capability provides a significant improvement over uncoded data with a modest bandwidth expansion but the lack of performance near threshold limits its use to high E_B/N_0 conditions.

4.4.3 Short Constraint Length, Rate 1/2 Convolutional Code

Short constraint length (k = 7), rate 1/2 convolutional code is a low-latency code that requires twice the bandwidth of uncoded data but provides coding gain for any input SNR. Its low latency makes it a good choice for low rate, emergency communications when recovery of data in real-time may outweigh the coding gain of higher-latency codes.

4.4.4 Concatenated Reed-Solomon and Rate 1/2 Convolutional Codes

When Reed-Solomon encoded spacecraft data is rate 1/2 convolutionally encoded before transmission, the resultant code has a slightly greater bandwidth expansion but significantly better performance at all SNRs than either of its components. This is because the convolutional decoder improves the input bit error rate to the Reed-Solomon decoder at low SNRs while the RS decoder improves the output error rate for all SNRs above its input threshold. As convolutional decoders tend to produce bursts of errors as they near their threshold, they can overwhelm the correction capability of the RS decoder. This can be alleviated by a technique called *interleaving* (See module 208) that trades improved performance for increased latency.

4.4.5 Turbo Codes

Turbo codes provide near Shannon-limit performance with bandwidth expansions from slightly more than 2 to slightly more than 6. Block sizes of 1784, 3568, 7136, and 8920 symbols are accommodated. The smaller block sizes are intended for lower data rates while using larger block sizes as the data rate increases reduces coding overhead. Their principal disadvantages are the amount of processing that must be done to decode them and the presence of an error floor at a Frame Error Rate of about 10^{-6}. The decoding complexity limits the maximum supported data rate.

4.4.6 Low-density Parity-Check Codes

Low-Density Parity-Check codes conforming to the code family specified in Section 7 of the CCSDS Recommended Standard 131.0-B-2 are supported by the DSN. The decoding complexity limits the maximum supported data rate.

4.4.7 Derandomization

If the telemetry data is randomized as defined in CCSDS 131.0-B-2, derandomization is applied prior to frame (Reed-Solomon, turbo or LDPC) decoding.

5 Proposed Capabilities

The following paragraph discusses capabilities that have not yet been implemented by the DSN but have adequate maturity to be considered for spacecraft mission and equipment design. Telecommunications engineers are advised that any capabilities discussed in this section cannot be committed to except by negotiation with the Customer Interface Management Office (910).

5.1 Bandwidth-efficient Modulation

Several bandwidth-efficient modulation schemes are in development to permit the maximum amount of data to be returned within the allocated frequency bands. The most likely candidate for implementation is Gaussian minimum-shift keying (GMSK). This would remove the additional losses mentioned in section 4.2.3.

207, Rev. A
34-m and 70-m Telemetry Reception

June 13, 2003

Document Owner:

Signature on file at DSMS Library

L. Paal, Date
Telemetry System Engineer

Approved by:

Signature on file at DSMS Library

J. B. Berner Date
Telecommunications Services
System Development Engineer

Author

Signature on file at DSMS Library

P. W. Kinman Date

Released by:

Signature on file at DSMS Library

DSMS Document Release Date

Change Log

Rev	Issue Date	Affected Paragraphs	Change Summary
Initial	11/30/2000	All	All
A	6/13/2003	Many	Revised to include concatenated codes, QPSK/OQPSK modulation, and to improve description of turbo code performance.

Note to Readers

There are two sets of document histories in the 810-005 document that are reflected in the header at the top of the page. First, the overall document is periodically released as a revision when major changes affect a majority of the modules. For example, the original release of this document was part of Revision E. Second, the individual modules also change, starting as an initial issue that has no revision letter. When a module is changed, a change letter is appended to the module number on the second line of the header and a summary of the changes is entered in the module's change log.

Contents

Paragraph **Page**

Illustrations

Figure **Page**

Figure **Page**

Tables

Table **Page**

Table **Page**

1 Introduction

1.1 Purpose

This module provides the performance parameters for telemetry reception at the Deep Space Network (DSN) 34-m and 70-m stations.

1.2 Scope

The scope of this module is limited to those features of the Downlink Channel at the 34-m and 70-m stations that relate to telemetry reception and demodulation. Under the Network Simplification Plan (NSP), each Block-V Receiver has been renamed the Receiver and Ranging Processor (RRP) and has become part of a Downlink Channel. The Downlink Channel also performs the frame synchronization and data decoding that are discussed in Module 208, Telemetry Data Decoding.

1.3 General Information

Figure 1 shows the architecture used in the 34-m and 70-m stations to process an arriving telemetry signal through the point at which it becomes a stream of data symbols. The arriving signal is routed from the Antenna Feed/Low Noise Amplifier (LNA) to the Downlink Channel. Within the radio-frequency (RF) to Intermediate-frequency (IF) Downconverter (RID) at the antenna, a local oscillator is generated by frequency multiplication of a highly stable frequency reference from the Frequency and Timing Subsystem (FTS), and the incoming downlink signal is heterodyned with this local oscillator. The Intermediate-Frequency (IF) signal that results is sent to the Signal Processing Center (SPC). Here, the Intermediate-frequency to Digital Converter (IDC) alters the frequency of the IF signal by a combination of up-conversion and down-conversion to a final analog frequency of approximately 200 MHz and then performs analog-to-digital conversion. The final analog stage of down-conversion uses a local oscillator supplied by the Channel-Select Synthesizer (CSS), that is also part of the Downlink Channel. The CSS is adjusted before the beginning of a pass to a frequency appropriate for the channel of the incoming downlink signal; during the pass, the frequency of the CSS remains constant. The frequency of the CSS (and, indeed, of all local oscillators in the analog chain of down-conversion) are synthesized within the Downlink Channel from highly stable frequency references provided by the FTS. The RRP accepts the digital signal and performs carrier, subcarrier, and symbol synchronization, Doppler compensation, and data demodulation (Reference 1). For purposes of telemetry, the output of the RRP is a stream of soft-quantized symbols, suitable for input to a decoder.

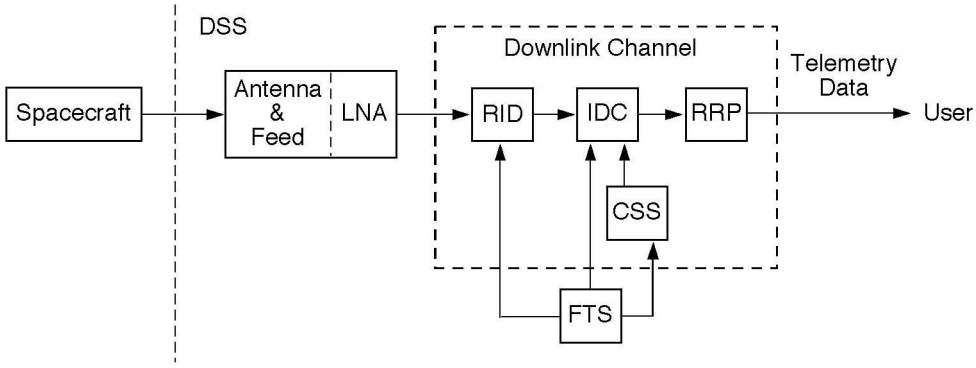

Figure 1. Receiver Architecture

2 *Telemetry Capability*

Table 1 shows the types of telemetry signals that can be tracked at the 34-m and 70-m stations. The new CCSDS bandwidth-efficient modulation schemes, which generally involve non-rectangular pulse shapes, are not shown. The Downlink Channel can, in fact, demodulate these new modulation schemes. However, there are large losses that result from using equipment that was designed for the optimum demodulation of rectangular pulse shapes to demodulate non-rectangular pulse shapes.

Table 1. Telemetry Capabilities

Parameter	Capabilities
Data Formats	NRZ (-L, -M, -N) Bi-ϕ (-L, -M, -N)
Modulation Types	Residual-carrier BPSK Suppressed-carrier BPSK QPSK, OQPSK
Subcarriers	Squarewave Sinewave
Symbol Rates	See Table 2
Carrier Loop Bandwidth	$B_L \leq 200$ Hz, residual carrier $B_L \leq \min(200 \text{ Hz}, R_{SYM}/20)$, suppressed carrier
Loop Types	2, 3

2.1 Modulation

Both residual-carrier and suppressed-carrier binary phase-shift keying (BPSK) can be coherently demodulated. A suppressed carrier is tracked with a Costas loop (Reference 2). Both squarewave and sinewave subcarriers can be coherently demodulated. Non-Return to Zero (NRZ) and Bi-ϕ (i.e., bi-phase or Manchester) data formats are supported.

Table 2. Symbol Rates

Data Type	Symbol Rates
Residual-Carrier	
Subcarrier Present	4 sps $\leq R_{SYM} \leq 0.67\ f_{subcarrier}$
Direct Modulation	
NRZ Bi-ϕ	4 sps $\leq R_{SYM} \leq$ 26 Msps 4 sps $\leq R_{SYM} \leq$ 13 Msps
Suppressed-Carrier	
Subcarrier Present	$20B_L \leq R_{SYM} \leq 0.67\ f_{subcarrier}$
Direct Modulation	
NRZ Bi-ϕ QPSK or OQPSK	$20B_L \leq R_{SYM} \leq$ 26 Msps $20B_L \leq R_{SYM} \leq$ 13 Msps 40 ksps $\leq R_{QSYM} \leq$ 26 Msps

When the incoming carrier has a quadriphase shift keyed (QPSK) or Offset QPSK (OQPSK), with symbols on both the in-phase and quadrature components of the carrier, the Downlink Channel can synchronize to the carrier and coherently demodulate and detect the symbols on both of its components. The four-fold phase ambiguity that arises in QPSK needs to be resolved downstream in the telemetry decoding operation. In Table 2, the limits on symbol rate for QPSK and OQPSK are written in terms of the quaternary channel symbol rate, R_{QSYM}. For QPSK and OQPSK, the information bit rate is $2rR_{QSYM}$, where r is the code rate.

2.2 Symbol Rate

When tracking a residual carrier, the smallest symbol rate that can be used is 4 sps. When tracking a suppressed carrier, there is an additional constraint on the relationship between symbol rate R_{SYM} and carrier loop bandwidth B_L of the Costas loop.

$$\frac{R_{SYM}}{B_L} \geq 20, \quad \text{suppressed carrier} \tag{1}$$

The reason that suppressed-carrier BPSK has a different minimum symbol rate than does residual carrier has to do with the implementation of the Costas loop that tracks the suppressed carrier. The effective update rate of this loop is equal to the smaller of 2 kHz or the symbol rate. The update rate must be large relative to the loop bandwidth otherwise good tracking will not be obtained.

For QPSK and OQPSK, the minimum symbol rate given in Table 2 represents a recommended minimum. The Downlink Channel can demodulate symbol rates smaller than this minimum but with an additional performance degradation that increases as the symbol rate decreases. There is no good reason to use QPSK or OQPSK for these smaller symbol rates since other modulation schemes offer better performance at small symbol rates and there is no pressing need for bandwidth efficiency under these circumstances.

Paragraph 5.5 provides information on symbol synchronization. This includes an equation for the Signal-to-Noise Ratio (SNR) in the symbol loop and the required value of symbol loop SNR.

It is recommended that the symbol transition density be greater than or equal to 0.25. (It is 0.5 for truly random data.) When the symbol transition density is less than 0.25, more signal-to-noise ratio will be required for symbol synchronization.

The baseband telemetry bandwidth is 36 MHz (half-power, i.e., –3 dB). In the absence of a subcarrier, the maximum symbol rate that can be demodulated and detected is 26 Msps for NRZ data and 13 Msps for Bi-ϕ (Manchester) data. Other limitations on symbol rate arise in the telemetry processing stages that are downstream from the RRP. Module 206, Telemetry General Information, should be consulted for greater detail.

If the symbol rate is derived from the same frequency source as the subcarrier frequency (i.e., synchronous), it is recommended that there be at least three subcarrier cycles per data symbol. If the subcarrier and symbol rate are asynchronous, a subcarrier frequency to symbol rate ratio of greater than 1.5 is recommended. Furthermore, it is recommended that all proposed combinations of subcarrier frequency and symbol rate be tested to ensure efficient subcarrier demodulation. If the subcarrier and symbol rate are asynchronous, the frequency difference between the subcarrier and any of the first ten harmonics of the symbol rate should be greater than the bandwidth of the subcarrier loop.

2.3 Carrier Loop Bandwidth

In this module, carrier loop bandwidth means the one-sided, noise-equivalent carrier loop bandwidth of the receiver. It is denoted B_L. There are limits on the carrier loop bandwidth. B_L can be no larger than 200 Hz. The lower limit on B_L is determined by the phase noise on the downlink. In addition, when operating in the suppressed-carrier mode, B_L is subject to the constraint given in Equation (1).

In general, the value selected for B_L should be small in order to maximize the carrier loop signal-to-noise ratio. On the other hand, B_L must be large enough that neither of the following variables becomes too large:

a) The static phase error due to Doppler dynamics,

b) The contribution to carrier loop phase error variance due to phase noise on the downlink.

The best B_L to select will depend on circumstances. Often, it will be possible to select a B_L of less than 1 Hz. A larger value for B_L is necessary when there is significant uncertainly in the downlink Doppler dynamics, when the Sun-Earth-probe angle is small (so that solar coronal phase scintillations are present on the downlink), or when the spacecraft transmitter (such as an auxiliary oscillator) has relatively poor frequency stability.

When tracking a spinning spacecraft, it may be necessary to set the carrier loop bandwidth to a value that is somewhat larger than would otherwise be needed. The loop bandwidth must be large enough to track out the variation due to the spin. Also, the coherent AGC in the receiver must track out the amplitude variations (Coherent AGC bandwidth is one-tenth of the carrier loop bandwidth).

The user may select either a type 2 or type 3 carrier loop. Both loop types are perfect, meaning that the loop filter implements a true accumulation.

3 *Definitions*

When a subcarrier is present, the modulation index of the data on the subcarrier is normally 90° so there is no residual subcarrier. There is no performance advantage to using a residual subcarrier since the Downlink Channel was designed to track the data and ignores the presence or absence of a residual subcarrier. Throughout this document, it is assumed that the modulation index of data onto the subcarrier is 90° and all subsequent references to modulation index refer to the modulation index of the carrier.

A residual carrier is present in each of the following cases:

a) With no subcarrier, the modulation index is less than or equal to 80°,

b) With a squarewave subcarrier, the modulation index is less than 80°,

c) With a sinewave subcarrier, the peak modulation index is less than 105°.

The carrier is considered to be suppressed when the modulation is BPSK and there is either no subcarrier or a squarewave subcarrier and the modulation index is greater than 80°.

P_T is the total received signal power at the input to the low-noise amplifier. N_0 is the one-sided noise spectral density referenced to the input to the low-noise amplifier. It equals the system noise temperature (referenced to the input to the low-noise amplifier) times

Boltzmann's constant, 1.380622×10^{-23} W/(Hz·K). In decibel units, Boltzmann's constant is −198.6 dBm/(Hz·K). The ratio P_T / N_0 is a useful parameter.

When there is only a single telemetry channel present and no ranging modulation, the carrier power P_C and data power P_D are given by

$$P_C = \begin{cases} P_T \cos^2\theta, & \text{no subcarrier or squarewave subcarrier} \\ P_T \, \mathrm{J}_0^2(\theta), & \text{sinewave subcarrier} \end{cases} \tag{2}$$

$$P_D = \begin{cases} P_T \sin^2\theta, & \text{no subcarrier or squarewave subcarrier} \\ P_T \, 2\mathrm{J}_1^2(\theta), & \text{sinewave subcarrier} \end{cases} \tag{3}$$

where θ is the peak modulation index and J_0 and J_1 are Bessel functions of the first kind of orders zero and one. In the case of a sinewave subcarrier, the Downlink Channel uses the power in the fundamental harmonics (upper and lower) of the subcarrier and does not use the power in the higher-order harmonics. In this case, P_D represents the power in just these harmonics.

When there is only a single suppressed carrier and there is no ranging modulation present, the total received signal power and the data power are the same.

$$P_D = P_T, \quad \text{suppressed carrier} \tag{4}$$

If two telemetry channels are present, or if one telemetry channel and a ranging code are present, more complicated expressions are needed. For example, with two telemetry channels, each of which has a squarewave subcarrier (or one with no subcarrier and one with a squarewave subcarrier), the carrier and data powers are given by

$$P_C = P_T \cos^2\theta_1 \cos^2\theta_2 \tag{5}$$

$$P_{D1} = P_T \sin^2\theta_1 \cos^2\theta_2 \tag{6}$$

$$P_{D2} = P_T \cos^2\theta_1 \sin^2\theta_2 \tag{7}$$

where P_{D1} and P_{D2} are the data powers for the first and second telemetry channels, and θ_1 and θ_2 are the corresponding modulation indices.

If ranging modulation is present on the downlink carrier, then the equations for residual-carrier power and data power need to be adjusted to reflect the fact that some of the downlink power is being allocated to ranging signal and noise that is present in the transponder ranging channel. The proper equations to use depend on the type of ranging signal. With sequential ranging, the equations are given in Reference 3.

The input energy per bit to noise spectral density ratio (bit SNR) is

$$\frac{E_b}{N_0} = \frac{P_D}{N_0 R_{BIT}} \tag{8}$$

where R_{BIT} is the bit rate (before encoding). The energy per symbol to noise spectral density ratio (symbol SNR) is

$$\frac{E_S}{N_0} = \frac{P_D}{N_0 R_{SYM}} \tag{9}$$

where R_{SYM} is the symbol rate (after encoding). For a convolutional code with code rate r (r=1/2, 1/4, or 1/6),

$$R_{SYM} = \frac{R_{BIT}}{r} \tag{10}$$

4 Receiver Acquisition

The following paragraphs describe normal receiver acquisition. There is also a Fast Acquisition algorithm, which is applicable to telemetry with low symbol rates. Fast Acquisition, which is similar in many respects to normal acquisition, has been described in Reference 4. Guidelines for estimating the receiver acquisition times are given in this section. These guidelines apply to residual carrier and suppressed-carrier BPSK. QPSK and OQPSK normally are used only for high data rates that have very short acquisition times.

The general procedure for normal acquisition is as follows. The carrier frequency is measured by searching the downlink signal spectrum in fixed bandwidth sections using a fast Fourier transform (FFT). This is true for both suppressed-carrier downlinks and residual-carrier downlinks. With a suppressed carrier, some signal processing that precedes the FFT causes a collapse of data modulation sidebands into a tone (located at the frequency of the phantom carrier) that can be identified by the FFT. Once a tone is found, FFTs are optionally computed for the adjacent bandwidth sections in order to verify that the true tone was found, as opposed to an alias from one of these adjacent bandwidth sections. Then a confirmation FFT, centered at the detected tone, may be computed if it is thought necessary to verify that the tone was not a strong signal that was just passing through. Such a set of FFTs produces an accurate measure of the carrier frequency.

When necessary, a set of FFTs can also be computed for determining the subcarrier frequency and symbol rate. Sometimes however, it is not necessary to measure the subcarrier frequency and symbol rate, since their predicts are usually quite accurate. Next, the numerically controlled oscillator (NCO) in the carrier loop is set with the aid of the information from the FFTs, and the carrier loop is closed (enabled). In the subcarrier loop and symbol loop, the NCOs are set and the loops closed (enabled). The loop closures may be selected to occur in parallel or in series. When the loops are initially closed, the loop gain normalizations are set in

accord with available predictions; but when phase-lock is indicated by the lock detectors, the coherent AGCs are enabled, allowing loop gain normalizations to be based on the actual received signal. This means that the power predicts are only required for acquisition.

4.1 FFT

The FFT is an optional part of the acquisition process. It is only needed when the signal's frequency uncertainty is greater than one-half the initial loop bandwidth of the tracking loop. Often, only the carrier loop requires the computation of FFTs. The subcarrier and symbol frequencies are usually well enough known that they need not be measured with FFTs.

An FFT takes a sequence of data points as its input. The sample frequency of these data points, here denoted f_s, depends in general on the type of data being processed and the symbol rate. Permissible values of f_s are given in Table 3. R_{SYM} is the symbol rate and R_{QSYM} is the quaternary channel symbol rate for QPSK/OQPSK.

For the residual-carrier FFT, f_s is independent of the tracking loop update rate and is selectable by the user from one of the values given in Table 3. (The most commonly used values are 10 kHz, 50 kHz, and 100 kHz.)

For the suppressed-carrier FFT, f_s is selectable by the user from the same set of values as for the residual-carrier case. However, f_s cannot exceed the symbol rate, R_{SYM}.

For the QPSK/OQPSK FFT, f_s is selectable by the user from the same set of values as for the residual-carrier case. However, f_s cannot exceed the symbol rate, R_{QSYM}.

Table 3. FFT Sample Frequencies

Data Type	Sample Frequency
Residual Carrier	2, 5, 10, 20, 50, 100, 200, 500, 1000, or 2000 kHz
Suppressed Carrier	Same as above if $f_S < R_{SYM}$; else R_{SYM}
QPSK and OQPSK	Same as above if $f_S < R_{QSYM}$; else R_{QSYM}
Subcarrier	minimum of 500 Hz and R_{SYM}
Symbol	minimum of 500 Hz and R_{SYM}

In general, a number of FFTs may need to be computed before the signal is found. The search bandwidth is explored in sections, with one FFT computed for each section. A section is selected by an appropriate setting of the NCO. This setting determines the center of the section. The bandwidth of each section is determined by the data type and by f_S, as shown in Table 4.

Table 4. FFT Section Bandwidths

Data Type	Section Bandwidth	Section Bandwidth Limits
Residual Carrier	f_S	$-f_S/2 \rightarrow +f_S/2$
Suppressed Carrier	$f_S/2$	$-f_S/4 \rightarrow +f_S/4$
QPSK and OQPSK	$f_S/4$	$-f_S/8 \rightarrow +f_S/8$
Subcarrier	$f_S/2$	$-f_S/4 \rightarrow +f_S/4$
Symbol	$f_S/2$	$-f_S/4 \rightarrow +f_S/4$

The tone representing the carrier (or subcarrier or symbol rate) will be considered detected within a given section when the corresponding FFT indicates the presence of a tone for which the power level falls within an acceptance range centered on the predicted tone power. The acceptance range is characterized by a lower limit delta, δ_{lower} in decibels and an upper limit delta, δ_{upper}, in decibels. The user will select the two parameters δ_{lower} and δ_{upper}.

Even after a tone is initially detected, more FFTs will, in general, be computed. An FFT for each of two adjacent sections is computed in order to check for aliases. Such an alias check is, however, optional; if the frequency predictions are quite good, the alias checks are unnecessary.

There is also an optional confirmation check. This consists of one FFT that is computed with the NCO set to the tone value detected in the previous FFTs. It is used to verify that the detected tone was not a noise spur (for weak signal acquisitions) and that the tone was not a very strong signal that was simply passing through.

The number of data points that should be selected for input to a particular FFT computation will depend on the predicted tone power. The algorithm that should be used in determining the number of data points is summarized here.

$$\text{Number of Data Points} = 2^M \tag{11}$$

M, the base 2 logarithm of the number of data points, is given by

$$M = \max\left\{9, \left\lceil 4.817 - 3.581 \cdot \log_{10}\left(\frac{P_{CTP}}{N_0} \cdot \frac{1}{f_S}\right)\right\rceil\right\} \tag{12}$$

where $\log_{10}(*)$ is the base 10 logarithm and $\lceil\cdot\rceil$ is the ceiling function. The ceiling function equals the smallest integer not less than its argument. The smallest permissible value for M is 9, corresponding to 2^9 (512) data points. P_{CTP}/N_0 is the computed tone power to noise spectral density ratio as calculated with Equation (13) for residual-carrier FFT or with Equation (14) for all other FFTs (see below). Figures 2 and 3 illustrate the dependence of the integer M on P_{CTP}/N_0 for f_s = 2000 Hz and f_s = 20 Hz, respectively.

For the FFT that measures the carrier frequency of a residual-carrier downlink, P_{CTP}/N_0 is given by

$$\frac{P_{CTP}}{N_0} = \left(10^{\delta_{lower}/10}\right) \cdot \frac{P_C}{N_0} \cdot \mathrm{sinc}^2\left(\frac{1}{2F_{ZP}}\right), \quad \text{residual - carrier FFT} \tag{13}$$

where δ_{lower} is a (negative) number representing the delta, in decibels, between the lower limit on acceptance and the predicted tone power level. P_C/N_0 is the residual carrier power-to-noise spectral density ratio. The sinc(∗) function is: $\mathrm{sinc}(x) = \sin(\pi x)/(\pi x)$. F_{ZP} is the zero pad factor. When $F_{ZP} = 1$, there is no zero padding in the FFT. When $F_{ZP} = 2$, there are as many zeros padded to the end of the data points as there are data points. The size of the sequence that is input to the FFT equals F_{ZP} times the number of data points.

For all other FFTs (i.e., for all FFTs except that for the carrier frequency of a residual-carrier downlink), P_{CTP}/N_0 is given by

$$\frac{P_{CTP}}{N_0} = \left(10^{\delta_{lower}/10}\right) \cdot \frac{R_{SYM}\left(E_S/N_0\right)}{\alpha_1 + \alpha_2\left(E_S/N_0\right)^{-1}} \cdot \frac{P_C}{N_0} \cdot \mathrm{sinc}^2\left(\frac{1}{2F_{ZP}}\right), \text{ all other FFTs} \tag{14}$$

where R_{SYM} is the symbol rate, and E_s/N_0 is the predicted energy per symbol to noise spectral density ratio. The coefficients α_1 and α_2 depend on the particular FFT. Table 5 lists these values. For example, for an FFT that is computed in order to identify the symbol rate, the coefficients α_1 and α_2 are 390 and 880, respectively, when there is a squarewave subcarrier present. For all loops besides the residual-carrier loop, the data modulation sidebands are employed. That is the reason Equation (14) is more complicated than Equation (13). Equation (14) is valid under the assumption that all loops are slipping (i.e., that none of the loops have acquired phase-lock) as the data points are being collected. If some loops have acquired phase-lock before the data points are collected for subsequent FFTs, then the P_{CTP}/N_0 given in Equation (14) will be somewhat pessimistic for these subsequent FFTs. Equations (13) and (14) are based on modifications to the theory presented in Reference 4. (The modifications are necessary since the theory of Reference 4 is for the Fast Acquisition algorithm, which is not described in this module.)

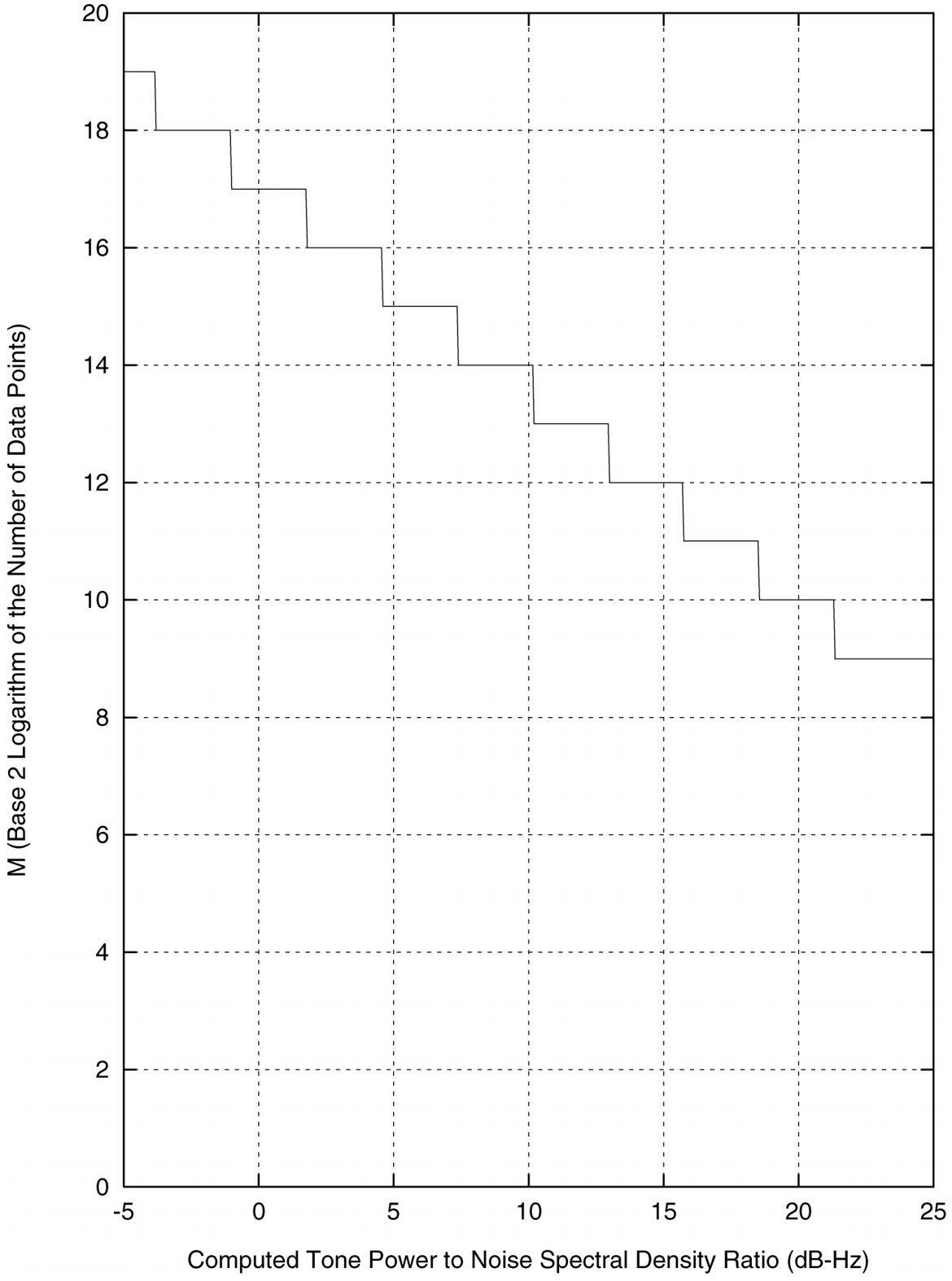

Figure 2. Number of Data Points for FFT; Sample Rate = 2000 Hz

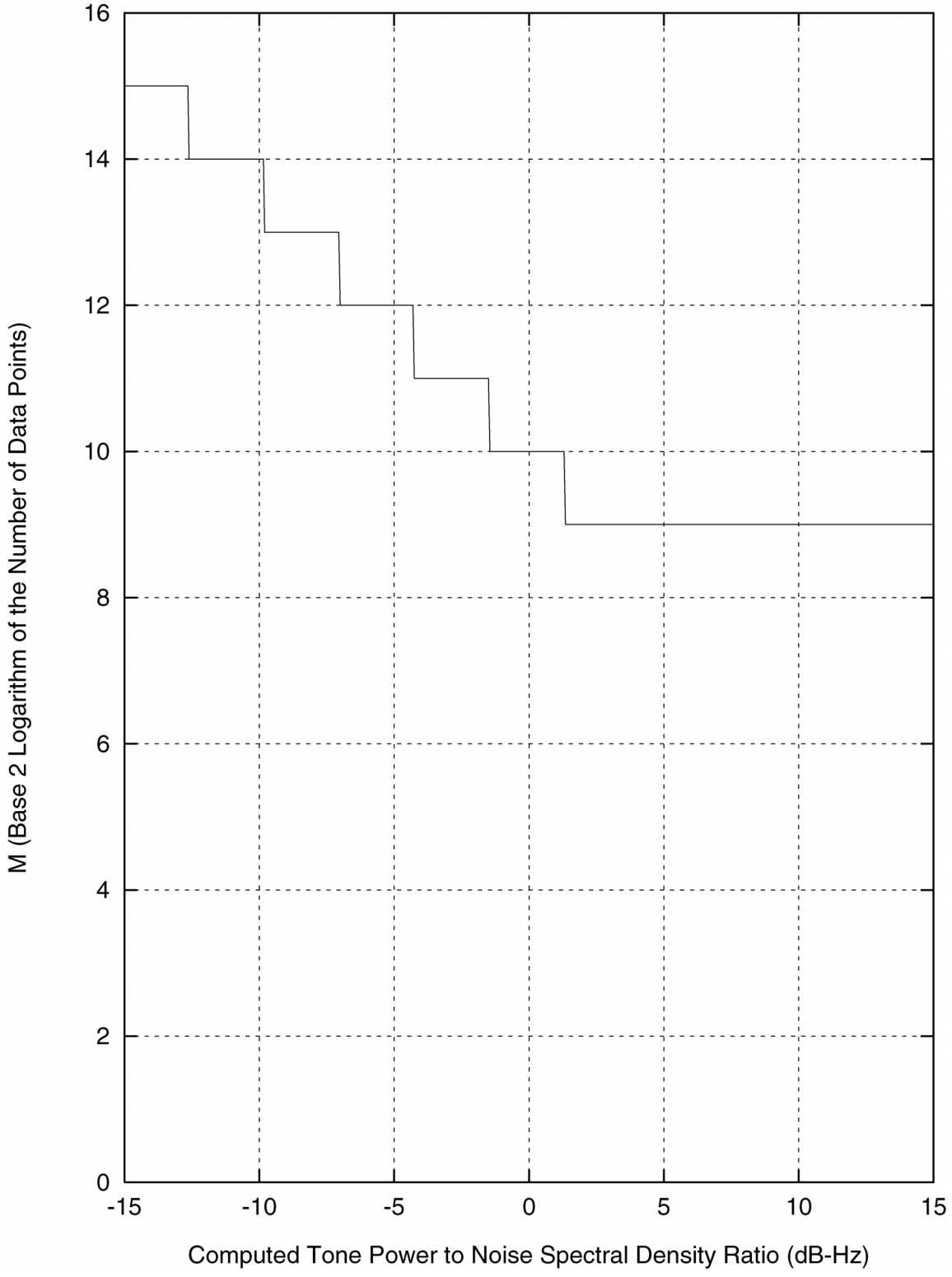

Figure 3. Number of Data Points for FFT; Sample Rate = 20 Hz

Table 5. Coefficients α_1 and α_2 in the Calculation of P_{CTP}/N_0

FFT	Subcarrier	α_1	α_2
Suppressed Carrier	none	6	4.5
Suppressed Carrier	square	18	41
QPSK and OQPSK	none	46	145
Subcarrier	square	18	41
Subcarrier	sine	12	18
Symbol	none	130	100
Symbol	square	390	880
Symbol	sine	260	390

4.2 Loop Locking

Once the carrier frequency has been found, the NCO in the carrier loop is set to the detected frequency and the carrier loop is closed (enabled). The loop starts at an initial bandwidth. The loop phase error, initially large, diminishes with time through the natural feedback action of the loop. Once phase-lock is declared at this bandwidth, the loop bandwidth is gradually reduced to its final value — the desired operational value — in a manner consistent with the retention of phase-lock. When the final bandwidth has been achieved and the degradation to effective signal level resulting from transient phase errors just drops below 0.1 dB, the loop is considered to be acquired. The initial and final bandwidths are controlled by the user, as are the parameters that control the rate at which the bandwidth is narrowed. Starting with loop closure, the time it takes for the lock detector to indicate phase-lock at the final bandwidth is approximately ten times the reciprocal of the final bandwidth. For purposes of estimating acquisition time, however, it is recommended that twenty times the reciprocal of the final loop bandwidth be used. This admits the possibility that phase-lock is not indicated in the first lock detection period. The final step in the procedure is for the coherent AGC loop to be enabled, providing an accurate estimate of the loop normalization constant.

The locking of the subcarrier and symbol loops is a similar process to that described in the previous paragraph for the carrier loop. The subcarrier and symbol loops may either be closed (enabled) at the same time that the carrier loop is closed (enabled) or be closed after the carrier loop has indicated phase-lock. It is the user's choice. In the former case, all three loops are simultaneously trying to achieve phase-lock. For the (squarewave) subcarrier and symbol loops, there is also a transition window, which has an initial value, a final value, and a parameter that controls the rate of narrowing.

4.3 Acquisition Time

The total receiver acquisition time is estimated as a sum of two components: the time required for the FFT stage of the acquisition process and the time required for locking the loops.

There is a time associated with the collection of enough data points as required for each FFT. For a given FFT, this time equals the number of data points divided by the sample frequency.

$$\text{Time for each FFT} = \frac{2^M}{f_S} \tag{15}$$

where M is given by Equation (12). For the carrier FFT, the time required to actually compute an FFT is often small compared with the time it takes to collect the data points for input to that FFT. (The time it takes to pad an input sequence with zeros is also small.) Hence, it is often a good approximation to use Equation (15) to estimate the time it takes to produce one FFT.

It is necessary to consider how many FFTs might be required and to sum together the individual FFT times in order to estimate the time spent on the FFT stage of the acquisition process. Consideration must be given to whether subcarrier or symbol FFTs will be required. Often, it is not necessary to compute FFTs in support of subcarrier and symbol acquisition. In the best possible scenario, in which carrier frequency, subcarrier frequency and symbol rate are all very accurately characterized by predicts, no FFTs are required. In a more typical scenario, however, at least two FFTs will be required for the carrier: an initial FFT and a confirmation FFT. In some cases, more FFTs will be required for carrier acquisition: the search bandwidth may be larger than a single section bandwidth and alias checking may be required.

A second component of receiver acquisition time is the time required for the loops to lock once their NCOs have been set. For each loop, phase-lock will be achieved and duly indicated by the lock detector in a time that may be estimated as

$$\text{Time for each loop} = \frac{20}{B} \tag{16}$$

where B represents the final loop bandwidth of the loop in question (carrier, subcarrier, or symbol). The numerator in this estimate is twenty, rather than ten, allowing for the possibility that phase-lock is not indicated in the first lock detection period. Figure 4 illustrates this dependence. If the loops are acquired in parallel, the loop-locking component of receiver acquisition time may be estimated from Equation (16) with the smallest of all loop bandwidths substituted for B. Typically, the smallest loop bandwidth is that of the symbol loop. If the loops are acquired in series, the loop-locking component of receiver acquisition time may be estimated as the sum of the individual loop-locking times, each of which may be estimated from Equation (16) with the substitution of the appropriate loop bandwidth. In general, the following factors will influence the user's choice of loop bandwidths: P_T/N_0, Doppler dynamics, oscillator stability, and acquisition time. For example, larger values of P_T/N_0 will permit larger loop bandwidths (for more details, see paragraph 5).

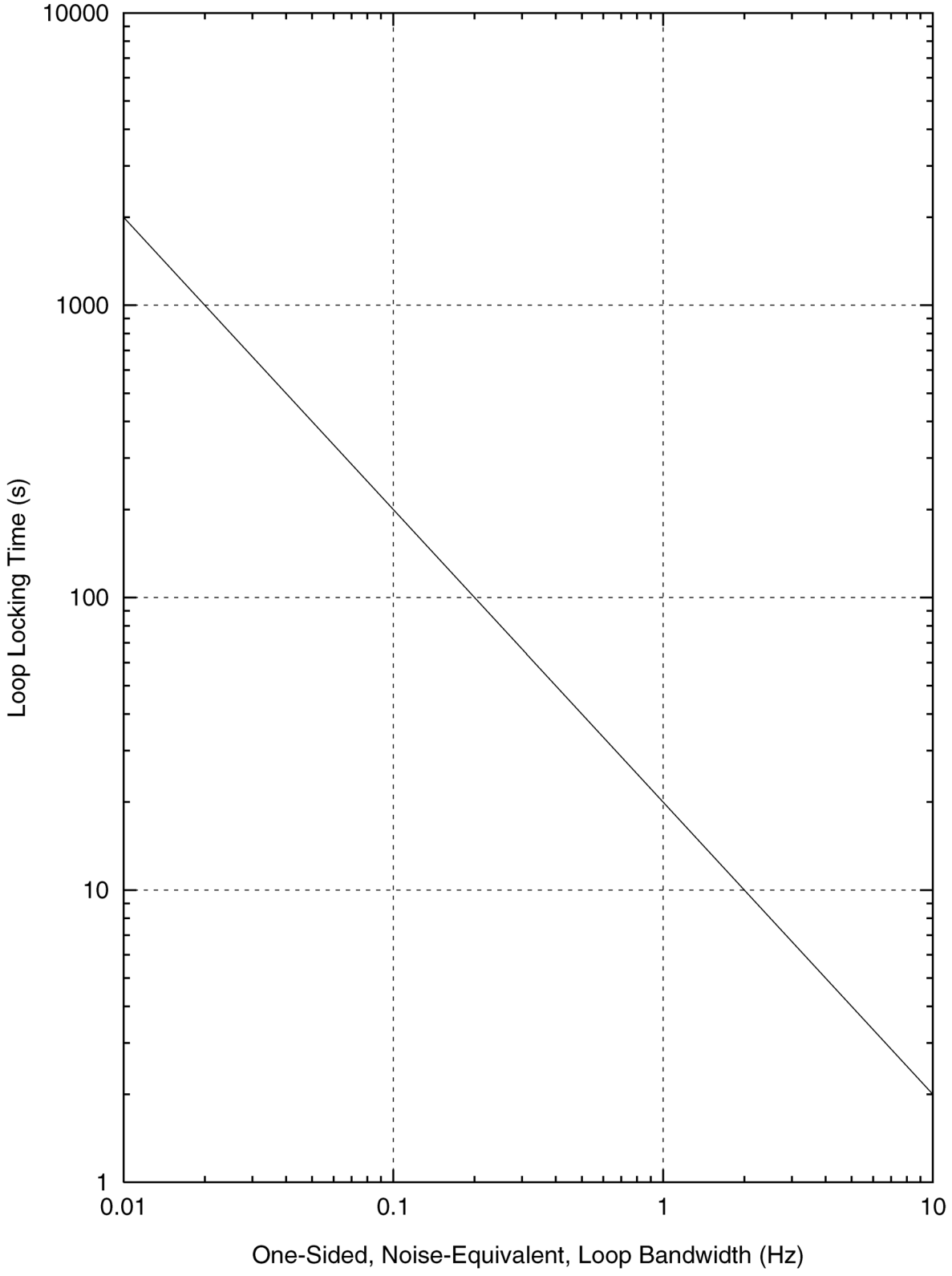

Figure 4. Loop Locking Time

For many applications, the receiver acquisition time will be one minute or less. This will be particularly true when the symbol rate is large and no particularly narrow loop bandwidths are employed. In such cases, it will not be necessary to estimate beforehand the receiver acquisition time. In other cases, particularly for small symbol rates and narrow loop bandwidths, it will take several minutes to accomplish receiver acquisition; and it may be important to characterize the receiver acquisition time with some degree of accuracy. Under such circumstances the discussion and equations of this paragraph should be used as a guide.

It would be very difficult to provide here a set of curves characterizing receiver acquisition time for all potential cases of interest. There are just too many possibilities. Not only are there a number of important variables (symbol rate, signal-to-noise ratio, loop bandwidths, quality of frequency predictions) with large dynamic ranges, but the flexibility of the Downlink Channel permits a wealth of different acquisition strategies. Alias-check FFTs and confirmation-check FFTs may or may not be used. Subcarrier FFTs and symbol rate FFTs may or may not be used. The loops may be acquired in parallel, in series, or in some other combination. (For example, the carrier loop might be acquired first, then the subcarrier and symbol loops might be acquired in parallel.) Although it is not practical to provide curves for all potential cases of interest, three sets of curves are provided in order to illustrate how receiver acquisition time varies with certain key parameters.

Figures 5, 6, and 7 show receiver acquisition time for a very specific set of assumptions. For all three of these figures, the frequency predicts are good enough that only two carrier FFTs (an initial FFT and a confirmation-check FFT) are necessary and that no subcarrier or symbol rate FFT is required. Furthermore, it is assumed that the loops are acquired in parallel. For these figures the receiver acquisition time is calculated as twice the "Time for each FFT", as given by Equation (15), plus $20/B$, where B is the smallest loop bandwidth (typically the symbol loop bandwidth). The integer M in Equation (15) is calculated from Equations (12) and (13) or (14). F_{ZP} is taken to be 1 (i.e., no zero padding) and δ_{lower} taken to be −2 dB.

Figure 5 shows the receiver acquisition time (in seconds) for a residual-carrier downlink as a function of P_C/N_0 with B, the smallest loop bandwidth, as a parameter. The frequency predicts have to be reasonably good to achieve the acquisition times shown in this figure: the carrier must lie within the section bandwidth of the first FFT and the subcarrier frequency and symbol rate must be well enough known to obviate the need for their measurement.

Figure 6 shows the receiver acquisition time (in seconds) for a suppressed-carrier downlink as a function of R_{SYM} with B, the smallest loop bandwidth, as a parameter. The energy per symbol to noise spectral density ratio is –3 dB. The frequency predicts have to be reasonably good to achieve the acquisition times shown in this figure: the collapsed carrier tone must lie within the section bandwidth of the first FFT, and the subcarrier frequency and symbol rate must be well enough known to obviate the need for their measurement.

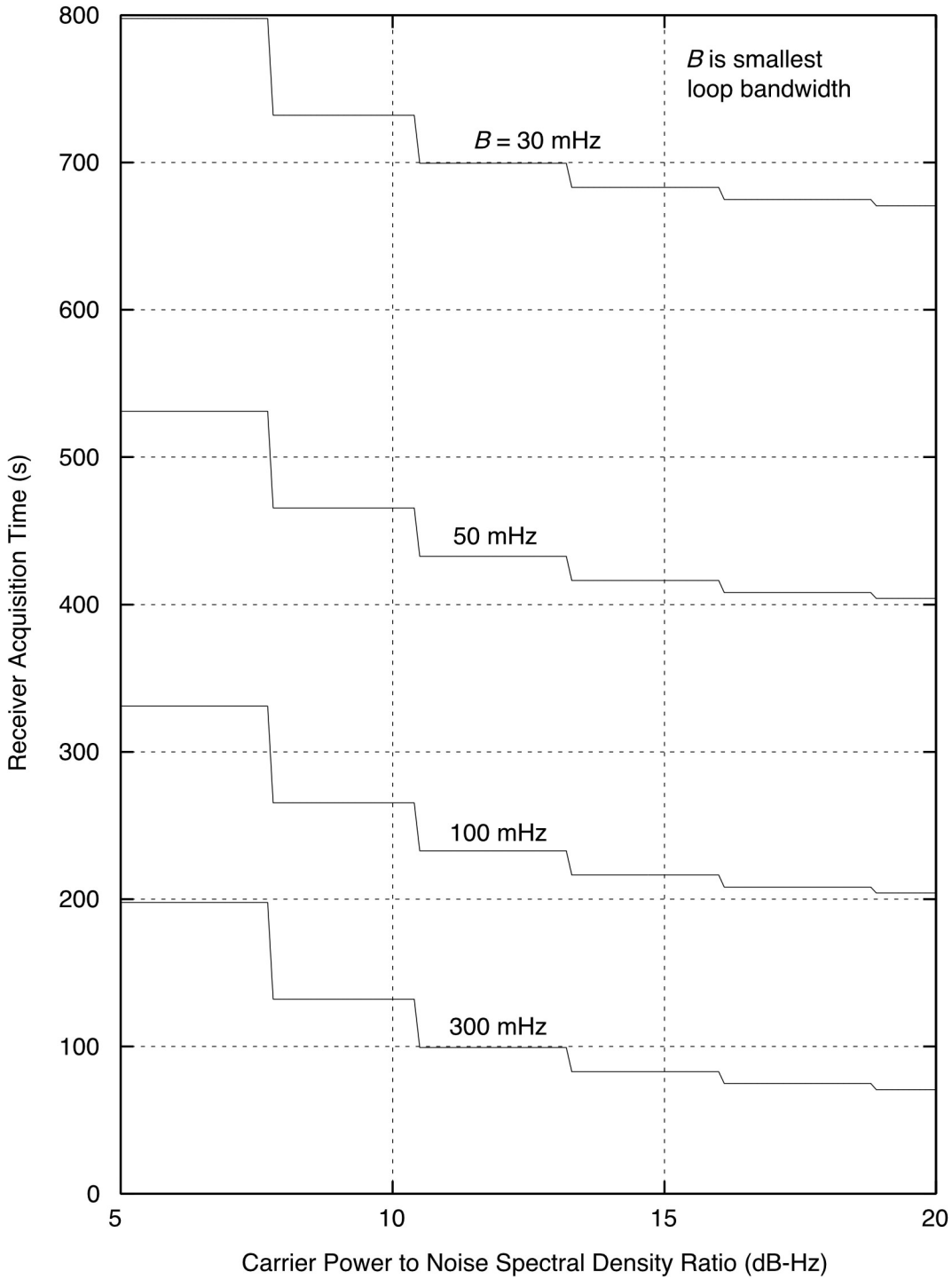

Figure 5. Receiver Acquisition Time; Residual Carrier

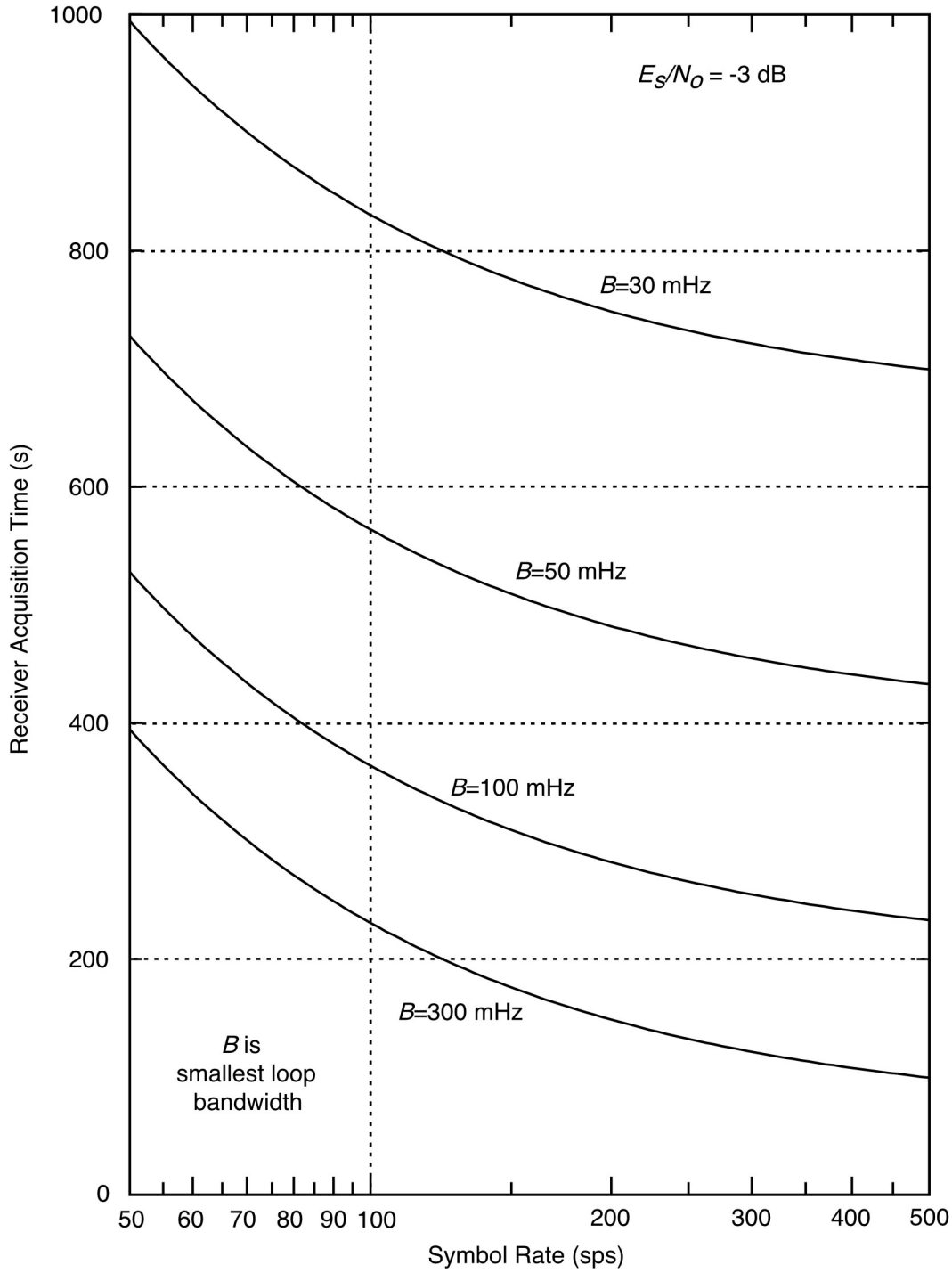

Figure 6. Receiver Acquisition Time; Suppressed Carrier, $E_s/N_0 = -3$ dB

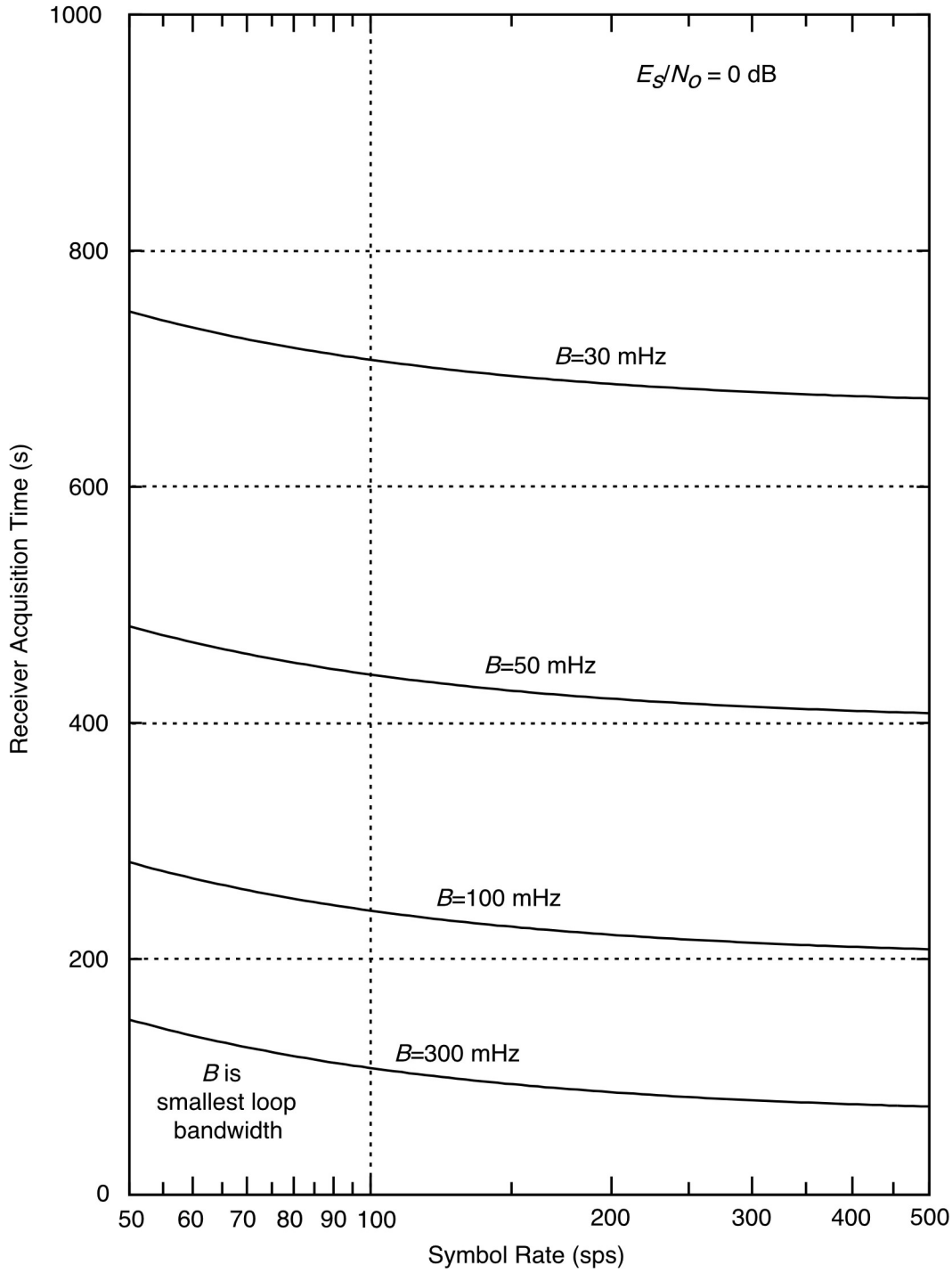

Figure 7. Receiver Acquisition Time; Suppressed Carrier, E_s/N_0 = 0 dB

Figure 7 shows the receiver acquisition time (in seconds) for a suppressed-carrier downlink as a function of R_{SYM} with B, the smallest loop bandwidth, as a parameter. The energy per symbol to noise spectral density ratio is 0 dB. The frequency predicts have to be reasonably good to achieve the acquisition times shown in this figure: the collapsed carrier tone must lie within the section bandwidth of the first FFT, and the subcarrier frequency and symbol rate must be well enough known to obviate the need for their measurement.

A comparison of Figures 5, 6, and 7 reveals that the receiver acquisition time increases as the symbol rate decreases, the signal-to-noise ratio decreases, or the loop bandwidths decrease. Also, the receiver acquisition time for suppressed-carrier operation will generally be larger than for residual-carrier operation.

5 Telemetry Performance

In general, four signal-to-noise ratios affect telemetry performance: the energy per bit to noise spectral density ratio and the signal-to-noise ratios in each of the three synchronization loops (carrier, subcarrier, and symbol). In some cases (especially with a suppressed carrier) there will be no subcarrier present. In order for telemetry to be supported at a given bit rate, P_T/N_0 must be large enough that these four (or three, if there is no subcarrier) signal-to-noise ratios are adequate. The following paragraphs offer guidance in this matter.

5.1 Comparison of Residual Carrier and Suppressed Carrier

The relative telemetry performance of residual-carrier operation and suppressed-carrier operation depends strongly on the bit rate. One scheme is said to have better telemetry performance than the other when it has a smaller required P_T/N_0 for the support of a given bit rate at a given threshold FER. In general, residual carrier has the better telemetry performance for the very low bit rates and especially for low bit rates coupled with larger carrier loop bandwidths (as would be necessary in the presence of significant phase noise or uncompensated Doppler dynamics). For intermediate bit rates, suppressed carrier offers a significant telemetry performance advantage over residual carrier. For high bit rates, suppressed carrier offers a telemetry performance advantage, but it is only about 0.1 dB. Of course, there will be times in which the decision between residual carrier and suppressed carrier is made on grounds having nothing to do with telemetry performance. For example, a residual carrier is sometimes needed for a radio science experiment. Also, in some applications it will important to minimize acquisition time. Then, the choice of residual carrier or suppressed carrier will be based on whichever scheme offers the quicker acquisition.

Figure 8 shows a typical case. It compares the required P_T/N_0 as a function of bit rate R_{BIT} for residual-carrier and suppressed-carrier operation in the case where a (1784, 1/3) turbo code is employed and the threshold FER is 1×10^{-4}. Three carrier loop bandwidths are considered: 0.5 Hz, 1 Hz, and 2 Hz.

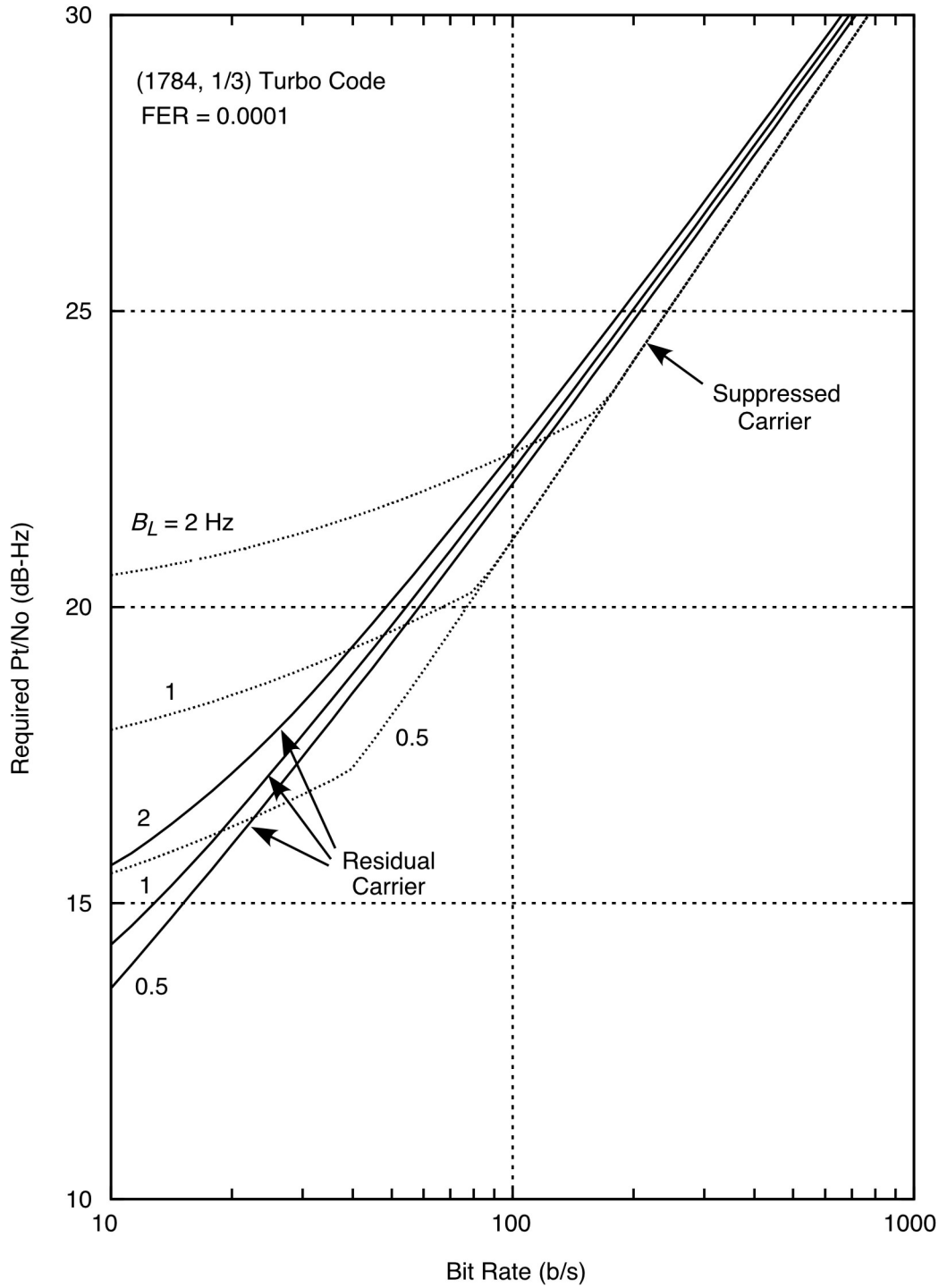

Figure 8. Comparison of Residual Carrier and Suppressed Carrier

For Figure 8, it has been assumed that there is no additional phase noise present in the carrier loop beyond that resulting from thermal noise. The required P_T/N_0 is, in this case, the minimum P_T/N_0 that simultaneously meets each of the following four constraints. First, the carrier loop signal-to-noise ratio (ρ_L, see paragraph 5.3) must be at least 10 dB if tracking a residual carrier or at least 17 dB if tracking a suppressed carrier. Second, the squarewave subcarrier loop signal-to-noise ratio (ρ_{SUB}, see paragraph 5.4) must be at least 20 dB. Third, the symbol loop signal-to-noise ratio (ρ_{SYM}, see paragraph 5.5) must be at least 15 dB. Fourth, the product $\eta_{SYS} \cdot E_b/N_0$ must be at least 0.8 dB, where η_{SYS} is system loss. For each residual-carrier performance curve, it is assumed that at each point on the curve the optimum modulation index is used. The subcarrier loop bandwidth and window factor are assumed to be 50 mHz and 0.25, respectively. The symbol loop bandwidth and window factor are assumed to be 50 mHz and 0.25, respectively.

For the case represented in Figure 8 with B_L = 0.5 Hz, residual carrier offers better telemetry performance than suppressed carrier for bit rates less than 20 bps, and suppressed carrier is better for bit rates greater than 20 bps. With B_L = 1 Hz, the performances of residual carrier and suppressed carrier cross at 50 bps. With B_L = 2 Hz, they cross at 100 bps. These numbers are specific to the example considered here. However, the essential qualitative features of the curves shown in Figure 8 are true in general. Residual carrier is better at low bit rates, suppressed carrier is better at intermediate bit rates, and there is not much difference at high bit rates. The bit rate for which the two performance curves cross increases with carrier loop bandwidth.

The reason residual carrier performs better than suppressed carrier at the low bit rates is because a residual-carrier loop is not subject to half-cycle slips. A suppressed-carrier loop, on the other hand, can slip a half-cycle and therefore requires a higher carrier loop signal-to-noise ratio in order to guard against these damaging slips. (A residual-carrier loop can slip a whole cycle, but this is both less likely and less damaging than a half-cycle slip.)

In order to get the best performance from residual-carrier operation, it is necessary that the modulation index be optimal or, at least, near optimal. Each residual-carrier performance curve of Figure 8 is based on the assumption that the modulation index is optimized at each point on the curve. Figure 9 shows what happens if this is not the case. In Figure 9, the lower curve (with the better telemetry performance) is the same as the residual-carrier curve with B_L = 1 Hz of Figure 8, with an optimized modulation index at each point on the curve. The upper curve of Figure 9 represents residual-carrier performance with B_L = 1 Hz under all the same circumstances except that the modulation index is not optimized at each point on the curve; instead, a single modulation index of 54° (the optimum modulation index for a bit rate of 10 bps) is used for the entire curve. The two curves of Figure 9 coalesce at R_{BIT} = 10 bps but, for R_{BIT} greater than 10 bps, a penalty is paid for not using the appropriate optimum modulation index. At R_{BIT} = 1000 bps, the penalty is about 2 decibels.

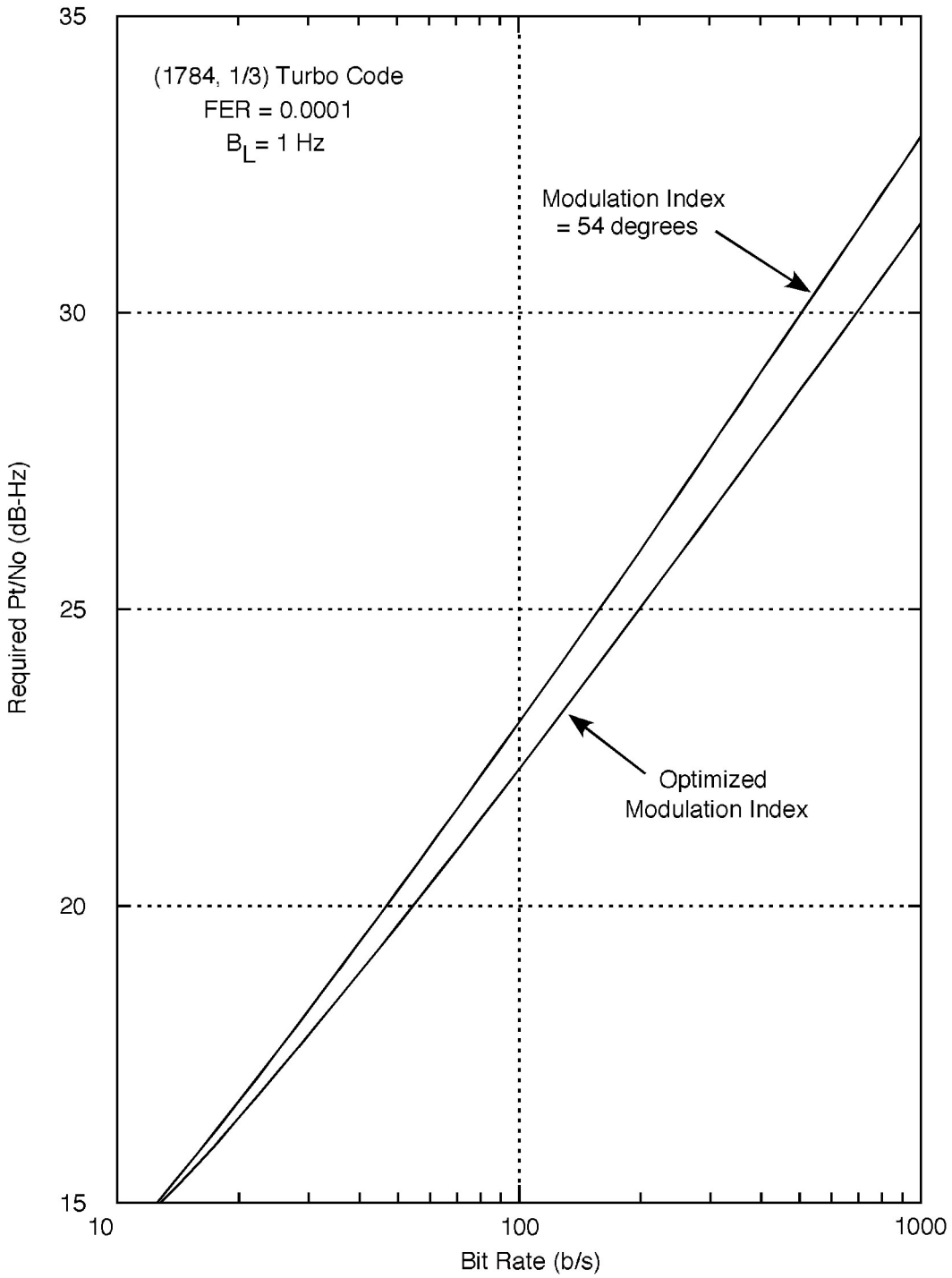

Figure 9. Comparison of Optimized and Non-optimized Modulation Index

5.2 *Decoding Threshold and System Loss*

Telemetry will not be properly decoded unless the product $\eta_{SYS} \cdot E_b/N_0$ (the effective E_b/N_0 after the available E_b/N_0 has been reduced by system losses) is greater than or equal to the effective threshold energy per bit to noise spectral density ratio, f^{-1}(BER) or f^{-1}(FER), that is required by the coding scheme. η_{SYS} is the system loss, BER is the threshold bit error rate, FER is the threshold frame error rate, and $f(*)$ is the ideal functional dependence of probability of bit (or frame) error on bit SNR (see Appendix A).

Table 6 lists the effective threshold energy per bit to noise spectral density ratio, f^{-1}(BER), in decibels, that is required by an uncoded link and by each of three different convolutionally coded links. These baseline values are valid for residual carrier, suppressed-carrier BPSK, and QPSK or OQPSK.

Table 6. Baseline E_b/N_0 for Uncoded and Convolutionally Coded Data, dB

Code	Threshold Bit Error Rate			
	5×10^{-3}	10^{-3}	10^{-4}	10^{-5}
Uncoded	5.2	6.8	8.4	9.6
(k=7, r=1/2)	2.3	3.0	3.8	4.5
(k=15, r=1/4)	0.5	0.9	1.5	2.0
(k=15, r=1/6)	0.3	0.7	1.3	1.8

Table 7 lists the effective threshold energy per bit to noise spectral density ratio, f^{-1}(FER), for a concatenated code (a Reed-Solomon outer code with one of two convolutional inner codes, the combination achieving a threshold frame error rate of 10^{-5}) using residual carrier, suppressed-carrier BPSK, QPSK and OQPSK. A frame error rate (as opposed to a bit error rate) is used because decoding failures of block-coded data result in the loss of the entire codeblock or data frame.

Table 7. Effective Threshold E_b/N_0 for Concatenated Codes, dB

Concatenated Code	FER	10 log [f^{-1} (FER)]
RS with (k=7, r=1/2) convolutional	1×10^{-5}	2.38 dB
RS with (k=15, r=1/4) convolutional	1×10^{-5}	1.24 dB
RS with (k=15, r=1/6) convolutional	1×10^{-5}	1.04 dB

Table 8 lists the effective threshold energy per bit to noise spectral density ratio, f^{-1}(FER), for a turbo-coded link in order to achieve a frame error rate of 1×10^{-4} using residual carrier, suppressed-carrier BPSK, QPSK or OQPSK. A frame error rate is used because turbo decoding failures result in the loss of the entire codeblock or data frame. The threshold FER specified with each turbo code is considered to be representative of what should be expected from a telecommunications link using that code.

Table 8. Effective Threshold E_b/N_0 for Turbo Codes, dB

Turbo Code	10 log [f^{-1} (FER)]	Turbo Code	10 log [f^{-1} (FER)]
(1784, 1/2)	1.5 dB	(7136, 1/2)	1.1 dB
(1784, 1/3)	0.8 dB	(7136, 1/3)	0.4 dB
(1784, 1/4)	0.6 dB	(7136, 1/4)	0.3 dB
(1784, 1/6)	0.3 dB	(7136, 1/6)	0.0 dB
(3568, 1/2)	1.3 dB	(8920, 1/2)	1.1 dB
(3568, 1/3)	0.6 dB	(8920, 1/3)	0.4 dB
(3568, 1/4)	0.4 dB	(8920, 1/4)	0.2 dB
(3568, 1/6)	0.1 dB	(8920, 1/6)	–0.1 dB

The system loss η_{SYS} ($0 < \eta_{SYS} < 0.93$) is a composite factor used in communication link budgets to account for the following influences on telemetry efficiency: imperfect carrier, subcarrier, and symbol synchronization, and waveform distortion.

$$\eta_{SYS} = \min\{0.93, \eta_{RADIO} \cdot \eta_{SUB} \cdot \eta_{SYM} \cdot \eta_{WD}\} \tag{17}$$

where η_{RADIO} is radio loss, η_{SUB} is subcarrier demodulation loss, η_{SYM} is symbol synchronization loss, and η_{WD} is waveform distortion loss. The models for the four loses are given in paragraphs 5.3.5 (Radio Loss), 5.4 (Subcarrier Synchronization), 5.5 (Symbol Synchronization) and 5.6 (Waveform Distortion). The component losses are estimated separately and the results multiplied (or their decibel equivalents added) to get the composite system loss. If the product of the component losses is not less than 0.93, then η_{SYS} should be estimated as 0.93 (i.e., $-10\log\eta_{SYS}$ = 0.3 dB).

5.3 Carrier Synchronization

Three different algorithms are used for carrier synchronization, depending on whether the tracking is residual carrier, suppressed-carrier BPSK, or QPSK/OQPSK.

5.3.1 Residual Carrier

A residual-carrier signal can be tracked whether or not there is a subcarrier (squarewave or sinewave) present and whether the symbols are non-return-to-zero or Bi-phase. When tracking a residual carrier, the carrier loop signal-to-noise ratio is

$$\rho_L = \frac{P_C}{N_0 B_L}. \tag{18}$$

There is an additional loss to the carrier loop signal-to-noise ratio when tracking a residual carrier with non-return-to-zero symbols in the absence of a subcarrier. This loss is due to the presence of data sidebands overlaying the residual carrier in the frequency domain and therefore increasing the effective noise level for carrier synchronization. ρ_L, in this case, must be calculated as (Reference 5)

$$\rho_L = \frac{P_C}{N_0 B_L} \cdot \frac{1}{1 + 2\,E_S / N_0}. \tag{19}$$

The model of Equation (19) is valid when the data bits are balanced. If the data bits are unbalanced (an unequal number of logical ones and zeroes), non-return-to-zero, and directly modulate the carrier (that is, no subcarrier), there will be a phase bias in the residual-carrier tracking loop that causes an additional loss in telemetry demodulation. This loss can be as great as 2 dB.

Imperfect carrier synchronization results in a higher bit error probability for the recovered telemetry data than would be the case if perfect tracking could be achieved. Radio loss is a measure of this discrepancy between the ideal and what is achieved in practice. Figures 10 through 19 show the effect of radio loss with residual carrier. Figure 10 is for uncoded telemetry. Figures 11, 12, and 13 are for convolutionally coded (k=7, r=1/2), (k=15, r=1/4) and (k=15, r=1/6) telemetry. Figures 14 and 15 are for concatenated codes using a Reed-Solomon outer code with either a (k=7, r=1/2) or (k=15, r=1/6) convolutional inner code. Figures 16, 17, 18, and 19 are for turbo-coded (1784, 1/2), (1784, 1/3), (8920, 1/4) and (8920, 1/6) telemetry. Turbo codes have an error floor in their performance that is not shown in these figures. The error floor is different for each code but, for each of the turbo codes shown here, the error floor lies below a frame error rate of 10^{-5} and therefore is not visible in the figure. Great care must be taken in evaluating the performance of these codes for frame error rates of less than 10^{-5}.

For the last six figures (14 through 19) the ordinate is Frame Error Rate rather than Bit Error Rate. For all figures, it has been assumed that subcarrier synchronization, symbol synchronization, and waveform symmetry are perfect and that transmitter and solar phase noise is negligible. Furthermore, it has been assumed that the bit rate is very large compared with the carrier loop bandwidth. The purpose of these six figures is to show the effect of imperfect carrier synchronization (due to thermal noise and static phase error) on telemetry performance. Appendix B summarizes the theory upon which the curves of Figures 10 through 19 are based.

The radio loss as a positive, decibel quantity (i.e., $-10\log\eta_{RADIO}$) is simply the horizontal distance between the baseline curve and the curve that represents performance in the presence of imperfect carrier synchronization. In comparing several curves from any one figure, it is evident that radio loss is a function of both ρ_L and the threshold BER (FER). In comparing different figures, it is evident that radio loss is a function of the coding scheme.

In each of Figures 10 through 19, there are three curves, corresponding to static phase errors of 0, 3, and 5 degrees, for each value of ρ_L. Static phase error is caused by uncompensated Doppler dynamics (Appendix C).

With residual-carrier tracking it is important to make an optimal selection of the modulation index. In general, the optimum value for modulation index is a function of the bit rate, the carrier loop bandwidth, the coding scheme, and the threshold BER. Figure 20 shows the optimum modulation index for uncoded telemetry. Figures 21 and 22 show the optimum modulation index for convolutionally coded (k=7, r=1/2) and (k=15, r=1/6) telemetry, respectively. The optimum modulation index for convolutionally coded (k=15, r=1/4) and (k=15, r=1/6) are approximately the same. Figure 23 shows modulation indices that are approximately optimum for use with any of the sixteen turbo codes listed in Table 8. For concatenated codes, it is recommended that the optimum modulation for the inner (convolutional) code be selected. Figures 20 through 23 are all based on the assumption that the carrier loop phase error variance is determined by thermal noise. If significant external phase noise is present, such as phase noise from the transmitter or phase scintillations from the solar corona, the optimum modulation index must be reconsidered.

The curves of Figures 20 through 23 are defined by two constraints: ρ_L should be greater than or equal to 10 dB and the product $\eta_{RADIO} \cdot E_b/N_0$ should be greater than the threshold effective energy per bit to noise spectral density ratio. Moreover, for effective residual-carrier tracking the modulation index must be no larger than 80 degrees.

Sometimes, it is important to take transmitter and solar phase noise into account. This is especially true for operation close to the Sun or for one-way or two-way noncoherent operation with an Auxiliary Oscillator (or some oscillator, serving as the source of the downlink carrier, that has relatively poor frequency stability).

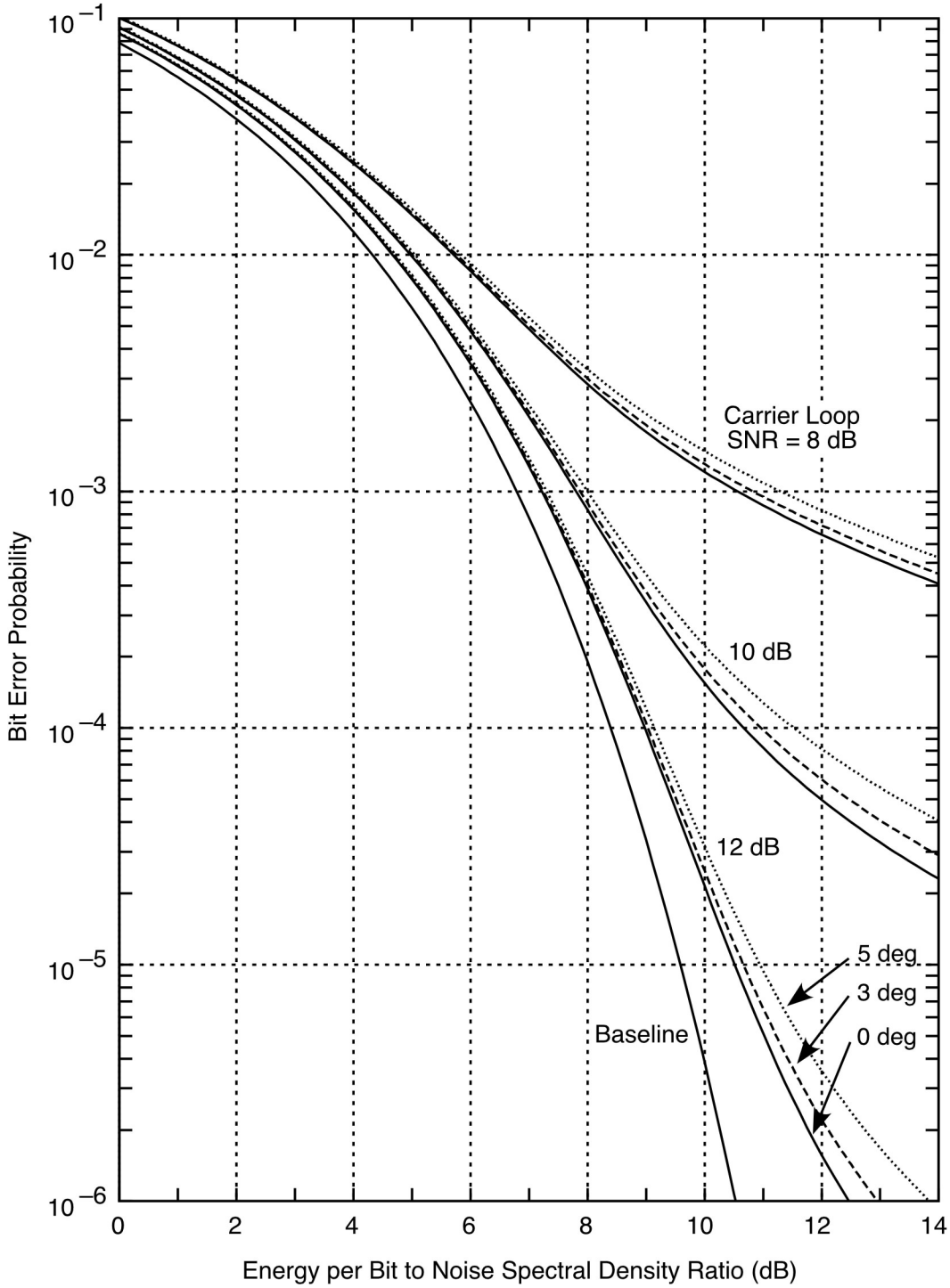

Figure 10. Telemetry Performance; Uncoded, Residual Carrier

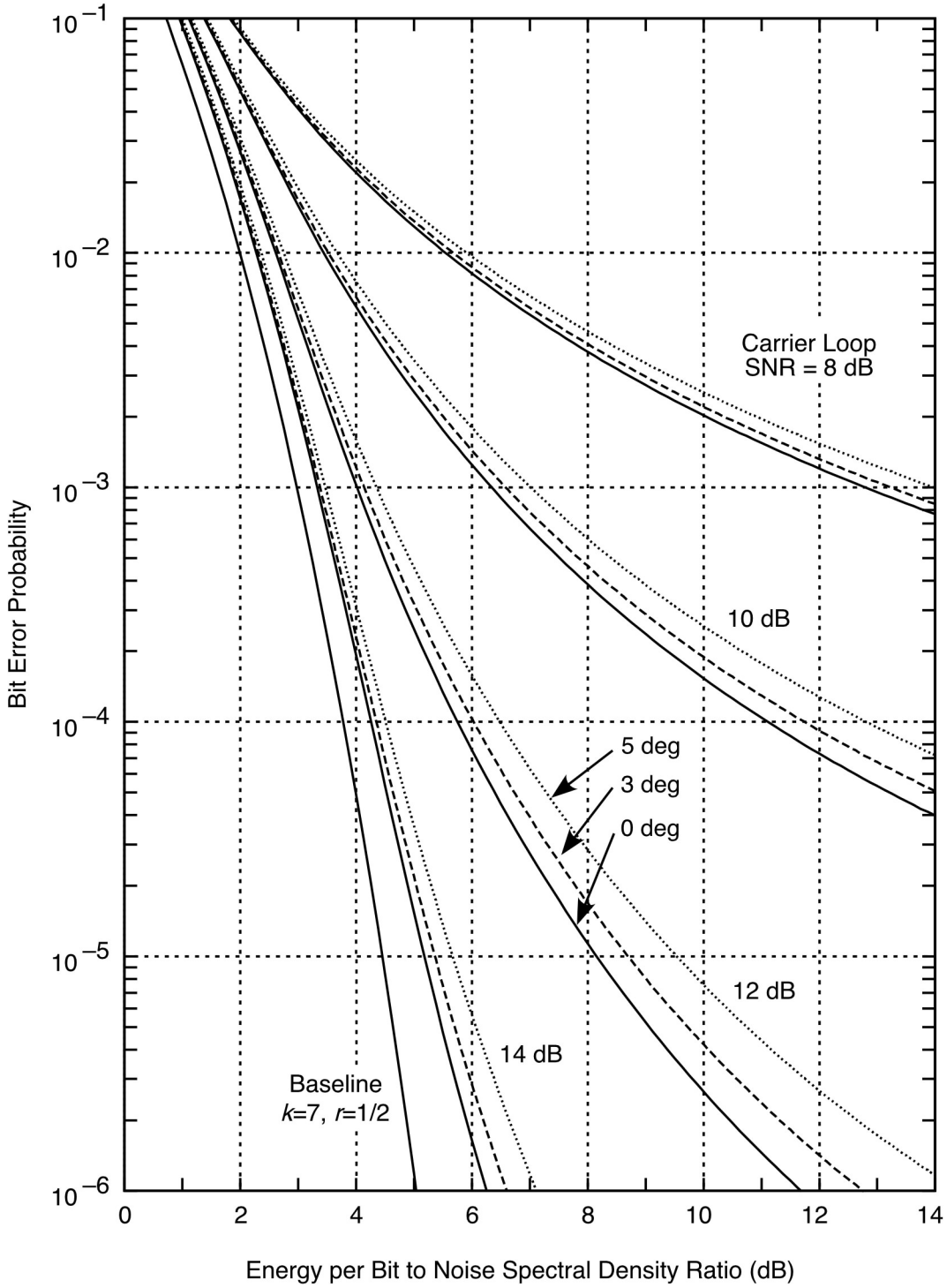

Figure 11. Telemetry Performance; (k=7, r=1/2) Convolutional Code with Residual Carrier

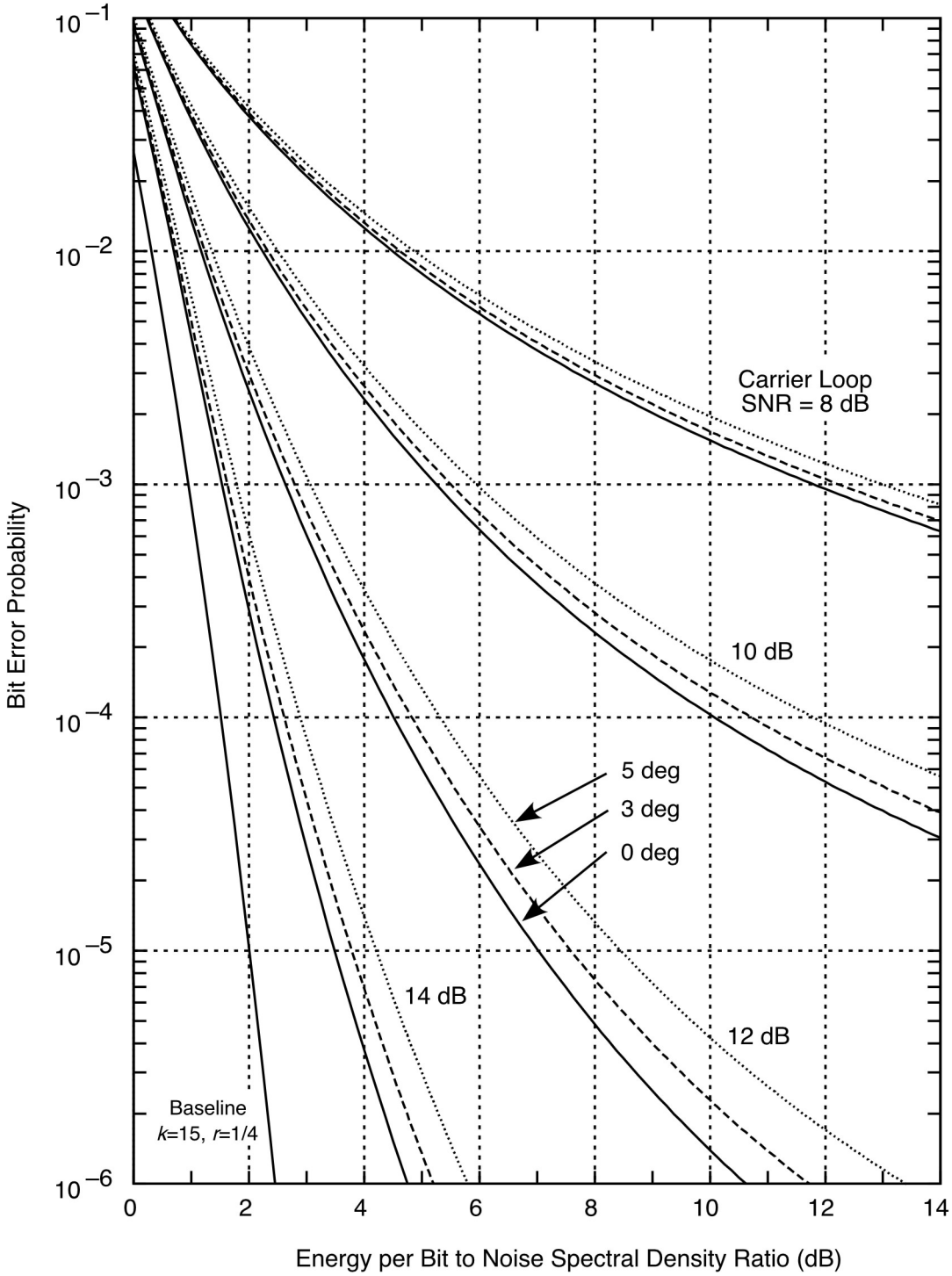

Figure 12. Telemetry Performance; (k=15, r=1/4) Convolutional Code with Residual Carrier

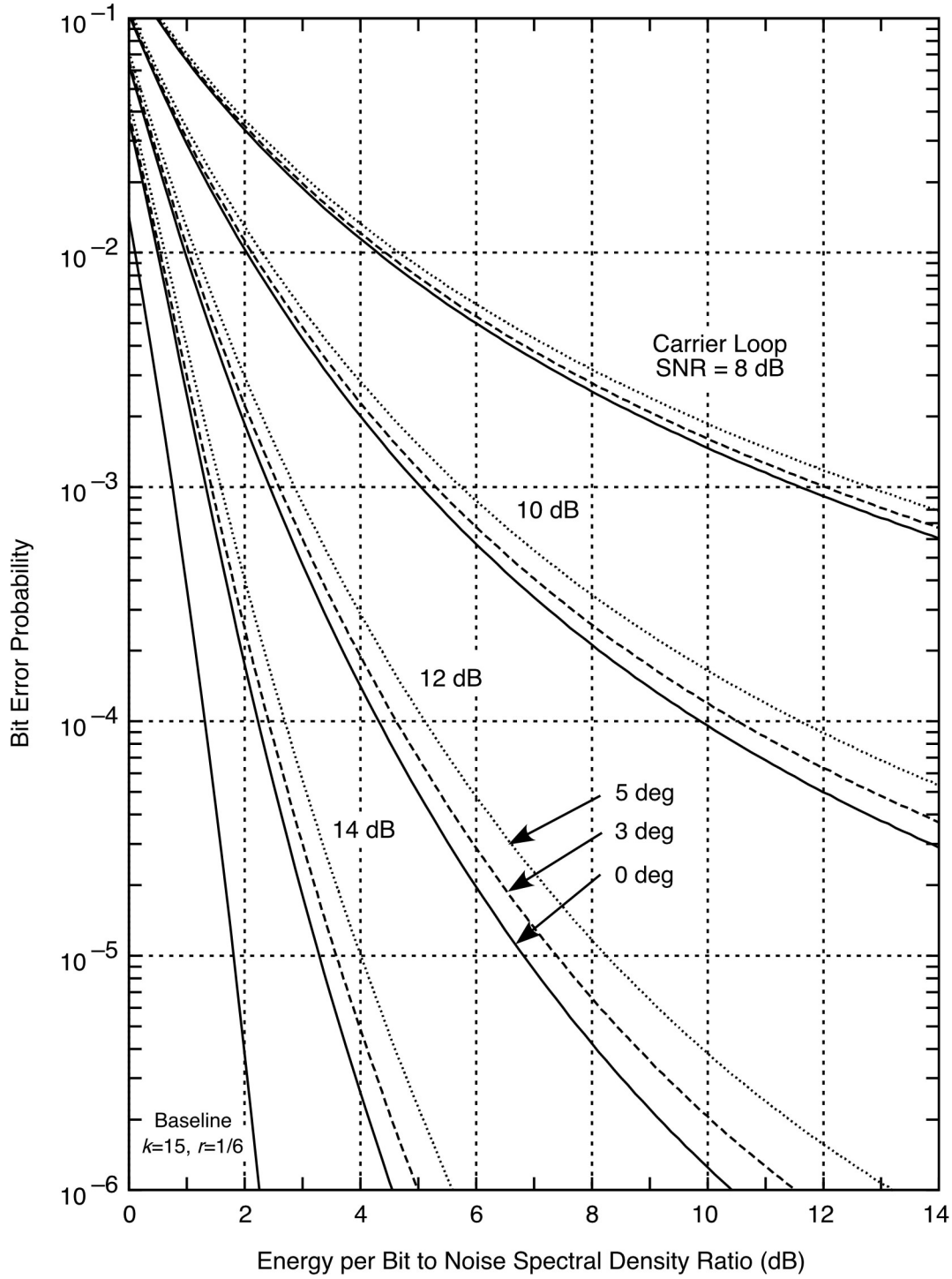

Figure 13. Telemetry Performance; (k=15, r=1/6) Convolutional Code with Residual Carrier

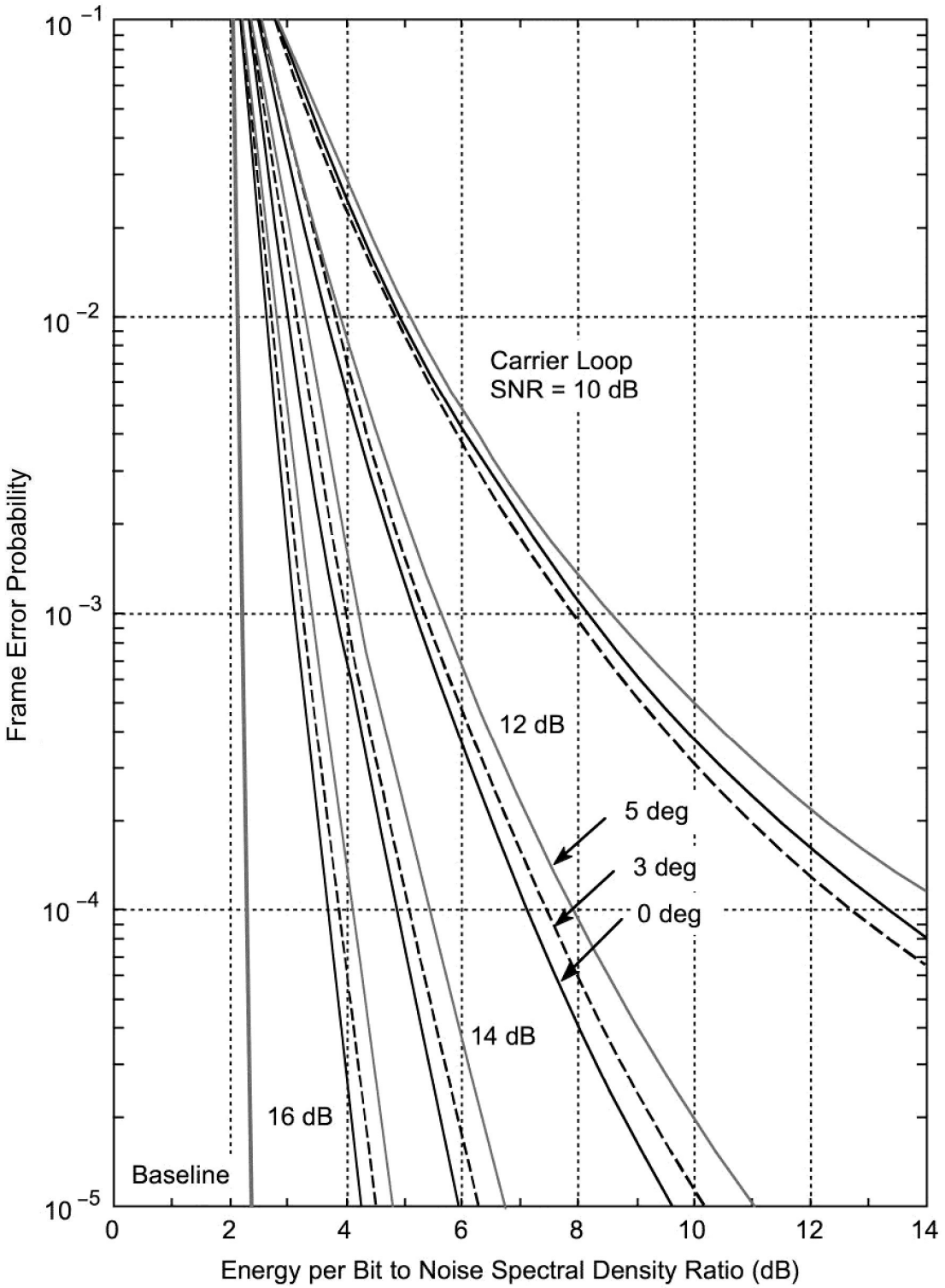

Figure 14. Telemetry Performance; Concatenated RS and (k=7, r=1/2), Convolutional Code with Residual Carrier.

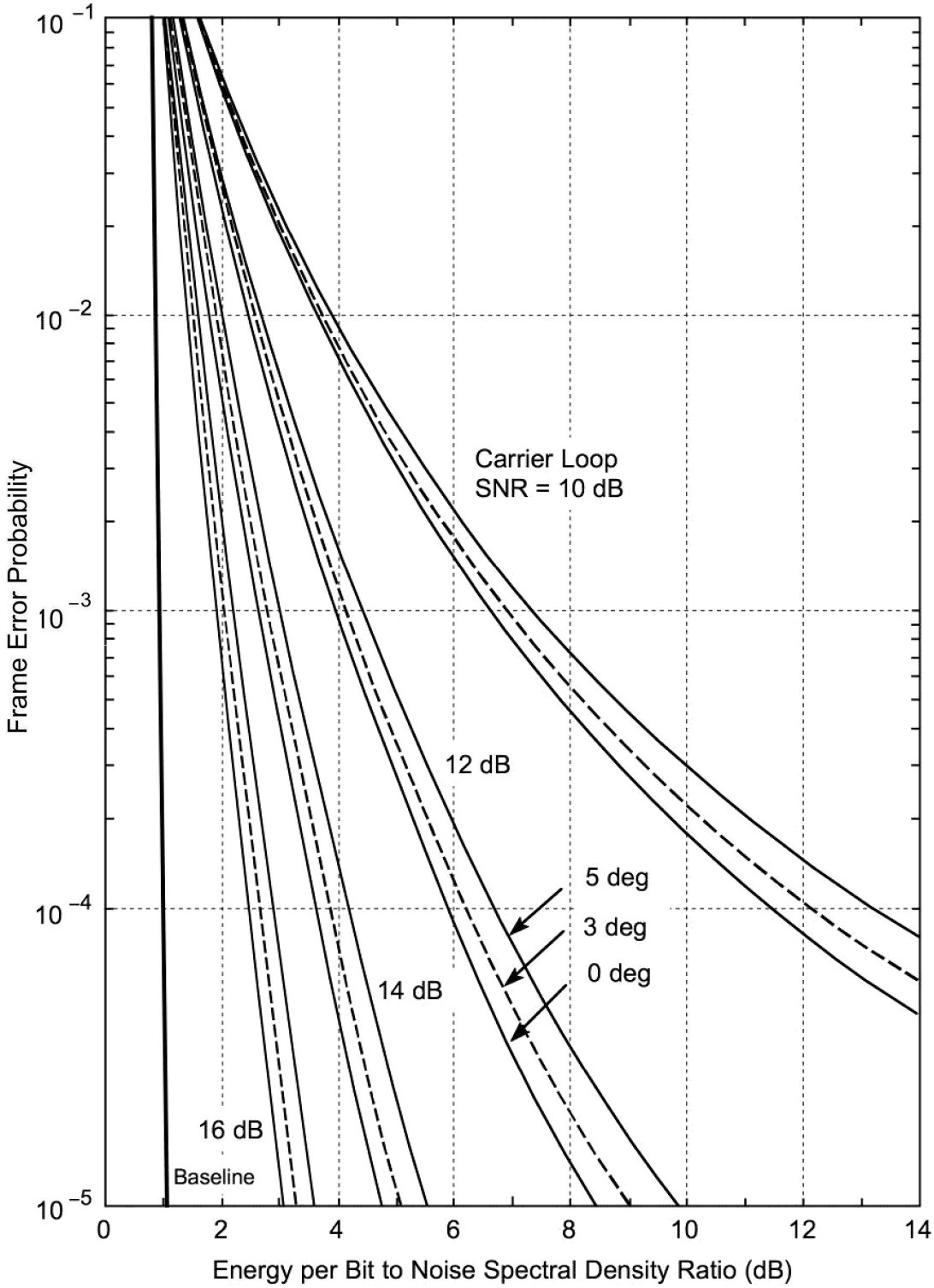

Figure 15. Telemetry Performance; Concatenated RS and (k=15, r=1/6) Convolutional Code with Residual Carrier.

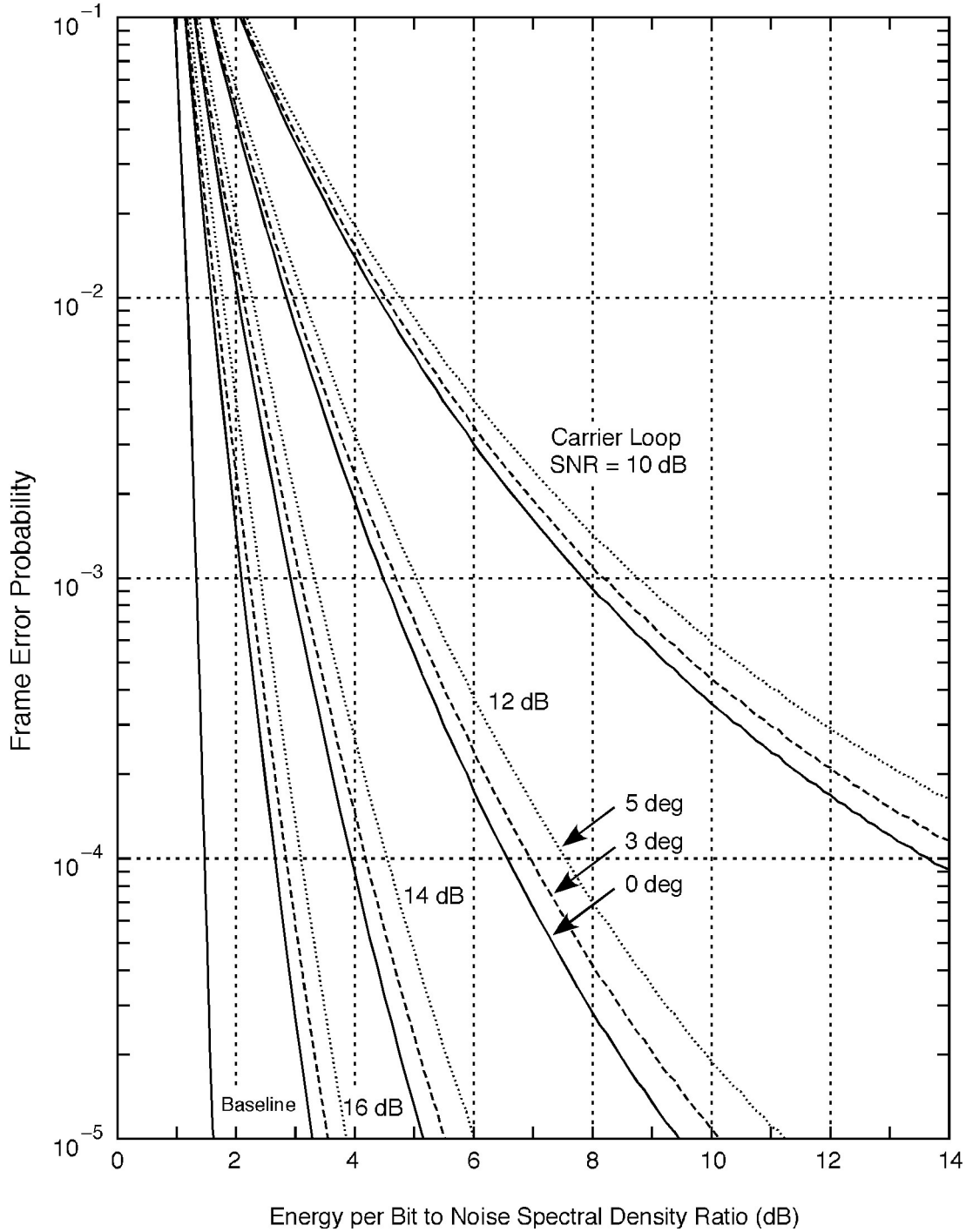

Figure 16. Telemetry Performance; (1784, 1/2) Turbo Code with Residual Carrier

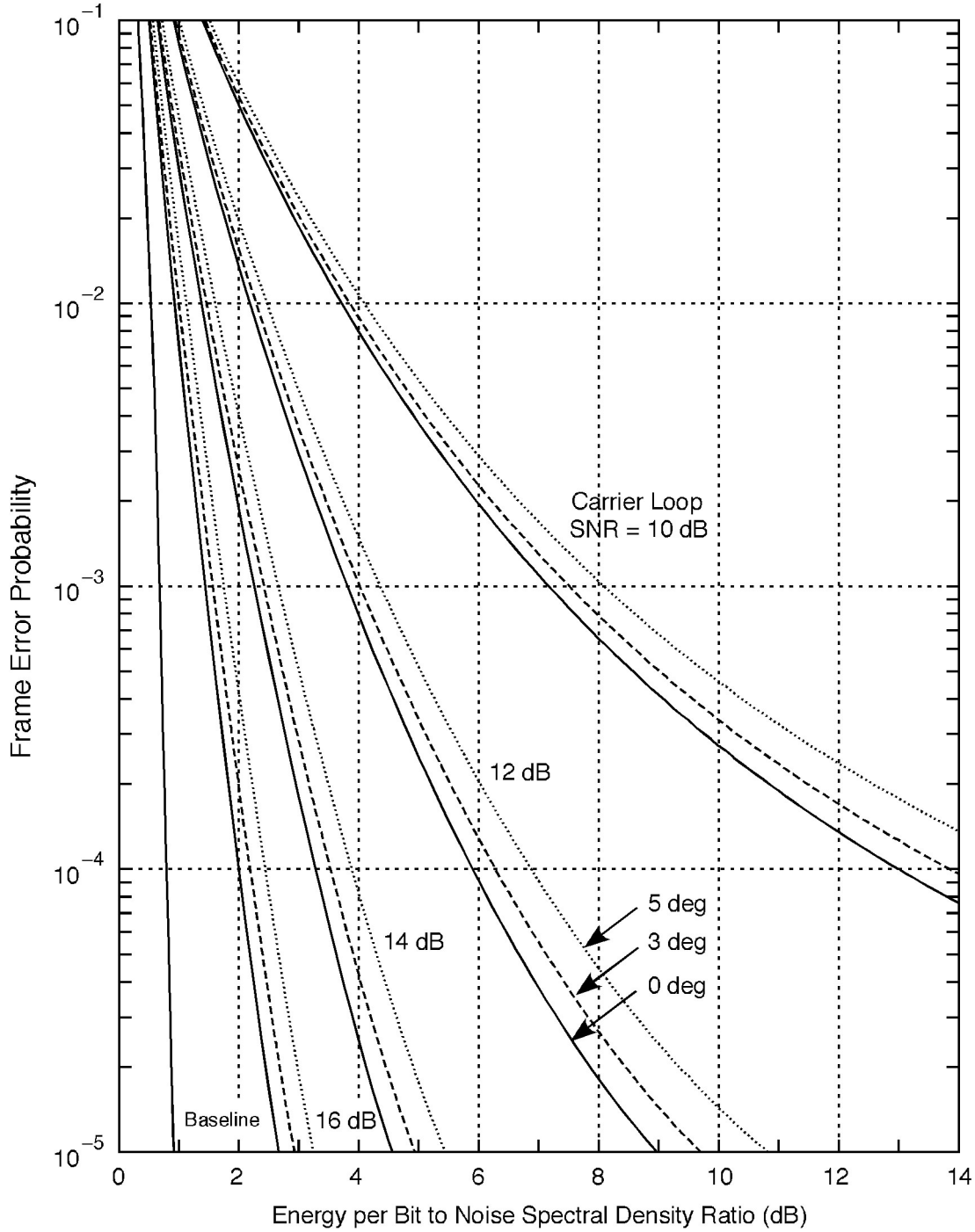

Figure 17. Telemetry Performance; (1784, 1/3) Turbo Code with Residual Carrier

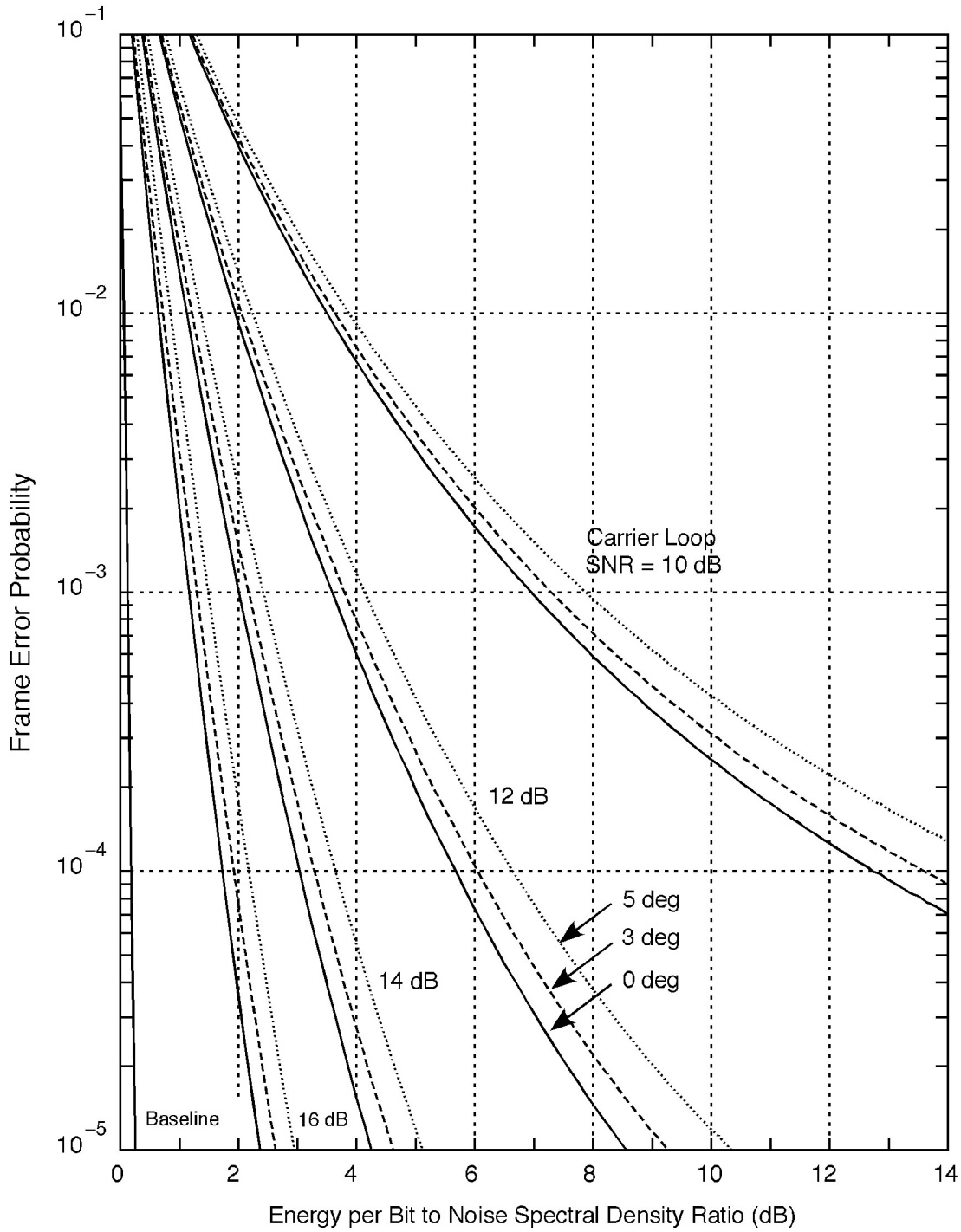

Figure 18. Telemetry Performance; (8920, 1/4) Turbo Code with Residual Carrier

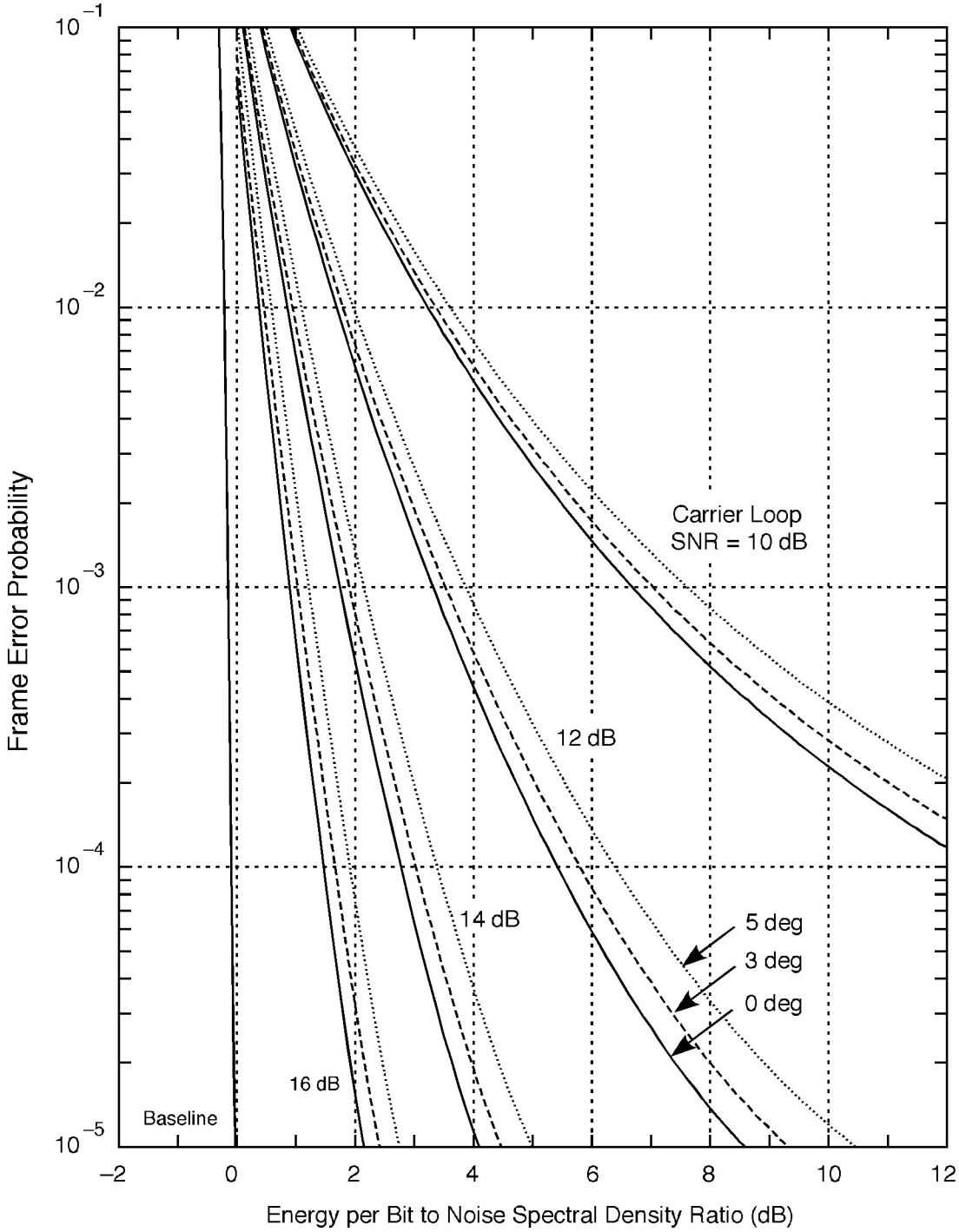

Figure 19. Telemetry Performance; (8920, 1/6) Turbo Code with Residual Carrier

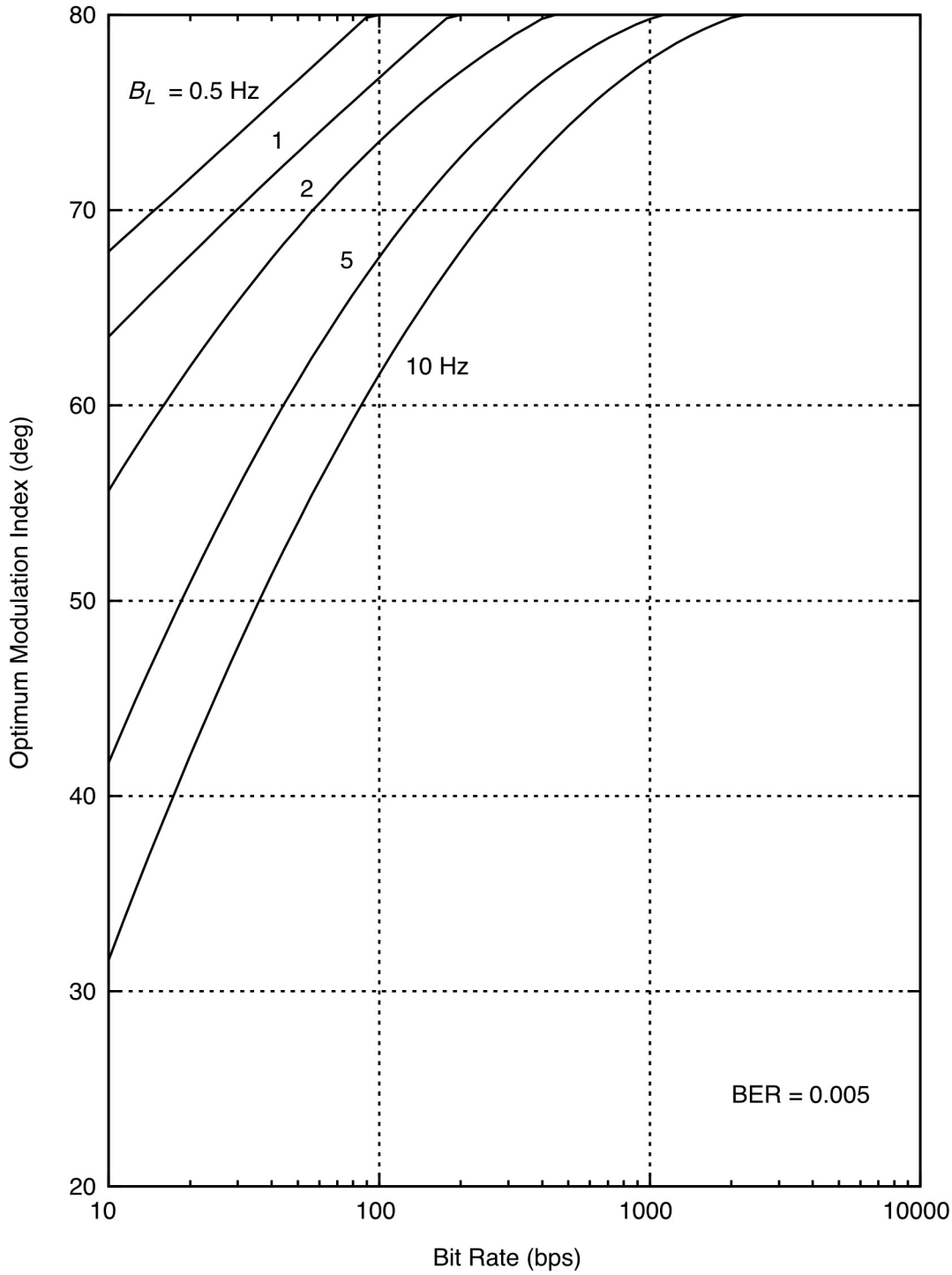

Figure 20. Optimum Modulation Index; Uncoded

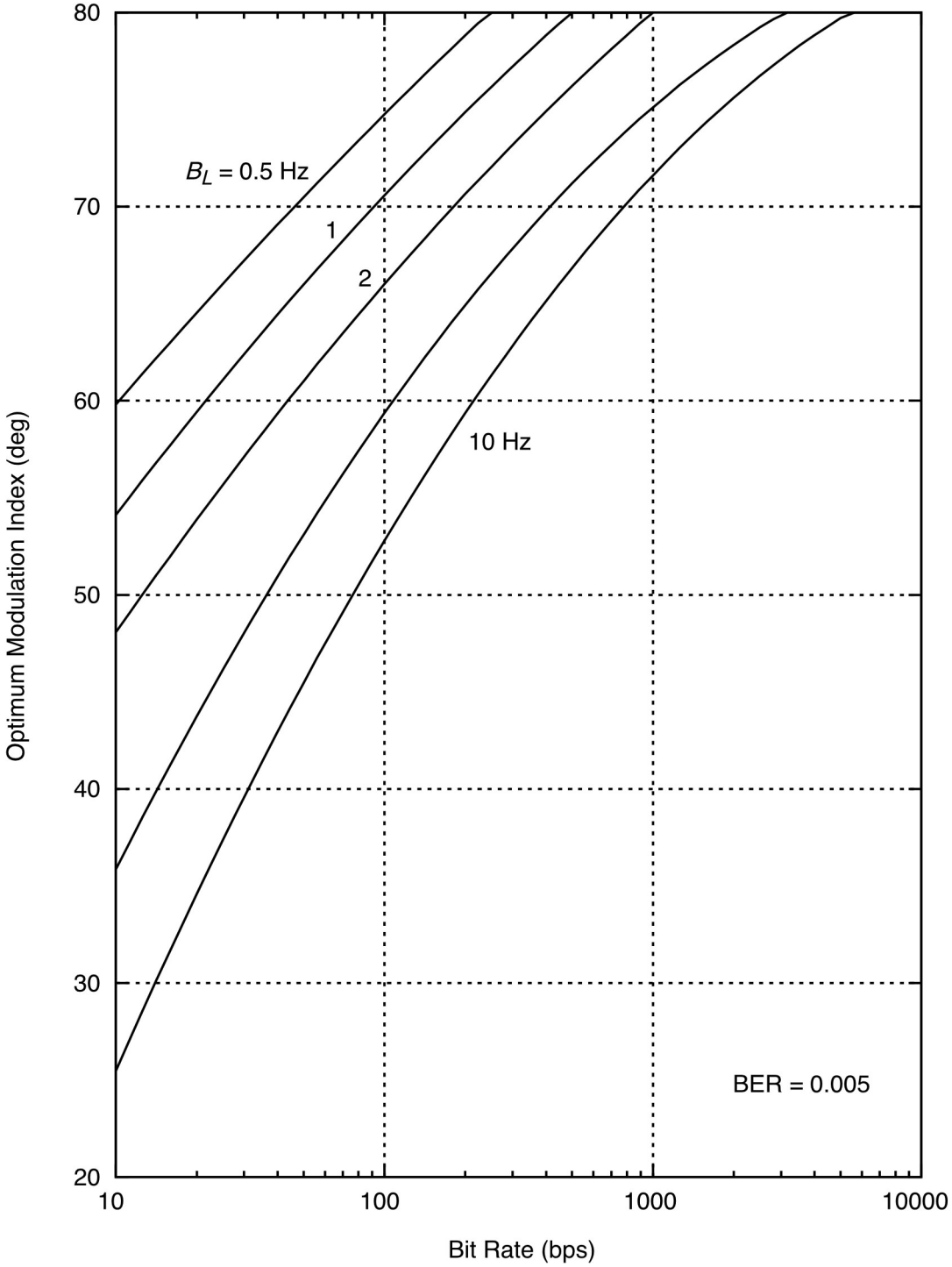

Figure 21. Optimum Modulation Index; (k=7, r=1/2) Convolutional Code

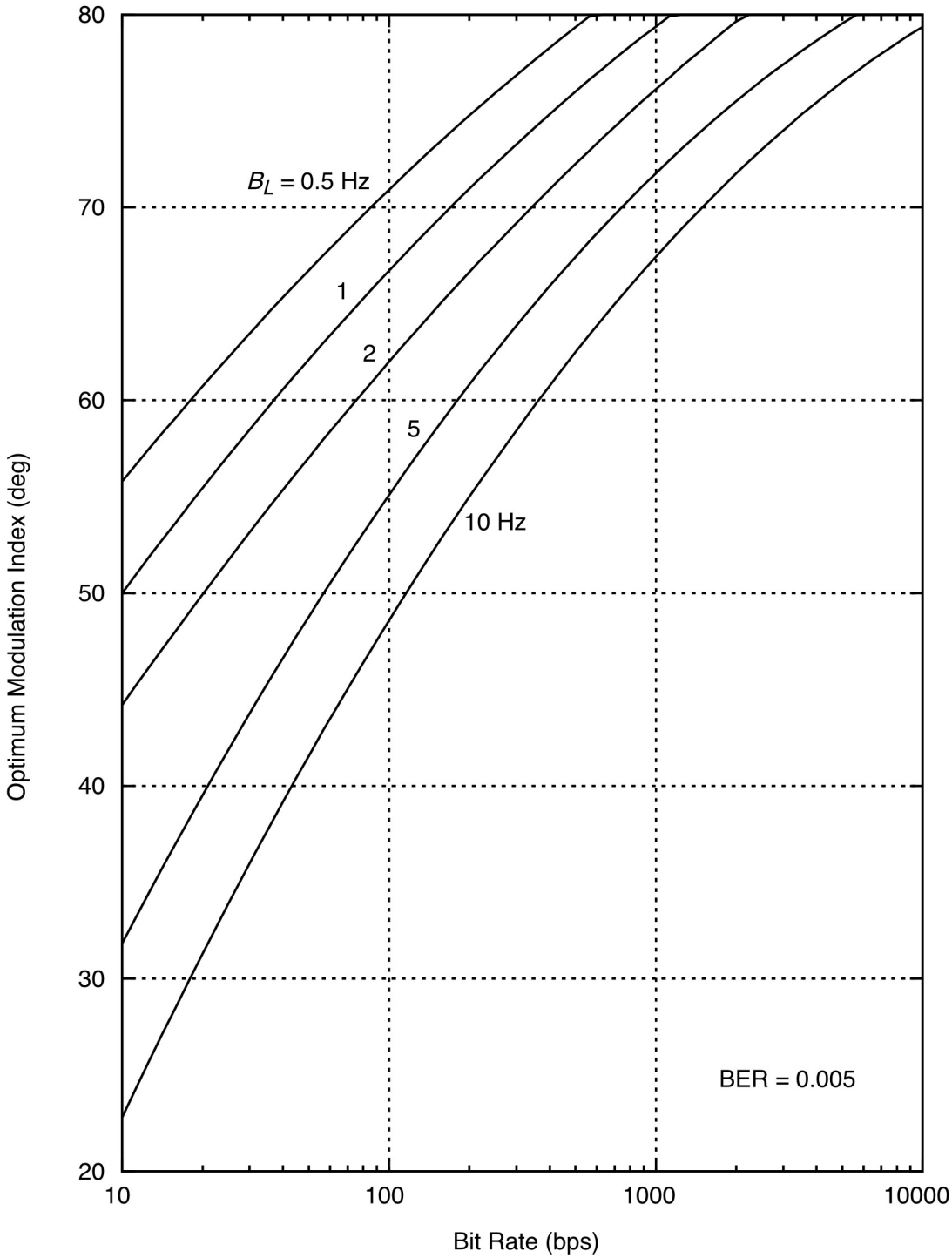

Figure 22. Optimum Modulation Index; (k=15, r=1/6) Convolutional Code

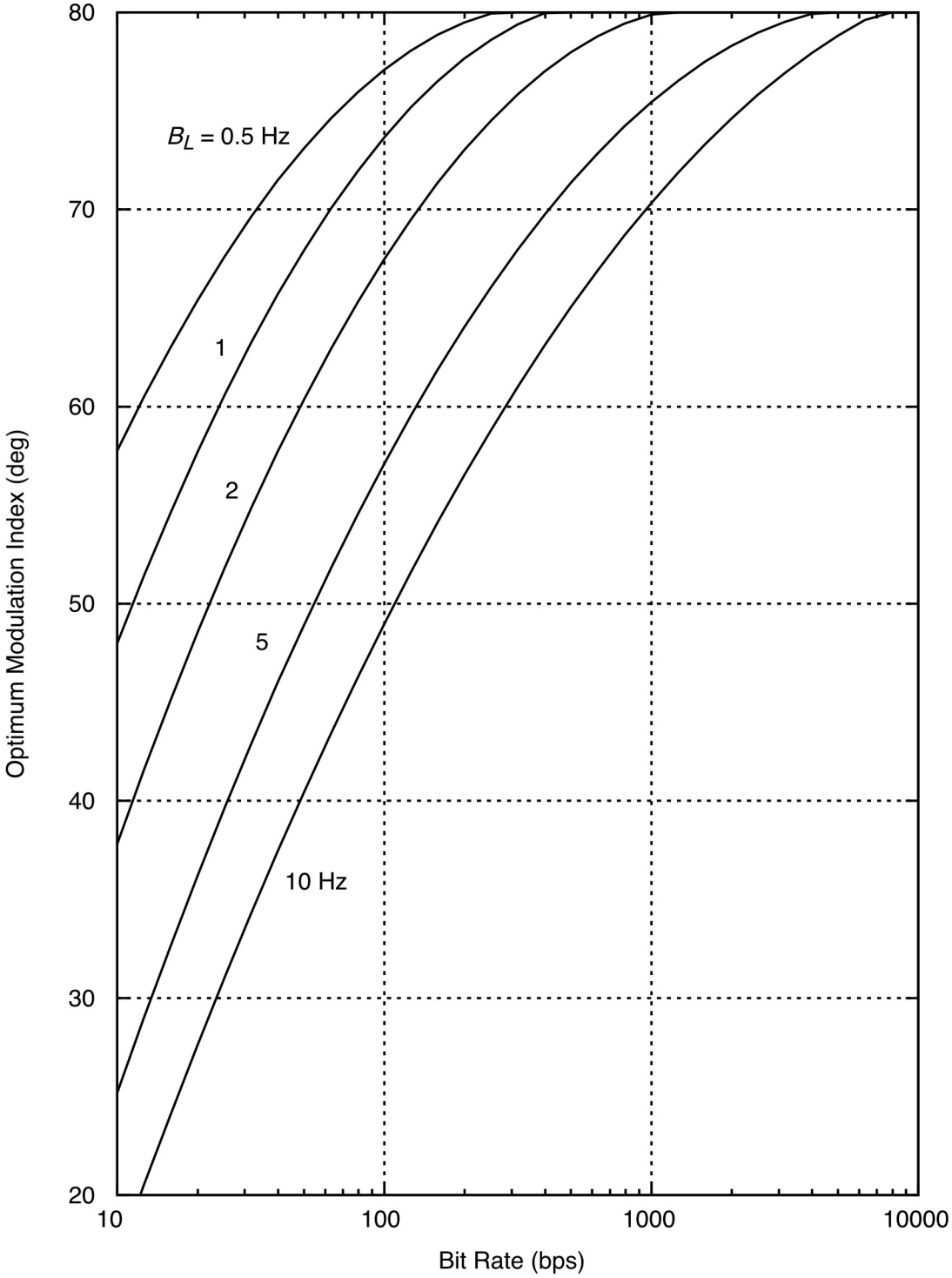

Figure 23. Optimum Modulation Index; Turbo Codes

Radio loss may, more generally, be regarded as a function of the carrier phase error variance σ_ϕ^2.

$$\sigma_\phi^2 = \frac{1}{\rho_L} + \sigma_T^2 + \sigma_S^2, \text{ rad}^2 \tag{20}$$

where σ_T^2 is the contribution of the transmitter phase noise to the phase error variance in the carrier loop and σ_S^2 is the contribution of solar phase noise. The contribution of thermal noise to phase error variance in the carrier loop equals the reciprocal of the carrier loop SNR; this is the first term on the right-hand side of Equation (20). σ_T^2 is a function of B_L and the statistical properties of the transmitter phase noise. Appendix D offers suggestions for estimating σ_T^2. If the Sun-Earth-probe angle is small, σ_S^2 will be significant and must be taken into account. Appendix E provides estimates of σ_S^2 as a function of Sun-Earth-probe angle and B_L.

In general, as a first step in estimating radio loss, the carrier phase error variance σ_ϕ^2 should be calculated using Equation (20). Then, radio loss will be calculated as a function of σ_ϕ^2.

It is recommended that the following constraint on residual-carrier tracking be observed.

$$\sigma_\phi^2 \leq 0.10 \text{ rad}^2 \tag{21}$$

This recommendation is based on simulations of cycle clipping in a phase-locked loop (Reference 12). In the absence of transmitter or solar phase noise, this becomes $\rho_L \geq 10.0$ (10 dB). In general, with transmitter or solar phase noise present, ρ_L needs to be larger yet.

The contributions of transmitter phase noise and of solar phase noise to the carrier phase error variance are computed as described in Appendices D and E, respectively. These computed contributions, together with Equations (20) and (21), define the minimum-acceptable carrier loop SNR for residual-carrier tracking.

5.3.2 Suppressed-Carrier BPSK

Suppressed-carrier BPSK is tracked with a Costas loop. This loop has different statistical properties than does the residual-carrier loop; thus, radio loss will be different in this case.

When tracking suppressed-carrier BPSK, the carrier loop signal-to-noise ratio is

$$\rho_L = \frac{S_L P_T}{N_0 B_L} \tag{22}$$

where S_L is the squaring loss of the Costas loop (Reference 6).

$$S_L = \frac{2\frac{E_S}{N_0}}{1+2\frac{E_S}{N_0}} \tag{23}$$

Radio loss can be regarded as a function of the carrier phase error variance $\sigma_\phi^{\ 2}$.

$$\sigma_\phi^2 = \frac{1}{\rho_L} + \sigma_T^2 + \sigma_S^2, \text{ rad}^2. \tag{24}$$

As before, σ_T^2 and σ_S^2 are the contributions of transmitter and solar phase noise, respectively, to the phase error variance in the carrier loop (see Appendices D and E).

It is recommended that the following constraint on suppressed-carrier BPSK tracking be observed.

$$\sigma_\phi^2 \le 0.02, \text{ rad}^2 \tag{25}$$

Violating this recommendation will lead to (at least) an occasional half-cycle slip. In the absence of transmitter or solar phase noise, inequality (25) corresponds to $\rho_L \ge 50.0$ (17dB), see Reference 7. In general, with transmitter or solar phase noise present, ρ_L needs to be larger yet.

5.3.3 QPSK and OQPSK

A QPSK or OQPSK signal is tracked by a loop designed for this purpose. The squaring loss is different than for the Costas loop used for suppressed-carrier BPSK.

When tracking a QPSK or OQPSK signal, the carrier loop signal-to-noise ratio is

$$\rho_L = \frac{S_{LQ} P_T}{N_0 B_L} \tag{26}$$

where S_{LQ} is the squaring loss of the QPSK/OQPSK loop.

$$S_{LQ} = \frac{1}{1+\frac{9}{2E_{SQ}/N_0}+\frac{6}{\left(E_{SQ}/N_0\right)^2}+\frac{3}{2\left(E_{SQ}/N_0\right)^3}} \tag{27}$$

Radio loss can be regarded as a function of the carrier phase error variance $\sigma_\phi^{\ 2}$.

$$\sigma_\phi^2 = \frac{1}{\rho_L} + \sigma_T^2 + \sigma_S^2, \text{ rad}^2 \tag{28}$$

As before, σ_T^2 and σ_S^2 are the contributions of transmitter and solar phase noise, respectively, to the phase error variance in the carrier loop (see Appendices D and E).

It is recommended that the following constraint on QPSK and OQPSK tracking be observed.

$$\sigma_\phi^2 \leq 0.005, \text{ rad}^2 \tag{29}$$

Violating this recommendation will lead to (at least) an occasional quarter-cycle slip. In the absence of transmitter or solar phase noise, inequality (29) corresponds to $\rho_L \geq 200.0$ (23dB), see Reference 7. In general, with transmitter or solar phase noise present, ρ_L needs to be larger yet.

5.3.4 Two/Three-Way Coherent

When the spacecraft is tracked in a two-way (or three-way) phase-coherent mode, the carrier phase error variance σ_ϕ^2 in the ground receiver is increased by a portion of the phase noise (of thermal origin) introduced onto the downlink by the spacecraft transponder.

$$\sigma_\phi^2 = \frac{1}{\rho_L} + \frac{G^2\left(B_{TR} - B_L\right)}{P_C / N_0\big|_{U/L}} + \sigma_S^2, \text{ rad}^2 \tag{30}$$

where G is the spacecraft transponder ratio and $P_C / N_0\big|_{U/L}$ is the uplink residual-carrier power-to-noise spectral density ratio. B_{TR} and B_L are the (one-sided) noise-equivalent carrier loop bandwidths of the transponder and ground receiver, respectively.

Equation (30) is a valid approximation only if $B_{TR} > B_L$. σ_S^2 is the contribution of solar phase noise to the phase error variance in the carrier loop; it will generally be larger for coherent operation than for one-way or two-way noncoherent operation (see Appendix E).

5.3.5 Radio Loss

For all of the carrier tracking modes discussed above—residual carrier, suppressed-carrier BPSK, QPSK/OQPSK, and two/three-way coherent—a common framework is used for modeling radio loss, the loss due to imperfect carrier tracking. That framework is summarized in the paragraphs that follow. Radio loss is a function of carrier loop phase error variance σ_ϕ^2. This variance must be calculated as described in the previous paragraphs. The radio loss models of this paragraph will be valid when σ_ϕ^2 satisfies the inequality:

$$\sigma_\phi^2 \leq \begin{cases} 0.1 \text{ rad}^2, & \text{Residual carrier} \\ 0.02 \text{ rad}^2, & \text{Suppressed - carrier BPSK} \\ 0.005 \text{ rad}^2, & \text{QPSK or OQPSK} \end{cases} \tag{31}$$

In the discussion that follows, a distinction is made between residual-carrier tracking and suppressed-carrier tracking where the latter includes both suppressed-carrier BPSK and QPSK/OQPSK.

Radio loss is modeled as an interpolation between a High-Rate Model (HRM) and a Low-Rate Model (LRM). This interpolation is

$$\eta^*_{RADIO} = a \cdot \eta^*_{HRM} + (1-a) \cdot \eta^*_{LRM} \tag{32}$$

where

η^*_{RADIO} = positive decibel radio loss ($\eta^*_{RADIO} = -10 \log \eta_{RADIO}$)

η^*_{HRM} = positive decibel HRM radio loss

η^*_{LRM} = positive decibel LRM radio loss

a = interpolation factor ($0 \le a \le 1$)

The interpolation factor a depends on the code. For uncoded and convolutionally coded telemetry, the interpolation factor is given by

$$a = \frac{1}{4B_L T_{SYM}} \left[1 - \frac{1}{8B_L T_{SYM}} \left(1 - e^{-8B_L T_{SYM}} \right) \right] \tag{33}$$

where B_L is the (one-sided, noise-equivalent) carrier loop bandwidth and T_{SYM} is the binary symbol period (the reciprocal of the binary symbol rate). For concatenated and turbo codes, the interpolation factor a is given by

$$a = \frac{1}{1 + c_1 \left(R / B_L \right)^{-c_2}} \tag{34}$$

where R is the bit rate. Computer simulations verify that Equation (34) yields an appropriate interpolation factor for concatenated and turbo codes (References 8 and 9). Table 9 gives the coefficients c_1 and c_2 for concatenated codes. The coefficients for turbo codes are provided in Table 10.

The HRM radio loss is modeled with a curve-fit of the form

$$\eta^*_{HRM} = c_{H0} \left[\exp\left(c_{H1} \sigma^2_\phi \right) - 1 \right] \tag{35}$$

and the LRM radio loss is modeled with a curve-fit of the same form (but with different coefficients)

$$\eta^*_{LRM} = c_{L0}\left[\exp\left(c_{L1}\sigma^2_\phi\right) - 1\right] \tag{36}$$

where $\sigma_\phi{}^2$ is the carrier loop phase error variance in units of rad^2.

Table 9. Interpolation Factor Coefficients c_1 and c_2 for Concatenated Codes

Concatenated Code	Tracking Mode	c_1	c_2
RS with (k=7, r=1/2) Convolutional	Residual	31,000.	1.3
RS with (k=15, r=1/4) or (k=15, r=1/6) Convolutional	Residual	52,400.	1.3
RS with (k=7, r=1/2) Convolutional	Suppressed	76,000.	1.3
RS with (k=15, r=1/4) or (k=15, r=1/6) Convolutional	Suppressed	129,000.	1.3

Table 10. Interpolation Factor Coefficients c_1 and c_2 for Turbo Codes

Turbo Code	c_1	c_2
(1784, 1/2), (1784, 1/3), (1784, 1/4), (1784, 1/6)	264.	0.84
(3568, 1/2), (3568, 1/3), (3568, 1/4), (3568, 1/6)	473.	0.84
(7136, 1/2), (7136, 1/3), (7136, 1/4), (7136, 1/6)	846.	0.84
(8920, 1/2), (8920, 1/3), (8920, 1/4), (8920, 1/6)	1020.	0.84

The HRM coefficients c_{HO} and c_{HI} of Equation (35) depend on the code, the threshold BER or FER, and the tracking mode. These coefficients are given in Table 11 for uncoded telemetry, in Table 12 for (k=7, r=1/2) convolutionally coded telemetry, and in Table 13 for both (k=15, r=1/4) and (k=15, r=1/6) convolutionally coded telemetry. For concatenated codes, the coefficients at a threshold FER of 1×10^{-5} are given in Table 14. The coefficients for the turbo codes listed in Table 8 at a threshold FER of 1×10^{-4} are given in Table 15 for residual carrier tracking and in Table 16 for suppressed carrier tracking. The LRM coefficients c_{LO} and c_{LI} are independent of the code and are given in Table 17.

Table 11. HRM Coefficients c_{H0} and c_{H1} for Uncoded Telemetry

Tracking Mode	Threshold BER	c_{H0}	c_{H1}
Residual	10^{-2}	0.53	8.1
Residual	5×10^{-3}	0.39	10.5
Residual	10^{-3}	0.21	17.5
Residual	10^{-4}	0.070	35.2
Residual	10^{-5}	0.030	55.5
Suppressed	10^{-2}	0.27	15.2
Suppressed	5×10^{-3}	0.21	18.5
Suppressed	10^{-3}	0.12	29.3
Suppressed	10^{-4}	0.031	62.7
Suppressed	10^{-5}	0.000023	244.

Table 12. HRM Coefficients c_{H0} and c_{H1} for (k=7, r=1/2) Convolutional Code

Tracking Mode	Threshold BER	c_{H0}	c_{H1}
Residual	10^{-2}	0.30	17.7
Residual	5×10^{-3}	0.24	21.6
Residual	10^{-3}	0.21	28.7
Residual	10^{-4}	0.11	45.8
Residual	10^{-5}	0.066	64.7
Suppressed	10^{-2}	0.11	34.6
Suppressed	5×10^{-3}	0.085	42.5
Suppressed	10^{-3}	0.041	65.2
Suppressed	10^{-4}	0.010	116.
Suppressed	10^{-5}	0.0030	174.

Table 13. HRM Coefficients c_{H0} and c_{H1} for k=15 Convolutional Codes

Tracking Mode	Threshold BER	c_{H0}	c_{H1}
Residual	10^{-2}	0.45	16.6
Residual	5×10^{-3}	0.45	18.8
Residual	10^{-3}	0.34	27.3
Residual	10^{-4}	0.21	43.1
Residual	10^{-5}	0.13	61.5
Suppressed	10^{-2}	0.13	38.4
Suppressed	5×10^{-3}	0.098	46.9
Suppressed	10^{-3}	0.067	65.4
Suppressed	10^{-4}	0.044	93.4
Suppressed	10^{-5}	0.021	135.

Table 14. HRM Coefficients c_{H0} and c_{H1} for Concatenated Codes

Concatenated Code	Tracking Mode	C_1	C_2
RS with (k=7, r=1/2) Convolutional	Residual	2.07	25.4
RS with (k=15, r=1/4) or (k=15, r=1/6) Convolutional	Residual	2.92	20.6
RS with (k=7, r=1/2) Convolutional	Suppressed	0.88	52.1
RS with (k=15, r=1/4) or (k=15, r=1/6) Convolutional	Suppressed	1.14	46.5

Table 15. HRM Coefficients c_{H0} and c_{H1} for Turbo Codes, Residual Carrier

Turbo Code	c_{H0}	c_{H1}
(1784, 1/2)	2.14	19.4
(1784, 1/3)	2.60	17.2
(1784, 1/4)	1.41	24.7
(1784, 1/6)	1.74	22.2
(3568, 1/2)	2.75	16.9
(3568, 1/3)	2.01	21.1
(3568, 1/4)	2.36	20.9
(3568, 1/6)	2.32	19.6

Turbo Code	c_{H0}	c_{H1}
(7136, 1/2)	3.25	15.7
(7136, 1/3)	2.45	18.9
(7136, 1/4)	2.03	21.1
(7136, 1/6)	3.51	16.0
(8920, 1/2)	3.39	15.3
(8920, 1/3)	3.19	16.1
(8920, 1/4)	3.29	15.6
(8920, 1/6)	3.67	14.5

Table 16. HRM Coefficients c_{H0} and c_{H1} for Turbo Codes, Suppressed Carrier

Turbo Code	c_{H0}	c_{H1}
(1784, 1/2), (1784, 1/3), (1784, 1/4), (1784, 1/6)	0.025	182.0
(3568, 1/2), (3568, 1/3), (3568, 1/4), (3568, 1/6)	0.22	99.8
(7136, 1/2), (7136, 1/3), (7136, 1/4), (7136, 1/6)	0.54	61.9
(8920, 1/2), (8920, 1/3), (8920, 1/4), (8920, 1/6)	0.75	50.7

Table 17. LRM Coefficients c_{L0} and c_{L1} for All Codes

Tracking Mode	c_{L0}	c_{L1}
Residual Carrier	4.0	1.1
Suppressed Carrier	0.56	7.3

5.4 *Subcarrier Synchronization*

Subcarrier demodulation loss η_{SUB} ($0 < \eta_{SUB} \leq 1$) is a contributor to system loss. It is the result of imperfect subcarrier synchronization. In general, the subcarrier demodulation loss is a function of subcarrier loop signal-to-noise ratio, the coding scheme, the threshold BER or FER, and the type of subcarrier (squarewave or sinewave).

The signal-to-noise ratio ρ_{SUB} in a subcarrier synchronization loop is given by (Reference 10)

$$\rho_{SUB} = \begin{cases} \left(\dfrac{2}{\pi}\right)^2 \cdot \dfrac{S_{SUB}}{W_{SUB} B_{SUB}} \cdot \dfrac{P_D}{N_0}, & \text{squarewave subcarrier} \\ \dfrac{S_{SUB}}{B_{SUB}} \cdot \dfrac{P_D}{N_0}, & \text{sinewave subcarrier} \end{cases} \tag{37}$$

where B_{SUB} is the (one-sided) noise-equivalent subcarrier loop bandwidth. S_{SUB} is the squaring loss of the subcarrier loop. For a squarewave subcarrier, P_D is the power in all the data modulation sidebands; whereas for a sinewave subcarrier, P_D is the power in the fundamental data modulation sidebands only. For a squarewave subcarrier, W_{SUB} is the subcarrier loop window factor ($W_{SUB} = 2^{-n}$, where $n = 0, 1, 2, 3$, or 4). A window is not used with sinewave subcarriers. The squaring loss S_{SUB} is, in the case of either squarewave or sinewave,

$$S_{SUB} = \frac{2\dfrac{E_S}{N_0}}{1 + 2\dfrac{E_S}{N_0}} \tag{38}$$

It is recommended that the following constraint on subcarrier tracking be observed.

$$\rho_{SUB} = \begin{cases} 100.0 \quad (20\text{ dB}), & \text{squarewave subcarrier} \\ 50.0 \quad (17\text{ dB}), & \text{sinewave subcarrier} \end{cases} \tag{39}$$

Subcarrier demodulation loss is modeled as an interpolation between a High-Rate Model (HRM) and a Low-Rate Model (LRM). This interpolation is

$$\eta^*_{SUB} = a \cdot \eta^*_{HSUB} + (1 - a) \cdot \eta^*_{LSUB} \tag{40}$$

where

η^*_{SUB} = positive decibel subcarrier demodulator loss
$\left(\eta^*_{SUB} = -10 \log \eta_{SUB}\right)$

η^*_{HSUB} = positive decibel HRM subcarrier demodulator loss

η^*_{LSUB} = positive decibel LRM subcarrier demodulator loss

a = interpolation factor ($0 \le a \le 1$)

The interpolation factor depends on the code. For uncoded and convolutionally coded telemetry, the interpolation factor a is given by

$$a = \frac{1}{4B_{SUB}T_{SYM}}\left[1 - \frac{1}{8B_{SUB}T_{SYM}}\left(1 - e^{-8B_{SUB}T_{SYM}}\right)\right] \tag{41}$$

where B_{SUB} is the subcarrier loop bandwidth and T_{SYM} is the symbol period (the reciprocal of symbol rate). For concatenated and turbo codes, the interpolation factor a is given by

$$a = \frac{1}{1 + c_1\left(R/B_{SUB}\right)^{-c_2}} \tag{42}$$

where R is the bit rate. The coefficients c_1 and c_2 depend on the code. Table 18 gives these coefficients for concatenated codes. The coefficients for turbo codes were provided in Table 10.

Table 18. Interpolation Factor Coefficients c_1 and c_2 for Concatenated Codes

Concatenated Code	c_1	c_2
RS with (k=7, r=1/2) Convolutional	76,000.	1.3
RS with (k=15, r=1/4) or (k=15, r=1/6) Convolutional	129,000.	1.3

The HRM subcarrier demodulation loss is modeled with a curve-fit whose form depends on whether the subcarrier is squarewave or sinewave.

$$\eta^*_{HSUB} = \begin{cases} c_0\left(\rho_{SUB}\right)^{c_1}, & \text{squarewave} \\ c_0\left(e^{c_1/\rho_{SUB}} - 1\right), & \text{sinewave} \end{cases} \tag{43}$$

The HRM coefficients c_0 and c_1 of Equation (43) depend on the code and the threshold BER as well as the type of subcarrier (squarewave or sinewave). Table 19 provides the coefficients for uncoded and convolutionally coded telemetry using a squarewave subcarrier. Table 20 provides the same information for a sinewave subcarrier. The coefficients given in Tables 19 and 20 for the (k=15, r=1/6) convolutional code also apply to the (k=15, r=1/4) code. Tables 21 and 22 provide the coefficients for concatenated codes using squarewave and sinewave

subcarriers at a threshold FER (from Table 7) of 1×10^{-5}. Tables 23 and 24 provide the coefficients for turbo codes listed in Table 8 at a threshold FER of 1×10^{-4} for residual carrier and suppressed carrier.

The LRM subcarrier demodulation loss is independent of the code and is modeled with a curve-fit of the form

$$\eta^*_{LSUB} = \begin{cases} 4.6\left(\rho_{SUB}\right)^{-0.50}, & \text{squarewave} \\ 5.8\left(\rho_{SUB}\right)^{-1.07}, & \text{sinewave} \end{cases} \tag{44}$$

Table 19. Subcarrier Demodulation HRM Loss Coefficients for Uncoded and Convolutionally Coded Data using Squarewave Subcarriers

Code	Threshold BER	Subcarrier Demodulation Loss Coefficient c_0	Subcarrier Demodulation Loss Coefficient c_1
Uncoded	10^{-2}	6.3	–0.55
Uncoded	5×10^{-3}	6.6	–0.56
Uncoded	10^{-3}	7.7	–0.58
Uncoded	10^{-4}	9.8	–0.61
Uncoded	10^{-5}	13.	–0.66
(k=7, r=1/2)	10^{-2}	12.	–0.65
(k=7, r=1/2)	5×10^{-3}	13.	–0.66
(k=7, r=1/2)	10^{-3}	16.	–0.69
(k=7, r=1/2)	10^{-4}	21.	–0.74
(k=7, r=1/2)	10^{-5}	29.	–0.78
(k=15, r=1/6)	10^{-2}	22.	–0.73
(k=15, r=1/6)	5×10^{-3}	25.	–0.76
(k=15, r=1/6)	10^{-3}	31.	–0.79
(k=15, r=1/6)	10^{-4}	40.	–0.83
(k=15, r=1/6)	10^{-5}	53.	–0.87

Table 20. Subcarrier Demodulation HRM Loss Coefficients for Uncoded and Convolutionally Coded Data using Sinewave Subcarriers

Code	Threshold BER	Subcarrier Demodulation Loss Coefficient c_0	Subcarrier Demodulation Loss Coefficient c_1
Uncoded	10^{-2}	0.27	15.2
Uncoded	5×10^{-3}	0.21	18.5
Uncoded	10^{-3}	0.12	29.3
Uncoded	10^{-4}	0.031	62.7
Uncoded	10^{-5}	0.000023	244.
(k=7, r=1/2)	10^{-2}	0.11	34.6
(k=7, r=1/2)	5×10^{-3}	0.085	42.5
(k=7, r=1/2)	10^{-3}	0.041	65.2
(k=7, r=1/2)	10^{-4}	0.010	116.
(k=7, r=1/2)	10^{-5}	0.0030	174
(k=15, r=1/6)	10^{-2}	0.13	38.4
(k=15, r=1/6)	5×10^{-3}	0.098	46.9
(k=15, r=1/6)	10^{-3}	0.067	65.4
(k=15, r=1/6)	10^{-4}	0.044	93.4
(k=15, r=1/6)	10^{-5}	0.021	135.

Table 21. Subcarrier Demodulation HRM Loss Coefficients for Concatenated Codes Using Squarewave Subcarriers

Concatenated Code	Subcarrier Demodulation Loss Coefficient c_0	Subcarrier Demodulation Loss Coefficient c_1
RS with (k=7, r=1/2) Convolutional	56.	–0.69
RS with (k=15, r=1/4) or (k=15, r=1/6) Convolutional	50.	–0.65

Table 22. Subcarrier Demodulation HRM Loss Coefficients for Concatenated Codes Using Sinewave Subcarriers

Concatenated Code	Subcarrier Demodulation Loss Coefficient c_0	Subcarrier Demodulation Loss Coefficient c_1
RS with (k=7, r=1/2) Convolutional	1260.	–1.70
RS with (k=15, r=1/4) or (k=15, r=1/6) Convolutional	643.	–1.51

Table 23. Subcarrier Demodulation HRM Loss Coefficients for Turbo Codes Using Squarewave Subcarriers

Turbo Codes	Subcarrier Demodulation Loss Coefficient c_0	Subcarrier Demodulation Loss Coefficient c_1
(1784, 1/2), (1784, 1/3), (1784, 1/4), (1784, 1/6)	62	–0.76
(3568, 1/2), (3568, 1/3), (3568, 1/4), (3568, 1/6)	53	–0.71
(7136, 1/2), (7136, 1/3), (7136, 1/4), (7136, 1/6)	48	–0.67
(8920, 1/2), (8920, 1/3), (8920, 1/4), (8920, 1/6)	46	–0.66

Table 24. Subcarrier Demodulation HRM Loss Coefficients for Turbo Codes Using Sinewave Subcarriers

Turbo Codes	Subcarrier Demodulation Loss Coefficient c_0	Subcarrier Demodulation Loss Coefficient c_1
(1784, 1/2), (1784, 1/3), (1784, 1/4), (1784, 1/6)	6490	–2.23
(3568, 1/2), (3568, 1/3), (3568, 1/4), (3568, 1/6)	2450	–1.97
(7136, 1/2), (7136, 1/3), (7136, 1/4), (7136, 1/6)	881	–1.67
(8920, 1/2), (8920, 1/3), (8920, 1/4), (8920, 1/6)	768	–1.63

5.5 *Symbol Synchronization*

Imperfect symbol synchronization results in a finite symbol synchronization loss, η_{SYM} ($0 < \eta_{SYM} \leq 1$), which is a contributor to system loss. The symbol synchronization loss is a function of symbol loop signal-to-noise ratio.

The signal-to-noise ratio ρ_{SYM} in the symbol synchronization loop is given by (Reference 11)

$$\rho_{SYM} = \frac{2}{(2\pi)^2} \cdot \frac{S_{SYM}}{W_{SYM} B_{SYM}} \cdot \frac{P_D}{N_0} \tag{45}$$

where B_{SYM} is the (one-sided) noise-equivalent symbol loop bandwidth, W_{SYM} is the symbol loop window factor ($W_{SYM}=2^{-n}$, where n = 0, 1, 2, 3, or 4), and S_{SYM} is the squaring loss of the symbol loop. In the case of QPSK/OQPSK, the P_D/N_0 of Equation (45) should be interpreted as 1/2 (P_T/N_0), since only the power in one of the two quadrature channels assists the symbol synchronization process. S_{SYM} takes on values from 0 to 1 and asymptotically equals 1 for large values of E_s/N_0. Figure 24 shows S_{SYM} (dB) as a function of E_s/N_0. Appendix G gives equations for calculating S_{SYM}.

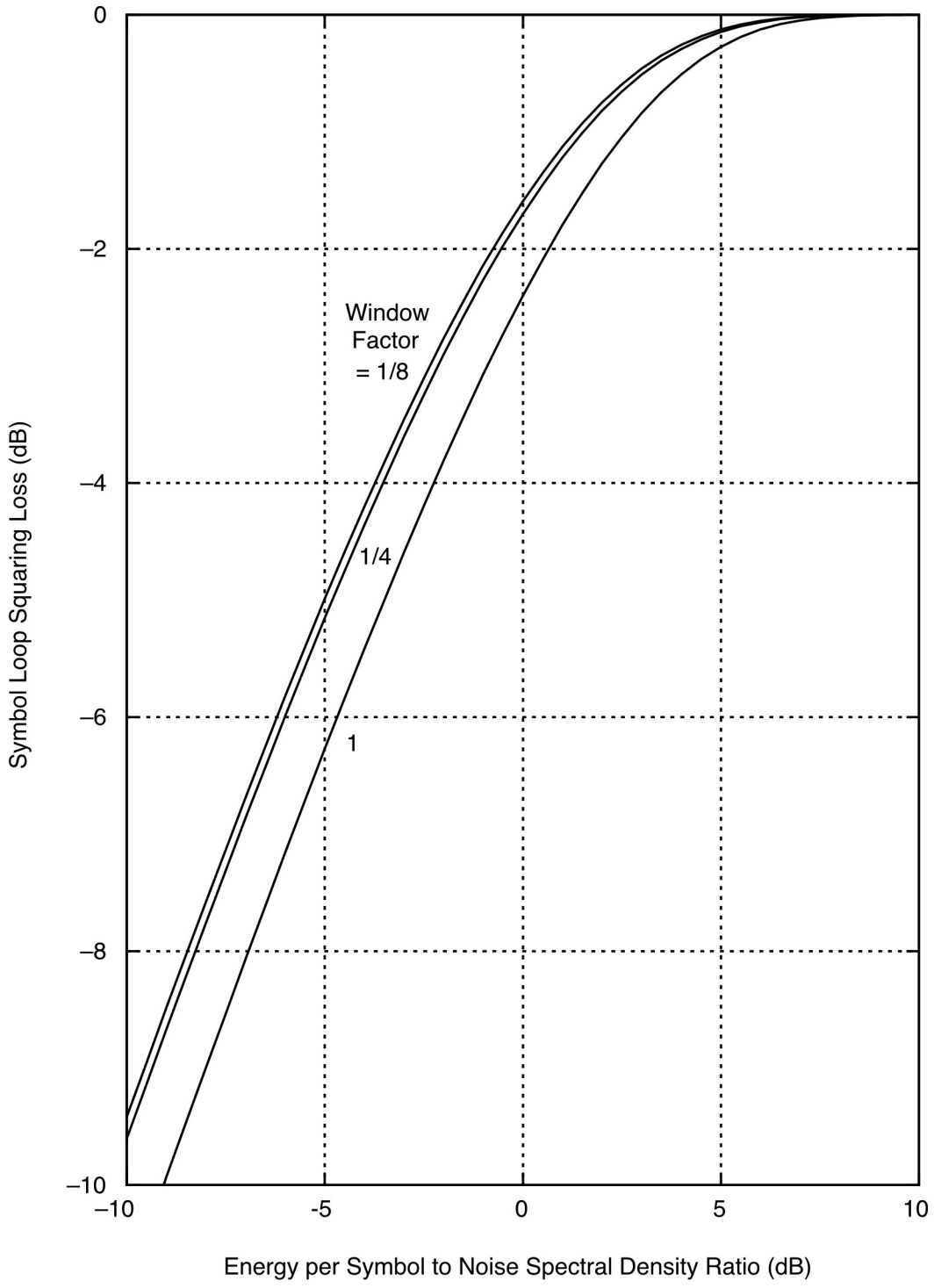

Figure 24. Symbol Loop Squaring Loss

It is recommended that the following constraint on symbol synchronization be observed.

$$\rho_{SYM} \geq 31.6 \text{ (15 dB)} \tag{46}$$

The inequality (46) is based on the assumption that the symbol transition density is approximately 0.5 or higher. If the symbol transition density is closer to 0.25, then it is recommended that ρ_{SYM} be at least 18 dB.

Symbol synchronization loss is modeled as an interpolation between a High-Rate Model (HRM) and a Low-Rate Model (LRM). This interpolation is

$$\eta^*_{SYM} = a \cdot \eta^*_{HSYM} + (1-a) \cdot \eta^*_{LSYM} \tag{47}$$

where

η^*_{SYM} = positive decibel symbol synchronizer loss $\left(\eta^*_{SYM} = -10 \log \eta_{SYM}\right)$

η^*_{HSYM} = positive decibel HRM symbol synchronizer loss

η^*_{LSYM} = positive decibel LRM symbol synchronizer loss

a = interpolation factor ($0 \leq a \leq 1$)

The interpolation factor depends on the code. For uncoded and convolutionally coded telemetry, the interpolation factor a is given by

$$a = \frac{1}{4B_{SYM}T_{SYM}}\left[1 - \frac{1}{8B_{SYM}T_{SYM}}\left(1 - e^{-8B_{SYM}T_{SYM}}\right)\right] \tag{48}$$

where B_{SYM} is the symbol loop bandwidth and T_{SYM} is the symbol period (the reciprocal of symbol rate). For concatenated and turbo codes, the interpolation factor a is given by

$$a = \frac{1}{1 + c_1\left(R/B_{SYM}\right)^{-c_2}} \tag{49}$$

where R is the bit rate. The coefficients c_1 and c_2 were provided in Table 18 for concatenated codes and in Table 10 for turbo codes.

The HRM symbol synchronization loss is modeled with a curve-fit of the form

$$\eta^*_{HSYM} = c_0\left(\rho_{SYM}\right)^{c_1} \tag{50}$$

where the HRM coefficients c_0 and c_1 depend on the code. For uncoded and convolutionally coded telemetry, the coefficients of Equation (50) are $c_0 = 2.2$ and $c_1 = -0.62$. In fact, an

excellent approximation for η^*_{SYM} may be obtained in this case (without the need for an interpolation) as follows

$$\eta^*_{SYM} = 2.2\left(\rho_{SYM}\right)^{-0.62}. \tag{51}$$

The HRM coefficients c_0 and c_1 of Equation (50) are given in Table 25 for concatenated codes at a threshold FER of 1×10^{-5} and in Table 26 for the turbo codes listed in Table 8 at a threshold FER of 1×10^{-4}.

Table 25. Symbol Synchronization HRM Loss Coefficients for Concatenated Codes

Concatenated Code	Symbol Synchronization Loss Coefficient c_0	Symbol Synchronization Loss Coefficient c_1
RS with (k=7, r=1/2) Convolutional	9.7	–0.77
RS with (k=15, r=1/4) or (k=15, r=1/6) Convolutional	8.2	–0.68

Table 26. Symbol Synchronization HRM Loss Coefficients for Turbo Codes

Turbo Codes	Symbol Synchronization Loss Coefficient c_0	Symbol Synchronization Loss Coefficient c_1
(1784, 1/2), (1784, 1/3), (1784, 1/4), (1784, 1/6)	6.6	–0.75
(3568, 1/2), (3568, 1/3), (3568, 1/4), (3568, 1/6)	7.3	–0.75
(7136, 1/2), (7136, 1/3), (7136, 1/4), (7136, 1/6)	7.4	–0.69
(8920, 1/2), (8920, 1/3), (8920, 1/4), (8920, 1/6)	6.8	–0.66

The LRM symbol synchronization loss is independent of the code and can be modeled with a curve-fit of the same form (but with different coefficients)

$$\eta^*_{LSYM} = 2.27\left(\rho_{SYM}\right)^{-0.50} \tag{52}$$

5.6 Waveform Distortion

Deviations of either the subcarrier waveform or the symbol waveform from ideal will adversely affect telemetry performance. In general, waveform distortion loss η_{WD} (fractional and dimensionless) is the composite loss factor that incorporates both of these deviations. η_{WD}, in turn, is a contributor to the system loss η_{SYS}.

In the case of no subcarrier, only the symbol waveform deviation is of concern.

$$\eta_{WD} = 1 - 2\left(\frac{\Delta T_{SYM}}{T_{SYM}}\right) + 2\left(\frac{\Delta T_{SYM}}{T_{SYM}}\right)^2 \tag{53}$$

T_{SYM} is the symbol period in seconds. The parameter ΔT_{SYM} is a measure of the finite risetime is recommended that ΔT_{SYM} be less than 2 percent.

In the case of a squarewave subcarrier,

$$\eta_{WD} = \left[1 - \frac{2\Delta T_{SUB}}{T_{SUB}}\right]^2 \cdot \left[1 - 2\left(\frac{\Delta T_{SYM}}{T_{SYM}}\right) + 2\left(\frac{\Delta T_{SYM}}{T_{SYM}}\right)^2\right] \tag{54}$$

where T_{SUB} is the subcarrier period in seconds and ΔT_{SUB} its asymmetry. Equation (54) is not applicable in the case of a sinewave subcarrer. The waveform distortion loss associated with a sinewave subcarrier should normally be negligible.

5.7 Amplitude Scintillation at Small Sun-Earth-Probe (SEP) Angles

When the Sun-Earth-Probe (SEP) angle is small and the spacecraft is beyond the sun, Rician fading of the signal occurs due to multipath propagation of the downlink signal within the solar corona. This is called amplitude scintillation. The effect is worse at lower carrier frequencies. For small SEP angels, the BER or FER increases dramatically as a result of amplitude scintillation. Appendix I summarizes the theory of amplitude scintillation. Figures 25, 26, and 27 illustrate the degradation to FER for a (1784, 1/3) turbo code due to amplitude scintillation for the cases of S-band, X-band and Ka-band, respectively.

Turbo codes have an error floor in their performance that are not shown in Figures 25 through 27. The error floor is different for each turbo code but, for each of the turbo codes shown here, the error floor lies below a frame error rate of 10^{-5} and therefore is not visible in the figures. Great care must be taken in evaluating the performance of these codes for frame error rates less than 10^{-5}.

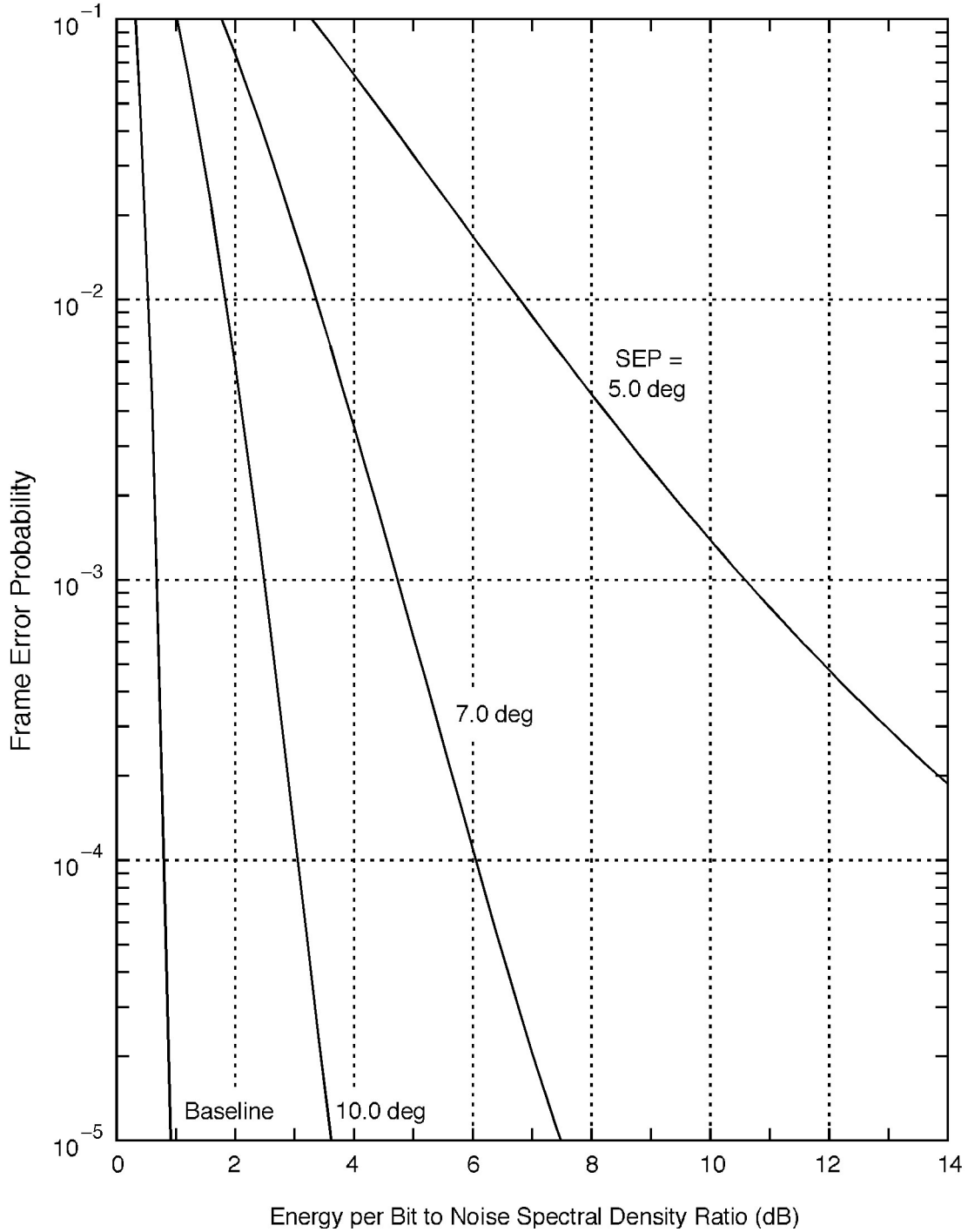

Figure 25. (1784, 1/3) Turbo Code Performance at S-Band With Amplitude Scintillation

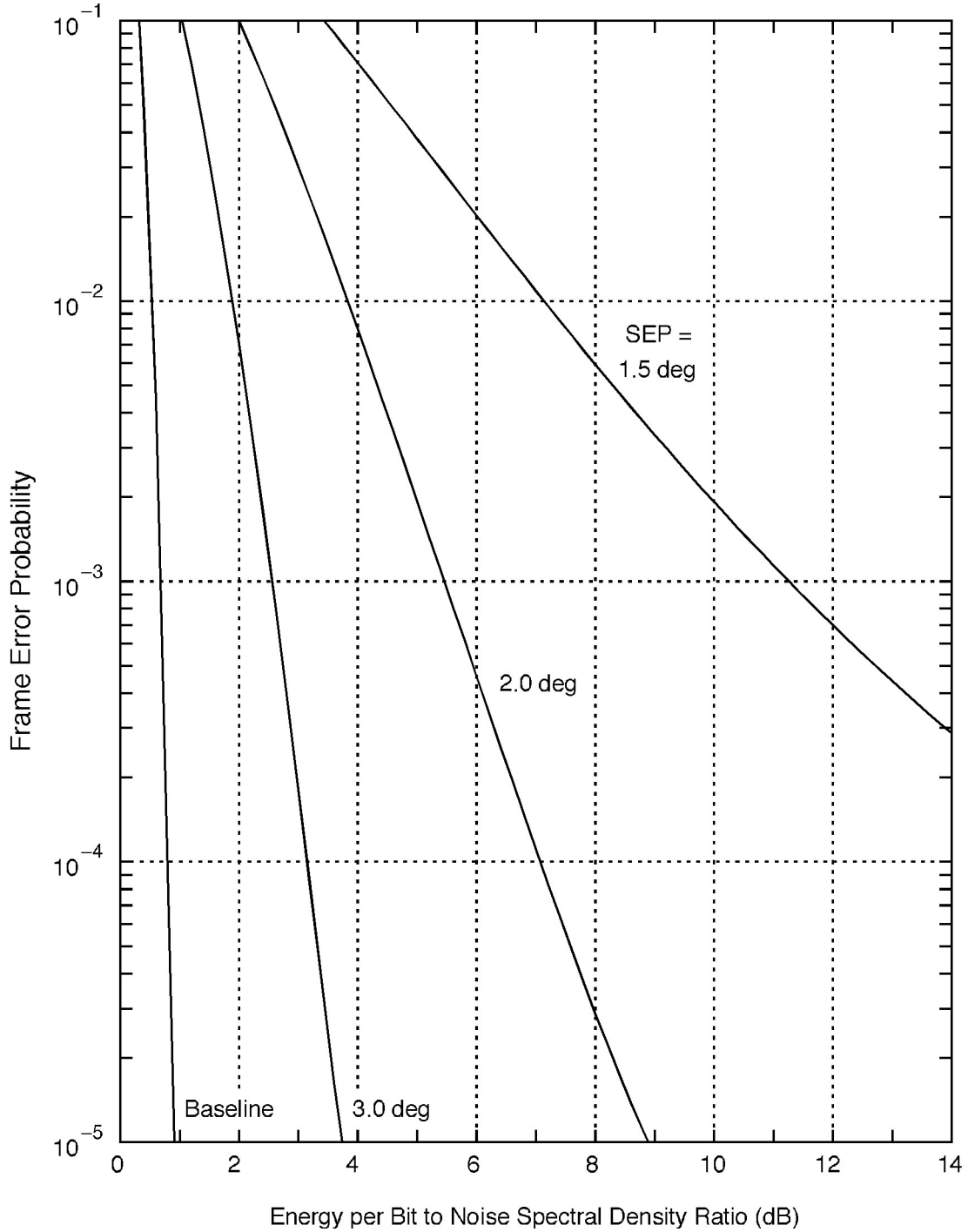

Figure 26. (1784, 1/3) Turbo Code Performance at X-Band With Amplitude Scintillation

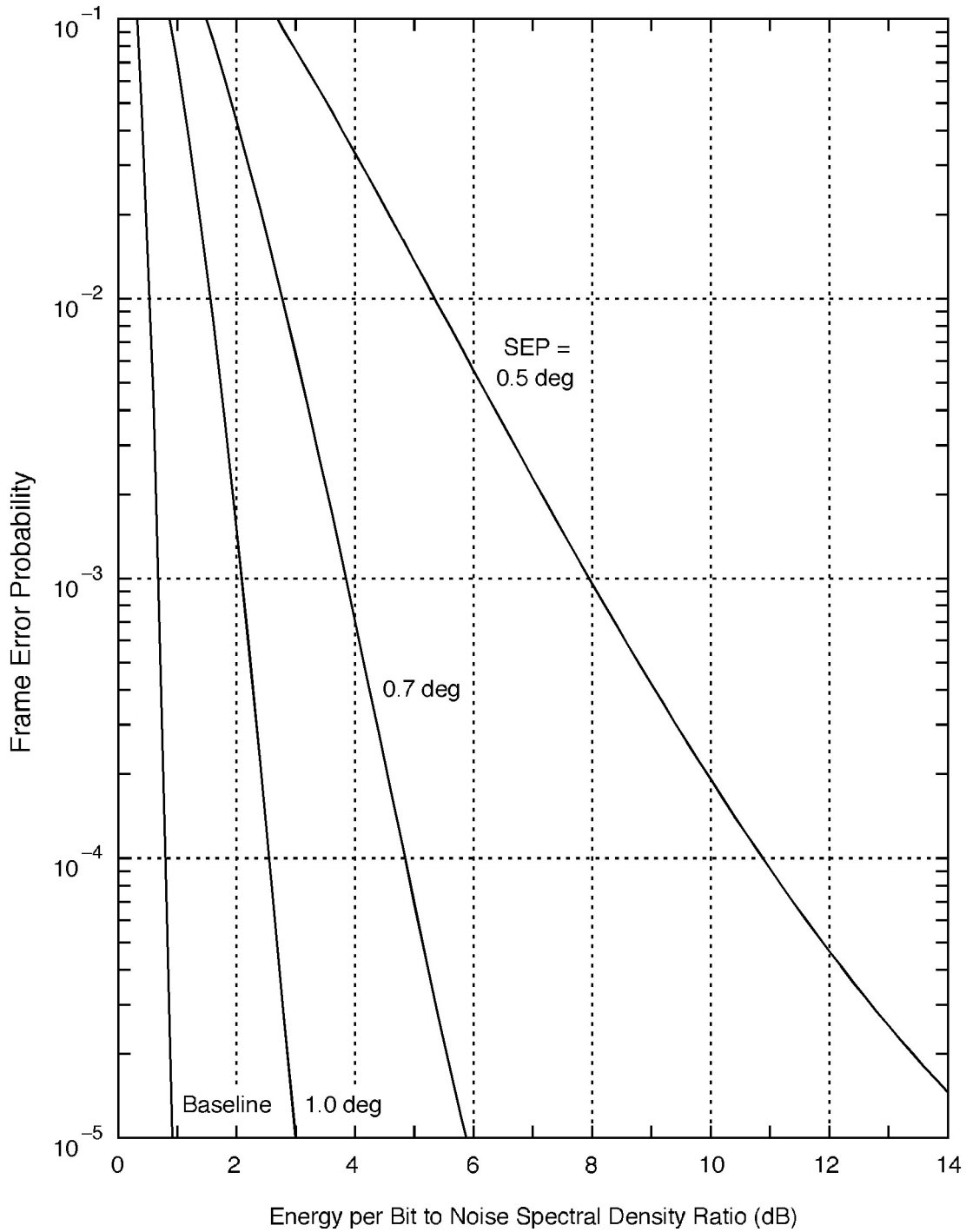

Figure 27. (1784, 1/3) Turbo Code Performance at Ka-Band With Amplitude Scintillation

Appendix A
Baseline BER and FER Performance

The baseline performance is the Bit Error Rate (BER) or Frame Error Rate (FER) when synchronization is perfect (i.e., with a system loss of 0 dB). For uncoded and convolutionally coded telemetry, BER is the appropriate figure of merit. For concatenated and turbo codes, FER is the appropriate figure of merit.

A.1 Uncoded and Convolutionally Coded Telemetry

For uncoded and convolutionally coded telemetry, the functional dependence of BER on E_b/N_0 in the ideal case of no system loss is here denoted

$$\text{Baseline:} \qquad \text{BER} = f(E_b/N_0) \tag{A-1}$$

In Equation (A-1), E_b/N_0 is a dimensionless quantity (i.e., it is the true ratio of bit energy to noise spectral density). This performance is never achieved in practice. Nonetheless, this idealized performance is a useful reference (baseline) from which to measure actual performance. For uncoded telemetry,

$$f(x) = \frac{1}{2}\operatorname{erfc}\left(\sqrt{x}\right) \tag{A-2}$$

where

$$\operatorname{erfc}(x) = 1 - \operatorname{erf}(x) = 1 - \frac{2}{\sqrt{\pi}}\int_0^x e^{-y^2}\,dy \tag{A-3}$$

For convolutionally coded telemetry, the baseline telemetry performance is approximated as

$$f(x) = \min\left\{\frac{1}{2}, \exp\left(a_0 - a_1 x\right)\right\} \tag{A-4}$$

where the coefficients a_0 and a_1 depend on the particular convolutional code, as indicated in Table A-1.

Table A-1. Coefficients a_0 and a_1 for Equation (A-4)

Code	a_0	a_1
$(k = 7, r = 1/2)$	4.4514	5.7230
$(k = 15, r = 1/4)$	9.8070	13.431
$(k = 15, r = 1/6)$	9.8070	14.064

A.2 Concatenated and Turbo-Coded Telemetry

For concatenated and turbo codes, the functional dependence of FER on E_b/N_0 in the ideal case of no system loss is here denoted

$$\text{Baseline:} \quad \text{FER} = f(E_b/N_0) \tag{A-5}$$

In Equation (A-5), E_b/N_0 is a dimensionless quantity (i.e., it is the true ratio of bit energy to noise spectral density). This performance is never achieved in practice. Nonetheless, this idealized performance is a useful reference (baseline) from which to measure actual performance.

The baseline telemetry performance for concatenated codes is approximated as

$$f(x) = \min\{1, \exp(a_0 - a_1 x)\} \tag{A-6}$$

where the coefficients a_0 and a_1 depend on the particular code, as indicated in Table A-2.

Table A-2. Coefficients a_0 and a_1 for Equation (A-6), Concatenated Codes

Concatenated Code	a_0	a_1
RS with (k=7, r=1/2) Convolutional	105.0019	67.4242
RS with (k=15, r=1/4) Convolutional	158.2971	127.5629
RS with (k=15, r=1/6) Convolutional	158.2971	133.5748

Simulations performed at JPL have characterized the baseline performance of the turbo codes. Tables A-3 through A-6 give the simulation data for these codes. This results were obtained by using 10 decoding iterations per frame. In this module, the baseline performance of the turbo codes is based on interpolations of the simulation data given below.

Table A-3. Rate 1/2 Turbo Code Baseline Data

E_b/N_0	Turbo Code			
	(1784, 1/2)	(3568, 1/2)	(7136, 1/2)	(8920, 1/2)
0.4		1.0000E+00		
0.5		—		1.0000E+00
0.6	7.5000E–01	8.0000E–01		8.8496E–01
0.7	—	—	5.5266E–01	5.9524E–01
0.8	3.8931E–01	2.6247E–01	1.8382E–01	1.8939E–01
0.9	—	—	2.5046E–02	2.0309E–02
1.0	7.5529E–02	2.2411E–02	1.4271E–03	8.4691E–04
1.1	—	—	7.7270E–05	3.5650E–05
1.2	7.9605E–03	3.1980E–04	7.6700E–06	1.5510E–05
1.3	—	—		1.2280E–05
1.4	3.2503E–04	4.0800E–06		6.7700E–06
1.5	—	—		
1.6	1.1620E–05	1.5800E–06		
1.7	—	—		
1.8	3.7500E–06	5.8000E–07		
1.9	—	—		
2.0	2.2500E–06	6.0000E–08		
2.1	—	—		
2.2	7.5000E–07	1.1000E–07		

Table A-4. Rate 1/3 Turbo Code Baseline Data

E_b/N_0	Turbo Code			
	(1784, 1/3)	(3568, 1/3)	(7136, 1/3)	(8920, 1/3)
–0.4	9.9020E–01			
–0.3	—			
–0.2	9.0090E–01			
–0.1	—			
0.0	6.8493E–01			8.3333E–01
0.1	—		4.3328E–01	4.9505E–01
0.2	2.9762E–01	1.8065E–01	1.0761E–01	9.7752E–02
0.3	—	5.1557E–02	1.0989E–02	8.9847E–03
0.4	4.7174E–02	9.0463E–03	4.4099E–04	2.0755E–04
0.5	—	9.5734E–04	1.0050E–05	2.8730E–05
0.6	4.4583E–03	4.1120E–05		1.4360E–05
0.7	—	4.5100E–06		1.1490E–05
0.8	9.2350E–05			
0.9	—			
1.0	1.9100E–06			

Table A-5. Rate 1/4 Turbo Code Baseline Data

E_b/N_0	Turbo Code			
	(1784, 1/4)	(3568, 1/4)	(7136, 1/4)	(8920, 1/4)
–0.4				
–0.3				9.9010E–01
–0.2				8.4746E–01
–0.1			3.3866E–01	3.7594E–01
0.0	2.3810E–01	1.3508E–01	6.7147E–02	7.3260E–02
0.1	1.4006E–01	3.1327E–02	5.5659E–03	2.9790E–03
0.2	3.8865E–02	4.1032E–03	2.9471E–04	5.4510E–05
0.3	9.9325E–03	4.9503E–04	1.0723E–04	2.5700E–06
0.4	2.1765E–03	6.0170E–05		2.0300E–06
0.5	4.9670E–04			1.7100E–06
0.6	7.7840E–05			7.8000E–07
0.7	1.0430E–05			
0.8	3.1900E–06			
0.9	1.7100E–06			
1.0	9.7000E–07			
1.1	5.1000E–07			
1.2	6.6000E–07			

Table A-6. Rate 1/6 Turbo Code Baseline Data

E_b/N_0	Turbo Code			
	(1784, 1/6)	(3568, 1/6)	(7136, 1/6)	(8920, 1/6)
–0.50				9.0909E–01
–0.45				7.2464E–01
–0.40			4.7659E–01	4.7619E–01
–0.35			—	2.8653E–01
–0.30	2.7855E–01		1.1924E–01	9.9701E–02
–0.25	—		—	3.2362E–02
–0.20	1.4793E–01	4.8632E–02	1.2559E–02	6.6542E–03
–0.15	—	—	—	1.1703E–03
–0.10	5.1203E–02	7.2787E–03	6.4147E–04	1.3089E–04
–0.05	—	—	—	1.6310E–05
0.0	1.1990E–02	9.2768E–04	4.5750E–05	5.5200E–06
0.05	—	—		4.3200E–06
0.10	3.5388E–03	5.9720E–05		2.4000E–06
0.15	—	—		
0.20	5.8113E–04	9.6500E–06		
0.25	—			
0.30	5.7830E–05			
0.35	—			
0.40	9.9500E–06			
0.45	—			
0.50	2.3400E–06			

Appendix B
High-Rate Model (HRM) Radio Loss

The High-Rate Model (HRM) is discussed in this appendix in terms of Bit Error Rate (BER); but for concatenated and turbo codes, Frame Error Rate (FER) is the proper figure of merit. So for these codes, the reader should regard BER in the following equations as being a stand-in for FER.

The HRM radio loss, η_{HRM} (fractional and dimensionless), is given by

$$\eta_{HRM} = \frac{f^{-1}(BER)}{E_b/N_0} \tag{B-1}$$

where $f(*)$ is the ideal functional dependence of probability of bit (frame) error on bit SNR (see Appendix A), corresponding to zero decibels of system loss. In the above equation, E_b/N_0 is the actual bit SNR needed to achieve a given threshold BER in the presence of imperfect carrier synchronization; it is the solution of the following equation (Reference 12)

$$BER = \int_{-\pi/2}^{\pi/2} f\left(\frac{E_b}{N_0}\cos^2\phi\right) p_\phi(\phi)\, d\phi \tag{B-2}$$

where $p_\phi(\phi)$ is the probability density function of the carrier loop phase error ϕ and BER is, as before, the threshold bit error rate.

When tracking a residual carrier,

$$p_\phi(\phi) = \frac{\exp\left[\dfrac{\cos\phi}{\sigma_\phi^2}\right]}{\displaystyle\int_{-\pi/2}^{\pi/2} \exp\left[\dfrac{\cos\psi}{\sigma_\phi^2}\right] d\psi}, \quad |\phi| \le \pi/2 \tag{B-3}$$

When tracking suppressed carrier BPSK,

$$p_\phi(\phi) = \frac{\exp\left[\dfrac{\cos\phi}{4\sigma_\phi^2}\right]}{\displaystyle\int_{-\pi/2}^{\pi/2} \exp\left[\dfrac{\cos 2\psi}{4\sigma_\phi^2}\right] d\psi}, \quad |\phi| \le \pi/2 \tag{B-4}$$

For either case, $p_\phi(\phi)$ is assumed to be zero for $|\phi| > \pi/2$. The parameter σ_ϕ^2 is the carrier loop phase error variance. The presence of $f(*)$ in Equation (B-2) means that the HRM radio loss depends on the coding scheme; it also depends on the threshold BER.

When there is a static phase error caused by Doppler dynamics, $p_\phi(\phi)$ has a different form. For a residual-carrier loop

$$p_\phi(\phi) = \frac{\exp\left[\dfrac{\cos\phi + \phi\sin\xi_{spe}}{\sigma_\phi^2}\right]}{\displaystyle\int_{-\pi/2}^{\pi/2} \exp\left[\dfrac{\cos\psi + \psi\sin\xi_{spe}}{\sigma_\phi^2}\right] d\psi}, \quad |\phi| \le \pi/2 \tag{B-5}$$

where ξ_{spe} is the static phase error.

Appendix C
Static Phase Error

The carrier loop, either as type 2 or type 3, has a very large tracking range; even a Doppler offset of several megahertz can be tracked. With a finite Doppler rate, however, there will be a static phase error in a type 2 loop.

Table C-1 shows the static phase error in the carrier that results from various Doppler dynamics for several different loops. These equations are based on the work reported in Reference 13 where standard underdamped and supercritically damped loops are defined. B_L is the (one-sided) noise-equivalent loop bandwidth of the carrier loop. The Doppler dynamics are here defined by the parameters α, β, and t where α is the Doppler Rate (Hz/s), β is the Doppler Acceleration (Hz/s^2), and t is the time since the beginning of the Doppler acceleration. (If the Doppler acceleration begins before carrier lock, t is the time since the loop acquired lock.)

The equations of Table C-1 are valid for either residual-carrier or suppressed-carrier BPSK, QPSK or OQPSK. In the presence of a persistent Doppler acceleration, a type 2 loop will periodically slip cycles.

Table C-1. Static Phase Error (rad)

Loop	**Constant Range-Rate**	**Constant Derivative of Range-Rate**	**Constant Second Derivative of Range-Rate**
	Constant Doppler Offset	**Constant Doppler Rate**	**Constant Doppler Acceleration**
type 2, standard underdamped	0	$\frac{9\pi}{16 B_L^2} \cdot \alpha$	$\left(\frac{9\pi\beta}{16 B_L^2}\right) t - \frac{27\pi\beta}{64 B_L^3}$
type 2, supercritically damped	0	$\frac{25\pi}{32 B_L^2} \cdot \alpha$	$\left(\frac{25\pi\beta}{32 B_L^2}\right) t - \frac{125\pi\beta}{128 B_L}$
type 3, standard underdamped	0	0	$\frac{12167\pi}{8000 B_L^3}\beta$
type 3, supercritically damped	0	0	$\frac{35937\pi}{16384 B_L^3}\beta$

Appendix D
Transmitter Phase Noise

Transmitter phase noise contributes to the phase error in the receiver's carrier loop. This contribution is a zero-mean random process, and its variance equals

$$\sigma_\phi^2 = \int_0^\infty S_\theta(f)\left|1 - H(j2\pi f)\right|^2 df \text{, rad}^2 \tag{D-1}$$

where $S_\theta(f)$ is the one-sided power spectral density of the transmitter phase noise and $H(j2\pi f)$ is the phase transfer function of the carrier loop. $S_\theta(f)$, with units of rad^2/Hz, is related to $L_\theta(f)$, the modulation sideband power spectral density relative to the carrier power, measured in the units dBc/Hz (Reference 14).

$$L_\theta(f) = 10\log\left(\frac{1}{2}S_\theta(f)\right) \tag{D-2}$$

For example, if the transmitter phase noise is flicker-of-frequency (i.e., $L_\theta(f)$ decreases with Fourier frequency f at a rate of 30 decibels per decade) in the frequency range of interest, and if $L_\theta(1\text{ Hz}) = -45$ dBc/Hz, then $S_\theta(f)$ may be modeled as S_3/f^3 with S_3 given by $2 \times 10^{-45/10} = 0.000063$.

For a type 2 loop, the phase transfer function $H(j2\pi f)$ is given by (Reference 13):

$$H(j2\pi f) = \frac{(j2\pi f)K_1 + K_2}{(j2\pi f)^2 + (j2\pi f)K_1 + K_2} \tag{D-3}$$

where

$$K_1 = \frac{8}{3}B_L, \quad K_2 = \frac{1}{2}K_1^2, \quad \text{(standard underdamped)}$$

$$K_1 = \frac{16}{5}B_L, \quad K_2 = \frac{1}{4}K_1^2, \quad \text{(supercritically damped)}$$

For a type 3 loop, the phase transfer function $H(j2\pi f)$ is given by (Reference 13):

$$H(j2\pi f) = \frac{(j2\pi f)^2 K_1 + (j2\pi f)K_2 + K_3}{(j2\pi f)^3 + (j2\pi f)^2 K_1 + (j2\pi f)K_2 + K_3} \tag{D-4}$$

where

$$K_1 = \frac{60}{23} B_L \,, \quad K_2 = \frac{4}{9} K_1^{\,2} \,, \quad K_3 = \frac{2}{27} K_1^{\,3}, \text{ (standard underdamped)}$$

$$K_1 = \frac{32}{11} B_L \,, \quad K_2 = \frac{1}{3} K_1^{\,2} \,, \quad K_3 = \frac{1}{27} K_1^{\,3} \text{ (supercritically damped)}$$

Table D-1 lists solutions to Equation (D-1) for several types of carrier loop and for two types of phase noise. These expressions are valid for residual-carrier, suppressed-carrier BPSK, or QPSK/OQPSK. B_L is the (one-sided) noise-equivalent carrier loop bandwidth.

Table D-1. Carrier Phase Error Variance, $\sigma_\phi^{\,2}$ (rad^2)

	type 2 standard underdamped	**type 2 supercritically damped**	**type 3 standard underdamped**	**type 3 supercritically damped**
$S_\theta(f) = \frac{S_2}{f^2}$	$\frac{3\pi^2}{8B_L} S_2$	$\frac{5\pi^2}{16B_L} S_2$	$\frac{23\pi^2}{50B_L} S_2$	$\frac{99\pi^2}{256B_L} S_2$
$S_\theta(f) = \frac{S_3}{f^3}$	$\frac{9\pi^3}{32B_L^{\,2}} S_3$	$\frac{25\pi^2}{32B_L^{\,2}} S_3$	$\frac{529\pi^2(\pi - \ln 2)}{1000B_L^{\,2}} S_3$	$\frac{1089\pi^3}{1024B_L^{\,2}} S_3$

Appendix E
Solar Phase Noise

When the Sun-Earth-probe angle is small and the spacecraft is beyond the Sun, microwave carriers pick up phase scintillations in passing through the solar corona. There is a resulting contribution to phase error in the carrier loop. The magnitude of the effect is highly variable, depending on the activity of the sun. Equation (E-1) below, based on the work reported in Reference 15, offers a coarse estimate of the average solar contribution, in units of rad^2, to carrier loop phase error variance. This equation is valid for residual-carrier, suppressed-carrier BPSK or QPSK/OQPSK, but only for sun-earth-probe angles between 5° and 27°.

$$\sigma_S^2 = \frac{C_{band} \cdot C_{loop}}{(\sin\beta)^{2.45} \cdot B_L^{1.65}}, \quad 5° \le \beta \le 27° \tag{E-1}$$

In Equation (E-1), β is the Sun-Earth-probe angle and B_L is the (one-sided) noise-equivalent carrier loop bandwidth. C_{band} is a constant for a given set of operating bands.

For one-way or two-way noncoherent operation,

$$C_{band} = \begin{cases} 2.6\times10^{-5}, & \text{S-down} \\ 1.9\times10^{-6}, & \text{X-down} \\ 1.3\times10^{-7}, & \text{Ka-down} \end{cases} \tag{E-2}$$

For coherent operation,

$$C_{band} = \begin{cases} 6.1\times10^{-5}, & \text{S-up / S-down} \\ 4.8\times10^{-4}, & \text{S-up / X-down} \\ 5.5\times10^{-6}, & \text{X-up / X-down} \\ 5.2\times10^{-5}, & \text{X-up / Ka-down} \\ 1.9\times10^{-6}, & \text{Ka-up / X-down} \\ 2.3\times10^{-7}, & \text{Ka-up / Ka-down} \end{cases} \tag{E-3}$$

where C_{loop} is a constant for a given carrier loop.

$$C_{loop} = \begin{cases} 5.9, & \text{standard underdamped type 2 loop} \\ 5.0, & \text{supercritically damped type 2 loop} \\ 8.2, & \text{standard underdamped type 3 loop} \\ 6.7, & \text{supercritically damped type 3 loop} \end{cases} \tag{E-4}$$

Appendix F
Subcarrier Demodulation Loss

The subcarrier demodulation loss is discussed in this appendix in terms of Bit Error Rate (BER); but for concatenated and turbo codes, Frame Error Rate (FER) is the proper figure of merit. So for these codes, the reader should regard BER in the following equations as being a stand-in for FER.

The subcarrier demodulation loss η_{SUB} (fractional and dimensionless) is

$$\eta_{SUB} = \frac{f^{-1}(BER)}{E_b / N_0} \tag{F-1}$$

where $f(*)$ is the ideal functional dependence of probability of bit (frame) error on bit SNR (see Appendix A), corresponding to zero decibels of system loss. In Equation (F-1) E_b/N_0 is the actual bit SNR needed to achieve a given threshold BER in the presence of imperfect subcarrier synchronization (with the assumption of perfect carrier and symbol synchronization); in the case of a squarewave subcarrier, it is the solution of the following equation

$$BER = \int_{-\pi/2}^{\pi/2} f\left(\frac{E_b}{N_0}\left[1-\frac{2}{\pi}|\phi|\right]^2\right) p_\phi(\phi)\, d\phi \tag{F-2}$$

where BER is, as before, the threshold bit error rate. The probability density function $p_\phi(\phi)$ of squarewave subcarrier loop phase error ϕ is modeled as having a Gaussian form within the limits $|\phi| \le \pi/2$ and as zero outside those limits.

$$p_\phi(\phi) = \frac{\exp\left(-\rho_{SUB}\phi^2/2\right)}{\int_{-\pi/2}^{\pi/2} \exp\left(-\rho_{SUB}\psi^2/2\right) d\psi} \tag{F-3}$$

where ρ_{SUB} is the squarewave subcarrier loop signal-to-noise ratio as computed from Equation (37). Equations (F-1), (F-2), and (F-3) define the subcarrier demodulation loss for a squarewave subcarrier. The presence of $f(*)$ in Equation (F-2) means that the subcarrier demodulation loss depends on the coding scheme; it also depends on the threshold BER.

For a sinewave subcarrier, the subcarrier demodulation loss is governed by Equations (B-1), (B-2), and (B-4), which also characterize the HRM radio loss with suppressed carrier, except that σ_ϕ^2 is replaced by $1/\rho_{SUB}$, where ρ_{SUB} is the sinewave subcarrier signal-to-noise ratio as defined in Equation (37).

Appendix G
Symbol Loop Squaring Loss

Symbol loop squaring loss S_{SYM} is given by (Reference 11)

$$S_{SYM} = \frac{\left[\operatorname{erf}\left(\sqrt{E_S/N_0}\right) - \frac{W_{SYM}}{2}\sqrt{\frac{E_S/N_0}{\pi}}\exp\left(-E_S/N_0\right)\right]^2}{1 + \frac{W_{SYM}}{2}E_S/N_0 - \frac{W_{SYM}}{2}\left[\frac{1}{\sqrt{\pi}}\exp\left(-E_S/N_0\right) + \sqrt{E_S/N_0}\operatorname{erf}\left(\sqrt{E_S/N_0}\right)\right]^2} \tag{G-1}$$

where the error function is given by

$$\operatorname{erf}(x) = \frac{2}{\sqrt{\pi}}\int_0^x e^{-y^2}\,dy \tag{G-2}$$

E_S/N_0 is the ratio of the energy in one binary symbol to the one-sided noise spectral density. In the case of suppressed-carrier BPSK, this is $(P_T/N_0)T_{SYM}$, where T_{SYM}, is the binary symbol period. In the case of QPSK/OQPSK, only half the total power is available for symbol synchronization but the quaternary symbol period is double the binary symbol period. So for QPSK/OQPSK, the same E_S/N_0 should be used as with suppressed-carrier BPSK, since

$$\frac{1}{2}\left(P_T/N_0\right)\cdot 2T_{SYM} = \left(P_T/N_0\right)\cdot T_{SYM}\,. \tag{G-3}$$

Appendix H
Symbol Synchronization Loss

The symbol synchronization loss is discussed in this appendix in terms of Bit Error Rate (BER); but for concatenated and turbo codes, Frame Error Rate (FER) is the proper figure of merit. So, for these codes, the reader should regard BER in the following equations as being a stand-in for FER.

The symbol synchronization loss η_{SYM} (fractional and dimensionless) is

$$\eta_{SYM} = \frac{f^{-1}(BER)}{E_b/N_0} \tag{H-1}$$

where $f(*)$ is the ideal functional dependence of probability of bit (frame) error on bit SNR (see Appendix A), corresponding to zero decibels of system loss. In Equation (H-1) E_b/N_0 is the actual bit SNR needed to achieve a given threshold BER in the presence of imperfect symbol synchronization (with the assumption of perfect carrier and subcarrier synchronization); it is the solution of the following equation

$$BER = \int_{-\pi/2}^{\pi/2} f\left(\frac{E_b}{N_0}\left[\frac{1}{2}\left\{1+\left(1-\frac{|\phi|}{\pi}\right)^2\right\}\right]\right) p_\phi(\phi)\,d\phi \tag{H-2}$$

where BER is, as before, the threshold bit error rate. The probability density function $p_\phi(\phi)$ of symbol loop phase error ϕ is modeled as having a Gaussian form within the limits $|\phi| \le \pi/2$ and as zero outside those limits.

$$p_\phi(\phi) = \frac{\exp\left(-\rho_{SYM}\phi^2/2\right)}{\int_{-\pi/2}^{\pi/2} \exp\left(-\rho_{SYM}\psi^2/2\right)d\psi} \tag{H-3}$$

In Equation (H-3) ρ_{SYM} is the symbol loop signal-to-noise ratio as computed from Equation (45).

Appendix I
Rician Fading at Small Sun-Earth-Probe (SEP) Angles

The discussion in this appendix is in terms of Bit Error Rate (BER); but for concatenated and turbo codes, Frame Error Rate (FER) is the proper figure of merit. So for these codes, the reader should regard BER in the following equations as being a stand-in for FER.

The BER of a signal subjected to Rician fading is given by

$$BER = \int_0^\infty f\left(x^2 E_b/N_0\right) p_r(x)\, dx \tag{I-1}$$

where $f(*)$ is the ideal functional dependence of probability of bit (frame) error on bit SNR (see Appendix A) in the absence of amplitude scintillation and system loss. Equation (I-1) represents an averaging over the random, normalized amplitude factor r, which is governed by the Rician probability density function

$$p_r(x) = 2x(1+K)\exp(-K)\exp\left[-(1+K)x^2\right] \mathrm{I}_0\left(2x\sqrt{K(1+K)}\right), \qquad r \geq 0 \tag{I-2}$$

where $\mathrm{I}_0(*)$ is the modified Bessel function of the first kind of order zero and K is the Rice factor ($K > 0$). A smaller Rice factor indicates more severe fading. This Rice factor K is related to the scintillation index m by

$$K = \left(\frac{1}{m^2} - 1\right) + \sqrt{\left(\frac{1}{m^2} - 1\right)^2 + \left(\frac{1}{m^2} - 1\right)} \tag{I-3}$$

A coarse approximation for the scintillation index is given by

$$m = \begin{cases} \dfrac{0.01}{(\sin\beta)^{1.55}}, & \text{S - band} \\ \dfrac{0.0016}{(\sin\beta)^{1.55}}, & \text{X - band} \\ \dfrac{0.00024}{(\sin\beta)^{1.55}}, & \text{Ka - band} \end{cases} \tag{I-4}$$

where β is the SEP angle. Equation (I-4) is based on the observations reported in Reference 16. In general, Equation (I-1) must be evaluated numerically.

Appendix J
References

(1) J. B. Berner and K. M. Ware, "An Extremely Sensitive Digital Receiver for Deep Space Satellite Communications," *Eleventh Annual International Phoenix Conference on Computers and Communications*, pp. 577-584, Scottsdale, Arizona, April 1-3, 1992.

(2) J. P. Costas, "Synchronous Communications," *Proceedings of the IRE*, Vol. 44, pp. 1713-1718, December 1956.

(3) P. W. Kinman and J. B. Berner, "Two-Way Ranging During Early Mission Phase," *2003 IEEE Aerospace Conference*, Big Sky, MT, March 8–15, 2003.

(4) M. Aung, W. J. Hurd, C. M. Buu, J. B. Berner, S. A. Stephens, and J. M. Gevargiz, "The Block V Receiver Fast Acquisition Algorithm for the Galileo S-Band Mission," *TDA Progress Report 42-118*, pp. 83-114, August 15, 1994.

(5) J. Lesh, "Tracking Loop and Modulation Format Considerations for High Rate Telemetry," *DSN Progress Report 42-44*, pp. 117-124, April 15, 1978.

(6) M. K. Simon and W. C. Lindsey, "Optimum Performance of Suppressed-Carrier Receivers with Costas Loop Tracking," *IEEE Transactions on Communications*, Vol. COM-25, No. 2, pp. 215-227, February 1977.

(7) L. C. Palmer and S. A. Klein, "Phase Slipping in Phase-Locked Loop Configurations That Track Biphase or Quadriphase Modulated Carriers," *IEEE Transactions on Communications*, pp. 984-991, October 1972.

(8) S. Shambayati, L. Tadjpour, and P. Kinman, "Turbo Code Carrier Synchronization Losses (Radio Losses)," *AIAA 19th International Communications Satellite Systems Conference and Exhibit*, Toulouse, France, April 17-20, 2001.

(9) S. Shambayati, "Radio Losses for Concatenated Codes," *IPN Progress Report* 42-151, November 15, 2002.

(10) W. J. Hurd and S. Aguirre, "A Method to Dramatically Improve Subcarrier Tracking," *TDA Progress Report 42-86*, pp. 103-110, August 15, 1986.

(11) M. Aung, "Tracking Performance and Cycle Slipping in the All-Digital Symbol Synchronizer Loop of the Block V Receiver," *TDA Progress Report 42-111*, pp. 179-191, November 15, 1992.

(12) J. H. Yuen, editor, *Deep Space Telecommunications Systems Engineering*, Plenum Press, New York, 1983.

(13) S. A. Stephens and J. B. Thomas, "Controlled-Root Formulation for Digital Phase-Locked Loops," *IEEE Transactions on Aerospace and Electronic Systems*, Vol. 31, No. 1, pp. 78-95, January 1995.

(14) D. Halford, J. H. Shoaf, and A. S. Risley, "Spectral Density Analysis: Frequency Domain Specification and Measurement of Signal Stability," *Proceedings of the 27th Annual Symposium on Frequency Control 1973*, Cherry Hill, New Jersey, 1973, pp. 421-431. (Also published as *NBS Technical Note 632*.)

(15) R. Woo and J. W. Armstrong, "Spacecraft Radio Scattering Observations of the Power Spectrum of Electron Density Fluctuations in the Solar Wind," *Journal of Geophysical Research*, Vol. 84, No. A12, pp. 7288-7296, December 1, 1979.

(16) J. W. Armstrong and R. Woo, "Solar Wind Motion Within 30 $R_{\odot}$: Spacecraft Radio Scintillation Observations," *Astronomy and Astrophysics*, Vol. 103, pp. 415-421, 1981.

Deep Space Network

208
Telemetry Data Decoding

Document Owner:

Signature Provided 01/09/2013

Andrew O'Dea Date
DSN TT&C System Engineer

Approved by:

Signature Provided 01/09/2013

Timothy. T. Pham Date
DSN Communications Systems Chief Engineer

Released by:

Signature Provided 01/09/2013

DSN Document Release Date

DSN No. **810-005-208, Rev. B**
Issue Date: January 10, 2013
JPL D-19379

Jet Propulsion Laboratory
California Institute of Technology

Users must ensure that they are using the current version in DSN Telecommunications Link Design Handbook website: http://eis.jpl.nasa.gov/deepspace/dsndocs/810-005/

Review Acknowledgment

By signing below, the signatories acknowledge that they have reviewed this document and provided comments, if any, to the signatories on the Cover Page.

Signature Provided	12/06/2012
Jeff Berner DSN Project Chief Engineer	Date

Document Change Log

Rev	Issue Date	Prepared By	Affected Paragraphs	Change Summary
Initial	11/30/2000	Robert Sniffin	All	Initial Release
Chg 1	03/31/2004	Robert Sniffin	Figures 3, 17	Corrects third generator polynomial hexadecimal representation in Figure 3. Removes implication in Figure 17 that Turbo code performance can be extrapolated below FER=10^{-5}
A	05/18/2009	Robert Sniffin	All	Deletes obsolete code types. Provides additional information on supported codes. Adds LDPC codes as a proposed capability
B	01/10/2013	Christine Chang Robert Sniffin	Table 1 Table 3 Table 5 Figure 21	Corrected the specification of the connection vectors for the (7, ½) convolutional code in Table 1. Added decoder throughput for the 26 GHz signal path in Table 1. Changed codeblock length from 17949 (rate 1/2) to 17848 (per CCSDS 131.0-B-1 "CCSDS TM Sync and Channel Coding") in Table 3. Changed codeblock length from 76772 (rate 1/3) to 26772 (per CCSDS 131.0-B-1 "CCSDS TM Sync and Channel Coding") in Table 3. Removed distinction of Turbo decoding in Table 5. Added Turbo rate 1/2 codes in Figure 21.

Contents

Illustrations

Figure **Page**

Tables

Table **Page**

1 Introduction

1.1 Purpose

This module describes the capabilities and performance of the telemetry decoding and frame synchronization equipment used by the Deep Space Network (DSN) in order to assist the telecommunications engineer in designing compatible spacecraft equipment.

1.2 Scope

The detailed discussion in this module is limited to the performance of equipment that is currently installed at the Deep Space Communications Complexes (DSCCs) and performs data extraction in real time. Additional factors that affect telemetry performance such as imperfect residual or suppressed carrier synchronization (radio loss), imperfect subcarrier and symbol synchronization, and waveform distortion are discussed in module 207.

2 General Information

Extracting data from spacecraft return link telemetry includes those processes that convert radio frequency energy into one or more bit or symbol streams (discussed in module 207) and those processes that convert the received symbol stream to a replica of the data collected onboard the spacecraft that are discussed in this module. Throughout this module, the term *bit* is used to represent the smallest unit of user data and the term *symbol* is applied to what is transmitted through the communications channel.

2.1 Telemetry Waveforms

All modern spacecraft utilize pulse code modulation (PCM) to transfer binary data between the spacecraft and the mission operations. The data are phase-modulated onto an RF carrier (PCM/PM) or used to switch the phase of a subcarrier by plus or minus 90-degrees. The subcarrier is then phase modulated on the carrier for transmission via the space link. This modulation scheme is referred to as PCM/PSK/PM. Phase modulation is used because it has a constant envelope that enables non-linear amplifiers to be used. Non-linear amplifiers tend to be more efficient than the linear amplifiers that would be necessary if the envelope (amplitude) were used to carry information. Phase modulation is also immune to most interference that corrupts signal amplitude.

Although these techniques are referred to as pulse code modulation, they do not use pulses in the conventional sense. They use non-return to zero waveforms that can be envisioned as a pulse starting as a transition from a zero voltage to some other voltage and not returning to zero until something happens. That “something” determines the characteristics and

name of the waveform. The simplest case is referred to as non-return to zero-level (NRZ-L) where the cause of the waveform returning to zero is the bit stream level changing from a one to a zero. Thus, the modulation waveform matches the data waveform. This is the most common modulation waveform used but suffers from the problem that it is impossible to tell which of the two levels is a one and which is a zero. It also has the problem that a long string of zeros or ones will prevent phase transitions from occurring that are necessary to keep the receiver symbol synchronizer in-lock.

The first of these problems can be solved by a technique called differential encoding. There are two differential encoding waveforms referred to as non-return to zero-mark (NRZ-M) and non-return to zero-space (NRZ-S). In the first case, the modulating waveform changes whenever the input is a “one” bit (or “mark” from teletypewriter terminology) and remains the same whenever the input is a “zero” bit (or “space” again, from teletypewriter terminology). The second is the opposite. The waveform changes whenever a “zero” bit occurs and remains the same whenever a “one” bit occurs. These waveforms enable the data polarity to be determined even if the detected waveform is inverted. However, a failure to properly detect a bit will always result in second error as the waveform restores itself. This causes an increase in error rate and these waveforms are not normally used for deep space communication where there is another method of determining waveform polarity (see the discussion of synchronization markers) and anything that unnecessarily increases error rate is unacceptable. Similar to NRZ-L, a long string of zeros when using NRZ-M or ones when using NRZ-S will suppress the phase transitions necessary to keep the receiver symbol synchronizer in lock

There are three other PCM modulating waveforms that have been used for spacecraft communication and solve the phase transition problem. These are bi-phase waveforms where every bit interval contains at least one phase transition. There is one bi-phase waveform corresponding to each NRZ waveform and they are referred to as Bi-ϕ-L, Bi-ϕ-M, and Bi-ϕ-S. Bi-ϕ-L is also referred to as Manchester or Split-phase encoding. The result of including a transition in every bit interval is to convert the transmitted spectrum to double-sideband having a total bandwidth twice that of the NRZ waveforms with the peak of each sideband at the bit rate and no energy at the center frequency. This leaves room for a residual carrier that can be detected with minimum interference from the data it carries. However, the increased bandwidth requirements of bi-phase modulation has normally limited its application to forward links where bandwidth requirements are less, the frequency of phase transitions permit a very simple (and low mass) symbol synchronizer onboard the spacecraft, and a residual carrier is useful for metric data measurements.

Figure 1 depicts the six telemetry waveforms discussed above. An inverted NRZ-M waveform is also included to illustrate its immunity to inversion. It is important to remember that these waveforms are not part of the telemetry encoding and decoding schemes that are used to improve telemetry performance. As mentioned above, differential encoding somewhat reduces telemetry performance. The DSN can receive any of these waveforms but uses hardware algorithms to convert them to NRZ-L either as part of the decoding process or before delivery to the customer.

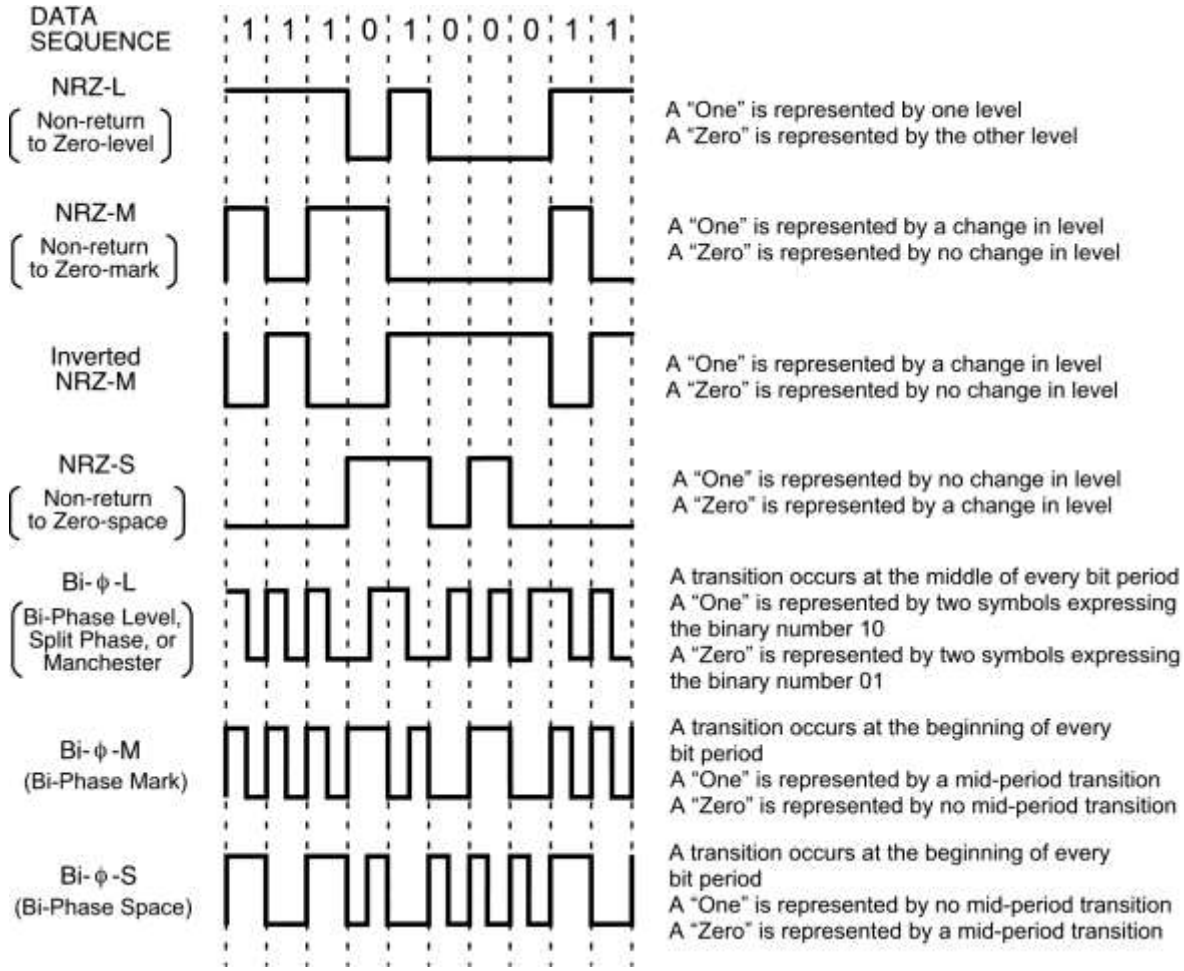

Figure 1. Telemetry Modulation Waveforms

2.2 Symbol Transition Density

The DSN derives symbol timing by observing successive phase transitions in the detected NRZ waveform and refining this estimate from additional phase transitions. This process requires that the received waveform have an adequate symbol transition density despite the nature of NRZ waveforms to produce long periods without transitions when delivering certain bit sequences. Transition density is defined as twice the probability that a symbol will be a one multiplied by the probability that it will be a zero. As, for truly random data both of these probabilities are 0.5, the transition density can have a value between 0 and 0.5. The DSN recommends that the transition density be between 0.25 and 0.5 (See Module 207) with the additional constraint that NRZ waveform has at least one phase transition every 64 symbol periods. It is the responsibility of the telecommunications designer to ensure that sufficient phase transitions are present in the transmitted data to maintain symbol synchronization. Several techniques for increasing the transition density are discussed below.

2.3 BPSK, QPSK and SQPSK

The binary NRZ waveform is used to shift the phase of the transmitted carrier or subcarrier in equal amounts from its rest phase. If the amount of phase shift is ±90 degrees, the carrier or subcarrier is fully suppressed and the modulation is referred to Binary Phase Shift Keying (BPSK). BPSK results in a 180-degree phase reversal at each NRZ waveform transition. When PCM/PSK/PM is being used, the phase transitions are normally synchronized with subcarrier zero-crossings. No such synchronization is attempted between the carrier and the data for PCM/PM.

The capacity of the communications channel can be doubled by splitting the data stream into two parts consisting of alternate symbols from the input data stream. These two parts are used to BPSK modulate carriers that are in phase quadrature with each other and the two modulated carriers are summed for transmission. This technique is referred to as Quadrature Phase Shift Keying (QPSK). Like BPSK, QPSK can produce 180-degree phase reversals when the two modulated carriers change phase at the same time. A 90-degree phase change will occur when only one of the two carriers changes phase.

Phase reversals of 180 degrees can be completely eliminated by employing Staggered QPSK (SQPSK), also referred to as Offset QPSK (QPSK). In SQPSK, one of the two waveforms is delayed by $^1/_2$ symbol period so that simultaneous phase transitions never occur and the greatest phase change in the transmitted waveform will be 90 degrees. SQPSK results in less degradation than QPSK in a bandwidth-limited channel.

The Consultative Committee for Space Data Systems (CCSDS) recommends that when a single data stream is being transferred, the stream be separated so that alternate symbols are transmitted on the two quadrature channels. The DSN supports this modulation format for all frequency bands and all supported data rates. The DSN also supports a modulation scheme for use in the near-Earth 26 GHz allocation at data rates in excess of 10 Mbps where the data stream is split into alternate bit streams, each bit stream is convolutionally coded, and the two symbol streams are delivered to the QPSK modulators. Upon reception, the two streams are separately decoded and then combined to recover the original data stream.

2.4 Symbol Quantization

Convolutional and Turbo codes, discussed below under Forward Error Correcting Codes, use decoding algorithms that are able to take into consideration not only that a symbol has been detected to be a one or a zero but also that a symbol is more likely to be a one than a zero. The DSN receivers produce symbol values (referred to as *soft symbols*) that are quantized as 8-bit values however the standard convolutional decoder only accepts 3-bit quantization. A mapping is provided at the input of the convolutional decoder to convert the 8-bit values to 3-bits. Figure 2 shows the effects of symbol quantization on convolutional decoder performance. This figure is included to illustrate the need to perform any conversion between NRZ-L and differential encoding prior to convolutional encoding and after convolutional decoding as the DSN does not include a decoder for differential NRZ waveforms nor a method of converting from differential

waveforms to NRZ-L without simultaneously converting them to one-bit quantization (*hard symbols*) which would result in a significant performance loss.

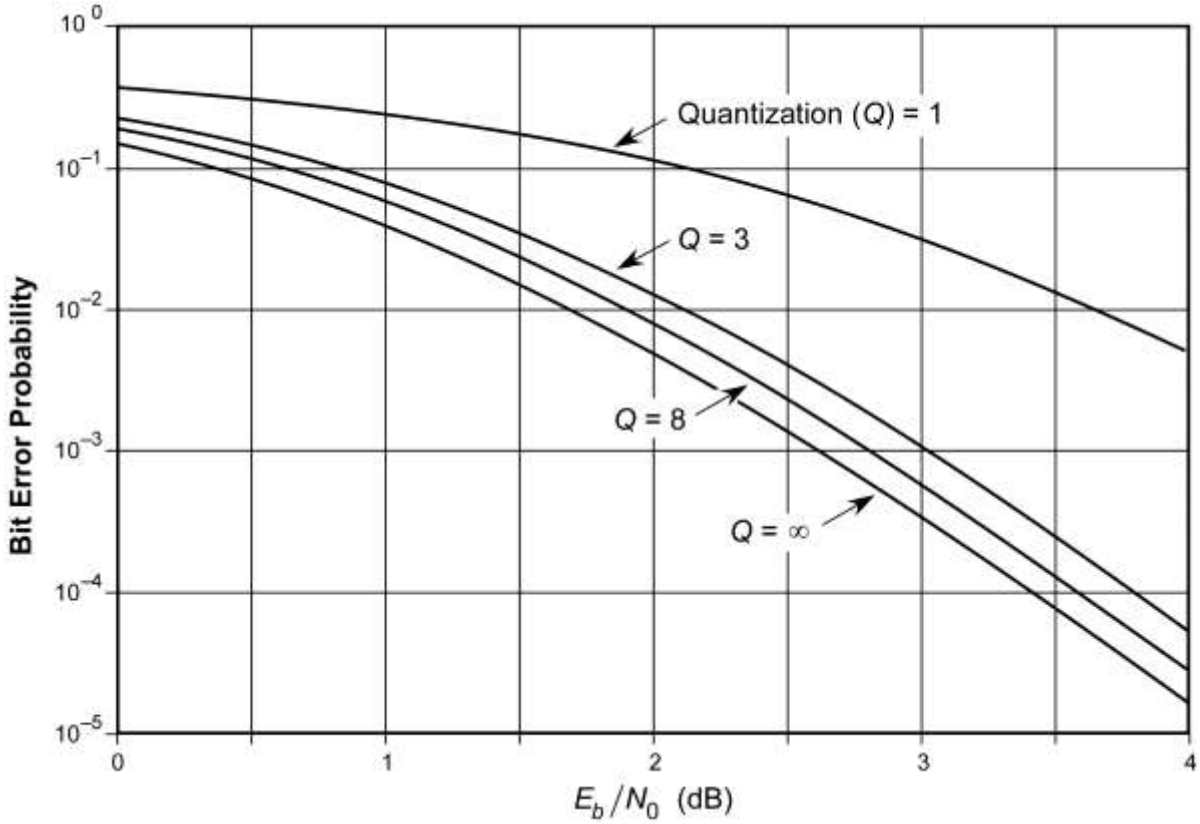

Figure 2. Quantization Effects on Decoder Performance

2.5 Forward Error Correcting Codes

Almost all spacecraft employ forward error correcting (FEC) codes to make more efficient use of the communications channel. Forward error correcting codes add additional symbols to the transmitted data stream that the decoder can use to improve its estimate of the encoded bit stream. The exceptions to FEC use would likely be extremely high data rate transmissions where adequate signal power is available to make the gain achieved by coding unnecessary and any bandwidth needed for the symbols added by coding is unavailable.

The DSN supports two convolutional codes, the Consultative Committee for Space Data Systems (CCSDS) standard Reed-Solomon code, and the CCSDS Turbo codes. Convolutional codes are used because they achieve significant coding gain with simple, highly reliable encoders and their decoders are of reasonable complexity. They also provide low latency and are useful when conditions may prevent a block of symbols from being received. The Reed-Solomon code provides excellent performance with minimum bandwidth expansion in a high signal-to-noise environment. It is most often used as an outer code in combination with a

convolutional inner code but may be used by itself under appropriate signal conditions. Turbo codes provide near-Shannon-limit error-correction performance with reasonable encoding and decoding complexity. The DSN presently includes an additional convolutional decoder that is used for the Cassini spacecraft support but it will be removed from service at the end of that mission.

2.5.1 Convolutional Codes

Convolutional codes are specified by their *constraint length* (*K*) and *rate* (*r*). Constraint length is the number of sequential input bits required to define the output symbols at any point in time. Rate is the number of data bits with respect to the number of coded symbols expressed as a fraction. In general, the performance of a convolutional code increases directly with *k* and inversely with *r*, but codes must be selected carefully because the channel bandwidth also varies inversely with *r* and decoder complexity increases exponentially with *k*.

The most common convolutional code is the CCSDS k=7, r= $^1/_2$ (7, $^1/_2$) code. This code falls into a category referred to as *transparent* codes meaning that if the input to the encoder or decoder is inverted, the output will be inverted. Thus, the phase ambiguity associated with BPSK modulation does not need to be resolved until the coding gain is achieved. A convolutional encoder consists of a *k*-stage shift register with the outputs of selected stages connected by *r* exclusive-OR connection vectors. The *r* outputs (in this case 2) are transmitted alternately through the communications channel. The recommended code inverts the output of one of the two connection vectors which ensures that sufficient transitions will be available to keep the receiver symbol synchronizer in lock. A diagram of the CCSDS (7, $^1/_2$) code is shown in Figure 3. Figure 3 also shows a variation of this code used on some legacy deep space missions. The only difference between the two codes is the order in which symbols from the two connection vector outputs are transmitted. The DSN can decode either variation with or without the alternate symbols being inverted. The capabilities of the DSN convolutional decoder are summarized in Table 1.

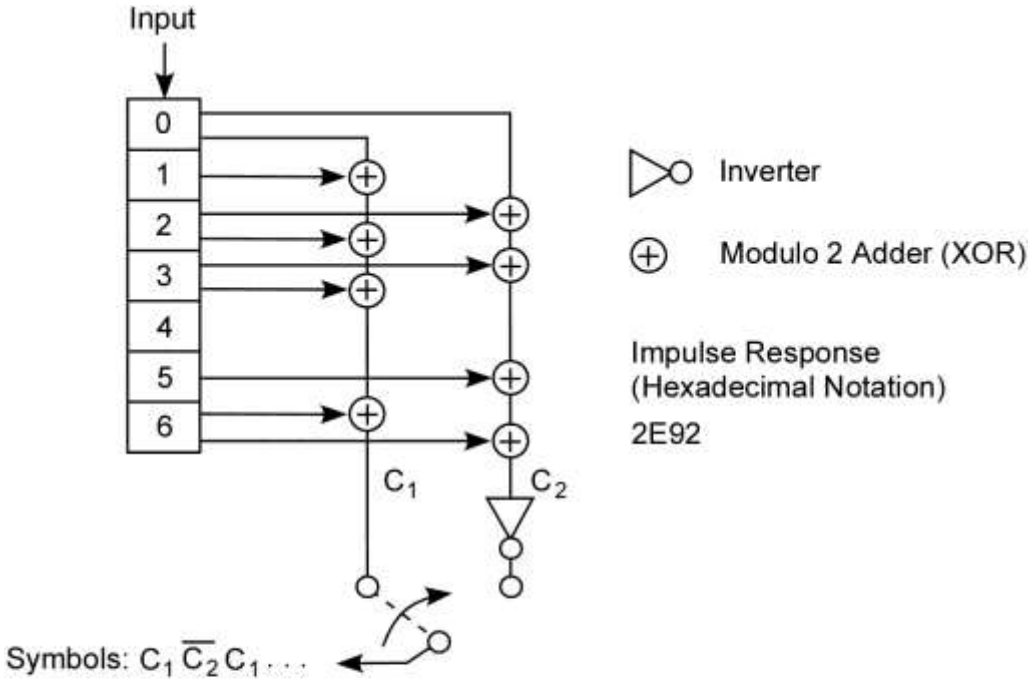

a) CCSDS (7, 1/2) Convolutional Encoder

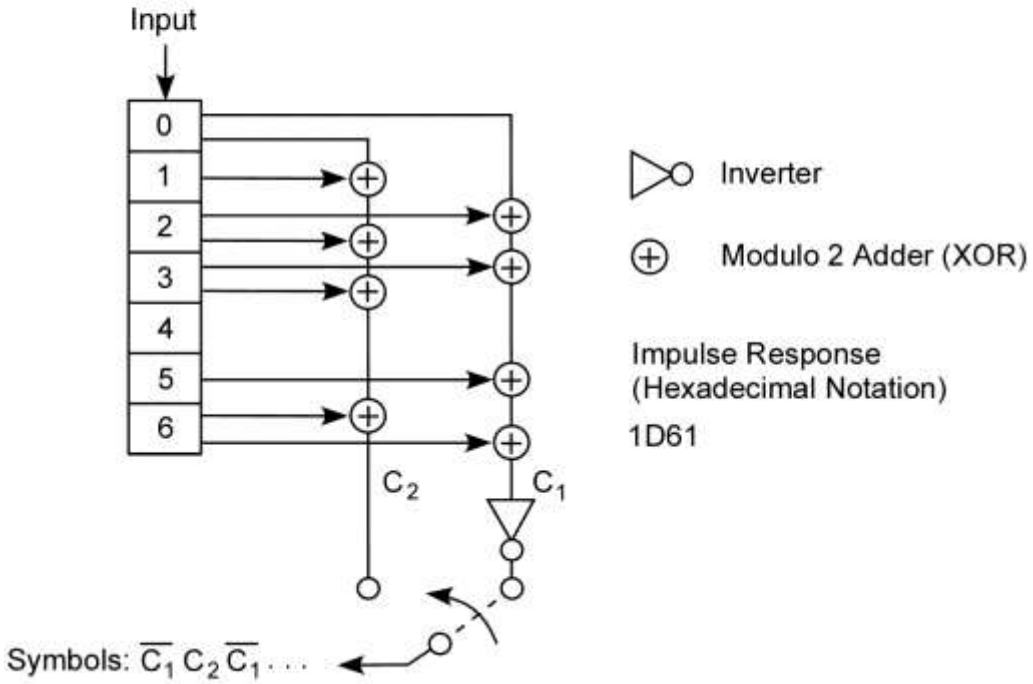

b) DSN Legacy (7, 1/2) Convolutional Encoder

Figure 3. *k*=7, *r*=1/2 Convolutional Encoder Connection Vector Schematics

Table 1. Convolutional Decoder Characteristics

Parameter	Value
Constraint length	7
Code rate	1/2
Connection vectors*	C1 = 1111001, C2 =1011011 or C1= 1011011, C2 = 1111001
Alternate symbol inversion**	Selectable
Input quantization**	3 bits (8 levels)
S, X, and Ka 32 GHz Symbol (Input) rate	4 s/s to 13.2 Ms/s (max.)
S, X, and Ka 32 GHz Bit (Output) rate	6.6 Mb/s (max.)
Node synchronization**	Symbol Error Rate or Metric Normalization Rate
Node sync acquisition**	≤ 5000 bit times for Eb/N0 ≥ 0.5 dB (99% probability)
Performance vs. theoretical** (for 3-bit quantization)	≤ 0.05 dB
Ka 26 GHz Symbol (Input) Rate	The (7, ½) Viterbi decoder input rate is limited to 240 Ms/s. Two Viterbi decoders can be used in parallel for QPSK/OQPSK to allow coded data up to 300 Ms/s (The 300 Ms/s limit comes from the demodulator, not the decoder.).*** Modulation is limited to 150 Ms/s (BPSK) or 300 Ms/s (QPSK/OQPSK).
Ka 26 GHz Bit (Output) Rate	Output bit rate is limited to: • 75 Mb/s for Viterbi-encoded BPSK • 150 Mb/s for uncoded BPSK • 120 Mb/s for single Viterbi-encoded QPSK/OQPSK • 150 Mb/s for dual Viterbi-encoded QPSK/OQPSK • 300 Mb/s for uncoded QPSK/OQPSK

Note:

* DSN currently only supports the first configuration (CCSDS convolutional encoder) for Ka 26 GHz

** Except for Ka 26 GHz reception.

*** The limitation of the upper range of the input rate is on how fast an instance of the convolutional decoder can decode. The implementation of the (7, ½) Viterbi decoder runs at a maximum symbol rate of 240 Ms/s. For higher symbol rates, the spacecraft needs to use QPSK/OQPSK and run two separate Viterbi encoders, one on "I" and one on "Q" channel. Each of these Viterbi decoders handles half of the symbols. For example at 300 Ms/s OQPSK, two Viterbi decoders would be running in parallel, with each decoder handling 150 Ms/s.

A convolutional decoder must establish node synchronization in order to correctly decode the incoming symbols. That is, which symbol of each received symbol pair represents the first symbol that was transmitted. For an $r = {}^1/_2$, transparent code, there are only two possibilities. The DSN decoder provides two methods for doing this, symbol error rate (SER) node synchronization and metric normalization rate (MNR) control.

The first method relies on the fact that when the decoder is operating properly the probability of the decoder falsely decoding a bit is at least two orders of magnitude less than the probability of a channel symbol error. The output can therefore be re-encoded and the resultant symbols compared with a delayed copy of the received symbols (to account for decoder delay). The number of differences between these two symbol streams will be an almost true count of the number of symbol errors received by the decoder. The maximum number of symbol errors and the interval over which these symbol errors are counted may be set over the range of 1 to 65535 at decoder initialization. Engineering research suggests that the decoder should obtain proper node sync alignment when the maximum number of symbol errors is set to 420 and the number of decoded bits in which this count is reached is set to 2000 provided the symbol SNR is greater than or equal to –2.5 dB. This same technique of re-encoding the output bits and comparing them to a suitably delayed version of the input symbol stream is used to provide an estimate of the E_b/N_0 with an accuracy of 0.1 dB provided that symbol errors are occurring. Under signal level conditions greater than E_b/N_0 = 12dB (where there are few symbol errors), the estimate of E_b/N_0 becomes unreliable.

The second method relies on the fact that decoders based on the Viterbi algorithm maintain state metrics that need to be normalized periodically to prevent register overflow. If normalizations are occurring more frequently than a preset interval, the decoder will switch to the alternate node sync and attempt reacquisition. Both the permitted number of normalizations and the interval (as a number of decoded bits) over which this permitted number is accumulated may be set during encoder initialization. The maximum number of normalizations may be set over the range from 4 to 2036, modulo 8 (4, 12, 20, …, 2036) and the interval used to detect this threshold may be set to the greater of 256 or 1 to 65535, modulo 256 bits. Engineering research suggests that the decoder should obtain proper node sync alignment with the maximum number of normalizations set to 180 and the interval set to 2048 bits provided the symbol SNR is greater than or equal to –2.5 dB.

For extremely low signal-to-noise ratios or if the received symbol stream is invalid, there is a possibility that the decoder will choose the wrong node sync position. If this is detected, the decoder can be commanded to attempt resynchronization but there is no guarantee that the resynchronization will result in the alternate node sync being chosen.

The output stage of the convolutional decoder can be set to perform the conversion to NRZ-L should another telemetry waveform have been employed on the RF channel. The decoder can be operated in a pass-through mode (no decoding) so the waveform conversion capability can be used for data that are not convolutionally coded.

The convolutional decoder presently used for the Cassini spacecraft support is capable of decoding constraint lengths up to k=15 and rates to $r={}^{1}/_{6}$. As noted earlier, this decoder will be removed at the end of the Cassini project.

2.5.2 Frame Synchronization

Frame synchronization must be established before processing any block code such as Reed-Solomon or Turbo codes or before formatting the data for delivery. Synchronization is accomplished by preceding each codeblock or transfer frame with a fixed-length Attached Synchronization Marker (ASM). This known bit pattern can be recognized to determine the start of the codeblocks or transfer frames. It also can be used to resolve the phase ambiguity associated with BPSK or QPSK (SQPSK or OQPSK) modulation. The DSN contains two frame synchronizers. The first of these operates in the bit domain and is used with convolutionally coded, Reed-Solomon coded, or uncoded data. The second operates in the symbol domain and is used with Turbo coded data.

2.5.2.1 Bit Domain Frame Synchronization

The Consultative Committee for Space Data Systems has adopted the 32-bit ASM shown in Figure 4 for synchronization in the bit domain. The pattern is represented in hexadecimal as 1ACFFC1D but any pattern having a length of 8 to 64 bits such as the Inter-range Instrumentation Group (IRIG) patterns can be accommodated.

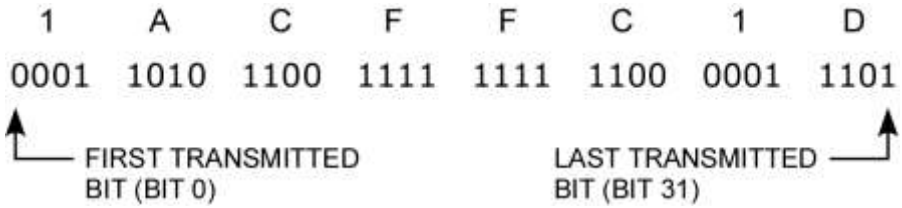

Figure 4. CCSDS Recommended 32-bit Attached Synchronization Marker

The DSN bit-domain frame synchronizer operation is defined by four operating modes: Search, Verify, Lock, and Flywheel. Parameters that affect the operation of the synchronizer are discussed in the following paragraphs and summarized in Table 2.

Table 2. Bit Domain Frame Synchronization Parameters

Parameter	Value
Frame length	8 – 65536 bits in multiples of 8
ASM length	8 – 64 bits
ASM search direction	Forward, Reverse, or Both
Bit-slip window	0 to 3 bits
In-lock bit error tolerance (permissible ASM bit errors while achieving lock)	0 to 31 bits
Number of verify frames	0 to 31
Automatic polarity correction	Enable or Disable
Out-of-lock bit error tolerance (permissible ASM bit errors while in-lock)	0 to 31 bits
Maximum flywheel frames	0 to 31
Maximum time to achieve lock	4 frames provided BER ≤ 10^{-2} (99.6% probability)

In the Search mode, the synchronizer assembles all received bits into blocks of the specified length while it attempts to find a pattern in the data that differs from the known ASM by less than a specified number of bit errors. The specified number of bit errors from the synchronization marker is called the In-lock Bit Error Tolerance (IL_BET) and can have a value from 0 to 31. It does this for the ASM as specified, the inverse of the ASM as specified and, if requested, both the normal and inverse of the ASM with the bit order reversed. When a suitable pattern is found, the block being assembled is flagged as a short block ending with the assumed sync marker and the subsequent received bits are collected into a new data block of the specified length for delivery to the next step in the telemetry processing process. At this point, the synchronizer advances to the Verify mode. Should an inverse of the ASM have been detected, the polarity of all bits is inverted at they are assembled in the data block. Thus, the ambiguity associated with BPSK modulation is automatically resolved.

In the Verify mode, the synchronizer starts looking for an acceptable ASM a few bit periods (referred to as the bit-slip window) before the specified length of the data block. An “acceptable” marker is one that has no more than IL_BET bit errors from the one previously detected. Should it find the pattern, it increments a counter towards declaring synchronization to be in-lock. Should it not find the pattern, it places the bits that it expected to be a sync maker at the front of the next data block and reverts to the Search mode until a suitable marker is found. The synchronizer remains in the Verify mode until the required number of sequential frames has been found at which time the synchronizer advances to the Lock mode. This number of frames that must be successfully detected before declaring lock can be set over the range of 0 to 31 with zero meaning that the Verify mode is skipped.

In the Lock mode, the synchronizer continues to examine the data stream for an acceptable ASM within the bit slip window using a bit error tolerance referred to as the Out-of-lock Bit Error Tolerance (OOL_BET) that can be set independently of IL_BET over the range of 0 to 31. The synchronizer remains in the Lock mode until no acceptable ASM is detected. Should this occur, the synchronizer places itself in the Flywheel mode.

In the Flywheel mode, the synchronizer discards the received bits that occurred where the ASM was anticipated and continues to place the remaining received bits into blocks of the specified frame size. It will continue this process until from 0 to 31 ASMs have been missed at which point it will switch to the Search mode. Should a frame with less than IL_BET errors be recognized at the appropriate place and before the maximum number of flywheel frames has occurred, the synchronizer will return to the Lock mode.

2.5.2.2 Symbol Domain Frame Synchronization

The symbol domain bit synchronizer is part of the DSN Turbo decoder and includes automatic polarity correction to resolve the BPSK phase ambiguity. Although the operation is essentially similar to the bit domain frame synchronizer, the parameters have been optimized through simulations and are not available for user modification.

Synchronization in the symbol domain requires longer synchronization markers because the lack of coding gain before synchronization can result in enough symbol errors occurring during a 32-bit sequence to prevent reliable recognition. In addition, the performance gain that is achieved by increasing the code rate comes at the expense of a further reduction of symbol signal to noise ratio resulting in a further increase in symbol errors. To accommodate these factors, the CCSDS has recommended synchronization markers having a length of 32 symbols divided by the code rate, r. The recommended CCSDS synchronization markers for Turbo codes are illustrated in Figure 5.

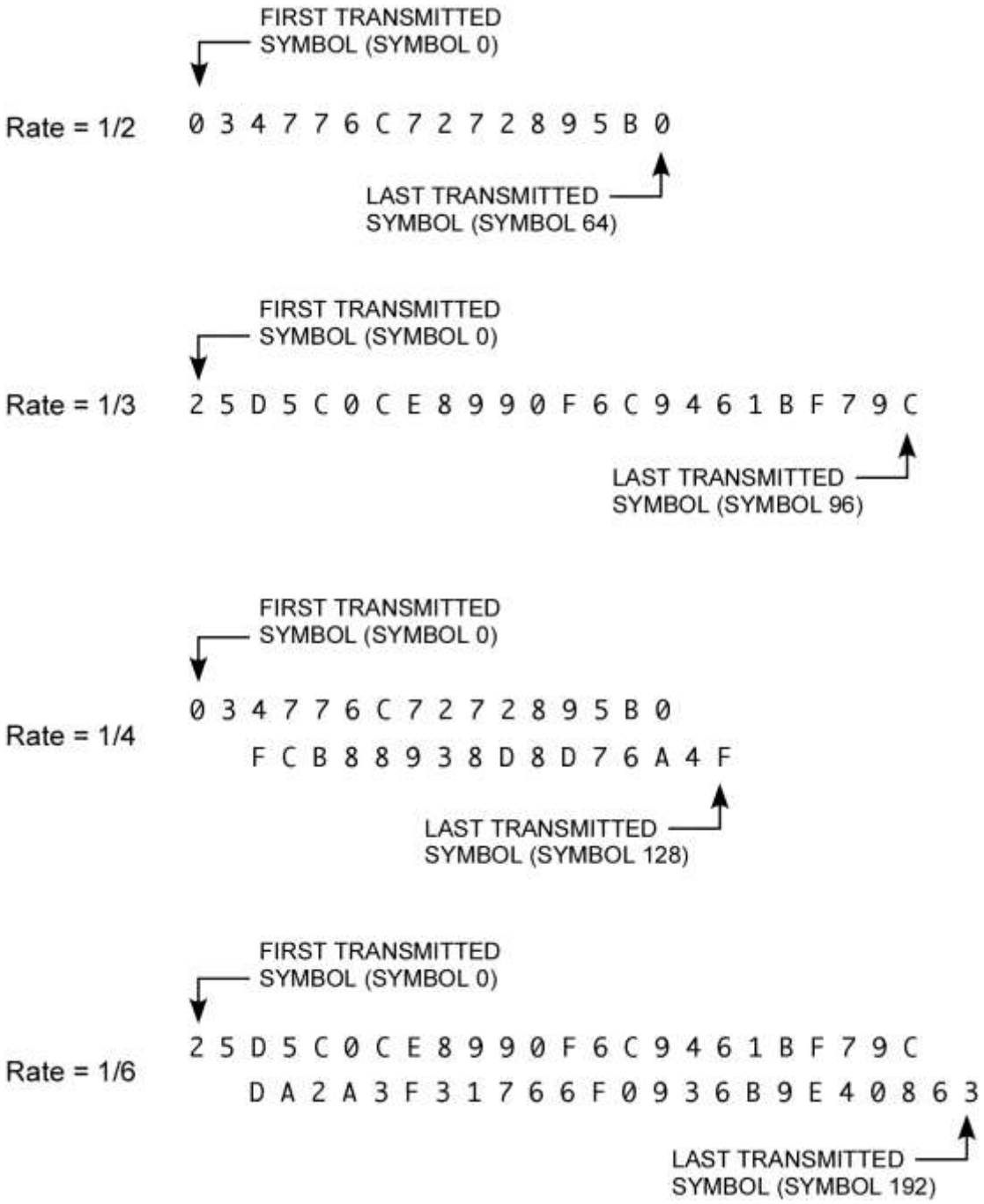

Figure 5. Attached Synchronization Markers for Turbo Codes

2.5.3 Randomization and De-randomization

The transition density of data may not be adequate for the receiver to maintain symbol synchronization if the data have not been convolutionally coded or when convolutional coding is used without alternate symbol inversion. This is especially true with NRZ-L uncoded data or when Reed-Solomon coding is used by itself as a sequence of consecutive ones or zeros for some period will provide no transitions.

The required transition density can be achieved for all data streams by modulo-two adding a standard pseudo-random, 255-bit sequence to the stream as it is formed into codeblocks or transfer frames for transmission and then modulo-two adding the same sequence to the received data in the received codeblocks. The code is arranged so that the first bit of the code is added to the first bit in the codeblock or transfer frame and the code is repeated as many times as necessary until the codeblock or transfer frame is completed. The DSN provides the capability to de-randomize uncoded, convolutionally coded, and Reed-Solomon coded data using the CCSDS pseudo-randomizer illustrated in Figure 6.

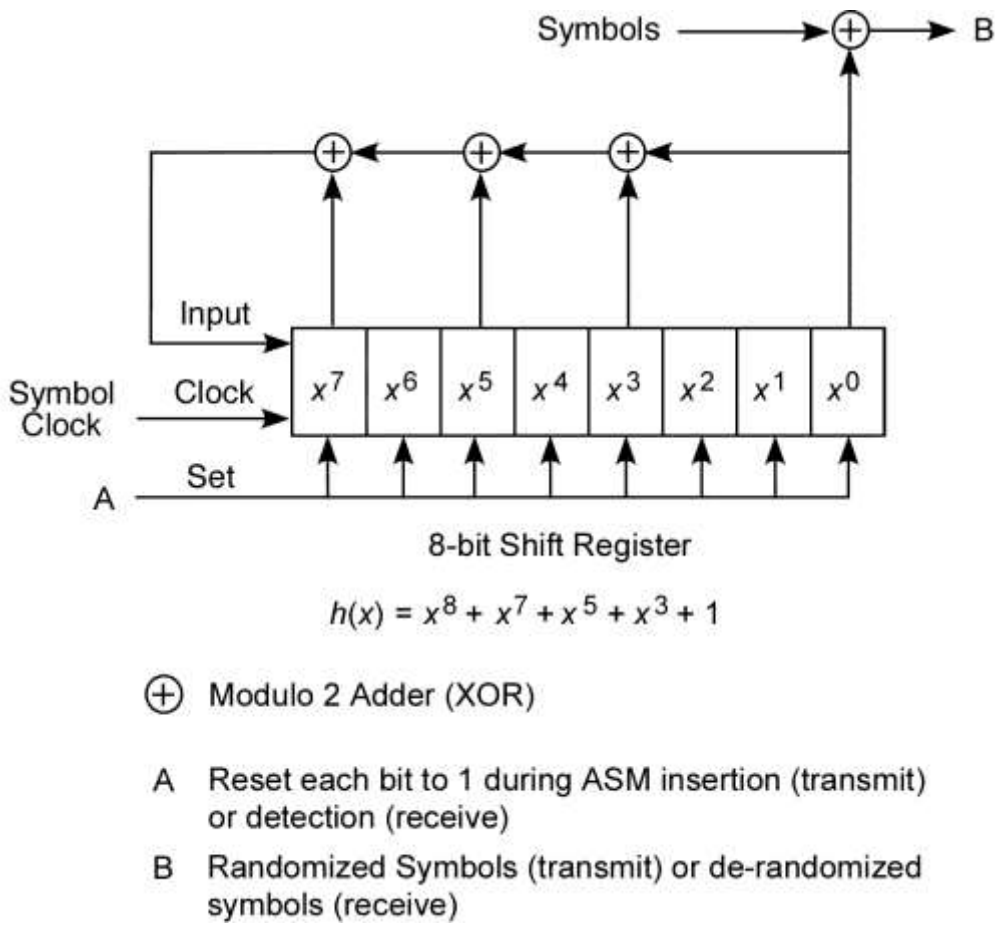

Figure 6. CCSDS Pseudo-Randomizer/De-randomizer

2.5.4 Reed-Solomon Code

Reed-Solomon (RS) codes are linear block codes for hard-coded (one-bit digitized) data streams. They are often used in combination with a convolutional inner code that is applied between the point at which the RS coding is complete and the communications channel and then removed prior to RS decoding. In high signal-to-noise environments the RS and convolutional codes can be used independently. The code is *systematic*, meaning that the input bits appear, unchanged, in the output stream followed by parity information that is used by the decoder to correct errors. This property can be useful in forensic analysis of corrupted data. The codes, themselves, are also transparent however, the DSN implementation will always resolve the BPSK phase ambiguity prior to RS decoding. This is important because use of *virtual fill*, described below, renders the code non-transparent.

The RS code adopted by the DSN is one of the two RS codes recommended by the CCSDS and is referred to as the RS (255,223) code. The code divides the input bits into 8-bit sequences to form symbols that are concatenated into a 255 symbol codeword. The RS encoder creates parity symbols from these information symbols that enable the decoder to correct any combination of E or fewer symbol errors in each codeword. The value E is referred to as the code redundancy and, for the supported code, has a value of 16. The output of the encoder consists of the 255 information symbols followed by 32 ($2E$) parity symbols. A complete description of this code is contained in references 3 and 4.

2.5.4.1 Reed-Solomon Encoder

The most common architecture for an RS encoder is named the Berlekamp Architecture, after its inventor. This architecture, in combination with appropriate selection of the RS code generator polynomial, enables parity symbols to be calculated using bit-serial multipliers constructed with a matrix of exclusive OR gates. Figure 7 shows the design of a Berlekamp encoder for producing the DSN/CCSDS standard RS code that includes support for interleaving and virtual fill as discussed below.

2.5.4.2 Concatenated Convolutional and Reed–Solomon Code

Errors in convolutionally coded channels tend to occur in bursts that result when noise causes the decoder to momentarily follow the wrong path through the decoding trellis. The combination of an outer Reed–Solomon (RS) code with an inner convolutional code provides good burst-error correction with minimal bandwidth expansion.

2.5.4.3 Interleaving

The burst errors associated with Viterbi decoding can be as long as several constraint lengths and equivalent to several consecutive RS symbols. Thus, several closely spaced error bursts can exceed an RS decoder's error correction capability. Interleaving is a technique that spreads the effects of burst errors across several RS codewords. The effect of interleaving RS coding performance is illustrated in Figure 8.

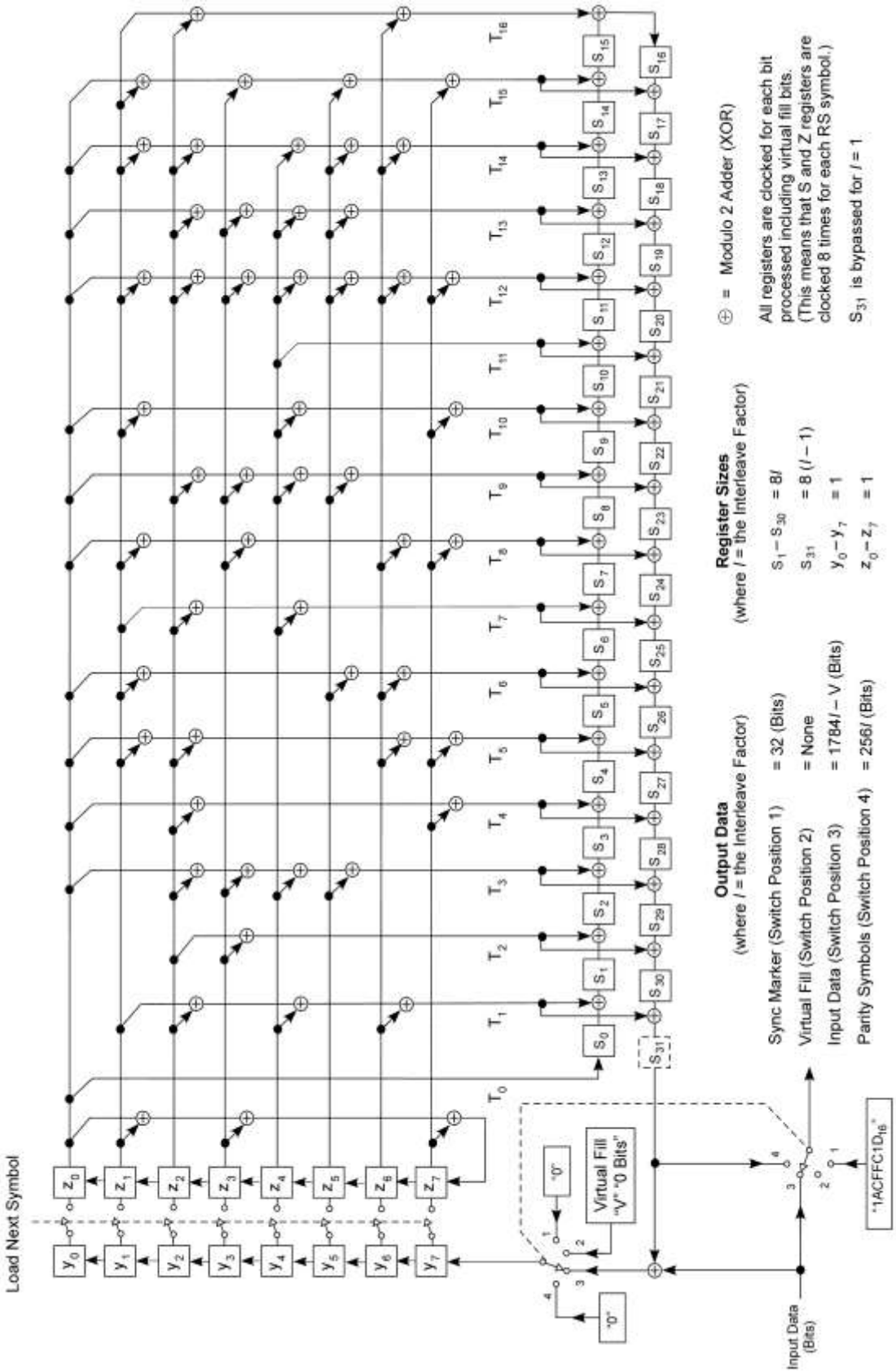

Figure 7. Reed–Solomon Encoder for RS (223, 255) Code

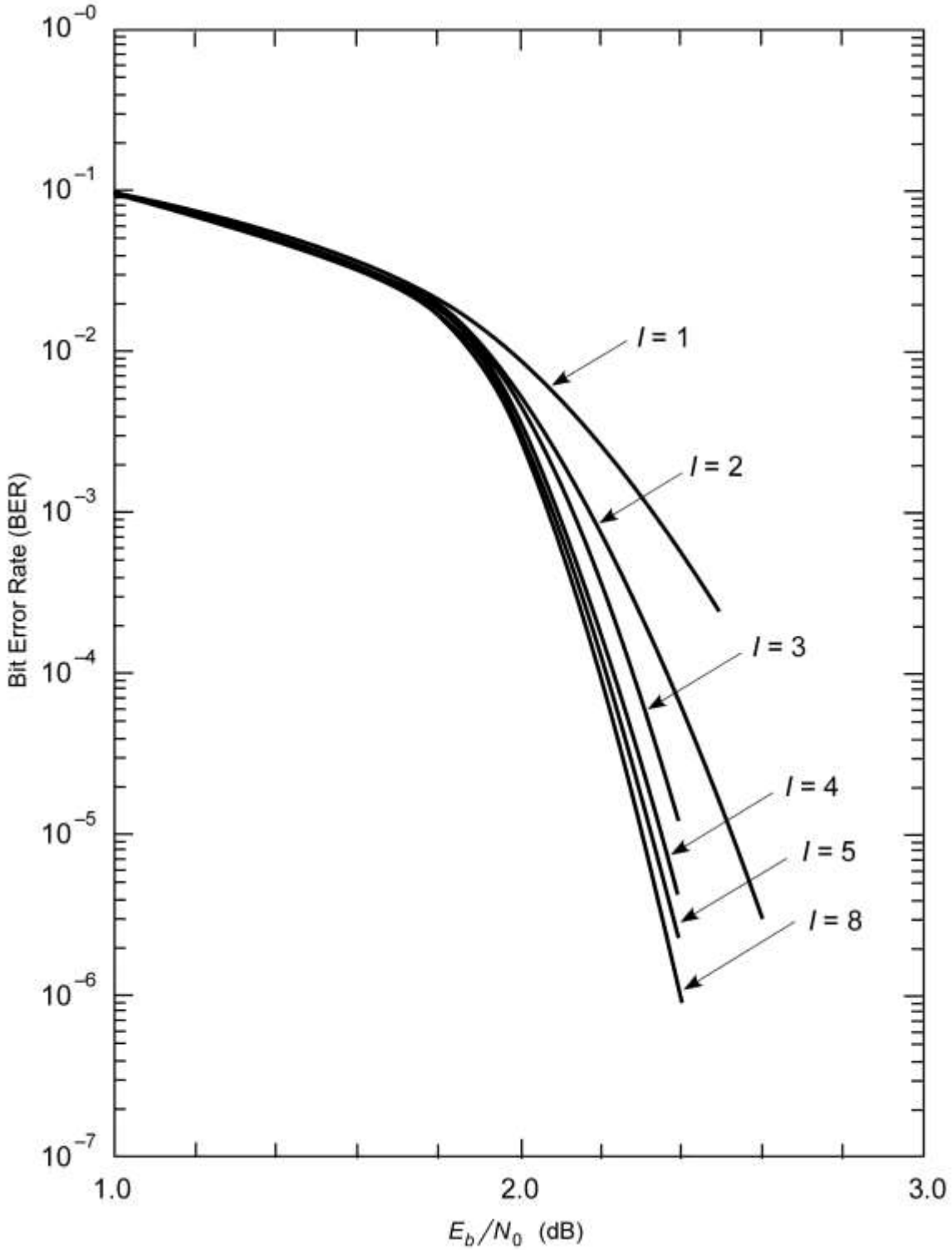

Figure 8. Effect of Interleaving on RS Performance

Interleaving is accomplished by storing partially completed parity symbols in 31, 8*I*-bit shift registers for parity symbols (I – 1) through 32*I* and one 8(I – 1)-bit shift register, where *I* is the *interleave factor* so that the parity symbols from any codeblock are not transmitted consecutively. The first 8 bits of input data are collected to form an RS symbol as these bits are being delivered to the convolutional encoder or the information channel. When the symbol is complete, it is transferred into the parity computer that computes the first bit of partial parity "instantaneously" so an output of the parity registers is available for modulo two addition (XOR) with the first bit of the next input symbol. This output will either be the result of the parity calculation if $I = 1$ or a zero if $I > 1$. As the remaining 7-bits of the second symbol are being collected, seven additional bits of partial parity are calculated from the first symbol and pushed into the parity registers resulting in additional bits being supplied for modulo two addition as the input bits are formed into symbols. This process continues until 223*I* symbols have been processed When *I* symbols have been processed, the output of the parity registers ceases to be the zeroes and each output bit includes the partial parity computed at all prior 8*I* intervals.

When 223*I* input symbols have been processed but before the last symbol is transferred to the parity calculation matrix, the input bit stream is set to all zeroes, guaranteeing that there will be no further changes to the collected parity symbols, and the output of the parity register array is connected to the convolutional encoder or the information channel. The last symbol is then processed resulting in the first parity symbol being delivered to the convolutional encoder or the information channel and the remaining symbols are clocked from the array while the array is filled with zeroes in preparation for processing the next codeblock.

Since the input data are passed directly to the convolutional encoder or information channel as the parity symbols are being calculated, the code remains systematic – independent of the interleave factor. The 32 parity symbols from the 223*I* blocks of information symbols are dispersed across the entire 32*I* parity symbol portion of the codeblock at *I*-symbol intervals. Figure 9 illustrates the symbol arrangement for an interleave factor of 5.

When the data are received, they are written into an array from which the parity symbols associated with each of the *I* RS codewords can be separated. DSN supports interleaving for values of *I* between 1 (no interleaving) and 8.

2.5.5 Virtual Fill

The maximum amount of input data that can be transmitted in a codeblock varies from 1784 bits (with no interleaving) to 14,272 bits (with an interleaving depth of 8). If a transfer frame has less data than 1784*I* bits (where *I* is the interleave factor), the codeblock can be completed by inserting virtual fill (all-zero RS symbols) between the ASM and the start of the input data. The amount of virtual fill (in units of 8-bits) must be fixed for a tracking pass and is inserted into the parity generator by the encoder and into the received symbol stream before it is decoded however these extra symbols are not transmitted. It is the fact that zeroes are inserted into the received data stream by the decoder that renders the code non-transparent because,

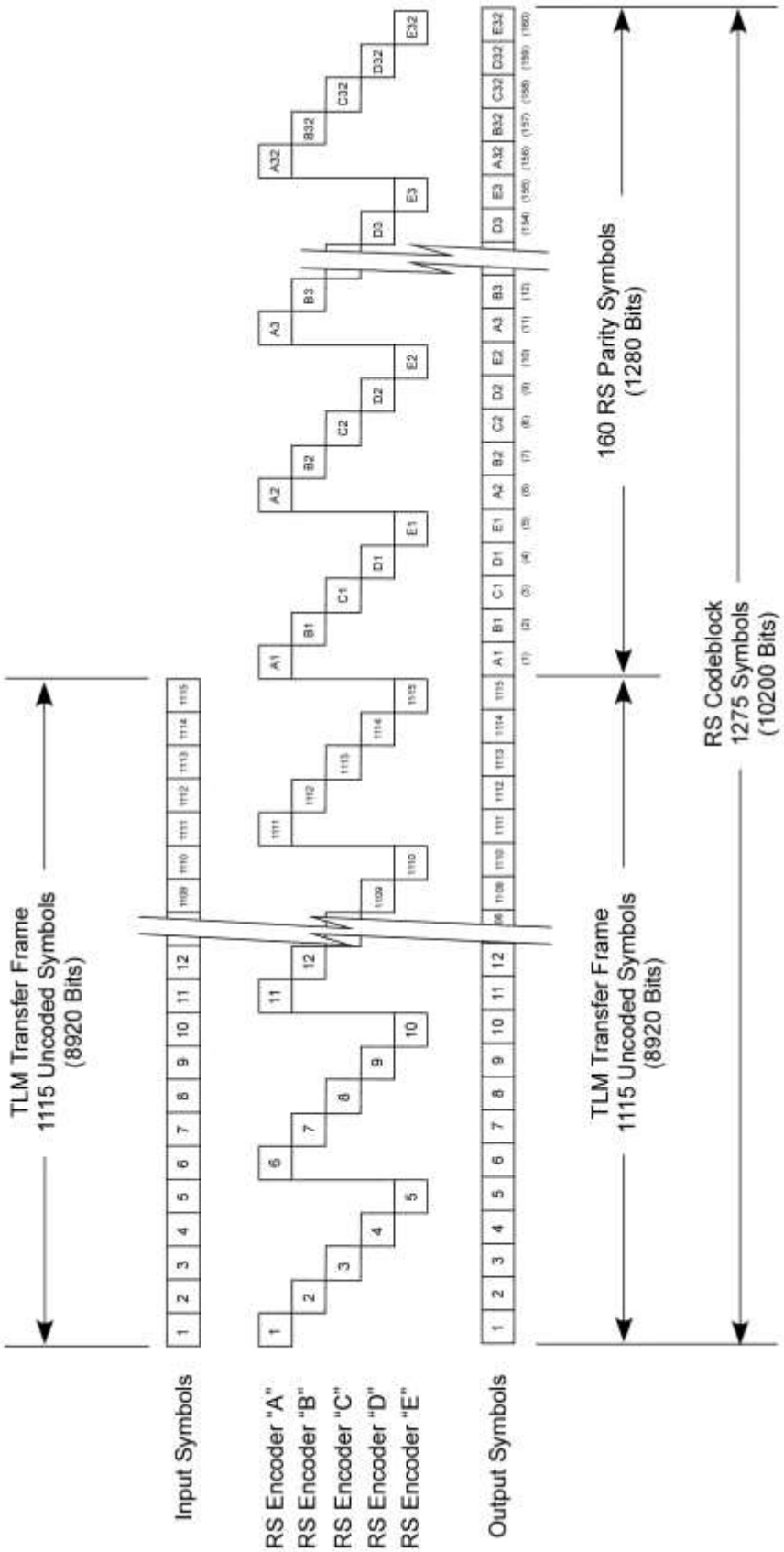

Figure 9. Reed–Solomon Symbol Arrangement for Interleave Factor (*I*) of 5

should an inversion have occurred, it would be necessary to insert ones instead of zeroes and this cannot be known. The efficiency of RS coding will decrease as the amount of virtual fill increases as the number of parity symbols remains fixed while the number of data symbols decreases. An illustration of virtual fill is shown in Figure 10.

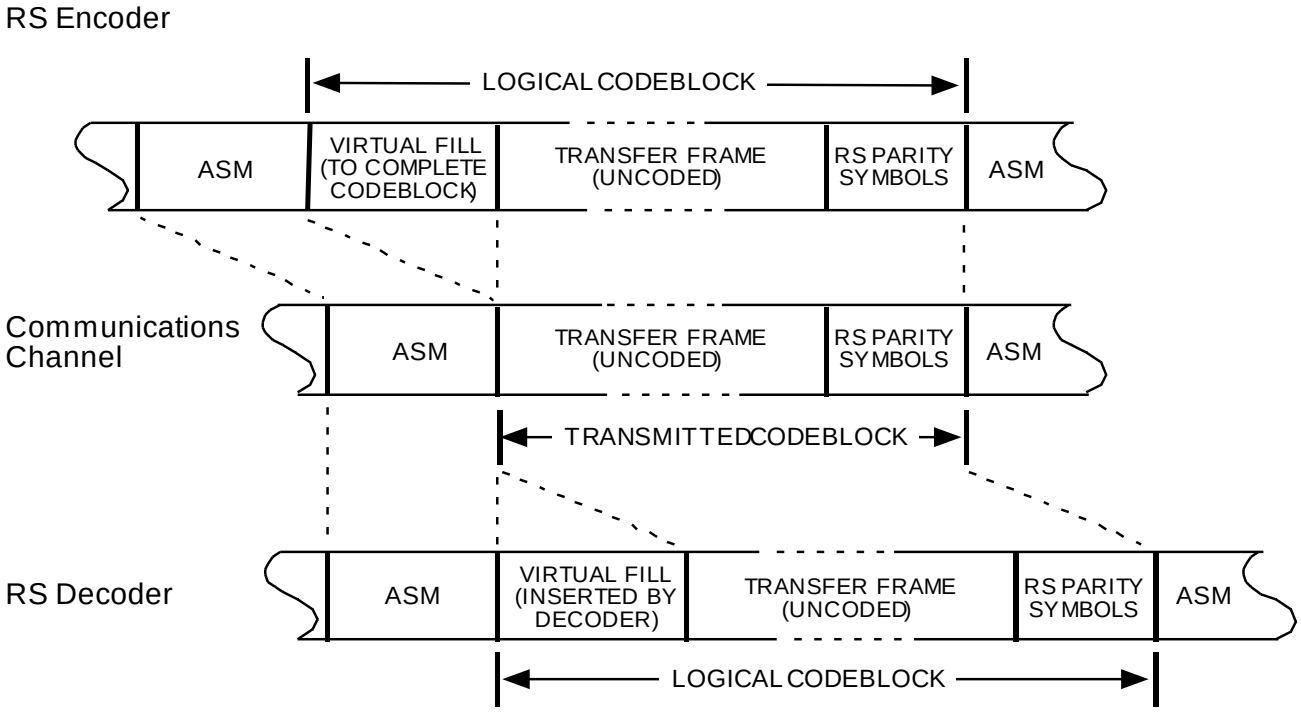

Figure 10. Illustration of Virtual Fill

2.5.6 Turbo Codes

Turbo codes provide error correction performance within approximately 0.8 dB of the theoretical limit at a BER of 10^{-6}. This performance is achieved using encoders and decoders of reasonable complexity but at the expense of increased latency. A turbo code is a systematic block code where two sets of parity symbols from independent recursive convolutional encoders are provided. The encoders employ trellis termination so that the codeblock both begins and ends in a known state.

The use of recursive convolutional encoders is one feature of turbo codes. The second is the presence of an interleaver at the input of one of the convolutional encoders that changes the order of the information bits before they are encoded. It is the presence of the interleaver that establishes the minimum latency as equaling the block size as an entire block of data must be assembled before the parity generation process can begin. Although the information bits appear, unchanged, in the encoded output, they do not appear contiguously as is the case with Reed Solomon codes.

The DSN provides support for the turbo code specified in CCSDS Recommendation 131.0-B-1 for information block lengths (*k*) of 1784, 3568, 7136, 8920 bits and nominal code rates (*r*) of $^1/_2$, $^1/_3$, $^1/_4$, and $^1/_6$. The recommendation also permits an information block length of 16,384 bits however the encoder for this block length has not been completely specified and it is not supported by the DSN, The four supported block lengths are the same as would be required for Reed-Solomon encoding using an interleave factor (*I*) of 1, 2, 4, or 5.

2.5.6.1 Turbo Code Encoder

Figure 11 illustrates the design of a CCSDS compliant turbo encoder. In actual practice, either the entire encoder or the information block buffer and interleaver (with appropriate changes to the input switching) must be duplicated to ensure a constant flow of symbols in the information channel. An actual implementation would also include the capability to preface each codeblock with the synchronization marker described above.

A block of information bits is entered into the information block buffer and the interleaver that stores them in accordance with the permutation algorithm defined by the recommendation. When the buffer and interleaver are full, the information is clocked into the encoders and the resultant symbols are transferred to the information channel in the order shown on the figure. When the last information bit has been transferred into each encoder, the switches at their inputs are placed in position 2 and the encoders permitted to run for four additional clock cycles. This causes four zeros to be entered into the encoders terminating the trellis. The encoder continues to output nonzero encoded symbols during trellis termination producing four extra symbols from the feedback line in addition to the *k* information bits.

The presence of the trellis termination symbols results in the channel code rates being slightly smaller than the nominal code rates. The information block and codeblock lengths for the 5 supported turbo codes are shown in Table 3. The structure of the turbo encoded data in the physical channel is illustrated in Figure 12.

Table 3. Turbo Code Information Block and Codeblock Lengths

Information block length, *k*, bits	Corresponding Reed-Solomon Interleave depth, *I*	Codeblock length			
		Rate $^1/_2$	Rate $^1/_3$	Rate $^1/_4$	Rate $^1/_6$
1784	1	3576	5364	7152	10728
3568	2	7144	10716	14288	21432
7136	4	14280	21420	28560	42840
8920	5	17848	26772	35696	53544
16384*	N/A	32776	49164	65552	98328

* Note: This information block length is not supported by the DSN.

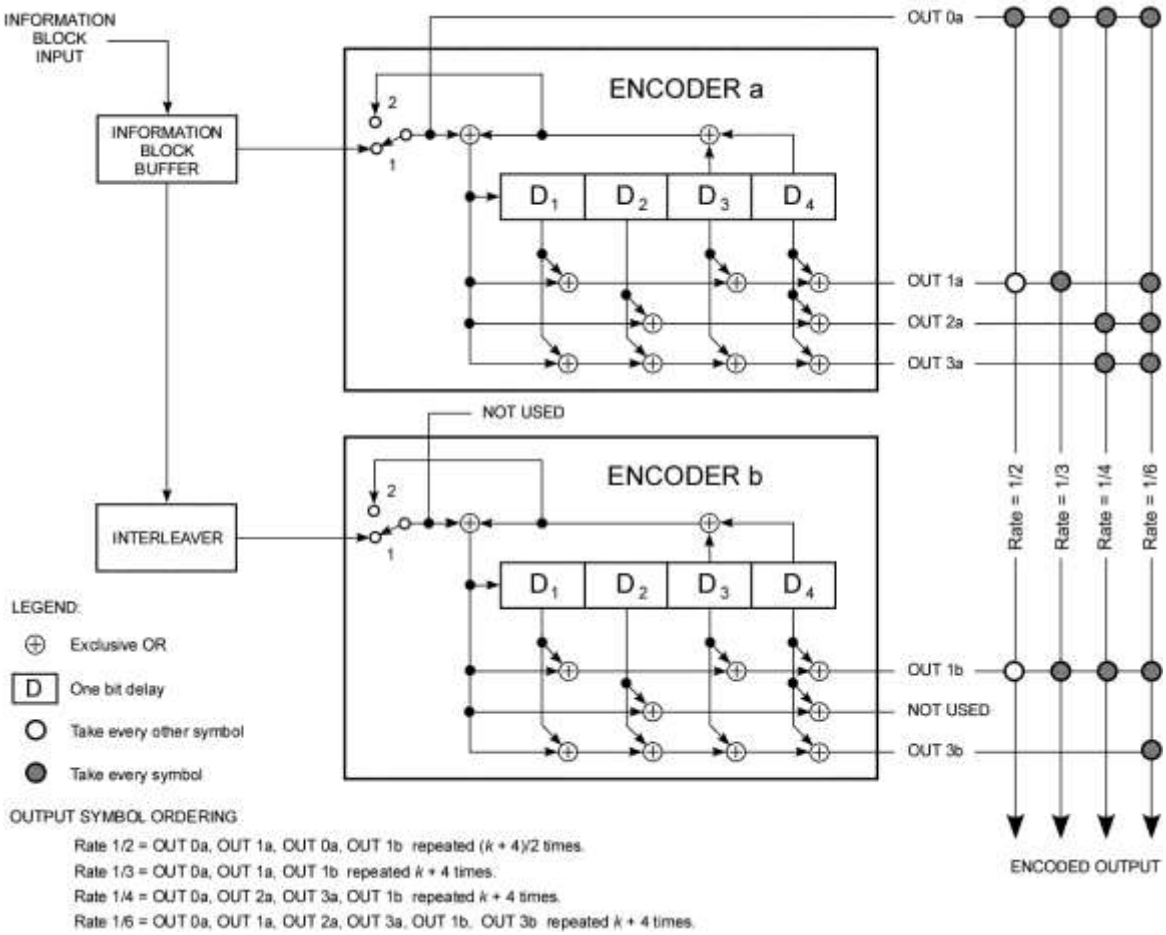

Figure 11. CCSDS Turbo Encoder

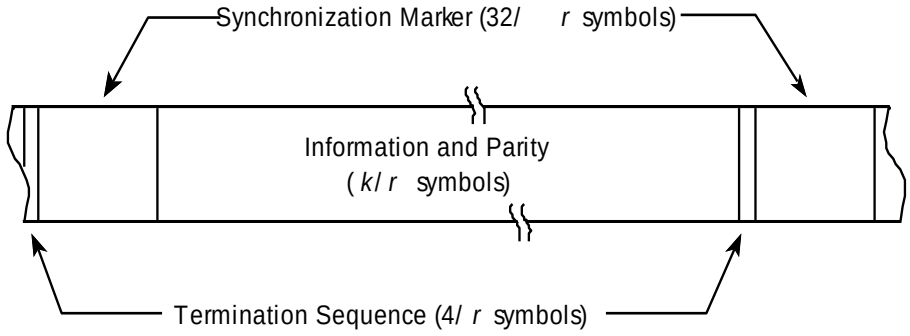

k = information block size (1784, 3568, 7136, 8920, or 16384 bits)

r = code rate (1/2, 1/3, 1/4, or 1/6)

Figure 12. Turbo Code Structure in the Physical Channel

2.5.6.2 Turbo Code Decoder

Upon recognizing the end of the synchronization marker, the turbo decoder uses a demultiplexer to separate the information symbols from the two sets of parity symbols and direct the information symbols and each of the parity streams into separate decoders. Each decoder makes a Maximum *A posteriori* Probability (MAP) estimate for each bit from the uncoded information symbols (in normal or permuted form, as appropriate) and the parity symbols generated by its corresponding encoder. The decoders exchange their MAP estimates via the appropriate permutation matrix to be used by the opposite decoder as *a priori* estimates for a second iteration. The exchange of MAP estimates continues for a specified number of times or until a satisfactory convergence is reached. Engineering research recommends 10 iterations and values as low as 6 have been successfully used in high data rate applications. The final output is a hard-quantized version of the likelihood estimates from either one of the decoders.

Unlike a Reed-Solomon decoder, there comes a point where a further increase in the E_b/N_0 does not significantly increase a turbo decoder's performance. This region is referred to as the turbo decoder error floor and, for the recommended codes, occurs at a BER of less than 10^{-7}. For operation near this region it is recommended that the data content of each information block be reduced to allow for a cyclic redundancy check (CRC) as an independent check on the decoding process to be inserted at the end of the codeblock. The DSN supports the 16-bit CRC specified in CCSDS Recommendation 132.0-B-1. A diagram of the CRC generator is shown in Figure 13. When CRC checking is enabled, the DSN decoder flags frames that are not successfully decoded but delivers all bits to the user.

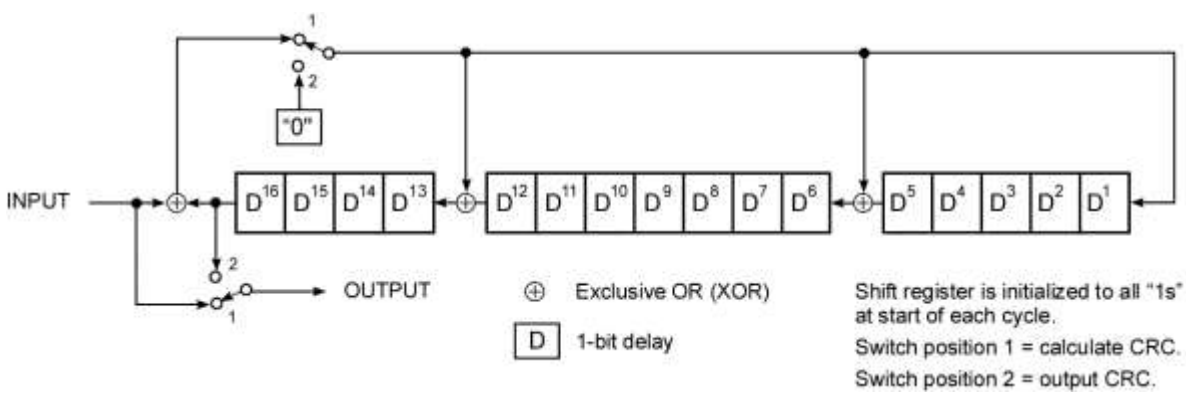

Figure 13. Cyclic Redundancy Check Generator

In addition to the latency required to create turbo-encoded data onboard the spacecraft, the DSN requires time to perform the iterative decoding process. The DSN turbo decoder is actually a set of parallel decoder modules where each module is filled with symbols while previously filled modules are either iterating or delivering their decoded results. The

decoder provides control over the number of iterations performed and a dimensionless convergence confidence threshold normally set at 100. The decoding process is considered complete if the confidence level at the end of an iteration exceeds the selected confidence threshold or if the specified maximum number of iterations is reached. The characteristics of the DSN Turbo Decoder are summarized in Table 4.

Table 4. DSN Turbo Decoder Characteristics

Parameter	Value
Code Supported	CCSDS
Information Block Lengths (*K*)	1784, 3568, 7136, 8920
Code Rates (*r*)	1/2, 1/3, 1/4, 1/6
ASM patterns	CCSDS compliant
Maximum Input Symbol Rates	Rate 1/2, 3.2 Msps Rate 1/3, 4.8 Msps Rate 1/4, 6.4 Msps Rate 1/6, 6.0 Msps
Number of Iterations	1 to 20 (nominal = 10)
Stopping Rule Threshold	0 (no confidence) to 32767 Nominal value = 100
Cyclic Redundancy Check	CCSDS 16-bit, Optional

2.5.7 Code Performance

The performance of a digital communications channel is expressed in the form of an error rate that is a function of the bit energy to noise spectral density ratio E_b/N_0. The two most common error rates used are the bit error rate (BER) and the frame error rate (FER). The FER, while being often the more significant of the two measures for judging performance, does not lend itself to comparison between code types because of its dependency on the code and the characteristics of the communications channel. On the other hand, BER is easily modeled for the additive white Gaussian noise (AWGN) channel which is a reasonable approximation for the deep space communications channel. Figure 14 provides a comparison of the BER performance for the codes supported by the DSN. Figure 15 shows the measured performance of the DSN Turbo Decoder for the same 8920 bit block size as Figure 14 but showing both the effects of increased code rate and the error floor.

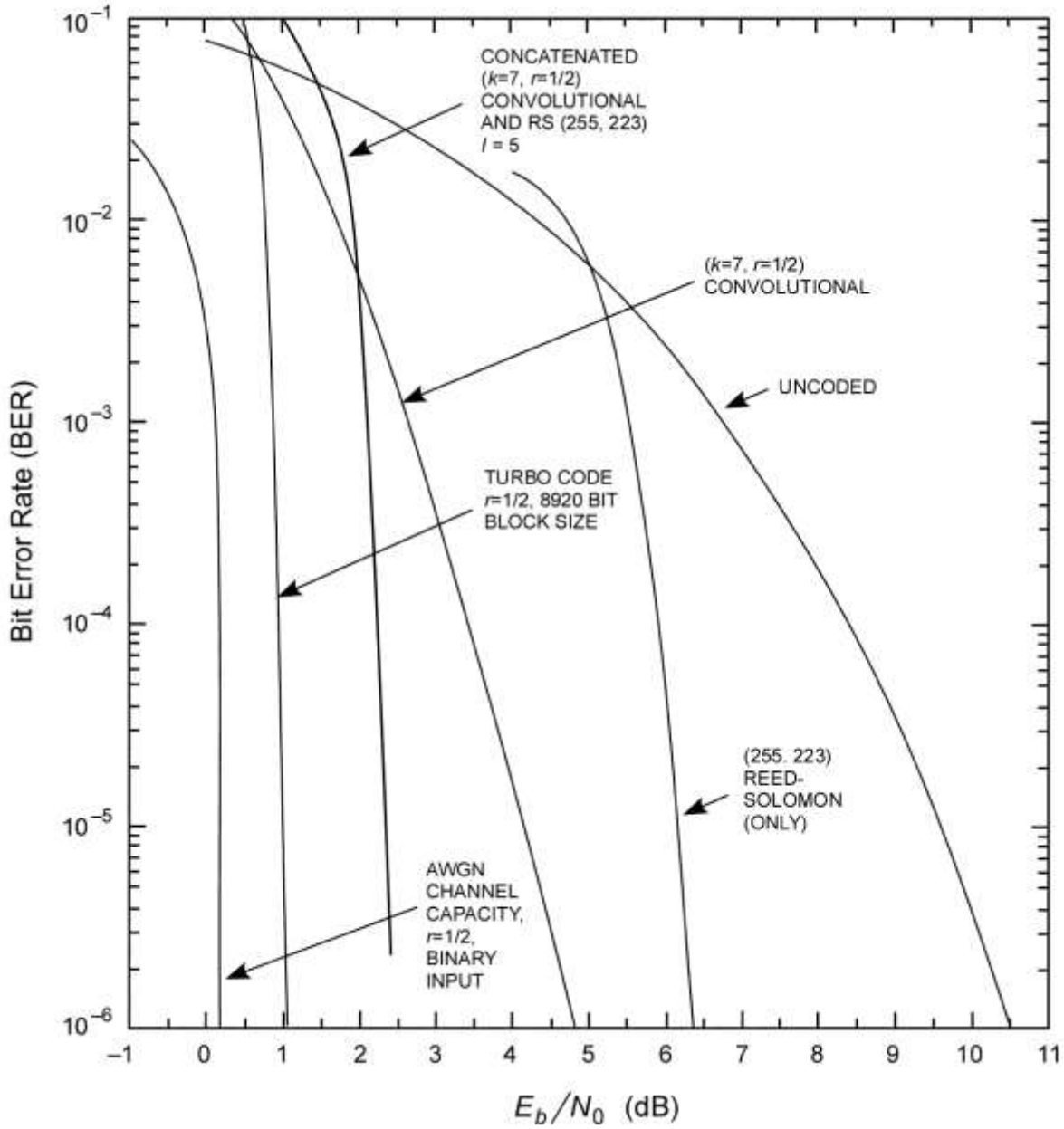

Figure 14. Relative Performance of Supported Codes

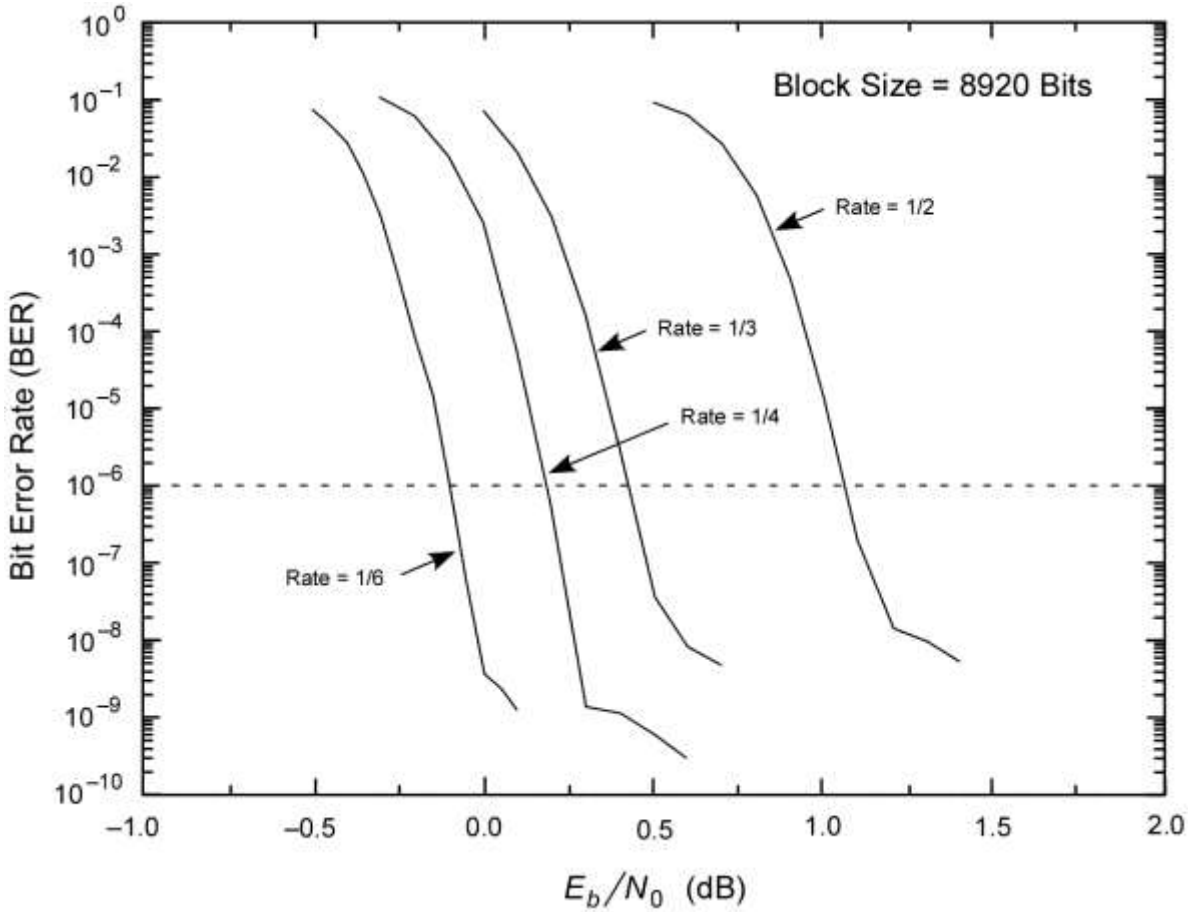

Figure 15. Measured Performance of DSN Turbo Decoder Showing Improvement with Code Rate and Error Floor Effects (Block Size = 8920 Bits)

2.6 Time Tagging

The DSN annotates every frame of data delivered to the user with its Earth-received time. The time may be specified as the beginning or end of each data frame depending on spacecraft data processing requirements. The time is calculated by determining the exact time the synchronization marker is recognized and adding a time delay measured when the equipment was installed to move the reference point to the input of the antenna's low noise amplifier. The normal precision of the time tag is 1 ms however additional precision can be provided by agreement between the DSN and users. Time tagging capability is summarized in Table 5.

Table 5. DSN Time Tagging

Parameter	Value
Normal Delivered Accuracy	Nearest ms
Station Reference	Test input port before LNA
Reference as Delivered	Leading edge of first bit of frame or trailing edge of last bit in frame
Accuracy	±5 usec (for symbol rates > 2000 sps and carrier loop SNR ≥ 20 dB)

2.7 Data Formatting

The result of the previously described processing is a series of fixed-length frames of telemetry data. The content of these frames may represent a single stream of telemetry data or a portion of several streams of telemetry data referred to as virtual channels, Virtual channels allocate the physical channel on a frame by frame basis identified by a virtual channel identifier. The DSN separates the frames based on the virtual channel identifier and creates independent streams of telemetry data. The use of virtual channels enables portions of the data stream to be delivered to different locations or with different latencies. Two types of telemetry frames are supported. *Version I Frames*, originally specified in CCSDS Recommendation 102.0-B, have the capability to support up to eight virtual channels numbered from 0 to 7. *Version II Frames*, originally specified in CCSDS Recommendation 701.0-B, have the capability to support up to sixty-four virtual channels. The DSN can combine from 1 to 16 of these channels into *virtual data streams* and the same virtual channel may appear in multiple virtual data streams. The number of virtual data streams that can be created for any one project is limited to 16.

Figure 16 provides an example of telemetry data flow when virtual channels are used. As shown in the figure, the contents of a virtual channel may be created by combining packets from multiple sources. The packets from each source are identified by a header that contains an Application Process ID (APID) and a packet length. This enables the user to separate the packets from each source. Since the virtual channel identifier and packet header fields within the transfer frames are not protected from errors, it is recommended that virtual channels not be used unless frames are known to be decoded correctly as can be determined if Reed-Solomon coding or a CRC field is used.

The DSN annotates each frame delivered to a user with received time and accountability information for each channel being delivered as opposed to the physical channel. The structure and detailed content of the data blocks as delivered is beyond the scope of this document but several standard formats are available and deviations to these formats can be negotiated as part of the establishment of detailed mission requirements.

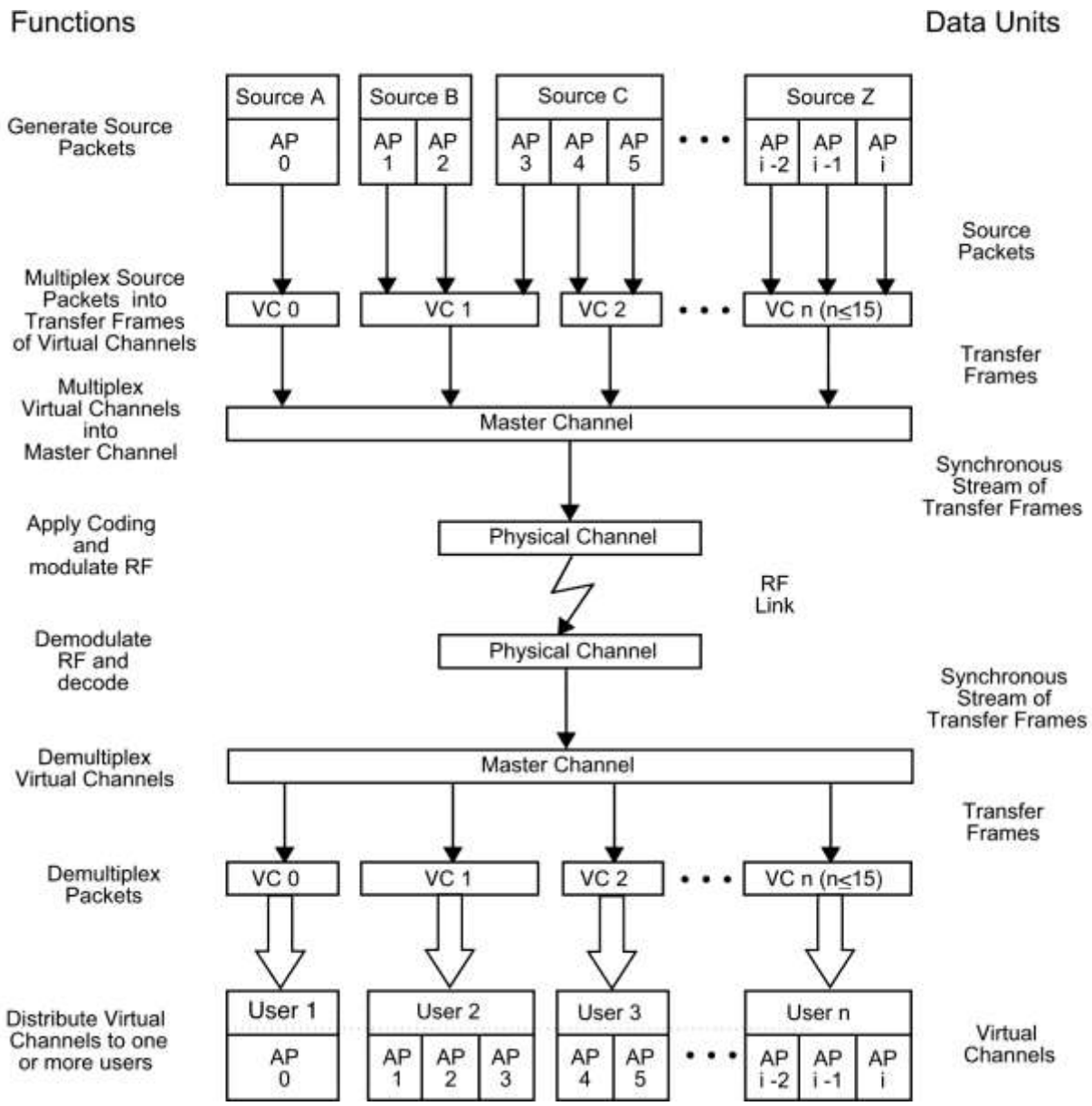

Figure 16. Example of Telemetry Data Flow Using Virtual Channels

2.8 Supported Telemetry Configurations

Figures 17 through 20 illustrate the telemetry coding configurations for spacecraft and ground equipment that are supported by the DSN. The order in which the steps in the coding and decoding process are performed are those recommended by the CCSDS and are fixed by hardware design.

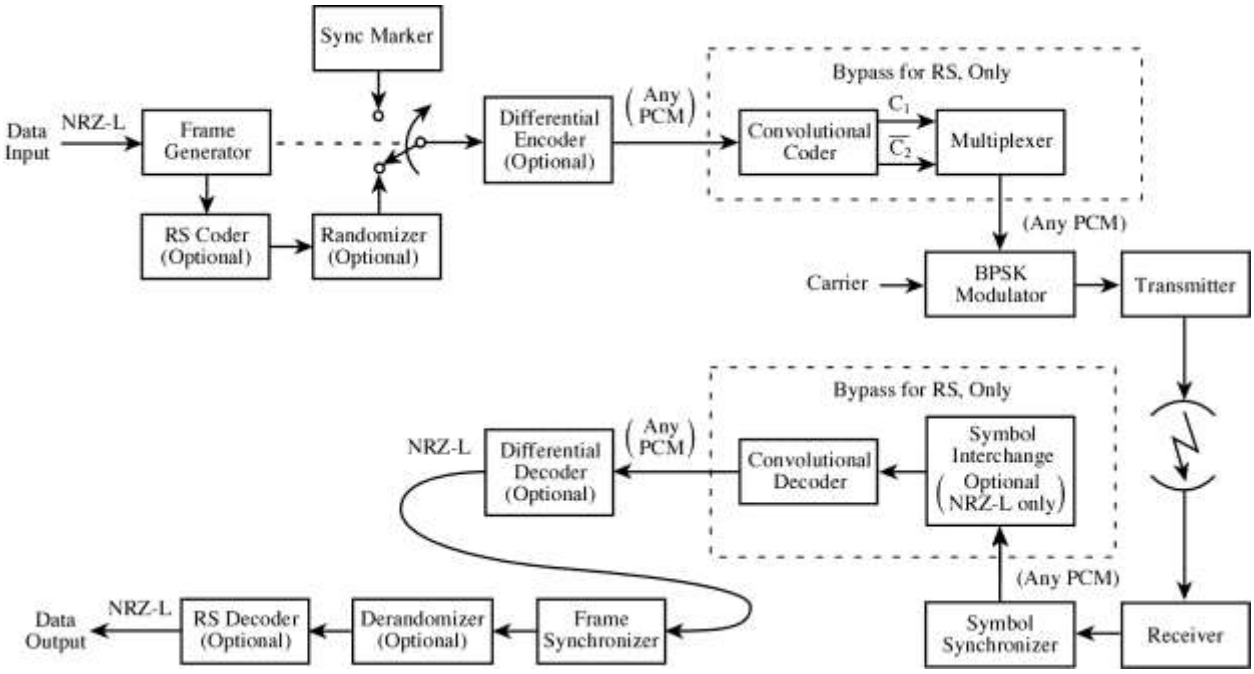

Figure 17. Spacecraft and Ground Configuration for BPSK Reed-Solomon, Convolutional, and Concatenated Coding

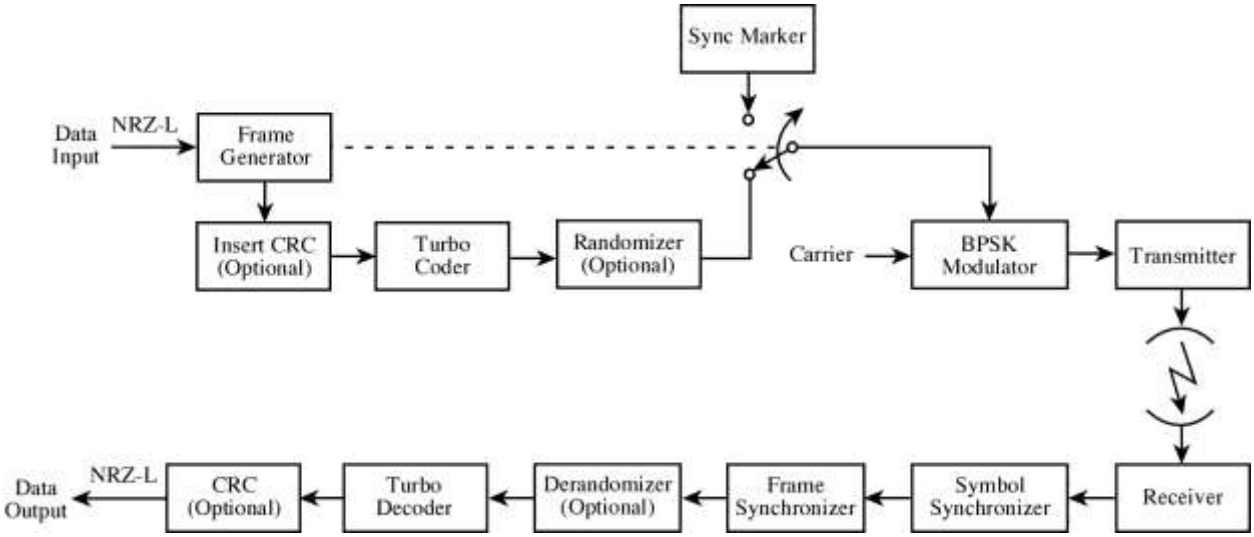

Figure 18. Spacecraft and Ground Configuration for BPSK Turbo Coding

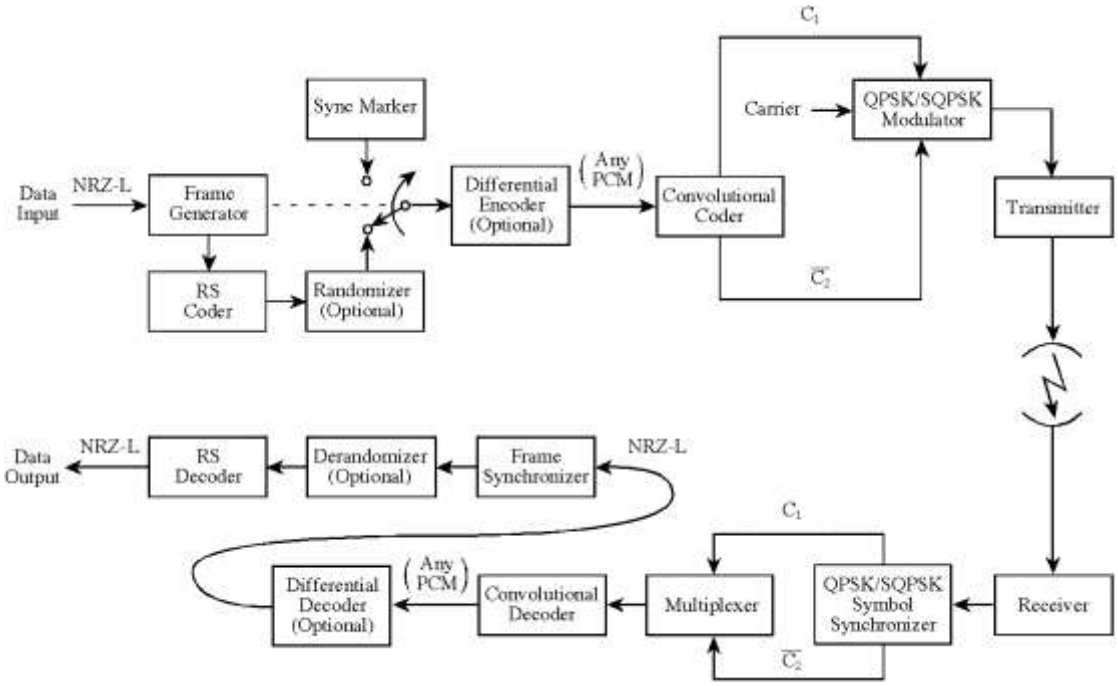

Figure 19. Spacecraft and Ground Configuration for QPSK/SQPSK Convolutional and Concatenated Coding

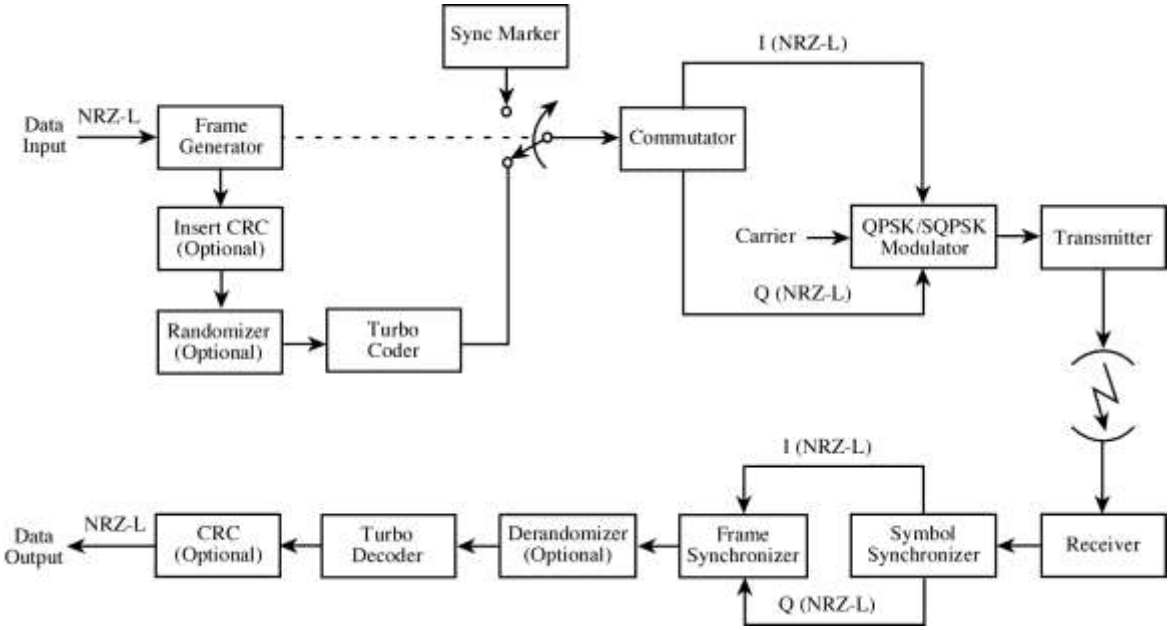

Figure 20. Spacecraft and Ground Configuration for QPSK/SQPSK Turbo Coding

3 Proposed Capability

The following paragraphs discuss capabilities that have not yet been implemented by the DSN but have adequate maturity to be considered for spacecraft mission and equipment design. Telecommunications engineers are advised that any capabilities discussed in this section cannot be committed to except by negotiation with the DSN System Engineering and Commitments Office.

3.1 Low-Density Parity-check (LDPC) Codes

Low-Density Parity-Check (LDPC) codes have been developed that provide near-theoretical limit performance at high code rates to complement the similar performance provided by Turbo codes at low code rates. They promise to be especially useful in applications where the bandwidth required to use a Turbo code is not available or would complicate spacecraft equipment design. LDPC codes have an additional benefit that their decoder structure is more appropriate for high-speed hardware implementation and, on the average, requires fewer computations per decoded bit.

LDPC codes were originally invented by R. Gallager in 1961 but were largely forgotten for 30 years. The discovery of an iterative decoding algorithm, now referred to as Belief Propagation (BP) decoding, in the mid 1990s coupled with advances in digital processing technology revived interest in the coding technique. LDPC codes are similar to turbo codes in that they are binary block codes with large code blocks of hundreds to thousands of bits. The codes selected for deep space applications are members of a class of LDPC codes referred to as quasi-cyclic. This class of codes has an advantage that encoder implementation can be accomplished with shift registers.

The particular codes selected for deep space application are described in the CCSDS Experimental Specification 131.1-0-2. They are systematic and non transparent requiring that phase ambiguities be resolved using the frame markers that are required for codeblock synchronization. Although these codes theoretically have error floors, they are typically at least two decades below those of Turbo codes so the CRC that is recommended with Turbo codes is unnecessary with LDPC codes. The codes cannot guarantee sufficient bit transitions to keep receiver symbol synchronizers in lock so the pseudo-randomizer described in section 2.5.3 of this document is required unless the system designer verifies that sufficient symbol transition density is assured by other means. Codeblock lengths for the supported code rates are provided in Table 6.

Figure 21 is included to show how LDPC codes compliment Turbo codes. The figure is in the symbol domain to make the effects of code rate more apparent and to prevent the curves from over-writing each other if they were presented in the bit domain in a single figure.

Table 6. Codeblock Lengths for LDPC Code Rates

Information Block Length, *k*	Codeblock Length, *n*		
	Rate = 1/2	Rate = 2/3	Rate = 4/5
1024	2048	1536	1280
4096	8192	6144	5120
16384	32768	24576	20480

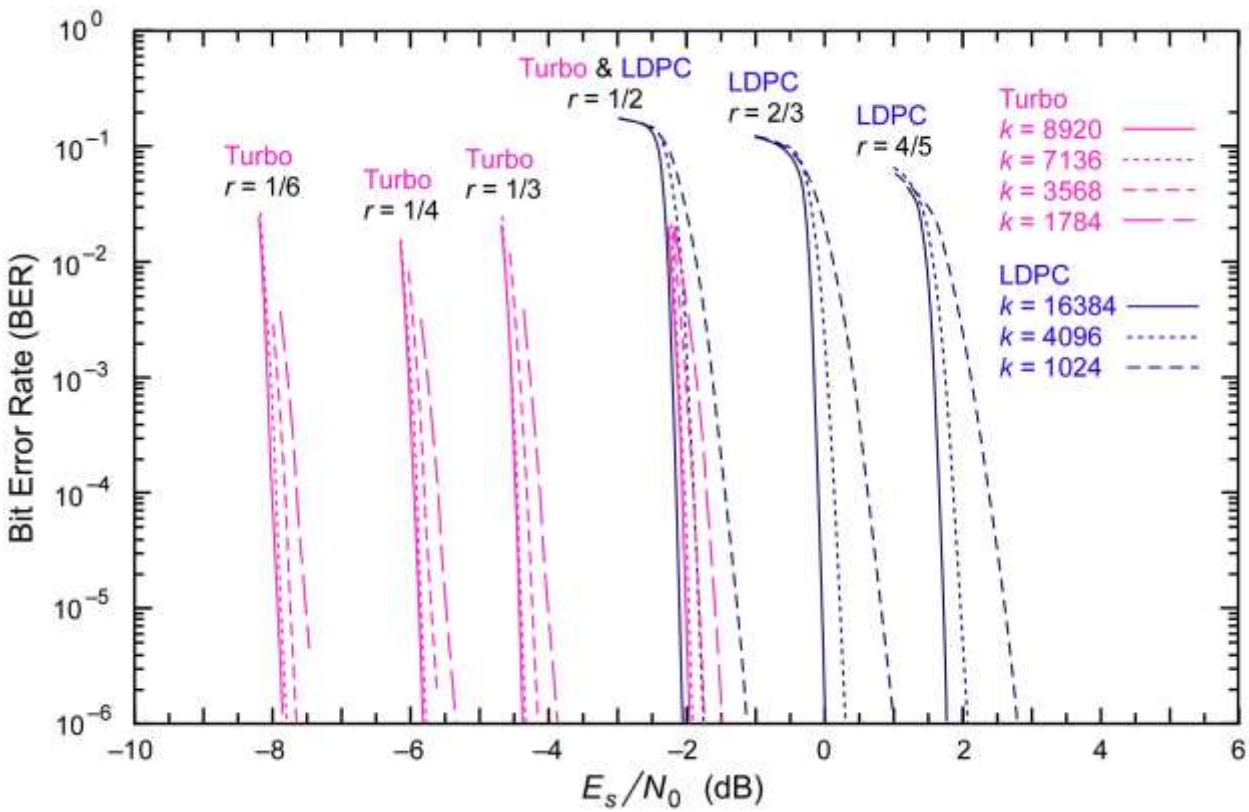

Figure 21. LDPC and Turbo Code Comparative Performance

References

1 FR. G. Gallager, “Low Density Parity Check Codes,” *IRE Transactions on Information Theory*, vol. IT-8, pp. 21–28, 1962.

2 CCSDS 102.0-B-5-S, Telemetry Channel Coding, Blue Book. Issue 5, November 2000.

3 CCSDS 130.0-G-1, Informational Report, TM Synchronization and Channel Coding – Summary of Concept and Rationale, June 2006

4 CCSDS 131.0-B-1, Recommendation, TM Synchronization and Channel Coding

5 CCSDS 131.1-O-2, Experimental Specification, Low Density Parity Check Codes for Use in Near-Earth and Deep Space Applications, September, 2007

6 CCSDS 701.0-B-2, Recommendation, Advanced Orbiting Systems, Networks and Data Links: Architectural Specification

Deep Space Network

209
Open-Loop Radio Science

Document Owner:		Approved by:	
Signature provided	11/14/2023	Signature provided	11/13/2023
Dong Shin OBD System Engineer	Date	Timothy Pham Communications Systems Chief Engineer	Date

Prepared By		Released by:	
Signature provided	11/19/2023	Signature provided	01/09/2024
Stephen Rogstad OLR Software CDE	Date	Christine Chang DSN Document Release Authority	Date

DSN No. **810-005, 209, Rev. F**
Issue Date: January 11, 2024
JPL D-19379; CL#24-0315

Jet Propulsion Laboratory
California Institute of Technology

Users must ensure that they are using the current version in DSN Telecommunications Link Design Handbook website:
https//deepspace.jpl.nasa.gov/dsndocs/810-005/

Review Acknowledgment

By signing below, the signatories acknowledge that they have reviewed this document and provided comments, if any, to the signatories on the Cover Page.

Signature provided	11/14/2023	Signature provided	11/14/2023
Jeff Berner DSN Project Chief Engineer	Date	Sue Finley OLR Subsystem Engineer	Date

Document Change Log

Rev	Issue Date	Prepared By	Affected Sections or pages	Change Summary
Initial	1/15/2001	R. Sniffin	All	All
A	6/1/2010	A. Kwok	All	Added Wideband VLBI Science Receiver (WVSR) and VLBI Science Receiver (VSR). Eliminated the Rev. E designation for the document series.
B	02/09/2015	A. Bedrossian S. Finley D. Shin	Section 2	Add DSS-35
C	11/17/2016	A. Bedrossian D. Shin	Section 2	Add DSS-36 Remove DSS-45 Updated Figures Some minor editorial corrections throughout the document
D	02/14/2019	S. Rogstad A. Bedrossian	All	Updates for OLR Delivery Remove DSS-15
E	02/05/2021	S. Rogstad A. Bedrossian S. Finley	Section 2	Added DSS-56 and DSS-53 Updated Table 2 and Table 3 information Some minor editorial corrections
F	01/11/2024	D. Shin S. Rogstad	Section 2	Updated DSS-53 status and added DDA annotation in Table 2

Contents

Figures

Figure **Page**

Tables

Table **Page**

1 Introduction

1.1 Purpose

This module describes the capabilities and performance of the Deep Space Network (DSN) open-loop receiving equipment used for supporting radio science (RS) experiments. Radio science experiments use the Open Loop Receiver (OLR) Subsystem.

1.2 Scope

This module discusses the open-loop radio science receiving equipment functions, architecture, operation, and performance. Although some RS experiments require uplink support and closed-loop Doppler and ranging data, this module only describes the open-loop recording capability that is used during radio science experiments. Open-loop recording is carried out by the OLR Subsystem. Details of the closed-loop Doppler tracking system can be found in module 202, Doppler Tracking. Details of the uplink functions can be found in the 70-m, the 34-m High Efficiency (HEF), and the 34-m Beam Waveguide (BWG) telecommunications interface modules 101, 103, and 104 respectively.

2 General Information

Radio science experiments involve measurements of small changes in the phase, frequency, amplitude, and polarization of the radio signal propagating from an interplanetary spacecraft to an Earth receiving station. By properly analyzing these data, investigators can infer characteristic properties of the atmosphere, ionosphere, and planetary rings of planets and satellites, measure gravitational fields and ephemerides of planets, monitor the solar plasma and magnetic fields activities, and test aspects of the theory of general relativity. Details of Radio Science System applications may be found in the JPL Publication 80-93, Rev. 1, written by S.W. Asmar and N.A. Renzetti, titled: *The Deep Space Network as an Instrument for Radio Science Research*. (https://ntrs.nasa.gov/search.jsp?R=19950015039).

2.1 Functions

The functions of the DSN with respect to conducting radio science experiments can be summarized as follows:

- Providing uplink carrier signals to the spacecraft with a pure spectrum, including low phase noise and stable frequency.
- Acquisition, down conversion, digitization, and recording of the downlink carrier with minimal changes to its frequency, phase, amplitude stability, and polarization.
- Assuring that the expected signals are being acquired and recorded.

2.2 Hardware Configuration

All radio science experiments require use of the antenna, microwave, antenna-mounted receiving equipment, and frequency and timing equipment at the stations, as well as the receivers in the signal processing center (SPC). They also require the Ground Communications Network (GCN) to deliver data from the stations to users at JPL, where experiments are monitored. A block diagram of the open-loop receiving capability is shown in Figure 1.

The receiving equipment on each DSN antenna produces one or more intermediate frequency (IF) signals with S-band producing an IF in the range 200 to 300 MHz; X-band 100-500 MHz and Ka-band 100-600 MHz. These IF signals are routed to an IF Gain Control (IGC) assembly and then digitized by the IF Digitizer (IFD). The IF digitizer channelizes the IF band and sends digital packets through the Digital IF Switch (DIS) to the OLR receivers.

Each of the 8 station OLRs can support up to 16 different IF inputs and each of the 16 possible configurable recording channels (see Table 1) can have a different BW, bit depth and static/predicted frequency configuration. However, limitations to this should be noted. An OLR should not be shared between users during a track, due to concerns about interference and having to divide up the available 16 channels. Users usually need multiple channels to record a given IF. Also, the total aggregate input bit rate of each OLR cannot exceed the 10Gbps Ethernet pipe.

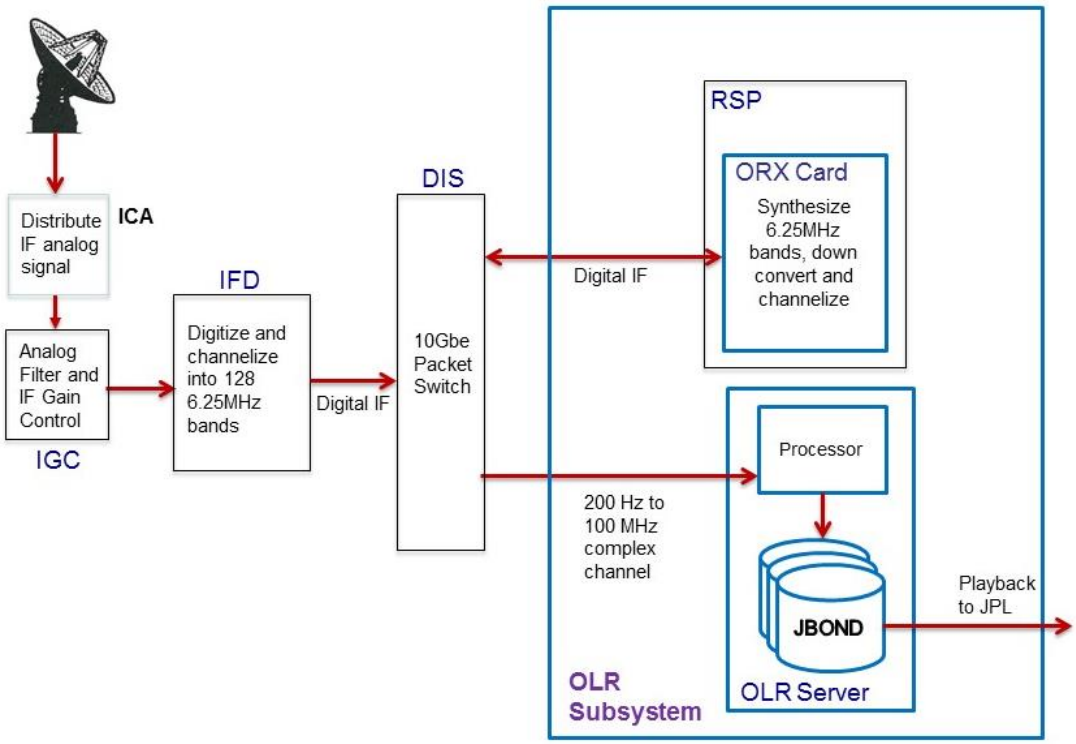

Figure 1. OLR Signal Flow

2.3 OLR Signal Processing

The IF signal is sampled in the IF Digitizer (IFD) where it is digitized and downconverted to 0-800MHz complex with a center frequency of 400MHz. However, the IF Gain Control (IGC) assembly filters the signal before entering the IFD to limit its bandwidth to the range of 85–609 MHz. This corresponds to a received frequency range of 2085-2609MHz at S-band, 8185-8709MHz at X-band, and 31785-32309MHz at Ka-band. However, the actual effective received frequency range will depend on the filter characteristics of the equipment on the selected antenna and may be narrower. Figure 2 illustrates the processing bandwidth through the OLR Subsystem.

The filtered IF signal is digitized at 3200 Ms/s with a 12-bit resolution, then downconverted to 0-800MHz complex with a center frequency of 400MHz and an equivalent resolution of 14 bits.

The recording channel filters are specified by their bandwidths, the desired resolution (bits/sample) and an offset from the predicted sky frequency predict file. This frequency predicts file is created by the DSN network support function and contains the spacecraft frequency altered by spacecraft trajectory and Earth-rotation. Table 1 lists a sample of the supported OLR filter bandwidths and resolutions. The OLR provides many other bandwidths and bit rates, however this table shows only those typically required by RS users. For a more exhaustive list of supported OLR channel bandwidths, see Section 3.2 of 820-013 0222-Science.

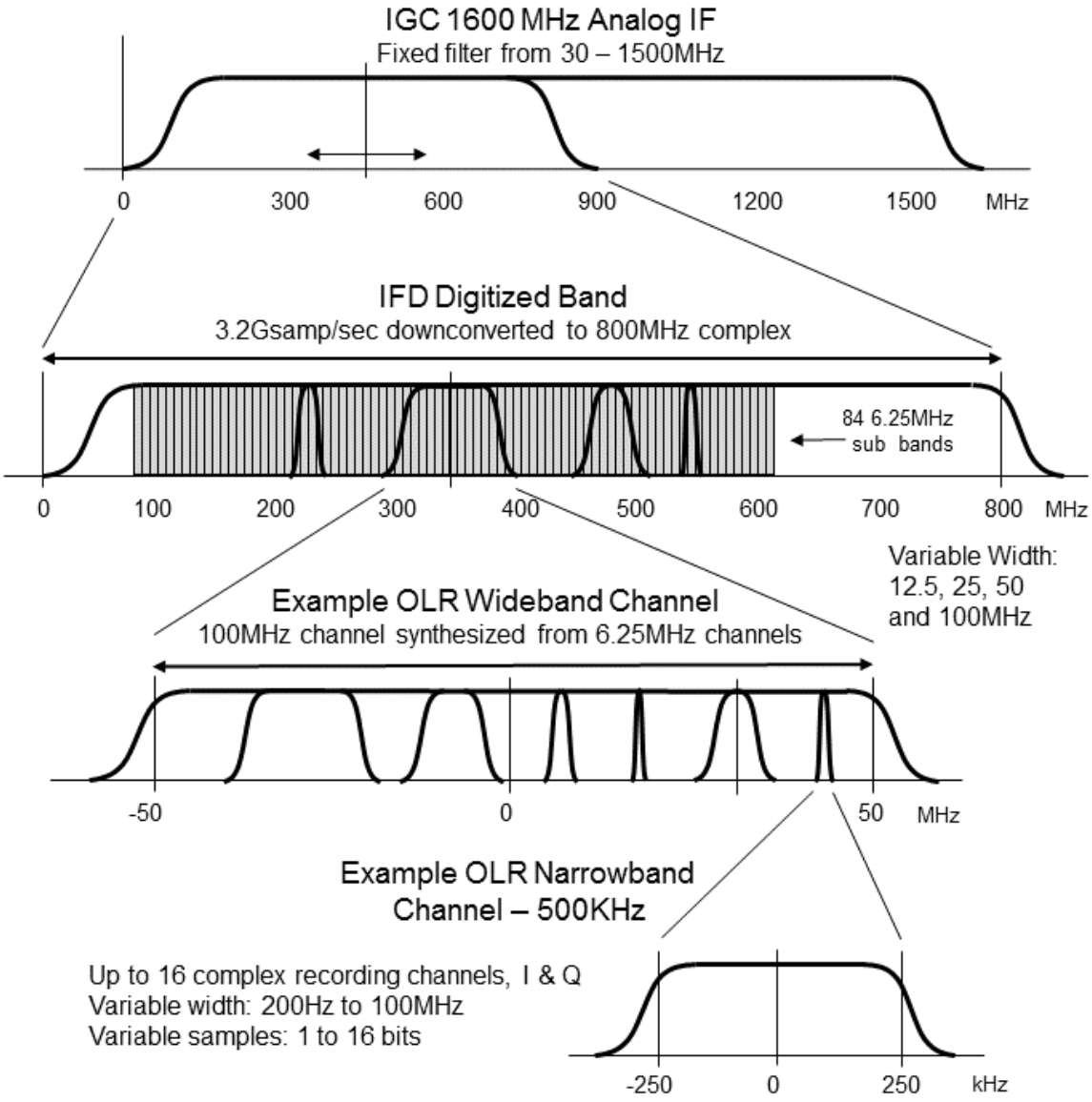

Figure 2. Relationships between Processing Bands for OLR

Table 1 - Sample of OLR Supported Bandwidths

Category	Bandwidth	Resolution (b/sample)	Upper Data Rate (b/s)
Narrowband	200 Hz	8,16	6400
	250 Hz	8,16	8000
	500 Hz	8,16	16000
	1 kHz	8,16	32,000
	2 kHz	8,16	64,000
	4 kHz	8,16	128,000
	8 kHz	8,16	256,000
	16 kHz	8,16	512,000
	25 kHz	8,16	800,000
	50 kHz	8,16	1,600,000
	80 kHz	8,16	2,560,000
	100 kHz	8,16	3,200,000
	250 kHz	8,16	8,000,000
	500 kHz	8,16	16,000,000
Wideband	1 MHz	8,16	32,000,000
	2 MHz	8,16	64,000,000
	1 MHz	2,4	8,000,000
	2 MHz	2,4	16,000,000
	4 MHz	2,4	32,000,000
	8 MHz	2	32,000,000
	16 MHz	2	64,000,000
	32 MHz	2	128,000,000
	40 MHz	2	160,000,000
	50 MHz	2	200,000,000

2.4 Available IF Inputs

Using a single client on a server, the OLR is capable of tracking and recording channels from up to 16 IF inputs at one time. These IF inputs available at each of the 3 DSN complexes are shown in Table 2.

2.5 OLR Signal Detection

The OLR does not have a mechanism to align its passband to (establish lock with, or track) the received signal. Instead, it relies on predicts to position its passband. This creates a risk that a predict error might result in the wrong portion of the received spectrum being processed. To assist in recognizing this, the OLR analyzes the data in each channel and provides a detected signal indication on the main display for that channel for diagnostic purposes only.

In addition to the detected signal indication, the OLR provides a frequency-domain representation of the bandpass being recorded in each channel using a Fast-Fourier Transform (FFT). Characteristics of the FFT such as number of points, averaging, and update rate are under user control.

Table 2 - Available IF Inputs at each complex

Goldstone IF Inputs	Madrid IF Inputs	Canberra IF Inputs
14_S1	63_S1	43_S1
14_S2	63_S2	43_S2
14_X1	63_X1	43_X1
14_X2	63_X2	43_X2
24_S1	65_S1	34_S1
24_X1	65_X1	34_X1
		34_K1*
25_X1	54_S1	34_K2*
25_X2	54_X1	
25_K1*	54_K1*	35_X1
25_K2*	54_K2*	35_X2
		35_K1*
26_S1	55_X1	35_K2*
26_X1	55_X2	
26_X2	55_K1*	36_S1
26_K1*	55_K2*	36_X1
26_K2*		36_X2
	56_S1	36_K1*
DDA1**	56_X1	36_K2*
	56_X2	
	56_K1*	DDA1**
	56_K2*	
	53_X1	
	53_X2	
	53_K1	
	53_K2	
	DDA1***	

*Software currently processes ‘K’ as ‘Ka’, Radio Science does not use K-band (25.5 – 26.0 GHz), only Ka-band.

**DDA1 is the downlink array subsystem, used occasionally by Radio Science. It will be replaced by DDA3 and DDA4 in middle of 2024 for dual array capability.

2.6 OLR Operation

Of the 8 OLRs per station, six operate in a connection (link-assigned) mode and two in a stand-alone mode. In the connection mode, the Network Monitor and Control (NMC) function receives monitor data from the OLR for displays at the NMC and provides a workstation from which the OLR can be operated. OLRs that are not assigned to a link are operated in a stand-alone mode without interference to any activities in process at the complex. Monitor data is not forwarded to the NMC by OLRs operating in the stand-alone mode.

The OLR employs a client-server architecture where each one acts as a server capable of accepting multiple connections from users operating the appropriate receiver client software at any time. In the link-assigned mode, one of these clients is the NMC workstation.

The OLR does not recognize any remote client as being superior to the others so it is up to the user to assign responsibility for control to one client with the other clients operating in a passive mode. NMC clients, on the other hand, have priority over remote clients and will terminate remote clients when brought up in a connection. Users who want to remotely monitor link-assigned OLR activities should bring up a remote client after it is put in the link.

All functions of the OLR may be performed from the OLR client in real time. Of special interest to the RS experimenter is the ability to adjust the predicted frequency profile, to slew the individual channel frequencies, to adjust FFT parameters, and to enable or disable recording for each channel.

2.7 Data Delivery

When recording is enabled, baseband samples and ancillary information, discussed below, are formatted into a file of one-second data records and stored on an OLR server for delivery via network playback to JPL or other users. A separate data file is created for each channel. Data delivery is via file transfer using Secure Shell (SSH) protocol. Data also may be obtained via Secure File Transfer Protocol (SFTP). The OLR is capable of playing data back in legacy 0159-Science format as well as 0222-Science format.

2.7.1 Ancillary Data

The following ancillary data are included as a header in each data record. A detailed description of the data is contained in DSN Document 820-013, module 0222-Science. The users will need to include the last two items in the filename for each channel to properly identify the supporting station, tracking pass, and spacecraft.

- Data record version
- Receiver configuration
- Channel identification
- Time tag for first sample in block
- Station and pass identification
- Spacecraft identification

2.8 Performance

The principal characteristics of the OLR are summarized in Table 3. In addition, radio science experiments are influenced by the overall stability of equipment at the stations. The following sections provide information on performance characterization in terms of frequency stability, phase noise, and amplitude stability for the ground stations.

Table 3. Open Loop Receiver Characteristics

Parameter	Value	Remarks
Frequency Ranges Covered		
At OLR Input (MHz)	100 - 600	
Referenced to S-band (MHz)	2,085 – 2,609	S-band downlink allocation is 2,200–2,290 MHz for near Earth application and 2,290–2,300 MHz for deep space applications
Referenced to X-band (MHz)	8,185 – 8,709	X-band downlink allocation is 8,400–8,450 MHz for deep space application and 8,450–8,500 MHz for near Earth applications
Referenced to Ka-band (MHz)	31,785 – 32,309	Ka-band downlink allocation is 31,800–32,300 MHz for deep space applications.
IF Attenuation		Applied by IGC
Range (dB)	0 – 31.75	
Resolution (dB)	0.25	
Doppler Compensation		
Maximum Doppler Shift (km/s)	30	At all downlink frequencies
Maximum Doppler Rate (m/s^2)	17	At all downlink frequencies
Maximum Doppler Acceleration (m/s^3)	0.3	At all downlink frequencies
Maximum Tuning Error (Hz)	0.5	At all downlink frequencies
Maximum Bitrate (Mb/sec)	512	Maximum recordable data rate per OLR with no performance degradation, assuming all 8 station OLRs are running at this rate.

Table 3. OLR Characteristics (Continued)

Parameter	Value	Remarks
Baseband Resolution (MHz)	1	
Configurable Recording Channels	16	Available on each of the 8 OLRs
Narrow Channel Tuning		
Tuning (MHz)	±262	
Resolution (Hz)	<1	
Recording Bandwidths	200 Hz – 50 MHz	
Resolutions (bits/sample)	1,2,4,8,16	
Time Tagging		
Resolution (s)	1	Data is time tagged once per second
Accuracy (μs)	1	With respect to station clock
Signal Detection Display		1 for each subchannel being recorded
Number of points in FFT	128 – 131,072	Default is 1024
Spectra Averaging	1 – 1000	Default is 10
FFT Interval (s)	1 – 10,000	Default is 10

2.8.1 Frequency Stability

DSN stations are designed to meet radio science requirements for stability. Frequency stability of the ground station is characterized by means of Allan deviation. RS System Performance Testing (SPT) has been conducted with the exciter, transmitter, the low noise amplifier (LNA), and the OLR receiving equipment. In this test configuration, an uplink signal generated by the exciter is frequency shifted via the test translator to a downlink frequency. The downlink signal is injected at the front-end of the LNA and passed through the RF-IF downconverter IGC and IFD which provides the IF signal to the OLR. SPT excludes instability in the frequency and timing equipment and the mechanical vibrations of the antenna. This is because frequency and timing instability is cancelled out, while the mechanical vibrations of the antenna are not included in the test configuration. Measurements of these items can be obtained via other means, making it possible to provide an estimate of the overall frequency stability for the stations.

Repeated SPT measurements have provided the basis of estimating the Allan deviation over a specified integration time for the ground station. Table 4 shows the 2-way Allan deviation numbers that any DSN ground station can achieve. These estimates include all elements in the ground station that constitutes the measurement path through which the OLR data are obtained. The values shown are meant to be the upper bound for performance (i.e., the not-to-exceed numbers). The measurements and analysis have accounted for the various station types (HEF, BWG, 70m), the different frequency band combinations (S, X, and Ka), and various system configurations.

2.8.2 Phase Noise

Phase stability (Spectral Purity) testing characterizes stability over very short integration times. The region of the frequency band where phase noise measurements are

performed can be as far as 10 kHz off the carrier frequency. Such measurements are reported in dB relative to the carrier (dBc), in a 1 Hz band at a specified distance from the carrier.

Phase noise data have also been captured as part of the SPT measurements. Table 5 shows the not-to-exceed phase noise levels for the different frequency bands, at specified offsets. As is the case with frequency stability testing, these numbers have been obtained through many repeated SPT measurements. They represent what the DSN can achieve under normal operation conditions.

2.8.3 Amplitude Stability

Amplitude stability tests measure the amplitude fluctuations produced by the open-loop receiving system relative to a constant (mean) amplitude input signal. The amplitude stability performance is specified in terms of a threshold on the amplitude fluctuations relative to the mean amplitude, and the corresponding probability that such fluctuations will not exceed such a threshold. Analyses with the collected data indicate that the 1-sigma number (67% of the time) of the amplitude stability at a given DSN station over a 30-minute observation at any frequency bands is less than 0.2 dB. This number includes the gain variation due to antenna pointing errors.

Table 4. Two-Way (Uplink and Downlink) Allan Deviation Estimates

Averaging Time, s	**Allan Deviation**			
	1	**10**	**100**	**1000**
Station				
34-m HEF / 34-m BWG / 70-m	7.0×10^{-13}	2.0×10^{-13}	3.0×10^{-14}	5.0×10^{-15}

Table 5. Uplink and Downlink Phase Noise Estimates

Offset from Carrier, Hz	**Phase Noise, dBc-Hz**		
	1	**10**	**100**
Frequency Band			
S-band (Uplink or Downlink)	–63	–69	–70
X-band (Uplink or Downlink)	–63	–69	–70
Ka-band (Uplink or Downlink)	–50	–55	–57

Deep Space Network

210
Delta Differential One-way Ranging

Document Owner:		Approved By:	
Signature Provided	11/16/2023	Signature Provided	11/28/2023
Chris Volk Delta-DOR System Engineer	Date	Timothy Pham Communications Systems Chief Engineer	Date

Prepared By:		Released by:	
Signature Provided	11/28/2023	Signature Provided	12/20/2023
Dong Shin OBD System Engineer	Date	Christine Chang DSN Document Release Authority	Date

DSN No. **810-005, 210, Rev. E**
Issue Date: January 11, 2024
JPL D-19379; CL#23-7139

Jet Propulsion Laboratory
California Institute of Technology

Users must ensure that they are using the current version in DSN Telecommunications Link Design Handbook website:
https://deepspace.jpl.nasa.gov/dsndocs/810-005/

Review Acknowledgment

By signing below, the signatories acknowledge that they have reviewed this document and provided comments, if any, to the signatories on the Cover Page.

Signature Provided	08/23/2023
Jeff Berner DSN Project Chief Engineer	Date

Document Change Log

Rev	Issue Date	Prepared By	Affected Sections or pages	Change Summary
Initial	07/15/2004	P. W. Kinman	All	New Module
A	02/09/2015	A. Bedrossian J. S. Border D. Shin	All	Replaced description of VSR with description of WVSR. Added DSS-35 interface. Updated error budget.
B	02/10/2017	J. S. Border D. Shin	Section 2	Add DSS-36 interface. Remove DSS-45 interface.
C	06/06/2019	J. S. Border	Section 2	Replaced description of WVSR with description of OLR in Section 2.1. Updated stations shown in Fig. 2. Updated error budget in Section 2.5.
D	02/05/2021	A. Bedrossian J. S. Border D. Shin	Figure 2	Added DSS-53 and DSS-56. Added DSS-65 decommission date.
E	01/11/2024	D. Shin	Figure 2	Updated DSS-53 and DSS-65 status.

Contents

Illustrations

Tables

Table **Page**

1 Introduction

1.1 Purpose

This module describes the capabilities and identifies the performance parameters for Delta-Differential One-way Ranging (ΔDOR) measurements at the Deep Space Network (DSN) 34-m and 70-m stations.

1.2 Scope

The document provides information on the Delta-Differential One-way Ranging (ΔDOR) technique. This document describes those parameters and operational considerations that are independent of the particular antennas being used. For antenna-dependent parameters, refer to the appropriate telecommunications interface module in DSN Document 810-005, modules 101, 103 and 104 of this handbook. The interpretation of any particular ΔDOR measurement is dependent on the precise locations of the tracking antennas. Station locations are provided in module 301, Coverage and Geometry. ΔDOR signals are received by the Open Loop Receiver (OLR). The quality of a ΔDOR measurement depends in part on solar wind velocity that is discussed in module 106, Solar Corona and Solar Wind Effects. Modules of 810-005 that cover DSN capabilities related to ΔDOR are listed in Appendix A.

2 General Information

Delta-Differential One-way Ranging is a radio-tracking technique that has proved very useful in the orbit determination of some spacecraft (References 1 and 2). A comprehensive review of ΔDOR development in the DSN is given in Reference 3. A comprehensive technical description including fundamentals, design trade-offs, and performance is given in Reference 4. Delta-DOR is an interferometric technique and therefore requires two Deep Space Stations located at different complexes for a single measurement.

2.1 Description of the Measurement

ΔDOR uses the differential one-way range technique to provide information about the angular location of a target spacecraft relative to a reference direction where the reference direction is defined by the direction of arrival of radio waves from a source whose direction is well known. This is the origin of the "Δ" in the name "ΔDOR". The term *reference source* is applied to the distant source of radio waves that define the reference direction. Typically, the reference source is a quasar whose angular position in the sky is well known and cataloged, having been previously measured and studied. Sometimes, the reference source is a second spacecraft whose position in the sky is better known than that of the target spacecraft.

DSN Document 810-005, Module 107 contains the current X-band radio source catalog. Work is in progress to publish the Ka-band radio source catalog as module 108. For further information on radio source catalog development, see References 5 and 6.

Since ΔDOR provides a direct geometric determination of spacecraft angular position, it is especially useful for cases where line-of-sight measurements have weaknesses such as spacecraft near zero declination and spacecraft with small, unmodeled dynamic forces affecting their motion. It can also provide an independent cross-check of orbits determined by other methods and, in combination with these methods, can improve the accuracy of trajectory determination. Further, ΔDOR measurements are of relatively short duration when compared to other orbit determination methods such as Doppler and two-way ranging (typically one hour or less compared with many hours). Thus, they can be used to reduce the total amount of tracking time necessary to attain the desired level of trajectory accuracy. The main disadvantages of ΔDOR are that it requires two stations for each measurement and, in most cases, will disrupt telemetry when the reference source is being viewed.

2.1.1 Differential One-Way Ranging

The name, differential one-way ranging, comes from the fact that only a range difference, rather than an absolute range, is determined and that only the downlink is used. It is because only a range difference is being measured that it is possible to make this measurement one-way. (Absolute range measurement requires a highly-accurate clock at the target spacecraft as any clock error would translate directly into a range measurement error. This is the reason that ordinary ranging measurements send a ranging code derived from the station clock to the spacecraft, see modules 203 and 214.)

The geometry of differential one-way range is depicted in Figure 1. The radio waves from the target spacecraft arrive in approximately parallel rays at the interferometer. An imaginary line that connects the two antennas forming the interferometer is called the baseline and is denoted B in Figure 1. Since the antennas of the interferometer are located in different complexes on separate continents, the baseline B passes through the Earth. Also in Figure 1, an imaginary line segment L is drawn that is perpendicular to the arrival direction of the incoming rays. The shaded area around L represents the *a-priori* uncertainty in angle A and, because L is perpendicular to R, the uncertainty of the angle of the incoming radio waves with respect to the baseline. The interferometer measures the path length difference, also known as differential one-way range and indicated as δR in the figure. This enables the accuracy of A to be significantly improved. It is important to note that this is not a complete solution for the angular position in the sky of the target spacecraft. A single measurement only provides information about the location of the target spacecraft in the plane defined by the interferometer baseline and the target spacecraft.

The path length distance (δR) is determined by recording the signals arriving at each station using an open-loop receiver. Later, when the signals from both stations are available at a common location, the two signals are correlated. The difference in group delay associated with the paths followed by the target spacecraft signal in propagating to the two stations is determined (τ_g) and converted into a path length difference by multiplying by the speed of electromagnetic waves in space (c). The path length difference and knowledge of the baseline orientation is used to refine the angular position of the of the target spacecraft in the sky. The errors inherent in the DOR and ΔDOR process are discussed in Paragraph 2.4 and summarized in

Paragraph 2.5. In discussing these errors, it is customary to use time units – that is, the units of differential group delay.

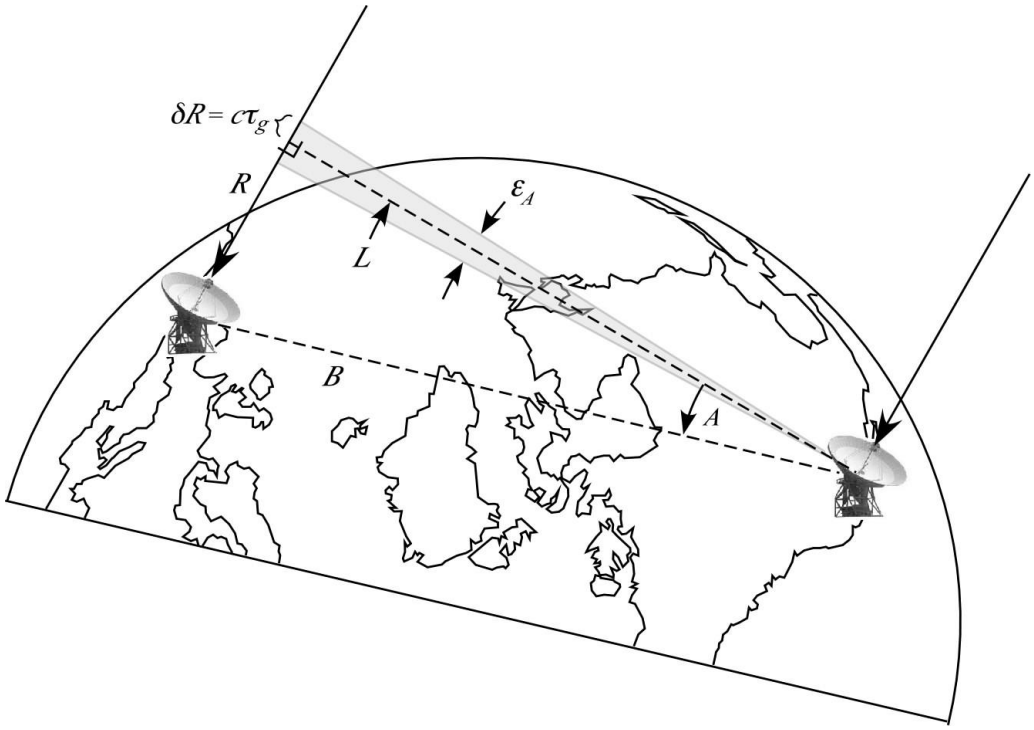

Figure 1. Geometry of Differential One-Way Ranging
(B = Baseline; L = perpendicular to incoming rays; A = angle between B and L;
δR = differential one-way range, ε_A = uncertainty in angle A)

The signals transmitted by the spacecraft should be high frequency sinewave or pseudo-noise (PN) waveforms to provide the best precision. These signals are commonly referred to as "DOR Tones". Lower frequency subcarrier harmonics can be substituted for DOR tones, with some loss of precision, if DOR tones are not available. The subcarrier harmonics may be pure tones or spread by telemetry. The lowest possible symbol rate is preferred to reduce the squaring loss that occurs during signal processing. Uplinked range tones provide even less precision, but may be used if no other components are available. Subcarrier harmonics or additional DOR tones may also be required in order to resolve the phase ambiguity, see Paragraph 2.3

2.1.2 ΔDOR

ΔDOR is a much more useful measurement for orbit determination than is plain DOR. In principle, a DOR measurement provides information about the angular position of the target spacecraft (within the plane of the interferometer plus target spacecraft). However, there are a number of measurement errors that prevent this form of measurement from being useful in

the solution of the typical deep space orbit determination problem. The sources of these measurement errors are (among others) station clock offsets, instrumental group delays, and media effects. To calibrate these effects, a plain DOR measurement is made on a reference source that is near the target spacecraft in an angular sense. The antennas are quickly moved to the target spacecraft and a similar measurement is made. Finally, the antennas are returned to the reference source to verify the calibration. This technique enables the effects of station clock offsets, instrumental group delay errors, and most of the media effects to be cancelled when the individual DOR results are differenced (which is a ΔDOR measurement). The result is that the errors in a ΔDOR measurement are much smaller than those for a plain DOR measurement and the technique becomes sufficiently accurate for orbit determination.

A number of missions have used ΔDOR measurements as part of their orbit determination. ΔDOR measurements played an important role in the orbit determination of 2001 Mars Odyssey (Reference 2) and the Mars Exploration Rovers (MER) (Reference 7). Those ΔDOR measurements were performed at X band. Delta-DOR measurements were also performed in the Ka band for the Mars Reconnaissance Orbiter using beam-waveguide stations (Reference 8). It should be noted that a VLBI measurement will always use two stations at different complexes; therefore stations 25 and 26 would not be used in the same measurement nor would stations 54 and 55.

2.1.3 DSN Equipment for ΔDOR Support

Differential one-way ranging is supported by the 34-m and 70-m antennas. Other equipment includes the OLRs in the complex Signal Processing Center (SPC), the ground communications infrastructure, and the DOR Correlators at Jet Propulsion Laboratory (JPL) and Goldstone Deep Space Communication Complex (GDSCC). Figure 2 depicts the DSN equipment used for ΔDOR support.

The input to the OLR is one or two digital Intermediate-Frequency (IF) signals that have been downconverted from the microwave sky frequency, also referred to as the radio frequency (RF). The IF signals cover the full usable signal bandwidth. The RF passbands are fixed and, in combination with the RF to IF downconverters, place restrictions on the frequency ranges in which the ΔDOR tones can be received. These restrictions, in terms of microwave sky frequency, are listed in Table 1. Additional restrictions based on the bandwidths of the antenna low noise amplifiers can be found in DSN Document 810-005, space link interfaces modules 101, 103, and 104.

Table 1. Microwave Sky Frequency Ranges for ΔDOR Tones

Band	Acceptable Frequency Range	Remarks
S-band	2,200–2,310 MHz	Deep Space Allocation is 2,290–2,300 MHz
X-band	8,200*–8,600 MHz	Deep Space Allocation is 8,400–8,450 MHz
Ka-band	31,800–32,300 MHz	Deep Space Allocation is 31,800–32,300 MHz

* DSS-35 X-band range is from 8,225 MHz-8,600 MHz

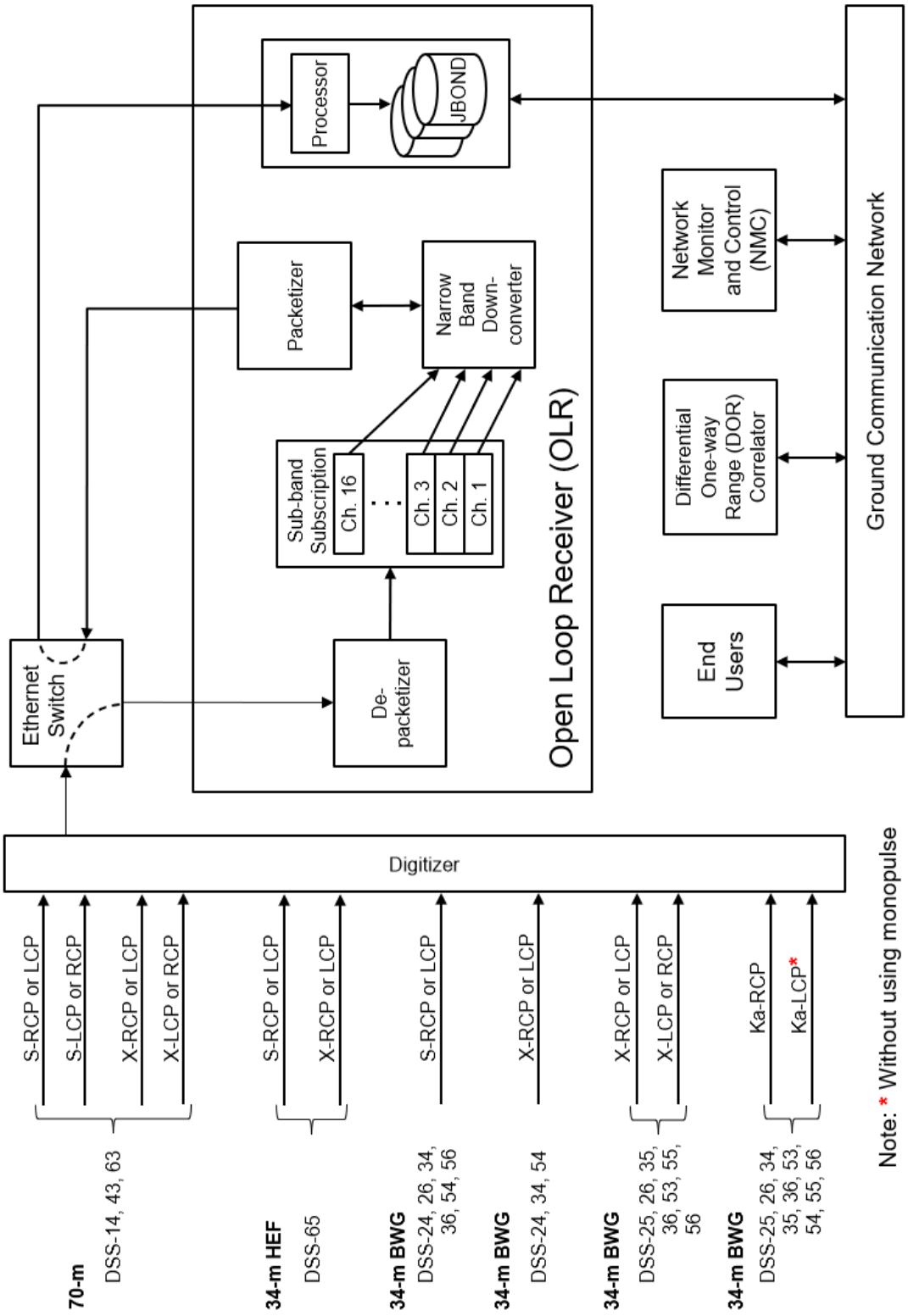

Figure 2. DSN Equipment for ΔDOR Support

The digital IF signals input to the OLR are in the range of 100 to 600 MHz. The OLR further downconverts and filters these IF signals to baseband channels for recording. Up to 16 baseband channels can be defined. The IF is downconverted to a specified center frequency and filtered to a specified bandwidth for each baseband channel. The downconversion can either be at a fixed frequency or can be optionally steered by predicts of the expected spacecraft sky frequency. Complex I/Q samples with 1 to 16 bit resolution are recorded. The supported bandwidths and sample resolutions are shown in Table 2. The OLR is capable of recording at other bandwidths also. Only the bandwidths and sample resolutions shown in Table 2 have been validated for use with the Delta-DOR processing system. The maximum aggregate record rate is 512 Mb/s.

Channels are typically defined for areas of interest that may include the carrier, the DOR tones and their harmonics, and harmonics of subcarriers. The composite data volume for all selected channels at each of the two stations involved in the measurement must be routed to one of the ΔDOR correlators at either JPL or GDSCC for processing. This is a large amount of data and the capability of the ground communications infrastructure is often a key factor in determining the overall time required to complete a ΔDOR measurement. At current effective transmission rates of about 80 Mb/s, (288 Gb/hr), the data from a typical one hour ΔDOR pass (32 minutes of six channels of 2-bit quantized quasar data with an 8 MHz bandwidth, and the associated narrower bandwidth channels for spacecraft signals), can be delivered to the correlator in about 1.3 hours.

Table 2. Supported Bandwidths and Resolutions with Resulting Data Rate

Type Filter	Bandwidth	Resolution (bits per sample)	Resultant Data Rate (b/s)
Narrowband	1 kHz	16	32,000
	2 kHz	16	64,000
	4 kHz	16	128,000
	8 kHz	16	256,000
	16 kHz	16	512,000
	25 kHz	16	800,000
	50 kHz	16	1,600,000
	100 kHz	16	3,200,000
	200 kHz	16	6,400.000
	500 kHz	16	16,000,000
	1 kHz	8	16,000
	2 kHz	8	32,000
	4 kHz	8	64,000
	8 kHz	8	128,000

Table 2. Supported Bandwidths and Resolutions with Resulting Data Rate (Continued)

Type Filter	Bandwidth	Resolution (bits per sample	Resultant Data Rate (b/s)
	16 kHz	8	256,000
	25 kHz	8	512,000
	50 kHz	8	800,000
	100 kHz	8	1,600,000
	200 kHz	8	3,200,000
	500 kHz	8	8,000,000
Wideband	1 MHz	8	16,000,000
	2 MHz	8	32,000,000
	4 MHz	8	64,000,000
	8 MHz	8	128,000,000
	16 MHz	8	256,000,000
	1 MHz	4	8,000,000
	2 MHz	4	16,000,000
	4 MHz	4	32,000,000
	8 MHz	4	64,000,000
	16 MHz	4	128,000,000
	32 MHz	4	256,000,000
	1 MHz	2	4,000,000
	2 MHz	2	8,000,000
	4 MHz	2	16,000,000
	8 MHz	2	32,000,000
	16 MHz	2	64,000,000
	32 MHz	2	128,000,000
	1 MHz	1	2,000,000
	2 MHz	1	4,000,000
	4 MHz	1	8,000,000
	8 MHz	1	16,000,000
	16 MHz	1	32,000,000
	32 MHz	1	64,000,000

2.1.4 Data Acquisition

ΔDOR measurements are conducted using either the Goldstone-Madrid baseline or the Goldstone-Canberra baseline. Two baselines with orthogonal components are needed to measure both the right ascension and declination coordinates of angular position. The Goldstone-Madrid baseline is oriented east-west and is most sensitive to right ascension for spacecraft near the ecliptic plane. The Goldstone-Canberra baseline is canted and has most sensitivity in the direction that splits the axes of right ascension and declination. Since declination is usually the most difficult component of spacecraft state to extract from line-of-sight measurements, the Goldstone-Canberra baseline may provide information that cannot otherwise be obtained. The Goldstone-Madrid baseline is still useful to evaluate small dynamic force modeling and improve overall trajectory accuracy.

Planning a measurement involves scheduling the stations, selecting DOR tones or signal frequencies to be used, and identifying the appropriate reference source(s). Each OLR can process up to 16 signal components. Spacecraft tones are typically recorded in narrow channels, while quasar noise and spacecraft PN signals must be recorded in wide channels.

Narrow channels range in bandwidth from 1 to 500 kHz. Sample resolution of 1 to 16 bits may be selected. Channels are centered on the predicted received frequency of the spacecraft signal component to be recorded. Channel bandwidth must be chosen wide enough to include margin for errors in prediction of the spacecraft transmitter frequency and Doppler shift. Enough bits should be used to protect against radio frequency interference and avoid loss of Signal-to-Noise ratio. The spacecraft data volume is usually much smaller than the quasar data volume. As a result, a wider bandwidth or greater sampling resolution may be selected for the narrow channels without significantly increasing the total amount of data.

Quasar channels range from 1 to 32 MHz. A sample resolution of 1 to 2 bits is usually selected. Channel bandwidth must be chosen wide enough to provide sensitivity to detect the faint signals from extra-galactic radio sources that are used to calibrate the DSN as an interferometer. A channel bandwidth of 8 MHz with 2 bit samples is adequate to detect a significant number of the sources in the JPL radio source catalog using a pair of DSN 34m antennas. A narrower bandwidth may be selected, and only stronger quasars observed, in order to reduce the volume of data that must be recorded.

To perform a measurement, the two Deep Space Stations forming the very long baseline interferometer make a series of observations to determine the differential one-way range to the target spacecraft and the reference source(s) that preferably has a small angular separation from the target spacecraft. (Differential one-way ranging with a quasar is similar to what has been described above for a target spacecraft; however, there are important differences since the nature of the quasar “signal” is quite different from that of a spacecraft with DOR tones.) Each observation is referred to as a *scan*. In a typical ΔDOR tracking pass of approximately one hour, the spacecraft and reference are alternately observed and a total of 5 to 10 scans, each lasting 5 to 10 minutes, are typically recorded. Some sources of measurement error can be reduced by making more observations, using shorter scans, and by more frequent switching between spacecraft and quasar. Only a slight improvement in the overall measurement accuracy can be obtained by increasing the measurement time beyond 1 hour in order to repeat the observations.

The following four scenarios are provided as examples of typical ΔDOR measurements made by the DSN.

2.1.4.1 Example 1, Spacecraft With One DOR Tone and Subcarrier Harmonics

- Tone frequency: 19.1 MHz
- Subcarrier frequency: 375 kHz
- Number of channels: 6 spacecraft and 6 quasar
- Narrow channel bandwidth: 50 kHz sampled with 8-bit resolution
- Wide channel bandwidth: 8 MHz sampled with 2-bit resolution

Table 3. Channel Assignments for Example 1

Channel	Spectral Component
1	Carrier
2	Upper 3rd harmonic of subcarrier
3	Lower 1st harmonic of DOR tone
4	Upper 1st harmonic of DOR tone
5	Lower 2nd harmonic of DOR tone
6	Upper 2nd harmonic of DOR tone

2.1.4.2 Example 2, Two Spacecraft With One DOR Tone and Subcarrier Harmonics

- Tone frequency: 19.1 MHz
- Subcarrier frequency: 375 kHz
- Number of channels: 4 for each spacecraft and 8 quasar
- Narrow channel bandwidth: 50 kHz sampled with 8-bit resolution
- Wide channel bandwidth: 2 MHz sampled with 2-bit resolution

Table 4. Channel Assignments for Example 2

Channel	Spectral Component
1	Carrier of spacecraft 1
2	Carrier of spacecraft 2
3	Upper 3rd harmonic of spacecraft 1 subcarrier
4	Upper 3rd harmonic of spacecraft 2 subcarrier
5	Lower 1st harmonic of spacecraft 1 DOR tone
6	Lower 1st harmonic of spacecraft 2 DOR tone

7	Upper 1st harmonic of spacecraft 1 DOR tone
8	Upper 1st harmonic of spacecraft 2 DOR tone

2.1.4.3 Example 3, Spacecraft With Only Subcarrier Harmonics

- Subcarrier frequency: 262 kHz
- Number of channels: 4 spacecraft and 4 quasar
- Narrow channel bandwidth: 50 kHz sampled with 8-bit resolution
- Wide channel bandwidth: 2 MHz sampled with 2-bit resolution

Table 5. Channel Assignments for Example 3

Channel	Spectral Component
1	Carrier
2	Lower 30th harmonic of subcarrier
3	Upper 26th harmonic of subcarrier
4	Upper 30th harmonic of subcarrier

In practice, squarewave subcarriers with finite risetimes have discrete spectral lines at the even harmonics of the subcarrier frequency whereas the odd harmonics may have data modulation. Therefore, even harmonics may be better choices for ΔDOR assuming they have sufficient power. It also may be necessary to select even harmonics if the telemetry symbol rate cannot be reduced sufficiently to be processed by the ΔDOR correlator.

2.1.4.4 Example 4, Spacecraft With Uplinked Range Tone

- Range Tone frequency: 1 MHz
- Number of channels: 3 spacecraft and 3 quasar
- Narrow channel bandwidth: 50 kHz sampled with 8-bit resolution
- Wide channel bandwidth: 2 MHz sampled with 2-bit resolution

Table 6. Channel Assignments for Example 4

Channel	Spectral Component
1	Carrier
2	Lower 1st harmonic of range tone
3	Upper 1st harmonic of range tone

2.2 Downlink Signal Structure and Power Allocation

The target spacecraft may use one or two DOR tones, phase-modulated onto the downlink carrier, for a ΔDOR measurement. For sinusoidal DOR tones, the mathematical form of the downlink carrier may generally be modeled as

$$\sqrt{2P_T}\sin\left[2pf_c t + qd(t) + q_1\sin(2pf_1 t) + q_2\sin(2pf_2 t)\right] \tag{1}$$

where P_T is the total downlink power, f_c is the carrier frequency, $d(t)$ is the telemetry and θ its modulation index. The DOR tones will have frequencies f_1 and f_2, and modulation indices of θ_1, and θ_2 if two tones are present, however the second DOR tone will sometimes be absent.

A detailed description of spacecraft signal structure used for ΔDOR observations is given in Section 3.2 of Reference 4.

Recommendations for DOR modulation are given in Reference 9. The recommendations include the number of DOR tones, DOR tone frequency, and DOR tone power.

2.3 DOR Tones and Phase Ambiguity

For each DOR tone that phase-modulates the downlink carrier, an upper and a lower fundamental harmonic are created. Thus, a (differential) group delay can be measured even when only one DOR tone modulates the carrier. However, it is sometimes advantageous to have two DOR tones. The DOR tones will normally be coherently related and may be coherently related to the carrier. Furthermore, if carrier-aided detection is to be used, the DOR tones must be coherently related to the carrier (Reference 9). If a DOR tone of about 20 MHz is used in the X band, then it is preferred for the downlink carrier to be assigned a channel near the center of the allocated band, in order that the upper and lower fundamental harmonics of the DOR tone lie within the allocated band.

When two DOR tones are present, the purpose of the additional DOR tone is to resolve the phase ambiguity that is inherent in any range (or differential range) measurement. For example, in two-way sequential ranging, the phase ambiguity associated with the range clock is resolved by sequentially sending a set of range components of decreasing frequency, see 810-005, module 203. With differential one-way ranging, the DOR tones are sent simultaneously rather than sequentially.

In order to make clear why two DOR tones are sometimes necessary, it is well to consider first the case of a single DOR tone. Corresponding to the single DOR tone, there are two fundamental harmonics (an upper and a lower). After each harmonic has been downconverted and recorded at the two stations, the differential phase between the two received copies of each harmonic may be plotted as indicated in Figure 3. The abscissa is the frequency of the observed harmonic as recorded at intermediate frequency. The ordinate is the differential phase. The column of points on the left side of Figure 3 represents the differential phase for the lower fundamental harmonic. The column of points on the right side of Figure 3 represents the differential phase for the upper fundamental harmonic. The horizontal separation between the

two columns of points is the spanned bandwidth, which equals twice the frequency of the DOR tone. The slope of the line labeled “True” is the differential group delay for the DOR tone.

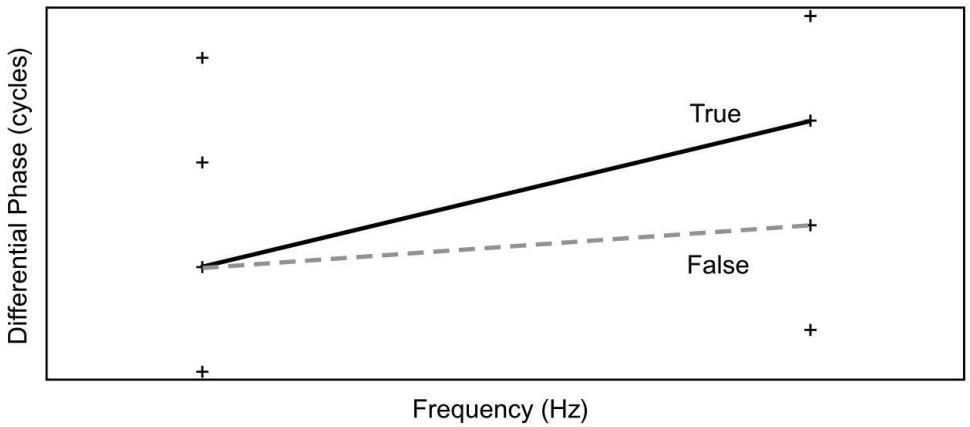

Figure 3. Phase Ambiguity with One DOR Tone

In Figure 3, there is a phase ambiguity since the DOR tone is a periodic signal. If the differential phase is regarded as having an integer number of cycles plus a fraction of one cycle, differential one-way ranging only measures the fractional part. That is why there is a column of points for the lower fundamental harmonic (and also for the upper fundamental harmonic). The points in each column are spaced by one cycle of phase. For the purpose of a ΔDOR measurement, it is not necessary to determine which point in the first column of points represents the true differential phase for the lower fundamental harmonic. However, it is necessary to distinguish the true slope, representing the actual differential group delay, from the false slope shown as a dashed line in Figure 3. The difference between these two slopes equals the reciprocal of the spanned bandwidth. (There are other false slopes than the one shown in Figure 3, but these other false slopes have a value at least as far from the true slope as the reciprocal of the spanned bandwidth.) If the *a priori* knowledge of the differential group delay is good enough to rule out a false slope corresponding to a delay that differs from the true differential group delay by the reciprocal of the spanned bandwidth, then there is no need for a second DOR tone.

Figure 4 illustrates how differential group delay is determined when there are two DOR tones. The leftmost column of Figure 4 represents the differential phase for the lower fundamental harmonic of the higher-frequency DOR tone. The rightmost column represents the differential phase for the upper fundamental harmonic of the higher-frequency DOR tone. The middle columns represent differential phase for the lower and upper fundamental harmonics of the other (lower-frequency) DOR tone. The horizontal separation between the two outermost columns of points is the spanned bandwidth, which equals twice the frequency of the higher-frequency DOR tone. The true and false slopes shown in Figure 3 are reproduced in Figure 4. It is now clear how the second (lower-frequency) DOR tone helps resolve phase ambiguity. The

true slope passes through legitimate points in the middle columns, whereas the false slope does not. On this basis, the false slope can be ruled out.

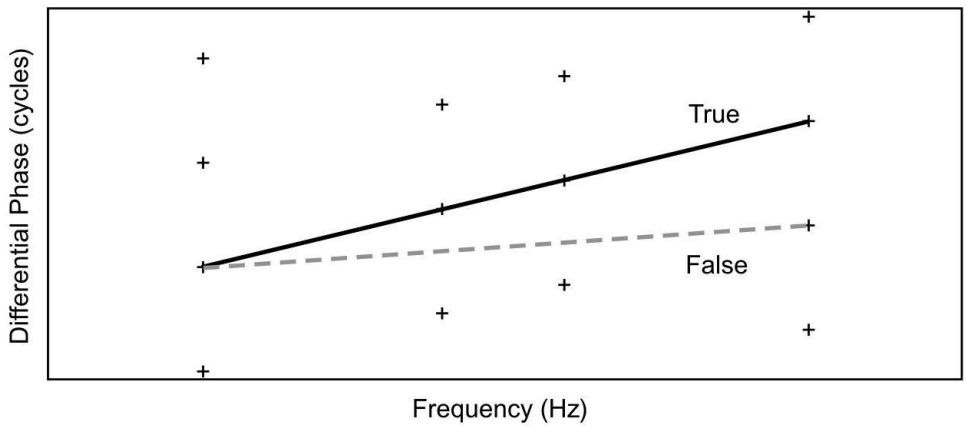

Figure 4. Resolution of Phase Ambiguity with a Second DOR Tone

It is important to use the largest possible spanned bandwidth because several measurement-limiting errors are inversely proportional to the spanned bandwidth. When selecting DOR tone frequencies, however, it is necessary to consider the problem of ambiguity resolution. Ambiguity resolution requires two signal components that are not widely separated in frequency. These two goals, achieving a large spanned bandwidth and resolving the ambiguity, are not contradictory. Generally, one DOR tone frequency is selected large enough that the desired measurement accuracy can be achieved. It will often be the case that the reciprocal of twice this frequency is smaller than the uncertainty in the *a priori* knowledge of differential group delay. This need not be a problem. The ambiguity can still be resolved by including one or more of the following in the measurement: a second (lower-frequency) DOR tone, the residual carrier, or telemetry subcarrier harmonics. The choice of how many signal components to use must be carefully considered because every signal that modulates the carrier consumes link power and produces intermodulation products that waste link power. These considerations are explored in Reference 4 and have been used to derive the recommendations in Reference 9.

2.4 ΔDOR Measurement Error Models

There are a number of important error sources for ΔDOR measurements. Precision for spacecraft delay depends on the power and spanned bandwidth of the DOR tones. Precision for quasar delay depends on the channel bandwidth and spanned bandwidth used to record the quasar signal. Instrumental error depends on clock stability, instrumental phase linearity, and spanned bandwidth. Errors in baseline length and orientation and errors in media delays scale with the angular separation between spacecraft and quasar. There is a natural trade-off between selecting a stronger source that might be at a larger angular separation from the spacecraft, or a weaker source that is angularly closer to the spacecraft. A denser radio source catalog provides more options to improve measurement geometry.

Section 3.4 of Reference 4 describes the significant error sources and gives quatitative models for estimating errors. Assumptions for model parameter values are presented that represent current DSN capabilities. The error budget presented in Reference 4 is summarized below in Paragraph 2.5 of this document. Section 4 of Reference 4 provides the trade-offs to consider when designing a measurement system and planning measurements.

It is important to note that these models assume that the measurements are in fact ΔDOR, and not plain DOR. (Some of the following errors would be much larger for plain DOR, since common-mode errors would then not be canceled.) Units of time delay are employed here to characterize ΔDOR measurement error.

The errors of ΔDOR measurement can be dramatically reduced if a spacecraft defines the reference direction and if this reference spacecraft and the target spacecraft are close in an angular sense. If the two spacecraft are close enough to be observed simultaneously in common receive antennas, then this is called *Same-beam Interferometry*. Many of the error models discussed in Reference 4 and summarized below either do not apply or must be drastically modified for the case of Same-beam Interferometry. For more information on this technique and the errors associated with it, the reader may wish to see References 1 and 10.

2.5 ΔDOR Measurement Error Budget

An example error budget based on current DSN capability and good observing geometry is given here. Note that DSN observing geometry is generally good for spacecraft near the ecliptic plane, if the Sun-Earth-Spacecraft angle is greater than 10 deg, and either

(i) observed from Goldstone-Canberra baseline; or

(ii) geocentric angular declination above -15 deg and observed from Goldstone-Madrid baseline.

The 3-complex DSN has a geometric weakness when spacecraft are at far southern declinations. Delta-DOR cross-support from Agencies with antennas at other sites may be required to support highly accurate navigation for this case.

The assumptions used for the error budget are given in Table 7. The reader is referred to Reference 4 for context of these parameters. The ΔDOR error budget based on these assumptions is given in Table 8, showing both random and systematic effects. Table 8 provides 1-sigma error estimates that are representative of geometric and atmospheric conditions typically encountered with DSN ΔDOR measurements. The full error models provided in Reference 4 can be used to estimate the ΔDOR error for other conditions, geometries or assumptions.

For navigational analysis it is common to break out errors into random and systematic models. Table 9 shows only the random error components for ΔDOR, that is the random error in the difference between the spacecraft and quasar delay measurements. The root-sum-square (RSS) random error is less than 0.06 ns, corresponding to an angular error of 1.9 nrad on an 8000 km baseline. This angular error projects to a cross-position error of 281 m in the plane-of-sky at a distance of 1 AU.

There are known systematic errors that affect all radiometric data types. It is common for navigation analysis software to include explicit models and parameters for systematic effects. Table 10 shows parameters based on current DSN capability, for systematic error models in common use. If ΔDOR data are used for estimation purposes, and these systematic effects are explicitly included in the analysis, then only the random error component should be used for deriving the ΔDOR data weight.

The DSN ΔDOR system performed very well for the Mars Science Laboratory cruise phase and final approach to Mars. The root-mean-square (RMS) of the ΔDOR residuals to the final reconstructed trajectory was 0.038 ns (Reference 11).

Table 7. Nominal Parameter Values for Evaluation of X-band ΔDOR Error Budget

Term	**Description**	**Nominal Value**
T_{QU}	Total quasar observation time	960 s
T_{SC}	Total spacecraft observation time	480 s
$\Delta\theta$	Angular separation between spacecraft and quasar	0.1 rad
$\Delta\theta_B$	Component of spacecraft-quasar angular separation in direction of baseline projection	0.1 rad
γ_{SC_i}	Spacecraft elevation angle at station *i*	20 deg
γ_{QU_i}	Quasar elevation angle at station *i*	25 deg
SEP	Minimum angle between Sun and spacecraft or quasar	20 deg
f_{BW}	Spanned bandwidth	38.25×10^6 Hz
$(G/T)_i$	G/T for antenna *i*	52.56 dB K^{-1}
D	Channel sampling rate	16×10^6 samples/s
S_c	Quasar correlated flux density	0.4 Jy
K_L	System loss factor	0.8
k	Boltzman constant	1.38×10^{-23} Joules/K
λ	Radio Frequency wavelength	0.0356 m
SNR_{QU}	Quasar voltage SNR (derived)	261
P_{tran}	Effective transmitted tone power	108 Watts
R	Distance from spacecraft to receiver	150×10^9 m
FL	Spacecraft tone flux (derived)	3.981×10^{-22} W/m^2
$\left(P_{DOR}/N_0\right)_i$	DOR tone power to noise spectral density, station *i* (derived)	27 dB•Hz

Term	Description	Nominal Value
SNR_{SC_i}	Spacecraft voltage SNR (derived)	695
$T_{SC\text{-}QU}$	Time between centers of spacecraft and quasar scans	600 s
$e_{\Delta f/f}$	Instrument frequency stability at 600 s	10^{-14}
e_f	Instrument phase ripple (nonlinearity across channel of few MHz bandwidth)	0.2 deg
e_{BL}	Baseline coordinate uncertainty, each component	0.02 m
e_{UTPM}	Baseline orientation uncertainty, each component (1 day prediction)	0.02 m
$r_{z_{wet_i}}$	Zenith wet troposphere delay uncertainty, station *i*	0.005 m
$r_{z_{dry_i}}$	Zenith dry troposphere delay uncertainty, station *i*	0.002 m
$r_{trop_{fluct}}$	Fluctuating troposphere uncertainty for 10 deg separation	0.01 m
$r_{iono_{day_i}}$	Daytime ionosphere model uncertainty (X-band level), station *i*	0.04 m
$r_{iono_{night_i}}$	Nighttime ionosphere model uncertainty (X-band level), station *i*	0.01 m
$r_{iono_{fluct}}$	Fluctuating ionosphere uncertainty for 10 deg separation (increase by ×2 near solar max)	0.01 m
f_{RF}	Signal Radio Frequency	8.42 GHz
B_s	Separation of raypaths from radio source to two stations, at plane of signal closest approach to Sun	6×10^6 m
n_{SW}	Solar wind velocity	4×10^5 m/s
e_J	Quasar coordinate uncertainty	0.75×10^{-9} rad
B_p	Length of baseline projection onto plane-of-sky	8×10^6 m

Table 8. Delta-DOR Error Budget (1 Sigma)—Both Random and Systematic Effects

Component	**Random/Systematic**	**Delay Error (ns)**
Quasar thermal noise	Random	0.023
Spacecraft thermal noise	Random	0.012
Clock instability	Random	0.006
Dispersive phase	Random	0.029
Station location	Systematic	0.007
Earth orientation	Systematic	0.007
Zenith troposphere	Systematic	0.012
Fluctuating troposphere	Random	0.019
Ionosphere shell	Systematic	0.019
Fluctuating ionosphere	Random	0.019
Solar plasma	Random	0.006
Quasar coordinate	Systematic	0.020
RSS total		**0.057**

Table 9. Delta-DOR Error Budget (1 Sigma)—Random Effects Only

Component	**Delay Error (ns)**
Quasar thermal noise	0.023
Spacecraft thermal noise	0.012
Clock instability	0.006
Dispersive phase	0.029
Fluctuating troposphere	0.019
Fluctuating ionosphere	0.019
Solar plasma	0.006
RSS random	**0.048**

Table 10. Common Parameters for Modeling Systematic Effects (1 Sigma)

Component		**Model Error**
Station Location*		2 cm with correlations
Earth Orientation		
	UT1 1-day prediction	2 cm
	UT1 after the fact	1 cm
	Polar Motion	1 cm
Zenith Troposphere		
	Wet	0.5 cm
	Dry	0.2 cm
Ionosphere Shell		
	Day (X-band level)	4 cm
	Night (X-band level)	1 cm
Quasar Coordinate		0.75 nrad
*Correlations among station coordinates may be accounted for in a covariance matrix.		

Appendix A
DSN Document 810-005

Module 101, 70-m Subnet Telecommunications Interfaces

Module 103, 34-m HEF Subnet Telecommunications Interfaces

Module 104, 34-m BWG Antennas Telecommunications Interfaces

Module 106, Solar Corona and Solar Wind Effects

Module 107, X-band Radio Source Catalog

Module 203, Sequential Ranging

Module 214, Pseudonoise and Regenerative Ranging

Module 301, Coverage and Geometry

References

1. C. L. Thornton and J. S. Border, Radiometric Tracking Techniques for Deep-Space Navigation, Wiley-Interscience, Hoboken, NJ, 2003.

2. P. G. Antreasian, et al., "2001 Mars Odyssey Orbit Determination During Interplanetary Cruise," AIAA/AAS Astrodynamics Specialist Conference and Exhibit, Monterey, CA, August 5-8, 2002.

3. David W. Curkendall and James S. Border, "Delta-DOR: The One-Nanoradian Navigation Measurement System of the Deep Space Network — History, Architecture, and Componentry," The Interplanetary Network Progress Report, vol. 42-193, Jet Propulsion Laboratory, Pasadena, California, pp. 1-46, May 15, 2013.

   https://ipnpr.jpl.nasa.gov/progress_report/42-193/193D.pdf

4. Delta-DOR -- Technical Characteristics and Performance, Report Concerning Space Data System Standards, CCSDS 500.1-G-2, Green Book, Issue 2. Washington, D.C.: CCSDS, November 2019.

   https://public.ccsds.org/Pubs/500x1g2.pdf

5. C. Ma, Chairman, "The Second Realization of the International Celestial Reference Frame by Very Long Baseline Interferometry," IERS Technical Note No. 35, Verlag des Bundesamts fur Kartographie und Geodasie, Frankfurt am Main 2009.

6. C. Jacobs, et al., "The JPL Extragalactic Radio Reference Frame: Astrometric Results of 1978-96 Deep Space Network VLBI," TMO Progress Report 42-133, Jet Propulsion Laboratory, Pasadena, CA, May 15, 1998.

   https://ipnpr.jpl.nasa.gov/progress_report/42-133/133E.pdf

7. T. P. McElrath, W. M. Watkins, B. M. Portock, E. J. Graat, D. T. Baird, G. G. Wawrzyniak, A. A. Attiyah, J. R. Guinn, P. G. Antreasian, R. C. Baalke, and W. L. Taber, "Mars Exploration Rovers Orbit Determination Filter Strategy," AIAA-2004-4982, paper presented at the AIAA/AAS Astrodynamics Conference, Providence, Rhode Island, August 15-20, 2004.

8. Shervin Shambayati, David Morabito, James S. Border, and Faramaz Davarian, Mars Reconnaissance Orbiter Ka-Band Demonstration: Cruise Phase Operations, Chapter 15 in Space Operations: Mission Management, Technologies, and Current Applications, Edited by Loredana Bruca, J. Paul Douglas, Trevor Sorensen, Progress in Astronautics and Aeronautics, Frank K. Lu, Editor-in-Chief, Volume 220, American Institute of Aeronautics and Astronautics, Inc., Reston, Virginia, 2007.

9. Radio Frequency and Modulation Systems—Part 1: Earth Stations and Spacecraft, Recommendation for Space Data System Standards, CCSDS 401.0-B-32, Blue Book, Issue 24, Washington, D.C.: CCSDS, October 2021.

https://public.ccsds.org/Pubs/401x0b32.pdf)

10. J. S. Border, et al., "Precise Tracking of the Magellan and Pioneer Venus Orbiters by Same-Beam Interferometry, Part I: Data Accuracy Analysis," TDA Progress Report 42-110, Jet Propulsion Laboratory, Pasadena, CA, August 15, 1992.

https://ipnpr.jpl.nasa.gov/progress_report/42-110/110A.PDF

11. T. J. Martin-Mur, G. L. Kruizinga, P. D. Burkhart, F. Abilleira, M. C. Wong, and J. A. Kangas, "Mars Science Laboratory Interplanetary Navigation," Journal of Spacecraft and Rockets, Vol. 51, Issue 4, pp. 1014-1028, July 2014.

Deep Space Network

211
Wideband Very-Long Baseline Interferometry

Document Owner:		Approved By:	
Signature provided	11/28/2023	Signature provided	11/13/2023
Lisa Mauger VRA Software CDE	Date	Timothy Pham Communications Systems Chief Engineer	Date

Prepared By:		Released by:	
Signature provided	11/18/2023	Signature provided	01/09/2024
Dong Shin OBD System Engineer	Date	Christine Chang DSN Document Release Authority	Date

DSN No. **810-005, 211, Rev. G**
Issue Date: January 11, 2024, 2023
JPL D-19379; CL# 24-0314

Jet Propulsion Laboratory
California Institute of Technology

Users must ensure that they are using the current version in DSN Telecommunications Link Design Handbook website https://deepspace.jpl.nasa.gov/dsndocs/810-005/

Review Acknowledgment

By signing below, the signatories acknowledge that they have reviewed this document and provided comments, if any, to the signatories on the Cover Page.

Signature provided	10/27/2023	Signature provided	12/20/2023
Jeff Berner DSN Project Chief Engineer	Date	Harvey Soldan Group Supervisor, DSN System Engineering	Date

Document Change Log

Rev	Issue Date	Prepared By	Affected Sections or pages	Change Summary
Initial	8/25/2006	Kurt Liewer	All	All
A	4/15/2011	Kurt Liewer	Section 2, 2.1, 2.3 Figure 2, 2.3.3, 2.3.5, and 2.4	• Removed references to Mark III VLBI DAT • Replaced all instances of “radio telescope” to “antenna” • Added text noting new DAT system will be replacing old in 2013. • Removed EAC references • Noted termination of Mark-IV tape support • Updated Figure 2 to reflect changes in the system
B	02/09/2015	A. Bedrossian J. S. Border D. Shin	Section 2 and Appendix	• Removed DTE, DAT and PCFS • Added DVP and Mark 5C • Added DSS—26, -35, -54 • Updated Figures, Tables, and Appendix
C	02/10/17	J. S. Border D. Shin	Section 2.3	Added DSS-36. Removed DSS-45.
D	07/03/18	D. Shin A. Bedrossian	Section 2 and 3	Remove DSS-15 and update section 2.3
E	12/23/2019	D. Shin A. Bedrossian	Section 2.2, 2.3, Figure 2, 2.3.4, Table 2 and 4	• 2.2: Example of the efficiency gain is updated • 2.3: Capacity of the open-loop receiver is updated. • 2.3.4: Tone generator availability at BWG antennas is updated • Figure 2, Table 2, Table 4: Updated
F	06/07/2022	D. Shin A. Bedrossian	Section 1.2, 2.3, 2.3.1, 2.3.3, 2.3.4, 2.3.5, and 2.4, Figure 1, 2 Table 1, 2, and 3	• 1.2: Added Module 108 (Ka-band source catalog) • 2.3: Updated for VRA/EJVC • 2.3.1: Added DSS-53, DSS-56, and K-band • 2.3.3: Updated for VRA/EJVC • 2.3.4: Updated for VRA/EJVC • 2.3.5: Updated for EJVC • 2.4: Updated for VRA/EJVC and added K-band • Figure 1: Updated for VRA/EJVC • Figure 2: Added DSS-53/56 and K-band and updated for VRA/EJVC • Table 1: Added DSS-53/56 and K-band

Rev	Issue Date	Prepared By	Affected Sections or pages	Change Summary
				• Table 2: Added supported bandwidths • Table 3: Updated and add DSS-53/56
G	01/11/2024	D. Shin	Figure 2 Table 1	• Figure 2: Added DSS-24 X-band and DSS-36 K-band • Table 1: Added DSS-24 X-band and DSS-36 K-band

Contents

Figures

Tables

1 Introduction

1.1 Purpose

This module introduces the Very-Long Baseline Interferometry (VLBI) astrometric measurement technique and identifies the capabilities and performance of Deep Space Network (DSN) equipment used to support wideband VLBI measurements.

1.2 Scope

The content of this module is limited to a discussion of the data gathering and data processing equipment used by the DSN to support VLBI. Experiment design and the quality of the results are influenced by many other factors that are discussed in Section 2.4. Among these factors are antenna performance parameters discussed in modules 101, 103 and 104, and frequency reference performance discussed in module 304. VLBI experimenters may also be interested in station locations discussed in module 301 and extra-galactic radio source positions provided in module 107 and 108. It should be noted that the equipment discussed in this module is the major contributor to the information content of modules 301, 107, and 108.

2 General Information

The DSN uses its VLBI capability to measure the earth orientation parameters that establish the relationship of the Terrestrial Reference Frame containing its stations to the Celestial Reference Frame used for spacecraft navigation. VLBI is also used to determine the relative locations of its stations and the locations of extra-galactic radio sources (EGRSs). The EGRSs are used as reference points for delta-differential one-way ranging (ΔDOR) spacecraft navigation (see module 210). Because the DSN uses equipment that is compatible with that used by the international VLBI community, other agencies can coordinate their observation schedules with DSN scheduled activities and the resultant data can be shared between the DSN and external experimenters.

2.1 Description of Very-Long Baseline Interferometry

Very-Long Baseline Interferometry is a technique for measuring the precise time difference between the arrivals of waveforms originating from an EGRS at two (or more) stations. Figure 1 provides an illustration of the technique. The stations simultaneously observe an EGRS. As they are widely separated, their baseline, B, passes through the Earth. At each station, the instantaneous voltage of the received signal (a random Gaussian process) is recorded in each of several channels; this is known as VLBI data acquisition. The measured difference in arrival time can be converted to an approximate path length difference by multiplying by c, the speed of electromagnetic waves in a vacuum. In actuality, the conversion is much more complex as the wave front must pass through several layers of the Earth's atmosphere – each of which has a different propagation speed.

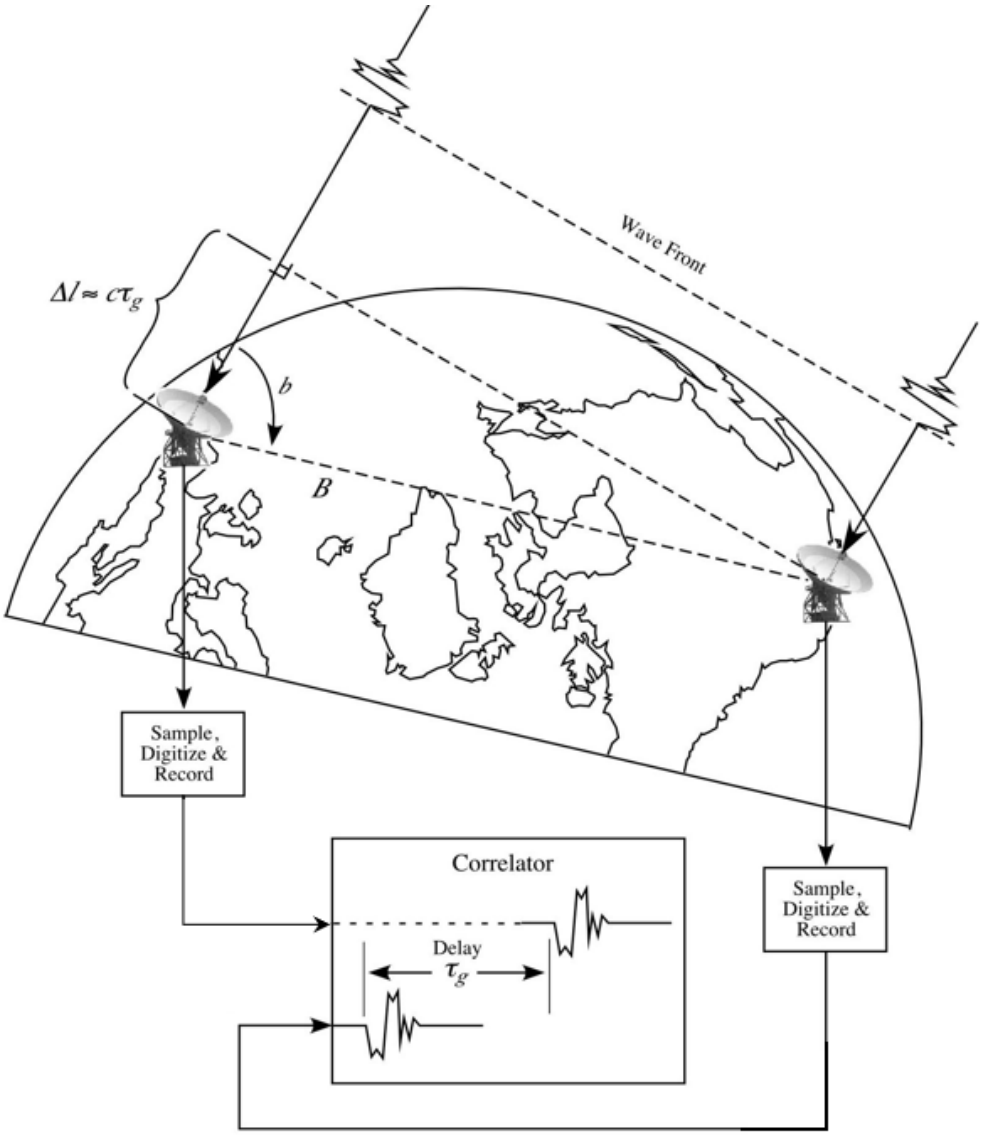

Figure 1. Very-Long Baseline Interferometry

The recorded data from the participating antennas are brought together at a correlator. The data from matching channels at the different radio telescopes are cross-correlated to determine the geometric time delay, τ_g; this is known as VLBI data correlation. After converting the time delay to a path length by a process that accounts for atmospheric delay and other effects, the angular relationship between the baseline of the two stations and the radio source can be determined by the relationship $b = \cos^{-1}\left(\Delta l / B\right)$. It is important to note that this is not a complete solution for the angular position in the sky of the radio source. This calculation only provides information about the location of the radio source in the plane defined by the interferometer baseline and the direction of arrival. The correlation of data from the observation of additional radio sources is necessary to completely define the baseline. By making sufficient

observations and assuming some reference, it is possible to calculate a singular solution that estimates each station's coordinates, the angular positions of all observed sources, the offset and rate differences between the two station frequency references, and several parameters relating to propagation. Additional observations above the minimum enable statistical uncertainties in the estimation to be reduced. A complete discussion of the process is contained in Reference 1.

The precision of a VLBI measurement improves with the length of the baseline. The location of the DSN stations provides baselines of 66% (Goldstone to Madrid) and 83% (Goldstone to Canberra) of the Earth's diameter. The third baseline, Canberra to Madrid, is 98% of the Earth's diameter but provides very limited mutual visibility (see module 301). To mitigate mutual visibility effects, additional antennas are often involved in VLBI measurements allowing a station between DSN locations to serve as a "relay" to tie-together observations made in different portions of the sky during an observation session.

2.2 Bandwidth Synthesis

The signal-to-noise ratio obtained by correlating the signals from two observing stations depends on the characteristics of the stations, the bandwidth of the channel being correlated and the observation time. It can be calculated from the following expression.

$$SNR_{CH} = 2.05 \times 10^{-4} \left(\gamma_\nu S\right) D_1 D_2 \sqrt{\frac{\eta_1 \eta_2 B_{CH} T}{T_{Sys1} T_{Sys2}}} \tag{1}$$

where

$(\gamma_\nu S)$	=	correlated flux density where S is the total flux density (jansky)
D_1, D_2	=	antenna diameters (m)
η_1, η_2	=	antenna efficiencies
B_{CH}	=	channel bandwidth (Hz)
T	=	observation time (s)
T_{Sys1}, T_{Sys2}	=	antenna system noise temperatures (K)

The factor 2.05×10^{-4} includes all normalization constants and allowances for degradation due to one-bit quantization and the fact that only one polarization is received.

When multiple channels are being correlated simultaneously and they have approximately the same SNR_{CH}, the post-correlation SNR for use in equation (3) can be calculated by

$$SNR = \sqrt{n} \cdot SNR_{CH} \tag{2}$$

where n is the number of channels in the correlation.

The error in delay measurement resulting from the correlation of data from two VLBI stations is expressed by

$$\sigma = \frac{c}{2\pi \cdot SNR \cdot BW} \tag{3}$$

where

c	=	the speed of electromagnetic propagation
SNR	=	the post-correlation signal-to-noise ratio
BW	=	the observation bandwidth

It can be seen from equation (3) that an extremely large data volume for transport to the common correlation site would be needed if the entire bandwidth were recorded. For example, if a post-correlation SNR of 40 (16 dB) is available, a bandwidth of 125 MHz would be required to achieve a delay error of 1 cm.

The data volume is significantly reduced by the technique of *bandwidth synthesis* (Reference 2). This technique uses several narrow channels spread across the observation bandwidth to achieve an *RMS bandwidth* of

$$BW_{RMS} = \sqrt{\frac{\sum_{CH=1}^{n} \left(f_{CH} - f_{AVG}\right)^2}{n}} \tag{4}$$

where

f_{CH}	=	center frequency of each channel used in the bandwidth synthesis
f_{AVG}	=	the average of all channel center frequencies used in the bandwidth synthesis
n	=	the number of channels

As an example of the efficiency gained by bandwidth synthesis, a typical Ka-band VLBI measurement will use the eleven 32-MHz double-sided channels shown in Table 4 corresponding to an RMS bandwidth of 168.314 MHz. By employing hard limiting, two-bit quantization, and a sampling rate equal to twice the bandwidth of each channel, the total recorded bandwidth is reduced to 128 MHz.

2.3 DSN VLBI Support Equipment

A diagram showing the major items of DSN equipment used to support wideband VLBI is provided by Figure 2. DSN 34-m BWG antennas and 70-m antennas are available for VLBI data acquisition. Note that 70-m antenna is not recommended for VLBI observations due to its slow slew rate.

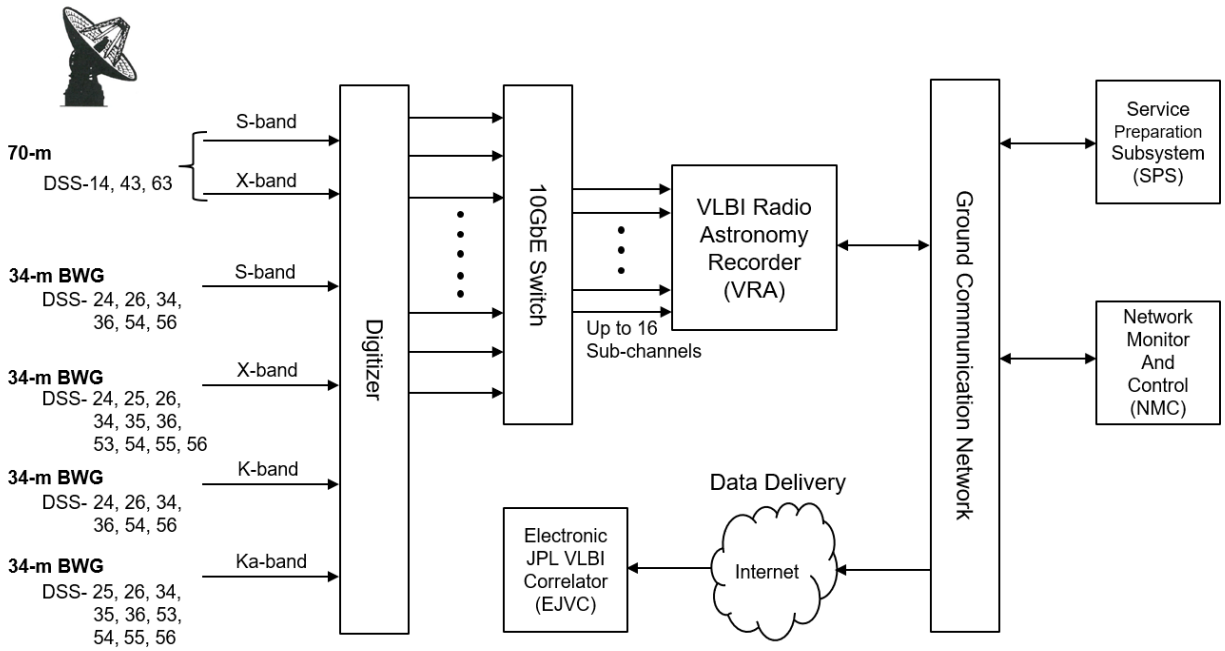

Figure 2. DSN Equipment for Wideband VLBI Support

Received signals are processed by the Deep Space Communication Complex (DSCC) VLBI Radio Astronomy Recorder (VRA). The VLBI data is electronically transmitting to the Electronic JPL VLBI correlator (EJVC) for the correlation. The VRA interfaces directly with the DSN Network Monitor and Control (NMC) Subsystem.

2.3.1 Signal Reception

Signals that are collected by the antenna are amplified by a cryogenically-cooled low-noise amplifier (LNA). For every observation band, the LNA is followed by a downconverter that translates the radio-frequency signal to an intermediate frequency (IF) to be forwarded to the Signal Processing Center (SPC). The downconverters are located on the antenna and are derived from the station frequency standard. Their local oscillator (LO) frequencies are 2.0 GHz for S-band, 8.1 GHz for X-band, variable 25.503 GHz +/- 487.5 MHz for K-band, and 31.7 GHz for Ka-band.

The frequency and polarization capabilities of the DSN for VLBI are summarized in Table 1.

Subnet	DSS	S-band	X-band	K-band	Ka-band
70-m	14, 43, & 63	RCP and LCP (2200–2300 MHz)	RCP and LCP (8200–8600 MHz)	–	–
34-m BWG	24	RCP or LCP (2200–2300 MHz)	RCP or LCP (8200–8600 MHz)	RCP or LCP (25.5–27.0 GHz)	–
	25, 35, 53, 55	–	RCP and LCP (8200–8600 MHz)	–	RCP and LCP (31.8–32.3 GHz)
	26, 36, 56	RCP or LCP (2200–2300 MHz)	RCP and LCP (8200–8600 MHz)	RCP or LCP (25.5–27.0 GHz)	RCP and LCP (31.8–32.3 GHz)
	34, 54	RCP or LCP (2200–2300 MHz)	RCP or LCP (8200–8600 MHz)	RCP or LCP (25.5–27.0 GHz)	RCP and LCP (31.8–32.3 GHz)

Table 1. Frequency and Polarization Support Capabilities for VLBI

2.3.2 Subreflector Position

Gravity deformation of the primary reflector and the structure that supports the subreflector as the antenna moves in elevation causes a change in the antenna focal position. To compensate for this, the subreflector undergoes a programmed motion relative to the feed to achieve the maximum antenna gain at every elevation angle. However, this motion introduces a time-varying phase delay to the received signal that is undesirable for wideband VLBI.

During wideband VLBI data acquisition at the 70-m antennas, the subreflector motion is usually disabled and the subreflector placed in a position that gives the best gain for a 45° elevation angle. This eliminates the time-varying phase delay associated with subreflector motion. However, it also causes some loss of antenna gain when the antenna is not at 45°.

Subreflector motion should not be disabled when a BWG antenna is used for wideband VLBI observations in the Ka-band. This is because gravity deformation also affects antenna pointing by an amount that is significant at Ka-band although not so at S- or X-bands and subreflector motion must be enabled in order to have the antenna point as commanded. The resultant phase delay changes can be modeled and removed in post processing.

2.3.3 Data Acquisition

The analog IF signals from each antenna are routed to an IF Gain Control (IFG) assembly and then digitized by the IF Digitizer (IFD). The IFD channelizes the IF band and sends digital packets through the Digital IF Switch (DIS) to the VRA. The VRA converts digital packets into digital baseband channels which are recorded to disk. The VRA can output up to 16 baseband channels. The VRA can record digital channels as either complex in-phase and quadrature (IQ) samples or real upper sideband and lower sideband (USB/LSB) samples.

The outputs of the baseband channel are placed into recording frames along with timing and parity data, and sent to the EJVC via internet. Supported channel bandwidths vary from 200 Hz to 100 MHz as shown in Table 2. Allowed channel bandwidths are enumerated by combining the multiplier in the top row and the first column, with units for each row in the right column. The x1 channel bandwidth column is shaded gray to indicate that these values are redundant with the final column.

Table 2. Supported Bandwidths

Multiplier	X 1	X 1.25	X 1.6	X 2	X 2.5	X 3.2	X 4	X 5	X 6.4	X 8	X 10	Unit
10 MHz	10	12.5	16	20	25	32	40	50	64	80	100	MHz
1 MHz	1	1.25	1.6	2	2.5	3.2	4	5	6.4	8	10	MHz
100 kHz	100	125	160	200	250	320	400	500	640	800	1000	kHz
10 kHz	10	12.5	16	20	25	32	40	50	64	80	100	kHz
1 kHz	1	1.25	1.6	2	2.5	3.2	4	5	6.4	8	10	kHz
100 Hz	--	--	--	200	250	320	400	500	640	800	1000	Hz

The maximum supported data rate is currently 2.048 Gbit/sec. For example, 16 complex channels with 32 MHz bandwidth and 2-bit sample resolution could be recorded. Bit configurations of 4 and 8 are also supported, as long as the maximum supported bitrate is not exceeded. For example, 4 complex channels with 8 bits is supported for channel bandwidth up to 32 MHz.

2.3.4 Phase Calibration Tones

The 70-m antennas include “S-band and X-band” tone generators (Reference 4). The tone generators inject a set of tones, uniformly spaced in frequency, into the receive signal path ahead of the LNA. The purpose of these tones is to permit calibration of irregularities in phase delay occurring along the signal path to the VRA. The tones are spaced 1.0 MHz apart and are derived from the station frequency reference. The power in the phase calibration tones is less than 1% of the signal power in any given bandwidth. With such a small power, the phase calibration tones do not interfere with the VLBI measurements. The 1.0 MHz spacing guarantees that at least one tone will be present in each 2-MHz or greater bandwidth normally used for VLBI. Selection of channel center frequencies will assure that one tone will be present in one sideband of each channel for narrower bandwidths.

The 34-m BWG antennas, DSS-25, -35, -53, and -55 have X/Ka (X-band and Ka-band) tone generators. The other BWG antennas, DSS-26, -34, -54, and -56 have both S/X (S-band and X-band) and X/Ka tone generators. The X/Ka tone generators have a tone spacing of 4.0 MHz. The tones are derived from the station frequency reference.

There is no simultaneous S/X and X/Ka-band tones available at any antennas. DSS tone generator availability is shown in Table 3.

Table 3. Tone Generator Availability

DSS	Tone Generator Availability	
	S/X	X/Ka
14	✓	
24**		
25		✓
26	✓*	✓
34	✓	✓*
35		✓
36	✓	
43	✓	
53		✓
54	✓*	✓
55		✓
56	✓*	✓
63	✓	

Note: * Preselected (default) configuration
** It does not have a tone generator

In the VLBI correlator, a measurement is made of the relative phase delay of the calibration tone in each channel. This is accomplished by correlating the recorded channel with a local (baseband) model of the individual calibration tone. These phase delay measurements enable the phase slope of the entire instrumentation system to be estimated and any phase offsets introduced across the analog RF and IF input to be removed. The result is a group delay calibration with a precision of 0.0015 ns for a 100-s integration time.

In addition to the precise measurement of phase delay in post processing at the VLBI correlator, the phase calibration tones are also monitored in near real-time by the VRA to detect instrument and configuration problems.

2.3.5 Correlation

The EJVC accepts VLBI data in Raw Data Exchange Format (RDEF) as specified in DSN external interface document 820-13, 0222-Science. The recorded data from two antennas may be cross-correlated. When the recorded data from one antenna are cross-correlated with that of another antenna, an interferometer is formed and the differential delay for that interferometer is determined. These correlated VLBI data are used for several purposes including navigation support, and reference frame support.

2.4 Experiment Design

The configuration and sequence of events for any wideband VLBI experiment are defined in a VLBI experiment (VEX) file as specified in DSN external interface document 820-

013, 0200-Science-VLBI. The VEX file is a format invented by members of the VLBI community to prescribe a complete description of a VLBI experiment, including scheduling, data-taking and correlation. For more information regarding these interface specifications users may contact their DSN Mission Interface Manager. Parameters from the VEX file are read by the EJVC, and the EJVC generates a recording script for the VRA and a .nmc file for antenna controller. The VRA creates an experiment log file and controls data recording.

The two observation bands (S, X, K, or Ka) for the experiment are chosen subject to the band availability on the antenna being used. A set of channels is defined for each observation band. In order to achieve high precision, the span of channel frequencies (within the band) should be wide. The two outermost channels determine this precision. The other channels are needed to resolve the phase ambiguity. Simultaneous measurements at "S- and X-band" or "X- and Ka-band" enable the differential delay in the ray path to the two observing stations caused by the Earth's ionosphere to be calibrated (Reference 1).

Baseband channels can be recorded as complex samples or as real samples from the corresponding pair of upper and lower sidebands. A lower sideband/upper sideband (LSB/USB) channel pair is created from an individual complex (I/Q) channel. At each complex, 16 complex channels may be used simultaneously resulting in a maximum of 32 real channels. Each of the 16 complex channels can be placed independently in either of the observational bands. A typical set of channel-pair frequencies is shown in Table 4 and Table 5 for simultaneous observation in the S- and X-bands or X- and Ka-bands. Also shown in Table 4 and 5 is the IF center frequency for complex channel that corresponds to the channel pair frequency. It may be noticed that the channel pair frequency equals the IF center frequency plus that of the first downconverter (2.0 GHz for S-band, 8.1 GHz for X-band, and 31.7 GHz for Ka-band).

Each channel is digitized with a selected depth of 2 bits per sample resolution. The sampling rate is at the nominal Nyquist rate (2 samples per period). The resultant parallel digital streams are formatted, time-tagged and recorded in the RDEF. The RDEF data can be translated to VLBI Data Interchange Format (VDIF), as specified in DSN external interface document 820-013 0200-Science-VLBI, for non-DSN correlators.

Table 4. Typical Channels (S- and X-Bands) for Wideband VLBI

Channel Pair	IF Center Frequency
2204.49 MHz LSB & USB	204.49 MHz
2212.49 MHz LSB & USB	212.49 MHz
2239.49 MHz LSB & USB	239.49 MHz
2259.51 MHz LSB & USB	259.51 MHz
2295.51 MHz LSB & USB	295.51 MHz
8214.49 MHz LSB & USB	114.49 MHz
8222.49 MHz LSB & USB	122.49 MHz
8238.49 MHz LSB & USB	138.49 MHz
8270.49 MHz LSB & USB	170.49 MHz
8353.51 MHz LSB & USB	253.51 MHz
8424.51 MHz LSB & USB	324.51 MHz
8520.51 MHz LSB & USB	420.51 MHz
8567.51 MHz LSB & USB	467.51 MHz
8575.51 MHz LSB & USB	475.51 MHz

Table 5. Typical Channels (X- and Ka-Bands) for Wideband VLBI

Channel Pair	IF Center Frequency
8218.01 MHz LSB & USB	118.01 MHz
8262.01 MHz LSB & USB	162.01 MHz
8346.01 MHz LSB & USB	246.01 MHz
8514.01 MHz LSB & USB	414.01 MHz
8598.01 MHz LSB & USB	498.01 MHz
31818.01 MHz LSB & USB	118.01 MHz
31850.01 MHz LSB & USB	150.01 MHz
31882.01 MHz LSB & USB	182.01 MHz
31914.01 MHz LSB & USB	214.01 MHz
31942.01 MHz LSB & USB	242.01 MHz
32014.01 MHz LSB & USB	314.01 MHz
32158.01 MHz LSB & USB	458.01 MHz
32190.01 MHz LSB & USB	490.01 MHz
32222.01 MHz LSB & USB	522.01 MHz
32254.01 MHz LSB & USB	554.01 MHz
32286.01 MHz LSB & USB	586.01 MHz

Appendix A
References

1. O. J. Sovers, J. L. Fanselow, and C. S. Jacobs, "Astrometry and Geodesy with Radio Inteferometry: Experiments, Models, Results," *Reviews of Modern Physics, Vol. 70, No. 4,* The American Physical Society, October, 1998

2. A. E. E. Rogers, "Very long baseline interferometry with large effective bandwidth for phase-delay measurements," *Radio Science Volume 5, Number 10, pp. 1239–1247*, October 1970.

3. A. R. Whitney, "Mark 5 Disk-Based Gbps VLBI Data System," in *New Technologies in VLBI*, edited by Y. C. Minh, ASP Conference Series, Vol. 306, Astronomical Society of the Pacific, San Francisco, CA, 2003.

4. R. Hamell, B. Tucker, M. Calhoun, "Phase Calibration Generator," *IPN Progress Report 42-154*, Jet Propulsion Laboratory, Pasadena, CA, October 15, 2003.

   https://ipnpr.jpl.nasa.gov/progress_report/42-154/154H.pdf

Deep Space Network

214
Pseudo-Noise and Regenerative Ranging

Document Owner:		Approved by:	
Signature Provided	07/10/2023	Signature Provided	5/17/2023
Andrew O'Dea Telemetry, Tracking, and Command System Engineer	Date	Timothy Pham Communications Systems Chief Engineer	Date
Prepared By:		**Released by:**	
Signature Provided	05/11/2023	Signature Provided	08/03/2023
Peter Kinman Telecommunications Technical Consultant	Date	Christine Chang DSN Document Release Authority	Date

DSN No. **810-005, 214, Rev. C**
Issue Date: August 03, 2023
JPL D-19379; CL#23-3965

Jet Propulsion Laboratory
California Institute of Technology

Users must ensure that they are using the current version in DSN Telecommunications Link Design Handbook website:
https://deepspace.jpl.nasa.gov/dsndocs/810-005/

Review Acknowledgment

By signing below, the signatories acknowledge that they have reviewed this document and provided comments, if any, to the signatories on the Cover Page.

Signature Provided	04/25/2023	Signature Provided	05/10/2023
Jeff Berner DSN Project Chief Engineer	Date	Scott Bryant DSN Ranging Cognizant Development Engineer	Date

Document Change Log

Rev	Issue Date	Prepared By	Affected Sections or pages	Change Summary
Initial	10/7/2003	P. W. Kinman	All	New Module
A	10/28/2015	P. W. Kinman	All	Added CCSDS range codes. Added curve fits for probability of acquisition. Added model for turn-around ranging channel with SDST AGC. Added performance comparison of PN and sequential ranging.
B	7/17/2019	P. W. Kinman	Many	Rewrote “Allocation of Link Power” section, including new models for downlink phase deviation for each of two types of turn-around ranging channels. Added new equation for chip rate. Added new information on DSS delay. Added glossary. Rewrote many paragraphs for improved clarity.
C	08/03/2023	P. W. Kinman	Sections 2.1, 2.2.1, 2.3, 2.3.2.1, 2.3.2.2, 2.5.2, 2.5.3, 2.5.3.1, 2.5.3.2, 2.5.4, 2.5.8 Figures 4, 10, 11	Modified Equation (34) of 214B, which is now Equation (40) of 214C. Added equations for filtering of feedthrough command by ranging channel. Added models for effect of interference on range measurement.

Contents

Illustrations

Figure **Page**

Tables

Table **Page**

1. Introduction

1.1 Purpose

This module describes capabilities of the Deep Space Network (DSN) for pseudo-noise (PN) ranging. These capabilities are available within the 70-m, the 34-m High Efficiency (HEF), and the 34-m Beam Waveguide (BWG) subnets. Performance depends on whether the spacecraft transponder uses a turn-around (non-regenerative) ranging channel or a regenerative ranging channel. Performance parameters are provided for both cases.

1.2 Scope

The material contained in this module covers the PN ranging system that may be utilized by both near-Earth and deep-space missions. This document describes those parameters and operational considerations that are independent of the particular antenna being used to provide the telecommunications link. For antenna-dependent parameters, refer to Module 101, 103, or 104 of this handbook. The other ranging scheme employed by the DSN is sequential ranging, described in Module 203.

An overview of the ranging system is given in Section 2.1. The parameters to be specified for ranging operations are explained in Section 2.2. The distribution of link power is characterized in Section 2.3. The spectrum of an uplink carrier modulated by a PN ranging signal is discussed in Section 2.4. The performance of turn-around and regenerative ranging is summarized in Section 2.5. Non-coherent ranging is also discussed there. Section 2.6 describes the corrections required to determine the actual range to a spacecraft. The total error for a range measurement is discussed in Section 2.7.

2. General Information

The ranging signal of interest in this module is a logical combination of a range clock and several PN codes; this signaling technique is called PN ranging. A different signaling technique, sequential ranging, is also supported by the DSN. The same instrumentation within the DSN supports both PN ranging and sequential ranging. However, there are performance differences between these two signaling techniques. This module only discusses PN ranging. Sequential ranging is discussed in Module 203.

A spacecraft transponder may have either a turn-around ranging channel or a regenerative ranging channel. The DSN processes a PN ranging signal in the same way for both types of transponder ranging channel. The performance of a PN range measurement will generally be better when the transponder uses a regenerative ranging channel. This module characterizes the performance of both regenerative ranging and non-regenerative (turn-around) ranging when the PN-ranging signaling technique is employed.

The range clock is coherently related to the carrier. The uplink carrier is often tuned during a tracking pass, in order to compensate for the Doppler effect on the uplink carrier, thereby reducing stress on the transponder's carrier-tracking loop. As the uplink carrier is tuned, the range-clock frequency varies proportionately.

In two-way ranging, one Deep Space Station (DSS) both transmits the uplink and receives the downlink. For two-way ranging, the user may calculate the round-trip light time (RTLT) from data provided by the DSN: phase measurements of the ranging signal and a record of the transmitted uplink carrier frequency.

Three-way ranging is also supported, for which one DSS transmits the uplink and a different DSS receives the downlink. As with two-way ranging, the DSN reports phase measurements of the ranging signal and a record of the uplink-carrier frequency. From these data, the user may calculate the light time for the travel of the ranging signal from the uplink DSS, through the spacecraft, to the downlink DSS.

To put matters in perspective, the measurements discussed here are phase measurements and the resulting data permit the user to calculate time delays. Range cannot be calculated directly and accurately from the time delays because the range changes significantly over the course of the signal travel time. Similar measurement techniques employed in terrestrial applications, where the distances and measurement times are much smaller, typically permit the calculation of the range as the two-way time delay times the speed of an electromagnetic wave divided by 2. That has been the justification for using the term range measurement for this class of measurement technique. The two-way and three-way time delays calculated for deep-space missions are useful in the orbit determination process. These calculated delays assist in the improvement of trajectory models; and so, indirectly, the delays assist in the estimation of range as a function of time.

It is customary to quote range measurement error in units of meters. For two-way ranging, the range error is defined as the error in the two-way time delay times the speed of electromagnetic waves in vacuum divided by 2. (The division by two accounts for the fact that range is a one-way distance but the time delay is two-way.)

2.1 System Description

The DSN ranging system records the phase of the ranging signal that is transmitted and measures the phase of the ranging signal that returns. For two-way ranging, both recorded phase values (that of the uplink ranging signal and that of the downlink ranging signal) apply to a common instant in time, an epoch of the 1-pulse per second timing reference, which becomes the common time tag. From the difference between the uplink and downlink phases and from the history of the transmitted range-clock frequency (which can be calculated from the history of the uplink-carrier frequency), a user may compute the RTLT (Reference 1). This two-way time delay applies to a signal arriving at the DSS at the instant specified by the time tag.

The architecture for the DSN ranging system is shown in Figure 1. The ranging signal originates in the Uplink Subsystem (UPL). The returned signal is processed in the Downlink Tracking and Telemetry Subsystem (DTT). Both the UPL and the DTT are located at the Deep Space Communications Complex (DSCC).

The signal processing in the UPL may be summarized as follows. The Uplink Signal Generator (USG) synthesizes the range clock such that it is coherently related to the uplink carrier. The range-clock frequency equals a rational factor times the uplink carrier frequency. The USG generates the ranging signal, which is the range clock modified by additional signal structure that makes possible resolution of the phase ambiguity. A sample of

the uplink phase, which is required for the delay measurement, is passed from the USG to the Uplink Processor Assembly (UPA). The USG modulates the uplink carrier with the ranging signal. The klystron supplies the final stage of power amplification for the uplink carrier.

The downlink carrier, after amplification within the Low-Noise Amplifier (LNA), passes to the DTT. Frequency down-conversion to an intermediate frequency (IF) takes place in the RF-to-IF Downconverter (RID). The IF signal is sent to an IF-to-Digital Converter (IDC). Demodulation of the IF carrier occurs in the Receiver, Ranging and Telemetry (RRT) processor. Also within the RRT, the correlation of the received, baseband ranging signal with a local model produces a measurement of the downlink phase. This downlink phase is passed to the Downlink Channel Controller (DCC).

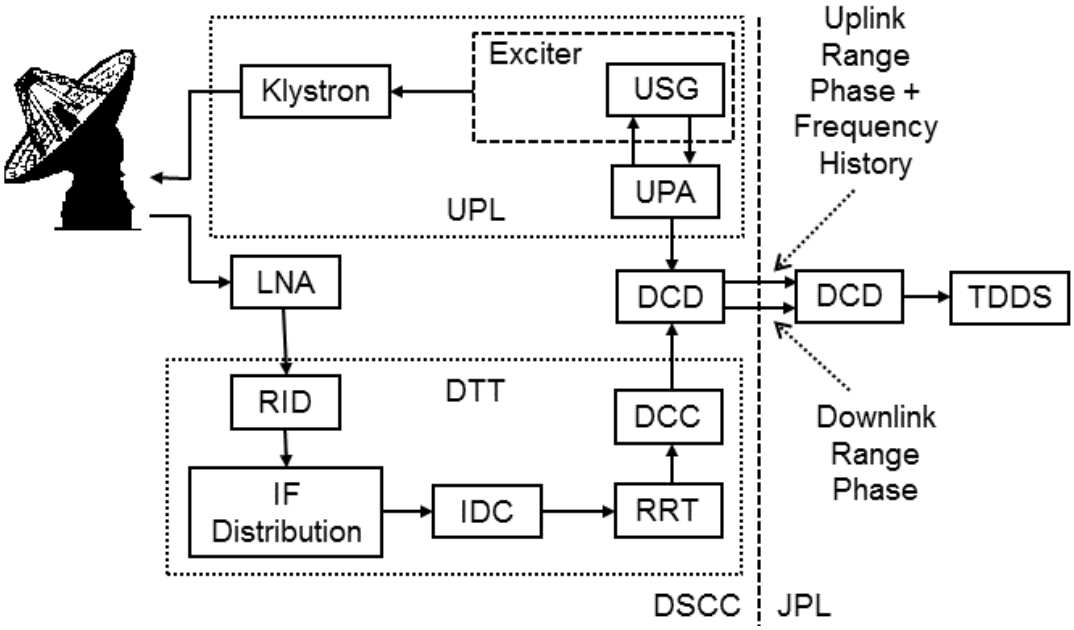

Figure 1. The DSN Ranging System Architecture

Uplink phase samples, each corresponding to an epoch of the 1-PPS (pulse per second) clock, are passed from the UPA, via the Data Capture and Delivery (DCD) software, to the Tracking Data Delivery Subsystem (TDDS), located in Pasadena. The DCC passes the downlink phase measurement and its time tag (an epoch of the 1-PPS clock), via the DCD, to the TDDS. A history of the uplink range clock's frequency is also needed for the calculation of the two-way time delay. Since the uplink range clock is coherently related to the uplink carrier, this necessary information can be derived from the history of the uplink carrier frequency, which is supplied by the UPA to the TDDS. All data required for the two-way delay calculation are archived by the TDDS for later use by a navigation team or other users.

The IDC, RRT, and DCC required for the processing of a downlink carrier are located within a Downlink Channel Processing Cabinet (DCPC). Each DCPC supports a single channel. For spacecraft with multiple channels (for example, X-band and Ka-band), or for

multiple spacecraft within a single antenna beamwidth, multiple DCPCs will be assigned to that antenna.

The DSN uses the Range Unit (RU) to deliver the difference of the ranging signal's uplink phase and downlink phase. Since the range clock and the carrier are coherently related, it is permissible to define the RU in terms of carrier phase. For an S-band uplink, the RU is defined as two cycles of the carrier. For an X-band uplink, one RU is $(749/221)$ times two cycles of the carrier. For a Ka-band uplink, one RU is $(3599/221)$ times two cycles of the carrier. Because the RU is defined with a factor (1 for an S-band uplink, $749/221$ for an X-band uplink, and $3599/221$ for a Ka-band uplink) that is proportional to frequency, the RU is proportional to time delay. (But the RU is a dimensionless unit.) One RU corresponds to approximately 0.94 ns of time delay.

A user may convert a two-way phase delay in RU into a two-way time delay as follows:

$$\text{Two-way Time Delay} = \begin{cases} \dfrac{2 \times RU}{f_S}, & \text{S-band uplink} \\ \dfrac{749}{221} \cdot \dfrac{2 \times RU}{f_X}, & \text{X-band uplink} \\ \dfrac{2407}{221} \cdot \dfrac{2 \times RU}{f_K}, & \text{K-band uplink} \\ \dfrac{3599}{221} \cdot \dfrac{2 \times RU}{f_{Ka}}, & \text{Ka-band uplink} \end{cases} \tag{1}$$

where f_S is the frequency of an S-band uplink carrier, f_X is the frequency of an X-band uplink carrier, f_K is the frequency of a K-band uplink carrier, and f_{Ka} is the frequency of a Ka-band uplink carrier. For example, if the uplink carrier is in the X band with a frequency of 7.16 GHz and the two-way phase delay is reported as 6,500,000 RU, then the two-way time delay is 6,153,467 ns.

2.2 Parameters Specified for Ranging Operations

The following subsections present the parameters that are required in ranging operations.

2.2.1 Chip Rate and Range-Clock Frequency

In the PN ranging system, the PN ranging signal is created by filtering a composite code, where timing is defined by the range clock. The chip rate f_{chip} for the composite code is defined in terms of a rational factor A/B (a ratio of two positive integers).

$$f_{\text{chip}} = \begin{cases} \dfrac{A}{B} \times f_S, & \text{S-band uplink} \\ \dfrac{221}{749} \times \dfrac{A}{B} \times f_X, & \text{X-band uplink} \\ \dfrac{221}{2407} \times \dfrac{A}{B} \times f_K, & \text{K-band uplink} \\ \dfrac{221}{3599} \times \dfrac{A}{B} \times f_{Ka}, & \text{Ka-band uplink} \end{cases} \tag{2}$$

f_S is the frequency of an S-band uplink carrier, f_X is the frequency of an X-band uplink carrier, f_K is the frequency of a K-band uplink carrier, and f_{Ka} is the frequency of a Ka-band uplink carrier. A/B is defined, in turn, by the whole numbers l_{CR} and k_{CR} (Reference 2).

$$\frac{A}{B} = \frac{l_{CR}}{128 \cdot 2^{k_{CR}}} \tag{3}$$

The chip rate is coherently related to the uplink carrier frequency, as suggested by Equation (2). l_{CR} and k_{CR} are whole numbers that together determine the rational factor A/B relating f_{chip} to the uplink carrier frequency. Table 1 lists the selections for l_{CR} and k_{CR}. This table also indicates the approximate value of the chip rate that corresponds to each pair of whole numbers l_{CR} and k_{CR}. The exact chip rate depends, as indicated in Equation (2), on the uplink carrier frequency (and, therefore, on the channel assignment and on any Doppler compensation that may be done on the uplink).

The range clock is a periodic signal. Each half-cycle of the range clock corresponds to one chip. Therefore, the range-clock frequency f_{RC} equals one-half of the the chip rate f_{chip}.

$$f_{RC} = \frac{f_{\text{chip}}}{2} \tag{4}$$

The approximate value of f_{RC} is given in Table 1 for numbers pairs l_{CR} and k_{CR} of that table. The exact value of f_{RC} depends on the uplink carrier frequency.

The DTT receiver uses the range clock in two ways. First, the phase of the range clock is measured; this determines the accuracy of the range measurement. Second, the receiver achieves chip synchronization using the range clock; this is a necessary precursor to resolving the ambiguity.

2.2.2 Ranging Signal Structure

In the PN ranging system, a filtered composite code is used for ranging. The timing of the composite code is set by the range clock. Three different composite codes are available: the DSN range code, the CCSDS T4B code, and the CCSDS T2B code. Each of these composite codes is built from a common set of component codes. The three composite codes differ from each other because of the manner in which the component codes are combined.

Table 1. CCSDS Chip Rates

l_{CR}	k_{CR}	A/B	Approximate value of f_{chip}	Approximate value of f_{RC}
94*	6	47/4096	24 MHz	12 MHz
64	6	1/128	16 MHz	8 MHz
32	6	1/256	8 MHz	4 MHz
16	6	1/512	4 MHz	2 MHz
12	6	3/2048	3 MHz	1.5 MHz
11	6	11/8192	2.8 MHz	1.4 MHz
10	6	5/4096	2.6 MHz	1.3 MHz
9	6	9/8192	2.3 MHz	1.15 MHz
8	6	1/1024	2 MHz	1 MHz
7	6	7/8192	1.8 MHz	900 kHz
6	6	3/4096	1.5 MHz	750 kHz
5	6	5/8192	1.3 MHz	650 kHz
4	6	1/2048	1 MHz	500 kHz
3	6	3/8192	750 kHz	375 kHz
2	6	1/4096	500 kHz	250 kHz
1	6	1/8192	250 kHz	125 kHz
2	8	1/16384	128 kHz	64 kHz
2	9	1/32768	64 kHz	32 kHz
2	10	1/65536	32 kHz	16 kHz

*This rate is used by the Bepi-Colombo mission and is outside defined CCSDS rates

2.2.2.1 Component Codes

Table 2 lists the component codes. In this table, a component code is represented as a finite-length sequence of bits. The length of the *n*-th component code is denoted λ_n for $1 \leq n \leq 6$. The lengths are: $\lambda_1 = 2$, $\lambda_2 = 7$, $\lambda_3 = 11$, $\lambda_4 = 15$, $\lambda_5 = 19$, and $\lambda_6 = 23$. (The first component code is the 2-bit sequence representing the range clock.) The *n*-th component code is denoted $b_n(i)$, where i represents a discrete-time index, $0 \leq i < \lambda_n$. The proper order of each of

these component codes is determined by reading the bits in each row from left to right. So, for example, the first three bits of $b_3(\cdot)$ are all 1s and the final bit is a 0.

It is also useful to represent each component code as a sequence of chips (with the bi-polar values ± 1).

$$c_n(i) = 2\, b_n(i) - 1 \tag{5}$$

where $c_n(i) = \pm 1$. Equation (5) translates a binary 1 into $+1$ and a logical 0 into -1.

Table 2. Component Codes

b_n	code	λ_n
b_1	1, 0	2
b_2	1, 1, 1, 0, 0, 1, 0	7
b_3	1, 1, 1, 0, 0, 0, 1, 0, 1, 1, 0	11
b_4	1, 1, 1, 1, 0, 0, 0, 1, 0, 0, 1, 1, 0, 1, 0	15
b_5	1, 1, 1, 1, 0, 1, 0, 1, 0, 0, 0, 0, 1, 1, 0, 1, 1, 0, 0	19
b_6	1, 1, 1, 1, 1, 0, 1, 0, 1, 1, 0, 0, 1, 1, 0, 0, 1, 0, 1, 0, 0, 0, 0	23

2.2.2.2 DSN Range Code

The DSN range code (also called the JPL range code) was the first composite code to be implemented and validated with the current ranging instrumentation in the DSN. Following is an explanation of how this composite code is generated from the component codes listed in Table 2.

For each finite-length PN code $b_n(i)$, a periodic code $b_n{}'(i)$ of period λ_n is formed by endless repetition:

$$b_n{}'(i) = b_n(i \bmod \lambda_n) \tag{6}$$

where $b_n{}'(i)$ is binary valued. In this document, the prime ($'$) indicates a periodic sequence (made from a finite-length sequence by periodic extension).

The composite code is

$$b'(i) = b_1{}'(i) \cup [b_2{}'(i) \cap b_3{}'(i) \cap b_4{}'(i) \cap b_5{}'(i) \cap b_6{}'(i)] \tag{7}$$

where $\cup$ and $\cap$ are the logical OR and logical AND operators, respectively. Since the component code lengths λ_n ($1 \le n \le 6$) are relatively prime, the period L (in bits) of the composite code is the product of the component code lengths. That is,

$$b'(i+L) = b'(i) \tag{8}$$

where

$$L = \prod_{n=1}^{6} \lambda_n = 1{,}009{,}470 \tag{9}$$

The periodic chip sequence corresponding to the periodic bit sequence $b'(i)$ is

$$c'(i) = 2\,b'(i) - 1 \tag{10}$$

where $b'(i)$ is the periodic bit sequence of Equation (7). $c'(i)$ is bi-polar, $c'(i) = \pm 1$.

In this design a large L is obtained from relatively small component code lengths. A large L is necessary for resolution of the range ambiguity, yet small λ_n are needed for a practical implementation of the correlators at the receiver. The ambiguity resolution of this code is given by

$$\text{ambiguity resolution} = \frac{c \cdot L}{4 f_{RC}} \tag{11}$$

where f_{RC} is the range-clock frequency and c is the speed of electromagnetic waves in vacuum. For a range clock of approximately 1 MHz, the ambiguity resolution is 75,660 km.

An important property of this composite code is that it approximates a sequence of period 2 bits. The composite code equals ${b_1}'(i)$, the first component with a period of 2 bits, most of the time. The effect of the other 5 component codes is to invert a small fraction (1/32) of the logical 0s in ${b_1}'(i)$. Since ${b_1}'(i)$ corresponds to the range clock, the composite code may be viewed as the range clock with an occasional inversion of a logical 0.

Most of this ranging signal's power lies at the range-clock frequency. This is desirable, since the accuracy of the range measurement is set by a correlation against a local model of the range clock. The occasional inversion is necessary to resolve the range ambiguity, but for this purpose the inversions need not be frequent.

2.2.2.3 CCSDS T4B Code

The Consultative Committee for Space Data Systems (CCSDS) recommends a composite code called T4B for use in deep-space ranging (Reference 2). The T4B code employs the same set of component codes that are used by the DSN range code (Table 2). The T4B code is constructed from the component chip sequences:

$${c_n}'(i) = c_n(i \bmod \lambda_n) \tag{12}$$

where $c_n(\cdot) = \pm 1$ is the chip sequence of length λ_n for the n-th component code, as given by Equation (5), and ${c_n}'(\cdot)$ is its periodic extension. The periodic, composite chip sequence $c'(i)$ is computed from the components ${c_n}'(i)$ as follows:

$$c'(i) = \text{sign}[4{c_1}'(i) + {c_2}'(i) - {c_3}'(i) - {c_4}'(i) + {c_5}'(i) - {c_6}'(i)] \tag{13}$$

where $c'(i) = \pm 1$ and where sign[·] is the algebraic sign of its argument. The period of the composite code $c'(i)$ equals L, as given in Equation (9). The ambiguity resolution of this code is the same as that for the DSN range code; this resolution is given in Equation (11).

As suggested by Equation (13), the range clock ${c_1}'(i)$ has a disproportionate influence on the composite code $c'(i)$. The composite code may be viewed as the range clock with an occasional inversion of a chip. (With the T4B code, unlike the DSN range code, the inversion may go in either direction: $-1 \rightarrow +1$ or $+1 \rightarrow -1$.) As with the DSN range code, most of the ranging signal's power lies at the range-clock frequency. As shown in Section 2.5, the performance of the T4B code is close to that of the DSN range code.

2.2.2.4 CCSDS T2B Code

The CCSDS recommends a second composite code, called T2B, which provides an alternative to the T4B code in performance trade-off space (Reference 2). The T2B code employs the same set of component codes (Table 2) that are used by the DSN range code and the T4B code. The periodic, composite chip sequence $c'(i)$ for the T2B code is computed from the components ${c_n}'(i)$ as follows:

$$c'(i) = \text{sign}[2{c_1}'(i) + {c_2}'(i) - {c_3}'(i) - {c_4}'(i) + {c_5}'(i) - {c_6}'(i)] \tag{14}$$

The period of the T2B code equals L, as given in Equation (9). The ambiguity resolution of this code is the same as that for the T4B code and the DSN range code; this resolution is given in Equation (11).

In the construction of the T2B code, using Equation (14), the range clock ${c_1}'(i)$ gets only 2 "votes", whereas in the construction of the T4B code, using Equation (13), the range clock gets 4 "votes". As a result, the T2B code places less power in the range clock. The T2B code will therefore generally produce a less accurate range measurement than the T4B code; however, the T2B code will achieve a better probability of acquisition for smaller received power levels.

2.2.2.5 PN Ranging Signal

The PN ranging signal is created by filtering the composite code. This is accomplished with the uplink ranging filter, which is digitally implemented within the USG. The uplink ranging filter is a low-pass filter with a configurable bandwidth. The default (and minimum) bandwidth is 1.2 MHz. The PN ranging signal, available at the output of the uplink ranging filter, is used to phase-modulate the uplink carrier. This modulation also happens in the USG.

The purpose of the uplink ranging filter is to limit the bandwidth of the modulated uplink carrier. Because phase modulation is a non-linear modulation, the bandwidth of a carrier that is phase-modulated by the PN ranging signal can be much wider than twice the bandwidth of the PN ranging signal. If the composite code were not low-pass filtered, but instead sent directly to the phase modulator, the bandwidth of the uplink carrier would, in general, be much wider yet. (The command signal, if present, also contributes to the bandwidth of the uplink carrier, but typically the command signal has a much smaller bandwidth than the PN ranging signal. The PN ranging signal, when present, is therefore the modulating signal that plays the dominant role in determining the bandwidth of the uplink carrier.)

The bandwidth of the uplink ranging filter has a default value of 1.2 MHz. This is also the minimum bandwidth. This filter can be configured for a larger bandwidth. For a range-clock frequency larger than 1 MHz, it will be necessary to use a larger bandwidth. The decision about what bandwidth to use will be based, in part, on the effect of the filter on the PN ranging signal but also must account for spectral occupancy of the uplink carrier.

The composite code, as it appears at the input to the uplink ranging filter, is a sequence of bi-polar chips, where each chip is represented by a rectangular pulse. The uplink ranging filter will remove the highest-frequency content from this chip stream, so the PN ranging signal at the filter output will have slower transitions and smooth features. In the case where the uplink ranging filter passes the fundamental harmonic of the range clock but blocks third and higher-order harmonics of the range clock, a square-wave range clock on the filter input becomes a sinewave range clock on the filter output. The composite code on the filter input becomes on the filter output, in this case, a sequence of bi-polar chips, where each chip may be represented approximately by a half-cycle of a sinewave. This is illustrated in Figure 2 for the first eight chips of the DSN range code. The parameter T_c is the chip period. The range-clock frequency equals $1/(2T_c)$. This is the desired situation for the purpose of minimizing the spectral occupancy of the uplink carrier.

The range clock is modeled, in this module, as a sinewave. The PN ranging signal is modeled as the composite code but with each chip a half-cycle of a sinewave, as depicted in Figure 2. These models are good approximations when the uplink ranging filter passes the fundamental harmonic of the range clock but blocks the third harmonic (and higher-order harmonics) of the range clock. Even if this condition is not strictly met, these models are useful as first-order approximations; they lead to performance equations that may be easily calculated. Trying to get more accurate results would typically involve computer simulations.

There is also the limiting case where the bandwidth of the uplink ranging filter is much larger than the range-clock frequency. In this limit, the range clock is a square-wave and the PN ranging signal is the composite code (with chips represented by rectangular pulses). This limiting case is only approached when the range-clock frequency is much smaller than 400 kHz (one-third of 1.2 MHz). Since the accuracy of the range measurement improves with increasing range-clock frequency, this scenario is not common.

2.2.3 Integration Time

The integration time T should be large enough that the probability of range measurement acquisition is close to 1.0 and the range error due to downlink thermal noise is small (see Section 2.5). In the special case of non-coherent ranging, the presence of a frequency mismatch between the received ranging signal and the local model means that there is also reason to keep T relatively small, so that an optimum T should be carefully chosen for non-coherent ranging.

2.2.4 Uplink Ranging Modulation Index

The uplink ranging modulation index is chosen to get a suitable distribution of power among the ranging and command sidebands and the residual carrier on the uplink (see Section 2.3). With turn-around (non-regenerative) ranging, the uplink ranging modulation index also affects the distribution of power on the downlink carrier. The analysis appearing below

employs an rms phase deviation of the uplink carrier. This rms phase deviation equals the peak modulation index divided by $\sqrt{2}$ for the usual case of a sinewave range clock.

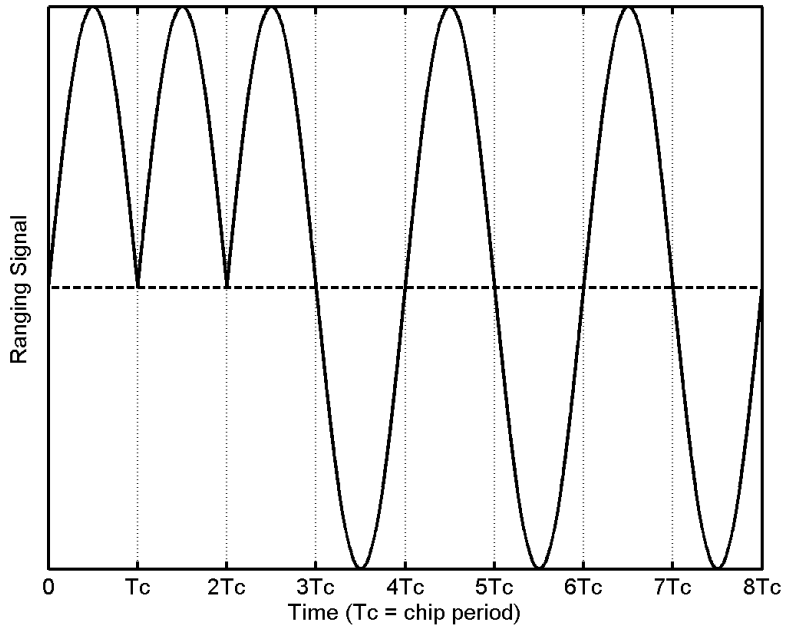

Figure 2. PN Ranging Signal When Third Harmonic of Range Clock is Blocked

2.2.5 Tolerance

The tolerance plays a role in deciding whether to judge range acquisitions as "in lock" or "out of lock". The ranging process does not use a phase-locked loop, so ranging lock status is estimated using the ranging probability of acquisition. For any given range acquisition, the ratio P_R/N_0 of the downlink ranging signal power to the noise spectral density is measured. From this measured P_R/N_0, an estimate of the probability of acquisition P_{acq} is calculated. Section 2.5 describes the calculation of the P_{acq} from P_R/N_0.

Tolerance may be selected over the range of 0.0% to 100.0%. The default value for tolerance is 99%. An acquisition lock status depends upon the following criteria:

$P_{\mathrm{acq}}(\%) \geq \mathrm{Tolerance}$ *results in* Acquisition declared "in lock"

$P_{\mathrm{acq}}(\%) < \mathrm{Tolerance}$ *results in* Acquisition declared "out of lock"

This procedure is explained for the example where the tolerance has the default value of 99%. For a given acquisition, P_R/N_0 is measured. From this measured value, the probability of acquisition P_{acq} is calculated; this number is the probability that the ambiguity is correctly resolved for this particular acquisition. Treating P_{acq} as a percentage, it is compared with the tolerance of 99%. If $P_{\mathrm{acq}}(\%)$ equals or exceeds 99%, the acquisition is declared "in lock". Otherwise, it is declared "out of lock". Note that the "out of lock" ranging data may be valid data, with a probability of $P_{\mathrm{acq}}(\%)$ of being correct.

2.3 Allocation of Link Power

The power allocation for a link is the distribution of power among the important link components: the residual carrier, the ranging sidebands, and the data (command or telemetry) sidebands. The following notation is used here for both the uplink and downlink:

P_C = power in residual carrier

P_R = usable power in ranging sidebands

P_D = usable power in data sidebands

P_T = total link power

P_C is the power in a single spectral line at the carrier frequency. When P_C is finite (greater than zero), carrier synchronization may be obtained at the receiver using a phase-locked loop that tracks this residual carrier. (Carrier synchronization may also be obtained with a Costas loop tracking the data sidebands, which are symmetrically located about the nominal carrier frequency.)

P_R is that portion of the power in the ranging sidebands that is used in the range measurement. P_R includes both the spread-spectrum content arising from the PN code components as well as the two discrete spectral lines (at f_{RC} Hz above and at f_{RC} Hz below the residual carrier) that correspond to the range clock's fundamental harmonic. Higher-order harmonics (beyond the fundamental harmonic) of the range clock are not used in a range measurement and are not included in P_R. The range measurement error is determined by the discrete spectral lines of the range clock's fundamental harmonic. Ambiguity resolution is achieved using the spread-spectrum content.

For the uplink, P_D is that portion of the power in the command sidebands that is employed in command detection in the transponder. In the most common signal design for a deep-space uplink, command data modulate a sinewave subcarrier and P_D only accounts for the power in the sidebands associated with the upper and lower fundamental harmonic of the subcarrier frequency. In the case of a sinewave subcarrier, the higher-order harmonics of the subcarrier frequency are not employed in command detection in the typical transponder and are not included in P_D.

For some missions, the command signal is bi-polar. The term "bi-polar" can mean either NRZ or bi-phase (Manchester encoded) pulses; for both of these pulse shapes, each symbol is conveyed using one of two algebraically opposite (antipodal) pulse shapes. An example of bi-polar commanding is when the command symbols, represented as NRZ or bi-phase pulses, directly phase-modulate the uplink carrier. In this case, the uplink P_D accounts for all power in command sidebands, since the command detection process in the typical transponder utilizes all command sidebands arising from a bi-polar command signal.

For the downlink, P_D is that portion of the power in the telemetry sidebands that is employed in telemetry detection at the station. Commonly, the telemetry signal is bi-polar. The term "bi-polar" can mean either NRZ or bi-phase (Manchester encoded) pulses; for both of these pulse shapes, each symbol is conveyed using one of two algebraically opposite (antipodal) pulse shapes. An example of bi-polar telemetry is when the telemetry symbols, represented as NRZ or

bi-phase pulses, directly phase-modulate the downlink carrier or when these symbols modulate a square-wave subcarrier that, in turn, phase-modulates the downlink carrier. In such cases, all of the power in the telemetry sidebands is employed in telemetry detection. This is a result of both the data and the subcarrier (if present) being bi-polar.

For some missions, the telemetry signal modulates a sinewave subcarrier and this composite signal phase-modulates the downlink carrier. In such a case, the downlink P_D is that portion of the power in the telemetry sidebands that is employed in telemetry detection at the station. Not included is the power in the higher-order harmonics of the subcarrier frequency.

P_T is not, in general, the sum of P_C, P_R, and P_D. In general, P_T is larger than that sum. There are multiple reasons for this. First, P_R does not account for power in the higher-order harmonics of the sinewave range clock. Second, when multiple signals (for example, a ranging signal and a telemetry signal) simultaneously phase-modulate a carrier, intermodulation products arise. These intermodulation products consume link power but do not contribute to either the range measurement or telemetry detection. Moreover, for the downlink, noise sidebands are present (in the case of turn-around ranging).

In calculating power allocations for a modulated carrier, it is necessary to characterize the level of the modulation. In this document, the root-mean-square (rms) phase deviation of the carrier will be used for this purpose. The following symbols are used in this module to represent rms phase deviation of the carrier:

uplink:	ϕ_r	=	rms phase deviation by ranging signal, rad rms
uplink:	ϕ_{cmd}	=	rms phase deviation by command signal, rad rms
downlink:	θ_{rs}	=	rms phase deviation by ranging signal (strong signal), rad rms
downlink:	θ_r	=	rms phase deviation by ranging signal, rad rms
downlink:	θ_{cmd}	=	rms phase deviation by feedthrough command signal, rad rms
downlink:	θ_n	=	rms phase deviation by noise, rad rms
downlink:	θ_{tlm}	=	rms phase deviation by telemetry signal, rad rms

On the uplink, ϕ_r and ϕ_{cmd} are parameters, constant for any given tracking pass. For a sinewave range clock, ϕ_r is related to the peak modulation index for uplink ranging by:

$$\phi_r = (\text{peak modulation index for uplink ranging, rad})/\sqrt{2} \tag{15}$$

When a sinewave subcarrier is used with command, ϕ_{cmd} is related to the peak modulation index for command by:

$$\phi_{cmd} = (\text{peak modulation index for command, rad})/\sqrt{2}, \quad \begin{matrix}\text{sinewave}\\ \text{subcarrier}\end{matrix} \tag{16}$$

However, for a bi-polar command signal, ϕ_{cmd} equals the peak modulation index for command.

On the downlink, θ_{rs} is a constant parameter that is determined by the AGC in the turn-around ranging channel. θ_{rs} is the rms phase deviation of the downlink carrier by the ranging signal in a strong-signal scenario. In such a scenario, the noise in the transponder's ranging channel is negligible compared with the ranging signal and there is no command. This

scenario occurs in a test facility before flight and in the early phase of flight when the ranging signal-to-noise ratio in the transponder's ranging channel is large. For a sinewave range clock, θ_{rs} is related to the peak modulation index (strong signal) by:

$$\theta_{rs} = (\text{strong-signal peak modulation index for downlink ranging, rad})/\sqrt{2} \qquad (17)$$

When PN ranging is done with a turn-around (non-regenerative) ranging channel, the variables θ_r, θ_{cmd} and θ_n become important. Within a turn-around channel the uplink carrier is demodulated, and the baseband signal plus noise that is the result of this demodulation is presented to a filter. The filter output is applied to an automatic gain control (AGC) circuit. The signal plus noise that exits the turn-around ranging channel is phase-modulated onto the downlink carrier.

For an arbitrary signal-to-noise ratio in a turn-around ranging channel, the rms phase deviation by ranging signal on the downlink, denoted θ_r, is less than or equal to θ_{rs}. Thus, θ_r is a variable, depending on both the parameter θ_{rs} and the ranging signal-to-noise ratio in the ranging channel. θ_{rs} is the limiting value of θ_r, corresponding to the strong-signal case. If command is present on the uplink and that command passes through the transponder's ranging channel, then θ_r also depends on the command signal-to-noise ratio in the ranging channel.

Uplink noise passes through the ranging channel and is phase-modulated onto the downlink carrier. θ_n is the rms phase deviation by this ranging-channel noise. θ_n, like θ_r, is a variable that depends on both the parameter θ_{rs} and the ranging signal-to-noise ratio (and, possibly, also the command signal-to-noise ratio) in the ranging channel.

θ_{tlm} is the rms phase deviation of the downlink carrier due to telemetry. When the telemetry signal is bi-polar, the rms phase deviation and the peak modulation index for telemetry are identical. When a sinewave subcarrier is used with telemetry, θ_{tlm} is related to the peak modulation index for telemetry by:

$$\theta_{tlm} = (\text{peak modulation index for telemetry, rad})/\sqrt{2}, \quad \begin{matrix}\text{sinewave}\\ \text{subcarrier}\end{matrix} \qquad (18)$$

2.3.1 Uplink

The equations of this subsection represent the case where a ranging signal and a command signal are simultaneously present on the uplink carrier. The range clock is taken here to be a sinewave. The ratio of P_C to P_T, the carrier suppression, is

$$\left.\frac{P_C}{P_T}\right|_{\mathrm{U/L}} = J_0{}^2\left(\sqrt{2}\,\phi_r\right) \cdot S_{cmd}(\phi_{cmd}) \qquad (19)$$

The ratio of P_R to P_T is

$$\left.\frac{P_R}{P_T}\right|_{\mathrm{U/L}} = 2J_1{}^2\left(\sqrt{2}\,\phi_r\right) \cdot S_{cmd}(\phi_{cmd}) \qquad (20)$$

The ratio of the fundamental command sideband power to P_T is

$$\left.\frac{P_D}{P_T}\right|_{\mathrm{U/L}} = J_0{}^2\left(\sqrt{2}\,\phi_r\right) \cdot M_{cmd}(\phi_{cmd}) \tag{21}$$

where $J_0(\cdot)$ and $J_1(\cdot)$ are Bessel functions of the first kind of order 0 and 1, respectively. These functions are plotted in Figure 3. When the argument x of $J_0(x)$ and $J_1(x)$ is small and positive, the following approximations may be used:

$$J_0(x) \cong 1, \qquad 0 \le x \ll 1 \tag{22}$$

$$J_1(x) \cong x/2, \qquad 0 \le x \ll 1 \tag{23}$$

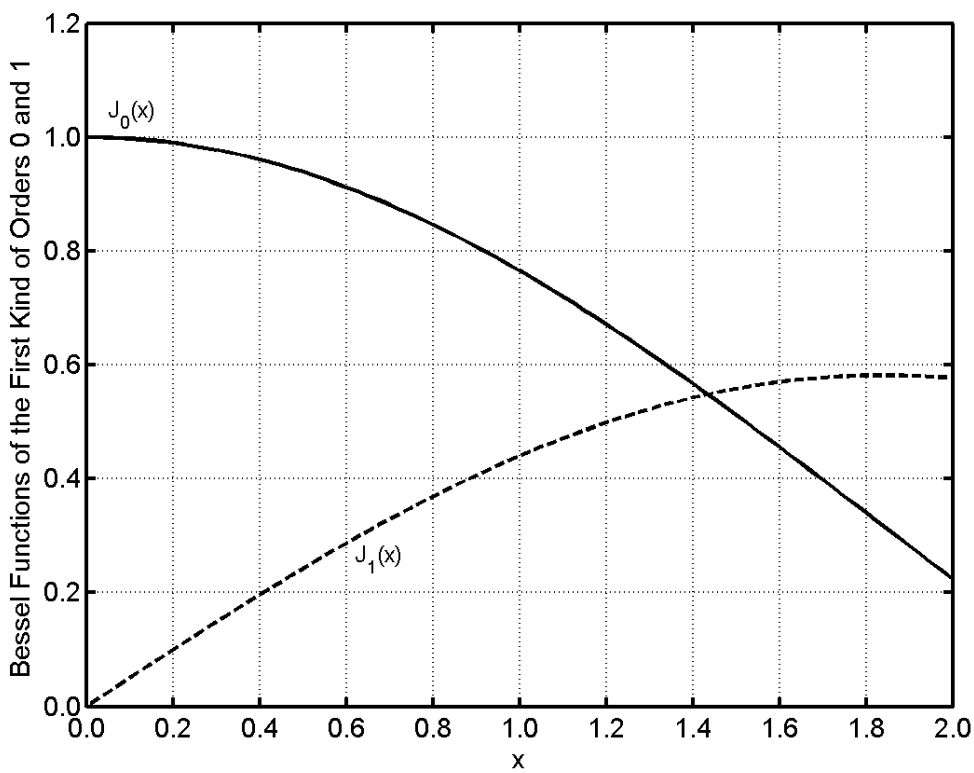

Figure 3. Bessel Functions of the First Kind of Order 0 and 1

The suppression factor $S_{cmd}(\phi_{cmd})$ in Equations (19) and (20) and the modulation factor $M_{cmd}(\phi_{cmd})$ in Equation (21) depend on whether the command signal is bi-polar or uses a sinewave subcarrier. These two factors are given by:

$$S_{cmd}(\phi_{cmd}) = \begin{cases} \cos^2(\phi_{cmd}), & \text{bi-polar} \\ J_0{}^2\left(\sqrt{2}\,\phi_{cmd}\right), & \text{sinewave subcarrier} \end{cases} \tag{24}$$

$$M_{cmd}(\phi_{cmd}) = \begin{cases} \sin^2(\phi_{cmd}), & \text{bi-polar} \\ 2{J_1}^2(\sqrt{2}\,\phi_{cmd}), & \text{sinewave subcarrier} \end{cases} \tag{25}$$

In the event that command is absent from the uplink, the factor $S_{cmd}(\phi_{cmd})$ in Equations (19) and (20) can be omitted, since $S_{cmd}(0) = 1$.

2.3.2 Downlink

The equations for power allocation on the downlink depend on whether the transponder has a turn-around (non-regenerative) ranging channel or a regenerative ranging channel.

2.3.2.1 Turn-Around (Non-Regenerative) Ranging

A turn-around ranging channel demodulates the uplink carrier, filters the baseband signal, applies automatic gain control, and then re-modulates the baseband signal onto the downlink carrier. The AGC serves the important purpose of ensuring that the downlink carrier suppression is approximately constant, independent of received uplink signal level. The bandwidth B_R of the transponder's ranging channel must be larger (typically about 50% larger) than the range-clock frequency, in order to pass the ranging signal with minimal distortion. For example, B_R is typically about 1.5 MHz when the transponder is intended to accommodate a range clock of 1 MHz. Substantial thermal noise from the uplink also passes through this channel. In many deep space scenarios, the thermal noise dominates over the ranging signal in this wideband, turn-around channel. Moreover, command signal from the uplink may pass through this ranging channel. In general, then, noise and command signal as well as the desired ranging signal are modulated onto the downlink carrier whenever the ranging channel is active (Reference 3).

The equations of this subsection represent the case where a ranging signal, a (feedthrough) command signal and noise are simultaneously present in the ranging channel, so that all three of these components, plus telemetry, phase-modulate the downlink carrier. The range clock is taken here to be a sinewave. The ratio of P_C to P_T, the carrier suppression, is

$$\left.\frac{P_C}{P_T}\right|_{\mathrm{D/L}} = {J_0}^2\left(\sqrt{2}\,\theta_r\right) \cdot S_{fth}(\theta_{cmd}) \cdot e^{-{\theta_n}^2} \cdot S_{tlm}(\theta_{tlm}) \tag{26}$$

The ratio of P_R to P_T is

$$\left.\frac{P_R}{P_T}\right|_{\mathrm{D/L}} = 2{J_1}^2\left(\sqrt{2}\,\theta_r\right) \cdot S_{fth}(\theta_{cmd}) \cdot e^{-{\theta_n}^2} \cdot S_{tlm}(\theta_{tlm}) \tag{27}$$

The ratio of the telemetry sideband power to P_T is

$$\left.\frac{P_D}{P_T}\right|_{\mathrm{D/L}} = {J_0}^2\left(\sqrt{2}\,\theta_r\right) \cdot S_{fth}(\theta_{cmd}) \cdot e^{-{\theta_n}^2} \cdot M_{tlm}(\theta_{tlm}) \tag{28}$$

The ratio of the command-feedthrough power to P_T is

$$\left.\frac{P_{fth}}{P_T}\right|_{\mathrm{D/L}} = J_0{}^2\left(\sqrt{2}\,\theta_r\right) \cdot M_{fth}(\theta_{cmd}) \cdot e^{-\theta_n{}^2} \cdot S_{tlm}(\theta_{tlm}) \tag{29}$$

where $J_0(\cdot)$ and $J_1(\cdot)$ are Bessel functions of the first kind of order 0 and 1, respectively.

The command-feedthrough suppression factor $S_{fth}(\theta_{cmd})$ that appears in each of Equations (26), (27) and (28) depends on whether the command signal is bi-polar or uses a sinewave subcarrier. This factor is given by:

$$S_{fth}(\theta_{cmd}) = \begin{cases} \cos^2(\theta_{cmd}), & \text{bi-polar} \\ J_0{}^2\left(\sqrt{2}\,\theta_{cmd}\right), & \text{sinewave subcarrier} \end{cases} \tag{30}$$

In the event that command feedthrough is absent from the ranging channel, the factor $S_{fth}(\theta_{cmd})$ in each of Equations (26), (27) and (28) can be omitted, since $S_{fth}(0) = 1$.

The command-feedthrough modulation factor $M_{fth}(\theta_{cmd})$ in Equation (29) depends on whether the command is bi-polar or uses a sinewave subcarrier. This factor is given by:

$$M_{fth}(\theta_{cmd}) = \begin{cases} \sin^2(\theta_{cmd}), & \text{bi-polar} \\ 2J_1{}^2\left(\sqrt{2}\,\theta_{cmd}\right), & \text{sinewave subcarrier} \end{cases} \tag{31}$$

The telemetry suppression factor $S_{tlm}(\phi_{tlm})$ in Equations (26), (27), and (29) and the telemetry modulation factor $M_{tlm}(\phi_{tlm})$ in Equation (28) depend on whether the telemetry signal is bi-polar or uses a sinewave subcarrier. These two factors are given by:

$$S_{tlm}(\theta_{tlm}) = \begin{cases} \cos^2(\theta_{tlm}), & \text{bi-polar} \\ J_0{}^2\left(\sqrt{2}\,\theta_{tlm}\right), & \text{sinewave subcarrier} \end{cases} \tag{32}$$

$$M_{tlm}(\theta_{tlm}) = \begin{cases} \sin^2(\theta_{tlm}), & \text{bi-polar} \\ 2J_1{}^2\left(\sqrt{2}\,\theta_{tlm}\right), & \text{sinewave subcarrier} \end{cases} \tag{33}$$

For a turn-around ranging channel, the downlink rms phase deviations θ_r, θ_n, and (if command feedthrough is present) θ_{cmd} depend on the ranging signal-to-noise ratio ρ_r and (if command feedthrough is present) the command signal-to-noise ratio ρ_{cmd} in the ranging channel.

$$\rho_r = \left.\frac{P_R}{P_T}\right|_{\mathrm{U/L}} \cdot \left.\frac{P_T}{N_0}\right|_{\mathrm{U/L}} \cdot \frac{1}{B_R} \tag{34}$$

$$\rho_{cmd} = \left.\frac{P_D}{P_T}\right|_{\mathrm{U/L}} \cdot \left.\frac{P_T}{N_0}\right|_{\mathrm{U/L}} \cdot \frac{1}{B_R} \cdot C_R(B_R T_{cmd}) \tag{35}$$

where

$P_T/N_0\|_{\mathrm{U/L}}$	=	uplink total power to noise spectral density ratio, Hz
B_R	=	noise-equivalent (one-sided) bandwidth of ranging channel, Hz
$C_R(B_R T_{cmd})$	=	fraction of command-signal power passing through ranging channel
T_{cmd}	=	command symbol period (reciprocal of command symbol rate), s

The factor $C_R(B_R T_{cmd})$, which is limited by $0 \leq C_R(B_R T_{cmd}) \leq 1$, accounts for the fact that some of the command-signal power might not pass through the transponder's ranging channel. This factor is a function of the product $B_R T_{cmd}$. If most of the command signal passes through the ranging channel, then the factor $C_R(B_R T_{cmd})$ may be approximated as 1.

With high-rate command, the factor $C_R(B_R T_{cmd})$ can be significantly less than 1. Models are given here for $C_R(B_R T_{cmd})$ in the case of bi-polar command (with either NRZ or bi-phase pulses) that directly phase-modulates the uplink carrier.

When high-rate command signaling consists of NRZ pulses that directly phase-modulate the uplink carrier, $C_R(B_R T_{cmd})$ may be modeled as

$$C_R(B_R T_{cmd}) = 2T_{cmd} \int_0^{B_R} \frac{\sin^2(\pi f T_{cmd})}{(\pi f T_{cmd})^2}\, df \qquad \text{NRZ} \qquad (36)$$

Equation (36) has no closed-form expression in terms of elementary functions. When the product $B_R T_{cmd} \ll 1$, $C_R(B_R T_{cmd}) \cong 2B_R T_{cmd}$. When $B_R T_{cmd} \gg 1$, $C_R(B_R T_{cmd}) \cong 1$. A general, approximate expression for $C_R(B_R T_{cmd})$ that is valid for high-rate command with NRZ pulses follows below. This approximation was obtained as a curve-fit of Equation (36) for intermediate values of the product $B_R T_{cmd}$.

$$C_R(B_R T_{cmd}) = \begin{cases} 2B_R T_{cmd}, & B_R T_{cmd} \leq 0.2 \\ \dfrac{1}{1 + \exp[-2.32 - 1.68 \cdot \ln(B_R T_{cmd})]}, & B_R T_{cmd} > 0.2 \end{cases} \qquad \text{NRZ} \qquad (37)$$

When high-rate command signaling consists of bi-phase (Manchester encoded) pulses that directly phase-modulate the uplink carrier, $C_R(B_R T_{cmd})$ may be modeled as

$$C_R(B_R T_{cmd}) = 2T_{cmd} \int_0^{B_R} \frac{\sin^4(\pi f T_{cmd}/2)}{(\pi f T_{cmd}/2)^2}\, df \qquad \text{bi-}\phi \qquad (38)$$

Equation (38) has no closed-form expression in terms of elementary functions. When the product $B_R T_{cmd} \ll 1$, $C_R(B_R T_{cmd}) \cong (\pi^2/6) \cdot (B_R T_{cmd})^3$. When $B_R T_{cmd} \gg 1$, $C_R(B_R T_{cmd}) \cong 1$. A general, approximate expression for $C_R(B_R T_{cmd})$ that is valid for high-rate command with bi-phase pulses follows below. This approximation was obtained as a curve-fit of Equation (38) for intermediate values of the product $B_R T_{cmd}$.

$$C_R(B_R T_{cmd}) = \begin{cases} \dfrac{\pi^2}{6} \cdot (B_R T_{cmd})^3, & B_R T_{cmd} \leq 0.6 \\ \dfrac{1}{1 + \exp[-0.35 - 2.10 \cdot \ln(B_R T_{cmd})]}, & B_R T_{cmd} > 0.6 \end{cases} \qquad \text{bi-}\phi \quad (39)$$

$C_R(B_R T_{cmd})$ is plotted as a function of $B_R T_{cmd}$ in Figure 4. This figure is for high-rate command that directly phase-modulates the uplink carrier. There is a curve for the case of NRZ pulses and second curve for the case of bi-phase pulses.

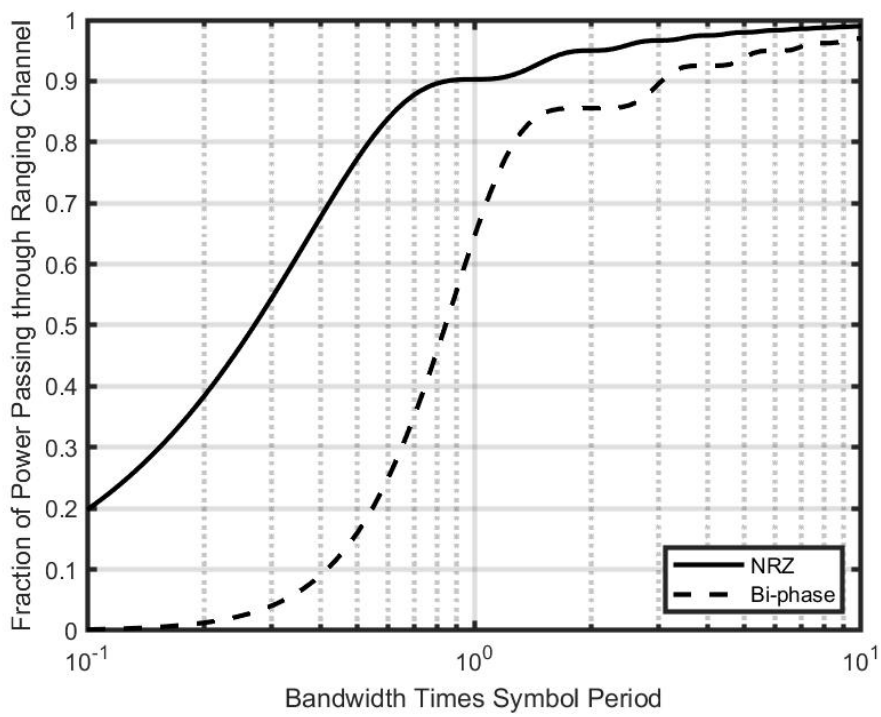

Figure 4. Fraction of Command Power Passing Ranging Channel

In some transponders with a turn-around ranging channel, the AGC is designed to keep constant the average of the absolute value of the voltage at the AGC output. In other transponders, the AGC is designed to keep constant the rms voltage at the AGC output. For both types of AGC, the downlink rms phase deviations θ_r, θ_n, and θ_{cmd} depend on ρ_r and ρ_{cmd} (as well as the parameter θ_{rs}). Turn-around ranging channels with both types of AGC are treated below.

2.3.2.1.1 AGC with Constant Average of Absolute Value of Voltage

When the transponder's ranging channel has an AGC that keeps constant the average of the absolute value of the channel voltage, there are no exact, analytical expressions for the rms phase deviations θ_r, θ_{cmd}, and θ_n. However, these rms phase deviations may be obtained by computer simulation. Curve fits to the simulations appear below.

$$\theta_r = \begin{cases} \theta_{rs} \cdot \dfrac{2\sqrt{2}}{\pi} \cdot \sqrt{\dfrac{\rho_r}{\rho_{cmd}}}, & \rho_{cmd} \geq 1 \text{ and } 0 < \rho_r \leq \rho_{cmd}/10 \\ \dfrac{\theta_{rs}}{1 + \exp[\gamma - 0.79 \cdot \ln(\rho_r)]}, & \text{otherwise} \end{cases} \tag{40}$$

where

$$\gamma = \begin{cases} -1.2, & \rho_{cmd} = 0 \\ \ln[0.3 + 0.27 \cdot {\rho_{cmd}}^{0.88}], & \rho_{cmd} > 0 \end{cases} \tag{41}$$

Here $\exp(\cdot)$ and $\ln(\cdot)$ are the exponential function and natural logarithm, respectively. In the event that there is no command feedthrough, $\rho_{cmd} = 0$ and θ_r depends only on the constant parameter θ_{rs} and the ranging signal-to-noise ratio ρ_r. The asymptotes for Equation (40) are $\lim_{\rho_r \to 0} \theta_r = 0$ and $\lim_{\rho_r \to \infty} \theta_r = \theta_{rs}$.

A similar set of equations are valid (approximately) for θ_{cmd}

$$\theta_{cmd} = \frac{\theta_{rs}}{1 + \exp[\chi - 0.79 \cdot \ln(\rho_{cmd})]} \tag{42}$$

where

$$\chi = \ln[0.3 + 0.27 \cdot {\rho_r}^{0.88}] \tag{43}$$

The asymptotes for Equation (42) are $\lim_{\rho_{cmd} \to 0} \theta_{cmd} = 0$ and $\lim_{\rho_{cmd} \to \infty} \theta_{cmd} = \theta_{rs}$.

A curve-fit to the simulation data for θ_n as a function of ρ_r and ρ_{cmd} is:

$$\theta_n = \frac{\theta_{rs} \cdot \left(2/\sqrt{\pi}\right)}{1 + \exp[-0.87 + 0.81 \cdot \ln(\rho_{rss})]} \tag{44}$$

where ρ_{rss} is the root-sum-square of ρ_r and ρ_{cmd}:

$$\rho_{rss} = \sqrt{{\rho_r}^2 + {\rho_{cmd}}^2} \tag{45}$$

The asymptotes for this curve are $\lim_{\rho_{rss} \to 0} \theta_n = \theta_{rs} \cdot \left(2/\sqrt{\pi}\right)$ and $\lim_{\rho_{rss} \to \infty} \theta_n = 0$.

Since θ_r is directly proportional to the parameter θ_{rs}, the ratio θ_r/θ_{rs} may be plotted as a function of ρ_r (and ρ_r alone when $\rho_{cmd} = 0$). This appears in Figure 5 for the case of no command feedthrough: $\rho_{cmd} = 0$ and $\theta_{cmd} = 0$. The solid curve labeled AAV is valid for a turn-around ranging channel whose AGC keeps constant the average of the absolute voltage (AAV). Figure 5 shows that the ratio θ_r/θ_{rs} increases monotonically as a function of ρ_r with a limiting value of 1. (In other words, the strong-signal value of θ_r is θ_{rs}.) The AAV curve of Figure 5 comes from Equations (40) and (41) with $\rho_{cmd} = 0$.

The ratio θ_n/θ_{rs} may also be plotted as a function of ρ_r when $\rho_{cmd} = 0$. This appears in Figure 6. The solid curve labeled AAV is valid for a turn-around ranging channel whose AGC keeps constant the average of the absolute voltage (AAV). Figure 6 shows that the ratio θ_n/θ_{rs} decreases monotonically as a function of ρ_r. The AAV curve of Figure 6 comes from Equations (44) and (45) with $\rho_{cmd} = 0$.

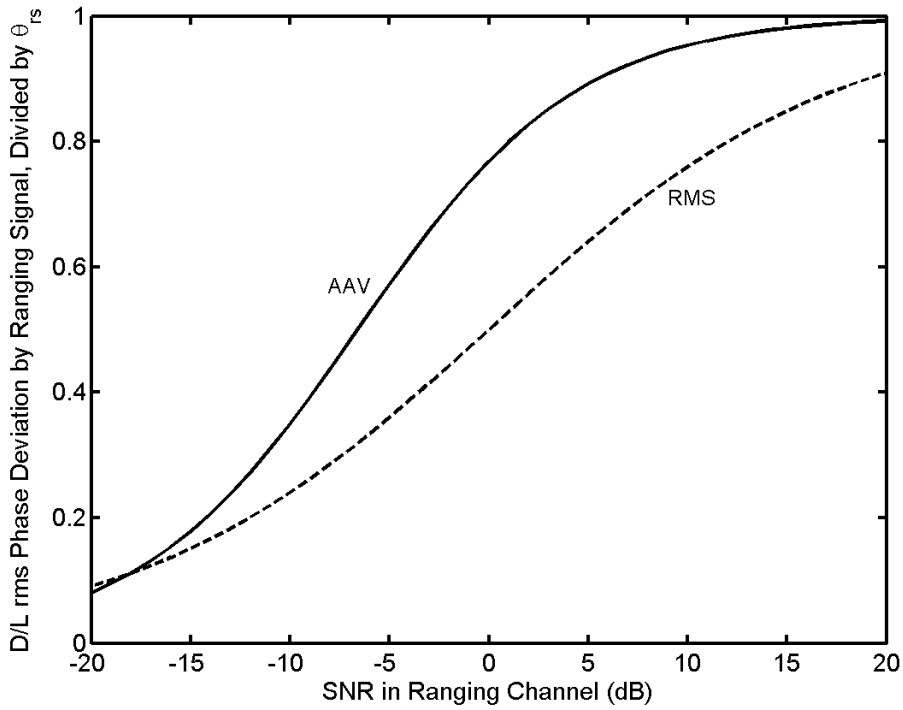

Figure 5. Downlink rms Phase Deviation by Ranging Signal (No Command Feedthrough)

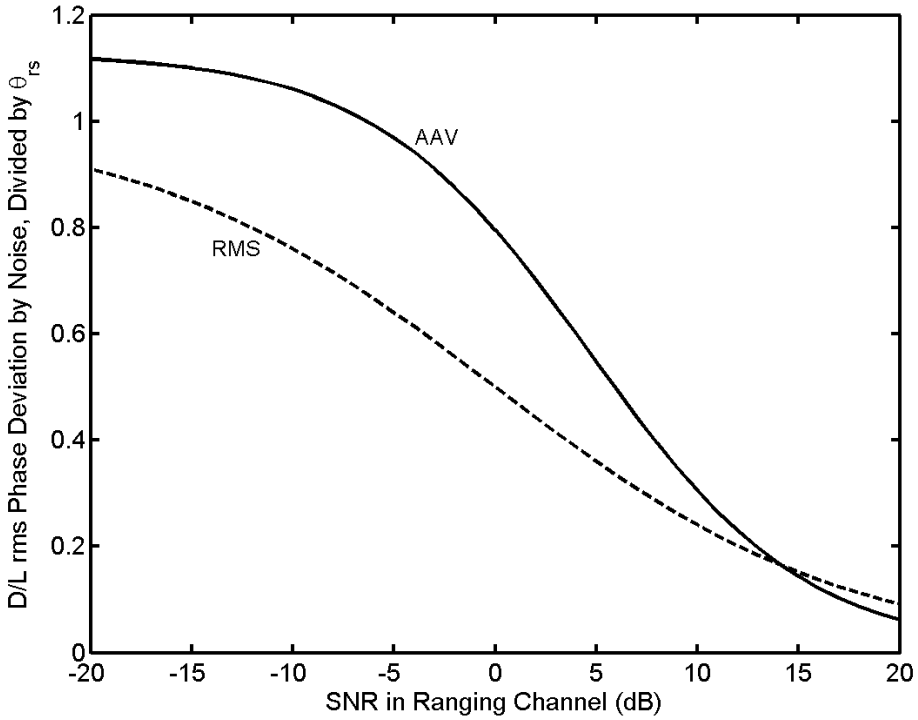

Figure 6. Downlink rms Phase Deviation by Noise (No Command Feedthrough)

2.3.2.1.2 AGC with Constant Root-Mean-Square Voltage

In some transponders, especially older designs, the ranging channel has an AGC that enforces a constant rms voltage at the AGC output. Since an unchanging rms voltage corresponds to an unchanging power, this type of AGC is also called a power-controlled AGC.

An AGC that enforces constant rms voltage (equivalently, constant power) at the AGC output is characterized by the following relationship among the rms phase deviations θ_r, θ_{cmd}, θ_n, and θ_{rs}.

$$\theta_r{}^2 + \theta_{cmd}{}^2 + \theta_n{}^2 = \theta_{rs}{}^2 \tag{46}$$

In other words, the total power in the turn-around ranging channel, which equals the ranging signal power plus the feedthrough command signal power plus the noise power in the channel bandwidth, equals a constant value. The rms phase deviations are given by

$$\theta_r = \theta_{rs} \cdot \sqrt{\frac{\rho_r}{1 + \rho_r + \rho_{cmd}}} \tag{47}$$

$$\theta_{cmd} = \theta_{rs} \cdot \sqrt{\frac{\rho_{cmd}}{1 + \rho_r + \rho_{cmd}}} \tag{48}$$

$$\theta_n = \frac{\theta_{rs}}{\sqrt{1 + \rho_r + \rho_{cmd}}} \tag{49}$$

The ratio θ_r/θ_{rs} is plotted as a function of ρ_r in Figure 5 for the case of no command feedthrough: $\rho_{cmd} = 0$ and $\theta_{cmd} = 0$. The dashed curve labeled RMS is valid for a turn-around ranging channel whose AGC enforces a constant rms voltage at the AGC output. The RMS curve of Figure 5 comes from Equation (47) with $\rho_{cmd} = 0$.

The ratio θ_n/θ_{rs} is plotted as a function of ρ_r in Figure 6 for the case of no command feedthrough: $\rho_{cmd} = 0$ and $\theta_{cmd} = 0$. The dashed curve labeled RMS is valid for a turn-around ranging channel whose AGC enforces a constant rms voltage at the AGC output. The RMS curve of Figure 6 comes from Equation (49) with $\rho_{cmd} = 0$.

2.3.2.1.3 Comparison of Two AGC Types

As explained above, there are two types of AGC that have been employed in transponders with turn-around ranging channels. These two AGCs differ in the quantity that is kept constant: either the average of the absolute voltage (AAV) or the root-mean-square (RMS).

Figure 7 plots $P_R/P_T|_{D/L}$ as a function of ρ_r for each of the two AGC types. For all curves in this figure, there is no telemetry and there is no command feedthrough. For each AGC type, there are two curves: one for $\theta_{rs} = 0.2$ rad rms and a second for $\theta_{rs} = 0.4$ rad rms. $P_R/P_T|_{D/L}$ was calculated using Equation (27). The phase deviations θ_r and θ_n needed within

Equation (27) were calculated using the equations of Subsection 2.3.2.1.1 for the AAV curves and Subsection 2.3.2.1.2 for the RMS curves.

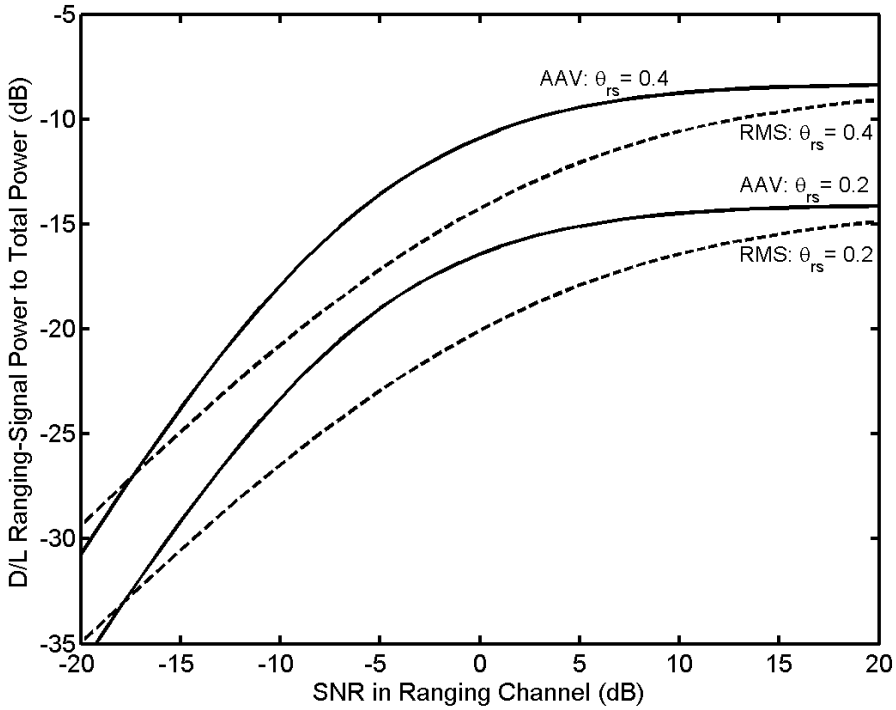

Figure 7. Downlink Ranging-Signal Power to Total Power (No Telemetry, No Command)

Figure 8 plots the carrier suppression $P_C/P_T|_{D/L}$ as a function of ρ_r for each of the two AGC types. For all curves in this figure, there is no telemetry and there is no command feedthrough. For each AGC type, there are two curves: one for $\theta_{rs} = 0.2$ rad rms and a second for $\theta_{rs} = 0.4$ rad rms. $P_C/P_T|_{D/L}$ was calculated using Equation (26). The phase deviations θ_r and θ_n needed within Equation (26) were calculated using the equations of Subsection 2.3.2.1.1 for the AAV curves and Subsection 2.3.2.1.2 for the RMS curves.

2.3.2.2 Regenerative Ranging

A regenerative ranging channel demodulates the uplink carrier, tracks the range clock, detects the range code, and modulates a ranging signal on the downlink. A regenerative ranging channel produces a clean ranging signal, free of command feedthrough and with little noise, because this channel has a small bandwidth. (This bandwidth is orders-of-magnitude smaller than the 1.5-MHz bandwidth of the typical turn-around ranging channel.)

A transponder that supports regenerative ranging will, of necessity, be designed to track a specific PN range code. This could be the DSN range code, the T4B range code, or the T2B range code. The equations appearing in this subsection are applicable to any of these three PN range codes, as long as the transponder in question is designed to support regenerative ranging with that particular range code.

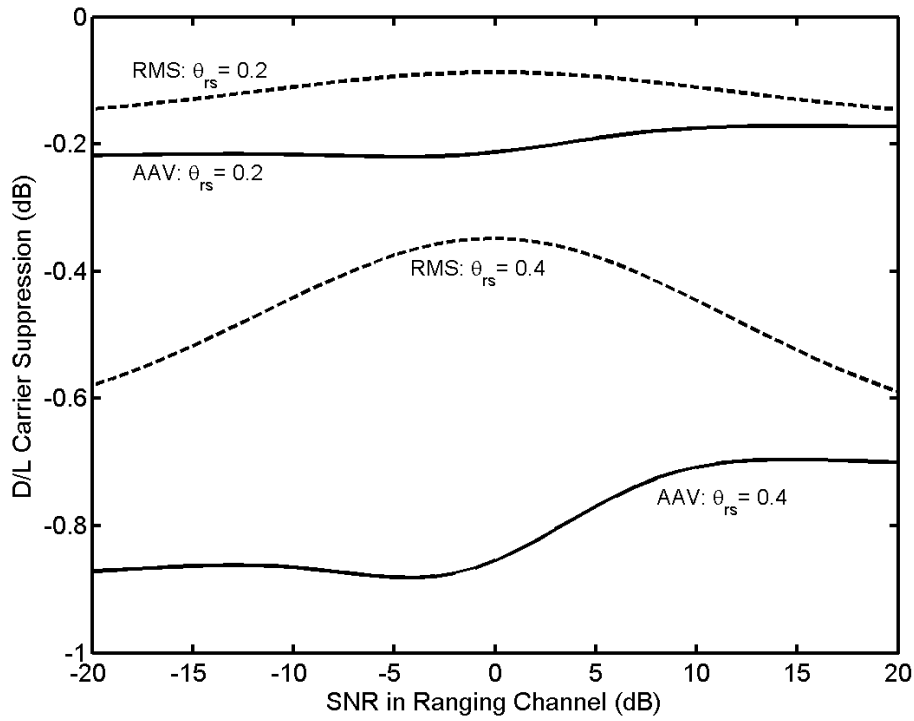

Figure 8. Downlink Carrier Suppression (No Telemetry, No Command)

For the purpose of calculating the distribution of power on the downlink in the case of regenerative ranging, the following equations may be used. There will, in general, be phase jitter on the downlink ranging signal that is caused by uplink thermal noise and this jitter is an error source for the two-way range measurement. This error is considered in Section 2.5.

The carrier suppression is

$$\left.\frac{P_C}{P_T}\right|_{\mathrm{D/L}} = J_0{}^2\left(\sqrt{2}\,\theta_{rs}\right) \cdot \cos^2(\theta_{tlm}) \tag{50}$$

The ratio of available ranging signal power to total power is

$$\left.\frac{P_R}{P_T}\right|_{\mathrm{D/L}} = 2\,J_1{}^2\left(\sqrt{2}\,\theta_{rs}\right) \cdot \cos^2(\theta_{tlm}) \tag{51}$$

The ratio of available telemetry (data) signal power to total power is

$$\left.\frac{P_D}{P_T}\right|_{\mathrm{D/L}} = J_0{}^2\left(\sqrt{2}\,\theta_{rs}\right) \cdot \sin^2(\theta_{tlm}) \tag{52}$$

In these equations, θ_{rs} is the (strong-signal) rms phase deviation of the downlink carrier by the ranging signal, and θ_{tlm} is the telemetry modulation index.

2.4 Uplink Spectrum

The spectrum of the uplink carrier is of some concern because of the very large transmitter powers used on the uplink for deep space missions. A mathematical model for this spectrum is given here for the case of a sinewave range clock and no command.

A PN ranging signal is periodic, so its spectrum consists of discrete spectral lines. The spectrum of an uplink carrier that has been phase modulated by only a PN ranging signal also consists of discrete spectral lines.

As described in Section 2.2, the composite chip sequence $c'(\cdot)$ is similar to the range clock $c_1{}'(\cdot)$, except that some chips are inverted. A discrepancy signal $d'(\cdot)$ is defined by

$$d'(i) = c_1{}'(i) \cdot c'(i) \tag{53}$$

$d'(i)$ equals $+1$ when the range clock and the composite code agree, which is most of the time. When the range clock and the composite code disagree, $d'(i)$ equals -1. The PN ranging signal may be mathematically modeled as $d(i)\sin(\pi t/T_c)$ for $iT_c \le t < (i+1)T_c$, where T_c is the chip period. In words, the PN ranging signal is a sinewave (range clock) of frequency $1/(2T_c)$ except that there is an occasional inversion of a half-cycle. When this signal phase modulates the uplink carrier with an rms phase deviation ϕ_r (radians rms), the fractional power in each discrete spectral line is given by

$$\frac{P_k}{P_T} = |X_k|^2 = \begin{cases} \text{fraction of uplink total power in the} \\ \text{discrete spectral line with frequency} \\ f_C + \dfrac{k}{LT_c} \end{cases} \tag{54}$$

where P_T is the total uplink power, f_C is the uplink carrier frequency, L is the period in chips of the composite code, k is an integer harmonic number, and X_k is given by

$$X_k = \frac{1}{L}\sum_{m=-\infty}^{\infty} \operatorname{sinc}\left(\frac{m}{2} - \frac{k}{L}\right) \sum_{n=0}^{L-1} J_m\left(\sqrt{2}\,\phi_r\, d'(n)\right) \exp\left[j\pi\left(n + \frac{1}{2}\right)\left(m - \frac{2k}{L}\right)\right] \tag{55}$$

where $J_m(\cdot)$ is the Bessel function of the first kind of order m, and

$$\operatorname{sinc}(x) = \frac{\sin(\pi x)}{\pi x} \tag{56}$$

Equation (55) may be evaluated numerically. The values of the Bessel functions decrease very rapidly with increasing $|m|$, so in practice it is possible to get good accuracy while including only a few terms from the sum over the integer m. In evaluating Equation (55), the following identity is useful.

$$J_{-m}(x) = \begin{cases} J_m(x), & m \text{ even} \\ -J_m(x), & m \text{ odd} \end{cases} \tag{57}$$

There is a symmetrical power distribution about the carrier. So for every discrete spectral line at $f_C + k/(LT)$ whose power is given by Equation (54), there is also a discrete spectral line at $f_C - k/(LT)$ with the same power.

Figure 9 illustrates the uplink spectrum for a sinewave range clock with the DSN range code and an rms phase deviation $\phi_r = 0.2$ rad rms. The horizontal axis represents the ratio of the frequency offset from the residual carrier to the range-clock frequency. The vertical axis is the ratio of the power in a discrete-spectral line to the total signal power, expressed in decibels. The residual carrier is located at the horizontal coordinate 0, and it has a power of -0.2 dB relative to P_T. In other words, the carrier suppression is -0.2 dB. The lower fundamental harmonic has a horizontal coordinate of -1 (a frequency of $f_C - f_{RC}$), and the upper fundamental harmonic has a horizontal coordinate of $+1$ (a frequency of $f_C + f_{RC}$); each of these has a power of -17.5 dB relative to P_T. The lower second harmonic has a horizontal coordinate of -2 (a frequency of $f_C - 2f_{RC}$), and the upper second harmonic has a horizontal coordinate of $+2$ (a frequency of $f_C + 2f_{RC}$); each of these has a power of -39.7 dB relative to P_T. The smaller spectral lines that lie between $f_C - 2f_{RC}$ and $f_C + 2f_{RC}$ arise from the occasional inversions of half-cycles as represented by $d'(i)$; this is the spectrum spreading that permits the amibiguity to be resolved.

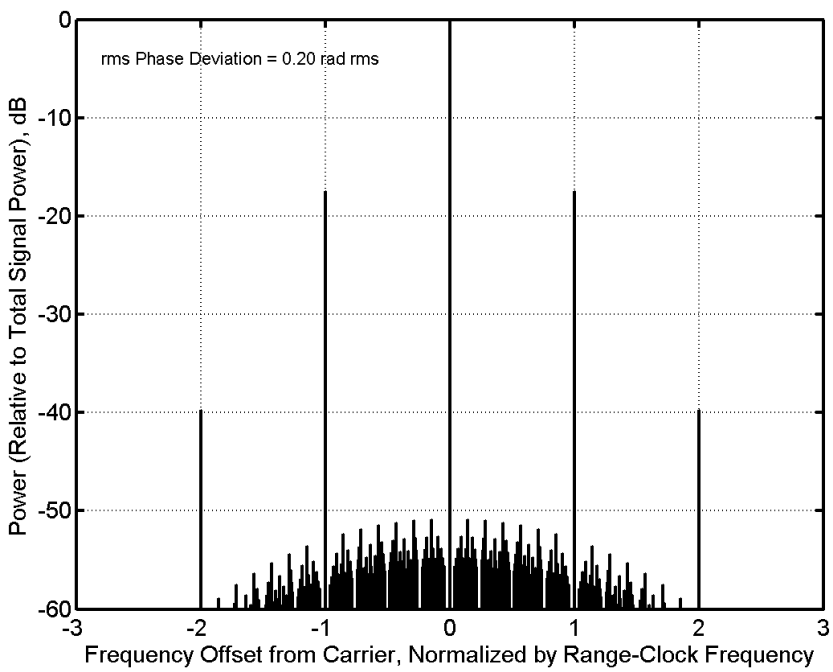

Figure 9. Uplink Spectrum for the DSN Range Code Ranging Signal

2.5 Range Measurement Performance

Thermal noise has two effects on range measurements. First, there is a standard deviation of range measurement error due to thermal noise. Second, there is a probability of acquisition of the range measurement that is less than 100% due to the presence of thermal noise. The cross-correlation factors of a composite code plays a role in the performance of PN ranging in the presence of thermal noise.

2.5.1 Cross-Correlation Factors

The cross-correlation factors R_n (with zero delay) are defined by

$$R_n = \frac{1}{L}\sum_{i=0}^{L-1} c'(i)c_n{}'(i) \tag{58}$$

where L is the period (in chips) of the composite code, $c'(i) = \pm 1$ is the chip sequence, and $c_n{}'(i) = \pm 1$ is the (periodic extension of the) chip sequence for the *n*-th component code. The cross-correlation factors are given in tables that follow: Table 3 for the DSN range code, Table 4 for the T4B code, and Table 5 for the T2B code.

Table 3. Cross-Correlation Factors, DSN Range Code

n	λ_n	R_n
1	2	0.9544
2	7	0.0456
3	11	0.0456
4	15	0.0456
5	19	0.0456
6	23	0.0456

Table **4**. Cross-Correlation Factors, T4B (Reference 4)

n	λ_n	R_n
1	2	0.9387
2	7	0.0613
3	11	0.0613
4	15	0.0613
5	19	0.0613
6	23	0.0613

Table 5. Cross-Correlation Factors, T2B (Reference 4)

n	λ_n	R_n
1	2	0.6274
2	7	0.2447
3	11	0.2481
4	15	0.2490
5	19	0.2492
6	23	0.2496

2.5.2 Downlink Ranging Signal Power to Noise Spectral Density

P_R/N_0, the ratio of the downlink ranging signal power to noise spectral density, is given by

$$\frac{P_R}{N_0} = \left.\frac{P_R}{P_T}\right|_{\mathrm{D/L}} \cdot \left.\frac{P_T}{N_0}\right|_{\mathrm{D/L}} \tag{59}$$

Equation (59) is applicable when there are no significant sources of interference (beyond the downlink thermal noise). Considered in the next subsection is the scenario where additional interference is present. $P_T/N_0|_{D/L}$ is the downlink total signal to noise spectral density ratio. $P_R/P_T|_{D/L}$ is the ratio of downlink ranging signal power to total power. $P_R/P_T|_{D/L}$ is given by Equation (27) for turn-around (non-regenerative) ranging and by Equation (51) for regenerative ranging.

2.5.3 Effect of Interference

In addition to the thermal noise that arises on the downlink, which is characterized by the noise spectral density $N_0|_{\mathrm{D/L}}$, there are sources of interference to the range measurement. Often the most important interference to the range measurement is telemetry; this interference occurs when there is spectral overlap of telemetry sidebands with the PN code components. When a non-regenerative (turn-around) ranging channel is used, the uplink noise and command signal can pass through the ranging channel and become modulated onto the downlink carrier. Finally, there are intermodulation products on the downlink.

In quantifying the effect of interference on range measurement, one considers the quadrature channel of the downlink receiver. It is in this quadrature receiver channel that the range correlations occur. The model employed here regards the interference in the quadrature channel as folding into the downlink thermal noise, so that the *effective* downlink noise spectral density is $N_0|_{\mathrm{D/L}} \cdot \Gamma_Q$, where $\Gamma_Q \geq 1$. In other words, Γ_Q is the factor by which the downlink noise floor increases in the downlink receiver's quadrature channel due to the presence of

telemetry, command feedthrough, uplink noise (that has been transponded to the downlink), and intermodulation products. This is the model used in Reference 3.

Another, equivalent way of stating the above is to define an effective P_R/N_0.

$$\text{effective } \frac{P_R}{N_0} = \left.\frac{P_R}{P_T}\right|_{\mathrm{D/L}} \cdot \left.\frac{P_T}{N_0}\right|_{\mathrm{D/L}} \cdot \frac{1}{\Gamma_Q} \tag{60}$$

When significant interference is present, the effective P_R/N_0 is smaller than that given by Equation (59). In this case, the effective P_R/N_0 should be calculated from Equation (60).

The various sources of interference in the quadrature channel may be taken into account in this manner:

$$\Gamma_Q = 1 + \mathrm{K}_{NQ} + \mathrm{K}_{tlm} + \mathrm{K}_{fth} \tag{61}$$

where

K_{NQ} = contribution from intermodulation products and transponded uplink noise
K_{tlm} = contribution from telemetry
K_{fth} = contribution from feedthrough command

For a non-regenerative ranging channel, K_{NQ} may be approximated as

$$\mathrm{K}_{NQ} = \frac{1}{B_R} \cdot \left.\frac{P_T}{N_0}\right|_{\mathrm{D/L}} \cdot \left.\frac{P_{NQ}}{P_T}\right|_{\mathrm{D/L}} \tag{62}$$

where $P_T/N_0|_{D/L}$ is the downlink total signal to noise spectral density ratio and B_R is the bandwidth of the transponder's ranging channel. The new term $P_{NQ}/P_T|_{D/L}$ is the power in uplink noise (transponded to the downlink) and quadrature-channel intermodulation products, relative to the total downlink power.

$$\begin{aligned} \left.\frac{P_{NQ}}{P_T}\right|_{\mathrm{D/L}} &= {\theta_n}^2 \\ &\cdot e^{-{\theta_n}^2} \\ &\times \left[{J_0}^2\left(\sqrt{2}\,\theta_r\right) \cdot \cos^2(\theta_{cmd}) \cdot \cos^2(\theta_{tlm}) \right. \\ &+ 2{J_1}^2\left(\sqrt{2}\,\theta_r\right) \cdot \cos^2(\theta_{cmd}) \cdot \sin^2(\theta_{tlm}) \\ &\left. + {J_0}^2\left(\sqrt{2}\,\theta_r\right) \cdot \sin^2(\theta_{cmd}) \cdot \sin^2(\theta_{tlm})\right] \end{aligned} \tag{63}$$

The variables θ_r, θ_{tlm}, θ_{cmd}, and θ_n have been defined previously. They are the rms phase deviations of the downlink carrier due to a ranging signal (θ_r), telemetry (θ_{tlm}), command feedthrough (θ_{cmd}), and transponded uplink noise (θ_n).

The following subsections provide models for K_{tlm} and K_{fth} that are applicable to bi-polar telemetry and bi-polar command. As before, "bi-polar" means either NRZ or bi-phase pulses that directly phase-modulate the carrier. These models for K_{tlm} and K_{fth}, in their most general form, are complicated. Therefore, curve-fit approximations are also given below; these curve-fit approximations should ease the task of implementing interference models in a spreadsheet.

2.5.3.1 Interference from Telemetry and Feedthrough Command (Bi-Polar Signaling)

The models for K_{tlm} and K_{fth} given here are applicable to bi-polar telemetry and bi-polar command. In other words, it is assumed here that NRZ or bi-phase symbols directly phase-modulate the carrier.

For each PN code component, the effect of the interference on that component's correlation is calculated. ${K^{(n)}}_{tlm}$ characterizes the telemetry interference to the correlation of component n, for $n = 1, 2, 3, 4, 5,$ or 6. Similarly, ${K^{(n)}}_{fth}$ characterizes the feedthrough-command interference to the correlation of component n. The six PN code components are listed in Table 2. All three of the range codes—DSN, T4B, and T2B—are built from this common set of PN code components. (The differences among the DSN, T4B, and T2B range codes arise from how the PN code components are combined.) Because the models given below are based on the correlations with the 6 PN code components and because these PN code components are the same for all three range codes—DSN, T4B, and T2B—these models are applicable to all three range codes.

K_{tlm} is taken to be the maximum of the six ${K^{(n)}}_{tlm}$, $n = 1, 2, 3, 4, 5,$ or 6.

$$\mathrm{K}_{tlm} = \max_{n} {K^{(n)}}_{tlm} \tag{64}$$

Equation (64) is an approximation; it is based on the idea that the weakest correlation defines, approximately, the performance of the range measurement in the presence of thermal noise plus telemetry interference.

In the model for the effect of command feedthrough, K_{fth} is taken to be the maximum of the six ${K^{(n)}}_{fth}$, $n = 1, 2, 3, 4, 5,$ or 6.

$$\mathrm{K}_{fth} = \max_{n} {K^{(n)}}_{fth} \tag{65}$$

Equation (65) is an approximation; it is based on the idea that the weakest correlation defines, approximately, the performance of the range measurement in the presence of thermal noise plus command-feedthrough interference.

The individual ${K^{(n)}}_{tlm}$ are calculated as

$${K^{(n)}}_{tlm} = \left.\frac{P_T}{N_0}\right|_{\mathrm{D/L}} \cdot \left.\frac{P_D}{P_T}\right|_{\mathrm{D/L}} \cdot \begin{cases} S_{tlm}(f_{1,1}), & n = 1 \\ \displaystyle\sum_{k=0}^{\infty} P_{n,k}\, S_{tlm}(f_{n,k}), & 2 \le n \le 6 \end{cases} \tag{66}$$

$P_T/N_0|_{D/L}$ is the downlink total signal to noise spectral density ratio. $P_D/P_T|_{D/L}$ is the ratio of telemetry power to total power, as given by Equation (28). $S_{tlm}(\cdot)$ is the one-sided, unity-power, power spectral density of telemetry, an expression for which appears below. The variables $f_{n,k}$ and $P_{n,k}$ are the frequencies and relative powers of discrete spectral lines associated with component PN code n.

The individual ${K^{(n)}}_{fth}$ are calculated as

$$K^{(n)}{}_{fth} = \left.\frac{P_T}{N_0}\right|_{\mathrm{D/L}} \cdot \left.\frac{P_{fth}}{P_T}\right|_{\mathrm{D/L}} \cdot \begin{cases} S_{cmd}(f_{1,1}), & n = 1 \\ \sum_{k=0}^{\infty} P_{n,k}\, S_{cmd}(f_{n,k}), & 2 \le n \le 6 \end{cases} \tag{67}$$

$P_{fth}/P_T\big|_{D/L}$ is the ratio of feedthrough-command power to total power, which is given by Equation (29). $S_{cmd}(\cdot)$ is the one-sided, unity-power, power spectral density of command, an expression for which appears below. The variables $f_{n,k}$ and $P_{n,k}$ are the frequencies and relative powers of discrete spectral lines associated with component PN code n.

The one-sided, unity-power, power spectral density of telemetry is

$$S_{tlm}(f) = \begin{cases} 2T_{tlm} \cdot \dfrac{\sin^2(\pi f T_{tlm})}{(\pi f T_{tlm})^2}, & \mathrm{NRZ} \\ 2T_{tlm} \cdot \dfrac{\sin^4(\pi f T_{tlm}/2)}{(\pi f T_{tlm}/2)^2}, & \mathrm{Bi-phase} \end{cases} \tag{68}$$

where T_{tlm} is the telemetry symbol period.

The one-sided, unity-power, power spectral density of command is

$$S_{cmd}(f) = \begin{cases} 2T_{cmd} \cdot \dfrac{\sin^2(\pi f T_{cmd})}{(\pi f T_{cmd})^2}, & \mathrm{NRZ} \\ 2T_{cmd} \cdot \dfrac{\sin^4(\pi f T_{cmd}/2)}{(\pi f T_{cmd}/2)^2}, & \mathrm{Bi-phase} \end{cases} \tag{69}$$

where T_{cmd} is the command symbol period.

Each PN code component $c_n{}'$ has a period of λ_n. The spectrum of $c_n{}'$ consists of discrete spectral lines. The k-th spectral line of $c_n{}'$ is denoted here by the ordered pair (n, k). The frequency of the (n, k) spectral line is denoted $f_{n,k}$. For example, the (1, 1) spectral line is the fundamental ($k = 1$) harmonic of the first code component; in other words, $f_{1,1}$ is the range-clock frequency. The general expression for $f_{n,k}$ is

$$f_{n,k} = \frac{k f_{\mathrm{chip}}}{\lambda_n} \qquad \begin{matrix} k \ge 0 \\ 2 \le n \le 6 \end{matrix} \tag{70}$$

where f_{chip} is the chip rate of the range code. The discrete Fourier transform (DFT) $\tilde{C}_n(k)$ of each $c_n{}'$ is required. The DFT of $c_n{}'$ is calculated using λ_n samples. The fractional power $P_{n,k}$ in the discrete spectral line at frequency $f_{n,k}$ is given by

$$P_{n,k} = 2 \cdot \frac{\sin^2(\pi k/\lambda_n)}{(\pi k)^2} \cdot \left|\tilde{C}_n(k)\right|^2 \qquad \begin{matrix} k \ge 0 \\ 2 \le n \le 6 \end{matrix} \tag{71}$$

The equations of this subsection permit calculation of K_{tlm} and K_{fth}. The only $S_{tlm}(f)$ and $S_{cmd}(f)$ models provided here are for the cases of NRZ or bi-phase pulses directly phase-modulated on the carrier.

2.5.3.2 Curve-Fit Approximations for Interference Models

The interference models of Subsection 2.5.3.1 are approximate models, but even those approximate models are rather complicated. Curve-fits to those models are given below. Of course, the curve-fits represent an additional layer of approximation.

The curve-fit for the telemetry interference model is accomplished by first rewriting Equations (64) and (66) as

$$\mathrm{K}_{tlm} = \left.\frac{P_T}{N_0}\right|_{\mathrm{D/L}} \cdot \left.\frac{P_D}{P_T}\right|_{\mathrm{D/L}} \cdot T_{tlm} \cdot \hat{S}_{tlm}(f_{\mathrm{chip}} T_{tlm}) \tag{72}$$

where

$$\hat{S}_{tlm}(f_{\mathrm{chip}} T_{tlm}) = \frac{1}{T_{tlm}} \cdot \max_n \begin{cases} S_{tlm}(f_{1,1}), & n = 1 \\ \sum_{k=0}^{\infty} P_{n,k}\, S_{tlm}(f_{n,k}), & 2 \le n \le 6 \end{cases} \tag{73}$$

$\hat{S}_{tlm}(f_{\mathrm{chip}} T_{tlm})$ is the maximum (over the six PN code components) of the weighted average of the one-sided, unity-power, telemetry power spectral density, normalized by the telemetry symbol period. The weighted average occurs over the frequencies ($f_{n,k}$) associated with the discrete spectral lines of each PN code component.

$\hat{S}_{tlm}(f_{\mathrm{chip}} T_{tlm})$ is a function of the product of the chip rate f_{chip} and the telemetry symbol period T_{tlm}. Both the input $f_{\mathrm{chip}} T_{tlm}$ and the output of the function $\hat{S}_{tlm}(f_{\mathrm{chip}} T_{tlm})$ are dimensionless. $\hat{S}_{tlm}(f_{\mathrm{chip}} T_{tlm})$ also depends on the nature of the telemetry spectrum. A curve-fit appears below both for NRZ telemetry symbols and for bi-phase telemetry symbols (directly phase-modulating the downlink carrier). For NRZ telemetry,

$$\hat{S}_{tlm}(f_{\mathrm{chip}} T_{tlm}) \cong 0.090 + 1.88 \exp(-0.46\, f_{\mathrm{chip}} T_{tlm}) \qquad \text{NRZ} \tag{74}$$

For bi-phase telemetry,

$$\hat{S}_{tlm}(f_{\mathrm{chip}} T_{tlm}) \cong \begin{cases} 2 \cdot \sin^4(\pi f_{\mathrm{chip}} T_{tlm}/4)/(\pi f_{\mathrm{chip}} T_{tlm}/4)^2, & f_{\mathrm{chip}} T_{tlm} \le 2.25 \\ 0.090 + 0.77 \exp(-0.20\, f_{\mathrm{chip}} T_{tlm}), & f_{\mathrm{chip}} T_{tlm} > 2.25 \end{cases} \tag{75}$$

Equation (72) can also be written as

$$\mathrm{K}_{tlm} = \left.\frac{E_S}{N_0}\right|_{\mathrm{D/L}} \cdot \hat{S}_{tlm}(f_{\mathrm{chip}} T_{tlm}) \tag{76}$$

where $E_S/N_0|_{\mathrm{D/L}}$ is the ratio of the telemetry symbol energy to the noise spectral density, and where this noise spectral density only accounts for thermal noise originating on the downlink.

$\hat{S}_{tlm}(f_{\mathrm{chip}} T_{tlm})$ is plotted as a function of $f_{\mathrm{chip}} T_{tlm}$ for both NRZ telemetry and for bi-phase telemetry in Figure 10. For the bi-phase curve, there is a slope discontinuity at $f_{\mathrm{chip}} T_{tlm} = 2.25$. This slope discontinuity originates with the approximation of Equation (64).

For $f_{\text{chip}}T_{tlm} \leq 2.25$, the largest term is that associated with the range clock; this dominant term is $K^{(1)}{}_{tlm}$. For $f_{\text{chip}}T_{tlm} > 2.25$, the largest term is one of the others: $K^{(n)}{}_{tlm}$ for $2 \leq n \leq 6$.

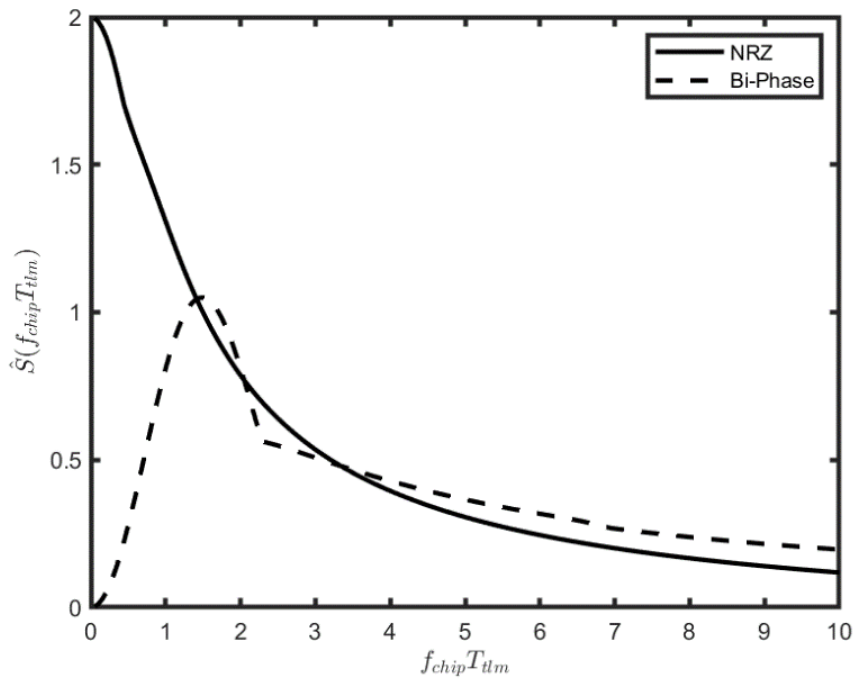

Figure 10. Curve-Fit Function for Modeling Increase in Quadrature-Channel Noise Floor

Once $\hat{S}_{tlm}(f_{\text{chip}}T_{tlm})$ is determined from a curve-fit, Equation (72) or (76) can be used to calculate K_{tlm}. In general, there can be other sources of interference (in addition to telemetry) that must be taken into account. Equation (61) is used to calculate Γ_Q.

Figure 11 plots Γ_Q, in decibels, as a function of $f_{\text{chip}}T_{tlm}$ with $E_S/N_0|_{\text{D/L}}$ as a parameter. This figure represents a scenario where telemetry is the only source of interference to the range measurement and the telemetry symbols are NRZ. The three curves in this figure correspond to the following values of $E_S/N_0|_{\text{D/L}}$: -3 dB, 0 dB, and $+3$ dB. The larger the $E_S/N_0|_{\text{D/L}}$, the larger is Γ_Q. Also, for NRZ telemetry, Γ_Q becomes larger as $f_{\text{chip}}T_{tlm}$ decreases.

The upper bound on K_{tlm} for NRZ telemetry is

$$\mathrm{K}_{tlm} \leq 2T_{tlm} \cdot \left.\frac{P_T}{N_0}\right|_{\text{D/L}} \cdot \left.\frac{P_D}{P_T}\right|_{\text{D/L}} \qquad \text{NRZ} \qquad (77)$$

$P_T/N_0|_{D/L}$ is the downlink total signal to noise spectral density ratio. $P_D/P_T|_{D/L}$ is the ratio of telemetry power to total power, as given by Equation (28). When the telemetry symbol rate is large compared with the range-code chip rate (that is, when $f_{\text{chip}}T_{tlm} \ll 1$), this upper bound on K_{tlm} for NRZ telemetry is tight and the upper bound is a good approximation for K_{tlm}.

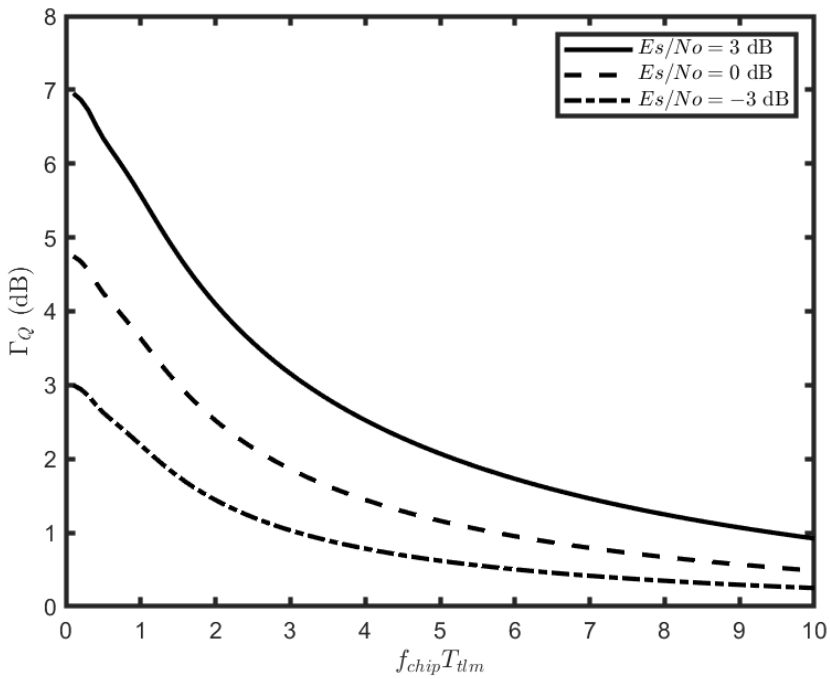

Figure 11. Increase (dB) in Range-Measurement Noise Floor Due to NRZ Telemetry

The upper bound on K_{tlm} for bi-phase telemetry is

$$\mathrm{K}_{tlm} \leq 1.1 \cdot T_{tlm} \cdot \left.\frac{P_T}{N_0}\right|_{\mathrm{D/L}} \cdot \left.\frac{P_D}{P_T}\right|_{\mathrm{D/L}} \qquad \text{bi-phase} \tag{78}$$

For bi-phase telemetry when $f_{\mathrm{chip}}T_{tlm} \ll 1$, the telemetry interference to a range measurement may be negligible.

The procedure for calculating K_{fth}, which is needed to estimate the effect of command-feedthrough interference on the range measurement, is very similar to the calculation of K_{tlm}. In order to take advantage of curve-fits, K_{fth} can be calculated by

$$\mathrm{K}_{fth} = \left.\frac{P_T}{N_0}\right|_{\mathrm{D/L}} \cdot \left.\frac{P_{fth}}{P_T}\right|_{\mathrm{D/L}} \cdot T_{cmd} \cdot \hat{S}_{cmd}(f_{\mathrm{chip}}T_{cmd}) \tag{79}$$

where $P_T/N_0|_{D/L}$ is the downlink total signal to noise spectral density ratio and $P_{fth}/P_T\big|_{D/L}$ is the ratio of feedthrough-command power to total power, as given by Equation (29). The dimensionless function $\hat{S}_{cmd}(f_{\mathrm{chip}}T_{cmd})$ is given by:

$$\hat{S}_{cmd}(f_{\text{chip}}T_{cmd}) = \frac{1}{T_{cmd}} \cdot \max_n \begin{cases} S_{cmd}(f_{1,1}), & n = 1 \\ \sum_{k=0}^{\infty} P_{n,k}\, S_{cmd}(f_{n,k}), & 2 \le n \le 6 \end{cases} \tag{80}$$

Equation (80) is of the same form as Equation (73). The differences are that Equation (80) uses the command symbol period T_{cmd} and the one-sided, unity-power, power spectral density $S_{cmd}(\cdot)$ that is appropriate for command.

The curve-fits for $\hat{S}_{cmd}(f_{\text{chip}}T_{cmd})$ are of the same form as those for $\hat{S}_{tlm}(f_{\text{chip}}T_{tlm})$. Of course, these curve-fits use the product of the chip rate f_{chip} and the command symbol period T_{cmd}. For NRZ command symbols,

$$\hat{S}_{cmd}(f_{\text{chip}}T_{cmd}) \cong 0.090 + 1.88 \exp(-0.46\, f_{\text{chip}}T_{cmd}) \qquad \text{NRZ} \tag{81}$$

Whereas for bi-phase command symbols,

$$\hat{S}_{cmd}(f_{\text{chip}}T_{cmd}) \cong \begin{cases} 2 \cdot \sin^4(\pi f_{\text{chip}}T_{cmd}/4)/(\pi f_{\text{chip}}T_{cmd}/4)^2, & f_{\text{chip}}T_{cmd} \le 2.25 \\ 0.090 + 0.77 \exp(-0.20\, f_{\text{chip}}T_{cmd}), & f_{\text{chip}}T_{cmd} > 2.25 \end{cases} \tag{82}$$

The upper bound on K_{fth}, for NRZ command, is

$$\mathrm{K}_{fth} \le 2T_{cmd} \cdot \left.\frac{P_T}{N_0}\right|_{\mathrm{D/L}} \cdot \left.\frac{P_{fth}}{P_T}\right|_{\mathrm{D/L}} \qquad \text{NRZ} \tag{83}$$

$P_T/N_0|_{D/L}$ is the downlink total signal to noise spectral density ratio. $P_{fth}/P_T|_{D/L}$ is the ratio of feedthrough-command power to total power, as given by Equation (29). When the command symbol rate is large compared with the range-code chip rate (that is, when $f_{\text{chip}}T_{cmd} \ll 1$), this upper bound on K_{fth} is tight and the upper bound is a good approximation for K_{fth}.

The upper bound on K_{fth} for bi-phase command is

$$\mathrm{K}_{fth} \le 1.1 \cdot T_{cmd} \cdot \left.\frac{P_T}{N_0}\right|_{\mathrm{D/L}} \cdot \left.\frac{P_{fth}}{P_T}\right|_{\mathrm{D/L}} \qquad \text{bi-phase} \tag{84}$$

For bi-phase command when $f_{\text{chip}}T_{cmd} \ll 1$, the command-feedthrough interference to a range measurement may be negligible.

2.5.4 Range Measurement Error Due to Thermal Noise

The standard deviation σ_ρ of range measurement error, in meters rms, due to downlink thermal noise is given by

$$\sigma_\rho = \frac{c}{f_{RC} \cdot A_c \cdot R_1 \cdot \sqrt{32\pi^2 \cdot T \cdot (P_R/N_0)}} \tag{85}$$

where

c = speed of electromagnetic waves in vacuum, $299{,}792{,}458\ \mathrm{m/s}$

A_c= fractional loss of correlation amplitude due to frequency mismatch ($A_c \leq 1$)

R_1 = cross-correlation factor for the correlation against the range clock

T = range measurement integration time

f_{RC} = frequency of the range clock

$A_c = 1$ under the normal circumstances, in which the range clock is coherently related to the carrier. In the special case of non-coherent ranging, $A_c < 1$.

P_R/N_0, the ratio of the downlink ranging signal power to the downlink noise spectral density, is given by Equation (59) when there is no significant interference present or by Equation (60) when interference must be taken into account.

P_R, as it appears in P_R/N_0, is that portion of the power in the downlink ranging sidebands that is used in the range measurement, either in the correlation that determines the range measurement error or in the resolution of the ambiguity. The power ${R_1}^2 P_R$ is utilized in the correlation that determines the range measurement error. It may be noted that ${\sigma_\rho}^2$, the square of the standard deviation given in Equation (85), is inversely proportional to ${R_1}^2 P_R$. In the spectrum of the modulated downlink carrier, the power ${R_1}^2 P_R$ is evenly divided between the discrete spectral line f_{RC} hertz below the residual carrier and the discrete spectral line f_{RC} hertz above the residual carrier.

For the DSN and T4B codes, the standard deviation of range measurement error (meters) due to thermal noise is plotted in Figure 12 against the product $T \cdot (P_R/N_0)$, expressed in decibels: $10 \log(T \cdot P_R/N_0)$. These curves were calculated from Equation (85) using the cross-correlation factor R_1 given in Table 3 for the DSN range code and Table 4 for the T4B code. Also, the range clock was taken to be a 1-MHz sinewave and A_c was taken to be 1. The factor R_1 depends on the range code. For the DSN range code, $R_1 = 0.9544$. For the T4B code, $R_1 = 0.9387$. This difference is the reason the two curves in Figure 12 do not overlap.

The T2B code was designed to operate at smaller values of $T \cdot (P_R/N_0)$. For the T2B code, the standard deviation of range measurement error (meters) due to thermal noise is plotted in Figure 13. This curve was calculated from Equation (85) using the cross-correlation factor R_1 given in Table 5. The range clock was taken to be a 1-MHz sinewave, and A_c was taken to be 1. The factor P_R in the product $T \cdot (P_R/N_0)$ is that portion of the power in the downlink ranging sidebands that is used in the range measurement, either in the correlation that determines the range measurement error or in the resolution of the ambiguity.

The standard deviation of the two-way time delay σ_τ, in seconds, is related to σ_ρ, as given in Eq. (85), by

$$\sigma_\tau = \frac{2}{c} \cdot \sigma_\rho \tag{86}$$

The factor of 2 in Eq. (86) accounts for the fact that σ_ρ characterizes the error in the *one*-way range, while σ_τ characterizes the error in a *two*-way time delay. The standard deviation of the two-way phase delay σ_{RU}, as measured in range units, is related to σ_τ by

$$\sigma_{RU} = \begin{cases} \frac{f_S}{2} \cdot \sigma_\tau, & \text{S-band uplink} \\ \frac{221}{749} \cdot \frac{f_X}{2} \cdot \sigma_\tau, & \text{X-band uplink} \\ \frac{221}{2407} \cdot \frac{f_X}{2} \cdot \sigma_\tau, & \text{K-band uplink} \\ \frac{221}{3599} \cdot \frac{f_{Ka}}{2} \cdot \sigma_\tau, & \text{Ka-band uplink} \end{cases} \tag{87}$$

where f_S is the frequency of an S-band uplink carrier, f_X is the frequency of an X-band uplink carrier, f_K is the frequency of a K-band uplink carrier, and f_{Ka} is the frequency of a Ka-band uplink carrier.

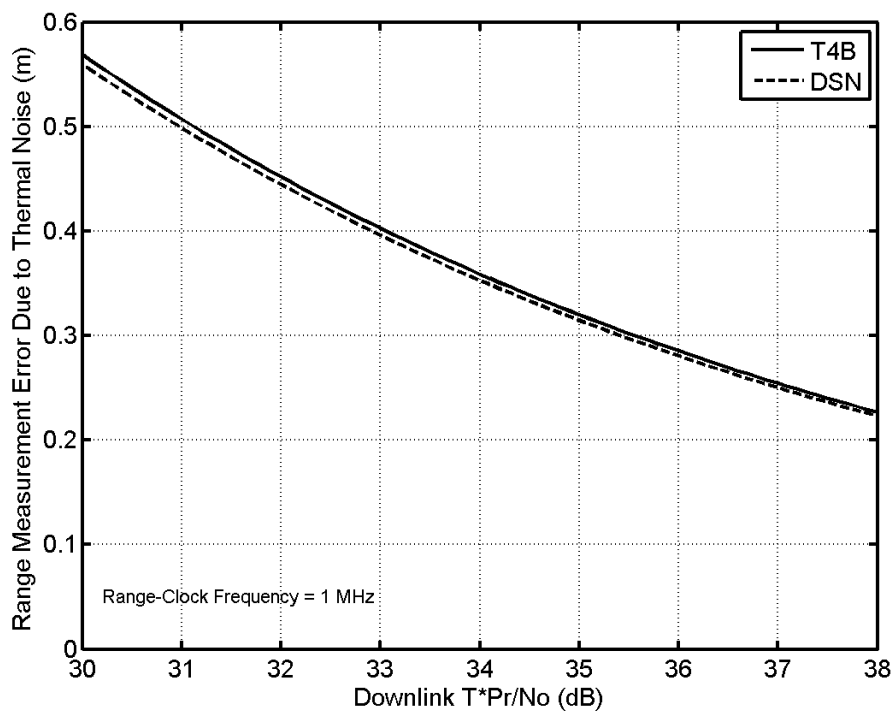

Figure 12. Standard Deviation of Range Measurement Error for the DSN and T4B Codes

2.5.4.1 Range Measurement Error for Turn-Around (Non-Regenerative) Ranging

For turn-around ranging, Equation (85) accounts for both uplink and downlink thermal noise. In this case, P_R is reduced by the effect of uplink noise and any command feedthrough. This can be understood from Equation (27) by noting that $P_R/P_T|_{D/L}$ depends on the rms phase deviations θ_r, θ_{cmd}, and θ_n.

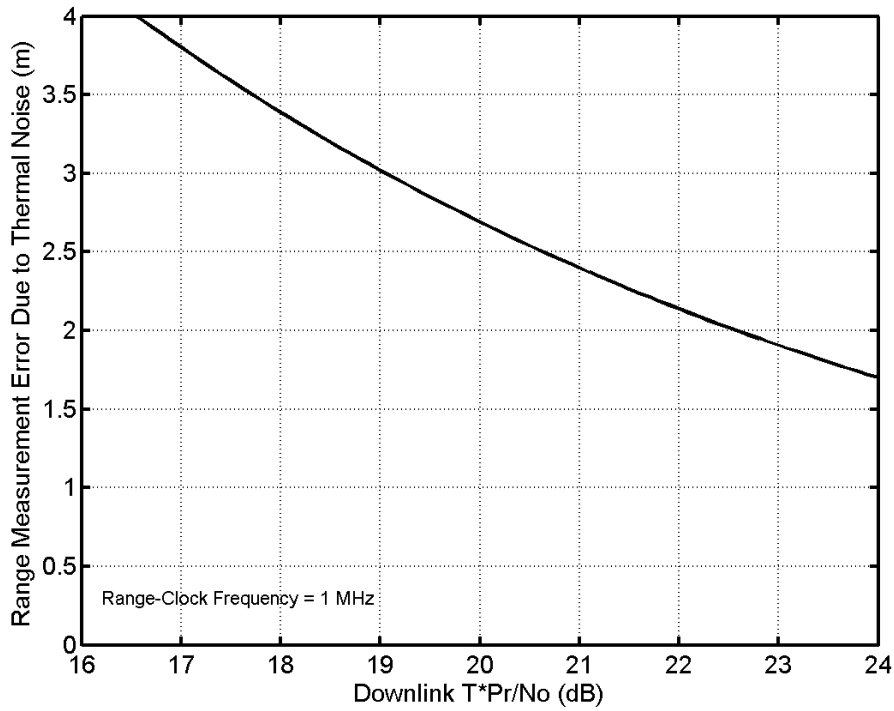

Figure 13. Standard Deviation of Range Measurement Error for the T2B Code

2.5.4.2 Range Measurement Error for Regenerative Ranging

For regenerative ranging, the standard deviation σ_{RR} of range measurement error, in meters rms, due to uplink and downlink thermal noise is given by

$$\sigma_{RR} = \sqrt{{\sigma_\rho}^2 + {\sigma_{\mathrm{U/L}}}^2} \tag{88}$$

${\sigma_\rho}^2$ is the square of the standard deviation σ_ρ of the range measurement error due to downlink thermal noise. σ_ρ is calculated from Equation (85). In the case of regenerative ranging, this calculation uses the $P_R/P_T|_{\mathrm{D/L}}$ that is defined in Equation (51). This (regenerative-ranging) $P_R/P_T|_{\mathrm{D/L}}$ contains no contribution from uplink thermal noise.

Uplink thermal noise causes phase jitter on the regenerated ranging signal. This phase jitter arises in the tracking loop that is part of the regeneration signal processing (Reference 5). This tracking jitter is a potential error source for the two-way range measurement. The standard deviation $\sigma_{\mathrm{U/L}}$ of range measurement error, meters rms, for this error source is given by

$$\sigma_{\mathrm{U/L}} = \frac{c}{4\pi R_1 f_{RC}} \sqrt{\frac{B_{RL}}{P_R/P_T|_{\mathrm{U/L}} \cdot P_T/N_0|_{\mathrm{U/L}}}} \tag{89}$$

where B_{RL} is the bandwidth of the loop that tracks the uplink range clock. The error $\sigma_{\mathrm{U/L}}$ only applies in the case of regenerative ranging. The range measurement error for a two-way, regenerative ranging measurement is computed as the root-sum-square of $\sigma_{\mathrm{U/L}}$ and σ_ρ, as indicated in Equation (88). For some missions it will be typical that $\sigma_{\mathrm{U/L}} \ll \sigma_\rho$, in which case σ_{RR} can be approximated as σ_ρ.

Regenerative ranging has better performance than turn-around ranging. A difference in bandwidth is the reason for this. With regenerative ranging, the bandwidth of the transponder's range-clock loop, B_{RL} in Equation (89), is typically small, perhaps a few hertz. With turn-around ranging, the bandwidth B_R of the transponder's ranging channel is typically about 1.5 MHz.

2.5.5 Probability of Acquisition

A correct determination of the range can only happen if the ambiguity is correctly resolved. This is accomplished with a set of correlations within the RRT between the received baseband ranging signal and local models of the component codes. A range measurement is successfully acquired when every code component is correctly acquired. The probability of acquisition P_{acq} for the range measurement is the product of the five probabilities P_n, $2 \le n \le 6$.

$$P_{\mathrm{acq}} = \prod_{n=2}^{6} P_n \tag{90}$$

P_n is the probability of acquiring the *n*-th component code ($2 \le n \le 6$). Each P_n is calculated by

$$P_n = \frac{1}{\sqrt{\pi}} \int_{-\infty}^{\infty} e^{-x^2} \left(\frac{1 + \mathrm{erf}\left(x + A_c\, R_n \sqrt{T \cdot (P_R/N_0)}\right)}{2} \right)^{\lambda_n - 1} dx \tag{91}$$

where λ_n and R_n are the code length (in chips) and cross-correlation factor for the *n*-th component code. Numerical integration is required to evaluate Equation (91). The error function $\mathrm{erf}(\cdot)$ is defined by

$$\mathrm{erf}(y) = \frac{2}{\sqrt{\pi}} \int_0^y e^{-t^2}\, dt \tag{92}$$

The value that Equation (90) gives for P_{acq} is, in general, greater than 0 and less than 1. P_{acq} is often characterized as a percentage (between 0% and 100%).

When interpreting Equation (91), it should be remembered that P_R is that portion of the power in the downlink ranging sidebands that is used in the range measurement. Not all of the power P_R is employed in acquisition (the resolution of the ambiguity). The power that helps with the code-component n correlation is ${R_n}^2 P_R$, where $2 \le n \le 6$.

Table 6 lists required values for $(A_c\, R_n)^2 \cdot T \cdot P_R/N_0$ (in decibels) as a function of λ_n (the code length) and P_n (the probability of acquiring the *n*-th component code). This table is based on Equation (91). The first column of Table 6 is $\log(P_n)$, where $\log(\cdot)$ is the common logarithm (the base-10 logarithm).

Table 6. Interpolation Table

Required $(A_c\, R_n)^2 \cdot T \cdot P_R/N_0$ (in decibels) for Given λ_n and P_n

$\log(P_n)$	$\lambda_n = 7$	$\lambda_n = 11$	$\lambda_n = 15$	$\lambda_n = 19$	$\lambda_n = 23$
-0.050	5.7	6.5	6.9	7.1	7.4
-0.040	6.2	6.9	7.2	7.5	7.7
-0.030	6.7	7.3	7.7	7.9	8.1
-0.020	7.4	7.9	8.3	8.5	8.7
-0.010	8.3	8.8	9.1	9.3	9.4
-0.009	8.4	8.9	9.2	9.4	9.5
-0.008	8.6	9.0	9.3	9.5	9.7
-0.007	8.7	9.2	9.4	9.6	9.8
-0.006	8.9	9.3	9.6	9.8	9.9
-0.005	9.1	9.5	9.8	9.9	10.1
-0.004	9.3	9.7	10.0	10.1	10.3
-0.003	9.6	10.0	10.2	10.4	10.5
-0.002	9.9	10.3	10.5	10.7	10.8
-0.001	10.5	10.8	11.0	11.1	11.3

Here is an example of how Table 6 can be used. If the desired P_n for a component code of length 19 is 0.99, then $\log(P_n) = -0.0044$. From Table 6, the decibel values 9.9 dB and 10.1 dB are found for $\log(P_n) = -0.005$ and $\log(P_n) = -0.004$, respectively. An interpolation suggests that $(A_c\, R_n)^2 \cdot T \cdot P_R/N_0$ must be about 10.0 dB in order to correctly acquire with probability $P_n = 0.99$ the component code having $\lambda_n = 19$. Of course, it is important to recall that $P_n = 0.99$ is not the probability of acquisition of the composite code. There are several component codes that must be correctly acquired before the range measurement is successfully acquired. P_{acq} is given by Equation (90), and it will be less than the value of any individual P_n.

For the DSN range code and the T4B code, P_{acq} is plotted in Figure 14 as a function of the product $T \cdot (P_R/N_0)$, in decibels: $10 \log(T \cdot P_R/N_0)$. For the T2B code, P_{acq} is plotted in Figure 15 as a function of the product $T \cdot (P_R/N_0)$, in decibels. The curves in these

two figures were calculated from Equations (90) and (91) using $A_c = 1$ and cross-correlation factors from Table 3, Table 4, and Table 5.

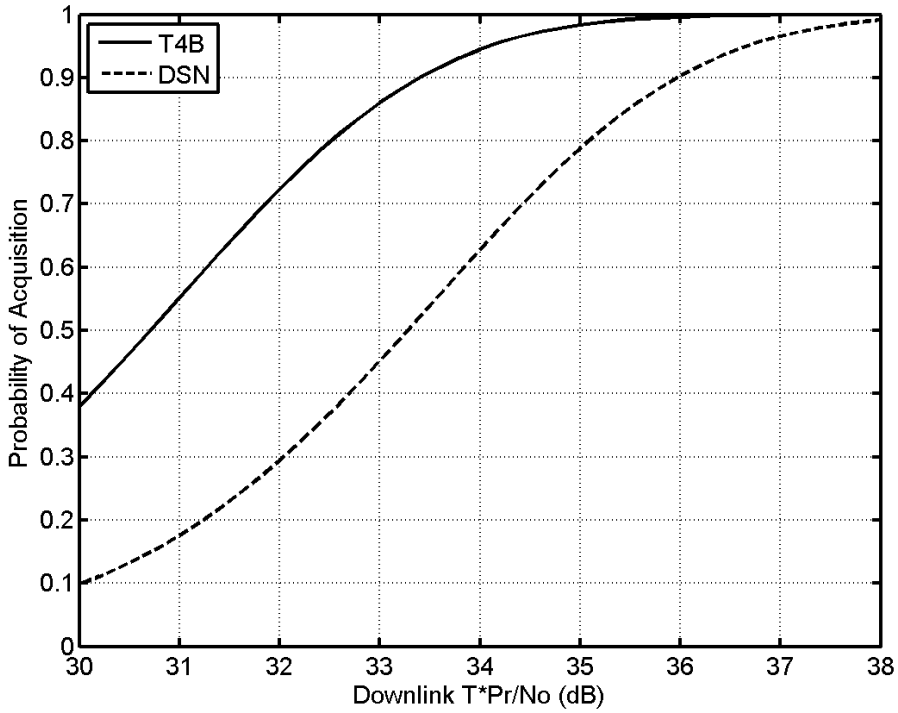

Figure 14. Probability of Acquisition for the DSN Range Code and the T4B Code

An approximation of P_{acq} may be calculated using the following curve fit:

$$P_{\text{acq}} = \begin{cases} c_3 Z^3 + c_2 Z^2 + c_1 Z + c_0, & Z_1 \le Z \le Z_2 \\ 1.00, & Z > Z_2 \end{cases} \tag{93}$$

where Z is the product $T \cdot (P_R/N_0)$ in units of decibels,

$$Z = 10 \log[T \cdot (P_R/N_0)] \quad \text{dB} \tag{94}$$

The parameters for the model of Equation (93) are given in Table 7. The correct set of parameters depends on the code (DSN range code, T4B, or T2B), as indicated in Table 7. The model of Equation (93) is not reliable for $Z < Z_1$ dB. For $Z > Z_2$ dB, the approximation $P_{\text{acq}} = 1$ may be used.

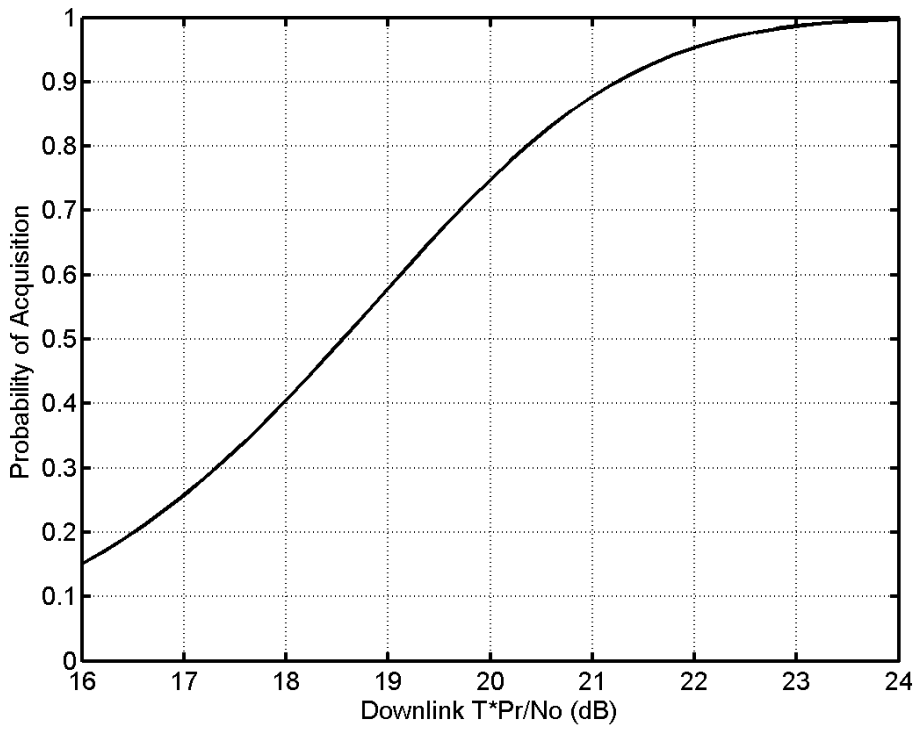

Figure 15. Probability of Acquisition for the T2B Code

Table 7. Parameters for Equation (93)

	DSN range code	T4B	T2B
Z_1	30 dB	28 dB	16 dB
Z_2	37 dB	35 dB	23 dB
c_3	-0.0039916	-0.0038441	-0.0037013
c_2	0.400534	0.356736	0.208431
c_1	-13.2253	-10.8645	-3.7427
c_0	144.154	109.048	21.833

Comparing Figure 12 and Figure 14, it becomes clear that the DSN range code was designed to give a σ_ρ of about 0.2 to 0.3 meter when the product $T \cdot P_R/N_0$ is just large enough (about 37 to 38 dB) to assure a high probability of acquisition. The T4B code has better acquisition performance than the DSN range code. Comparing Figure 13 and Figure 15, it can

be seen that the T2B code achieves a high P_{acq} for considerably smaller $T \cdot P_R/N_0$, but the price paid is a larger σ_ρ, about 2 meters.

2.5.6 Processing a Set of Range Measurements

For a given PN range code, a minimum $T \cdot (P_R/N_0)$ product is needed to achieve a high P_{acq}, and there is an approximate range measurement error (standard deviation) corresponding to this $T \cdot (P_R/N_0)$. In the example discussed above, the DSN range code ordinarily requires that $T \cdot (P_R/N_0)$ be about 37 to 38 dB in order to assure a high P_{acq}, and the corresponding range measurement error is about 0.2 to 0.3 meter.

Sometimes the available $T \cdot (P_R/N_0)$ is smaller than the minimum value for which a range code was designed to work. It is still possible to acquire range measurements with the correct resolution of the ambiguity even under the circumstance of a low $T \cdot (P_R/N_0)$. This is accomplished by using a large set of range measurements (obtained from one station tracking one spacecraft).

Reference 6 describes the "Plurality Voting Method" for accomplishing range acquisitions for a large measurement data set when $T \cdot (P_R/N_0)$ is low. This method employs range residuals for the given set of range measurements. A range residual is the difference between the measured two-way delay and the predicted two-way delay, where the predicted value is computed from a spacecraft ephemeris. Doppler velocity residuals can also be used. The Plurality Voting Method, making use of a large set of range measurements, increases the acquisition probability beyond that given in Eq. (90). This method does not, however, improve the standard deviation of acquired range measurements. The Plurality Voting Method has value in scenarios where $T \cdot (P_R/N_0)$ is adequate for the required range accuracy (standard deviation) but is inadequate (in the absence of this special method) for the required acquisition probability.

2.5.7 Comparison of PN Ranging and Sequential Ranging

It is instructive to compare the performance of turn-around PN ranging with sequential ranging (Reference 7). For both techniques, a minimum integration time T can be calculated as a function of P_R/N_0 for a given range measurement error σ_ρ (due to thermal noise) and a given P_{acq}. For the purpose of the present comparison, σ_ρ is taken to be 0.2 m and P_{acq} is taken to be 0.99. Furthermore, the range-clock frequency f_{RC} is taken to be 1 MHz.

For the analysis presented here, the minimum T is calculated for the DSN range code by finding, for a given P_R/N_0, the smallest T that satisfies the two constraints: $\sigma_\rho < 0.2$ m, as calculated with Equation (85), and $P_{\text{acq}} > 0.99$, as calculated with Equations (90) and (91).

For sequential ranging, the number of sinewaves in the sequence is taken to be 20; this gives an ambiguity resolution of 78,590 km, comparable with the 75,660 km ambiguity resolution offered by the DSN range code. The minimum T for sequential ranging is the minimum cycle time consistent with a range error (due to thermal noise) of 0.2 m and a probability of acquisition of 0.99. The cycle time includes the range-clock integration time T_1 plus 19 times the ambiguity integration time T_2 plus the required deadtime seconds.

Figure 16 shows the ratio of the minimum T (cycle time) for sequential ranging to the minimum T (integration time) for PN ranging as a function of P_R/N_0. This figure is intended

as a performance comparison of sequential ranging and turn-around PN ranging. The underlying assumption is that P_R/N_0 is approximately the same for these two ranging techniques for a given set of link parameters.

In principle, a plot like this also applies to regenerative PN ranging. However, P_R/N_0 will not be the same for regenerative PN ranging and (non-regenerative) sequential ranging. In general, it is expected that regenerative PN ranging will out-perform (non-regenerative) sequential ranging.

The results of Figure 16 suggest that sequential ranging has a small performance advantage over turn-around PN ranging for small P_R/N_0 (less than about 12 dB-Hz for the parameters used here) but that PN ranging has a performance advantage for P_R/N_0 larger than this. When the sequential ranging minimum T is larger than the PN ranging minimum T (that is, when P_R/N_0 is larger than about 12 dB-Hz), the choice to use PN ranging means that more range measurements can be made in a given period than can be made with sequential ranging.

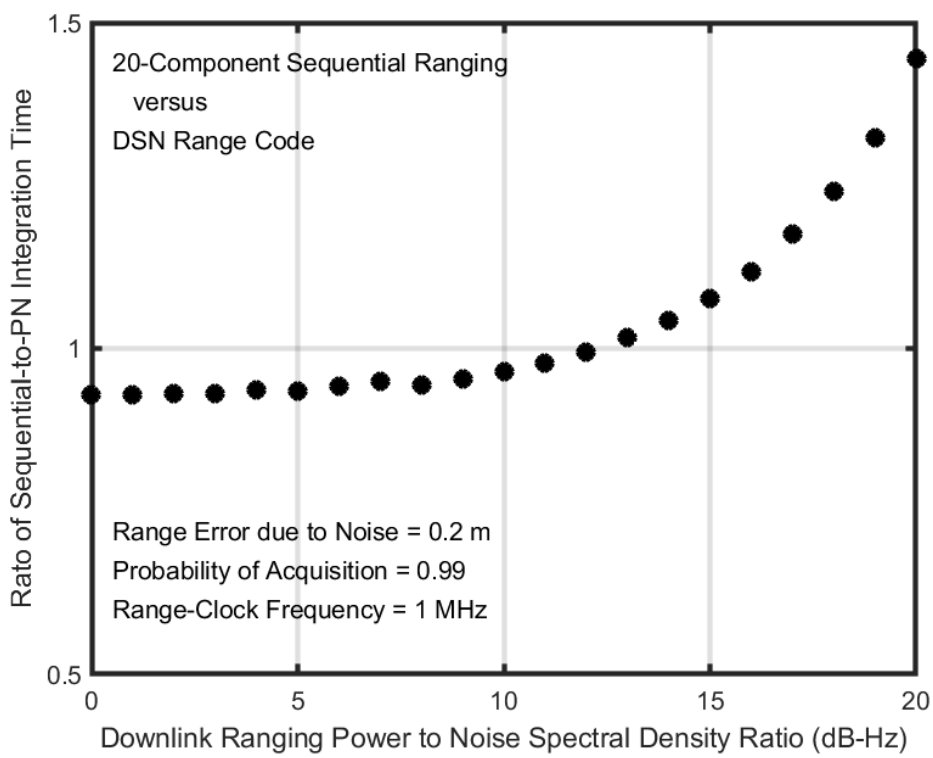

Figure 16. Comparison of Sequential Ranging and PN Ranging

PN ranging has an operational advantage over sequential ranging. With sequential ranging, a large increase in the RTLT during the tracking pass forces a measurement restart. This is not an issue for PN ranging. The PN range code has a period of approximately 0.5 second when the range clock has its typical frequency of about 1 MHz. (The measurement integration time T is larger, as the measurement comprises multiple periods of the PN range code.) With PN ranging, the downlink can start processing at any 1-second boundary.

2.5.8 Comparison of the Different PN Ranging Techniques

There are three PN range codes supported by the Deep Space Network: the heritage DSN range code and the T4B and T2B range codes. The CCSDS recommends the T4B and the T2B range codes. These three range codes are all built from the same set of component PN codes. (See Table 2.) The differences between these three range codes arise because each combines the component PN codes in its own way. For all three of these range codes (DSN, T4B, and T2B), the range-clock equals one-half of the chip rate. A turn-around ranging channel within a spacecraft transponder is compatible with all three of these range codes, assuming its bandwidth is sufficiently large.

The DSN range code and the T4B range code offer similar range-measurement precision as a function of downlink $T \cdot P_R/N_0$. (See Figure 12.) However, the T4B range code outperforms the DSN range code in acquisition. For example, the DSN range code requires that the downlink $T \cdot P_R/N_0$ be 37.9 dB for an acquisition probability of 99%, whereas the T4B range code only requires 35.3 dB for the same acquisition probability. (See Figure 14.)

Compared to the DSN and T4B range codes, the T2B range code can be reliably acquired with a much smaller downlink $T \cdot P_R/N_0$. For example, the T2B range code only requires a downlink $T \cdot P_R/N_0$ of 23.2 dB for an acquisition probability of 99%. (See Figure 15.) The disadvantage of the T2B range code is that it cannot achieve the same range-measurement precision as the other two range codes. (Compare Figure 12 and Figure 13.)

Regenerative ranging offers, in principle, a performance improvement over non-regenerative (turn-around) ranging for a given range code. Whether this performance improvement is significant depends on the link parameters. The performance advantage of regenerative ranging comes at the expense (to the mission) of needing special regenerative signal processing in the ranging channel of the transponder. The signal processing in a regenerative-ranging transponder is specific to the exact range code being used. Within the Deep Space Network, the processing of a range measurement is independent of whether the transponder employs regenerative or non-regenerative ranging.

2.5.9 Non-Coherent Operation

A non-coherent ranging technique has been described in Reference 8. For the sake of economy, this technique employs a transceiver, rather than a transponder, at the spacecraft. With such a technique, the downlink carrier is not coherent with the uplink carrier, and the downlink range clock is not coherent with the downlink carrier. This means that there will ordinarily be a frequency mismatch between the received downlink range clock and its local model. This mismatch is to be minimized by Doppler compensation of the uplink carrier, but it will not be possible, in general, to eliminate completely the frequency mismatch. With this non-coherent technique, range measurement performance will not be as good as that which can be achieved with coherent operation using a transponder. Nonetheless, non-coherent range measurement performance is expected to be adequate for some mission scenarios.

The frequency mismatch inherent in non-coherent ranging has two effects on performance. One is a loss A_c of correlation amplitude, which increases the thermal noise contribution to measurement error. The other is a direct contribution to range measurement error. This direct contribution is much the more important of these two effects.

The loss of correlation amplitude is represented by A_c where $0 < A_c < 1$. The standard deviation σ_ρ of range measurement error due to thermal noise is given by Equation (85), and the probability of acquisition (considering the effect of thermal noise) is given by Equations (90) and (91). The amplitude loss factor A_c is, for non-coherent operation, given by

$$A_c = |\mathrm{sinc}(2\Delta f_{RC} T)| \tag{95}$$

where Δf_{RC} is the frequency mismatch between the received range clock and its local model. The function $\mathrm{sinc}(\cdot)$ is defined by Equation (56). For coherent operation, $\Delta f_{RC} = 0$ and $A_c = 1$.

The direct contribution of frequency mismatch to range measurement error is given by

$$\text{range error due to } \Delta f_{RC} = \frac{c}{4} \cdot \frac{\Delta f_{RC}}{f_{RC}} \cdot T, \qquad \text{m} \tag{96}$$

The range error given by Eq. (96) is in meters (with c in m/s, T in seconds, and with Δf_{RC} and f_{RC} sharing the same units). It is worth noting that this measurement error is directly proportional to both the fractional frequency mismatch $\Delta f_{RC}/f_{RC}$ and the measurement integration time T. The fractional frequency error will, in general, comprise two terms: a fractional frequency error due to uncertainty in the spacecraft oscillator frequency and a fractional frequency error due to imperfect uplink Doppler predicts.

Non-coherent ranging measurements should be done with regenerative ranging using PN signals. The reason for this follows. The direct error contribution due to frequency mismatch is directly proportional to the measurement integration time, as can be seen in Equation (96). So, for non-coherent operation, it is important to make T as small as possible. This is achieved with regenerative ranging, and regenerative ranging is only available with a PN ranging signal.

With non-coherent operation, the range error due to frequency mismatch increases with T and the range error due to thermal noise decreases with T. Therefore, it is important to seek an optimal value for T, in order to get the best possible performance. Reference 8 offers guidance in this matter.

2.6 Range Corrections

Range is defined to be the distance from the reference point on the DSS antenna to the reference point on the spacecraft antenna. The reference point of a DSS antenna is the intersection of the azimuth and elevation axes. When the two-way time delay is measured, the result includes more than just the two-way delay between the reference points of the DSS and spacecraft antennas. The measured two-way delay also includes station delay and spacecraft delay. These extra delays must be determined through calibration and then removed from the measured two-way time delay. The spacecraft delay is measured during DSN compatibility testing prior to launch. The station delay is determined in two parts: the DSS delay and the Z-correction.

A range measurement (that has not yet been corrected) provides the two-way delay through the station uplink path, starting from the USG, to and from the spacecraft, and through the station downlink path, ending in the RRT. Figure 17 illustrates the two-way signal

path at the station. It is necessary to determine the uplink station delay for the path from the USG to the antenna reference point, to determine the downlink station delay for the path from the antenna reference point to the RRT, and to remove these delays from the measured two-way delay.

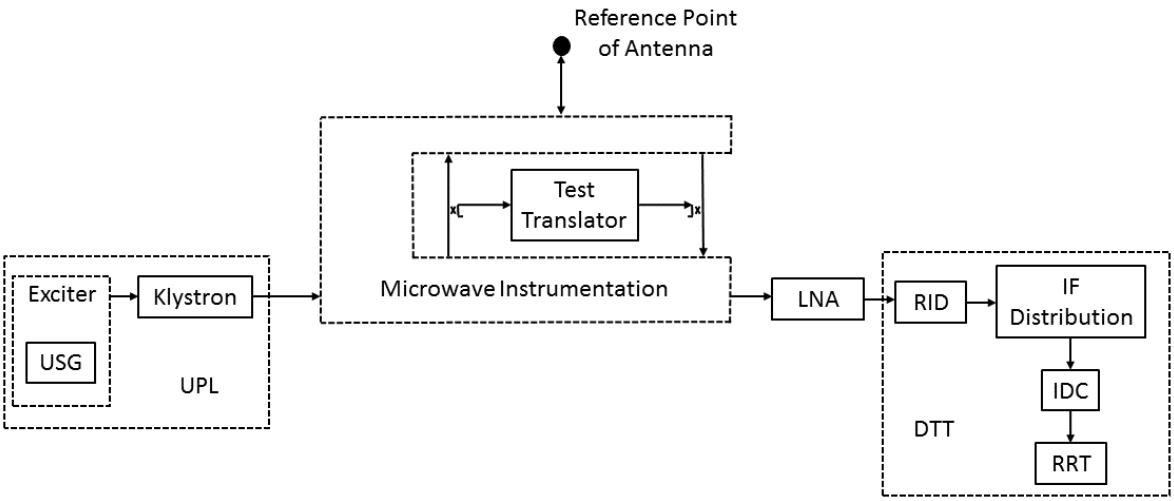

Figure 17. DSS Delay Calibration

2.6.1 DSS Delay

The DSS delay is obtained by a calibration that mimics an actual two-way range measurement, except that the signal path lies entirely within the station. A portion of the uplink carrier is diverted through a coupler to a test translator. The test translator shifts the carrier to the downlink frequency (while not altering the modulation) and feeds this frequency-shifted carrier to a coupler that places it on the downlink path within the station. The DSS delay contains most of the station delay. To be precise, the DSS delay comprises the delay from the USG to the ranging coupler on the uplink, the delay through the test translator (and its cables), and the delay from the ranging coupler on the downlink to the RRT.

Figure 17 is a somewhat abstract representation of the configuration. The microwave instrumentation shown in this figure is not an official subsystem, rather it is a conceptual grouping of microwave signal paths and microwave devices. On the uplink, the uplink carrier that is output from the klystron passes through the microwave instrumentation on its way to the reference point of the antenna. On the downlink, the downlink passes through the microwave instrumentation on its way to the LNA. Along the uplink path, a portion of the uplink carrier is coupled to the test translator. The portion of the carrier that has been frequency shifted to the downlink band inside the test translator is then coupled to the downlink path. The specific details of the microwave instrumentation are generally different at different DSSs and for different bands within a given DSS. Modules 101, 103 and 104 should be consulted for those details.

The DSS delay is station and configuration dependent. It should be measured for every ranging pass. This measurement is called precal for pre-track calibration and postcal for post-track calibration. The former is done at the beginning of a ranging pass; the latter is only

needed when there is a change in equipment configuration during the track or precal was not performed due to a lack of time.

The DSS delay varies significantly as a function of carrier frequency. This is illustrated in Figure 18 for an X-band (uplink and downlink) calibration at DSS 63. The vertical axis on this plot is the DSS delay, labeled STDL in this plot. The difference between the largest and smallest delays over the 8400—8450 MHz band is about 18 ns in this case. On both the lower and upper ends of this band, the rise in station delay originates in the klystron on the uplink side of the station. The ripple in the station delay arises from impedance mismatches; every transmission line that has some mismatch at both ends will introduce ripple in the group delay.

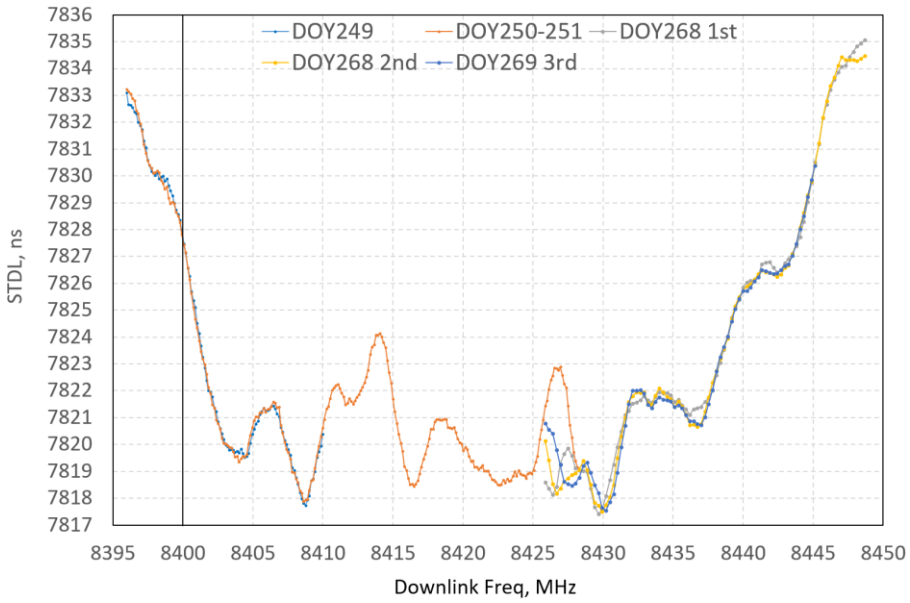

Figure 18. DSS Delay as a Function of Downlink Frequency

2.6.2 Z-Correction

The DSS delay itself must be corrected. This is accomplished with the Z-correction. The DSS delay includes the delay through the test translator (and its cables), but the test translator is not in the signal path of an actual range measurement. Moreover, the DSS delay does not include, but should include, the delays between the ranging couplers and the antenna reference point.

The Z-correction is defined as the delay through the test translator (and its cables) minus the uplink and downlink delays between the ranging couplers and the antenna reference point. The DSS delay minus the Z-correction therefore gives the delay between the USG and the antenna reference point plus the delay between the antenna reference point and the RRT. This is exactly the quantity that must be subtracted from a range measurement in order to produce a two-way delay relative to the antenna reference point.

The test translator delay is measured by installing a zero delay device (ZDD) in place of the test translator. Since the ZDD delay is measured in the laboratory, the signal delay contributed by the test translator can be calculated to a known precision. This measurement is made approximately once each year or when there are hardware changes in this portion of the signal path. The delays between the ranging couplers and the antenna reference point are stable and need not be updated often; they are determined by a combination of calculation and measurement.

2.7 Total Error for Range Measurement

Several error sources contribute to the total error for a range measurement. For two-way range measurement, the two most important error sources are typically thermal noise and station calibration error. The error due to thermal noise is discussed in Section 2.5. The error in calibrating and removing the station delay is often the dominant error source for two-way ranging. For two-way range measurements in the X band, there is typically about 6 ns of station calibration error in the two-way delay, corresponding to a (one-way) range error of about 1 meter.

The error in calibrating and removing the spacecraft delay is stable for a given spacecraft and a given band pairing (for example, X band on the uplink and X band on the downlink). The orbit determination program can, given enough range measurements for this spacecraft and band pairing, solve for this error.

There are error contributions, usually small compared to the station calibration error, due to the passage of the uplink and downlink through the troposphere, ionosphere and solar corona (Reference 9). When the angle between the sun and the spacecraft, as seen from the station, is small and the spacecraft is beyond the sun, the error contribution from the solar corona can become the dominant contributor to error in the range measurement.

For three-way ranging (in which one station transmits the uplink and a second station receives the downlink), the total delay measurement error is larger than for two-way. There are two reasons for this. First, there is a clock offset between the transmitting and receiving stations. Second, the calibration of the station delays is more difficult to achieve accurately in this case.

Appendix: Glossary of Parameters

$P_T/N_0\|_{\mathrm{U/L}}$	ratio of uplink total power to noise spectral density, Hz
$P_C/P_T\|_{\mathrm{U/L}}$	ratio of uplink residual-carrier to total power
$P_R/P_T\|_{\mathrm{U/L}}$	ratio of uplink ranging-signal to total power
$P_D/P_T\|_{\mathrm{U/L}}$	ratio of uplink command-signal to total power
$P_T/N_0\|_{\mathrm{D/L}}$	ratio of downlink total power to noise spectral density, Hz
$P_C/P_T\|_{\mathrm{D/L}}$	ratio of downlink residual-carrier to total power
$P_R/P_T\|_{\mathrm{D/L}}$	ratio of downlink ranging-signal to total power
$P_D/P_T\|_{\mathrm{D/L}}$	ratio of downlink telemetry to total power
$P_{fth}/P_T\|_{\mathrm{D/L}}$	ratio of command-feedthrough power to total power on downlink
$E_S/N_0\|_{\mathrm{D/L}}$	ratio of telemetry symbol energy to noise spectral density
P_R/N_0	ratio of downlink ranging-signal power to noise spectral density, Hz
P_k/P_T	ratio of discrete spectral line power to total power
Z	$T \cdot (P_R/N_0)$ in decibels
ρ_ρ	ranging signal-to-noise ratio in transponder's ranging channel
ρ_{cmd}	command-feedthrough signal-to-noise ratio in transponder's ranging channel
$C_R(B_R T_{cmd})$	fraction of command-signal power passing through ranging channel
T_{cmd}	command symbol period, s
T_{tlm}	telemetry symbol period, s
B_R	noise-equivalent bandwidth of transponder's ranging channel, Hz
B_{RL}	noise-equivalent bandwidth of uplink code-tracking loop, Hz
T	integration time for range measurement, s
T_c	chip period, s
f_{chip}	chip rate, Hz
f_{RC}	range-clock frequency, Hz
f_C	frequency of residual carrier, Hz
f_S	S-band carrier frequency, Hz

f_X	X-band carrier frequency, Hz
f_K	K-band carrier frequency, Hz
f_{Ka}	Ka-band carrier frequency, Hz
Δf_{RC}	difference between the received range-clock frequency and its local model, Hz
A/B	rational factor that, together with the uplink carrier frequency, sets the chip rate
c	speed of electromagnetic waves in vacuum, m/s
λ_n	period of n-th component code
L	length of composite code
R_n	cross-correlation factor of code component n against composite code
A_c	fractional loss of correlation amplitude due to non-coherent frequency mismatch
ϕ_r	phase deviation of uplink carrier by ranging signal, rad rms
ϕ_{cmd}	phase deviation of uplink carrier by command signal, rad rms
θ_{rs}	phase deviation of downlink carrier by ranging signal (strong signal), rad rms
θ_r	phase deviation of downlink carrier by ranging signal, rad rms
θ_{cmd}	phase deviation of downlink carrier by command feedthrough, rad rms
θ_n	phase deviation of downlink carrier by noise, rad rms
θ_{tlm}	telemetry modulation index, rad
$S_{cmd}(\phi_{cmd})$	suppression factor on uplink due to command
$M_{cmd}(\phi_{cmd})$	modulation factor on uplink for command
$S_{fth}(\theta_{cmd})$	suppression factor on downlink due to command feedthrough
$M_{fth}(\theta_{cmd})$	modulation factor on downlink for command feedthrough
$S_{tlm}(\theta_{tlm})$	suppression factor on downlink due to telemetry
$M_{tlm}(\theta_{tlm})$	modulation factor on downlink for telemetry
P_n	probability of acquiring the n-the component code
P_{acq}	probability of acquisition
σ_ρ	standard deviation of range measurement error due to downlink noise, m
$\sigma_{\mathrm{U/L}}$	standard deviation of range measurement error due to uplink noise, m

σ_{RR}	standard deviation of range measurement error due to all noise, m
σ_{τ}	standard deviation of two-way delay, s
σ_{RU}	standard deviation of the two-way phase delay, RU
Γ_Q	factor by which downlink noise floor increases in quadrature receiver channel
K_{NQ}	contribution to Γ_Q from uplink noise and downlink intermodulation products
K_{tlm}	contribution to Γ_Q from telemetry interference
K_{fth}	contribution to Γ_Q from feedthrough command interference
$P_{NQ}/P_T\big\vert_{\mathrm{D/L}}$	ratio of power from K_{NQ} sources to total power on downlink
$S_{tlm}(f)$	one-sided, unity-power, power spectral density of telemetry, 1/Hz
$S_{cmd}(f)$	one-sided, unity-power, power spectral density of command, 1/Hz
$\hat{S}_{tlm}(\cdot)$	maximum of weighted average of $S_{tlm}(f)$, normalized by T_{tlm}
$\hat{S}_{cmd}(\cdot)$	maximum of weighted average of $S_{cmd}(f)$, normalized by T_{cmd}
$f_{n,k}$	frequency of spectral line at frequency index k for component PN code n, Hz
$P_{n,k}$	relative power of spectral line at frequency index k for component PN code n
$\tilde{C}_n(k)$	DFT of component PN code n, as calculated from λ_n samples

References

1. J. B. Berner, S. H. Bryant, and P. W. Kinman, “Range Measurement as Practiced in the Deep Space Network,” *Proceedings of the IEEE*, Vol. 95, No. 11, November 2007.
2. Consultative Committee for Space Data Systems, "Pseudo-Noise (PN) Ranging Systems," CCSDS 414.1-B-2, February 2014.
3. P. W. Kinman and J. B. Berner, “Two-Way Ranging During Early Mission Phase,” *2003 IEEE Aerospace Conference*, March 8-15, 2003, Big Sky, MT.
4. J. L. Massey, G. Boscagli, and E. Vassallo, "Regenerative Pseudo-Noise (PN) Ranging Sequences for Deep-Space Missions," *Int. J. Satellite Communications and Networking*, Vol. 25, No. 3, pp. 285-304, May/June 2007.
5. J. B. Berner, J. M. Layland, P. W. Kinman, and J. R. Smith, “Regenerative Pseudo-Noise Ranging for Deep-Space Applications,” *TMO Progress Report 42-137*, Jet Propulsion Laboratory, Pasadena, CA, May 15, 1999.
6. J. R. Jensen, “A Plurality Voting Method for Acquisition of Regenerative Ranging Measurements,” *2013 IEEE Aerospace Conference*, March 2-9, 2013, Big Sky, MT.
7. J. B. Berner and S. H. Bryant, “Operations Comparison of Deep Space Ranging Types: Sequential Tone vs. Pseudo-Noise,” *2002 IEEE Aerospace Conference*, March 9-16, 2002, Big Sky, MT.
8. M. K. Reynolds, M. J. Reinhart, R. S. Bokulic, and S. H. Bryant, “A Two-Way Noncoherent Ranging Technique for Deep Space Missions,” *2002 IEEE Aerospace Conference*, March 9-16, 2002, Big Sky, MT.
9. C. L. Thornton and J. S. Border, *Radiometric Tracking Techniques for Deep-Space Navigation*, Monograph 1 of the *Deep-Space Communications and Navigation Series*, Jet Propulsion Laboratory, Pasadena, CA, 2000.

Deep Space Network

301
Coverage and Geometry

Document Owner:		Approved by:	
Signature Provided	02/28/2022	Signature Provided	03/31/2022
Stephen D. Slobin Antenna System Engineer	Date	Timothy Pham Communications Systems Chief Engineer	Date
Prepared by:		**Released by:**	
Signature Provided	02/28/2022	Signature Provided	04/15/2022
Stephen D. Slobin Antenna System Engineer	Date	Christine Chang DSN Document Release Authority	Date

DSN No. **810-005, 301, Rev. N**
Issue Date: April 15, 2022
JPL D-19379; CL#22-1842

Jet Propulsion Laboratory
California Institute of Technology

Users must ensure that they are using the current version in DSN Telecommunications Link Design Handbook website:
https://deepspace.jpl.nasa.gov/dsndocs/810-005/

Review Acknowledgment

By signing below, the signatories acknowledge that they have reviewed this document and provided comments, if any, to the signatories on the Cover Page.

Signature Provided	02/26/2022	Signature Provided	02/27/2022
Jeff Berner DSN Project Chief Engineer	Date	John Cucchissi Antenna System Engineer	Date
Signature Not Provided			
Harvey Soldan Technical Group Supervisor, DSN System Engineering Group	Date		

Document Change Log

Rev	Issue Date	Prepared By	Affected Sections or Pages	Change Summary
Initial	11/30/2000	Robert Sniffin	All	New Module
A	4/15/2003	Robert Sniffin	2.1.1, 2.1.4, 2.2.3, 3.	Identified 11-m subnet as non-operational. Corrected equations 4, and 7. Added DSS 55. Documented improved coverage for MDSCC antennas. Expressed Geodetic coordinates in terms of WGS84 ellipsoid. Revised Proposed Capabilities.
B	2/5/2004	Robert Sniffin	2.1.2, 2.1.2.1, 2.11.2.2, 2.1.5, 2.2.3.6, 2.2.3.10, 2.2.4	Corrects locations of DSS 26, 54 and DSS 55. Revises locations of other stations. Adds Table 7 (location uncertainties). Provides final receive and transmit masks for DSS 55. Adds Figure 8 and renumbered subsequent figures.
C	8/20/2005	Robert Sniffin	Tables 2, 5,& 6.	Documents new location and masking of DSS 65.
D	9/19/2008	Robert Sniffin	2.1.1, 2.2.3.7 – 2.2.3.10, Tables 1, 2, 5 – 7, Figures 9 & 10	Deleted references to 11-m antenna subnet stations and DSS 16 that have been decommissioned. Revised Figures 9 and 10 and titles of Figures 11 and 12. Deleted Figure 15 and renumbered subsequent figures.
E	12/15/2009	Robert Sniffin	Tables 1, 2, 5 – 7, Figures 9, 10, 22, & 27	Deleted references, the affected Figures, and information in the Tables due to the 26-m stations decommissioning. Renumbered the Figures.
F	6/1/2010	Andrew Kwok	Page 18	Corrected DSS-27 cable wrap limits in Table 8. Eliminated the Rev. E designation for the document series.
G	10/1/2011	Robert Sniffin Christine Chang	2.2.2, 2.2.3, 2.2.4, Figures 5 and 11 – 23	Corrected transmit mask of DSS-65 and revised 34-m HEF transmit coverage chart. Revised all horizon masks to show wrap limits and locations of nearby antennas. Merged 2.2.2.1 into 2.2.2. Added explanation of difference between land mask and mask used for calculating spacecraft rise and set times. Updated discussion of Spacecraft Visibility plot program in 2.2.3.
H	10/17/2012	Robert Sniffin Christine Chang	2.2.3.6, Figures 7, 8,10, 20 and 21	Incorporated changes in transmit limits at DSS-54 and DSS-55.
I	6/12/2014	Stephen Slobin Christine Chang Robert Sniffin	Figure 16 Figure 17 Tables 2, 5, 6, 7 Table 8	Removed references to DSS 27 and DSS 65 (old). Added new transmit horizon mask for DSS-34. Added new figure for DSS-35. Added coordinates for DSS-35. Added wrap limits for DSS-35.
J	9/10/2014	Stephen Slobin Christine Chang Robert Sniffin	2.2.4 Figure 17	Clarified description of horizon mask plotted values. Updated receive horizon mask for DSS-35. Added L/P transmit horizon mask for DSS-35.

Rev	Issue Date	Prepared By	Affected Sections or Pages	Change Summary
K	9/13//2016	Stephen Slobin Christine Chang	Tables 1, 8 Tables 2, 5, 6, 7 Tables 2, 5, 6, 7 Figure 16 Figure 17 Figure 18 Figures 18-23 Sec. 2.2.4	DSS-36 added. Updated position values for DSS-35. New position values for DSS-36. New transmit and receive horizon masks for DSS-34. New receive horizon mask for DSS-35. New DSS-36 horizon masks. Renumbered 19-24. Expanded description of DSS-34, -35, -36 horizon masks.
L	07/3/2018	Stephen Slobin Christine Chang	Table 1 Tables 2, 5, 6, 7 Table 8 Figure 15 Figure 16 Download Spreadsheet	Future antennas DSS-53 and DSS-56 added. Added coordinates for DSS-53 and DSS-56. New cable wrap limits for all antennas. Added high power transmit mask for DSS-26. New transmit horizon mask for DSS-34. Updated with new DSS-34 transmit horizon mask.
M	09/04/2020	Stephen Slobin Christine Chang	810-005 Downloads 810-005 Downloads Figures 11-24 Sec. 2.2.3 Sec. 2.2.4 Sec. 2.2.1 & 2.2.4 Tables 2, 5, 6, 7	New Download Spreadsheet for Spacecraft Coverage and Visibility. New Download Spreadsheet for Antenna Horizon Masks. New for DSN antenna horizon masks. Update to coverage charts. Update to horizon masks. Updated references to DSS-43 100 kW S-band and 80 kW X-band transmitters. Updated with latest DSS-56 location.
N	04/15/2022	Stephen Slobin Christine Chang	Sec. 2.2.4 Tables 2, 5, 6, 7 Table 8	Description of new DSS-53 location on masks and blockages. Updated with latest DSS-53 location. Notes added regarding station location accuracy. Updated DSS-53 cable wrap limits.

Contents

Illustrations

Tables

Table **Page**

1 Introduction

1.1 Purpose

This module describes the geometry and coverage visibility provided by the DSN for support of spacecraft telecommunications.

1.2 Scope

This module provides the Deep Space Network (DSN) station coordinates that are required for spacecraft navigation and to locate the stations with respect to other points on the Earth's surface. Coverage charts are provided to illustrate areas of coverage and non-coverage from selected combinations of stations for spacecraft at selected altitudes. Horizon masks are included so the effects of terrain masking and antenna blockage can be anticipated.

2 General Information

2.1 Station Locations

The following paragraphs discuss the important concepts relating to establishing the location of the DSN antennas.

2.1.1 Antenna Reference Point

The coordinates provided by this module refer to a specific point on each antenna. For antennas where the axes intersect (AZ/EL antennas), the reference point is the intersection of the axes. For antennas for which the axes do not intersect (HA/DEC antennas), the reference point is the intersection of the primary (lower) axis with a plane perpendicular to the primary axis and containing the secondary (upper) axis. This antenna type has an axis offset, which must be accounted for in the range observable as a function of antenna positioning. There are currently no operational HA/DEC antennas in the DSN. Table 1 lists the DSN antennas by type.

Although the antenna reference point is fixed, the path length between this point and a spacecraft normally increases as the antenna elevation is changed from the horizon to zenith. This results from the antenna subreflector being moved to provide maximum gain as gravity distorts the antenna geometry. The effect can be modeled as a decrease in antenna height and a latitude/longitude position change as a function of azimuth and elevation angle for orbit determination purposes. The effect is greatest on the 70-m antennas (approximately 6.7 cm) and is discussed in the appropriate Telecommunications Interface modules of this handbook. Subreflector movement can be disabled for activities such as very-long baseline interferometry (VLBI) where a constant path length is more important than maximum gain.

Table 1. DSN Antenna Types

Antenna Type	Station Identifiers	Primary and Secondary Axes
70-m	14, 43, 63	AZ/EL
34-m High Efficiency (HEF)	15, 45, 65	AZ/EL
34-m Beam Waveguide (BWG)	24, 25, 26, 34, 35, 36, 53, 54, 55, 56	AZ/EL

2.1.2 IERS Terrestrial Reference Frame

To use station locations with sub-meter accuracy, it is necessary to clearly define a coordinate system that is global in scope. The International Earth Rotation and Reference Systems Service (IERS) has been correlating station locations from many different services and has established a coordinate frame known as the IERS Terrestrial Reference Frame (ITRF). The IERS also maintains a celestial coordinate system and coordinates delivery of Earth-orientation measurements that describe the motion of station locations in inertial space. The DSN has adopted the IERS terrestrial system to permit its users to have station locations consistent with widely available Earth-orientation information.

The IERS issues a new list of nominal station locations each year, and these locations are accurate at the few-cm level. At this level of accuracy, one must account for ongoing tectonic plate motion (continental drift), as well as other forms of crustal motion. For this reason ITRF position coordinates are considered valid for a specified epoch date, and one must apply appropriate velocities to estimate position coordinates for any other date. Relative to the ITRF, even points located on the stable part of the North American plate move continuously at a rate of about 2.5 cm/yr.

The coordinates in this module are based on the 1993 realization of the ITRF, namely ITRF93, documented in IERS Technical Note 18 (Reference 1). ITRF93 was different from earlier realizations of the ITRF in that it was defined to be consistent with the Earth Orientation Parameters (EOP) distributed through January 1, 1997. Earlier realizations of the ITRF were known to be inconsistent (at the 1-3 cm level) with the Earth orientation distributions.

After ITRF93 was published, the IERS decided to improve the accuracy of the EOP series and make it consistent with the ITRF effective January 1, 1997. This date was chosen because it enabled a defect in the definition of universal time to be removed at a time when its contribution was zero. In anticipation of this change, ITRF94 and ITRF95 were made consistent with the pre-ITRF93 definition of the terrestrial reference frame, and all prior EOP series were recomputed in accordance with the new system.

The DSN continues to deliver Earth-orientation calibrations to navigation teams that are consistent with the earlier definition and using the ITRF93 reference frame because it is impractical for planetary navigators to adopt an IERS standard that changes approximately every

year. Users interested in precise comparison with other systems should keep in mind the small systematic differences.

Position values and uncertainties for the all DSN antennas are given in Tables 2, 5, 6, and 7. Position values for decommissioned antennas are given for historical reference only.

2.1.2.1 Cartesian Coordinates

Figure 1 illustrates the relationship between the Cartesian coordinates and geocentric coordinates discussed below. The Cartesian coordinates of the DSN station locations are fits to many years of tracking and Very-Long Baseline Interferometry data and are expressed in the ITRF93 reference system in Table 2.

2.1.2.2 Estimated DSN Site Velocities

The locations given in Table 2 are for the epoch 2003.0. To transform these locations to any other epoch, the site velocities should be used. Table 3 gives the site velocities for the DSN stations, in both Cartesian (x, y, z) and east-north-vertical (e, n, v) components.

2.1.3 Geodetic Coordinates

Locations on the Earth’s surface are defined with respect to the geoid, the surface around or within the Earth that is normal to the direction of gravity at all points and coincides with mean sea level (MSL) in the oceans. The geoid is not a regular surface because of variations in the Earth's gravitational force. To avoid having to make computations with respect to this non-mathematical surface, computations are made with respect to an ellipsoid, the surface created by rotating an ellipse around one of its two axes. The ellipsoid is uniquely defined by specifying the equatorial radius and the flattening (that is, the amount that the ellipsoid deviates from a perfect sphere). The relationship between the polar and equatorial axes is given by the following expression:

$$(\text{polar axis}) = (\text{equatorial axis}) \times (1 - 1/\text{flattening}) \qquad (1)$$

In the past, the ellipsoid used was chosen to be a best fit to the geoid in the area of interest. However, the presence of the Global Positioning System (GPS) has resulted in a single ellipsoid, named the WGS 84 Ellipsoid, being adopted for most geodetic measurements. This ellipsoid, while providing a good fit to the entire Earth, results in larger differences between the

geoid and the ellipsoid than could be obtained when ellipsoids were chosen to fit only a

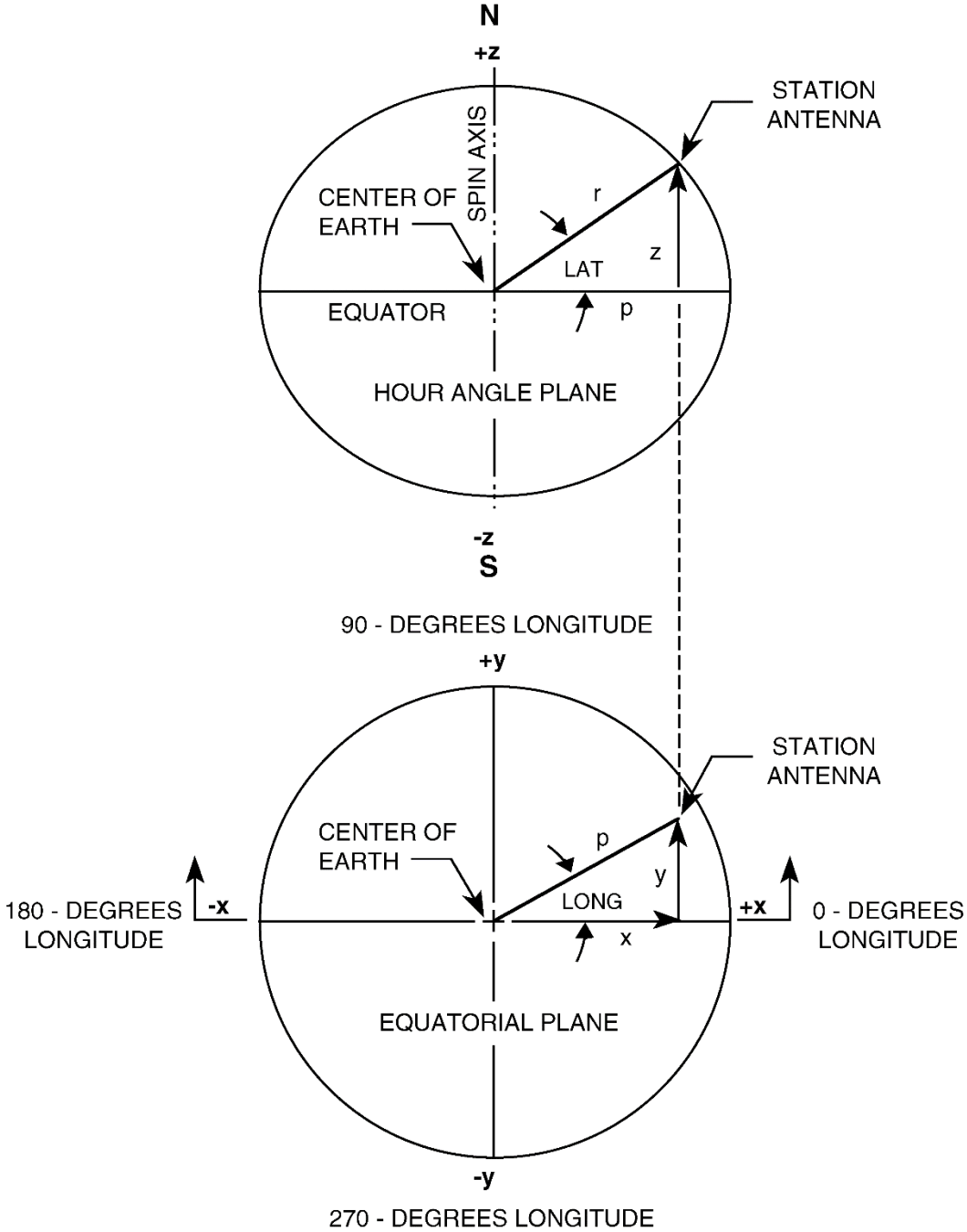

Z = Height above (+z) or below (-z) equatorial plane.
Y = Distance in front of (+y) or behind (-y) plane (Hour Angle plane) established by spin axis and Greenwich meridian.
X = Distance from spin axis towards Greenwich meridian (+x) or towards 180-degree meridian (-x).

Figure 1. Cartesian and Geocentric Coordinate System Relationships

Table 2. Cartesian Coordinates for DSN Stations in ITRF93 Reference Frame, Epoch 2003.0[3]

Antenna		Cartesian Coordinates		
Name	**Description**	**x(m)**	**y(m)**	**z(m)**
DSS 13	34-m R & D	–2351112.659	–4655530.636	+3660912.728
DSS 14	70-m	–2353621.420	–4641341.472	+3677052.318
DSS 15[2]	34-m HEF	–2353538.958	–4641649.429	+3676669.984
DSS 24	34-m BWG	–2354906.711	–4646840.095	+3669242.325
DSS 25	34-m BWG	–2355022.014	–4646953.204	+3669040.567
DSS 26	34-m BWG	–2354890.797	–4647166.328	+3668871.755
DSS 34[1]	34-m BWG	–4461147.093	+2682439.239	–3674393.133
DSS 35[1]	34-m BWG	−4461273.090	+2682568.925	−3674152.093
DSS 36[1]	34-m BWG	−4461168.415	+2682814.657	−3674083.901
DSS 43	70-m	–4460894.917	+2682361.507	–3674748.152
DSS 45[2]	34-m HEF	–4460935.578	+2682765.661	–3674380.982
DSS 53[1]	34-m BWG	+4849338.209	−360657.812	+4114746.173
DSS 54	34-m BWG	+4849434.488	–360723.8999	+4114618.835
DSS 55	34-m BWG	+4849525.256	–360606.0932	+4114495.084
DSS 56[1]	34-m BWG	+4849421.679	−360549.659	+4114646.987
DSS 63	70-m	+4849092.518	–360180.3480	+4115109.251
DSS 65	34-m HEF	+4849339.634	–360427.6637	+4114750.733

NOTES:

1. Position absolute accuracy estimated to be +/−3 cm (0.030 m) (1-sigma) for each coordinate.
2. Decommissioned. For historical reference only.
3. See NOTE, Table 7.

Table 3. Site Velocities for DSN Stations

Complex	x(m/yr)	y(m/yr)	z(m/yr)	e(m/yr)	n(m/yr)	v(m/yr)
Goldstone (Stations 1x & 2x)	–0.0180	0.0065	–0.0038	–0.0190	–0.0045	–0.0003
Canberra (Stations 3x & 4x)	–0.0335	–0.0041	0.0392	0.0208	0.0474	–0.0012
Madrid (Stations 5x & 6x)	–0.0100	0.0242	0.0156	0.0234	0.0195	0.0012

portion of the Earth. This difference, the *Geoidal Separation*, must be subtracted from the WGS 84 height measurements to give the height with respect to mean sea level.

Geoidal separations are typically determined from satellite altimetry and gravity measurements and maintained as a grid of points in longitude and latitude. Modern GPS equipment uses a sixteen point interpolation routine to estimate the surface curvature in the grid-square of interest and the geoidal separation at the specific point within the grid-square. Table 4 provides the average geoidal separation for the three DSN complexes. These numbers do not take into consideration such things as topography within the complex and grading that was done when the antennas were installed.

Table 4. Average Geoidal Separations for the DSN Complexes

Complex	Geoidal Separation (m)
Goldstone (Stations 1x & 2x)	–30.6
Canberra (Stations 3x & 4x)	19.3
Madrid (Stations 5x & 6x)	54.1

Once the Cartesian coordinates (x, y, z) are known, they can be transformed to geodetic coordinates in longitude, latitude, and height (λ, ϕ, h) with respect to the ellipsoid by the following non-iterative method (Reference 2):

$$\lambda = \tan^{-1}\frac{y}{x} \tag{2}$$

$$\phi = \tan^{-1}\left(\frac{z(1-\mathrm{f}) + e^2 \mathrm{a}\sin^3\mu}{(1-\mathrm{f})\left(p - e^2 \mathrm{a}\cos^3\mu\right)}\right) \tag{3}$$

$$h = p\cos\phi + z\sin\phi - a\left(1 - e^2\sin^2\phi\right)^{\frac{1}{2}} \tag{4}$$

where:

$$\mathrm{f} = \frac{1}{\text{flattening}} \tag{5}$$

$$e^2 = 2\mathrm{f} - \mathrm{f}^2 \tag{6}$$

$$p = \left(x^2 + y^2\right)^{\frac{1}{2}} \tag{7}$$

$$r = \left(p^2 + z^2\right)^{\frac{1}{2}} \tag{8}$$

$$\mu = \tan^{-1}\frac{z}{p}\left[(1-\mathrm{f}) + \frac{e^2\mathrm{a}}{r}\right] \tag{9}$$

Table 5 provides geodetic coordinates derived by the preceding approach using the WGS84 ellipsoid that has a semi-major axis (a) of 6378137 m and a flattening of 298.2572236. In this table, for stations in the southern hemisphere (negative latitude) the tabular values for latitude (degrees, minutes, seconds) are ALL negative, although the minus sign is shown associated only with the degree value, as is conventionally done.

2.1.4 Geocentric Coordinates

Geocentric coordinates are used by navigation analysts when corrections to station locations are being investigated. They relate the station location to the Earth's center of mass in terms of the geocentric radius and the angles between the station and the equatorial and hour angle planes. Geocentric coordinates for the DSN stations are provided in Table 6.

2.1.5 Station Location Uncertainties

The primary reference antennas at each complex in the past have been the 34-m HEF antennas. Their location has been established by very-long baseline Interferometry (VLBI) measurements over a period of many years and their location uncertainty is that of the VLBI technique. With the decommissioning of DSS-15 and DSS-45, and the future decommissioning of DSS-65, the location references are being migrated to BWG antennas at the same complexes. The uncertainty of station locations depends on the method used to link their position to that of the reference antennas. The estimated location uncertainties for all stations are provided in Table 7.

Table 5. Geodetic Coordinates for DSN Stations With Respect to the WGS 84 Ellipsoid[5]

Antenna		latitude (ϕ) [3]			longitude (λ)			height(h)[1]
Name	**Description**	**deg**	**min**	**sec**	**deg**	**min**	**sec**	**(m)**
DSS 13	34-m R & D	35	14	49.79131	243	12	19.94761	1070.444
DSS 14	70-m	35	25	33.24312	243	6	37.66244	1001.390
DSS 15[4]	34-m HEF	35	25	18.67179	243	6	46.09762	973.211
DSS 24	34-m BWG	35	20	23.61416	243	7	30.74007	951.499
DSS 25	34-m BWG	35	20	15.40306	243	7	28.69246	959.634
DSS 26	34-m BWG	35	20	8.48118	243	7	37.14062	968.686
DSS 34[2]	34-m BWG	–35	23	54.52383	148	58	55.07191	692.020
DSS 35[2]	34-m BWG	−35	23	44.86387	148	58	53.24088	694.897
DSS 36[2]	34-m BWG	−35	23	42.36634	148	58	42.75912	685.503
DSS 43	70-m	–35	24	8.72724	148	58	52.56231	688.867
DSS 45[4]	34-m HEF	–35	23	54.44766	148	58	39.66828	674.347
DSS 53[2]	34-m BWG	40	25	37.50154	355	44	47.74405	842.806
DSS 54	34-m BWG	40	25	32.23805	355	44	45.25141	837.051
DSS 55	34-m BWG	40	25	27.46525	355	44	50.52012	819.061
DSS 56[2]	34-m BWG	40	25	33.47285	355	44	52.58149	835.746
DSS 63	70-m	40	25	52.35510	355	45	7.16924	864.816
DSS 65	34-m HEF	40	25	37.94289	355	44	57.48397	833.854

NOTES:

1. Geoidal separation must be subtracted from WGS 84 height to get MSL height.
2. Latitude, longitude, and height absolute accuracy estimated to be +/-0.001 sec and +/-3 cm (0.030 m) (1-sigma)
3. For southern hemisphere antennas deg, min, sec should all be treated as negative numbers.
4. Decommissioned. For historical reference only.
5. See NOTE, Table 7.

Table 6. Geocentric Coordinates for DSN Stations[3]

Antenna		Geocentric Coordinates			
Name	**Description**	**Spin Radius (m)**	**Latitude (deg)**	**Longitude (deg)**	**Geocentric Radius (m)**
DSS 13	34-m R & D	5215524.541	35.0660180	243.2055410	6372125.096
DSS 14	70-m	5203996.968	35.2443523	243.1104618	6371993.267
DSS 15[2]	34-m HEF	5204234.338	35.2403129	243.1128049	6371966.511
DSS 24	34-m BWG	5209482.543	35.1585346	243.1252056	6371973.601
DSS 25	34-m BWG	5209635.569	35.1562591	243.1246368	6371982.537
DSS 26	34-m BWG	5209766.354	35.1543409	243.1269835	6371992.264
DSS 34[1]	34-m BWG	5205508.011	-35.2169824	148.9819644	6371693.538
DSS 35[1]	34-m BWG	5205682.820	-35.2143051	148.9814558	6371697.358
DSS 36[1]	34-m BWG	5205719.750	-35.2136127	148.9785442	6371688.208
DSS 43	70-m	5205251.840	-35.2209189	148.9812673	6371688.998
DSS 45[2]	34-m HEF	5205494.965	-35.2169608	148.9776856	6371675.873
DSS 53[1]	34-m BWG	4862731.241	40.2372333	355.7465956	6370030.706
DSS 54	4-m BWG	4862832.157	40.2357726	355.7459032	6370025.490
DSS 55	34-m BWG	4862913.938	40.2344478	355.7473667	6370007.988
DSS 56[1]	34-m BWG	4862806.461	40.2361152	355.7479393	6370024.058
DSS 63	70-m	4862450.835	40.2413554	355.7519915	6370051.198
DSS 65	34-m HEF	4862715.598	40.2373555	355.7493011	6370021.709

NOTES:

1. Latitude, longitude, and radius absolute accuracy estimated to be +/-0.0000003 deg and +/-3 cm (0.030 m) (1-sigma) for each coordinate.
2. Decommissioned. For historical reference only.
3. See NOTE, Table 7.

Table 7. DSN Stations Location Uncertainties

Antenna		Location Uncertainties (m, 1-sigma))		
Name	**Description**	**Spin Radius**	**Longitude**	**z**
DSS 13	34-m R & D	0.025	0.036	0.031
DSS 14	70-m	0.024	0.035	0.030
DSS 15	34-m HEF	0.023	0.035	0.030
DSS 24	34-m BWG	0.029	0.036	0.033
DSS 25	34-m BWG	0.029	0.036	0.033
DSS 26	34-m BWG	0.030	0.038	0.034
DSS 34	34-m BWG	0.030	0.030	0.030
DSS 35	34-m BWG	0.030	0.030	0.030
DSS 36	34-m BWG	0.030	0.030	0.030
DSS 43	70-m	0.026	0.035	0.032
DSS 45	34-m HEF	0.024	0.035	0.031
DSS 53	34-m BWG	0.03	0.03	0.03
DSS 54	34-m BWG	0.032	0.036	0.034
DSS 55	34-m BWG	0.050	0.037	0.048
DSS-56	34-m BWG	0.03	0.03	0.03
DSS 63	70-m	0.027	0.035	0.031
DSS 65	34-m HEF	0.026	0.034	0.030

NOTE:
The numbers in this table represent the uncertainties in location at the time of VLBI measurements. In the years since the measurements, a number of occurrences have conspired to increase the uncertainties to as much as 0.1 meter, 1-sigma. This is due to events such as the 2019 Ridgecrest earthquake, which affected Goldstone at the level of several centimeters, as well as uncertainty in tectonic plate velocities integrating up over the years.

2.2 Coverage and Mutual Visibility

The coverage and mutual visibility provided for spacecraft tracking depends on the altitude of the spacecraft, the particular antenna being used, the blockage of the antenna beam by the land mask and structures in the immediate vicinity of the antennas, and whether simultaneous uplink coverage is required. Receive limits are governed by the mechanical capabilities of the antennas and the terrain mask. Transmitter limits, on the other hand, are based on radiation hazard considerations to on-site personnel and the general public and are set above the terrain mask and the antenna mechanical limits.

2.2.1 Use of Transmitters Below Designated Elevation Limits

Requests for coordination to relinquish the transmitter radiation restrictions will be considered for spacecraft emergency conditions or for critical mission support requirements (conditions where low elevation or high-power transmitter radiation is critical to mission objectives). In either event, the uplink radiation power should be selected as the minimum needed for reliable spacecraft support. In general, there is no transmission allowed below 10.2-10.5 degrees elevation by any antenna at any power level. DSS-43 (Canberra) will have new S-band (100 kW) and X-band (80 kW) transmitters operational as of February 2021. These transmitters cannot be used below 17.4 degrees elevation angle at any power level above 20 kW. JPL internal document 842-40-321 (Rev. C and later) should be consulted when it is necessary to determine the airspace restrictions and azimuth and elevation limits for the various stations.

2.2.1.1 Spacecraft Emergencies

The need for violation of transmitter radiation restrictions to support a spacecraft emergency will be determined by the DSN. The restrictions will be released after assuring that appropriate local authorities have been notified and precautions have been taken to ensure the safety of both on-site and off-site personnel.

2.2.1.2 Critical Mission Support

If critical mission activities require the transmitter radiation restrictions to be violated, the project is responsible for notifying the DSN through their normal point of contact three months before the activity is scheduled. The request must include enough information to enable the DSN to support it before the appropriate authorities. Requests made less than three months in advance will be supported on a best-efforts basis and will have a lower probability of receiving permission to transmit. Requests will be accepted or denied a minimum of two weeks before the planned activity.

2.2.2 Mechanical Limits on Surveillance Visibility

All DSN antennas have areas of non-coverage caused by mechanical limits of the antennas. The first area is the mechanical elevation limit, which is approximately six degrees for antennas using an azimuth-elevation mount. A second area of non-coverage is an area immediately above the antenna referred to as the *keyhole*.

The keyhole of the DSN azimuth-elevation antennas is directly overhead and results from the fact that high azimuth angular rates are needed to track spacecraft passing nearly overhead, at zenith. For the 70-m antennas, with a maximum azimuth tracking rate of 0.25 deg/sec, spacecraft can be tracked continuously to an elevation of about 89 degrees. For the 34-m antennas, with a maximum azimuth tracking rate of 0.8 deg/sec, spacecraft can be tracked continuously to a maximum elevation of about 89.7 degrees. Thus, the size of the keyhole depends on how fast the antenna can be slewed in azimuth. Specifications on antenna motion are contained in module 302, Antenna Positioning. The locations of the DSN antennas are such that overhead tracks are not required for spacecraft operating near the plane of the ecliptic.

The DSN AZ/EL antennas have an additional restriction on antenna motion caused by the routing path of cables and hoses between the fixed and rotating portions of the antenna. This azimuth cable wrap has no effect on surveillance visibility but does place a restriction on the time between tracks due to the requirement to unwind the cables. Table 8 provides the approximate cable wrap limits for the DSN AZ/EL antennas. Users with appropriate access should also refer to the following link for the latest updates to the cable wrap limits:

https://spsweb.fltops.jpl.nasa.gov
(Select “SPS Support Files” tab and then select “view Station Parameters” tab.)

Table 8. Approximate Cable Wrap Limits for Azimuth-Elevation Antennas

Antenna		Azimuth Position (Degrees)		
Name(s)	Description	Counterclockwise (CCW) Limit	Neutral	Clockwise (CW) Limit
DSS 14	70-m	140.0	45	309.9
DSS 43	70-m	230.2	135	39.8
DSS 63	70-m	142.0	45	309.5
DSS 15 (see Note)	34-m HEF	271.3	135	358.9
DSS 45 (see Note)	34-m HEF	181.1	45	268.9
DSS 65	34-m HEF	271.3	135	358.9
DSS 24	34-m BWG	270.2	135	359.7
DSS 25	34-m BWG	270.2	135	359.7
DSS 26	34-m BWG	270.2	135	359.7
DSS 34	34-m BWG	180.0	45	269.7
DSS 35	34-m BWG	159.3	45	271.4
DSS 36	34-m BWG	159.3	45	268.0
DSS 53	34-m BWG	275.0	135.1	359.9
DSS 54	34-m BWG	269.9	140	359.7
DSS 55	34-m BWG	263.4	135	359.6
DSS 56	34-m BWG	270.0	135.05	359.0

NOTE: DSS-45 decommissioned as of 10/2016. DSS-15 decommissioned as of 5/2018.

2.2.3 Coverage Charts

Figures 2-10 provide examples of coverage for various combinations of stations, spacecraft altitudes, and type of support. The coverage limits in these figures were plotted by a program written as a collection of Microsoft Excel macros with shading and labels added for publication. The coverage areas shown are the locations on earth over which a spacecraft must be so that it is visible by all the stations at an antenna complex, subject to the altitude and receive/transmit elevation limits given for that particular case. The latest version of this program combines the capability to draw the coverage charts and is available for download from the 810-005 web sites:

https://deepspace.jpl.nasa.gov/dsndocs/810-005/downloads/ .

The coverage charts are available from "Download Spacecraft Coverage and Visibility Spreadsheet for 301". The file includes a spreadsheet with the antenna coordinates used to create the figures. For antennas grouped closely at each complex (e.g. the BWG antennas at Goldstone), the visibility differences among the antennas are insignificant. This

download spreadsheet should not be used for generating the horizon masks. Horizon mask plots are available from the 301N download spreadsheet (see Section 2.2.4). The spacecraft coverage spreadsheet uses generic elevation limits for the receive and transmit elevations. These are 6.0 degrees for receive, 10.0 degrees for low-power transmit, and 13.5 degrees for high-power transmit. There is no azimuth variation of these elevation limits, and the coverages thus shown will be the maximum available for spacecraft at the given altitude values, including geosynchronous and deep-space spacecraft, subject to the minimum elevation limits given in the specific antenna horizon masks (Section 2.2.4). The following coverage cases were drawn in Figures 2-10 for specific elevation limits somewhat different from the generic elevation limits given in the coverage and visibility download spreadsheet.

2.2.3.1 70-m Receive Coverage of Planetary Spacecraft

Figure 2 illustrates the receive coverage of planetary spacecraft by the DSN 70-m antenna subnet. The small ovals at each antenna location on the figure represent the 70-m antenna keyholes above each station and are approximately to scale.

2.2.3.2 70-m Transmit Coverage of Planetary Spacecraft

Figure 3 illustrates the transmit coverage of planetary spacecraft by the DSN 70-m antenna subnet using a 10.4-degree transmit elevation limit at DSS 14 and a 10.2-degree transmit elevation limit at DSS 43 and DSS 63. The small ovals at the antenna locations on the figure represent the 70-m antenna keyholes. The reduced coverage to the west of DSS 63 (seen over the western United States) is caused by the need to have a 20.2-degree elevation limit to protect the high ground to the northwest of the station.

2.2.3.3 34-m HEF Receive Coverage of Planetary Spacecraft

Figure 4 illustrates the receive coverage of planetary spacecraft by the DSN 34-m HEF antenna subnet. The keyhole above each 34-m HEF antenna is very small and is somewhat exaggerated for clarity on the maps. This chart is very similar to Figure 2 but is included to show that the location of DSS 65 shifts the apparent position of the high ground to the north and west of where it is observed from DSS 63.

2.2.3.4 34-m HEF Transmit Coverage of Planetary Spacecraft

Figure 5 illustrates the transmit coverage of planetary spacecraft by the DSN 34-m HEF antenna subnet. As is the case in Figure 4, the size of the circles used to indicate the keyholes on the map are larger than the actual size of the 34-m HEF antenna keyholes. The transmit elevation limit is 10.6-degrees at DSS 15 and 10.5-degrees at DSS 45. At DSS 65, the transmit limit is 10.3 degrees but it is increased to 14.0 degrees when the antenna is pointed in a northerly direction from 326.6 to 355.1 degrees azimuth and again from 24.1 to 50.9 degrees azimuth. This is done to clear the hills to the north, north-west and other antennas to the north, north-east of DSS 65's new location.

2.2.3.5 34-m BWG Receive Coverage of Planetary Spacecraft

Figure 6 illustrates the receive coverage of planetary spacecraft by a subnet of DSN 34-m BWG antennas capable of supporting X and Ka bands. As is the case with the other 34-m antennas, the size of the keyhole circles on the map is larger than the actual size of the antenna keyholes. This chart is very similar to Figures 2 and 4 but is included to show that the location of DSS 55 shifts the apparent position of the high ground to where it does not significantly affect tracking coverage.

2.2.3.6 34-m BWG Transmit Coverage of Planetary Spacecraft

Figure 7 illustrates the transmit coverage of planetary spacecraft by the same subnet of 34-m BWG antennas (DSS 26, 34, and 55) shown in Figure 6. DSS 55 is sited south-east of DSS 54 at a slightly lower elevation. To allow an adequate clearance above DSS 54 for the DSS 55 transmitter pencil beam, an 18.36-degree lower elevation limit is placed on the DSS 55 transmitter between 304.9 and 360 degrees. Figure 8 is included primarily to show the effect of substituting DSS 54 for DSS 55. There is no significant coverage difference between any of the 3 Goldstone BWG stations. Coverage by DSS 54 between 344.4 and 8.5 degrees azimuth is limited to elevations above 13.3 degrees in order to protect the high ground northwest of the station.

2.2.3.7 34-m BWG Receive Coverage of Near Earth Spacecraft

Figure 9 illustrates the receive coverage of near-Earth spacecraft by the DSN 34-m BWG antennas at altitudes of 500 km, 5000 km, and geosynchronous (35789 km) using the near-Earth support stations, DSS 24, 34, and 54. As is the case with the other 34-m antennas, the size of the keyhole circles on the map is larger than the actual size of the antenna keyholes. It should be noted that at lunar distance the coverage is essentially the same as the planetary coverage shown in Figure 6.

2.2.3.8 34-m BWG Transmit Coverage of Near Earth Spacecraft

Figure 10 illustrates the transmit coverage of near-Earth spacecraft by the DSN 34-m BWG antennas at altitudes of 500 km, 5000 km, and geosynchronous (35789 km) using the near-Earth support stations. As is the case with other figures, the keyholes are shown larger than actual size and coverage at lunar distance is essentially the same as the planetary coverage shown in Figure 7.

2.2.4 Horizon Masks and Antenna Limits

Horizon mask data and plots are available from the 810-005 download website at

https://deepspace.jpl.nasa.gov/dsndocs/810-005/downloads/.

The horizon mask charts are available from “Download Horizon Mask Spreadsheet for 301N”. These horizon mask charts should be considered valid beginning May 1, 2020, until further notice, and are presently being used for planning mission telecom sequences. Figures 11 through 24 show the receive and transmit horizon mask limits for all DSN stations.

For this revision (Rev. N) the masks for the MDSCC (Madrid) stations have not been updated to show the effects (masks plus blockages) due to the updated 2-meter lower DSS-53 location. The effects on the DSS-53 mask are believed to be small (horizon mask less than 0.1 deg higher, and blockage by other antennas less than 0.7 degrees higher). As seen from other antennas, DSS-53 will appear to be less than 0.7 degrees lower.

The receive limits are governed generally by the physical terrain surrounding the antenna and blockage by neighboring antennas, or by the mechanical lower limit of approximately 6 degrees elevation. The transmitter limits are governed by statutory restrictions of approximately 10 degrees for low power (typically 20 kW) transmission, and approximately 13.5 degrees (by analysis) for high power (typically 80 kW) transmission. Most antenna horizon masks differ slightly from these values.

In general, the absolute lower elevation limit for uplink transmission is 10.0 degrees, unless a higher limit is required to clear terrain or some other obstruction. DSS-65 has a lower transmit limit of 10.8 degrees, which includes interlock position uncertainties of as much as 0.5 degrees, so as to guarantee that there is no transmission at an elevation angle less than 10.0 degrees or closer than some safe distance (at least several meters) above an elevated horizon. At DSS-43 neither the 100-kW S-band transmitter nor the 80-kW X-band transmitter can be used below 17.4-degrees elevation angle at any power level above 20 kW.

The receive horizon masks for DSS-34, DSS-35, and DSS-36, Figures 15 thru 17, were measured by radiometric techniques to determine the actual antenna elevation angle where the increase in system noise temperature due to the beam impinging upon the terrain, and the accompanying blockage of the beam, would create an antenna G/T degradation that would make reliable spacecraft tracking impossible. The noise temperature increase chosen to define the receive horizon was +50 K, which would result in an approximately 3 dB increase in system noise temperature, and a 1 dB decrease of gain, resulting in a total G/T degradation of about 4 dB. Because of configuration changes to DSS-35, only the DSS-34 and DSS-36 receive horizons are determined by this method. The DSS-35 receive horizon was modeled from the existing +2.5 K noise contour (the transmit horizon) by lowering that profile by 2 degrees.

The transmit horizon masks for the Canberra BWG antennas were determined by the azimuth profile where the system noise temperature increase was +2.5 K, where it is thought the lower edge of the beam is just touching the terrain. An additional 0.5 degrees in azimuth and elevation was added to account for interlock position uncertainties. The transmit profile for DSS-35 was squared-off so that the beam clearance was 0.5 degrees above the highest obstacle, dropping down to 10.5 degrees at azimuths where the 10.5 degree elevation was 0.5 degrees above the +2.5 K profile, or about 2-3 degrees above the receive mask. The transmit horizon masks for DSS-34 and DSS-36 were also measured by radiometric means, but the transmit mask is now a continuous function of azimuth, and the transmitter lower limits are defined by a set of polynomials, each over a small range of azimuth. These polynomial transmit masks are used in the ATMC (Antenna Transmit Mask Controller).

A DSS-26 high-power (80 kW) transmit horizon mask at 13.5 degrees elevation has been added to Figure 14, in addition to the low-power mask at 10.5 degrees.

Transmit and receive horizon masks for the Madrid antennas (DSS-53, -54, -55, -56, -63, and -65) have been calculated from SRTM (Shuttle Radar Topography Mission) data.

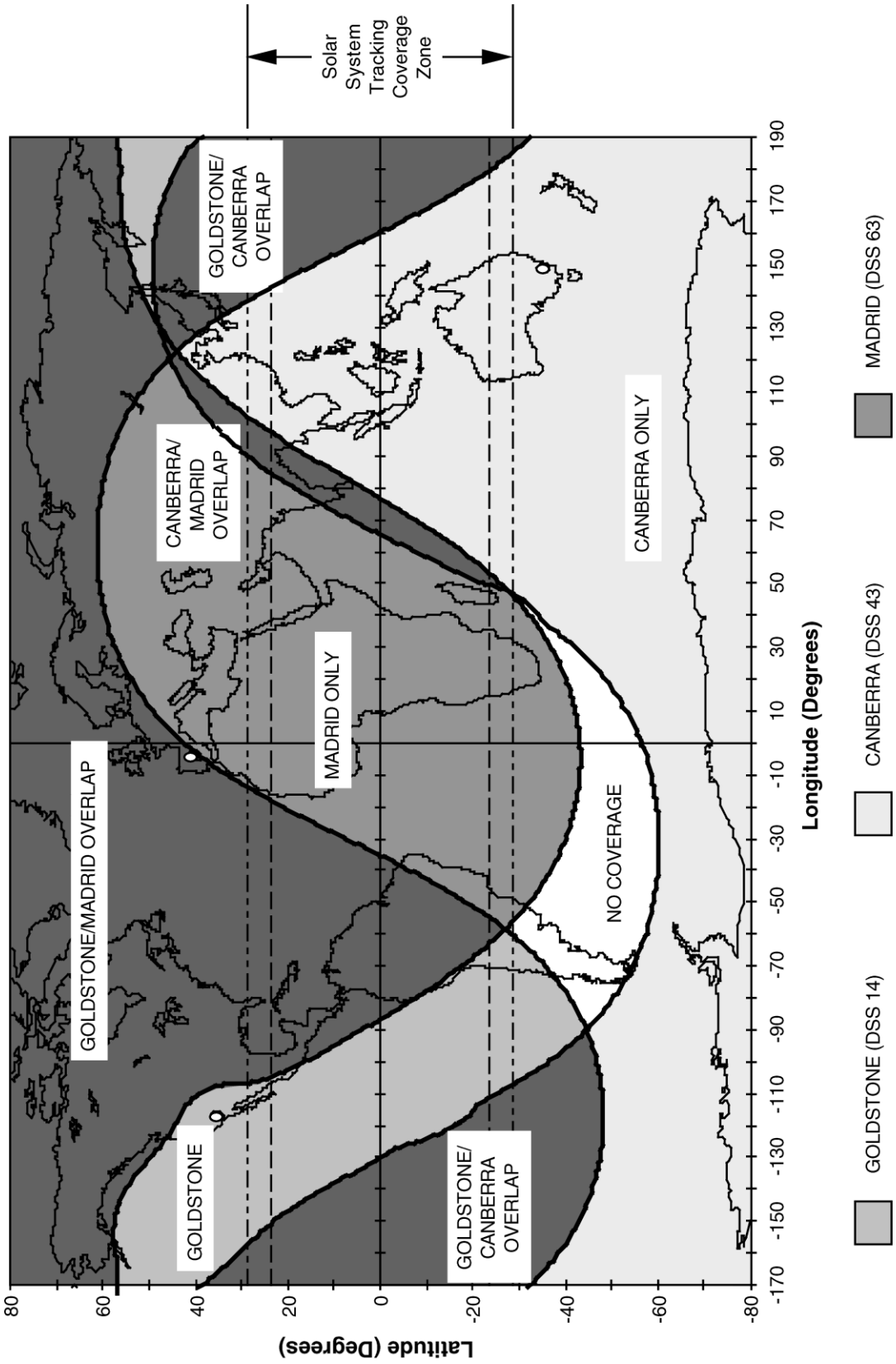

Figure 2. DSN 70-m Subnet Receive Coverage, Planetary Spacecraft

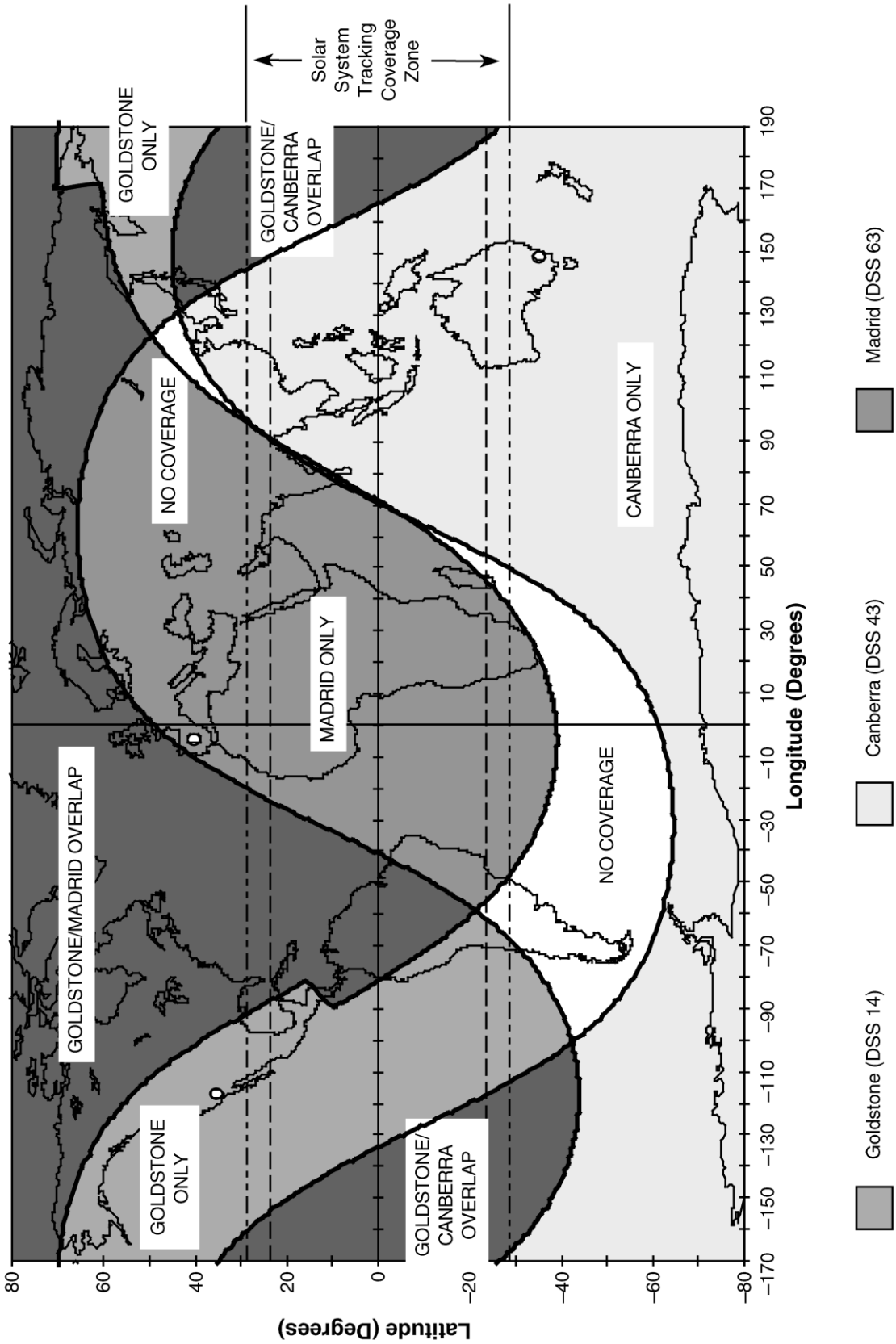

Figure 3. DSN 70-m Subnet Transmit Coverage, Planetary Spacecraft.

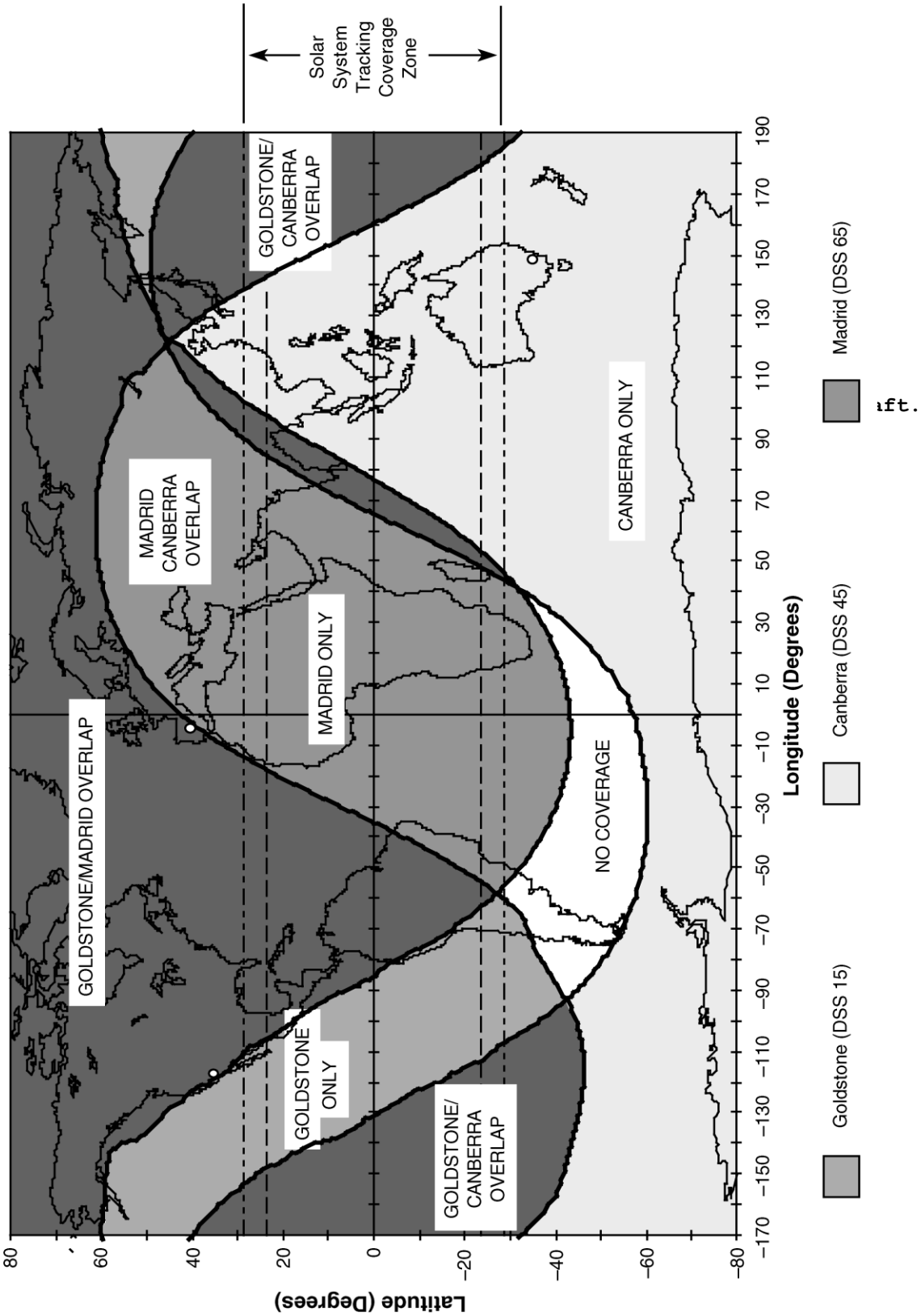

Figure 4. DSN 34-m HEF Subnet Receive Coverage, Planetary Spacecraft.

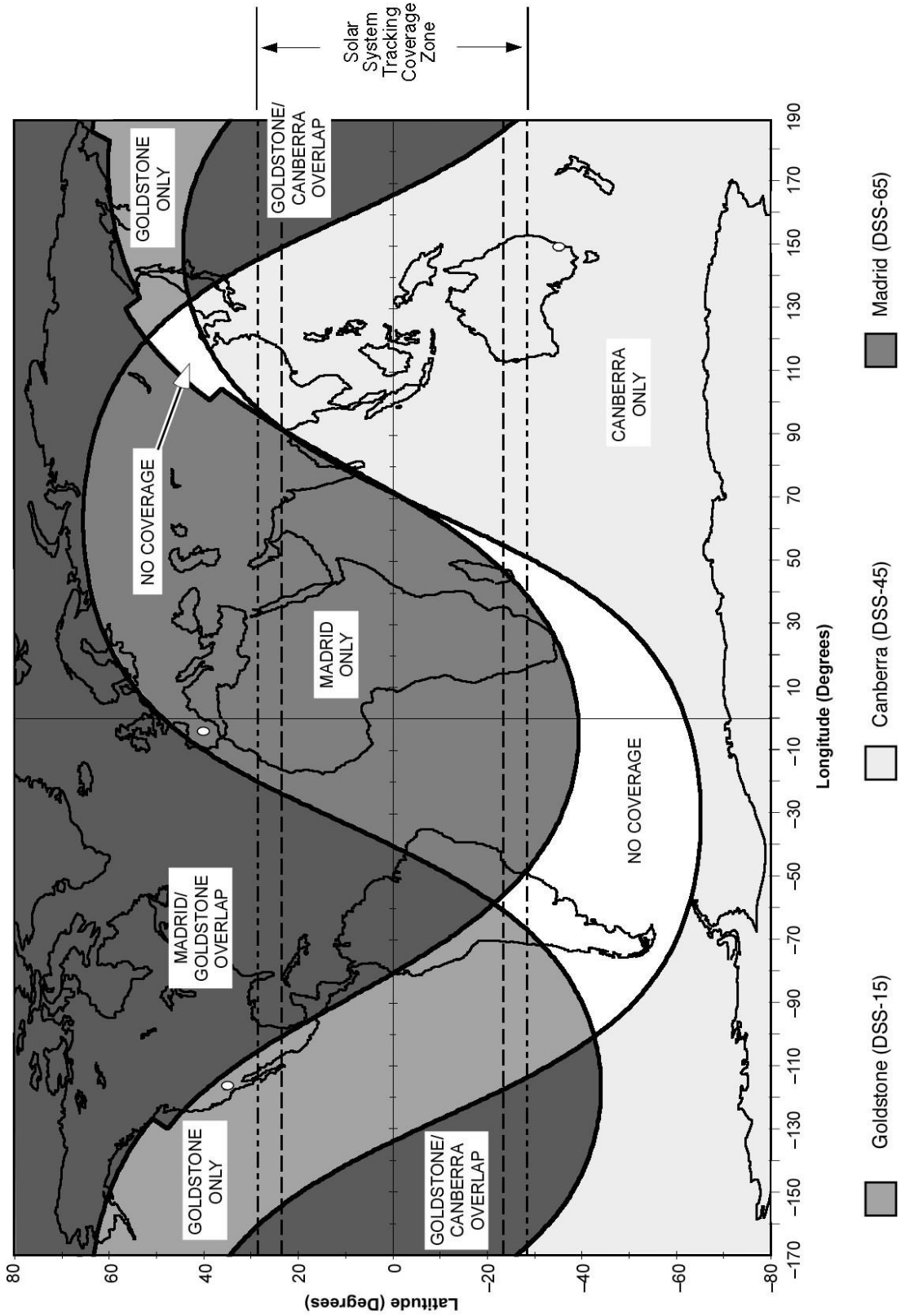

Figure 5. DSN 34-m HEF Subnet Transmit Coverage, Planetary Spacecraft

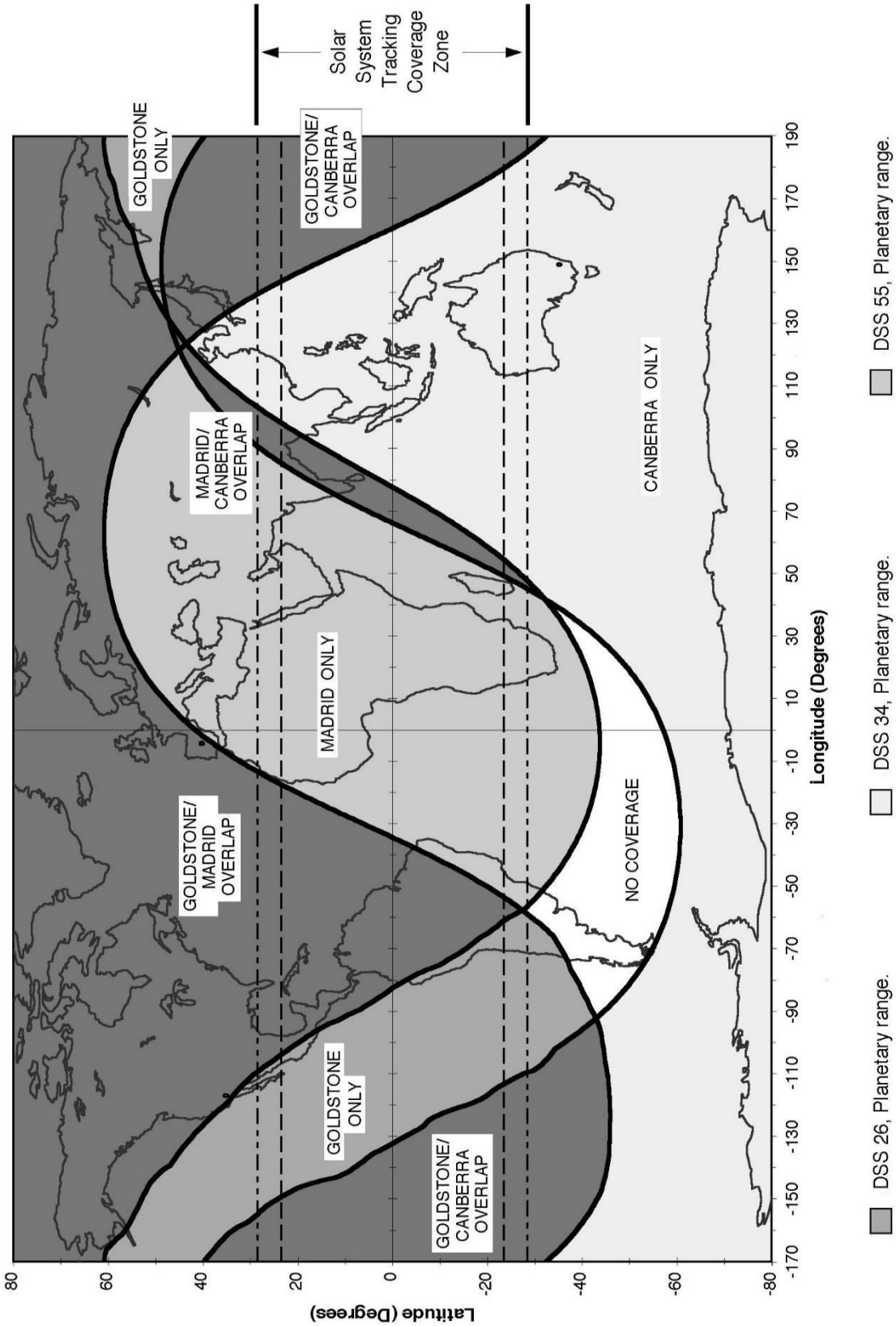

Figure 6. DSN 34-m BWG Antennas Receive Coverage, Planetary Spacecraft, Using DSS 26, 34, and 55

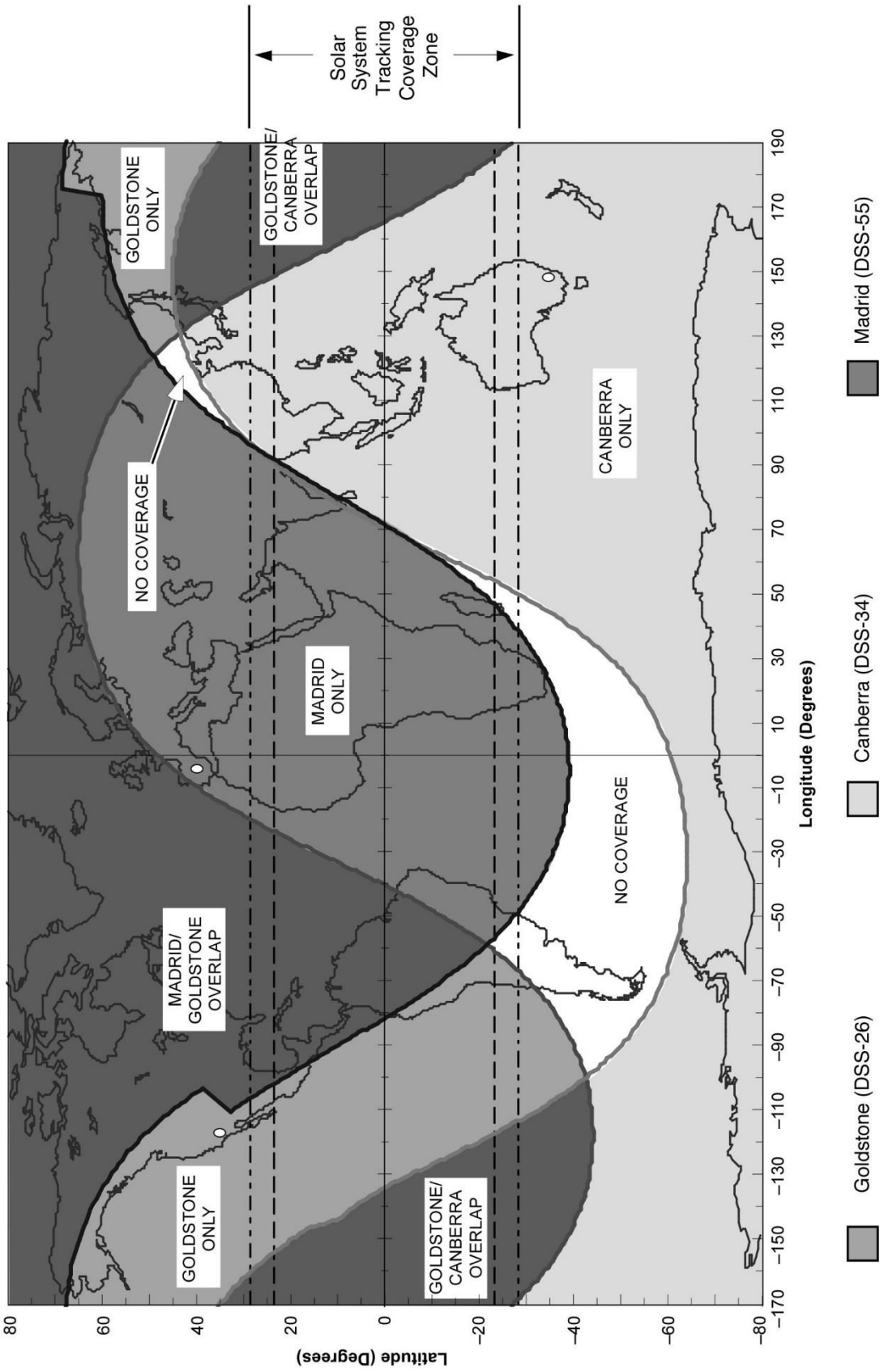

Figure 7. DSN 34-m BWG Antennas Transmit Coverage, Planetary Spacecraft, Using DSS 26, 34, and 55.

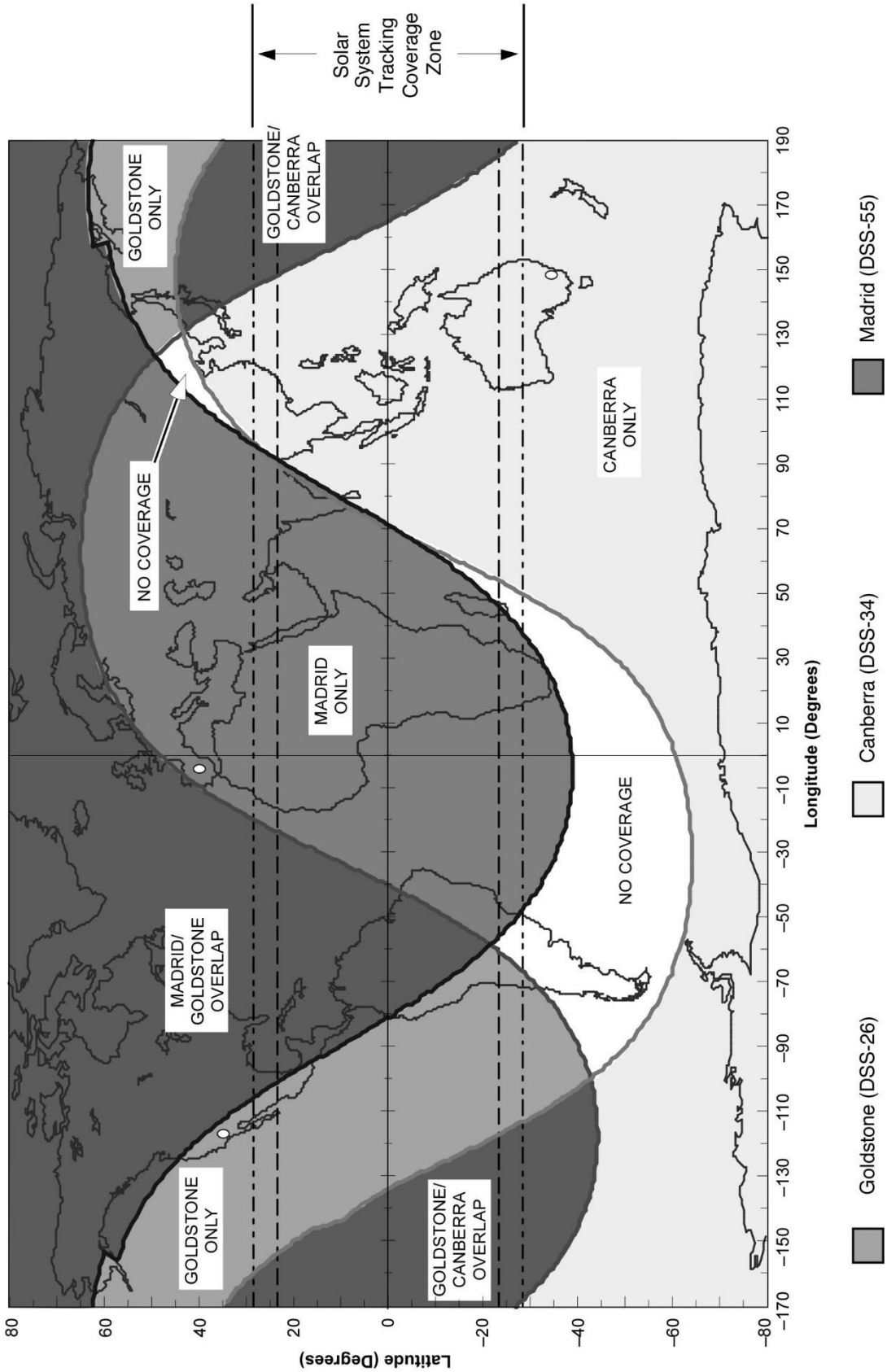

Figure 8. DSN 34-m BWG Antennas Transmit Coverage, Planetary Spacecraft, Using DSS 26, 34, and 54.

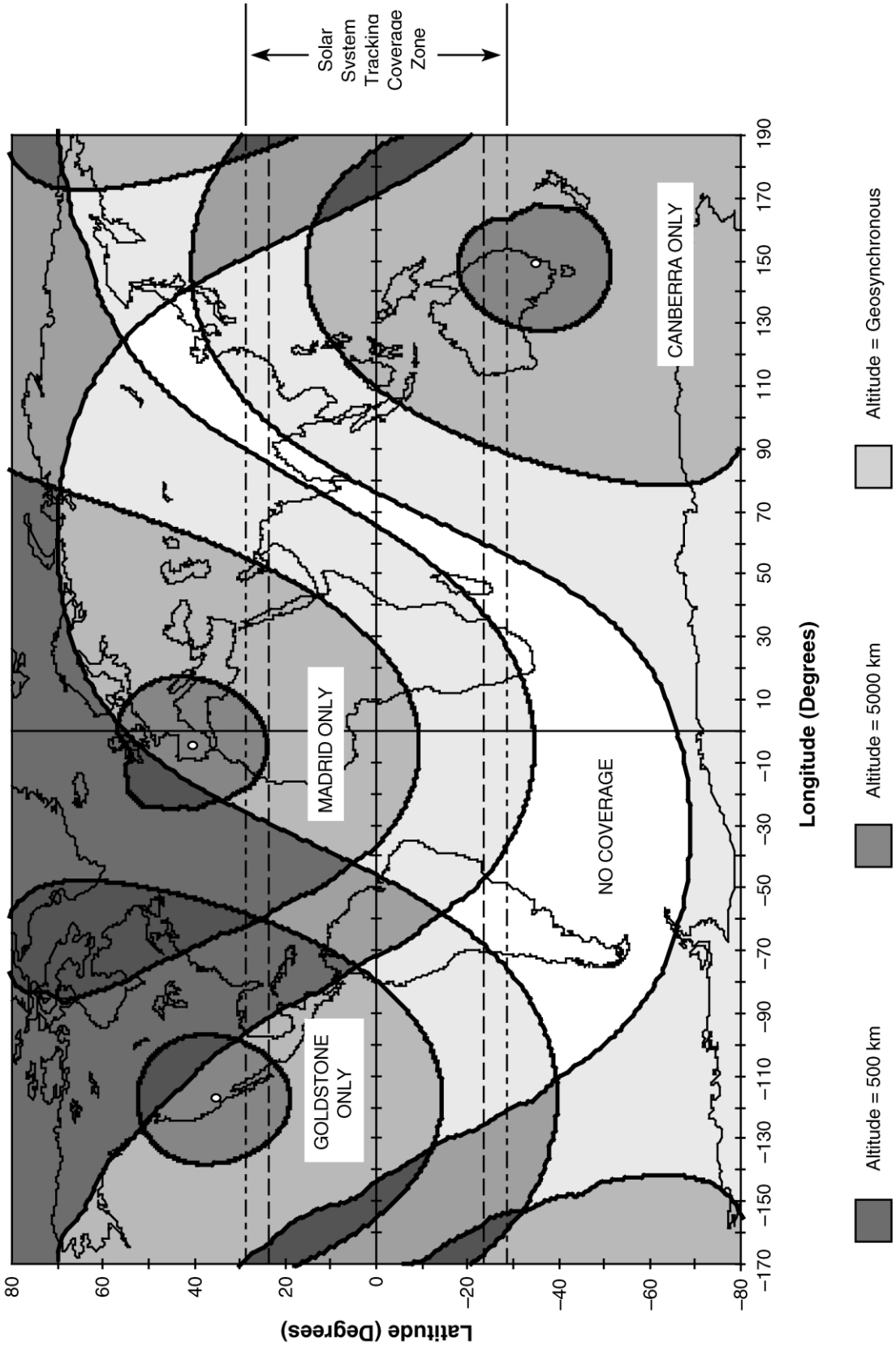

Figure 9. DSN 34-m BWG Antennas Receive Coverage, Near-Earth Spacecraft

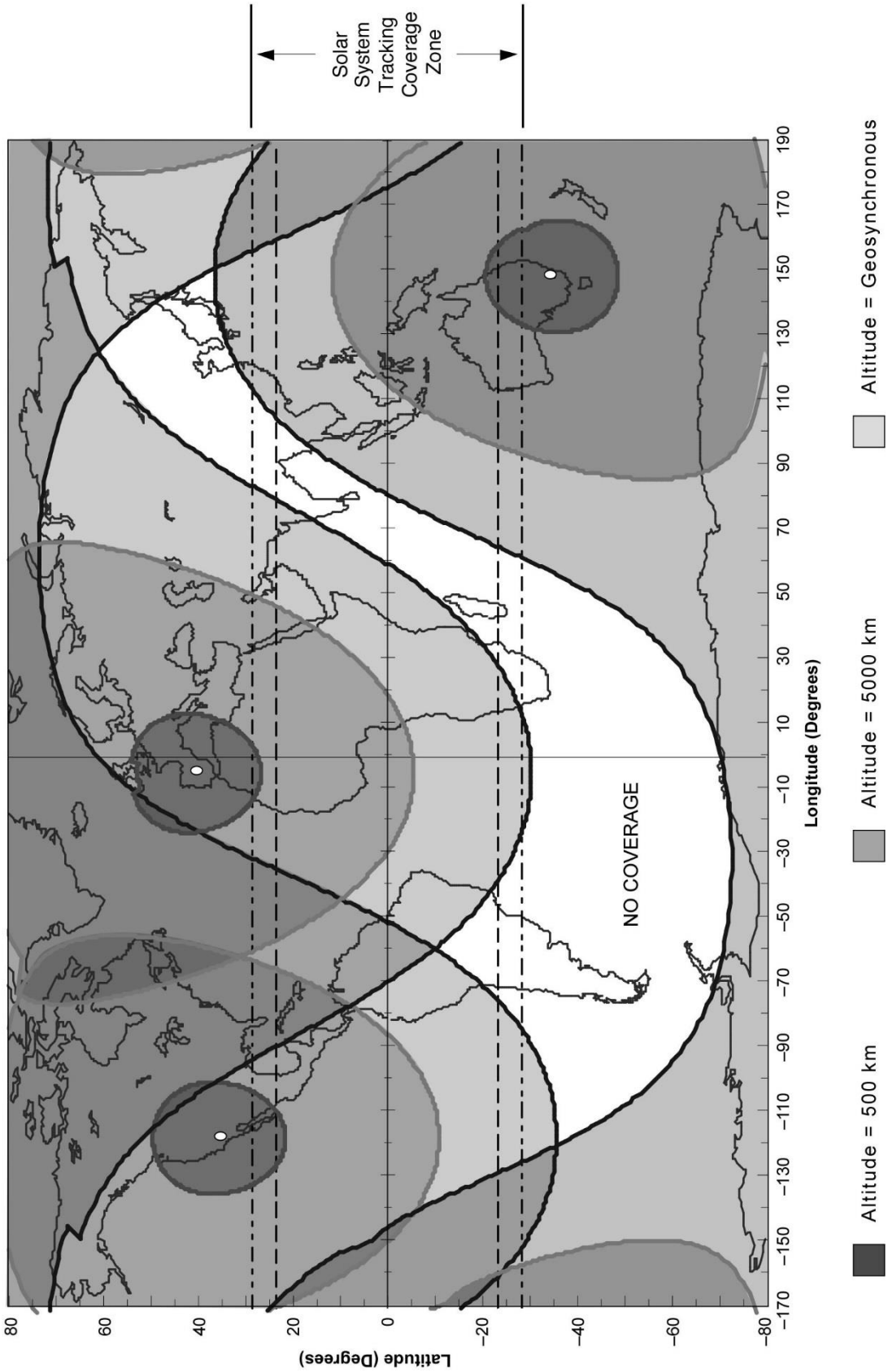

Figure 10 DSN 34-m BWG Antennas Transmit Coverage, Near-Earth Spacecraft

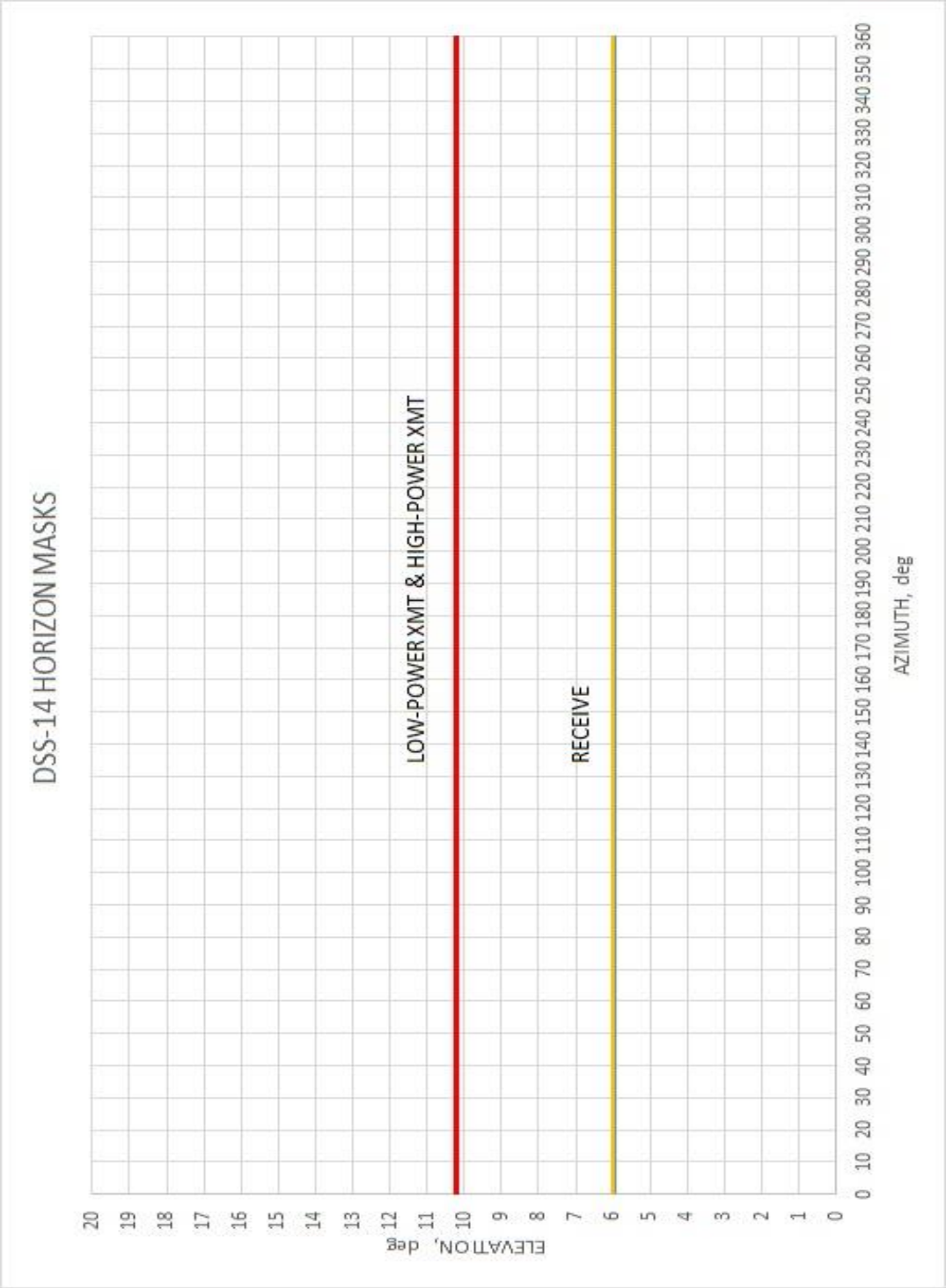

Figure 11. DSS-14, 70-m, Receive, Low-Power Transmit, and High-Power Transmit Horizon Masks

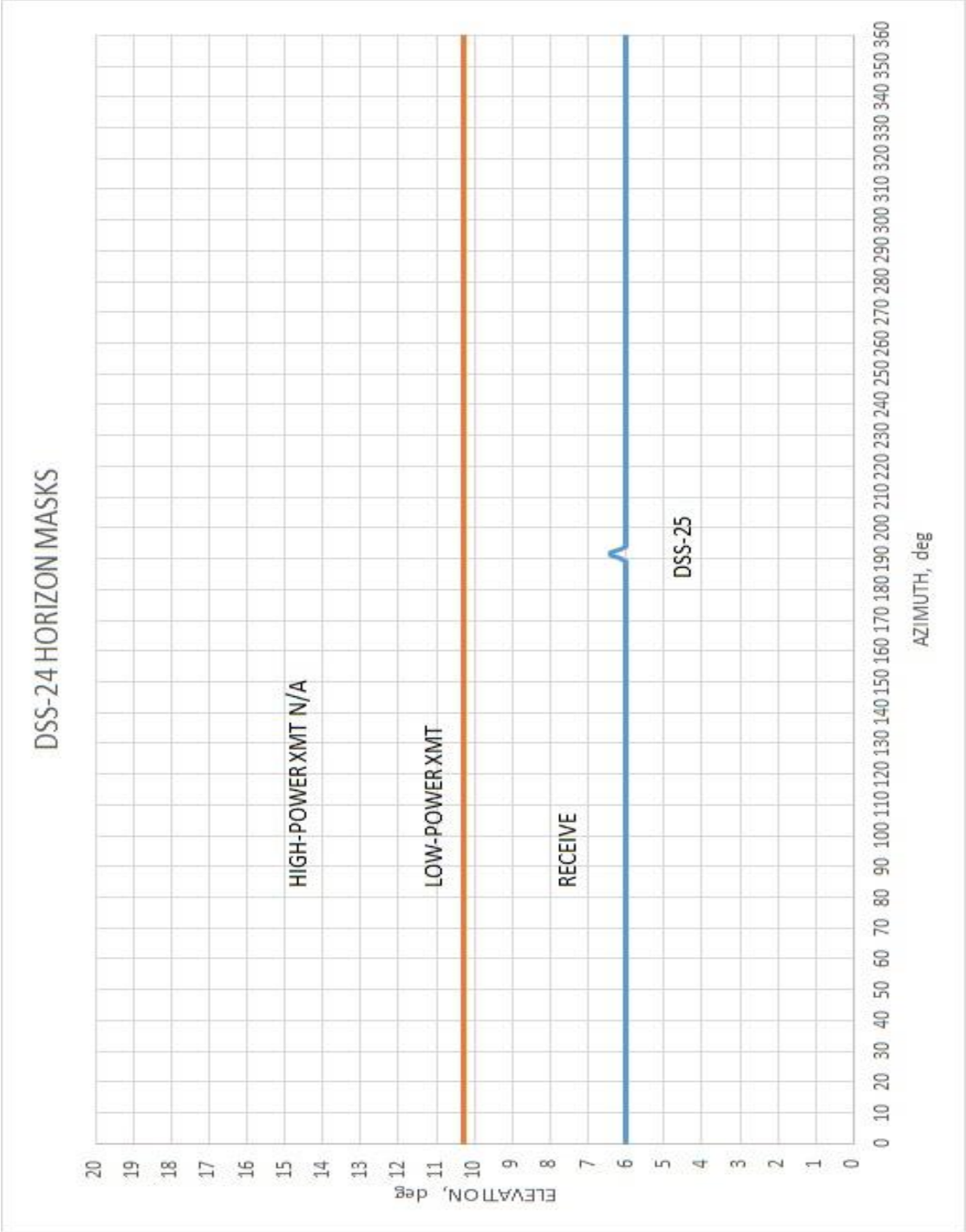

Figure 12. DSS-24, BWG, Receive and Low-Power Transmit Horizon Masks

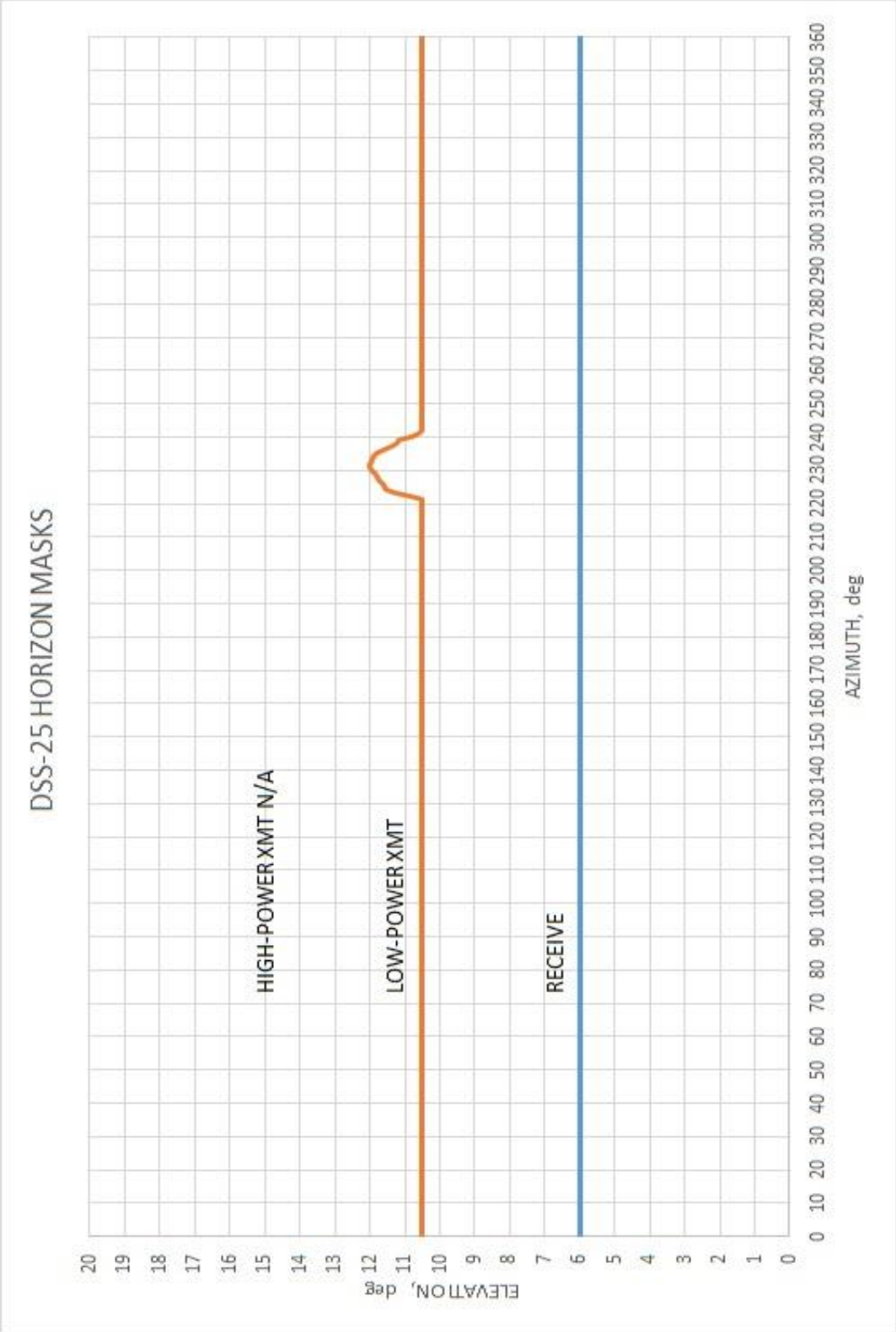

Figure 13. DSS-25, BWG, Receive and Low-Power Transmit Horizon Masks

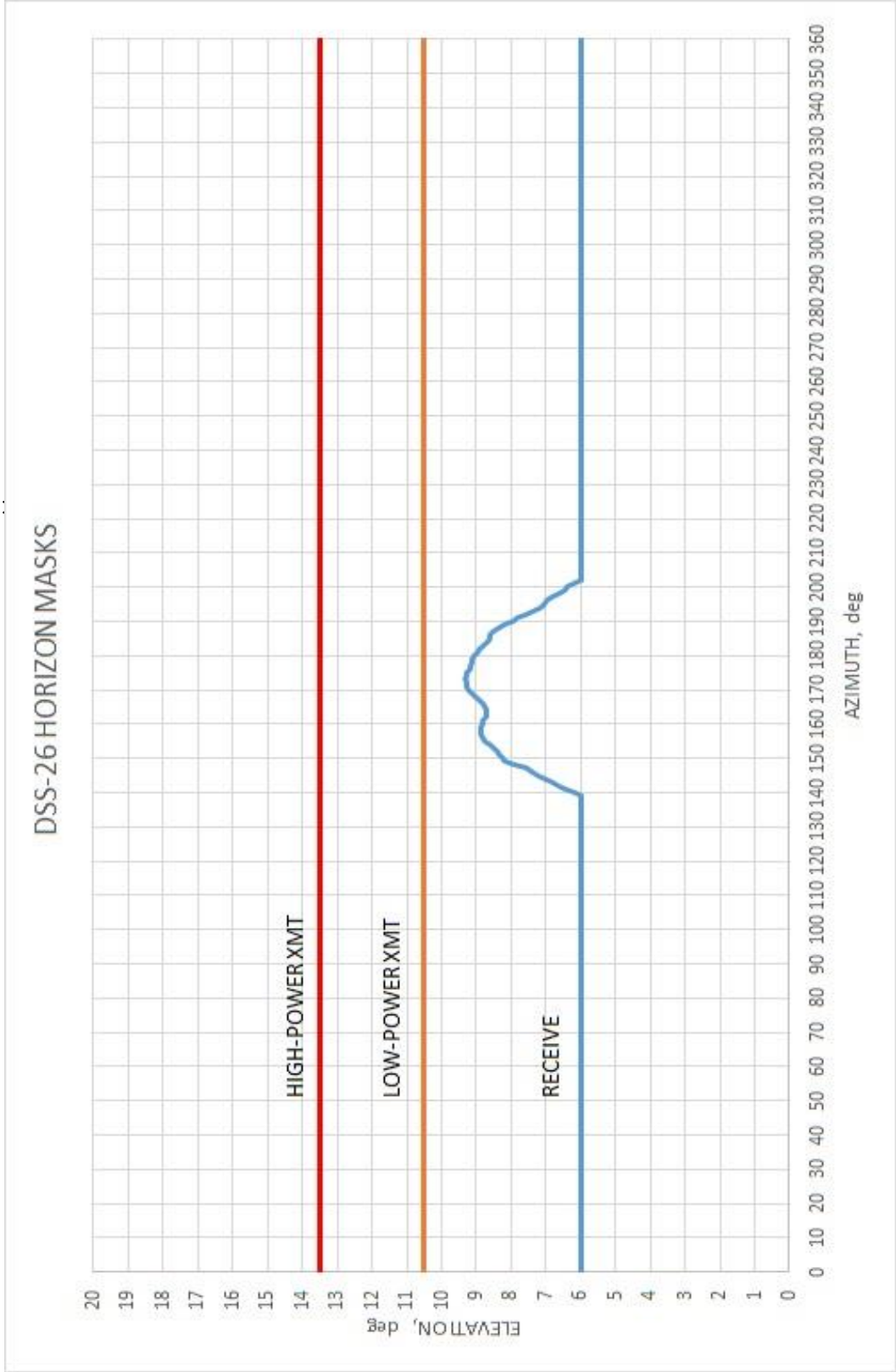

Figure 14. DSS-26, BWG, Receive, Low-Power Transmit, and High-Power Transmit Horizon Masks

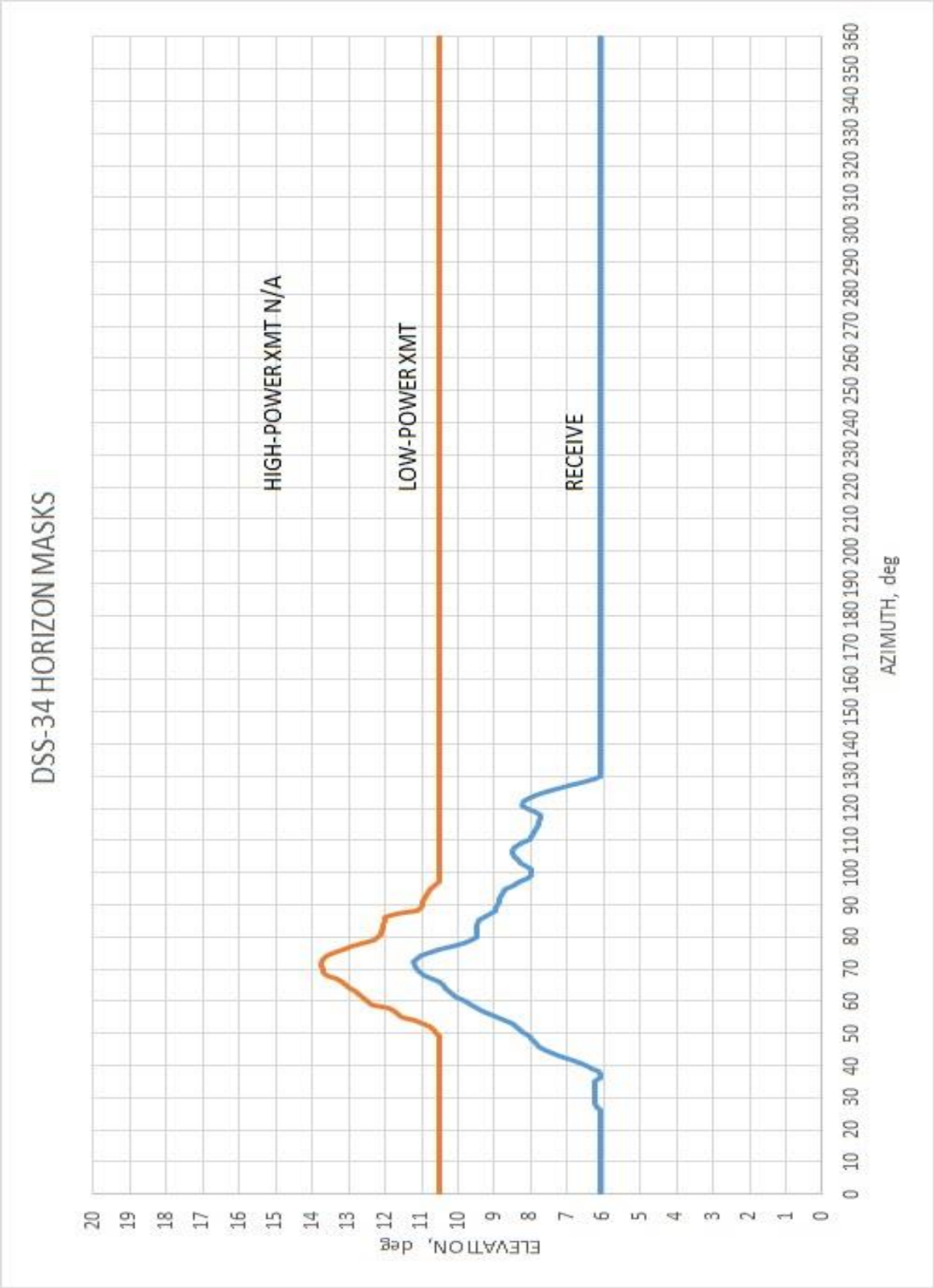

Figure 15. DSS-34, BWG, Receive and Low-Power Transmit Horizon Masks

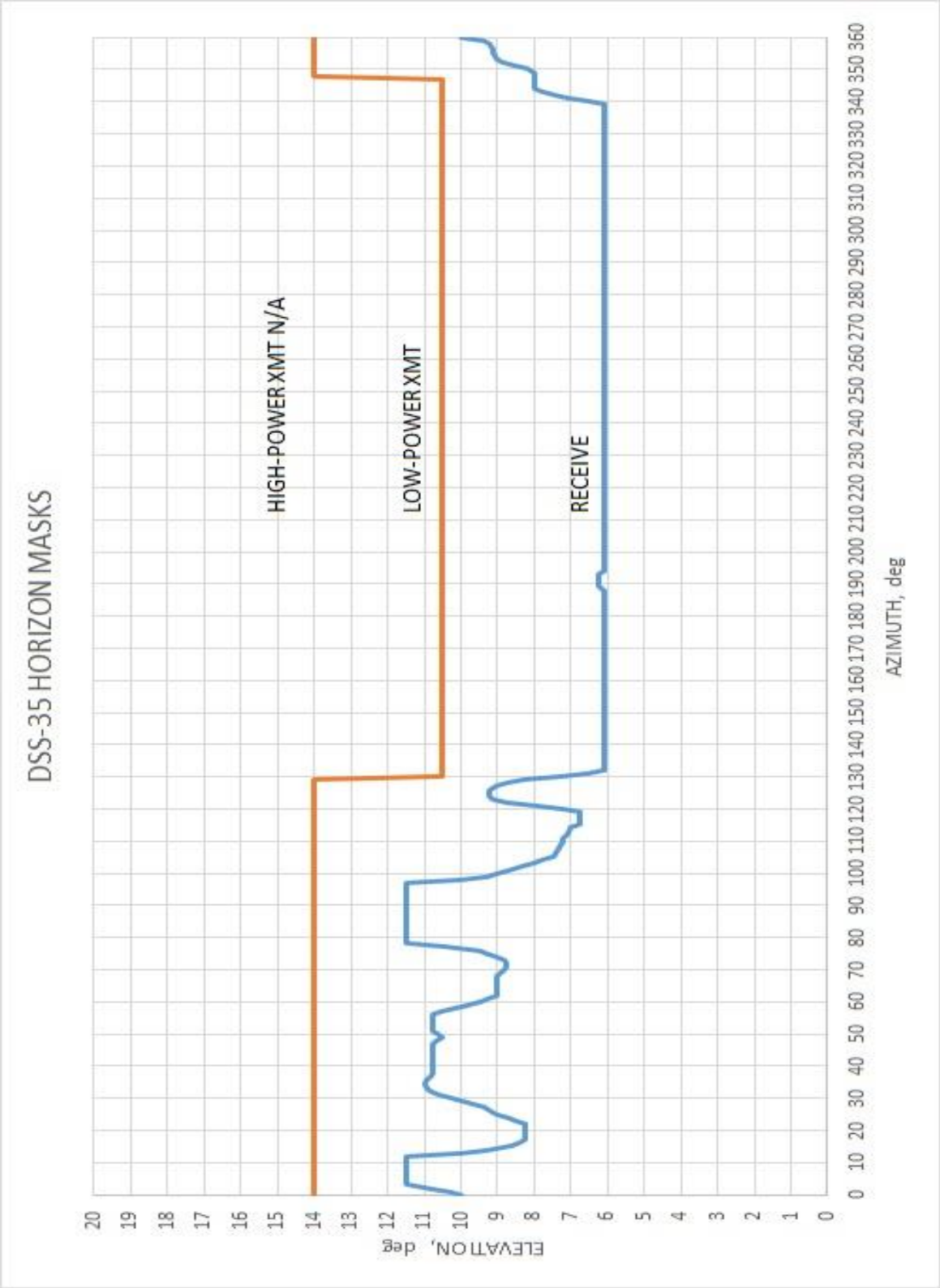

Figure 16. DSS-35, BWG, Receive and Low-Power Transmit Horizon Masks

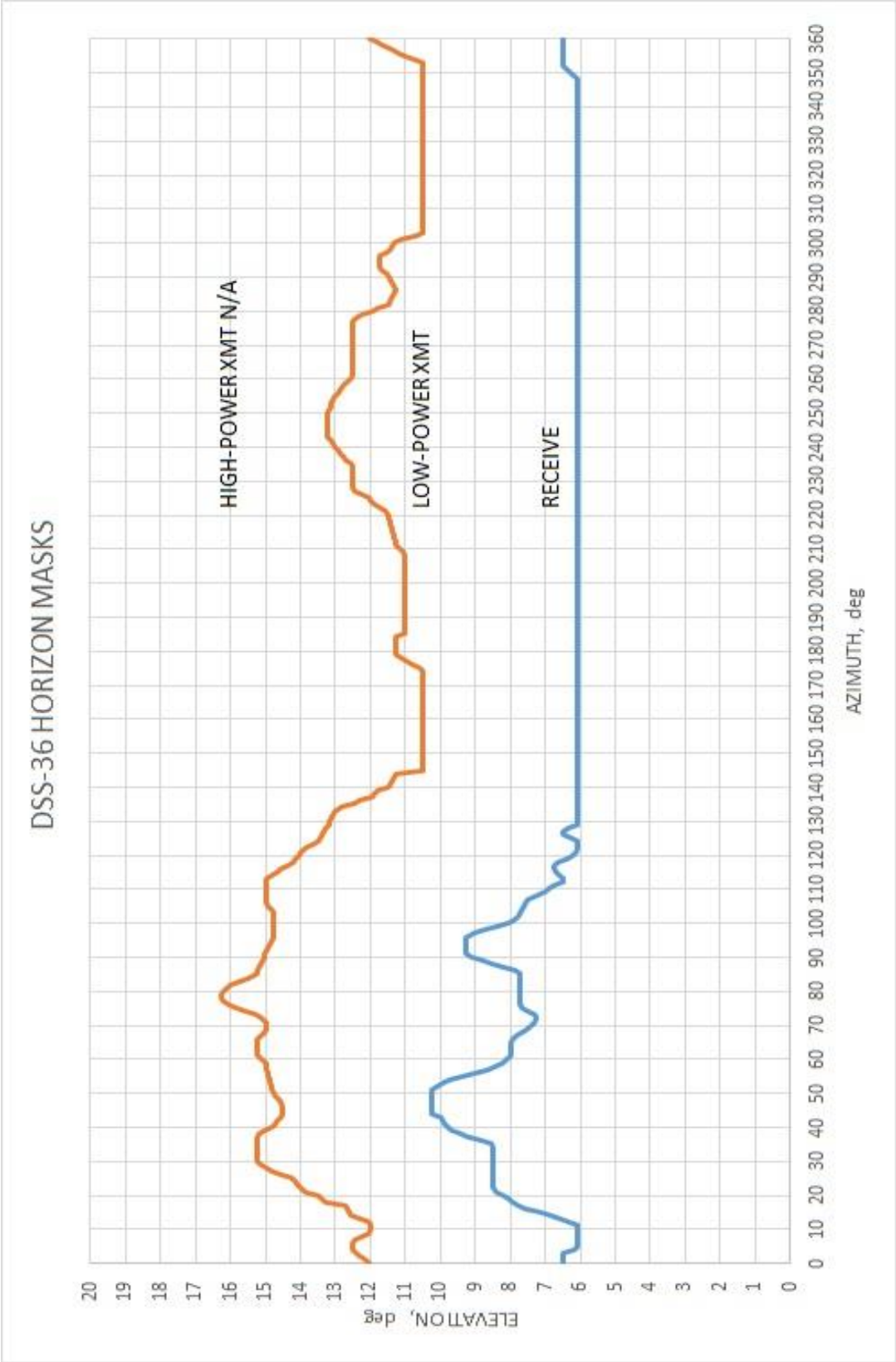

Figure 17. DSS-36, BWG, Receive and Low-Power Transmit Horizon Masks

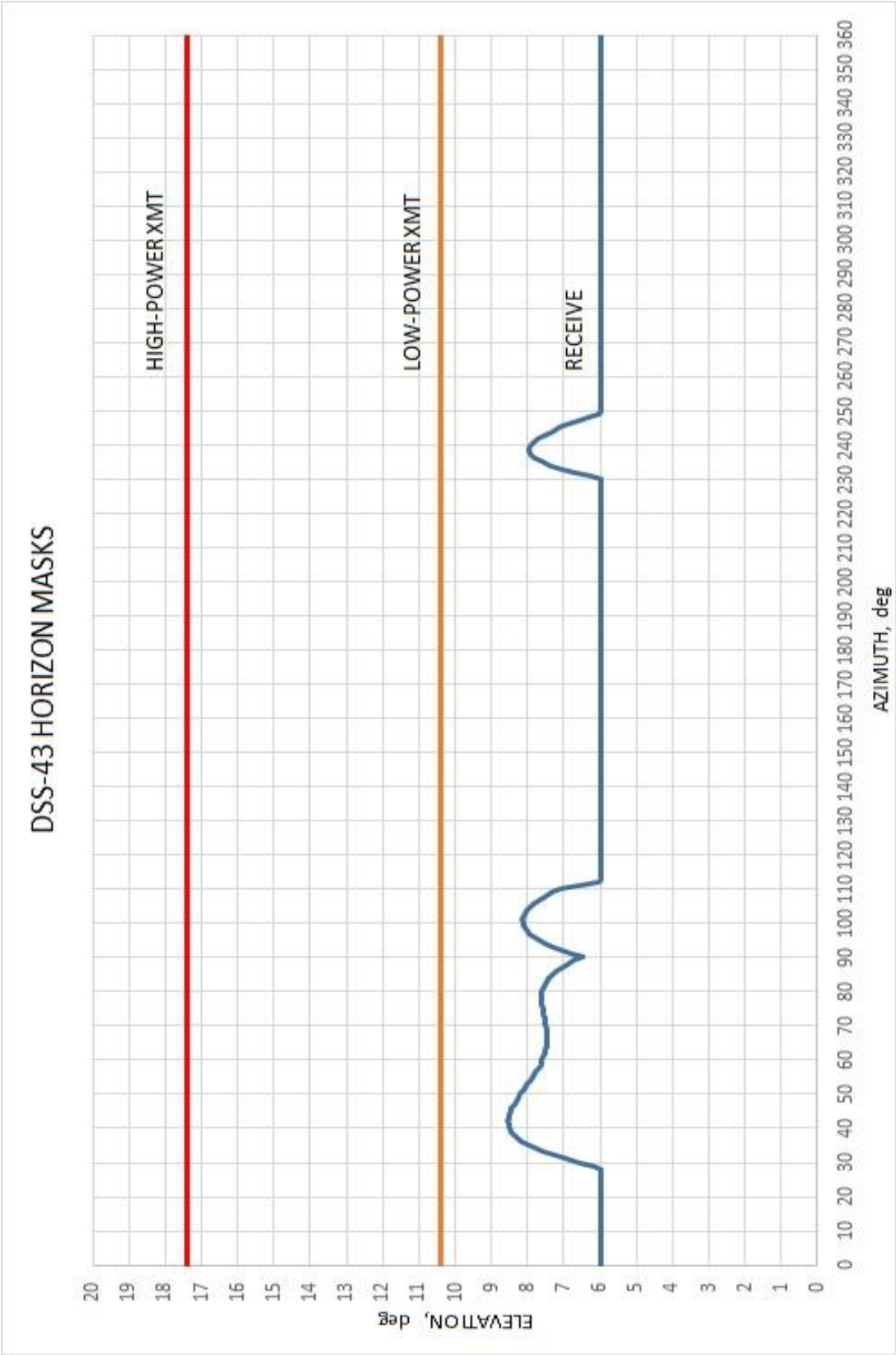

Figure 18. DSS-43, 70-m, Receive, Low-Power Transmit, and High-Power Transmit Horizon Masks

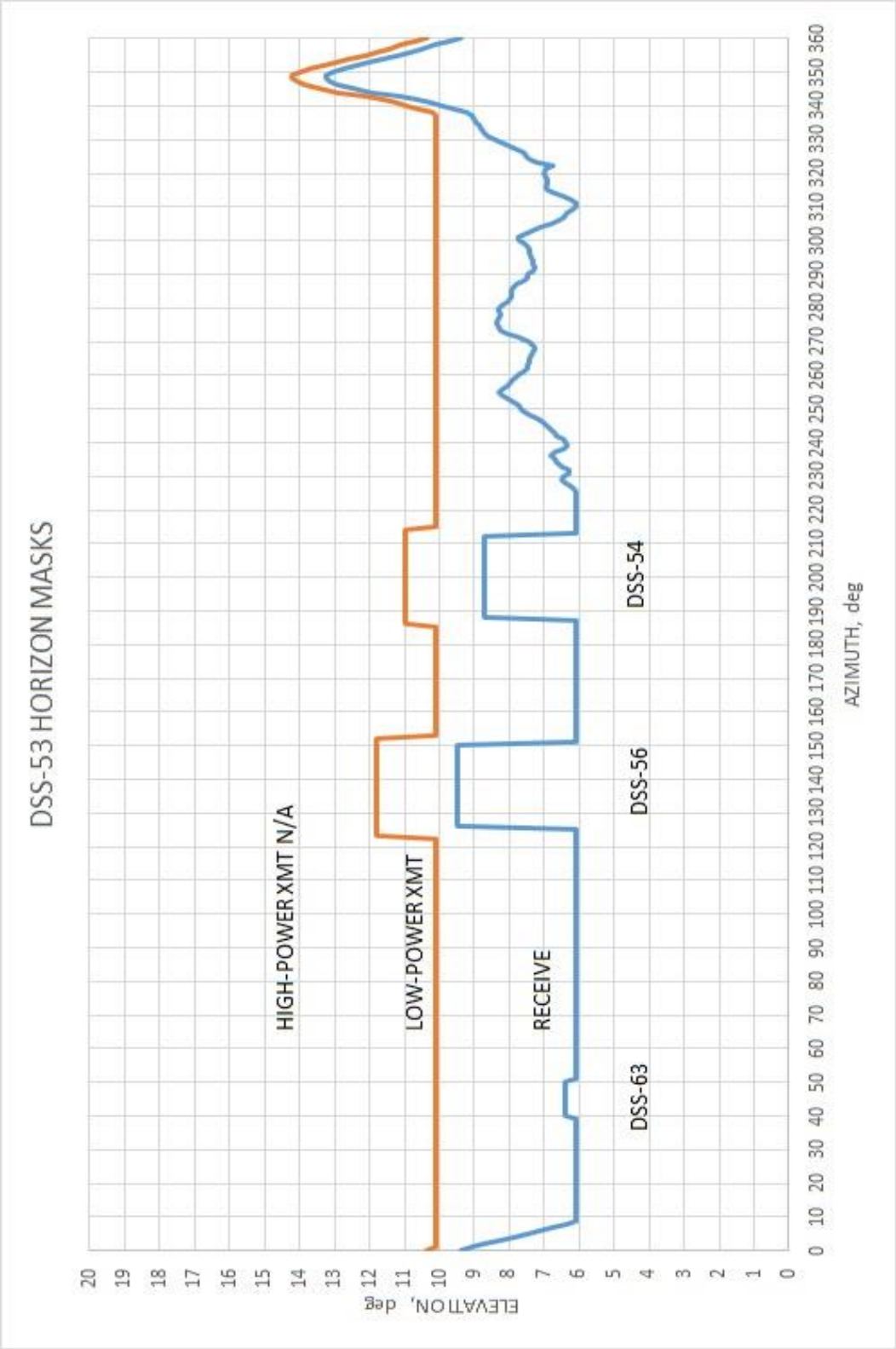

Figure 19. DSS-53, BWG, Receive and Low-Power Transmit Horizon Masks

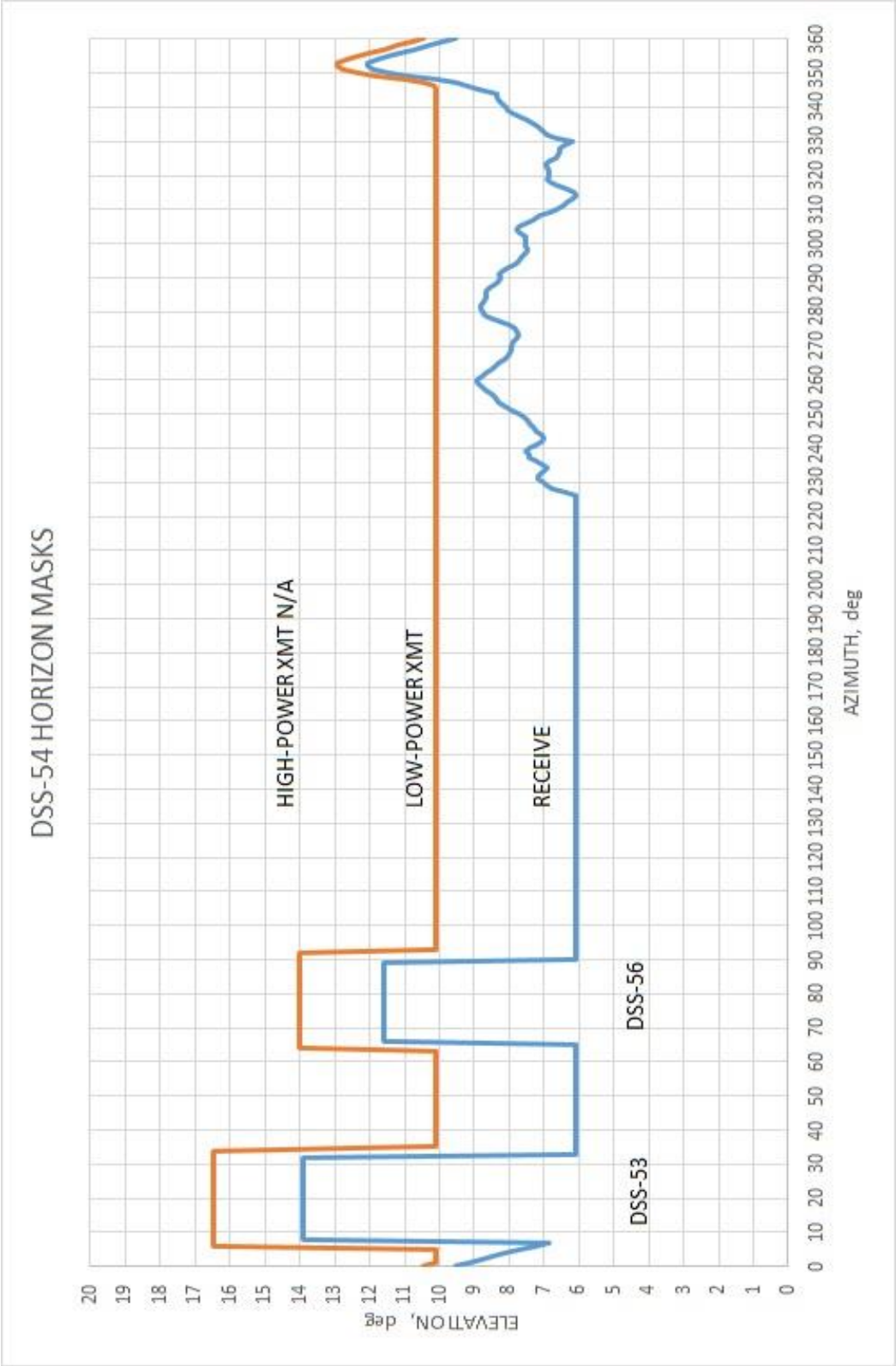

Figure 20. DSS-54, BWG, Receive and Low-Power Transmit Horizon Masks

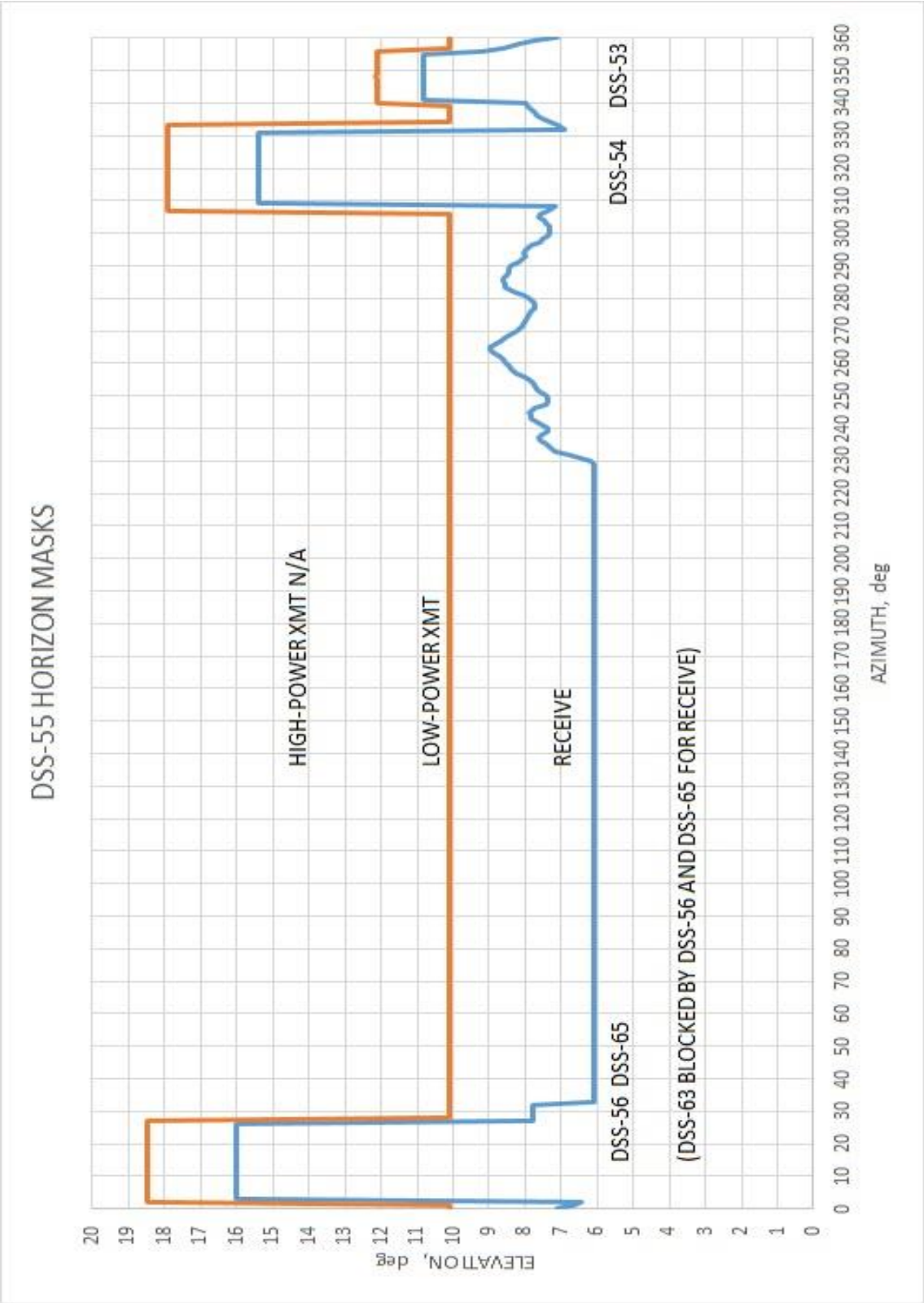

Figure 21. DSS-55, BWG, Receive and Low-Power Transmit Horizon Masks

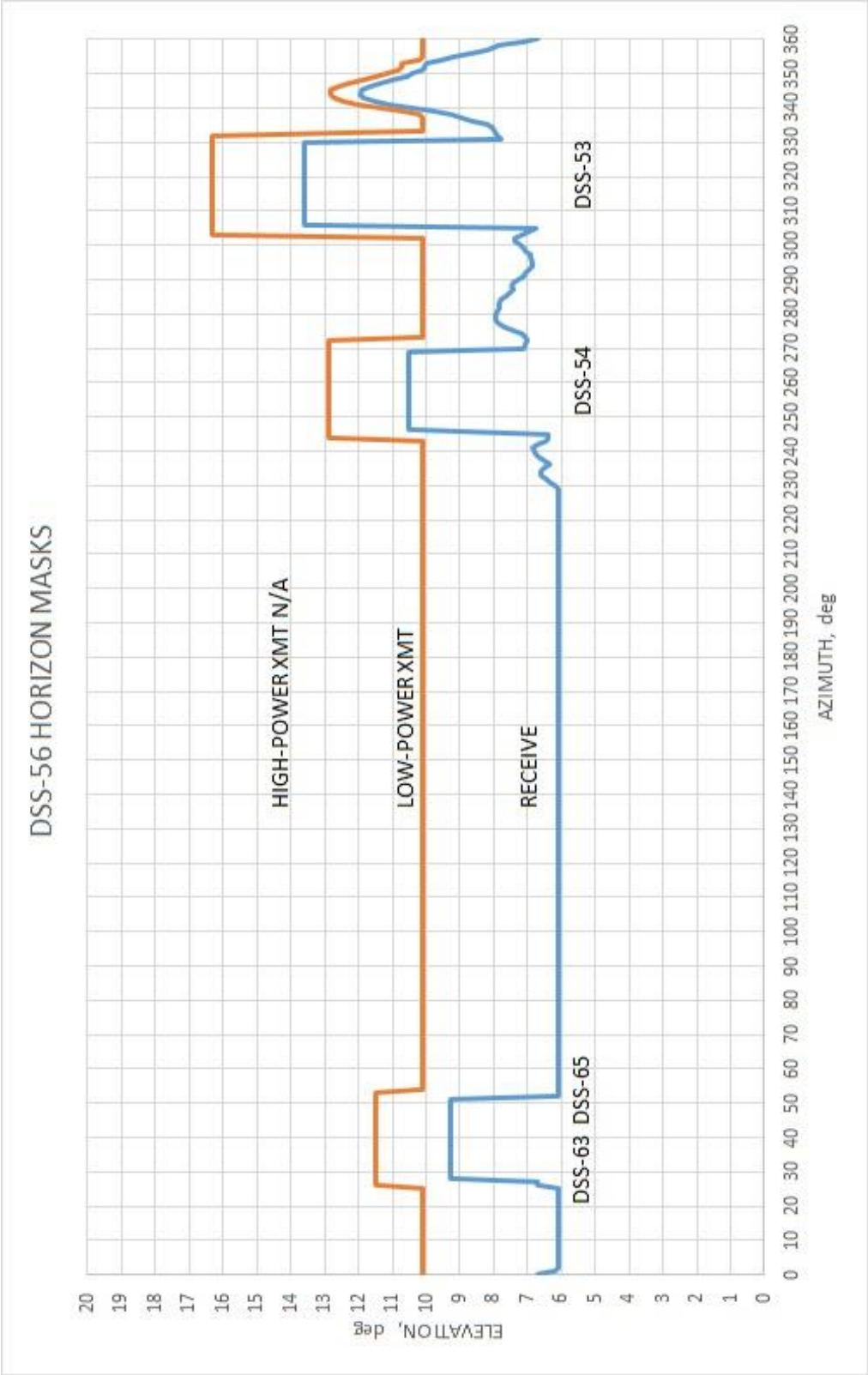

Figure 22. DSS-56, BWG, Receive and Low-Power Transmit Horizon Masks

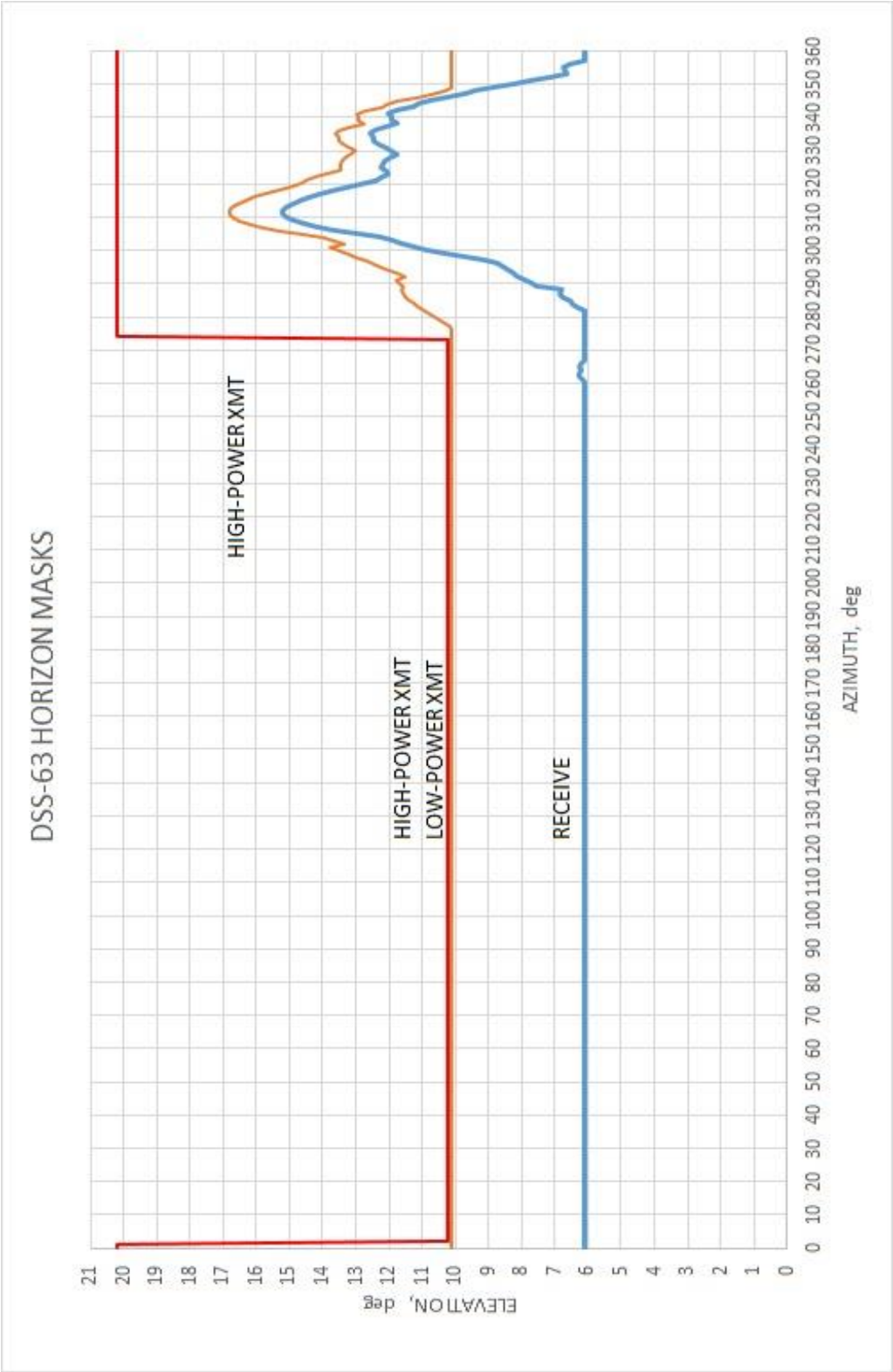

Figure 23. DSS-63, 70-m, Receive, Low-Power Transmit, and High-Power Transmit Horizon Masks

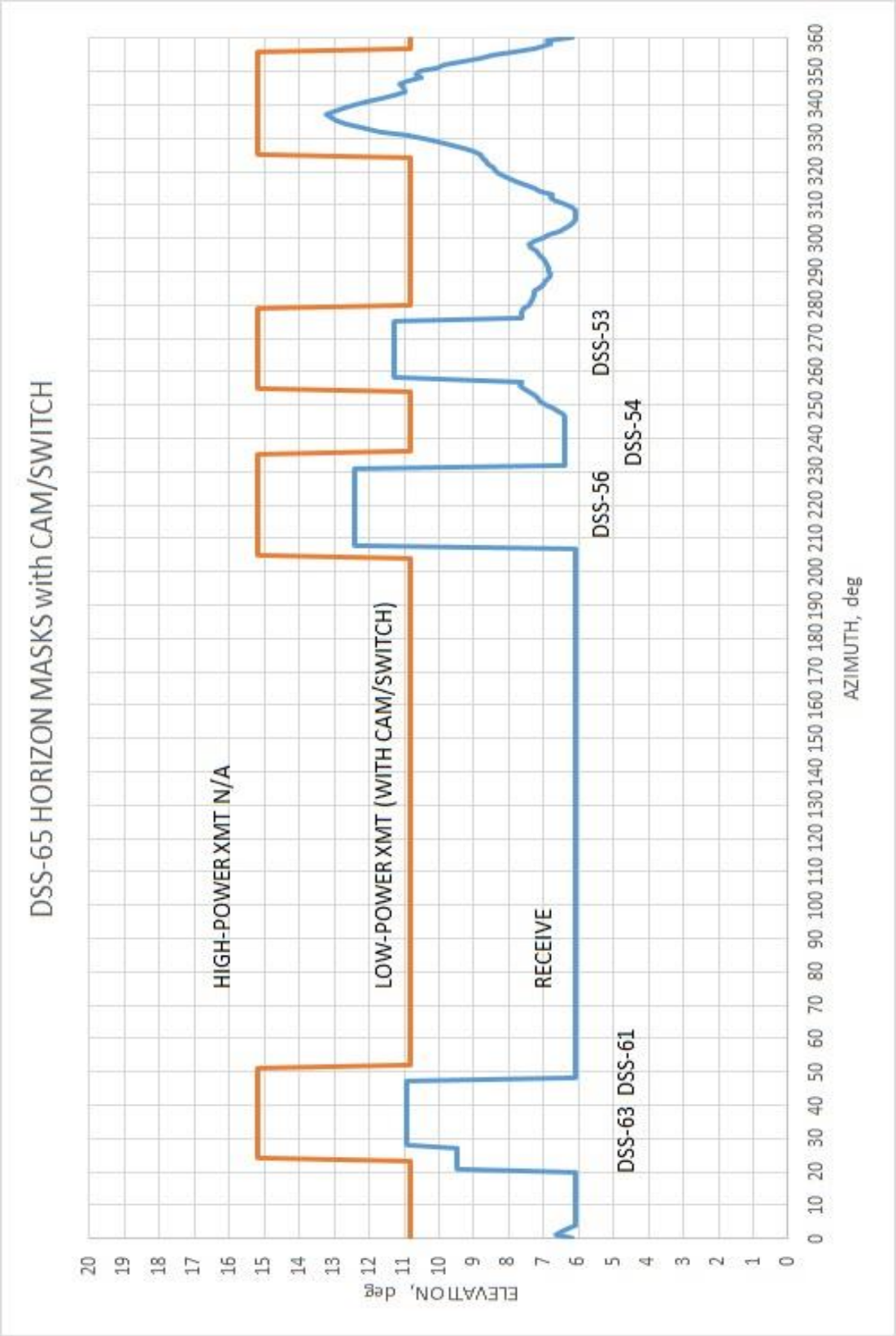

Figure 24. DSS-65, HEF, Receive and Low-Power Transmit Horizon Masks

Appendix A
References

1 C. Boucher, Z. Altamimi, and L. Duhem, *Results and analysis of the ITRF93*, IERS Technical Note 18, Observatoire de Paris, October 1994

2 B. R. Bowring, "The accuracy of geodetic latitude and height equations," *Survey Review*, 28, pp. 202-206, 1985.

Deep Space Network

302
Antenna Positioning

Document Owner:		Approved by:	
Signature Provided	01/17/2017	Signature Provided	01/17/2017
Stephen D. Slobin Antenna System Engineer	Date	Timothy Pham Communications Systems Chief Engineer	Date
Prepared by:		Released by:	
Signature Provided	01/17/2017	Signature Provided	02/10/2017
Stephen D. Slobin Antenna System Engineer	Date	Christine Chang DSN Document Release Authority	Date

DSN No. **810-005, 302, Rev. D**
Issue Date: February 10, 2017
JPL D-19379; CL #17-0712

Jet Propulsion Laboratory
California Institute of Technology

Users must ensure that they are using the current version in DSN Telecommunications Link Design Handbook website:
http://deepspace.jpl.nasa.gov/dsndocs/810-005/

Review Acknowledgment

By signing below, the signatories acknowledge that they have reviewed this document and provided comments, if any, to the signatories on the Cover Page.

Signature Provided	01/17/2017	Signature Not Provided	
Jeff Berner DSN Project Chief Engineer	Date	David Rochblatt Antenna System Engineer	Date

Change Log

Rev	Issue Date	Prepared By	Affected Paragraphs	Change Summary
Initial	10/7/2004	Stephen Slobin Robert Sniffin	All	New Module
A	12/15/2009	Stephen Slobin Robert Sniffin	Many	Removed references and information related to the decommissioned 26-m antennas.
B	6/1/2010	Stephen Slobin Robert Sniffin	Table 1	Changed Azimuth Motion Limits to Travel Range and Corrected DSS-27 cable wrap center value. Eliminated the Rev. E designation for the document series.
C	02/09/2015	Stephen Slobin Christine Chang	Table 4 Figures 4,5,6,7 Section 2.1 Rev. B, Section 2.3.2 Section 2.5.2 Section 2.6	Updated MRE values – added DSS-35. Added to show wind effect on pointing loss. DSS-27 HSB antenna decommissioned. Removed, IIRV no longer supported in DSN. Expanded description of blind pointing errors. Expanded description of CONSCAN and monopulse.
D	02/10/2017	Stephen Slobin Christine Chang	Sec. 2.6.2 Table 4	Ka-band monopulse MRE at DSS-36 added. Added DSS-36 blind pointing performance. Noted that DSS-45 is decommissioned.

Contents

Illustrations

Figure **Page**

Tables

Tables **Page**

1 Introduction

1.1 Purpose

This module describes the pointing capabilities of the antennas used by the Deep Space Network (DSN) in sufficient detail to enable a telecommunications engineer to design spacecraft missions that are compatible with these capabilities.

1.2 Scope

This discussion in this document is restricted to the mechanical limitations of the antennas, their control algorithms, and the error sources that influence the ability to point the radio frequency (RF) beam in the desired direction. Wind velocity statistics that can be used to estimate the effects of wind on antenna pointing are presented in module 105. Coverage and restrictions to coverage caused by terrain masking are discussed in module 301.

2 General Information

Antenna positioning or pointing is the process of directing the antenna beam towards the desired target. The target may be a spacecraft or radio source that is producing a receivable signal. The target may also be a spacecraft other object at a known or suspected position that is not producing a signal but to which RF energy must be directed. The antenna must keep its RF beam properly aimed for the scheduled duration of the spacecraft or other observation, often referred to as a pass.

There are two types of antenna beam pointing. The first of these is blind pointing, sometimes referred to as open loop pointing, that relies on the ability to model the direction of the antenna beam in the presence of systematic and random processes. The second is closed-loop pointing that derives corrections from the received signal. Blind pointing produces larger errors, but is the only method available in the absence of a received signal or during radio science observations when the data quality would be adversely affected by closed loop positioning.

Antenna pointing is not only influenced by random errors due to wind and thermal effects, but also due to imperfect modeling of systematic pointing errors that vary unpredictably throughout the sky or along a particular path in the sky when tracking a spacecraft. Standard first-order systematic error pointing models (used for blind pointing) may not be adequate to describe “high frequency” (e.g., 2 or more cycles per 360 degrees movement in azimuth or elevation) variations in pointing. Fourth-order blind pointing models exist for all antennas and frequency bands.

2.1 Antenna Characteristics

The DSN employs three general types of antennas. At least one of each type antenna exists at each DSN complex. The antenna types are the 70-m antennas, the 34-m high-efficiency (HEF) antennas, and the 34-m beam waveguide (BWG) antennas. All of these

antennas employ an azimuth-elevation (AZ-EL) mount. The Goldstone high-speed beam waveguide (HSB) antenna (DSS-27) has been decommissioned.

The antennas are pointed by variable-rate servo systems that use the antenna pointing commands as input and the axis position encoders (azimuth and elevation) as feedback. The 70-m antennas also have a *precision mode* where the main reflector is slaved to a small hour-angle/declination instrument, referred to as the *Master Equatorial (ME)*, using optical collimation techniques. The ME is mounted at the intersection of the 70-m azimuth and elevation axes in a controlled environment and on a separate foundation to eliminate vibration and thermal effects. Servo performance is generally a function of antenna size, with higher tracking and slew rates being available from the smaller antennas. Table 1 summarizes the primary mechanical characteristics of the various antennas.

2.2 Coverage Restrictions and Servo Performance Limits

DSN antennas have restrictions to their coverage from two sources other than terrain masking. The first of these is the antenna *keyholes* – areas where coverage in not possible because the reflector would need to be positioned about the secondary (upper) axis in such a way that it would run into the primary (lower) axis or its supporting structure. The sizes of the keyholes can be inferred from the elevation motion limits given in Table 1 and are illustrated on the horizon mask charts in module 301. The second restriction occurs near the ends of the primary axis where the amount of motion required to correctly position the antenna beam exceeds the capability of the primary axis servo should the orbital path pass near an imaginary extension of the lower axis.

Azimuth-elevation antennas have an area of non-coverage directly above the antenna resulting from the fact that should a spacecraft pass directly overhead, the antenna would have to instantaneously rotate 180 degrees in azimuth to follow it. Clearly, this is not possible but, for spacecraft passing nearly overhead, the azimuth rate is finite and can be calculated from the equation.

$$r_{AZ} = \frac{r_{SC}}{\cos(EL_{Peak})} \tag{1}$$

where

r_{AZ} = the peak azimuth rate required of the antenna

r_{SC} = the cross-elevation rate of the spacecraft as seen from the antenna

EL_{Peak} = the maximum elevation reached by the spacecraft.

Table 1. DSN Antenna Mechanical Characteristics

Parameter	70-m	34-m HEF	34-m BWG
Antenna Mount	AZ-EL	AZ-EL	AZ-EL
Slew Rate, each axis (deg/s)	0.25	0.8	0.8
Minimum Tracking Rate, each axis (deg/s)	0.0001	0.0001	0.0001
Maximum Tracking Rate, each axis (deg/s)	0.25	0.4	0.4
Acceleration each axis (deg/s^2)	0.2	0.4	0.4
Deceleration (braking) each axis (deg/s^2)	2.5	5.0	5.0
Axis Encoder Resolution (mdeg)	0.021	0.021	0.021
Axis Encoder Accuracy (mdeg)	±0.171	±0.171	±0.171
Master Equatorial Axis Encoder Resolution (mdeg)	0.021	–	–
Master Equatorial Axis Encoder Accuracy (mdeg)	±0.343	–	–
Azimuth Travel Range from Wrap Center (deg)	±265	±225	±225
GDSCC Wrap Center (deg)	45	135	135
CDSCC Wrap Center (deg)	135	45	45
MDSCC Wrap Center (deg	45	135	135
Elevation Motion Limits (deg)	6 – 89.5	6 – 89.5	6 – 89.5

For spacecraft tracked at near-sidereal rates, the areas of non-coverage are not large but must be avoided by appropriate scheduling. The maximum peak spacecraft elevation is limited to 89 degrees for continuous tracking when using the 70-m antennas. For the HEF and BWG antennas, the maximum peak elevation for continuous tracking is limited to 89.4 degrees.

Formula (1) can be used for Earth-orbiter spacecraft; however, the rate of spacecraft as seen from the antenna will be a function of orbit altitude. Figure 1 illustrates the effect of orbit altitude on peak azimuth rate for several circular orbits.

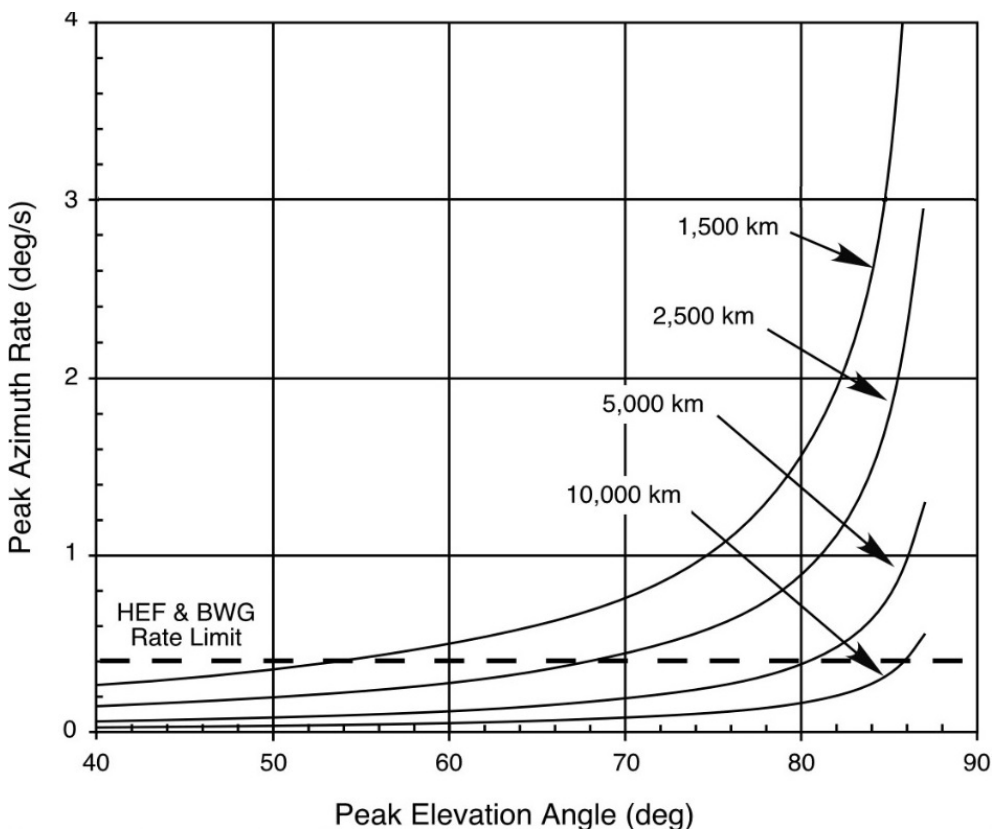

Figure 1. Azimuth Rates for Selected Circular Orbits.

2.3 Pointing Modes

DSN antennas are normally operated by aiming their RF beams in accordance with a pre-determined set of instructions referred to as antenna pointing predictions or *predicts*. The format and contents of the predicts depends on their source, the type of support being provided, and the antenna being used. In addition to predict-driven modes, there are specialized pointing modes available for the antenna type. All pointing is provided in terms of the actual

direction to the target. The antenna controller adds whatever corrections are required to compensate for the atmosphere and imperfections in the antenna response, calculates the rate at which each axis must move to reach the next point at the desired time and delivers this information to the antenna servos. Position feedback from the selected axis position encoders is constantly monitored and used to adjust the axis tracking rates.

The 34-m BWG antennas have a single predict-driven mode, the direction cosine mode. The Improved Inter-Range Vector (IIRV) mode is no longer supported in the DSN. The 34-m HEF and 70-m antennas have the direction cosine predict-driven mode. In addition, the 70-m antennas also have the precision tracking mode. Common to all antennas are the planetary and sidereal tracking modes. These pointing modes are further described below.

2.3.1 Direction Cosine Mode

Target positions are delivered to the station as a binary file of predict points, where each point contains time, target range, and topographic direction cosines (X, Y, and Z) with their 2nd and 4th differences for use in an Everett Interpolation algorithm within the antenna controller. The points may represent the location of a single spacecraft from which data is to be acquired for an entire pass, a collection of radio sources that are to be observed on a pre-determined schedule, or in the case of delta-differential one-way ranging (ΔDOR), a series of observations alternating between a spacecraft and one or more radio sources. The direction cosine predict-driven mode is commonly available for all DSN antennas.

2.3.2 Planetary Mode

Planetary mode is used to track an object with slowly varying right ascension and declination. Pointing commands are interpolated from three planetary predict points (typically one per day) entered from the control position or read from a locally-created file of at least four predict points. The points may be geocentric or topocentric and should include precession and nutation corrections. Each point contains time, right ascension, declination, and range. Parallax correction is available for use with geocentric points when a non-sidereal object (such as a planet) is to be tracked.

2.3.3 Sidereal Mode

This mode, also called Star Track Mode, is used to track a celestial object at a fixed position (fixed at least for a number of days) described by geocentric right ascension (RA) and declination (DEC) coordinates, including precession and nutation. The points may be entered from the local control position or may be read from a locally-created file containing time, RA, and DEC. A capability to boresight the antenna after arriving on point is included. The boresight algorithm performs a small cross-elevation (XEL) scan centered on the expected target location followed by a small elevation (EL) scan. Pointing corrections are estimated from signal strength measurements. This mode is mainly used for evaluating antenna performance and collecting very-long baseline interferometry (VLBI) data.

2.3.4 70-m Precision Tracking Mode

The 70-m antennas have a precision tracking mode that makes use of an instrument called the *master equatorial* (ME). The master equatorial is a 7-inch (17.8 cm) mirror

on an hour-angle/declination mount. The mount is attached to the top of a concrete and steel tower on a separate foundation in an environmentally controlled area within the antenna pedestal and alidade structure. The mirror can be positioned to better than 1 mdeg in each axis and the 70-m reflector is optically slaved to it. The precision tracking mode is available with any of the above modes but should only be used when needed because of its extra complexity.

2.4 Statistics of Pointing Errors

If an antenna has EL and XEL random pointing errors due to any number of causes that are normally (Gaussian) distributed, it can be shown that for equal EL and XEL standard deviations, σ, the radial pointing error (two dimensional) becomes Rayleigh distributed. The characteristics of the Rayleigh distribution are that the probability density function (PDF) is zero at zero pointing error, rises to a maximum value at the EL and XEL σ, and decreases with a long tail out to large values of radial pointing error. The cumulative distribution (CD) of the pointing error at a particular value is the integral of the PDF from zero to that value. The mean radial error (MRE) for the Rayleigh distribution of radial pointing errors is related to the standard deviation of the axial (XEL and EL) distributions as:

$$\mathrm{MRE} = \sqrt{\pi/2} \cdot \sigma = 1.2533\sigma \tag{2}$$

and the cumulative distribution at the MRE is 0.545. This means that 54.5% of the pointing errors are less than or equal to the MRE. Conversely, 45.5% of the pointing errors are larger than the MRE. Once the MRE is known, the radial error associated with any CD can be calculated from the properties of the Rayleigh distribution. Table 2 provides the factors by which the MRE must be multiplied to obtain the radial error at the selected CD.

Table 2. Mean Radial Error Multipliers for a Rayleigh Distribution.

CD	Mean Radial Error Multiplier	CD	Mean Radial Error Multiplier
0.0	0.000	0.6	1.080
0.1	0.366	0.7	1.238
0.2	0.533	0.8	1.431
0.3	0.673	0.9	1.712
0.4	0.806	0.95	1.953
0.5	0.939	0.98	2.232
0.545	1.000 (MRE)	0.99	2.421

Figure 2 shows a graph of the PDF and cumulative distribution function (CDF) for a Rayleigh distribution with axial (XEL and EL) σ of 3.19 mdeg, chosen to yield a mean radial error of 4.00 mdeg. Pointing performance such as this would be acceptable for a 34-m DSN antenna operating at X-band where the pointing loss (see module 104) would be less than

0.13 dB 90% of the time. It would be not be acceptable pointing for the same antenna operating at Ka-band antenna where the beamwidth is substantially smaller. The resulting Ka-band pointing loss (see module 104) would be greater than 0.7 dB 45.5% percent of the time and greater than 2 dB 10% of the time.

Figure 3 shows cumulative distributions of pointing error for values of mean radial error ranging from 2 to 20 mdeg and includes the pointing loss curves from modules 101 (70-m Telecommunications Interfaces) and 104 (34-m BWG Telecommunications Interfaces). As an example of the use of this figure, consider the inverse of the preceding example. Assuming it has been determined that a 90% probability of having no more than 2 dB of pointing loss for a Ka-band experiment is acceptable, the chart is entered from the right along the 2-dB line until it intersects the Ka-band Pointing Loss curve. The line is extended vertically to the CD = 0.9 line where it intersects the MRE = 4 curve. Thus, to accomplish the experiment with the desired pointing performance will require an antenna with an MRE capability of 4 mdeg.

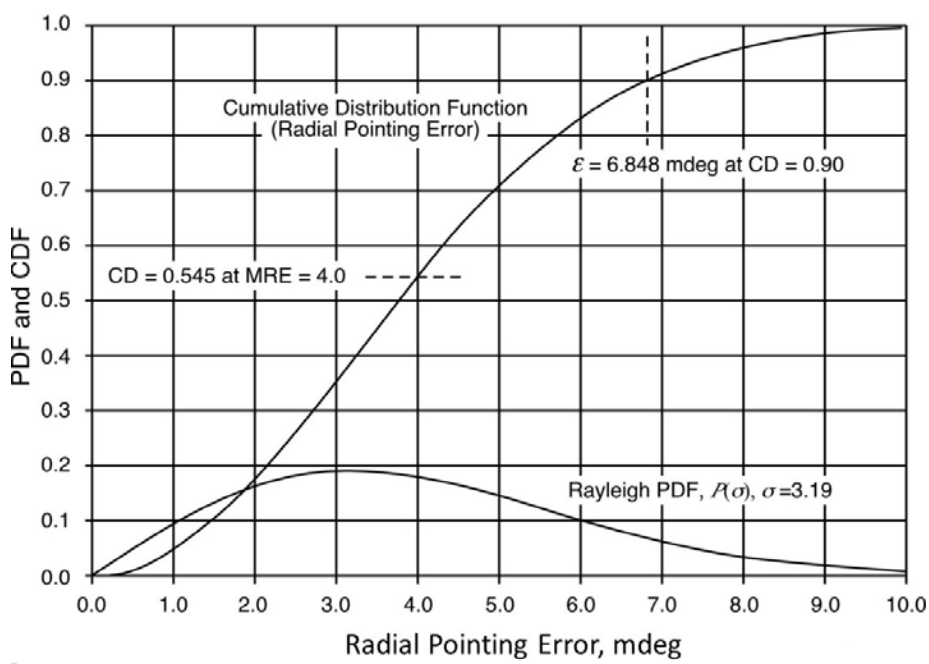

Figure 2. Rayleigh PDF and CDF for a Mean Radial Pointing Error = 4.0 mdeg.

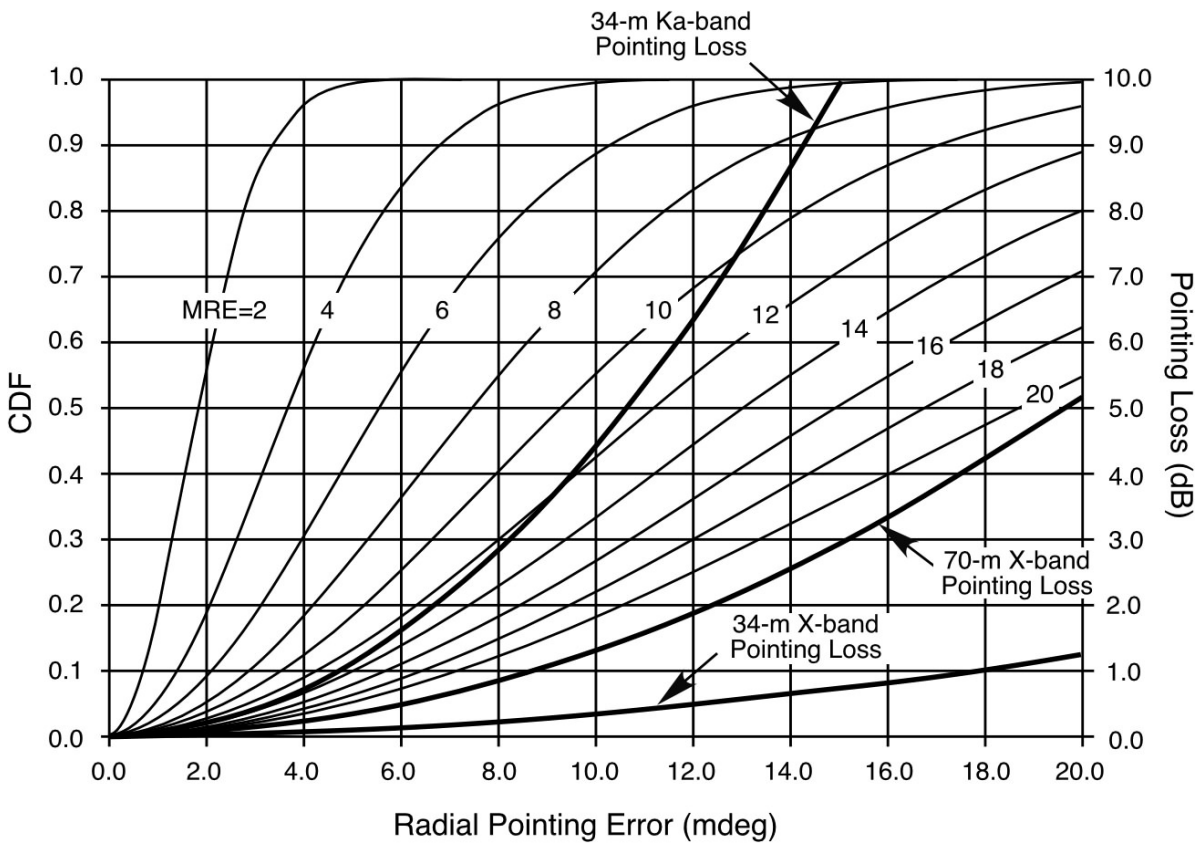

Figure 3. Cumulative Distributions of Pointing Errors for Selected MREs

2.5 Blind Pointing

Blind pointing relies on calibration and computer modeling to compensate for errors between the antenna beam direction and the direction as reported by the antenna axis position encoders. Blind pointing errors result in a pointing loss that is most severe on the BWG antennas when operating at Ka-band because of the extremely narrow beamwidth. The 70-m antennas have a relatively narrow X-band beamwidth, but this is mitigated by use of the precision tracking mode. The BWG antennas' beam waveguide tube at the center of the antenna prevents use of a master equatorial, and there are additional error sources. The BWG error sources, their magnitude, and the degree to which they can be reduced by modeling are tabulated in Table 3 and discussed in the following paragraphs.

Table 3. 34-m BWG Antenna Pointing Error Sources

Error Source	Estimated Size (mdeg)	Correction Method	Residual Error (mdeg)
Atmospheric refractivity	83 at EL = 10°	Surface weather model	0.8, 1σ at EL=10°
Gravity deformation of dish and quadripod	100, EL (max)	Subreflector lookup table	5 – 10 P-P (≅ 6σ)
Systematic errors	100, EL (max)	12 term, first order trigonometric model	1 – 8 (range)
Azimuth track level	8 P-P (≅ 6σ	Lookup table	0.3 XEL, 0.1 EL
Azimuth encoder gear noise	0.44, 1σ	Uncorrected	0.44, 1σ
Elevation encoder	0.2	Uncorrected	0.2, 1σ
Thermal deformation	8 P-P (≅ 6σ EL & XEL)	Uncorrected	8 P-P (≅ 6σ
Wind displacement of foundation	1.1 (30 mph wind)	Uncorrected	1.1 (30 mph wind)
Wind distortion of structure	6 – 9 (30 mph wind)	Uncorrected	6 – 9 (30 mph wind)
Calibration measurements	1, 1σ	Uncorrected	1, 1σ
Mean pointing error (without wind)			2.3 – 8.4 (range)
Mean pointing error (with 30 mph wind)			6.5 – 12.4 (range)

2.5.1 Pointing Corrections

2.5.1.1 Atmospheric Refraction Correction

The antenna controller uses local surface weather measurements to calculate and apply a pointing correction in elevation to compensate for atmospheric refraction. The weather data normally is provided from a local weather station but may be manually entered, if necessary.

2.5.1.2 Gravity Deformation Correction

The main reflector and the quadripod structure that supports the subreflector change shape slightly when the antenna moves in elevation. Because of this, the subreflector must be moved continuously during a pass in both the up and down as well as the in and out directions to optimize the gain. The up-down component of the motion causes a shift in antenna

pointing referred to as *squint*. This is compensated for by a squint correction algorithm that adjusts the elevation pointing depending on how far the subreflector has been moved.

2.5.1.3 Systematic Error Correction

All antennas, no matter how well they are designed and how carefully they are built, have certain repeatable pointing errors that can be measured by referencing well-known radio sources. Among the causes for these errors are imperfections such as angle-encoder offsets, azimuth axis tilt, gravitational flexure, axis skew, structure aging, etc. The DSN models these using constants and spherical harmonic functions of the antenna pointing angle in what is called a first-order pointing model. This model works reasonably well over the entire sky at S-band and X-band. However, experiments requiring extremely accurate pointing can benefit by special calibrations and adjusting the model for optimum performance in the portion of the sky where the experiment will occur. Antenna calibrations are performed periodically and the best model for the planned activity is always used.

The addition of Ka-band to the network has made the first order model inadequate as an all-sky model. As a result, a 4th order systematic error model has been developed to handle pointing variations that are not directly traceable to physical imperfections in the antenna. More frequent calibration and possible use of different models for day and night operation are also being investigated to improve Ka-band pointing.

2.5.1.4 Azimuth Track Level Compensation

The BWG antenna azimuth tracks are composed of eight, precision-machined segments. Extremely small irregularities in the track, coupled with the four-wheeled rectangular support structure for the antenna, result in a 32-node signature that is more complex than can be modeled by the 1st order or 4th order systematic error correction model. The antenna controller employs a lookup table and applies appropriate corrections to both elevation and azimuth axes.

2.5.2 Measured Blind Pointing Performance of DSN Antennas

Table 4 presents measured X-band blind-pointing pointing performance of DSN antennas. S-band pointing is provided only for DSS-36. X-band pointing models are good enough to be used for S-band, due to the much larger S-band beamwidth. The blind pointing performance presented here is deduced from the pointing errors measured at X-band by CONSCAN and at Ka-band by monopulse (see below) during tracks on numerous spacecraft over a period of 3 to 9 months during 2014, and at DSS-36 during 2016. Although the pointing was maintained nearly perfectly on the spacecraft by use of the closed-loop systems, the running sum of the individual pointing corrections gives a measure of how much the blind pointing error varies over a track − in other words, how far the commanded antenna position varies from the actual spacecraft position. Additionally, reported pointing calibrations at the Madrid station include measurements made by ACME (Antenna Calibration and Measurement Equipment) on radio sources.

Table 4. Measured Blind Pointing Performance of DSN Antennas

Antennas	Mean Radial Error, mdeg	Remarks (see NOTE)
70-Meter		
DSS-14, Goldstone	3.2	X-band
DSS-43, Canberra	2.2	X-band
DSS-63, Madrid	2.9	X-band
	2.0	X-band, ACME
34-Meter HEF		
DSS-15, Goldstone	5.4	X-band
DSS-45, Canberra	See NOTE	
DSS-65, Madrid	6.0	X-band
	4.7	X-band, ACME
34-Meter BWG		
DSS-24, Goldstone	4.4	X-band
DSS-25, Goldstone	3.5	X-band
	2.7	Ka-band
DSS-26, Goldstone	5.3	X-band
	3.1	Ka-band
DSS-34, Canberra	5.9	X-band
	3.9	Ka-band
DSS-35, Canberra	7.7	X-band, preliminary
	2.5-3.4	Ka-band
DSS-36, Canberra	6.3	S-band
	5.8	X-band
	3.4	Ka-band
DSS-54, Madrid	3.2	X-band
	4.4	X-band, ACME
	3.2	Ka-band
DSS-55, Madrid	3.9	X-band
	3.5	X-band, ACME
	4.2	Ka-band

NOTE: X-band = CONSCAN measurements of blind pointing
Ka-band = monopulse measurements of blind pointing
ACME = Antenna Calibration and Measurement Equipment
DSS-45 decommissioned as of October 2016.

2.6 Closed-loop Pointing

Closed-loop pointing relies on the signal being received to provide corrections for antenna pointing. The DSN employs two methods of closed-loop pointing, CONSCAN and monopulse. Table 4 (above) presents the deduced blind pointing performance of DSN antennas as determined by closed-loop CONSCAN (X-band) and monopulse (Ka-band) pointing measurements.

2.6.1 CONSCAN

CONSCAN is available on all 70-m and 34-m antennas. It consists of performing a circular scan (as seen looking at the spacecraft) with the center at the predicted source position and a radius that reduces the received signal level by a small amount, typically 0.1 dB. If the target is at the expected location and antenna pointing model is perfect, no variation in the received signal level will be detected, although it will be down 0.1 dB from the maximum possible received signal level. If the initial pointing is imperfect or the target is not at the predicted location, each CONSCAN cycle will see a variation in amplitude from which the radial error and clock angle of the mis-pointing can be calculated. The typical time for a CONSCAN cycle is 120 seconds and the pointing is corrected after each cycle. The process is repeated continuously during the pass. Various amounts of CONSCAN "gain" can be applied for making the pointing correction, ranging from 0 (no correction applied) to 1 (full detected correction applied). A gain of less than 1 is usually applied to reduce the effect of noise during the CONSCAN cycle. This results in some time delay (perhaps 20 minutes) before fully corrected pointing is obtained.

CONSCAN is available at all frequency bands but is usually not necessary at S-band and is not recommended for Ka-band, since monopulse (see below) is usually available.

The relatively long CONSCAN cycle coupled with the much more severe Ka-band atmospheric effects can provide misleading information to the pointing correction algorithm resulting in the antenna being driven off-point.

The mean pointing error (used for estimating pointing loss) using CONSCAN should be considered as the 0.1 dB point on the antenna pattern for the antenna and frequency in question. For a 34-meter antenna at X-band, this value is 6 mdeg and for a 70-meter antenna at X-band it is 3 mdeg. Considering CONSCAN pointing to be Rayleigh distributed, the pointing error for various CDs can be calculated from Figure 3. Antenna beam patterns for the various DSN antennas are given in modules 101 through 104.

The most critical pointing requirements in the DSN are for the use of Ka-band on the 34-m BWG antennas. This is because the half-power beamwidth is about 0.017 degrees, half the width of the X-band beam on the 70-m antennas. Tracking results using CONSCAN indicate that the center of the CONSCAN circle can typically be kept pointed to within 6 mdeg of a spacecraft at X-band, and somewhat less at Ka-band.

Figure 4 shows the X-band pointing errors as measured by CONSCAN during a Kepler spacecraft track on the DSS-34 BWG antenna in August, 2012. Wind speeds up to about 45 km/hr were experienced during the track, and it is felt that significant pointing errors resulted. A straight-line fit through the data indicates a mean pointing error of as much as 0.004 degrees for 45 km/hr wind speed, although individual points are as much as 0.008 degrees. Each radial pointing error is the resulting measurement of one two-minute CONSCAN circle. The average X-band pointing loss over the CONSCAN cycle is small, less than 0.3 dB for the points shown in Figure 5.

Assuming that the pointing errors determined using Ka-band CONSCAN would be the same as what were measured at X-band, the average pointing losses over the Ka-band CONSCAN cycle are shown in Figure 6. In this case, at 50 km/hr the straight-line fit gives 1.0 dB, although individual points are as much as 2.8 dB. Because of the wider X-band beamwidth, it is felt that the X-band CONSCAN measurements are noisier (in degrees) than what would be experienced at Ka-band, so estimates of the maximum Ka-band pointing losses are probably exaggerated to some degree.

There may be some conditions under which it might be necessary to use X-band CONSCAN while tracking at both X- and Ka-bands. Possibilities include unavailability of Ka-band monopulse (Section 2.6.2), or gusty wind conditions which introduce excessive pointing "noise" into the Ka-band CONSCAN cycle. For the case of Ka-band tracking using X-band CONSCAN (for coincident X- and Ka-band beams), the Ka-band losses will be greater than those using Ka-band CONSCAN, as the Ka-band beam is "dragged around" in the X-band CONSCAN process, and thus is generally further away from the spacecraft than it would be using Ka-band CONSCAN alone. In this case the Ka-band pointing losses are shown in Figure 7, and individual points are as large as 3.4 dB, with a minimum of 1.44 dB. The straight-line fit gives an average pointing loss over the CONSCAN cycle of about 2.0 dB at a wind speed of 50 km/hr.

Each pointing loss value shown in the figures is the average pointing loss over the two-minute CONSCAN cycle; thus there is a portion of the CONSCAN cycle where the pointing loss is significantly worse than the average, which might result in the spacecraft signal being lost. The straight-line fits are not intended to suggest a model, but rather to indicate the trends of pointing error and loss as a function of wind speed.

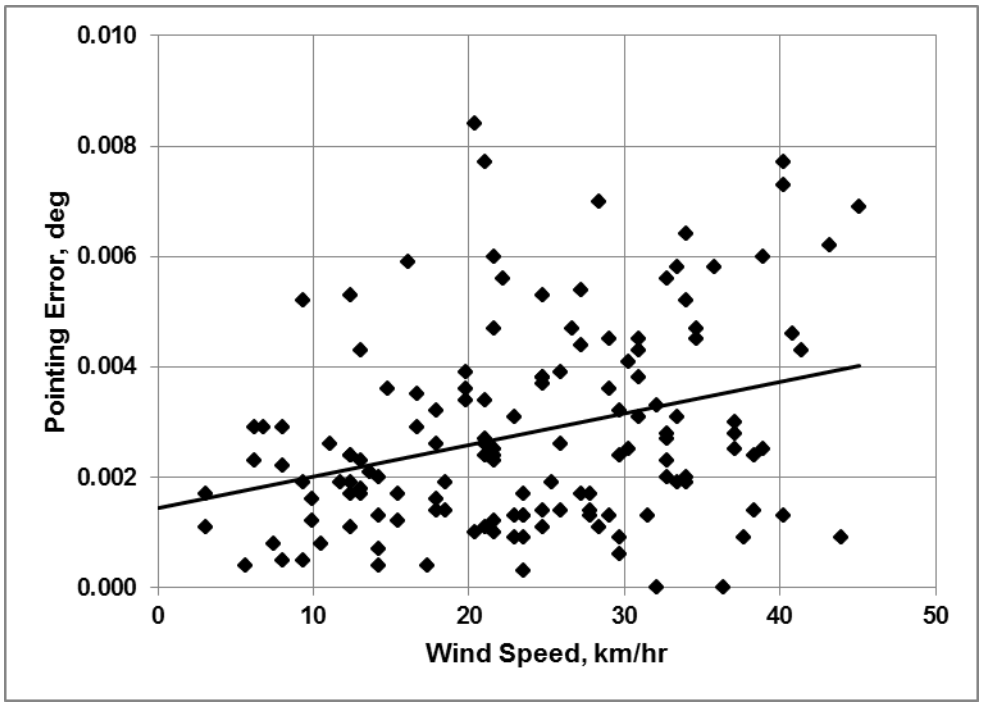

Figure 4. 34-m BWG Antenna X/Ka-band Pointing Error vs. Wind Speed

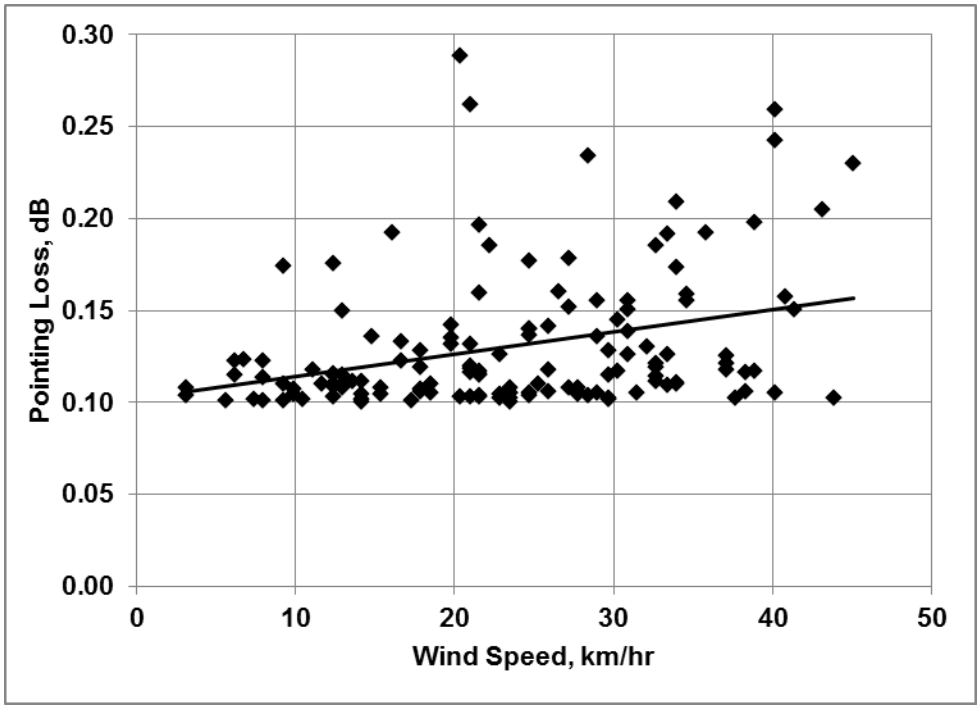

Figure 5. X-band CONSCAN Average Pointing Loss vs. Wind Speed

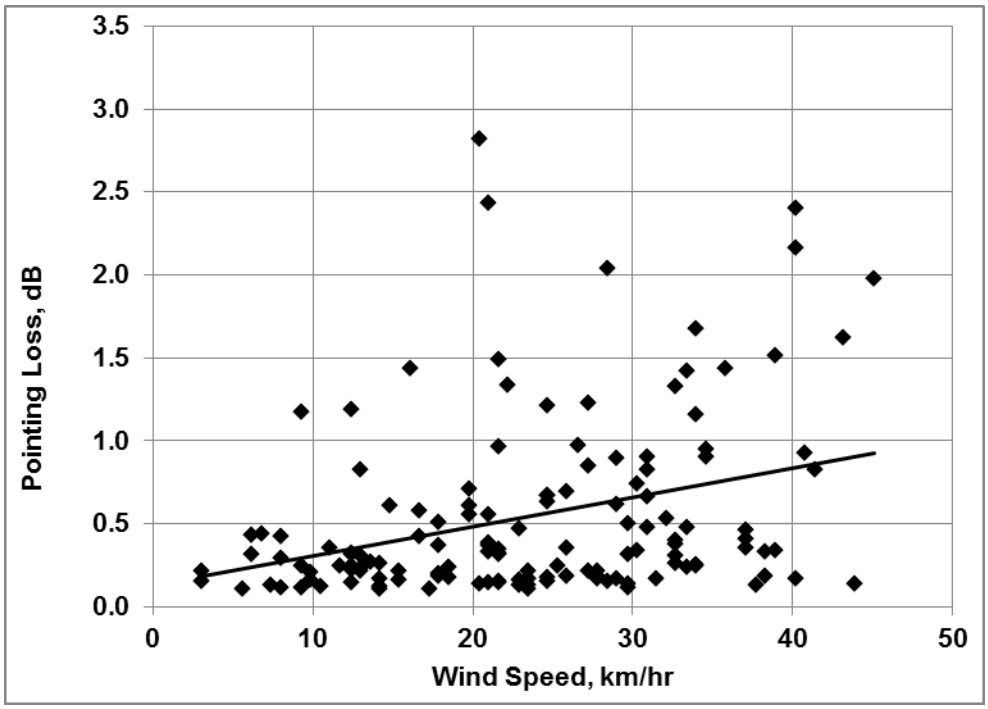

Figure 6. Ka-band CONSCAN Average Pointing Loss vs. Wind Speed

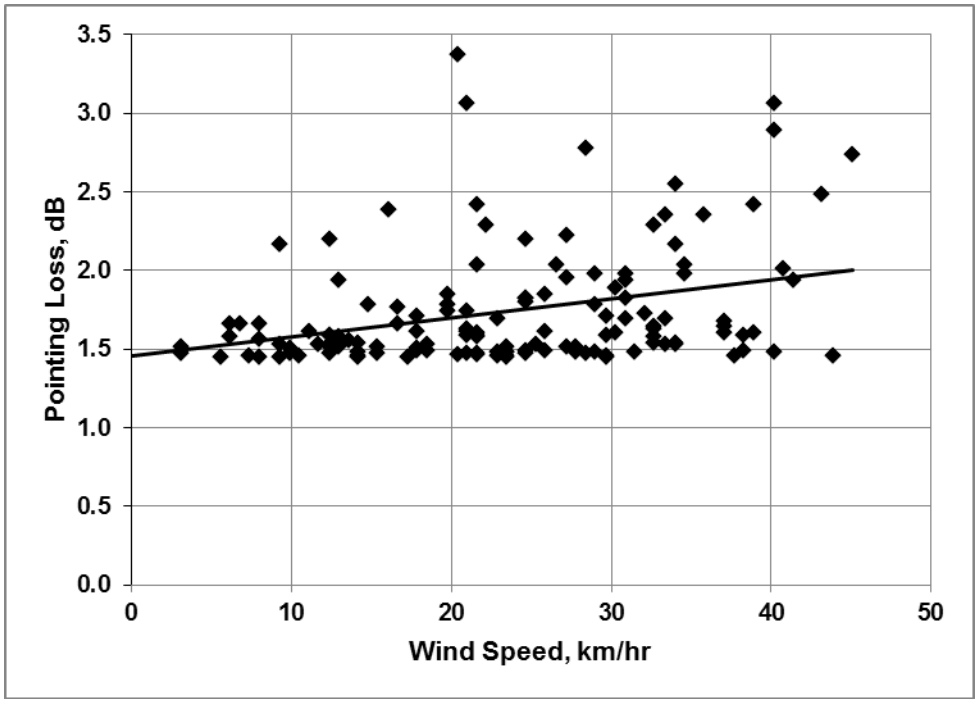

Figure 7. Ka-band Average Pointing Loss using X-band CONSCAN vs. Wind Speed

2.6.2 Monopulse

Monopulse is a technique for extracting pointing information from the phase of the received signal while maintaining the source at the peak of the antenna pattern. This technique relies on the presence of a carrier signal to provide a reference for the error channel(s). As a result, it is not suitable for suppressed carrier signals or radio sources.

The monopulse capability is available to support deep space Ka-band (32-GHz) at DSS-25, DSS-26, DSS-34, DSS-35, DSS-36, DSS-54, and DSS-55. The Ka-band feeds of these 34-m BWG antennas include a cryogenically cooled TE_{21} mode coupler that extracts a signal whose phase, with respect to the main beam signal, indicates the direction of the target with respect to the center of the beam and whose amplitude indicates the angular displacement from the beam center. The advantage of such a system over a conventional amplitude monopulse system is that only a single receiver channel is required for the error signal as opposed to two. The monopulse receiver measures the phase and amplitude of the signal in the error channel, calculates elevation and cross-elevation corrections, and forwards this information to the antenna controller 25 times a second. The antenna controller translates the errors into the local antenna coordinate system, integrates them, and applies the corrections to the predicted azimuth and elevation positions. During most Ka-band tracks using monopulse the pointing is maintained to with 2 mdeg, resulting in a maximum pointing loss of less than 0.2 dB. Monopulse pointing at DSS-36 was measured to be 1.5 mdeg MRE. Monopulse used at Ka-band is also used to determine the blind pointing errors for the 34-meter BWG antennas.For initial acquisition using blind pointing, monopulse should be able to “pull-in” when the pointing is within about 10 mdeg. For larger pointing errors and/or low signal to noise ratios (SNRs), CONSCAN is used to get on target.

For extremely high signal-to-noise ratios (SNR > 40 dB-Hz), the monopulse system is capable of pointing the antenna within 1 mdeg of a stationary target. As SNR decreases, this performance is degraded by servo jitter resulting from noise in the selected servo bandwidth. A study has shown that the mean radial error using monopulse varies with SNR approximately as

$$MRE = 0.2 + 12e^{-0.13SNR} \text{, mdeg} \tag{3}$$

where SNR is the monopulse signal-to-noise ratio, dB-Hz (signal in the main channel divided by noise in the error channel). For example, for SNR = 20 dB-Hz, MRE = 1.1 mdeg. SNRs below 10 dB-Hz will probably yield unacceptably poor pointing performance.

2.7 Beam Alignment

Most DSN antennas that support more than one frequency accomplish this by having multiple feedhorns. The exceptions to this are the 34-m HEF antennas that have a single S- and X-band coaxial feedhorn and the BWG antennas (with the exception of DSS-25) where there is a coaxial X- and Ka-band feedcone. When multiple feedcones are used, it is likely that there will be a small misalignment between the peak of the two antenna beams. However, if good pointing is achieved at the higher frequency, it virtually guarantees nearly perfect performance at the lower frequency due to the larger beamwidth. For example on the DSS-43, 70-m antenna

(Canberra), the S- and X-band beams have a pointing difference of about 4 mdeg in the EL direction. Because the S-band beam has a half-power beamwidth of about 118 mdeg, perfect pointing at X-band would give an S-band pointing loss of less than 0.02 dB.

2.8 X-band Beam Shift on 70-m Antennas

The 70-meter antennas have an S/X dichroic plate that is retractable to provide an X-band only low-noise mode. There is an 8.5 mdeg (approximately) beam movement in the negative XEL direction (to the left, when looking outward from the antenna) when it is retracted. Separate systematic error models are maintained for each position of the dichroic plate and are selected automatically by the antenna controller.

2.9 DSS-25 Ka-band Transmit Aberration Correction

The extremely narrow beamwidth at Ka-band requires that the DSS-25 Ka-band uplink signal be aimed at the RA and DEC where the spacecraft will be when the signal arrives, while simultaneously receiving a signal that left the spacecraft one light-time previously. This is accommodated by mounting the Ka-band transmit feed on a movable X-Y platform that can displace the transmitted beam as much as 30 mdeg from the received beam. The reduction in gain caused by the feed not being located at the optimum focus of the antenna is discussed in module 104.

DSMS Telecommunications Link
Design Handbook

303
Media Calibration

Effective November 30, 2000

Document Owner:

P. H. Richter 12/11/00

P. H. Richter, Date
Senior Engineer

Approved by:

12/13/00

A. Kwok Date
Tracking and Navigation Service
Systems Development Engineer

Released by:

[Signature on file at TMOD Library]

TMOD Document Release Date

Change Log

Rev	Issue Date	Paragraphs Affected	Change Summary
Initial	11/30/2000	All	All

Note to Readers

There are two sets of document histories in the 810-005 document, and these histories are reflected in the header at the top of the page. First, the entire document is periodically released as a revision when major changes affect a majority of the modules. For example, this module is part of 810-005, Revision E. Second, the individual modules also change, starting as an initial issue that has no revision letter. When a module is changed, a change letter is appended to the module number on the second line of the header and a summary of the changes is entered in the module's change log.

This module supersedes module MED-10 in 810-005, Rev. D.

Contents

Tables

1 Introduction

1.1 Purpose

This module describes the capabilities of the equipment used by the Deep Space Network (DSN) to obtain data from which correction factors can be determined for media effects that limit navigational accuracy. The data are forwarded from each Deep Space Communications Complex (DSCC) to the Network Operations Control Center (NOCC) where they are processed and archived.

1.2 Scope

The functional performance and data characteristics of the Deep Space Station (DSS) Media Calibration Subsystem (DMD) are described. The DMD is responsible for obtaining Global Positioning System (GPS) and ground weather data for the NOCC Tracking Subsystem (NTK) and Navigation Subsystem (NAV).

2 General Information

The DMD provides two types of data:

- GPS data consisting of L-band carrier phase and group delay of GPS satellite signals, in addition to ephemeris and almanac data for the GPS satellites.
- Weather data, consisting of temperature, barometric pressure, relative humidity, precipitation rate, total precipitation, wind speed, and wind direction.

2.1 Global Positioning System Data

The Global Positioning System GPS Operational Constellation consists of at least 24 satellites that orbit the earth with a 12 sidereal-hour period. There are often more than 24 as new satellites are launched to replace the older ones. The orbit is such that the satellites repeat the same track and configuration over any point approximately each 24 hours (4 minutes earlier each day). There are six orbital planes (with nominally four satellites in each), equally spaced (60 degrees apart), and inclined at about fifty-five degrees with respect to the equatorial plane. This constellation provides the user with between five and eight satellites visible from any point on the earth. A minimum of four satellite signals must be received to estimate the four unknowns of position in three dimensions and time.

The DSCC GPS Receiver/Processor Assembly (GRA), which is part of the DMD, makes use of the GPS data to provide carrier phase and group delay for the GPS signals. These

data may then be used to characterize the Earth's ionosphere and troposphere along the line of sight from a given satellite to the DSCC.

2.1.1 GPS Signal Structure

The GPS satellite signals are complex in structure, with each L-band frequency being binary biphase-modulated with two pseudo-random noise codes, the Coarse Acquisition (C/A) and Precision (P) codes, and a navigation message.

The complete signal broadcast by a satellite may be represented as:

$$\begin{aligned} s(t) &= \left[A_C\, C(t) D(t) \sin(2\pi f_1 t) + A_P\, P(t) D(t) \cos(2\pi f_1 t)\right] \\ &\quad + \left[A_P P(t) D(t) \cos(2\pi f_2 t)\right] \end{aligned} \tag{1}$$

where the first square bracket is the L1 signal at frequency f_1, and the second square bracket is the L2 signal at frequency f_2. The terms appearing above have the following definitions:

A_c and A_p	=	the constant amplitudes of the Coarse Acquisition (C/A) and Precision (P) codes
$C(t)$	=	the C/A-code modulation (= ±1)
$P(t)$	=	the P-code modulation (= ±1)
$D(t)$	=	the navigation message modulation (= ±1)
f_1	=	154 f_0 = 1575.42 MHz
f_2	=	120 f_0 = 1227.60 MHz

The $C(t)$, $P(t)$, and $D(t)$ modulations are all synchronized to the fundamental clock frequency, f_0, such that they have the following frequencies:

f_0	=	10.23 MHz (Note 1)
$C(t)$	=	$f_0/10$ = 1.023 Mbps
$P(t)$	=	f_0 = 10.23 Mbps
$D(t)$	=	$f_0/204600$ = 50 bps.

Note (1): To partially compensate for general and special relativistic effects on the satellite clock (gravitational red shift and time dilation), the actual value of f_0 is 10.23 MHz – 4.55 mHz.

The complete C/A code contains 1023 cycles (or "chips"), has a total period of 1.0 ms, and is different for each satellite.

The P-code is more complicated and consists of two code segments (X1 and X2), which differ in length by 37 chips. These are added modulo 2 and timed in such a way that

exactly 403,200 X1 code segments correspond to exactly one week, the period of the P-code. (The P-code actually has a total period of 37 weeks, with each satellite using only a single one-week segment of the total.) The duration of the X1 code segment is thus 1.5 seconds and contains exactly 15,345,000 chips at 10.23 Mbps. As is the case with the C/A code, the P-code is different for each satellite.

The navigation message also has a complex structure, with a total period of 12.5 minutes (one master frame) and is divided into frames, subframes, words, and bits. The first three subframes (lasting 6 seconds each) repeat every 30 seconds, while the last two subframes are different in each of 25 consecutive frames (pages), after which the entire message repeats.

2.1.2 GPS Receiver/Processor Assembly (GRA)

The GRA provides the following functional capabilities:

1) Automatically acquire and track the L1 and L2 GPS signals for specified satellites, usually all of those transiting

2) Extract and store GPS almanac and ephemeris data from the navigation message

3) Measure the differential P-code group delay between the L1 and L2 GPS signals

4) Measure the differential carrier phase between the L1 and L2 GPS signals.

The almanac data, contained in subframe 5 of the GPS navigation message, consist of approximate ephemeris data for all satellites and are used by the GRA for signal acquisition.

The ephemeris data for a specified satellite (subframes 2 and 3) provide a complete description of the orbit. When the data are combined with measured signal delays, the local position and atmospheric path that the signal has traversed can be determined.

Since the Department of Defense, which controls the GPS signal content, may elect at any time to encrypt the P-code (resulting in what is termed an anti-spoofing (A/S) mode of operation in which the encrypted, or Y-code, is unavailable to civilian users of the system) the GRA operates in two distinct modes to determine the differential group and phase delays of the satellite signals.

In the normal, coded mode, the known P-code is used to determine the carrier phase and group delay of each signal (L1 and L2) separately. The computed differences may then be used to characterize the propagation medium over the path of the signals. This provides the most precise determination due to the length of the P-code.

In the codeless mode, advantage is taken of the fact that the same unknown Y-code is transmitted on both the L1 and L2 channels with an unknown delay. The product of the two signals is formed and the differential group and phase delays are determined by cross-correlation. This method results in a somewhat reduced accuracy.

The GRA simultaneously receives and processes the signals from up to eight satellites selected to provide the longest unbroken tracks at any given time. In addition to the data described above, the system provides various status and health data on the signals being processed. Tables 1 through 4 list the GPS parameters measured, their ranges and accuracy, and the sample intervals provided.

2.1.3 Relation of Phase and Group Delay to Atmospheric Properties

The Earth's atmosphere may conveniently be divided into three regions according to the effects produced on the propagation of electromagnetic radiation:

(1) troposphere, stratosphere, and lower part of mesophere— region between the Earth's surface and about 60 km altitude consisting of neutral (unionized) gases

(2) ionosphere — region from about 60 km to between ~500 and 2000 km, depending on the extent of extraterrestrial ionizing radiation, consisting of partially ionized gases

(3) plasmasphere — ionized region extending from ~2000 km to about four Earth radii (26,000 km), where it blends into the solar wind of the Earth's magnetosphere

At the frequencies in which the DSN operates, tropospheric dispersion may be neglected and the refractivity represented by a dry and a wet component whose approximate total zenith phase and group delays are:

$$\Delta t_D \sim 7.6 \text{ ns},$$

$$\Delta t_W \sim 0.3 \text{ ns} - 1.4 \text{ ns}.$$

The first varies linearly with pressure at the Earth's surface; the second increases as the tropospheric moisture content increases.

Since tropospheric dispersion is negligible at L-band, these delays cancel when differential delays are computed or measured between f_1 and f_2.

In the ionized portion of the Earth's atmosphere, the medium displays anomalous dispersion at microwave frequencies. This causes the phase velocity to exceed, and the group velocity to be less than, the speed of light in a vacuum, c. Specifically, to a good approximation at L-band:

$$\frac{v}{\mathrm{c}} = 1 + \frac{x}{2} \tag{2}$$

$$\frac{v_g}{\mathrm{c}} = 1 - \frac{x}{2} \tag{3}$$

Table 1. GPS Metric Data, Code Mode

Parameter	Units (1)	Approximate Decimal Range
Delay Calibration	2^{-7} ns	±255 ns
Output Interval	sec	1–300 s
L1-C/A Doppler Phase	2^{-16} cycles	±2.1 x 10^9 cycles
L1-C/A Doppler Phase Noise	2^{-16} cycles	0–1 cycle
L1-P Doppler Phase	2^{-16} cycles	±2.1 x 10^9 cycles
L1-P Doppler Phase Noise	2^{-16} cycles	0–1 cycle
L2-P Doppler Phase	2^{-16} cycles	±2.1 x 10^9 cycles
L2-P Doppler Phase Noise	2^{-16} cycles	0–1 cycle
L1-C/A Group Delay	2^{-11} ns	±0.27 sec
L1-C/A Group Delay Noise	2^{-11} ns	0–32 ns
L1-P Group Delay	2^{-11} ns	±0.27 sec
L1-P Group Delay Noise	2^{-11} ns	0–32 ns
L2-P Group Delay	2^{-11} ns	±0.27 sec
L2-P Group Delay Noise	2^{-11} ns	0–32 ns
C/A SNR (1 sec)	2^{-4} volt/volt	0–4096
P1 SNR (1 sec)	2^{-4} volt/volt	0–4096
P2 SNR (1 sec)	2^{-4} volt/volt	0–4096
Receiver Clock Error	2^{-32} sec	±0.5 sec
L1-C/A Residual Phase	2^{-10} cycles	0–0.25 cycle

Note (1): Least significant bit transmitted by the GRA.

Table 2. GPS Metric Data, Non-Code Mode

Parameter	Units (1)	Approximate Decimal Range
Delay Calibration	2^{-7} ns	±255 ns
Output Interval	sec	1–300 sec
L1-C/A Doppler Phase	2^{-16} cycles	±2.1 x 10^9 cycles
L1-C/A Doppler Phase Noise	2^{-16} cycles	0–1 cycle
L1-L2 Doppler Phase	2^{-16} cycles	±2.1 x 10^9 cycles
L1-L2 Doppler Phase Noise	2^{-16} cycles	0–1 cycle
L1-C/A Group Delay	2^{-11} ns	±2.1 x 10^9 cycles
L1-C/A Group Delay Noise	2^{-11} ns	0–32 ns
P2-P1 Group Delay	2^{-9} ns	±1.1 s
P2-P1 Group Delay Noise	2^{-9} ns	0–128 ns
C/A SNR (1 s)	2^{-4} volt/volt	0–4096
P2-P1 SNR (1 s)	2^{-6} volt/volt	0–1024
Receiver Clock Error	2^{-32} s	±0.5 s
L1-C/A Residual Phase	2^{-10} cycles	0–0.25 cycle

Note (1): Least significant bit transmitted by the GRA.

Table 3. GPS Ephemeris Data

Parameter	Units (1)	Approximate Decimal Range
Sample Year (Modulo 100)	Year	0–99 yrs
Sample Day-of-Year	Days	0–366 days
Sample Hours	Hours	0–24 hrs
Sample Minutes	Minutes	0–60 minutes
Sample Seconds	seconds	0–60 s
GPS Week Number	N/A	
Satellite Number	N/A	
L2 Code Type/L2 Code On	N/A	
User Range Accuracy	N/A	
Issue of Data (Clock)	N/A	
Clock Data Reference Time (t_{oc})	2^4 s	0–6.0 x 10^5 s
Time Correction Coefficient (a_{f2})	2^{-55} s/s^2	±3.6 x 10^{-15} s/s^2
Time Correction Coefficient (a_{f1})	2^{-43}s/s	±3.7 x 10^{-9} s/s
Time Correction Coefficient (a_{f0})	2^{-31}s	±3.9 ms
Issue of Data (Ephemeris)	N/A	
Amplitude of Sine Harmonic Correction to the Orbit Radius (C_{rs})	2^{-5}m	±1.0 km
Mean Motion Difference From Computed Values (Delta N)	2^{-43} semicir/s	±1.2 x 10^{-5} mrad/s
Mean Anomaly at Reference Time (M_o)	2^{-31} semicir	±180 deg
Amplitude of Cosine Harmonic Correction to the Argument of Latitude (C_{uc})	2^{-29} radians	±6.1 x 10^{-2} mrad
Eccentricity (e)	2^{-33}	0–0.03
Amplitude of Sine Harmonic Correction to the Argument of Latitude (C_{us})	2^{-29} radians	±6.1 x 10^{-2} mrad
Square Root of Semi-Major Axis ($A^{1/2}$)	2^{-19} m$^{1/2}$	0–8200 m$^{1/2}$
Ephemeris Reference Time (t_{0E})	2^4 s	0–6.0 x 10^5 s

Note (1): Least significant bit transmitted by the GRA.

Table 3. GPS Ephemeris Data (Continued)

Parameter	Units (1)	Approximate Decimal Range
Amplitude of Cosine Harmonic Correction to Inclination (C_{ic})	2^{-29} radians	$\pm 6.1 \times 10^{-2}$ mrad
Right Ascension at Reference Time ($Omega_0$)	2^{-31} semicir	±180 deg
Amplitude of Sine Harmonic Correction to Inclination (C_{is})	2^{-29} radians	$\pm 6.1 \times 10^{-2}$ mrad
Inclination at Reference Time (i_0)	2^{-31} semicir	±180 deg
Amplitude of Cosine Harmonic Correction to the Orbit Radius (C_{rc})	2^{-5} m	±1.0 km
Argument of Perigee (Omega)	2^{-31} semicir	±180 deg
Right Ascension Rate (Omega DOT)	2^{-43} semicir/s	$\pm 3.0 \times 10^{-3}$ mrad/s
Issue of Data (Ephemeris)	N/A	
Inclination Angle Rate (IDOT)	2^{-43} semicir/s	$\pm 1.2 \times 10^{-5}$ mrad/s

Note (1): Least significant bit transmitted by the GRA.

Table 4. GPS Almanac Data

Parameter	Units (1)	Approximate Decimal Range
Sample Year (Modulo 100)	Year	0–99 yr.
Sample Day-of-Year	Days	0–366 days
Sample Hours	Hours	0–24 hrs
Sample Minutes	Minutes	0–60 minutes
Sample Seconds	s	0–60 s
GPS Week Number	N/A	
Satellite Number	N/A	
Data and Space Vehicle ID	N/A	
Eccentricity (e)	2^{-21}	0–0.03
Reference Time (t_{OA})	2^{+12} s	0–6.0 x 10^5 s
Delta Inclination (δ_i)	2^{-19} semicir	±11 deg
Right Ascension Rate (Omega DOT)	2^{-38} semicir/sec	±3.7 x 10^{-4} mrad/s
Square Root of Semi-Major Axis ($A^{1/2}$)	2^{-11} $m^{1/2}$	0–8200 $m^{1/2}$
Right Ascension at Reference Time ($Omega_0$)	2^{-23} semicir	±180 deg
Argument of Perigee (Omega)	2^{-23} semicir	±180 deg
Mean Anomaly (M_0)	2^{-23} semicir	±180 deg
Correction Term (a_{f0})	2^{-20} s	±0.03 deg
Correction Term (a_{f1})	2^{-38} s	±1.2 x 10^{-7} s/s

Note (1): Least significant bit transmitted by the GRA.

where:

v	=	phase velocity = ω/k
v_g	=	group velocity = $d\omega/dk$
k	=	*wave vector* ($\lambda/2\pi$)
x	=	$(f_p/f)^2 << 1$
f	=	frequency of interest
f_p	=	plasma frequency = $(Ne^2/m\varepsilon_0)^{1/2}/2\pi$
N	=	electron density (electrons/m^3)
e	=	electronic charge
m	=	electronic mass
ε_o	=	permittivity of free space.

In terms of the above, the phase (Δt) and group (Δt_g) delays at frequency f may be written:

$$\Delta t_g = -\Delta t = \left(\frac{1.345\times10^{-7}}{f^2}\right)\times \mathrm{TEC}, \text{ s} \tag{4}$$

where $\mathrm{TEC} = \int N\,dl$ is the total electron content (TEC) along the propagation path (electrons/m^2).

The corresponding differential delays are given by:

$$\delta t_g = -\delta t = 1.345\times10^{-7}\left(\frac{1}{f_2^{\,2}} - \frac{1}{f_1^{\,2}}\right)\times \mathrm{TEC}, \text{ s} \tag{5}$$

where $\delta t_g = \Delta t_g\,(f_2) - \Delta t_g\,(f_1)$.

Since the TEC along the satellite line of sight may vary between ~10^{16} and 4×10^{18}m^{-2}, the group and phase delays typically range between ~0.5 ns and 90 ns, and the differential delays between ~0.35 ns and 35 ns, although larger values are often observed during periods of high solar activity.

2.2 Ground Weather Data

The ground weather data are generated by instruments located near the Signal Processing Centers (SPC) at each DSCC. In particular, the wind speed and direction sensors are adjacent to the 34m HEF antennas.

All data are asampled once per second by the instruments, and the resulting data stream is transmitted to the Subsystem Control and Monitor Assembly (SCA) of the DMD. Here the data are packaged and transmitted to the NTK and NAV at regular intervals and stored for up to five days for later recall. Table 5 lists the weather parameters measured, their ranges and accuracy, and the interval of transmission to the NTK, NAV, and DMC.

Table 5 Weather Data Transmitted from the SCA

Parameter	Range	Accuracy	Transmission Interval	
			Default	Range
Temperature	-50 to +50 °C	±0.1 °C	60 s	10 s to 1 hr
Barometric Pressure	600 to 1100 mbar	1.0 mb	60 s	10 s to 1 hr
Relative Humidity(1)	0 to 100%	2%	60 s	10 s to 1 hr
Dew Point Temperature	–40 to 50°C	±0.5°C	60 s	10 s to 1 hr
Precipitation Rate	0 to 250 mm/hr	5%	60 s	10 s to 1 hr
Total Precipitation	>0 mm	5%	60 s	10 s to 1 hr
Wind Speed(2)	0 to 100 km/hr	±0.6 km/hr	60 s	10 s to 1 hr
Wind Direction(2)	0 to 360 deg	±3.6 deg	60 s	10 s to 1 hr

See notes on following page.

(1) Relative humidity is calculated from the measured weather parameters according to the formula:

$$\mathrm{RH} = 10^{x} \text{ percent,} \tag{6}$$

where:

$x = 2 + 2300\,(1/T - 1/T_d)$,

T = temperature in Kelvins

T_d = dew point temperature in Kelvins

(2) Wind data are averaged over 10-s intervals by converting the polar velocity vector:

$$\mathbf{v_w} = S_w \hat{\mathbf{e}}(\theta) \tag{7}$$

where

S_w = wind speed,

$\hat{\mathbf{e}}(\theta)$ = wind direction unit vector,

to rectangular form,

$$\mathbf{v_w} = S_x \hat{\mathbf{i}}(\theta) + S_y \hat{\mathbf{j}}(\theta) \tag{8}$$

and computing $\langle S_W \rangle$ and $\langle \theta \rangle$, where

$\langle S_w \rangle^2 = \langle S_x \rangle^2 + \langle S_y \rangle^2$,

$\langle \theta \rangle = \tan^{-1}(\langle S_x \rangle / \langle S_y \rangle)$,

$S_x = S_w \cos\theta$,

$S_y = S_w \sin\theta$.

Deep Space Network

304
Frequency and Timing

Document Owner:		Approved by:	
Signature Provided	12/10/2020	Signature Provided	11/30/2020
Andrey Matsko Frequency & Timing System Engineer	Date	Timothy Pham Communications Systems Chief Engineer	Date

Prepared by:		Released by:	
Signature Provided	12/10/2020	Signature Provided	12/21/2020
Andrey Matsko Frequency & Timing System Engineer	Date	Christine Chang DSN Document Release Authority	Date

DSN No. **810-005, 304, Rev. C**
Issue Date: February 05, 2021
JPL D-19379; CL#20-6547

Jet Propulsion Laboratory
California Institute of Technology

Users must ensure that they are using the current version in DSN Telecommunications Link Design Handbook website:
https://deepspace.jpl.nasa.gov/dsndocs/810-005/

Review Acknowledgment

By signing below, the signatories acknowledge that they have reviewed this document and provided comments, if any, to the signatories on the Cover Page.

Signature Provided	12/07/2020	Signature Provided	11/30/2020
Jeff Berner DSN Project Chief Engineer	Date	Rabi Wang Frequency & Timing Subsystem Engineer	Date

Change Log

Rev	Issue Date	Prepared By	Paragraphs Affected	Change Summary
–	3/1/2004	B. Benjauthrit	All	New Module
A	9/30/2010	Robert Tjoelker	All	Replaced DSMS with DSN. Eliminated the Rev. E designation for the document series. Deleted references to the decommissioned 26 m station, DSS 16. Updated performance information to match current capabilities.
B	12/15/2014	John Lauf	Sections1, 2, 3 Figures 1, 2, 3 Tables 1, 2	Corrected configuration information at DTF-21, MIL-71 and CTT-22. Removed references to DSS-27. Replaced references to FODA with PFD and S-FODA with S-PFD. Replaced references to NIST with USNO.
C	02/05/2021	Andrey Matsko	Figure 2 2.2.12 3.1, 3.2	Added DSS65, DSS56 and DSS53 Removed DSS15 and DSS45 Section 3.1 was moved to Section 2.2.12; Section 3.2 was renamed to Section 3.1

Contents

Illustrations

Figure **Page**

Tables

Table **Page**

1 Introduction

1.1 Purpose

This module provides information to assist Deep Space Network (DSN) customers in understanding the limits placed on navigation, quality of science observations, and telecommunications performance by the Frequency and Timing Subsystem (FTS) equipment installed in the DSN.

1.2 Scope

The discussion in this module is limited to the accuracies and stabilities of frequency and time within the DSN including the effects of implementations that are unique to each site. The module deals primarily with general system information of the operational DSN FTS capability. Performance information that pertains only to specific users, such as performance for the radio science community, may be found in the modules for these topics. A brief discussion of potential enhancements is included at the end of the module.

2 General Information

Figure 1 provides an overview of Frequency and Timing in the DSN. The frequency reference for the three Deep Space Communications Complexes (DSCCs) at Goldstone (GDSCC), Canberra (CDSCC) and Madrid (MDSCC) respectively, is derived from one of at least four, redundant atomic frequency standards (AFSs). The Development and Test Facility (DTF-21) has one AFS while the other two sites, the Merritt Island Launch Annex (MIL-71) and the Compatibility Test Trailer (CTT-22) use disciplined GPS receivers as a frequency reference source.

At each DSCC, a single (prime) atomic frequency standard serves as the source for all coherent, precision, station frequencies and provides the reference for the station Master Clock. The other AFSs serve as backups to the prime standard, should it fail, indicate instability or require maintenance. Each station synchronizes its clock to the United States Naval Observatory (USNO) realization of Coordinated Universal Time (UTC), referred to as UTC (USNO), via the Global Positioning System (GPS). Time offset data measured at the DSCCs are forwarded to the DSN Time Analyst who is responsible for verifying that station frequency and time offsets, relative to UTC (USNO), are within specified limits. The frequency and time performance for the test facilities is the responsibility of their respective operations organizations.

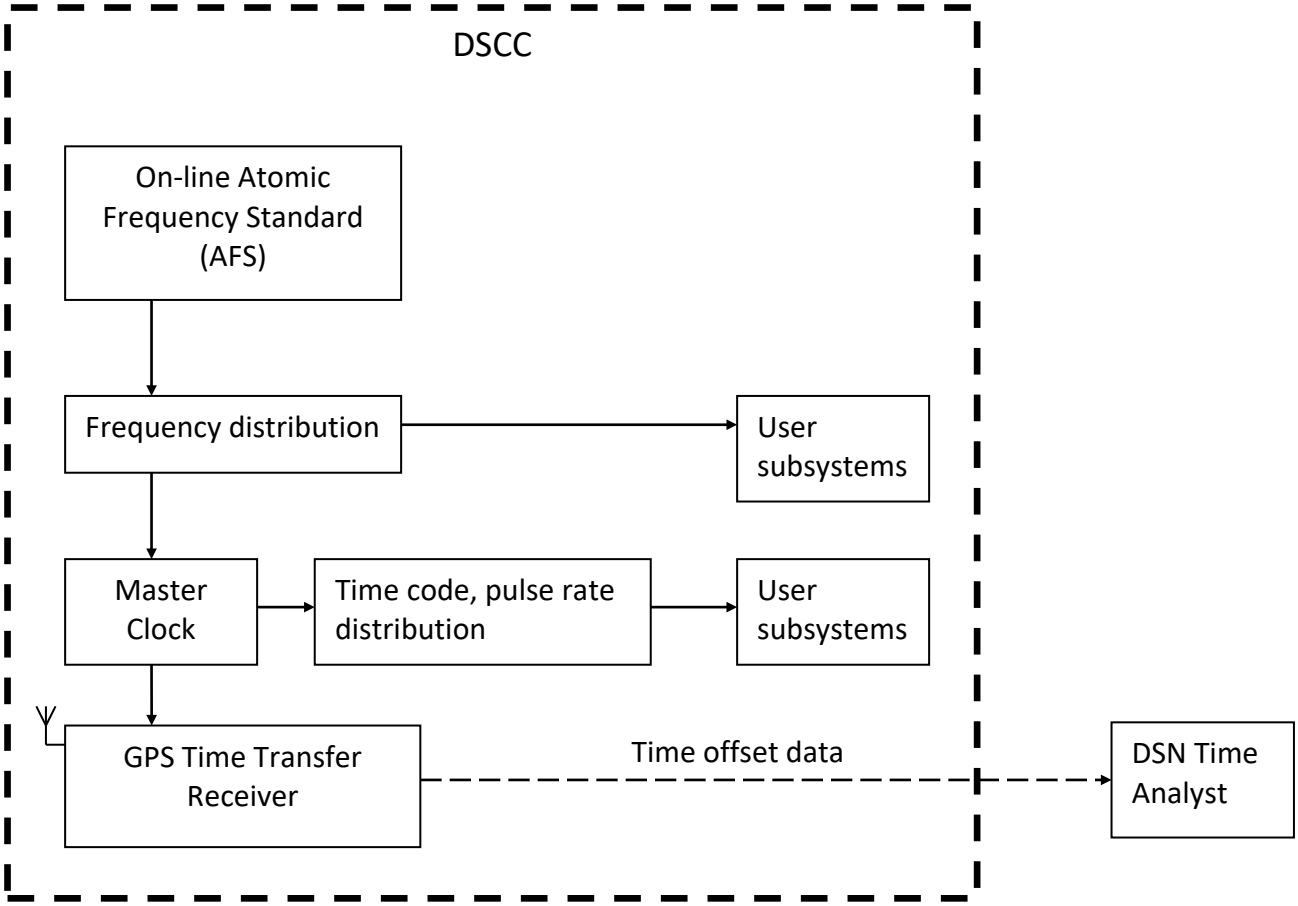

Figure 1. DSN Frequency and Timing – Simplified Block Diagram

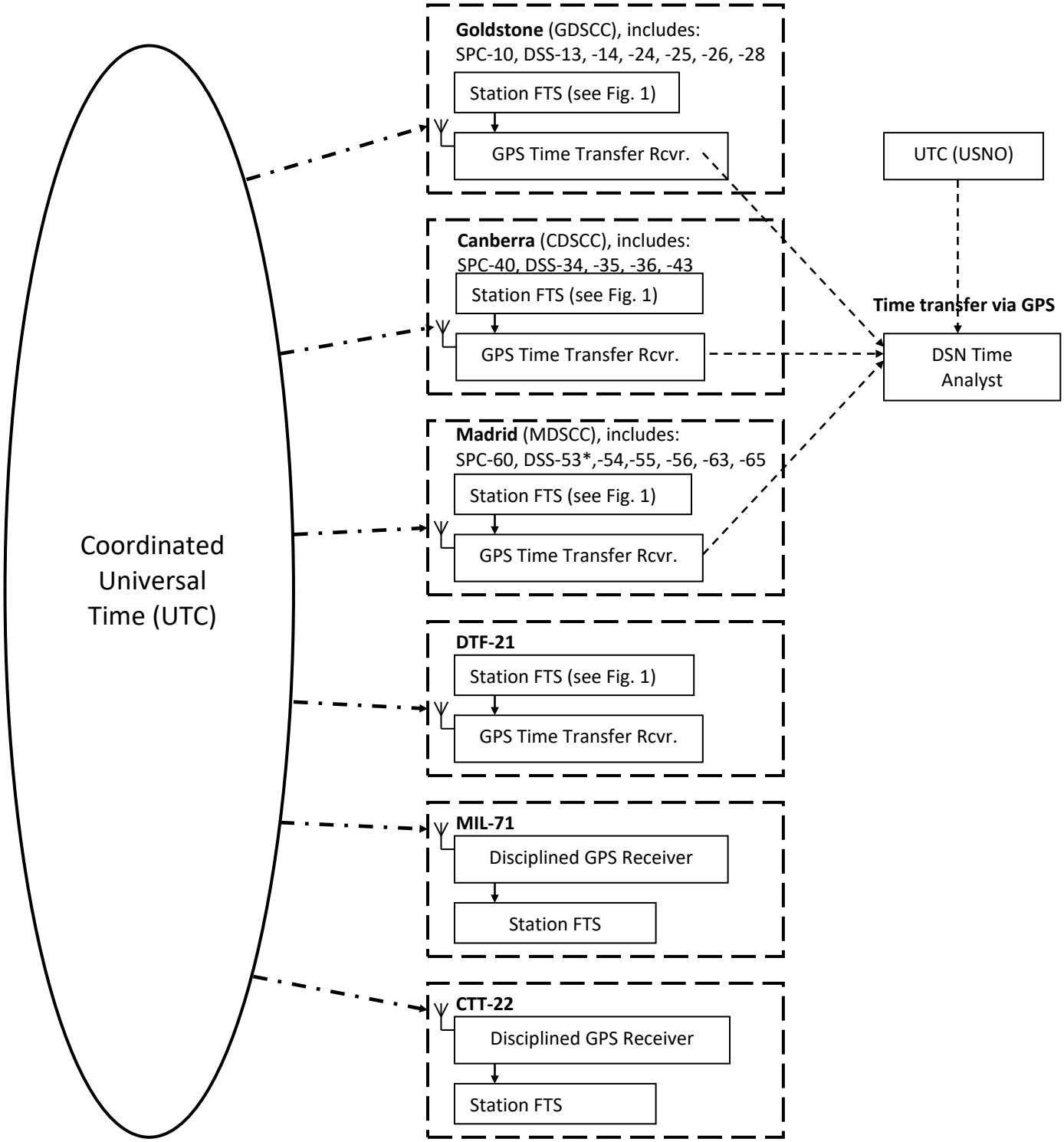

*DSS-53 is expected operational by end of 2021

Figure 2. DSN Time Transfer

2.1 Functions

The FTS provides the following major functions:

1) Generate and distribute very stable reference frequencies, time codes, and timing pulses to other equipment
2) Provide measurements of clock synchronization (time) and syntonization (frequency) traceable to UTC (USNO)
3) Generate phase calibration tones for very-long baseline interferometry (VLBI) via phase calibration generators. See paragraph 2.2.12 for further details.

2.2 Components

Principal components of the FTS include frequency standards, clocks, frequency and time distribution equipment, phase calibration generators, and performance measurement equipment.

2.2.1 Atomic Frequency Standards

Two types of atomic frequency standards are nominally deployed at the DSCCs. They are the hydrogen maser and the cesium-beam standard. The performance of these standards is a function of multiple factors including model, configuration, and the environment. Figure 3 shows the range of performance routinely available in the DSN in terms of Allan Deviation, σ, over the averaging time, τ. The lower bound of the range in the figure captures the optimum performance that should be expected in the implemented configuration. The upper bound can be considered as the worst case. This figure also shows the performance of the cryogenic sapphire oscillator (CSO), a non-atomic oscillator that may be made available for special experiments. See paragraph 2.2.3 for additional details.

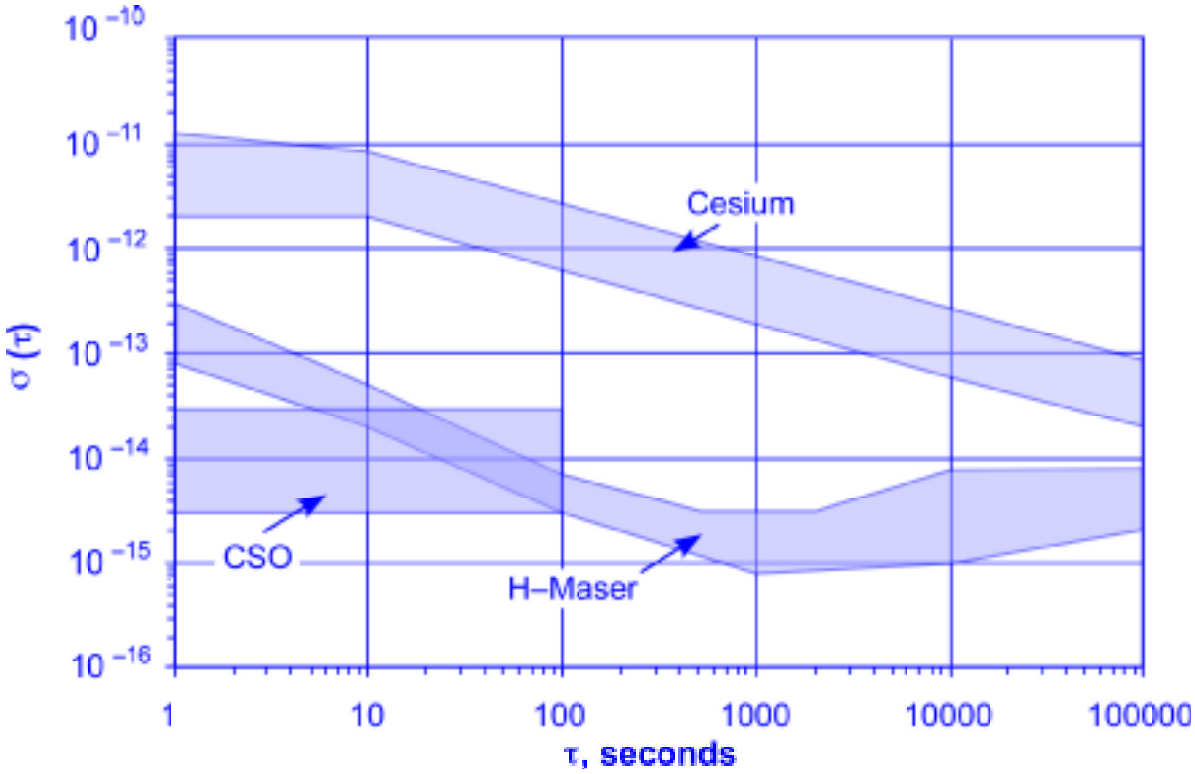

Figure 3. Allan Deviation of Frequency Standards.

Hydrogen masers have been employed as the prime DSN frequency standard for some years. They provide spectral purity commensurate with a very good quartz crystal oscillator and frequency stability that is optimal for measurement periods between 1000 and 10,000 seconds. Spectral purity is especially important because the frequency reference must be multiplied up to local oscillator frequencies as required by DSN transmit and receive equipment. The frequency multiplication degrades the spectral purity (expressed as a signal-to-noise ratio) by 6 dB per octave or 20 dB per decade. Noise injected by a local oscillator has the same effect on receiver performance as noise from any other source and can significantly degrade radio science investigations. Stability for measurement times through 10,000 seconds is important for navigation, where frequencies and timing signals are compared delayed by the round-trip light time to the spacecraft. Another driver for stability at medium-to-long measurement times is radio science and VLBI investigations that normally are performed over a period of 8 to 12 hours. Table 1 summarizes the performance of the DSN frequency standards in the implemented configuration.

Table 1. DSN Frequency Standard Performance

Parameter	Value
Frequency Offset Relative to UTC Typical Resolution reconstructed by analysis (3 σ)	 $<3 \times 10^{-13}$ $<1 \times 10^{-13}$
Fractional Frequency Drift Specified Typical	 1×10^{-13} /10 days $<3 \times 10^{-14}$ /10 days
Harmonic distortion (sine waves)	<5%
Stability (Allan Deviation)	See Figure 3
SSB Phase Noise at 100 MHz, in 1Hz bandwidth, 1Hz from the carrier Hydrogen Maser Cesium Standard	 –97 to –104 dBc/Hz –65 to –85 dBc/Hz For other frequencies, add 20 log (f/100) to these values, where f is the desired frequency in MHz.
Availability	> 0.9999

2.2.2 Frequency Standards at the DSCCs

The present complement of standards at each DSCC nominally comprises two hydrogen masers and two cesium standards. The standards are located in an environmentally controlled area of the Signal Processing Center (SPC).

2.2.3 FSTL and DSS-25 Cryogenic Sapphire Oscillator

Cryogenic oscillators provide the ultra-high short-term stability and low phase noise for measurement times less than 200 seconds. The cryogenic sapphire oscillator achieves long-term operation using commercial cryogenic cooling systems. A CSO with the performance shown in Figure 3 has been installed at DSS-25 to provide an improved reference for radio science investigations and the JPL FSTL for low phase noise characterization. The CSO is currently only available for use at DSS-25 through special arrangements.

2.2.4 Frequency References for Test Facilities

Reference frequencies at DTF-21 are derived from a Cesium Beam standard (see Figure 3 for nominal stability). Reference frequencies at MIL-71 and CTT-22 are derived from a disciplined GPS Receiver. For testing at JPL locations that requiring high performance, a signal from a hydrogen maser, similar to those used at the complexes, can be made available from the JPL Frequency Standards and Test Laboratory (FSTL) via a fiber optic link. The calibration of this hydrogen maser can be traced to UTC via GPS.

The Network Operations Control Center (NOCC) at JPL does not require reference frequencies but receives time code via the JPL Calibration Laboratory.

2.2.5 Signal Processing Centers

Reference frequencies at the DSCCs are distributed via a system of high-quality distribution amplifiers and coax cables that are designed to minimize degradation to the frequency standard performance. Outputs from the selected frequency standard are routed to the *Frequency Reference Selection* (FRS) Assembly. The FRS provides a switching capability, a frequency flywheel, and standard coherent reference outputs at 100, 10, and 5 MHz. These reference signals are routed from the frequency standards room to an assembly within the SPC control room referred to as the *Frequency Reference Distribution* (FRD) Assembly. The FRD provides 5, 10, and 100 MHz distribution to all control room equipment.

2.2.6 34-m High Efficiency Antennas and 70-m Antennas

The frequency references for the Receiver Downconverters at the 34-m High Efficiency (HEF) and 70-m antennas are provided by a fiber optic transmission system, the *Photonic Frequency Distribution* (PFD), designed to preserve the stability equivalent to that of a hydrogen maser at the distribution point within the antennas. The PFD installation at these stations uses special low temperature coefficient fiber optic cabling to transport the reference frequency from the SPC to the tilting structure of the antennas. This is important because the cables on the antennas can experience significant changes in temperature both from the environment and when antenna motion exposes them or shields them from the sun.

2.2.7 34-m Beam Waveguide Antennas

The frequency references for the Exciters and Receiver Downconverters at the 34-m beam waveguide (BWG) antennas are provided via PFDs. Standard temperature coefficient, single mode fiber is used for frequency distribution to all of the DSN BWG antennas. However, it is buried 1.2 m below the surface where there are no significant diurnal changes for antennas located near the SPCs. The diurnal phase change for DSS-26, located 15.5 km from the SPC, has been measured as 1-degree at 100 MHz over a 12-hour period and ~8 ns peak to peak over an annual cycle. Diurnal phase variations at DSS-24 and DSS-25 are nominally the same as DSS-26 as the signal distribution follows an almost identical path to that of DSS-26. All equipment requiring frequency references at the BWG antennas is located within the antenna pedestals so antenna motion has no effect on frequency stability.

2.2.8 Time Standards

All DSN facilities use a single time source, traceable to UTC, for all operational equipment within the facility that requires precision timing. The accuracy and availability of this time source depends on the requirements of the facility at which it is installed.

2.2.9 DSCC Time Standard

Each DSCC contains a Master Clock whose rate is determined by the selected on-line frequency standard. In the rare circumstance of a switchover between online standards, an in-series, low noise flywheel oscillator continues to provide a frequency reference to the Master Clock during the switching period (typically < 5ms). This technique ensures that the maximum clock error after a frequency standard switchover does not exceed a clock cycle (10 ns with a 100 MHz reference). Characteristics of the DSCC time standard are provided in Table 2.

Time offset from UTC (USNO) is maintained at < 3 μs from UTC with a knowledge < 20 ns. Synchronization between the DSCCs and UTC is accomplished using “common-view” or “all-in-view” GPS time transfer between USNO and the DSCCs.

Table 2. DSCC Time Standard Characteristics

Parameter	Value
Time Reference	UTC (USNO)
Setability	10 ns
Offsets from UTC Requirement Resolution from UTC, reconstructed by analysis (3 σ)	 < 3 μs < 1 μs
Offsets between DSCCs Requirement Resolution between DSCCs, reconstructed by analysis (3 σ)	 < 6 μs < 100 ns
Availability	> 0.9999

2.2.10 DTF-21, CTT-22, MIL-71 and NOCC Time Standards

Timing signals and day-of-year at DTF-21 and CTT-22 are derived from a Master Clock identical to that operating in each DSCC. At DTF-21 the clock rate is derived from a Cesium frequency standard. The Master Clock may be calibrated to GPS receivers that reference GPS Time and are traceable to UTC with an accuracy of $\leq$ 100 ns. At MIL-71 and CTT-22, clock rates are determined by disciplined GPS receivers.

Time and date at the NOCC are obtained via the Network Time Protocol (NTP) that is derived from UTC. The time is referenced to GPS Time and is traceable to UTC with an accuracy of $\leq$ 100 ns. NTP enables all computers at the NOCC to be synchronized within 0.1 s of UTC.

2.2.11 Time Distribution

Station time information is distributed from the Master Clock, via fiber optic cables up to 30km in length, to Time Code Translators (TCTs) that are typically located in racks of user subsystems that require precision time or pulse rate signals. TCTs can be calibrated to compensate for fixed distribution path length delays with a resolution of 10 ns so the offset knowledge of synchronization from the Master Clock to a specific user is < 10 ns. The typical jitter stability at the output of the TCTs is < 30 ps (RMS).

Certain monitor and control computers that do not require precision timing (> 0.1s accuracy) are synchronized to local NTP servers, independent of the station FTS.

2.2.12 Phase Calibration Generators

The stability of the receivers used to detect signals from extra-galactic radio sources at the various DSN antenna sites is critical, but often difficult to control because of the extreme and exposed environment of the antenna and its electronics. Performance of VLBI measurements can be improved by comparing phase variations in received signals to a stable calibration tone locally generated in the detection bandwidth. The Phase Calibration Generator (PCG) provides these high stability calibration comb tones.

On the 70-m and DSS-65 HEF antennas, a comb spectrum with a fixed 1.0 MHz line spacing can be injected into the feedcone or microwave waveguide ahead of the S-band and X-band low noise amplifiers (LNAs). On the 70-m antennas, a similar spectrum can also be injected into the waveguide ahead of the L-band LNAs.

Receiver and comb generator stability tests on the S- and X-band PCGs were performed at the JPL Frequency Standards Test Laboratory both in a stabilized temperature environment and with temperature cycling. The averaged Allan Deviation from the 15 units tested is shown in Figure 4. Based on knowledge of temperature sensitivity of the PCG and the environmental requirements for the locations where they are installed, a curve showing the estimated installed performance of the S- and X-band PCG at a typical DSN site has been calculated and is also shown in Figure 4.

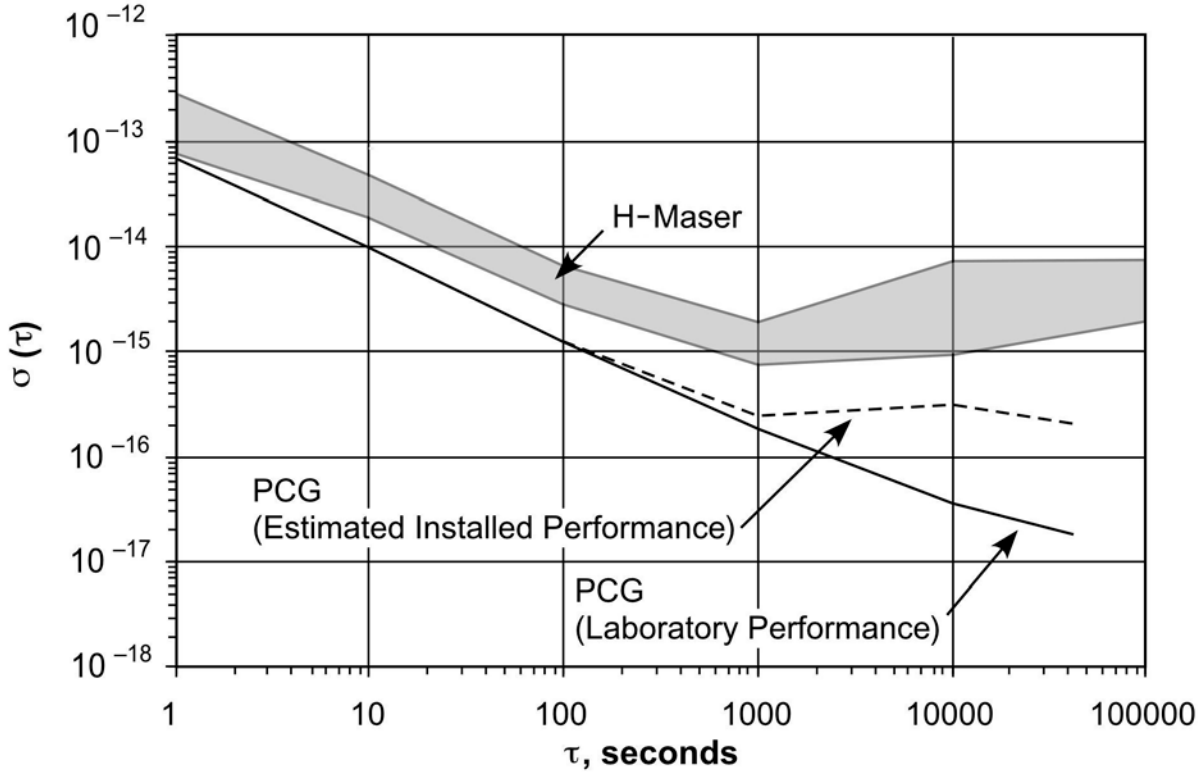

Figure 4. S-band and X-band Phase Calibration Generator Stability.

A newer X/Ka-band phase calibration generator has been developed and deployed at all BWG antennas except DSS-24. This design generates stable comb tones spanning the frequency range from 3 GHz to 40 GHz. The performance capabilities are summarized in Table 3.

Table 3. X/Ka-band Phase Calibration Generator.

Parameter	Capability
Stability (Allan Deviation)	
1 s	5×10^{-14}
10 s	8×10^{-15}
100 s	1.0×10^{-15}
1000 s	1.2×10^{-16}
10,000 s < τ < 100,000 s	$<5 \times 10^{-17}$
Amplitude Flatness	±1.7 dB, 32-33 GHz
Comb Spacing	1 MHz, 2 MHz, or 4 MHz selectable

2.3 Frequency and Time Synchronization

DSN frequency and time synchronization is referenced to UTC using "common-view" or "all-in-view" GPS time transfer. This technique allows the direct comparison of two clocks at widely separated locations by canceling out the effect of GPS clock performance and most media effects (see Figure 5). The DSN GPS receiver takes the time difference between the DSN Master Clock and the time obtained from one or more GPS satellites (including propagation delay) and creates a data file. USNO maintains a similar database between UTC (USNO) and all GPS satellites. The USNO database is queried periodically and the DSN Time Analyst uses the data and a weighted averaging technique to derive time offsets. Frequency offsets are derived using a moving average barycentric filter. The resultant information is used to adjust the DSN frequency standards to keep them within the required frequency and time specification limits.

2.4 Adjustment of DSN Time to UT1

The Earth's rate of rotation is not uniform. It is affected by gravitational effects of the sun, moon, and planets, tidal effects, and several other mechanisms. The time scale based on the earth's rotation, corrected for polar motion, is called UT1 and is maintained by the International Earth Rotation Service (IERS), http://www.iers.org/. UT1 enables proper aiming of telescopes and radio-telescopes (including DSN antennas) at celestial objects.

The mean solar day as determined from the UT1 time scale is approximately 2 ms longer than 86,400 SI seconds established by atomic clocks. By international agreement, the UT1 and UTC time scales are kept synchronized within ±0.9 seconds by step-time adjustments of exactly one second (leap seconds). Notification to perform this adjustment is received from the IERS between 30 and 60 days before the adjustment is required. Leap seconds are added or subtracted, usually at the end of December or June, at the end of the day and set, as described below. DSN users must be aware of the potential for interference between time adjustments and sequences of time-critical events. Table 4 provides the sequences of time codes that occur during leap second adjustments.

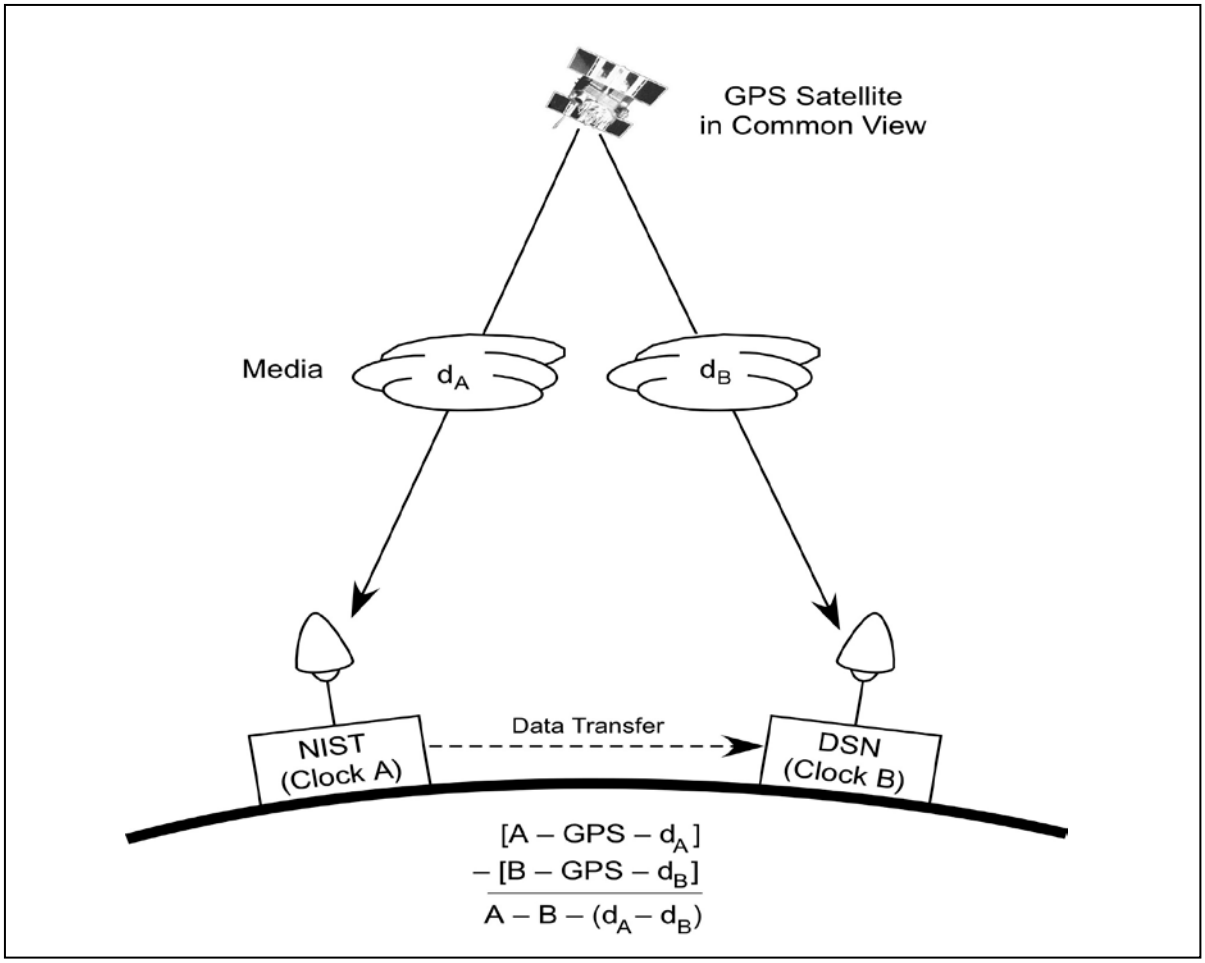

Figure 5. Common-View GPS Time Transfer

Table 4. DSN Leap Second Adjustments.

Day	Second	Time
Leap Second Add		
n	*t*	23:59:59
n + 1	*t* + 1	23:59:60
n + 1	*t* + 2	00:00:00
n + 1	*t* + 3	00:00:01
Leap Second Subtract		
n	*t*	23:59:58
n + 1	*t* + 1	00:00:00
n + 1	*t* + 2	00:00:01

3 Proposed Capabilities

The following paragraphs discuss capabilities that have not yet been fully implemented by the DSN but have adequate maturity to be considered for spacecraft mission and equipment design. Telecommunications engineers are advised that any capabilities discussed in this section cannot be committed to except by negotiation with the Interplanetary Network Directorate (IND) Plans and Commitments Program Office.

3.1 Stabilized Photonic Frequency Distribution (S-PFD)

The existing PFD implementation for frequency reference distribution to the antennas provides a return link that facilitates performance verification at the user port. Nevertheless, the PFD frequency distribution system is open loop. I.e. there is no provision to actively compensate for distribution link induced phase variations (e.g. due to environmental thermal variations) – potentially significant at the remote antennas at Goldstone where the distribution link can be up to 30 km. A closed-loop modification to the PFD hardware has been developed which does actively compensate for induced phase variations on the distribution link. Initial testing at JPL indicates a 50- to 100-times improvement in stability at averaging times greater than 100s.

DSN Telecommunications Link
Design Handbook

305, Rev. B
Test Support

Released October 31, 2009

Prepared by:

10/29/09

A. Kwok Date

Approved by:

10/30/09

T. T. Pham Date
DSN Chief System Engineer

Released by:

Signature on File at DSN Library 10/31/2009

DSN Document Release Date

Change Log

Rev	Issue Date	Paragraphs Affected	Change Summary
–	7/30/2003	All	New Module
A	5/26/2006	Many	Documents revised capabilities due to relocation of DTF-21 and MIL-71.
B	10/31/2009	Many	Replaced DSMS with DSN. Removed references to the decommissioned 26-m stations.

Note to Readers

There are two sets of document histories in the 810-005 document that are reflected in the header at the top of the page. First, the entire document is periodically released as a revision when major changes affect a majority of the modules. For example, this module is part of 810-005, Revision E. Second, the individual modules also change, starting as an initial issue that has no revision letter. When a module is changed, a change letter is appended to the module number on the second line of the header and a summary of the changes is entered in the module's change log.

Contents

Illustrations

Figure **Page**

Tables

Table **Page**

1 Introduction

1.1 Purpose

This module provides information to enable Deep Space Network (DSN) customers design tests that use the DSN test instrument and identify the appropriate site to conduct the tests. These tests are used primarily during the mission implementation process to validate spacecraft, spacecraft components, and spacecraft support.

1.2 Scope

This module deals solely with test support for flight projects currently available in the DSN. It provides characteristics of equipment that are unique to the test environment. It does not provide information about the capability of the operational equipment that is installed at each test support site. Characteristics of operational equipment may be found elsewhere in this Design Handbook.

2 General Information

The DSN exists to provide communication between a project control center and its spacecraft. Commands are relayed to the spacecraft on the forward link and the transmitted data from the spacecraft is extracted from the return link. This involves both a ground link and a space link. Trouble free communications on both links are important for mission success. The DSN provides extensive capability to demonstrate the performance of the ground link in combination with project control centers and with spacecraft hardware in a test environment. Test support is available from the three Deep Space Communications Complexes located at Goldstone, California; Madrid, Spain; and Canberra, Australia. In addition, the DSN includes three facilities that exist primarily for test support. These are the Development and Test Facility (DTF) 21 in Monrovia, California; the Compatibility Test Trailer (CTT) 22; and the Merritt Island Launch Annex (MILA) facility (MIL-71) at the Kennedy Space Center (KSC), Florida.

2.1 Functions

The DSN has three primary functions with respect to test support:

1) To support data flow testing between the DSN stations and project control centers,
2) To validate the compatibility between spacecraft or spacecraft subsystems and the DSN,
3) To provide communication between a spacecraft and its project control center during pre-launch activities.

Figure 1 provides an overview of the DSN test support that is available both at the stations and at the compatibility test sites. This support may involve elements of the Microwave, Uplink and Downlink equipment, the Telemetry Simulation Assembly (TSA), the System Performance Test (SPT) Assembly, and Service Management.

The TSA generates test data in the format specified by the customer subject to the restrictions described in this document. The data may be coupled directly into the station downlink equipment or it may be modulated on a radio frequency (RF) carrier (or on a subcarrier that is modulated on the RF carrier) by the uplink equipment, injected into the station microwave equipment, and received by the downlink equipment before being processed as if it had come from a spacecraft. The received data and any other data subscribed to by the project are forwarded to the project control center and to the SPT Assembly for analysis. The analyzed results from the SPT Assembly are made available to the project. Service Management is responsible for scheduling and the non-real-time interfaces between the DSN and the customers.

The links to and from the spacecraft are accomplished by direct cabling although Ka-band signals are normally downconverted near the spacecraft and transferred to the downlink equipment at the DSN intermediate frequency (100 – 600 MHz). The uplink equipment at the compatibility test sites may be used to relay project-originated commands that can be acted on by the spacecraft or spacecraft subsystems under test.

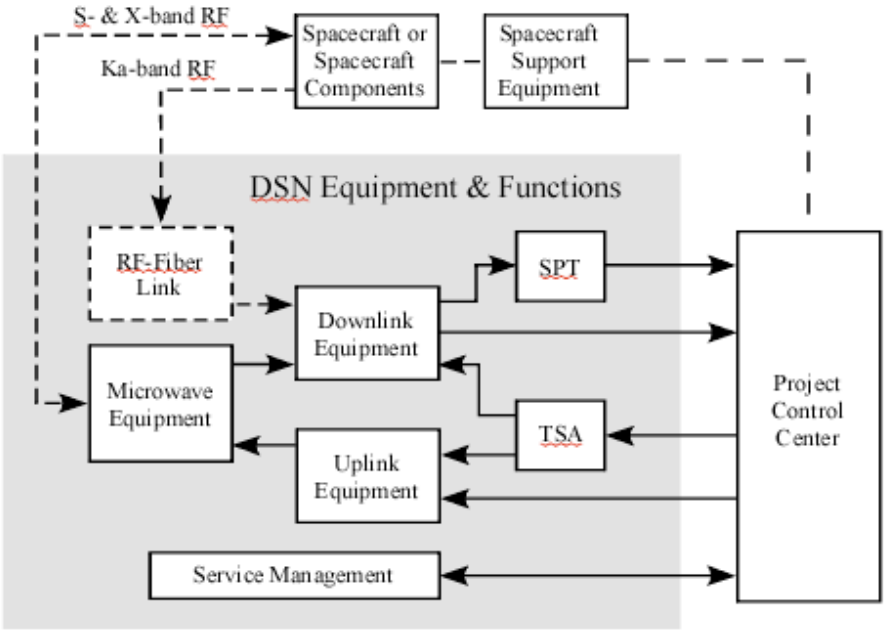

Note: Interfaces appearing as dashed lines only exist at Compatibility Test Facilities.

Figure 1. DSN Test Support Overview.

2.2 Station Test Support Equipment

Each DSN location includes a TSA, an SPT Assembly, and appropriate equipment to generate simulated spacecraft signals.

2.2.1 Telemetry Simulation Assembly

The TSA enables telemetry testing to be performed without the need for a spacecraft. It includes either two or four independent channels that can be controlled locally or remotely. Each channel can replay pre-recorded data from disk or generate telemetry data in real time without using disk storage. Pre-recorded data can be uncoded or can be symbols in any coding scheme acceptable to the equipment under test. Pre-recorded data is the only way turbo coded data can be simulated at this time.

Pre-recorded or real-time data can be converted to any pulse code modulation (PCM) format, have any convolutional coding acceptable to the DSN applied, have Reed-Solomon (RS) coding added, modulate the data onto a subcarrier, add Gaussian (noise amplitude decreases with increasing frequency in output bandwidth) or white noise (noise amplitude is uniform across output bandwidth), and simulate Doppler frequency shifts of the subcarrier frequency and data rate. The capabilities and limitations of the TSA are summarized in Table 1.

Table 1. TSA Capabilities and Limitations.

Capability	Limitations
RECORDED DATA	
Spacecraft ID (used for locating recorded data)	1–255
Data Types	No Restrictions – Examples are Uncoded, RS coded, Convolutional Coded, Turbo Coded, etc.
Starting Byte Offset for Playback	1–1,000,000,000
REAL-TIME DATA	
Data Types	Uncoded, RS coded, Convolutional Coded, concatenated RS and Convolutional Coded
Data Pattern	All 1s, all 0s, alternating 1s & 0s, PN sequences, 1–128 1s followed by 1–128 0s
DATA FRAME OPERATIONS (each channel)	
Frame Length	8–128000 bits (any multiple of 8)
Frame Sync Word	
Length	8–32
Pattern	Hexadecimal, limited by length
Frame Counter	Starts at 0. Repeats upon overflow.
Starting Bit	1–128000 or disabled
Field Length (bits)	3–32
Time Tag	
Length (bits)	50 (9 day-of-year, 17 second-of-day, 24 millisecond-of-day)
Starting Bit	1–127951
Fixed Fields (Content does not change from frame to frame)	Fields may not overlap any other fixed or variable field.
Number of Fields	0–32
Starting Bit (each field)	1–128000
Field Length (bits, each field)	3–32
Contents (each field)	Hexadecimal or unsigned integer value
Variable Fields (Content changes from frame to frame as described below)	Fields may not overlap any other fixed or variable field.
Number of Fields	0–32
Starting Bit (each field)	1–128000
Contents (each field)	Data file, ramp function, sinusoidal function, triangular function, Taylor series expansion

Table 1. TSA Capabilities and Limitations (Continued).

Capability	Limitations
Fixed Frame Errors	
Number of Errors	0–32
Starting Bit (each error)	1–128000
Error Mask (each error)	6 hexadecimal digits
DATA RATE	
Uncoded Data (b/s)	3.0000 – 25,000,000.0000
Coded Data (s/s)	3.0000 ÷ Code Rate to 25,000,000.0000
Doppler Simulation (data & subcarrier)	Carrier Doppler Predict File Must Exist
DATA ENCODING	
PCM Formats	NRZ-L, NRZ-M, NRZ-S, Bi-ϕ-L, Bi-ϕ-M, Bi-ϕ-S
Convolutional Coding	
Rate (*r*)	1/2, 1/3, 1/4, 1/5, 1/6
Constraint Length (*k*)	3–15
Connection Vectors	2–6 vectors expressed as 4 hexadecimal digits
$k = 7$, $r = 1/2$ Symbol Order	CCSDS or DSN
Alternate Symbol Inversion	Optional
Reed-Solomon Encoding	
Code Supported	RS (255,223)
Interleave Factor	1–8
Virtual Fill	Provided for short frames (< 223 x Interleave)
Sync Word	Attached or Embedded
OUTPUT (each channel)	
Subcarrier (bi-phase modulated)	
Frequency (Hz)	100.000 – 1,000,000.000
Waveform	Sine or Square
Noise	Gaussian (frequency dependent) or white (frequency independent)
Signal/Noise Ratio (dB)	–60.0 to +40.0

Real-time data includes the capability for frame generation with fixed or pseudo-noise (PN) data patterns, optional frame counter, time-tag, programmable data fields, and systematic frame error generation. Real-time data generation starts by filling a suitable data structure from which a continuous data stream can be produced with the selected data pattern. Next, the data pattern is overlaid with the Attached Synchronization Marker (ASM), for frame-synchronized data, and other fixed and variable fields at appropriate intervals if required. If Reed-Solomon (RS) coding is required, sufficient space is allowed between the end of one frame and the start of the next ASM to permit the RS parity symbols to be inserted as the frame is coded. RS frame sizes specified as having a data length of less than 223 bytes multiplied by the interleave factor will result in an appropriate amount of virtual fill being inserted at the beginning of each frame. The completed data may be convolutionally coded prior to being converted to PCM. Figure 2 illustrates this process for a 1784 bit data frame using a PN11 fill pattern, a standard 32-bit ASM, no additional data fields, and RS encoding.

Each TSA channel functions independently and each DSN location can support as many test activities as the number of channels in the TSA. Initial configuration of each channel is from a pre-programmed configuration file that can be modified using operator directives (ODs). The revised configuration can then be saved under a new file name for later use.

2.2.2 System Performance Test Assembly

The SPT assembly operates as a stand-alone system test tool. It is used to collect and analyze test data from the test equipment and present the results to the project. The SPT functions include:

1) Telemetry bit error rate (BER) tests,
2) Telemetry time delay tests,
3) Data stream continuity tests,
4) Data stream extraction tools,
5) Data analysis tools.

2.2.2.1 Telemetry Bit Error Rate Tests

Telemetry BER tests evaluate the performance of the Telemetry Service by comparing the telemetry data output when supplied with a known (TSA generated or, in the case of turbo codes, previously recorded) input to the system. A desired E_b/N_0 (energy-per-bit to noise spectral density ratio) or E_s/N_0 (energy-per-symbol to noise spectral density ratio) is established using the received noise as a reference for RF testing or the additive noise capability of the TSA for data testing. The bit or symbol error rate determined by the SPT is used to calculate the theoretical input E_b/N_0 or E_s/N_0 for a lossless system employing the specified code. The difference between the actual input and the theoretical input is the system loss. The following codes can be used for BER tests.

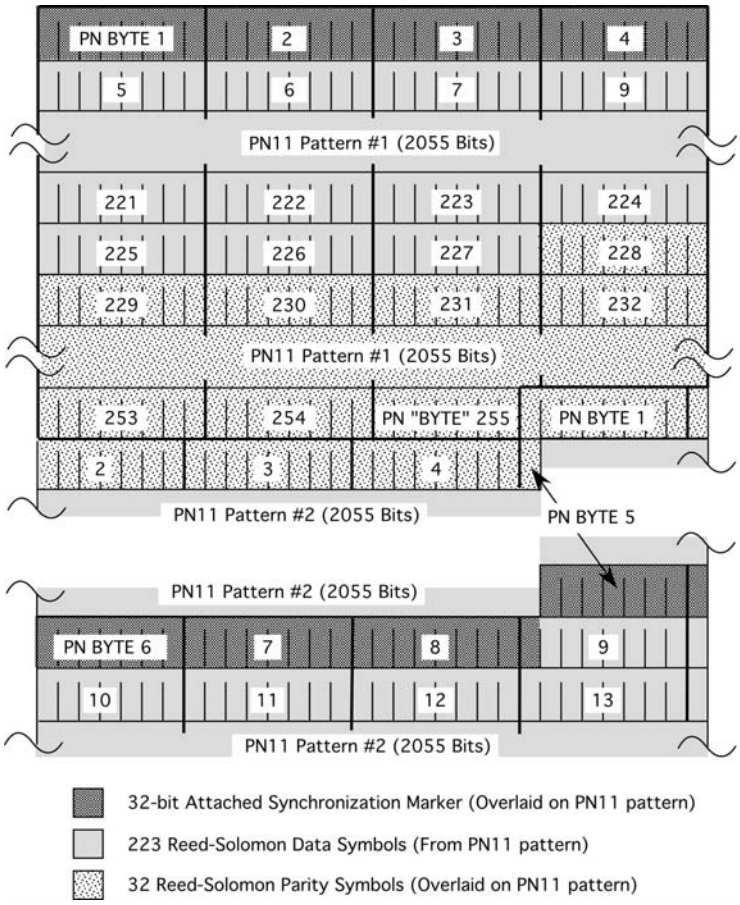

Figure 2. TSA Real-time Data Generation Process.

1) None (Uncoded)

2) Convolutional (k=7, r=1/2)

3) Convolutional (k=15, r=1/4),

4) Convolutional (k=15, r=1/6),

5) Concatenated Reed-Solomon and any of above convolutional codes,

6) CCSDS turbo codes for block sizes of 8920 bits and smaller (using recorded data prepared in accordance with the frame generation process described above).

The SPT operates with the data patterns specified below. To do real time data validation, the SPT needs a frame description; fill pattern used, and location and content of fields. It is important to note that the SPT expects the type of frame generation process employed by the TSA, where the fields overlay the fill pattern. Frames generated with a different process cannot be checked in real time.

1) Alternating 1s and 0s,

2) Alternating 00 and FF bytes,

3) PN11 through PN16 data with operator modifiable connection vector,

4) Frame sync word or other user specified pattern only,

5) User data file that includes frame sync and frame sequence number;

2.2.2.2 Telemetry Time Delay Tests

The telemetry time delay test compares the time-tag applied to each data frame header by the telemetry system with the time-tag inserted into the simulated telemetry data by the TSA. The test provides the mean, standard deviation, and number of blocks exceeding a user specified tolerance between these two times. This test is not available for turbo coded or other previously coded playback data.

2.2.2.3 Data Stream Continuity Tests

The SPT can monitor any data stream routed through the Reliable Network Server (RNS). The SPT evaluates data stream continuity by detecting missing or duplicate block serial numbers and by detecting time gaps within the headers of the data blocks.

The SPT has the capability to record the data being processed during BER tests for off-line analysis of data stream continuity.

2.2.2.4 Data Stream Extraction Tools

The SPT can extract user-specified data items from any data stream routed through the RNS. The extraction mechanism permits the user to specify the structure of the data block including position, length, and conversion units of each item to be extracted. The extracted data is stored in a delimited, user-specified format and is accessible for real-time and post-test analysis.

2.2.2.5 Data Analysis Tools

The SPT includes a complete set of graphical and mathematical tools for analysis of data extracted from any data stream visible from its network port. These tools include the capability to:

1) Provide the capability to graph real-time or stored data by specifying the inputs for the X- and Y-axes. This capability includes the ability to modify the axis scales and provide text notations to the graph and its components.

2) Calculate the mean, variance, standard deviation, and standard error of a sample when provided with the initial and end point of the data.

3) Determine the 90% and 95% confidence intervals for the mean when the sample size is greater than 30

4) Perform a linear squares fit to the data and determine the correlation coefficient

5) Perform a null hypothesis test.

2.2.3 RF Signal Generation

The principal RF signal source is the DSN exciter equipped with appropriate attenuators to generate an uplink signal with command and ranging modulation as expected by the spacecraft. For tests not involving a spacecraft, the exciter can be modulated by simulated telemetry from the TSA, ranging modulation, or both. The RF output of the exciter is translated to the downlink frequency and can be attenuated to whatever level is appropriate to simulate the expected signal-to-noise ratio for the spacecraft signal during its various mission phases. The ability of the exciter to follow a pre-determined frequency profile can be used to simulate Doppler effects.

A secondary frequency source for spacecraft simulation (the Receiver Test Signal Generator) exists at all sites except CTT-22 and MIL-71. It is capable of producing an adjustable output with modulation from one of the TSA channels and can be used independently of the exciter to simulate a second S-band or X-band telemetry downlink or possibly an interfering spacecraft.

2.3 DSN Compatibility Test Facilities

There are three DSN facilities that are provided primarily to support compatibility testing. Each of these facilities has its own unique capabilities and contains both operational and specialized test equipment. The equipment available in each of the facilities is summarized in Table 2.

2.3.1 DTF-21

DTF-21 is located near JPL in Monrovia, CA. It is equipped with simulated front ends for the DSN 70-m and 34-m stations, uplink and downlink equipment, and at least one set of all data processing equipment found in the Signal Processing Centers (SPCs). Simulators for the antennas, transmitters, and microwave control equipment are provided to mimic their responses. Communications are provided by standard JPL/NASA Integrated Service Network (NISN) ground communications interfaces and a Cesium Beam Frequency Standard provides station timing. DTF-21 may be configured to simulate any station at a DSCC. This capability provides a convenient environment for Project/DSN interface testing. DTF-21 includes an RF shielded room in order to isolate devices under test.

Table 2. Equipment at Compatibility Test Facilities

Equipment	DTF-21	CTT-22	MIL-71
34-M/70-M EQUIPMENT			
Antenna Pointing Assy	1	–	–
Uplink Assembly Command Modulation Generators (2), Exciter and ranging control)	2	1	1
Block V Exciter (with uplink ranging)	1	1	1
Downlink Channel Processors	3	2	2
Receiver Test Signal Generator	1	–	–
Microwave Switch Control	1	–	–
SPC EQUIPMENT			
Full Spectrum Receiver	1	–	–
Frequency and Timing Assembly	1	1	1
NETWORK MONITOR AND CONTROL EQUIPMENT (NMC)			
Operator Consoles	3	1	1
GROUND COMMUNICATIONS FACILITY (GCF) EQUIPMENT			
GCF Monitor Processor	2	1	1
Router	2	2	2
Reliable Network Server (RNS)	2	1	1
Operational Voice	Yes	No	Yes
Telephone	Yes	Yes	Yes
COMPATIBILITY TEST EQUIPMENT			
S-band Microwave	Yes	Yes	Yes
X-band Microwave	Yes	Yes	Yes
Ka-band Reception	No	1 as required	1 as required
TSA	4-channel	2-channel	2-channel
SPT Assembly	1	1	1
Y-factor detector	1	1	1

2.3.2 CTT-22

CTT-22 is a 14.6-m (48-foot) towable trailer designed and implemented specifically to perform compatibility and telemetry data flow testing at spacecraft manufacturing facilities and to provide launch support of spacecraft from locations other than Cape Canaveral. It provides capabilities representative of those found at a DSCC. It can be relocated to any

convenient location around the world. However, special arrangements would be required for locations outside the continental United States.

The trailer requires an 18.6 m by 6.6 m (61 ft by 21.6 ft) area for parking and access that is connected via roadways for delivery. Recommended setup time is 24 hours to allow for parking, connection, and equipment stabilization. Interfaces between the CTT and spacecraft are normally made with low-loss coaxial cable. A router is included to enable communication with networks or leased communication circuits. A photograph of the trailer is provided as Figure 3. Significant characteristics and the recommended parking site dimensions can be found in Appendix A.

Figure 3. Compatibility Test Trailer, CTT-22.

2.3.3 MIL-71

MIL-71 is located in the Mission Operations Support Building (MOSB) at the Kennedy Space Center in Florida, USA. The facility is normally maintained in a caretaker status between launches and is implemented as needed, usually to simulate a 34-m Beam Waveguide (BWG) station, for pre-launch project and DSN compatibility. MIL-71 RF interfaces are via fiber optic links to various launch support facilities and to project control centers via NISN ground communications circuits. Use of the facility must be planned and scheduled early enough to allow for temporary relocation of personnel and re-verification of equipment.

2.3.4 Specialized Test Support Equipment

The equipment requirements for the compatibility test facilities differ from DSN tracking sites – the most obvious difference is the lack of a large antenna. Characteristics of the compatibility test equipment that are significantly different from equipment at the tracking sites are summarized in Table 3.

3 Test Activities

The following paragraphs provide a brief discussion of the test activities for which the DSN provides support.

3.1 Data Flow Testing

Data flow tests are usually conducted at the Deep Space Communications Complexes. They include Ground Data System (GDS) tests, Mission Operations System (MOS) tests, and Operations Readiness Tests (ORTs).

3.1.1 GDS Tests

GDS tests are conducted under the direction of the project Mission Manager, who will delegate the responsibility to either the GDS Integration Engineer or the End-to-End Information System (EEIS) Test Engineer who is responsible for scheduling and running the tests and for documenting the results. The emphasis of these tests is on the end-to-end integrity of the GDS, that is, the DSN, the Ground Communications Facility (GCF), the Advanced Multi-mission Operations System (AMMOS), end user devices, and all the associated interfaces. GDS testing normally starts with a minimum number of components and gradually builds up in complexity to involve all elements of the GDS.

3.1.2 MOS Tests

MOS tests address the state of training and readiness of the project mission operations personnel to carry out their assigned responsibilities on a realistic mission time line using the GDS facilities. Similarly to GDS tests, the Mission Manager is responsible for the MOS test program. The MOS Test and Training Engineer has responsibility for the design, scheduling, and execution of the MOS tests. At the successful completion of MOS testing, the flight team is certified as “flight ready.”

Table 3. Characteristics of Compatibility Test Equipment.

Parameter	Value*	Remarks
SHIELDED ENCLOSURE		DTF 21, only
Dimensions		
Width [m (ft)]	3.7 (12)	
Depth [m (ft)]	3.7 (12)	
Height [m (ft)]	3.0 (10)	
Entry Door		
Width [m (ft)]	1.2 (4)	
Height [m (ft)]	2.1 (7)	
Isolation (dB)	140	
Available Power		Within enclosure
Voltage (VAC)	120	Single Phase, nominal
Current (A)	30	
RF INTERFACES		
S-band Direct Input		
System Temperature (K)	500 ±50	
S-band Fiber Optic Input		
Noise (dB)	49	
Nominal input signal level (dBm)	13	
X-band Direct Interface		
System Temperature (K)	500 ±50	
X-band Fiber Optic Input		
Noise (dB)	59	
Nominal input signal level (dBm)	13	
Ka-band Interface		Downconverted to fiber optic IF
System Temperature (K)	725 ±50	Includes follow-on contribution
Output signal levels (dBm)	+3	Maximum, S- and X-band
Output (Exciter) Power Stability (dB)	< 0.5	Over 12-h period
Attenuator step size (dB)	0.1	Independent for input and output

* All values are manufacturer's specifications.

Table 3. Characteristics of Compatibility Test Equipment (Continued).

Parameter	Value	Remarks
FREQUENCY STABILITY		DTF 21, only. CTT 22 and MIL 71 do not have thermal controls and stability is unknown
1 s	5.0×10^{-12}	
10 s	3.5×10^{-12}	
100 s	8.5×10^{-13}	
1000 s	2.7×10^{-13}	
10000 s	8.5×10^{-14} *	
86400 s (1 day)	3.0×10^{-14} *	
TIME ACCURACY		
Reference Time (μs)	1.0	With respect to Global Positioning Satellite (GPS) Time
Time Distribution (ns)	100	With respect to reference time

* Excluding environmental effects

3.1.3 GDS Tests

GDS tests are conducted under the direction of the project Mission Manager, who will delegate the responsibility to either the GDS Integration Engineer or the End-to-End Information System (EEIS) Test Engineer who is responsible for scheduling and running the tests and for documenting the results. The emphasis of these tests is on the end-to-end integrity of the GDS, that is, the DSN, the Ground Communications Facility (GCF), the Advanced Multi-mission Operations System (AMMOS), end user devices, and all the associated interfaces. GDS testing normally starts with a minimum number of components and gradually builds up in complexity to involve all elements of the GDS.

3.1.4 MOS Tests

MOS tests address the state of training and readiness of the project mission operations personnel to carry out their assigned responsibilities on a realistic mission time line using the GDS facilities. Similarly to GDS tests, the Mission Manager is responsible for the MOS test program. The MOS Test and Training Engineer has responsibility for the design, scheduling, and execution of the MOS tests. At the successful completion of MOS testing, the flight team is certified as “flight ready.”

3.1.5 ORTs

ORTs are conducted to demonstrate the readiness of the MOS to support flight operations. The successful completion of these tests demonstrates that all elements of the MOS (hardware, software, people, procedures, and facilities) work together to accomplish routine and mission critical activities. The DSN considers ORTs to be real-time mission activities and provides full support with all committed resources.

3.2 Demonstration Tracks

From time to time, the DSN requests the support of flight projects to verify that a newly implemented capability provides the required support in an actual tracking environment. These activities are referred to as *Demonstration Tracks* and are scheduled with projects that can tolerate data loss should something not work as planned. They are very similar to GDS tests except that they are planned and conducted by DSN personnel who are also responsible for analyzing the results. Demonstration Tracks are always conducted prior to committing a DSN capability for operational support.

3.3 Compatibility Tests

The DSN recommends compatibility testing with all spacecraft for which support is committed. If the project waives compatibility testing, the DSN cannot assume responsibility for spacecraft/DSN interface compatibility. In such cases, DSN support would be provided on a “best-efforts” basis.

Compatibility testing validates the compatibility between the spacecraft radio frequency subsystem and its telecommunications capabilities as they interface with DSN RF and data systems. This testing is conducted at DTF-21, at MIL-71, or at a spacecraft manufacturing facility using CTT-22. Compatibility testing is normally conducted in three phases depending on project requirements: spacecraft subsystem design, spacecraft system design, and system compatibility verification. Figure 4 illustrates the major steps in the compatibility test process.

3.3.1 Subsystem Design Compatibility Tests

The objective of these tests is to demonstrate design compatibility between the spacecraft radio subsystems and the DSN telecommunications subsystems. The tests are performed as early as practical in the spacecraft development program (typically 1-3 years before spacecraft integration). DTF-21 is equipped with an RF shielded enclosure and supporting facilities to accommodate project equipment needed for testing.

The spacecraft telecommunications subsystems are likely be in the form of engineering-level (breadboard or prototype) hardware at this point in the design process. If a new DSN capability is being verified, the test facility (DTF-21 or CTT-22) will be configured with valid (but not necessarily DSN operationally ready) subsystem equipment and software. The types of tests performed during this phase include:

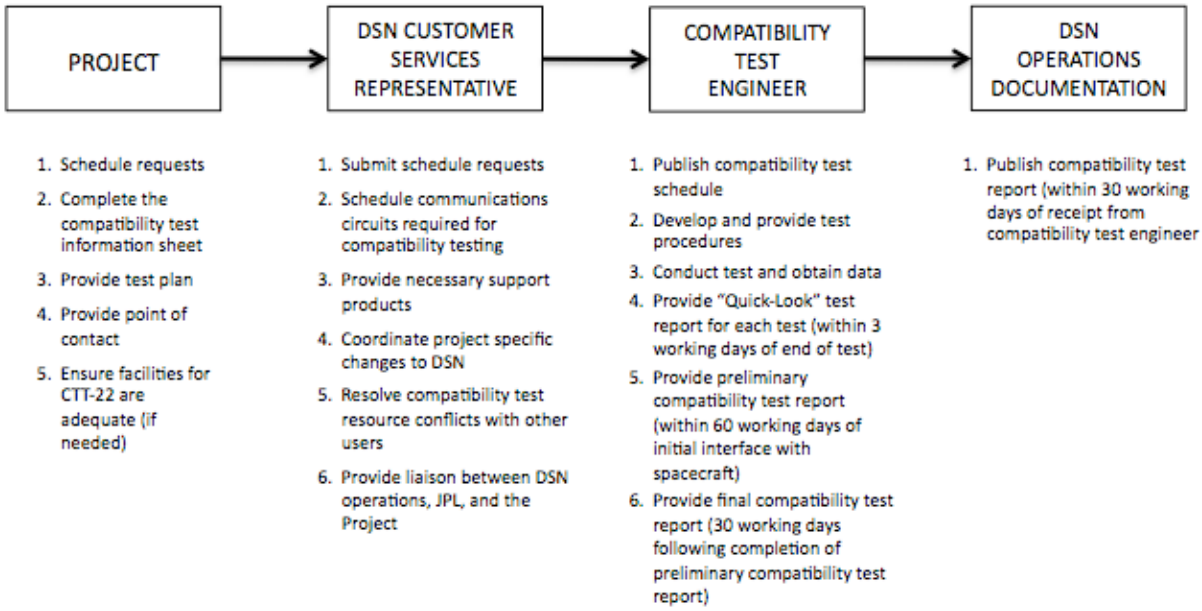

Figure 4. Compatibility Test Process

1) Radio frequency tests including maximum acquisition sweep rates, RF spectrum, transponder rest frequency determination, threshold signal levels, and ranging delay calibration.

2) Telemetry tests including bit error rate, modulation index measurement, and acquisition time.

3) Command tests including performance with ranging modulation and performance with Doppler.

3.3.2 System Design Compatibility Tests

The objective of these tests is to demonstrate the compatibility between the DSN and spacecraft telecommunications system designs and that these designs are in accordance with negotiated flight project/DSN agreements. The tests involve a fully assembled spacecraft and are usually supported by CTT-22. When appropriate, the tests may utilize AMMOS or the Deep Space Operations Center (DSOC). The types of tests performed during this phase are:

3.3.3 System Design Compatibility Tests

The objective of these tests is to demonstrate the compatibility between the DSN and spacecraft telecommunications system designs and that these designs are in accordance with negotiated flight project/DSN agreements. The tests involve a fully assembled spacecraft and are usually supported by DTF-21 for JPL spacecraft or by CTT-22 for non-JPL spacecraft. When appropriate, the tests may utilize AMMOS or the Deep Space Operations Center (DSOC). The types of tests performed during this phase are:

1) RF tests including two-way phase jitter measurements,

2) Repeats of selected subsystem design tests,

3) Data flow compatibility tests with the Project Operations Control Center (POCC).

3.3.4 System Compatibility Verification Tests

The objective of these tests is to ensure that the design compatibility (established during system-level tests) is maintained after equipment implementation and transportation of the spacecraft to the launch site. System verification tests are usually a subset of the tests run in the previous phases and are normally supported by MIL-71. The tests may be performed as part of the DSN Operational Verification Test (OVT) or as a project end-to-end test. Both the spacecraft and the DSN facilities must be in a mission-ready status for these tests to ensure that the final decision of compatibility status is valid. Formal waivers are required to permit substitution of non-operational DSN equipment or software for the tests.

Appendix A
Compatibility Test Trailer Significant Characteristics

Table A-1. CTT-22 Significant Characteristics.

Parameter	Value	Remarks
DIMENSIONS AND WEIGHT		Highway Configuration
Length [m (ft)]	14.6 (48)	Rear stairs removed and stowed
Width [m (ft)]	2.6 (8.5)	Side stairs removed and stowed
Height [m (ft)]	4.1 (13.5)	
Weight [kg (lbs)]	22,700 (50,000)	Maximum
Rear Access Door		
Width [cm (in)]	107 (42)	
Height [cm (in)]	227 (89.5)	
Side Access Door		
Width [cm (in)]	91 (36)	
Height [cm (in)]	208 (82)	
ENVIRONMENTAL REQUIREMENTS		
Slope of parking pad (deg)	5	Maximum
Exterior Temperature [C (F)]	–18 to 41 (0 to 105)	Interior is climate controlled
POWER REQUIREMENTS (60 Hz)		Two 30.5 m (100 ft) cables and 3 m (10 ft) pigtails provided for each circuit
Voltage (VAC)	120/208	60 Hz, 3-Phase, 4-wire plus ground
Equipment Buss		
Service Rating (A)	100	Per phase
Connector	AR61047-S22	Crouse-Hinds Reversed Contacts
Utility Buss		
Service Rating (A)	125	Per phase
Connector	AR2041-S22	Crouse-Hinds Reversed Contacts
RF INTERFACES		Two 30.5 m (100 ft) Type N (male) to Type N (male) low-loss cables provided
RF Connectors	4 Type N, Female 6 Type TNC, Female	Connector impedance is 50 ohms.
DATA INTERFACES		One 30.5 m (100 ft) cable provided for each interface
Serial Data	RS-449 and RS-530	Several circuits, data rates from 9.6 to 3.0 Mb/s, DB25S or DB37P connectors. Data rates above 1.4 Mb/s are supported via MLPP routing protocol and multiple circuits.
Local Area Network (data)	10/100 MB/s	RJ-45 Connector
Local Area Network (monitor)	10/100 MB/s	RJ-45 Connector (Used at JPL, only)
Telephone	2/4 wire	Several circuits, RJ11 and RJ45 female connectors
Intercom	4 wire/channel	Analog intercom voice instrument provided

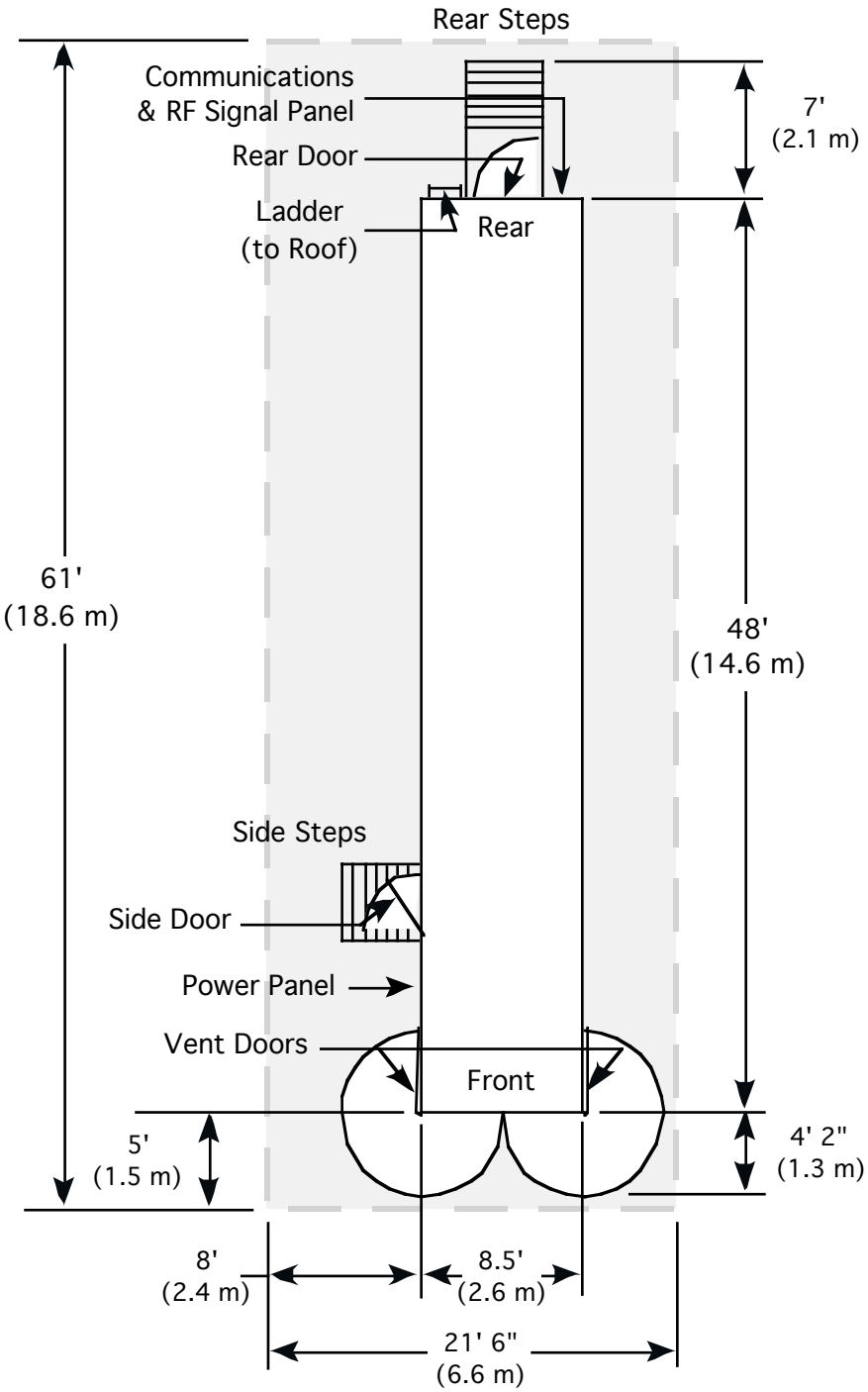

A-1. Recommended CTT Parking Site Dimensions.

Deep Space Network

901
Handbook Glossary

Document Owner:		Approved by:	
Signature Provided	12/17/2020	Signature Provided	11/20/2020
Christine Chang Support System Engineer	Date	Timothy T. Pham Communications Systems Chief Engineer	Date

Prepared by:		Released by:	
Signature Provided	12/17/2020	Signature Provided	12/21/2020
Christine Chang Support System Engineer	Date	C. Chang DSN Document Release Authority	Date

DSN No. **810-005, 901, Rev. H**
Issue Date: February 05, 2021
JPL D-19379; CL#20-6546

Jet Propulsion Laboratory
California Institute of Technology

Users must ensure that they are using the current version in DSN Telecommunications Link Design Handbook website::
https://deepspace.jpl.nasa.gov/dsndocs/810-005/

Review Acknowledgment

By signing below, the signatories acknowledge that they have reviewed this document and provided comments, if any, to the signatories on the Cover Page.

Signature Provided	12/17/2020
Jeff Berner DSN Project Chief Engineer	Date

Change Log

Rev	Issue Date	Prepared by	Affected Sections or Pages	Change Summary
-	11/30/2000	R. Sniffin	All	Initial Release
A	8/15/03	R. Sniffin	2	Corrected units of Boltzmann's constant and other typographical errors. Added abbreviations for new and revised modules.
B	10/7/04	R. Sniffin	2	Revised abbreviation list for new and revised modules.
C	10/21/05	R. Sniffin	2	Revised abbreviation list for new and revised modules.
D	10/31/2009	A. Kwok	Many	Replaced DSMS with DSN. Removed all references related to the 26-m stations.
E	4/29/2011	C. Chang	2	Revised abbreviation list for revised modules.
F	3/22/2012	C. Chang	2	Modified the abbreviation IERS
G	02/10/2017	C. Chang	Sections 1.1, 1.2, 1.4.3, & 2	Added terms used by various 810-005 modules. Obsoleted unused items.
H	02/05/2021	C. Chang	Section 2 Removed section 1.4.3	Updates terms/abbreviation: • Added DSS-53, DSS-56, AOS, DCD, FEC, HSB, IRIG, MNR, SQPSK, USG • Deleted DSS-15, AM, AMMOS, DDC, DN, FSP, L/P, MB, MGSS, MRN, MOCC, MRT, NB, TSDA, WB, WD

Contents

1 Introduction

1.1 Purpose

The purpose of this document is to present a useful glossary of commonly used terms and abbreviations that are current and applicable to the Deep Space Network (DSN).

1.2 Scope

This scope of this document is limited to providing terms and abbreviations that are used within Document 810-005 and especially those that may be different from usage in other organizations.

Terms and abbreviations are included in this document if they meet any of the following criteria:

- used within the DSN but with a meaning that may be unique to the DSN,
- used within 810-005 in place of equivalent terms and abbreviations that may be used elsewhere, or
- commonly used in the field of telecommunications engineering but not necessarily known to all users of 810-005.

1.3 Revisions

This glossary will be periodically revised with changes, improvements, or additions. Usually, these revisions will be coincident with the publication of new or revised 810-005 modules that contain new or revised terminology.

1.4 Definitions

The following paragraphs define the types of items that appear in this glossary and give general rules for their formation.

1.4.1 Terms

A *term* is any word or expression that has a precise meaning in a particular field, in this case, telecommunications engineering.

1.4.2 Abbreviations

An *abbreviation* is a shortened or contracted form of a word or phrase. In a strict sense, the letters are individually pronounced (for example, rpm or DSN) or the reader might

visualize and pronounce the complete form of the word (for example, "assembly" for "assy" or "telemetry" for "TLM").

2 Abbreviations and Terms

Abbreviation or Term	Definition
A	
A-D	analog-to-digital
A/S	anti-spoofing mode of operation (Global Positioning System) in which the encrypted, or Y-code, is unavailable to civilian users of the system
ACME	Antenna Calibration and Measurement Equipment
AFC	automatic frequency control
AFS	atomic frequency standard
AGC	automatic gain control
AIU	Antenna Interface Unit
alidade	The rotating but non-tilting portion of the DSN azimuth-elevation antennas.
AMP	amplifier
AOS	Advanced Orbiter System
APID	Application Process Identifier
ASM	Attached Synchronization Marker
atm	atmospheric
ATSE	Antenna Test Signal Equipment
AWGN	additive white Gaussian noise
az or AZ	azimuth
AZ-EL	azimuth-elevation
A_{zen}	Zenith Atmospheric Attenuation
B	
B3MCD	Block III Maximum Likelihood Convolutional Decoder
B/W or BW	bandwidth
b/s	Bits per second
BCH	Bose-Chaudhuri-Hocquenghem (code)
BER	bit error rate

Abbreviation or Term	***Definition***
BET	bit error tolerance
Bi-φ	Bi-phase
Bi-φ-L	Bi-phase, level
Bi-φ-M	Bi-phase, mark
Bi-φ-S	Bi-phase, space
B_L	loop bandwidth
Boltzmann's constant	–198.6 dBm/(Hz · K)
BP	Belief Propagation
bps	Bits per second
BPSK	binary phase shift keyed
BVR	Block V Receiver (part of DTT Subsystem)
BWG	Beam Waveguide (antenna or subnet)

C

c	speed of light, 299,792.458 km/s
Category A	missions within 2 million km of Earth
Category B	missions at distances greater than 2 million km from Earth
C/A	Coarse Acquisition (GPS code)
CCSDS	Consultative Committee for Space Data Systems
CCW	counter-clockwise
CD	cumulative distribution
CDF	cumulative distribution function
CDSCC	Canberra (Australia) Deep Space Communications Complex
CFDP	CCSDS file Delivery Protocol
CLTU	Communications Link Transmission Unit
CLTUF	Communications Link Transmission Unit File
CMD	command
CONSCAN	conical scanning
CRC	Cyclic Redundancy Check
CRG	Coherent Reference Generator
cryo	cryogenic

Abbreviation or Term	***Definition***
CSO	Cryogenic Sapphire Oscillator (frequency standard)
CSS	Channel-Select Synthesizer
CTT	Compatibility Test Trailer
CV	connection vector
CVCDU	Coded Virtual Channel Data Unit
CW	clockwise
D	
D/C	downconverter
D/L	downlink
DAT	Data Acquisition Terminal
dB	decibel(s)
dBc	decibel(s) with respect to carrier
dBi	decibel(s) with respect to isotropic
dBm	decibel(s) with respect to one milliwatt
dBV	decibel(s) with respect to one Volt
dBW	decibel(s) with respect to one Watt
DCC	Downlink Channel Controller
DCD	Data Capture and Delivery
DCPC	Downlink Channel Processing Cabinet
DCT	design control table
DDC	Digital Downconverter
dec or DEC	declination
deg	degree(s)
ΔDOR	Delta-Differential One-way Ranging
DIG	digitizer (assembly)
DMD	DSS Media Calibration (subsystem) or Data Monitor and Display (assembly)
DOR	differential one-way range
DRVID	differenced range versus integrated Doppler
DSCC	Deep Space Communications Complex
DSG	Downlink Signal Generator (a DSN assembly)
DSN	Deep Space Network
DSOC	Deep Space Operations Center

Abbreviation or Term	***Definition***
DSS	Deep Space Station
DSS-13	34-m research & development antenna at Goldstone DSCC
DSS-14	70-m antenna at Goldstone DSCC
DSS-24	34-m BWG antenna at Goldstone DSCC
DSS-25	34-m BWG antenna at Goldstone DSCC
DSS-26	34-m BWG antenna at Goldstone DSCC
DSS-34	34-m BWG antenna at Canberra DSCC
DSS-35	34-m BWG antenna at Canberra DSCC
DSS-36	34-m BWG antenna at Canberra DSCC
DSS-43	70-m antenna at Canberra DSCC
DSS-53	34-m BWG antenna at Madrid DSCC
DSS-54	34-m BWG antenna at Madrid DSCC
DSS-55	34-m BWG antenna at Madrid DSCC
DSS-56	34-m BWG antenna at Madrid DSCC
DSS-63	70-m antenna at Madrid DSCC
DSS-65	34-m HEF antenna at Madrid DSCC
DTF	Development and Test Facility
DTT	Downlink Tracking and Telemetry (Subsystem)
DVP	DSN VLBI Processor
E	
Eb/N0	energy per bit divided by noise power spectral density
EEIS	End-to-End Information System
EGRS	extra-galactic radio source
EIRP	effective isotropic radiated power
el, EL, elev	elevation
EOP	Earth Orientation Parameters (of the International Earth Rotation Service [IERS]) or Earth Orientation and Polar motion
F	
F/O	fiber optic
FER	frame error rate
FEC	Forward Error Correcting
FET	field effect transistor

Abbreviation or Term	***Definition***
FFT	Fast Fourier transform
FM	frequency modulation
FODA	Fiber-optic Distribution Assembly
FOM	figure of merit
FRD	Frequency Reference Distribution (a DSN Assembly)
FSTL	Frequency Standards Test Laboratory (at JPL)
FTP, ftp	file transfer protocol
FTS	Frequency and Timing Subsystem
G	
G/T	(antenna) gain divided by (operating system) temperature
GCF	Ground Communications Facility
GCN	Ground Communications Network
GCR	Ground Communications Router
GDS	Ground Data System
GDSCC	Goldstone (California) Deep Space Communications Complex
GMSK	Gaussian minimum-shift keying
GPS	Global Positioning System
GRA	GPS Receiver/Processor Assembly
GSFC	Goddard Spaceflight Center
GSSR	Goldstone Solar System Radar
H	
H/P	high power
HA	hour angle
HEF	high efficiency (antenna)
HEMT	high electron-mobility (field-effect) transistor
HPBW	half-power beamwidth
HRM	high-rate (radio loss) model
HSB	High-Speed Beam waveguide
Hz	hertz
I	
I/F	interface

Abbreviation or Term	***Definition***
IF	intermediate frequency
ICRF	International Celestial Reference Frame
ID	identifier or identification
IDC	IF-to-Digital Converter
IERS	International Earth Rotation and Reference Systems Service
IF	intermediate frequency
IIRV	Improved Inter-range Vector
IL_BET	In-lock Bit Error Tolerance
IPN	Interplanetary Networks (JPL Directorate)
IRIG	Inter-Range Instrumentation Group
ITRF	International Terrestrial Reference Frame
ITU	International Telecommunications Union
IVS	International VLBI Service for Geodesy and Astrometry
J-K	
JPL	Jet Propulsion Laboratory
J_y	Janskys
K	Kelvin
KEOF	Kalman Earth Orientation Function
km	kilometer
KSC	Kennedy Space Center
kW	kiloWatts
kHz	kilohertz
L	
LAN	local area network
LDPC	Low-Density Parity-Check
LCP	left (-hand) circular polarization
LITS/VCXO	Linear Ion-trap/Voltage Controlled Crystal Oscillator (frequency standard)
LNA	low noise amplifier
LO	local oscillator
LRM	low-rate (radio loss) model
M	

Abbreviation or Term	***Definition***
m	meters
MAP	maximum *a posteriori* probability
MASER	microwave amplification by stimulated emission of radiation
max	maximum
MB/s	Megabyte per second
MCD	Maximum Likelihood Convolutional Decoder
mdeg	millidegree
MDSCC	Madrid (Spain) Deep Space Communications Complex
ME	Master Equatorial
MGC	manual gain control
MHz	megahertz
MIL-71	Merritt Island Launch Area at the Kennedy Space Center
MILA	Merritt Island Launch Area
min	Minimum or Minute
MJD	Modified Julian Day
MNR	Metric Normalization Rate
MOC	Mission Operations Center
mod	modulation, module
MOS	Mission Operations System
mph	miles per hour
MRE	mean radial error
Ms/s	Mega samples per second
MSL	mean sea level
MSPA	multiple spacecraft per antenna
N	
NA, N/A	not applicable
NASA	National Aeronautics and Space Administration
NAV	Navigation
NCO	numerically controlled oscillator
NISN	NASA Integrated Service Network
NIST	National Institute of Standards and Technology
NMC	Network Monitor and Control (Subsystem)
NOAA	National Oceanic and Atmospheric Administration

Abbreviation or Term	***Definition***
NOCC	Network Operations Control Center
NRZ	non-return to zero
NRZ-L	non-return to zero, level
NRZ-M	non-return to zero, mark
NRZ-S	non-return to zero, space
NTIA	National Telecommunications and Information Administration
NTP	Network Time Protocol
O	
OD	Operator Directive
OOL_BET	Out-of-lock Bit Error Tolerance
OQPSK	offset quadrature phase-shift keyed
ORT	Operational Readiness Test
OVT	Operational Verification Test
P	
PCG	Phase Calibration Generator
PCFS	Personal Computer Field System
PCM	pulse-code modulation
PDF	probability density function portable document format (type or extension of computer file)
PDRVID	pseudo-DRVID
PDU	Protocol Data Unit
PFD	Photonic Frequency Distribution
PLL	phase-locked loop
PM	phase modulation
PN	pseudo-random noise
POCC	Project Operations Control Center
PSK	phase-shift keyed
Q	
QPSK	quadrature phase-shift keying
QQCL	quantity, quality, continuity, and latency

Abbreviation or Term	***Definition***
R	
R/T	real-time
R&D	Research and Development
RA	right ascension
RCP	right (-hand) circular polarization
rev	revision
RF	radio frequency
RH	relative humidity
RID	RF-to-IF Downconverter
RMDC	Radio-Metric Data Conditioner
RMS; rms	root-mean-square
RNG	range
RRP	Receiver and Ranging Processor
RRT	Receiver, Ranging and Telemetry
RS	Reed-Solomon (code), radio science
RSR	Radio Science Receiver
rss, RSS	root-sum-square
RTLT	round-trip light time
RU	range unit
S	
S/C	spacecraft
S/X	S-band or X-band
S/N	Signal-to-Noise
SCMF	Spacecraft Command Message File
sec	seconds
SEP	Sun-Earth-Probe (angle)
SER	Symbol error rate
SETSI	Secretaria de Estado de Telecomunicaciones para la Sociedad de la Informacion
SFDU	Standard Formatted Data Unit
SFODA	Stabilized Fiber-optic Distribution Assembly
SFTP	Secure File Transfer Protocol

Abbreviation or Term	***Definition***
SFU	solar flux units (one SFU = 1 □ 10^{-22} W/m^2/Hz)
SGA	Signal Generation Assembly
SLE	Space Link Extension
SMS	Service Management System (a DSN system)
SNR	signal-to-noise ratio
SPC	Signal Processing Center
SPD	S-Band Polarization Diplexed (feedcone)
sps	symbols per second
SPS	Service Preparation Subsystem (a DSN subsystem)
SPT	System Performance Test or System Performance Test Assembly
SQPSK	Staggered QPSK
SSH	Secure Shell
STEC	slant total electron content
stowed	With respect to an antenna, aimed near zenith for protection from the wind.
sub, subcarr	subcarrier
SYM	symbol
SYS	system
T	
T_{AMW}	Antenna-Microwave Noise Temperature
TBD	to be determined
TCT	Time Code Translator
TDDS	Tracking and Data Delivery System
TDM	Time-division multiplex
TDRSS	Tracking and Data Relay Satellite System
TDS	Telemetry Delivery Subsystem
TEC	total electron content
TLM	telemetry, Telemetry Service
TLP	Telemetry Processor
T_{OP}	T sub OP (operating system noise temperature)
T_{sky}	sky noise
TXR	transmitter or Transmitter Subsystem

Abbreviation or Term	***Definition***
U	
U/C	upconverter
U/L	uplink
UPA	Uplink Processor Assembly
UPL	Uplink (Subsystem)
URA	Uplink Ranging Assembly
USG	Uplink Signal Generator
USNO	United States Naval Observatory
USO	Ultra-Stable Oscillator
UTC	Universal Time, Coordinated
UTPM	Universal Time and Polar Motion
V	
VAC	vacuum
VC	virtual channel
VCDU	Virtual Channel Data Unit
VCO	voltage controlled oscillator
VCXO	voltage-controlled crystal oscillator
VEX	VLBI experiment
VLBI	Very-Long Baseline Interferometry
VMF	Vienna Mapping Function
VSR	VLBI Science Receiver
W	
WGS	World Geodetic System
WRMS	Weighted Root Mean Square
WVSR	Wideband VLBI Science Receiver
X	
X/KA	X-band or Ka-band
X-EL, XEL	cross-elevation
XMIT	transmit

Abbreviation or Term	***Definition***
XOR	modulo two addition
XRO	X-band receive only (feedcone)
XTR	X-band transmit-receive (feedcone)
Y-Z	
yr	year
ZDD	Zero-delay Device
ZEN	zenith